Osama M. Musa *Editor*

Handbook of Maleic Anhydride Based Materials

Syntheses, Properties and Applications

Springer

Handbook of Maleic Anhydride Based Materials

Osama M. Musa
Editor

Handbook of Maleic Anhydride Based Materials

Syntheses, Properties and Applications

Springer

Editor
Osama M. Musa
Ashland Inc.
Bridgewater, New Jersey
USA

ISBN 978-3-319-29453-7 ISBN 978-3-319-29454-4 (eBook)
DOI 10.1007/978-3-319-29454-4

Library of Congress Control Number: 2016952878

Printed on acid-free paper

This Springer imprint is published by Springer Nature
The registered company is Springer International Publishing AG Switzerland

Preface

Within the chemical industry, the chemical compound known as maleic anhydride is a critical material that is globally produced at significant and increasing volumes. The wide availability of this compound is due to a precious coupling of low cost and high functionality. This *functionality* easily bridges the domains of chemical synthesis and transformation to extreme market application and diversification. This functionality is further reflected in the tens of thousands of peer-reviewed journal articles and granted patents that highlight some form of maleic anhydride utility.

This book is written from the perspective of an industrial scientist. By bridging the science and technology found in both academia and industry, a comprehensive and contemporary picture of maleic anhydride's impact on the world today, as well as tomorrow, emerges. Perhaps the most unique aspect of this work is the group of scientists that prepared and contributed to this manuscript. They are all members of the Research and Development community at Ashland, Inc., where maleic anhydride is a *core technology*. This team closely collaborated and debated the most relevant technical topics, which should be of great benefit to the reader.

Remembering that in 1982, B.C. Trivedi and B.M. Culbertson coauthored the seminal book entitled "Maleic Anhydride," covering topics such as its production, chemical reactions, and polymerizations. This comprehensive treatise was a truly ambitious achievement. Our book seeks to build upon this foundation, built 34 years ago, by focusing on many of the key technical insights and commercial developments since 1982. It is my hope that the reader will obtain a deeper and more comprehensive understanding of the beauty, nuances, and complexities of maleic anhydride through our exploration of production, synthesis and transformation, and diverse application topics that are incorporated into these ten chapters.

Chapter 1 reviews the main production processes, analyzes the current understanding of catalyst structure/function in the butane oxidation process, and reviews a variety of contemporary research topics such as catalyst additives that improve yield and purity, catalyst dimensional strength, morphology, porosity, shape, regeneration, reactor designs, and improvements in product quality and safety.

Chapter 2 reviews virtually all maleic anhydride chemical reactions, including its acid form, in the context of the influence the parent structure imparts on the molecule's final behavior and properties.

Chapter 3 reviews small molecule chemistry and applications such as maleated-vegetable oil derivatives and its oligomeric products. Modern topics such as maleimide-based compounds are also detailed in elegant fashion.

Chapter 4 is a detailed review of the maleic anhydride-*co*-alkyl vinyl ether copolymer family of materials discussing polymerization, architecture, physical properties, and attributes.

Chapter 5 reviews other industrially significant polymers, ranging from unsaturated polyester and alkyd resins to styrenic, acrylic, and N-vinyl amide copolymers. Incorporated into this overview are recent advances in controlled free radical polymerization materials.

Chapter 6 highlights higher molecular weight maleic anhydride-derived polymers. Polymerization processes, including alternating copolymers by conventional free-radical methods, as well as newer approaches such as ROMP methodologies are discussed.

Chapter 7 discusses the colloidal and physicochemical properties for maleic anhydride-based polymers in addition to providing insight into how such material features can relate to application performance.

Chapter 8 provides an in depth discussion of key Personal Care applications of maleic anhydride in markets ranging from Hair Care and Skin Care to Transdermal Delivery and Oral Care. Maleic anhydride chemistry is paramount in many commercially available consumer products in this arena and where it has become an essential key ingredient.

Chapter 9 reviews the utility of maleic anhydride in industrial adhesive and coating applications in markets ranging from coatings, boats, and electronics through the exploitation of materials including alkyd resins, reactive polymeric surfactant, unsaturated polyester resins, bismaleimides, and epoxy resins. Insights into printing and imaging materials are also incorporated into this discussion.

Chapter 10 is a continuation of Chap. 9, where the variety of different application areas of maleic anhydride chemistry is expanded into lubricants, fuels, and biologically active compounds as well as pharmaceutical compositions, microencapsulation, thermoplastics, films, and water treatment materials.

This book provides the reader with a broad and in-depth resource on maleic anhydride and its derivatives, enabling a more complete understanding of the science and technology of maleic anhydride.

Bridgewater, NJ Osama M. Musa

Acknowledgements

I would like to gratefully acknowledge the authors and their families, who sacrificed significant time and effort to make this text possible. I would also like to thank my family for their tremendous patience and encouragement.

Finally, on behalf of the authors, I would like to thank the management of Ashland Inc. for their support in bringing this manuscript to fruition.

Contents

Part IV Applications

Biography

Osama M. Musa Ph.D. Dr. Osama M. Musa is currently Vice President and Chief Technology Officer for Ashland Inc. (NYSE: ASH). He leads Ashland's Global Research and Development focusing on consumer and industrial markets including pharmaceutical, personal care, beverage, nutrition, agricultural, coatings, adhesives, and energy applications. Dr. Musa has overall responsibility for the global technology platforms including Molecular Science, Measurement Science, Process Research, Biofunctionals, Acrylates & Microencapsulation, Preservatives & Microbial Technology, as well as the R&D Stage-Gate development process. He also leads the R&D Council and Multifunctional Innovation Engagement Team, which are charged with managing and enhancing new product development processes. In addition to these technical roles, he has the commercial and technical responsibility for Ashland's Advanced Materials business.

Dr. Musa is a strategic R&D leader with broad experience in the specialty chemicals business sector. He utilizes a wide-ranging network, cooperating with partners both in the industry and in academia. Dr. Musa joined Ashland in 2011 following the company's acquisition of International Specialty Products (ISP) Incorporated. Previously, he held technical and leadership positions with the National Starch and Chemical Company.

As a passionate leader, Dr. Musa is committed to addressing customer needs through the application of innovative chemistry. He holds more than 50 issued U.S. patents and has authored numerous technical publications. From Ashland's Open Innovation platform, he cultivates student scholarship through numerous collaborations with universities, providing encouragement and motivational mentoring to the next generation of young, promising scientists. He serves as a

member of the Board of Advisors at Manhattan College's Department of Electrical and Computer Engineering.

Dr. Musa earned a Ph.D. in organic chemistry from Wayne State University, where he also completed a postdoctoral fellowship. In addition, he received an M.S. in macromolecular chemistry from the University of Detroit Mercy, an M.S. degree in heterocyclic organic chemistry from the University of Jordan, and a B.S. in chemistry from Yarmouk University.

Part I
Introduction

Chapter 1
Progress in Maleic Anhydride Production

David K. Hood and Osama M. Musa

1.1 Introduction

Maleic anhydride (furan-2,5-dione) is a key component to an incredibly diverse group of chemistries and commercial applications. The ability of maleic anhydride to achieve such great diversity is a direct result of the maleic anhydride's industrial complex capacity to develop economical production routes in the face of ever-increasing governmental scrutiny, fierce pricing pressures, and tremendous technical requirements (at significant volumes) coupled to high demand for quality fundamental product properties.

What is it about maleic anhydride that creates such demand, utility, and value? The two critical success factors are chemistry and economics. Both are truly connected, intertwined, and inseparable. First, the basic chemical structure of maleic anhydride is inherently versatile. Maleic anhydride, based upon a five-member heterocyclic ring, comprises a double bond at the C_3–C_4 position and two carbonyl groups, one at the C_2 position and the other at the C_5 position (see Scheme 1.1, Left). The double bond is well known to be very reactive. Maleic anhydride is a powerful electron-accepting monomer due to the electron-deficient character of double bond. The electronic deficiency originates from the two C = O substituent group's strong electron-withdrawing forces.

Upon exposure to water, maleic anhydride can hydrolyze to yield a dicarboxylic acid structure known as maleic acid. The chemical structure of maleic acid is presented in Scheme 1.1 (Right). In addition to the reactive double bond, these carboxylic acid groups are also well known for high reactivity coupled to two distinct acid dissociation constants. Dehydration of maleic acid enables the reformation of maleic anhydride. Key physical properties for these two chemical compounds are presented in Table 1.1.

D.K. Hood (✉) • O.M. Musa
Ashland Inc., 1005 Route 202/206, Bridgewater, NJ 08807, USA
e-mail: dhood@ashland.com

O.M. Musa (ed.), *Handbook of Maleic Anhydride Based Materials*,
DOI 10.1007/978-3-319-29454-4_1

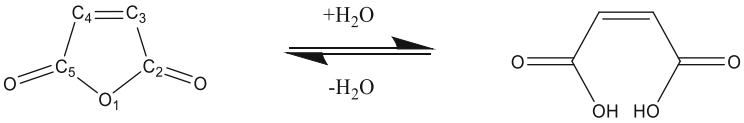

Scheme 1.1 Maleic anhydride and maleic acid, respectively

Table 1.1 Key physical properties for maleic anhydride and maleic acid

Property	Maleic anhydride	Maleic acid
CAS number	108–31–6	110–16–7
EINECS number	203–571–6	203–742–5
Molecular formula	$C_4H_2O_3$	$C_4H_4O_4$
Molecular weight (g/mol)	98.06	116.07
Physical state	Solid	Solid
Color	Colorless to white [1]	White [2]
Odor	Irritating, choking [1]	Odorless [2]
Density	1.48 [3]	1.59 [3]
Melting point (°C)	53.58 [1]	132.5 at 101.3 kPa [2]
Boiling point (°C)	200.1 [1]	157.8 at 99.7 kPa [2]
Vapor pressure	0.033 kPa [1]	9×10^{-7} kPa at 20 °C [2]
Refractive index [$d^{20}{}_{20}$ (solid)]	NA	1.590 [4]
Heat of formation (kJ/mol)	−470.4 [5]	−788.3 [6]
Heat of fusion (kJ/mol)	12.26 [7]	26.9 [7]
Heat of sublimation (kJ/mol)	71.5 ± 5.0 [7]	105.4 ± 1.7 [7]
Heat of combustion (kJ/mol)	−1391.2 [6]	−1358.9 [6]
Specific heat (liquid) (kJ mol^{-1} K^{-1})	−1.67 [6]	NA
Heat of evaporation (kJ/mol)	54.8 [6]	NA
Solubility in water	~400 g/L at 20 °C [1]	478.8 g/L at 20 °C [2]
pKa	NA	$pK_1 = 1.910$; $pK_2 = 6.332$ [8]
Biodegradation	Readily biodegradable [1]	Readily biodegradable [2]

Within these two chemical compounds are a wide variety of possible chemical transformations. From free radical and charge transfer polymerization processes to Diels–Alder, esterification, and amidation reactions, these thematic transformations form the basis of the tremendously flexible synthetic platform provided to the myriad of chemical technology implementers.

Second, the economics of maleic anhydride are particularly attractive. Maleic anhydride is largely derived from butane gas, especially in North America, but can also be produced from benzene. Both production routes remain the most relevant feedstocks in global product supply. Butane, C_4H_{10}, is a colorless, odorless gas that is normally shipped under pressure in the form of a liquefied gas. Common synonyms for butane are n-butane, butyl hydride, diethyl, liquefied petroleum

Table 1.2 Examples of compositional variation of natural gas with geographical location [11]

	Example 1	Example 2	Example 3
State	Colorado	New Jersey	New Mexico
County	Cheyenne	Offshore	Chaves
Field	Cheyenne Wells	Mid-Atlantic	Buffalo Valley
Methane (mole %)	9.2	94.1	89.1
Ethane (mole %)	3.0	2.0	6.6
Propane (mole %)	25.5	0.8	2.2
n-Butane (mole %)	20.9	0.1	0.7
Isobutane (mole %)	10.2	Trace	0.1
n-Pentane (mole %)	3.7	0.0	0.2
Isopentane (mole %)	9.4	0.1	0.3
Cyclopentane (mole %)	1.1	Trace	0.1
Hexanes plus (mole %)	2.6	Trace	0.1
Nitrogen (mole %)	10.0	1.1	0.4
Oxygen (mole %)	0.1	0.0	0.0
Argon (mole %)	0.1	Trace	Trace
Hydrogen (mole %)	0.0	0.2	0.0
Hydrogen sulfide (mole %)	1.8	0.0	0.0
Carbon dioxide (mole %)	2.4	1.7	0.2
Helium (mole %)	0.12	0.02	0.04
Heating value	2605	1018	1135
Specific gravity	1.713	0.596	0.639

gas, and methylethylmethane [9]. This chapter will employ the term "C_4" to mean butane. C_4 is produced by refining materials that originate from either crude oil or natural gas. Natural gas is often found in geological shale deposits and tight sands. Recent advancements in horizontal drilling and well-completion technologies, particularly in low-permeability formations, have liberated tremendous reservoirs of supply in large sections of the North American continent [10]. Geographic regions spanning from Western Canada to Appalachia and the Gulf Coast are producing significant quantities of natural gas [10]. Natural gas as such is comprised of regionally varied amounts of gases, which is often, but not always, dominated by methane gas. Examples of compositional variations are presented in Table 1.2.

With existing pipeline infrastructures, very large volumes of natural gas as well as discrete, refined gases, such as C_4, can be transported to key downstream facilities. C_4 is commonly stored in underground caverns, such as the 1MM barrel (bbl) cavern recently constructed near Neal, West Virginia [12]. More modest volumes, ranging from 800 bbl to 1600 bbl, are stored in aboveground pressurized vessels [13]. Thus, economies of global scale and positive supply chain dynamics exist in significant ways for continued maleic anhydride growth potentials.

In 1982, Trivedi and Culbertson's *Maleic Anhydride* published a broad overview of maleic anhydride production technology in a chapter entitled *Production of*

Maleic Anhydride [14]. The processes detailed in this chapter spanned the three main production routes: benzene, C_4, and phthalic anhydride. Benzene routes designed by Scientific Design, Ruhrol-Lurgi, Ruhrol-Bayer, and Sava were discussed in detail. C_4 routes by Mitsubishi and BASF were previewed followed by a brief discussion of phthalic anhydride by-product sourcing. In 2001, *Maleic Anhydride, Maleic Acid, and Fumaric Acid* was published in the Kirk-Othmer Encyclopedia of Chemical Technology [15]. C_4 routes by Huntsman (formerly Monsanto), ALMA, and DuPont were discussed in detail. This author is fortunate to use these chapters as a backdrop to efficiently analyze more recent technical trends and accomplishments that have empowered the maleic anhydride product, as it nears its ninth decade in commercial production. It is hoped that the reader will benefit from the wide-ranging discussion, enabling a broader appreciation for the scope of technologies, challenges, and current solution strategies that exist in current maleic anhydride production.

1.2 Historical Overview

Historically, the two main commercial routes to maleic anhydride production are by the thermal oxidation of benzene or C_4 feedstocks via heterogeneous catalysis. In 1982, it was reported that the benzene route was favored due to the lack of efficient catalysts and purification processes for suitable C_4 process implementation. However, it was also noted that increasing environmental regulations on the benzene route were expected to lead to significant research efforts in the field in order to develop new, more environmentally sustainable processes. In a time frame of about 15 years, the C_4 route evolved into the preferred production process, certainly within the USA. Today, C_4 is the dominant commercial route for maleic anhydride production and is recognized for its superior economics [16].

Stoichiometry favors the C_4 route, where 100 kg of C_4 should yield 168.9 kg of maleic anhydride. Conversely, 100 kg of benzene is only expected to yield 125.6 kg of maleic anhydride [17]. During the C_4 oxidation process, there are a number of less desirable but significant side products: butadiene, furan, crotonaldehyde, and C_4 isomers. Principally, the main products are maleic anhydride [Eqs. (1.2) and (1.3)] and unstable intermediates (Eq. 1.1). The reaction schemes for various oxidation process steps are presented below [18]:

$$C_4H_8 + \frac{(12-m)}{2}\,O_2 \rightarrow m\mathrm{CO} + (4-m)CO_2 + 4H_2O \tag{1.1}$$

$$C_4H_8 + 3O_2 \rightarrow C_4H_2O_3 + 3H_2O \tag{1.2}$$

$$C_4H_2O_3 + \frac{(6-n)}{2}\,O_2 \rightarrow n\mathrm{CO} + (4-n)CO_2 + H_2O \tag{1.3}$$

$$CO + \frac{1}{2}O_2 \rightarrow CO_2 \tag{1.4}$$

1.2.1 Early Maleic Anhydride (via C_4) Production Examples

The literature is imprecise as to when the first maleic anhydride (via C_4) production process was fully implemented. Some point to 1975, where Amoco deployed a Chem Systems process [19]. However, other literatures present published examples prior to 1975. For example, Mitsubishi Chemical Industries announced a fluid-bed reactor capable of 18,000 tons/year operating in Mizushima, Japan, as of 1970 [20]. BASF announced a fixed-bed reactor plant capable of 3000 tons/year operating in Ludwigshafen, Germany, in May 1968 [21]. The earliest process was likely Petro-Tex in a Scientific Design-engineered plant in 1962 (near Houston, Texas) [22]. Reportedly, this effort struggled in the early years due to competition from cheaper benzene and was eventually stopped in favor of the overall benzene economics [22]. The earliest plants typically state a capability to interchange feedstock between benzene and C_4 enabling economic forces to balance the basic plant operating conditions.

Because of the basic interchangeability of feedstock, the key production technologies comprise very similar design concepts and equipment schemes. The two main production processes employ either fixed-bed or fluid-bed oxidative designs. Every major maleic anhydride production process is equipped with a reactor, gas cooler, separator, scrubber, refiner/condenser, and product column collector. To better understand the role of each step, we will first examine a Halcon–Scientific Design (HSD) process.

1.2.1.1 Halcon–Scientific Design (HSD) Fixed-Bed Process [23]

Early maleic anhydride production processes were benzene based. The existing capital equipment was then converted to C_4-based processes. A prime example of a convertible feedstock plant is the Halcon–Scientific Design (HSD) process for maleic anhydride manufacture. A schematic of this process is presented in Scheme 1.2.

Interpreting the HSD process, from left to right, either benzene or C_4 is fed into a compressed air line to be presented into a carbon steel reactor comprised of numerous tubes nominally 3.7 m long and 25 mm in diameter [25]. In this case, the process is fixed bed, where the C_4 and air are mixed, normally 1.0 to 2.0 mol percent of C_4, prior to introduction to the reactor, which houses the catalyst. The reactor is often positioned in an upflow configuration. The pressure in the operating reactor, ranging from 20 to 50 psi, [26, 27] is close to atmospheric requiring only enough pressure to move the gas through the catalyst bed [1800–2800 gas hourly

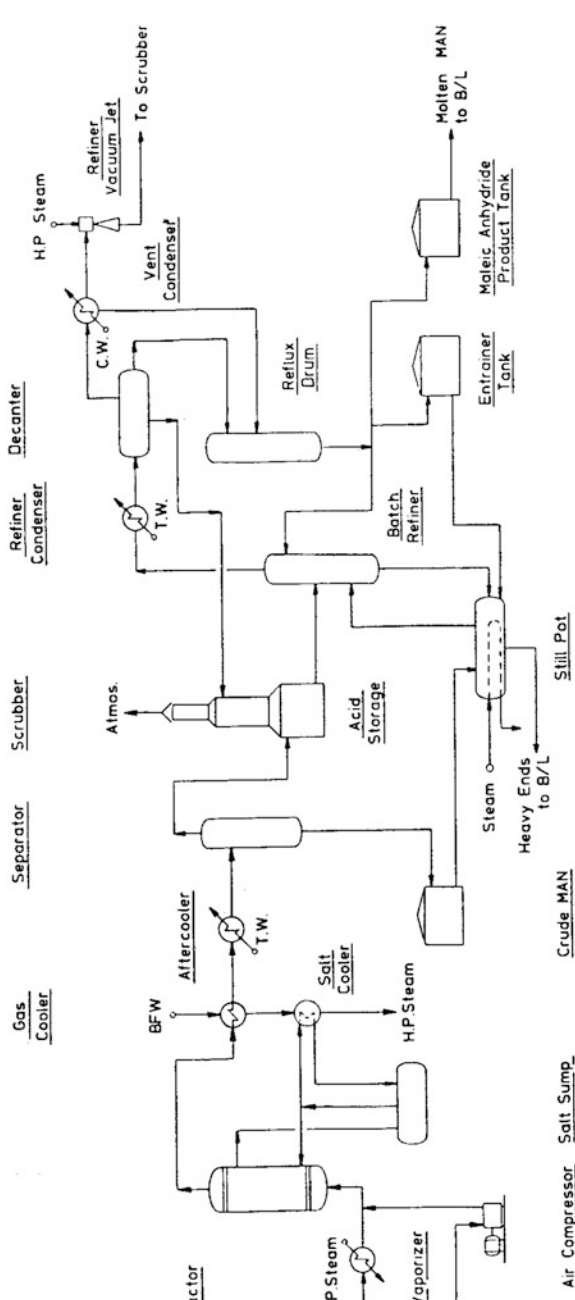

Scheme 1.2 Halcon–Scientific Design (HSD) process for maleic anhydride [24] (Adapted from Environmental Progress, Malow, M., Vol. 4, No. 3, Maleic Anhydride via Butane Oxidation Substitution of n-butane for benzene in the production of maleic anhydride has led to the solution of a serious environmental problem, 151–154, Copyright August **1985** with permission from John Wiley and Sons)

space velocity (GHSV)] [28]. The catalyst is housed in tubes, often numbering in thousands, and surrounded by a heat transfer fluid system. Typically, the catalyst tubes are first packed with an inert material, i.e., metal or ceramic balls, to preheat the gas flow prior to exposure to the catalyst [28]. The reactor heat and heat exchanger are supplied by molten salts. The temperature range of these salts is typically between 390 and 430 °C. These eutectic salt mixtures comprise salts such as potassium nitrate, sodium nitrate, and sodium nitrite (i.e., HITEC®) [25]. Many processes recycle this heat in the form of steam generation for additional energy supply. Upon exiting the reactor, the process stream enters a gas cooler, often fabricated from carbon steel [25]. Partial cooling is applied to the process stream in order to reduce its temperature to just below maleic anhydride dew point (53–60 °C). The cooled materials then enter a separator, constructed of stainless steel, enabling a crude separation between the partially condensed maleic anhydride and other gases and uncondensed vapors. The condensed maleic anhydride is destined for the still pot. It is critical to monitor the temperature at this stage. If the maleic anhydride solidifies, the process can experience blockages coupled to pressure and temperature challenges. The gas flow continues onto a scrubber unit, which is constructed of a grade of stainless steel that includes molybdenum. The gas flow is contacted with a countercurrent of water to absorb remaining maleic anhydride in the hydrolyzed form of maleic acid [29]. Remaining, unabsorbed overhead gases are exhausted either to the atmosphere or an incinerator. Maleic acid is collected and later pumped to the refiner for further purification processing. In the stainless steel refiner/condenser batch unit, maleic acid solution is first dehydrated (azeotropically) with xylenes or toluene. This remaining solution is then combined with the maleic anhydride from the still pot for refining. The crude maleic anhydride is refined via vacuum distillation. Normally, a forecut at high reflux is removed followed by collection of product at lower reflux. The molten maleic anhydride is collected for sale or further converted into pastilles or briquettes for easier handling. Typical product impurities from such processes include acrylic acid and acetic acid [30].

During the operation of this process, two challenges must be understood and controlled: hot spots and gas mixtures. First, as gases are fed into the reactor tubes, these gases are generally cooler than the mixed salts in the heat exchanger, leading to a cooling effect of the salt mixture in the heat exchanger. A more significant problem is if the gas temperature in the reactor tubes is greater than the salt mixture in the heat exchanger. Under this scenario a hot spot can be generated in the catalyst tubes. If not controlled, these hot spots can negatively affect the catalyst life and reactor maintenance and decrease the reactor yield. Operational control of the temperature is challenging because there are normally thousands of tubes and only a few points of temperature measurement [25]. Hot spots can also lead to possible runaway process conditions. It is critical that the operator understand the hot spot effect, employing modeling and empirical observations in detail, to achieve the maximum operating efficiency [31]. Second, careful monitoring of the gas mixtures is required, thereby ensuring operation at the appropriate temperatures relative to the inherent flammability limit of the process gas mixture. Typically, the

reactor inlet is set for the lower flammability limit of butane in air, and the exit line is set for the lower flammability of the combustible composition at the reactor exit [25]. For additional safety, the reactors are equipped with rupture disks at both the reactor inlet and exit areas in case of a runaway event [25].

1.2.1.2 ALMA Fluid-Bed Process

In early 1984, Alusuisse Italia/Lummus Crest (ALMA) began operating a 3000 ton per year maleic anhydride reactor system in Scanzorosciate, Italy [32]. A key element to this plant was the implementation of a fluid-bed reactor. A schematic of this plant is presented in Scheme 1.3:

In this reactor configuration, C_4 and air are fed separately, from 2 to 8 volume percent C_4 in air, into the bottom of the reactor for presentation to the fluidized catalyst bed [34]. The reactor is typically operating at 360–460 °C [35]. Fluidized-bed reactors tend to operate at higher C_4 concentrations and process stream residence times versus typical fixed-bed processes [15]. Heat generated during the oxidative process is removed from the reactor via steam coils that are in intimate contact with the fluidized solid materials. Reactors of this type are known to exhibit

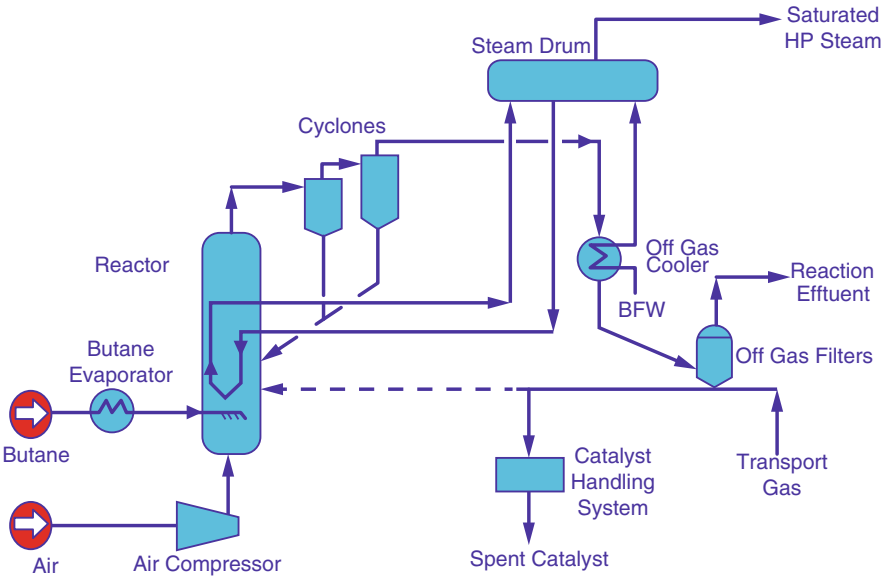

Scheme 1.3 Simplified flow sheet of the reaction section of the Lonza ALMA process for maleic anhydride production [33] (Springer and Topics in Catalysis, Vol. 38, Nos. 1–3, 2006, page 148, "VPO catalyst for n-butane oxidation to maleic anhydride: A goal achieved, or a still open challenge?," Ballarini, N.; Cavani, F.; Cortelli, C.; Ligi, S.; Pierelli, F; Trifiro, F.; Fumagalli, C.; Mazzoni, G.; Monti, T., Fig. 1.1, Copyright 2006 with kind permission from Springer Science and Business Media)

excellent heat transfer between fluidized solids and steam coils enabling smaller heat transfer zones as compared to a typical fixed-bed reactor. As a result, hot spots are typically less problematic. As with fixed-bed processes, the process heat generated is often recycled to drive reboiling and turbine drives. One interesting component to the process is the ability to change catalyst during operation by intermittently adding a virgin catalyst to maintain stable activities and particle size distributions (~80–150 μm) [15, 34]. Gas flow patterns are generally back-mixed, a reverse circulation flow pattern for a material in a process, and are a common challenge that leads to enhanced impurity profiles and reduced yields [34]. For equipment, a large volume of space is required above the catalyst fluid bed to enable separation of solids and gases. Partitioning of the solids is achieved by cyclone and filter separation. Once separated, the product gas stream is cooled prior to the collection and refining stages. As in the fixed-bed processes, any tail gases are incinerated prior to venting. The process employs solvent adsorption to selectively remove maleic anhydride from the cooled reactor effluent. Typically, the solvent is a cycloaliphatic acid dialkyl ester such as dibutylhexahydrophthalate [36]. From there, the maleic anhydride solvent mixture is pumped to the stripper where crude maleic anhydride is separated as distillate. This material is fed to the light ends column where small amounts of impure light ends are removed and incinerated. The remaining materials are fed to the product column where the maleic anhydride product is recovered as distillate and residuals are pumped back to the stripper. There is also a solvent purification loop to prevent the buildup of impurities in the solvent. Process impurities typically consist of carbon monoxide and acetic and acrylic acids [34].

1.2.2 Fixed-Bed and Fluid-Bed Comparisons

In analyzing these two established reactor technologies, a comparison scheme proposed in 1985 by Wellauer is presented in Table 1.3.

Table 1.3 presents a logical map to determine where the key areas of development are required to improve such processes. For fixed-bed reactors, topics ranging from

Table 1.3 Comparison of reactor technologies [37, 38]

	Fixed-bed reactor	Fluid-bed reactor
Capital requirements	Large	Less significant
Design knowledge	Clear	Emerging
Increasing scale	Straightforward	Challenging
Ease of operation	Straightforward	Challenging
Pressure drop	Major	Minor
Back-mixing	Insignificant	Challenging
Heat transfer	Not good	Good
Catalyst attrition	Insignificant	Challenging
Catalyst pore diffusion	Critical	Minor
Regeneration of catalyst during operation	Challenging	Minor

heat transfer, pressure control, catalyst porosity/geometry, as well as catalyst regeneration would be expected to be of keen interest to manufacturers that employ such processes. Likewise, process modeling for increasing production scale, back-mixing, and catalyst attrition are topics that would be of particular interest to fluid-bed reactor designers and operators. As we will see later, this map was effective in identifying the relevant, thematic topics of research that have since emerged.

1.2.3 Industry Response

In 1978, the majority of maleic anhydride manufacturing in the USA was by the benzene route. Within 8 years, this manufacturing had been largely converted to C_4 feedstocks [37]. This shift becomes even more apparent by reviewing the data presented in Table 1.4.

Despite a trend toward fewer major North American (NA) suppliers (a few major plant acquisitions are reflected in Table 1.4 by arrows) and reductions in plant numbers, not only did the feedstock shift but overall industrial production volumes increased. Such trends suggest that the current facilities have been able to operate more efficiently and more competitively in an increasingly global marketplace.

The industry has transitioned from benzene to C_4. What are the main technical insights that have emerged to enable a successful transition to C_4 feedstocks? How have the general plant operating efficiencies been enhanced? Beyond the obvious importance of plant engineering is the requirement for optimized materials, especially catalysts. It is the catalyst that is the real keystone to the entire maleic anhydride industry. We must have a deeper, more fundamental understanding of these specialized materials and their behavior in order to appreciate the current industrial improvement efforts that are under way. Consequently, we now transition the discussion into the world of catalytic oxidation science to understand the basic structure of these materials and their resulting function, remembering to keep in mind that these materials are critical to all of the manufacturing environments we have previously discussed.

Table 1.4 Annual production capacity of NA maleic anhydride in the USA (tons/year) [37, 39, 40]

Company	1978		1981		1986		2007		2012	
	Benzene	C_4	Benzene	C_4	Benzene	C_4	Benzene	C_4	Benzene	C_4
Amoco	--	27,000	--	27,000	--	27,000	--	--	--	--
Ashland	27,000	--	14,000	14,000	--	23,000	--	45,000	--	45,000
Denka	23,000	--	--	20,000	--	23,000	--	--	--	--
Flint Hills Resources	--	--	--	--	--	--	--	50,000	--	50,000
Huntsman	--	--	--	--	--	--	--	110,000	--	155,000
Koppers	15,000	--	--	--	--	--	--	--	--	--
Lanxess	--	--	--	--	--	--	--	75,000	--	75,000
Monsanto	42,000	10,000	42,000	10,000	--	97,000	--	--	--	--
Reichhold	45,000	--	27,000	--	--	--	--	--	--	--
Tenneco	12,000	--	12,000	--	--	--	--	--	--	--
USS	36,000	--	36,000	--	--	16,000	--	--	--	--
Total	200,000	37,000	131,000	71,000	--	186,000		280,000		325,000

1.3 Catalysis: Progress in Structure and Function

Thermal, oxidative catalysis is an essential component to the success of commercial maleic anhydride production. It is a complex topic to which significant research resources, both in industry and academia, are dedicated. To better understand the fundamental elements of this catalytic process, we will break this topic down into two distinct discussions: inorganic catalyst structure and proposed C_4 catalytic oxidation mechanisms. With this background, the reader is expected to gain a more representative insight to the current trends in this field.

1.3.1 Inorganic Catalyst Structure

Vanadium oxides represent the most important catalyst class in C_4 oxidation. Vanadium found in vanadium oxides can exist in a variety of oxidation states (+5, +4, +3, and +2). This broad range of oxidation states enables vanadium to form numerous coordination polyhedral structures that can include tetrahedron, trigonal bipyramid, square pyramid, distorted octahedra, and rectilinear octahedra [41]. Specifically toward maleic anhydride production, the key oxidation states are V^{5+} and V^{4+} [42]. Perhaps the most important form of vanadium oxide is vanadyl pyrophosphate which is considered the common template. Remembering that the typical maleic anhydride process occurs at high temperature (i.e., ~400 °C), where the catalytic precursor is in a dehydrated state and effectively in a catalyst heat treatment environment, the active component responsible for the oxidation process is attributed to $(VO)_2P_2O_7$ [42]. Literature nomenclature references to $(VO)_2P_2O_7$ include both vanadyl diphosphate and vanadyl pyrophosphate [43, 44]. We will employ VPO to refer to this inorganic composition. VPO is comprised of two polyhedra that are connected through oxygen-bridging: VO_6 and PO_4. The basic polyhedra structures, which are depicted in the most common illustration styles, are presented in Scheme 1.4.

VO_6 is often referred to as a distorted octahedron, where the centrally located vanadium atom is coordinated to six oxygen atoms. Other references cite a VO_5 square pyramid that is weakly coordinated to another O from a neighboring VO_5 square pyramid. The distinct feature of this structure is the vanadyl group (Scheme 1.4a) that forms a double bond to oxygen, denoted as V = O. This particular bond is shorter than the others resulting in a distortion of the octahedron. Bond lengths determined on single green crystals are present in three ranges: ~1.6 A (V = O, "short"), ~2 A (~coplanar V–O), and ~2.3 A (V–O, "long") [45]. The structure for PO_4 (Scheme 1.4b) is a tetrahedron where the centrally located phosphorus atom is coordinated to four oxygen atoms. Bond lengths are found to be ~1.5 A [45]. Bond valence calculations yield ~4.1 for V and ~4.9 for P, corresponding to V^{4+} and P^{5+}, respectively [45].

From these two basic structures, the VPO catalyst architecture begins to emerge, as illustrated in Fig. 1.1. Vanadium polyhedra are equatorially

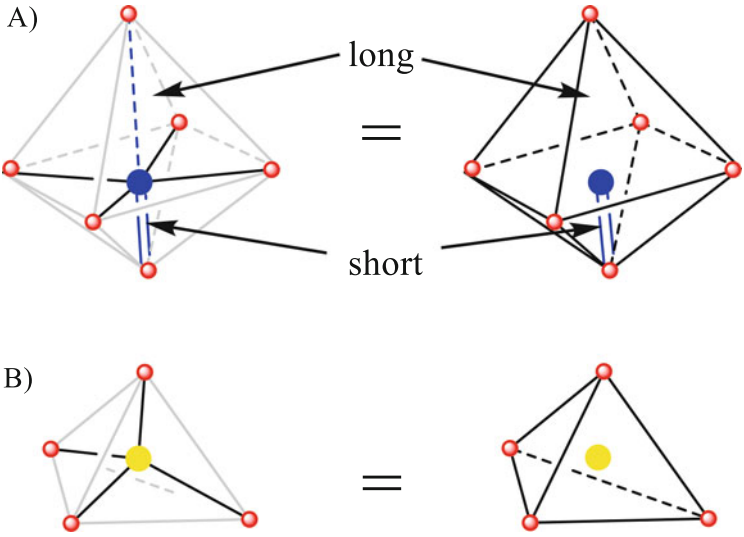

Scheme 1.4 VO_6 and PO_4 crystal structures [41, 43] (*filled blue circle* is vanadium; *filled yellow circle* is phosphorus; *open red circle* is oxygen)

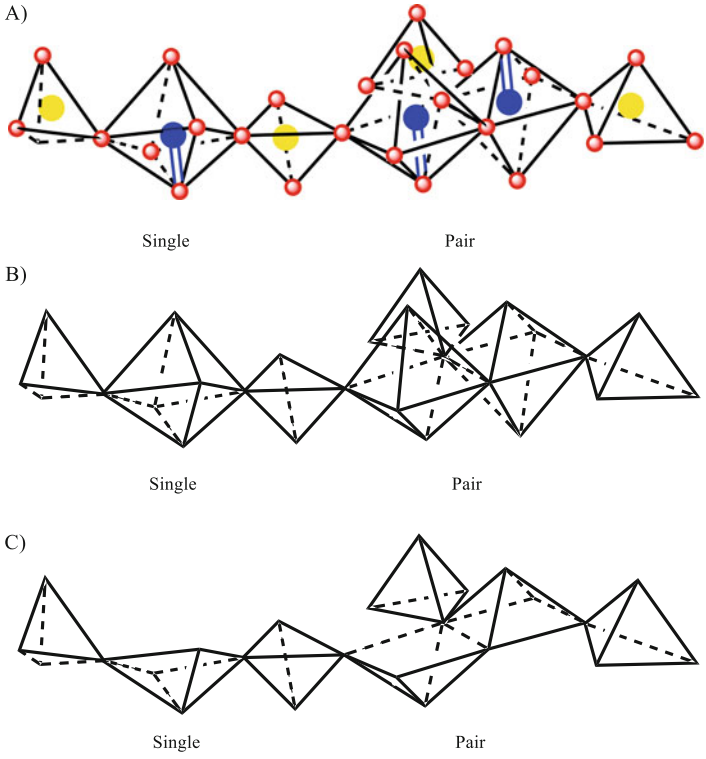

Fig. 1.1 Various VO_6 and PO_4 connective structures in an idealized VPO strand (*filled blue circle* is vanadium; *filled yellow circle* is phosphorus; *open red circle* is oxygen)

connected, in a *trans*-oriented manner, exhibiting an oscillating structure due to the spatial arrangements of the short V = O and long V–O bonds. The four nearly coplanar oxygen atoms bonded to the central vanadium atom are linked to P via either single PO_4 groups or double tetrahedral pyrophosphates (P_2O_7), where the oxygen atoms are shared [42]. Because V^{3+} is not known to be common to mild oxidation catalysis, it is generally not represented. Consequently, two general structures prevail: one single distorted octahedron and a pair of distorted octahedra [42]. Examples of these various connective structures are presented in Fig. 1.1 for an idealized VPO strand. Note that Fig. 1.1 presents these idealized strands in three common illustration styles found in the literature. Also note that the bond angles are not actualized and these structures are only to be considered a general representation.

Figure 1.1a presents formal oxygen atoms to highlight oxygen bridging between the polyhedral, while Fig. 1.1b presents such bridges through implication. Perhaps least intuitively, Fig. 1.1c eliminates the long V–O bond contribution from the distorted octahedron, presenting VO_6 as a square pyramidal polyhedron to simplify the vanadium environment for visual interpretation.

From visualizing simple individual strands, a more complete VPO can be confidently presented and investigated. Negating the long V–O bond from VO_6, as previously discussed, and presenting the square pyramidal polyhedron (dark gray) and including tetrahedral (light gray), PO_4 crystals enable the presentation of the ideal orthorhombic VPO crystal structure in Fig. 1.2.

Upon further examination of Fig. 1.2, one finds crystalline sheets comprised of VO_6 polyhedra with alignments that are further distorted by variations in the group arrangements of tetrahedral phosphate. Unlike previous results, which demonstrated a low degree of symmetry and eight distinct V atoms, more recent results yield improved accuracy and four distinct V atoms. This ideal structure is expected to differ from commercial VPO catalyst structures due to additional defects caused by impurities as well as other inherent structural complications [45].

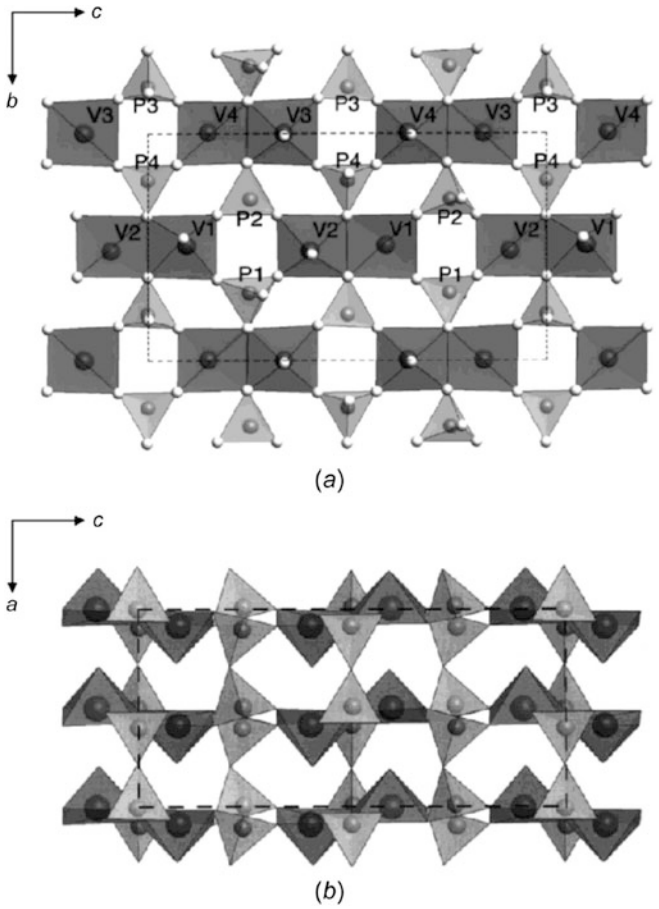

Fig. 1.2 Polyhedral representation of the crystal structure of $(VO)_2P_2O_7$ viewed (**a**) along the [100] direction and (**b**) along the [010] direction. The VO_5 square pyramids are drawn in dark grey, the PO_4 tetrahedra in light grey. Large circles represent V atoms and medium circles represent P atoms. *Small circles* in (**a**) denote O atoms, which are not shown in (**b**). [46] (Geupel, S., Pilz, K., Smaalen, S. van, Büllesfeld, F., Prokofiev, A., Assmus, W. (2002) Acta Cryst. C58, 9-13. Reproduced with permission of the International Union of Crystallography)

1.3.2 Proposed C_4 Catalytic Oxidation Mechanisms

The catalytic activity of VPO is considered to be located at the interface of the (100) plane, to where we will focus our attention on its finer surface details. In 1987, Bordes proposed a model of the VPO surface which is presented in Fig. 1.3.

A key feature to this VPO surface model is its apparent amorphous structure which is a result of localized γ-$VOPO_4$ micro-domains formed via surface topotactic reoxidative processes. These features, when coupled to inherent variations in topography from the various atomic contortions, account for the irregular structure [42]. During maleic anhydride production, the catalyst is continuously exposed to

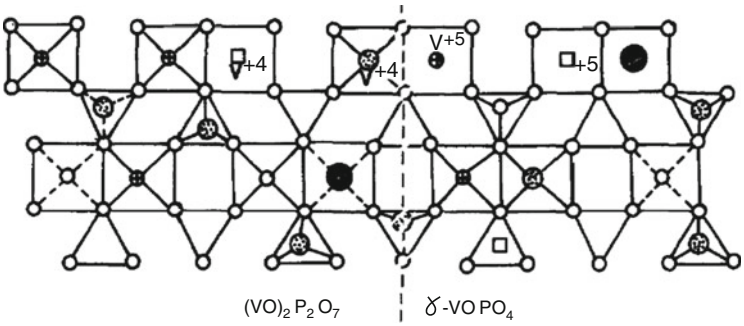

Fig. 1.3 Model (100) plane crystal surface of VPO and γ-$VOPO_4$ [42] (Reprinted from Catalysis Today, 1, Bordes, E., "Crystallochemistry of V–P–O Phases and Application to Catalysis," 499–526, Copyright **1987** with permission from Elsevier)

oxygen/air, C_4/hydrocarbons, heat, and water. Such an environment, when linked to the inherent *trans* orientations of the paired distorted VO_6 octahedra, suggests a redox-type coupling for the paired crystals. A closer inspection of Fig. 1.3 reveals five different oxygen sites. These sites are V = O, V–O, $V_{(1)}$–O–P, $V_{(2)}$–O–P, and P–O–P. Vanadium oxygen vacant sites (denoted by an □ in Fig. 1.3) are considered to be Lewis acid (electron pair acceptor) sites. Such sites can be reoccupied by oxygen, water (denoted by an ● which is OH_2 free or coordinated to V), or –OH resulting in the formation of Bronsted acid (proton donor) sites. Additionally, it is also possible for oxygen from PO_4 moieties to be abstracted from the surface (also denoted by an □ in Fig. 1.3), which can further alter the crystalline framework. As such, there is a slight excess in PO_4 (~P/V = 1.2). Interestingly, note that when the P/V ratio decreases to ~1, the reactivity rate was found to diminish significantly. This effect can be considered an indication of PO_4's contribution to the overall catalyst activity enhancement [42].

With this model surface in hand, a visualized interface between VPO crystalline phases and C_4 intermediates has been suggested. Bordes envisioned that C_4 activation was achieved by available oxygen sites at the exposed surfaces of vanadium and phosphorus. Envisioned arrangements of hydrocarbon orientations are included in Scheme 1.5.

Scheme 1.5 (1) suggests C_4 activation at the V^{4+} site resulting in hydrogen abstraction from methylene and methyl groups which protonates oxygen on V = O and P–O, respectively. The protonations yield V–OH and P–OH moieties at the catalyst surface and absorbed "ene" hydrocarbons. Ultimately, desorption of water molecules, resulting from this process, results in new vacancies. These vacancies can be replenished by two pathways: lower catalyst layers, via gliding processes, and gaseous oxygen, forming γ-$VOPO_4$ micro-domains. Scheme 1.5 (2) suggests another possibility that V^{4+} can abstract both hydrogens resulting in adsorbed butadiene molecule, depicted in either *cis* or *trans* conformations [42]. Scheme 1.5 (3) suggests that adsorbed butadienes on γ-$VOPO_4$ can cyclize via incorporation of oxygen from a P–O moiety yielding 2,5-dihydrofuran (DHF) or furan. Finally, Scheme 1.5 (4) presents the concept of dehydrogenation of furan by acid phosphate groups which can then receive oxygen which is on top of V^{5+} leading to the formation of maleic anhydride

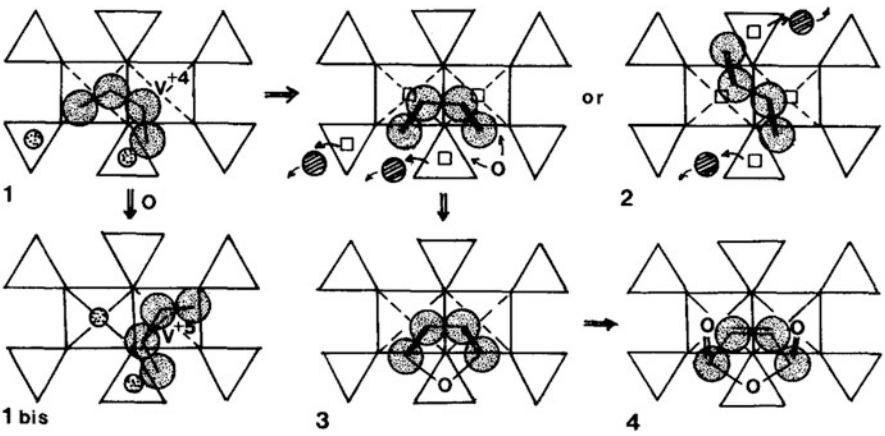

Scheme 1.5 Possible molecular orientations during maleic anhydride production [42] (Reprinted from Catalysis Today, 1, Bordes, E., "Crystallochemistry of V–P–O Phases and Application to Catalysis," 499–526, Copyright **1987** with permission from Elsevier)

[42]. These mechanistic concepts were more recently explored by other techniques to develop a more comprehensive picture to the nature of VPO catalytic behavior.

In 1989, Busca and Centi employed steady-state and transient reactivity measurements, Fourier transform infrared (FTIR) studies, and stopped-flow desorption (SFD) measurements to study the surface dynamics of absorbed species on the VPO catalyst surface during C_4 oxidation. Some of their key experimental observations include: (1) Steady-state oxidation studies reveal decreasing selectivity as maleic anhydride conversion rates increase to greater than ~80 % in combination with enhanced formation of carbon oxides. (2) C_4 oxidation behavior follows a Langmuir–Hinshelwood dependence on oxygen concentration. (3) Comparing non-steady state pulsed reactor (anaerobic conditions) flow to steady-state flow reactor (aerobic conditions) presented similar results suggesting that under these conditions, the C_4 oxidation is not affected by the rate of catalyst surface reoxidation by gaseous oxygen. (4) C_4 oxidation is increased significantly if the catalyst is initially treated at higher temperatures under inert helium gas flow conditions. (5) FTIR hydrocarbon absorption experiments produced results enabling the formation of a hydrocarbon reactivity scale where butadiene (most reactive) > butene > C_4 (least reactive). (6) Behavior of C_4 hydrocarbons under aerobic or *in vacuo* comparative conditions suggests that maleic anhydride can form on the oxidized VPO surface in the absence of gas-phase oxygen. (7) Furan was found to strongly absorb to the VPO surface at room temperature while at higher temperatures exhibits absorbed species similar to DHF and C_4 reactive absorption conditions. (8) Stopped-flow desorption methods revealed much stronger interactions for butadiene compared to other C_4 hydrocarbons. (9) Stopped-flow desorption measurements suggest furan disproportion hydrogen transfer reactions from furan to form crotonaldehyde and butadiene [47]. Using these numerous experimental observations, Busca and Centi proposed a reaction mechanism for C_4 conversion to maleic anhydride that is presented in Scheme 1.6.

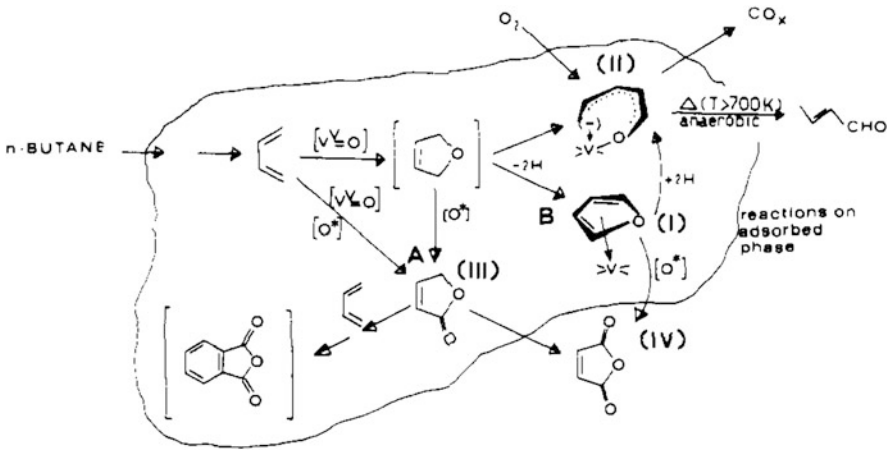

Scheme 1.6 Proposed reaction mechanism of C_4 conversion to maleic anhydride with VPO [47] (Reprinted with permission from Busca, G.; Centi, G., *J. Am. Chem. Soc.* **1989**, 111, 46–54. Copyright **1989** American Chemical Society)

As presented in Scheme 1.6, there are two main pathways for maleic anhydride formation, both of which occur predominately via transformation of absorbed species on the catalyst surface. Route A is believed to be the faster reaction due to higher reactivity found in the presence of gaseous oxygen. Thus, C_4 proceeds to butadiene which is then converted to dihydrofuran (DHF) via oxygen insertion from $V^v = O$. This oxidation is believed to occur via 1,4-electrophilic addition. Once the DHF intermediate is formed, the presence of labile oxygen species [O*] can promote its transformation to γ-crotonolactone (III). Butadiene can also transform directly to γ-crotonolactone by coupling the insertion of oxygen from both $V^v = O$ and labile oxygen species [O*]. Upon γ-crotonolactone formation, additional oxidation yields maleic anhydride. From γ-crotonolactone it is also possible to form phthalic anhydride, which can result from an enhanced lifetime of this intermediate on the catalyst surface in the presence of butadiene. Route B similarly proceeds through the formation of the DHF intermediate. DHF can then be dehydrogenated to yield a furan (I) intermediate. Furan can yield maleic anhydride when further oxidized by labile oxygen species [O*]; however, due to strong Lewis acid site interactions at the VPO surface, furan can also serve as a hydrogen transfer agent promoting hydrocarbon surface species (II) that are potentially capable of forming both crotonaldehyde and carbon oxides [47].

A 1991 study of VPO's electronic structure and properties by Schiott, Jorgensen, and Hoffmann developed a mechanism for the formation of maleic anhydride that focused on the more selective DHF to lactone route to maleic anhydride. Techniques such as density of states (DOS) and crystal orbital overlap populations (COOP) were employed to suggest models of the VPO surface and interaction schemes between various VPO sites and C_4 molecules. Also incorporated in the study were +4 and +5 oxidation states for VPO, for structures comprising $V_2O_8^{8-}$, analogs that incorporate $P(OH)_3$ moieties, and molecular orientations between organic/inorganic interfaces. Importantly, they point out that in this reaction, bulk oxygen is not significant; but it is more essential for molecular oxygen to become

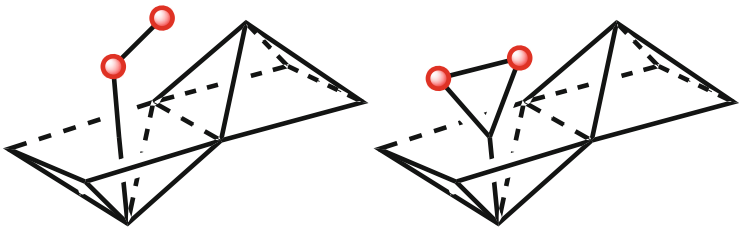

Fig. 1.4 Proposed coordinated structures of molecular oxygen to VPO superoxo (*Left*) and peroxo (*Right*) [49] (*open red circle* is oxygen)

activated from the surface of VPO, an effect that is still not clear. They found only minor variations for comparative electronic surface properties, with and without phosphorus, leading them to conclude that the $V_2O_8^{8-}$ structure was a suitable structural model for the catalytic transformation of DHF [48].

The important intermediate is the formation of DHF, which they suggest is derived from molecular oxygen inserting from the vanadyl group, in a concerted [2 + 4] cycloaddition-type process, to the 1,4-positions of butadiene. How molecular oxygen becomes available for C_4 coordination is a feature of the mechanism to explore in more detail. The molecular oxygen molecule is capable of coordinating with VPO in two forms, known as superoxo and peroxo. Remembering the *trans* configuration of neighboring VO_6 distorted octahedra, molecular oxygen coordinates to vanadium trans to the V = O. The two proposed coordinated structures are presented in Fig. 1.4.

Using extended Huckle approaches, it was not possible to distinguish energy-level differences between these structures. However, upon further consideration, where orbitals were rotated, the peroxo form was perceived to be more favorable [48]. As we will learn later, both structures, when abstracting hydrogen from DHF, lead to O–O–H surface species.

DHF is thought to be formed by insertion of molecular oxygen from the vanadyl group (V = O) to butadiene. With this in mind, once in the appropriate configuration of surface species is achieved, electron donation from DHF to the peroxo σ^* orbitals becomes possible. A sequence of various proposed intermediate structures are described in more detail in Fig. 1.5 [50].

From the Fig. 1.5a intermediate, formation of a new O–O–H bond via hydrogen transfer is possible (see Fig. 1.5b). A similar process is also envisioned to be suitable for the superoxo intermediate, yielding an identical structure. From the Fig. 1.5b intermediate, interaction between the newly formed O–O–H and C_1 is favorable, enabling the formation of the 2-hydroxy derivative of DHF (see Fig. 1.5c). Rotation leads to Fig. 1.5d, enabling enhanced interaction with the oxygen atom on the adjoining vanadium atom. Another hydrogen abstraction from this 2-hydroxy derivative results in the formation of a new vanadium-hydroxyl functionality pictured in Fig. 1.5e. Concurrently, the oxygen atom on the C_1 is beginning to transition to C = O bond formation. Finally, hydrogen is transferred to the V–OH resulting in the formation of a V–H_2O species and a coordinated γ-crotonolactone species on the VPO surface, depicted in Fig. 1.5f [48]. Once γ-crotonolactone has been formed, there are two required steps envisioned to

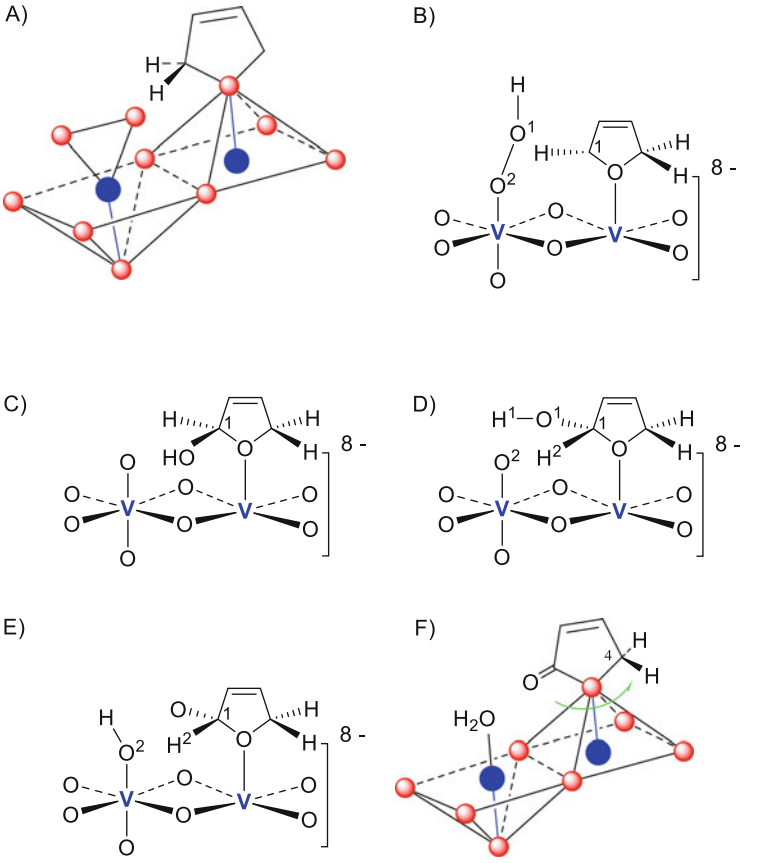

Fig. 1.5 Sequence of proposed intermediate structures in transformation of DHF in the presence of molecular oxygen and the vanadyl pyrophosphate surface [48] (Figs. 5B, 5C, 5D, and 5E adapted with permission from Schiott, B.; Jorgensen, K.A.; Hoffman, R., *J. Phys. Chem.* **1991**, *95*, 2297–2307. Copyright 1989 American Chemical Society) (*filled blue circle* is vanadium; *open red circle* is oxygen)

complete the formation of maleic anhydride. First, the water molecule (depicted in Fig. 1.5f) is exchanged for molecular oxygen. Second, the coordinated γ-crotonolactone rotates 180° enabling another CH_2 moiety to be in close proximity to the activated di-oxygen species derived from reabsorption of molecular oxygen. Thus, with these two steps completed, the maleic anhydride formation process then proceeds in a similar manner to the steps previously highlighted in Fig. 1.5, ultimately resulting in the formation of a second carbonyl moiety, at the 4-position (see Fig. 1.5f), and maleic anhydride [48].

In 2013, M. Cheng and W. A. Goddard employed density functional theory (DFT) techniques to study the mechanism of C_4 oxidation by VPO. They propose a more essential role for phosphorus, pointedly remarking that unlike previous studies where phosphorus moieties are presumed to be "innocent linked ligand (s)" in the catalytic process, the phosphorus–oxo bonds [P = O] are actually highly reactive and activate C_4 by decoupling hydrogen from the methylene groups. The

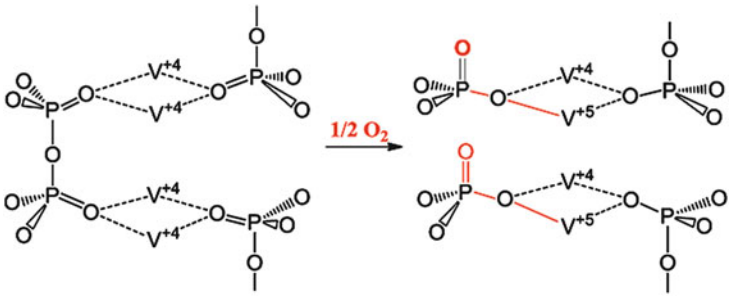

Scheme 1.7 Schematic of VPO surface oxidation [50] (Reprinted with permission from Cheng, M.; Goddard, W.A., *J. Am. Chem. Soc.* **2013**, *135*, 4600–4603. Copyright **2013** American Chemical Society)

first step in their proposed process is the molecular oxygen's oxidation of the VPO surface. A schematic of this reaction is presented in Scheme 1.7 [50].

In Scheme 1.7, the VPO surface is depicted in a manner that eliminates the oxygen atoms coordinated to the vanadium atom in order to make the process more clear. In this reaction scheme, oxygen adds to phosphorus, converting the pyrophosphate (P–O–P) moiety into two orthophosphate. In concert, V^{4+} is oxidized to a new V^{5+} state.

Once VPO has been oxidized, the newly formed P = O moiety is thought to be capable of abstracting a hydrogen atom from the C_4 methylene as depicted in Scheme 1.8a.

This hydrogen abstraction, which results in the formation of a P–OH moiety in the catalyst surface, overcomes a potential energy barrier of 0.0 kcal/mol and a reaction barrier of 13.6 kcal/mol. Such an energy barrier is reported to be consistent with experimental determinations suggesting this transformation is the origin of the VPO catalytic cycle. The next step in the proposed mechanism is trapping the resulting methylene radical by a V–O surface moiety. A subsequent hydrogen atom abstraction by a neighboring P = O surface group yields a second P–OH and a reduction of V–O to a V = O moiety (see Scheme 1.8a). This step concludes with the formation of the intermediate butene. Similar processes are repeated to enable the formation of the intermediates butadiene (Scheme 1.8b), DHF (Scheme 1.8c), and γ-crotonolactone (Scheme 1.8d). The conversion of γ-crotonolactone to maleic anhydride is the final step in the transformation of C_4, as presented in Scheme 1.8e. For each step in this proposed mechanism, M. Cheng and W. A. Goddard envisioned that the intermediate species desorbs from the catalyst surface to then re-adsorb to a fresh catalyst surface for the next step in their specific transformation [50].

From the myriad of fundamental research, we learn that the structural, perhaps even architectural, catalyst features and surface properties are essential to the inherent oxidation capabilities. We will find later that, even now, researchers are continuing to adjust formulations and compositions in addition to catalyst preparation processes to develop even deeper understanding of these structure/function relationships to further improve maleic anhydride manufacturing processes. Beyond purely compositional considerations, maintaining the compositional

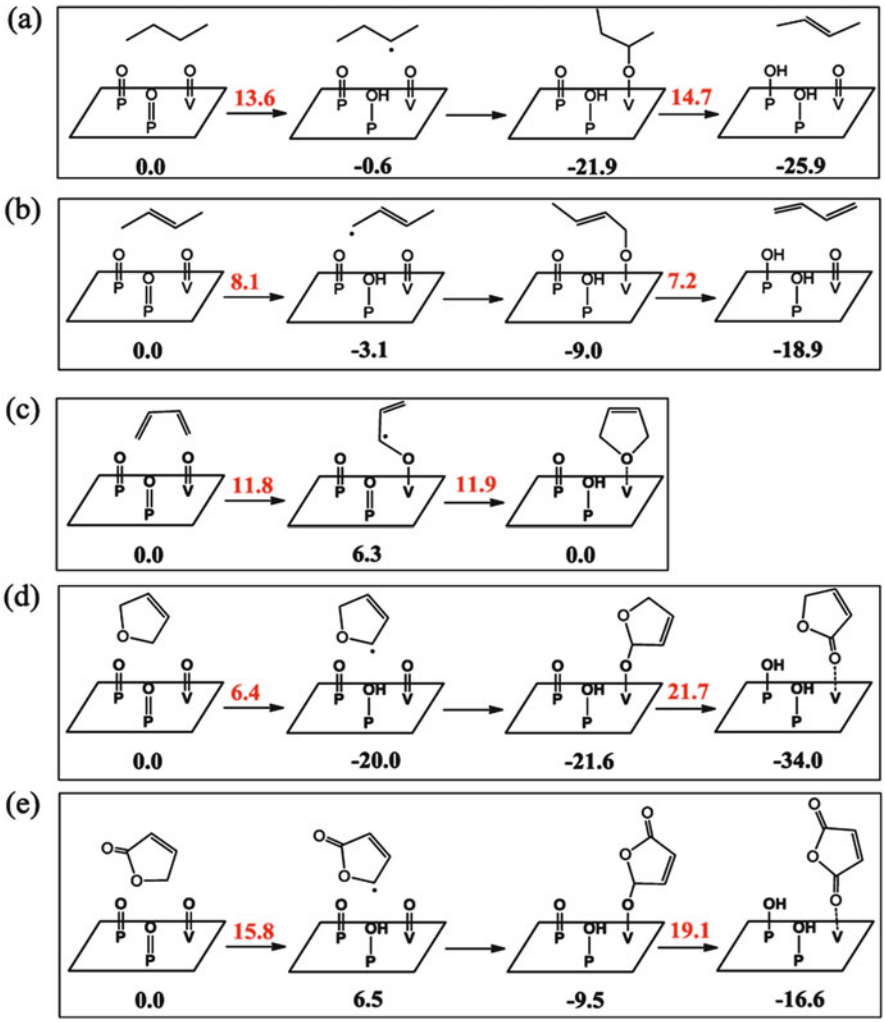

Scheme 1.8 Proposed initial mechanistic steps of C_4 activation by $VOPO_4$ [50] (Reprinted with permission from Cheng, M.; Goddard, W.A., *J. Am. Chem. Soc*. **2013**, *135*, 4600–4603. Copyright **2013** American Chemical Society)

balance (~P/V = 1.2) of the catalyst has been suggested as critical to the long-term performance behavior. As a result, strategies to maintain this compositional balance during production have emerged. Thus, while we continue to learn more about the basic nature of these materials, our ability to improve manufacturing processes based on current understandings has been fruitful, and this background should improve our appreciation for the technical approaches yet to be discussed.

1.3.3 Catalyst Improvement and Implementation Strategies in Manufacturing

Common improvement strategies in the industrial application of maleic anhydride catalyst technology include insertion of enhancement agents, co-metal inclusions, multiple catalytic zones, halide removal, pretreatment and purity, dimensional stability, morphology and porosity, and shape and regeneration. Note that in the case of insertion agents, where the discourse may not be obviously linked to the catalyst material per se, this topic is incorporated into this section due to the inherent exposure of such chemistries to the catalysts featured in the process.

1.3.3.1 Insertion of Enhancement Agents

Autoignition Suppression Agents

Gas compositions for C_4 oxidation processes must be carefully monitored to minimize the possibility of autoignition. Manufacturing conditions may require operation within, or at least near, potentially hazardous conditions, wherein the feed compositions may result in exposure to ignition sources, combustion, and possibly explosive combustion. The consequences of autoignition include loss of product yield, productivity, and personnel safety. Without an ignition source, the flammable process mixtures are still subject to autoignition if exposed to conditions suitable for oxidation chain reactions, such as prolonged exposure to elevated temperatures and pressures [51]. In addition to developing a method for estimating the autoignition temperature of the gaseous flammable mixture, incorporating the influencing factors such as pressure, concentration, volume, and other conditions, a method to suppress the autoignition temperature was developed by utilizing a pyrophoric suppression agent. In deploying the suppression agent, the process stream contains an autoignition suppression agent in contact with the gases and catalyst. The autoignition suppression agent is comprised of acidic sites or trivalent phosphorus which results in associated deposits along the plant walls of the process stream. These agents maintain contact with oxygen and iron at the wall interface at temperatures suitable for decomposition enabling the formation of polyphosphate acidic polymers or trivalent phosphorus as an inhibitor to autoignition [51].

Additions of Process Gases

In addition to air and C_4, it is also possible to inject other gases to further modify the process behavior. For example, additional mixing of a substantially pure carbon monoxide into the reactor gaseous feed streams, which comprise C_4 and an oxygen-containing gas, in a fixed-bed reactor has been found to improve the process yield and selectivity. The continuous addition of at least one trialkyl phosphite or trialkyl

phosphate component to this new gas combination, in amounts ranging from 0.5 to 4 ppm based on the weight of elemental phosphorus to the total amount of the gaseous feed, is also considered. This reactant combination results in a conversion rate of C_4 to maleic anhydride of about 75 % or more [52].

To improve the C_4 conversion rates and maleic anhydride yields, another approach has been to operate the oxidation process in the presence of an inert gas, i.e., nitrogen, helium or neon, and molecular oxygen (in the form of air). Critically, the thermal conductivity of the inert gas mixtures is designed to be not less than 800 ($10^{-4}Wm^{-1}K^{-1}$) at ~427 °C (700 K). The inert gas is recovered by separating for reuse as reactor feed. The total concentration of gases in the reactor feed ranges from 75 to 90 % by volume (inert gas mixtures), 1 to 5 % (C_4), and 5 to 25 % (molecular oxygen as air). Using helium in this approach, a process conversion of 83.2 (mol. %), selectivity of 73.9 (mol. %), and yield of 61.5 (mol. %) were achieved. Helium was recovered at 95.0 (mol. %). In contrast, in the absence of helium, the process conversion of 81.5 (mol. %), selectivity of 62.0 (mol. %), and yield of 50.5 (mol. %) were achieved, indicating significant process improvement for the inert gas strategy [53].

Addition of Phosphates

The reaction temperature profile within the oxidative reaction zone in a fixed-bed reactor can be controlled by aqueous phosphorus compound additions, even if the process was operating in a known flammability zone. Consequently, the ability to control hot spots translated to an enhancement of the catalyst life and production rates. To achieve these benefits, a phosphorus compound, such as triethyl phosphate (TEP), in water, is continuously added to the feed stream. The weight ratio of water to phosphorus ranges from 6500:1 to 35,000:1. The temperature throughout the entire effective reaction zone is maintained to be no greater than 30–50 °F above the salt bath temperature. Under these conditions, a uniform isothermal method of operation enabled high product yields using catalysts for extended periods of time. Using this approach, process conversions of 85 ± (%), selectivity of 65 ± (mol. %), and yield of 95 ± (wt. %) are achievable [54].

A similar improved process for continuously distributing phosphorus agents [i.e., trimethyl phosphate (TMP)] in fixed-bed reactors, at levels of 7–14 ppmw, that incorporates a strategy for enhancing the interfacial contact between the liquid TMP and the gaseous C_4 (ranging from 85 to 95 °C) by reducing the average size of the liquid droplets, enhancing the phosphorus agent's vaporization behavior, was developed. To reduce the droplet size, the liquid TMP (optionally with water) is first warmed, typically by wrapping the TMP feed line around the warm C_4 pipe. Then, during continuous insertion, the TMP is passed through an in-line filter medium which promotes its vaporization and distribution into the gaseous feed stream. The residence time for this mixture is typically 8–15 s prior to contact with the air feed. The increasing mixing time further improves the uniformity of the feed stream prior to contact with the reactor catalyst. In the case of multiple reactors,

similar strategies can be practiced prior to each reactor to permit individual phosphate level adjustments and good mixing. Reduction in reactor surface wear, maintenance, and improvements to reactor longevity are benefits of this approach [55].

Addition of Peroxides

Other oxidative compounds, i.e., hydrogen peroxide, have been found to be beneficial. In one example, where H_2O_2 was added directly to the C_4/air feedstock, an equivalent yield was observed coupled to a lower salt bath temperature (~20–30 °F lower). The preferred amount of H_2O_2 ranged from 5 to 1000 ppmw. A lower salt bath temperature can prolong the catalyst lifetime, resulting in longer production runs between maintenance of the catalyst bed. While not limited to H_2O_2, H_2O_2 has provided additional benefits such as additional water during decomposition and oxygen supply for the oxidation reaction [56].

1.3.3.2 Catalytic Co-metal Inclusions

Another very popular strategy has been to develop new inorganic catalyst compositions. Catalyst compositions comprising composite metal oxides of molybdenum, vanadium, tellurium, and certain other types of metals have been found to be effective in the maleic anhydride oxidation process. Other elements include Nb, Ta, W, Ti, Al, Zr, Cr, Mn, Fe, Ru, Co, Rh, Ni, Pd, Pt, Sb, Bi, B, In, P, and Ce. In a specific example, 90 wt% of $Mo_1V_{0.3}Te_{0.23}Nb_{0.12}O_n$ and 10 wt% of SiO_2 were found to exhibit conversion of 96.6 %, selectivity of 37.0 %, and a yield of 35.7 % when operating the oxidation reactor, where the molar ratio of C_4–air = 1:24, at 1000 SV (hr^{-1}) at 422 °C [57].

In a recent VPO catalyst modification from BASF, compositions comprising vanadium, phosphorus, iron, and oxygen were developed. The iron, typically iron phosphate, is present at an atomic ratio of 0.005:<0.05 (iron–vanadium). Properties of the typical catalysts include BET surface area from >15 to 40 m^2/g, pore volume from 0.15 to 0.4 mL/g, and bulk density from 0.5 to 1.0 kg/L [58]. In another catalyst approach employing iron, a polynary vanadyl pyrophosphate composition, such as $(VO)Fe_2(P_2O_7)_2$, was designed. The powder product exhibits a BET surface area, ranging from 1 to 4 m^2/g, depending on the catalyst preparative procedure [59].

1.3.3.3 Multiple Catalytic Zones

The performance of the oxidation reactor can be modified by deploying at least two different catalysts, where the catalyst activities are designed to be packed into the tubes in a gradient manner to enable improved reactor performance and control

Table 1.5 Mixed catalyst loading schedule in a fixed-bed reactor [60]

Bed function	% of tube length in reactor	Catalyst activity
Preheat	19–23	0.9–1.0
Critical	23–29	0.7–0.9
Downstream	48–56	1.0

[60]. By deploying a catalytic gradient, the operator is capable of running the reactor at an initial (feed gas) hydrocarbon concentration of $> 1.5\,\%$ by volume, to maintain a temperature difference between the gas and cooling fluid $> 15\,^{\circ}C$ in the reactor tube area where the gas temperature exceeds the fluid temperature, and a maleic anhydride productivity of at least about 5.0 lbs. per hour. Critically, during the reaction, the temperature difference between the gas and cooling fluids does not exceed 80 °C. The catalyst activity and the gas permeability of the bed vary in the general direction of the gas stream. In this manner, the catalyst activity and the pressure drop are lower in the critical region, or hot spot. An example of a catalyst loading schedule is presented in Table 1.5.

Assembly of the catalyst bed in this fashion results in significant improvement in reactor performance and reduced catalyst degradation [60].

Other researchers found success in designing two successive catalytic reaction zones. In the first reaction zone, catalysts suitable for producing 1,3-butadiene from C_4 via oxydehydrogenation were employed. Examples of suitable catalysts include $Mo_{12}BiNi_8Pb_{0.5}Cr_3K_{0.2}O_x$ and $Mo_{12}BibNi_7Al_3Cr_{0.5}K_{0.5}O_x$ [61]. In the second reaction zone, catalysts suitable for the oxidation of 1,3-butadiene to maleic anhydride were deployed. Suitable catalysts include $SbMo_3V_{0.1}Fe_{0.2}W_{0.06}O_x$ [62]. In demonstrating this process, the process was configured so that the first reaction zone was 330 °C and the second zone was 400 °C. The maleic anhydride yield was determined to be 62 %. Conversely, operating the process under isothermal conditions of either 330 °C or 400 °C resulted in maleic anhydride yields of 32 % or 54 %, respectively [63].

1.3.3.4 Halide Removal

The concept of halide removal from the catalyst composition has received attention. To achieve this goal involves utilizing glycol ether solvents and phosphoric acid in a slurry of vanadium and other metals and metal oxides with no chlorides present. Water can be introduced during the catalyst preparation and/or presented during the oxidation process. In a specific example where water was part of the preparative process, comparing a chloride-containing catalyst to a chloride-free catalyst, both based upon VPO–Mo compositions, results for a pilot reactor run are presented in Table 1.6 [64].

Results presented in Table 1.6 demonstrate that the chloride-free catalyst improves the overall performance of the oxidative reactor, as indicated by greater conversion, selectivity, and yields, coupled to operating the process at lower reactor

Table 1.6 Performance of chloride-free catalyst in a pilot reactor [64]

Hours on stream	Reactor temperature (°C)	Chloride-containing catalyst (VPO–Mo)	Reactor temperature (°C)	Chloride-free catalyst (VPO–Mo)
1000	406	Conversion (mol%) = 84.6	399	Conversion (mol%) = 87.7
		Selectivity (mol%) = 62.7		Selectivity (mol%) = 64.6
		Yield (wt.%) = 89.5		Yield (wt.%) = 95.6

temperatures. All of these features combined to improve the overall efficiency and economics of the process.

1.3.3.5 Pretreatment and Purity

Not surprisingly, pretreatment of VPO catalysts was shown to boost the activity of various catalyst compositions. Chemical pretreatment can be accomplished by contacting the catalyst precursor to dry inert gas to remove any residual oxygen, then introducing acetic anhydride vapors, at a temperature of 150 °C, at 2–5 % by volume, for about 8 h of exposure. Residual acetic anhydride vapors were removed by sweeping the system with nitrogen gas. The powder from this product was formulated with 4 % graphite and pressed into tablets in preparation for calcination. The calcination process is critical to the overall performance of this strategy. The atmosphere during this process is typically a mixture of steam, inert gas, and oxygen. In general, slower heating rates result in better catalyst performance. In the example provided, the optimal heating rates are <1 °C per minute to a temperature 420 °C coupled to isothermal temperature dwell time, suitable for achieving a vanadium oxidation state no greater than +4.5, after 8 h [65].

In modifying the previous catalyst preparation strategy, a step was added for the removal of water formed during the catalyst preparation to achieve < 0.5 % residual water content by volume. The water is removed via an entrainer, such as cyclohexane, toluene, or xylenes. Crude amounts of water were removed by a water separator followed by additional water removal during reflux. Heating schedules for calcination are in four distinct steps: step 1, purge the furnace with nitrogen at 20–100 °C to reduce oxygen to <5 % by volume; step 2, hold temperature ranging from 150 to 250 °C, heating rate from 5 °C to 20 °C/min, for an isothermal hold up to 3 h; step 3, hold temperature ranging from 200 to 300 °C, heating rate from 1 °C to 10 °C/min, for an isothermal hold up to 3 h; step 4, hold temperature ranging from 380 to 460 °C, heating rate from 0.1 °C to 3 °C/min, for an isothermal hold from 2 to 8 h. Mixtures of air, nitrogen, and water vapor (0.1–0.5:0.1–0.5:0.0–0.8 volume ratios) are fed in the furnace during these temperature steps. The treated catalysts are cooled to < 100 °C under nitrogen prior to removal from the furnace for storage in a tightly closed container. The performance of the catalyst was judged

to be superior to the previous catalyst treatment, particularly in terms of yield improvement [66].

Phosphorus additions to fluidized-bed catalysts have developed for suitable TEP insertion techniques. Previous methods demonstrated that vapor-phase addition of TEP led to increased operating temperatures, which limit reactor throughput and accelerate catalyst degradation [67]. An alternative approach is to add phosphorus by impregnating the catalyst with TEP prior to adding the catalyst to the reactor. Impregnated VPO catalyst enables lower TEP use levels and increased yield of maleic anhydride at lower operating temperatures. The amount of TEP added to the catalyst is from about 0.9 mg to about 0.454 kg of TEP per 45.4 kg of total catalyst bed per day [68].

Lonza researchers report negative performance effects to catalyst activity related to remaining carbonaceous materials trapped inside the catalyst. To control the carbon content in the VPO catalyst precursor, and catalyst purity, the catalyst is prepared in an organic medium comprising (a) isobutyl alcohol or a mixture of isobutyl alcohol and benzyl alcohol and (b) a polyol, such as 1,3-propandiol and 1,4-butanediol. The preparation of the catalyst precursor in such organic mediums results in carbon content ranges from 0.7 to 4 wt%. The catalyst precursor is transformed into the active catalyst by an activation process that includes a heat treatment that includes applying a temperature of up to 600 °C. The performance of the final catalyst improved for conversion, selectivity and yield [68].

Another process for preparing pure VPO catalyst precursors which exhibit low residual organic material is based upon the following steps: (1) reacting VPO with 102–110 % strength H_3PO_4 in the presence of isobutanol in a temperature range from 80 to 160 °C. It includes the option of additional alcohols, such as a primary or secondary, noncyclic or cyclic, unbranched or branched, saturated alcohol, and having 3–6 carbon atoms; (2) isolating precipitated product; (3) (a) drying the precipitate to <5 wt% residual isobutanol or other alcohols; (b) passing gases, at temperatures ranging from 130 to 200 °C, such as nitrogen comprised of 0.1–9 % by volume of oxygen through the dried precipitate, directly or after isolation. The powder product exhibits BET surface areas, ranging from 20 to 40 m^2/g, pore volumes ranging from 0.2 to 0.4 mL/g, and bulk density ranging from 0.5 to 1.0 kg/L, depending on the catalyst preparative procedure [69].

1.3.3.6 Dimensional Stability

Dimensional stability of the catalyst is critical to the ability to implement a commercially viable catalytic material. The material must be strong enough to withstand handling, abrasion, and other physical forces. One critical physical attribute is catalyst expansion. Amoco studied the manufacture of VPO catalysts and developed techniques to alter their fabrication in order to minimize the tendencies of the catalyst toward expansion. In this approach, the VPO was prepared with a co-metal, such as molybdenum trioxide (MoO_3). Critically, in the preparative process, water is added, ranging from 2.5 to 3.5 moles H_2O per mole of P. This

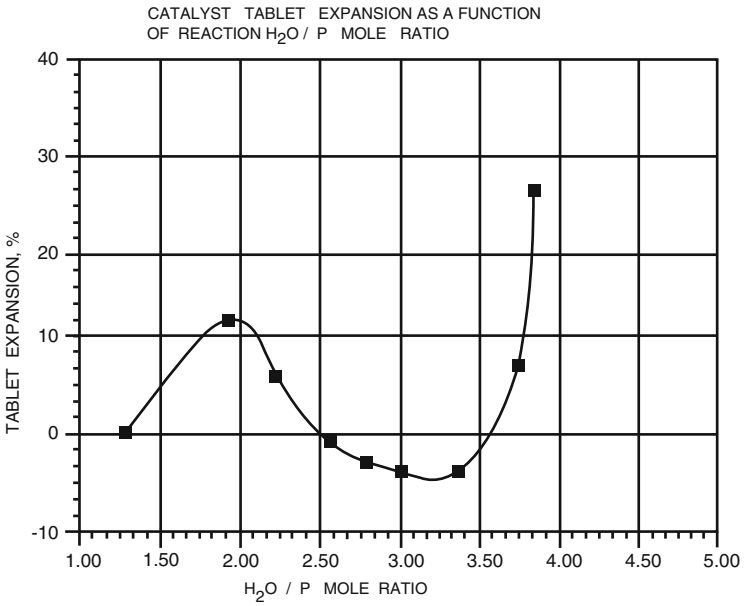

Fig. 1.6 Catalyst tablet expansion as a function of reaction water/P mole ratio [70]

water reacts to form phosphoric acid and esters. If the water is outside this range, the catalyst tablet will exhibit undesirable expansion properties. Additionally, to achieve the final catalyst form, additives such as inert supports (i.e., alumina, titania, silicon carbide, kieselguhr, pumice, or silica) and binders (i.e., starch and polyvinyl alcohol) can be employed to improve physical properties and shape forming processes. In developing this approach, a tablet expansion test was designed, where tablets were dimensionally analyzed prior to being placed in a 900 °F oven equipped with a humid air stream for 2 h. The tablets are allowed to cool in a desiccator and are dimensionally reevaluated. Results of these tests are presented in Fig. 1.6.

The results from these tests indicate that optimal range for the water/P mole ratio is 2.5–3.5, where the tablet either does not expand or slightly contracts. Thus, by controlling the water in the catalyst preparation, catalyst expansion can be minimized enabling longer production runs and catalyst cycle life [70].

Other strategies toward improving catalyst expansion properties include the production of coated catalysts. Coated catalysts are achieved by applying a catalytic composition in a coatable form to a shaped structural support body. The structural support is comprised of materials such as aluminum oxide, aluminates, silicon carbide, silicon oxide, silicates, steatite, duranite, porcelain, or stoneware [71]. An important feature to this approach is to first calcine the catalyst prior to applying the coating composition, enabling the binder to be present upon introduction of the coated catalyst to the oxidation reactor. This approach will enhance the adhesion of the oxidation catalyst to the support body. For the coating composition,

additives include binder, inert fillers, and promoters. Binders, such as polyvinyl acetate, are effective at 10–20 % (wt% based on solids) use levels. Inert fillers, such as SiO_2, TiO_2, SiC, and graphite, can be added at 0.5–25 % (by wt% based on the calcined precursor). These inert fillers can aid in activity control of the catalyst. Promoters, such as $(NH_4)_2MoO_4$, Li_2CO_3, and $Co(NO_3)_2{\cdot}6H_2O$ which are water-soluble compounds, can also be added to the coating slurry. The coating slurry is typically applied using a spray coater or coating drum, where support bodies in the shape of spheres, rings, or saddles are coated in the temperature range of 50–100 °C. Using this strategy, the coating mechanical stability was significantly increased even after removal of the binder during maleic anhydride production. Thus, sufficient adhesion of the active catalyst composition to the inert support material existed during the entire maleic anhydride production. Another advantage of this approach is reduced catalyst dusting enabling easier change-over processes in the plant [71].

1.3.3.7 Morphology and Porosity

As discussed earlier, VPO is considered to be the active phase. The catalyst microstructure, or morphology, has been found to exhibit significant influence on its selectivity and reactivity. Empirically, selectivity is found on platelike particles versus particles comprising more roselike shapes. By implication, the crystallographic (100) plane is likely the active surface of the catalyst on these platelike particles [72]. To accentuate the formation of these platelike catalysts, a synthetic process was designed. The key features of this product by process are [73]:

1. An aqueous solution of $NH_2OH{\cdot}HCl$, including H_3PO_4, is employed to reduce V_2O_5 solid, which is indicated by forming a blue solution.
2. The solution is allowed to evaporate to form a pasty mass.
3. The pasty mass is aged to yield a blue solid.
4. The blue solid is washed with boiling water, removing any water-soluble materials.
5. The remaining solid is dried to form $VOHPO_4{\cdot}0.5H_2O$ product.
6. The dry product, $VOHPO_4{\cdot}0.5H_2O$, is ground to a fine powder.
7. The $VOHPO_4{\cdot}0.5H_2O$ powder is slurried with a mixture of dimethylformamide (DMF) and water (H_2O).
8. The dispersed $VOHPO_4{\cdot}0.5H_2O$ powder is recovered from the slurry and washed with hot water.
9. The remaining $VOHPO_4{\cdot}0.5H_2O$ is dried to a solid, which exhibits an enhanced (001) plane.
10. The $VOHPO_4{\cdot}0.5H_2O$ solid is calcined to yield $(VO)_2P_2O_7$ with the selectively exposed (100) plane [73].

Other researchers at Huntsman have sought to affect the catalyst morphology by controllably altering the catalyst porosity. Their concept is that VPO catalysts containing a high concentration of pores can enable a more rapid diffusion of

product and reactant gases within its structure, improving the overall activity of the catalyst. To form pores, a solvent-removable pore-building agent, such as 1,1,1-tris (hydroxymethyl)ethane, is incorporated in the activated catalyst, at 10 wt%, and then removed by submersing the pellets in acetone for 6–24 h. By enhancing the porosity of the catalyst, the maleic anhydride yield also is improved [74].

Other methods for adjusting the surface area of the catalyst, such as incorporating inorganic promoters, have been found to be useful in enhancing the catalytic activity. For catalyst produced in organic mediums via precipitation, a typical BET surface area ranges from 10 to 20 m^2/g after activation and rarely beyond 22–23 m^2/g. The incorporation of a copromoter, such as zirconium, enables the catalyst to develop surface areas greater than 28 m^2/g. For example, when Zr $(C_4H_9O)_4{\cdot}C_4H_9OH$ (zirconium butoxide) is incorporated into the catalyst, where the Zr/V ratio ranges from 0.005 to 0.0375 and is evaluated comparatively, the conversions improve ~15 %, and yields increase by ~5 %. Such enhancements are significant in commercial environments [75].

Molybdenum-modified VPO catalyst shaped bodied structures can also yield improved surface area, activity, selectivity, and productivity. The catalyst shaped body has a volume > 0.02 mL and a BET surface area > 15 m^2/g. The molar ratio of molybdenum to vanadium ranges from 0.0020 to 0.0060 (Mo/V). Catalyst compositions tend to slightly lower the maleic anhydride yield %, ranging from 0 to ~2 %, but also significantly lower acrylic acid production, ranging from 35 to 65 % reductions in gas stream [76].

Adjusted micropore structures, where the pore diameter ranges from 0.01 to 0.6 μm, can enable improved performance of the catalyst structure and morphology by reducing the catalyst's internal resistance to diffusion. The total pore volume of the catalyst structure is comprised of >55 % micropores which exhibit a volume of > 0.2 mL/g. In one example, propylene glycol was added to enhance the formation of micropores. As a result the BET surface area (m^2/g) increased from 18.09 to >30.0 with the pore volume increase > 20 %. The increase in the micropore volume was found to be > 30 %. It was found that these improved catalyst structures enabled a 2.1 % yield improvement over the original catalyst structures [77].

1.3.3.8 Shape Considerations in Production

The kinetic rate of catalysis is limited by the ability of the reactant gases to internally diffuse into the pore structure of the catalyst body. By increasing the porosity of the catalyst body, the catalytic activity can be enhanced. As a result, pore formers, i.e., organic compounds, which burn out during later heating and sintering, are added. However, this strategy is subject to limitation because excessively porous shaped catalyst bodies will lack sufficient mechanical strength to exhibit commercial utility.

The control of the macroscopic catalyst body shape in a way that optimizes its performance in the reactor is another approach. For fixed-bed reactors, there are at least four factors that control the process behavior of the catalyst bed: particle

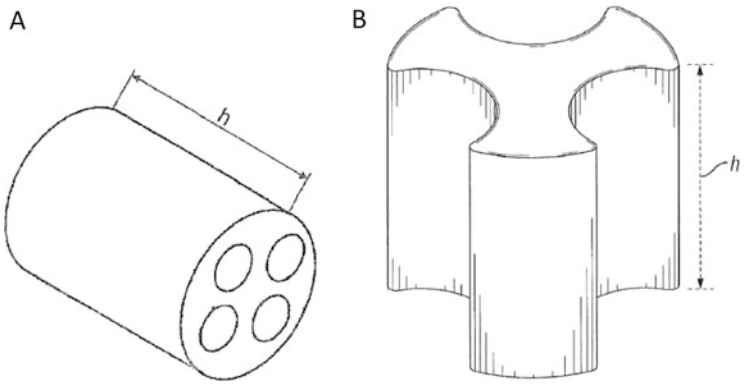

Fig. 1.7 Recent examples of shaped bodies suitable for VPO catalysts [79, 80]

properties (i.e., shape, size, mass, etc.), container properties (i.e., shape, size, surface properties), charging techniques (i.e., intensity, speed, methods), and post-charging (i.e., vibration, etc.) processes [78]. In general, it is known that catalyst activity increases as the catalyst particle size decreases and exposed surface area increases. The pressure drop across the fixed catalyst bed tends to increase as this particle size decreases, as the bed becomes more and more closely packed. As the pressure drops, the amount of reactant gases that can pass through the bed becomes more limited. The process gas flow can be improved by increasing the catalyst size, but the activity of the catalyst can be somewhat compromised as a result. Consequently, the focus shifts to catalyst shape. Often, the catalyst shape is designed based upon cylindrical bodies comprising at least two parallel internal holes which are parallel to the cylinder body axis and go right through the catalyst structure. An example of this shaped body concept is presented in Fig. 1.7a [81].

Additional examples of common shapes include spheres, cubes, hollow cubes, solid cylinders, hollow cylinders, single rings, cross-webs, grooved cylinders, pall rings, Intalox saddles, and Berl saddles [78]. Recently, a shaped body structure comprised of a solid cylinder with three void spaces running along the cylinder height to yield three lobes was designed by Huntsman. An example of this shaped body concept is presented in Fig. 1.7b [82]. Shape and size are optimized to achieve enhanced surface area properties. Ultimately, a proper optimization of surface area can contribute to minimization of required reactor volume, leading to reduced capital expenditures.

Beyond purely shape and size, general mechanical properties are known to be important to proper shape body selection. In shape body manufacturing, the side crush strength is a critical factor to quality, since it is directly related to the product durability during handling, shipment, and catalyst loading [82]. Greater crush strengths are generally preferred. Another challenge for shape catalyst bodies is their tendency to exhibit high attrition behavior. The term attrition describes the amount of catalyst lost to disintegration after some amount of process wear and tear and, as an aside, is an especially crucial property in fluid-bed reactors. Attrition

measurements are important because shaped bodies that exhibit high attrition percentages generally yield increased, undesirable pressure drops in the commercial reactor tubes.

Methods employed to load catalysts into reactor tubes are also critical to process performance. Especially in maleic anhydride production, where thousands of reactors tubes are often utilized, charging the shaped catalyst body must be consistent, tube to tube, in order to maintain uniform pressure drops. One common technique for charging a reactor is to fill a properly shaped sock with the catalyst, then completely slip the sock into the tube. Once fully inserted, the sock is released from the bottom enabling the catalyst to be placed in the tube in a controlled manner, minimizing catalyst body motions in the tube. Another common technique is to "pour" the catalyst into the tube. In one study, fast filling, slow filling, and "snow storm" filling were comparatively evaluated for effectiveness in bed packing weight and bed voidage via a "pour" filling process. "Snow storm" filling (SSF) is a process which involves passing the packing material over wires that have been either staggered or meshed to enable the falling particle to be interrupted prior to reaching the bed face. This process causes the particles to radially disperse enabling the bed face to be filled uniformly and align particles such that more are able achieve a minimal contact area. Consequently, the SSF process can consistently achieve greater packing weights and smaller bed voidages [78]. Once the deposition of catalyst is achieved, further densification of the bed can be achieved by vibration techniques in a post-deposition procedure.

Once the shaped catalyst bodies are charged into the reactor housing, the possibility of expansion must be considered. Minimal dimensional change is preferred. Catalyst compositions and molding processes must be evaluated for dimensional change. For example, Amoco researchers designed a process for preparing and shaping solid catalysts that exhibited minimal expansion characteristics. Upon synthesis, the catalyst formed is a powdery material by grinding and passing through a 30-mesh screen. This powder was calcined suitably in air or a nitrogen–air combination at temperatures ranging from 300 to 370 °C. The resulting product is then formed into geometric shapes, such as cylinders, by incorporating additional ingredients such as lubricants (i.e., graphite, Sterotex, stearic acid, zinc stearate) and binders (i.e., starch and polyvinyl alcohol). The shaped catalyst is then heated in a nitrogen atmosphere at temperatures ranging from 343 to 704 °C. The catalyst, in its final geometric shape, must be treated in the inert atmosphere prior to being exposed to an oxygen-containing gas at an elevated temperature in order to minimize its expansion characteristics. The specific size and shape of the tablets, such as right cylinders, are critical since the available void fraction in the reactor is determined by these parameters. The void fraction must be large enough to avoid any large pressure drops inside the reactor. To determine if the catalyst exhibits desirable properties, the catalyst is subjected to a standard expansion test. In a standard expansion test, the dimensions, length and diameter, of 10 tablets are determined. Also, the length and diameter of 10 tablets are measured with a caliper. An average volume is estimated based upon the volume determination of a cylinder. The tablets are placed in an oven at 482 °C in the presence of a humid air stream

Table 1.7 Expansion test results for pretreated tablets exposed to different atmospheres [83]

Tablet	Pretreatment (°C)	Volume change	Hours on stream	Reactor temperature (°C)	Conversion % (mol)	Selectivity % (mol)
A	427 (air)	+2.18	192	422	84	64
B	427 (nitrogen)	−2.23	192	422	83	64
C	427 (helium)	−5.41	192	421	82	64

for 2 h. The tablets are then removed and allowed to cool inside a desiccator. The tablet dimensions are remeasured and average volumes are reestimated. By comparing the average volume of the tablets, before and after thermal treatment, the effect of the pretreatment process can be assessed. To determine effects of the pretreatment process on the catalytic activity, the pretreated tablets were tested in a mini-reactor test, exposing a charge of pretreated tablets to a feed of C_4 in synthetic air (1.1 mol%) at 1200 h^{-1} VHSV with a continuous addition of 10,000 ppm water. The data are shown in Table 1.4. The results of the expansion test are presented in Table 1.7 [83].

Results presented in Table 1.7 indicate that the performance of pretreated catalyst is equivalent but the expansion characteristics are superior for the catalysts that were treated in inert atmospheres.

Solid shaped oxidation catalyst was designed by Monsanto to include at least one void space, which results in a shape exhibiting a volume that is 30–67 % of a comparable shape comprising no voids. In addition, the shaped catalyst, with at least one void, exhibits an external geometric surface to volume ratio of > 20 cm^{-1} coupled to a bulk density ranging from 0.4 to 1.4 g/cm^3 [84]. Importantly, the voided shape still must exhibit sufficient mechanical integrity to be applicable in commercial process. Thus, the side crush strength should range from 13.3 N to 89 N. The effect of shape on the maleic anhydride oxidation process is illustrated in Table 1.8.

In general, as more void space becomes available, the % conversion improves. Interestingly, when the external geometric surface to volume ratio is maximized at 27.0, the % conversion and % yield are optimal. Similar trends are followed within other examples from this research [84].

1.3.3.9 Regeneration

Catalyst materials contribute a significant and necessary expense to the maleic anhydride process. Enhancing the longevity of catalyst when already loaded in a reactor is very desirable to plant operators. One approach to improving reduced catalyst activity is to regenerate, in situ, and stabilize the catalyst. In this approach, first treatment of the aged catalyst is with a carbon halide compound, such as CCl_4. The treatment enables the old surface of the catalyst to be removed. Typically,

Table 1.8 Comparison of cylinder shape effects on the performance of $VP_{1.15}O_x$ catalyst [84]

Tablet	Void space no.	Height (mm)	Width (mm)	Side crush strength (N)	Geometric volume ratio	External surface/vol. (cm^{-1})	Bulk density (g/cm^3)
A	None	3.73	3.18	66.75	100	18.0	0.84
B	Center Core hole	4.76	4.76	35.60	89.0	17.0	0.87
C	Grooves, 6	5.36	5.56	48.95	67.0	20.0	0.66
D	Grooves, 3	3.97	3.96	35.60	61.0	27.0	0.64
E	Grooves, 3	5.56	5.56	35.60	45.0	20.0	0.66

Tablet	On stream time, hr	Reactor catalyst charge (kg)	Reactor charge density ($kg/m^3 \times 10^2$)	Bath temperature (°C)	Hot spot temperature (°C)	% conversion (mol. %)	% yield (mol %)	Wt/Wt production g maleic anhydride (kg cat hr)
A	3679	0.336	7.96	410	465	74.0	51.0	77.7
B	1657	0.303	7.18	439	490	79.0	50.0	84.5
C	536	0.241	5.71	424	471	77.3	50.0	106.2
D	1500	0.253	5.99	421	474	80.0	53.0	107.3
E	1042	0.261	6.18	424	488	78.0	51.0	100.0

0.01 g to 0.1 g CCl_4/g catalyst is added to a nitrogen gas carrier. This composition is passed through the catalyst bed at 350–500 °C, at 100–1000 VHSV for 10–30 min. Once the catalyst is reactivated, phosphorus compounds, such as TEP, are added to the catalyst feed stream to optimize the P/V atomic ratio at the active catalyst sites, thus regenerating the catalyst. It is also possible to add TEP in the presence of water ranging from 1000 ppm to 40,000 ppm (by weight % of the reactor feed gas stream). It was found that this approach was superior to those approaches where the catalyst was regenerated by either process alone. This efficient technique for catalyst regeneration leads to significant economic savings, since downtime, labor costs, and requirements for new catalysts are minimized [85].

As we have now seen, there are many techniques and strategies researchers employ to optimize the catalyst, the process, and the processing window. Interestingly, the material selections, beyond the inorganic catalyst composition itself, are relatively narrow in scope. The practical awareness of the key variables is high, such as phosphate addition, shape, composition, mechanical properties, etc. The critical challenge remains to develop an even more comprehensive understanding of the interrelationship of these variables to the actual manufacturing processes, and the corresponding product yield, to enable further improvements to production processes.

1.4 Strategic Design Improvements in Existing Plants

Returning to the manufacturing facility, a number of strategies have been found to exist in recently improved processing designs for maleic anhydride plants. More common examples include additional reactor modifications, gas recycling, and column preparation and improvement to solvent absorption and distillation processes. We'll examine each of these examples in more detail.

1.4.1 Reactor Design Modifications

1.4.1.1 High-Purity Maleic Anhydride Insertion

Insertion of process improvement agents is a popular strategy. In an effort to improve the recovery of maleic anhydride from the oxidation reactor, researchers at Amoco found that the addition of maleic anhydride, with critically a minimum melting point of 52.5 °C and 99.9 wt% + purity, into the reactor effluent stream and before the stream enters the condenser can increase the recovery of maleic anhydride from 40–45 wt% to 50–60 wt%. In addition, the fouling rate of the condenser, due to maleic anhydride deposits on condenser surfaces, is significantly reduced, enhancing production rates and reducing plant downtime. The maleic anhydride is typically injected, by means of a fogging-jet spray nozzle, into the gas stream at temperatures ranging from 93 to 177 °C resulting in a maleic anhydride gas-phase addition. The amount of maleic anhydride added to the reactor effluent stream is at least 1 wt% of the maleic anhydride effluent stream content [86].

1.4.1.2 Fixed-Bed Modifications

Scientific Design (SD) modified the original HSD process by inserting a second fixed-bed reactor, in a series configuration, to improve plant yield and process efficiency. This type of reactor configuration is commonly known as a "Series Reactor." The first type of series modification involved the critical insertion of a cooling step to the C_4 process after the process stream exits the first reactor. Thus, the gas effluent from the first reactor is moderated under pressure- and temperature-controlled conditions to a range of 50–300 °C and more closely to 200 °C. Then a new, controlled amount of C_4 is added to this process stream prior to the introduction into the second reactor for further oxidation. Importantly, no additional oxygen is required at this point, indicating that the oxygen content of the second reactor is actually lower than the first reactor. The net result is a reduction in the flammability of the process stream. The new cooling step is essential to preventing "cold flame" effects. The term "cold flame" is used to describe processes where the C_4 reacts

with oxygen, in the absence of a catalyst, resulting in the production of polyglot mixtures of oxidation products. Such undesirable reactions reduce the process yield and cause problems in downstream purification processes. Operating two reactors in series in this manner is reported to increase the effective conversion rate above what would be possible for a single reactor. The yield of maleic anhydride can increase 8–10 wt% and reduce waste gases, power consumption, steam usage, and capital costs. Based on laboratory work, a parallel reactor approach was also evaluated by operating two reactors at a 20 psig inlet pressure. This approach was found to demand significantly more power resulting in an unrealistic economic operation model. The series process typically yields 85–90 % butane conversion and 94–99 % of maleic anhydride weight yield percent [27].

In a second modification to the Series Reactor concept, SD inserted a maleic anhydride removal step between the reactors [87]. Thus, once the process stream from the first reactor is cooled, the process stream can be treated for partial condensation maleic anhydride products and their removal from the process stream. Another possibility is the first reactor process stream can be scrubbed with liquid, i.e., water, removing maleic anhydride formed in the first reactor. The gases from this intermediate scrubber, which comprise C_4 and oxygen, are subsequently passed, along with additional, new C_4 to the second reactor for further oxidative processing [87]. From there, the process continues to treat the process stream as previously described in the HSD process. This approach is reported to demonstrate significant improvements to reducing raw material costs (particularly reduced C_4 consumption), power demands, and general operating expenses [87]. It was also found that oxygen-enriched air results in improved conversions and yields. In the case of oxygen-enriched air, the overall conversion was reported to be 90.54 %, selectivity 70.88 %, and reaction yield 108.30 % (wt%) [87].

In another modified fixed-bed process, which can include Series Reactor designs, two successive reaction zones are cooled such that the temperature range of the first reaction zone is 350–450 °C and the temperature range of the second reaction zone is 350–480 °C. Importantly, the temperature differential between the hottest reaction zone and the coolest upstream reaction zone is > 2 °C. In addition, the hot spot for the second, upstream reaction zone is hotter than any previous hot spots. Numerous results present a process that is capable of achieving high conversion, high selectivity, and high yield of maleic anhydride. High space-time yield (150 g/L*h) coupled to high space velocity of hydrocarbon over the catalyst bed reportedly enabled several thousand operating hours under stable reaction conditions [62].

1.4.1.3 Reduction in Fluid-Bed Back-Mixing

Back-mixing is a significant challenge for fluid-bed reactors. Back-mixing describes an effect where, within a given reactor, some of the reaction products are recirculated throughout the bed, forward and backward. The back-mixing,

also known as backflow or reverse circulation, results in increased contact time between the product, catalyst, and process environment. The increased contact time can enhance degradation effects in the product [34]. In efforts to prevent this effect in fluidized-bed reactors, a process in which both the gaseous fluid phase and the fluidized solids move simultaneously through at least two fluid-bed compartments in a plug flow manner was envisioned [34]. Back-mixing, which remains a possibility within each compartment, is reduced in the total process because the fluidized gases and catalyst advance in parallel, plug flow. At the final stage of the reactor, the solid particles are removed from the fluid phase and returned to initial reactor compartment [34]. To achieve the proper process flow conditions, the linear velocity of the fluid phase ranges from 2 to 50 times higher than the minimum fluidization velocity in each compartment. In addition, the fluid phase within the free area of the partition(s) exhibits a linear velocity ranging 0.8–2.0 times greater than inherent entrainment velocity of the solid particles [34]. The various linear velocities of the system must be carefully balanced to avoid systematic pressure drops and mechanical attrition of particles while maintaining plug flow [34].

1.4.1.4 Process Gas Recycling

Gas recycling has been an important development to maleic anhydride production and offers several ecological advantages leading to more sustainable production processes. In one approach for fixed-bed reactors, the feed stream is water scrubbed, under pressures ranging from 121 to 304 kPa, to remove maleic anhydride. The resulting process stream is then recycled back to the reactor feed stage of the process, again under at least 121 kPa [88]. Typical processing conditions for this type of fixed-bed plant design are presented in Table 1.9.

Under the conditions described in Table 1.9, typical conversion rates range from 75 to 90 % and conversion selectivity ranging from 55 to 75 %. Any remaining exhaust gases are incinerated, producing water and carbon dioxide. The benefit of recycling becomes apparent when evaluating the specific parameters presented in Column B. Under those conditions, operating the plant without recycling was found to reduce process yields from 1.03 to 0.94 Kg. The decrease in performance was

Table 1.9 Processing conditions for a fixed-bed gas recycling plant design [88]

Process parameter	A	B
Reactor temperature (°C)	370–440	400
Reactor inlet pressure (kPa)	203–608	344
Space velocity (h^{-1})	1000–3000	1500
Total C_4 concentration fed to reactor (% volume)	1.6–3.0	2.1
% oxygen in reactor feed (% volume)	11–16	12.2
Total yield (kg of maleic anhydride/kg of C_4)	0.9–1.05	1.03
Yield (% mol)	NA	60.7

attributed to recovering C_4 which would otherwise be lost to incineration and, curiously, reducing the available oxygen in the reactor to ranges of 11–14 % versus air, which is 21 % by volume. The net result of recycling is that only a fraction of the reaction gases are conveyed to the incinerator. Advantages to gas recycling can include reduced incinerator dimensions, compression energy savings (~30 %), and a significant reduction of carbon dioxide release into the atmosphere (~270 kg per ton of maleic anhydride produced) in addition to the previously mentioned yield improvement [88].

In considering the above approach, it was noted that a disadvantage of the process was its proximity to the explosive-range boundary conditions [89, 90]. It was also noted that only by using an oxygen concentration closer to 10 % (volume) and/or C_4 concentrations at the lower end of the range (~1.6 % by volume) was a safe condition possible [90]. However, since the potential value of exhaust gas recycling was clearly demonstrated, more efforts to demonstrate safer parameters were undertaken.

To further develop a recycling approach, where exhaust gases are recirculated after removing maleic anhydride product, new processing parameters were considered. These parameters are presented in Table 1.10.

Under the conditions described in Column D of Table 1.10, including addition of 1.5 ppm TEP (by volume) and converting between 50 and 75 % of C_4 within each reactor pass, similar process yields were achieved at 79.4 % recycling rates. Importantly, this process operates within safer operational parameters [90]. A comparative proximity of these processes to the flammability region is more easily seen in Fig. 1.8.

Figure 1.8 graphically presents the flammability region of gaseous mixtures comprising molecular oxygen, C_4, and balanced with nitrogen at 100 kPa at 20 °C. As previously indicated, Point B is very near the boundary, whereas Point D is comfortably located some distance from the flammable region.

Table 1.10 Processing conditions for a fixed-bed gas recycling plant design [90]

Process parameter	C	D
Reactor temperature (°C)	380–440	419
Reactor inlet pressure (kPa)	600–1000	850
Space velocity (h^{-1})	3000–6000	4400
Total C_4 concentration fed to reactor (% volume)	1–1.3	1.2
% oxygen in reactor feed (% volume)	8–13	8.7
Total yield (kg of maleic anhydride/kg of C_4)	NA	NA
Yield (%, mol)	NA	59.2

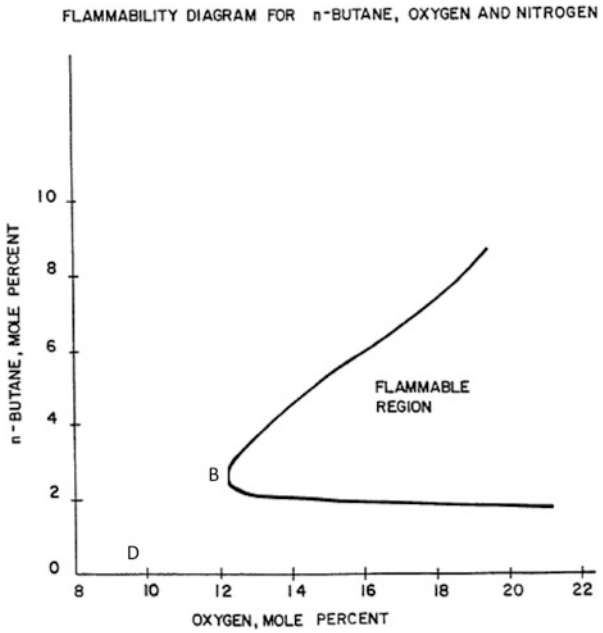

Fig. 1.8 Flammability diagram for mixtures of C_4 and oxygen balanced with nitrogen [89]

1.4.1.5 Solvent Absorption and Distillation

Efficient separation of the maleic anhydride product from the process stream is an essential feature to any economical plant process. As we saw earlier, strategies for separating some maleic anhydride product include partial cooling of the reactor effluent, cooling to the maleic anhydride dew point, and removing some maleic anhydride product. Water absorption is also employed to remove maleic anhydride product from the reactor effluent. However, some have noted drawbacks to water absorption [91]. These include expensive distillation processes, where water and dehydration of maleic acid requires significant energy, and loss of product, where maleic acid conversion to fumaric acid reduces process yields. Equipment fouling can also increase which leads to more plant maintenance [91]. Conversely, organic solvent processing can eliminate many of these drawbacks. Previous processes have demonstrated the effectiveness of maleic anhydride solvent-based recovery operations [92]. However, solvent methods are also known to accumulate undesirable by-products in the absorbing and stripping loops. Contaminants such as acrylic acid, fumaric acids, maleic acids, etc. as well as polymeric tars can build up and cause significant problems over time.

In one approach to improving solvent processing, the reactor effluent is brought in contact with an organic solvent, such as dibutyl phthalate. The water found in the maleic anhydride-enriched solvent is removed by stripping it off with a low-relative humidity gas and/or adsorbing agent. In the case of a low-humidity gas, the gas is

brought into contact with the enriched solvent at elevated temperature (>80 °C) and between 1 kPA and 200 kPa. These conditions enable the water to evaporate from the maleic anhydride-enriched solvent. Suitable gases, with water less than 15 %, are air, carbon dioxide, and/or nitrogen. Adsorbing agents, such as zeolites, are also effective in the dehydration process. This process is reported to reduce decomposition of the solvent, improve yields of maleic anhydride, and enable commercial production of maleic anhydride-enriched solvent streams with water contents less than 0.1 % [91].

Observers found that the process above typically resulted in maleic anhydride purity in the range of 97–99 %. The main residual was found to be trace levels of solvent, organic by-products (i.e., acrylic acid and carbonyl compounds), and water. To reach even higher levels of purity, another process was designed which incorporates a three-stage distillation process. In a simplified version of this solvent process, the maleic anhydride effluent from the reactor is brought into contact with organic solvent in the absorber. From the base of the first absorber, the maleic anhydride-enriched solvent stream is sent to a first vacuum separation column. In this first column, the top section is separated under stripping conditions, enabling the overhead vapors that form condensates to be fed to a second absorber, which is also countercurrently fed with the same organic solvent. Vapors that do not condense here are sent to disposal. The condensed solvent phase is sent on to the first fractionation column. The overhead containing impurities such as acrylic acid from the first fractionation column is sent directly to the second absorber. The bottoms of this absorber are returned to the original oxidation reactor absorber for recycling. The bottoms of the first fractionation column feed to the second fractionation column. It is from this second fractionation column that the high-purity maleic anhydride is obtained. Purities of 99.0 + % are achieved [93].

In another approach, purification of the oxidation gas stream, which comprises maleic anhydride, is again absorbed by a solvent, i.e., dibutyl phthalate. The maleic anhydride is then separated from the solvent by stripping in the presence of hydrogen gas in a column. The advantage of this approach is that the hydrogen gas cools the liquid phase which reduces the formation of by-products like fumaric acids. Another reported benefit is that the overall column diameter can be smaller, which reveals significant cost advantages [94].

Other research efforts enabled the development of a polymeric tar removal strategy. The approach was to first cool the effluent from the oxidation reactor and bring it into contact with the maleic anhydride solvent absorbent, i.e., dibutyl phthalate, in the absorber. The enriched solvent comprises maleic anhydride and contaminants. Maleic anhydride is then stripped from enriched solvent resulting in two process streams: one mainly maleic anhydride and the other comprised of solvent and contaminants. The solvent/contaminant mixture is brought into contact with agitated water, which is largely immiscible with the solvent. Polymeric tars present in the solvent are hydrolyzed and extracted into the aqueous phase. The solvent raffinate phase is substantially reduced of the polymeric tars and recycled back to the maleic anhydride absorption zone [95].

The formation of tars in the absorber and the degradation of solvent have also been found to be affected by the presence of catalyst fines. These catalyst fines, which result from attrition of the shaped catalyst body, exhibit an ability to

promote hydrolytic degradation of solvents such as alkyl phthalates. This degradation leads to tar formation in the solvent circuit. The process of catalyst attrition, once under way, can become accentuated and self-accelerating as the fines are continuously removed from a reactor tube. As the numbers of reactor tube fines become reduced, resulting in greater void spaces in the upper tube zone, there can be a decrease in the resistance inside the reactor tube. The increase in the tube gas flow, or gas velocity, coupled to a catalyst loss in the upper portion can ultimately lead to a fluidization of the fixed-bed or shaped catalyst expansion leading to greater abrasion effects, against both the tube walls and neighboring catalyst shaped bodies, further promoting catalyst attrition. To overcome these issues, two strategies are employed. First, a restraining bed composed of discrete material substantially denser than the catalyst is placed on the catalyst column top in each reactor tube. For example, 0.25-inch spherical Norton Denstone bodies exhibiting a density of 1.44 g/mL are placed on top of the VPO catalyst with a bulk density of 0.65 g/mL [96]. This will help to immobilize the catalyst bed. Tension springs, or other mechanical means, can also be employed to apply as a supplemental immobilizing force to the fixed catalyst bed. Second, fines typically < 1000 μm are removed from the catalyst bed by deploying a purging gas that is capable of dislodging and removing catalyst fines from the bed. A temporary, porous filter in direct communication with the exiting purge gas is employed to remove the fines from the process stream. The most effective removal of fines is utilizing the purging gas in an intermittent manner, effectively pulsing the purge gas in the catalyst bed. By passing pulsing gas through the tubes, one removes not only the fines capable of finding a clear exit path but also particles which are entrapped in various crevices of the catalyst bed. Essentially, this process is a de-dusting of the catalyst bed [96].

In a recent development, a process was designed by BASF with the intent to simplify maleic anhydride purification while maintaining high-purity levels. An important feature to this process is the dividing wall purification column presented in Scheme 1.9.

The purification column is comprised of three chambers, labeled 1, 2, and 3. The column is fed with crude maleic anhydride, via inlet #10, into chamber 2A. The purified maleic anhydride is collected in the chamber labeled 2B. Chamber 2A and 2B are separated from each other. Both chambers are open at the top to chamber 3 and bottom to the lower chamber 1. Within chambers 2A and 2B are a dividing wall and trays for amassing and dispersing materials, in rectified regions, ensuring distilling-type flow through the column. Vapors at the top of chamber 3 are fed into an overhead condenser labeled #4, where the condensate can be recycled. Remaining gases and liquids are discharged via #13. Material bottoms in chamber #1 are either recycled or discharged via #12. In Example #1, five theoretical plates are found in chambers #1 and #3, and chambers #2A and #2B comprised 12 theoretical plates, due to packing elements from Montz (A3-750 Hilden). The chamber pressure was operated at 30 mbar. The temperature of the chamber 1 was 200 °C

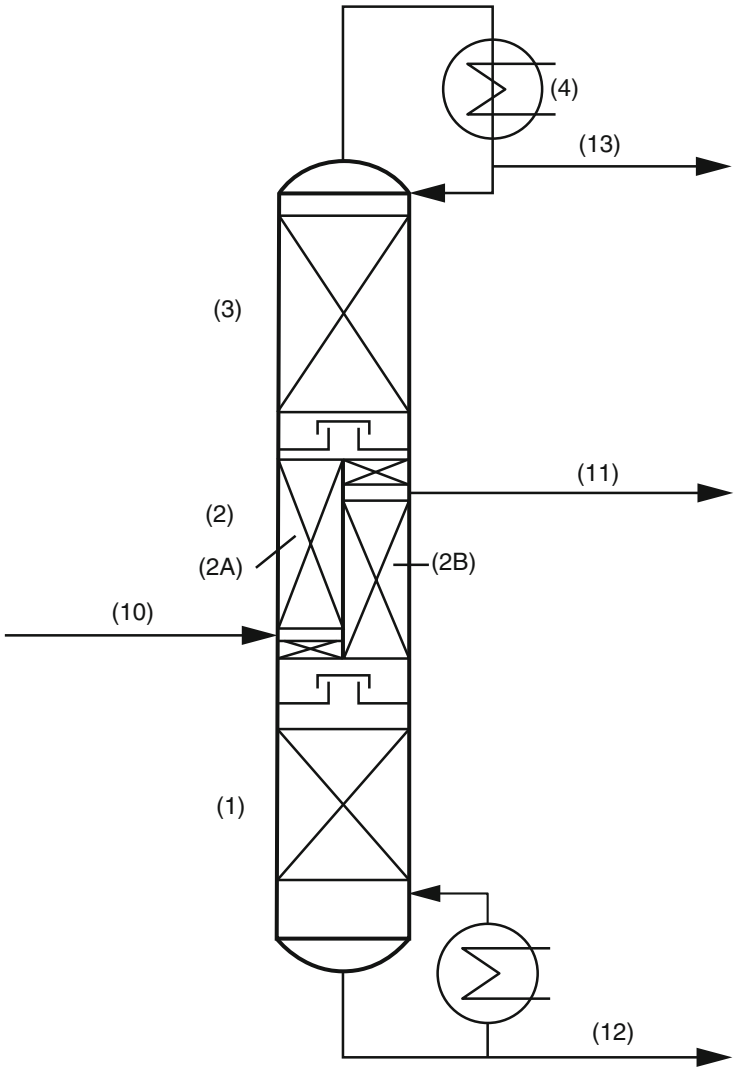

Scheme 1.9 A dividing wall column for maleic anhydride purification [97]

and 3 was 93 °C. Dibutyl phthalate solvent absorbent was employed where the feed rate of the enriched solvent was 1400 g/h and draw rate was 86 g/h. Under these general conditions, the collected material exhibited the properties found in Table 1.11.

As illustrated above, the distillation process yields 99.9+ % maleic anhydride, with very low levels acrylic acid and acetic acid. Additionally, the overall simplification of the equipment scheme is of great benefit to plant personnel [97].

Table 1.11 Maleic anhydride distillation purity from a divided wall column [97]

Compound	Collected result	Compound	Collected result
Acetic acid	NA	Monobutyl maleate	0.0185
Acrylic acid	NA	Monobutyl fumarate	NA
Maleic anhydride	99.9162	Phthalic anhydride	0.0027
Citraconic anhydride	NA	Dibutyl maleate	NA
Benzoic acid	0.0001	Dibutyl fumarate	NA
Dimeric acrylic acid	NA	Phthalic acid	0.0014
Maleic acid	0.0070	Monobutyl phthalate	0.0002
Fumaric acid	0.0006	Dibutyl phthalate	0.0528
Citraconic acid	NA	Unknown	0.0528
Color (APHA)	15	Water	NA

1.5 Improving Product Quality and Safety

Efforts to improve the quality of maleic anhydride by reducing color and improving thermal stability in addition to increasing purity are of critical industrial importance. The treatment of maleic anhydride with chemical additives can be technically complicated and leads to "impurities" that are intentionally introduced into downstream maleic anhydride production processes. As a result, strategies that focus on additives and/or processes continue to be developed in efforts to improve product quality.

1.5.1 Distillation in Designed Atmospheres

To improve the quality of crude maleic anhydride obtained from production of phthalic anhydride via o-xylene, the material was distilled in the presence of air, which contains molecular oxygen. The oxygen ratio to crude maleic anhydride ranges from 1 mmol/mol to 15 mmol/mol and is performed at temperatures ranging from 60 to 180 °C, in vacuo. After separation from the bottoms, comprised of maleic anhydride, citraconic anhydride, phthalic anhydride, benzoic acid, and other miscellaneous impurities (at a ratio of 27:18:23:27.5:4.5), the molten maleic anhydride was found to exhibit improved color stability, even over several days [98].

Highly pure, color-stable maleic anhydride with long shelf life stability was also prepared by fractional distillation of crude maleic anhydride, separating the desired product from low-boiling and high-boiling materials. The high-boiling materials are removed by partially condensing the maleic anhydride vapor, so 0.5–15 % by weight of maleic anhydride vapor is separated off as a liquid pre-condensate. The remaining vapor, which is highly pure maleic anhydride vapor, is then condensed into the product. This process is carried out downstream of conventional distillation of crude maleic anhydride. The process yields a maleic anhydride product which is color stable, a purity 98 + % by weight, and a color number (Hazen) < 40 on heating. Stored in liquid form, this product is shelf stable for 6–8 weeks [99].

In another distillation process, the crude maleic anhydride is introduced into the stripper column while removing the overhead stream from the stripper column. Meanwhile, the bottom stream is removed from the stripper column and introduced into the refining column where portions of the overhead low- and middle-boiling vapors are removed. Low-boiling materials range from 45 to 155 °C at 760 mm Hg, while middle-boiling materials exhibit boiling temperatures ranging from 160 to 285 °C at 760 mm Hg. A portion of this overhead vapor originating from the middle-boiling materials is condensed and directed to a refining column as a reflux. Finally, in the refining column, a side draw stream is collected and is at least 99.90 wt% maleic anhydride, while the overhead vapor is removed. The process is operated in an inert gas, such as nitrogen, and can also employ oxygen (<5 mol%). The inert gas treatment aids in purging the non-condensable materials from the crude maleic anhydride [100].

1.5.2 Additives for Distillates

An additive approach to product quality improvement, where maleic anhydride is distilled in the presence of tridecyl phosphate (TDP) ranging from 100 to 200 ppm as an antioxidant, was developed. After TDP addition, the crude maleic anhydride is thermally treated at 120–190 °C for 1–10 h. After thermal treatment, the distillation process begins at pressures of 50–100 mm Hg. The bottom temperature of the distillation tower ranges from 120 to 160 °C. To the distillate are the additions of n-propyl gallate (1–100 ppm), cuprous chloride (0.1–5 ppm), and zinc chloride stabilizers (0.1–5 ppm). Key to their effectiveness is good mixing. Zinc chloride is added to improve the maleic anhydride thermal stability. The effect of these stabilizer packages on maleic anhydride color and thermal stability are presented in Table 1.12.

In Table 1.12 Example B, the specific addition levels of n-propyl gallate (10 ppm), cuprous chloride (1 ppm), and zinc chloride stabilizers (0.5 ppm) enabled molten maleic anhydride color (APHA) results as follows when directly compared to no additive package [101].

The prior additive method was observed to be insufficient in meeting the stringent quality requirements when solid maleic anhydride is stored for long time periods. Phenols and catechols additives are known to have discoloration tendencies, especially if used in large quantities, and may become ineffective over time by exposure to light and oxygen [102]. As a result, monochloro-substituted aliphatic alcohols, such as 2-chloro-1,3-propanediol and 3-chloro-1,2-propanediol, were found to be effective stabilizing additives, when used in the presence of cuprous chloride and zinc chloride stabilizers. Additive use levels for chlorine-substituted alcohols range from 5 to 60 ppm, copper compounds from 0.25 to 1 ppm, and zinc compounds from 0.1 to 0.5 ppm. In a specific example, presented in Table 1.12, additive levels for Example C were 20 ppm for 5-chloro-1-pentanol, 1 ppm for copper acetate, and 0.2 ppm for zinc acetate [102]. Again, it was found that the stabilizer package improved the thermal and color stability of the purified maleic anhydride product.

Another method to improve maleic anhydride production quality is to minimize the amount of impurities generated in the oxidative reactor stream. For example,

Table 1.12 Results of additives for color and thermal stability [101, 102]

Example	Stabilizer	Molten color (APHA)		Heat-melted color (APHA)		
		Immediately after addition	After 30 days	Immediately after addition	Stored in liquid state (30 days)	Stored in solid state (30 days)
A	–	5	1	300	>500	>500
B	Added	5	10	10	10	15
C	Added	5	5	10	NA	35

trialkyl phosphite or trialkyl phosphate can be continuously added to reactor feed gases, in amounts ranging from 0.5 to 4 ppm (by wt. of elemental phosphorus). The reactor temperature is ranging from 400 to 440 °C, with a maximum temperature of 480 °C. Operating the reactor under these conditions results in conversion to maleic anhydride of ~84 + % and acrylic acid formation of < ~1.5 % [103].

1.5.3 Removal of Impurities via Precipitation

BASF employed a precipitation concept, where the reduction of fumaric acid deposits on plant equipment was envisioned to significantly improve product efficiency, reduce downtime and cleanup efforts, as well as improve product quality. Fumaric acid is formed from the isomerization of maleic acid, which is formed from the reaction of water and maleic anhydride. A key element to this process is a controlled precipitation of fumaric acid, where maleic anhydride-enriched phthalate-derived absorbent in temperatures ranging from 100 to 150 °C is cooled to a range of 30 to 70 °C. Fumaric acid exhibits a temperature-dependant solubility limit in dibutyl phthalate, the maleic anhydride-absorbing solvent in this case. As a result, cooling the solvent liquor enables significant amounts of fumaric acid precipitate to be removed from the purification and production process [104].

1.6 Safety

Mitsubishi Chemical has worked to establish safer operating processes for fluidized-bed reactors by studying a variety of process parameters and their inter-relationships. This effort has enabled the determination of a safety index, F. The safety index, F, is defined in Eq. (1.5): [105]

$$F = F_{\mathrm{L}} - F_{\mathrm{R}} > 0 \tag{1.5}$$

where F_{L} is determined by Eq. (1.6):

$$F_{\mathrm{L}} = C/C_{\mathrm{T}}/C_{\mathrm{o}} \tag{1.6}$$

where C is concentration (volume %) of flammable gas in the reaction product gas. Due to the numerous gases in this feed stream, C is actually the summation of each concentration flammable gas, i.e., C_1, C_2, etc. or $C = \sum_{i=1}^{n} C_i$. C_o represents the concentration of oxygen gas (volume %) in the reaction product gas as represented in Eq. (1.7):

$$C_o = \frac{\text{Concentration } (Vol.\ \%) of\ Oxygen\ in\ Reaction\ Product\ Gas}{(100 - C)} \times 100 \quad (1.7)$$

C_T is defined as the concentration of the flammable gas components in the reaction product gas which can be completely combusted with the amount of oxygen present in the gas feed. It is determined from Eq. (1.8):

$$C_T = \frac{100}{\left[1 + \left\{\left\{\sum_{i=1}^{n}(RixC_i)/\sum_{i=1}^{n} C_i\right\}/C_o\right\} \times 100\right]}, \quad (1.8)$$

and F_R is determined from Eq. (1.9):

$$F_R = 2.319 \times 10^{-5} \times T^2 - 1.688 \times 10^{-2} \times T + 3.288 + (P - 0.15) \times 0.3 \quad (1.9)$$

where T is the reaction product gas temperature (°C) and P is the gauged reaction pressure in MPa. In numerous experimental examples, using these relationships, it was possible to discern between explosive and nonexplosive processes, providing another technique for improving the safe operation of fluidized-bed reactors. Substantial data was also reported for a variety of experimental process conditions coupled to safety index data in support of this research effort [105].

To further develop the fluid-bed process, process parameters were developed that were constrained to empirical mathematical relationships. First, a safety coefficient (α) was developed, where α ranges between 0 and 10. The safety coefficient is determined by equations presented in (1.10):

$$\alpha = -10.51 + 51.22D - 35.35D^2 - E \text{ where}$$
$$D = \frac{C}{B + C} \text{ and } E = \frac{100A}{100 - B - C} \quad (1.10)$$

where the reactor exit gas stream is comprised of, in volume %, a maleic anhydride concentration > 2 %, an oxygen concentration (A), a hydrocarbon concentration (B), and a CO concentration (C) that satisfies the constraints of $0 < \alpha < 10$. Using these relationships enhances the overall process safety and efficiency of the fluid-bed maleic anhydride plant [106].

1.7 Other Production Routes

Within the known reactor technologies, numerous challenges remain unmet. While there is continuing focus on hot spot control, minimization of catalyst thermal degradation, catalyst attrition, and avoidance of thermal runaway episodes, the basic conditions and challenges of current reactor technology are relatively stable relying on operation in safe operation reaction zones to achieve economically viable results. Within these confines, there has been renewed effort to design even more capable processes for maleic anhydride production. Among these processes are circulating fluidized-bed reactors, microchannel technology, and bio-based production.

1.7.1 Circulating Fluidized-Bed (CFB) Reactor

Other processes are known for maleic anhydride production. Perhaps the most well-known alternative process is the circulating fluidized-bed (CFB) reactor developed and commercially demonstrated by DuPont [107]. Scheme 1.10 presents a schematic of the CFB reactor.

Interpreting Scheme 1.10 beginning at the reactor feed, C_4 and nitrogen gases in tandem with the catalyst rise through the riser pipe in plug flow. Upon their exit, the gases are separated from the catalyst in the separator/stripper, where any carbonaceous species are removed. The product stream continues on as in the other processes once completely separated. The reduced catalyst, on the other hand, is fed to the fluid-bed regenerator to be reoxidized to then return to the base of the riser. In this manner, the process is continuously deploying "fresh" catalyst. The CFB approach sought to eliminate several challenges for typical fixed-bed and fluid-bed systems. As with fluid-bed processes, the CFB heat transfer is very good, but, in this case, the system operates in plug flow within the riser resulting in minimal back-mixing. One key improvement is the reduction in catalyst attrition, which results in selectivity losses when attrition becomes severe, a common issue in fluid-bed reactors. The selectivity of the catalyst to C_4 to maleic anhydride is preferred to be in an inert atmosphere, such as nitrogen. Note that the process in the riser is substantially free of oxygen, but in the fluid-bed regenerator, where the catalyst is oxidized (regenerated), there is 20 mol% oxygen and 80 mol% helium. But before the regenerated catalyst returns to the riser, the catalyst must be stripped to minimize the amount of gas-phase oxygen when the catalyst communicated with C_4. In one specific example, where the CFB process is operated at 438 °C, the residence time for C_4/nitrogen [3:97 (mol %)] gases in catalyst contact contained in the riser was 4 s, and the fluid-bed regenerator feed gas was O_2/helium [20:80 (mol %)] with a residence time of 3 s, enabling 83.3 % conversion and 60.8 % selectivity [108]. In 1996, an 82,000 tons/year CFB plant was started in Asturias, Spain, for producing THF using this process for C_4 to maleic acid [109].

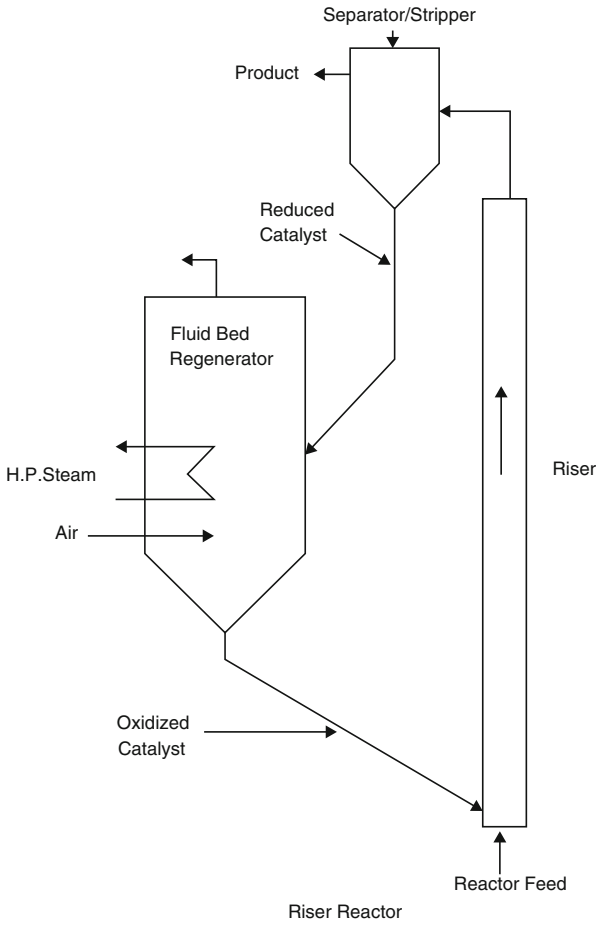

Scheme 1.10 Circulating fluidized-bed (CFB) reactor schematic [107] (Reprinted from Chemical Engineering Science, 54, Contractor, R.M., "Dupont's CFB technology for maleic anhydride," 5627–5632, Copyright **1999** with permission from Elsevier)

1.7.2 Microchannel Reactor

In 2007, BASF employed a microchannel reactor for C_4 oxidation demonstrating that a reactor could be safely operated in the explosive range and produce an above-average yield of maleic anhydride [110]. Because the microchannel reactor is dimensionally so small, where in at least one direction the reactor is <3 mm, the ability of fire to spread is not possible, implying a much safer process. With flammability issues minimized or significantly reduced, there is a significant increase in the design freedom for the processing parameters: gaseous ratios (organic/oxygen), reactor pressure design beyond maximum explosion pressures, and improved mass/heat transfer (enabling suppression of hot spots) [110]. A general comparison of fixed-bed and microchannel process parameters is presented in Table 1.13.

Table 1.13 Comparison of fixed-bed and microchannel process parameters [88, 110]

Process parameter	Fixed-bed B (see Table **1.9**)	Microchannel
Reactor temperature (°C)	400	380–440
Reactor inlet pressure (MPa abs)	0.344	~0.101
Space velocity (h^{-1})	1500	3000–8000
Total C_4 concentration fed to reactor (% volume)	2.1	2–20
% oxygen in reactor feed (% Volume)	12.2	20–98
Total yield (kg of maleic anhydride/kg of C_4)	1.03	NA
Yield (%, mol)	60.7	~70 %

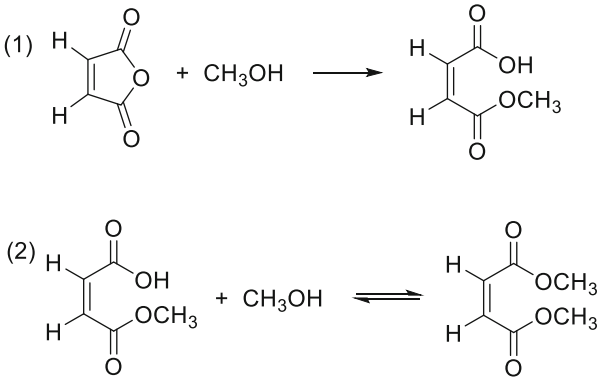

Scheme 1.11 Transformation of maleic anhydride to dimethyl maleate [111]

1.7.3 Bio-based Reactants

To generate even more value from existing maleic anhydride production facilities, plants capable of producing other commercially relevant compounds than can be derived from maleic anhydride, such as butane-1,4-diol (B1D), γ-butyrolactone (BLO or GBL), and tetrahydrofuran (THF), are envisioned. To accomplish this additional production, an important intermediate step is to react maleic anhydride with an alkyl alcohol, such as methanol, to ultimately produce dimethyl maleate. This chemical reaction scheme is presented in Scheme 1.11.

Once the dimethyl maleate is formed, the maleated material can undergo a vapor-phase hydrogenation using a copper chromite catalyst or a promoted copper catalyst [111, 112]. The result of this key hydrogenation step is the production of B1D, GBL, and THF [111].

In 2013, Arkema revealed a process for maleic anhydride production based on butanol via a fermentation process versus the now more traditional C_4 approach. In developing the bio-based strategy, organic matters, such as sugars, starches, and cellulosics, as well as vegetable matter, which are all renewable raw materials, are fermented in the presence of microorganisms, such as *Closlridium* and *Closlridium*

acelobuzylicum. Among the mixture of products produced are butanol and acetone, which are separated, usually by distillation, to isolate butanol. Butanol is then oxidized to maleic anhydride at temperatures ranging from 300 to 600 °C using traditional VPO catalysts. To determine the actual source of the maleic anhydride products, maleic anhydride prepared from renewable sources contains ^{14}C, which is a component of the Earth's atmosphere. Thus, isotopes are convenient compositional feature to determine the ultimate source of the maleic anhydride product [113].

Acknowledgments The authors would like to express their sincere gratitude to Frank Fusiak, Larry Lake, Jude Ruszkay and Laurence Senak, all of Ashland, Inc., and Professor Robert D. Pike, of The College of William and Mary, for their many helpful conversations/suggestions and thorough review of the manuscript prior to publication.

References

1. Ashland Product Stewardship Summary, Maleic Anhydride, 16 Sept 2013
2. DSM Product safety summary, Maleic Acid, 8 Aug 2011
3. The Merck index, 9th edn. Merck & Co, Rahway, NJ (1976)
4. Lohbeck K, Haferkorn H, Fuhrmann W, Fedtke N (2012) Maleic and fumaric acids. Ullmann's Encycl Ind Chem 22:145–155
5. Wilhoit RC, Shiao D (1964) J Chem Eng Data 9(4):595–599
6. Lohbeck K, Haferkorn H, Fuhrmann W, Fedtke N (2012) Maleic and fumaric acids. Ullmann's Encycl Ind Chem 22:145–155
7. Acree W, Chickos JS (2010) J Phys Chem Ref Data 39(4)
8. Dahlgren G, Long FA (1960) J Am Chem Soc 82(6):1303–1308
9. OSHA (1992) n-Butane
10. Paper #1-13 Natural Gas Liquids (2011) Working document of the National Petroleum Council North American Resource Development Study made available 15 Sept 2011
11. Moore BJ, Sigler S (1987) Analyses of natural gases, 1917–85. Bureau of Mines, Information Circular 9129
12. Marathon Petroleum Corp (2012) Annual Report
13. Ashland Performance Materials Neal Plant (2011) Title V Fact Sheet R30-09900009-2012 to the State of West Virginia, 2011
14. Trivedi BC, Culbertson BM (1982) Maleic anhydride. Plenum Press, New York
15. Felthouse TR, Burnett JC, Horrell B, Mummey MJ, Kuo Y-J (2001) Maleic anhydride, maleic acid, and fumaric acid. In: Kirk-Othmer encyclopedia of chemical technology. Wiley, New York
16. Mirasol F (2012) US chemical profile: maleic anhydride. ICIS.com. Accessed 23 Apr 2012
17. Trivedi BC, Culbertson BM (1982) Maleic anhydride. Plenum Press, New York, p 17
18. Sunderland P (1976) Ind Eng Chem Prod Res Dev 15(2):90–99
19. Chemical Weekly (2010) 11 May 2010, pp 185–190
20. Hydrocarbon Process 176 (1971)
21. Hydrocarbon Process 175 (1971)
22. Malow M (1980) Hydrocarbon Process 149–153
23. Malow M (1985) Environ Prog 4(3):151–154
24. Malow M Environ Prog 4(3):151–154
25. Burnett JC, Keppel RA, Robinson WD (1987) Catal Today 1:537–586
26. Doshi BM (1999) Production of maleic anhydride. US 6,194,587 B1

27. Padia AS, Click, GT (1994) Two stage butane maleic anhydride process. US 5,360,916
28. Padia AS, Bortinger A, Mazzoni G, Monti T (2009) Reduction of acrylic acid in the production of maleic anhydride. US 7,619,099 B2
29. Schmidt J (1978) Two stage maleic anhydride process. US 4,116,983
30. Daniel C (1984) Manufacture of maleic anhydride. US 4,429,136
31. Wellauer TP, Cresswell DL, Newson EJ (1986) Chemical Eng Sci 41(4):765–772
32. Hydrocarbon Process 142 (1985)
33. Ballarini N, Cavani F, Cortelli C, Ligi S, Pierelli F, Trifiro F, Fumagalli C, Mazzoni G, Monti T (2006) Topics Catal 38(1–3)
34. Suciu GD, Paustian JE (1987) Process for preventing backmixing in a fluidized bed vessel. US 4,691,031
35. Suciu GD, Stefani G, Fumagalli C (1986) Production of maleic anhydride. US 4,594,433
36. Neri A, Sanchioni S (1982) Process for the continuous separation of maleic anhydride from process gases. US 4,314,946
37. Emig G, Martin F (1987) Catal Today 1:477–498
38. Wellauer TP (1985) Optimal policies in maleic anhydride production through detailed reactor modelling. Dissertation, ETH Zurich
39. Emig G, Martin F (2007) ICIS Chem Bus:58, 17–23 Sept
40. ICIS (2012) US chemical profile: maleic anhydride
41. Zavalij PY, Whittingham MS (1999) Acta Cryst B55:627–663
42. Bordes E (1987) Catal Today 1:499–526
43. Bordes E (1987) Catal Today 1:499–526
44. Boudin S, Guesdon A, Leclaire A, Borel M-M (2000) Int J Inorg Mat 2:561–579
45. Nguyen PT, Hoffman RD, Sleight AW (1995) Mater Res Bull 30(9):1055–1063
46. Geupel S, Pilz K, van Smaalen S, Büllesfeld F, Prokofiev A, Assmus W (2002) Acta Cryst C58:9–13
47. Busca G, Centi G (1989) J Am Chem Soc 111:46–54
48. Schiott B, Jorgensen KA, Hoffman R (1991) J Phys Chem 95:2297–2307
49. Schiott B, Jorgensen KA, Hoffman R (1991) J Phys Chem 95:2297–2307
50. Cheng M, Goddard WA (2013) J Am Chem Soc 135:4600–4603
51. Keppel RA, Mitchell SF, Mummey MJ (1998) Supression of autoignition in maleic anhydride production. US 5,734,066
52. Padia AS, Sachs H, Millman M (2009) Yield improvement in the production of maleic anhydride. US 7,589,217 B2
53. Takayasu O, Nakajima A, Hashiba H (2001) Method for production of maleic anhydride. US 6,194,588 B1
54. Taheri H (1992) Continuous process for the production of maleic anhydride from a C4-hydrocarbon feedstock. US 5,117,007
55. Burnett JC, Alumbaugh WH, Reeves LA (2001) Method and apparatus for improving the uniformity of distribution of a phosphorous-containing agent throughout a maleic anhydride catalytic reactor. US 6,300,505 B1
56. McCandless HA, Cearley JL, Taheri H (1990) Process for the manufacture of maleic anhydride utilizing peroxides to improve catalytic activity. US 4,950,769
57. Ushikubo T, Oshima K (1995) Method for the production of maleic anhydride. US 5,449,792
58. Dobner C, Duda M, Raichle A, Wilmer H, Rosowski F, Holzle M (2008) Catalyst and methods for producing maleic anhydride. US 2008/0227992 A1
59. Hibst H, Glaum R, Benser E (2010) Polynary vanadyl pyrophosphate. US 2010/0105927 A1
60. Ebner JR, Keppel RA, Mummey MJ (1999) High productivity process for the production of maleic anhydride. US 6,005,121
61. Yamamoto H, Yoneyama N (1983) Process for producing conjugated diolefins. US 4,423,281
62. Weiguny J, Storck S, Tenten A, Ruppel (2004) Method for producing maleic acid anhydride. US 6,803,473 B2
63. Hibst H, Noe R, Exner KM, Duda M (2006) Method for producing maleic anhydride. US 6,989,454 B2

64. Haddad MS, Meyers BL, Taheri H, Wolfe PA (1998) Catalysts for the production of maleic anhydride by the oxidation of butane. US 5,792,722
65. Bertola A, Cassarino S, Nsunda VK (2001) Process for the preparation of improved vanadium-phosphorus catalysts and use thereof for the production of maleic anhydride. US 6,174,833 B1
66. Groke D, Bosch R, Lotz J, Eberle HJ (2002) Method for producing catalysts for synthesizing maleic anhydride by means of gas phase oxidation. US 6,407,030
67. Haddad MS, Goeden GV (2009) Phosphorus addition process for improvement of catalysts suitable for maleic anhydride production. US 7,629,286 B2
68. Albonetti S, Cavani F, Ligi S, Mazzoni G (2005) Vanadium/phosphorous mixed oxide catalyst. US 6,956,004 B2
69. Altwasser S, Dobner CK, Wilmer H, Rosowski F (2012) Maleic anhydride synthesis catalyst precursor and process for its preparation. US 2012/0149919 A1
70. Haddad MS, Eryman WS (1992) Maleic anhydride catalysts. US 5,134,106
71. Groke D, Ruedinger C, Eberle HJ, Jering R, Bosch R (2000) Process for producing coated catalysts for the synthesis of maleic anhydride by gas-phase oxidation. US 6,048,987
72. Okuhara T, Misono M (1993) Catal Today 16:61–67
73. Datta A, Dasgupta S, Agarwal M (2004) Process for preparing vanadyl pyrophosphate catalyst. US 6,774,081
74. Forkner MW (2012) Maleic anhydride catalyst and method for its preparation. US 8,143,461 B2
75. Andrews WJ, Ebner JR, Felthouse TR (1994) Catalysis for the production of maleic anhydride containing vanadium-phosphorous oxide with selected promoter elements. US 5,364,824
76. Felthouse TR, Keppel RA, Schaefer CJ (1999) Molydenum-modified vanadium-phosphorous oxide catalysts for the production of maleic anhydride. US 5,945,368
77. Shan Z (2011) High pore volume vpo catalyst for maleic anhydride production. US 2011/0201830 A1
78. Afandizadeh S, Foumeny EA (2001) Appl Thermal Eng 21:669–682
79. Dobner CK, Altwasser S, Wilmer H, Rosowski F (2011) Catalyst and method for producing maleic anhydride. US 2011/0257413 A1
80. Melde LE, Smith WA (2011) Modified trilobe shape for maleic anhydride catalyst. US 2011/0201829 A1
81. Dobner CK, Altwasser S, Wilmer H, Rosowski F (2011) Catalyst and method for producing maleic anhydride. US 2011/0257413 A1
82. Melde LE, Smith WA (2011) Modified trilobe shape for maleic anhydride catalyst. US 2011/0201829 A1
83. Haddad MS, Meyers BL, Eryman WS (1992) Maleic anhydride production. US 5,095,125
84. Ebner JR, Keppel RA (1992) Shaped oxidation catalyst structures for the production of maleic anhydride. US 5,168,090
85. Edwards RC (1990) Process for preparation of maleic anhydride. US 4,918,201
86. Ceisel SC, Conrad JF, Lestan EM, Nelson AP (1990) Process for the continuous separation of maleic anhydride from process gases. US 4,941,895
87. Doshi BM (2001) Production of maleic anhydride. US 6,194,587 B1
88. Ruggieri R, Cassarino S (1997) Process to recycle exhaust gases from n-butane conversion into maleic anhydride. US 5,688,970
89. Palmer DA, Holzhauer JK (1987) Process for production of maleic anhydride. EP0099431 B1
90. Duda M, Machhammer O, Weck A (2008) Method for the production of maleic anhydride. US 7,345,167 B2
91. Bertola A, Ruggieri R (1991) Process of recovery of maleic anhydride from reaction gaseous mixtures. US 5,069,687
92. White JE (1978) Recovery of maleic anhydride. US 4,118,403
93. Ruggieri R, Conni S (1996) Process and plant for the purification of raw maleic anhydride recovered from gaseous reaction mixtures. US 5,585,502

94. Windecker G, Weck A, Steiniger M, Bredehoft JP, Bender B, Knappik P, Hautte DV, Pierre B, Haffner B (2008) Method for separating maleic anhydride from mixtures containing the same by means of stripping. US 2008/0182996 A1
95. Brown HC, Alumbaugh WH (1997) Process for the preparation and recovery of maleic anhydride. US 5,631,387
96. Mummey MJ, Keppel RA, Reeves AL (2000) Prevention of catalyst attrition and tar formation in the manufacture of maleic anhydride. US 6,046,343
97. Windecker G, Kaibel G, Steiniger M, Buntrock T, Weiguny J, Hautte DV, Lurquin T (2013) Process for obtaining maleic anhydride by distillation. US 8,461,356 B2
98. Michl G, Seubert R, Schmidt JE (1990) Obtaining maleic anhydride not prone to discolor. US 4,921,977
99. Zimmerling D, Schmidt JE, Seubert R, Fischer K, Sauer F (1990) Obtaining very pure maleic anhydride from crude maleic anhydride. US 4,961,827
100. Brown HC, Alumbaugh WH, Burnett JC (2000) Process for the purification of maleic anhydride. US 6,120,654
101. Sugawara H, Okawa T (1991) Process for producing maleic anhydride. US 5.026,876
102. Sugawara H, Ohkawa T (1992) Method of preventing discoloring of maleic anhydride. US 5,157,130
103. Padia AS, Bortinger A, Mazzoni G, Monti T (2009) Reduction of acrylic acid in the production of maleic anhydride. US 7,619,099 B2
104. Windecker G, Weiguny J, Weck A, Dahlhoff E, Weibker WS, Heilek J, Krug T, Freyberger R (2013) Process for separating off fumaric acid and other minor components during the production of maleic anhydride. US 8,476,463 B2
105. Iizuka Y, Ihara T, Yamauchi Y, Sawano M, Sawaki I (2002) Process for the production of maleic anhydride. US 6,458,971
106. Sawaki I, Suwa H, Ishimura Y, Iizuka Y, Izumi M (2003) Process for the preparation of maleic anhydride. US 6,620,948
107. Contractor RM (1999) Chem Eng Sci 54:5627–5632
108. Contractor RM (1991) Vapor phase catalytic oxidation of butane to maleic anhydride. US 5,021,588
109. Contractor RM (1999) Chem Eng Sci 54:5627–5632
110. Wilmer H, Maurer T, Rosowski F, Schuch R (2007) Process for preparing maleic anhydride in a microchannel reactor. US 2007/0270597 A1
111. Sutton DM, Hiles AG, Backes AF (2003) Process for the simultaneous production of maleic anhydride and its hydrogenated derivatives. US 6,620,949
112. Scarlett J, Wood MA (1995) Process for the production of hydroxy compounds by hydrogenation of oxygenates. EP0656336A1
113. Dubois JL (2013) Manufacture of maleic anhydride from renewable materials, maleic anhydride obtained, and uses thereof. US 8,394,973

Part II
Reactions and Derivatives

Chapter 2
Reactions Involving Maleic Anhydride

Michael A. Tallon

2.1 Introduction

2.1.1 Physical Properties of Maleic Anhydride and Its Derivatives

The rich chemistry that maleic anhydride can participate in makes it the quintessential building block for a variety of small and polymeric molecules that are in use today. This is derived from the electron-deficient conjugated double bond and the cyclic anhydride functionality present. This activated double bond allows it to take part in Michael reactions, electrophilic addition, formation of Diels–Alder adducts, alkylation and acylation reactions, sulfonation, halogenations, reduction, photodimerization, hydroformylation, or free-radical polymerization reactions to generate poly-anhydride copolymers.

Likewise, the reactive anhydride functionality permits a whole host of organic reactions like esterification, amidation, imidation, hydrolysis, decarboxylation, and metal chelation to name a few. This chapter begins with the basic chemistry of maleic anhydride due to its molecular structure and the types of reactions it can participate in, as well as its physical and chemical properties. For instance, the bond angles and bond lengths for maleic anhydride are depicted in Fig. 2.1, and this results in a very compact and particularly planar structure [1].

Even though the double bond in maleic anhydride is quite electron deficient and would be expected to be slightly shorter than 1.1 Å for the C–H and 1.3 Å for the C=C bond length, they are still comparable to a typical alkene like ethylene that corresponds to 1.08 Å and 1.33 Å, respectively. The anhydride bond lengths are typical of anhydrides like acetic anhydride. However, the bond angles are significantly

M.A. Tallon (✉)
Ashland Inc., 1005 Route 202/206, Bridgewater, NJ 08807, USA
e-mail: mtallon@ashland.com

O.M. Musa (ed.), *Handbook of Maleic Anhydride Based Materials*,
DOI 10.1007/978-3-319-29454-4_2

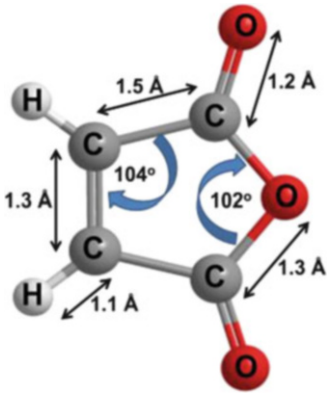

Fig. 2.1 Bond angles and bond lengths for maleic anhydride

different from 120° reflecting the internal ring strain of the cyclopentane ring structure. With the exception of the C–O–C bond angle of 102°, the remaining four carbon–carbon bond angles are all 104°, Fig. 2.1. The cumulative effect of all these factors forces all the atoms within the maleic anhydride molecule to lie in one plane.

The true nature of this extreme planarity and compact nature for the maleic anhydride molecule can be depicted by the ball–stick and space-filling models illustrated in Fig. 2.2, where the oxygen's lone pairs are depicted in pink [2]. This molecular structure also allows for efficient packing of the molecules into its crystal lattice resulting in a relatively high density value of 1.48 g/cc.

The olefinic double bond within maleic anhydride is quite electron deficient and can be better portrayed by its resonance structures shown in Fig. 2.3a, which results in its potent electron-acceptor behavior. This electron deficiency is particularly important in free-radical polymerization reactions and is responsible for the creation of a charge-transfer complex between an electron-rich comonomer and an electron-poor monomer like maleic anhydride. This charge-transfer complex results in activating maleic anhydride to participate in free-radical copolymerization thereby resulting in an alternating copolymer. In contrast, homopolymerization of maleic anhydride is not particularly favored so that only low molecular weight oligomers are generated.

The electron-density map of maleic anhydride is depicted by the electropositive (red) nature of the conjugated double bond and by the electronegative (blue) anhydride functionality in Fig. 2.3b. The maleic anhydride molecule exhibits a very strong dipole moment of 3.96 debye and strong coulombic attractions between maleic anhydride molecules. This results in its high melting (53 °C) and boiling (202 °C) points than expected by its neutral structure alone [1, 3, 4].

Maleic anhydride crystallizes as orthorhombic needlelike crystals, while maleic acid and fumaric acid form monoclinic crystals. The crystal structure for maleic anhydride was first deduced by Marsh and coworkers in 1962 [2]. They found that it forms an orthorhombic crystal structure, with a $P2_12_12_1$ unit cell that contains four

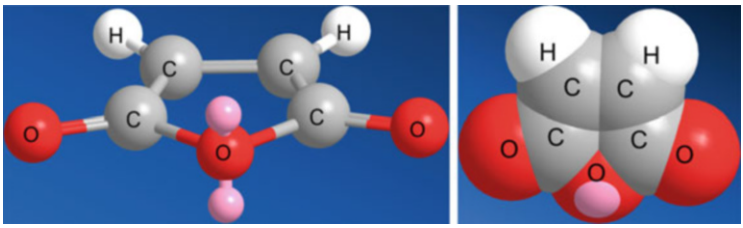

Fig. 2.2 Ball–stick (**a**) and space-filling (**b**) models for maleic anhydride

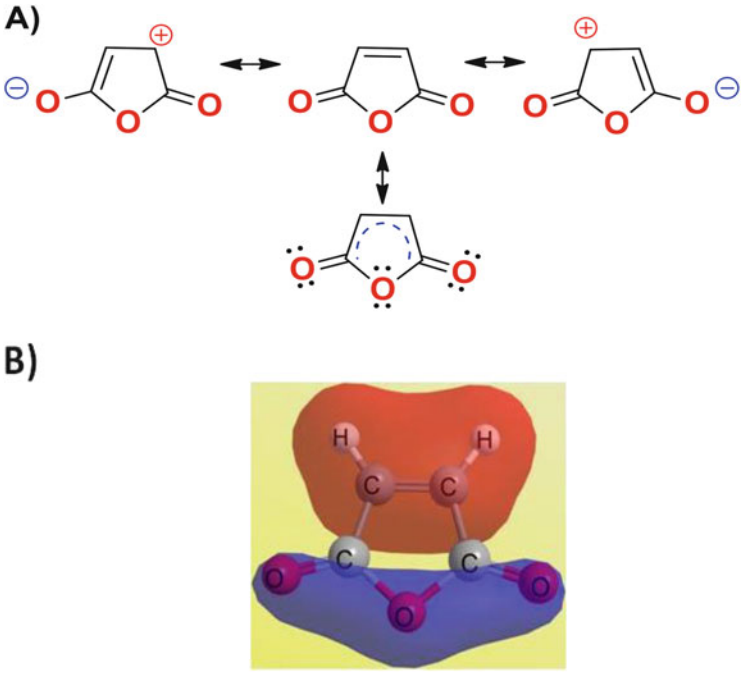

Fig. 2.3 Resonance structures (**a**) and electron density were partially positive (*red*) and partially negative (*blue*) for maleic anhydride (**b**)

molecules of maleic anhydride. This is schematically depicted in Fig. 2.4, in the ball–stick (2.4a) and space-filling (2.4b) models.

It should be noted that the electrophilic double bonds align themselves in close spatial proximity to the electron-rich anhydride atoms of adjacent molecules thereby giving rise to the strong coulombic attraction between maleic anhydride molecules thereby increasing its melting point. These interactions are denoted by the yellow arrows in Fig. 2.4a.

The corresponding dimensions of each unit cell, as defined by axes a, b, and c, the number of maleic molecules within each unit cell (Z), and its corresponding volume are summarized in Table 2.1. The numbering system used for individual

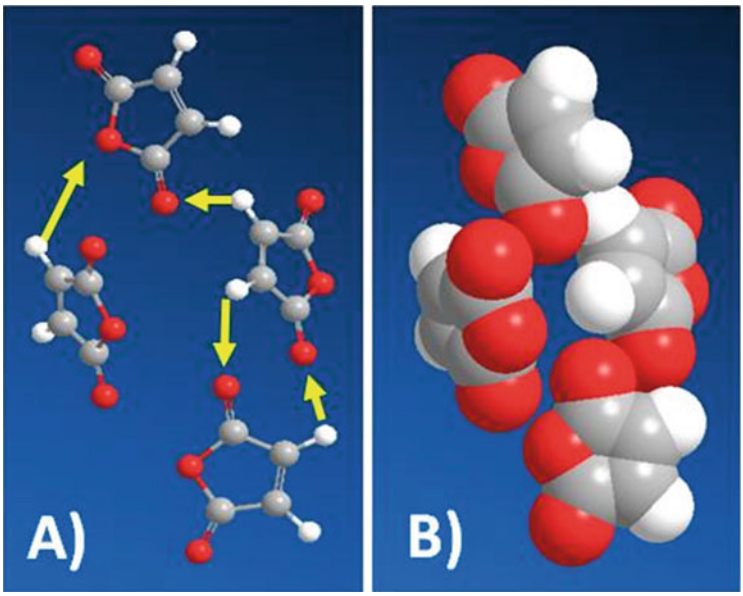

Fig. 2.4 Maleic anhydride's $P2_12_12_1$ unit-cell crystal structure, (**a**) ball–stick and (**b**) space-filling models

Table 2.1 Crystallographic data for maleic anhydride at 295°K

Lattice	Orthorhombic	Numbering system
Space Group	$P2_12_12_1$	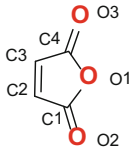
a	7.18 Å	
b	11.23 Å	
c	5.39 Å	
Unit-cell Volume	434.60 Å^3	
Density	1.505 g/ml	
Z	4 molecules	

Molecule volume 108.65 Å^3, Actual density=1.48g/cc

atoms, bond lengths, and bond angles of the maleic molecule are reported in Table 2.2.

This molecular structure further results in some practical consequences toward its physical properties, as summarized in Table 2.3 [3, 4]. For instance, this planar structure with conjugated double bond, along with its compact electron cloud, makes it a very *efficient mirror* with visible light thereby resulting in a very high refractive index value of 1.55 [1, 3, 4].

The dipolar nature of the maleic anhydride molecule not only affects the physical properties of the molecule, but this electron-deficient double bond is activated to reactions with nucleophilic reagents, thereby enabling it to participate in Michael-type reactions. Similarly, maleic anhydride is a potent dienophile in Diels–Alder reactions.

Table 2.2 Bond angles/distances for maleic anhydride crystal structure

Bonds	Angle (°)	Bond	Distance (Angstrom)
C2–C1–O1	107.9	C2–C3–H3	130
C2–C1–O2	131.2	C4–C3–H3	121
O1–C1–O2	120.9	C1–O1	1.396
C1–C2–C3	108.4	C1–C2	1.476
C2–C3–C4	108.5	C2–C3	1.317
C1–C2–H2	119	C1–O2	1.200
C3–C2–H2	133	C2–H2	1.085
C3–C4–O1	107.8	C3–C4	1.480
C3–C4–O3	131.6	C4–O1	1.389
O1–C4–O3	120.6	C4–O3	1.203
C1–O1–C4	107.4	C3–H3	1.01

Table 2.3 Select physical and toxicological properties of maleic anhydride, maleic acid, and fumaric acid

Property	Maleic anhydride	Maleic acid	Fumaric acid
Chemical formula	$C_4H_2O_3$	$C_4H_4O_4$	$C_4H_4O_4$
Molecular weight (g/Mole)	98.06	116.07	116.07
[a]Physical form	White solid	White solid	White solid
Refractive index	1.55	1.35	1.34
[a]Melting point	52.9 °C	138–139 °C	287 °C
[a]Boiling Point	202 °C	138(dec)	290 °C
Density, g/cc 20 °C	1.48	1.59	1.64
Dipole moment, Debye	3.96	3.18	2.45
Crystalline form	Orthorhombic	Monoclinic	Monoclinic
Solubility in H_2O@ 25 °C	Hydrolyzes	30.6 %	0.7 %
Acidity pK_a @ 25 °C	NA	pK_{a1}= 1.5 pK_{a2}= 6.5	pK_{a1}= 3.0 pK_{a2}= 4.5
Acid number (mg KOH/g)	Hydrolyzes	966	966
Flash point Open cup	110 °C	Decomposes @ 135 °C	282 °C
Closed cup	102 °C	ND	230 °C
Viscosity centipoises @ 70 °C	1.5	ND	ND
Oral rat LD_{50} mg/Kg	400	708	10,700
Skin rabbit LD_{50} mg/Kg	2620	1560	20,000
Intraperitoneal rat LD_{50} mg/Kg	97	ND	587
Subcutaneous rat LD_{50} mg/Kg	1220	ND	ND

[a]At 25 °C and 760 torr, *NA* not applicable, *ND* not determined

Films of maleic anhydride and its copolymers, or its derivatives, tend to exhibit very high gloss or shine. Hydrolysis of maleic anhydride yields maleic acid, which can be isomerized to its sister-isomer, fumaric acid. Table 2.3 presents the comparative properties between maleic anhydride, maleic acid, and fumaric acid. All three molecules are hygroscopic solids at room temperature.

Maleic anhydride slowly sublimes around 40–50 °C and exhibits a relatively high vapor pressure that is partially responsible for its acrid odor. Maleic anhydride slowly hydrolyzes into maleic acid by absorption of moisture and therefore exhibits a slight deliquescence behavior. Molten maleic anhydride exhibits an absolute viscosity of 1.5 centipoise at 70 °C.

OSHA's threshold for inhalation is 0.25 ppm (1 mg/M^3), while dermal limits to prevent contact dermatitis are approximately around 100–500 ppm depending on the global regulatory body involved [3, 5]. In summation, the chemical reactivity of maleic anhydride is best described by its electrophilic conjugated *cis*-double bond and its reactive anhydride functionality in a compact five-membered planar ring structure. These attributes are the foundation for its versatility in organic syntheses.

The thermodynamic properties for maleic anhydride are listed in Table 2.4. The two most practical properties in manufacturing are the heat of hydrolysis and heat of neutralization. These values are needed to determine if the reactor size has the correct cooling capacity to handle the heat generated by hydrolyzing, reacting the anhydride ring, and/or neutralization. Process engineers use this data by converting these values to British thermal units (BTU) and comparing them to the cooling capacity rate of the chiller in the reactor.

For instance, 1 kJ (kilojoule) is equal to 0.9478 BTU, meaning that neutralizing 5000 Kg of maleic acid to disodium maleate will generate 3.7 million BTUs of heat. That will raise the temperature of a 50 % aqueous solution by 95 °C. Therefore, even if you started at room temperature, say about 25 °C, the neutralization would result in a temperature increase of the solution to roughly 120 °C, well above the boiling point of water.

Maleic acid begins to decompose at 120 °C by decarboxylation into CO_2 gas. Significant formation of gas can ultimately result in a substantial explosive potential. Such a large energy release from the enthalpy of neutralization requires dilute solutions of maleic acid to be used for neutralization coupled to a slow rate of addition of neutralizer. In addition, a low temperature glycol chiller must be used for safety and practical reasons.

Since maleic anhydride is a solid at room temperature, a solvent is often used to dissolve it prior to any syntheses operations. Table 2.5 summarizes maleic anhydride, maleic acid, and fumaric acid solubilities in different solvents. Interestingly, maleic anhydride is not readily soluble in water even though it exhibits a strong dipole moment, but instead it slowly hydrolyzes to form maleic acid at room temperature, which is readily soluble in water.

Usually mild heating is applied ≈ 60–70 °C to accelerate hydrolysis and prevent off-gassing by decarboxylation. This will be discussed more fully in the following hydrolysis section. Maleic anhydride is extremely soluble in polar aprotic solvents

Table 2.4 Thermodynamic properties of maleic anhydride, maleic acid, and fumaric acid

Property	Maleic anhydride	Maleic acid	Fumaric acid
Heat of formation kJ/Mol	−470.41	−790.57	−811.03
Heat of combustion kJ/Mol	−1389.5	−1355.2	−1334.7
Specific heat (solid) kJ/Mol °K	−0.1199	−0.1356	−0.1418
Heat of evaporation kJ/Mol	54.8	NA	NA
Heat of fusion kJ/Mol	13.55	NA	NA
Heat of hydrolysis kJ/Mol	−34.9	NA	NA
Heat of neutralization kJ/Mol	−126.9	−92	−92
Heat of sublimation kJ/Mol	71.5	105.4	123.6

NA not applicable

Table 2.5 Solubilities of maleic anhydride, maleic acid, and fumaric acid

Solvent	Maleic anhydride wt%	Maleic acid wt%	Fumaric acid wt%
Acetone @ 20 °C	>69	27.8	ND
Acetone @ 29.7 °C	>70	20.8	1.66
Benzene 25 °C	50	0.02	0.003
Chloroform 25 °C	34.4	0.10	0.02
Ethanol 22.5 °C	Esterifies	34.4	ND
Ethyl acetate 25 °C	52.8	ND	ND
Kerosene 25 °C	0.25	ND	ND
Methanol 22.5 °C	Esterifies	29.1	ND
1-Propanol 22.5 °C		24.3	ND
Water @ 25 °C	Hydrolyzes into maleic acid	30.6	0.7
40 °C		34.6	1.04
60 °C		37.1	2.28
97.5 °C		44.4	ND
100 °C		ND	8.19
Toluene 25 °C	19	ND	ND
o-Xylene 25 °C	16	ND	ND

ND not determined

like acetone, methyl ethyl ketone, and ethyl acetate (Table 2.5). It is also moderately soluble in apolar solvents like benzene, xylene, and toluene.

Solubility parameters in protic solvents like alcohols are meaningless since maleic anhydride will slowly react with them to form half esters. This results in a new composition with different solubility characteristics. Therefore, its Log *P* coefficient is a somewhat misleading value in octanol, since it is capable of reacting with the alcoholic component. In contrast, maleic acid is practically insoluble in apolar solvents like benzene and toluene and only moderately soluble in acetone and in water.

2.1.2 *Spectroscopic Properties of Maleic Anhydride*

The spectroscopic profiles for maleic anhydride are illustrated in Figs. 2.5, 2.6, 2.7, and 2.8. The UV trace (see Fig. 2.5) depicts the UV absorption of the conjugated double bond and carbonyl group spanning 220–250 nm region.

The FT-IR profile of maleic anhydride is shown in Fig. 2.6. Typical absorption bands at 3130 cm^{-1} for the olefinic =C–H stretch, the antisymmetrical and symmetrical C=O stretches at 1856 and 1774 cm^{-1}, C=C stretch at 1630 cm^{-1}, C–O

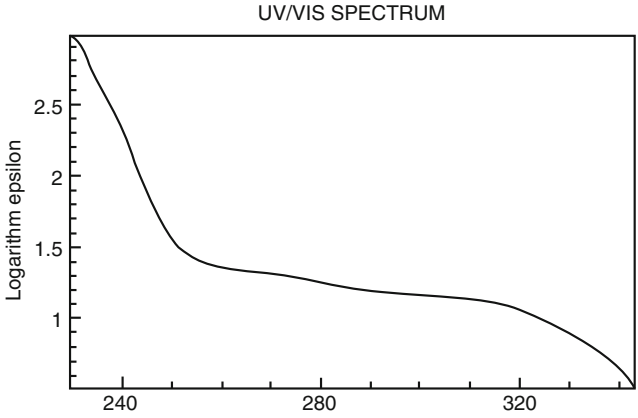

Fig. 2.5 UV profile for maleic anhydride

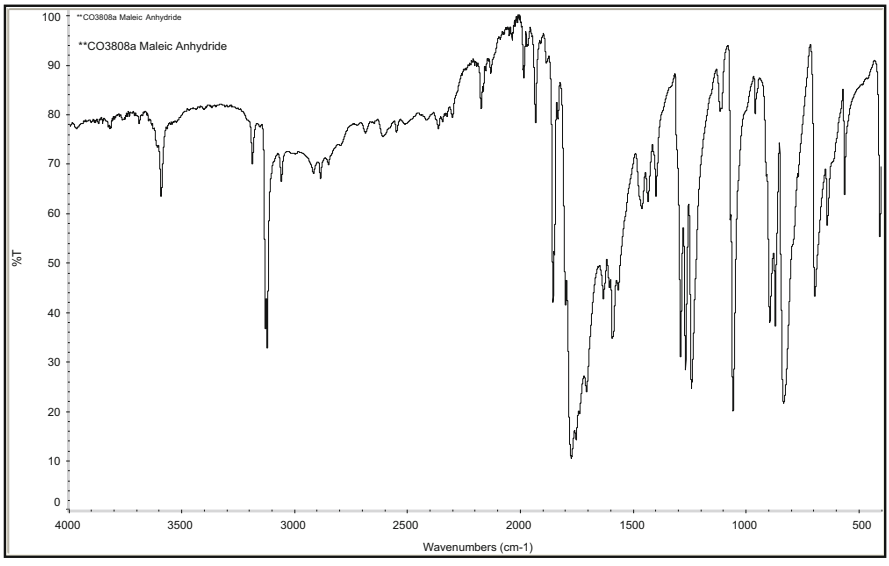

Fig. 2.6 FT-IR profile for maleic anhydride

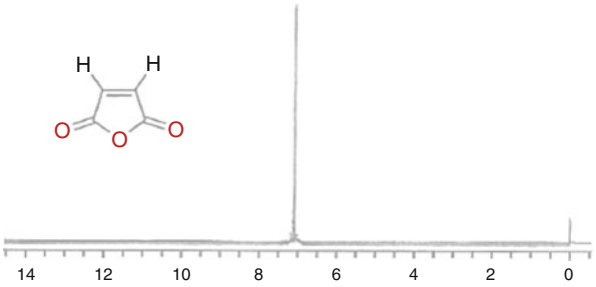

Fig. 2.7 Proton-NMR profile for maleic anhydride

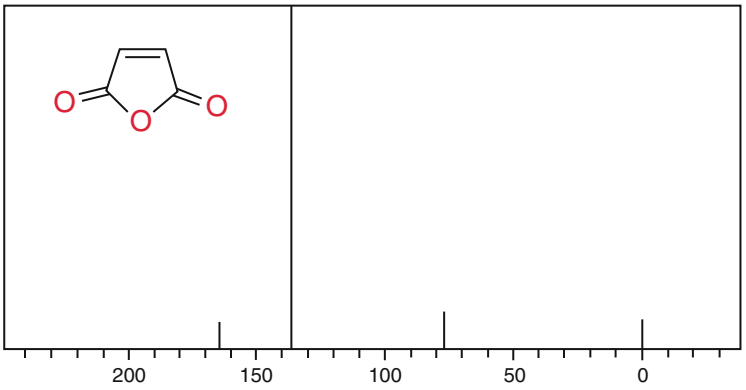

Fig. 2.8 Carbon-NMR profile for maleic anhydride

stretch at 1030 cm^{-1}, and the *cis*-C=C wag band 700 cm^{-1}, all characteristic of the maleic anhydride structure.

The proton-NMR profile for maleic anhydride is depicted in Fig. 2.7. The sharp singlet at 7.1 ppm is consistent with the olefinic =C–H proton signal, while the absence of a broad carboxylic acid signal at 12–10 ppm indicates the anhydride functionality in the aprotic $CDCl_3$ solvent.

The carbon-NMR profile for maleic anhydride is portrayed in Fig. 2.8. The sharp singlet at 136 ppm is consistent with the olefinic =C–H proton signal, while the carboxylic anhydride signals O–C=O at 165 ppm are both consistent with the maleic anhydride structure in $CDCl_3$ solvent. The carbon signal at 77 ppm is deuterochloroform, while the carbon peak at 0 ppm is attributable to tetramethylsilane as an internal reference standard.

2.2 Reactions of the Anhydride Functionality

2.2.1 Hydrolysis and Acidity

Maleic anhydride will slowly hydrolyze to maleic acid at room temperature at a rate slower than typical anhydrides like acetic anhydride, which generally occurs very rapidly when mixed with water. This effect is due in part to the strong intermolecular columbic attraction between maleic anhydride molecules. However, once hydrolyzed to maleic acid, it exhibits some rather unique stability and acidity characteristics [6].

Note the double-sided equilibrium arrows in Scheme 2.1. The hydrolysis reaction of maleic anhydride into maleic acid and the dehydration reaction of maleic acid into maleic anhydride are in equilibrium and can be interconverted under rather mild conditions. For example, the forward reaction will occur in water at 60 °C to form maleic acid; however, the reverse reaction in vacuum occurs at 55 °C to generate maleic anhydride up to 50–60 % by weight. This is due to the *cis*-double bond *locking in* the diacid groups in close special proximity as depicted in Fig. 2.9.

The close spatial proximity of the diacid group, resulting from the *cis*-double bond, has another consequence with regard to acidity. The acidity of maleic acid is roughly thirty times stronger than its *trans*-counterpart fumaric acid, for the first proton dissociation step (Scheme 2.2a), notably due to the anionic charge stabilization by the neighboring acid proton that can transfer back and forth between the two *cis*-carboxyl groups, denoted by structures 1–3 in Scheme 2.2a.

Therefore, resonance structures 1–4 actually delocalize the proton from the first dissociation across six atoms. This extreme resonance stabilization results in very acidic $pK_{a1} = 1.5$ value (Table 2.1).

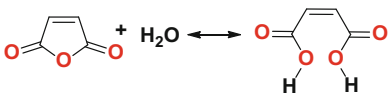

Scheme 2.1 Aqueous hydrolysis of maleic anhydride to form maleic acid

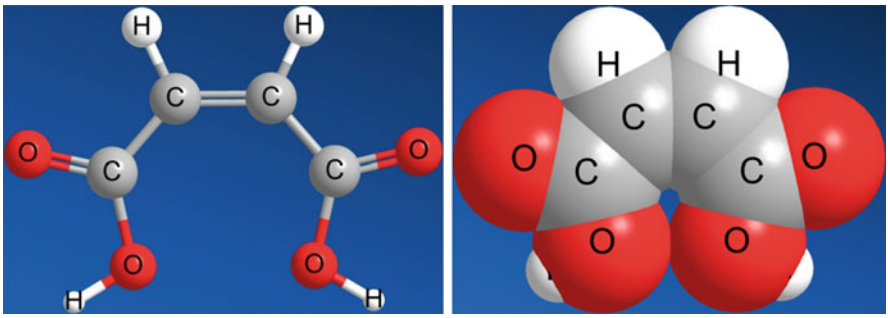

Fig. 2.9 Ball–stick (**a**) and space-filling (**b**) models for maleic acid

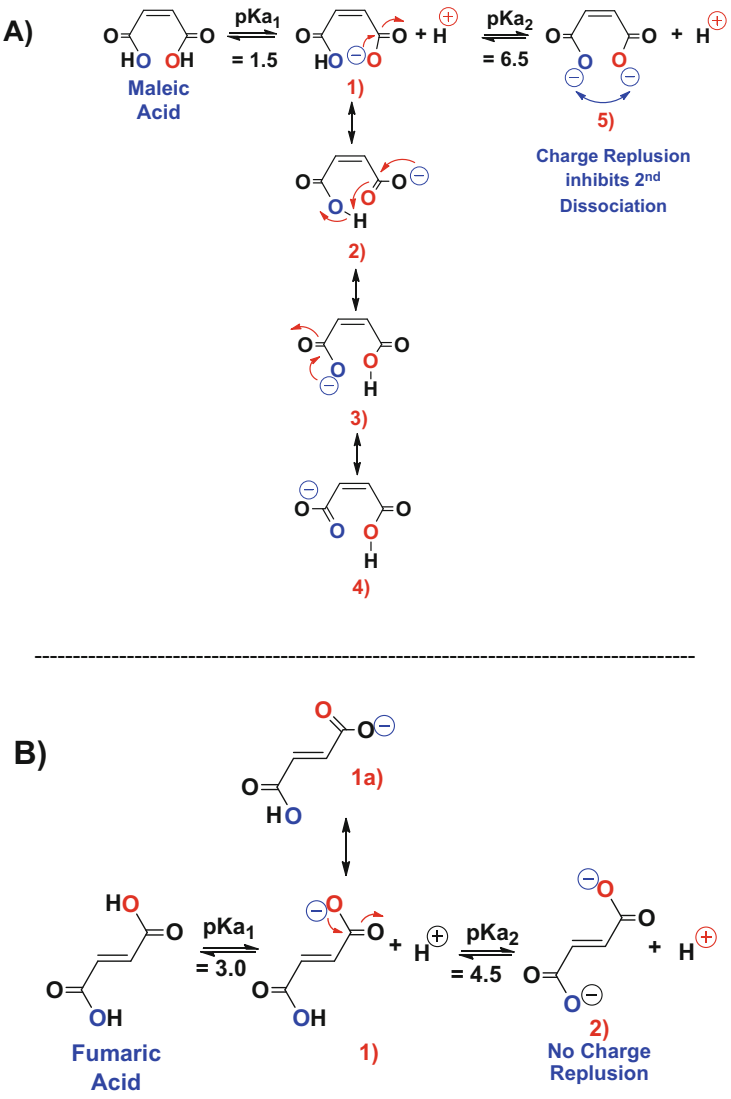

Scheme 2.2 Acidity of maleic acid (**a**) versus fumaric acid (**b**)

In contrast, the *trans*-configuration of fumaric acid positions these two carboxyl groups further apart. This increased separation suggests the second neighboring carboxyl group is less capable of stabilizing the first dissociated proton. As a result there is less resonance stabilization (Scheme 2.2b structures 1-1a) which generates an increase in the pK_a value for fumaric acid, to that more typical of an organic acid, p$K_{a1} = 3.0$ (Table 2.1).

Fumaric acid (p$K_{a2} = 4.5$) is a hundred times stronger acid for the second ionization step than maleic acid (p$K_{a2} = 6.5$). This effect arises from the charge repulsion of the *cis*-di-anion that is formed in maleic acid. The second dissociation

is inhibited by the first proton dissociation, because the two anionic charges are in close spatial proximity to each other and they are *locked in* by the *cis*-double bond. This effect is illustrated in Scheme 2.2a structure 5. Conversely, the *trans*-configuration of fumaric acid places these two carboxyl groups far apart so that the di-anion formed is not destabilized by charge repulsion (Scheme 2.2b structure 2), and occurs at much lower pH values.

An additional consequence of the *cis*- versus *trans*-configuration for the diacid group is manifested in their respective melting and boiling points. Experimentally fumaric acid exhibits a melting point (287 °C) versus maleic acid (138–139 °C) (Table 2.1). (This arises because each fumaric acid molecule can hydrogen bond to multiple partners within the crystal lattice and therefore requires more energy to break them apart for the melting point transition to occur.)

This becomes apparent when looking at the crystal structure of maleic acid versus fumaric acid, Fig. 2.10a, b. The *cis*-diacid group of maleic acid enables strong hydrogen bonding corresponding to one intramolecular H-bond per molecule and either two or three intermolecular H-bonds. In contrast, fumaric acid's *trans*-configuration permits only strong intermolecular hydrogen bonding corresponding up to eight potential H-bonds per molecule. (One would expect a higher melting point for fumaric as compared to maleic.)

In addition, better packing due to the *trans*-configuration results in a slightly higher solid density than maleic acid (1.64 vs. 1.59 g/mole). The enhanced packing also permits for more efficient intermolecular hydrogen bonding across multiple fumaric molecules, as depicted in Figs. 2.10, 2.11, and 2.12. Hence, fumaric acid can H-bond in all three dimensions across multiple "chains" as depicted in Fig. 2.10b, while maleic acid can only hydrogen bond mostly in two dimensions, Fig. 2.10a. Therefore, less energy is required to fracture the interactions between maleic acid molecules for its melting transition to occur. This notion is further corroborated by the ball and stick and space-filling models for maleic acid versus fumaric acid illustrated in Figs. 2.11 and 2.12, respectively. The dotted lines represent H-bonding between atoms in Figs. 2.11a and 2.12a.

Besides H-bonding, additional factors involved for the increase in melting arises from the columbic attraction of the partial positive charge related to the olefinic methine group, to the partial negative charge ascribed to the carbonyl functionality, denoted in red and blue, respectively. For fumaric acid, the symmetry of the *trans*-configuration allows for better packing and better overlap between these partial charges across multiple fumaric molecules. In contrast, maleic acid is much less efficient in overlapping these partial charges because of the anisotropy exhibited where only one side of the molecule is partially positive (*cis*-olefinic methines) and the opposing side attributable to the *cis*-carbonyl groups is partially negative.

Therefore, the spatial group of the crystal structure caused by the atomic coordinates of the atoms prevents maximum overlap between the partial charges within the maleic acid crystal lattice, while for fumaric acid the symmetry of the *trans*-configuration does allow for better packing and overlap within its crystal lattice. This notion is illustrated by the number and orientation of blue and red partial charges depicted in Fig. 2.10a versus 2.10b for a pair of neighboring chains,

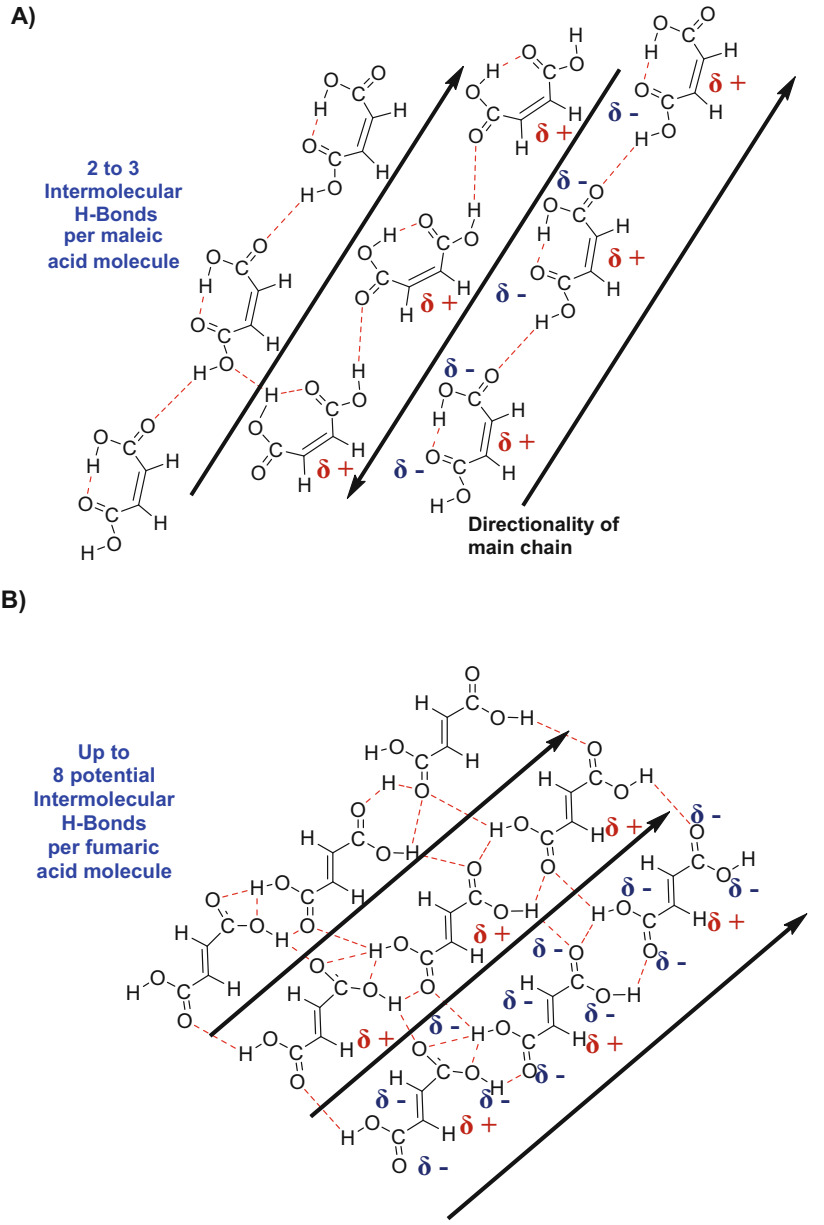

Fig. 2.10 Hydrogen bonding and coulombic attraction of partial charges for (**a**) maleic acid versus (**b**) fumaric acid in their crystal lattice (Adapted from [7])

as well as the H-bonding network generated for maleic acid in Fig. 2.11a versus fumaric acid in Fig. 2.12a.

With regard to the crystal structures of maleic and fumaric acid, both individual molecules exhibit multiple crystal forms known as polymorphs. Polymorphism is

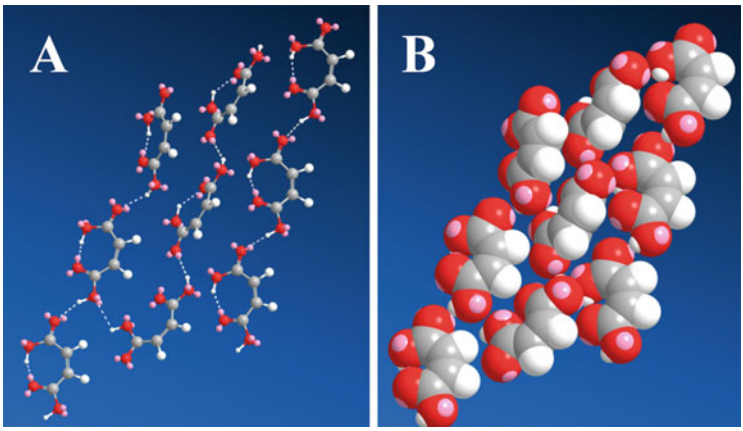

Fig. 2.11 Maleic acid $P2_1/c$ unit-cell crystal structure, (**a**) ball–stick and (**b**) space-filling models

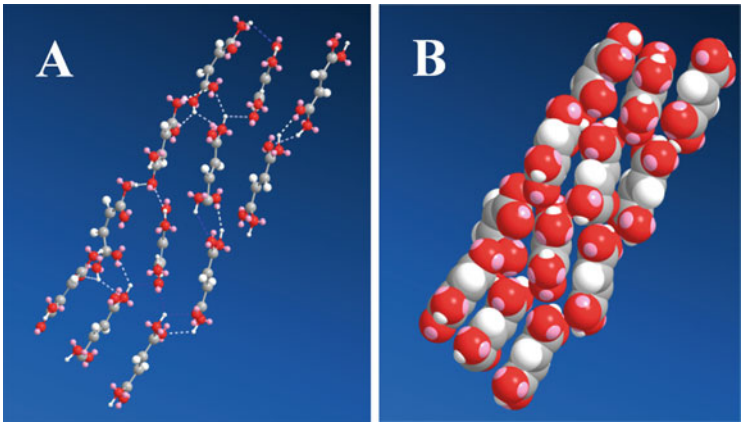

Fig. 2.12 Fumaric acid $P2_1/c$ unit-cell crystal structure, (**a**) ball–stick and (**b**) space-filling models

the ability of a single chemical substance to adopt more than one crystal structure. Maleic acid is an example of one such compound that exhibits polymorphism. Both the pure substance itself and as a conjugate salt with pharmaceutical actives are capable of forming polymorphs. As far back as 1881, interest in maleic acid prompted the analysis of its crystal structure, which was first reported by Bodewig [8]. X-ray analysis followed to define its space group [9], while additional analyses confirmed the crystal structure for the monoclinic crystal form-I [10, 11]. 125 years later a second polymorphic monoclinic form-II was reported [12, 13].

The polymorphic forms of maleic acid are built up from molecular sheets or planes wherein molecules interact with each other via OH···O=C hydrogen bonds, thereby forming 1D chains that alternate in directionality within one plane. As these chains oscillate in direction back and forth as depicted by the black arrows in Fig. 2.10a, they also H-bond through close special contacts between the antiparallel aligned chains through their hydroxyl groups. The α-form-I forms sheets or planes

Table 2.6 Crystallographic data for maleic acid at 295°K

Lattice	Monoclinic α-Form-I	Monoclinic β-Form-II
Space Group	$P2_1/c$	Pc
a	7.47 Å	3.69 Å
b	10.15 Å	7.48 Å
c	7.65 Å	8.49 Å
Unit-cell volume	580.02 $Å^3$	234.33 $Å^3$
Density	1.59 g/ml	1.55 g/ml
Z	4 molecules	2 molecules
Molecule volume	145.01 $Å^3$	117.17 $Å^3$

that alternate in directionality from plane to adjacent plane, such as ABAB, while the β-form-II forms sheets that are all in the same directionality, AAAA.

Form-I is the most prevalent structure reported for maleic acid in the literature today. The crystallographic data for each polymorphic form can be summarized by Tables 2.6 and 2.7, with the corresponding dimensions of each unit cell as defined by axes a, b, and c, as well as the number of maleic molecules within each unit cell (Z), and its corresponding molecular volume per maleic anhydride molecule is listed. Since Z exhibits 2–4 molecules per unit cell depending on the polymorph type, the molecular volume per molecule was listed so that a direct comparison to the density of each type can be made.

Similarly, fumaric acid also exhibits polymorphism. In general, fumaric acid crystals in their α-form contain six molecules per unit cell, while β-form contains only one molecule per unit cell [7]. Like maleic acid, sheets or planes are formed for both polymorphic forms of fumaric, but both are unidirectional with respect to the 1D chain orientation, as well as the polarity of the planes, such as AAAA. The crystallographic data for both forms are summarized in Table 2.7.

Table 2.8 summarizes the crystallographic bond lengths found for the different polymorphic forms of fumaric acid and maleic acid. Maleic acid is basically planar and exhibits compact intramolecular hydrogen bonds (2.46 Å). Additionally, both polymorphic forms of maleic acid exhibit very similar bond lengths for both the single- and double-bond carbon–carbon backbone thereby reflecting more pseudo-aromatic character within these molecules. In contrast, both the α- and β-forms of fumaric acid, the "single" and "double" carbon–carbon bond lengths, are more typical for an alkylene system (Table 2.8).

2.2.2 Isomerization and Stability

At this point it should be noted that the solubility of fumaric acid in water at 25 °C is 0.7 % while maleic acid is 30.6 weight% (Table 2.3). This provides a means to manufacture fumaric acid from maleic anhydride. Specifically, maleic anhydride is manufactured by oxidation of butane as outlined in Chap. 1 and then hydrolyzed to maleic acid in water (Scheme 2.3). Then an 80 weight% aqueous solution of maleic

Table 2.7 Crystallographic data for fumaric acid at 295°K

Lattice	Monoclinic α-Form-I	Triclinic β-Form-II
Space group	$P2_1/c$	$P\,\bar{1}$
a	7.60 Å	5.26 Å
b	15.11 Å	7.62 Å
c	6.61 Å	4.49 Å
Unit-cell volume	759.06 $Å^3$	179.97 $Å^3$
Density	1.63 g/ml	1.62 g/ml
Z	6 molecules	1 molecules
Molecule volume	126.51 $Å^3$	179.97 $Å^3$

Table 2.8 Bond distances for fumaric acid versus maleic acid crystal structures

Bond	Bond length α-Fumaric acid in angstroms	Bond length β-Fumaric acid in angstroms	Bond length α-Maleic acid in angstroms
–C–C–	1.46	1.49	1.44
–C=C–	1.34	1.32	1.43
C–OH	1.29	1.29	1.28
C=O	1.23	1.23	1.20
O···HO	2.68	2.67	2.46, 2.75

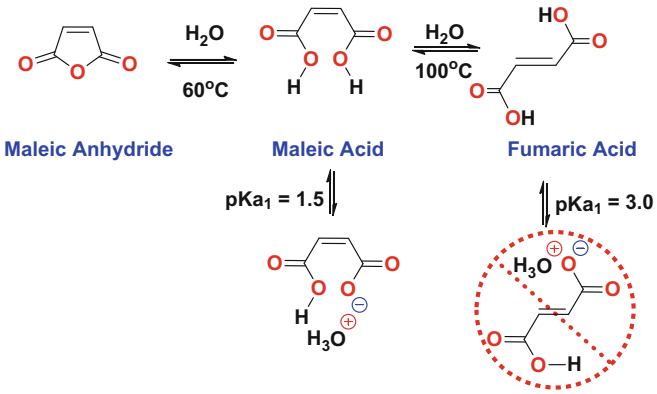

Scheme 2.3 Isomerization of maleic acid into fumaric acid by hydrolysis of maleic anhydride

acid is refluxed in water for several hours upon which fumaric acid begins to crystallize out of solution. The resulting solution is then cooled and filtered to obtain fumaric acid crude that is subsequently washed with water and dried as pure monoclinic crystals. The process washes are combined with the mother liquor and the process can be repeated over again. This simple procedure is even practiced in undergraduate organic chemistry labs today.

This procedure works so well because the *cis*-double bond of maleic acid can be isomerized into the more thermodynamically stable *trans*-double bond of fumaric

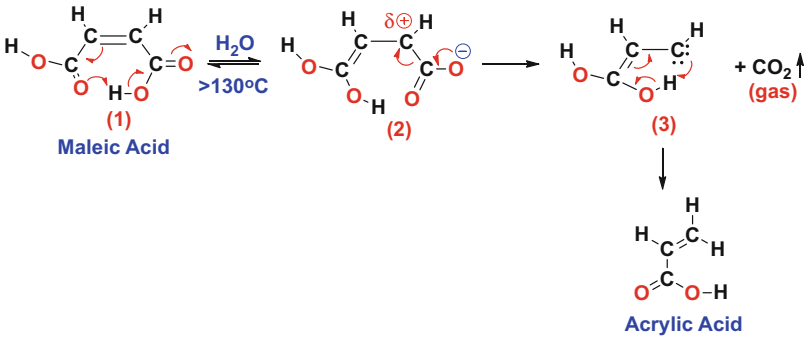

Scheme 2.4 Decarboxylation of maleic acid due to excess heat

acid by moderate heating (Scheme 2.3). The fumaric acid so formed then crystallizes out of the aqueous solution to drive the reaction further to the right. This difference in solubility between maleic acid and fumaric acid arises because of their difference in acidity. Maleic acid having a $pK_{a1} = 1.5$ would be partially ionized (≈30 %) and hydrated in its hydronium maleate salt form at a pH around 1–2. In contrast, fumaric acid would only be ≈0.1 % ionized at the same pH. So as maleic acid is isomerized into fumaric acid, which is not readily soluble in water because of its weaker ionization potential, fumaric acid therefore crystallizes out of the solution.

Both maleic anhydride and maleic acid are unstable at high temperatures. Exposure to elevated temperature should be avoided because of the potential for decarboxylation side reactions that *off-gas* these materials. This effect is analogous to beta-keto-esters or malonic acid decarboxylation, whereby the formation of an enolate-transition state results in carbon–carbon bond fission. This degradation can occur in excess of 130 °C under highly acidic conditions, as depicted in Scheme 2.4.

For maleic anhydride, decarboxylation usually originates from the adsorption of moisture enabling the formation of some maleic acid to provide the prerequisite acidic catalyst. Because of maleic acid extreme acidity, it is easy to protonate the neighboring *cis*-carboxyl group at high temperatures. In doing so, an enolate is formed due to electronic rearrangement, as depicted in Scheme 2.4 structure 2. Carbon–carbon bond fission follows to release CO_2, along with proton transfer to the intermediate carbene that is formed (Scheme 2.4 structure 3) with the net result to convert maleic acid into acrylic acid with the release of CO_2. It should also be noted that in Scheme 2.4 structure 2 can isomerize to interconvert into fumaric acid for the arrangement of the transitional double bond, as depicted by the bold blue oxygen atom for clarity in Scheme 2.4. However, the outcome is the same regardless of the orientation, and both routes still form acrylic acid once the enolate-transition state is formed.

Fumaric acid can also undergo decarboxylation, but because it's a much weaker acid ($pK_{a1} = 3.0$) than maleic acid ($pK_{a1} = 1.5$), the formation of the enolate-transition state requires a much higher temperature in excess of 240 °C as compared to 130 °C for maleic acid. The temperature at which decarboxylation occurs can be significantly lowered to 100 °C by the presence of a weak tertiary base such as pyridine or dioctyl-methylamine, but this is generally accompanied by

polymerization to yield an intractable resinous mass. Likewise, maleate/fumarate half esters form alkyl acrylates and/or dialkyl maleate esters and free maleic acid, the latter of which transforms into acrylic acid as outlined above [3, 14].

2.2.3 Peroxidation

The peroxidation of linear anhydrides with concentrated hydrogen peroxide has been well known since the late 1950s [9]. However, it was not until 1962 that White and Emmons demonstrated the formation of maleic peracid from maleic anhydride and hydrogen peroxide, as shown in Scheme 2.5 [15, 16].

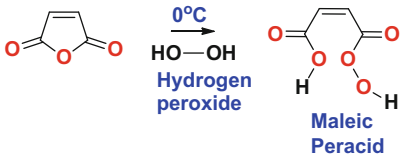

Scheme 2.5 Peroxidation of maleic anhydride into maleic peracid

The synthesis of maleic peracid was carried out in methylene chloride at 0 °C by means of an ice bath as depicted in Scheme 2.5. Other inert solvents for this reaction include benzene, dioxane, DMF, and formamide. At 0 °C, the peroxidation reaction predominates and little to no epoxide is formed with the double-bond functionality. However, Saotome et al. [17, 18] demonstrated that at 70 °C, aqueous solutions of maleic acid can be epoxidized. Therefore, the peroxidation reaction is extremely sensitive to temperature, and the heat released upon treatment with aqueous hydrogen peroxide must be maintained as low as possible. This can be achieved by controlling the addition rate of the peroxide to maleic anhydride to keep the overall reaction temperature well below 30 °C to prevent this side reaction.

In 1967, Rohm and Haas patented the use of maleic peracid as an excellent oxidizing agent for conversion of monoketones to their esters by the Baeyer–Villiger reaction, such as the conversion of benzophenone into phenyl benzoate in near-quantitative yield in 2 h [16, 19]. Maleic peracid is also an excellent oxidizer of primary amino compounds into their nitro-derivatives, as well as conversion of olefins into their epoxide end product [15, 20].

It was demonstrated that the maleic peracid was not as potent as trifluoroperacetic acid, but was stronger than all other organic peracids, such as performic, peracetic, and perphthalic acids, and was reasonably stable in methylene chloride where it decomposes approximately 5 % in 6 h at room temperature. An additional benefit in performing the synthesis of maleic peracid in methylene chloride was the ease of removal for the unwanted maleic acid that precipitates out from the reaction medium because of its insolubility in this solvent.

It was postulated by White and Emmons that the strength of maleic peracid in the Baeyer–Villiger oxidation could be attributed to its lower basicity and higher stability of the maleic peracid monoanion intermediate, as the second acid group

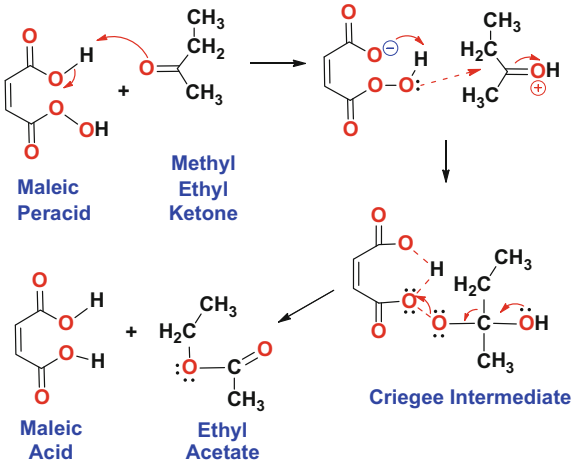

Scheme 2.6 Baeyer–Villiger oxidation of a ketone by maleic peracid in its transition state and conversion from ketone to an ester

protonates the adjoining peroxide oxygen as depicted in Scheme 2.6. This is analogous to the acidity of maleic acid previously described by its resonance structures distributing the anionic charge across both carbonyl groups.

A carbon rearrangement ensues to transfer one of the alkyl groups onto the geminal oxygen atom as an electronic rearrangement completes the ester transformation. When different alkyl groups are attached to the keto-functionality, then the more substituted group proceeds to migrate onto the oxygen atom thereby producing the more substituted ester due to the stabilization of the transition-state intermediate.

2.2.4 Friedel–Crafts Acylation

Over 130 years ago, Von Pechmann can be credited for first observing that in the presence of Lewis acid catalysts like $AlCl_3$, maleic anhydride can be used to acylate aromatic compounds under anhydrous conditions, as outlined in Scheme 2.7 [21]. If an excess of $AlCl_3$ is present, addition of another molecule of aromatic functionality can occur, but this time to the double bond of maleic anhydride to form α-aryl-*β-aroylacrylic* acids. In the case of substituted-benzene derivatives, acylation takes place at the *para*-position to generate *β-aroylacrylic* acids in very good yields, ranging from 70 to 90 % [22, 23]. Furthermore, the *trans*-isomer predominates as the acylation end product instead of the *cis-isomer*.

In many cases, the aromatic reactant is also the solvent that is used in excess to drive the reaction to these 70–90 % yields and that the *trans-isomers* are inclined to be yellow in color, while the minor *cis-isomers* are usually white. However, chlorinated solvents such as 1,2-dichloroethane tend to give the best yields for this type of reaction.

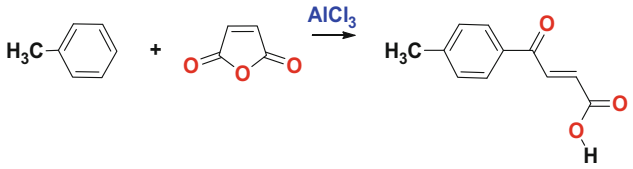

Scheme 2.7 Friedel–Crafts acylation with maleic anhydride

Similarly, modification of pendant side chains of aromatic monomers [24], or of aromatic polymers [25], can be achieved by this approach, and carboxylic acid/salt functionality can be tailored onto the molecule, so that the physical and chemical properties are further enhanced to either reactivity, solubility, or other potential derivatives to specifically design the desired properties onto the resultant polymer. Hence, as summarized in Scheme 2.8, there are at least three ways to incorporate the maleoyl functionality onto a polymer. The first is to simply copolymerize the maleic anhydride into the polymeric backbone with an aromatic comonomer such as styrene (Scheme 2.8a) [24]. A second approach is to synthesize a *β-aroylacrylic* acid monomer and then polymerize it (Scheme 2.8b) [21, 25]. Thirdly, it can hang off as a pendant group on the polymer (Scheme 2.8c) [26]. Therefore, this simple acylation reaction summarized in Scheme 2.8b,c is quite powerful in the versatility of molecules and polymers that can be made.

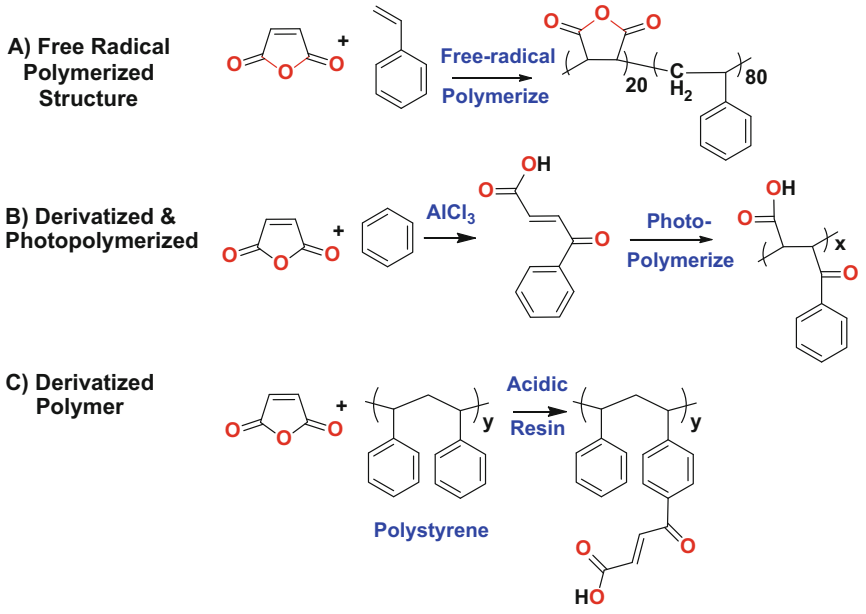

Scheme 2.8 Formation of polymeric derivatives of maleic anhydride by copolymerization (**a**) or by Friedel–Crafts acylation (**b**, **c**) reactions

2.2.5 *Acid Halide Formation*

The formation of monoacid halides from maleic anhydride or from maleic acid is not readily obtained. This is primarily due to the preference of such compounds to regenerate maleic anhydride instead. Treatment of maleic anhydride with reagents

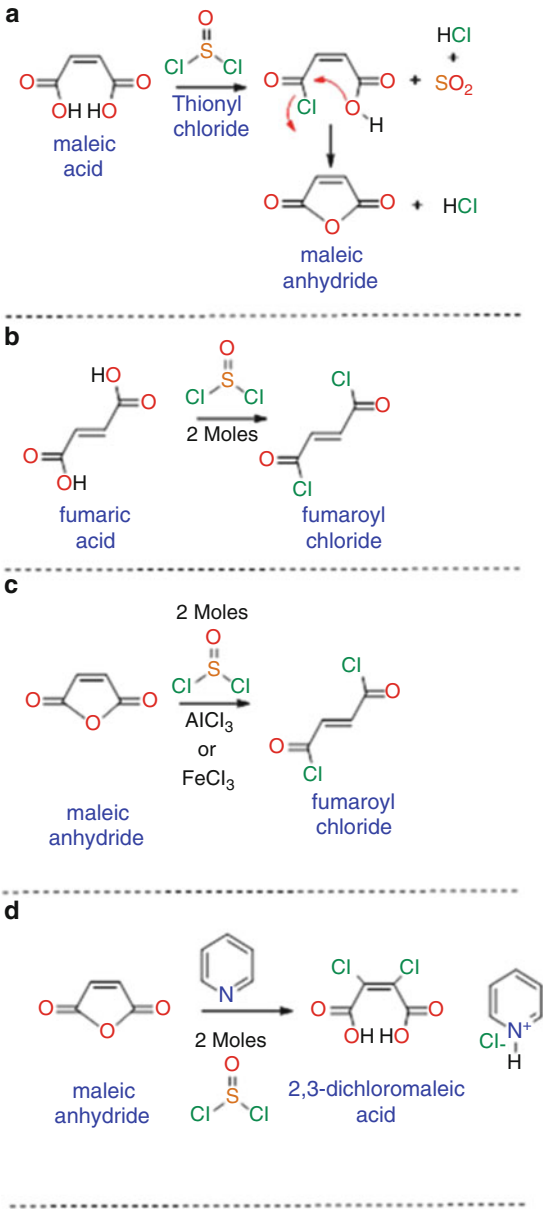

Scheme 2.9 Formation of maleate derivatives from maleic anhydride and acid-chloride reagents

such as phthaloyl chloride, thionyl chloride, or PCl_5 also converts maleic anhydride into a number of different entities depending on the catalyst used in conjunction with these reagents, as outlined in Scheme 2.9. Likewise, acid dichlorides and maleoyl chlorides do not form either, but the acid dichlorides from fumaric acid, fumaroyl chloride, are achievable in high yields.

The reason for the lack of mono- and diacid-chloride formation from maleic acid is quite simple. Once the first acid chloride is formed on the maleic molecule, its neighboring sister acid spontaneously intramolecularly ring-closes to reform maleic anhydride (Scheme 2.9a). This process cannot occur for fumaric acid as it is in the *trans*-configuration, so the carbonyl groups are too far apart to react intramolecularly (Scheme 2.9b). Therefore, fumaroyl dichloride is readily formed upon treatment with thionyl chloride with fumaric acid.

With regard to the actual reaction between maleic anhydride and thionyl chloride, there appear to be some discrepancy and inconsistencies in the literature. For example, Kyrides claimed the synthesis of fumaroyl chloride from maleic anhydride–$SOCl_2$ in the presence of ZnCl and heat [27, 28], while a Union Carbide patent by Brotherton made fumaroyl chloride using $AlCl_3$ or $FeCl_3$ (Scheme 2.9c) [29].

In contrast, Trivedi and Culbertson and others claimed a structure that is highly unstable for maleoyl chloride [1, 3, 30]. US Patent 3,810,913 from General Electric claims the 2,3-dichloromaleic acid is formed in the presence of pyridine catalyst (Scheme 2.9d) [29].

The reaction pathway to the product appears to be dictated by the promoter/catalyst used in conjunction with maleic anhydride–$SOCl_2$ pair. Simply put, maleic acid dichlorides do not readily exist. But fumaroyl chloride can be made from maleic anhydride [27, 30], as well as 2,3-dichloromaleic acid [31], while 2,3-dichloromaleic dichloride can be obtained by thermal decomposition of ethyl perchlorocrotanate [32].

2.2.6 *Alkali Metal Salt Formation, Organic Neutralizer, and Metal Chelation*

Hydrolysis of maleic anhydride followed by neutralization with an alkali metal hydroxide provides the simplest reactions outlined in this chapter, as depicted in Scheme 2.10a. Since maleic acid is a diacid, it can neutralize and complex multivalent metals too, but this can occur both intramolecularly and intermolecularly as shown in Scheme 2.10b,c. Simple hydrolysis and neutralization really is an oversimplification of the true complexity that exists.

Maleic acid itself can also be used to neutralize pharmaceuticals and other basic compounds to increase their stability and solubility in water or blood plasma for

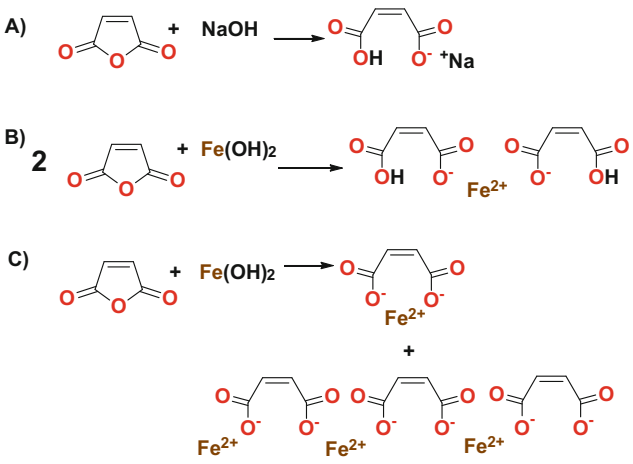

Scheme 2.10 Maleate salt formation by neutralization

gastrointestinal adsorption. Maleic acid can be used for making maleate salts of bulk drugs like pheniramine maleate, fluvoxamine maleate, timolol maleate, chlorpheniramine maleate, enalapril maleate, and others [33]. The monosodium maleate salt can also be used as a buffer in the pH range 5.2–6.8 [34]. Zirconium and other esoteric salts can also be made by entropic factors with the use of ion-exchange resins.

Note that this scheme is a two-dimensional representation. In particular, maleic and fumarate mono- and dibasic salts are very important representatives of the β-dicarboxylic acid class for their complexation or chelating ability to metal ions. When two electron-rich carbonyl groups are conjugated to the electron-deficient double bond, the electron-acceptor character of the olefinic C=C particularly increases [35]. Maleic anhydride has the best acceptor properties among derivatives of the α,β-unsaturated dicarboxylic acids in part due to their ionization potential of their respective pK_as, as previously described in Sect. 2.1.

Stable metal chelates form with maleic salts. This is particularly evident for divalent and multivalent metal ions chelating with the planar mono- and dibasic salts of maleic acid. In doing so, the interaction between the 3D orbital of the metal cation with the anionic maleic carboxylate group is optimized geometrically resulting in stabilization of the ionic salt as a whole. This stabilization is not just a consequence of the local environment around the individual metal atom, but it extends to the whole complex formed as a unit cell in the crystal structure [35].

For example, monobasic maleates with cobalt, iron, zinc, nickel, manganese, and magnesium having the general formula of (mono-metal-maleate)$_2$•tetrahydrate are typical representatives of this group of molecules. In this centrosymmetrical complex, the metal atom is linked to two monodentate maleic molecules, where, for instance, the Fe•••O distance is 2.157 Å and the octahedron structure being completed by the four water molecules, as depicted in Fig. 2.13.

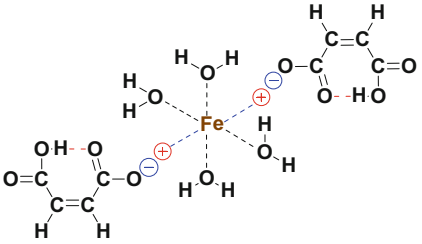

Fig. 2.13 Structure of iron(II)-hydrogen maleate tetrahydrate salt/chelate, where *red dashes* are hydrogen bonds, *black dashes* are columbic attractions, and *blue dashes* are ionic attractions

The planar structure of the maleate ligand in these complexes is further stabilized by an intramolecular hydrogen bond of the maleate carboxyl groups as illustrated in Fig. 2.13. In fact, the Fe-maleate hydrogen bond depicted in red is H ••O = 1.87 Å, while the O•••O distances within the maleate moiety are within the range of 2.39–2.44 Å. The symmetry of these hydrogen bonds presented in Fig. 2.13 can vary significantly, from perfectly symmetrical to completely asymmetric.

In contrast, the dianionic form of maleic can play a dual role in the Fe(III) complex. First, there is an axial ligand binding the metal atom with the monodentate carboxyl group, while the other carboxyl group acts as a counterion, as illustrated in Fig. 2.14. Furthermore, the presence of a broad net of intramolecular columbic forces and ionic attractions occurs around the individual iron atom, in addition to these same interactions bridging neighboring Fe atoms to form the stabilized network structure depicted as the result [36]. The potassium iron(III)-tri-maleate hydrate also has the same overall structure, in addition to hydrogen bonding by water inside the crystal lattice as in Fig. 2.14.

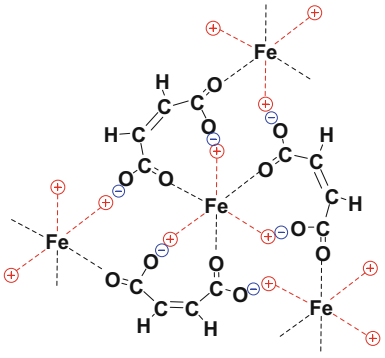

Fig. 2.14 Structure of iron(III)-tri-maleate salt/chelate, where *blue* anions indicate bridging carboxylate group, *black dashes* are columbic attractions, and *red dashes* are ionic attractions

The two maleate salts or chelates just described demonstrate that formation of maleate salts is not as simple as one would expect. There is a higher-order structuring of the metal cation with the maleate anion that forms an anisotropic system both intramolecularly and intermolecularly. These attractive forces form an associative network of columbic and ionic interactions, sometimes further stabilized by hydrogen bonding from water, and as a whole stabilize the overall structure derived.

For iron, an octahedron array is generated, while for copper, a pyramidal–square–planar array is formed, thereby generating a whole host of structural or geometric arrays of interaction between the particular metal cations used and the mono- or dibasic maleate anions that resultantly form these higher ordered structures.

Not only do these polymorphs have different solubilities and melting points, but they are also recognized as different structural entities from an intellectual property point of view.

The polymeric analog for the maleate salts in copolymers of maleic anhydride also exhibits similar interactions and has effect to its physical properties too. While many polymers are amorphous, the incorporation of metallic cations can induce higher-order structuring.

2.2.7 *Esterification*

Reactions involving the reactive anhydride functionality allow for a diverse group of compounds that can be made out of maleic anhydride. Maleic anhydride esterification with alcohols proceeds readily at moderate temperatures, approximately 80–90 °C for 6 h, to generate monoalkyl esters (Scheme 2.11). The acidity of monoalkyl maleate esters are significantly lower than the diacid form of maleic acid as there is no delocalization of the anionic charge across both carbonyl groups, and therefore the pK_a approaches that of typical monoalkyl esters around 5.5.

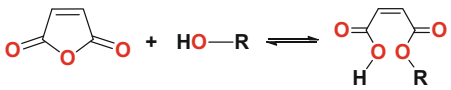

Scheme 2.11 Esterification of maleic anhydride to form monoalkyl esters

As expected, the highest reactivity occurs with primary alcohols, followed by secondary, and lastly tertiary alcohols due largely to steric factors. Note the double-sided arrows in Scheme 2.11, as this is an equilibrium reaction and is reversible depending on the conditions.

Primary alcohols react the quickest at lower temperatures. But they are also the least stable to hydrolysis or transesterification, transforming at temperatures of 20–40 °C over the course of several months. This result is due to the anhydride functionality reforming under acidic condition liberating free alcohol at moderate

temperatures slowly. These processes can proceed over several hours when temperatures are in excess of 80–90 °C.

Alpha-branched alcohols such as 2-ethyl-hexanol, 2-methyl-1-propanol, and *sec*-butanol are slower to react. But they are more stable, inhibiting reformation of anhydride functionality by ring closure. Other secondary alcohols like menthol and cyclohexanol behave similarly.

Esterification by tertiary alcohols is the most difficult and requires even higher temperatures, in excess of 100–120 °C. These reactions are rarely quantitative unless a large excess of alcohol, usually 4–5 stoichiometric equivalents over that of the anhydride. Catalysts are sometimes used to lower the temperature of the esterifications, speed up the rate of the reaction, and improve yields.

A number of catalysts can be used. Acidic catalysts (such as *p*-toluene sulfonic acid, methane-sulfonic acid, or trifluoroacetic acid), inorganic acids like sulfuric or phosphoric acid, and metal catalysts (copper based or tin oxalate or dibutyl-tin) can be used to accelerate this reaction. The most common catalysts are sulfuric and hydrochloric acids, boron trifluoride, organo-tin, zinc salts, and aluminum halides.

In commercial practice *p*-toluene sulfonic acid, or methane-sulfonic acid, is preferred because it tends to be less corrosive to the reactor. Sometimes phosphoric acid is used but this leads to slower reaction rates. Soluble metal salts or their insoluble counterparts minimize side reactions, but require higher temperatures [37–41].

The use of acid-regenerated cation-exchange resins have grown in popularity over the years. They are easily removed by simple filtration and can be regenerated over again [42, 43]. These are typically based on styrene, ethylvinylbenzene, and divinylbenzene copolymers that are sulfonated and cross-linked to provide the macroporous nature of these types of catalysts.

These catalysts provide rapid reaction rates for esterification because of their high surface area of highly acidic sulfonic acid groups [44]. Typical resins such as Amberlite IR-116 and Amberlite IR-120B are used because despite their higher cost compared to inorganic acids, they provide better selectivity and can be used in continuous bed reactors or stir tanks, increasing throughput compared to batch reactors [45–48].

Typically, dialkyl maleate esters can be produced from maleic anhydride with alcohols, such as methanol with sulfuric acid acting as acid catalyst. The reaction proceeds via a nucleophilic acyl substitution to synthesize the monomethyl ester. This is followed by a Fischer esterification reaction for generation of the dimethyl ester. Both reactions are well known.

However, dialkyl maleate esters can also be formed from monoalkyl maleate esters as well. This requires high temperature usually >100 °C. Primarily because one of the two molecules of monoalkyl ester is capable of reverting back into maleic anhydride and free alcohol (Scheme 2.12a) followed by the attack of the second molecule of monoalkyl maleate to form an acyclic anhydride (Scheme 2.12b), then the free alcohol can attack this acyclic mixed anhydride to form the diester and maleic acid, as illustrated in Scheme 2.12c [49].

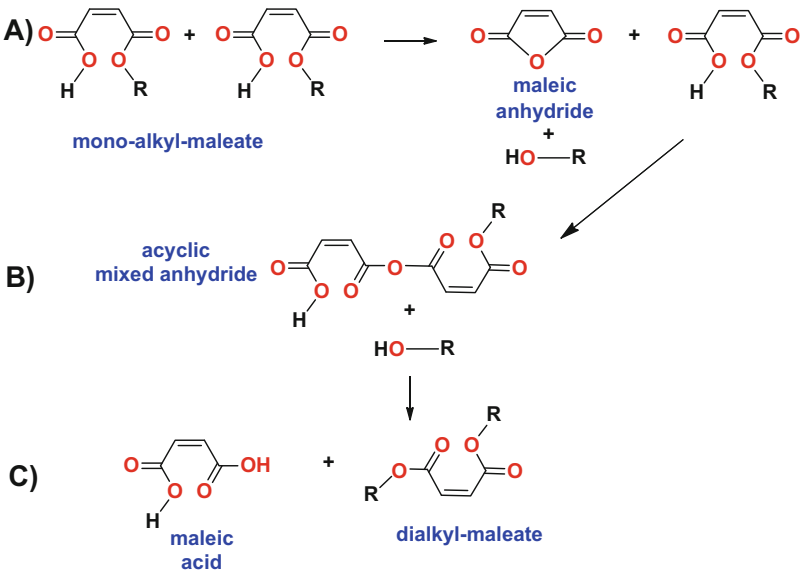

Scheme 2.12 Formation of dialkyl esters of maleic anhydride during esterification reaction or distillation

Care needs to be exercised during distillation or purification procedures of the half esters to prevent such side reactions from occurring. Another side reaction observed at high temperatures is the unwanted isomerization of the maleate into its sister-isomer fumarate. Usually temperatures below 100 °C are employed to prevent this from happening.

The synthesis of diesters utilizing the reaction of carboxylic acids with dialkylcarbonates in the presence of weak Lewis acids such as $MgCl_2$ and optionally with the corresponding alcohol as solvent is depicted in Scheme 2.13 [50]. This approach is effective for more energy-intensive synthetic processes as described in Scheme 2.12.

The mechanism generally thought to arise from a double addition of the carboxylic acid to the alkyldicarboxylate resulting in the formation of a mixed carboxylic/carbonic anhydride and CO_2, as presented in Scheme 2.13. The first step is activation by Mg^{2+} ion with the dialkylcarbonate. In the second step, maleic acid (A) reacts with the activated carbonate to form the mixed anhydride (B), CO_2, and alcohol. In the third step, the released alcohol attacks the mixed anhydride to form monoalkyl maleate (C), CO_2, and another molecule of free alcohol. Fourth, another molecule of activated dicarbonate reacts with the monoalkyl maleate to regenerate the mixed anhydride (D). In the fifth and final step, another molecule of free alcohol reacts with the mixed anhydride (D) to form the dialkyl maleate (E). Esterification of the carboxylic acid with the correct choice of alkyl group on the dialkyl dicarbonate results in esters with only CO_2 as process by-product.

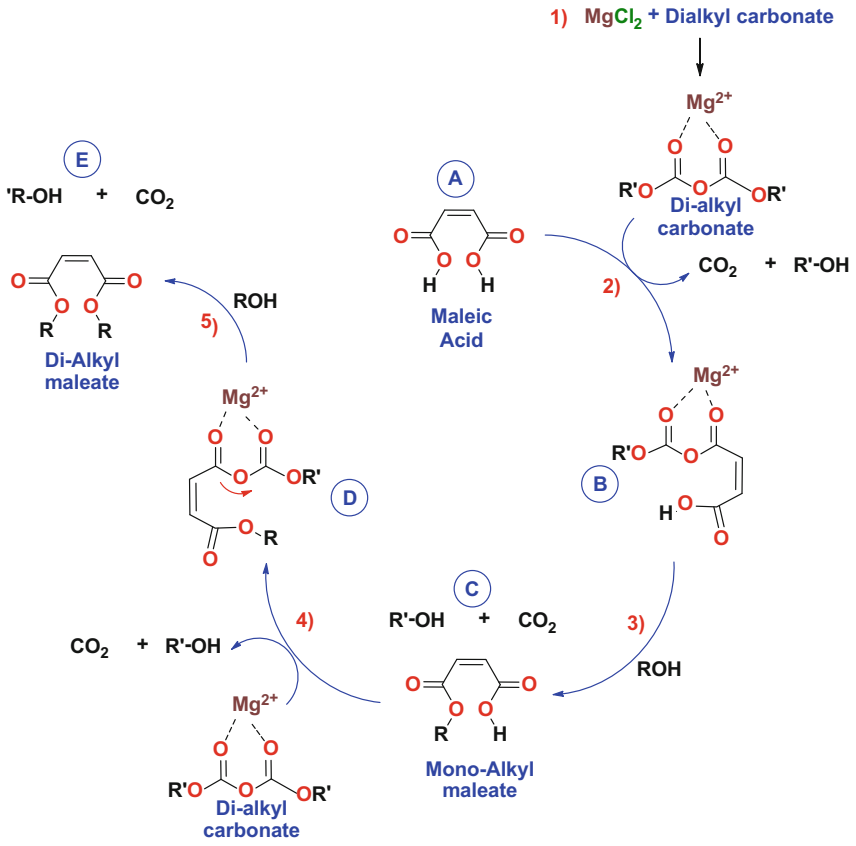

Scheme 2.13 Maleic acid conversion to a diester with dialkyl dicarbonate and $MgCl_2$

The reaction of maleic anhydride with epoxides deserves special mention here and will be discussed in more detail in Chap. 5. These reactions lead to the synthesis of polyesters [51, 52]. In general, the reaction can be carried out at ~45 °C, with little to no side reactions. While ether formation or cross-linking is possible, the majority of product is an alternating polyester of maleic/glycol comonomer units ranging in molecular weight around 15–20 kDa, with a low polydispersity around 1–2 [53]. If a catalytic amount of organic base is added, some of the maleate units can isomerize to a fumarate/maleate polyester. Such isomerizations lead to increasing the T_g by roughly 10 °C. A general reaction scheme is presented in Scheme 2.14.

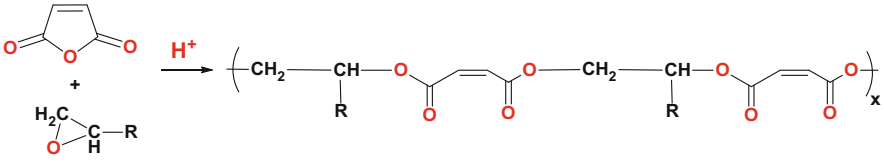

Scheme 2.14 Polyester formation from the reaction of maleic anhydride with epoxides

2.2.8 *Stabilization of Maleate Monoesters*

To increase the stability of newly formed monoalkyl maleate esters, quick neutralization of the half acid immediately after the esterification reaction can inhibit anhydride reformation by ring closure. In this way, the formed alkoxy anion will rapidly reopen the transient anhydride to reform the monoester. This process is depicted in Scheme 2.15. A unique feature of regenerating the anhydride functionality is the *cis*-carbonyl structure of maleic acid and monoesters. This *cis*-configuration only inhibits the anhydride from forming and does not prevent it. Under dilute concentrations in water or another alcohol, hydrolysis or transesterification still proceeds but only at a slower rate.

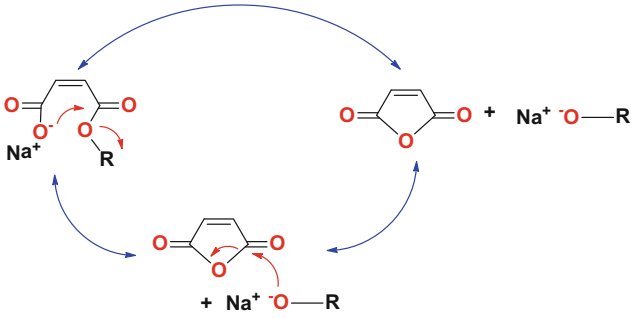

Scheme 2.15 Stabilization of monoalkyl esters of maleic anhydride by neutralization

Esterification reactions can also be achieved indirectly. For example, maleic acid at temperatures in excess of 90–100 °C enables ring closure of the diacid to form the anhydride functionality, which then can proceed to esterification as previously described. However, removal of water is essential for this reaction to achieve any quantitative result.

The use of azeotropes is often employed to remove water during the esterification of maleic acid. With the exception of methanol, many smaller chain-length aliphatic alcohols with chain lengths up to C20 alcohols form binary azeotropes with water. The removal of these higher alcohols drives the equilibrium in favor of the ester product [54]. Under certain conditions, gases are entrained to facilitate the removal of water, like bubbling air into the liquid solutions [55].

Use of desiccants and other chemical means to dehydrate the reaction has also been employed. Typically, these strategies are utilized toward the end of the reaction process to drive it to completion. In one example, the reaction solution is continually pumped through a drying bed of calcium carbide/chloride and then back into the reactor by means of a recirculating loop over the course of the reaction [56, 57].

2.2.9 *Thioester Formation*

The procedures just described for simple esters can also be applied for the synthesis of simple alkyl mono-thioesters from maleic anhydride. Addition of an aliphatic thiol to maleic anhydride proceeds more rapidly than alcohols due to the polarizable electron-rich sulfur moiety. As a result, thio-esterification can occur at much lower temperatures.

However, the reaction mechanisms are much more complicated due to the presence of the activated double bond in the maleate functionality. This activated double bond is very susceptible to nucleophilic reagents, capable of participating in Michael-type reactions. Hence, attack at the anhydride is often accompanied by addition to the double bond as well, resulting in a myriad of side products as illustrated in Scheme 2.16. Nevertheless, given the labile thioester group present in intermediate-A, it is possible to drive the reaction to the thermodynamically stable alkyl-thio-succinate as the major product [58, 59].

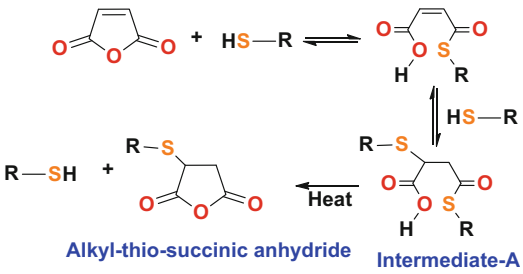

Scheme 2.16 Thioester and S-alkylation formation of maleic anhydride with an alkyl thiol

One special case worth mentioning is the use of mercaptoethanol with maleic anhydride. The kinetic product is the thioester and not the oxy-ester. This thioester is not thermodynamically stable and spontaneously rearranges to the oxy-ester. One can obtain a free thiol esterified by its alcoholic group to the maleic functionality as depicted in Scheme 2.17. But this reaction is not yet completed, as demonstrated by addition of the free thiol to the activated double bond in Scheme 2.17. Allowed to proceed, a poly-(ester-thioether) copolymer is formed, as outlined in Scheme 2.17 [60]. It is noteworthy to note that the offensive stench from these thio-based products has prevented their widespread use.

The esterifications described so far have been under acidic conditions. Basic catalysis is not practical with maleic anhydride or its acid derivatives for a number of reasons. They tend to require more expensive catalysts and their selectivity is not very good. In addition, the presence of the activated double bond makes it very susceptible to nucleophilic reagents. In general, a multitude of by-products is observed with basic catalytic processes.

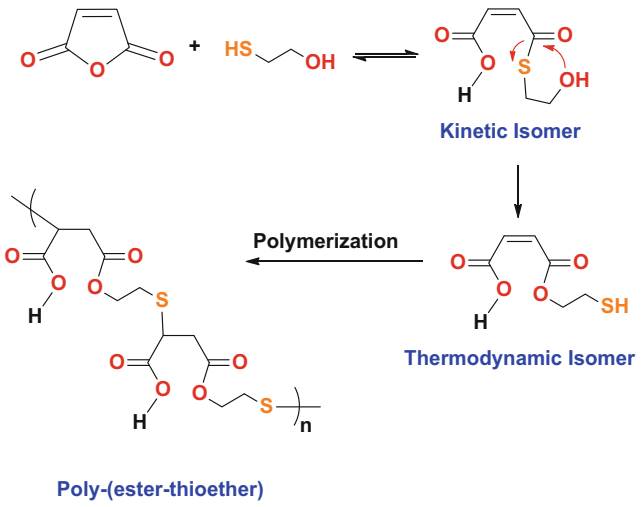

Scheme 2.17 Esterification of maleic anhydride with mercaptoethanol

2.2.10 Amidation Reactions

Addition of ammonia, primary, or secondary amines to maleic anhydride enables the formation of an amide derivatives. These amide compounds are commonly called maleamic acids, or amic acids, or half-amides. If the organic substituent is an aromatic, it is generally referred to as a maleamic acid derivative, as depicted in Scheme 2.18. Because of the presence of the activated double bond in maleic anhydride, addition across the double bond can also take place, via a Michael-type reaction. This reaction pathway lowers the overall yield of amide and generates many side products.

In general, when a Michael addition derivative is wanted, maleic diesters or its salts are used. When the half amide is desired, then maleic anhydride can be used. For this approach, temperature control is critical to the success of this reaction. In particular, if the reaction temperature is maintained at 50 °C for 5 h, 95 % yield of half amide is obtained for both aliphatic and aromatic amines [58, 59]. When temperatures exceed 50 °C, then both Michael additions and half amide formation occur simultaneously.

Hydroxylamine and hydrazine, as well as their organic counterparts such as alkyloxyamines (NH_2OR) and hydrazides, react in a similar fashion with maleic anhydride. The reaction of maleic anhydride with hydrazine is of considerable

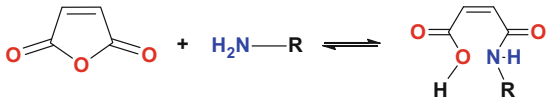

Scheme 2.18 Amidation of maleic anhydride by amines

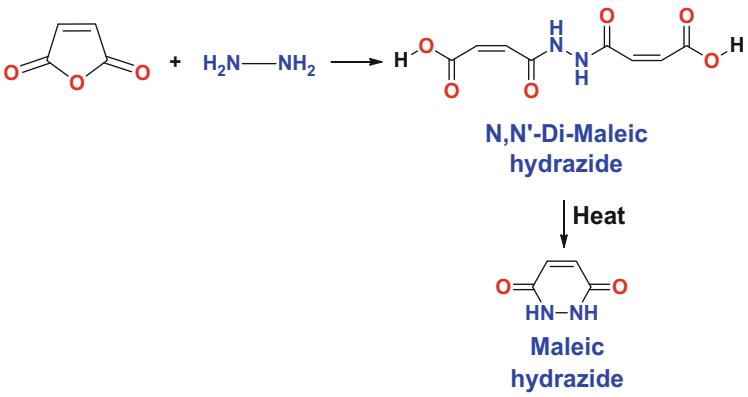

Scheme 2.19 Reaction of maleic anhydride with hydrazine

importance synthetically and commercially. For example, Feuer and coworkers demonstrated that two reactions can occur with hydrazine depending on the conditions employed for the reaction [61]. When maleic anhydride and hydrazine in a 1:1 ratio are dissolved in acetic acid, the mono-hydrazide is not formed. But the *N*, *N*′-dimaleic hydrazide is the major product at 96 % yield. Yet, upon heating this product, it can cyclize upon itself, intramolecularly rearranging to maleic hydrazide in 83 % yield. These processes are depicted in Scheme 2.19.

Interestingly, this reaction occurs only under weakly acidic conditions, such as acetic acid or in refluxing water. Under highly acidic conditions such as in polyphosphoric acid, the cyclization reaction does not readily occur and only the intermolecular *N*,*N*′-dimaleic hydrazide is formed. A similar result is found when the maleic anhydride to hydrazine ratio is 2:1, under highly acidic condition. When a hydrazinium salt such as hydrazine hydrochloride, sulfate, or phosphate is used, then cyclization into the intramolecular hydrazide readily proceeds [62].

2.2.11 Maleimides and Imidation Reactions

Maleimides can be produced by dehydration/cyclization of maleamic acids/esters (Scheme 2.20) [63]. Simple heating of maleamic acid derivatives with concomitant water removal or use of its ester offers the simplest way to produce maleimides. An acid catalyst, such as those employed for esterifications, can also be employed [64]. In particular, maleamic acids can be converted to maleimides with strongly acidic cation-exchange resins, in conjunction with vacuum or azeotropic distillation of the water. Once the reaction is complete, then the acidic resin is simply filtered off [65].

In the absence of a strongly acidic catalyst, the thermal dehydration reaction requires very high temperature, 130 °C or higher. To reduce this temperature,

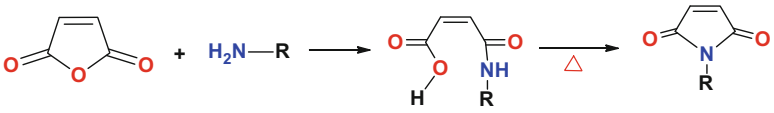

Scheme 2.20 Maleimide formation from maleamic acids by dehydration using high temperature or an acidic catalyst

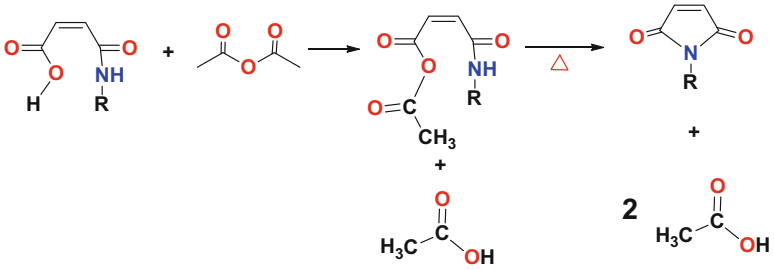

Scheme 2.21 Maleimide formation using a mixed anhydride scheme

100 °C or less, requires removal of water by vacuum or azeotropic distillation and addition of an acidic catalyst. Other catalytic imidation methods include the addition of acetic anhydride with triethylamine to form the mixed anhydride. This approach leads to cyclization and dehydration and is presented in Scheme 2.21 [65]. In the case of very hydrophobic imides, the removal of the ammonium acetate salt can be achieved by washing the biphasic mixture with water and/or recrystallization from hydroalcoholic blends.

Commercial tactics employed often include air sparging during the reaction, or super-heated steam/nitrogen sparge, to facilitate water removal. Vapor-phase reaction of maleic anhydride with anhydrous ammonia over a dehydration catalyst like Al_2O_3, and zeolites, is another commercial approach.

Similarly, bis-maleimide cross-linkers can be produced from di-amines. The length of the spacer between the maleimide units can impart either rigidity or flexibility as in six or more linear methylene groups (this feature has been exploited in the manufacture of liquid-based maleimide precursors that after heat treatment polymerize into a solid adhesive for electronic circuitry boards. Mixtures of metals and the liquid maleimides have also been used to form conductive adhesives between silicon wafers in the manufacture of computer chips too), as outlined in Scheme 2.22 [66, 67].

Another indirect approach to imidation is the reaction of maleic anhydride with urea or alkylurea to obtain the *N*-carbamoylmaleic acid in the presence of acetic acid solvent up to 80 °C, as summarized in Scheme 2.23 [68]. This *N*-carbamoylmaleic acid can be ring closed to form the *N*-carbamoyl-maleimide at 100 °C or at 140 °C upon which thermolysis in DMF produces maleimide, ammonia, and isocyanate by-products, as summarized in Scheme 2.24 [69].

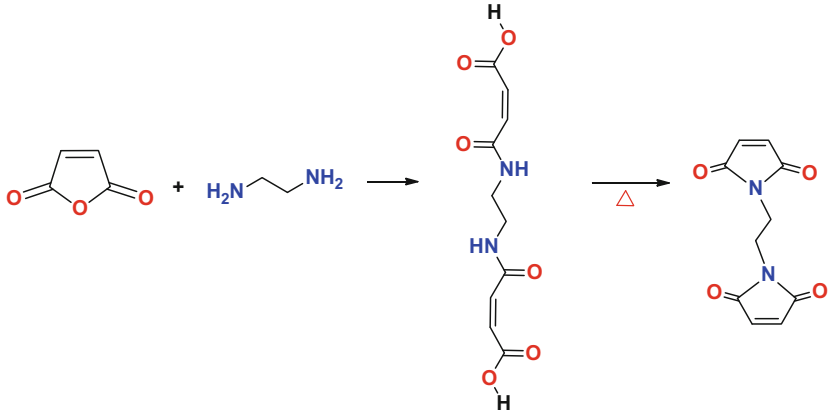

Scheme 2.22 Bis-maleimide formation from maleamic acids by dehydration using high temperature and/or an acidic catalyst

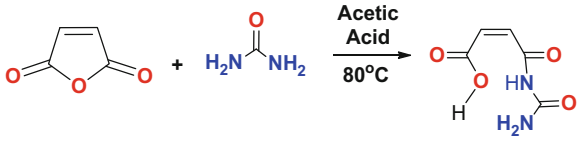

Scheme 2.23 Reaction of maleic anhydride with ureas

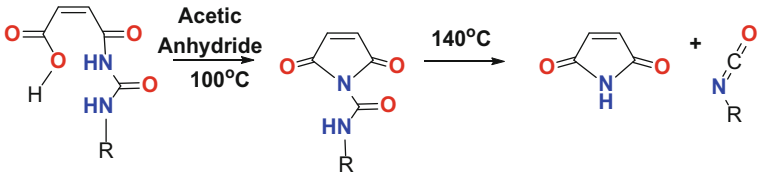

Scheme 2.24 Maleimide formation using thermolysis of the *N*-carbamoyl-maleimide

For temperature-sensitive and/or chiral substituents, activation of the amic acid can be achieved using more sophisticated strategies. For instance, imide formation can be achieved at much lower temperature (25 °C) when using acyl halide formation on the free acid functionality with thionyl halides ($SOCl_2$) or phosphorous halides (PCl_5, PBr_3). Likewise, mixed anhydrides with the use of phosphorous pentoxide, or chloroformates, or carbodiimides can also achieve the same result. However, these reagents are more costly and impractical for most large commercial syntheses.

The synthesis of maleimido-hydrazide can be achieved by the use of a protected-hydrazide like *t*-butoxycarbonyl-hydrazide (Boc-hydrazide) with maleic anhydride followed by thermal dehydration/cyclization. Subsequent deprotection with an acid enables the generation of gaseous CO_2 and isobutylene. This reaction is outlined in Scheme 2.25 [70].

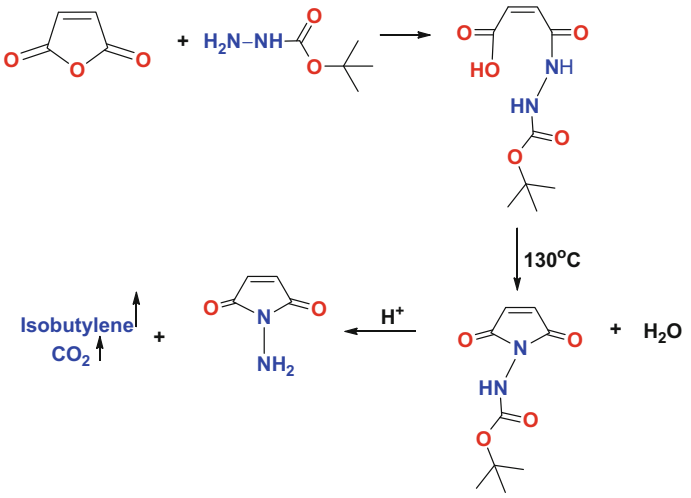

Scheme 2.25 Maleimido-hydrazide formation using thermal dehydration of BOC-hydrazide with maleic anhydride

2.3 Hydrogenation of the Electron-Deficient Double-Bond Functionality

2.3.1 Catalytic Hydrogenation of Maleic into Succinic Derivatives

In principle, hydrogenation of maleic anhydride can be the most direct, environmentally safe, and economical route to manufacture succinic acid. Maleic anhydride is readily available and low price is the result of large production plants in use today. There are several approaches to the hydrogenation of maleic anhydride: catalytic, electrolytic, and transfer hydrogenation.

Maleic or fumaric acids or its salts, as well as their esters, or (thio)esters, amides, and its imides can be reduced to their succinate counterparts [71, 72]. A number of hydrogenation catalysts can accomplish this task. For example, disodium maleate can be reduced with Raney Nickel at 100 °C and 156 bar [73]. After acidification, the yield is nearly quantitative. Milder conditions for hydrogenation are often employed with more expensive metal catalysts like platinum or palladium. These approaches suffer from side reactions to form γ-butyrolactone (BLO) and tetrahydrofuran (THF), as depicted in Scheme 2.26 [74]. In some cases, these side reactions are desired for the production of useful downstream chemicals.

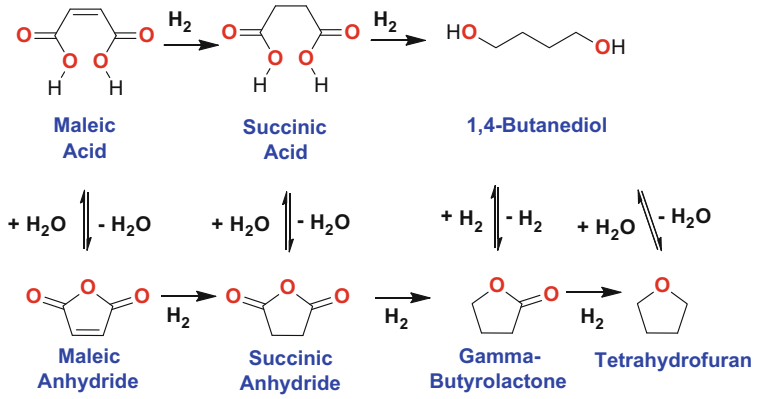

Scheme 2.26 Hydrogenation reactions of maleic anhydride

Maleic anhydride provides a route for many industrially significant chemicals and intermediates: succinic anhydride, 1,4-butanediol, γ-butyrolactone, and THF. The production routes are depicted in Scheme 2.26 [75, 76]. These molecules are produced by both hydrogenation and hydrogenolysis reactions.

There are basically four processes to produce these industrially significant molecules: (1) the Reppe process is based on the condensation of acetylene with formaldehyde; (2) the Davy McKee process is based on hydrogenation of maleate diesters [77]; (3) the Mitsubishi-Kasei process (MKC) is based on diacetoxylation of 1,3-butadiene; (4) and the Arco process is based on isomerization of propylene oxide to allyl alcohol, followed by hydroformylation [78]. Each of these processes has shortcomings. For example, the Reppe process uses explosive acetylene as a starting reagent under rather severe temperature and pressures (140–280 bar, 250–350 °C); hence, specialized knowledge and equipment are required to follow this route [79]. Likewise, the Arco process uses explosive propylene oxide, while the Davy McKee and Mitsubishi processes use costly reagents and precursors.

Maleic anhydride hydrogenation employing different noble metal or copper-based catalysts in either the vapor phase or liquid phase has also been reported [75, 77–83]. Nickel promotes the hydrogenation reaction of maleic toward succinic anhydride, while small amounts of copper are used to prevent the side reaction of maleic anhydride to form γ-butyrolactone. But the catalysts tend to be expensive and are susceptible to deactivation. Typically, the deactivation is a result of homopolymerization of γ-butyrolactone into a viscous poly-butyrolactone polyester that deposits onto the catalyst surface. Metal/clay composites have also been studied like Pd-Al_2O_3, Ni/$(NO_3)_2$, or Ni$(NO_3)_2$ hexahydrate for hydrogenation of maleic anhydride into succinic anhydride. Under the most optimized conditions of 190 °C at 10 bar, it was demonstrated that these nickel-based systems are good alternatives [84].

More recent academic and patent literature explores sol–gel formation to increase the surface area of the different types of catalysts for the hydrogenation of maleic anhydride [85], as well as using different solvents [86, 87]. Various products, including 1,4-butanediol, γ-butyrolactone, THF, and butyric acid, can be obtained, depending on the catalyst choice and reaction conditions employed

[88–92]. In particular, Palladium on carbon can be used for the hydrogenation of maleic anhydride in supercritical carbon dioxide, achieving 97.3 % selectivity for gamma-butyrolactone, or 100 % conversion into maleic anhydride can be achieved at an H_2 pressure of 40 bar and reaction temperature of 100 °C [93].

Newer catalysts have been investigated for hydrogenation of maleic anhydride to succinic anhydride. For example, complete selectivity was achieved when employing $RhCl(PPh_3)_3$, also known as Wilkinson's catalyst, in the liquid phase during maleic anhydride hydrogenation in ethylene glycol dimethylether [85]. In another approach which avoids the high cost of removing the solvent from the reaction mixture, solvent-free hydrogenation of maleic anhydride has been carried out using metallic nickel catalyst [94].

Many catalysts have also been explored in fixed bed reactors. For example, Ni/SiO_2, Co/SiO_2, and Cu/SiO_2 have been used as hydrogenation catalysts with maleic anhydride [95]. However, partial deactivation occurred, primarily due to polymer deposition onto the metallic phase. Nickel–platinum catalysts are commonly employed in maleic anhydride hydrogenation, where a Pt-adjunct has been found to increase the stability of the catalyst. In one example, only a 4 % loss in activity was detected after 120 hours of use [75, 95].

One pathway for catalytic hydrogenation is summarized in Scheme 2.27 as observed for hydrogenation of ethylene. Hydrogen adsorbs onto the surface of metal catalyst followed by formation of an activated metal-hydride intermediate. This process is reversible. The maleic molecule can also adsorb onto the catalyst through π bonding with the catalyst surface. Then in a stepwise fashion, one hydrogen atom is transferred from catalyst to organic acceptor. This is followed by addition of a second hydrogen atom from catalyst to the partially hydrogenated acceptor to complete the hydrogenation reaction.

This sequential addition of hydrogen was invoked to explain the lack of stoichiometry observed when deuterium gas D_2 was used in the hydrogenation reaction of ethylene with Pd. In particular, it was observed that the average reaction product

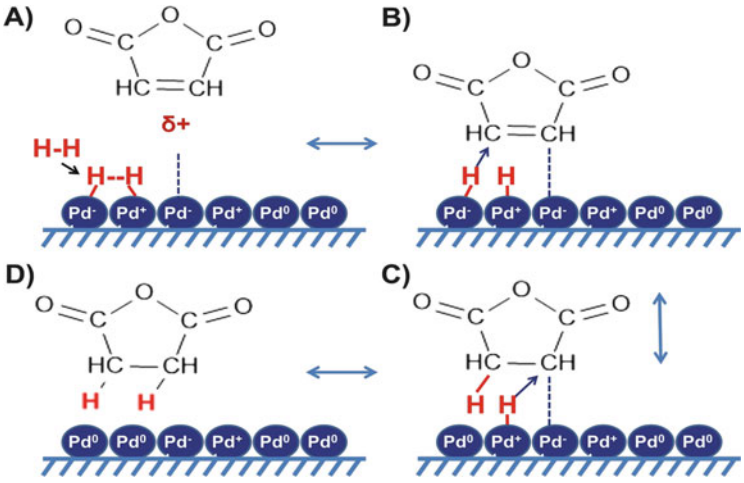

Scheme 2.27 Catalytic hydrogenation mechanism of maleic into succinic (Adapted from [96])

was $C_2H_{2.63}D_{1.37}$ instead of the expected $C_2H_2D_2$ [96]. Therefore, the surface atoms of the catalyst can be in three different oxidation states, with a net change of −1, 0, +1. This partially explains why an electron-rich double bond would adsorb onto an electron-rich catalyst. The net +1 site on the metal exerts a columbic attraction to the electron-rich double bond of the ethylene moiety. Similarly, the electron-deficient double bond of maleic anhydride or its acid can be attracted to the net −1 site of the metal by this columbic attraction, as depicted in Scheme 2.27. Then a shuffling of electrons between the surface metal atoms acts in concert to form the transient organometallic intermediate for hydrogenation to ensue.

2.3.2 *Electrolytic Hydrogenation of Maleic into Succinic Derivatives*

Succinic acid can be also produced by an electrolytic reduction method using maleic acid or maleic anhydride. The production of succinic acid with electrolytic technology had been industrialized since the 1930s. After nearly 85 years of development of this technology, the mature electrolytic synthesis technology continues to accomplish higher and higher conversion ratios, yield, purity, and current efficiency in producing succinic acid. In the meantime, zero discharge of wastewater has been realized by recycling the mother liquor. Electrolytic technology has long been considered as a green chemical synthesis technology.

Electrolytic hydrogenation is another method for the conversion of maleic/fumaric derivatives. These processes generally employ less hazardous protic solvents. For instance, Takahashi and Elving reported that maleic and fumaric behaved identically in this reaction [97]. However, since pyridine (a known isomerization agent to convert maleic acid into fumaric acid) is employed as a catalyst, some have speculated that isomerization of maleic acid into fumaric acid has occurred and then hydrogenation follows to describe this behavior.

The literature presents two primary routes using electrolytic technology of succinic acid production, namely, a membrane technique or a membrane-free approach. At present, the membrane-free method is more widely adopted, as indicated by the number of increasing patent applications from 2006 onward.

As a result, the electrooxidation pathway with oxygen evolution has been adopted as the most preferred anodic reaction for production of succinic acid today [97]. Some manufactures have chosen PbO_2 as the preferred anode material. The disadvantage in this method is the high cell voltage, the short life of PbO_2 anode, and the costly initial investment of the anode. Other than the oxygen evolution reaction, it was also reported that the electrooxidation reaction of glyoxal to glyoxylic acid had been employed as the anodic reaction by one Chinese manufacture of fine chemicals. But the yields of glyoxylic acid and succinic acid were still relatively low.

US patent application 20130134047 A1 (Zhejiang University of Technology) teaches a new technology for the electrolytic synthesis of both succinic acid and sulfuric acid in the redox couple from a waste stream of SO_2 gas in water [98]. The process creates sulfuric acid that can be used as a beneficial chemical reagent.

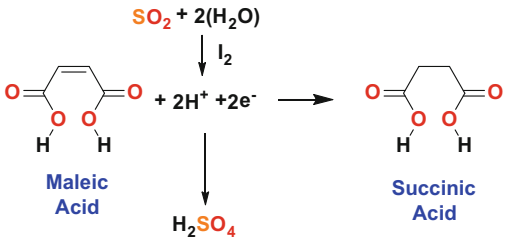

Scheme 2.28 Electrolytic reduction of maleic acid into succinic acid

Remediation of this waste stream while generating a useful reagent is environmentally attractive. Either sulfurous or sulfuric acid formed by oxidation of SO_2 transfers electrons that are mediated through the redox reaction of I_2 (or I_3^-) into the anode-lyte. Iodine (or I_3^-) is generated through the electrooxidation reaction of iodide. Their present invention is a novel technology in producing succinic acid and sulfuric acid at the same time with this paired electrolytic technology.

Maleic acid or maleic anhydride can be used as the raw material for the cathodic reaction. In this process sulfuric acid is the cathodic reactant and the supporting electrolyte of the reaction system. The electrolyte solution in the anode and cathode compartments of the electrochemical cell is separated by a cation-exchange membrane. The resultant reaction on the cathode is described by the following redox reaction presented in Scheme 2.28.

In the anodic compartment, sulfuric acid is produced and iodide ion is regenerated through the redox coupling reaction of I_2 and I_3^-, with sulfur dioxide as the following electrooxidation reactions take place.

$$2I^- \rightarrow I_2 + 2e \text{ (or } 3I^- \rightarrow I_3^- \rightarrow 2e) \tag{2.1}$$

$$I_2 + SO_2\,(\text{gas}) + 2H_2O \rightarrow H_2SO_4 + 2HI \tag{2.2}$$

$$H_2SO_3 + I_2 + H_2O \rightarrow 4H^+ + 2I^- + SO_4^{2-} \tag{2.3}$$

$$I_3^- + SO_2 + 2H_2O \rightarrow 4H^+ + 3I^- + SO_4^{2-} \tag{2.4}$$

In the above anodic reaction, the iodide ion is regenerated through the following chemical redox reaction of I_2 and I_3^- with SO_2 or H_2SO_3, represented by Eqs. (2.1) and (2.2). Concurrently, sulfuric acid is produced. The net reactions can be expressed as follows. In the anodic compartment, sulfur dioxide gas is fed into the anolyte where sulfurous acid is formed through the reaction of SO_2 and water.

Compared with the related technologies, the beneficial results of the this process include (1) reducing the energy consumption of succinic acid electrolytic synthesis significantly by adopting appropriate paired anodic and cathodic reactions; (2) decreasing the initial investment and production cost by using inexpensive anode material, overcoming the problem of short lifetime of anode; (3) providing a new wet technology to produce sulfuric acid at lower temperatures; and (4) increasing

current efficiency, recycling electrolyte, and achieving green production. The technology of this approach is suitable for industrial scale production [98].

After 10 h at constant current density, the electrolysis reaction is stopped, and the catholyte is taken out for post-processing. After posttreatment which includes cooling, crystallization, filtration, rinsing with icy deionized water, and drying, 68.4 g succinic acid is obtained finally. The cathodic current efficiency is calculated to be 95.1 %.

2.3.3 *Transfer Hydrogenation of Maleic into Succinic Derivatives*

Safety in an industrial plant is of paramount importance. The use of explosive hydrogen gas to hydrogenate maleic into succinic derivatives is only employed by specialized and experienced manufacturers. An alternative and safer process to hydrogenate organic molecules is the use of transfer hydrogenation where hydrogen-donor molecules are used instead of H_2 gas, as depicted in Scheme 2.29. Generally, these donors are special solvents which enhance the efficiency of the overall process. Some typical hydrogen donors include hydrazine, cyclohexene or its diene, isopropanol, dihydronaphthalene, dihydroanthracene, and formic acid to name a few. The commercially preferred hydrogen donors tend to be formic acid or its formates, or a combination of formic acid and organic base, hydroquinone, cyclohexene, phosphorus acid, or alcohols like isopropanol [97].

The catalysts can be a solid for heterogeneous catalysis or an organometallic for liquid homogenous catalysis. Recent advances in asymmetric transfer hydrogenation enable stereospecific addition of hydrogen in the reduction step for synthesis of chiral intermediates [99, 100].

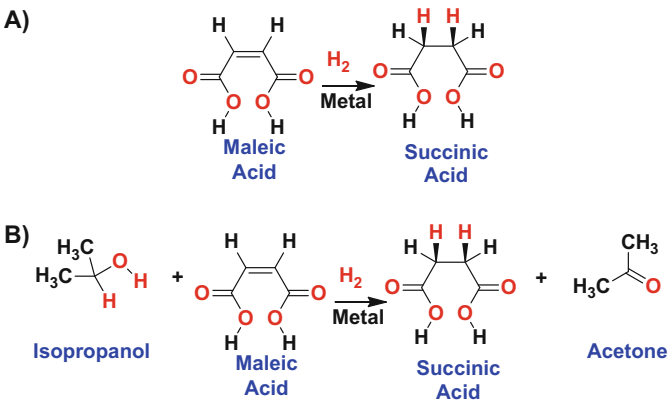

Scheme 2.29 Catalytic hydrogenation (**a**) versus (**b**) transfer hydrogenation of maleic acid into succinic acid

Typically, solid catalysts used include Pd black; Pd/carbon, Pd or Ni on alumina, and Raney nickel. Homogenous organometallic catalysts like Ru, Rh, Ir, and Pt complexes can also be employed. Besides temperature and pressure, other variables affecting hydrogenation rates include mechanical agitation and flow rates. Commercial processes usually use Pd/carbon since only the double bond is reduced with this catalyst. These catalysts do not affect the carbonyl groups. Chemical selectivity should also be considered prior to the reduction step to obtain the desired product.

Catalytic transfer hydrogenation employing platinum group metals (pgms) Ru, Rh, and Ir has been the most successful. While other metal catalysts or organocatalysts have been employed, their rates are generally slower. Most often, the metal-catalyzed transfer hydrogenation reactions are performed in isopropanol, or in an azeotropic mixture of formic acid (HCOOH) and triethylamine (Et_3N) with a molar ratio 2.5:1. This admixture can act as both the solvent and the reductant. Transfer hydrogenation reactions can be carried out in water in a highly efficient manner [101]. The use of water in these processes is environmentally advantageous. These reductions are simple to perform, requiring no ligand modification or organic solvents, and often do not require an inert gas headspace. These processes use one of the most easily available and inexpensive hydrogen sources, sodium formate (HCOONa), thus providing a new viable tool for carbonyl or double-bond reduction.

It should be pointed out that catalytic transfer hydrogenation is not just a regular catalytic hydrogenation where the hydrogen donor replaces H_2 gas as the hydrogen source. But the process is mechanistically different. For example, Pt black and Rh/carbon are very efficient hydrogenation catalysts with H_2. However, they do not work with hydrogen donors under the same set of conditions. Instead, the metal activates the donor for the hydrogen transfer event in a stepwise fashion. This sequential addition of hydrogen was invoked to explain the isomerization of olefinic double bonds from *cis* to *trans* and *trans* to *cis*, as well as the positioning of the double bond via allylic isomerization along the chain during the hydrogenation of oils with Pd. Kinetically, a ternary complex of metal, donor, and acceptor is required for the transfer hydrogenation as the preformed metal hydride is the active species.

2.4 Oxidation Reactions of the Electron-Deficient Double Bond

2.4.1 Epoxidation

Epoxidation of suitable maleate and fumarate derivatives can be performed in a variety of ways. The primary use of maleic epoxidation has been in the production of tartaric acid, where R is hydrogen, as depicted in Scheme 2.30. Since the (*d*,*d*)-isomer is the natural form, routes to produce this isomer in highest yields were sought. Synthetic tartaric acid is mainly the *meso*-(*d*,*l*)-isomer, but sometimes the (*l*,*l*)-isomer is also referenced.

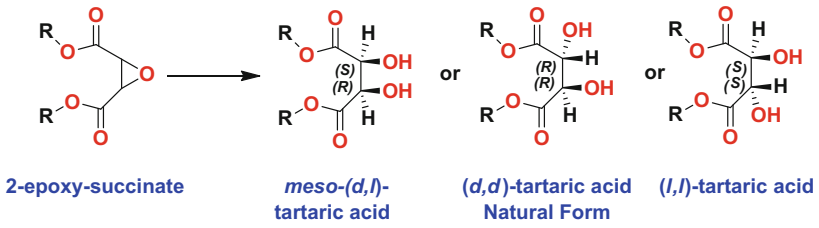

Scheme 2.30 Conversion of 2-epoxysuccinate into tartaric acid

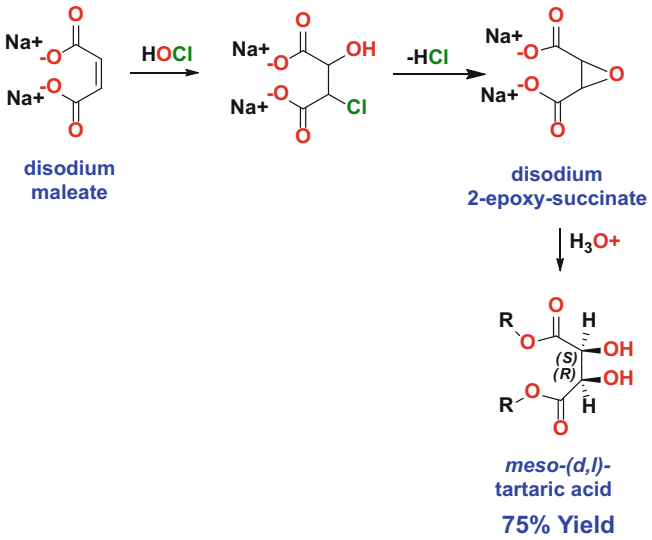

Scheme 2.31 Hypochlorite epoxidation of maleate into *meso*-tartaric acid

Epoxidation of disodium maleate with hypochlorite followed by acidification is one route to this product that has been isolated in 75 % yield, as outlined in Scheme 2.31 [102].

There are many routes to the dihydroxylation of maleates and fumarates into dihydroxy compounds [103]. These include OsO_4-based routes for *cis*-hydroxylation, either directly or with a co-oxidant, such as hydrogen peroxide, or many transition-metal variants. The hazardous nature and high cost of OsO_4-based routes have precluded their widespread use in commercial processes.

Using hydrogen peroxide with catalysts, such as titanium, tungsten, molybdenum, vanadium, and composites with silicates and combinations of these metals, has been used more recently. Modern oxidation methods have been reported with in-depth details [103].

In 1959, Payne and Williams reported the selective epoxidation of crotonic, fumaric, and maleic acids using aqueous hydrogen peroxide with a catalytic amount of sodium tungstate (2 mol%) [104]. The control of pH (4–5.5) was essential in the reaction media. Electron-deficient substrates like maleates, fumarates, and

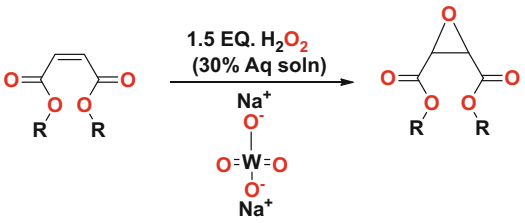

Scheme 2.32 Sodium tungstate epoxidation of maleate

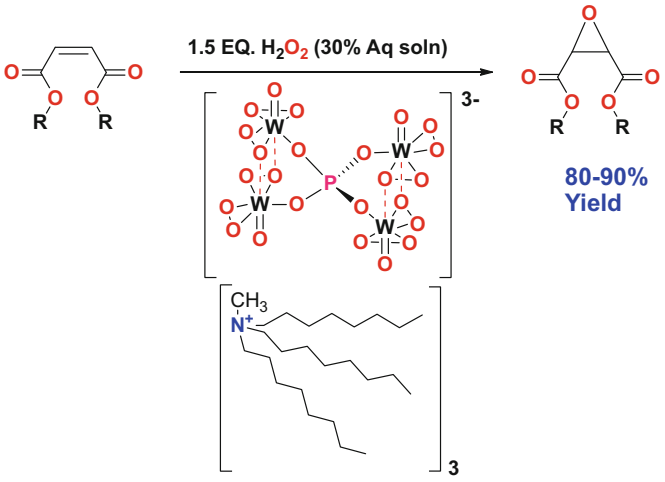

Scheme 2.33 Tungstate complex for epoxidation of maleate

crotonates were difficult to selectively oxidize using common techniques like peroxy acids. Earlier attempts using this combination failed because of rapid hydrolysis of the newly formed epoxide (Scheme 2.32) [103].

Addition of phosphoric acid and quaternary ammonium salts substantially improved the epoxidation of maleates [105]. Active tungstate catalysts are typically produced in situ. Noyori and coworkers reported conditions for the selective epoxidation of aliphatic terminal alkenes employing toluene, or absolutely solvent-free system [106]. One shortcoming with the previous systems was the use of chlorinated solvents. Their approach provided for a *greener* process. In the media, 2 mole% sodium tungstate, aminomethylphosphonic acid, and methyltrioctylammonium bisulfate were used at 90 °C with no solvent, which resulted in high yields directly from the reaction medium. The use of these additives was essential for epoxidation, as presented in Scheme 2.33.

Replacement of aminomethylphosphonic acid with other phosphonic acids, or simply phosphoric acid itself, significantly lowered the conversion. The phase-transfer catalyst trioctyl-methyl-ammonium bisulfate (HSO_4) generated better results than the corresponding chloride or hydroxide salts [105, 106]. The size of the alkyl group on the ammonium quat was found to be important, since C6 or less was inferior to C8 or higher

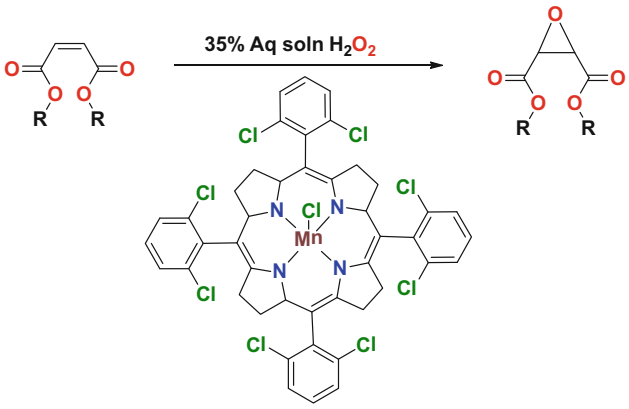

Scheme 2.34 Manganese(III) complex for epoxidation of maleate (Adapted from [108])

chain lengths. This system was further optimized by addition of more aminomethylphosphonic acid and Na_2WO_4 and the pH adjusted closer to 4.2–5.5 [106].

Another highly efficient tungsten-based system for epoxidation was introduced by Mizuno and coworkers who used the tetrabutylammonium salt of a Keggin-type silicon cotungstate $[\gamma\text{-}SiW_{10}O_{34}(H_2O_2)]^{4-}$ that was found to catalyze epoxidation with aqueous hydrogen peroxide with 99 % selectivity and 99 % yield [107]. Furthermore, the catalyst could be recycled at least five times without loss in selectivity or efficiency.

Other catalysts based on manganese complexes with porphyrins have also been used (Scheme 2.34). Co-oxidants that are compatible with manganese include sodium hypochlorite, alkyl peroxides or hydroperoxides (*t*-butylhydroperoxide in *t*-butanol), N-oxides, $KHSO_5$, and molecular O_2. These catalysts can be used in the presence of an electron-donor source [108].

Another effective catalyst system uses rhenium with hydrogen peroxide to form a bis-peroxorhenium complex. This catalyst is intensely yellow in color and has been used to epoxidize olefinic compounds. One preferred type of oxidation catalyst comprises an alkyl trioxorhenium-based material. The size of the alky group can range from 1 to 4 carbons in length that is attached to the rhenium catalyst complex. Methyltrioxorhenium (MTO) has been found to perform the best in these types of oxidations [109]. MTO is a well-known catalyst because of its commercial availability and it stability in air.

MTO reacts with H_2O_2 to generate an equilibrium mixture with the formation of monoperoxo- and diperoxo-rhenium (VII) species, as presented in Scheme 2.35. The diperoxo-rhenium species structure (III) in Scheme 2.35a is the most reactive toward maleic anhydride resulting in epoxidization and hydroxylation by this process (Scheme 2.35b). Notably, the MTO/H_2O_2 system employs nontoxic reagents, the work-up is simple, and water is the only by-product. Moreover, MTO does not decompose H_2O_2, unlike other transition-metal-based catalysts [110].

Generally, the MTO/H_2O_2 system exhibits high acidity and can promote hydrolysis of the epoxidized products to unwanted diol side products. Addition of one or

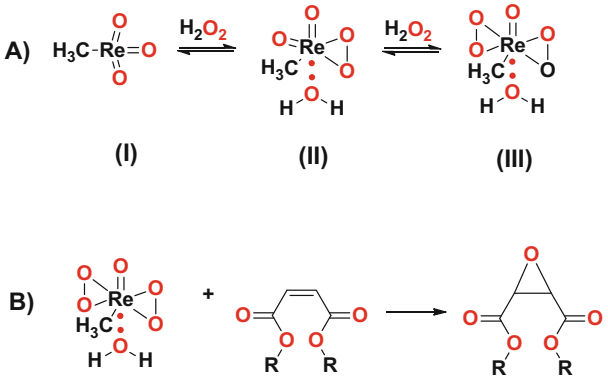

Scheme 2.35 (**a**) Catalyst preparation of rhenium complex. (**b**) Epoxidation of maleate by this catalyst (Adapted from [109])

more basic ligands to the MTO complex reduces the acidity and improves yields. Ammonia, alkyl amines, pyridine, bipyridine, or other pyridine derivatives can all be used as the basic ligand. Typically, the level of hydrogen peroxide oxidant can range from about 1.05 to about 10 moles per equivalent of olefinic double bond, while the catalyst level used ranges from 0.001 to 0.1 mole% [111].

Ruthenium catalysts have also been employed, as depicted in Scheme 2.36. Late transition metals, such as cobalt(II) Schiff bases, have been used with molecular oxygen with reported yields up to 98 %. Additionally, nickel- and platinum(II)-based catalysts have also been used.

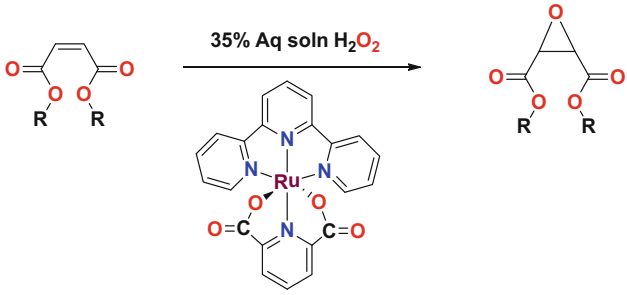

Scheme 2.36 Ruthenium complex for epoxidation of maleate

Other factors that influence the epoxidation process have included solvents to replace methylene chloride. Solubilizing the organometal catalysts in solvents like trifluoroethanol or hexafluoro-isopropanol (HFIP) has been used but requires at least 60 % hydrogen peroxide to be efficient. Additionally, immobilization of catalysts onto a solid support for easier removal and reuse is becoming important. Also Iron salts and complexes as catalysts have also been used. For water-sensitive epoxides, the use of anhydrous hydrogen peroxide as its urea complex has been quite beneficial. Likewise, percarbonate- or persulfate-based derivatives can be used as well.

2.4.2 *Ozonolysis*

Ozonolysis of maleic acid was first reported by Harries in 1903 [112]. Since then, a deeper understanding of this complex chemistry has been revealed, as illustrated in Scheme 2.37. Ozone forms a five-membered tri-oxo ring structure with maleate followed by hemolytic cleavage of the tri-oxo species to generate a diradical species, pathway (A). An internal rearrangement yields glyoxylic acid as one product and the peroxy-glyoxylate diradical

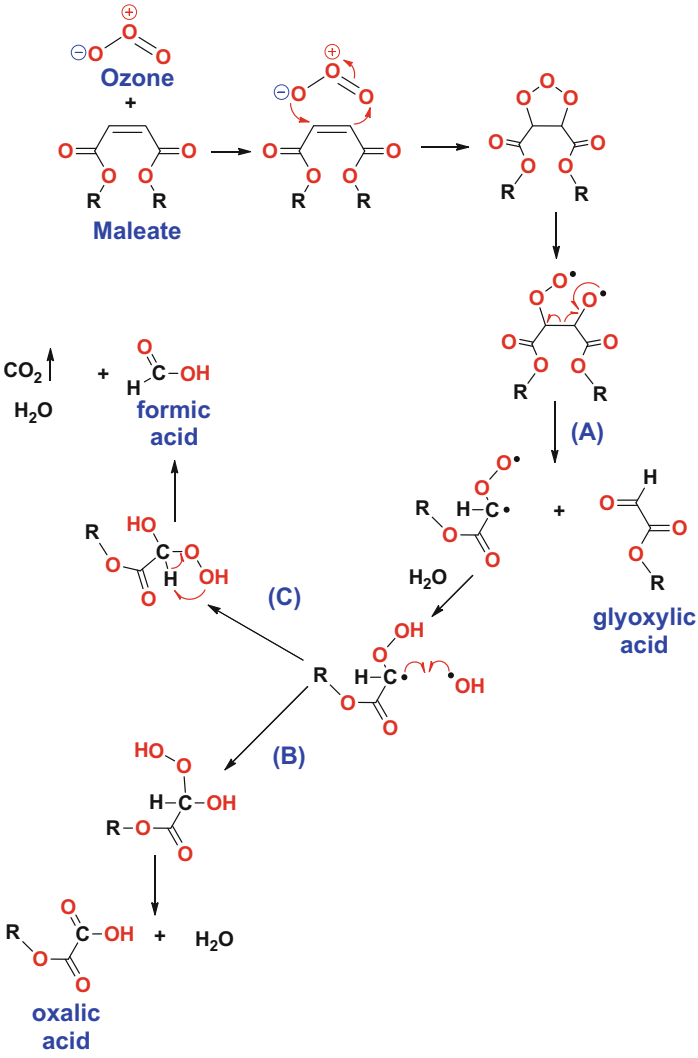

Scheme 2.37 Ozonolysis of maleate

adduct as the other. Attack of this adduct by a hydroxyl radical can yield a variety of products. In one route, the adduct forms oxalic acid and water as depicted in pathway (B), while in the other route formic acid and CO_2 are formed (pathway (C)).

These two routes are not mutually exclusive. Both pathways can proceed concurrently. Only the reaction conditions dictate which predominates over the other.

2.5 Addition Reactions to the Electron-Deficient Double Bond

2.5.1 Hydroformylation Reaction

Besides hydrogen or oxygen addition across the double bond of maleic anhydride, a number of other reactants exhibit utility. For example, diethyl fumarate generated by esterification and isomerization of maleic anhydride can be hydroformylated with carbon monoxide and H_2 gas employing a cobalt catalyst at 150 °C and 300 bar with a reported yield of 51 % [113]. Better yields were obtained by Umemura and Ikada using lower temperatures and pressures 70–120 °C at 115 bar or 25 °C at 150 bar in the presence of a 1:1 ratio of CO: H_2 using dimethyl maleate generating 83 % yield of formyl product and 17 % dimethylsuccinate, as depicted in Scheme 2.38 [114].

Other catalysts including rhodium with aryl phosphine or aryl phosphite ligands (e.g., $HRh(CO)(PPh_3)_3$) have been proposed as the active species in the hydroformylation reaction to generate aldehydic derivatives. The conditions can be exploited for whole range of olefin conversion into aldehydes as well, operating at 70–100 °C and 35 bar, with less than 5 % hydrogenation by-products [113, 114].

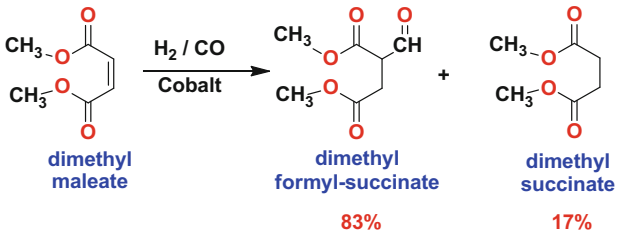

Scheme 2.38 Hydroformylation of dimethyl maleate

2.5.2 Addition of Water for Conversion of Maleic into Malic Compounds

Conversion of aqueous solutions of maleic acid into malic acid is achieved by contacting with a steam sparge under pressure. Optionally, partially neutralized maleic sodium salts up to 50 mole% can be used to enhance hydration. This process is summarized in Scheme 2.39 and proceeds through a fumaric acid intermediate [113]. Note that (*l*)-malic acid is the naturally occurring form while this process yields a racemic mixture.

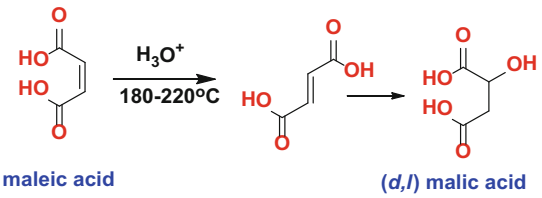

Scheme 2.39 Conversion of maleic acid into malic acid

Another route to convert maleic acid into (*l*)-malic acid is the use of biological enzymes and/or bacteria. For instance, when the enzyme fumarase is added to an aqueous solution of calcium fumarate and the enzyme acts on water-dissolved fumarate converting a portion to calcium malate. Due to the lower solubility of the malate, it crystallizes and precipitates out from the system before the reaction has reached chemical equilibrium.

This precipitation process enables the continuous production of calcium malate. In a typical hydration reaction, maleic acid is hydrated in the presence of various catalysts including sulfuric acid. Aluminum and chromium hydroxide catalysts have been found to increase yields of malic acid in the aqueous hydration of maleic acid. Smaller amounts of fumaric acid were also found in the hydration product [114].

2.5.3 Addition of Halo Acids for Conversion of Maleic into Halosuccinate Compounds

Halosuccinic acid can be directly prepared by addition of HBr or HCl with maleic anhydride, or its diacid under anhydrous conditions. These processes have not found much commercial use. Similarly, fumaric acid in the presence of acetic acid saturated with HCl or HBr will also form the halosuccinate derivatives, as outlined in Scheme 2.40. Other routes are also known.

For example, chlorosuccinic acid can be obtained through the reaction of malic acid and phosphorous pentachloride at room temperature [115]. Chlorosuccinic acid can also be derived from malic acid with thionyl chloride, as well as through

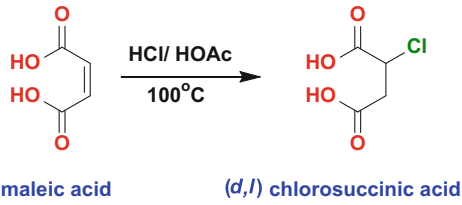

Scheme 2.40 Conversion of maleic acid into a halosuccinic acid

the addition of hydrogen chloride to maleic acid in acetic acid at 100 °C [116]. Additionally, chlorosuccinic acid can be obtained by reduction of 2-chlorobutenedioic acid with chromium powder in perchloric acid at 25 °C [117] and from the reaction of chloroacetic acid with lithium diisopropylamide at −80 °C and then heating to 50 °C [118]. Similar reactions are expected from similar brominated derivatives, such as thionyl bromide, etc.

To achieve a stereoselective form of one enantiomer of chlorosuccinic acid, such as (S)-chlorosuccinic acid, the use of thionyl chloride with (S)-malic acid should be used for retention of configuration. To produce (R)-chlorosuccinic acid, the use of thionyl chloride with pyridine, a weak nucleophile, would be employed. Likewise, the R-isomer can be produced from (S)-malic acid using PCl_5, for inversion of configuration as presented in Scheme 2.41.

The mechanism by which inversion of configuration is obtained was first elucidated by Paul Walden in 1896 and was dubbed the Walden Inversion. It proceeds by an S_N2 reaction mechanism when using PCl_5 resulting in inversion of configuration, as outlined in Scheme 2.42. In contrast, the use of thionyl chloride proceeds via an S_N1 mechanism with retention of configuration.

Assuming complete conversion of malic acid into its cyclic anhydride form (Scheme 2.42 panel b). The alcohol of the malic anhydride in panel b attacks the PCl_5 to form the activated intermediate shown in panel c, and the chloride anion then attacks the opposing face of the molecule forming the chlorosuccinic compound, panel d, resulting in inversion of configuration from the (S)-enantiomer into the (R)-enantiomer. Meanwhile, rearrangement of the protonated phosphorous oxychloride, panel d, occurs to form HCl and $O{=}PCl_3$, panel d. In the last step, water opens the anhydride to generate the (−) R-chlorosuccinic acid molecule (Scheme 2.42-panel e).

Walden proposed that retention of configuration can result from a double inversion. For instance, an *l*-isomer is converted to a *d*-isomer that is an intermediate in the reaction, and then the *d*-isomer is converted back into its *l*-isomer by a second reaction as the final product.

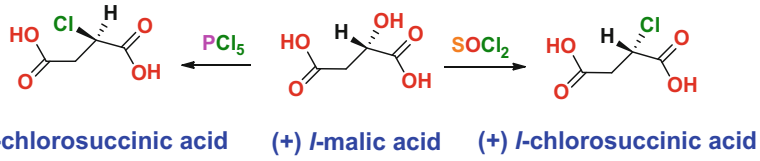

Scheme 2.41 Conversion of malic acid into a halosuccinic acid

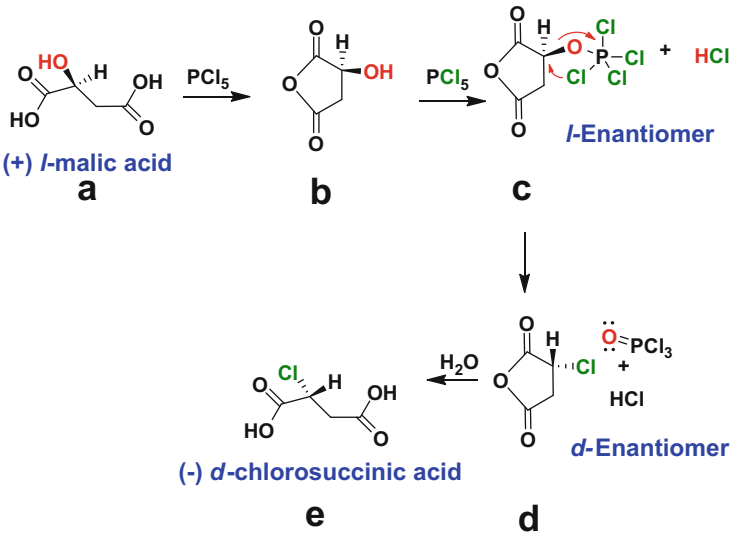

Scheme 2.42 Inversion of configuration by S_N2 displacement by PCl_5 chloride ion converting malic acid into (−) R-chlorosuccinic acid

His hypothesis is correct for the reaction of silver hydroxide with R-chlorosuccinic as the second reaction, converting it back to S-malic acid. Remember, S-malic acid was the starting reagent for the synthesis of R-chlorosuccinic acid as the first reaction/intermediate. However, not all reactions proceed with inversion of configuration; one such example is the reaction of S-malic acid with thionyl chloride that proceeds with retention of configuration, as illustrated in Scheme 2.43.

Again, assuming complete conversion of malic acid into its cyclic anhydride form as the first step (Scheme 2.43-panel b). The alcohol of malic anhydride attacks thionyl chloride to form the protonated chlorosulfite intermediate (panel c). Electronic rearrangement ensues to release hydrogen chloride (panel d). There is some debate as to the intermediate formed proceeding from panel d to panel f.

Some assert that a formal charge is formed on the chlorosulfite moiety as depicted in panel e, to form an "intimate ion pair" with the carbon cation malic intermediate. Others assert that a concerted reaction ensues in which that as the carbocation is forming on the malic intermediate, while simultaneously the chloride anion is forming a bond with this cation center, resulting in an exchange reaction of oxygen for chloride in only one step. In either case, the observed product is S-chlorosuccinic acid (Scheme 2.43-panel g).

In summary, three reactions have been discussed to illustrate the capability of various reactions to retain or invert configuration of chlorosuccinic acid. These compounds are usually intermediates for further reactions, requiring a high degree of stereospecificity.

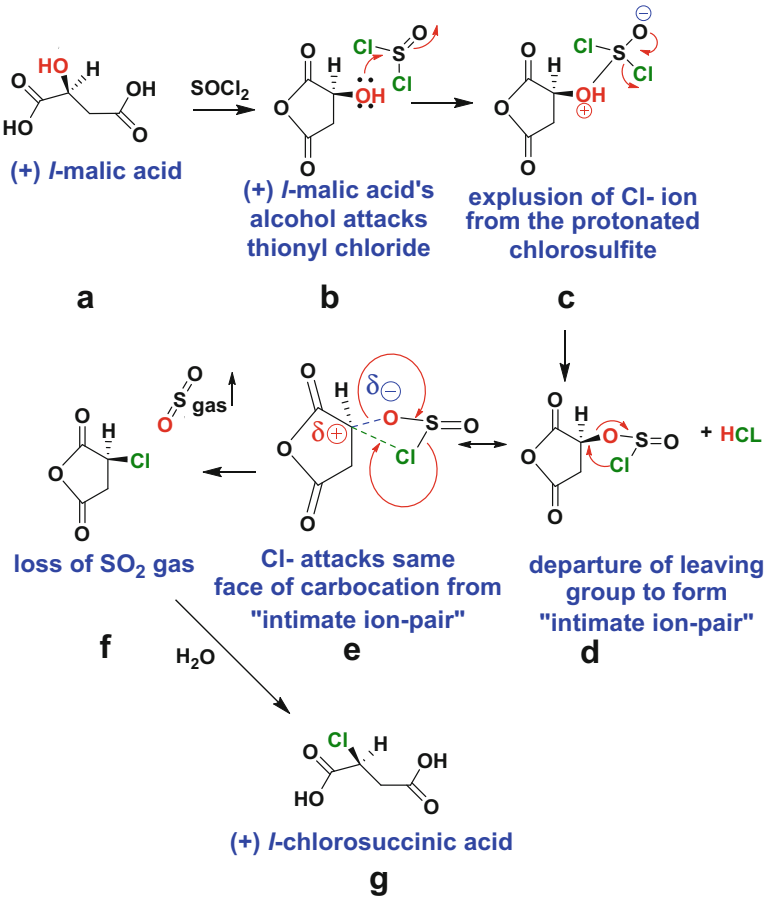

Scheme 2.43 Retention of configuration by S_N1 reaction mechanism using thionyl chloride converting malic acid into (+)*l*−chlorosuccinic acid

2.5.4 *Addition of Halogens for Conversion of Maleic into Dihalosuccinate Compounds*

The addition of halogens directly to maleic anhydride forming dihalosuccinic anhydrides is another important chemical reaction. Chlorination of molten maleic anhydride yields α,β-dichlorosuccinic anhydride that can be subsequently hydrolyzed in water to form the dichlorosuccinic acid molecule, as outlined in Scheme 2.44 [119].

When maleic anhydride in water or its corresponding diacid is used, then a pair of diastereomers is produced, (*d*,*d*) and (*l*,*l*)-dichlorosuccinic acid (Scheme 2.44-panel a). Fumaric acid can be chlorinated but generates only one diastereomer, specifically (*d*,l)-dichlorosuccinic acid (panel b). The reaction is an anti-addition for both fumaric and maleate. The *trans*-configuration of fumarate along with *trans*-

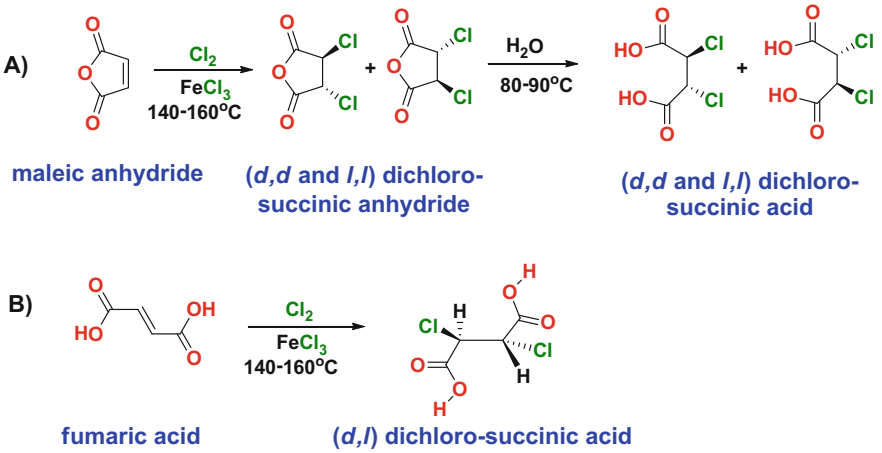

Scheme 2.44 (**a**) Chlorination of maleic anhydride to form (*dd* and *l*,*l*)-dichloro-succinic anhydride or its diacid form, (**b**) while chlorination of fumaric acid generates (*d*,*l*)-dichloro-succinic acid

addition gives the net result of a syn-addition product, more properly named as the *meso*-isomer, as depicted in Scheme 2.44-panel b.

Maleic and fumarate can be brominated as well. Both maleic and fumarate preferentially form the *meso*-isomer as the major product at lower temperature ≈ −5 °C. In contrast, at 65 °C, only 46 % of the maleic product is in its *meso*-form [119]. The *meso*-isomer is the thermodynamically more stable form of this dibromo-derivative.

Mechanistically, the *trans*-addition of bromine to the fumarate electron-deficient double bond is straightforward, like that of chlorination of fumarate in Scheme 2.45-panel b. Unexpectedly, bromination of maleic generates the same product too, especially, given the results from the chlorination of maleic depicted in Scheme 2.45-panel a.

Isomerization of the double bond for maleic acid must occur during the bromine addition reaction onto maleic acid. It has been observed that increasing the level of bromide anion in the medium from 0.2 M to 4.0 M results in an increase in *meso*-isomer from 32 % to 73 %, respectively. Bromide and bromine, at lower temperatures, are known to isomerize double bonds. But the real driving force for this result is the large van der Waals radius of the bromine atom. In the meso-configuration(*d*, *l*), the bromine atoms are farther apart, residing on opposite faces of the molecule. In contrast, the (*d*,*d*)- and (*l*,*l*)-isomers can only assume a gauche orientation to prevent overlap of functional groups present. Therefore, these isomers have their bromine atoms in close spatial proximity to each other, thereby increasing the overall energy of the molecule due to electronic repulsion of the electron cloud surrounding both bromine atoms.

Molecular modeling results support this conclusion, that the meso-isomer is more thermodynamically stable. In this configuration, the two bromine atoms

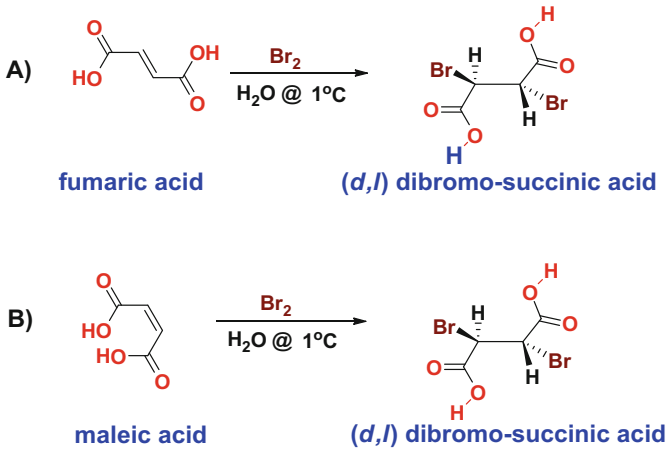

Scheme 2.45 (**a**) Bromination of fumaric acid *to meso*-(*d*,*l*)-dibromo-succinic diacid, (**b**) while bromination of maleic acid mainly generates *meso*-(*d*,*l*)-dibromo-succinic diacid too

(brown) can adopt an anti-configuration (Fig. 2.15a), while the (*d*,*d or l*,*l*)-dibromo-succinic acid isomers can only adopt a gauche orientation as their lowest energy state (Fig. 2.15c).

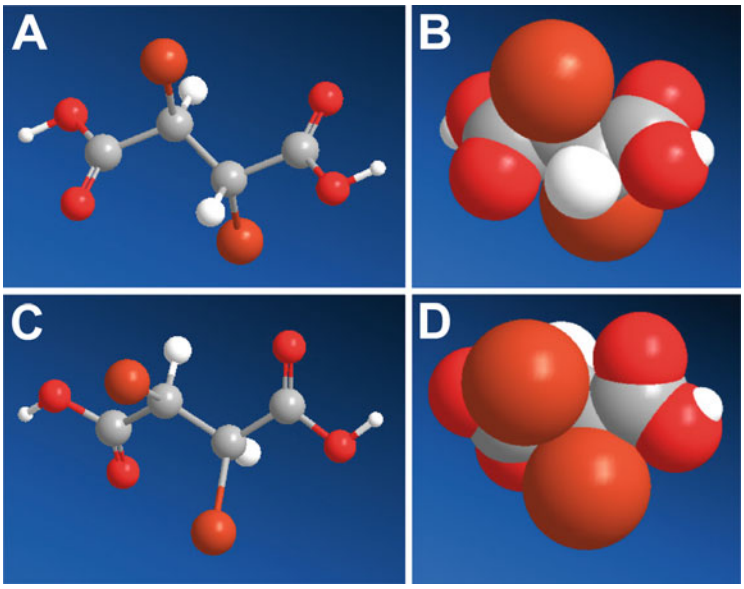

Fig. 2.15 (**a**) *meso*-(*d*,*l*)-dibromo-succinic acid in anti-configuration, (**b**) space-filling model of meso-isomer versus (**c**) (*d*,*d or l*,*l*)-dibromo-succinic acid in gauche configuration, (**d**) space-filling model of (*d*,*d*)-isomer

This is even more apparent in the space-filling models, where the (*d*,*d*)-isomer exhibits more steric clutter between the bromine atoms in the gauche conformation (Fig. 2.15d), compared to the meso-isomer in the anti-orientation (Fig. 2.15b). The energy difference between these two conformers are 12 Kcal/Mole versus 15 Kcal/Mole for the *meso*-(*d*,*l*)-dibromo-succinic acid versus the (*d*,*d or l*,*l*)-dibromo-succinic acid isomers, respectively.

2.5.5 *Michael Additions to the Electron-Deficient Double Bond*

Dialkyl maleates and fumarates, as well as their monoalkyl salts, or any nonacidic form of maleates and fumarates can participate in Michael addition reactions due to the electrophilic character of the conjugated double bond. Resonance structures can be drawn that tacitly indicate the *beta*-carbon exhibits partial positive character, meaning that the *beta*-carbon also has the potential to be an electrophilic target (Scheme 2.46-panels a and c).

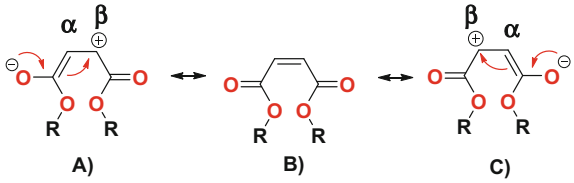

Scheme 2.46 Maleate behaves as a Michael acceptor due to electrophilic character at the β-position

It was demonstrated that the structure of the activated *ene* such as the maleic double bond is crucial to the degree of activation [120, 121]. Inorganic catalysts have also been used to further activate the *ene* in this reaction. For example, Lewis acids such as $ZnCl_2$, ZnI_2, and $AlCl_3$ have been used as catalysts in Michael additions [122].

Nucleophilic (Nu) attack at the *beta*-carbon of the activated *ene* results in formation of an enol or enolate intermediate (Scheme 2.47-panels a or c). Usually, this intermediate collapses and the alpha-carbon is protonated (Scheme 2.46-panel d). This type of reaction is known as a "conjugate addition" or a "Michael addition."

Maleic and fumaric are well-known Michael acceptors and react with a variety of nucleophilic Michael donors, or inorganic nucleophiles. Regardless if the nucleophile is a Michael donor or not, the addition reaction is stabilized through an enolate-transition state, and protonation by solvent or directly with acid completes the reaction, as outlined in Scheme 2.47.

The reverse of a Michael addition can occur and is called a *beta-e*limination. This is often referred to as an "E1cb" mechanism. The E stands for "elimination"; the numeral 1 refers to the fact that, like the S_N1 mechanism, it is a stepwise

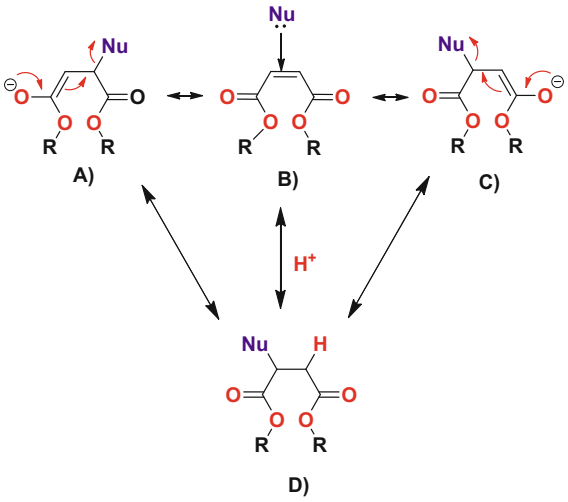

Scheme 2.47 Michael addition of nucleophile (Nu) with dialkyl maleate, salt

reaction with first-order kinetics. The "cb" designation refers to the intermediate, which is the *c*onjugate *b*ase of the starting compound, as depicted in Scheme 2.48.

Because both Michael additions and *beta*-elimination or E1cb reactions proceed through a resonance-stabilized carbanion intermediate, it is essential that a carbonyl group be located in an appropriate position. This requirement is evident in the *beta*-elimination below to stabilize the carbanion intermediate (Scheme 2.48b–c).

Both Michael additions and *beta*-elimination are intimately related to one another. The reaction product is really dictated by the reaction conditions employed. Generally, Michael additions are performed at lower temperature in neutral to mildly basic conditions. *Beta*-eliminations are usually performed at higher temperature under highly basic conditions. Case in point, in 1948 Kloetzel reported that the nature of the reaction product of 2-nitropropane with diethyl fumarate depends on the level of diethylamine employed [123].

In particular, when using a catalytic amount of 0.2 mole of diethylamine, the simple Michael addition product is obtained in 90 % yield (Scheme 2.49 pathway A). However, when 1.25 equivalent of diethylamine is used, then a *beta*-elimination of the nitro-group occurs with 83 % yield (Scheme 2.49 pathway B). This reaction has been revisited by Ballini and coworkers in 2002 using dimethyl maleate to generate (E)-3-alkylidene succinic anhydrides and 3-alkyl succinic anhydrides [124].

Not all *beta*-elimination reactions generate a retro-Michael addition product of the starting reagents. It is possible that a Michael addition followed by a b*eta*-elimination can generate a whole new entity, as outlined in Scheme 2.49 pathway B.

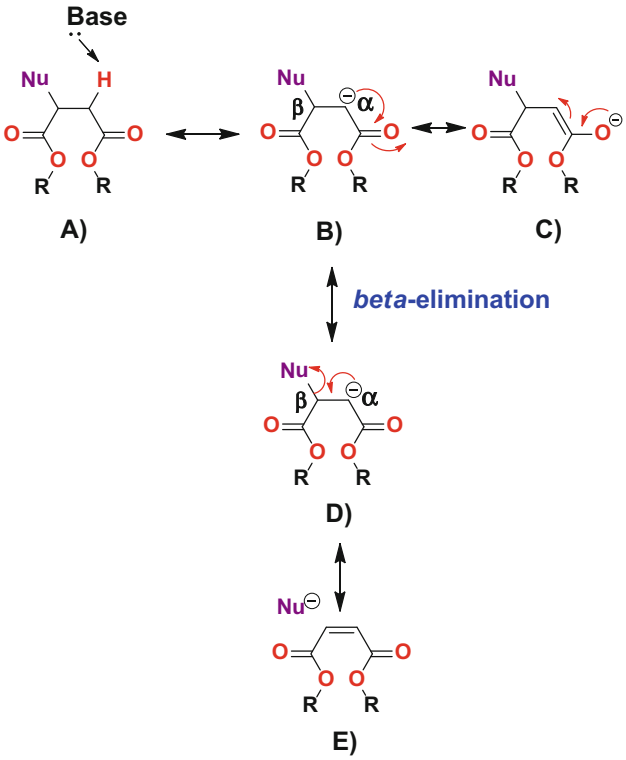

Scheme 2.48 *Beta*-elimination or E1cb of nucleophile (Nu) with dialkyl maleate salt

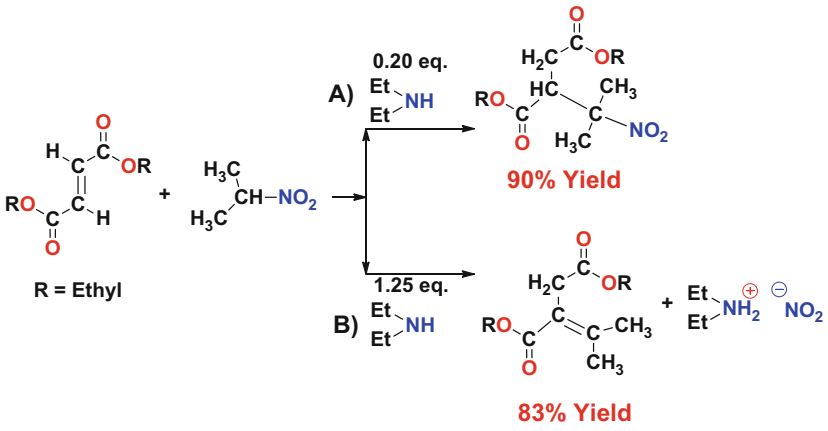

Scheme 2.49 Michael addition of diethyl fumarate with 2-nitropropane using (**a**) 0.20 eq diethyl amine versus (**b**) using 1.25 eq diethyl amine followed by *beta*-elimination reaction

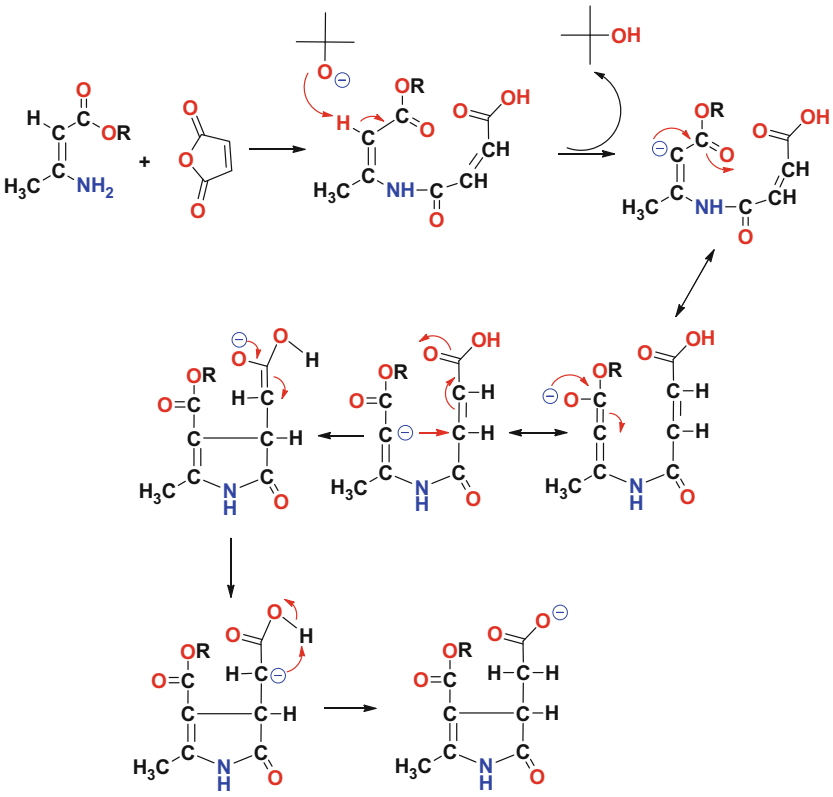

Scheme 2.50 Cyclization of β-aminocrotonic ester with maleic anhydride

In some cases, an internal Michael reaction can occur and cause ring closure similar to the Robinson annulation. For instance, Szilagyi and Wamhoff reported the cyclization of β-aminocrotonic ester with maleic anhydride to form a highly substituted unsaturated pyrrolidone derivative, as depicted in Scheme 2.50 [125].

Another interesting reaction is the oligomerization of maleates and fumarates to form polycarboxylic esters using malonic or acetoacetate enolates as the polymerization initiator. Hence, the first step of the reaction is the Michael addition to maleate/fumarate, followed by anionic homopolymerization of maleate and/or fumarate diesters [126]. The resultant structures for these homopolymers are depicted in Scheme 2.51.

The remainder of this chapter will focus on the addition reactions to the activated and electron-deficient double bond of maleate and fumarate. But one should keep in mind that retro-reactions and *beta*-elimination reactions are also possible.

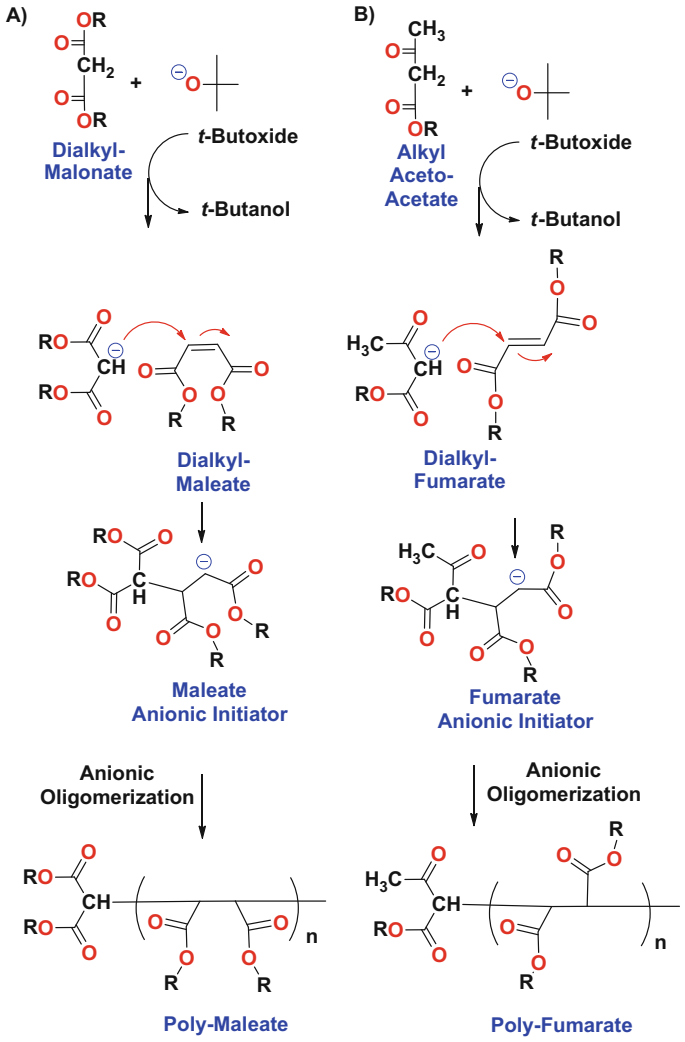

Scheme 2.51 Poly-maleate or poly-fumarate initiated by malonic or acetoacetate enolates

2.5.6 Sulfonation and Thiol Additions

The base-catalyzed thiol addition to the polarized double bond of maleic anhydride has been well known since the early 1960s [54, 127]. These processes are known as thiol–ene reactions. Thiol–ene reactions proceed through a thiolate anion addition mechanism, where the dielectric of the solvent indirectly plays a role in thiol dissociation, followed by a Michael addition of the thiolate anion onto maleic anhydride. These mechanisms are presented in Scheme 2.52.

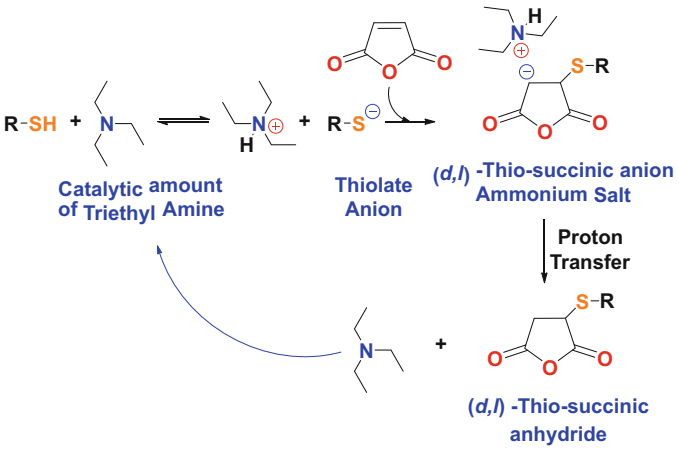

Scheme 2.52 The thiol–ene reaction with maleic anhydride

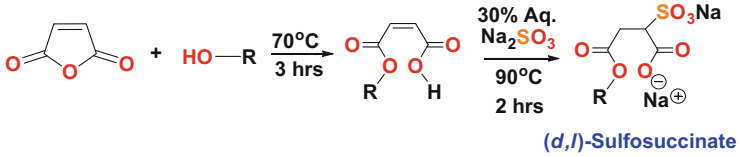

Scheme 2.53 Formation of sulfo-succinates with maleic anhydride

Both alkyl and aryl thiols participate in this reaction in a straightforward manner. The greater the acid strength of the thiol, the quicker addition occurs, primarily due to a higher population of thiol present in its anionic form. The reaction proceeds readily under anhydrous conditions. Under aqueous conditions, the reaction becomes quite complicated, due to hydrolysis of maleic anhydride into maleic acid, enabling a number of side reactions.

Sulfonation of maleic anhydride proceeds in a similar fashion to thiol additions, where the nucleophilic alkali metal sulfonate moiety adds to the electron-deficient double bond, as illustrated in Scheme 2.53. The typical reaction is a two-step process, where the maleic anhydride is first reacted with an alcohol, usually a fatty alcohol, to form the monoester, and then the alkali metal salt of sulfite is added to form the well-known surfactant class of sulfo-succinates [128, 129].

2.5.7 Alkoxylation Reactions to the Double Bond

As seen in the previous section on thiols, base-catalyzed alkoxy addition to the polarized double bond of dialkyl maleates can occur to generate a racemic mixture of alkoxy-succinates, as depicted in Scheme 2.54. This reaction readily proceeds at

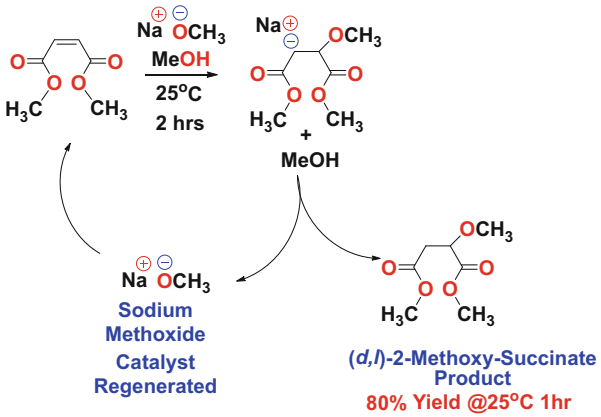

Scheme 2.54 Formation of alkoxy-succinates from catalytic amount of sodium methoxide in methanol and dimethyl maleate

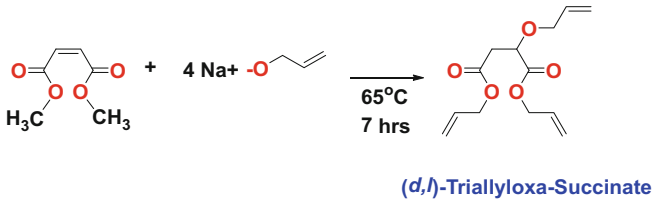

Scheme 2.55 Formation of alkoxy-succinates from sodium allyloxide and dimethyl maleate (Adapted from [131])

room temperature with a reported yield of 80 % in 1 h [130]. Typically this reaction is carried out with an alkoxy anion identical in structure to the ester functionality, minimizing the complexity of the product that is formed by transesterification side reactions that cannot be completely controlled under the typical reaction conditions employed.

It must be recognized that not only does the alkoxy anion participate in a Michael addition reaction, it also reacts with the ester functionality and can transesterify. This is evidenced by the tri-allyloxa-succinate cross-linker structure depicted in Scheme 2.55 [131]. In particular, addition of the alkoxy anion of allyl alcohol to dimethyl maleate not only results in the addition across the double bond, but the methyl esters also participate in an exchange reaction to replace the methyl ester with the diallyl ester too.

2.5.8 *Amination, Amino-Acid Formation, and Biopolymer Synthesis*

Michael additions of ammonia, alkyl, and aryl amines to maleate salts and esters generate racemic amino-acid products. In fact, two out of the 20 naturally occurring amino acids found in proteins can be manufactured from maleic anhydride. These compounds are aspartic acid and asparagine. For example, addition of ammonium hydroxide to maleic or fumaric acid forms a racemic mixture of (*d*,*l*)-aspartic acid ammonium salt, while addition of ammonia in methanol to maleic anhydride generates the racemic amino-acid asparagine ammonium salt, as depicted in Scheme 2.56 [132].

Biodegradable polymers based on aspartic acid or asparagines have significance in the marketplace. For instance, poly-aspartic acids can be used as anti-scaling agents for heating and cooling water systems and corrosion inhibition [133–135], super-swelling hydrogels in diapers and feminine hygiene products [136], a builder in detergents, and as a dispersant [137]. As a polyelectrolyte, it has replaced poly-acrylic acid in many applications due to its benign nature and potential biodegradability as a more ecologically friendly alternative and *greener* product.

Synthetically, it is manufactured much like that of aspartic acid in Scheme 2.57, but requires much higher temperatures for condensation to occur [139]. The thermal polymerization is actually a condensation reaction instead for aspartic acid, or precursors of aspartic acid, and proceeds through a polyimide intermediate followed by mild alkaline hydrolysis to produce the polyamide poly-aspartate.

As NMR techniques were applied to characterize the intermediates and products, a mixture of the α, β nature of the residues became well known, and a preference for

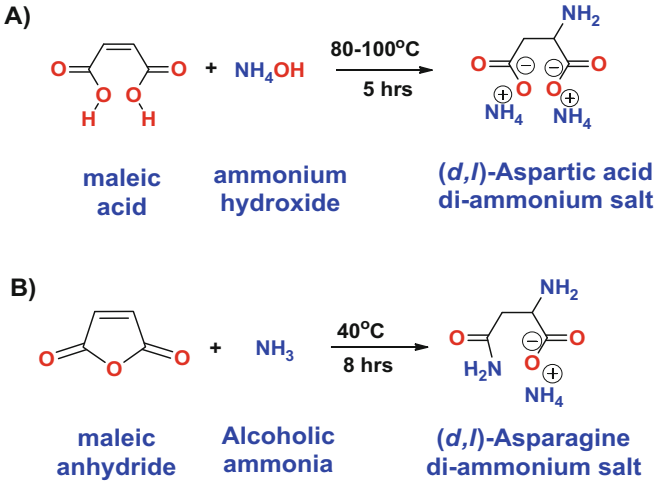

Scheme 2.56 Formation of racemic amino acids; (**a**) aspartic and (**b**) asparagine from maleic anhydride

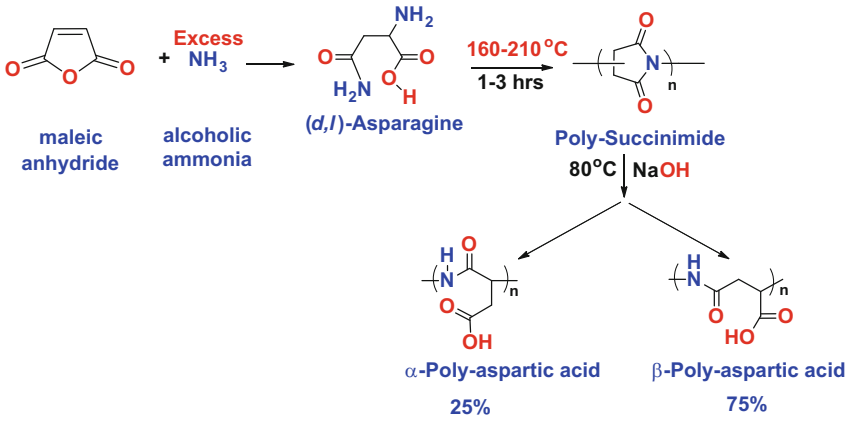

Scheme 2.57 Formation of biopolymers poly-(*d*,*l*)-aspartate/asparagine from maleic anhydride (Adapted from [138])

the more flexible β-linkage was observed over the α-linkage by a 3:1 margin [140]. These configurational and structural isomers are related to isomeric structures generated along the polymer backbone, two related to the ring opening of the α, or β-carboxyl group, and two related to the *d*, or *l*-stereocenter.

Fox and Harada (1962) further demonstrated that the copolymerization of aspartic acid, or its precursors to aspartic acid, with other amino acids by heating admixtures at 160–210 °C for 1–3 h or a time sufficient to form a polyimide, resulted in branched poly-aspartates. If H_3PO_4 was added in an equimolar or lesser amount relative to the amounts of amino acids used, linear products with higher molecular weights were achieved at lower reaction temperatures. The polyimide was then decomposed by mild alkaline at 80 °C for 10 min, as outlined in Scheme 2.57 [138].

2.6 Cycloaddition (Diels–Alder) Reactions of Maleic Anhydride

Maleic anhydride is a potent dienophile in cycloadditions. These reactions are better known as Diels–Alder reactions. In fact, this type of reaction was discovered in the late 1920s by Otto Diels and Kurt Alder using maleic anhydride with dienes and trienes [141]. This reaction can synthesize complex chiral compounds related to natural products such as terpenes, sesquiterpenes, and alkaloids.

Diels and Alder reaction is extremely useful in forming cyclic rings in high yield and high stereospecificity. Diels–Alder reactions are also known to be reversible under certain conditions. The reverse reaction is known as the retro-Diels–Alder reaction. Most Diels–Alder adducts are aromatic, which is an additional driving force within this type of reaction.

The Diels–Alder reaction has been extensively used in the synthesis of complex natural molecules due to the formation of numerous chiral centers in one reaction, which are governed by the Woodward–Hoffmann rules. These theoretical rules involve the correlation of orbital symmetry to the outcome of a Diels–Alder reaction, as well as other electrocyclic reactions [142–144].

This reaction is neither polar nor ionic or radical-based either. It is known as a concerted pericyclic reaction, a reaction in which several bonds in the cyclic transition state are formed and severed simultaneously. A pericyclic reaction is a type of reaction wherein the transition state of the molecule(s) has a cyclic geometry, and the reaction proceeds in concerted fashion. Pericyclic reactions are usually rearrangement reactions. Some other major classes of pericyclic reactions include electrocyclizations (Nazarov) and sigmatropic rearrangements (Cope, Claisen) and group transfer.

When a diene and dienophile react with each other, sometimes more than one stereoisomer can be produced. The isomer that predominates is the one which involves maximum overlap of the pi-electrons in the cyclic transition state [144]. This reaction runs quickly when the diene bears an electron-donating group (EDG), while the dienophile contains an electron-withdrawing group (EWG), as summarized in Scheme 2.58. In general, the dienophile must have an

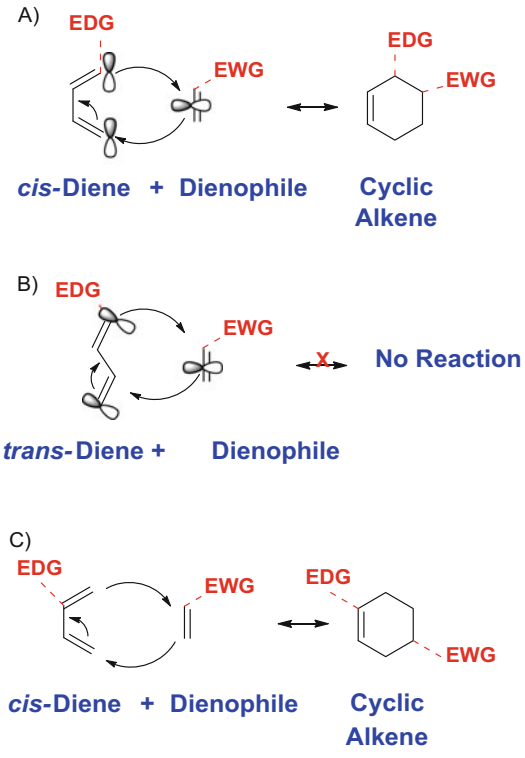

Scheme 2.58 Diels–Alder reaction of a diene with a dienophile (Adapted from [145])

electron-withdrawing substituent for the reaction to readily proceed. Ethylene itself does not easily form Diels–Alder adducts. For ethylene to participate in a Diels–Alder reaction, extremes of pressure 1800 psi and temperature 185 °C are required [146]. Furthermore, the diene must be in the *s-cis*-conformation for proper alignment of the molecular orbitals to form the prerequisite bonds between the diene and dienophile, as shown in Scheme 2.58a.

Dienes in the *trans*-conformation do not form Diels–Alder adducts because of improper overlap of their molecular orbitals with the dienophile (Scheme 2.58b). Positioning of the electron-donating group (EDG) on the diene can also affect the alignment between the two reactants such that the terminal EDG will be vicinally attached to the carbon bearing the EWG in the dienophile (Scheme 2.58a). In contrast, internally positioned EDG will be positioned further apart from the EWG group, analogous to a *para*-orientation in the ring (Scheme 2.58c).

Dienes with bulky terminal substituents in the C1 and C4 positions decrease the rate of reaction, while bulky substituents at the C2 or C3 position of the diene actually increase reaction rate by presumably destabilizing the *trans*-conformation and forcing the diene into the more reactive *cis*-conformation [145].

The Diels–Alder cycloaddition reaction involves the 1,4-addition of a conjugated diene to a *cis*-alkene, resulting in two new sigma bonds, formed from two *pi* bonds. The resultant adduct thereby forms a six-membered ring. This reaction is quickest when the diene has two conjugated bonds locked within a ring system, such as cyclopentadiene or cyclohexadiene, enabling a fixed alignment of the requisite molecular orbitals in space. The molecule can also be an acyclic diene that can assume a *cis*-conformation. These isomers tend to react slower, since it must achieve the correct conformation before the reaction can proceed, as outlined in Scheme 2.58a versus 2.58b.

Maleic anhydride is a potent dienophile because of the electron-withdrawing substituents of the anhydride carbonyls. These resonance structures of maleic anhydride are further stabilized by the presence of the neighboring lone-pair electrons on the carbonyl group's oxygen atoms denoted by a blue-δ as outlined in Scheme 2.59. Hence, maleic anhydride's pi bond is clearly electron deficient and behaves as an electrophile to electron-rich dienes.

Retention of configuration for the reactants in the products implies that both new sigma bonds are formed simultaneously [145]. The stereochemical information in

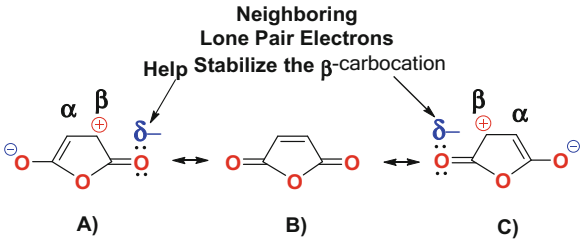

Scheme 2.59 Resonance structures for maleic anhydride as a dienophile

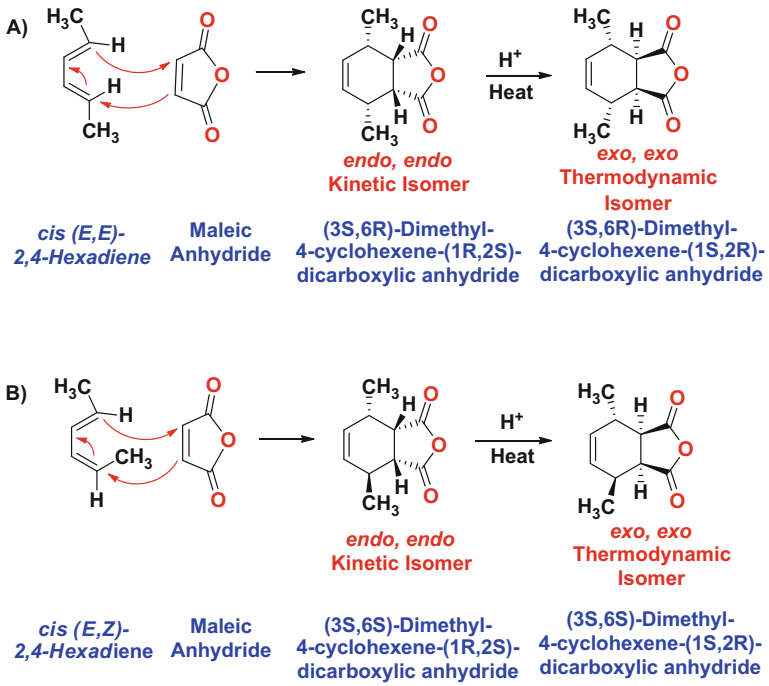

Scheme 2.60 Retention of configuration between 2,4 hexadiene and maleic anhydride

the reactants is therefore retained within the products. For instance, (*E*)- and (*Z*)-dienes give rise to the adducts with corresponding *syn*- or a*nti*-stereochemistry, as presented in Scheme 2.60.

When the diene (*E*,*E*)-2,4-hexadiene reacts with maleic anhydride, the *pseudo-cis*-isomer for (3S,6R)-dimethyl-4-cyclohexene-1,2-dicarboxylic anhydride is formed (Scheme 2.60a); however, when (*E*,*Z*)-2,4-hexadiene is used, the pseudo-*trans*-isomer (3S, 6R)-dimethyl-4-cyclohexene-1,2-dicarboxylic anhydride is formed (Scheme 2.60b).

The kinetic *endo*,*endo*-isomer is formed first for both molecular entities (Scheme 2.60a, b). However, when application of an isomerization agent such as heat or acid is used, then the thermodynamically more stable *exo*,*exo*-isomer predominates [147]. The *exo*,*exo*-isomer has been found to be more reactive in ring-opening metathesis polymerization (ROMP), a topic that will be addressed in-depth in Chap. 6 [148].

The retention of configuration is also observed for the dienophile. Specifically, if the alkene is in the *trans*-configuration such as fumaroyl chloride (Scheme 2.61), then only the *endo*,*exo*-isomer (3S, 6R)-dimethyl-4-cyclohexene-(1R,2R)-diacyl chloride is formed due to symmetry factors within the molecule (Scheme 2.61a). In contrast, when maleoyl chloride is used, then the predisposed kinetic and thermodynamic isomers are again observed highlighting the retention of

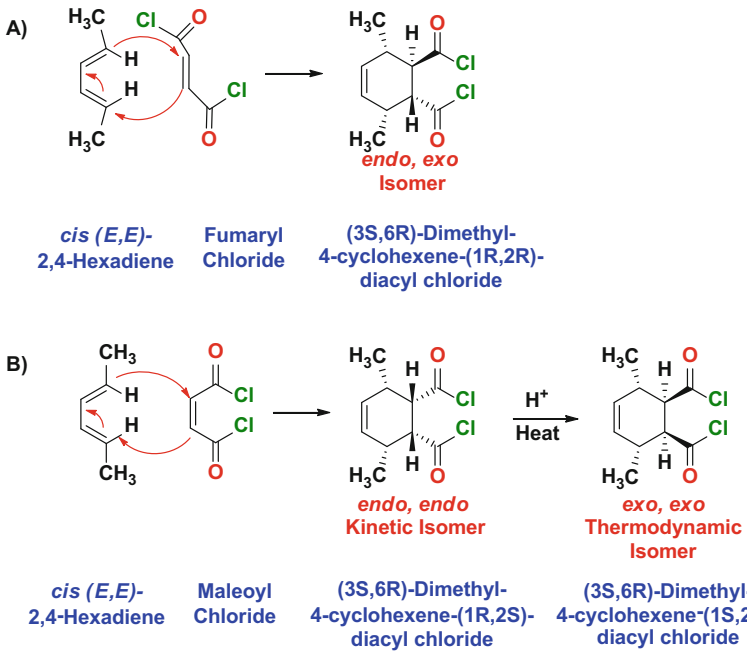

Scheme 2.61 Retention of configuration between 2,4-hexadiene and fumaryl chloride or maleoyl chloride

configuration within the product (Scheme 2.61b). The reason for this can be explained by the mechanistic factors involved in the Diels–Alder reaction itself [148, 149].

For a pericyclic reaction to proceed, the p-orbitals for each reactant must overlap with each other and that the sign of the terminal orbitals in the HOMO of the diene and the LUMO of the dienophile must match. This happens naturally with the HOMO/LUMO overlap in the $[4\pi + 2\pi]$ Diels–Alder cycloaddition. In contrast, this fails with the HOMO/LUMO overlap in the analogous $[2\pi + 2\pi]$ cycloaddition reaction. Mechanistically, the cyclic transition state for the formation of the *endo*-isomer in this reaction involves a sandwich with the diene directly above the dienophile (Scheme 2.62) [150].

In such an arrangement, the electron-withdrawing group on the dienophile is geometrically placed under the diene. Furthermore, the electrons of the *pi* bonds are on the same face to each other and are called suprafacial. For instance, in the Diels–Alder addition of cyclopentadiene with maleic anhydride, the two molecules approach each other in the orientation depicted in Scheme 2.62b, as this orientation provides maximal overlap of pi bonds between the two reactants and favors formation of an initial *pi*-complex resulting in the final *endo*-product.

Illustrated in Fig. 2.16 is the endo- and exo-molecular orbital interactions between cyclopentadiene and maleic anhydride. The endo-product is favored

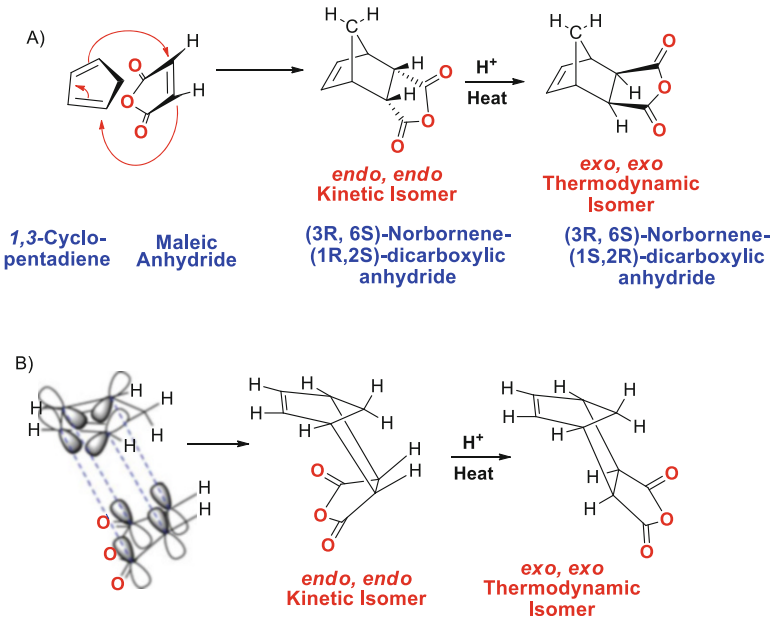

Scheme 2.62 Diels–Alder reaction between cyclopentadiene and maleic anhydride (Adapted from [150])

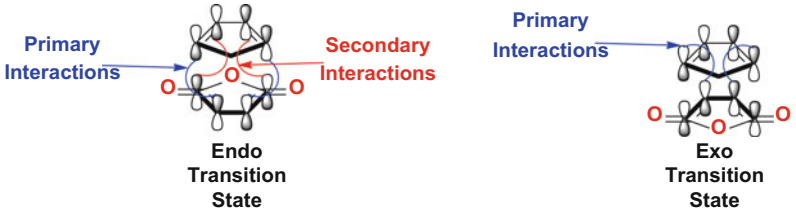

Fig. 2.16 Diels–Alder molecular orbital interactions between the endo- and exo-orientations for cyclopentadiene and maleic anhydride (Adapted from [150])

because of secondary interactions highlighted in red that are absent in the exo-orientation. Therefore, this lowers the activation energy, and kinetically this isomer is favored over the more thermodynamically stable exo-isomer.

A consideration of the reactants' frontier molecular orbitals (FMO) makes it clearer why this occurs, as portrayed in Scheme 2.63. This reaction proceeds quickest when the HOMO and LUMO orbitals are energetically similar. Since the antibonding LUMO orbital is always higher in energy than the bonding HOMO orbital, anything to raise the energy of the HOMO orbital and/or lower the energy of the LUMO orbital can make Diels–Alder reactions even more facile. This can be achieved by adding electron-donating groups (EDGs) to the diene and/or electron-withdrawing groups (EWGs) to the dienophile [151].

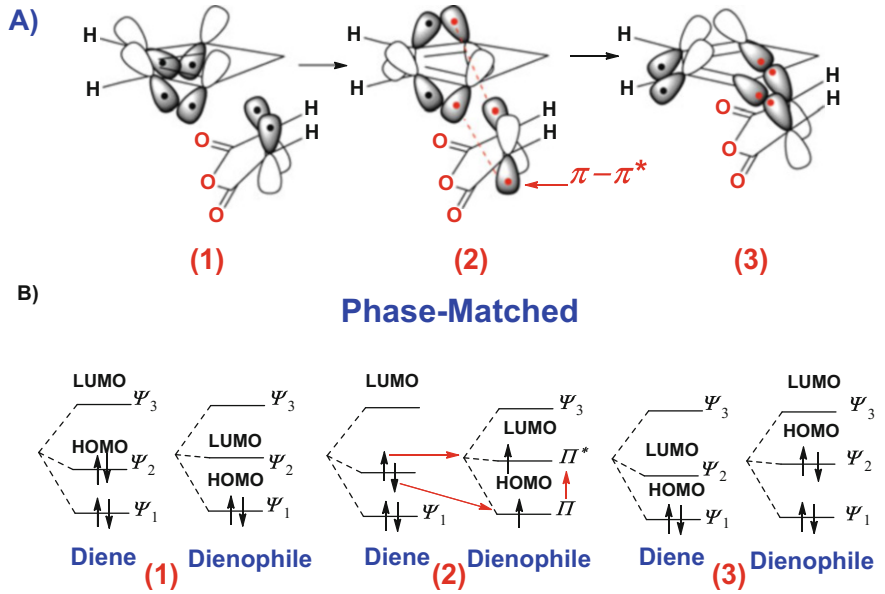

Scheme 2.63 Frontier molecular orbital theory of Diels–Alder reaction between cyclopentadiene and maleic anhydride

Scheme 2.63 summarizes some of the reaction's major features involved. Panels 63 A1–A3 correspond to the approach of the diene and dienophile. Scheme 2.63-a1 illustrates the orientation of the diene's ether and the dienophile's anhydride group that are facing each other. The dienophile is partially under the diene so that their orbitals overlap. The electronic rearrangement between the two entities as a consequence of thermal energy (Scheme 2.63-a2) and the bond formation between the HOMO orbital of the diene to the LUMO orbital of the dienophile are phase matched so electrons can flow from HOMO to LUMO during bond formation (Scheme 2.63-a3). The corresponding energy diagram for each partner is directly under their respective figure panel, such as the b1 energy diagrams are directly under a1 orbital profiles, while b2 corresponds to a2, and b3 corresponds to a3.

Complexation between the diene and dienophile occurs with the diene aligning its orbitals over the dienophile in Scheme 2.63-a1 and b1. Upon thermal activation, a $\Pi \rightarrow \Pi^*$ transition occurs in the dienophile, denoted by the red electrons in Scheme 2.63-a2, while the diene's pi-electrons assume an antiparallel arrangement, corresponding to Scheme 2.63-b2. Note that in this transition state, the diene's C1 and C4 electrons and their corresponding orbitals are in phase with the dienophile orbitals, so that upon decay in Scheme 2.63-b2–3, the new sigma bonds may form.

The electrons flow from the HOMO orbitals to the LUMO orbitals to form the two new sigma bonds between the two reactants converting it to the Diels–Alder adduct product (Scheme 2.63-a3). Because the HOMO and LUMO of the two components are in phase, a bonding interaction occurs as depicted in Scheme 2.63-

a2–a3. Since the reactants are also in their ground state, the reaction is initiated thermally and does not require activation by UV light [152]. Using frontier molecular orbital theory, one can also predict which centers with the largest frontier-orbital coefficients will react more quickly, thereby enabling one to predict the major regioisomer that will result from a given diene–dienophile pair [153, 154].

Lewis acids such as zinc chloride, boron trifluoride, tin tetrachloride, and aluminum chloride among others can act as catalysts for Diels–Alder reactions by coordination to the dienophile. The complexed dienophile thereby becomes more electrophilic and more reactive toward the diene, increasing the reaction rate and often improving the regioselectivity and stereoselectivity. Lewis acid catalysis also enables Diels–Alder reactions to proceed at low temperatures [152–156].

Many other additives have been developed for influencing the stereoselectivity of the Diels–Alder reaction. These include chiral auxiliaries, chiral Lewis acids, Evans' oxazolidinones, oxazaborolidines, bis-oxazoline Cu chelates, and imidazoline catalysis, for affecting the diastereoselectivity and enantioselectivity of Diels–Alder reactions [157–163].

2.6.1 *Ring-Opening Metathesis Monomers from Maleic Anhydride*

Endo-selectivity is typically higher when employing maleic anhydride in the Diels–Alder reaction with cyclopentadiene or furan (Scheme 2.64). The most widely accepted explanation for this effect is due to a favorable interaction between the dienophile substituent's π electron system and the diene's (termed secondary orbital effects), though dipolar and van der Waals attractions [152, 164].

A number of new monomers are useful for ring-opening metathesis polymerization. These monomers can be made from many conjugated dienes, like cyclopentadiene, to form norbornene dicarboxylic anhydride (Scheme 2.62), or its esters from dialkyl maleates, amides, or maleimides, and 7-oxanorbornene derivatives from furan (Scheme 2.64). Other monomers include thiophene or

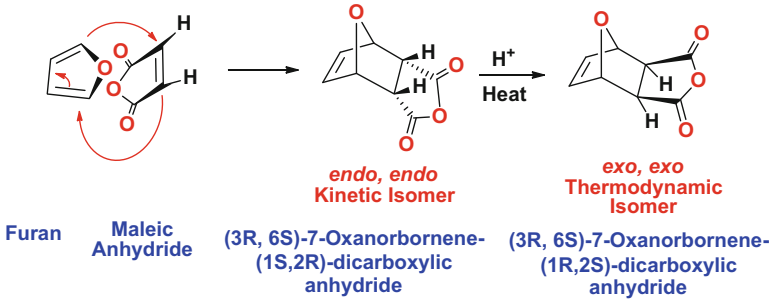

Scheme 2.64 Diels–Alder reaction between furan and maleic anhydride

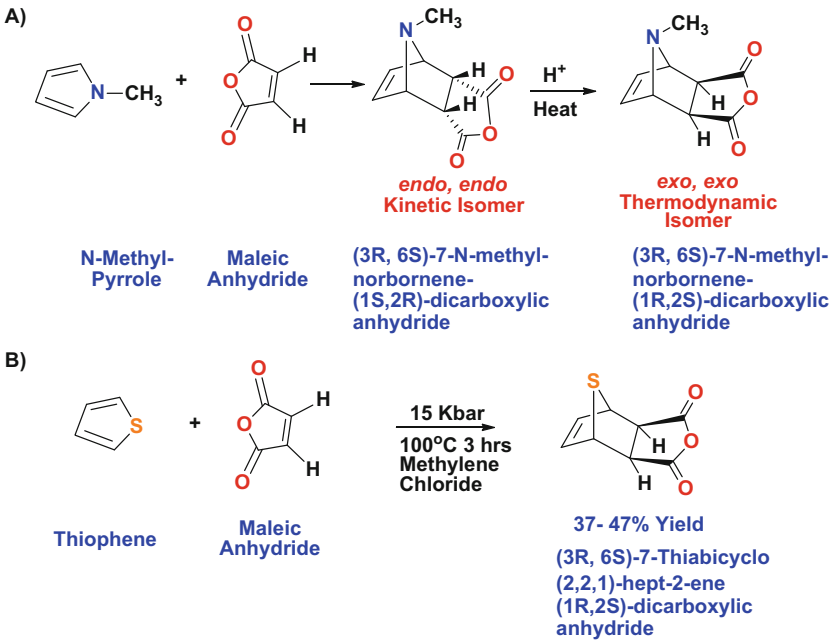

Scheme 2.65 Diels–Alder reaction between *N*-methyl-pyrrole or thiophene with maleic anhydride

pyran-based derivatives (Scheme 2.65a, b). However, the thiophene adduct requires extreme temperature and pressure to obtain a moderate 37–47 % yield of Diels–Alder adduct [162]. These molecules can be further reacted to form a host of derivatives such as the diacid, mono- and di-alkali salts, esters, amides, imides, and more.

2.6.2 Maleated Fatty Acids and Vegetable Oils

An especially useful transformation of the conjugated olefin system in fatty acids is the Diels–Alder reaction. Many conjugated fatty acids like sorbic acid can react with maleic anhydride to form Diels–Alder adducts. These adducts possess greater functional diversity due to the anhydride functionality, which can react further into a whole host of derivatives. An example of this transformation is presented in Scheme 2.66.

Normally, fatty acids derived from vegetable oils do not have conjugated double bonds. Three typical unsaturated fatty acids from triglycerides, namely, oleic acid, linoleic acid, and linolenic acid, are depicted in Fig. 2.17. These molecules do not participate in Diels–Alder reactions.

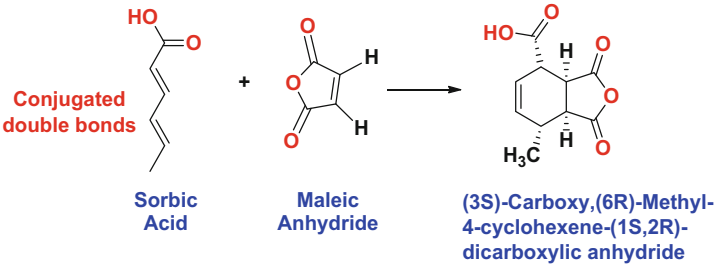

Scheme 2.66 Diels–Alder reaction between sorbic acid with maleic anhydride

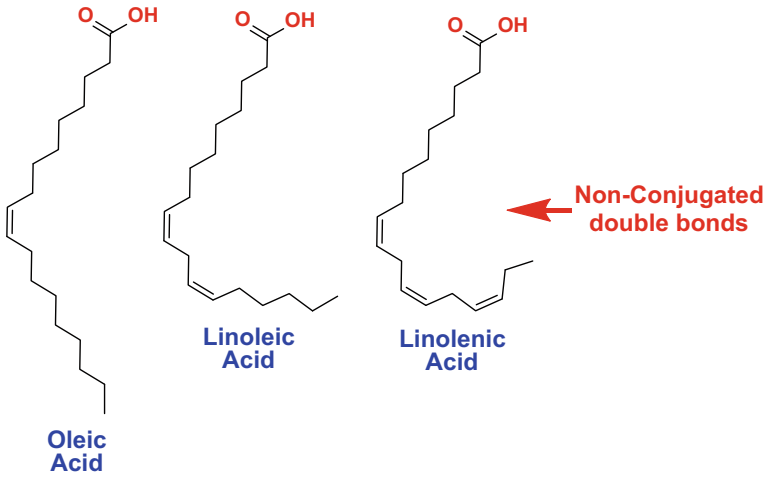

Fig. 2.17 Chemical structures for typical non-conjugated fatty acids found in plants and animals

Linoleic and linolenic fatty esters can be isomerized from their non-conjugated state into a conjugated one by the treatment with alcoholic base, as depicted in Scheme 2.67 [165]. In doing so, the non-conjugated linoleic fatty ester is converted into conjugated linoleic fatty ester. Once formed, this conjugated linoleic fatty ester can now participate in a straightforward Diels–Alder reaction.

This reaction enables derivation and enhanced functionality of the fatty acids in several ways. For example, maleic anhydride will react with a conjugated fatty acid or ester to form the (3S)alkyl carboxy, (6R) alkyl-4-cyclohexene-(1S,2R)-dicarboxylic anhydride (Scheme 2.68). By this relatively simple reaction [166], which can be carried out at about 100 °C, one can obtain a trifunctional acid in near-quantitative yield.

Other dienophiles or activated monoolefins that have been transformed into Diels–Alder adducts with conjugated linoleic acids are listed below [167]. Not all of them react as readily as maleic anhydride. For example, acrolein gives a 97 % yield of the Diels–Alder adduct at 100 °C, as does maleic anhydride. Acrylonitrile

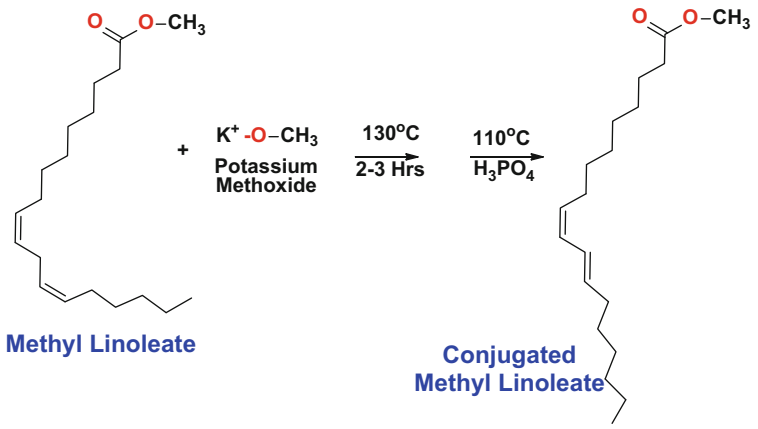

Scheme 2.67 Isomerization of methyl linoleate into a conjugated methyl linoleate by base treatment followed by neutralization

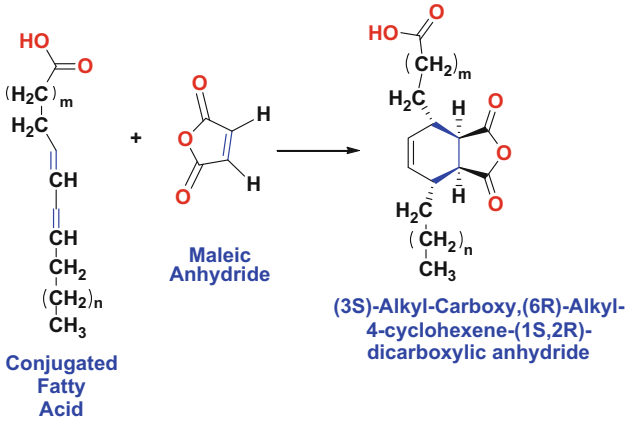

Scheme 2.68 Diels–Alder reaction between conjugated fatty acid with maleic anhydride

and β-nitrostyrene give only a 27 % yield of adduct at 200 °C, while acrylic acid at this temperature gives a 96 % yield. Fumaric acid reacts to the same extent and under the same conditions as acrylic acid. Methyl vinyl sulfone gives an 80 % yield of adduct at 200 °C. Tetracyanoethylene, an extremely reactive dienophile, will react quantitatively with conjugated linoleic acids at about 50 °C [168].

Adduct reactions, such as those just mentioned, are generally carried out in chloroform or benzene solution in a closed reactor in the presence of a small amount of a polymerization inhibitor, such as hydroquinone. Acetic acid, or even water, in catalytic amounts has been reported to increase the rate of adduct formation with conjugated linoleic acids [169]. Use of a polar solvent such as acetonitrile, with no added water or acid, facilitates adduct formation.

The preferred isomer for the Diels–Alder reaction has the *trans–trans* configuration. It has been reported that the use of small amounts of sodium or potassium

bisulfites [170], sulfur [171], selenium, iodine, or noble metals will isomerize the *cis–trans*-isomer to the *trans–trans* form. Accordingly, optimum utilization of the conjugated system in the feedstock of fatty acids for adduct formation under mild conditions is obtained by the use of one of these isomerization catalysts. The addition of the dienophile itself can be promoted with a little acid, as mentioned earlier. The multifunctional Diels–Alder reaction product illustrated in Scheme 2.68 is characterized by a substituted cyclohexene ring in a long-chain fatty acid.

The polyfunctional Diels–Alder adducts of these fatty acids can serve as intermediates for further derivation. For example, the adduct with maleic anhydride can be reacted with primary amines or ammonia to give imides that may be water dispersible. The aldehyde group of the acrolein adduct can be reduced to an alcohol group. A derivative such as this has the complete functionality for a polyester in one molecule, yet the hydroxyl and carboxyl groups are separated enough to avoid lactone formation.

Ethylene, propylene, and even-numbered *alpha*-olefins from C_4 to C_{20} have been adducted to the diene system of conjugated linoleic acid. These reactions are carried out at 260 °C under pressure and result in branched-chain, high molecular weight fatty acids [172].

2.7 "Ene" Reactions of Maleic Anhydride: "Ene" Reaction

A reaction closely related to the Diels–Alder reaction, and one that can be used to increase the functionality of unsaturated fatty acids, is the "ene" reaction. This reaction is also known as the "Alder-ene" reaction. This reaction is not as facile as Diels–Alder because much higher reaction temperatures are needed, usually 200–230 °C without solvent, and it requires a more highly reactive enophile, such as maleic anhydride. The ene reaction typically requires higher temperatures due to the stereo-electronic requirement of breaking the allylic C–H σ-bond.

The enophile can be an alkene or alkyne that couples to the "ene" to form a new sigma bond between the two molecules, along with a migration of the "ene" double bond and a concomitant 1,5 hydride shift from the ene to the enophile. This reaction is best summarized by Scheme 2.69.

Enes are π-bonded molecules that contain at least one active hydrogen atom at the allylic, or α-position. Possible ene components include olefinic, acetylenic,

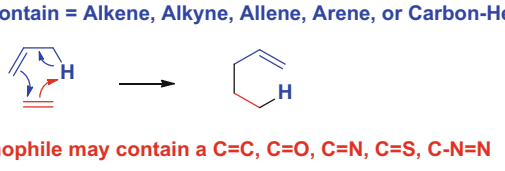

Scheme 2.69 The "ene" or Alder-ene reaction between an "ene" with an enophile (Adapted from [173])

allenic, aromatic, cyclopropyl, and carbon-hetero bonds [173]. Typically the allylic hydrogen of an allenic component will participate in the ene reaction.

Enophiles are also π-bonded molecules, which have electron-withdrawing substituents that significantly lower the LUMO orbital of the π bond. Possible enophiles contain carbon–carbon multiple bonds (olefins, acetylenes, benzynes), carbon-hetero multiple bonds (C=O in the case of carbonyl-ene reactions, C=N, C=S, C≡P), hetero–hetero multiple bonds (N=N, O=O, Si=Si, N=O, S=O), cumulene systems (N=S=O, N=S=N, C=C=O, C=C=S, SO_2), and charged π systems (C=N+, C=S+, C≡O+, C≡N+). The enophile may also be an aldehyde, ketone, or imine, in which case β-hydroxy or β-aminoolefins are obtained. These compounds may be unstable under the reaction conditions, so that at elevated temperature (>400 °C), the reverse reaction takes place—the retro-ene reaction.

Lewis acids catalyze the ene reaction and can produce high yields and superior selectivities at much lower temperatures. The main frontier-orbital interaction occurring in an ene reaction is between the HOMO of the ene and the LUMO of the enophile (Scheme 2.70) [171]. The HOMO of the ene results from the combination of the π-bonding orbital in the vinyl moiety and the C–H bonding orbital for the allylic hydrogen and proceeds in a concerted fashion [174].

If the enophile becomes more polar, as in the presence of heteroatoms, its LUMO orbital has a larger influence on the carbon atom of the enophile, yielding a better C–C overlap and a poorer H–X one. This translates into a lowering of the activation barrier. The concerted nature of the ene process has been supported experimentally [175, 176], and the reaction can be designated as [σ2s + π2s + π2s] in the Woodward–Hoffmann notation [132–144]. For example, the ene reaction of cyclopentene and cyclohexene with diethyl azodicarboxylate can be catalyzed by free-radical initiators. As seen in Scheme 2.71, the stepwise nature of the process is favored by the stability of the cyclopentenyl or cyclohexenyl radicals [177, 178].

The success of any ene reaction is largely influenced by the steric accessibility to the ene's allylic hydrogen. In general, methyl and methylene H atoms are abstracted more easily than methine hydrogens. In thermal ene reactions, the order of reactivity for the abstracted H atom is primary > secondary > tertiary, irrespective of the thermodynamic stability of the internal olefin product. In Lewis-acid-promoted reactions, the enophile–Lewis acid pair employed determines largely the relative

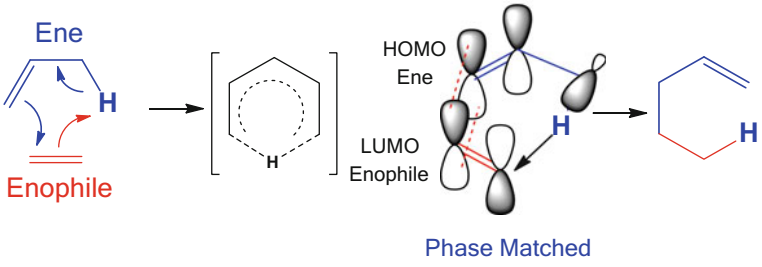

Scheme 2.70 Concerted mechanism for the ene reaction (Adapted from [173])

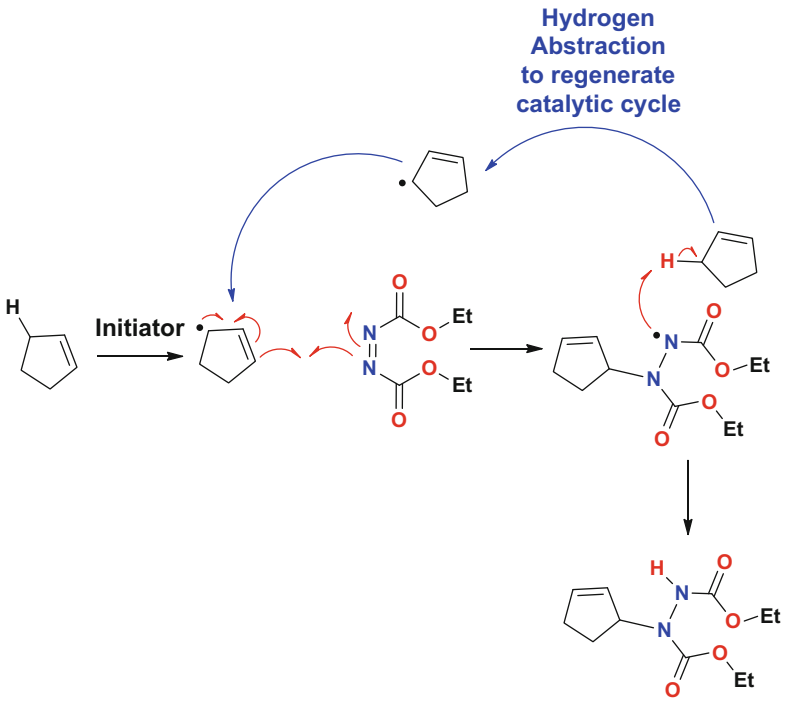

Scheme 2.71 Stepwise, free-radical pathway for the ene reaction (Adapted from [177])

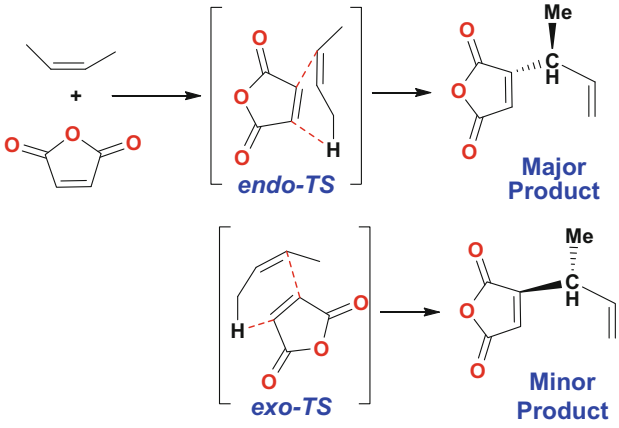

Scheme 2.72 Endo-preference for the ene reaction (Adapted from [180])

ease for abstraction of methyl versus methylene hydrogens [179, 180]. In terms of the diastereoselection with respect to the newly created chiral centers, an *endo*-preference has been qualitatively observed, but steric effects can easily modify this preference, as depicted in Scheme 2.72.

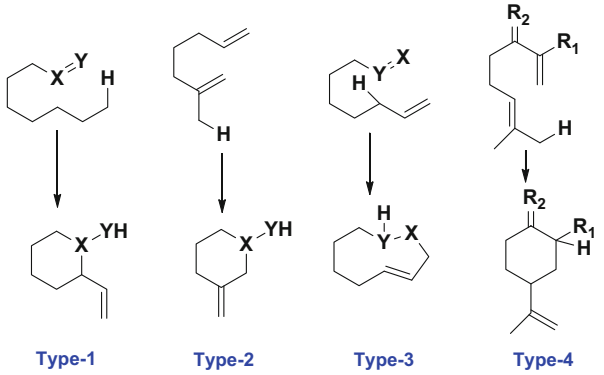

Scheme 2.73 Types of intramolecular ene reactions (Adapted from [180])

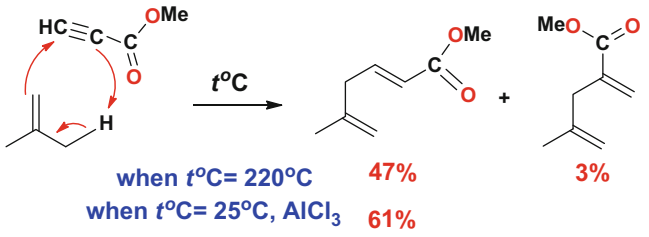

Scheme 2.74 Improvements brought to the ene reaction by Lewis acid catalysis

In the position of attachment between the ene and enophile, Oppolzer [180] has classified both thermal and Lewis-acid-catalyzed intramolecular ene reactions as types I, II, and III, and Snider [181] has added a type IV reaction (Scheme 2.73) [173].

Thermal ene reactions have several shortcomings, such as the need for very high temperatures and the possibility of side reactions, like proton-catalyzed olefin polymerization or isomerization reactions. Since enophiles are electron deficient, it was rationalized that their complexation with Lewis acids should accelerate the ene reaction, as observed for the reaction shown in Scheme 2.74.

As seen in Scheme 2.75, Lewis-acid-catalyzed ene reactions can proceed either through a concerted mechanism that has a polar transition state or through a stepwise mechanism with a zwitterionic intermediate. The ene, enophile, and choice of catalyst can all influence which pathway is the lower energy process. In broad terms, the more reactive the ene or enophile-Lewis acid complex is, the more likely the reaction is to be stepwise [181].

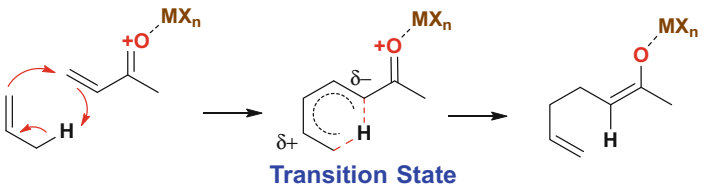

Scheme 2.75 Mechanisms of Lewis-acid-catalyzed ene reactions (Adapted from [181])

2.7.1 *Ene Reactions of Fatty Acids and Oils with Maleic Anhydride*

The use of the ene reaction has been exploited to add functionality and polarity to simple olefins like unsaturated fatty acids or vegetable oils especially when using maleic anhydride. Maleic anhydride reacts with one mole of non-conjugated linoleic acid to form the ene adduct as depicted in Fig. 2.18a. This reaction provides

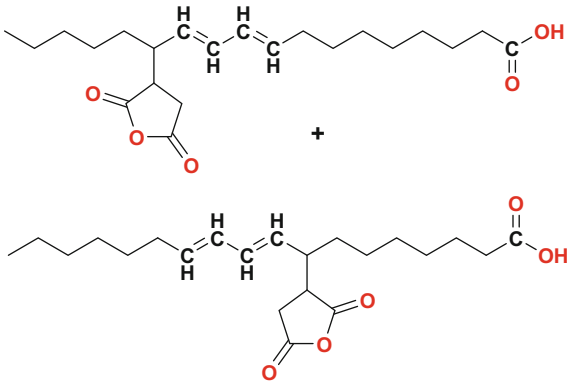

A) Reaction Product of Linoleic Acid with Maleic Anhydride thereby forming conjugated double-bonds

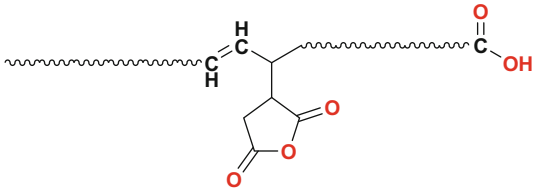

B) Reaction Product of Oleic Acid with Maleic Anhydride

Fig. 2.18 Chemical structures for ene adduct of (**a**) maleic anhydride with non-conjugated linoleic acid (**b**) and that with oleic acid

a conjugated diene that can be further functionalized through the Diels–Alder reaction, as depicted in Fig. 2.18a.

By use of the "ene" reaction, it is possible to attach more than one mole of maleic anhydride onto the fatty acid chain. If the reaction is stopped after addition of one mole of maleic anhydride, a polycarboxylic alkyd intermediate can be obtained whose conjugated site provides good "built-in" air-drying properties. With the addition of more than one mole of maleic anhydride to linoleic acid, one can obtain a highly acidic material capable of further reaction with a primary amine or ammonia to yield imides that could be water dispersible.

In contrast, when oleic acid is used as the ene component, there is still one double bond in the product after one mole of maleic anhydride has been added, as depicted in Fig. 2.18b. However, this double bond is sterically hindered by the maleic anhydride group. Thus, addition of a second mole of maleic anhydride is unfavorable.

2.7.2 *Grafted Polyethylene or Polypropylene with Maleic Anhydride*

Similarly, polymers like polyethylene or polypropylene can be grafted with maleic anhydride via the ene reaction, instead of free-radical process that tends to lower the molecular weight due to chain scission reactions, as illustrated in Scheme 2.76.

Polypropylene is a very large volume product (8,013,000 metric tons in the USA in 2003). One of the major problems with its use is that there are no polar functional groups in the polymer to provide reactive sites. A typical way to solve this problem is to add in a small amount of material which contains polar groups attached to a low molecular weight polypropylene backbone. The polypropylene backbone bonds to the bulk polypropylene and the polar groups allow reactivity with external materials.

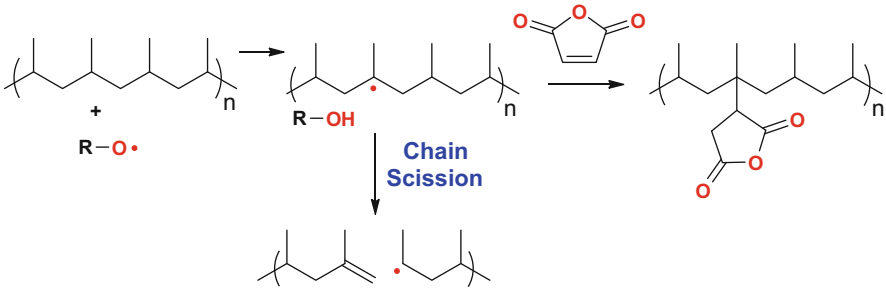

Scheme 2.76 Free-radical addition of maleic anhydride onto polypropylene also results in chain scission

The most common polar group that is incorporated is maleic anhydride. Typical of this approach is Eastman® E43, Eastman® AP550, or Arkema Orevac® grafted polypropylenes. A major problem with these materials is that they contain relatively low amounts of functional groups. The amount of maleic anhydride is determined by its acid number or SAP number. This is defined as the number of milligrams of KOH required to neutralize 1 g of the polymer. The polymers mentioned above have acid numbers of about 40–45. This corresponds to approximately 4 wt% of the polymer being from maleic anhydride.

It is difficult to increase the amount of maleic anhydride. The maleic anhydride is typically attached by grafting initiated by a radical chain process. It has been found that polypropylene undergoes chain scission via radical processes [182, 183]. This chain scission results in significant loss of physical properties due to decreases in the molecular weight of the polypropylene and consequent decreases in viscosity.

This method employs succinic-terminated polypropylene formed via the ene reaction onto vinylidene-terminated polypropylene. This polypropylene is often, but not exclusively, prepared by metallocene catalysis. It has been discovered that grafting maleic anhydride onto this polymer does not result in significant chain scission or polymerization (Scheme 2.76).

The process involves heating maleic anhydride in the presence of a polypropylene that has been formed using a metallocene catalyst in such a way that a single terminal vinylidene group results on each molecule. The subsequent ene addition of maleic anhydride onto this polymer chain end affords the desired product, as shown in Scheme 2.77 [182].

Polymerization of this maleic anhydride/polypropylene ene adduct would then yield a highly maleated polypropylene polymer, as summarized in Scheme 2.78.

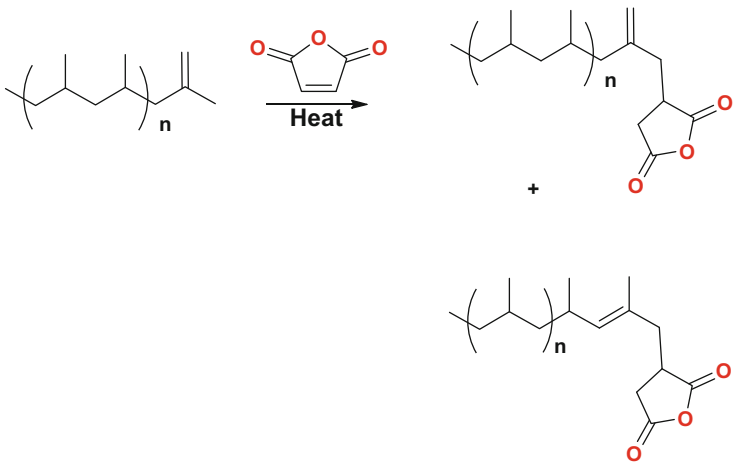

Scheme 2.77 Ene addition of maleic anhydride onto polypropylene (Adapted from [182])

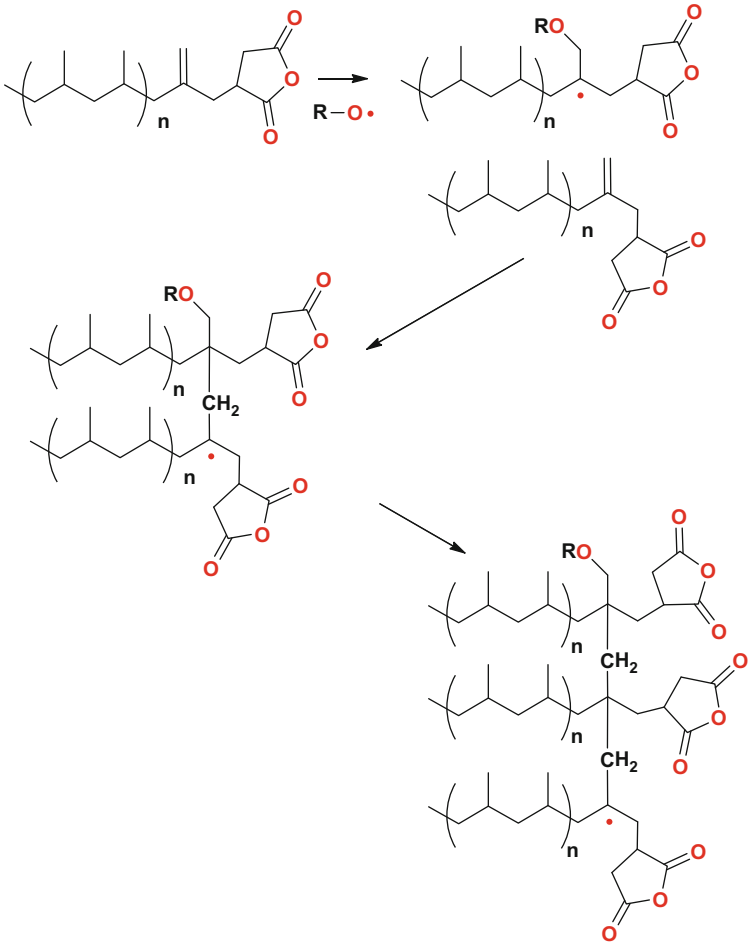

Scheme 2.78 Oligomerization of maleic anhydride/polypropylene ene adduct (Adapted from [182])

It is also known that olefins will form alternating polymers with maleic anhydride in the presence of radicals [1, 3]. This has been shown to happen for polypropylenes prepared via metallocene catalysts. This happens because metallocene catalysts produce polypropylenes that have a single vinylidene group on the end of each molecule. Such polymerization is schematically shown in Scheme 2.79.

As can be seen from the end result shown above where polypropylene chains are joined by succinic anhydride moieties, the molecular weight greatly increases as does the viscosity of the material. Likewise, a number of structural isomers of oligomeric-maleated-polypropylene can be generated, Schemes 2.77–2.79.

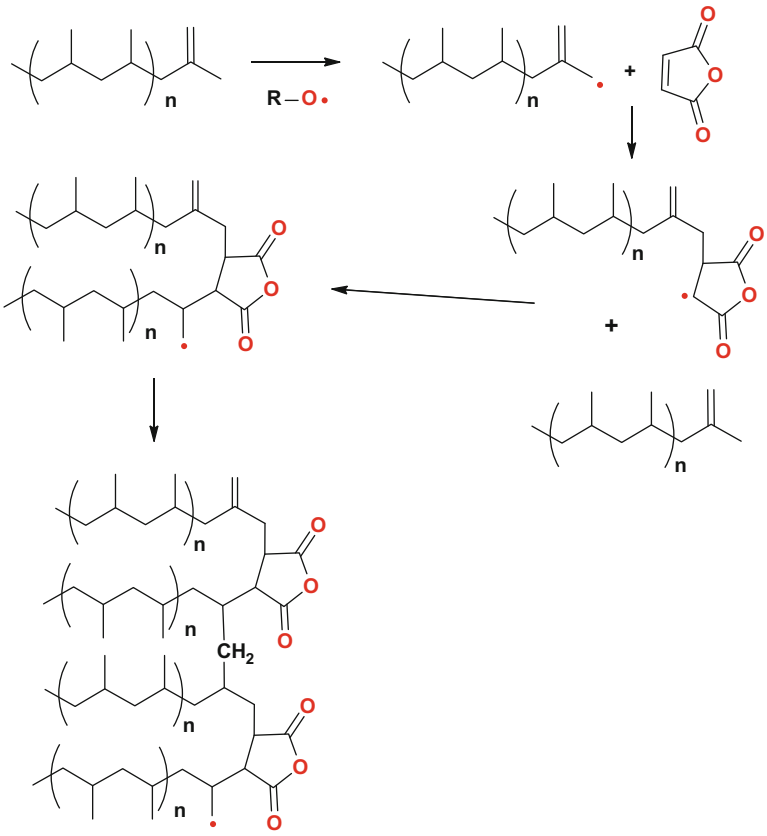

Scheme 2.79 Oligomerization of in situ formed maleic anhydride/polypropylene graft (Adapted from [182])

2.8 Photochemistry of Maleic Anhydride

The photochemistry of maleic anhydride is diverse and highly complex. One of the simplest examples is the photoaddition of maleic anhydride to ethylene. In the first step of the reaction, a $(2\pi + 2\pi)$ photoaddition occurs (Scheme 2.80). According to Woodward–Hoffmann rules, this addition is thermally disallowed, but it is photochemically allowed.

The frontier molecular orbital argument is that the LUMO and the HOMO of ethylene are phase mismatched to maleic anhydride and cycloaddition is symmetry forbidden. But a photon promotes one of the electrons into the LUMO making a transient diradical species. The excited state HOMO is now phase matched to combine with the LUMO, and cycloaddition is symmetry allowed.

Maleic anhydride is also known to form two different classes of adducts with benzene versus alkylbenzenes, depending on the conditions of excitation. At reflux temperatures, in the presence of catalytic amounts of peroxides, adducts of Type-I

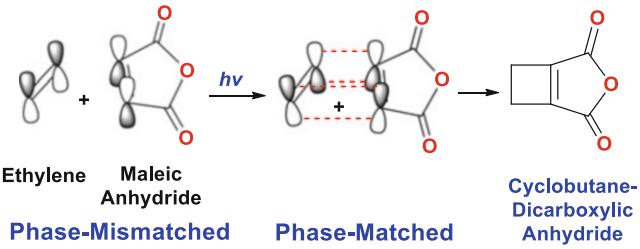

Scheme 2.80 Photo-cycloaddition of ethylene with maleic anhydride

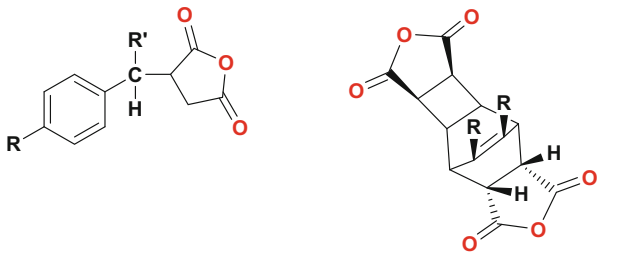

Fig. 2.19 Photochemical reactions yielding Type-I and Type-II structures

are formed (Fig. 2.19) [183, 184]. A free-radical chain reaction is thought to be involved via abstraction of the benzylic hydrogen, and then a oligomerization/polymerization ensues. The oligomeric chain-length based on the ratio of product to peroxide varied from 20 to 100.

In contrast, at 25–35 °C and in the presence of UV radiation, Type-II adducts are formed instead (Fig. 2.19) [185–190]. Excited aromatic molecules or charge-transfer complexes are thought to be involved as the reaction intermediates. This addition reaction is sensitized by addition of benzophenone, which accelerates the rate of reaction, but not required for the reaction to proceed. It appears that benzophenone is essential if only sunlight is used as the source of radiation [191].

Interestingly, benzene adducts of maleic anhydride form readily, while alkyl-substituted-benzene adducts are sluggish and only partially react as poly-maleic anhydride oligomers are formed as the major reaction product under Type-II reaction conditions. Type-II adducts were also formed under gamma radiation but only 4 % incorporation of maleic anhydride occurred [192]. The main product was a mixture of poly-maleic anhydride oligomers.

The photoaddition of maleic anhydride to benzene generates a very stable 2:1 adduct (II) formed in a formal sense by an exo-1,2- and endo-1,4-additions (Scheme 2.81) [190]. Note that it is also aromatic too.

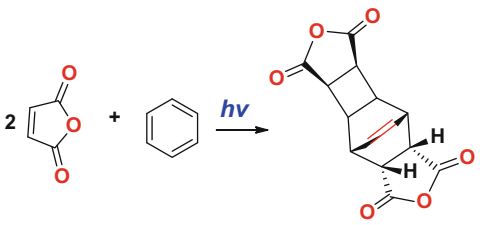

Scheme 2.81 Photochemistry of maleic anhydride in benzene

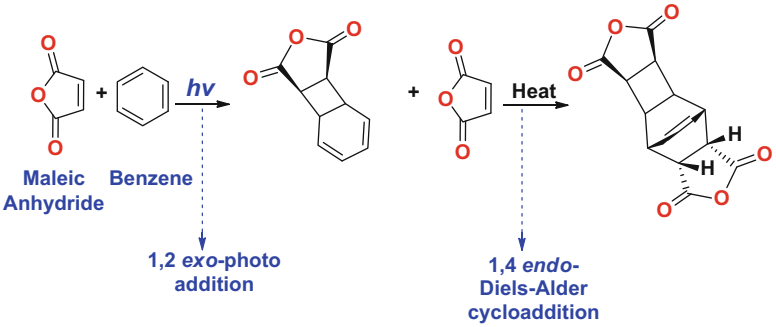

Scheme 2.82 Reaction sequence of photochemical/Diels–Alder reactions for maleic anhydride in benzene

The reaction sequence is believed to follow a (2+2)-1,2-photochemical exo-cycloaddition, followed by a (4+2)-1,4-Diels–Alder endo-cycloaddition reaction, as summarized in Scheme 2.82. The finding of a 1,2-exo-photocycloaddition is surprising rather than the exo-2,3-addition which would be expected on purely steric grounds. It is both the stereospecific orientation of the donor–acceptor charge-transfer complex that is formed, along with the steric factors involved that account for this result.

Reactions of this type have been shown to involve charge-transfer excitation within a weak complex formed between the reactants in the first step of this photoaddition reaction [183, 192]. Relatively electrophilic benzene derivatives such as benzonitrile or nitrobenzene show no such excitation with maleic anhydride and do not photoadd to these types of molecules [193]. It is readily apparent that in the maleic anhydride-benzene versus alkyl-benzene reactions, two types of reactions are prevalent, one by free-radical processes yielding oligomeric compounds. The other involves excited molecules or charge-transfer complexes forming monomeric Type-II adducts.

2.8.1 Photodimerization of Maleic Anhydride

Photodimerization of maleic anhydride has been well known since the early 1960s. The process for the preparation of the di-anhydride by dimerizing maleic anhydride

by subjecting a solid-state layer of maleic anhydride directly to light having a wave length between about 175 and 400 nm, and can be photosensitized with benzophenone [194]. Like the photo-adduct of maleic anhydride with benzene, the (2+2) exo-photocycloaddition was obtained. The maleic rings are in the *trans*-orientation to the cyclobutane ring, as presented in Scheme 2.83.

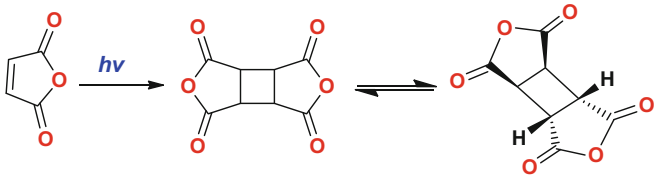

Scheme 2.83 Photodimerization of maleic anhydride in the solid state

2.8.2 *Photochemistry of Maleimide*

Maleimide behaves similarly to maleic anhydride with respect to photocycloadditions with itself and with benzene (Schemes 2.84 and 2.85, respectively) [195]. But unlike maleic anhydride, maleimides readily photopolymerize. Bis-maleimides are also useful photo-cross-linkers. In fact, photopolymerizations can be carried out in both the liquid and the solid state [196].

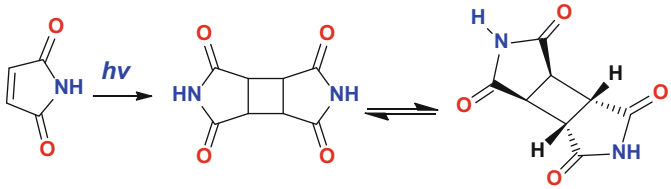

Scheme 2.84 Photodimerization of maleimide in the solid state

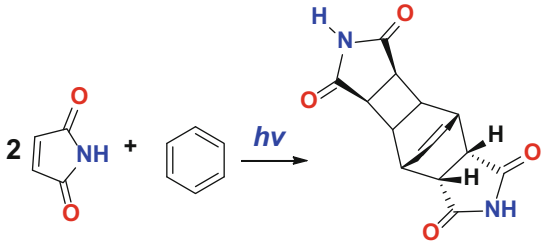

Scheme 2.85 Photochemistry of maleimide in benzene

2.8.3 *Photoinitiation and Photopolymerization of Maleimide*

Photo-induced free-radical polymerization of N-substituted maleimides with vinyl ethers has been extensively studied [197–199]. These UV curable systems do not require any external photoinitiator and are not susceptible to oxygen inhibition enabling polymerization in air. The mechanism of initiation in the case of maleimide/vinyl ether system involves an electron transfer followed by a proton transfer. It was found that the rate of polymerization and degree of conversion are highly dependent on presence of labile hydrogens [197]. Mechanistically this can be summarized by Scheme 2.86.

The first step involves excitation of maleimide by 308 nm laser, since maleimide has two lambda maxima at 260 nm and 320 nm. This results in the formation of a diradical species as depicted in Scheme 2.86 structure-A. Resonance stabilizes this

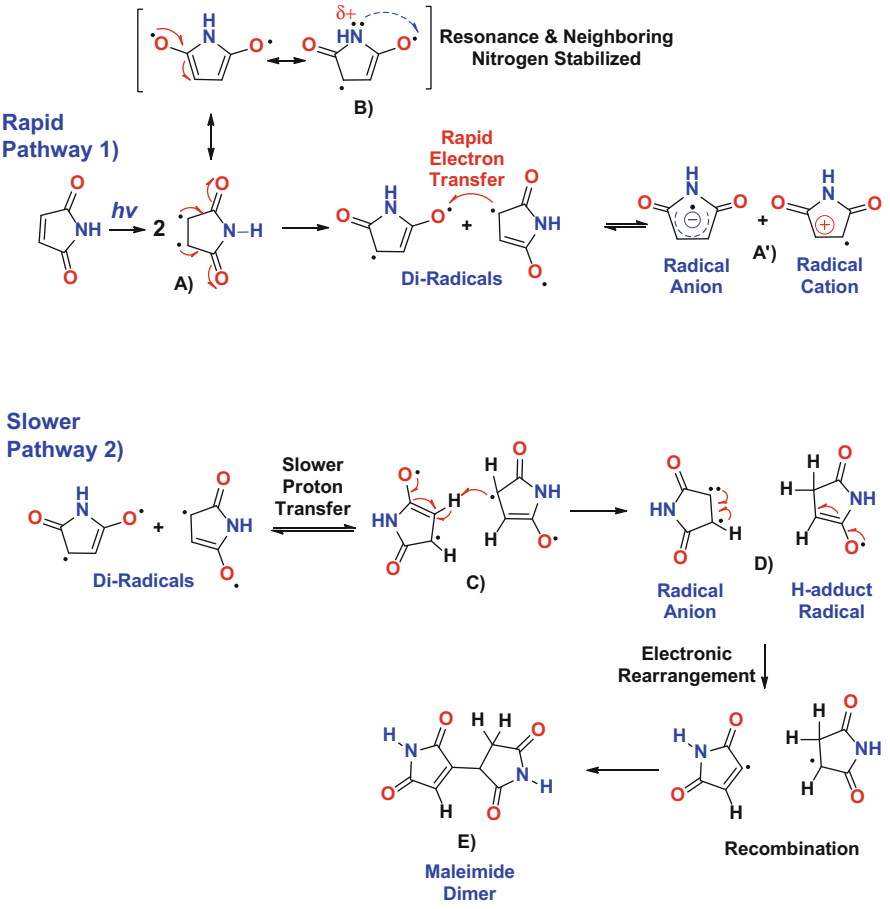

Scheme 2.86 Photoinitiation by maleimide in water or monomer

diradical across six atoms onto the carbonyl-oxygen atoms, shown in Scheme 2.86 structure-B, thereby lowering the activation energy needed to achieve this transient intermediate. The combination of the nitrogen's lone-pair electrons and nitrogen's electronegativity allows these electrons to stabilize the oxygen diradical illustrated in Scheme 2.86 structure-B.

Once the diradical is formed, there are two potential directions for the cyclic pathway to proceed. The most rapid pathway is an electron-transfer event with maleimide itself, forming a radical anion and radical cation pair (Scheme 2.86 structure-A′). Chain-transfer solvents or other monomers that may be present can also have an effect. The radical anion was definitively observed in this reaction as observed by electron-spin resonance (ESR) results [200]. The radical cation rapidly isomerizes to generate a neutral radical and a proton (Scheme 2.86 structure-A′).

Meanwhile, the oxygen diradical can proceed along the slower pathway to generate the H-adduct radical by hydrogen abstraction from another oxygen diradical as shown in Scheme 2.86 structure-C, or from other chain-transfer agents that may be present. The H-adduct radical was also definitively observed in this reaction as observed by ESR experiments [200]. Note that formation of this H-adduct radical is accompanied by the formation of another molecule of radical anion too.

This anion can further propagate the radical polymerization, or it can recombine with the proton released from the radical cation to generate another molecule of neutral radical. The lack of observable neutral radicals in this study may suggest rapid dimerization to generate maleimide dimers (Scheme 2.86 structure-E). There are multiple radical species that can easily be formed from maleimide for free-radical polymerization to occur by this photoinitiator-free system.

Similarly, the photocyclodimerization of bis-maleimides can be carried out under the influence of ultraviolet radiation. These reactions can be activated by adding to the solution sensitizing agents, such as carbonyl-containing aromatic compounds, (e.g., benzophenone or Michler's ketone). The concentration of the bis-maleimides in the solvent may vary widely. However, the best results are obtained with approximately 5-to-10 moles of bis-maleimide per liter of solvent used. ln this case, the concentration of the sensitizing agent averages 50 moles per liter. While irradiation of the bis-maleimides may be carried out with a high-pressure mercury vapor lamp or any other light source emitting in the range of 300–400 nm [201–205], their usefulness will extend well into the future.

References

1. Trivedi BC, Culbertson BM (1982) Maleic anhydride. Plenum, New York
2. Marsh RE, Ubell E, Wilcox HE (1962) Acta Crystallogr 15:35
3. Felthouse TR, Burnett JC, Horell B, Mummey M, Kuo Y (2001) Kirk Online. Wiley Interscience, New York, pp 1–58
4. Considine G (ed) (2006) Van Nostrand's scientific encyclopedia. Wiley, New York

5. Pohanish RP (ed) (2012) Sittig's handbook of toxic and hazardous chemicals and carcinogens, 6th edn. Elsevier, Oxford, UK
6. Acton QA (ed) (2013) Anhydrides-advances in research and application. Scholarly Editions, Atlanta, GA
7. Bednowitz AL, Post B (1966) Acta Crystallogr 21:566
8. Bodewig C (1881) Z Kristallogr 5:559–560
9. Yardley K (1925) J Chem Soc Trans 1:2207–2219
10. Lonsdale K (1939) Proc R Soc Lond Ser A 171:541–568
11. Shahat M (1952) Acta Crystallogr 5:763–768
12. Williams JGB (1974) Acta Crystallogr B Struct Crystallogr Cryst Chem 30:1249–1257
13. Day GM, Trask AV, Motherwell WDS, Jones W (2006) Chem Commun 1:54
14. Back RA, Parsons JM (2011) Can J Chem 59(9):1342
15. Swern D (1957) In: Adams R (ed) Organic reactions, vol 7. Wiley, New York, p 378
16. White RW, Emmons WD (1962) Tetrahedron 17:31
17. Saotome M, Itoh Y, Terashi M (1973) Japan Kokai 73:38435
18. Saotome M, Itoh Y, Terashi M (1973) Japan Kokai 73:39436
19. White RW, Emmons WD (1965) UK Patent No. GB-986,058
20. Pechmann HV (1882) Ber Dtsch Chem Ges 15:881
21. Pets AG (1964) In: Olah G (ed) Friedel-Crafts and related reactions, vol 3. Wiley, New York
22. Aslan T, Ozarslan AE, Ridvanoglu N, Sahbaz F, Yurdakul A (2005) EP Patent 1513868
23. Li H, Chen H, Shen Z, Lin S (2002) Polymer 43:5455
24. Cutter LA, Nunn RE (1979) US Patent 4,145,375A
25. Winey DA (1979) US Patent 4,148,987A
26. Okudan A, Baktir S, Sagdic A (2013) Adv Polym Technol 32:E451
27. Relles HM (1974) US Patent 3,810,913
28. Brotherton TK (1967) US Patent 3,337,662
29. Dean JA (ed) (1992) Langes handbook of chemistry, 14th edn. McGraw-Hill Book, New York
30. Roedig A, Bernemann P (1956) Liebigs Ann Chem 600:1
31. Maahs G (1964) Angew Chem Int Ed Engl 3:316
32. O'Niel MJ (ed) (2013) Merck Index, 15th edn. RSC Publishing, Cambridge, UK
33. Temple J (1929) J Am Chem Soc 51(6):1754
34. Pomogailo AD, Dzhardimalieva GI, Kestelman VN (eds) (2010) Macromolecular metal carboxylates and their nanocomposites, Chap 4.2.1, Springer series in material science, vol 138. Springer, Berlin
35. Prasad R, Kumar S, Kumar A (2005) J Therm Anal Calorim 81:441
36. (2005) Kirk-Othmer encyclopedia of chemical technology, vol 15, 5th edn. Wiley, Hoboken, NJ, pp 1–49
37. (2012) Ullmann's encyclopedia of industrial chemistry, vol 22. Wiley-VCH, Weinheim, pp 145–155
38. Lange N, Sinks M (1930) J Am Chem Soc 1:2602–2604
39. Burnop VC (1963) UK Patent No. GB-933,102
40. Harrison IT, Harrison S (1971) Compendium of organic synthetic methods, vol 1. Wiley-Interscience, New York
41. Harrison IT, Harrison S (1974) Compendium of organic synthetic methods, vol 2. Wiley-Interscience, New York
42. Hegedus LS, Wade L (1977) Compendium of organic synthetic methods, vol 3. Wiley-Interscience, New York
43. Nakashima S et al (1989) US Patent 4,833,267
44. Bhagade SS, Nageshwar GD (1978) Chem Petro-Chem J 9(7):3
45. Pietrzyk DJ (1990) Chromatogr Sci 47:585

46. Bartoli G, Bosco M, Carlone A, Dalpozzo R, Marcantoni E, Melchiorre P, Sambri L (2007) Synthesis 22:3489
47. Robert C, de Montigny F, Thomas CM (2011) Nat Commun 2:586
48. DiCiccio AM, Coates GW (2011) J Am Chem Soc 133:10724
49. Gomzi Z, Zrncevic S (1980) Croat Chem Acta 53(1):25
50. (1989) Chem Abstr 110:137443f
51. Wilmott M et al (1990) World Patent WO-9,008,121
52. Vera-Castaneda E et al (1987) US Patent 4,740,272-A
53. Sogah DY et al (1987) Macromolecules 20:1473
54. Horsley LH (1973) In: Gould RF (ed) Azeotropic data-III. American Chemical Society, Washington, DC
55. Konen JC, Clocker ET, Cox RP (1945) Oil Soap 22:57
56. Thielpape E, Flude A (1454) Chem Ber B66:1454
57. Dmuchovsky B, Vineyard BD, Zienty FB (1964) J Am Chem Soc 86:2874
58. Sanders GC, Duchateau R, Lin CY, Coote MI (2012) Macromolecules 45:5923
59. Kosmin M, Butler JM (1952) US Patent 2,610,202
60. Coleman LE, Bork JF, Dunn H (1959) J Org Chem 24:135
61. Mizzoni RH, Spoerri PE (1951) J Am Chem Soc 73:1873
62. Tawney PO, Snyder RH, Bryan CE, Congr RP, Dovell FS, Kelly RJ, Stitler CH (1960) J Org Chem 25:56
63. Deshpande SR, Maybhate SP, Likhite AP, Chaudhary PM (2010) Indian J Chem 49B:487
64. Doi S, Takayanagi Y (1989) US Patent 4,812,579
65. Parsons CF (1989) US Patent 5,115,061A
66. Musa OM (2008) US Patent 7,456,280
67. Dershem S (2011) US Patent 8,043,534 B2
68. Synder RH (1955) US Patent 2,717,908
69. Synder RH (1957) US Patent 2,788,349
70. Swartz DA (2008) US Patent 7,462,689 B2
71. Allen BB, Wyatt B, Henze HR (1939) J Am Chem Soc 61:843
72. Freudenberger D, Wunder F, Fernoltz H (1978) (Hoechest) US Patent 4,096,156
73. Schwenk E, Papa D, Witman B, Ginsberg HF (1944) J Org Chem 9:175
74. Gao S, Tian W, Shi L (2012) Trans Met Chem 37:757
75. Li J, Tian WP, Shi L (2011) Catal Lett 141:565
76. Brownstein AM (1991) Chem Tech 21:506
77. Castiglioni GL, Ferrari M, Guercio A, Vaccari A, Lancia R, Furnagalli C (1996) Catal Today 27:181
78. Lancia R, Vaccari A, Fumagalli C, Armbruster E (1977) US Patent 5,698,713
79. Thomas WD, Taylor PD, Tomfohrde HF (1992) US Patent 5,149, 836
80. Thakur DS, Roberts BR, Sullivan TJ, Vichek AL (1992) US Patent 5,155,086
81. Wegman RW, Bryant DR (1993) US Patent 5,191,091
82. Bjornson G, Sturk J (1992) US Patent 5,086,030
83. Hara Y, Kusaka H, Inagaki H, Takahashi K, Wada K (2000) J Catal 194:188
84. Liu P, Liu Y, Yin YQ (1999) J Mol Catal A 138:129
85. Yuan HJ, Zhang C, Huo W, Ning C, Tang Y, Yi Z, Cong D, Zhang W, Luo J, Li S, Wang Z (2014) J Chem Sci 1:141
86. Pillai UR, Demessie ES, Young D (2003) Appl Catal B Environ 43:131
87. Li J, Tian WP, Wang X, Shi L (2011) Chem Eng J 175:417
88. Zhang RC, Yin HB, Zhang DZ, Qi L, Lu HH (2008) Chem Eng J 140:488
89. Yu Y, Guo YL, Zhan WC, Guo Y, Wang YQ (2011) J Mol Catal A Chem 337:77
90. Herrmann U, Emig G (1998) Ind Eng Chem Res 37:759
91. Lu WJ, Lu GZ, Guo Y, Guo YL, Wang YS (2003) Catal Commun 4:177
92. Wang Q, Cheng HY, Liu RX, Hao JM, Yu YC, Zhao FY (2009) Catal Today 148:368
93. Liu P, Liu Y, Yin Y (1999) J Mol Catal A Chem 138:129

94. Feng YH, Yin HB, Wang AL, Xie T, Jiang TS (2012) Appl Catal A Gen 425:205
95. Meyer CI, Marchi AJ, Monzon A, Garetto TF (2009) Appl Catal A Gen 367:122
96. Bond GC, Phillipson JJ, Wells PB, Winterbottom JM (1966) Trans Faraday Soc 62:443
97. Takahashi R, Elving PJ (1967) Electrochim Acta 12:213
98. Gao Y (2013) US Patent Application 20130134047 A1
99. Brieger G, Neslrick TJ (1974) Chem Rev 74(5):567
100. Vaclavik J, Sot P, Vilhanova B, Pechacek J, Kuzma M, Kacer P (2013) Molecules 18:6804
101. Wu X, Wang C, Xiao J (2010) Platinum Met Rev 54(1):3
102. Kuhn R, Ebel F (1925) Ber Dtsch Chem Ges 58B:919
103. Backvall JE (ed) (2010) Modern oxidation methods, 2nd edn. Weinheim, Wiley-VCH
104. Payne G, Williams P (1959) J Org Chem 24:54
105. Venturello C, Alneri E, Ricci M (1983) J Org Chem 48:3831
106. Sato K, Aoki M, Ogawa M, Hashimoto T, Noyori R (1983) J Org Chem 61:8310
107. Yoshida A, Yoshimura M, Uehara K, Hikichi S, Mizuno N (2006) Angew Chem Int Ed 45:1956
108. Anelli PL, Banfi S, Montanari F, Quici S (1989) J Chem Soc Chem Commun 779
109. Patil AO, Zushma S (2013) US Patent 8,519,057-B2
110. Adkins H, Krsek G (1948) J Am Chem Soc 70:383
111. Umemura S, Ikada Y (1975) Japan Patent 50-101320
112. Dennis AJ, Harrison GE, Wyber JP (1985) European Patent EP0096987 B1
113. Ramsey SH, Schultz RG (1993) US Patent 5,210,295 A
114. Kitahara K (1961) US Patent 2,972,565
115. McKenzie B (1911) J Chem Soc 99:1923
116. Gawron O, Glaid AJ, Fondy TP, Bechtold MM (1962) J Am Chem Soc 84:3877
117. Katakis D, Vrachnou-Astra E, Konstantatos J (1986) J Chem Soc Dalton Trans Inorg Chem 1:1491
118. Johnson CR, Bade TR (1982) J Org Chem 47:1205
119. Clifford AM, Long JR (1947) US Patent 2,425,509
120. Weiss H (1977) J Am Chem Soc 99:1670
121. Chan JW, Hoyle CE, Lowe AB, Bowman M (2010) Macromolecules 43(15):6381
122. Baik W, Yoon CH, Koo S, Kim H, Kim J, Kim J, Hong S (2004) Bull Korean Chem Soc 25 (4):491
123. Kloetzel MC (1948) J Am Chem Soc 70:3571
124. Ballini R, Bosica G, Fiorini D, Righi P (2002) Synthesis 5:681
125. Szilagyi G, Wamhoff H (1974) Acta Chim Acad Sci Hung 82:375
126. Bergmann ED, Ginsburg D, Pappo R (1959) The Michael reaction. In: Adams R (ed) Organic reactions, vol 10. Wiley, New York, p 179
127. Zienty FB, Schleppnik BD, Vineyard (1962) J Org Chem 27:3140
128. Nguyen VG, Alexander M (2012) EP Patent EP2480070 A2
129. Patil HV, Kulkarni RD, Mishra S (2013) Int J Chem Chem Eng 3:69
130. Gusmeroli M, Mormile SM, Gironda R, Mirenna L, Osti S (2004) World Patent WO 2004/103041 A1
131. Rothrock HS (1944) US Patent 2,346,612
132. Mazo GY, Mazo J, Vallino B, Ross RJ (1999) US Patent 5,872,285
133. Hirbrunner P, Berthlet R (1976) US Patent 3,979,449
134. Hasson D, Shemer H, Sher A (2011) Ind Eng Chem Res 50:7601
135. Zahuriaan-Mehr MJ, Pourjavadi A, Salimi H (2009) Poly Avd Technol 20:655
136. Thombre SM, Sarwade BD (2005) J Macromol Sci A 42:1299
137. Boehmke G, Schmitz G (1995) US Patent 5,468,838
138. Fox S, Harada WK (1962) US Patent 3,052,655 A1
139. Saudek V, Drobnik J (1981) Polym Bull 9:473
140. Wolk SK, Swift G, Paik YH, Yocom KM, Smith RL, Simon ES (1994) Macromolecules 27:7613

141. Diels O, Alder K (1929) Chemische Berichte 62(8):2081
142. Woodward RB, Hoffmann R (1965) J Am Chem Soc 87(2):395
143. Hoffmann R, Woodward RB (1965) J Am Chem Soc 87(9):2046
144. Woodward RB, Hoffmann R (1969) Angew Chem Int Ed 8(11):781
145. Craig D, Shipman JJ, Fowler RB (1961) J Am Chem Soc 83(13):2885
146. Houk KN, Lin YT, Brown FK (1986) J Am Chem Soc 108(3):554
147. Gajewski JJ, Peterson KB, Kagel JR (1987) J Am Chem Soc 109(18):5545
148. Bailey ME (1960) US Patent 2,959,599
149. Benedicto A, Novack BM, Grubbs RH (1992) Macromolecules 25:5893
150. Kloetzel MC (1948) Org React 4:1
151. Holmes HL (1948) Org React 4:60
152. Carey FA, Sundberg RJ (2007) Advanced organic chemistry: Part B: Reactions and synthesis, 5th edn. Springer, New York
153. Hyung Woo S (1994) Tetrahedron Lett 35(23):3957
154. Schrock RR, Lewis JJ (1973) J Am Chem Soc 95:4102
155. Houk KN, Luskus LJ (1971) J Am Chem Soc 93(18):4606
156. Fernandez I, Bickelhaupt FM (2014) J Comput Chem 35(5):371
157. Williamson KL, Hsu YFL (1970) J Am Chem Soc 92(25):7385
158. Evans DA, Chapman KT, Bisaha J (1988) J Am Chem Soc 110(4):1238
159. Corey EJ, Loh TP (1991) J Am Chem Soc 113(23):8966
160. Corey EJ, Shibata T, Lee TW (2002) J Am Chem Soc 124(15):3808
161. Ryu DH, Corey EJ (2003) J Am Chem Soc 125(21):6388
162. Johnson JS, Evans DA (2000) Acc Chem Res 33(6):325
163. Ahrendt KA, Borths CJ, MacMillan DWC (2000) J Am Chem Soc 122(17):4243
164. Kobuke Y, Sugimoto T, Furukawa J, Fueno T (1972) J Am Chem Soc 94(10):3633
165. Midland MM, Tramontano A (1978) J Org Chem 43(7):1471
166. Danzig MJ, O'Donnell JL, Bell EW, Cowan JC, Teeter HM (1957) J Am Oil Chem Soc 34:136
167. Teeter HM, O'Donnell JL, Schneider WJ, Gast LE, Danzig MJ (1957) J Org Chem 22:512
168. Miller WR, Cowan JC (1962) J Am Oil Chem Soc 39:380
169. Gast LE, Bell EW, Teeter HM (1956) J Am Oil Chem Soc 33:278
170. Silverstone GA (1968) GB Patent 1,141,690
171. Toseland P, Ord AJL (1967) GB Patent 1,046,207
172. Friedrich JP, Bell EW, Beal RE (1962) J Am Oil Chem Soc 39:420
173. Paderes GD, Jorgensen WL (1992) J Org Chem 57(6):1904
174. Inagaki S, Fujimoto H, Fukui KJ (1976) J Am Chem Soc 41(16):4693
175. Fernandez I, Bickelhaupt FM (2012) J Comput Chem 33(5):509
176. Stephenson LM, Mattern DL (1976) J Org Chem 41(22):3614
177. Thaler WA, Franzus BJ (1964) J Org Chem 29(8):2226
178. Hoffmann HMR (1969) Angew Chem Int Ed 8(8):556
179. Mikami K, Shimizu M (1992) Chem Rev 92(5):1021
180. Oppolzer W, Snieckus V (1978) Angew Chem Int Ed Engl 17(7):476
181. Snider BB (1980) Acc Chem Res 13(11):426
182. Hanna PK, Truong (2009) European Patent EP1805238 A4
183. Biokford WC, Fisher GS, Dollear F, Swift CE (1948) J Oil Chem Soc 25:251
184. Beavers EM (1954) US Patent 2,692,270
185. Bryce-Smith D, Gilbert A (1965) J Chem Soc 1:918
186. Hammond GS, Hardham WH (1963) Proc Chem Soc 1:63
187. Bryce-Smith D, Lodge JE (1962) J Chem Soc 1:2675
188. Groveinstein R, Rao DV, Taylor JW (1961) J Am Chem Soc 83:1705
189. Schenk GO, Steinmetz R (1960) Tetrahedron Lett 21:1
190. Angus HJF, Bryce-Smith D (1960) J Chem Soc 1:4791
191. Vickery B, Gilbert A, Bryce-Smith D (1965) GB Patent 986,348

192. Raciszewski Z (1966) Chem Ind (Lond) 1:418
193. Hardham WH, Hammond GS (1967) J Am Chem Soc 89(13):3200
194. Walter GG (1964) US Patent 3,203,886 A1
195. Shim SC, Pill-Hoon B (1982) Bull Kor Chem Soc 3(3):115
196. Yamada M, Takase I, Koutou N (1968) J Polym Sci B Polym Lett 6(12):883
197. Andersson H, Hult A (1997) J Coat Technol 69(885):91
198. Lee CW, Kim JM, Han DK, Ahn KD (1999) J Macromol Sci A Pure Appl Chem 36(10):1387
199. De Schurijver FC, Smets GJ (1971) US Patent 3,622,321 A1
200. Von Sonntag J, Beckert D, Knolle W, Mehnert R (1999) Radiat Phys Chem 55:609
201. Kohli P, Scranton AB, Blanchard GJ (1998) Macromolecules 31(17):5681
202. Jonsson S, Viswanathan K, Lindgren K, Swami SN, Ng LT (2003) Polym Preprint 44(1):7
203. Kyrides LP (1940) Org Synth 40:51
204. Liwschitz Y, Zilkha A (1955) J Am Chem Soc 77:1265
205. Feuer H, White EH, Wyman JE (1958) J Am Chem Soc 80:3790
206. Tzoganakis C, Vlachopoulos J, Hamielec AE (1988) Chem Eng Prog 1:47
207. Suwanda D, Lew R, Balke ST (1988) J Appl Polym Sci B 35(4):1033

Chapter 3
Vegetable Oil–Maleic Anhydride and Maleimide Derivatives: Syntheses and Properties

Fan Wu and Osama M. Musa

3.1 Syntheses and Properties of Maleic Anhydride Derivatives with Vegetable Oil

The marriage of maleic anhydride and vegetable oils as a unique class of environmentally benign macromonomers and sustainable polymers has attracted a great deal of interests in the last few decades. The rich chemistry and versatile reactivity of maleic anhydride, combined with the biodegradable and renewable nature of vegetable oils, have rendered infinite possibilities for the maleic anhydride–vegetable oil derivatives. This section provides a survey of the recent literatures on the synthetic routes of the various maleic anhydride derivatives based on the reactive sites in the vegetable oil, as well as the properties and applications of these novel macromonomers and polymers.

3.1.1 Introduction on Vegetable Oil

The production of synthetic polymers and chemicals consumes approximately 7 % of the world's fossil fuels, which, based on recent studies, may be depleted in the next 50–100 years [1, 2]. Moreover, petroleum-based materials exert a negative impact on the environment, such as CO_2 emission and pollution caused by improper waste management. Therefore, there is a compelling need for the switch from fossil feedstock to renewable resources for the production of synthetic polymers and chemicals. Vegetable oils from plants (soy, castor, linseed, palm, sunflower, etc.) are the most widely used renewable resource for future bio-based fuels due to their

F. Wu (✉) • O.M. Musa
Ashland, Inc., 1005 Route 202/206, Bridgewater, NJ 08807, USA
e-mail: fanwu@ashland.com

O.M. Musa (ed.), *Handbook of Maleic Anhydride Based Materials*,
DOI 10.1007/978-3-319-29454-4_3

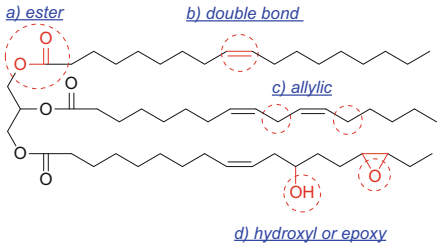

Fig. 3.1 Vegetable oil structure and reactive sites

universal availability, sustainability, inherent biodegradability, minimal toxicity, and low cost. Worldwide vegetable oil production has seen a consistent 4 % annual increase in the past several decades, indicative of the significant growth in industrial use [1].

Vegetable oils are mostly comprised of triglycerides of different fatty acids, with minor amounts of di- and monoglycerides. The properties and the reactivity of the vegetable oils are largely dependent on the structural features of the fatty acids. Most fatty acids are straight chain with an even number of carbons. The C–C double bonds in unsaturated fatty acids typically adopt "cis" configuration. Other functional groups that may be present in vegetable oils are hydroxyl or epoxy groups. Figure 3.1 depicts the structure of a triglyceride and the various reactive sites: (a) the ester group, (b) the double bond, (c) the allylic positions (both monoallylic and bisallylic), and (d) the other functional groups (such as hydroxyl or epoxy).

Vegetable oil can be readily modified to a polymerizable macromonomer and further polymerized to synthesize polymers, such as polyester, polyurethane, polyether, and polyolefin. These vegetable oil macromonomers are suitable for the synthesis of hydrophobic polymer, complementary to other bio-based materials that are naturally hydrophilic, namely, carbohydrates and proteins.

The rich chemistry and versatile reactivity of maleic anhydride make it a prime candidate for the modification of vegetable oils. Esterification reactions occur when the anhydride functionalities react with the ester bond or the hydroxyl groups in the vegetable oil. The ene reaction happens between the double bond in maleic anhydride ("enophile") and the mono- or diallylic protons in vegetable oil ("ene"). The double bond in maleic anhydride can participate in Diels–Alder reaction in the presence of conjugated double bonds in the vegetable oil.

3.1.2 Esterification of Maleic Anhydride with Hydroxyls in the Fatty Acid Chain of Vegetable Oil

Castor oil, as shown in Scheme 3.1, is the triglyceride of ricinoleic acid which is a monounsaturated, 18-carbon fatty acid. Among fatty acids, ricinoleic acid is unusual in that it has a hydroxyl functional group on the 12th carbon. Castor oil is therefore a unique vegetable oil that contains the hydroxyl functionality in the fatty acid chain. This functional group enables the chemical derivatization of castor

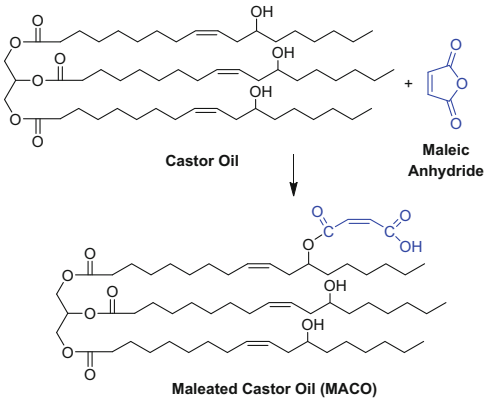

Scheme 3.1 Idealized synthesis of maleated castor oil

oil through esterification of the hydroxyl group to maleated half esters, which is not possible with most other seed oils.

The idealized reaction scheme of castor oil with maleic anhydride in a 1:1 hydroxyl to maleic anhydride stoichiometric ratio is depicted in Scheme 3.1. The esterification reaction can occur without adding catalysts due to the weak acidity of the resulting half carboxylic acid; however, the reaction is extremely slow. Strong inorganic acids, such as HCl, H_2SO_4, or HI, have been used as conventional catalysts to protonate the carbonyl oxygen in maleic anhydride, to promote the nucleophilic attack of the hydroxyl group to ring open, and to yield the half ester more efficiently. The separation and disposal of these inorganic salts resulting from the neutralization of the acid catalysts have raised some environmental concerns. The use of microwave heating as an alternative to catalytic inorganic acids has been reported in literature, with the advantage of reaction rate enhancement due to the higher reaction temperature caused by microwave irradiation. Recently, the kinetics of esterification of castor oil with maleic anhydride was studied using both conventional and microwave heating [3]. The reaction was found to be non-catalytic and first order with respect to each reactant. Activation energy and enthalpy, entropy, and free energy of activation were similar regardless of the heating method. The conclusion of this study suggests that the effects of microwave heating in the maleation of castor oil are mainly thermal effects, and nonthermal effects are not observed.

The uncatalyzed esterification reaction of castor oil with maleic anhydride was carried out at a 1:1 molar ratio of the hydroxyl group to the carboxyl group at 100 °C for 6–8 h [4, 5]. The chemical structure of maleated castor oil (MACO) was characterized by IR spectroscopy, i.e., the decrease of the –OH band at 3400 cm^{-1} and the presence of the C–C double bond at 1657 cm^{-1}. ^1H NMR spectroscopy also confirmed the molar ratio of the reactants and the presence of the C–C double bond. Some physical properties of castor oil (CO) and the synthesized MACO are listed in Table 3.1 [4].

Table 3.1 Physical properties of castor oil (CO) and the maleated castor oil (MACO)

Property	CO	MACO
Appearance	Viscous yellow	Viscous yellow
Specific gravity at 40 °C	0.946	0.983
Acid value (mg KOH/g)	3.1	48.6
Hydroxyl value (mg KOH/g)	164.5	24.4
M_n	854	969
M_w	978	1390
M_w/M_n	1.14	1.43
Viscosity η (cP) at 40 °C	160	600
Electrical conductivity (S/cm) at 40 °C	2×10^{-12}	2×10^{-10}

The electrical properties, such as the permittivity and conductivity, were studied as a function of frequency at various temperatures and are considered to be in the range of electrical insulation. The electrical conductivity, which describes the ionic mobility of the MACO adduct, was found to be 2×10^{-12} S/cm, suggesting potential antistatic applications. The antimicrobial activity toward two soilborne sugar beet pathogens indicated improved antifungal properties by the maleation of the castor oil [4].

Recently, a series of biodegradable plastic foams were prepared by chemical modification of the hydroxyl groups in castor oil with maleic anhydride [6]. The reaction was performed with a 1:2.5 molar ratio of castor oil–maleic anhydride at various temperatures (85–130 °C) for 0.5–9 h without any catalysts. At higher temperature and longer reaction times, it was found that complete esterification of maleic anhydride may occur to form single maleated castor oil (MACO) and dimer/oligomers of MACO as shown in Fig. 3.2. The mixture of complete esterification products was confirmed by multiple peaks in the gel permeation chromatography (GPC) profile. In addition, isomerization of maleate to fumarate (*cis* to *trans* C–C double bond) may occur under prolonged heating conditions. Fumarate has a higher free-radical polymerization reactivity than maleate in the subsequent foaming procedure.

Since maleates or fumarates are unreactive for homopolymerization, the MACO was copolymerized with styrene to form plastic foams through free-radical polymerization. The MACO/styrene ratio and the type of curing initiator were varied in this work, so the mechanical properties of the MACO/styrene foam could be easily tuned. A simplified illustration of the MACO/styrene copolymer structure is shown in Fig. 3.3.

On the whole, the MACO foams synthesized in the above manner are softer and tougher than commercial semirigid polyurethane forms, with comparable compressive stress at 25 % strain. The content of castor oil can be as high as 61 % in this biofriendly plastic foam. The soil burial tests further confirmed that the MACO-based biofoams maintained the biodegradability of the renewable vegetable oil. The diluent monomer styrene, on the other hand, favors the foams with higher compressive stress but slows down the biodegradation.

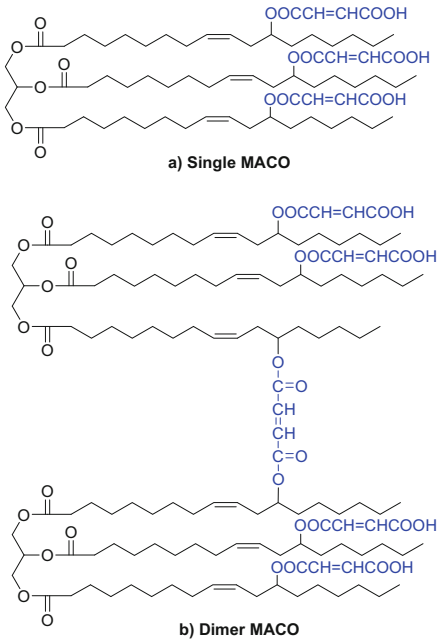

Fig. 3.2 Idealized products of complete esterification of MACO

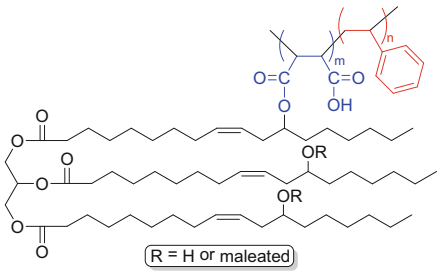

Fig. 3.3 Simplified structure of MACO/styrene copolymer

Furthermore, a macromonomer based on castor oil (*CO*) modified with both maleic anhydride (*MA*) and β-hydroxyethyl acrylate (*HEA*) was synthesized [7]. The half ester *HEA-MA* was first synthesized between maleic anhydride and β-hydroxyethyl acrylate and then further reacted with the hydroxyl groups in the castor oil to yield modified *HEA-MA-CO* (an idealized structure of the macromonomer shown in Fig. 3.4). This macromonomer can be copolymerized with diluent monomer styrene to form novel biodegradable HEAMACO plastic foams. Compared with MACO-based plastic foams, the HEAMACO foam plastics have higher compressive properties, which can be attributed to more reactive acrylate double bonds in the macromonomer and higher cross-link density.

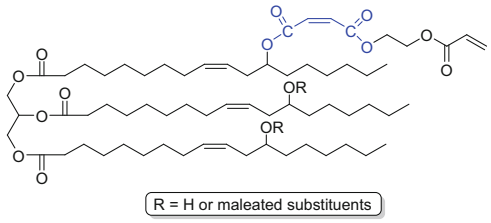

Fig. 3.4 Idealized structure of HEAMACO macromonomer

Flexible polyurethane foams based on maleated castor oil (MACO) were synthesized, and their biodegradation characteristics and mechanisms were studied [8]. The MACO was synthesized without catalysts at 100 °C for 2 h, with 1:1 molar ratio of the maleic anhydride and castor oil. In a single-stage process, the resulting MACO was further mixed with castor oil (at 25:75 or 75:25 weight ratios) and 2,4-toluene diisocyanate (TDI) in stoichiometric amount of OH versus NCO functionalities. There are many reactive sites for this polycondensation reaction. For instance, one of the isocyanate groups in TDI can be added to either the –OH group in the castor oil, or the carboxylic acid groups in the MACO, and the other isocyanate group in TDI can react similarly with another molecule of castor oil or MACO for effective chain propagation and cross-linking. Scheme 3.2 illustrates a simplified reaction scheme of this polycondensation reaction to form MACO-based polyurethane foams.

The polyurethane foam made with higher MACO content (75:25 MACO: CO) exhibited a significant increase in the biodegradation rate. It is hypothesized that the higher content of the ester functionalities in the hydrophilic polymer is more susceptible to enzymatic attack and chemical hydrolysis, thus increasing the degradation rate. The biodegradation mechanism, involving the generation of toxic amines and oligomers with different molecular weights, was proposed and further supported by GC-MS and NMR analysis.

3.1.3 Esterification Reaction of Maleic Anhydride with the Glycerides of Vegetable Oil

Vegetable oils (triglycerides) can readily undergo alcoholysis reaction to form monoglycerides, important chemicals used in the food industry as emulsifiers. Of particular interest is the alcoholysis reaction with glycerol. The general glycerolysis reaction scheme is shown in Scheme 3.3. Both mono- and diglycerides can be formed depending on the stoichiometry of the reactant, and higher content of glycerol favors the formation of monoglycerides. The reaction glycerolysis is generally catalyzed by alkaline solutions at over 200 °C.

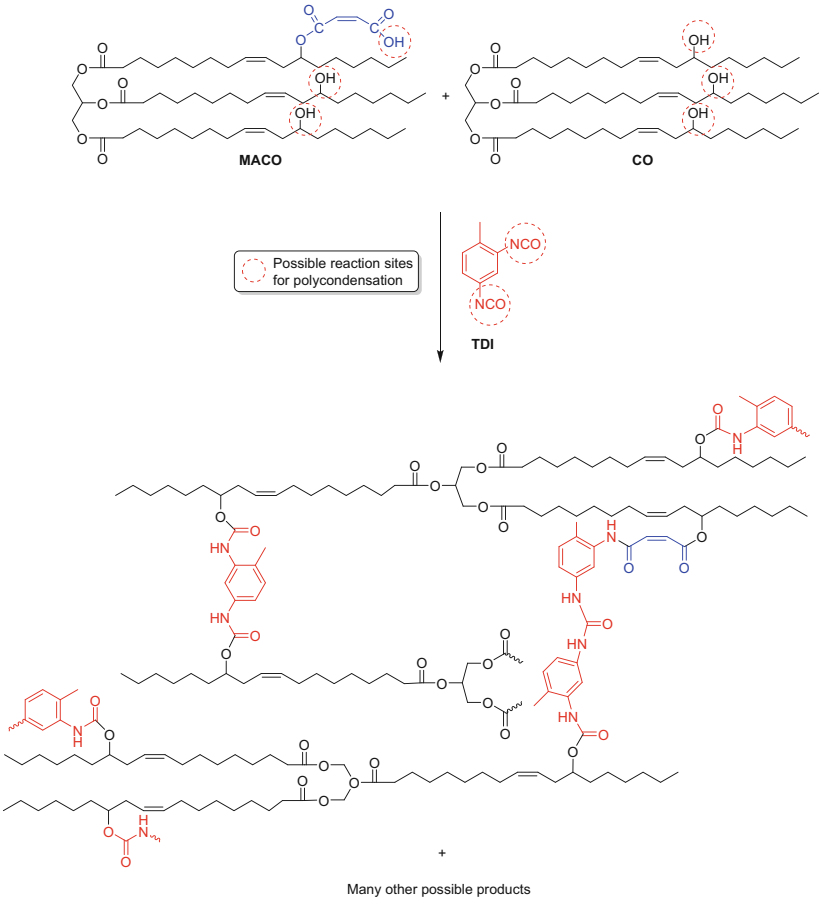

Scheme 3.2 Simplified reaction scheme to form polyurethane based on MACO

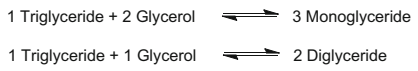

Scheme 3.3 General reaction scheme of glycerolysis of vegetable oil

After glycerolysis, any resulting monoglycerides can be further modified by maleic anhydride to form maleated monoglycerides, with or without catalysts at about 100 °C.

Soybean oil mono- and diglycerides were obtained from the glycerolysis of the cost-effective, biodiesel-derived crude glycerol and further acrylated with maleic anhydride at 80–100 °C [9–11]. The glycerolysis reaction was self-catalyzed since crude glycerol contains alkaline impurities such as sodium hydroxide and sodium methoxide. The maleation reactions were conducted without the use of catalysts or

polymerization inhibitor and afforded over 95 % conversion of the hydroxyl groups and a product with over 1.9 maleates per glyceride molecule. A simplified reaction scheme of the glycerolysis of soybean oil (only soybean oil monoglyceride is shown) and the subsequent maleation reaction is illustrated in Scheme 3.4.

Additionally, the maleated half esters of castor oil were synthesized by the glycerolysis of castor oil or castor oil methyl esters using crude alkaline glycerol. The subsequent maleation of castor oil glycerides were uncatalyzed and afforded 87 % conversion and over 2.6 maleate groups per molecule. An idealized structure of maleated castor oil monoglyceride is shown in Fig. 3.5.

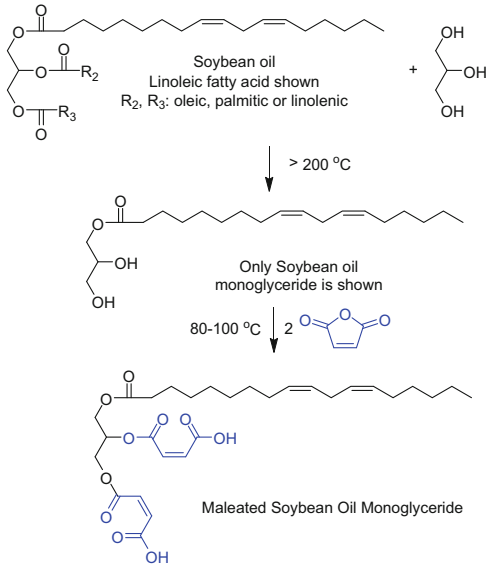

Scheme 3.4 Simplified reaction scheme of glycerolysis and maleation of soybean oil

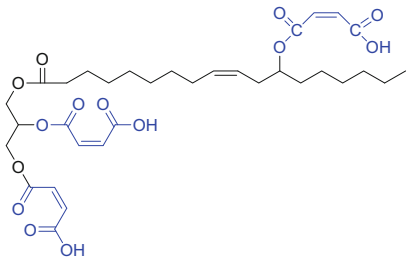

Fig. 3.5 Idealized structure of maleated castor oil monoglyceride

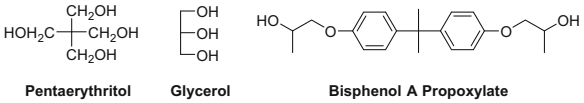

Fig. 3.6 Polyol species used in the alcoholysis of vegetable oils

In other communications, the maleation of soybean oil monoglyceride (SOMG) was performed at 100 °C with several catalysts, such as sodium hydroxide, sulfuric acid, 2-methylimidazole, and *p*-toluenesulfonic acid [12–14]. This work was further extended to other vegetable oils and other polyol species. Both soybean oil (SO) and castor oil (CO) were alcoholyzed with aliphatic and aromatic polyols, such as pentaerythritol (PER), glycerol (GLY), and bisphenol A propoxylate (BPAPR) in Fig. 3.6 [12].

The alcoholysis reactions were carried out at a 1:2 molar ratio (oil–alcohol) at 230–240 °C under N_2 atmosphere for 2 h, in the presence of catalytic amount of Ca $(OH)_2$, to yield the corresponding monoglyceride, as well as the transesterified alcohol. The hydroxyl groups in the alcoholysis products, the monoglyceride, and the transesterified alcohol can both react with maleic anhydride to form the maleated monoglyceride. The maleation reaction was carried out in a large excess of maleic anhydride, at 98 °C for 2–5 h, with 1 % *N*,*N*-dimethylbenzylamine as a catalyst, in the presence of a polymerization inhibitor 0.1 % hydroquinone. A small amount of fumarate may be formed at the maleation step, since the maleate to fumarate isomerization is generally favored at temperatures higher than 160 °C. Idealized alcoholysis reaction of soybean oil with pentaerythritol and subsequent maleation reaction are depicted in Scheme 3.5.

In the case of castor oil, the hydroxyl group in the aliphatic chain also participates in the maleation reaction. The idealized reaction scheme of the castor oil with glycerol followed by maleic anhydride in a molar ratio of 1:2:9 is shown in Scheme 3.6.

Another example of the alcoholysis of castor oil by bisphenol A propoxylate (BPAPR), followed by reaction with maleic anhydride to yield the corresponding macromonomer MA-CO-BPAPR, is exemplified in Scheme 3.7.

The resulting maleated vegetable oil macromonomers, such as MA-SO-PER in Scheme 3.5, MA-CO-GLY in Scheme 3.6, and MA-CO-BPAPR in Scheme 3.7, are solids at room temperature. They can undergo free-radical copolymerization with diluent styrene to yield rigid thermoset polymers (Scheme 3.5). These resins showed viscosity in range to be suitable for liquid molding processes, when the styrene content is fixed at 33 wt%. Table 3.2 listed some of the physical properties of the vegetable oil-based resins with 33 wt% of styrene. The effects the monomer identity and styrene content on the polymerization conversion were also explored.

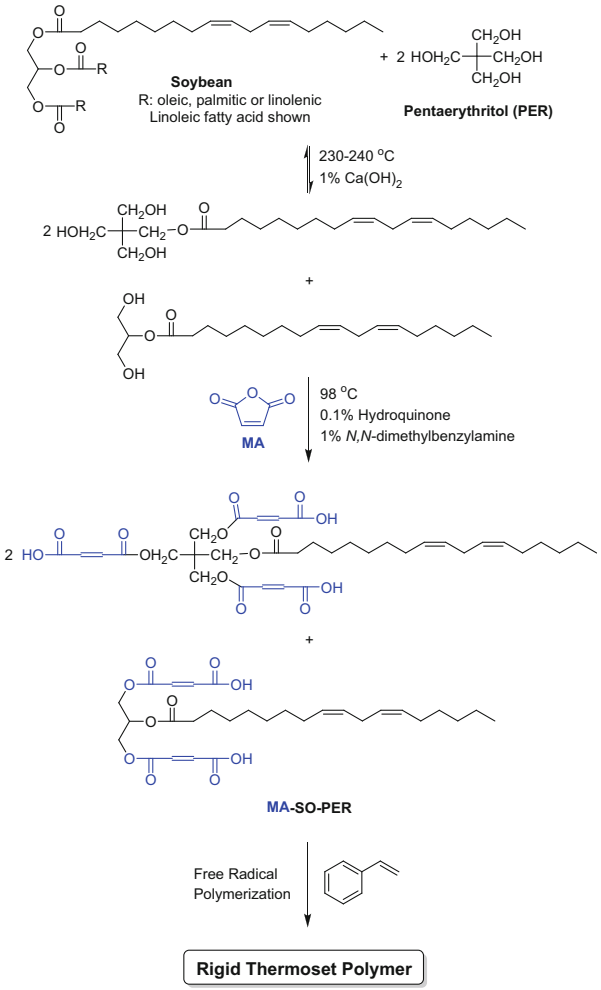

Scheme 3.5 Idealized reaction scheme of alcoholysis and maleation of soybean oil with pentaerythritol

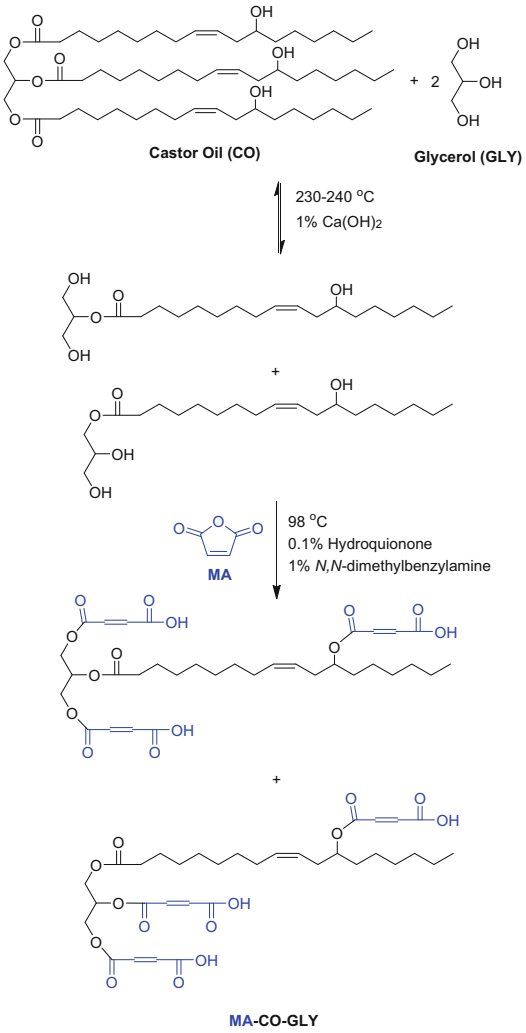

Scheme 3.6 Idealized reaction scheme of alcoholysis and maleation of castor oil with glycerol

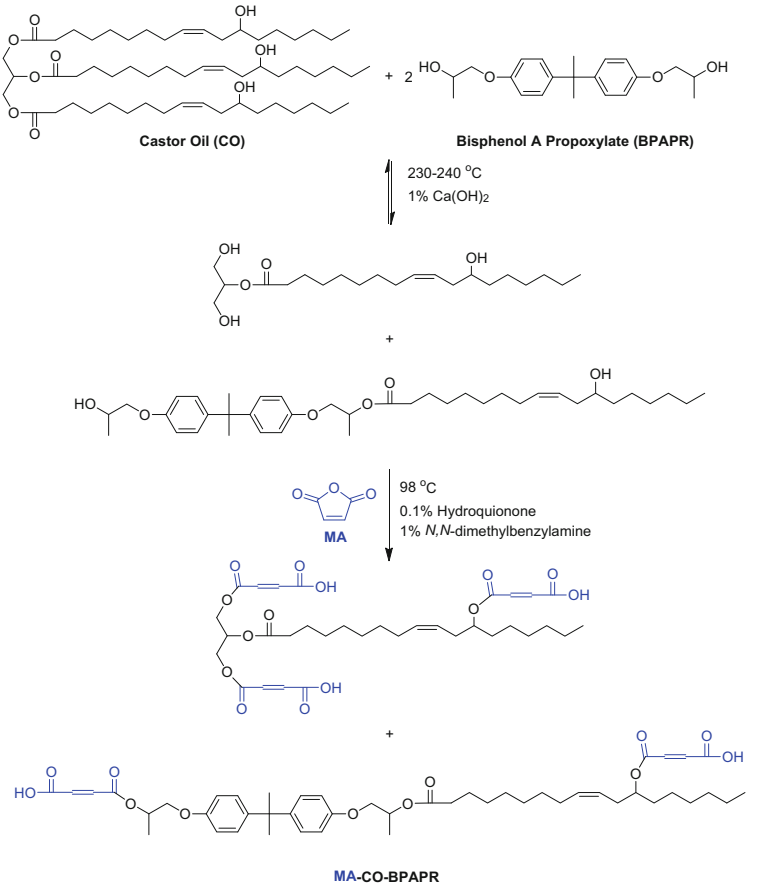

Scheme 3.7 Idealized reaction scheme of alcoholysis and maleation of castor oil with bisphenol A propoxylate

Table 3.2 Physical properties of the vegetable oil-based resins with 33 wt% of styrene

Resin	Specific gravity (g/mL)	Viscosity (cP)	Surface energy (mN/m)
MA-SO-PER	0.94	343	27.38
MA-CO-PER	1.06	363	28.84
MA-CO-GLY	1.04	213	26.36
MA-CO-BPAPR	0.98	183	27.20
MA-CO	0.90	92	26.02

3.1.4 Polyesterification of Maleic Anhydride with the Glycerides of Vegetable Oil

Unsaturated polyesters are an important class of specialty polymers that are used for coatings, paint, insulating, and adhesive materials. They are generally derived from the

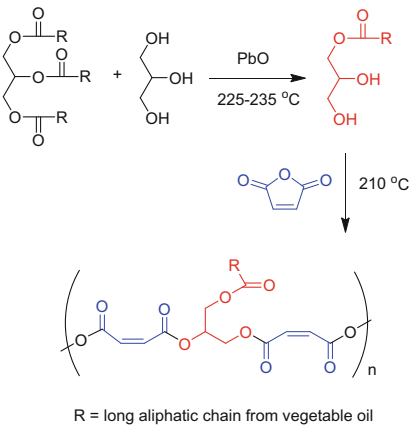

Scheme 3.8 Polycondensation of vegetable oil monoglyceride with maleic anhydride

Fig. 3.7 Yellow oleander (*Thevetia peruviana*) plant, fruit, and seed [15]

polycondensation reactions between a diprotic acid and a polyhydric alcohol. Recently, the use of edible and nonedible vegetable oils and their alcoholysis products (monoglycerides) as polyhydric alcohol have attracted a great deal of research due to the renewability and the biodegradability of the resulting polyester resin, also known as alkyd resin. The most widely used unsaturated diprotic acid in unsaturated polyesters is maleic anhydride, which introduces unsaturated moieties into the polymer that are critical for an efficient curing process. A general scheme of polycondensation of a monoglyceride of vegetable oil and maleic anhydride is shown (Scheme 3.8).

The synthesis and characterization of yellow oleander seed oil-based alkyd resin was recently reported [15]. Yellow oleander (*Thevetia peruviana*), shown in Fig. 3.7, is an evergreen, ornamental, dicotyledonous shrub belonging to the Apocynaceae family. The oil content, extracted with petroleum ether, was found to be over 60 %.

The glycerolysis reaction was carried out with 1:2 molar ratio of the extracted yellow oleander oil and glycerol, in the presence of a catalytic amount of PbO at 230 °C for 1 h. Then the reaction mixture was cooled to 120 °C and mixed with the excess (3 molar equivalents) of acid anhydride (phthalic and maleic anhydride) and glycerol and heated to 210 °C to conduct the polycondensation reaction. The reaction is followed by acid value until it reduced to below 20 mg KOH/g, indicating the completion of the polycondensation reaction. It was reported that the amount of maleic anhydride in the synthesized resin plays an important role in altering the properties of these alkyd resins. The yellow oleander oil can be classified as nondrying oil, and thus the derived alkyd resins were cured by blending with epoxy resin for coating performance. The resins possess gratifying gloss, hardness, adhesion, chemical resistance, and thermal stability which make them suitable for surface coating, as binder for composites, etc.

Similar two-stage glycerolysis–polyesterification reactions were utilized in the synthesis of other alkyd resins based on nonedible, nondrying renewable plant seed oils, such as the Karanja (*Millettia pinnata*) seed oil [16], *Jatropha curcas* seed oil [17], and *Mesua ferrea* seed oil [18]. These plant oils provide renewable sources of raw materials for the production of alkyd resin and subsequent use as coating material.

Over the last decade, poly(ester amide)s with a combination of aliphatic and aromatic moieties have generated significant interest in biomedical and environmental applications due to their apt biodegradability, biocompatibility, and favorable physical properties. These characteristics may be attributed to synergistic properties of the ester and amide linkages in the same polymer network. Vegetable oil-based poly(ester amide) resin can be prepared from the polycondensation of *N*,*N*-bis(2-hydroxyethyl) fatty amides obtained by base-catalyzed aminolysis of various vegetable oils, such as linseed [19], *Pongamia glabra* [20], and *Mesua ferrea* [21], with different dibasic acid moieties such as phthalic, maleic anhydride, tartaric acid, etc.

The synthesis of poly(ester amide) resin from *N*,*N*-bis(2-hydroxyethyl) fatty amides of castor oil was reported in a recent communication [22]. The reaction Scheme 3.9 started with a transesterification of the castor oil with methanol in the presence of sodium methoxide to form the methyl ester of castor oil at almost quantitative yield. Furthermore, the isolated methyl ester was subject to the aminolysis reaction with diethanolamine, catalyzed by sodium methoxide, at 110–115 °C, to afford the diethanol amide of castor oil, at 95 % yield. The polycondensation reaction of the diethanol fatty amide of the castor oil with the maleic/phthalic anhydride and isophthalic acid resulted in the desired poly(ester amide) resin. The formation of ester–amide linkages in the polycondensation reaction was confirmed by the FT-IR study. The hydroxyl group of the diethanol amide reacted with carboxyl ester group of the anhydride and diacid to form the poly(ester amide) resin.

The use of sodium methoxide as polycondensation catalyst improves the polyesterification rate, as compared to conventional catalysts. The anhydrides/diacids were charged in a mole ratio of 30:70 unsaturated (maleic) to saturated (phthalic) to control the gelation. The isophthalic acid moiety in the polymer network is the most hydrophobic and enhances the hydrolytic stability and durability of the resulting resin. On the other hand, the amide moiety with the long hydrocarbon chain introduces flexibility into the structure. Finally, the presence of the aromatic moieties contributes to the thermal stability of the thermosets. The rheological

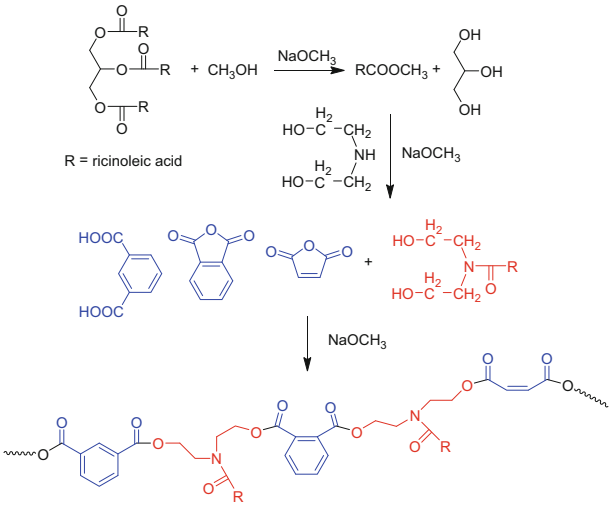

Scheme 3.9 Synthesis of poly(ester amide) resin based on castor oil, diacid/acid anhydride, and diethanolamine

behavior, studied in the steady shear mode, showed shear-thinning behavior of the resin. Various physical properties such as acid value, saponification value, iodine value, specific gravity, and viscosity of the resin were also determined.

This study also showed that the nature of the curing system has a significant effect on the properties of the thermoset. The epoxy–poly(amido amine)-cured thermoset exhibited superior scratch hardness, gloss, chemical resistance, and enhanced thermal behavior than the epoxy–cycloaliphatic amine-cured one. The epoxy–poly(amido amine)-cured thermoset exhibited biodegradation after six weeks of inoculations by broth culture technique using *P. aeruginosa*, thus showing its potential to be explored as biodegradable thin-film material.

Hyper-branched poly(ester amide) was similarly synthesized using *N*,*N*′-bis (2-hydroxyethyl) castor oil fatty amide, maleic/phthalic anhydride/acids as A2 monomer, and diethanol amine (with varying weight percentages) as B3 monomer for hyper-branching [23]. The resulting hyper-branched poly(ester amide) HBPEA was characterized by FT-IR and NMR. It was found that the degree of branching, as well as thermal stability, increases with the amount of B3 monomer. The rheological study revealed differential flow behavior with respect to the degree of branching. The desirable adhesion strength, abrasion resistance, scratch hardness, gloss, impact strength, mechanical properties, renewability, and biodegradability of the HBPEA render it as an advanced surface coating material.

3.1.5 "Ene"-Grafting of Maleic Anhydride onto the Allylic Position in the Fatty Chain of the Vegetable Oil

The ene reaction (also known as the Alder–ene reaction) is a chemical reaction between an alkene with an allylic hydrogen (the ene, vegetable oil and its

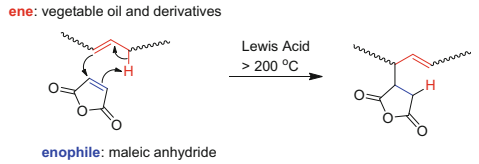

Scheme 3.10 Generalized reaction between maleic anhydride and unsaturated vegetable oils

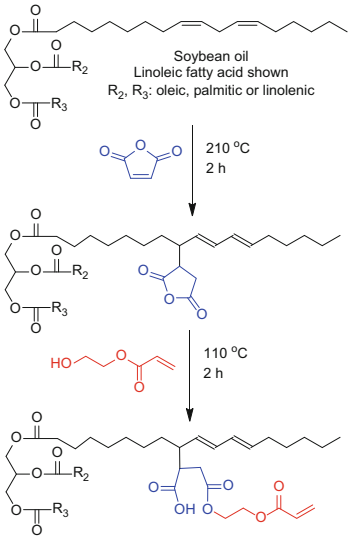

Scheme 3.11 Idealized ene reaction of soybean oil with maleic anhydride and subsequent modification with acrylate monomer

derivatives in this chapter) and a compound containing a multiple bond (the enophile, maleic anhydride in this chapter). During the ene reaction, as shown in Scheme 3.10, a new bond is created between two unsaturated termini, with migration of the ene double bond and transfer of the allylic hydrogen to the enophile. The ene reaction requires a Lewis acid and/or high temperature (>200 °C) to overcome its high activation energy (E_a, >80 kJ/mol). The ene reaction product is also known as an alkenyl succinic anhydride.

A series of vegetable oil macromonomers were synthesized by the ene reaction of unsaturated vegetable oil with maleic anhydride [24]. The grafted anhydride functionality can further react with a hydroxyl, amine, thiol, oxirane, or other functional vinyl monomers to form the corresponding vegetable oil macromonomers. For example, soybean oil was reacted with maleic anhydride at 1:2.5 molar ratio at 210 °C for 2 h to form the maleated soybean oil. The idealized reaction Scheme 3.11 illustrates the ene reaction of soybean oil with maleic anhydride. Please note that only the linoleic acid side chain is depicted for soybean oil, while the other possible fatty acid chains, such as oleic, palmitic, or linolenic acids, are abbreviated as R_2 and R_3 in the scheme.

As shown in the Scheme 3.11, the maleated soybean oil can further react with a functional monomer, such as hydroxyethyl acrylate, to form vegetable oil-based macromonomers. The reaction was carried out at 110 °C for 2 h, in the presence of polymerization inhibitor phenothiazine. Other functional vinyl monomers, such as 2-(*t*-butylamino)ethyl methacrylate, glycidyl (meth)acrylate, allyl amine, hydroxybutyl vinyl ether, can be used to react with the grafted maleic anhydride moieties to form the corresponding macromonomer. Another staged polymerization process to synthesize latex and coating compositions from these macromonomers was reported. In addition, the copolymerization with conventional functionalized monomers in emulsion polymerization process was described to make vinyl copolymers [24].

A variety of performance-boosting UV absorber compounds can be derived from at least one UV absorber having at least one functional group (hydroxyl group, primary amine group, or secondary amine group) and a maleated vegetable oil [25]. The maleated vegetable oil was synthesized based on ene reaction of maleic anhydride and an unsaturated triglyceride, with or without an initiator, such as di-*tert*-butyl peroxide (DTPO). The initiator route can be conducted at a lower temperature (130 °C), as compared to the conventional non-initiator route. Subsequently, one or more UV-A or UV-B absorber, utilizing the hydroxyl or amine functional groups, can be grafted onto the maleated vegetable oil by ring opening of the anhydride functionality. An exemplary reaction between the maleated soybean oil and a UV-A absorber (2-aminobenzophenone) and a UV-B absorber (2-aminobenzoate) is shown in the Scheme 3.12. The reaction was carried out at 130 °C in the presence of DTPO from the maleation step. The anhydride ring opening yielded the half amide–half acid first, and this intermediate may further cyclize to form the imide form. Both the UV-A and the UV-B moiety in the reaction product can be in either form, as illustrated in the Scheme 3.12.

These UV absorber compounds provide better resistance (permanence) and offer broad and customizable UV-A or UV-B spectrum protection. The maleated vegetable oil host exhibits low toxicity, sustainability, and renewability and also contributes to the improved water resistance. The increase in molecular weight of these UV absorbers reduced or essentially eliminated the risk of skin penetration of these compounds, therefore providing formulation flexibility. Remarkably, labile UV absorbers, such as avobenzone, may be stabilized when blended with these UV absorber compounds, thus further increasing their use in personal care, especially sun care, applications.

Other vegetable oil derivatives, such as fatty acids or fatty esters, can also undergo ene reactions with maleic anhydride to form alkenyl succinic anhydrides (ASA).

The ene reaction between n-alkyl (C1 to C5) oleates and maleic anhydride was conducted at 220 °C for 8 h under static nitrogen atmosphere [26]. The reaction products were purified by vacuum distillation and characterized by FT-IR, NMR, and MS. Two isomers, with ene reaction occurring at either C9 or C10 of the alkyl oleate, are formed as shown in Scheme 3.13.

Structure–property relations were established for viscosity, m.p., and density. The combination of a long hydrophobic chain and a highly polar group with density values close to that of water implied good emulsification properties. The grafting of maleic anhydride afforded ASA with low melting temperatures (less than –60 °C)

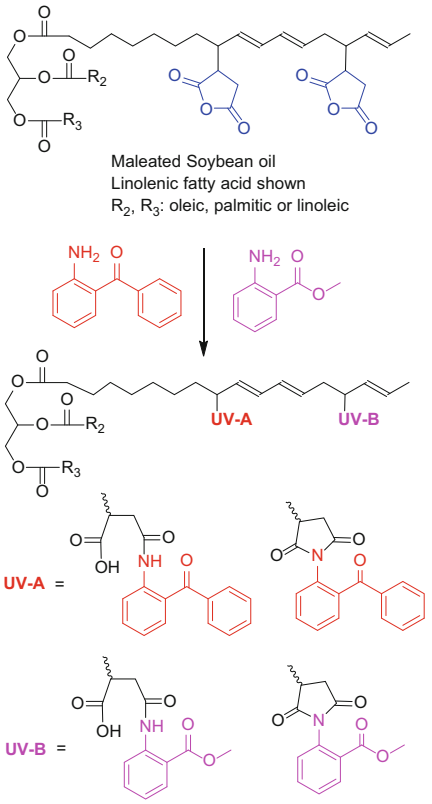

Scheme 3.12 Illustrative synthetic route to UV absorber compounds derived from maleated soybean oil

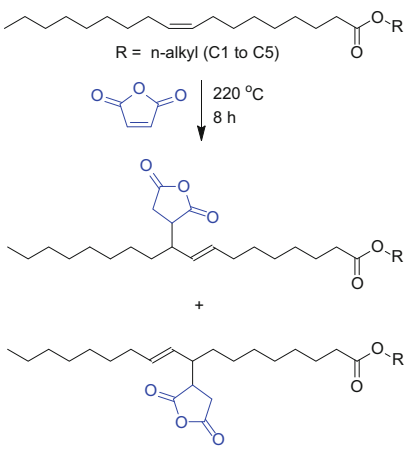

Scheme 3.13 Ene reaction between n-alkyl (C1 to C5) oleates and maleic anhydride

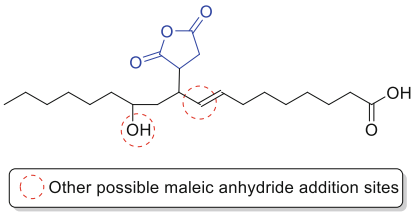

Fig. 3.8 Possible ene adduct of maleic anhydride with ricinoleic acid

and improved stability at high temperatures (greater than 350 °C) under both air and helium, as compared with alkyl oleates. All these properties suggest a strong potential for application in the biolubricant or surfactant fields.

The preparation of the maleic anhydride "ene" adducts with various hydroxyl higher fatty acids, such as ricinoleic acid, 12-hydroxystearic acid, and their oligomers, was reported [27]. The ene reaction, as the unsaturated addition of maleic anhydride at the double bond, was carried out at 160–170 °C for 8 h under partial vacuum at 50 mm Hg. Other maleic anhydride adducts are possible, and one example of the possible "ene" adduct with ricinoleic acid is depicted in Fig. 3.8. This "ene" adduct was isolated by column chromatography and structurally confirmed in this work. The solutions of triethanolamine salts of crude reaction mixture displayed good antirust properties for water-based cutting fluids.

3.1.6 Syntheses of Vegetable Oil-Based Resins Using Maleic Anhydride as Cross-Linking Agent

Maleic anhydride, a polycarboxylic acid (PCA), can be used as a cross-linking agent via ester linkage for polymers that possess hydroxyl functionalities, such as cellulosic polymers. Maleic anhydride reacts initially with the hydroxyl group in the polymer precursor to form a half acid half ester, and the generated half acid can further react with another hydroxyl group from another molecule of the polymer precursor; hence, cross-linking occurs via condensation to form the second ester linkage.

Castor oil contains a hydroxyl group on the 12th carbon of the fatty acid chain. It was recently reported that in the reaction of castor oil with maleic anhydride, cross-linking was observed as an undesirable by-product and was detected by size exclusion chromatography (SEC) [28]. The cross-linking, or the second esterification reaction, occurs at a temperature above 125 °C, while the desired single esterification reaction occurs around 100 °C. The other side reaction is the dehydration and subsequent Diels–Alder reaction, which only occurs at above 150 °C. Accordingly, the reaction was carefully controlled at 100 °C to minimize the cross-linking and Diels–Alder reactions and yielded predominantly the desired half acid, half ester product (see Sect. 3.1.2).

Epoxidized soybean oil can also be cross-linked/cured by maleic anhydride by base-catalyzed ring opening of the oxirane moiety. The cross-linking can be

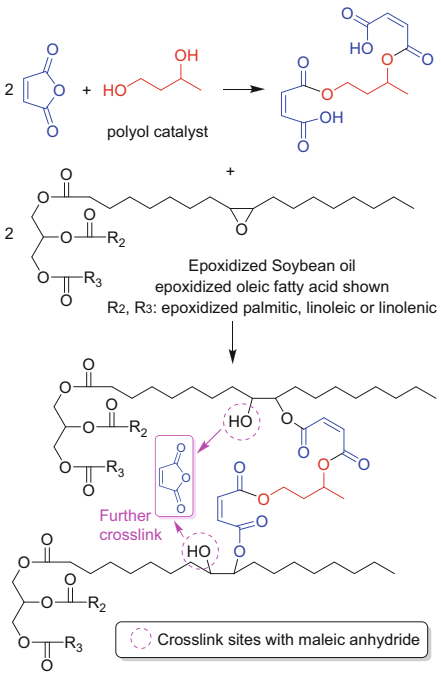

Scheme 3.14 Idealized mechanism for the cross-linking of epoxidized soybean oil via maleic anhydride and catalyzed by 1,3-butanediol

initiated with catalytic amount of a polyol species. An idealized schematic drawing of the maleic anhydride cross-linking of the epoxidized soybean oil, catalyzed by 1,3-butanediol, is shown in Scheme 3.14.

An epoxidized soybean oil (ESO) resin was cured for 5 h with maleic anhydride in the presence of a catalytic amount of 1,3-butanediol and dimethylbenzylamine [29]. Depending on the ratio of ESO versus maleic anhydride, the resin exhibits different mechanical and thermal properties. By using maleic anhydride as a hardener, which is characterized by a relatively low equivalent weight, it is feasible to obtain fully cured materials with a renewable content higher than 60 wt%, which represents values from environment, sustainability, and renewability aspects.

The mechanical and thermal properties of materials prepared by curing epoxidized soybean oil with maleic anhydrides in the presence of catalytic amount of trimethylamine were described in a recent communication [30]. The cross-linking was conducted at the melting temperature of maleic anhydride (53 °C). The cured epoxy resin exhibited thermosetting characteristics, and the study showed the influence of anhydride/epoxy molar ratio and the degree of epoxidation in soybean oil on the mechanical and thermal properties. Cured resins exhibited thermal stability up to 300 °C and were chemically resistant to acid and base solutions.

Polymeric materials from epoxidized vegetable oils, such as epoxidized soybean oil, epoxidized linseed oil (ELO), and different mixtures of the two oils, were recently developed and reported [31]. The curing of the epoxidized vegetable oils

was conducted at 90–115 °C for up to 90 min, with phthalic anhydride (17 mol%) and maleic anhydride (83 mol%) as the cross-linking agents in the presence of benzyl dimethyl amine (BDMA) and ethylene glycol as the catalyst and initiator, respectively. The anhydride-cured epoxy resin showed excellent mechanical properties for use as a green matrix composite.

3.1.7 *Diels–Alder Reaction of Maleic Anhydride with Conjugated Diene in Vegetable Oil*

Maleic anhydride, as a dienophile, can readily react with a conjugated diene or polyene in the fatty acid chain of the vegetable oil to undergo Diels–Alder reaction and yield a cyclohexene derivative. Common vegetable oils with conjugated diene are tung oil and dehydrated castor oil as depicted in Fig. 3.9. Tung oil, a Chinese wood oil, is a major product from the seeds of tung trees. The major component of tung oil is a triglyceride comprised of alpha-eleostearic acid, i.e., *cis*-9, *trans*-11, *trans*-13-octadecatrienoic acid. The major component in dehydrated castor oil is a triglyceride of *cis*-9, *trans*-11, octadecadienoic acid. It is also noted that a competing ene reaction may occur at a higher temperature, in addition to the Diels–Alder reaction. The Diels–Alder reaction for conjugated diene is favored at lower temperature (<150 °C).

The synthesis of the maleated tung oil was conducted at 120 °C for 3 h in the presence of polymerization inhibitor MEHQ and a catalytic amount of stannous octoate [32]. Depending on the molar ratio of the tung oil versus maleic anhydride, either one or two maleic anhydride molecules can be grafted onto one molecular of the tung oil. The final product is obtained as a yellow liquid. The hypothesized reaction Scheme 3.15 (with 1:1 tung oil to maleic anhydride molar ratio) is depicted below with the Diels–Alder reaction occurring with the conjugated double bonds at the 11th and 13th carbon positions of the fatty acid chain in tung oil.

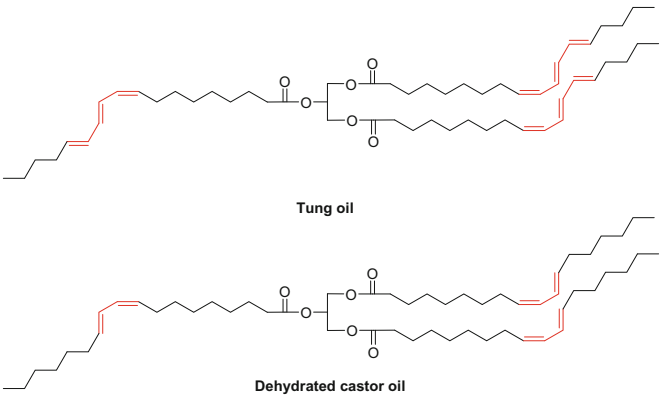

Fig. 3.9 Structures of vegetable oils with conjugated diene

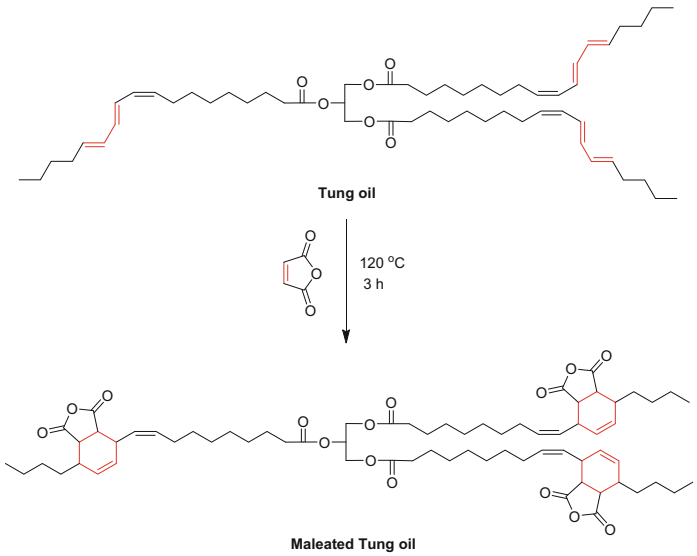

Scheme 3.15 Idealized Diels–Alder reaction of Tung oil with maleic anhydride in 1:1 molar ratio

The synthesized maleated tung oil underwent polycondensation reactions with polyols, such as piperazine-1,4-dicarboxylic acid bis-(2-hydroxy-ethyl) ester (PCD) or isophoronediamine-1,4-dicarboxylic acid bis-(2-hydroxy-ethyl) ester (ICD), to form nonisocyanate polyurethane (NIPD). The NIPD was further modified with glycidyl methacrylate (GMA) to afford a UV-curable tung oil-based resins, implying the potential utilization in UV coatings.

A similar Diels–Alder modification of tung oil with maleic anhydride was performed without catalysts, followed by the free-radical (azobisisobutyronitrile)-initiated grafting of methyl methacrylate, butyl acrylate, and hydroxypropyl acrylate at 80 °C [33]. The hypothesized grafting reaction and the structure of the tung oil grafted, waterborne insulation varnish resin, is shown in Scheme 3.16.

The varnish could be solidified at a relatively low temperature with blocked hexamethylene diisocyanate as a curing agent. As the maleic anhydride content increased, the thermal stability of the film improved. However, the electrical insulation strength, volume resistivity, and surface resistivity decreased. At maleic acid content less than 25 %, the resin showed good potential as an effective immersion insulation varnish for the spindle of electric motor.

The Diels–Alder maleation of a nonconjugated diene in soybean oil was recently reported [34]. The free-radical maleation was conducted in a closed Parr reactor system at elevated temperatures (100–150 °C) and pressures in the presence of a peroxide initiator, such as bis(*tert*-butylperoxy)-2,5-dimethylhexane peroxide (L-101), and di-*tert*-butyl peroxide (DTBP). Such a free-radical maleation process can be completed in as little as 30 min. As illustrated in Scheme 3.17, it was hypothesized that the linoleic moiety (9,12-diene) in soybean oil first undergoes

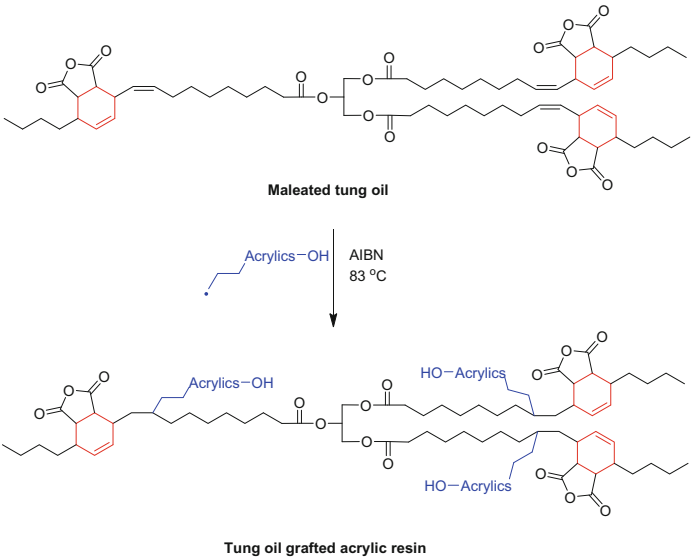

Scheme 3.16 Hypothesized grafting reaction of maleated tung oil with acrylic resins

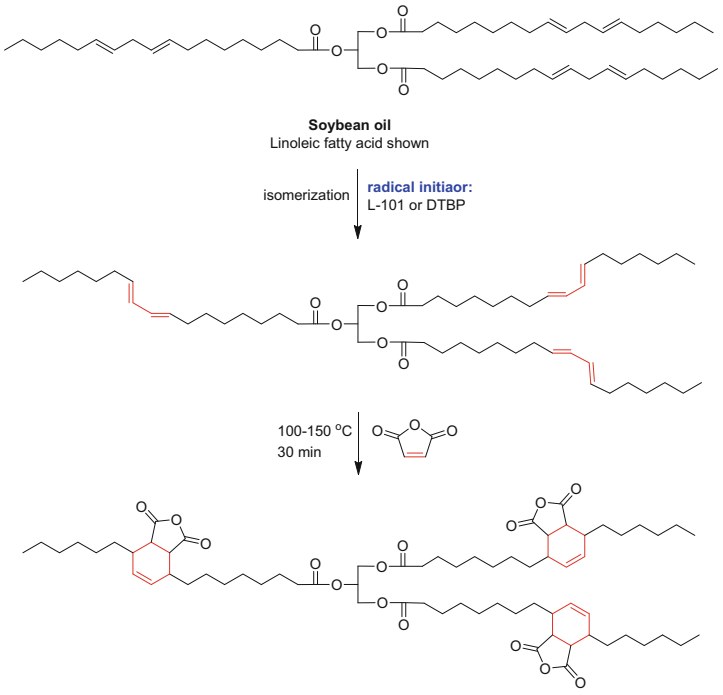

Scheme 3.17 Free-radical-initiated Diels–Alder reaction of soybean oil with maleic anhydride

free-radical-initiated isomerization to form 9,11-conjugated diene, followed by the Diels–Alder reaction with maleic anhydride. It was found that independent of the stoichiometry of the maleic anhydride, reaction temperature, or type of the initiator, the maleic functionality in the final product did not exceed one equivalent. The maleated soybean oil was characterized using acid value, iodine value, and FT-IR. The data strongly suggest that Diels–Alder addition of maleic anhydride is favored when a peroxide initiator is present, while the competing ene reaction is favored in the absence of peroxide initiator, in the presence of Lewis acid catalysts and at higher temperatures (>200 °C).

Similarly, the Diels–Alder maleation reaction of nonconjugated polyunsaturated fatty acid triglycerides, such as soybean oil, was performed [35]. These vegetable oil adducts were made by first conjugating and elaidinizing the nonconjugated polyene fatty acid moiety, such as in linoleic and linolenic acids, in the vegetable oil, followed by Diels–Alder reaction with maleic anhydride in the presence of catalytic amounts of iodine (the conjugation and elaidinization agent). The conjugation, elaidinization, and Diels–Alder reaction can all take place in one step in a sealed, pressurized reaction vessel at 200–250 °C for 4 h. These adducts are an important class of emollients in human skin and hair preparations by providing persistent softening effects.

3.2 Maleimide Derivatives and Their Properties

Maleimides and derivatives are important building blocks in chemical synthesis, and some of them demonstrate biological activity. A special feature of the reactivity of maleimides is their susceptibility to additions across the double bond, either by Michael additions or via Diels–Alder reactions. The carbon–carbon double bond in maleimide is also capable of free-radical or anionic polymerization or copolymerization to produce functional polymers that are utilized in high temperature applications, such as adhesives in the semiconductor industry. Biological applications of maleimide derivatives result from their high and specific reactivity/binding toward the thiol groups in biological substrate (e.g., chemical probes), site-directed modification for proteins and peptides, bioconjugates, and prodrugs.

3.2.1 Recent Advances in the Synthesis of Maleimide Derivatives

The classical synthesis of maleimide derivatives was carried out via a two-step route as illustrated in Scheme 3.18. First, reaction of maleic anhydride with an alkyl or aryl amine readily produces a maleamic acid (maleic acid monoamide) at room temperature. Subsequently, the maleamic acid undergoes dehydration ring-closure/

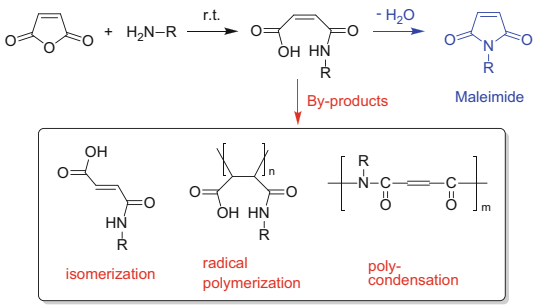

Scheme 3.18 Classical synthesis of maleimide derivatives and possible by-products

cyclization reaction to form the corresponding N-substituted alkyl or aryl maleic maleimide.

The dehydration ring-closure reaction generally requires high temperature heating and/or a stoichiometric amount of acidic dehydrating agent (such as acetic anhydride) and/or water removal via vacuum or azeotropic distillation. However, these classical reaction conditions can cause undesirable effects on the dehydration ring closure, and several by-products may form (Scheme 3.18). The high reaction temperature and long reaction time can cause the isomerization of the maleamic acid to the thermodynamically more stable fumaric analogue, therefore, lowering the yield for the maleimide. In addition, the high temperature may cause other side reactions, such as polymerization to occur. The use of stoichiometric amount of dehydrating agent can be costly for the chemical process and will often require laborious and repetitive workup procedures to purify the final maleimides. The azeotropic distillation often requires a toxic organic solvent, such as toluene or xylene, and is not environmentally benign. Recent advances in the synthesis of maleimide have been focused on the optimization of the synthetic methodologies to improve yield and selectivity, shorten reaction times, and to be more environmentally friendly.

The *N*-arylmaleimide compounds, which are useful as pharmaceutical and agrochemical intermediates and as additives for polymers, were prepared by a method which is less costly and less toxic using cyclohexanone as solvent at 120–155 °C and H_3PO_4 as acid catalysts, with removal of water of reaction by azeotropic distillation with xylene in the presence of diphenylnitrosamine as polymerization inhibitor [36]. It was also reported that the reaction of maleic anhydride with aniline in an aprotic polar solvent (such as *N*-methyl-2-pyrrolidone) in the presence of an acid catalyst (such as sulfuric acid) and azeotropic removal of water yielded *N*-phenylmaleimide (Fig. 3.10) at 97.1 %. Moreover, the sulfuric acid and the *N*-methyl-2-pyrrolidone are recycled and reused [37].

Repetitive washing process can also be eliminated from the synthesis of *N*-methylmaleimide [38, 39]. A mixture of xylene and concentrated sulfuric acid was stirred at 135–140 °C for 30 min with removal of water to produce xylenesulfonic acid, which was subsequently cooled and mixed with maleic anhydride and

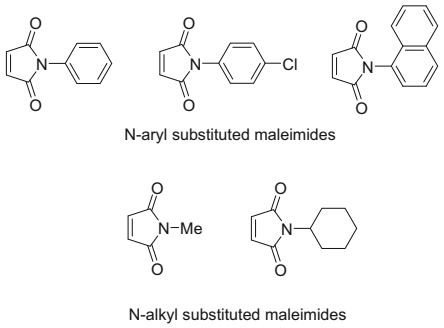

Fig. 3.10 N-substituted maleimide derivatives

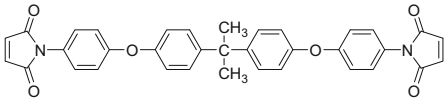

Fig. 3.11 N-substituted bismaleimide

methylamine. The reaction mixture was purified by evaporation of xylene under reduced pressure (40 mmHg) and direct distillation at 10 mmHg to afford *N*-methylmaleimide (Fig. 3.10) at 90.5 % yield. The pot residue left after separation of the *N*-methylmaleimide by distillation was repeatedly used as the dehydration catalyst. This process does not require a procedure for removing the acid catalyst such as water and alkali washing. It allows the easy recovery of the pot residue by dissolving it in an aromatic hydrocarbon solvent, recycles it as the acid catalyst, and gives N-substituted maleimide of high purity in a good yield.

Metal and metal salts, such as copper, tin, iron, and their salts, were used as catalysts or cocatalysts in the dehydration process to improve the reaction selectivity and inhibit the formation of by-products. For instance, a stirred mixture of maleic anhydride, p-toluenesulfonic acid (organic acid catalyst), $CuSO_4$ (metal cocatalyst), and 4-$MeOC_6H_4OH$ (polymerization inhibitor) in toluene/DMF was treated with aniline, refluxed for 3 h, and further purified to afford *N*-phenylmaleimide of 99.9 % purity at 95.4 % yield [40]. Additionally, *N*-phenylmaleimide was prepared at 94.0 % yield by dehydration–imidation of N-substituted maleamic acids in xylene/DMF in the presence of SnO or Sn salts under azeotropic dehydration while feeding maleic anhydride [41]. Similarly, bismaleimide shown in Fig. 3.11 was formed with high selectivity and yield (86.8 %) when $FeCl_3$ was added to the reaction of 2,2-bis-[4-(4-aminophenoxy) phenyl]propane with maleic anhydride in toluene and *N*-methyl-2-pyrrolidone [42].

Haloiminium salts, such as 2-chloro-1,3-dimethylimidazolinium chloride (Fig. 3.12), can be used as dehydrating agents in the reaction of maleic anhydride with NH_2-containing compounds or polymers, or the condensation of maleamic acids, to improve the reaction efficiency [43]. For instance, the condensation

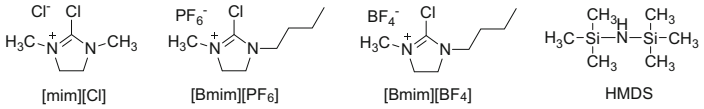

Fig. 3.12 Haloiminium salts and hexamethyldisilazane

reaction of aniline with maleic anhydride can occur at lower temperature (90 °C), shorter reaction time (1 h), and high yield (98.4 %) due to the presence of 2-chloro-1,3-dimethylimidazolinium chloride.

The use of room temperature ionic liquids, such as 1-butyl-3-methylimidazolium hexafluorophosphate [Bmim][PF_6] or tetrafluoroborate [Bmim][BF_4] (Fig. 3.12), have demonstrated reaction rate acceleration and increased yield for the synthesis of maleimides [44]. The *N*-arylmaleimides, such as *N*-phenylmaleimide, *N*-*p*-chlorophenylmaleimide, *N*-(1-Naphthyl)maleimide (Fig. 3.10), etc., were synthesized from maleic anhydride with a variety of primary amines in accelerated reaction time (20 min) and excellent yield (>90 %) when [Bmim][PF_6] or [Bmim][BF_4] was used as the reaction medium. In addition, the ionic liquids can be readily recovered by extraction of the maleimide products and drying the residue under vacuum and reused with no appreciable decrease in yield.

Lewis acids, such zinc halides, in the presence of hexamethyldisilazane (HMDS, shown in Fig. 3.12), prompted the dehydration/cyclization reaction of the maleamic acid to form the corresponding maleimides. A series of aromatic and aliphatic primary amines were reacted with maleic anhydride in refluxing benzene in the presence of a Lewis acid and HMDS and resulted in over 90 % yield of maleimide in 1–4 h of reaction time in most cases [45]. It was hypothesized that the formation of thermodynamically stable hexamethyldisiloxane or trimethylsilanol, alongside maleimide, makes this reaction feasible under mild conditions. This demonstrated an economical and practical method for the synthesis of maleimide derivatives by using inexpensive and readily available reagents under mild conditions.

Heterogeneous ion-exchange resin was used as the catalyst for the manufacturing of N-substituted maleimides by treatment of maleic anhydride with a primary aromatic or aliphatic amine in the presence of an organic solvent and a strongly acidic ion-exchange resin. For example, reaction of maleic anhydride, aniline, and Amberlyst 15 in xylene gave 90.3 % *N*-phenylmaleimide. The resin can be filtered off and reused [46].

Solid acidic heterogeneous catalysts, such as diatomite-supported acid catalyst [47] and phosphoric acid on zirconia [48], were utilized to achieve high production yield with high purity of maleimides. The reaction of maleic anhydride with aniline, catalyzed by the diatomite-supported aniline salt of H_3PO4, occurred at 135 °C for 2 h to give 97.6 % *N*-phenylmaleimide. It was also reported that maleimides (e.g., *N*-cyclohexylmaleimide shown in Fig. 3.10) are prepared at over 90 % by reacting maleic anhydride and primary amine, such as cyclohexylamine at 100–180 °C in xylene and in the presence of a solid, acidic catalyst which consists of an inorganic acid (phosphoric acid) supported on an inorganic metal oxide (zirconia). The solid

catalysts used in these reactions can be readily separated by filtration, washed, and recycled for subsequent use. This synthetic approach provided a low-cost, environmentally friendly, and efficient alternative to the classical synthesis of maleimide.

Microwave-assisted synthesis was reported to provide improvements to the cyclization of maleamic acid to maleimides. A mixture of maleic anhydride and aromatic primary amines undergo solvent-free dehydration in the presence of acetic anhydride under microwave irradiation to afford the corresponding *N*-aryl maleimides in 80–90 % yield within minutes [49].

A new source and reaction scheme to form maleimide, namely, the dehydrochlorination of chlorosuccinimides, appeared in recent literature [50, 51]. A variety of aryl or alkyl α-chlorosuccinimides were formed by the reaction of the corresponding maleamic acid with phosgene ($COCl_2$), followed by dehydrochlorination in the presence of dimethylbenzylamine at 50–70 °C for one hour. The yield of the maleimides under these mild conditions was over 90 %. It was also reported, as depicted in Scheme 3.19, that *N*-aryl-α-chlorosuccinimides are formed by the reaction of maleamic acid with thionyl chloride in refluxing methylene chloride. Subsequent dehydrochlorination with triethylamine at 25 °C produced *N*-aryl-maleimides in excellent yield (>85 %). Moreover, further reduction of the C–C double bond in refluxing acetic acid by zinc hydrogenation catalysts afforded the respective *N*-aryl-succinimides.

Alkylation of maleimide with a variety of alcohols via the Mitsunobu reaction to form the corresponding *N*-alkylmaleimides is a more general and direct synthetic route to maleimides [52]. The Mitsunobu reaction, which utilizes maleimide as a nucleophile, can be carried out under essentially neutral conditions and at ambient temperature and enable the use of alcohols, instead of amines, as the synthetic precursor to the maleimides. As shown in Scheme 3.20, the typical reaction condition involves the overnight reaction of the alcohol and maleimide, in equal molar ratio, in THF in the presence of triphenylphosphine and an azodicarboxylate such as diisopropyl azodicarboxylate (DIAD). The yields were modest, and the

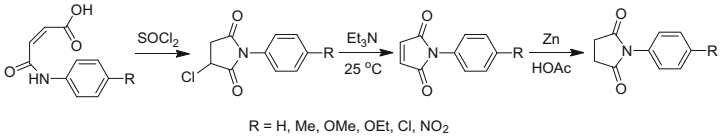

Scheme 3.19 Direct synthesis of maleimides via the dehydrochlorination of chlorosuccinimides

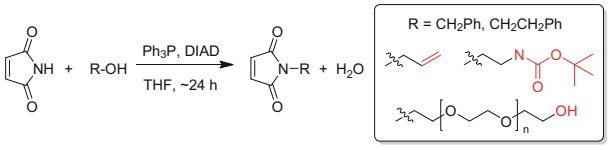

Scheme 3.20 Direct synthesis of N-substituted maleimides via the Mitsunobu reaction

best yield was obtained for primary alcohols with an adjacent SN2 activating group. This reaction is especially useful when the primary alcohol reagent contains another functional group, such as double bond and hydroxyl group, resulting in multifunctional maleimides.

As noted from one of the Mitsunobu reactions in Scheme 3.20, the *tert*-butyloxycarbonyl (*t*-BOC) group is commonly used in the synthesis of N-substituted maleimide derivatives when the substituent contains another functional group, such as hydroxyl or amine. *tert*-Butyloxycarbonyl (*t*-BOC)-protected maleimide monomers were synthesized from the corresponding N-substituted maleimides with di-*t*-butyl dicarbonate (DTBDC) in the presence of pyridine [53]. The deprotection reaction can be catalyzed by acids or initiated by heat, with concurrent evolution of isobutylene and carbon dioxide. Two examples of such protected maleimides with the labile t-BOC group are shown in Scheme 3.21. The polymers originated from these N-protected maleimides are especially interesting in the context of chemically amplified resists, due to the low activation energy and the appreciable change in resist properties displayed in the deprotection process.

Another direct route to *N*-alkyl-maleimides involves the protection of the carbon–carbon double bond via a reversible Diels–Alder reaction with furan, an example of which is displayed in Scheme 3.22. When the alkyl substituent contains a tertiary amine, it may react with the double bond in maleic anhydride via nucleophilic attach, or initiate polymerization. The reversible Diels–Alder reaction

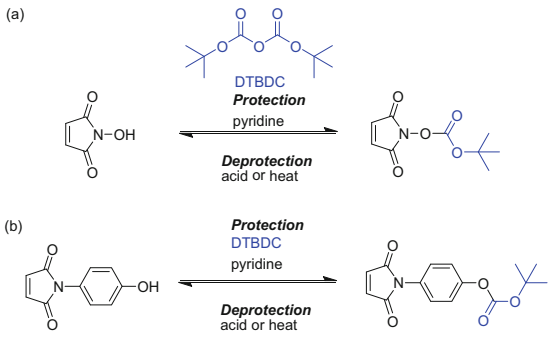

Scheme 3.21 Syntheses of *tert*-butyloxycarbonyl-protected maleimide derivatives

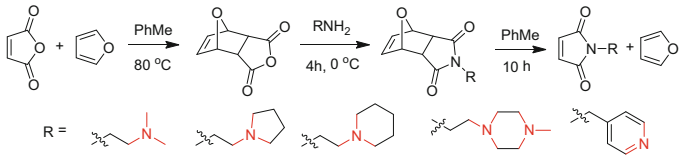

Scheme 3.22 Synthesis of *N*-alkyl-maleimides via the reversible Diels–Alder reaction with furan

with furan protects the double bond and provides a one-step reaction to the maleimide derivative without the use of acid catalysts. Another advantage of this route is the furan-protected maleimide derivatives which are crystalline solids at room temperature and thus facilitate the purification of the final products.

3.2.2 *Syntheses of Novel Maleimide Derivatives and Their Uses*

A novel electron-deficient semiconductor family for organic thin-film transistors (OTFT), based on core-unsubstituted (R′=H) and core-cyanated (R′= CN) anthracenedicarboximides as shown in Fig. 3.13, was synthesized from the Diels–Alder cycloaddition/aromatization of the brominated 1,2,4,5-tetramethylbenzene with the corresponding primary (R = *n*-octyl or benzyl) or tertiary (R = cyclohexyl) maleimides [54]. By tuning electron affinity, these materials exhibit good electron-transport properties and stability in ambient as well as very high I_{on}/I_{off} ratios. Compared with anthracene-based OTFT, the introduction of the N-substituted diimide is crucial for the enhancement of n-channel conductivity and charge transport.

A range of heterocyclic dyes and pigments in Fig. 3.14 were synthesized by nucleophilic substitution reactions of halide derivatives of phenylmaleimide or

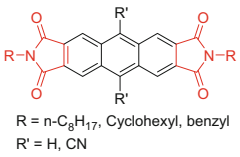

Fig. 3.13 N-substituted anthracenedicarboximides as organic thin-film transistors

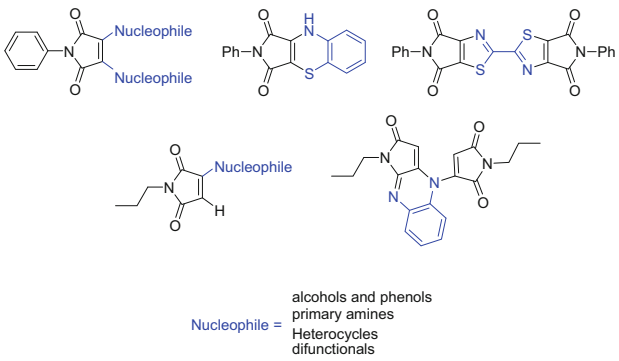

Fig. 3.14 Heterocyclic dyes and pigments based on maleimide derivatives

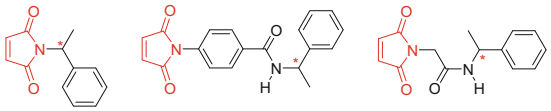

Fig. 3.15 Chiral and optically active N-substituted maleimide derivatives

n-propylmaleimide with mono-nucleophiles such as primary amines, phenols, and heterocycles (pyrazole, 4-pyridone, imidazole, etc.) and difunctional nucleophiles, such as *o*-aminothiophenol, *o*-phenylenediamine, dithiooxamide, etc. [55]. These maleimide derivatives showed intense colors that may be attributed to the merostabilization of free radicals in the excited state and offer potential in new dyestuff chemistry.

Novel chiral and optically active N-substituted maleimide derivatives reported in literature are displayed in Fig. 3.15 [56–59]. These molecules, containing a polymerizable double bond in the maleimide ring, can therefore produce optically active polymers and copolymers. It was found that the chiroptical properties of these polymers can be attributed not only to the chiral substituent in the pendant maleimides, but also to the asymmetric inductions to the polymer backbone. Examples of maleimide derivatives bearing alpha-methylbenzyl group are shown. The synthesis of *N*-[4-*N*′-(alpha-methylbenzyl)aminocarbonylphenyl] maleimide was achieved by multistep reactions of maleic anhydride, glycine, and (R)-(+)-alpha-methylbenzylamine.

3.2.3 Syntheses of Fluorescent Maleimide Derivatives and Their Properties

The maleimide moiety possesses an activated C–C double bond and is well known to undergo specific alkylation reactions with the sulfhydryl/thiol group to form stable thioethers. It is also known that a series of non-fluorescent maleimides with aromatic side chains give rise to strongly fluorescent products when treated with thiols. Through this reaction, the maleimide derivatives can be selectively attached to biological species with sulfhydryl functionalities, such as lipids, peptides, and proteins, to introduce fluorescence sensors.

A maleimide bearing electron-donating chromophore, *N*-(4-*N*′,*N*′-dimethylaminophenyl)maleimide (DMAPMI) was synthesized from *N*,*N*-dimethylaminoaniline and maleic anhydride in the classical two-step reaction in the presence of acetic anhydride and sodium acetate [60]. It was observed that the fluorescence emission intensity of the DMAPMI monomer was much lower than those of its polymers. This phenomenon of "fluorescence structural self-quenching," as illustrated in Scheme 3.23, may be attributed to the intra- or intermolecular charge transfer between the electron-donating dimethylaminophenyl moiety and the electron-accepting

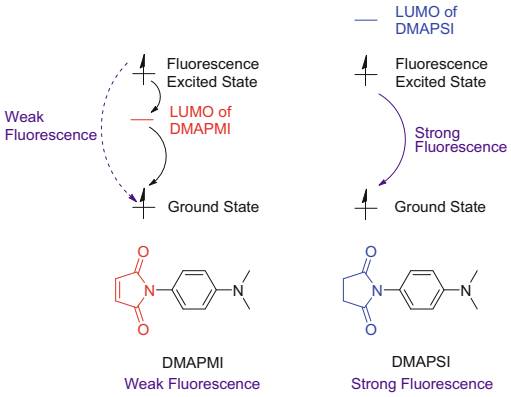

Scheme 3.23 Illustration of the phenomenon of "fluorescence structural self-quenching"

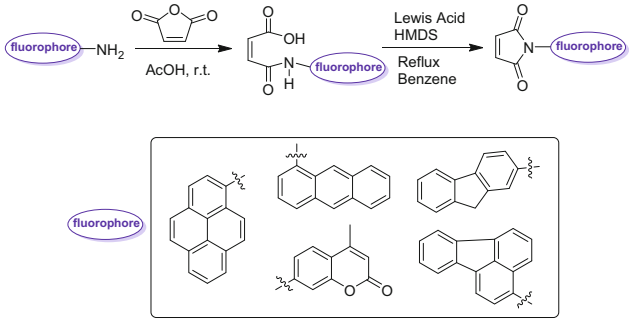

Scheme 3.24 Synthesis of fluorophore-linked *N*-aryl-maleimide derivatives

carbon–carbon double bond in the monomer. Such a hypothesis was validated by the much stronger fluorescence emission intensity of the *N*-(4-*N*′,*N*′-dimethylaminophenyl)succinimide (DMAPSI) when carbon–carbon double bond in the monomer is absent. As illustrated in Scheme 3.23, the presence of the C=C lowers the LUMO energy of the DMAPMI with respect to the DMAPSI, diverting the electron transfer from the fluorescence excited state directly to the ground state to produce weak fluorescence. While in the succinimide analogue, the LUMO of DMAPSI is energetically inaccessible, and all the electron transfer occurs from the fluorescence excited state to the ground state to emit strong fluorescence.

A series of fluorophore-linked *N*-aryl-maleimides were synthesized using the Lewis acid ($ZnCl_2$), and hexamethyldisilazane (HMDS) promoted the reaction of maleic acid with respective aryl amines [61]. This one-pot synthesis in Scheme 3.24, discussed earlier in this chapter, has proven to be efficient and high yielding. These fluorogenic maleimide derivatives are of interest as markers for biological substrates due to a number of characteristics, such as the reactivity toward the sulfhydryl group, fluorescence off–on switching nature, and long–lived fluorescence.

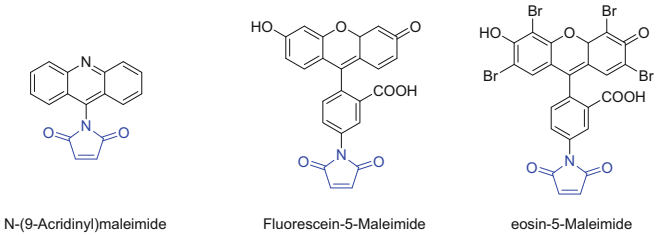

Fig. 3.16 Commercial fluorescent labeling reagents based on maleimide derivatives

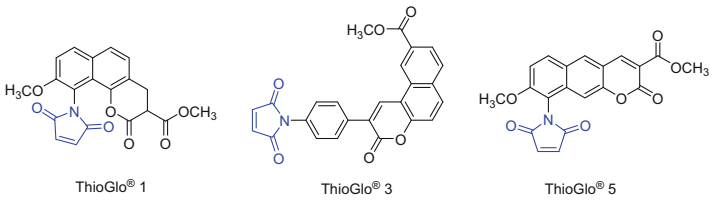

Fig. 3.17 ThioGlo® fluorescent probes

Fluorescent organic compounds, such as fluorescein [62], eosin [63–70], and acridine [71] shown in Fig. 3.16, have been functionalized with maleimide moiety to produce specific fluorescent labeling reagents that are commercially available. For example, eosin-5-maleimide was used to bind specifically to the anion transport protein lysine-430 in the red cell membrane as a diagnostic screening tool for membrane disorders such as hereditary spherocytosis [68]. Similarly, eosin-5-maleimide has been used to determine the orientation of human erythrocyte band 3 by fluorescence polarization microscopy [67], to characterize cysteine residues and transport activity of mitochondrial ADP/ATP carrier [63–66].

ThioGlo® reagents (Fig. 3.17) have been commercialized as thiol-reactive fluorescent probes for the derivatization, detection, and determination of thiol groups in biological molecules. They have little or no fluorescence prior to reaction with thiols and high quantum yields after fast reaction with active –SH groups in proteins, enzymes, and simple peptides resulting in superior thiol sensitivity and reaction efficiency.

As illustrated in Scheme 3.25, ThioGlo® 3 has been used to stereospecifically derivatize and determine captopril, a well-known angiotensin converting enzyme inhibitor, for the treatment of arterial hypertension [72]. In addition, ThioGlo® 3 has also been used to quantify the trace amount of *N*-(2-mercaptopropionyl)-glycine and 2-mercaptoethane sulfonate in biological samples using fluorescence detection [73, 74].

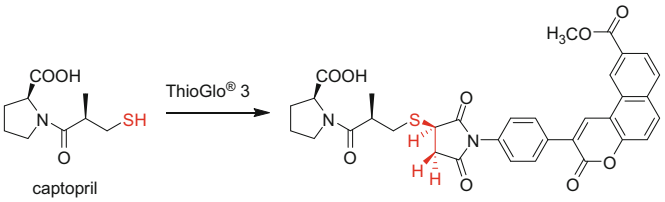

Scheme 3.25 Stereo-specific derivatization of captopril by ThioGlo® 3

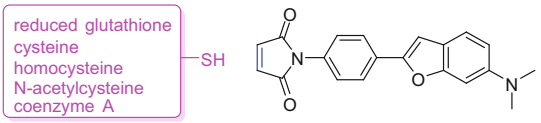

Fig. 3.18 Selective determination of thiols in biological samples using maleimide derivative

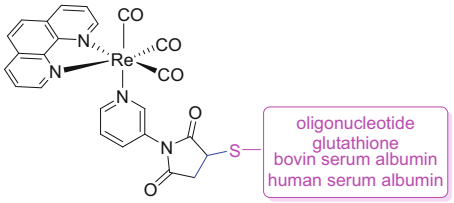

Fig. 3.19 Rhenium(I) polypyridine maleimide complexes as luminescent labels

The selective determination of thiols in biological samples was also investigated by high-performance liquid chromatography using *N*-[4-(6-dimethylamino-2-benzofuranyl)phenyl] maleimide in Fig. 3.18, which was found to give fluorescent products when treated with certain thiols. Six kinds of thiol (cysteine, *N*-acetylcysteine, homocysteine, cysteamine, reduced glutathione, and coenzyme A) could be separated simultaneously within ca. 12 min and determined at final level of sensitivity. The method was successfully applied to the determination of thiols in rat tissues and plasma and in human normal serum [75].

A series of rhenium(I) polypyridine maleimide complexes, as depicted in Fig. 3.19, were synthesized and utilized as luminescent labels for a thiolated oligonucleotide, glutathione, bovine serum albumin, and human serum albumin [76].

As shown in Scheme 3.26, the reaction of maleic anhydride with 2-ferrocene ethylamine proceeded through ring opening to form maleamic acid intermediate and subsequent dehydration to afford the electroactive *N*-(2-ferrocene-ethyl)

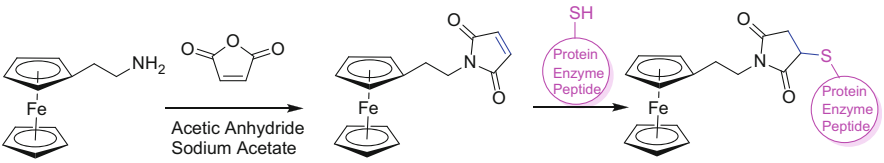

Scheme 3.26 Synthesis of *N*-(2-ferrocene-ethyl)maleimide and reaction with thiols

maleimide [77]. The activated double bond in the maleimide moiety enabled the labeling of enzymes, peptides, and proteins via the sulfhydryl groups thereof. The ferrocene moiety introduced excellent redox and electrochemical properties to the enzymes (e.g., cytochrome P450) and peptides (e.g., cysteine-containing glutathione) that are originally electroinactive.

3.2.4 Syntheses and Properties of Maleimide Derivatives Based on the Diels–Alder Reaction

Diels–Alder reaction, [4+2] system, generally consists of a coupling of a diene and a dienophile by intra- or intermolecular fashion. The activated carbon–carbon double bond in maleimide has made it an attractive dienophile in many applications of the Diels–Alder reaction. The efficient Diels–Alder reaction enables quantitative C–C bond formation without side reactions or purification and offered molecules ranging from block copolymers and graft copolymers to complexed macromolecular structures [78].

A number of diblock copolymers were successfully prepared by Diels–Alder reaction, between maleimide- and anthracene-end functionalized poly (methyl methacrylate) (PMMA), polystyrene (PS), poly(*tert*-butyl acrylate) (PtBA), and poly(ethylene glycol) (PEG) [79]. An exemplary scheme of PMMA-*b*-PS is shown in Scheme 3.27. Both the maleimide and the anthracene terminal groups were introduced into the polymer through the atom transfer radical polymerization (ATRP) of PMMA and PS, using 2-bromo-2-methyl-propionic acid 2-(3,5-dioxo-10-oxa-4-azatricyclo[5.2.1.02,6]dec-8-en-4-yl)-ethyl ester and 9-anthyryl-methyl 2-bromo-2-methyl propanoate, respectively, as the initiators, in the presence of Cu(I) salt and pentamethyldiethylenetriamine (PMDETA). During this ATRP process, the maleimide group has to be protected to avoid undesired copolymerization of maleimide with MMA. The Diels–Alder reaction of the two polymeric precursors in refluxing toluene yielded block copolymer of PMMA-*b*-PS, while the deprotection of the maleimide group occurred in situ.

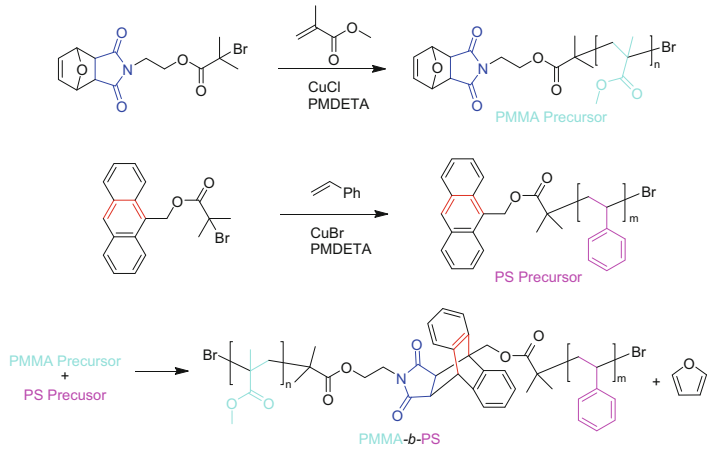

Scheme 3.27 Synthesis of PMMA-*b*-PS copolymer based on Diels–Alder reaction

In a similar fashion using the Diels–Alder "click chemistry" between anthracene and maleimide functionalities, well-defined polystyrene-*g*-poly(ethylene glycol) (PS-*g*-PEG) and polystyrene-*g*-poly(methyl methacrylate) (PS-*g*-PMMA) graft copolymers were successfully prepared in quantitative yield and without an additional purification step [80]. In another example, the Diels–Alder ligation between cyclopentadienyl end-capped poly(3-hexylthiophene) (P3HT) and maleimide-functionalized polydopamine was employed to fabricate conductive surface tethered polymer brushes. The efficient nature of the Diels–Alder ligation was further combined with a biomimetic polydopamine-assisted functionalization of surfaces, making it an access route of choice for P3HT surface immobilization [81].

3.2.5 Syntheses of Multifunctional Maleimide Derivatives and Their Uses

The electron-accepting maleimide moiety can undergo free-radical-initiated polymerization. Combining the maleimide functionalities with another polymerizable functionality to produce dual functional monomers has attracted a lot of interest recently. These functionalities include benzoxazines [82–84], oxazolines [85], oxetanes [86], and cycloaliphatic epoxy [87], which undergo ring-opening polymerizations. A common maleimide precursor to these novel monomers is 6-maleimidocaproic acid (MCA), obtained by the reaction of maleic anhydride with 6-aminocaproic acid. The illustrative Scheme 3.28 shows the reaction products of MCA with oxazoline, oxetane, and cycloaliphatic epoxy precursors. These dual functional compounds have the capability of undergoing both thermal and radiation cure processing and offer a new spectrum of performance materials for use within the adhesive, coating, and semiconductor fabrication industries.

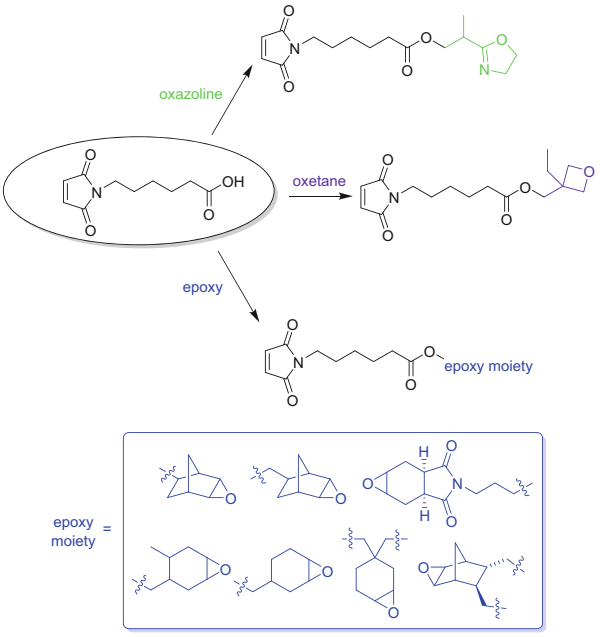

Scheme 3.28 Multifunctional maleimide derivatives derived from 6-maleimidocaproic acid

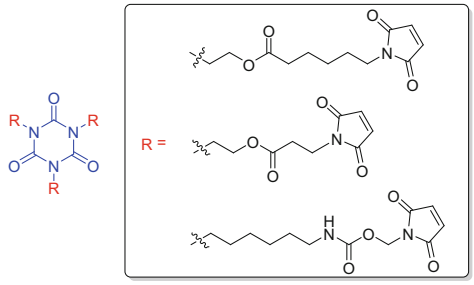

Fig. 3.20 Maleimide derivatives with cyanurate core

In the fabrication of semiconductor packages, maleimide derivatives with cyanurate core and the polymeric resins of these novel monomers are useful materials that show improved adhesion and improved modulus at high temperature [88]. A schematic drawing of these monomers with various pendent maleimide arms are shown in Fig. 3.20. The side arms contain a maleimide group at one end and a divalent organic linker (aliphatic or aromatic) connecting the maleimide and the cyanurate core. For every cyanurate core, there could be 1–3 side arms depending on the stoichiometry of the reactions. A typical reaction scheme consists of the reaction of maleic anhydride with an amino acid to form the maleimide with the carboxyl functionality. Subsequently, the reaction of the carboxyl group with the hydroxyl or isocyanate group on the 1,3,5-tris(2-hydroxyethyl)cyanuric acid affords these maleimide monomers with a cyanurate core.

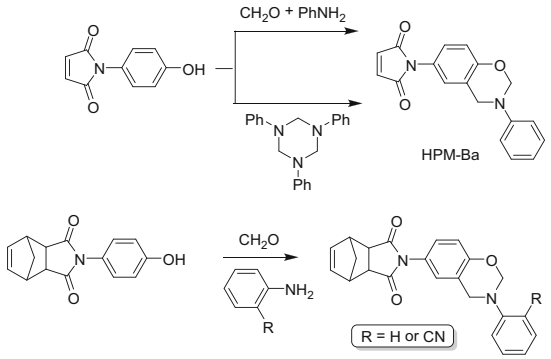

Scheme 3.29 Multifunctional maleimide derivatives that contain benzoxazine moiety

Benzoxazine derivatives that contain maleimide groups were studied in recent literatures [82–84]. Both maleimides and benzoxazine are polymerizable monomers, and their polymers exhibit good thermal, mechanical, and electrical properties, as well as the versatility in molecular design. The marriage of these two functional moieties in one monomer offers new candidates for high-performance composites. A benzoxazine compound with a maleimide group, 3-phenyl-3,4-dihydro-2H-6-(*N*-maleimido)-1,3-benzoxazine (HPM-Ba), was prepared from *N*-(4-hydroxyphenyl) maleimide with either formaldehyde/aniline in solution, or the intermediate 1,3,5-triphenylhexylhydro-1,3,5-trizine via paraformaldehyde and aniline (Scheme 3.29). As expected, HPM-Ba showed a two-stage process of thermal polymerization. The first stage was the polymerization of maleimides at 130 °C, while the second stage was attributed to the ring opening of the benzoxazine. The other example in Scheme 3.29 was the maleimide and norbornene functionalized benzoxazine, which can be synthesized from the corresponding norbornene maleimides with formaldehyde and aniline. Incorporation of both norbornene and maleimide into the originally monofunctional benzoxazine resulted in an increase in char yield and glass transition temperature without significant increase of the monomer viscosity. The extent and the type of the polymerization pathway in these novel monomers affect the final network structure and application of the benzoxazine polymer.

Maleimide derivatives with multiple functionalities have been extensively studied for use in curable compositions in the fabrication of semiconductor materials [86, 89–92]. A reactive oligomer was prepared from a bisphthalic anhydride linked by an aliphatic/aromatic linker, an amino alcohol, and a carboxylic acid terminated with maleimide functionality, as shown in the exemplary Scheme 3.30 [93]. The resulting reactive maleimide monomers with both imide and ester functionalities can be cured under different conditions and provide tunability of the cured adhesive materials by varying the functional groups and linkers.

Another multifunctional maleimide derivative, which contains diphenyl backbone, ester functionality, and terminal maleimide, was prepared from the reaction of diphenyl oxide, formaldehyde or paraformaldehyde, and maleimides with carboxylic acid terminal group (Scheme 3.31) [90]. The resulting oligomeric maleimide derivative has a high molecular weight and fewer reaction points than a maleimide monomer

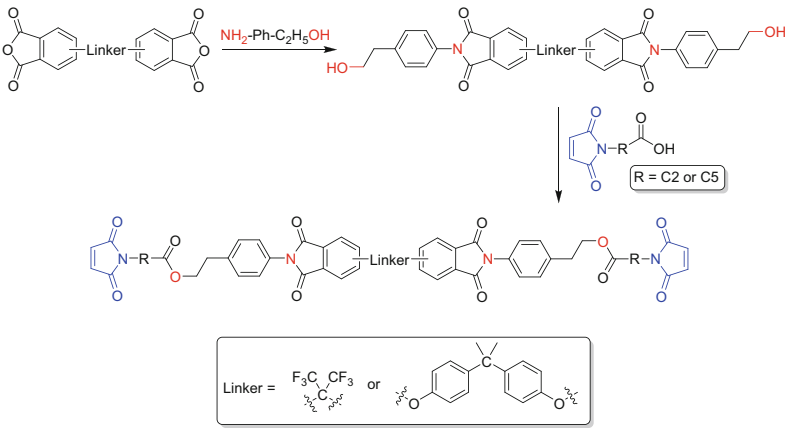

Scheme 3.30 Maleimide derivatives that contain multiple functionalities

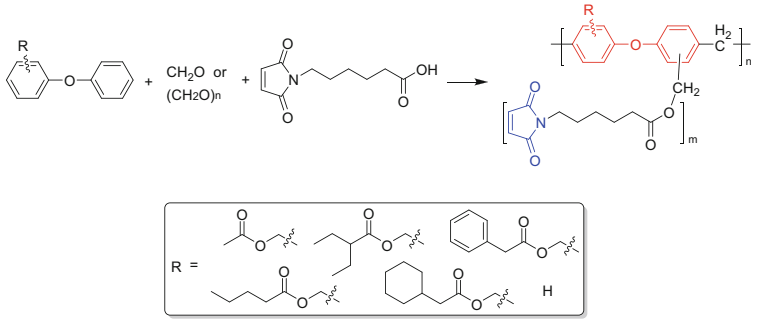

Scheme 3.31 Oligomeric maleimide derivatives that contain diphenyl backbone

and can be beneficial as curable compositions in the fabrication of semiconductor materials for shrinkage void performance, high T_g, and high thermal conductivity.

Oligomeric maleimide derivatives, resulting from the Michael addition product of a thiol with a compound having internal ester functionality and maleimide terminal group, can be formulated into curable compositions to improve adhesion to metal substrates [94]. As shown in Scheme 3.32, the reaction was carried out between a maleimide/bismaleimide and linear or branched mercaptans with various stoichiometry, using 3-aminopropyltrimethoxy silane as the catalyst. Depending on the stoichiometry, the oligomer can be either maleimide terminated or thiol terminated. The terminal S–H group can initiate premature polymerization of the adhesive to cause gelation and short work life. Thus, it is advantageous to use the maleimide-terminated oligomer to promote adhesion to the metal surface so that the internal sulfur functionality can bond to the metal via covalent bonding or van der Waals interactions.

Similarly, the Michael addition between a diamine and a bismaleimide affords a series of oligomeric maleimide adducts, as shown in Scheme 3.33. These amine adducts, as well as the thiol adducts described in Scheme 3.32, are suitable for use

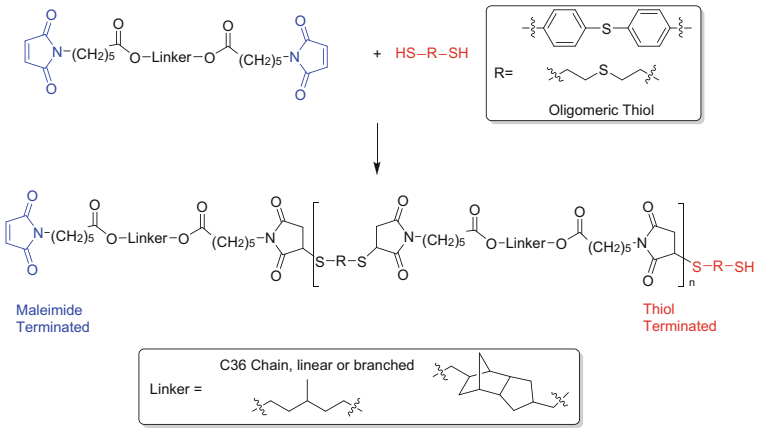

Scheme 3.32 Oligomeric maleimide derivatives resulting from the Michael addition of thiol moiety

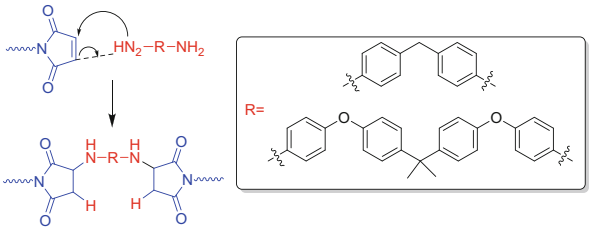

Scheme 3.33 Oligomeric maleimide derivatives resulting from the Michael addition of amine moiety

as a coating for the inactive face of a silicon wafer in the microelectronics packaging industry.

3.2.6 Syntheses of Liquid Maleimide Compounds and Their Properties

Maleimide compounds, especially bismaleimide-based resins, have been known as high-performance thermosetting resins since the 1960s. They possess a wide range of desirable physical properties: heat and chemical resistance, high mechanical stability, high cross-link density, low moisture absorption, and good adhesive and electrical properties. The broad applications of bismaleimide resins in the adhesive and packaging industries can be attributed to these properties. However, the disadvantages of the bismaleimide resin, brittleness and poor process ability, are also originated from their unique physical properties. Most maleimide compounds and the polymerized resins are solids at room temperature, which are difficult to process and to cure rapidly. Moreover, most bismaleimide compounds have poor solubility in organic solvents and thus limit the choice of organic diluents to

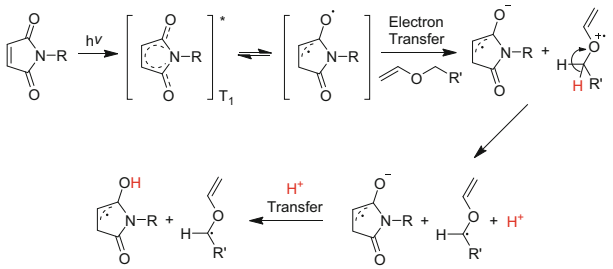

Scheme 3.34 Proposed mechanism for the maleimide photoinitiation

ones with high polarity in the curing process. The high cross-link density of the bismaleimide resins result in their brittleness. Therefore, research has been focused recently on various approaches to overcome such shortcomings.

One approach that generated a lot of research interest is the use of reactive liquid diluents, such as divinyl ethers [95–98] and diacrylates [99–101] in the copolymerization with maleimide compounds. The use of reactive diluents as comonomers is advantageous in that they become part of the cured resin and do not pose disposal and environmental issues. The other distinct feature of these curing systems is the dual effect of maleimide compounds as both photoinitiators and polymerizable monomers. The maleimide photoinitiation mechanism is proposed in Scheme 3.34 [96]. As the reactive comonomer (such as a divinyl ether in Scheme 3.34) is UV transparent at >250 nm wavelength, UV radiation can only be absorbed by maleimide compound to form the excited maleimide. Subsequent electron transfer and proton transfer from the vinyl ether can yield the initiating maleimide and α-ether radicals.

The polymer chain propagates either by a cross-over process or by homopolymerization of the donor–acceptor complex. The cross-over process is when the vinyl ether radical reacts with the maleimide double bond, or the maleimide radical attacks the vinyl ether double bond. Regardless of the chain propagation mechanism, alternating copolymers of maleimide and vinyl ether will be formed [96].

Figure 3.21 exhibits the variety of reactive diluents/comonomers that were reported in recent literature, which are primarily divinyl ethers, diacrylates, and many other simple alkyl acrylates/methacrylates, some with long aliphatic chain linkages [95–101]. All of these reactive monomers are liquid at room temperature, and the corresponding maleimide/bismaleimide compounds can be readily dissolved. UV radiation will then initiate the copolymerization of maleimide and the vinyl compounds in liquid form.

A variety of maleimide and bismaleimide compounds have been studied for photocuring with a reactive liquid vinyl diluent. They include simply hydroxyalkylmaleimides and aliphatic or aromatic-linked bismaleimides. Examples of commercially available maleimides compounds are depicted in Fig. 3.22.

Many other bismaleimides can be synthesized with aliphatic chains linked through carbonate/urethane functional groups. For instance, in Scheme 3.35 [97], the reaction of ethanolamine with 3,6-endoxo-1,2,3,6-tetrahydrophthalic anhydride in a 1:1 molar

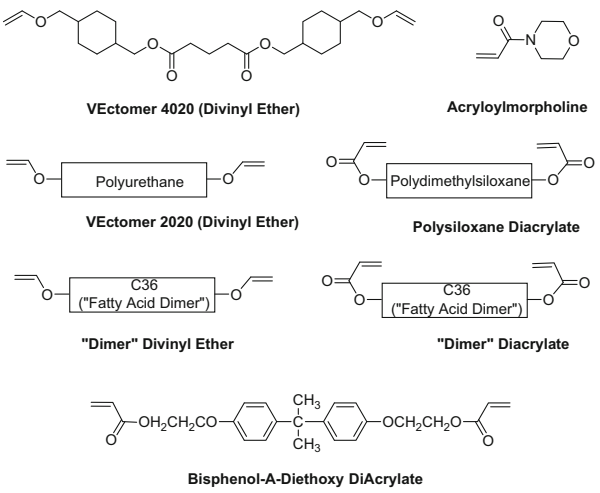

Fig. 3.21 Reactive liquid diluents/comonomers: divinyl ethers and diacrylates

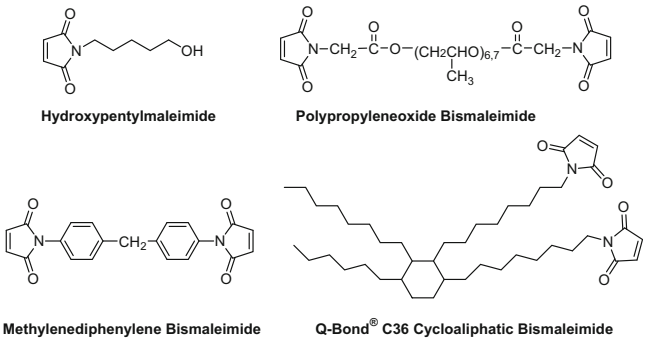

Fig. 3.22 Commercial maleimide compounds that can be photocured with reactive diluents

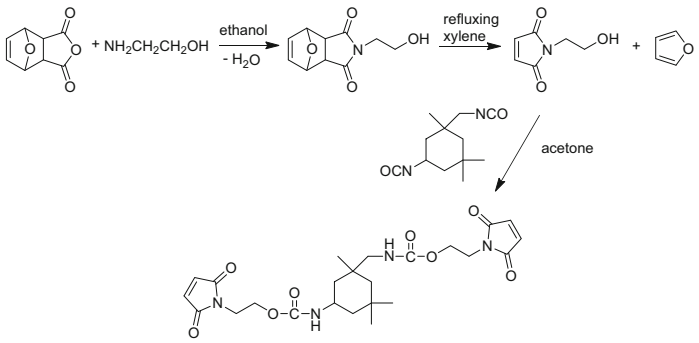

Scheme 3.35 Synthesis of bismaleimide linked through urethane functional group

ratio in ethanol affords the furan-protected maleimide. The deprotection in refluxing xylene yields the desired hydroxyethylmaleimide as white crystalline solid with an overall 50 % yield. Further reaction with isophorone diisocyanate in the presence of dibutyl dilaurate catalyst in acetone produces isophorone bisurethane bisethylmaleimide as a white precipitate in nearly 80 % yield.

As a majority of the maleimide compounds discussed above are solids at room temperature, a liquid, reactive comonomer is needed in order to obtain a liquid co-photocuring system that facilitates the handling of these maleimide resins at room temperature. However, the number of suitable liquid comonomer is limited by the volatility, odor, toxicity, viscosity, and solubility of the maleimides. In addition, since the reactive diluents become an integral part of the copolymer thermosetting resin, they will definitely affect the physical properties of the maleimide-based resin. Consequently, another approach to enhance the processability, the ease of handling of maleimide compounds at room temperature, and rapid curing is strongly desired.

The liquid maleimide compounds emerge in the literature as a promising approach to meet the above needs. As a liquid at room temperature, they are easy to handle, do not require any diluent, and are 100 % reactive. In fact, two bismaleimides in Fig. 3.22, Q-Bond® C36 cycloaliphatic bismaleimide and polyoxypropylene bismaleimide, are commercially available and liquid at room temperature; however, they have not been extensively studied in a rapid curing application.

Liquid bismaleimide based on the C36 aliphatic chain originated from the dimer of oleic acid was synthesized in a recent invention [102]. As exemplified in Scheme 3.36, the reaction of 6-maleimidocaproic acid (MCA) with the commercial C36 aliphatic dimer diol (Pripol 2033) in refluxing toluene resulted in the desired bismaleimide as a liquid at room temperature in 68 % yield. Remarkably, the viscosity of this dimer diester bismaleimide is only ~2500 cps at room temperature.

Another liquid bismaleimide, shown in Scheme 3.37, was synthesized in a moderate yield by the classical two-step maleation reaction of maleic anhydride

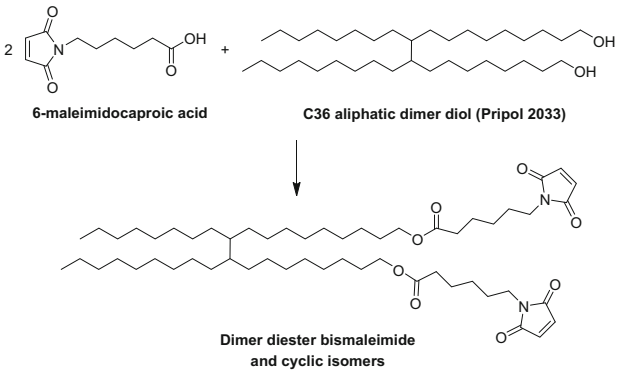

Scheme 3.36 Synthesis of dimer diester bismaleimide

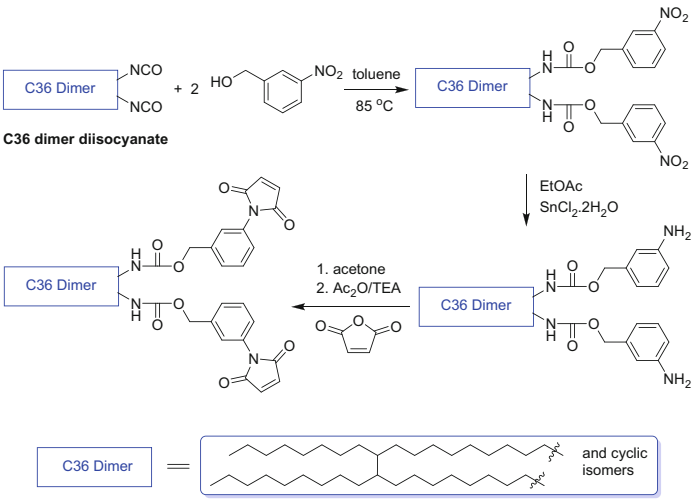

Scheme 3.37 Synthesis of bis(*m*-maleimidobenzyl) dimer dicarbamate

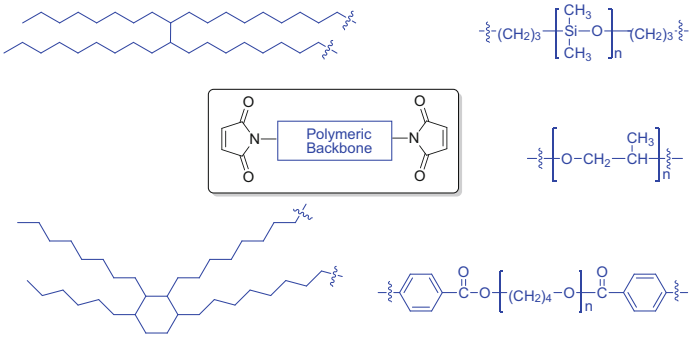

Fig. 3.23 Liquid bismaleimide compounds with polymeric backbone

with the diamine precursor of the C36 dimer core structure [102]. The diamine precursor, bis(*m*-aminobenzyl carbamate) of C36 dimer, was made by reacting *m*-nitrobenzyl alcohol with the "C36 dimer diisocyanate" in toluene at 85 °C, followed by the reduction of the nitro group to the amine by stannous chloride dihydrate in ethyl acetate. This bis(*m*-maleimidobenzoyl) dimer dicarbamate is a viscous orange oil at ambient temperature.

A series of liquid bismaleimides were synthesized by the maleation reactions of commercial polymeric diamines and maleic anhydride in a recent invention [103]. The polymeric diamines include aliphatic C36 dimer (linear or cyclic) diamine, aminopropyl-terminated dimethyl siloxanes, polyoxypropylene amines, and polytetramethylene-di-*p*-aminobenzoate. Schematic drawings of these liquid bismaleimide compounds are shown in Fig. 3.23.

These liquid bismaleimide compounds have suitable viscosities at ambient temperature for the ease of handling and processing. They can undergo rapid curing with or without the presence of a reactive comonomer, either by UV radiation or by a radical initiator. The resulting thermosetting resins are highly resistant against heat or chemicals, are highly flexible, exhibit low moisture absorption, and have shown promising applications as adhesives in the microelectronics and packaging industries [102, 103].

3.2.7 *Syntheses of Maleimide Derivatives with Reworkable Acetal Linkage and Their Properties*

Novel maleimide derivatives that contain an acid-sensitive acetal or ketal moiety were synthesized, and the polymers and copolymers thereof have been explored in formulating positive photoresist compositions [104, 105]. As depicted in Scheme 3.38, the reaction of maleimide with formalin produced methylol maleimide in good yield. Subsequent reaction of methylol maleimide with the carbon–carbon double bond in 2-methoxypropene, alkyl vinyl ether, and dihydropyran formed the corresponding acetal and ketal containing maleimide monomers. This two-step reaction is reversible, particularly in the polymers of these maleimides. Under a catalytic amount of photoacid generated by radiation, the acetal/ketal will deblock. Upon subsequent exposure to aqueous alkaline solution, the remaining methylol group can be removed.

Thermosetting materials have been widely used in a variety of applications, such as coatings, encapsulations, and adhesives. However, they generally exhibit poor tractability after curing, which limits their use in applications where degradable, recyclable, and reworkable polymers are preferred. New thermosetting materials were developed for reworkable adhesive applications by introducing thermally breakable acetal ester linkages into maleimide compounds [106–108]. The synthesis of such compounds was carried out by a one-step neat reaction from a commercially available maleimide precursor with a terminal carboxylic acid group and a

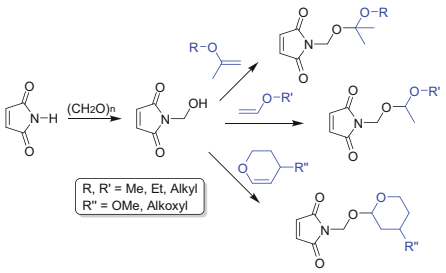

Scheme 3.38 Synthesis of maleimide derivatives that contain an acid-sensitive acetal moiety

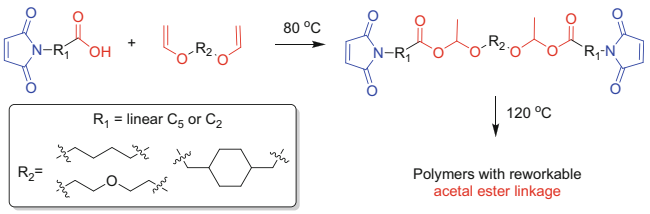

Scheme 3.39 Multifunctional maleimide derivatives that contain a reworkable acetal ester linkage

divinyl ether, as shown in the illustrative Scheme 3.39. These multifunctional derivatives can be radically polymerized at 120 °C into highly cross-linked networks with the acetal ester groups intact. Upon further heating the polymer to above 225 °C, the acetal ester linkage completely degraded, resulting in a significant reduction of the adhesive strength from the original intact maleimide-acetal ester polymer.

The degradation mechanism, displayed in Scheme 3.40, was hypothesized based on molecular modeling. The decomposition of the C–O bond adjacent to the C–O yielded a carboxylic acid and vinyl ether. Subsequent hydrolysis of the vinyl ether under the acidic condition afforded an alcohol and acetaldehyde. Finally, the –OH group in the alcohol can backbite the other acetal ester linkage to form cyclic acetal and another molecule of the carboxylic acid. The degradation products were mainly the cyclic acetal, with minor amounts of acetaldehyde and butanediol [106].

The hypothesized degradation mechanism was further supported by hot-stage FT-IR and GC-MS. In particular, Fig. 3.24a shows the hot-stage FT-IR spectra of the bismaleimide compound with acetal linkage plotted as a function of temperature ranging from 25 to 275 °C. At about 250 °C, the intensities of the acetal C–O peak (~1135 cm^{-1}) and C–H stretching of the maleimide (831 and 698 cm^{-1}) decreased significantly, suggesting the decomposition at acetal linkage and self-polymerization upon heating. In addition, Fig. 3.24b examined the thermal IR profile of the acetal C–O peak, in which the frequency shift of the breaking acetal C–O bond was observed due to the decomposition.

The reworkable acetal ester linkage can also be incorporated into norbornene dicarboximide, a derivative of maleimide and cyclopentadiene [108]. These mono-, di-, or mixtures of mono- and difunctional norbornene monomers undergo efficient, controllable, and reproducible ring-opening metathesis polymerization (ROMP) to afford thermosetting polymeric materials with the acetal ester group intact (Scheme 3.41), using Grubbs ruthenium first-generation catalyst in chloroform at ambient temperature.

Thermal gravimetric analysis of the cross-linked materials with various difunctional norbornene monomer content showed that they are stable up to 150 °C and that they exhibit rapid degradation above 200 °C, resulting from the thermolysis of the acetal ester linkage. The more acetal ester linkage in the ROMP polymer, the

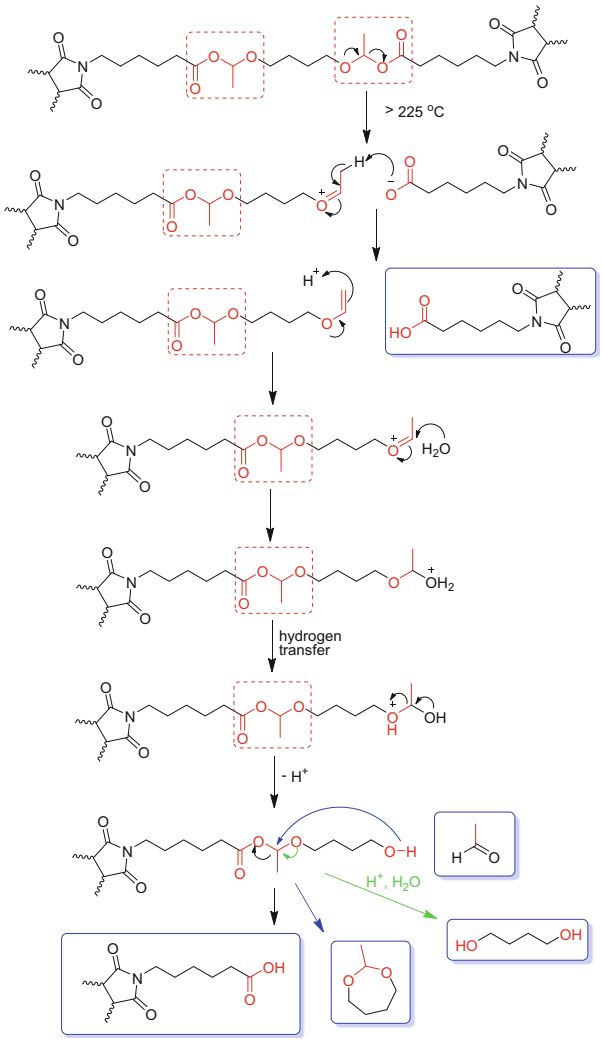

Scheme 3.40 Hypothesized degradation mechanism of reworkable maleimide derivatives

more weight loss was observed in the TGA profile in Fig. 3.25 (ROMP polymers (a) to (d) are designated in Scheme 3.41). This is consistent with difunctional ROMP polymer (a) having the highest difunctional content and cross-linking.

The degradation products of the acetal ester linkage, as determined by TGA-MS, were acetaldehyde, butadiene, butenyl alcohol, and pentenoic acid. A plausible degradation mechanism is shown in Scheme 3.42.

These multifunctional monomers that contain both maleimide/norbornene and acetal ester functionalities are precursors to reworkable thermosetting polymers,

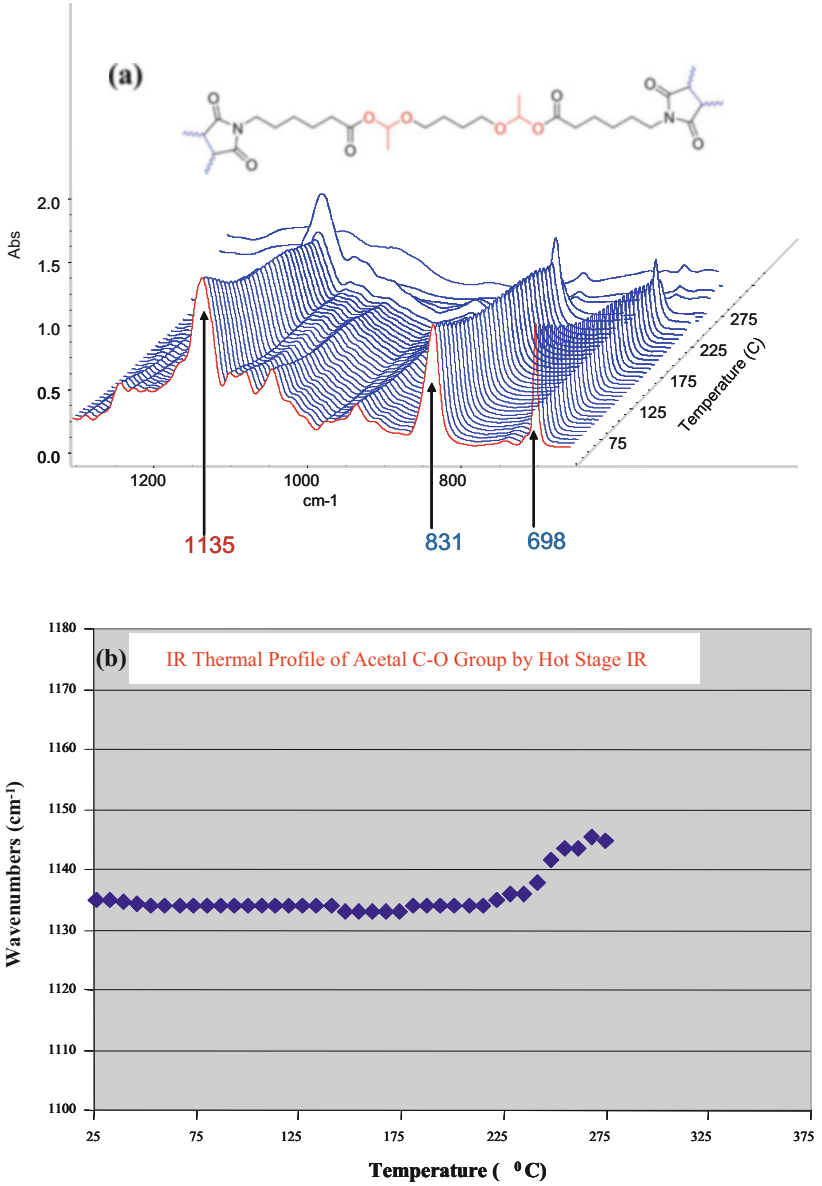

Fig. 3.24 Hot-stage FT-IR spectra of the bismaleimide compound with acetal linkage

with application as adhesives in semiconductor industry. The decomposition of the acetal ester functionality upon heating at higher temperature is expected to lead to a decrease in cross-linking density and modulus of the adhesive, thus allowing the chip removal and replacement.

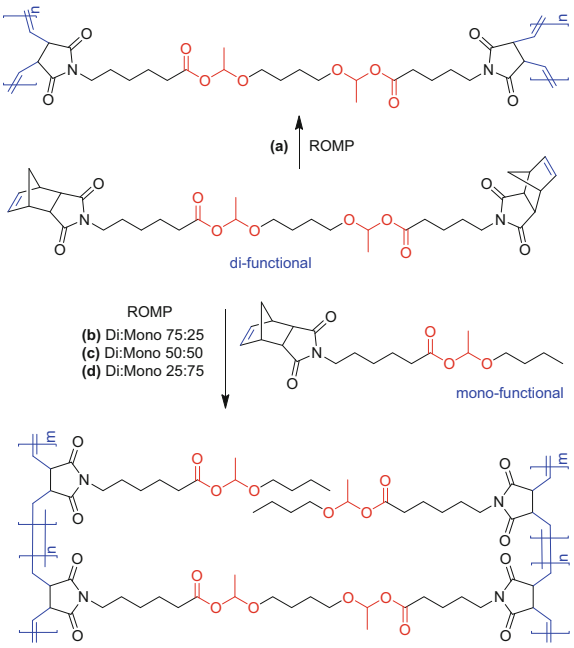

Scheme 3.41 Norbornene dicarboximide with acetal ester linkage: monomers and ROMP polymers

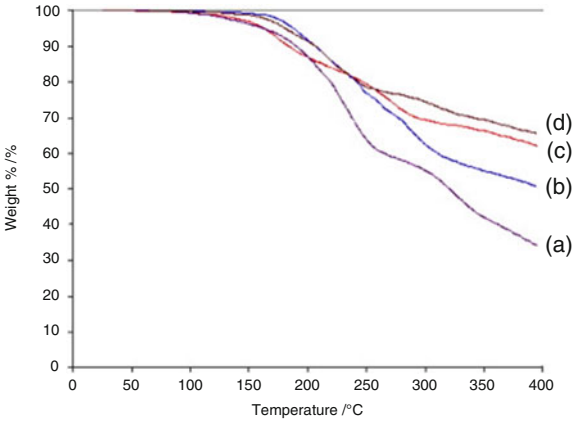

Fig. 3.25 TGA thermographs of the ROMP polymers of norbornene dicarboximide with acetal ester linkage

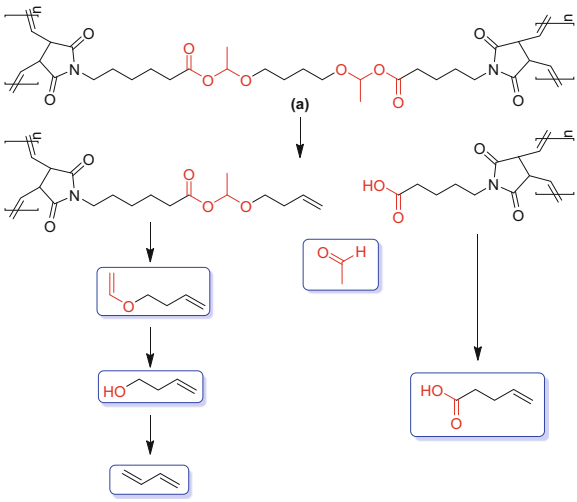

Scheme 3.42 Degradation mechanism of norbornene dicarboximide with acetal ester linkage

3.2.8 Syntheses of Maleimide Derivatives Based on Reversible Diels–Alder Reaction

Cross-linked polymeric materials based on the Diels–Alder reaction between a diene (furan) and dienophile (maleimide derivative) have attracted a great deal of interest in recent literature [109–113]. This can be mostly attributed to the reversible nature of the maleimide–furan Diels–Alder reaction. Retro Diels–Alder reaction occurs at elevated temperature to debond the chemical linkages at the cross-linked polymer network, hence reversing the cross-linking process. As exemplified in Scheme 3.43, the mixture of polystyrene substituted with maleimidomethyl group and poly [styrene-*co*-(maleic anhydride)] substituted with furfuryl ester underwent thermally reversible Diels–Alder cross-linking at 65 °C, and the retro Diels–Alder reaction occurred rapidly at 150 °C [109]. It was also demonstrated that the Diels–Alder cross-linking process was truly reversible by repeatedly cycling the reaction temperatures.

Thermally labile dendrimers based on the reversible furan–maleimide Diels–Alder reaction were also reported [110, 111]. As depicted in Scheme 3.44, the reaction of a bismaleimide central linker with benzyl aryl ether-based dendrons (first through fourth generation) that contained furan functionalities at their focal point yielded the corresponding dendrimers. These dendrimers efficiently undergo retro Diels–Alder cleavage and Diels–Alder reassembly at relatively milder temperatures. Appropriate selection of dendron, functionalized dienes (furan), and dienophile (bismaleimide) will lead to a variety of nanoscopic materials that can be activated through a noninvasive thermal trigger.

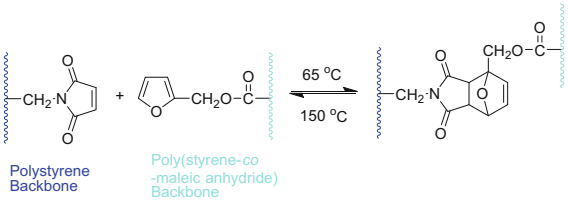

Scheme 3.43 Reversible Diels–Alder cross-linking of maleimide and furan graft polymers

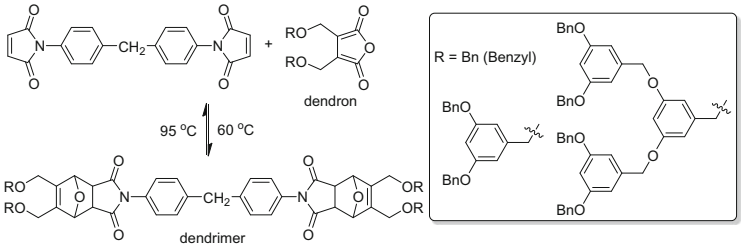

Scheme 3.44 Thermally labile dendrimers based on the reversible furan–maleimide Diels–Alder reaction

Similarly, an epoxy-like thermally reversible cross-linked resin was prepared from a trifunctional maleimide and a trifunctional furan derivative. The resin displayed thermal remendability and removability through Diels–Alder (DA) and retro-DA reactions and can be applicable in advanced encapsulants and structural materials [113]. In addition, the reversible furan–maleimide Diels–Alder reaction has been applied to thermally cleavable encapsulates, foams, and surfactants [78, 111].

3.2.9 Bioconjugates Containing Maleimides and Their Uses

Maleimide derivative, through the highly selective and efficient reaction with the thiol group, has been widely used to form bioconjugates to peptides, proteins, DNA, and even monoclonal antibodies [114]. Simple stirring of the two reactants at room temperature is often sufficient to achieve complete conversion without the need of heat or catalyst. Two maleimide-based lipidating reagents in Fig. 3.26 were prepared to anchor thiol-containing peptides and polypeptides into phospholipid bilayers and membranes [115]. These amphiphilic reagents were applied to the anchoring of a C-terminal cysteamine-modified polypeptide which comprises the extracellular N-terminal domain of the human thrombin receptor, a transmembrane protease-activated receptor (PAR-1). These maleimide derivatives are useful to

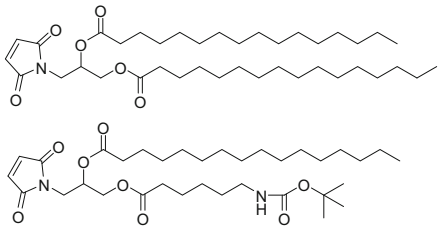

Fig. 3.26 Maleimide-based lipidating reagents

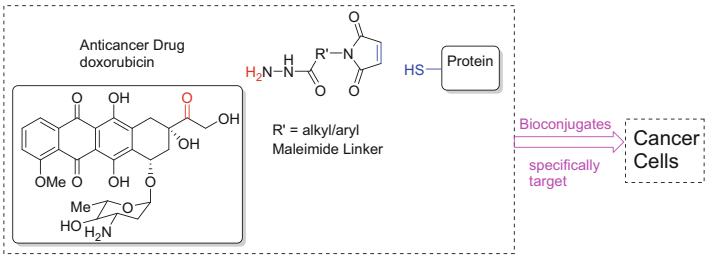

Scheme 3.45 Maleimide derivatives that bind to anticancer drug and protein carrier

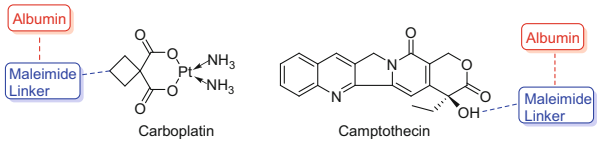

Fig. 3.27 Water-soluble maleimide derivatives as thiol-reactive prodrugs

study the structure and function of peptides and polypeptides at phospholipid bilayer surfaces.

Maleimide derivatives have been extensively used to improve the pharmacokinetic properties and target drug delivery of anticancer drugs via the specific conjugation of the maleimide–drug complex to the carrier protein [116]. An example of the drug–maleimide–carrier protein bioconjugates is shown in Scheme 3.45. The maleimide linker molecule binds to the anticancer drug doxorubicin in a labile manner at one end, while conjugates to the carrier protein at the other end to form a bioconjugate complex. This complex delivers the drug specifically to the targeted cancer cell and liberates the drug as delivered.

In another example in Fig. 3.27, the water-soluble maleimide derivatives of the anticancer drugs carboplatin and camptothecin were employed as thiol-reactive prodrugs to bind to the cysteine-34 position of circulating albumin and showed improved drug delivery and antitumor effect [117, 118]. In addition, the maleimide

scaffold was reported to reactivate Mutant p53 and induce apoptosis on human tumor cells [119].

Finally, the use of the high and specific reactivity of maleimide-thiol coupling reaction has yielded an efficient oligonucleotide–enzyme conjugate hybridization probe. Such a probe demonstrated superior sensitivities in detecting complementary DNA sequences [120].

Acknowledgments The authors would like to express our sincere gratitude to Helen Gerardi, Tian Lu, Guanglou Cheng and Chi-san Wu of Ashland, Inc. for many helpful conversations/suggestions for the contents, and their thorough review of the manuscript and valuable feedback prior to publication.

References

1. Lu Y, Larock RC (2009) Novel polymeric materials from vegetable oils and vinyl monomers: preparation, properties, and applications. ChemSusChem 2(2):136–147
2. Miao S, Wang P, Su Z, Zhang S (2014) Vegetable-oil-based polymers as future polymeric biomaterials. Acta Biomater 10(4):1692–1704
3. Mazo P, Estenoz D, Sponton M, Rios L (2012) Kinetics of the transesterification of castor oil with maleic anhydride using conventional and microwave heating. J Am Oil Chem Soc 89 (7):1355–1361
4. Saied MA, Mansour SH, Eweis M, El-Sabee MZ, Saad ALG, Abdel Nour KN (2008) Some biophysical properties of castor oil esterified with some acid anhydrides. Eur J Lipid Sci Technol 110(10):926–934
5. Saied MA, Mansour SH, El Sabee MZ, Saad ALG, Abdel-Nour KN (2012) Some electrical and physical properties of castor oil adducts dissolved in 1-propanol. J Mol Liq 172:1–7
6. Wang HJ, Rong MZ, Zhang MQ, Hu J, Chen HW, Czigany T (2008) Biodegradable foam plastics based on castor oil. Biomacromolecules 9(2):615–623
7. Wang H, Rong M, Zhang M (2014) Plastic foams based on castor oil modified with the reaction product of maleic anhydride and β-hydroxyethyl acrylate. Gaofenzi Cailiao Kexue Yu Gongcheng 30(2):21–26
8. Sponton M, Casis N, Mazo P, Raud B, Simonetta A, Rios L, Estenoz D (2013) Biodegradation study by *Pseudomonas* sp. of flexible polyurethane foams derived from castor oil. Int Biodeterior Biodegrad 85:85–94
9. Echeverri DA, Perez WA, Rios LA (2013) Maleinization of soybean oil glycerides obtained from biodiesel-derived crude glycerol. J Am Oil Chem Soc 90(12):1877–1882
10. Echeverri DA, Jaramillo F, Rios LA (2015) Curing copolymerization kinetics of styrene with maleated castor oil glycerides obtained from biodiesel-derived crude glycerol. J Appl Polym Sci 132(4)
11. Echeverri DA, Perez WA, Rios LA (2013) Synthesis of maleated-castor oil glycerides from biodiesel-derived crude glycerol. Ind Crops Prod 49:299–303
12. Can E, Wool RP, Kusefoglu S (2006) Soybean and castor oil based monomers: synthesis and copolymerization with styrene. J Appl Polym Sci 102(3):2433–2447
13. Can E, Kusefoglu S, Wool RP (2001) Rigid, thermosetting liquid molding resins from renewable resources. I. Synthesis and polymerization of soybean oil monoglyceride maleates. J Appl Polym Sci 81(1):69–77
14. Can E, Kusefoglu S, Wool RP (2002) Rigid thermosetting liquid molding resins from renewable resources. II. Copolymers of soybean oil monoglyceride maleates with neopentyl glycol and bisphenol A maleates. J Appl Polym Sci 83(5):972–980

15. Bora MM, Gogoi P, Deka DC, Kakati DK (2014) Synthesis and characterization of yellow oleander (*Thevetia peruviana*) seed oil-based alkyd resin. Ind Crops Prod 52:721–728
16. Bora MM, Deka R, Ahmed N, Kakati DK (2014) Karanja (*Millettia pinnata* (L.) Panigrahi) seed oil as a renewable raw material for the synthesis of alkyd resin. Ind Crops Prod 61:106–114
17. Boruah M, Gogoi P, Adhikari B, Dolui SK (2012) Preparation and characterization of *Jatropha curcas* oil based alkyd resin suitable for surface coating. Prog Org Coat 74 (3):596–602
18. Dutta N, Karak N, Dolui SK (2004) Synthesis and characterization of polyester resins based on Nahar seed oil. Prog Org Coat 49(2):146–152
19. Ahmad S, Ashraf SM, Zafar F (2007) Development of linseed oil based polyesteramide without organic solvent at lower temperature. J Appl Polym Sci 104(2):1143–1148
20. Ahmad S, Ashraf SM, Naqvi F, Yadav S, Hasnat A (2003) A polyesteramide from *Pongamia glabra* oil for biologically safe anticorrosive coating. Prog Org Coat 47(2):95–102
21. Mahapatra SS, Karak N (2004) Synthesis and characterization of polyesteramide resins from Nahar seed oil for surface coating applications. Prog Org Coat 51(2):103–108
22. Pramanik S, Sagar K, Konwar BK, Karak N (2012) Synthesis, characterization and properties of a castor oil modified biodegradable poly(ester amide) resin. Prog Org Coat 75(4):569–578
23. Pramanik S, Konwarh R, Sagar K, Konwar BK, Karak N (2013) Bio-degradable vegetable oil based hyperbranched poly(ester amide) as an advanced surface coating material. Prog Org Coat 76(4):689–697
24. Thames SF, Smith OW, Evans JM, Dutta S, Chen L (2005) Functionalized vegetable oil derivatives used in latex and coating compositions and their preparation. US7361710
25. Musa OM, Shih JS (2010) Performance-boosting UV-absorbing compounds for personal care and performance compositions. US8557226
26. Candy L, Vaca-Garcia C, Borredon E (2005) Synthesis and characterization of oleic succinic anhydrides: structure-property relations. J Am Oil Chem Soc 82(4):271–277
27. Tomoda H, Sugimoto Y, Tani Y, Watanabe S (1998) Characteristic properties of cutting fluid additives derived from the reaction products of hydroxyl fatty acids with some acid anhydrides. J Surfact Deterg 1(4):533–537
28. Bertz SH, Miksza FM, Zucker E (2001) Adduct characterized by absence of free maleic anhydride; personal care products. 4p
29. Espana JM, Sanchez-Nacher L, Boronat T, Fombuena V, Balart R (2012) Properties of biobased epoxy resins from epoxidized soybean oil (ESBO) cured with maleic anhydride (MA). J Am Oil Chem Soc 89(11):2067–2075
30. Gerbase AE, Petzhold CL, Costa APO (2002) Dynamic mechanical and thermal behavior of epoxy resins based on soybean oil. J Am Oil Chem Soc 79(8):797–802
31. Samper MD, Fombuena V, Boronat T, Garcia-Sanoguera D, Balart R (2012) Thermal and mechanical characterization of epoxy resins (ELO and ESO) cured with anhydrides. J Am Oil Chem Soc 89(8):1521–1528
32. Huang Y, Pang L, Wang H, Zhong R, Zeng Z, Yang J (2013) Synthesis and properties of UV-curable tung oil based resins via modification of Diels-Alder reaction, nonisocyanate polyurethane and acrylates. Prog Org Coat 76(4):654–661
33. Ge Q, Wang H, She Y, Jiang S, Cao M, Zhai L, Jiang S (2015) Synthesis, characterization, and properties of acrylate-modified tung-oil waterborne insulation varnish. J Appl Polym Sci 132(10):41608/1–41608/8
34. Tran P, Seybold K, Graiver D, Narayan R (2005) Free radical maleation of soybean oil via a single-step process. J Am Oil Chem Soc 82(3):189–194
35. Force CG, Starr FS (1988) Vegetable oil adducts as emollients in skin and hair care products. US4740367
36. Bidulescu G, Stere EA, Tarko L (1986) Manufacture of maleimides from aromatic primary amines. RO89171A2
37. Yamamoto T, Mizuno S, Watanabe M (1994) Preparation of N-arylmaleimides from maleic anhydride and aromatic amines. JP06184104A

38. Yamamoto T, Mizuno S, Watanabe M (1995) Preparation and purification of N-substituted maleimide. JP07109258A
39. Yamamoto T, Mizuno S, Watanabe M (1995) Preparation of maleimide derivatives. JP07053513A
40. Fujita T, Irie T, Takayanagi Y, Narita T, Yano Y (1989) Preparation of N-substituted maleimides. DE3905872A1
41. Sudo I, Watabe Y (1992) Preparation of maleimides. JP04198167A
42. Oonuma Y, Chiba H, Kanayama K (1994) Preparation of maleimides. JP06016627A
43. Ikeda I, Yamashita W, Tamai S (1998) Preparation of (poly)maleimides as monomers. JP10175952A
44. Le Z-G, Chen Z-C, Hu Y, Zheng Q-G (2004) Organic reactions in ionic liquids: ionic liquid-promoted efficient synthesis of N-alkyl and N-arylimides. Synthesis 7:995–998
45. Reddy PY, Kondo S, Toru T, Ueno Y (1997) Lewis acid and hexamethyldisilazane-promoted efficient synthesis of N-alkyl- and N-arylimide derivatives. J Org Chem 62(8):2652–2654
46. Doi S, Takayanagi Y (1986) N-substituted maleimides. EP177031A1
47. Ueda H, Kita J, Kishino K (1993) Preparation of maleimides. JP05213869A
48. Wu K-C, Tung Y-L, Lee C-H, Dai J-C, Huang C-H (2003) Imidation method and catalysts for the production of maleimides from maleic anhydride and primary amines. US6630595
49. Manjula KS, Rai KML, Umesha KB, Babu MS, Jagadeesha RL (2003) Microwave-assisted synthesis of N-aryl maleimide under solvent free conditions. Bulg Chem Commun 35 (3):192–194
50. Matsukawa M, Wada M, Minazu H, Furuya M, Nagata T (1991) Preparation of N-substituted maleimides. JP03011060A
51. Gaina V, Gaina C (2004) Dehydrochlorination of α-chlorosuccinimides, a new method for synthesis of high-purity maleimides. Mater Plast (Bucharest) 41(3):169–172
52. Walker MA (1994) The Mitsunobu reaction - a novel method for the synthesis of bifunctional maleimide linkers. Tetrahedron Lett 35(5):665–668
53. Ahn KD, Koo DI, Willson CG (1995) Synthesis and polymerization of t-Boc protected maleimide monomers - N-(t-butyloxycarbonyloxy) maleimide and N-p-(t-butyloxycarbonyloxy) phenyl-maleimide. Polymer 36(13):2621–2628
54. Wang ZY (1990) Syntheses of some N-alkylmaleimides. Synth Commun 20(11):1607–1610
55. Katritzky AR, Fan WQ, Li QL, Bayyuk S (1989) Novel chromophoric heterocycles based on maleimide and naphthoquinone. J Heterocyc Chem 26(4):885–892
56. Oishi T, Fujimoto M (1992) Synthesis and polymerization of N-4-N′-(alpha-methylbenzyl) aminocarbonylphenyl maleimide. J Polym Sci A Polym Chem 30(9):1821–1830
57. Oishi T, Kagawa K, Fujimoto M (1993) Synthesis and polymerization of N-N′-(alpha-methylbenzyl)amino carbonyl methyl maleimide. Macromolecules 26(1):24–29
58. Kitagawa O, Izawa H, Sato K, Dobashi A, Taguchi T, Shiro M (1998) Optically active axially chiral anilide and maleimide derivatives as new chiral reagents: synthesis and application to asymmetric Diels-Alder reaction. J Org Chem 63(8):2634–2640
59. Yanase M, Kagawa T (2005) Optically active polymaleimides, their manufacture, and uses for separation of optically active compounds. JP2005255795A
60. Cai H, He XH, Zheng DY, Qiu JA, Li ZC, Li FM (1996) Vinyl monomers bearing chromophore moieties and their polymers. 2. Fluorescence and initiation behavior of N-(4-N′, N′-dimethylaminophenyl)maleimide and its polymer. J Polym Sci A Polym Chem 34 (7):1245–1250
61. Reddy PY, Kondo S, Fujita S, Toru T (1998) Efficient synthesis of fluorophore-linked maleimide derivatives. Synthesis 7:999–1002
62. Palmer M, Buchkremer M, Valeva A, Bhakdi S (1997) Cysteine-specific radioiodination of proteins with fluorescein maleimide. Anal Biochem 253(2):175–179
63. Majima E, Shinohara Y, Yamaguchi N, Hong YM, Terada H (1994) Importance of loops of mitochondrial ADP/ATP carrier for its transport activity deduced from reactivities of its cysteine residues with the sulfhydryl reagent eosin-5-maleimide. Biochemistry 33 (32):9530–9536

64. Houstek J, Pedersen PL (1985) Adenine nucleotide and phosphate transport systems of mitochondria. Relative location of sulfhydryl groups based on the use of the novel fluorescent probe eosin-5-maleimide. J Biol Chem 260(10):6288–6295
65. Liu SQJ, Knauf PA (1993) Lys-430, site of irreversible inhibition of band-3 Cl(-) flux by eosin-5-maleimide, is not at the transport site. Am J Physiol 264(5):C1155–C1164
66. Majima E, Koike H, Hong YM, Shinohara Y, Terada H (1993) Characterization of cysteine residues of mitochondrial ADP/ATP carrier with the SH-reagents eosin 5-maleimide and N-ethylmaleimide. J Biol Chem 268(29):22181–22187
67. Blackman SM, Cobb CE, Beth AH, Piston DW (1996) The orientation of eosin-5-maleimide on human erythrocyte band 3 measured by fluorescence polarization microscopy. Biophys J 71(1):194–208
68. Kedar PS, Colah RB, Kulkarni S, Ghosh K, Mohanty D (2003) Experience with eosin-5′-maleimide as a diagnostic tool for red cell membrane cytoskeleton disorders. Clin Lab Haematol 25(6):373–376
69. King MJ, Smythe JS, Mushens R (2004) Eosin-5-maleimide binding to band 3 and Rh-related proteins forms the basis of a screening test for hereditary spherocytosis. Br J Haematol 124 (1):106–113
70. Girodon F, Garcon L, Bergoin E, Largier M, Delaunay J, Feneant-Thibault M, Maynadie M, Couillaud G, Moreira S, Cynober T (2008) Usefulness of the eosin-5′-maleimide cytometric method as a first-line screening test for the diagnosis of hereditary spherocytosis: comparison with ektacytometry and protein electrophoresis. Br J Haematol 140(4):468–470
71. Kamata T, Akasaka K, Ohrui H, Meguro H (1993) A sensitive fluorometric assay of glutathione reductase activity with N-(9-acridinyl)maleimide. Anal Sci 9(6):867–870
72. Aykin N, Neal R, Yusof M, Ercal N (2001) Determination of captopril in biological samples by high performance liquid chromatography with ThioGlo(TM)3 derivatization. Biomed Chromatogr 15(7):427–432
73. Penugonda S, Wu W, Mare S, Ercal N (2004) Liquid chromatography analysis of N-(2-mercaptopropionyl)-glycine in biological samples by ThioGlo 3 derivatization. J Chromatogr B Anal Technol Biomed Life Sci 807(2):251–256
74. Mare S, Penugonda S, Ercal N (2005) High-performance liquid chromatography analysis of MESNA (2-mercaptoethane sulfonate) in biological samples using fluorescence detection. Biomed Chromatogr 19(1):80–86
75. Nakashima K, Umekawa C, Yoshida H, Nakatsuji S, Akiyama S (1987) High-performance liquid chromatography-fluorometry for the determination of thiols in biological samples using N-4-(6-dimethylamino-2-benzofuranyl) phenyl-maleimide. J Chromatogr 414 (1):11–17
76. Lo KKW, Hui WK, Ng DCM, Cheung KK (2002) Synthesis, characterization, photophysical properties, and biological labeling studies of a series of luminescent rhenium(I) polypyridine maleimide complexes. Inorg Chem 41(1):40–46
77. DiGleria K, Hill HAO, Wong LL (1996) N-(2-ferrocene-ethyl)maleimide: a new electroactive sulphydryl-specific reagent for cysteine-containing peptides and proteins. FEBS Lett 390(2):142–144
78. Gandini A (2013) The furan/maleimide Diels-Alder reaction: a versatile click-unclick tool in macromolecular synthesis. Prog Polym Sci 38(1):1–29
79. Durmaz H, Colakoclu B, Tunca U, Hizal G (2006) Preparation of block copolymers via diels alder reaction of maleimide- and anthracene-end functionalized polymers. J Polym Sci A Polym Chem 44(5):1667–1675
80. Gacal B, Durmaz H, Tasdelen MA, Hizal G, Tunca U, Yagci Y, Demirel AL (2006) Anthracene-maleimide-based Diels-Alder “click chemistry” as a novel route to graft copolymers. Macromolecules 39(16):5330–5336
81. Yameen B, Rodriguez-Emmenegger C, Preuss CM, Pop-Georgievski O, Verveniotis E, Trouillet V, Rezek B, Barner-Kowollik C (2013) A facile avenue to conductive polymer

brushes via cyclopentadiene-maleimide Diels-Alder ligation. Chem Commun 49 (77):8623–8625
82. Liu YL, Yu JM, Chou CI (2004) Preparation and properties of novel benzoxazine and polybenzoxazine with maleimide groups. J Polym Sci A Polym Chem 42(23):5954–5963
83. Ishida H, Ohba S (2005) Synthesis and characterization of maleimide and norbornene functionalized benzoxazines. Polymer 46(15):5588–5595
84. Chaisuwan T, Ishida H (2006) High-performance maleimide and nitrile-functionalized benzoxazines with good processability for advanced composites applications. J Appl Polym Sci 101(1):548–558
85. Musa OM, Xhang R, Zhang R Curable liquid composition used as adhesive or encapsulant for affixing semiconductor devices onto substrate, comprises bisoxazoline resin, and resin having one or more reactive carbon to carbon double bonds e.g. 1,6-hexanediol diacrylate. WO2005085384-A1; EP1716215-A1; US2007032578-A1; US7390430-B2; TW200606231-A; EP1716215-B1; DE602004027549-E; TW384045-B1; SG116203-B
86. Musa OM, Sridhar LM, Yuan-Huffman QW Synthesizing product having triazole functionality, useful in film adhesive, comprises bulk polymerization of reactants having e.g. azide functionality using copper without a reducing agent in the absence of solvent. WO2008048733-A1; TW200829625-A; EP2078050-A1; KR2009088371-A; JP2010506940-W; CN101652405-A; US2010121022-A1
87. Musa OM (2004) Cycloaliphatic epoxy compounds containing styrenic, cinnamyl, or maleimide functionality. US6716992
88. Musa OM (2008) Maleimide resin with cyanurate core. US7456280
89. Phelan JC, Sung CSP (1997) Cure characterization in bis(maleimide)/diallylbisphenol A resin by fluorescence, FT-IR, and UV-reflection spectroscopy. Macromolecules 30 (22):6845–6851
90. Marr B, Musa OM (2010) Diphenyl oxide compound for forming curable composition used as, e.g. coating, has diphenyl oxide backbone and pendant from backbone which is hydrocarbon chain containing ester functionality and terminated with maleimide functional group. US2010311207
91. Marr B, Musa OM, Zhuo Q (2009) Curable composition useful as adhesives, coatings, and encapsulants for various fabrication steps in the semiconductor packaging industry comprises oligomeric adduct of bismaleimide, diamine and dithiol; and a curing initiator. WO2009145779-A1
92. Olsen LC, Boyce BJ, Musa OM Vibrating screen assembly for separating e.g. rock in aggregate business, has screen deck and three cross braces diagonally disposed within frame, where one cross brace is positioned in center portion of deck to stiffen deck. US2004222135-A1; WO2004098797-A2; US6953121-B2; CN100344674-C; WO2004098797-A3
93. Musa OM, Marr B (2010) Alcohols containing imide moieties and reactive oligomers prepared therefrom. US20100190998-A1
94. Musa OM (2009) New oligomeric compound obtained by Michael addition reaction of a thiol with a maleimide compounds useful as a curable composition, adhesives, coatings and encapsulants, and for various fabrication steps in semiconductor packaging. US2010036136-A1
95. Molly H, Askym FS, Charles EH, Joe BW, Charles MW, Garfield TW (2005) Maleimide—Vinyl ether-based polymer dispersed liquid crystals, in stimuli-responsive polymeric films and coatings. American Chemical Society, Washington, DC, pp 195–213
96. Decker C, Bianchi C, Morel F, Jonsson S, Hoyle C (2000) Mechanistic study of the light-induced copolymerization of maleimide/vinyl ether systems. Macromol Chem Phys 201 (13):1493–1503
97. Hoyle CE, Clark SC, Jönsson ES (2005) Polymerization processes using aliphatic maleimides. Google Patents

98. Jonsson S, Viswanathan K, Hoyle CE, Clark SC, Miller C, Nguyen C, Zhao W, Shao L, Morel F, Decker C (2000) Recent development in free radical photopolymerization. Direct and sensitized excitation of maleimides. J Photopolym Sci Technol 13(1):125–143
99. Fan SL, Boey FYC, Abadie MJM (2007) UV curing of a liquid based bismaleimide-containing polymer system. eXPRESS Polym Lett 1(6):397–405
100. Hoyle CE, Viswanathan K, Clark SC, Miller CW, Nguyen C, Jonsson S, Shao LY (1999) Sensitized polymerization of an acrylate/maleimide system. Macromolecules 32 (8):2793–2795
101. Bongiovanni R, Sangermano M, Malucelli G, Priola A (2005) UV curing of photoinitiator-free systems containing bismaleimides and diacrylate resins: bulk and surface properties. Prog Org Coat 53(1):46–49
102. Herr D, Schultz RA, Xu P, McLaughlin SR (2001) Die attach adhesives for use in micro-electronic devices. US6265530
103. Dershem SM, Patterson DB, Osuna JA (2006) Maleimide compounds in liquid form. US7102015
104. Horai A, Funaki K (2002) Maleimides for photoresist monomers, and their manufacture. JP2002069056A
105. Osuch CE, McFarland MJ (1990) Blocked monomer and polymers therefrom for use as photoresists. US 4962171
106. Zhang X, Chen G-C, Collins A, Jacobson S, Morganelli P, Dar YL, Musa OM (2009) Thermally degradable maleimides for reworkable adhesives. J Polym Sci A Polym Chem 47(4):1073–1084
107. Khosravi E, Musa OM (2011) Thermally degradable thermosetting materials. Eur Polym J 47 (4):465–473
108. Khosravi E, Iqbal F, Musa OM (2011) Thermosetting ROMP materials with thermally degradable linkages. Polymer 52(2):243–249
109. Canary SA, Stevens MP (1992) Thermally reversible cross-linking of polystyrene via the furan-maleimide Diels-Alder reaction. J Polym Sci A Polym Chem 30(8):1755–1760
110. McElhanon JR, Wheeler DR (2001) Thermally responsive dendrons and dendrimers based on reversible furan-maleimide Diels-Alder adducts. Org Lett 3(17):2681–2683
111. Szalai ML, McGrath DV, Wheeler DR, Zifer T, McElhanon JR (2007) Dendrimers based on thermally reversible furan-maleimide Diels-Alder adducts. Macromolecules 40(4):818–823
112. Ondrus V, Fisera L, Polborn K, Ertl P, Pronayova N (1995) Diels-Alder reaction of fulvenes with N-(3,5-dichlorophenyl)-maleimide. Monatshefte Fur Chemie 126(8-9):961–969
113. Liu YL, Hsieh CY (2006) Crosslinked epoxy materials exhibiting thermal remendability and removability from multifunctional maleimide and furan compounds. J Polym Sci A Polym Chem 44(2):905–913
114. Stenzel MH (2013) Bioconjugation using thiols: old chemistry rediscovered to connect polymers with nature's building blocks. ACS Macro Lett 2(1):14–18
115. Elliott JT, Prestwich GD (2000) Maleimide-functionalized lipids that anchor polypeptides to lipid bilayers and membranes. Bioconjug Chem 11(6):832–841
116. Le Sann C (2006) Maleimide spacers as versatile linkers in the synthesis of bioconjugates of anthracyclines. Nat Prod Rep 23(3):357–367
117. Warnecke A, Fichtner I, Garmann D, Jaehde U, Kratz F (2004) Synthesis and biological activity of water-soluble maleimide derivatives of the anticancer drug carboplatin designed as albumin-binding prodrugs. Bioconjug Chem 15(6):1349–1359
118. Warnecke A, Kratz F (2003) Maleimide-oligo(ethylene glycol) derivatives of camptothecin as albumin-binding prodrugs: synthesis and antitumor efficacy. Bioconjug Chem 14 (2):377–387
119. Bykov VJN, Issaeva N, Zache N, Shilov A, Hultcrantz M, Bergman J, Selivanova G, Wiman KG (2005) Reactivation of mutant p53 and induction of apoptosis in human tumor cells by maleimide analogs. J Biol Chem 280(34):30384–30391
120. Ghosh SS, Kao PM, McCue AW, Chappelle HL (1990) Use of maleimide-thiol coupling chemistry for efficient syntheses of oligonucleotide-enzyme conjugate hybridization probes. Bioconjug Chem 1(1):71–76

Part III
Maleic Anydride-Derived Polymers

Chapter 4
The Quintessential Alternating Copolymer Family: Alkyl Vinyl Ether co-Maleic Anhydride Copolymers

Krystyna Plochocka, Xuejun (Jay) Liu, Michael A. Tallon, and Osama M. Musa

4.1 Maleic Anhydride-*co*-Alkyl Vinyl Ether Copolymer

4.1.1 Composition of Maleic Anhydride-co-Alkyl Vinyl Ether Copolymers

From the viewpoint of polymerization behavior, a characteristic property of both maleic anhydride and alkyl vinyl ethers is their low reactivity in homopolymerization under common conditions of radical polymerization. Yet, together they can be easily copolymerized to create alternating maleic anhydride/alkyl vinyl ether copolymer with high molecular weight (Fig. 4.1) [1, 2]. These copolymers prove to be extremely versatile, making possible molecular structure modifications to adjust their properties by varying the R group in the vinyl ether monomer units. Some of the C_1–C_{18} alkyl vinyl ethers are commercially available. The practical importance of maleic anhydride–alkyl vinyl ether copolymers is related to the versatility of the chemical reactions that can be performed on the anhydride unit, yielding a variety of useful derivatives via and/or post-polymerization.

4.1.1.1 Maleic Anhydride-*co*-Methyl Vinyl Ether Copolymer

The simplest form of alkyl vinyl ethers is methyl vinyl ether. Copolymers based on maleic anhydride and methyl vinyl ether are commercially available and are supplied by Ashland Inc. under the Gantrez® AN, Gantrez® S, Gantrez® ES, and Gantrez® MS trade names [3].

K. Plochocka • X.(J). Liu • M.A. Tallon (✉) • O.M. Musa
Ashland Inc., 1005 Route 202/206, Bridgewater, NJ 08807, USA
e-mail: MTallon@ashland.com

O.M. Musa (ed.), *Handbook of Maleic Anhydride Based Materials*,
DOI 10.1007/978-3-319-29454-4_4

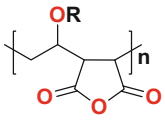

Fig. 4.1 Molecular structure of alternating maleic anhydride-*co*-alkyl vinyl ether copolymers

These high molecular weight poly(maleic anhydride-*co*-methyl vinyl ether) copolymers can be synthesized by free-radical processes in organic solvents [4–8]. To achieve high molecular weight, the process can employ non-chain-transfer-type solvents [9]. These solvents can then be removed by azeotropic distillation of the hydrolyzed copolymer in water, if it is not desired in the final product.

Polymerization processes in nonpolar solvents typically yield a copolymer with a specific viscosity of about 2–4, measured as 1 wt/v % in methyl ethyl ketone by Eq. (4.1):

$$\text{Specific viscosity } \eta_{sp} = (t - t_0)/t_0 \tag{4.1}$$

where t is the efflux time of the polymer solution and t_0 is the efflux time of the solvent through a capillary-type viscometer (Table 4.1).

This yields an alternating maleic anhydride/methyl vinyl ether copolymer with a specific viscosity in a range from about 2 to 4, as deduced from ^{13}C-NMR and Size-Exclusion Chromatography techniques. Chain transfer agents can also be employed to target specific viscosity within the polymerization process as well.

In contrast, the polymerization of maleic anhydride–methyl vinyl ether in solvents like acetone yields copolymers having lower viscosities [10–17]. The copolymer obtained by this process has a low intrinsic viscosity ($\leq$0.3, 1 g/100 ml in methyl ethyl ketone at 25 °C). After polymerization, the copolymer is reacted with alcohol to form monoester products, and the acetone is distilled off. The monoester derivatives have been demonstrated to be suitable for use in hairspray products.

Furthermore, a low specific viscosity grade of maleic anhydride–methyl vinyl ether copolymer has been made in sterically hindered ether, such as methyl *t*-butyl monoether [15]. The use of a sterically hindered ether as the solvent avoids any potential solvent peroxide formation in the reaction medium, thereby providing a safer process. In particular, acetone peroxide is a well-known explosive that can potentially form if any moisture is present in the acetone/peroxide combination employed in the polymerization. The copolymer obtained has a specific viscosity of less than 0.4.

4.1.1.2 Maleic Anhydride–Methyl Vinyl Ether–Isobutylene Terpolymer

Partial replacement of the alkyl vinyl ether monomer in maleic anhydride-*co*-alkyl vinyl ether copolymers with α-olefin monomers yields terpolymers with increased

Table 4.1 Specific viscosities of maleic anhydride–methyl vinyl ether copolymer synthesized from different processes

Solvent type	Solvent	Chain-transfer constant[a]	Specific viscosity[b]
Apolar	Benzene	0.028	1–5
Apolar	Toluene	0.105	2–4
Slightly polar	Ethyl acetate	15.5	2–3.5
Slightly polar	Ethyl acetate/acetone	15.5/4.1	1.0–3.5
Polar	Acetone	4.1	$\leq$0.3
Apolar	Methyl *t*-butyl monoether	n/a	<0.4

[a]Brandrup, Polymer Handbook, 3rd edition, $C_S \times 10^4$ for polymerization of styrene
[b]1 wt/v% in methyl ethyl ketone at 25 °C

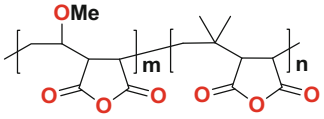

Fig. 4.2 Molecular structure of alternating poly(methyl vinyl ether-*co*-maleic anhydride-co-isobutylene terpolymer

hydrophobicity. Varying the ratio of alkyl vinyl ether and α-olefin enables for fine-tuning the hydrophobic/hydrophilic balance in the final polymer.

For example, maleic anhydride in combination with methyl vinyl ether and isobutylene readily undergoes radically induced polymerization to produce a terpolymer where maleic anhydride forms equimolar units with the combined monomers of methyl vinyl ether and isobutylene in the polymer chain [18, 19].

Since the homopolymers of methyl vinyl ether and isobutylene can only be formed by a cationic mechanism, the terpolymers thus obtained are of alternating molecular structure between (maleic anhydride/methyl vinyl ether units) or (maleic anhydride/isobutylene units), similar to that of the well-known poly(maleic anhydride-*co*-methyl vinyl ether) and poly(maleic anhydride-*co*-isobutylene) copolymers themselves, as presented in Fig. 4.2.

The terpolymer of maleic anhydride–methyl vinyl ether–isobutylene can be synthesized in a variety of organic solvents to produce terpolymers that exhibit a molecular weight of 30,000–400,000 daltons (Da). Copolymerization in a mixture of methyl vinyl ether with isobutylene as a reaction medium results in polymers with molecular weight above 2,000,000 Da [19].

Methyl vinyl ether has been shown to exhibit higher reactivity than isobutylene towards maleic anhydride enabling polymerization to proceed rapidly for the methyl vinyl ether/maleic anhydride pair over that of the isobutylene/maleic anhydride pair, when both pairs are present within the reaction medium at the same time [19]. This finding is demonstrated in Fig. 4.3, wherein a higher molar ratio of methyl vinyl ether over that of isobutylene is found in the terpolymer than that employed in the reaction charge.

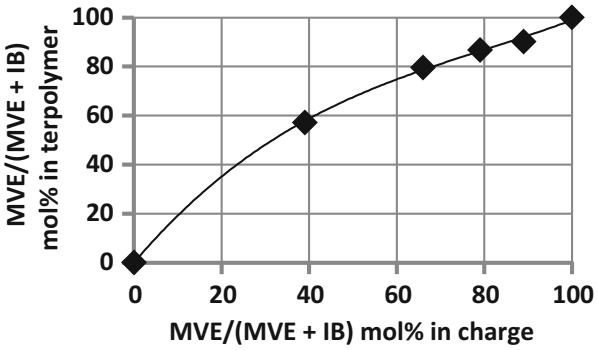

Fig. 4.3 The molar ratio of methyl vinyl ether/isobutylene in the charge and that found in the terpolymer [13]. *MVE* methyl vinyl ether, *IB* isobutylene (Adapted from [19])

4.1.1.3 Cross-Linked Copolymer of Maleic Anhydride–Methyl Vinyl Ether

Cross-linked maleic anhydride–alkyl vinyl ether copolymers can be synthesized in the presence of cross-linking agents. The selection of solvent has a significant impact on the final viscosity, stability, salt tolerance, and clarity of the hydrolyzed polymers in aqueous formulations [20]. Furthermore, the cross-linked copolymers have demonstrated excellent thickening and rheological properties that have been shown to be suitable for use in personal care formulations. Cross-linked copolymers based on maleic anhydride and methyl vinyl ether are commercially available and are supplied by Ashland Inc. under the Stabileze® brand name.

4.1.1.4 Branched Copolymer of Maleic Anhydride–Methyl Vinyl Ether

Similarly, high molecular weight and homogeneously branched maleic anhydride–methyl vinyl ether copolymers can be synthesized in the presence of a small amount of cross-linker, which at this concentration behaves as a branching agent (Fig. 4.4) [21–23]. When larger amounts of cross-linker are employed, an insoluble cross-linked polymer results. Therefore, the concentration of cross-linker employed will dictate if a soluble branched polymer or a highly cross-linked insoluble polymer is obtained [20, 24].

The branched maleic anhydride/methyl vinyl ether copolymers are typically soluble in acetone. The branched copolymers also exhibit different oscillatory and shear rheological properties than the fully linear or fully cross-linked copolymer counterparts [23]. For example, the branched maleic anhydride–methyl vinyl ether copolymers do not exhibit a substantial storage modulus *G*', as compared to their cross-linked counterparts.

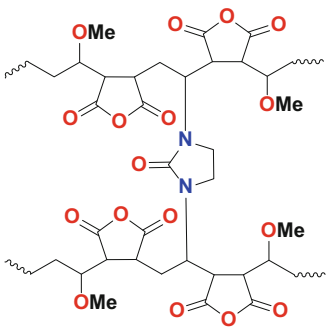

Fig. 4.4 Molecular structure of branched maleic anhydride–methyl vinyl ether copolymers

4.1.1.5 Maleic Anhydride–Mixed Alkyl Vinyl Ether Copolymers

The copolymerization of maleic anhydride with mixed alkyl vinyl ethers enables modulation of the polymer's hydrophobicity and glass transition temperature, as depicted in Fig. 4.5. Typically, short chain alkyl vinyl ethers, such as methyl vinyl ether, are employed as the major component. When small amounts of long chain alkyl vinyl ethers are introduced, the film properties of these terpolymers exhibits increased water resistance and enhanced flexibility [25, 26].

The cross-linked terpolymers of C_1–C_4 alkyl vinyl ether–maleic anhydride and a hydrophobic C_6–C_{18} alkyl vinyl ether also demonstrate improved salt tolerance as thickening agents, when compared to those based on soluble short chain alkyl vinyl ethers and maleic anhydride alone [27]. This result is achieved by an additional interaction mechanism between Alkyl chains, namely, hydrophobic interactions.

Therefore, hydrophobically modified water soluble polymers poly(methyl vinyl ether-*co*-maleic acid-*co*-dodecyl vinyl ether) tend to exhibit more stable viscosity profiles than their hydrophilic poly(methyl vinyl ether-*co*-maleic acid) counterpart as pH and ionic strength increase. For instance, as the pH is increased from pH 2 to pH 8, the viscosity of the polymer solution rises to a plateau for both types of polymers.

However, as the pH rises above pH = 9+, the hydrophilic-type copolymer such as (poly-methyl vinyl ether-*co*-maleic anhydride), viscosity drops as the polymer no longer can hydrogen bond to adjacent chains, and ionic repulsion between the highly negative charged polymers occurs. In contrast, the longer hydrophobic chain-length vinyl ethers do not exhibit this viscosity drop but remain constant instead, since hydrophobic association between hydrophobes on different chains still remains.

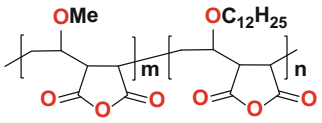

Fig. 4.5 Molecular structure of methyl vinyl ether–maleic anhydride–dodecyl vinyl ether terpolymer

4.1.1.6 Maleic Anhydride–Divinyl Ether Copolymer

Maleic anhydride reacts with divinyl ether to form divinyl ethyl–maleic anhydride copolymer (DIVEMA), also known as Pyran® copolymer. The polymer is synthesized through a unique free-radical cyclopolymerization process (Scheme 4.1) in which a soluble copolymer is formed (rather than an insoluble cross-linked copolymer). This copolymer possesses a 2:1 alternating backbone structure. DIVEMA has shown a broad spectrum of biological activities in its sodium salt form [28].

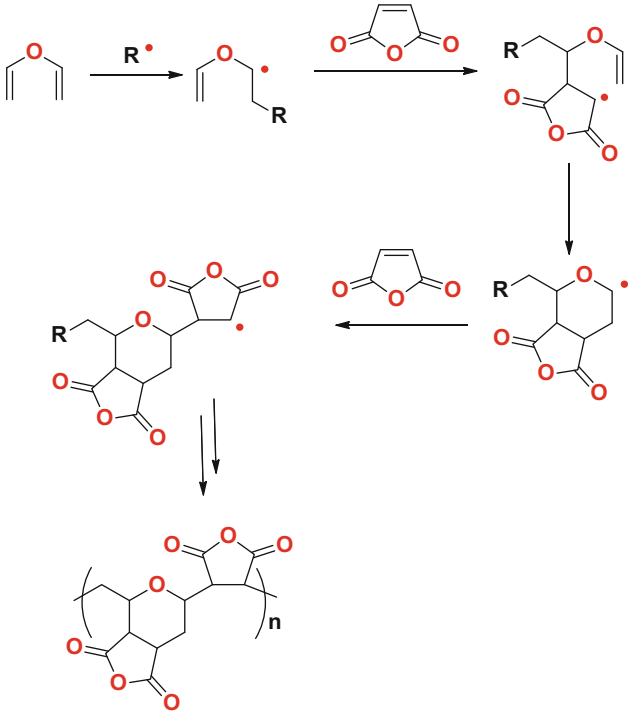

Scheme 4.1 Polymerization of maleic anhydride and divinyl ether to form DIVEMA ("Pyran® copolymer")

4.1.2 Mechanism of Copolymerization of Maleic Anhydride and Alkyl Vinyl Ethers

4.1.2.1 Radical Copolymerization of Non-homopolymerizable Monomers

In an alternating radical copolymerization, the reactivity ratios, r_1 and r_2, of the two monomers, M_1 and M_2, are characterized by $1 > r_1 \times r_2 = 0$, and both r_1 and r_2 are less than one [29]. The parameters r_1 and r_2 are defined by

$$r_1 = \frac{k_{11}}{k_{12}}$$

and

$$r_2 = \frac{k_{22}}{k_{21}}$$

where k_{11} is the rate constant for a growing radical chain ending in M_1 adding to monomer M_1, k_{12} is that for a growing radical chain ending in M_1 adding to monomer M_2, while k_{22} is that for a growing radical chain ending in M_2 adding to monomer M_2, and k_{21} is that for a growing radical chain ending in M_2 adding to monomer M_1. In the extreme alternating behavior, both r_1 and r_2 are equal to 0, and the two monomers enter into the polymer chain in 1:1 molar composition in a nonrandom, alternating arrangement. That is to say the growing radical species will only add the other monomer during the chain propagation step resulting in an alternating structure.

~$M_1M_2M_1M_2M_1M_2M_1M_2M_1M_2M_1M_2M_1M_2M_1M_2M_1M_2$~

In the moderate alternating behavior, three cases can occur: (1) both r_1 and r_2 are small values and the product $r_1 \times r_2$ is close to zero; (2) r_1 is small and $r_2 = 0$; or (3) r_2 is small and $r_1 = 0$. In all these cases, the polymer chain structure tends to be alternating.

Alkyl vinyl ethers and maleic anhydride also belong to a broad category of monomers yielding alternating copolymers by radical polymerization.

In alternating copolymerization, at least one monomer is incorporated into a polymer exclusively as a single unit. The other monomer can be also attached as a single unit, if it is not capable of homopolymerization at the reaction conditions, or as a longer monomer sequence in the event that it readily undergoes homopolymerization.

Based on the terminal copolymerization model, the simplest model in which propagation in copolymerization depends only on the rates of reactions of two monomers (M_1 and M_2) with corresponding growing macroradicals ending with –M_1 and –M_2, the reactivity ratios of the monomers are

$$r_1 = k_{11}/k_{12} \text{ and } r_2 = k_{22}/k_{21}$$

where k_{ij} is a rate constant of a corresponding propagation reaction. The terminal model predicts rate of copolymerization and monomer sequence distributions dependent only on the rates of propagation as described above.

If neither of the monomers are able to homopropagate, the resulting copolymer has an equimolar comonomer composition, 1:1 alternating molecular structure, and the monomer in excess in the feed remains unreacted. In addition to that, monomer reactivity ratios for the terminal copolymerization model are $r_1 = r_2 = 0$ (or very close to zero) and $r_1 \times r_2 = 0$.

However, if one of the comonomers (M_2) can homopolymerize, then its reactivity ratio $r_2 > 0$ and only $r_1 \times r_2 = 0$. Therefore, the copolymer consists of single –M_1—monomer units and potentially longer –$(M_2)_n$—runs, and the monomer M_2 can be completely reacted [30–33].

According to Braun and Hu[30], two non-homopolymerizable monomers can readily copolymerize by radical mechanism if they significantly differ in polarity, i.e., their *e*-values (from Alfrey's-Price Q, *e* scheme) have opposite signs and differ by one or two units, as it is in the case for the systems consisting of vinyl ethers having *e*-values in the range of −0.68 for dodecyl vinyl ether to −2.16 for phenyl vinyl ether and maleic anhydride with $e = 2.25$ (quoted from [30]). This important relationship is in agreement with the terminal model which assumes that reactivity ratios r_1 and r_2 depend on resonance stabilization of monomer and macroradical (Q) and on polar interactions between growing macroradical ends and monomers (e), with a prevailing importance of *e*-value in the case of electron donor (ED)–electron acceptor (EA) pairs.

Radical copolymerization of electron-donor monomers with electron-acceptor monomers tends to form an alternating copolymer chains. Electron-donor vinyl monomers include alkyl vinyl ethers, α-olefins, and vinyl aromatic monomers, among others. Some examples of electron-acceptor monomers are maleic anhydride, itaconic anhydride, citraconic anhydride, dialkyl citraconates and mesaconates, dialkyl maleates and fumarates, *N*-substituted maleimides, chlorotrifluoroethylene, and fumaronitrile [30]. Bulky vinyl ethers, such as adamantyl vinyl ether and norbornyl vinyl ether, yield equimolar alternating copolymers with tetrafluoroethylene as well [31]. Optically active aliphatic vinyl ethers can also form alternating copolymers with maleic anhydride [32, 33].

Braun and coworkers have investigated binary copolymerization between non-homopolymerizable electron-donor monomers such as chloroethyl vinyl ether, *iso*-butyl vinyl ether, or *trans*-anethole and non-homopolymerizable electron-acceptor monomers such as maleic anhydride or fumaronitrile [30, 34]. It was demonstrated that in all binary systems investigated, the reactivity ratios, r_1 and r_2, are close to zero, suggesting that predominantly 1:1 alternating copolymers were generated.

On the other hand, as reported by Bevington et al. [35, 36], in binary systems involving a variety of vinyl ethers (M_1) as non-homopolymerizable electron-donor

monomers paired with either methyl methacrylate or styrene as homopolymerizable monomers (M_2), reactivity ratios r_1 were always very close to zero, and reactivity ratios (r_2) were always higher than one, which means that vinyl ethers were incorporated into the polymer as single units, while styrene or methyl methacrylate could have formed longer monomer sections. Reactivity ratios (r_2) displayed significant differences as dependent on a vinyl ether partner.

4.1.2.2 Charge-Transfer Complex

The Terminal model has been widely used to characterize reactivity of monomers in copolymerization. However, its inability to fully describe all copolymerization systems was questioned since its inception. Major issues that are frequently raised regarding the terminal model is its inability to predict at the same time the copolymer composition, monomer sequence distributions, and the rate of propagation in copolymerization. Deviations from the terminal model are ascribed to the effect of the penultimate unit in a growing macroradical and to a variety of other interactions in the reaction system, such as complex formation between comonomers, complexation of monomers and growing macroradicals with solvents, physical separation of the environment of growing macroradical from the bulk of the reaction, and others. Therefore, more recently developed copolymerization models frequently comprise monomer reactivity ratios and equations describing copolymerization rates that include the effects listed above.

Charge-Transfer Complexes (CTCs) between pairs of monomers proved to be of particular interest in copolymerization research. CTC is usually described as a complex of an electron-donor monomer (ED), such as vinyl ether with an electron-acceptor monomer (EA), such as maleic anhydride in which electrons from the double bond of ED are partially transferred to the double bond of EA. ED–EA complex (otherwise known as EDA complex or CTC) was postulated by Mulliken [37] in order to interpret UV/Vis spectra of mixtures of ED and EA organic compounds (Scheme 4.2).

The presence of charge-transfer complexes in a reaction system often results in the appearance of colors from yellow to blue, where yellow tends to signify a weaker interaction, while blue indicates stronger interactions between the electron-donor and electron-acceptor pair. Color intensity of the reaction mixture typically weakens as the polymerization proceeds due to the consumption of the charge-transfer complex monomer pairs. In a solution, an equilibrium exists between the free electron-donor monomer, free electron-acceptor monomer, and the charge-transfer complex. The equilibrium constant K can be obtained by UV–Vis and ^{1}H NMR spectroscopy techniques.

$$K = \frac{[\text{charge transfer complex}]}{[\text{electron donor}] \times [\text{electron acceptor}]}$$

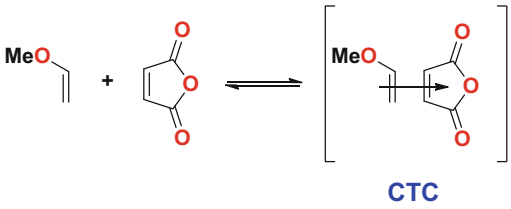

Scheme 4.2 Formation of charge-transfer complex (CTC) between methyl vinyl ether and maleic anhydride (adapted from [34])

In UV–Vis spectroscopy, the equilibrium constant can be determined by measuring the absorbance at various monomer concentrations. The equilibrium constant K is calculated using the Benesi–Hildebrand equation [38]. In ^{1}H NMR spectroscopy, the chemical shifts of the double bond protons, due to partial charge transfer, are employed to calculate the equilibrium constant [39].

Higher K values are frequently considered to indicate stronger interactions between electron-donor and electron-acceptor monomers, which results in the formation of a more stable charge-transfer complex. However, it should be noted that higher values of the equilibrium constant (K) do not necessarily mean that the charge-transfer complex will polymerize faster. This notion will be become quite clear in the following discussions of terpolymerization, as well as initiation of spontaneous polymerization. The K values for charge-transfer complexes of maleic anhydride with various comonomers in different solvents and at different temperatures are summarized in Tables 4.2, 4.3, 4.4, and 4.5 [33–49].

The participation of a charge-transfer complex in radical copolymerization was first proposed by Bartlett and Nozaki in 1946 for the system allyl acetate–maleic anhydride (Scheme 4.3) [40]. Since then, the effect of monomer–monomer complexes has become of significant interest in the field of radical copolymerization studies [30, 41, 42].

Equilibrium constants, K, for charge-transfer complexes of maleic anhydride with electron-donor monomers depend on the molecular structure of the monomers, solvent, and temperature. Solvent-monomer complexes can compete with the formation of charge-transfer complexes [42]. Solvent effect on the equilibrium constant, K, depends on its dielectric constant.

Rätzsch noted that K values tend to increase with increasing difference in "e-values," which represent the polar factor in the monomer reactivity, between maleic anhydride and the electron-donor monomers [41].

Increasing temperature often results in a reduced concentration of charge-transfer complex, because the stabilization energy afforded by the formation of a charge-transfer complex is not as significant at higher temperatures.

Research focused on charge-transfer complexes of monomers; their interactions with solvents and other solvent effects resulted in the development of more complex copolymerization models that are included in the following general list:

Table 4.2 Equilibrium constants, *K*, for charge-transfer complexes of maleic anhydride with various comonomers

Comonomer	Solvent	Temp (°C)	*K* (L/mol)	Method
n-Butyl vinyl ether	Cyclohexane/1,2-dichloroethane (9:1)	20	0.116	UV
n-Butyl vinyl ether	Cyclohexane/1,2-dichloroethane (9:1)	28	0.108	UV
n-Butyl vinyl ether	Cyclohexane/1,2-dichloroethane (9:1)	36	0.102	UV
n-Butyl vinyl ether	Cyclohexane/1,2-dichloroethane (9:1)	44	0.098	UV
n-Butyl vinyl ether	Cyclohexane/1,2-dichloroethane (9:1)	52	0.092	UV
n-Butyl vinyl ether	Cyclohexane/1,2-dichloroethane (9:1)	60	0.084	UV
n-Butyl vinyl ether	CCl_4	20	0.56	UV
iso-Butyl vinyl ether	CCl_4	20	1.11	UV
iso-Butyl vinyl ether	CCl_4	37	0.052	NMR

Adapted from [33–49]

Table 4.3 Equilibrium constants, *K*, for charge-transfer complexes of maleic anhydride with various comonomers

Comonomer	Solvent	Temp (°C)	*K* (L/mol)	Method
iso-Butyl vinyl ether	$CDCl_3$	37	0.036	NMR
iso-Butyl vinyl ether	$CHCl_3$	23	0.033	UV
iso-Butyl vinyl ether	Methyl ethyl ketone	25	0.023	UV
iso-Butyl vinyl ether	Acetonitrile-d_3	~23	0.135	NMR
iso-Butyl vinyl ether	$CDCl_3$	~23	0.066	NMR
iso-Butyl vinyl ether	CCl_4	~23	0.110	NMR
tert-Butyl vinyl ether	Acetone-d_6	35	1.78	NMR
tert-Butyl vinyl ether	CCl_4	20	2.12	UV
2-Chloroethyl vinyl ether	Benzene	10	0.11	UV
2-Chloroethyl vinyl ether	Benzene	30	0.10	UV
2-Chloroethyl vinyl ether	Benzene	51	0.07	UV
2-Chloroethyl vinyl ether	$CHCl_3$	10	0.13	UV
2-Chloroethyl vinyl ether	$CHCl_3$	30	0.10	UV

Adapted from [33–49]

- Terminal, in which the rate of propagation depends only on the molecular structure of the terminal radical and on the monomer it reacts with.
- Penultimate, where the rate of propagation depends on the molecular structure of the terminal radical and on the preceding monomer unit, i.e., penultimate unit, as well as the molecular structure of the monomer it reacts with (either implicit or explicit).

- Monomer complex participation (MCP), in which the rate of propagation depends on terminal or both terminal and penultimate units, and the reactivity of CTC that reacts with the growing macroradical as a whole, i.e., CTC plays role of a monomer.
- Monomer complex dissociation (MCD), where the rate of propagation depends on the terminal or terminal and penultimate unit, but CTC undergoes dissociation before it is attached, i.e., CTC serves as a source of both monomers.
- MCP and MCD models that allow also participation of free monomers in propagation.
- Monomer partitioning or the bootstrap effect, in which the monomer can be partitioned between the vicinity of growing macroradical and the bulk of the reaction.

Table 4.4 Equilibrium constants, *K*, for charge-transfer complexes of maleic anhydride with various comonomers

Comonomer	Solvent	Temp (°C)	*K* (L/mol)	Method
2-Chloroethyl vinyl ether	$CHCl_3$	51	0.09	UV
1,4-Dioxene	Benzene	10	0.074	UV
1,4-Dioxene	Benzene	25	0.069	UV
1,4-Dioxene	Benzene	51.5	0.058	UV
1,4-Dioxene	Toluene	10	0.042	UV
1,4-Dioxene	Toluene	25	0.040	UV
1,4-Dioxene	Toluene	51.5	0.035	UV
1,4-Dioxene	Chlorobenzene	25	0.051	UV
1,4-Dioxene	$CHCl_3$	10	0.055	UV
1,4-Dioxene	$CHCl_3$	25	0.054	UV
1,4-Dioxene	$CHCl_3$	51.5	0.040	UV
1,4-Dioxene	Acetone	25	0.047	UV

Adapted from [33–49]

Table 4.5 Equilibrium constants, *K*, for charge-transfer complexes of maleic anhydride with various comonomers

Comonomer	Solvent	Temp (°C)	*K* (L/mol)	Method
Styrene	$CHCl_3$	25	1.4	UV
Styrene	Methyl ethyl ketone	25	0.045	n/a
Styrene	Cyclohexane	60	0.25	NMR
Styrene	Cyclohexane-d_{12}	50	0.30	NMR
N-Vinyl pyrrolidone	$CHCl_3$	25	0.15	UV
Acrylic acid	Acetone-d_6	25	0.056	NMR
Acrylic acid	Dioxane-d_6	25	0.16	NMR

Adapted from [33–49]

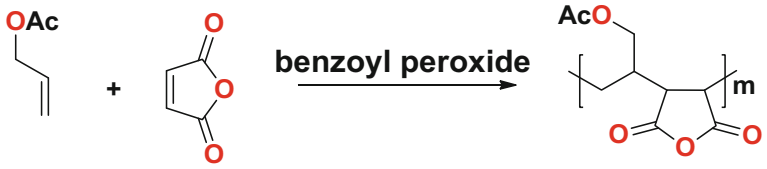

Scheme 4.3 Equimolar copolymerization of maleic anhydride and allyl acetate (adapted from [40])

Table 4.6 Correlation between CTC equilibrium constant (K) and expected outcome of polymerization

K (L/mol)	Copolymerization behavior
<0.01	Negligible CTC formation and no alternating copolymerization
0.01–0.1	Alternating copolymerization with radical initiator
0.1–1.0	Spontaneous alternating copolymerization near room temperature
1.0–5.0	(Spontaneous) ionic copolymerization
>5.0	Formation of stable charge-transfer complexes that can be isolated

Adapted from [46]

Some of the copolymerization models above were further developed to include contributions of complexation with solvents and complexes containing more than two entities.

Copolymerization models are reviewed and discussed in depth in references [30, 31, 47–49].

Studies on the monomer–monomer complex were extensively reviewed by Hill et al. [42] and Fukuda et al. [56]. However, despite the interest in the CTC role in copolymerization that continues until today, many questions still remain unanswered, the most critical being the issue of choosing the right kinetic model for a given reaction system.

Fitting of the copolymerization system to the terminal or penultimate model generally requires data on polymer composition and monomer sequence distributions vs. monomer feed. Models involving CTC, possible contributions of free monomers, and solvent effects also require also CTC equilibrium constants and kinetics of copolymerization.

Kokubo et al. have suggested that the value of the CTC equilibrium constant might be employed as a guideline to predict the outcome of charge-transfer copolymerizations in a binary system (Table 4.6) [46]. However, in the case of terpolymers, this suggestion is of limited utility, as the empirically derived reaction rate is required to compare the polymerization kinetics of the two charge-transfer complexes relative to each other to predict the outcome.

4.1.2.3 Copolymerization with Monomer Complex Participation

In a binary system where maleic anhydride copolymerizes with non-homopolymerizable electron-donor monomers, as in the case of seminal work of Bartlett and Nozaki [40], the copolymerization may be considered as a homopolymerization of the charge-transfer complex (Scheme 4.4) [30]. Therefore, the resulting copolymers always have an equimolar comonomer composition in an alternating molecular structure, as deduced from comonomer ratios and ^{13}C-NMR results.

In a ternary system, that includes maleic anhydride and two electron-donor monomers, two charge-transfer complexes can be formed, and the equilibrium constants can sometimes be employed to calculate reactivity ratios of the individual complexes. Kokubo et al. [46] interpreted the terpolymerization of maleic anhydride–chloroethyl vinyl ether–*p*-dioxene as a copolymerization between two monomer complexes: maleic anhydride–chloroethyl vinyl ether complex and maleic anhydride–*p*-dioxene complex (Scheme 4.5) [46]. Reactivity ratios of the complexes were found to be $r_1 = 1.52$ and $r_2 = 0.46$, respectively. Since, however, no data concerning rate of polymerization of the CTC complexes were available, it was not possible to predict the sequence distribution of the resulting terpolymer.

Since the CTC equilibrium constant involves concentrations of both complex and of the free monomers, the concept of CTC participation in copolymerization leads to an obvious question on the role of free monomers in propagation.

Therefore, in realistic *Monomer Complex Participation model* (MCP), it is assumed that CTC competes with both individual monomers in the chain propagation step, and that the rate of propagation depends on the reactivity ratios and the reaction rates of the monomers, monomer complexes, and the growing macroradicals, as well as the equilibrium constant, *K* [29, 30].

At constant temperature, concentration of the charge-transfer complex depends on the monomer feed composition, conversion, and solvent. If the stoichiometry of

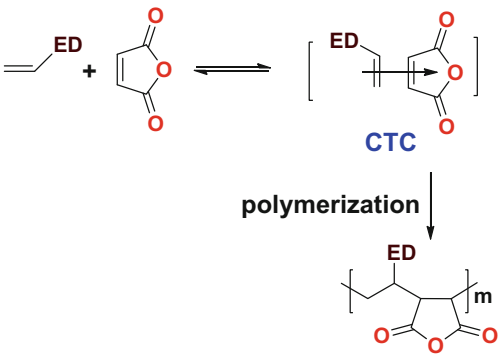

Scheme 4.4 Homopolymerization of charge-transfer complex formed between maleic anhydride and electron-donor (ED) monomer (adapted from [30])

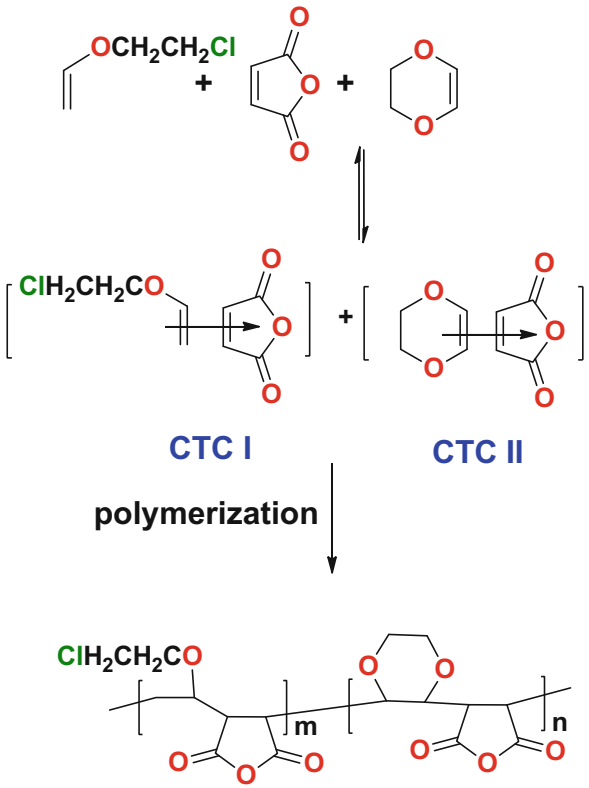

Scheme 4.5 Copolymerization of two charge-transfer complexes (CTC I and CTC II) formed in a ternary system containing chloroethyl vinyl ether, *p*-dioxene, and maleic anhydride (adapted from [46])

the complex is not well defined, such as the involvement of more than two monomers or solvents, this kinetic model becomes even more complicated.

In a *binary* copolymerization system, the impact of monomer concentration $[M_1]$ on the rate of propagation (R_p) helps to differentiate between the free monomers and the monomer complex [30, 57–60].

For the free monomers, the propagation rate, R_{pF}, is proportional to the monomer concentration $[M_1]$. However, for the monomer complex, the chain growth rate, R_{pCTC}, is second order dependent on the monomer concentration $[M_1]$. Therefore, at lower monomer concentration, R_{pF} dominates the overall polymerization process, while at higher monomer concentration, R_{pCTC} becomes more important. The critical monomer concentration $[M_1]_C$ is where the two partial propagation rates are equal.

$$X = \frac{[M_2]}{[M_1]}$$

$$A(X) = \frac{2k_{12}R_i^{0.5}X}{\left(k_{t11} + 2k_{t12}\,\frac{k_{12}}{k_{21}}X + k_{t22}\left(\frac{k_{12}}{k_{21}}X\right)^2\right)^{0.5}}$$

$$F(X) = K\left(\frac{k_{1CTC}}{k_{12}} + \frac{k_{2CTC}}{k_{21}}X\right)$$

$$R_{pF} = A(X)[M_1]$$

$$R_{pCTC} = A(X)F(X)[M_1]^2$$

$$R_p = R_{pF} + R_{pCTC}$$

In the equations provided, X is the ratio of free monomer concentrations, R_i is the initiation rate, k_{ij}'s are the propagation rate constants, k_t's are the termination rate constants, K is the CTC equilibrium constant, R_{pF} is the propagation rate for the free monomers, R_{pCTC} is the propagation rate for the monomer complex, and R_p is the overall propagation rate.

Work by Fujimori et al. provides support to the idea that both CTC and free monomers take part in the propagation in a *binary* system [39]. In the case of an exclusive cross-propagation of free monomers, the maximum initial rate of the alternating copolymerization should always occur at the same ratio of monomers, X, *a*nd this rate should be independent of total monomer concentration.

On the other hand, if homopolymerization of charge-transfer complex would be the only propagation reaction in the system, the maximum initial rate of reaction should occur at the 1:1 monomer ratio in the feed ($X = 0.5$). The pattern expected for the CTC only system was actually identified in copolymerization of maleic anhydride and *iso*-butyl vinyl ether ($CHCl_3$, AIBN, 50 °C), but only at the highest total monomer concentration of 1.5 mol/L (Fig. 4.6) [39].

However, at lower total monomer concentrations the positions of the rate maxima occurred at, correspondingly, 35 % maleic anhydride at total monomer feed of 0.5 mol/L and 43.5 % maleic anhydride at total feed of 1 mol/L. This indicates that both the 1:1 charge-transfer complex and the free monomers add to the growing macroradical terminals.

Spectroscopic analysis of linkage configuration and monomer unit distribution of maleic anhydride and *iso*-butyl vinyl ether copolymer by ^{13}C NMR also support the participation of the complex [44]. The copolymers formed were predominantly alternating. The copolymerization led to the same microstructure independent of polymerization conditions.

It was also observed that a significant proportion, i.e., 48 ± 4 %, of *cis* linkage configuration at the cyclic maleic anhydride units was present in the copolymer, which can only be explained by the complex participation mechanism (Fig. 4.7). If only free monomers participated in the copolymerization, predominantly *trans* linkage configuration should have been observed at cyclic maleic anhydride units in the copolymers due to steric hindrance.

The formation of a *cis* linkage configuration can be rationalized by an edge-on or orthogonal attack at the maleic anhydride side of a monomer complex followed by a

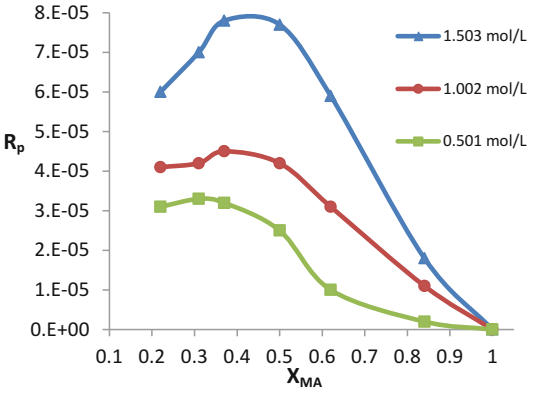

Fig. 4.6 Initial rate of copolymerization (R_p in mol/Ls) of maleic anhydride (MA) with isobutyl vinyl ether in chloroform at 50 °C. X_{MA}: molar fraction of maleic anhydride in the feed. Total monomer concentration *square*: 0.5010 mol/L; *circle*: 1.002 mol/L; *triangle*: 1.503 mol/L (adapted from [39])

concerted addition of the *iso*-butyl vinyl ether monomer unit within the complex (Fig. 4.7).

The simplified MCP model was also applied to copolymerization of maleic anhydride and *trans*-anethole (ANE) [61]. At fixed monomer concentration ratio X_{MA}, the plot of R_p/[ANE] against [ANE] gives a straight line, which is consistent with the MCP model (Fig. 4.8).

In methyl ethyl ketone, the equilibrium constant of donor–accepter complexation of the comonomers is small, $K = 0.057$/M at 26 °C. However, the ratios of the propagation rate constants were $k_{1CTC}/k_{12} = 2$ and $k_{2CTC}/k_{21} = 6$, which means that the charge-transfer complex of maleic anhydride–*trans*-anethole is more reactive than the free monomers. Similar results were also observed when the copolymerization was carried out in either chloroform or tetrahydrofuran.

In terpolymerization of one EA monomer (maleic anhydride) with two ED monomers (*trans*-anethole and *iso*-butyl vinyl ether), investigated by Braun et al. [30, 57], it has been found that a polymerization product contained always 50 mol % of donor and 50 mol % of acceptor units in an alternating sequence. Reactivity ratios were obtained for both complexes r_1 and r_2, in tetrachloromethane, chloroform, acetonitrile, and tetrahydrofuran used as polymerization solvents (Scheme 4.6) (Table 4.7).

As it is evident from data in Table 4.7, the tendency for cross polymerization of the two monomer complexes varied as a function of the reaction solvent. Unfortunately, no clear-cut correlation between the CTC equilibrium constants and the CTC reactivity ratios could be deduced.

Nevertheless, as proposed by Braun et al. [30, 57], careful examination of polymerization rates, K constants, and reactivity ratios leads to a conclusion that in terpolymerization as above, both free monomers and CTC complexes take part. At low monomer concentrations, the overall polymerization rate is dominated by

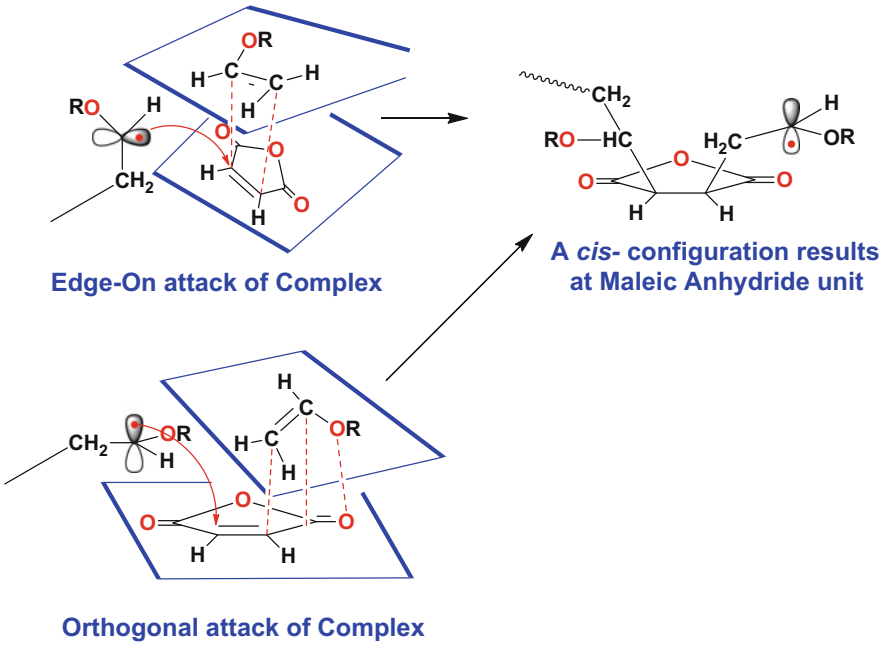

Fig. 4.7 Proposed pathways for reaction of *iso*-butyl vinyl ether with maleic anhydride-*iso*-butyl vinyl ether complex leading to a *cis* configuration at maleic anhydride (MA) unit (Adapted from [44]. Copyright 2000 with permission from Elsevier)

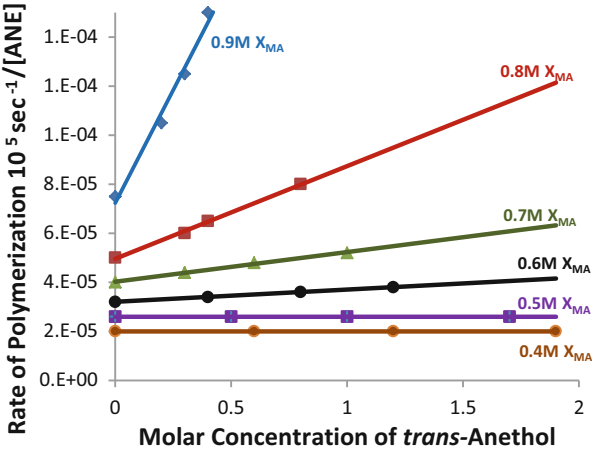

Fig. 4.8 Plot of R_p/[ANE] vs. [ANE] at various ratios of monomer concentration X_{MA} in the copolymerization of maleic anhydride (MA) and ANE in methyl ethyl ketone at 50 °C using 2,2′-azobisisobutyronitrile (AIBN) as the initiator. ANE: *trans*-anethole (adapted from [61])

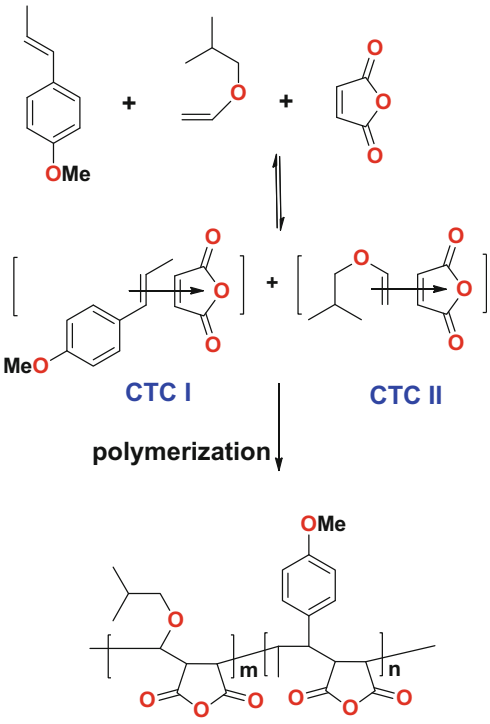

Scheme 4.6 Copolymerization of two charge-transfer complexes, CTC I and CTC II, formed in a ternary system containing *trans*-anethole, *iso*-butyl vinyl ether, and maleic anhydride (adapted from [30, 57])

Table 4.7 Reactivity ratios according to the MCP copolymerization model for the radical polymerization of maleic anhydride, *trans*-anethole, and *iso*-butyl vinyl ether at 60 °C with AIBN as initiator

	CTC equilibrium constant, K (L/mol)		Reactivity ratios of CTC	
Solvent	Maleic anhydride/*trans*-anethole (CTC I)	Maleic anhydride/*iso*-butyl vinyl ether (CTC II)	r_1	r_2
CCl_4	0.480	0.110	0.45	1.59
$CHCl_3$	0.086	0.066	0.56	0.94
CH_3CN	0.034	0.135	1.05	0.23
THF	0.116	0.091	0.90	1.70

Adapted from [30, 57]

free monomers, whereas at high monomer concentrations, CTCs determine the polymerization process.

In contrast to the findings above, in a system of two EA monomers (maleic anhydride and methyl α-cyanocinnamate) with one ED monomer (chloroethyl vinyl ether) in CCl_4, Braun and coworkers [60] found that terpolymerization results best fit with the terminal model of two CTC complexes, having reactivity ratios of

$r_{CTC1} = 1.17$ and $r_{CTC11} = 1.02$ for maleic anhydride–chloroethyl vinyl ether complex and methyl α-cyanocinnamate–chloroethyl vinyl ether complex, respectively. Equilibrium constants for both complexes were the same: 0.16. See Scheme 4.7.

Systematic investigations of the copolymerization of maleic anhydride with electron-donor monomers by other researchers have raised more questions concerning the critical role of a charge-transfer complex in the propagation step [62–64]. Hall and Padias [62, 63] indicated that the monomer interactions in the charge-transfer complex are weak, the CTC has no identifiable chemistry, and it cannot be isolated from the system. Considering CTC participation in copolymerization is not necessary to explain alternating behavior that can be adequately interpreted as the system of free monomers differing in polarity [62, 63]. The alternating polymer structure is thought to be the result of the preferential addition to the terminal radical of a monomer having opposite polarity, rather than the participation of charge-transfer complex.

Ito et al. [64] showed that the binary system norbornene–maleic anhydride yields an equimolar alternating polymer. Introducing *t*-butyl methacrylate into the system, a homopolymerizable monomer, produced a terpolymer having significantly less norbornene than maleic anhydride and not in 1:1 ratio of norbornene/maleic

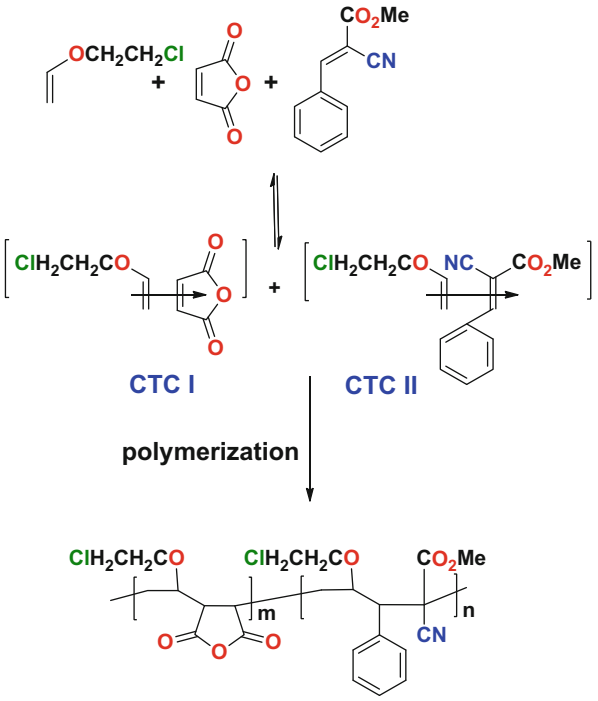

Scheme 4.7 Copolymerization of two charge-transfer complexes CTC I and CTC II formed in a ternary system containing chloroethyl vinyl ether, maleic anhydride, and methyl α-cyanocinnamate (adapted from [60])

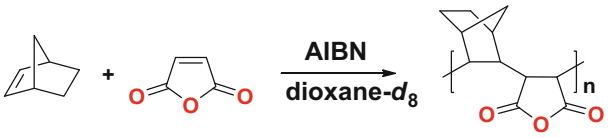

Scheme 4.8 Copolymerization of maleic anhydride and norbornene in dioxane-d_8

anhydride as expected with CTC participation. Reaction of the mixture of both monomers with the electron-rich cyclohexyl radical gave only cyclohexyl-succinic anhydride (i.e., the product of addition of cyclohexyl to maleic anhydride), instead of the expected product of concerted addition to CTC. These results suggest that norbornene and maleic anhydride reacted as free monomers rather than as a CTC (Scheme 4.8) [64].

Reactions of chloroethyl vinyl ether (ED)/*N*-phenylmaleimide (strong EA) blends with electron-rich butyl or benzyl radicals yield only simple adducts of the radicals with *N*-phenylmaleimide. These results, as concluded by Jones et al. [65–67], provide evidence against concerted addition of CTC to the growing macroradical in copolymerization reactions. Given these findings, one can conclude that maleic anhydride-based polymers undergo a variety of complex polymerization schemes depending on the comonomer used. In the case of copolymerization with a vinyl ether, maleic appears to predominantly favor an alternating structure in most reported cases.

4.1.2.4 Spontaneous Copolymerizations Involving Maleic Anhydride and Alkyl Vinyl Ethers

Spontaneous polymerization is defined as polymerization that occurs readily without the addition of an initiator. The mechanism of initiation and propagation in spontaneous copolymerization generated great interest in the research community.

Electron-accepting maleic anhydride and its derivatives can readily undergo spontaneous alternating copolymerization with a number of electron-donating monomers, such as vinyl ethers [46], styrene [68], and vinyl sulfide [69].

As dependent on monomers involved, spontaneous copolymerization in electron-donor and electron-acceptor comonomer blends can yield alternating copolymers, homopolymers of electron-donor and electron-acceptor monomers, low molecular weight adducts, such as cyclobutanes, cyclohexanes, and Diels–Aldrich adducts, and linear dimers of both monomers. Cationic homopolymerization seems to be more likely with the comonomers having larger disparity of polarity as in vinyl ethers.

In 1968, Kokubo et al. [46] found that maleic anhydride and vinyl ethers, such as *p*-dioxene, 2-chloroethyl vinyl ether, and 1,2-dimethoxyethylene, copolymerize spontaneously.

At a constant monomer feed concentration and at an equimolar monomer ratio in benzene, the observed polymerization rate for the maleic anhydride/vinyl ether pair increased in parallel to the corresponding CTC equilibrium constants, K: *p*-dioxene < 2-chloroethyl vinyl ether < 1,2-dimethoxyethylene (Table 4.8).

Table 4.8 Comparison of spontaneous copolymerization rate and K for maleic anhydride and vinyl ethers

Alkyl vinyl ether	*p*-dioxene	2-chloroethyl vinyl ether	1,2-dimethoxyethylene		
Solvent	Benzene	Benzene	Benzene	Toluene	*m*-Xylene
CTC equilibrium constant K (L/mol, 25 °C)	0.069	0.10 (30 °C)	0.29	0.16	0.73
Mean polymerization rate (%/min)	0.0027 (60 °C)	0.089 (60 °C)	0.093 (30 °C)	0.080 (30 °C)	0.110 (30 °C)

Adapted from [46]

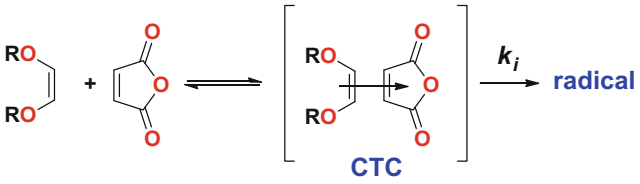

Scheme 4.9 Charge-transfer complex initiated spontaneous free-radical polymerization of maleic anhydride and vinyl ether (adapted from [43])

The larger the equilibrium K values obtained, the faster the polymerization rates observed. Similar effects of the equilibrium constant, K, on the polymerization rate have been observed when the solvent was varied for the maleic anhydride–1,2-dimethoxyethylene pair (Table 4.8).

Kokubo and coworkers (1969) proposed that in the case of spontaneous copolymerization of maleic anhydride with 1,2-dimethoxyethene and *p*-dioxene, a charge-transfer complex participated in both initiation and propagation steps (Scheme 4.9) [70].

Hallensleben (1971) reported that the copolymerization of maleic anhydride with *n*-butyl vinyl ether, *iso*-butyl vinyl ether, or *t*-butyl vinyl ether in CCl_4 yields 1:1 alternating copolymers both with and without the addition of AIBN initiator [43]. Inhibition of spontaneous copolymerization by a radical polymerization inhibitor confirmed that the copolymerization of maleic anhydride with vinyl ethers is radical in nature.

Initiation (R_i) and propagation (R_p) rates depend on monomer concentrations as expected in the case of CTC participation in both initiation and propagation steps:

$$R_i \propto [\text{maleic anhydride}]^1[\text{vinyl ether}]^1$$

$$R_p \propto [\text{maleic anhydride}]^{3/2}[\text{vinyl ether}]^{3/2}$$

The activation energy of initiation, E_i, in the system of maleic anhydride and *p*-dioxene was considerably smaller than that in the spontaneous polymerization of styrene. From this result, it was hypothesized that a high energy biradical formation was not involved in the initiation step, as believed to be the case with

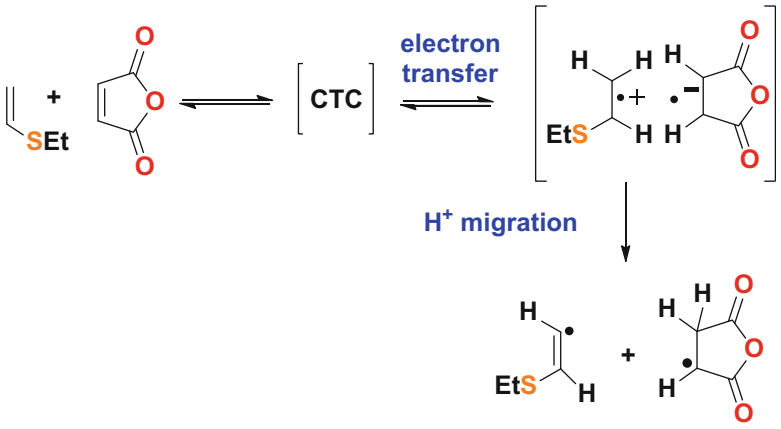

Scheme 4.10 Postulated initiation mechanism for spontaneous free-radical polymerization of maleic anhydride and ethyl vinyl sulfide (adapted from [69])

styrene; however, the authors were not clear whether the chain growth proceeded via biradicals or not and suggested further study was needed.

In related work, Sato et al. (1981) suggested that a vinyl radical and a substituted alkyl radical from electron/proton transfer between maleic anhydride and vinyl sulfides could initiate the spontaneous copolymerization (Scheme 4.10) [69]. In order to prove this, a spin trapping agent, 2-methyl-2-nitrosopropane, was employed to capture transient radicals, and the products were analyzed by electron-spin resonance (ESR) spectroscopy. The spin trapped radicals that initiated the copolymerization were assumed to be generated by the charge-transfer complex formed from maleic anhydride and vinyl sulfide via electron transfer within the charge-transfer complex resulting in an anion–radical and a cation–radical. Subsequent proton migration from the cation–radical to anion–radical yielded two radicals: a vinyl radical and a substituted alkyl radical, as depicted in Scheme 4.10.

In their groundbreaking paper, Stille and Chung [71] reported that blends of vinylidene cyanide $CH_2=C\text{-}(CN)_2$ (VdCN, a strong EA) with a range of unsaturated ethers, such as ethyl vinyl ether, *iso*-propyl vinyl ether, di-hydropyran, and di-ethoxyethene, at 25 ° C, yield mixtures of three types of products: homopolymers of VdCN, homopolymers of unsaturated ethers, and cycloadducts of VdCN with unsaturated ethers. Reactions were performed in a variety of solvents differing in polarity, such as benzene, toluene, CH_2Cl_2, and acetonitrile, as well as at a variety of monomer ratios.

When AIBN was added and the reactions were heated to 80 ° C, they still obtained 1:1 alternating VdCN-unsaturated ether copolymers, side-by-side with the formerly listed homopolymers and cycloadducts. The alternating 1:1 copolymers were obtained in the presence of AIBN at a variety of VdCN/ether monomer ratios employed [71].

All unsaturated ethers except di-hydropyran reacted to yield head-to-tail homopolymers as expected for their cationic polymerization. Homopolymers of VdCN

obtained from its blends with all unsaturated ethers studied had also a head-to-tail molecular structure as expected for its anionic polymerization.

The mechanism proposed by Stille et al. [71] involves participation of CTC complex, which can either homopolymerize by radical mechanism (initiated by AIBN) to yield a 1:1 alternating copolymer or through complete electron transfer from ED to EA can generate a radical–cation and radical–anion pair that separately initiate the cationic and anionic homopolymerizations, respectively. Additionally, the radical–anion may react with the radical–cation to generate cycloadducts.

Hall, Padias et al. [62, 63, 72–74], performed an in-depth, comprehensive research in the field of spontaneous polymerizations of a variety of ED–EA monomer pairs, with a particular focus on reactions of increasingly electrophilic EA, such as tri- and tetrasubstituted ethylenes with ester (E) and cyano (–CN) groups (Fig. 4.8).

The spontaneous reactions yielded homopolymers of ED monomers by cationic polymerization, alternating copolymers of EA and ED monomers by radical copolymerizations, and low molecular weight adducts. The adducts comprised cyclobutanes, cyclohexanes, and, occasionally, linear dimers of both monomers.

The proportion of cationic homopolymerization was higher in the case of olefins with a larger difference in their EA and ED character than in the case of olefins close to each other. In order to interpret these results, Hall postulated a new mechanism based on a unified stepwise 2 + 2 cycloaddition of EA and ED monomers, leading to a spontaneous initiation of polymerization [62, 63, 72–74].

The first step in the initiation mechanism postulated by Hall [62, 63] and his group involves generation of a tetramethylene intermediate, which can initiate cationic and anionic homopolymerizations, as well as a radical alternating copolymerization. The tetramethylene intermediate mechanism is shown below in Scheme 4.11 [63]:

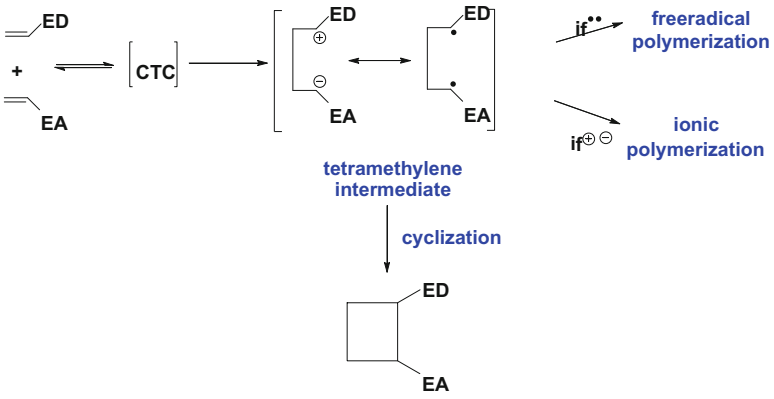

Scheme 4.11 Initiation of a spontaneous polymerization by tetramethylene intermediate (adapted from [63])

According to Hall [63], Huisgen [75], and Huisgen et al. [76], the tetramethylene intermediates are resonance hybrids of two extremes, namely, 1,4-diradical and a zwitterion, and their ionic or radical character depends in a continuous way on polarity of the substituents attached to the olefins. The tetramethylene intermediates of similar kind were first proposed by Huisgen [75] to account for stepwise cycloaddition reactions of EA and ED olefins.

The occurrence of the specific polymerization mechanism in the reaction depends on the polarity of the EA and ED monomers and their ability to homopropagate by a cationic or anionic mechanism or to copolymerize by a radical mechanism. Although Hall's work did not involve spontaneous anionic homopolymerization, results reported by Stille et al. [71] for a VdCN-unsaturated ether system fit well with the tetramethylene intermediate initiation hypothesis.

As reported by Eberson et al. [77], spin trapping of radicals from the reactions of styrenic ED monomers combined with tri-substituted ethylenes with three –CN and $–CO_2Me$ groups supported tetramethylene diradicals as initiators in spontaneous copolymerization.

4.1.3 Physical Properties of Maleic Anhydride–Alkyl Vinyl Ether Copolymers

4.1.3.1 Molecular Weight

Absolute molecular weights of maleic anhydride–methyl vinyl ether copolymers have been analyzed by size exclusion chromatography coupled with low angle laser light scattering (SEC/LALLS), and the results are summarized in Table 4.9 [78, 79].

Table 4.9 Intrinsic viscosities, absolute molecular weights, and molecular weight distributions of maleic anhydride–methyl vinyl ether copolymers

Copolymer	Intrinsic viscosity	M_w (Da)	M_n (Da)	M_w/M_n
Gantrez® AN 119	1.719	2.16×10^5	7.98×10^4	2.71
Gantrez® AN 139	5.650	1.08×10^6	3.11×10^5	3.47
Gantrez® AN 149	6.000	1.25×10^6	4.85×10^5	2.58
Gantrez® AN 169	8.530	1.98×10^6	9.60×10^5	2.06
Gantrez® AN 179	8.939	2.40×10^6	1.13×10^6	2.12

Gantrez® is a registered trade name of maleic anhydride–methyl vinyl ether copolymers by Ashland Specialty Ingredients

4.1.3.2 Glass Transition Temperature of Maleic Anhydride–Alkyl Vinyl Ether Copolymers

Most of the maleic anhydride–alkyl vinyl ether copolymers are amorphous solids at ambient temperature. In contrast, maleic anhydride–dodecyl vinyl ether copolymer

is a waxy material due to the presence of long chain hydrophobic alkyl groups. For the same copolymer composition, the glass transition temperature (T_g) is mostly independent of molecular weight over a broad range. For maleic anhydride–methyl vinyl ether copolymer, T_g ranges from 151 to 154 °C as the polymer's specific viscosity increases from 0.31 to 2.67 (Table 4.10) [80]. Thermal degradation of maleic anhydride–methyl vinyl ether copolymer starts at about 275 °C, as reported by a DSC and TGA study [80].

Table 4.10 Glass transition temperature (T_g) of maleic anhydride–methyl vinyl ether copolymers vs. specific viscosity

Copolymer	Specific viscosity[a]	T_g (°C)
Gantrez® AN 119	0.31	152
Gantrez® AN 139	1.10	151
Gantrez® AN 149	1.76	153
Gantrez® AN 169	2.67	154

[a]1 wt/v% of polymer in methyl ethyl ketone (MEK) at 25 °C

4.1.3.3 Solubility of Maleic Anhydride–Alkyl Vinyl Ether Copolymers

The solubility of maleic anhydride–methyl vinyl ether copolymer in a variety of solvents is summarized in Table 4.11 below.

Table 4.11 Solubility of Gantrez® AN at 10 wt% at ambient temperature

Solvent	Soluble	Insoluble
Alcohol[a]	Methanol, ethanol, *n*-propanol, *i*-propanol, butanol	1,4-butanediol, cyclohexanol, diethylene glycol
Ether	Tetrahydrofuran, 1,4-dioxane	Diethyl ether, methyl *t*-butyl ether, methyl vinyl ether
Ester	Methyl acetate, ethyl acetate	Butyl acetate, isopropyl acetate
Ketone	Acetone, methyl ethyl ketone, cyclohexanone	Methyl isobutyl ketone
Hydrocarbon	n/a	Benzene, toluene, xylene, cyclohexane, hexane, heptane, petroleum ether, isobutylene
Chlorinated hydrocarbon	n/a	Chloroform, carbon tetrachloride, methylene chloride, chlorobenzene
Other organic solvent	*N*-methyl-2-pyrrolidone, dimethyl formamide, dimethyl sulfoxide	n/a

[a]Ester formation in soluble alcohols
Adapted from [3]

4.1.3.4 Stability of Maleic Anhydride–Alkyl Vinyl Ether Copolymers in the Solid State

The copolymers of maleic anhydride and alkyl vinyl ethers are stable solids under ambient conditions. However, the copolymers from the solution process do not exhibit the desired viscosity shelf life for unspecified reasons [81]. However, the copolymers from these processes can be rendered stable by treatment with dry inert gas.

At elevated temperature, the copolymers of maleic anhydride and alkyl vinyl ethers are stable in the absence of oxygen [82, 83]. There is no loss in specific viscosity for the maleic anhydride–methyl vinyl ether copolymers treated at 110 °C or 140 °C for up to 12 h in an oxygen-free environment. However, the presence of oxygen significantly accelerates the degradation of the polymer backbone as can be seen from the drop of specific viscosity over time at 110 °C (Fig. 4.9). The exact reaction mechanism for decomposition by oxygen in the copolymer of maleic anhydride–alkyl vinyl ether has not yet been elucidated.

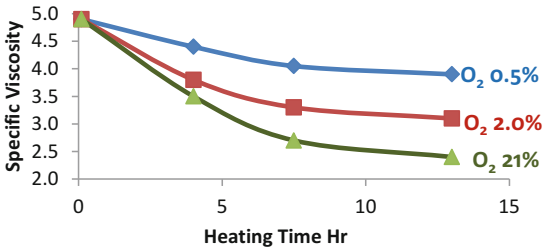

Fig. 4.9 Relationship between heating time and specific viscosity of maleic anhydride–methyl vinyl ether copolymer under an oxygen concentration of 0.5 %, 2.0 %, and 21 % at 110 °C (adapted from [83])

4.1.3.5 Stability in Aqueous Solution

The stability study of maleic anhydride–alkyl vinyl ether copolymer in aqueous solution has attracted significant interest due to its commercial importance. In aqueous solution, the maleic anhydride–alkyl vinyl ether copolymer hydrolyzes to maleic acid–alkyl vinyl ether copolymer (Scheme 4.12). Plochocka et al. showed that high molecular weight, i.e., 1.2×10^6 Da, maleic acid–methyl vinyl ether copolymer is stable in an aqueous system at ambient temperature and in darkness [84].

The polymer degradation was accelerated by visible light, UV, elevated temperature, and oxygen. The decrease in molecular weight or specific viscosity was observed, accompanied with the formation of methanol, formaldehyde, and formic acid. In aqueous solution, maleic acid-ethyl vinyl ether and maleic acid–butyl vinyl ether copolymers underwent similar degradation at 60 °C.

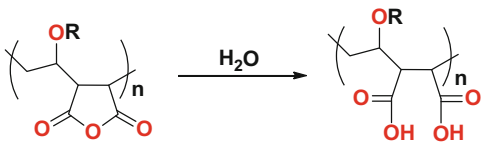

Scheme 4.12 Hydrolysis of maleic anhydride–alkyl vinyl ether copolymers to form maleic acid–alkyl vinyl ether copolymers. R = alkyl

In contrast, under the same set of conditions, the molecular weight of maleic acid–ethylene copolymer was almost unchanged, and no aldehyde formation was observed [84]. Therefore, chain scission appears to be dependent upon the vinyl ether component rather than the maleic component within the copolymer and is believed to proceed through a radical degradation mechanism.

Studies have found that the stability of the maleic acid–alkyl vinyl ether copolymer in aqueous solutions can be significantly improved by the presence of reducing agents, radical trapping agents/antioxidants, or chelating agents. Login et al. (1983) [85] found that a stabilizing additive of sulfur dioxide and its salt at 10–500 ppm was effective to prevent oxygen from the air and peroxide impurities contained within the polymer system from degrading the copolymer [85].

Mayer et al. (1999) [86] discovered that phosphinic acid was also very effective to stabilize the copolymer in aqueous solution. If the additive is added, the copolymer solution retains at least 85–90 % of its original viscosity after 3 months. The antioxidants/free-radical scavengers were selected from *t*-butylhydroquinone, propyl gallate, butylated hydroxy-anisole (BHA), butylated hydroxy-toluene (BHT), 4-hydroxymethyl-2,6-di-tert-butylphenol, 2,4,5-trihydroxy-butyrophenone (THBP), and *N*,*N*-diethylhydroxylamine [84, 88].

The instability of maleic acid–alkyl vinyl ether copolymers in aqueous solution is interpreted as the result of attack by free radicals. The free radicals can be generated from dissolved oxygen or residual polymerization initiator and can be promoted by elevated temperature, UV light, or trace transition metals [84].

The alkyl vinyl ether bond in the polymer is most susceptible to free-radical attack. For example, dissolved oxygen can attack the tertiary carbon to form alkyl hydroperoxide which initiates further degradation (Scheme 4.13) [84–88]. This can explain the formation of low molecular species such as alkyl alcohols, which can be further oxidized into aldehydes and acids.

On the other hand, the insertion of a single oxygen between the tertiary carbon of the polymer backbone and the adjacent alkoxy group can yield a peroxide fragment, which undergoes decomposition in a way similar as an alkyl peroxide initiator does. The presence of trace levels of transition metals accelerates thermal oxidative degradation by catalyzing hydroperoxide decomposition. The presence of stabilizing additives retards the activities of free radicals, thus reducing the extent of polymer backbone scission.

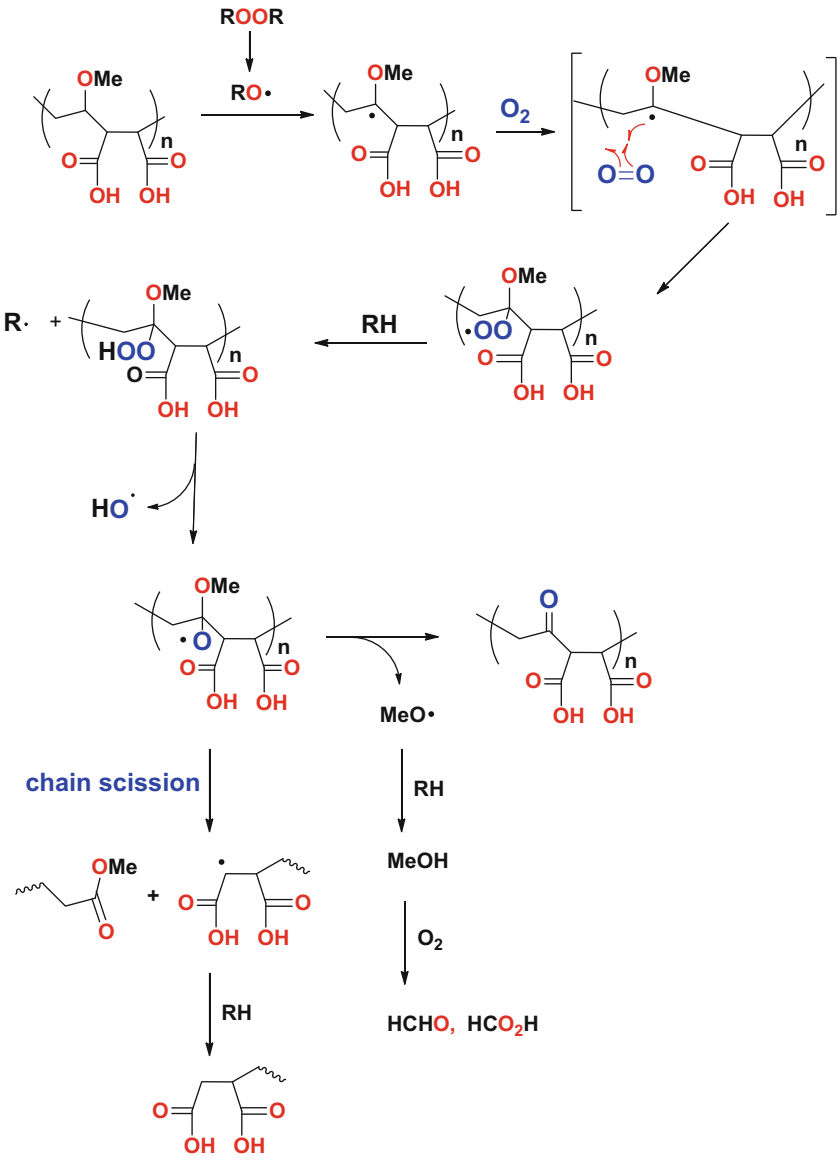

Scheme 4.13 Proposed mechanism of degradation of maleic acid–methyl vinyl ether copolymer in aqueous solution (adapted from [84])

The cleavage of methoxy groups from maleic acid–methyl vinyl ether copolymer backbone can also be catalyzed by the neighboring acid groups (Scheme 4.14). The cleavage results in the formation of methanol, in which subsequent oxidation leads to formaldehyde and formic acid.

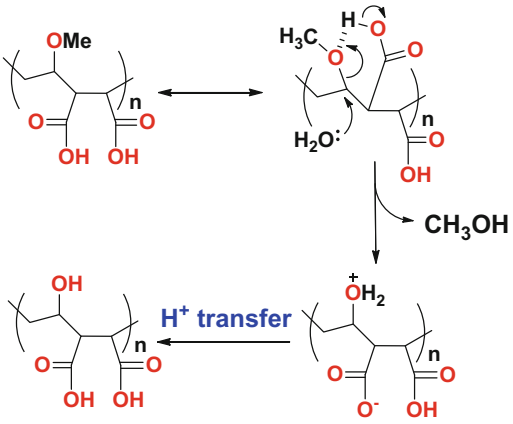

Scheme 4.14 Intramolecularly acid-catalyzed cleavage of methoxy groups from maleic acid–methyl vinyl ether copolymer backbone (adapted from [84])

However, Ladaviere et al. (1999) [89] postulated that the thermal degradation of maleic acid–methyl vinyl ether copolymer in aqueous solution was due to decarboxylation and a *retro-Claisen* rearrangement (Scheme 4.15). They compared the thermal stability of maleic acid–methyl vinyl ether copolymer with that of maleic anhydride–styrene or maleic anhydride–ethylene copolymers in the temperature range of 37–130 °C.

It was demonstrated that maleic acid–methyl vinyl ether copolymer was less stable than maleic anhydride–styrene or maleic anhydride–ethylene copolymers. They also observed the formation of methanol and CO_2 in the degradation of maleic acid–methyl vinyl ether copolymer in water. In the proposed mechanism, methanol and CO_2 are formed through an intramolecular decarboxylation step (Scheme 4.15, step a).

Then the decarboxylated/demethoxylated unit undergoes *retro-Claisen* rearrangement and tautomerization to form an ester linkage in the copolymer backbone (Scheme 4.15, step b). Subsequent ester hydrolysis results in polymer chain scission. No involvement of free-radical oxidation was considered in the degradation mechanism as reported by Ladaviere et al. [89].

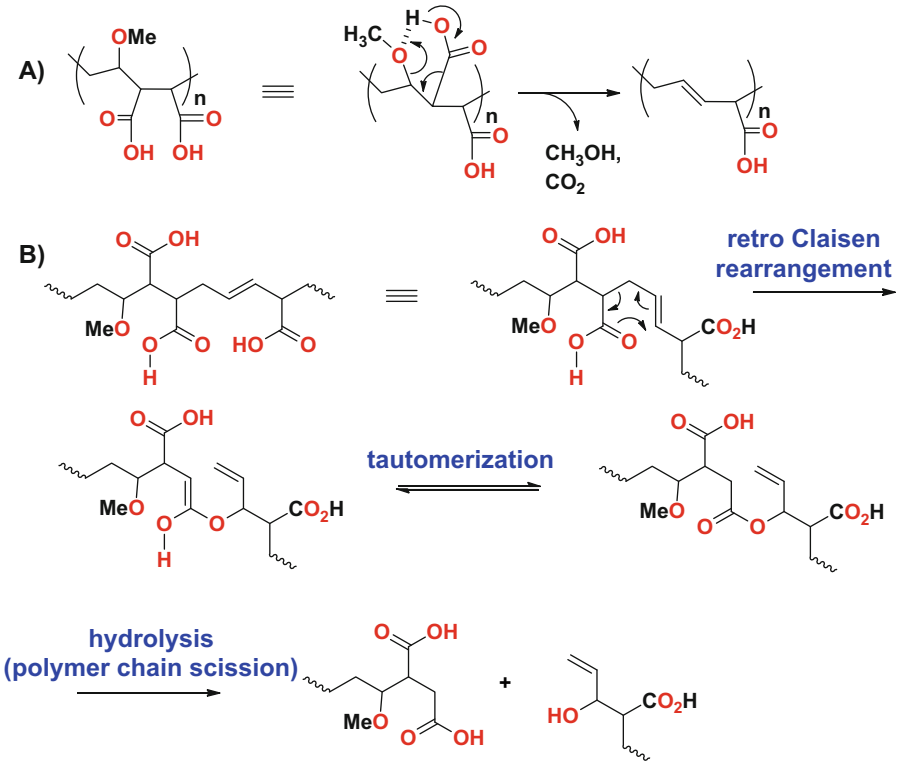

Scheme 4.15 Proposed mechanism for the degradation of maleic acid–methyl vinyl ether copolymer in aqueous solution (adapted from [89])

4.1.4 Derivatives of Maleic Anhydride/Alkyl Vinyl Ether Copolymers

Benefited by the versatile reactivity of the anhydride ring in maleic anhydride, the copolymers of maleic anhydride–alkyl vinyl ether are able to react with water, alcohols, and amines to yield many interesting derivatives (Scheme 4.16). In aqueous solution, the anhydride rings undergo hydrolysis to yield polyacids or their salts. The anhydride rings can also react with alcohols to form either monoalkyl maleate or dialkyl maleate ester derivatives.

The reactions with amines will yield amic acids, imides, and ammonium salts, depending on the reaction conditions employed. If polyols or polyamines are involved, the derivatizations will form cross-linked systems. Therefore, derivitization of the anhydride groups in the copolymers makes it possible to develop a wide variety of tailor-made products for specific applications.

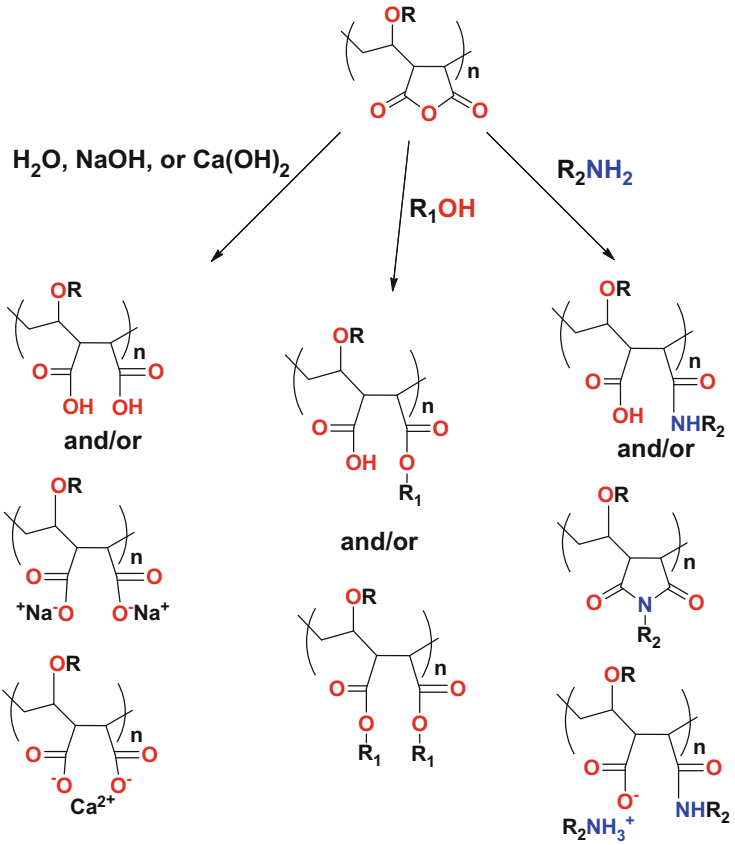

Scheme 4.16 Derivatives of maleic anhydride–alkyl vinyl ether copolymers. R_1 and R_2 are alkyl, cycloalkyl, or aryl substituents

4.1.4.1 Polyacids and Their Salts from Maleic Anhydride–Alkyl Vinyl Ether Copolymers

In aqueous solution, maleic anhydride–alkyl vinyl ether copolymers react with water to form maleic acid–alkyl vinyl ether copolymers (Scheme 4.16). The maleic acid–methyl vinyl ether copolymers thus obtained are soluble in water, DMSO, or DMF but insoluble in most other organic solvents such as acetone. The maleic acid–alkyl vinyl ether copolymers with longer chain alkyl vinyl ethers typically require neutralization to be rendered soluble in water.

The rate of hydrolysis of maleic anhydride–methyl vinyl ether copolymer in water depends on molecular weight, pH, and temperature. The hydrolysis/dissolution rate decreases with both increasing molecular weight and decreasing pH in the range of pH 7.5–2.3 [90]. Ladaviere et al. [91] found that the hydrolysis rate

constant of maleic anhydride–methyl vinyl ether copolymer is on the order of 10^{-4}/s with an activation energy of 14 kJ/mol.

The maleic acid–alkyl vinyl ether copolymer exhibits two pK_a values: p$K_{a1} = 3.5$ and p$K_{a2} = 6.5$ in the case of alkyl groups ranging from methyl to hexyl. However, the titration behavior of the maleic acid–alkyl vinyl ether copolymers is dependent on the nature of the alkyl groups [78]. The maleic acid–methyl vinyl ether and maleic acid–ethyl vinyl ether copolymers behave as typical weak polyacids. On the other hand, at low pH, the butyl and hexyl copolymers exhibit a hypercoiled state due to hydrophobic interactions. As the degree of neutralization increases, they undergo conformational transitions to extended states.

The thermal analysis of maleic acid–methyl vinyl ether copolymer indicates that the anhydride units are rebuilt during the heating process [80]. In the thermogravimetric (TGA) curves of maleic acid–methyl vinyl ether copolymer, three distinct peaks at 80, 175, and 325 °C were observed and assigned to free water removal, anhydride formation, and polymer degradation, respectively. The anhydride formation at 175 °C, about 30 °C above its T_g of 144 °C, is facilitated in the glassy state. The dehydrated product has a T_g of 153 °C, indicating that the maleic anhydride–methyl vinyl ether copolymer was reconstituted. FTIR and DSC analysis showed that the anhydride formation was exclusively intramolecular cyclization, which is different from the dehydration of polyacrylic acid.

A kinetic study by isothermal TGA showed that the reconstitution of the maleic anhydride unit is endothermic and first order with an activation energy of 18.8 kcal/mol. Partial dehydration of maleic acid–methyl vinyl ether copolymer yields a terpolymer of maleic acid–methyl vinyl ether–maleic anhydride. This terpolymer is difficult to obtain by traditional free-radical polymerization approach [93].

Maleic acid–alkyl vinyl ether copolymers form salts with caustic and alkaline earth metals. With divalent cations, the complex formation between the metal center and maleic acid may be superimposed on the electrostatic interaction [94]. The chelate formation constant K_f with alkaline earth metals is shown in Table 4.12, while the values for succinic acid are presented as a comparison. Even with a similar unit structure, the complexation with the polyacids is two to three times stronger than that with succinic acid. Likewise, due to its chelating ability, the binding with divalent cations is also much stronger than that for polyacrylic acid. This arises due to the *cis*-diacid as described in Chap. 2, in that the copolymer's maleic acid unit (p$K_a = 3.5$) is a much stronger acid than polyacrylic acid (p$K_a = 4.2$). The Ca/Na salt of maleic acid–methyl vinyl ether copolymer,

Table 4.12 Chelate formation constant, K_f, of maleic acid–ethyl vinyl ether copolymer with alkaline earth metals

log K_f	Mg^{2+}	Ca^{2+}	Sr^{2+}	Ba^{2+}
Maleic acid–ethyl vinyl ether copolymer	2.30	2.45	1.96	2.00
Succinic acid	1.02	1.16	0.75	0.97

Adapted from [94]

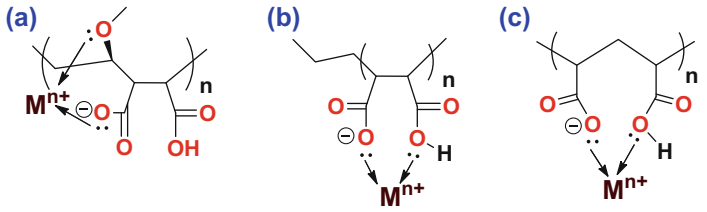

Fig. 4.10 Binding geometry of alkaline and alkaline earth cations with (**a**) maleic anhydride–methyl vinyl ether copolymer, (**b**) maleic anhydride–ethylene copolymer, and (**c**) polyacrylic acid, $M^{n+} = Mg^{2+}$, Ba^{2+}, Li^{+}, or K^{+} (adapted from [95])

commercially known as Gantrez® MS-955, have been widely employed in oral care applications.

The binding geometry of certain cations with maleic acid–alkyl vinyl ether copolymers involves both the ether oxygen and the adjoining carboxylate group. In a comparison study of counterion binding by dilatometry, it was observed that the degree of binding of Mg^{2+}, Ba^{2+}, Li^{+}, and K^{+} cations with maleic acid–methyl vinyl ether polyanion was significantly larger than that with either polyacrylic acid or poly(maleic acid–ethylene) anions [95]. This difference was ascribed to the binding coordination.

It has been proposed that the binding of a metal ion with maleic acid–methyl vinyl ether copolymer involves both the methoxy group and the nearest carboxylate group, yielding a stable six-membered ring conformation (Fig. 4.10a) [96]. In contrast, the binding with polyacrylic acid or poly(maleic acid-ethylene) anions involves only carboxylic groups and leads to the formation of a less stable seven- or eight-membered ring conformation (Fig. 4.10b, c). A computational modeling study of the complexation of metal ions, such as Ca^{2+}, Mg^{2+}, Mn^{2+}, and Fe^{3+}, with maleic acid–methyl vinyl ether copolymer also indicates that the energetically most favorable binding coordination involves the carboxylate oxygens and the ether oxygen acting in a concerted fashion [96].

4.1.4.2 Half Esters from Maleic Anhydride–Alkyl Vinyl Ether Copolymers

Maleic anhydride–alkyl vinyl ether copolymers react with aliphatic alcohols to form either monoalkyl maleate or dialkyl maleate derivatives (Scheme 4.16). The reaction with lower alkyl alcohols, such as methanol or ethanol, can be performed directly in the corresponding alcohol at ambient temperature. The reaction with secondary alcohols, such as isopropyl alcohol, requires higher temperature. On the other hand, the hydrolytic stability of the half-esters in hydroalcoholic solution

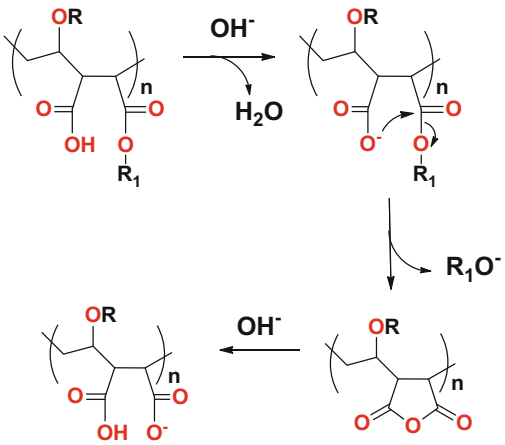

Scheme 4.17 Enhanced hydrolysis of monoesters of maleic anhydride–alkyl vinyl ether copolymers by *neighboring-group effect*

follows the opposite order [97], where the more substituted alkyl group is most stable due to steric factors:

primary normal < primary branched < secondary alkyl ester and butyl ester < pentyl ester

The dissolution properties of aliphatic monoesters of maleic anhydride–methyl vinyl ether copolymer in aqueous solutions depend on several factors [90]. In general, the dissolution rate in water increases with higher pH, lower molecular weight, less degree of derivatization, and shorter alkyl chain length. The monoester derivatives can undergo further reactions. Partial neutralization using either inorganic bases or organic amines renders diverse solubility profiles in alcohol–water systems. Partial neutralization can also impact the polymer film properties, and other useful characteristics, while hydrolysis or transesterification of the monoester in aqueous solution can be catalyzed by inorganic base.

Interestingly, the ester hydrolysis is significantly enhanced by the *neighboring-group effect*. Instead of being attacked directly by hydroxide ions in solution, the ester groups undergo hydrolysis by the neighboring carboxylate anion (Scheme 4.17). The rate enhancement is due to the formation of a favored 5-membered ring intermediate. As a result, the maleic anhydride unit is yielded, which further reacts with hydroxide anions to form the salts of maleic acid–alkyl vinyl ether copolymers.

Half-esters of aliphatic alcohols tend to form tough, clear, glassy films that are tack-free and have excellent substantivity to hair. The mono-ethyl, isopropyl, and *n*-butyl ester derivatives, commercially known as Gantrez® ES from Ashland, have

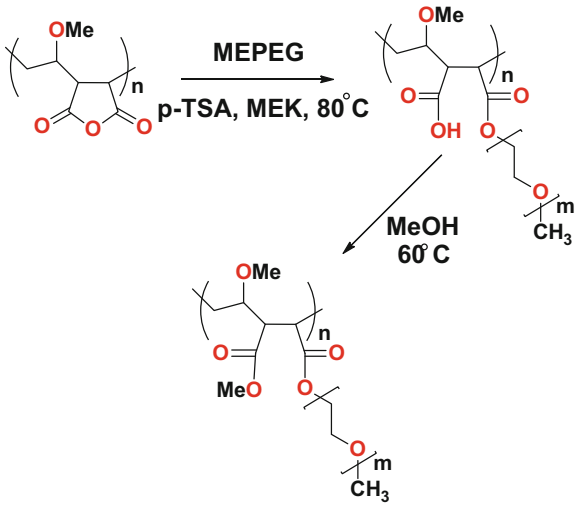

Scheme 4.18 Esterification of maleic anhydride–methyl vinyl ether copolymer with MEPEG to form its half ester. MEPEG: poly(ethylene glycol) monomethyl ether; p-TSA: *p*-toluenesulfonic acid; MEK: methyl ethyl ketone (adapted from [101])

been widely employed in hair fixative products [3]. Partially neutralized half-esters of maleic acid-alkyl vinyl ether copolymers also find use as dispersing agents for aqueous suspension concentrates of agricultural actives [98]. The hydrolyzable nature of the half-esters is utilized to slowly release certain actives such as menthol in oral care applications as well [99, 100].

PEG-grafted comb polymers are formed by esterification of maleic anhydride–methyl vinyl ether copolymer with poly(ethylene glycol) monomethyl ether (MEPEG) (Scheme 4.18) [101], in conjunction with esterification by alkyl alcohols. The properties of these hybrid polymer derivatives can be fine-tuned in terms of hydrophobic and hydrophilic balance, T_g, and solubility. The unreacted carboxyl group can then be endcapped with methanol.

In the solid state, the MEPEG/methyl esters of maleic anhydride–methyl vinyl ether copolymer form complexes with Li^+, thereby exhibiting ion conductive properties as well.

Maleic anhydride–alkyl vinyl ether copolymers also react with polyols to yield cross-linked polyesters [102]. If the esterifications are performed in aqueous solution, the products are obtained as hydrogels which are hydrophilic polymers that are swellable but not soluble in water [103–105]. One of the most interesting hydrogels is from the cross-linking of maleic anhydride–methyl vinyl ether copolymer with poly(ethylene glycol) (Scheme 4.19) [106]. The physical properties of these

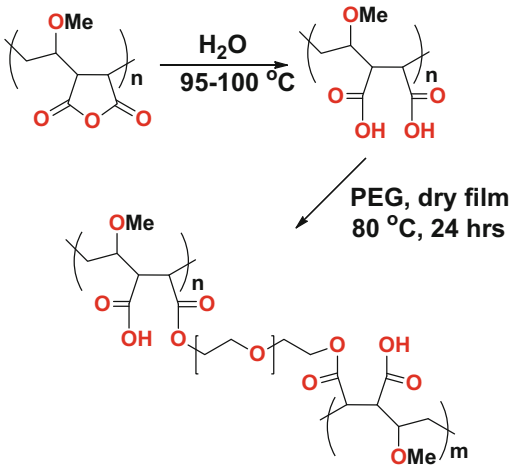

Scheme 4.19 Cross-linking of maleic anhydride–methyl vinyl ether copolymer with PEG. PEG: poly(ethylene glycol) (adapted from [106])

hydrogels render them very useful in biomedical, drug delivery, and personal care applications [107].

4.1.4.3 Polyamides and Imides from Maleic Anhydride–Alkyl Vinyl Ether Copolymers

Maleic anhydride–alkyl vinyl ether copolymers can also react with amines to form polyamic acids and polyimides (Scheme 4.16). The relative ratio of amic acid vs. imide units in the modified polymer can be controlled by reaction temperature. Lower reaction temperatures such as 90–100 °C give predominantly amic acid units. Higher reaction temperatures (≈130 °C) promote the formation of the more thermodynamically stable imide units. The reaction of maleic anhydride–alkyl vinyl ether copolymers with hydrophobic amines provides a convenient way for hydrophobic modification as well [108]. The resultant copolymer derivatives are hydrolytically stable, compared to the derivatives from esterification. Polysoaps can additionally be obtained after unreacted anhydride units are hydrolyzed with caustic, alkaline earth metals, and amines.

Reactions of maleic anhydride–methyl vinyl ether copolymer with substituted aminophenols yield imide groups (Scheme 4.20) at 130 °C. The reaction results exclusively in imides containing *N*-phenol substituents and not phenyl esters, due to the higher thermodynamic stability [109]. As expected, these materials display antimicrobial properties useful in barrier film formation in oral care, as well as hard surface cleaner applications.

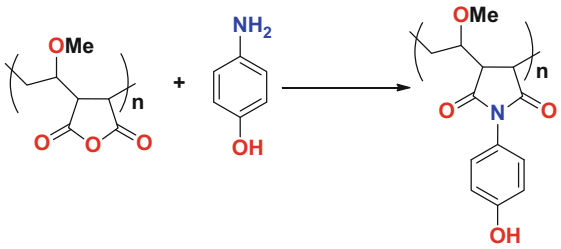

Scheme 4.20 Reaction of maleic anhydride–methyl vinyl ether copolymer with *p*-aminophenol to form polyimides (adapted from [107])

References

1. Trivedi BC, Culbertson BM (1982) Maleic anhydride. Plenum Press, New York
2. Culbertson BM (1987) Maleic and fumaric polymers. Encyclopedia of polymer science and engineering. Wiley, New York, p 225
3. Ashland (2014) Ashland [Online]. http://www.ashland.com/products/gantrez-copolymers. Cited 30 June 2014
4. Robert MV (1957) US Patent 2,782,182
5. Jones JF (1962) US Patent 3,030,343
6. Field ND, Williams EP (1970) US Patent 3,499,876
7. Field ND, Lorenz DH (1971) US Patent 3,553,183
8. Field ND, Lorenz DH (1970) US Patent 3,532,771 US
9. Tazi M, Ardan JJ (1991) US Patent 5,034,487
10. Fujikawa H, Katsui H, Ogawa H (1995) US Patent 5,385,995
11. Tazi M, Kundel N (1990) US Patent 4,948,848
12. Pehlah Z, Potencsik I, Kopp W, Urmann E (1991) US Patent 5,047,490
13. Plochocka K (2001) US Patent 6,214,956
14. Tazi M, Nikhil K (1990) US Patent 4,939,198
15. Tazi M, Harwood HJ (1991) US Patent 4992517
16. Tazi M, Ardan JJ (1991) US Patent 5,003,014
17. Goertz H-H, Straub F, Vogel F, Frosch F, Naegle P, Raubenheimer HJ (1990) US Patent 4,908,413
18. Tazi M, Login RB, Kwak YT (1992) US Patent 5,082,913
19. Plochocka K (1999) US Patent 5,939,506
20. Tazi M, Kwak YT, Login RB (1991) US Patent 5,034,488
21. Ulmer HW (2001) US Patent 6,197,908
22. Ulmer HW (2001) US Patent 6,252,026
23. Grigoras C (2013) World Patent Application 2013/082359 WO
24. Prencipe M, Durga GA (1993) US Patent 5,202,112
25. Block J, Sokol PE (1976) US Patent 3,974,128
26. Field ND, Lorenz DH (1971) US Patent 3,625,924
27. Kwak Y, Narayanan KS, Kopolow SL (1996) US Patent 5,567,787
28. Butler GB, Xing Y, Gifford GE, Flick DA (1985) Ann NY Acad Sci 446:149
29. Odian G (2004) Principles of polymerization. Wiley, Hoboken, NJ, p 473
30. Braun D, Hu F (2006) Prog Polym Sci 31(3):239
31. Feiring AE, Wonchoba ER, Fischel BE, Thieu TV, Nassirpour MR (2002) J Fluor Chem 118:95

32. Chiellini E, Marchetti M, Villiers C, Braud C, Vert M (1978) Eur Polym J 14(4):251
33. Barner-Kowollik C, Davis TP, Coote ML, Matyjaszewski K, Vana P (2004) Encycl Polym Sci Technol 9:394
34. Braun D, Hu F (2004) Polymer 45:61
35. Bevington JC, Huckerby TN, Jenkins AD (1999) J Macromol Sci A 36:1907
36. Bevington JC, Hunt BJ, Jenkins AD (2000) J Macromol Sci A 37:609
37. Mulliken RS (1952) J Phys Chem 56:801
38. Schmidt-Naake G, Drache M, Leonhardt K (1998) Macromol Chem Phys 199:353
39. Fujimori K (1986) J Macromol Sci A Chem 23:647
40. Bartlett PD, Nozaki K (1495) J Am Chem Soc 68:1495
41. Rätzsch M (1988) Prog Polym Sci 13:277
42. Hill DJT, O'Donnell JJ, O'Sullivan, PW (1982) Prog Polym Sci 8:215
43. Hallensleben ML (1971) Makromol Chem 144:267
44. Hao X, Fujimori K, Tucker DJ, Henry PC (2000) Eur Polym J 36:1145
45. Denizli BK, Can HK, Rzaev ZMO, Guner A (2006) J Appl Polym Sci 100:2455
46. Kokubo T, Iwatsuki S, Yamashita Y (1968) Macromolecules 1:482
47. Rzaev ZMO (2000) Progr Polym Sci 25:163
48. Coote ML, Davis TP, Klumperman B, Monteiro MJ (1998) J Macromol Sci Chem Phys C38:567
49. Coote ML, Davis TP (1999) Progr Polym Sci 24:1217
50. Andrews LJ, Keefer RM (1953) J Am Chem Soc 75:3776
51. Fujimori K, Craven IE (1986) J Polym Sci A Polym Chem 24:559
52. Dodgson K, Ebdon JR (1977) Eur Polym J 13:791
53. Deb PC, Meyerhoff G (1984) Eur Polym J 20:713
54. Fehérvári F, Azori M, Berezsnich TF, Tudos F (1987) Polymer Bull 18:225
55. Can HK, Rzaev ZMO, Güner A (2004) J Mol Liquids 111:77
56. Fukuda T, Kubo K, Ma Y-D (1992) Progr Polym Sci 17:875
57. Braun D, Elsässer H (2000) Macromol Theory Simul 9:177
58. Yoshimura M, Nogami T, Yokoyama M, Mikawa H, Shirota Y (1976) Macromolecules 9:211
59. Braun D, Schacht M, Elasser H, Tudos F (1997) Macromol Rapid Commun 18:335
60. Braun D, Elsässer H, Hu F (2001) Eur Polym J 37:1779
61. Fujimori K, Schiller WS, Crave IE (1988) Polym Bull 20:355
62. Hall HK, Padias AB (2001) J Polym Sci A Polym Chem 39:2069
63. Hall HK, Padias AB (2004) J Polym Sci A Polym Chem 42:2845
64. Ito H, Miller D, Sveum N, Sherwood M (2000) J Polym Sci A Polym Chem 38:3521
65. Jones SA, Tirrell DA (1987) J Polym Sci A Polym Chem 25:3177
66. Jones SA, Tirrell DA (1986) Macromolecules 19:2080
67. Prementine GS, Jones SA, Tirrell DA (1989) Macromolecules 22:770
68. Mota-Morales JD, Gutierrez MC, Ferrer ML, Jimenez R, Santiago P (2010) Macromol React Eng 4:222
69. Sato T, Abe M, Otsu T (1981) J Macromol Sci A Chem A15:367
70. Kokubo T, Iwatsuki S, Yamashita Y (1969) Makromol Chem 123:256
71. Stille JK, Chung DC (1975) Macromolecules 8:114
72. Hall HK, Padias AB (1997) Acc Chem Res 30:322
73. Hall HK (1983) Angew Chem Int Ed Engl 22:440
74. Hall HK, Padias AB (1995) Aldrichim Acta 28:37
75. Huisgen R (1977) Acc Chem Res 10:199
76. Huisgen R, Penelle J, Mloston G, Padias AB, Hall HK (1992) J Am Chem Soc 114:266
77. Eberson L, Persson O, Hall HK, Padias AB, Steel PJ (2000) Macromolecules 33:2021
78. Wu CS, Senak L, Malawer EG (1989) J Liquid Chromatogr 12:2901
79. Wu CS, Senak L, Malawer EG (1989) J Liquid Chromatogr 12:2919
80. Chung KH, Wu CS, Malawer EG (1990) J Appl Polym Sci 41:793
81. Kittrell JR, Quinlan CW (1994) US Patent 5,340,918

82. Saito M (2004) US Patent 6,800,696
83. Endo T, Fujii T, Tsuji Y, Saito M (2005) US Patent 6,881,803
84. Plochocka K, Login RB, Chuang JC (1996) Degradation and stabilization of alkyl vinyl ether maleic acid copolymers in aqueous systems. In: Book of abstracts, 211th ACS national meeting, vol 37. American Chemical Society, New Orleans, LA, pp POLY-127
85. Login RB, Plochocka K, Chuang JC (1993) US Patent 5,214,089
86. Meyer H, Sanner A, Frosch F, Richter H (1999) US Patent 6,008,274
87. Wu CS, Curry J, Cullen JP, McEwan, JS (1998) US Patent 5,739,183
88. Plochocka K, Chuang JC (1995) US Patent 5,449,715
89. Ladavière C, Delair T, Domard A, Pichot C, Mandrand B (1999) Polym Degrad Stabil 65:231
90. Woodruff CW, Peck GE, Banker GS (1972) J Pharm Sci 61:1916
91. Ladaviere C, Delair T, Domard A, Pichot C, Mandrand B (1999) J Appl Polym Sci 71:927
92. Dubin PL, Strauss UP (1970) J Phys Chem 74:2842
93. Plochocka K (2003) US Patent 6,562,928
94. Morawetz H, Kotliar AM, Mark H (1954) J Phys Chem 58:619
95. Begala AJ, Strauss UP (1972) J Phys Chem 76:254
96. Pesonen H, Sillanpaa A, Aksela R (2005) Polymer 46:12653
97. Plochocka K, Chuang JC, Tallon M (1997) Alkyl half-esters of methyl vinyl ether/maleic acid copolymers in ethanol/water systems. In: Book of abstracts, 214th ACS national meeting. American Chemical Society, Las Vegas, NV, pp POLY-115
98. Curry JF, Goehner RH, Narayanan KS, Jon D (2000) US Patent 6,156,803
99. Plochocka K (2001) US Patent 6,315,987
100. Plochocka K (2002) US Patent 6,464,961
101. Ding LM (1997) Polymer 38:4267
102. Hassan M, Dixit N, Bentley M, Viscio DB (1997) US Patent 5,661,221
103. Khutoryanskiy V, Khutoryanskaya O, Cook JP, Goodall GB (2013) US Patent Application 2013/0018110
104. Plochocka K, Lynn J (2003) US Patent 6,583,225
105. Plochocka K, Lynn J (2004) US Patent 6,706,817
106. Singh TRR, Woolfson AD, Donnelly RF, McCarron PA (2009) Eur Polym J 45:1239
107. Garreta JMI, Yoncheva KP (2008) US Patent Application 2008/0248125
108. McCormick CL, Hoyle CE, Clark MD (1992) Polymer 33:243
109. Plochocka K, Winkowski K, Lynn J (2007) US Patent Application 2007/0036743

Chapter 5
Industrially Significant Copolymers Containing Maleic Anhydride

Michael A. Tallon and Xuejun (Jay) Liu

5.1 Introduction to Unsaturated Polyester Resins Based on Maleic Anhydride

In the United States, the commercial use of unsaturated polyester resins accounts for the major consumption of maleic anhydride. Approximately 2.2 billion kilograms/year of unsaturated polyester resins are employed to manufacture a variety of products. In the fiber-reinforced plastic (FRP) industry, unsaturated polyester resins are widely employed as thermoset resins. The broad applications of unsaturated polyester resins are due to their low cost, ease of processability, fast curing, and excellent mechanical properties.

5.2 Production of Unsaturated Polyester Resins

Unsaturated polyester resins are produced by condensation of dibasic organic acids and dihydric alcohols that are subsequently cured in the presence of diluent monomers (Scheme 5.1) [1]. The commonly employed dibasic organic acids include maleic anhydride, fumaric acid, phthalic anhydride, isophthalic acid, and terephthalic acid. The dihydric alcohol is primarily propylene glycol. Other diols are also employed including ethylene glycol, 2-methyl-1,3-propanediol, and diethylene glycol. The linear unsaturated polyesters that still contain a reactive double bond are then free to radically or thermally cross-link with other diluent monomers(such as styrene, at 18–40 wt%) to form thermoset polyester resins, as depicted in Scheme 5.1.

M.A. Tallon (✉) • X.(J). Liu
Ashland Inc., 1005 Route 202/206, Bridgewater, NJ 08807, USA
e-mail: mtallon@ashland.com

O.M. Musa (ed.), *Handbook of Maleic Anhydride Based Materials*,
DOI 10.1007/978-3-319-29454-4_5

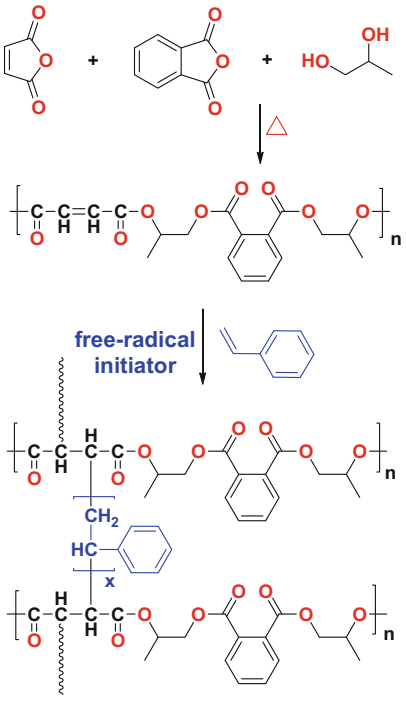

Scheme 5.1 Condensation of propylene glycol with maleic anhydride and phthalic anhydride, along with subsequent curing with styrene (adapted from [1])

The condensation portion of the polymerization is typically performed at 210–225 °C [1]. A slight excess of polyols (10 %) are employed to compensate for their evaporative loss. The reaction progress can be monitored by acid value. The obtained polyesters are linear polymers with an average molecular weight of about 700–5000 Da with an acid number of approximately 40 [2]. To bring down the acid value below 30, vacuum can be applied to remove water and further accelerate the condensation reaction. To further drop the acid number to 0–10, catalysts such as titanate, zirconate, or stannous salts are required.

Another way to control the completion of the condensation step is to monitor its number-average molar mass (M_N) [3]. For example, in a condensation reaction starting from equal moles of propylene glycol, diethylene glycol with maleic anhydride, and isophthalic acid, Eisenberg and coworkers demonstrated that increasing the reaction time from 1 to 9 h resulted in an increase of M_N from 484 to 1712 g/mol [3]. In this study, increasing M_N resulted in an increase in the resin's' compatibility with styrene, presumably due to the lower overall polarity of the resin that is attributable to a lower concentration of polar end groups in higher M_N polymers.

An important consequence occurring during the high temperature 210–225 °C condensation process is the substantial conversion of maleate to fumarate by

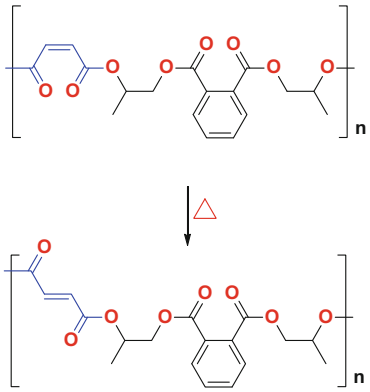

Scheme 5.2 Maleate-to-fumarate isomerization during the condensation process (adapted from [1])

isomerization (Scheme 5.2). It is also well known that cross-linking maleate polyesters with styrene is slow, but the copolymerization reactivity of fumarate with styrene is almost 20 times higher than that for maleate [4]. Fumarate-containing polyesters have less steric hindrance in the *trans* form and can adopt more planar conformations [3]. The degree of isomerization increases in the presence of aromatic diacids and if sterically more hindered glycols are employed [1]. Higher reaction temperatures also lead to more isomerization.

The subsequent curing process of the condensation product is affected by several factors: (1) the extent of maleate-to-fumarate isomerization, (2) the nature of saturated and unsaturated acid monomers and their relative ratio, (3) the relative ratio of diluent monomers to the unsaturated polyester resins, and (4) the nature and use level of catalysts and accelerators [1].

For the curing of these resins, the reactive diluent monomers should be inexpensive and readily available, and the resin shrinkage should be low to prevent cracking of the resin. They should have high boiling points to avoid evaporative losses during the condensation process, and the polymerization reactivity should be high but controllable. In the presence of diluent monomers such as styrene, the curing rate is about 30 times higher [5]. Styrene forms linear oligomeric chains between the double bonds in the polyester backbones. Typically, about one to five styrene units are observed as cross-linking tethers between adjacent polyester chains in the cured resins [6]. However, there is still a small amount of unsaturated groups (3–7 %) from the polyester chain that remain unreacted. At very low styrene concentration, fumarate-fumarate cross-linking can potentially occur as well.

The curing of unsaturated polyester resins with diluent monomers, such as styrene, is typically initiated by a free radical initiator and an accelerator [7]. The combination of an initiator and an accelerator is to obtain a reasonable gel time (<20 min) [8]. Free radical polymerization initiators such as methyl ethyl ketone peroxide (MEKP) are normally employed. The accelerator promotes the decomposition of the initiators and lowers the overall curing temperature.

Typically, organocobalt salts, such as cobalt naphthenate or cobalt octoate, are employed as the accelerator. During the storage of unsaturated polyester resin-styrene mixtures, a low level of inhibitors such as hydroquinone is added to the blend to ensure its shelf life. The inhibitors inhibit premature gelation and reduce peak exotherm temperatures.

The commercial general-purpose grade (GP) of unsaturated polyester resins are mixtures of styrene and condensation products from maleic anhydride, phthalic anhydride/acid, and propylene glycol. The compositions of commercial condensation products vary from different manufacturers, and most are considered proprietary [9]. One commercial example contains a molar ratio of propylene glycol, maleic anhydride, and phthalic anhydride, of 2.7:1:1.6 in one of the general-purpose-grade resins from Bakelite Hylam, India.

5.2.1 Composition of Unsaturated and Saturated Dicarboxylic Anhydride/Acid

The type and proportion of unsaturated and saturated dicarboxylic anhydride/acid inevitably influence the final properties of the cured polyester resins. Among the dicarboxylic anhydrides acids, phthalic anhydride is the least expensive and enhances the resin's compatibility with styrene. Phthalic anhydride also reduces the tendency of the resin to crystallize and make it brittle. Isophthalic acid has a relatively higher cost; however it gives very good structural and corrosion properties. Terephthalic acid is employed in small volumes to make certain specialty resins. In general-purpose-grade unsaturated polyester resins, maleic anhydride and phthalic anhydride/acid are primarily employed.

The relative composition of maleic anhydride and phthalic anhydride affects the curing behavior and mechanical properties of the cured resins. T_{max} is the maximal curing temperature, while t_{max}, is the time required to reach T_{max}, both of which are very important curing parameters [2]. In the presence of equal molar ratio of propylene glycol and diethylene glycol, T_{max} increases as maleic anhydride concentration increases (Table 5.1), but $t_{max,}$ decreases as maleic anhydride concentration increases.

Table 5.1 Composition of unsaturated polyester resins and their curing behavior and tensile modulus of corresponding cured resins; equal molar ratio of propylene glycol and diethylene glycol were employed (adapted from [2])

Sample #	Dicarboxylic anhydride (wt%)		T_{max} (°C)	t_{max} (min)	Tensile modulus (GPa)
	Maleic anhydride	Phthalic anhydride			
1	18.1	81.9	37.0	25	–
2	39.8	60.2	43.7	16	0.728
3	66.5	33.5	56.5	14	1.372

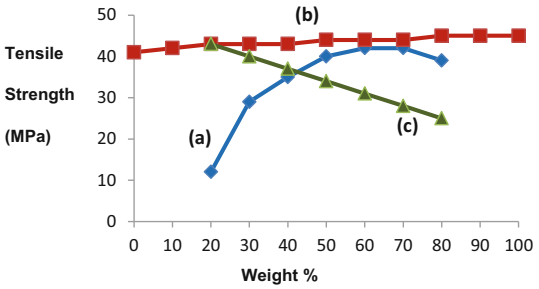

Fig. 5.1 Effect of reactant compositions on tensile strength of the cured resins: (**a**) wt% of maleic anhydride in maleic anhydride/phthalic anhydride, (**b**) wt% of ethylene glycol in propylene glycol/ethylene glycol, and (**c**) wt% of diethylene glycol in propylene glycol/diethylene glycol (adapted from [8])

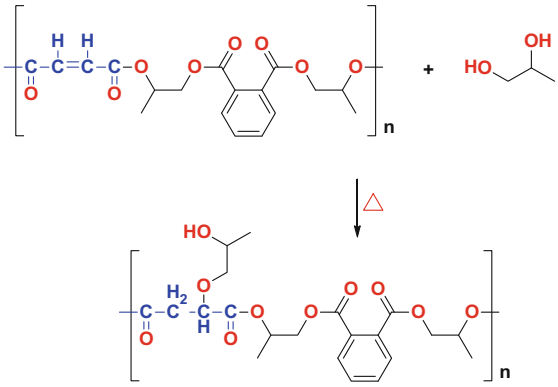

Scheme 5.3 The Ordelt reaction—the addition of propylene glycol to the maleate double bond

Furthermore, it has been observed that the tensile strength of the cured resin reaches a maximum at around 60 % maleic anhydride composition in a blend of phthalic anhydride and maleic anhydride, if propylene glycol is employed as the diol (Fig. 5.1a) [8], while its tensile strength, the maximum stress that a material can withstand while being stretched before breaking or failure, tends to increase. As the maleic anhydride concentration increases from 20 to 60 %, the rise in the cross-linking density leads to higher tensile strength. At too high concentration of maleic anhydride, a side reaction, known as the Ordelt reaction, reduces the unsaturation by about 10–20 % through the addition of glycols onto the double bond (Scheme 5.3). Ultimately, the Ordelt reaction affects the cross-linked polymer structure and final mechanical properties of the cured resins.

The tensile modulus shows a similar dependence on the maleic anhydride composition. The tensile modulus, or Young's modulus, is a measure of the stiffness of an elastic isotropic substance. If only propylene glycol is employed,

the tensile modulus of the cured resin peaks at about 50–60 % maleic anhydride [8]. In the presence of equal molar quantity of propylene glycol and diethylene glycol, the tensile modulus reaches a maximum at 66.5 % maleic anhydride concentration (Table 5.1, sample 3) [2]. Below 20 % maleic anhydride concentration, the resins are more flexible material and their tensile moduli cannot be measured (Table 5.1, sample 1) with any reasonable accuracy.

The Izod impact strength of the cured resins measures the suddenly applied energy load required to fracture a material sample. For the cured resins, the Izod impact strength gradually increases to about 60 % maleic anhydride composition and then it drops slowly. Cross-linking protects the resins from impact failure; however, at too high maleic anhydride concentration, it becomes more brittle [8].

On the contrary, the elongation at break measures the strain on a material when it breaks under stress, of which the cured resins drops significantly as maleic anhydride increases from 20 to 40 % [8] and plateaus at higher than 40 % maleic anhydride concentrations. At low concentrations of maleic anhydride, due to low cross-linking density, the cured resins are flexible and thus have high elongation at break.

The resin's toughness follows a similar trend as elongation at break does [8]. Material toughness is the ability to absorb energy and plastically deform without breaking. It can be calculated by integration of the stress-strain curve. For the cured resins, higher elongation at break gives the resins better toughness, since the energy absorption capability is higher at lower cross-linking density.

The type of (un)saturated anhydride/acid excluding phthalic anhydride can further influence the curing process and the mechanical properties of the cured resins. The saturated acids including succinic acid, adipic acid, and sebacic acid were employed to prepare unsaturated polyesters with maleic anhydride and glycols [10].

It has been demonstrated that as the molecular weight of the dibasic acid increases, T_{max} decreases while the time t_{max} increases. It is rationalized that lower-molecular-weight dibasic acid results in shorter spacing between the unsaturation and faster curing rates. The materials made from lower-molecular-weight dibasic acids also showed higher tensile modulus due to the denser cross-linking network [8–10].

5.2.2 Composition of Dihydric Alcohols

The type and proportion of dihydric alcohols also have an influence on both the curing behavior and mechanical properties of the cured resins. In general-purpose-grade unsaturated polyester resins, propylene glycol is mainly employed because of the cost advantage over all the other diols. The unsaturated polyester resins prepared from propylene glycol are also compatible with styrene and demonstrate good water resistance and flexibility.

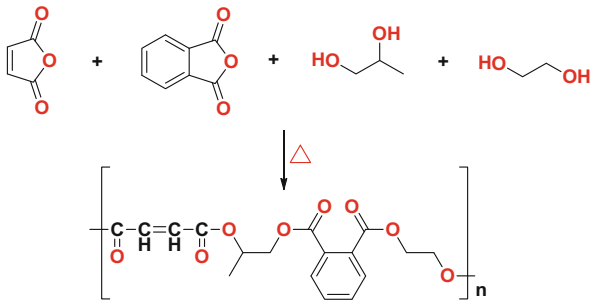

Scheme 5.4 Condensation of propylene glycol and ethylene glycol with maleic anhydride and phthalic anhydride (adapted from [8])

The incorporation of ethylene glycol results in higher maximal curing temperature and faster curing rate, presumably due to the increased exotherm per unit mass (Scheme 5.4) [2]. Among all the possible diols, ethylene glycol has the lowest molar mass. Therefore the most exothermic curing reaction is observed when ethylene glycol is employed as the sole glycol. Higher-molecular-weight glycols lead to lower T_{max} and longer t_{max} (time to reach T_{max}) [10].

Compared to propylene glycol, the incorporation of ethylene glycol marginally improves tensile strength (Fig. 5.1b) [8]. With ethylene glycol, the tensile modulus increases considerably, although not as significantly in Abd-El-Azim's study [2]. Therefore, ethylene glycol-based resins are surprisingly stiffer than propylene glycol-based resins. However, the incorporation of ethylene glycol is detrimental for elongation at break, resin toughness, impact strength, and water absorption, due to the greater stiffness and/or higher hydrophilicity of ethylene glycol-based resins [8].

Diethylene glycol has a longer chain length between the diols, so diethylene glycol-based resins are more flexible but have a lower tensile strength and tensile modulus (Fig. 5.1c) [2]. Incorporation of diethylene glycol leads to lower hardness, higher abrasion loss, and higher water absorption [8]. However, the incorporation of diethylene glycol is beneficial for elongation at break, resin toughness, and impact strength. The use of poly(ethylene glycol)s, which have even longer chain length between the chain-end diols, yield cured resins with decreased tensile and flexural properties [11].

Compared to propylene glycol, unsaturated polyester resins made from 2-methyl-1,3-propanediol have shown improved processability and better mechanical properties of the cured products (Scheme 5.5) [13]. 2-Methyl-1,3-propanediol contains two very reactive primary alcohols, and the boiling point of 2-methyl-1,3-propanediol is 30 °C higher than propylene glycol, making it possible to run the condensation reaction at higher temperatures and in shorter time [12]. The cured resins have demonstrated improved mechanical strength, good ductility, and excellent corrosion resistance.

In the theme of "greener chemistry," bio-based monoglycerides have been employed to partially replace propylene glycol to render bio-based unsaturated polyester resins (Scheme 5.6) [14, 15]. These studies demonstrated that the optimal properties could be achieved when the resin contains 30 % soybean oil-based

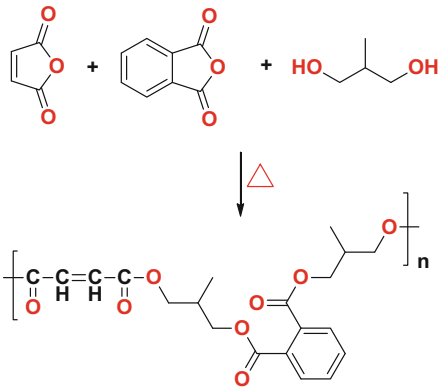

Scheme 5.5 Condensation of 2-methyl-1,3-propanediol with maleic anhydride and phthalic anhydride (adapted from [12])

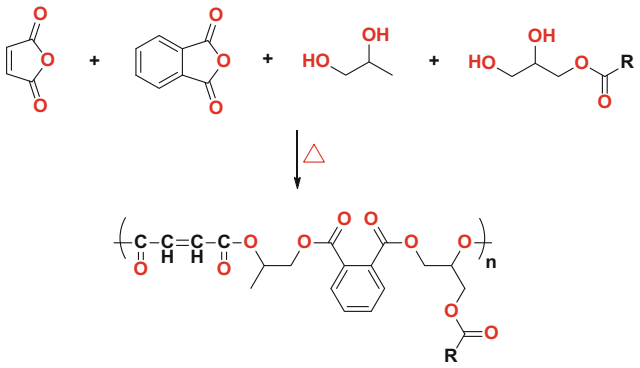

Scheme 5.6 Condensation of propylene glycol and monoglyceride with maleic anhydride and phthalic anhydride. R has 0–3 double bonds and ranges from 14 to 22 carbons in length (adapted from [14, 15])

monoglyceride. Due to steric hindrance of the fatty ester group, the Ordelt-type side reaction was not observed.

Nonetheless, the curing reactivity of the monoglyceride-containing polyester was lower than that without monoglyceride. Therefore, lower cross-linking density was obtained, which led to decreased tensile strength of the cured resins but improved impact strength of the cured resins.

Isosorbide has also been employed as the structural component to synthesize bio-based unsaturated polyesters (Scheme 5.7) [16]. Isosorbide is produced commercially from bio-based feedstocks, such as starch or glucose. In typical commercial unsaturated polyester resins, phthalate is employed to bring stiffness in the cured resins due to the rigidity of the aromatic rings.

With the fused bicyclic ring structure, isosorbide was chosen as a bio-based rigid diol to replace both phthalic anhydride and propylene glycol. However, the

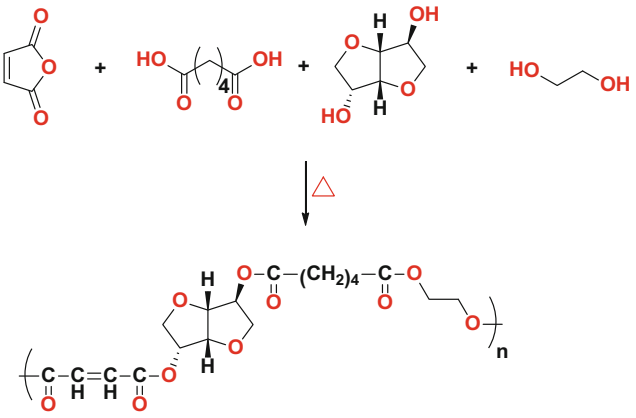

Scheme 5.7 Condensation of maleic anhydride, adipic acid, isosorbide, and ethylene glycol (adapted from [16])

resultant unsaturated polyester has very low solubility in styrene. Therefore, additional studies are required to improve the formulation's compatibility with reactive diluent monomers.

5.2.3 *Addition Sequence of Dibasic Acids and Dihydric Alcohols*

Cherian and Thachil studied five potential sequences for addition of reactants to prepare general-purpose-grade unsaturated polyester resins [10]. The three components, phthalic anhydride, propylene glycol, and maleic anhydride, were charged by: (1) reacting maleic anhydride, phthalic anhydride, and propylene glycol at one stage; (2) reacting phthalic anhydride and a stoichiometric amount of propylene glycol first, followed by maleic anhydride and the rest of the propylene glycol; (3) reacting maleic anhydride and a stoichiometric amount of propylene glycol first, followed by phthalic anhydride and the rest of the propylene glycol; (4) reacting phthalic anhydride with all the propylene glycol first, followed by maleic anhydride; and (5) reacting maleic anhydride with all the propylene glycol first, followed by phthalic anhydride.

The mechanical properties of the cured resins from these five methods were evaluated in terms of: impact strength, elongation at break, tensile strength, tensile modulus, and toughness [11, 13]. The different addition sequences did not show any significant impact on most of the test properties. However, method IV gave the shortest reaction time and produced unsaturated polyester resins that have comparatively higher bulk viscosity and molecular weight.

The modest difference observed for the method IV process yielded cured resins exhibiting marginally better tensile strength and modulus. They explained that method IV yielded polyesters with optimal spacing between the double bonds in the polyester backbone and therefore an optimal cross-linking profile during the

curing step. The poor distribution of the cross-linking sites (such as too closely spaced) may lead to poorer mechanical properties of the cured resins.

5.3 Unsaturated Polyester Resins from Polyethylene Terephthalate Waste

In the same theme of "greener chemistry," unsaturated polyester resins have been produced from glycolyzed polyethylene terephthalate (PET) waste [9, 17]. Polyethylene terephthalate is widely employed in synthetic fibers, beverage, food, and other liquid containers. Glycolysis has been performed by the chain scission of fiber- or fabric-grade polyethylene terephthalate waste with propylene glycol using zinc acetate as the catalyst (Scheme 5.8).

Recycling can also be performed from postconsumer polyethylene terephthalate bottles [18]. Alternative glycols, such as ethylene glycol, propylene glycol, diethylene glycol, or triethylene glycol, have been employed for the chain-scission process through a transesterification process.

The glycolyzed products are then reacted with maleic anhydride to form unsaturated polyester resins. Subsequent curing with styrene is performed using a similar process as virgin resins. The propylene glycol-based glycolyzed products are compatible with styrene [18]. The resins have shown comparable processability and mechanical properties against the conventional general-purpose-grade resin [8]. Due to the presence of terephthalate linkages, the cured resins have demonstrated improved heat deflection temperature (HDT, 80–85 °C) compared to the general-purpose-grade resins (65 °C). The mechanical properties and thermal stability of the cured resin products are most improved with long glycolysis time (8 h) [8, 17].

The nature of glycols has shown significant impact on the characteristics of the resins before and after curing. Before curing, ethylene glycol-based recycled resins

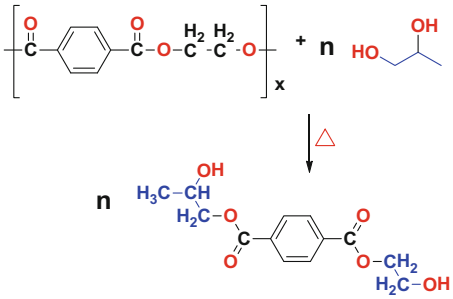

Scheme 5.8 Glycolysis of poly (ethylene terephthalate) with propylene glycol (adapted from [17])

are soft solids at room temperature, while the ones from propylene glycol or diethylene glycol are viscous liquids [18].

The glycolysis products are mostly composed of mixtures of hydroxyl-ended terephthalate monomers and dimers [19]. After curing, ethylene glycol-based resins are hard and brittle plastics, presumably due to their most regular polymer chain structure [20]. The cured propylene glycol-based resins have mostly amorphous regions and elongate as the load increases.

For the cured diethylene glycol-based resins, strain-induced crystallization has been observed. Again, the curing behaviors and mechanical properties of the cured resins from the glycolyzed polyethylene terephthalate resins are comparable with the control resins prepared from the identical glycols. Interestingly, the cured resins from either soft-drink bottles, water bottles, or a mixture of both do not show any difference in terms of their mechanical properties.

5.4 Condensation Kinetics of Dibasic Acid and Diol

Extensive studies have been performed to investigate the kinetics of condensation by a dibasic acid and a diol. In 1982, by introducing additional considerations into conventional rate equations, Chen and Wu have presented reaction mechanisms and rate equations that fit quite well with the experimental data observed [21].

They proposed: (1) ionization of the acids, either the acid monomer or the acid catalyst, through an ion pair mechanism in which the diols act as hydrogen ion carriers, (2) change of the dielectric constants of the reaction media as the polymerization proceeds (the decrease in the dielectric constant as the conversion increases has a significant impact on the ionization of the acids, which can affect the polymerization rate), and that (3) the produced water from the condensation, if not completely removed from the reaction system, also affects the rates. The presence of water also impacts the polymerization rate especially in the latter stage.

From the Chen and Wu studies, the following rate equations were derived. For a typical self-catalyzed condensation reaction,

$$\mathrm{RCO_2H} + \mathrm{R'OH} \rightleftharpoons \mathrm{RCO_2R'} + \mathrm{H_2O},$$

the rate equation is

$$\frac{d\left[\mathrm{RCO_2R'}\right]}{dt} = kK_e 0e^{(\propto p)}[\mathrm{RCO_2H}]^2\left[\mathrm{R'OH}\right] - k_h[\mathrm{H_2O}]\left[\mathrm{RCO_2R'}\right]$$

If catalyzed by a foreign acid catalyst HA, then the rate equation is

$$\frac{d\left[\mathrm{RCO_2R'}\right]}{dt} = k_c K_{ec0} e^{\propto p}[\mathrm{HA}][\mathrm{RCO_2H}]\left[\mathrm{R'OH}\right] - k_{hc}[\mathrm{H_2O}]\left[\mathrm{RCO_2R'}\right]$$

in which k or k_c is the condensation rate constant (kg/mol-min); K_{e0} or K_{ec0} is the ionization equilibrium constant at zero conversion ($p = 0$) (kg/mol) for acid monomer or foreign acid catalyst, respectively; α is a constant; p is the degree of conversion of the acid group, $p = ([CO_2H]_0 - [CO_2H])/([CO_2H]_0$; and k_h or k_{hc} is the ester bond hydrolysis rate constant (kg/mol-min).

5.4.1 Condensation Kinetics of Maleic Anhydride and Phthalic Anhydride with Propylene Glycol

For the system composed of maleic anhydride, phthalic anhydride, and propylene glycol, Zetterlund and coworkers have modified Chen and Wu's model to investigate the condensation kinetics [21, 22]. They have taken into consideration: (1) the reactivity difference between the primary and secondary alcohols on the propylene glycol molecule itself [as determined that a primary alcohol $(OH)_1$ is 2.6 times more reactive than a secondary one $(OH)_2$] [21] and (2) cross-catalysis in which one acid monomer catalyzes the esterification of the other.

In the absence of foreign acid catalyst, the rate equations for maleic anhydride and phthalic anhydride and propylene glycol have been established [22]. For example, the rate equation for maleic anhydride is

$$\begin{aligned}\frac{d[\mathrm{CO_2H}]_y}{dt} = & -2.6k_y K_{e0y} e^{\propto p}[\mathrm{CO_2H}]_y^2[\mathrm{OH}]_1 - k_y K_{e0y} e^{\propto p}[\mathrm{CO_2H}]_y^2[\mathrm{OH}]_2 \\ & -2.6k_{xy} K_{e0x} e^{\propto p}[\mathrm{CO_2H}]_y[\mathrm{CO_2H}]_x[\mathrm{OH}]_1 \\ & -k_{xy} K_{e0x} e^{\propto p}[\mathrm{CO_2H}]_y[\mathrm{CO_2H}]_x[\mathrm{OH}]_2 \\ & +(k_h[\mathrm{H_2O}])_y[\mathrm{E}]_y\end{aligned}$$

in which y stands for maleic anhydride, x stands for phthalic anhydride, k_y is the esterification rate constant catalyzed by maleic acid, k_{xy} is the esterification rate constant catalyzed by phthalic acid, and $E_y = p_y[CO_2H]_{0y.}$

Zetterlund and coworkers discovered that after ring opening, the maleic acid unit is more reactive than phthalic acid toward propylene glycol. The relative reactivity ratio, maleic acid and propylene glycol vs. phthalic acid and propylene glycol, increased from 1.7 to 2.3, as the polymerization temperature rose from 160 to 22 °C.

An anti-synergist effect is also observed. The total reaction rate of the carboxylic acid groups in the ternary system is lower than the sum of the reaction rates for the individual acids, while all the reaction conditions were kept the same. Hence, their simulated results were in good agreement with the experimental data obtained [22].

5.4.2 Condensation Kinetics of 2-Methyl-1,3-Propanediol with Maleic Anhydride and Phthalic Anhydride

The kinetics for the condensation involving 2-methyl-1,3-propanediol has also attracted considerable interest due to the two equally reactive primary alcohols [22]. The simplified kinetic models for self-catalyzed condensation have been proposed. For example, the rate equation for the disappearance of maleic anhydride is

$$\frac{d[\mathrm{CO_2H}]_y}{dt} = -k_y K_{e0y} e^{\propto p} [\mathrm{CO_2H}]_y^2 [\mathrm{OH}] - k_{xy} K_{e0x} e^{\propto p} \left[\mathrm{CO_2H}\right]_y \mathrm{CO_2H}]_x [\mathrm{OH}] + (k_h [\mathrm{H_2O}])_y [\mathrm{E}]_y$$

in which y stands for maleic anhydride and x stands for phthalic anhydride and the other parameters as previously defined.

Experimentally, the condensation of 2-methyl-1,3-propanediol with maleic anhydride and phthalic anhydride, employing a temperature range of 180–200 °C, was performed [22]. The relative reactivities for maleic anhydride or phthalic anhydride with 2-methyl-1,3-propanediol were measured by monitoring the disappearance of carboxylic acid groups. Similarly, maleic anhydride is more reactive than phthalic anhydride toward 2-methyl-1,3-propanediol [23]. However, as the polymerization temperature increased from 180 to 200 °C, the relative reactivity ratio decreased from 2.26 to 1.70 [22, 23].

The activation energies for the condensation reaction of some of the dicarboxylic acids and dihydric alcohols are listed in Table 5.2. In the absence of foreign acid catalyst, the activation energy falls in the range of 60–90 kJ/mol. Likewise, 2-methyl-1,3-propanediol is more reactive toward maleic anhydride than propylene glycol, as is expected from its two primary alcohols. However, for the reactions involving phthalic anhydride, the activation energies for the condensation reactions with propylene glycol and 2-methyl,3-propanediol are similar, 81.7 and 82.3 KJ/mol.

Table 5.2 Activation energies for the condensation of dicarboxylic anhydride/acids and dihydric alcohols (adapted from [13, 21])

Dicarboxylic acid	Dihydric alcohol	External acid catalyst	Activation energy (kJ/mol)
Maleic anhydride	Propylene glycol	None	89.6
	2-Methyl-1,3-propanediol	None	65.2
Phthalic anhydride	Propylene glycol	None	81.7
	2-Methyl-1,3-propanediol	None	82.3
Adipic acid	Ethylene glycol	None	62.3
	Ethylene glycol	*p*-Toluenesulfonic acid	38.5

5.5 Mechanical Properties of Cured Unsaturated Polyester Resins

In North America and Europe, the major producers for unsaturated polyester resins include Ashland Inc., AOC, CCP Composites, Reichhold, Royal DSM, and Scott Bader. The unsaturated polyester resins can be utilized in various manufacturing processes such as open molding, closed molding, hot molding, and continuous processes. The cured resins provide excellent mechanical and impact properties. Table 5.3 gives the mechanical properties of cured unsaturated polyester resins from several major suppliers in pultrusion applications [23–26].

Table 5.3 Mechanical properties of cured unsaturated polyester resins in pultrusion applications (adapted from [18–20])

Supplier	Product	Tensile strength (MPa)	Tensile modulus (GPa)	Elongation at break (%)	Flexural strength (MPa)	Flexural modulus (GPa)
Ashland	Aropol™ 2036C	81.4[a]	3.4[a]	4.5[a]	138.6[b]	3.7[b]
	Aropol™ A 3058	58.6	3.4	2.1	100.7	3.4
	Aropol™ L 2450	58.6	3.9	1.8	88.3	4.0
	Aropol™ MR 14,029	69.0	3.7	2.4	112.4	3.6
DSM	Palatal® P 69-02	75[c]	3.8[c]	3.4[c]	na	na
	Synolite™ 2155-N-1	60[c]	4.0[c]	2.0[c]	na	na
	Synolite™ 0152-N-2	88[c]	3.8[c]	4.2[c]	na	na
	Synolite™ 1717-N-1	65[c]	3.6[c]	3.5[c]	na	na
CCP composites	Stypol® 040-2988	64.1	6.4	1.9	120.7	4.5
	Stypol® 040-9322	65.5[a]	3.7[a]	2.3[a]	94.5[b]	5.3[b]
	Stypol® 040-9341	67.2[a]	3.6[a]	2.3[a]	89.6[b]	4.5[b]
	Stypol® 040-9342	69.6[a]	3.8[a]	2.3[a]	153.1[b]	3.8[b]

Test method: [a]ASTM D638; [b]ASTM-D790; [c]ISO 527-2; the rest are not available

5.6 Introduction to Alkyd Resins

Alkyd resins are widely employed as binders in solvent-based coating applications [27] and are found in architectural, industrial, and special-purpose coatings. Alkyd resins provide unique properties including film flexibility and durability, excellent adhesion to substrates, and good color and gloss retention. Although alkyd resins are gradually being replaced by water-based acrylic resins for environmental concerns, they remain the primary binders in surface coating applications.

Alkyd resins are typically produced from the condensation of polybasic acids, polyols, and fatty acids or triglyceride oils. Polyol monomers containing at least three functionalities are employed, such as glycerol, 1,1,1-trimethylolpropane, and pentaerythritol. Glycerol and phthalic anhydride are the most common raw materials employed due to economical and process considerations.

The fatty acids employed in alkyd manufacturing are usually produced from saponification of their respective triglyceride oil. The triglyceride oils from linseed, castor, soybean, sunflower, safflower, tung, coconut, and tall oil are most commonly employed. The incorporation of fatty acids or glyceride oils improves the resin's flexibility, adhesion, water resistance, and chemical resistance.

The typical processes to manufacture alkyd resins can be categorized into two types: (1) direct condensation of phthalic anhydride, glycerol, and fatty acids and (2) saponification of triglyceride oils into monoglycerides followed by condensation with phthalic anhydride and glycerol (Scheme 5.9) [27]. Monoglycerides are usually mixtures of monoglyceride, diglyceride, triglyceride, and glycerol.

Slight excess of polyols are typically employed to guarantee the complete conversion of the carboxylic acid groups and regulate the degree of polymerization and bulk viscosity to their desired level. In these processes, small amounts of commercial xylenes are added to aid in water removal through azeotropic distillation.

Depending on the curing behaviors, alkyd resins are grouped into drying alkyd resins and nondrying alkyd resins [27]. For drying alkyd resins, the curing is achieved through auto-oxidation by air, which can be catalyzed by peroxide and transition metals. Chemically, the curing process is due to free radical cross-linkable double bonds in the fatty acid components. In contrast, nondrying alkyd resins do not polymerize substantially in air because of the lower concentration of unsaturation present within the monoglyceride. Instead, they can be cured with aminoplasts at elevated temperature.

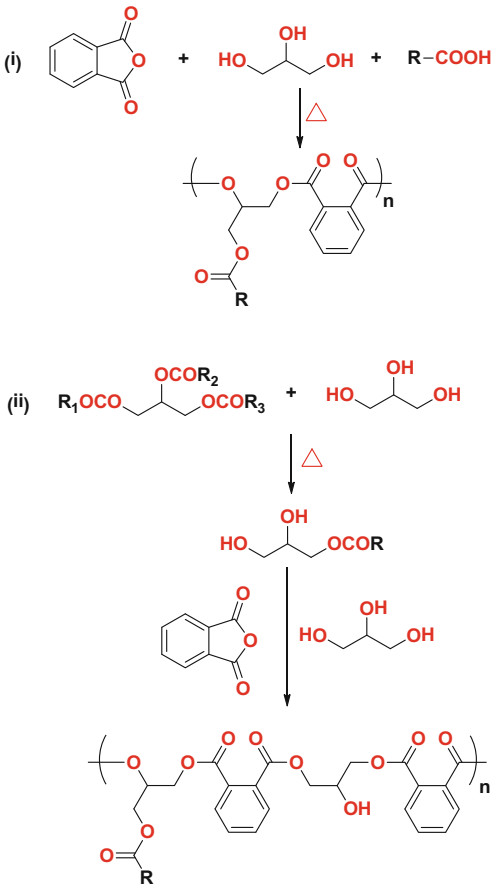

Scheme 5.9 Two typical processes to manufacture alkyd resins: (1) direct condensation of phthalic anhydride, glycerol, and fatty acids and (2) saponification of triglyceride oils into monoglycerides followed by condensation with phthalic anhydride and glycerol (adapted from [27])

5.6.1 Alkyd Resins Containing Maleic Anhydride

Many alkyd resins contain small amounts of maleic anhydride. The incorporation of maleic anhydride enhances water resistance, resin color, and processing time within the final coatings [28].

The use level of maleic anhydride has a significant impact on the physical properties of the alkyd resin, its curing behavior, and the mechanical properties of the final coating. Different alkyd resins have been prepared from various ratios of maleic anhydride and phthalic anhydride. The resins were synthesized by glycerolysis of *Jatropha curcas* oil, yellow oleander seed oil, or Nahar seed oil and subsequent condensation with phthalic anhydride and maleic anhydride (Scheme 5.10) [28–31].

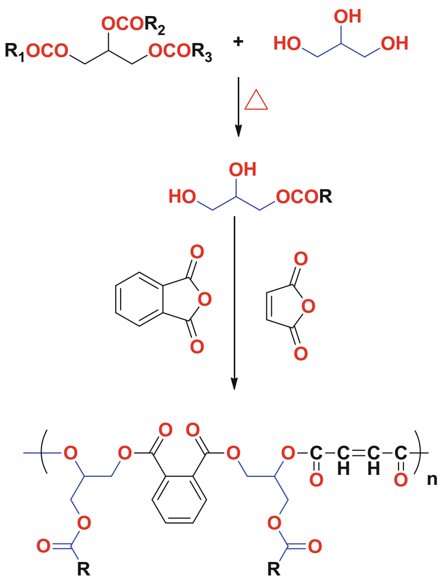

Scheme 5.10 Glycerolysis of *Jatropha curcas* oil and subsequent condensation with phthalic anhydride and maleic anhydride to form alkyd resins (adapted from [28])

It was demonstrated that a higher-molecular-weight polymer and higher bulk viscosity can be obtained with higher maleic anhydride content within the alkyd resin. During the curing process, a shorter curing time was achieved with higher maleic anhydride content. Hence, maleate can participate in cross-linking reactions by a free radical mechanism (Scheme 5.11) [27]. In terms of the mechanical properties of the cured film, the resin without maleic anhydride showed the highest pencil hardness (a test that correlates the maximum hardness of the pencil grade ranging from 1H (soft) to 9H (very hard), without scoring the test film at a thickness of 1.0–1.5 mils) owing to the highest concentration of stiff aromatic functionality within the polymer chain, whereas all the cured resins have shown good adhesion characteristics and possess good gloss properties as well.

For chemical resistance, all the resins are very good against distilled water, 10 % NaCl aqueous, and 10 % HCl aqueous. Pure phthalic anhydride-based resins demonstrate the best resistance against 1 % aqueous NaOH compared to the other resins. Aromatic esters typically have better alkali hydrolysis stability than aliphatic esters. The higher concentration of maleic anhydride also helps the thermostability of the cured alkyd resin due to increased cross-linking density.

The effects of a broader variety of anhydrides on the preparation of low-viscosity alkyd resins and their film properties have also been investigated [30, 31]. Anhydrides including phthalic anhydride, maleic anhydride, glutaric anhydride, or succinic anhydride were employed to react with monoglycerides to form alkyd resins. Compared to the other resins, maleic anhydride-based resins tend to have higher viscosity.

The physical and chemical properties of a succinic anhydride-, phthalic anhydride (PA)-, and maleic anhydride (MA)-based alkyd resins from cottonseed oil

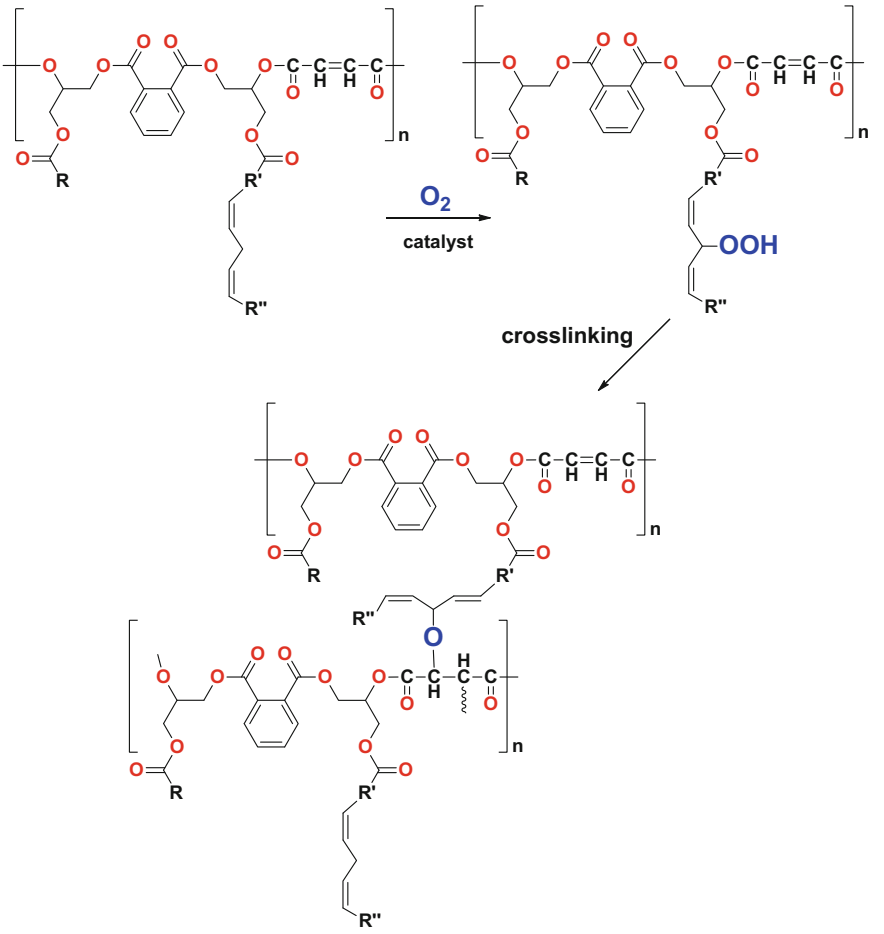

Scheme 5.11 Participation of maleate in the cross-linking of alkyd resins (adapted from [27]). R, R′, and R″ are fatty groups

were evaluated, and these results are summarized in Table 5.4. The resins were synthesized with 35 wt% of each respective anhydride: 50 % cottonseed oil, 15 wt% glycerol, and 0.015 % lead oxide. All the alkyd resins were chemically resilient to 5 % brine and 1 % acid, but were still alkali instable in 1 % KOH, as expected [29].

In most cases, the phthalic anhydride-based alkyd resin performed better than the maleic alkyd, and the maleic alkyd performed better than the succinic alkyd.

In some of the maleic anhydride-based resins, even gelation has been observed. At very high maleic anhydride concentration, Diels-Alder reactions between maleic anhydride and conjugated fatty acids in triglycerides can form polyfunctional components which promote gelation (Scheme 5.12) [32–34].

On the other hand, this gelation could involve the products of the Ordelt reaction, via the addition of hydroxyl groups to the maleate double bond as proposed by some investigators (Scheme 5.13) [35]. This may explain why only a low level of maleic

Table 5.4 Physiochemical properties of succinic anhydride-, phthalic anhydride (PA)-, and maleic anhydride (MA)-based alkyd resins (adapted from [29])

Physical property	Phthalic anhydride-based alkyd	Maleic anhydride-based alkyd	Succinic anhydride-based alkyd
Color	Brown	Light brown	Light brown
Specific gravity at 30 °C ml/g	1.025	1.011	1.002
Acid value (mg KOH/g)	5.09	8.82	9.41
Saponification value	254	358	283
% solids	73	85	91
% volatile organic	27	15	8
Adhesion	Excellent	Excellent	Good
Dry to touch Time (min)	14	17	28
Complete dry (h)	8.1	8.6	11
Scratch resistance by pencil hardness	4H	3H	2H
Gouge resistance by pencil hardness	5H	4H	3H

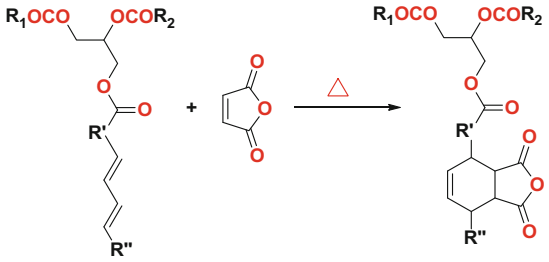

Scheme 5.12 Diels-Alder reactions between maleic anhydride and conjugated fatty acids in triglycerides (adapted from [32–34]). R_1, R_2, R', and R'' are fatty groups

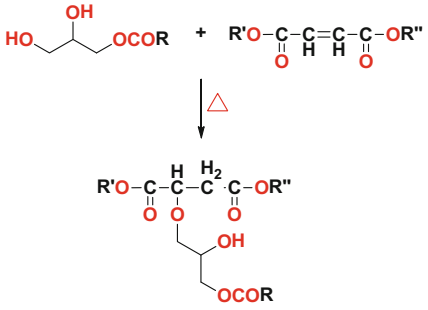

Scheme 5.13 Ordelt reactions between maleate and hydroxyl groups in monoglycerides (adapted from [35]). R is a futty group

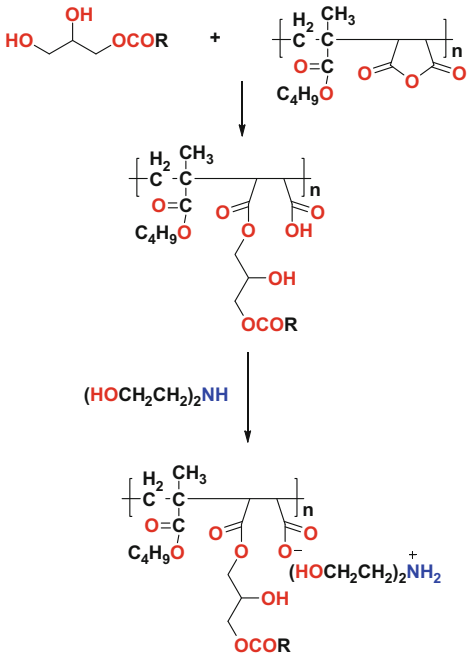

Scheme 5.14 Synthesis of water-dispersible acrylic-alkyd resins by modification of copolymer of maleic anhydride and *n*-butyl methacrylate with monoglycerides (Adapted from [36])

anhydride is typically employed in commercial alkyd resins. After curing the maleic anhydride-based alkyd resins, exhibit the shortest drying time and best water resistance.

The push for low-VOC (volatile organic compound) and environmentally friendly coatings has driven the development of water-dispersible alkyd resins. After production, the traditional alkyd resins are typically diluted in organic solvents, such as mineral spirits, to make them flowable [27]. During the drying stage, the volatile organic solvents in the coatings evaporate into the atmosphere, so they are not considered environmentally friendly. Water-dispersible alkyd resins are delivered in a cosolvent system of water and water-miscible solvents. Hydrophilic functional groups, most commonly carboxylic acids, are employed to modify alkyd resins into a water-dispersible form.

Maleic anhydride-based copolymers have been utilized to synthesize water-dispersible acrylic-alkyd resins [36]. The monoglycerides from palm oil and tung oil were modified by the copolymer of maleic anhydride and *n*-butyl methacrylate via esterification onto the polymer (Scheme 5.14). The resultant acrylic-alkyd resins were then neutralized with diethanolamine at reduced temperature. No organic solvent was employed in the process. The optimal content of acrylic copolymers was 20–35 %. The water-dispersible acrylic-alkyd resin could not be

cured well in air for 10 days. It is believed that the presence of water and diethanolamine inhibited the requisite auto-oxidation and cross-linking reactions.

The films can be dried at elevated temperature using a small amount of transition metal catalysts. The cured films have shown good flexibility, excellent adhesion, and high impact strength utilizing similar approaches; water-dispersible hyperbranched acrylic-alkyd resins have also been synthesized [37].

Waterborne coatings from maleated rubber seed oil and its alkyd resins have been prepared as well [38]. Maleated rubber seed oil or its alkyd resin was synthesized by treating the oil or the alkyd resin with various amounts of maleic anhydride, followed by neutralization with triethylamine. The final resin emulsion was made in a water/isopropanol mixture.

Compared to traditional solvent-based rubber seed oil alkyd resins that have a volatile organic compound content of about 30 %, these maleated resins have a much lower VOC content: 1.5 % and 10 % for maleated rubber seed oil or maleated alkyd resin, respectively. The final curing process was then performed by oven-baking at elevated temperature using cobalt and calcium catalysts. The maleated alkyd resins exhibited better chemical resistance than the maleated oil itself. However, the film stability in alkali solutions (0.1 M NaOH) was still low.

5.7 Olefin/Maleic Anhydride Copolymers

Ethylene, propylene, butene, and virtually most of the other unsaturated olefins have been copolymerized with maleic anhydride. These types of copolymers follow the typical charge-transfer complex intermediate through a free-radical polymerization mechanism, discussed in depth in Chap. 4, and results in an alternating copolymer structure with respect to the maleic anhydride unit.

High molecular weight grafted maleic anhydride/olefin copolymers are commercially available. For example, maleic anhydride can be grafted onto a high or low density polyethylene, or polypropylene, to impart better adhesion and thermoplastic properties to the polyolefin polymer. In general, only 4 weight percent of maleic anhydride incorporation can be achieved by free-radical grafting since the radical processes also can result in unwanted chain-scission side reactions, Scheme 5.15) [39, 40]. These maleic anhydride-grafted polyolefins provide excellent adhesion to ethylene/vinyl alcohol copolymers, nylon, metals, polyolefins, cellulose, polyesters, polycarbonates, and glass, as offered by Dow. The improved mechanical properties of these grafted copolymers can be evidenced by the increase in the Shore-D hardness as summarized in Table 5.5.

Key attributes found in these maleic anhydride-grafted polyolefins are superior adhesion to cellulose, polyethylene terephthalate (PET), metal, polycarbonate, glass, foil, and polyolefins. A high level of functionality and diversification can be realized when these polymers are employed as modifiers in other systems due to the anhydride functionality present within these copolymers. Likewise, improved

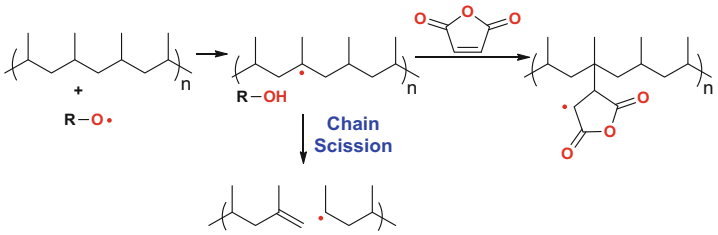

Scheme 5.15 Free radical addition of maleic anhydride onto polypropylene or any other unsaturated olefin can result in chain-scission side reactions (adapted from [39, 40])

Table 5.5 Properties of polyethylene-maleic anhydride graft copolymers

Polyethylene-grafted maleic anhydride	Density g/cm of base resin	Melt index	Durometer hardness Shore-A vs. Shore-D @ 1 s
Maleic anhydride graft (very high)	0.953 (high-density polyethylene)	12.0	97 (64)
Maleic anhydride graft (very high)	0.962 (high-density polyethylene)	2.0	96 (67)
Maleic anhydride graft (medium)	0.8985 (very low-density polyethylene)	3.3	96 (36)
Maleic anhydride graft (high)	0.8985 (very low-density polyethylene)	2.0	96 (35)
Maleic anhydride graft (high)	0.8985 (very low-density polyethylene)	1.25	77 (22)
Maleic anhydride graft (low)	0.920 (low-density polyethylene)	3.0	95 (49)

temperature stability/good heat resistance enables these polymers to maintain strong performance through extreme changes in temperature.

Maleic anhydride and its isostructural analog, fumaric acid, and citraconic anhydrides are hydrophilic monomers. When unsaturated dicarboxylic acids and their anhydrides are grafted onto polymers, they convey a denser distribution of carbonyl or free carboxylic acid groups. These reactive groups can further serve as sites for macromolecular reactions on the copolymers or grafted polymers, especially for compatibilization of immiscible polymer blends. Additionally, they have been employed in reactive blends with better performance, including better mechanical properties, higher engineering performance, and controlled morphology [41].

Such maleic-grafted polyethylene copolymers have found utility as adhesion promoters, packaging films and coatings, injected molded parts, improved polymer compatibilizer and fillers, increased impact modulators, and protective metal coatings in powder coatings and composite pipe applications.

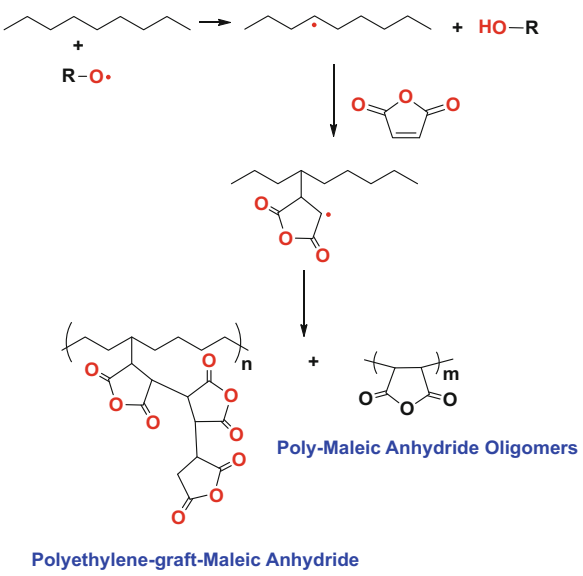

Scheme 5.16 Free radical addition of maleic anhydride onto polyethylene (adapted from [42])

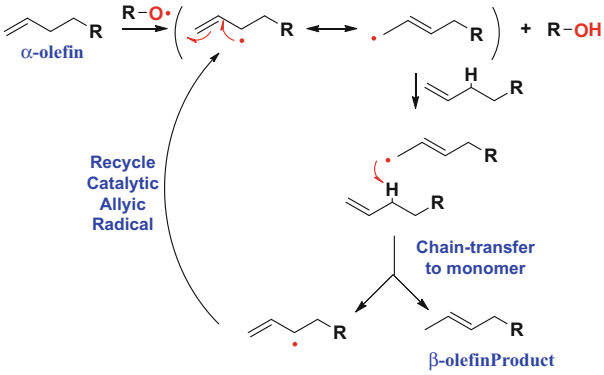

Scheme 5.17 Catalytic free radical isomerization of an α-olefin into a β-olefin

The structure of the grafting points of maleic anhydride onto polyethylene indicates that maleic anhydride forms oligomers, in addition to short-chain branching of poly-maleic anhydride onto the polyethylene backbone, as depicted in Scheme 5.16. Therefore, a blend of unreacted polyethylene, poly-maleic anhydride oligomers, and the desired polyethylene-grafted maleic anhydride is formed under the free radical conditions used [42].

In contrast to ethylene and/or propylene polymers that typically graft maleic anhydride onto the higher-molecular-weight polyolefin, longer-chain alpha-olefin monomers such as 1-butene, 1-octene, and 1-octadecene generate low-molecular-weight oligomers due to their steric bulk and catalytic isomerization from a reactive alpha-olefin to the more stable beta-olefin (Scheme 5.17). Hence, lower-molecular-

weight oligomers tend to be produced from these longer-chain olefin monomers under free radical conditions.

Maleic anhydride and longer-chain alpha-olefins are generally copolymerized to produce higher-molecular-weight alternating copolymers instead, ranging from 20 to 50 kDa [42]. Typical physical properties of the copolymer are as follows: T_g range 115–119 °C., acid no. 337, anhydride content 24.4 % by weight, acid content 2.8 % by weight, density 0.973, and inherent viscosity (based on 5.0 g/dl in methyl isobutyl ketone at 77°F) 0.144.

Interestingly, octadecene-*alt*-maleic anhydride copolymers have found utility as oil additives in the automotive industry. These include multifunctional lube oil additives (viscosity index improvers and detergent/dispersant additives) as reported by Abd-El-Azim and coworkers [43]. This octadecene-maleic anhydride copolymer was further esterified with various alcohols (dodecyl, hexadecyl, octadecyl, and docosanol) to create four different types of esters that were then amidated with three alkylamines (dodecyl, hexadecyl, and octadecyl) to form ester/amide copolymer additives.

The efficacies of the prepared esters, and the ester/amide composites, were investigated as detergents, dispersants, and viscosity index improvers. A viscosity index improver is a compound that, when added in small quantities, improves the rheological properties such as flow characteristics, but does not affect other important attributes such as chemical and thermal stability.

It was found that the efficacy of all the ester and ester/amide polymers as viscosity index improvers increases with increasing concentration of the modified copolymers, along with growing alkyl chain length of the ester/amide pair. Likewise, all the poly-octadecene-maleic esters and amides also showed excellent dispersion power [43, 44].

These properties can be rationalized by the presence of more hydrophobic characters due to the presence of the long hydrocarbon side chain that overshadows an otherwise highly polar copolymer. This property makes poly-octadecene-*alt*-maleic anhydride copolymers and their derivatives effective in the ensuing applications:

- Lube oil additives
- Adhesives
- Chelants and surfactants
- Corrosion preventatives
- Dispersing agents
- Epoxy curing agents
- Imparting lightfastness to basic dyestuffs
- Release agents and coatings
- Thickening agents
- Water and paper treating chemicals and coatings
- Waterproofer for personal care products

Reactions identical to that of the polystyrene-maleic copolymers can also be obtained with poly-octadecene-*alt*-maleic anhydride copolymers. Reactions with

amines to form the ammonium salts of the amic acid of poly-octadecene-maleic anhydride copolymer can be prepared from ammonium hydroxide to a solution of poly-octadecene-maleic anhydride copolymer in THF [44]. Similarly, substituted amides can be obtained using alkylamines.

Imides may be synthesized by heating the amic acid to 130 °C or treatment with acetic anhydride. Under anhydrous conditions, amines and ammonia, particularly in hydrocarbon solvents or oils, can result in intractable gelation and should be avoided. But this finding is suggestive that poly-octadecene-maleic anhydride copolymer could also be employed as a thickening agent [44].

Half-ester derivatives of poly-octadecene-maleic anhydride copolymer can be formed with an appropriate alcohol to a solution of poly-octadecene-maleic anhydride copolymer in acetone or methyl isobutyl ketone using an acid catalyst. Suitable catalysts include phosphoric acid, sulfuric acid, methanesulfonic acid, and p-toluenesulfonic acid. To prepare the diester, an excess of alcohol can be added with meticulous removal of water as it is formed [42, 43].

Poly-octadecene-maleic anhydride copolymers can also participate in cross-linking reactions. In fact, the solubility properties and its anhydride functionality make this copolymer an ideal cross-linking agent for thermosetting resins composed of epoxy and/or hydroxy functionality [44]. In particular, poly-octadecene-maleic anhydride copolymer can be an effective curing agent for epoxy resins. Cross-linking may also be realized by heating poly-octadecene-maleic anhydride copolymer with metal oxides and hydroxides such as calcium oxide or calcium hydroxide. Poly-octadecene-maleic anhydride copolymer can also cross-link polyols, such as polyvinyl alcohol, to form a cross-linked polyester material that can be molded at temperatures above 80 °C.

Aqueous solutions of poly-octadecene-*alt*-maleic anhydride copolymer form free acids that are compatible with modest levels of monovalent cations. However, precipitation does occur with polyvalent cations.

Poly-octadecene-*alt*-maleic anhydride copolymer is soluble in an assortment of organic solvents, including benzene, acetone, methyl isobutyl ketone, ethyl acetate, chloroform, carbon tetrachloride, and ligroin. In contrast, poly-octadecene-*alt*-maleic anhydride is somewhat insoluble with alcohols such as propanol and ethanol but will slowly dissolve as the anhydride esterifies [44].

Poly-octadecene-maleic anhydride copolymers are good clear film formers. Typically, these anhydride-containing films use common plasticizers, such as phthalate esters. The resultant films cast from an acetone solution containing 20 wt% dimethyl phthalate are glossy, smooth, and continuous [44].

5.8 Acrylic/Maleic Anhydride Copolymers

Copolymers of maleic acid and acrylic acid can be produced by polymerizing these monomers in water in the presence of a radical initiator at 70–100 °C (Scheme 5.18). Peracid salts are particularly useful for initiation and include potassium and sodium salts of persulfate, percarbonates, perborates, and perphosphates [45].

These catalysts or free radical initiators may be utilized alone to initiate the polymerization process or can be combined with a reducing agent to form a redox catalyst system, which results in faster reactions at lower temperatures. The reducing agents may be iron compounds such as the ferrous salts from sulfates, acetates, or phosphates to name a few.

Table 5.6 summarizes some of the physical characteristics as one varies the concentration of the maleic comonomer and the reaction temperature at which polymerization occurs [45]. As expected, poly-acrylic acid exhibits a large reactivity coefficient toward free radical polymerization, while maleic acid is very slow to react under the same conditions [45]. Hence, as the maleic acid content in the copolymer decreases, the molecular weight and viscosity rise, 13–30 wt% @ 96 °C.

In all cases, varying the maleic content from 13 to 36 wt% does not alter the flexibility of the air-dried films. Therefore, maleic concentrations ranging from 10 to 40 %, producing molecular weights with resultant Brookfield viscosities spanning 562–43,000, do not affect this flexibility either (even though it has been thoroughly documented that corresponding poly-acrylic acid films are brittle). Consequently, addition of ≈ 10 wt% and above of maleic acid functionality is more responsible for the flexibility than its molecular weight and overall acidity (Table 5.6) [45].

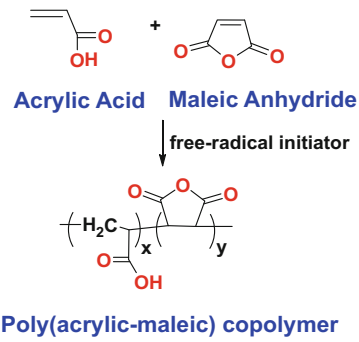

Scheme 5.18 Acrylic acid-*co*-maleic anhydride copolymer

Table 5.6 Polymerization characteristics of poly-acrylic-maleic copolymer (adapted from Reference [45])

Wt% maleic	Brookfield viscosity cPoise @ 25 °C	Acid number mg KOH/g sample	Flexible film
13 % @ 96 °C	900	804	Yes
25 % @ 96 °C	625	827	Yes
30 %@ 96 °C	562	835	Yes
30 % @ 72 °C	30,000	835	Yes
36 % @ 70 °C	43,000	847	Yes
Poly-acrylic acid	40,000	779	No

The copolymers produced in this manner are water soluble, clear, flexible, and useful as surface coatings. The copolymers are particularly useful as textile and paper sizing compositions for fibers and yarns such as cotton, nylon, or Dacron.

Acrylic acid/maleic anhydride copolymers have also been fashioned to impart select benefits in industrial, household, and institutional cleaning formulations too. The average molecular weight and its comonomer ratio have also been optimized to deliver optimum performance in laundry and dishwashing applications.

Additionally, acrylic acid/maleic anhydride copolymers are useful additives as an antifouling agents and corrosion inhibitors for boiler systems due to their chelating ability to alkali and transition metals. In particular, maleic acid contains a *syn*-diacid that, when neutralized, can efficiently chelate monovalent, divalent, and trivalent cations by its geometric positioning of the two carboxylate groups (Fig. 5.2). This removes corrosive or water-insoluble cations from the recirculating water and prevents fouling due to precipitation of alkali metal salts, such as calcium and barium, within the heating system that otherwise reduces the efficiency of heat transfer within the heating system as a whole [45].

This calcium-binding capability is also employed in the laundry detergent market. For instance, the use of sodium carbonate continues to increase in the powdered laundry segment as a phosphate replacement and a means to create low-cost detergents. Their use poses a significant problem in many laundry applications as the result of calcium ions present in certain geographical areas (water hardness) causes the in situ formation of calcium carbonate that deposits onto the clothes and makes them appear gray and rough (Fig. 5.3a).

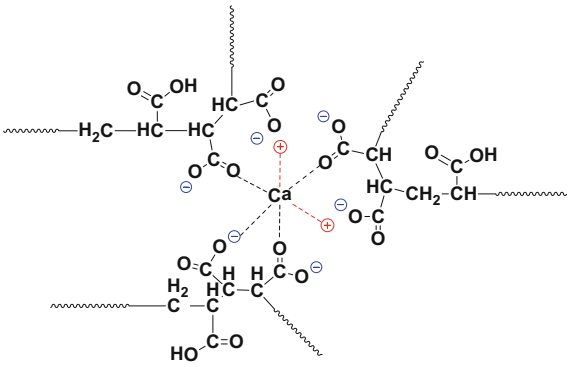

Fig. 5.2 Chelation of divalent calcium by poly-acrylic-maleic salt (adapted from [45])

Fig. 5.3 Before and after washing with a sodium carbonate-containing laundry detergent using water with high calcium content

Calcium carbonate is a water-insoluble mineral that deposits onto fabric causing both graying of fabrics and an abrasive texture, as evidenced by Fig. 5.3b. However, the chelating ability exhibited by poly-acrylic-maleic copolymers is employed to prevent this deposition of calcium carbonate from the laundry detergent onto clothes during the wash cycle so that clothes appear brighter and softer.

Table 5.7 summarizes the acidity and complexation strength of poly-acrylic acid/maleic acid copolymers in varying ionic strength media, as determined by Bretti and coworkers by potentiometric titrations [46]. As expected, the higher maleic-containing (50 mol%) copolymer is more acidic than the 33 mol% maleic copolymer due to the diacid functionality.

Addition of salt to increase the ionic strength of the medium results in less dissociation of each copolymer. Furthermore, the 50 mol% maleic copolymer is six times stronger at binding with sodium than the 33 mol% copolymer and seven times stronger at complexing with calcium, again probably due to the stronger diacid functionality. However, the lower 66 % acrylic/33 % maleic copolymer is ten times stronger at binding with magnesium than the 50/50 acrylic/maleic copolymer.

The coordination geometry of the magnesium cation toward the acrylic acid functionality is favored over that of the acid strength of the maleic functionality. This finding highlights how the monomer functionality alone does not completely describe the behavior of a polymer, but its geometric/sequence distribution needs to

Table 5.7 Acidity and complexation strength of poly-acrylic acid/maleic acid copolymers (adapted from [46])

Copolymer sample	Poly(50 %-acrylic-50 %-maleic acid)	Poly(66 %-acrylic-33 %-maleic acid)
Mean pK_a value	5.40	5.54
pK_a value @ 0.05 N NaCl	5.08	5.25
pK_a value @ 0.10 N NaCl	4.93	5.09
pK_a value @ 0.25 N NaCl	4.73	ND
pK_a value @ 0.50 N NaCl	4.64	4.82
pK_a value @ 1.00 N NaCl	4.50	4.65
pK_a value @ 0.10 N Et_4N^+I	5.17	5.44
pK_a value @ 0.25 N Et_4N^+I	5.11	5.33
pK_a value @ 0.50 N Et_4N^+I	5.04	5.29
K_{form} for Na^{1+} -complex M/L	0.018	0.003
K_{form} for Ca^{2+} -complex @ 0.10N NaCl	0.022	0.003
K_{form} for Mg^{2+} -complex @ 0.10N NaCl	0.003	0.030

Table 5.8 Typical physical properties of acrylic acid/maleic acid copolymers as their completely neutralized sodium salts

Appearance	Clear to slightly yellow solution
Solvent	Water
Total solids	40 %
Average M. Wt.	70,000
Specific gravity (ml/g)	1.30
pH as is	7.2
Brookfield viscosity (mPa/s)	1600
Residuals	<10 ppm for each monomer

be considered with respect to the coordination geometry of the alkali metal salt as well.

Some of the typical physical properties that acrylic acid/maleic acid copolymers exhibit when completely neutralized by sodium hydroxide are summarized in Table 5.8. The aqueous product appears clear to slightly yellow with a moderate molecular weight and a moderate Brookfield viscosity, but contains very low levels of acrylic and maleic monomers, less than 10 ppm each.

Based on these properties, a neutralized copolymer of acrylic acid/maleic anhydride with a molecular weight around 70,000 was optimized for the following applications:

- Anti-precipitation: This copolymer increases the solubility of calcium and magnesium salts (carbonates, sulfates) to prevent precipitation in the wash

water that will otherwise deposit onto fabrics and give rise to graying and stiffness of the apparel.
- Suspending properties: This copolymer suspends insoluble or partly insoluble builders (such as layered silicate or zeolite) homogeneously in the wash water to prevent them from settling on fabrics.
- Dispersing properties: This copolymer is an outstanding dispersant for protein stains that have been removed from fabrics and keeps them suspended in the wash water to inhibit redeposition back onto the fabric.
- Processing aids: Produces coated/agglomerated detergent particles that are non-dusty.

The benefits of this optimized copolymer include reduced phosphate levels or its elimination in laundry, industrial and institutional formulations, and automatic dishwashing detergents, to manage the development of insoluble scale (encrustation), while maintaining fabric softness and whiteness.

5.9 *N*-Vinyl Amide/Maleic Anhydride Copolymers

Up to this point, we have discussed many alternating copolymer compositions of maleic anhydride with an electron-donating comonomer. This is due to the formation of a charge-transfer complex that activates both comonomers to react as a single entity in free radical polymerizations, such as vinyl ether/maleic anhydride copolymers. *N*-vinyl amide or lactam monomers can also participate in a charge-transfer complex to activate copolymerization so that an alternating copolymer is formed. Examples include *N*-vinyl pyrrolidone-maleic anhydride (as depicted in Scheme 5.19), vinyl caprolactam, *N*-methyl *N*-vinyl acetamide, and vinyl piperidone.

This feature arises because the pyrrolidone ring exhibits a large dipole moment due to the cyclic lactam functionality of 4.1 Debye, whereas most linear amides are 3.6 Debye [47]. Therefore, resonance structures for *N*-vinyl-2-pyrrolidone can be constructed such that a partial positive charge is located on the nitrogen atom and a partial negative charge is on the carbonyl-oxygen atom (Scheme 5.20a-(I)). Since the *N*-vinyl group is conjugated with the lactam amide, an electron-pushing

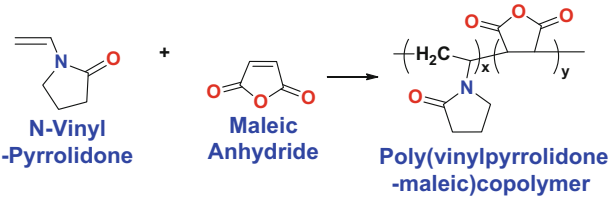

Scheme 5.19 Poly (*N*-Vinyl-2-pyrrolidone-*co*-maleic anhydride) copolymer

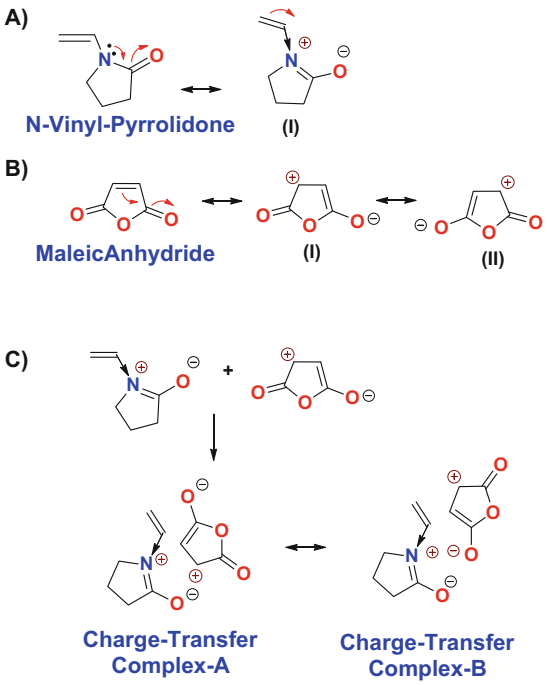

Scheme 5.20 Resonance-stabilized structures leading to the formation of a vinyl pyrrolidone-maleic anhydride charge-transfer complex (adapted from [48, 49])

inductive effect leading to further stabilization of the pseudo-cationic nitrogen atom can be achieved by the vinyl group (Scheme 5.20a-(I)).

Maleic anhydride exhibits an electron-deficient double bond and an electron-rich anhydride group, resulting in a dipole moment of 3.95 Debye [47], whereas linear anhydrides are approximately 2.8 Debye, as displayed in Scheme 5.20b. When combining these two monomers together, a charge-transfer complex is formed that activates both monomers toward free radical polymerization as illustrated in Scheme 5.20c.

The complexes shown are derived from a simple electronic rearrangement of the maleic anhydride unit itself that is extremely rapid. The charge-transfer complex formed in situ is probably a hybrid of the two shown for maleic anhydride (Scheme 5.20b-I and II) and the two shown for vinyl pyrrolidone (Scheme 5.20a). These complexes arise both geometrically and electronically so that both monomers are oriented in the right spatial configuration and that both monomers are electronically stabilized by each other's dipoles thereby activating both monomers toward alternating free radical polymerization.

Despite the ambiguity that exists in the literature regarding the actual structure of the charge-transfer complex between vinyl pyrrolidone and maleic anhydride [48, 49], it is well documented that they form a charge-transfer complex in which

the growing macroradical has vinyl pyrrolidone as its chain end. This charge-transfer complex provides a route to alternating copolymers with equal stoichiometry for each comonomer. Block copolymers can also be constructed, where an alternating block of maleic anhydride/electron-donating comonomer are easily formed, followed by a homopolymer block of free radical-polymerized electron-donating comonomer as well.

Typically, the slower-reacting monomer, in this case, maleic anhydride, will be charged up-front into the reactor, and then polymerization is initiated and the faster-reacting monomer is fed over time to remove all the residual maleic anhydride from the reactor. In this way, one can control the exothermic heat of polymerization by the feed rate of the faster-reacting comonomer to prevent a runaway polymerization. Alternatively, one can also feed maleic anhydride at a much faster rate than the other comonomer to achieve the same result when higher maleic anhydride concentrations approaching 30–40 mol% are employed.

One salient feature needs to be recognized here, particularly when using slower-reacting monomers such as *N*-vinyl-pyrrolidone (VP) or *N*-vinyl-caprolactam in free radical polymerizations. In particular, the reactivity of the vinyl pyrrolidone-maleic anhydride charge-transfer complex reacts at least an order of magnitude faster than vinyl pyrrolidone itself. Therefore, one cannot expect to homogenously distribute the maleic functionality across the polymer backbone by just simple dilution with vinyl pyrrolidone monomer.

Instead, Georiev, Konstantinov, and Kabaivanov demonstrated that regardless of the VP concentration employed in a batch reaction where the VP concentration was employed in great excess, the initial kinetics of the reaction were such that the charge-transfer complex formed by vinyl pyrrolidone-maleic anhydride reacted at least ten times faster in the free radical polymerization at the onset of the polymerization until all the charge-transfer vinyl pyrrolidone-maleic anhydride intermediate was consumed. After total consumption of the charge-transfer complex, then vinyl pyrrolidone homopolymerization ensued [49].

The copolymer sequence distribution along the polymeric backbone can generate alternating comonomer sequences, gradient comonomer sequences or blocks, or random comonomer sequences depending on how the monomers are fed.

The resultant molecular weight of *N*-vinyl-pyrrolidone/maleic anhydride copolymers produced in dioxane with AIBN initiator at 65 °C is affected by the comonomer composition. In particular, as the maleic anhydride composition rises within the *N*-vinyl-pyrrolidone/maleic anhydride copolymers, the rate of polymerization slows from 1.5 to 19 h and the molar mass drops (Table 5.9). This arises because the slower-reacting maleic comonomer decreases the propagation rate for polymerization as the maleic concentration increases thereby increasing both the polymerization time and increasing the probability that termination side reactions will ensue [50, 51]. This results in an increased polydispersity as well, varying from 1.7 at 15 wt. % Maleic anhydride incorporation up to 2.9 when the Maleic content of 75 weight % was obtained (Table 5.9).

Table 5.9 Molecular weight distributions for *N*-vinylpyrrolidone/maleic anhydride copolymers (adapted from [50])

% *N*-vinylpyrrolidone within the copolymer	% maleic anhydride within the copolymer	Weight-average molecular weight (kDa)	Number-average molecular weight (kDa)	PDI[a]	Time[b] (h)
85	15	122	73	1.7	1.5
76	24	134	74	1.8	1
70	30	129	67	1.9	3
65	35	113	51	2.2	4
50	50	90	34	2.6	3
25	75	48	18	2.9	19

[a]Polydispersity index
[b]Polymerization time

Some of the physical properties exhibited by these types of polymers have been exploited as polymeric chelants. For instance, many of these N-vinyl amide/maleic anhydride copolymers have found utility as anticorrosion additives for heating/cooling systems. Corrosion may occur resulting in deposition of the corrosion products on surfaces within the heating/cooling system reducing its heat-transfer efficiency. Additionally, deposits may form as a result of crystallization or precipitation of salts from solutions employed in these systems.

These crystallized or precipitated salts are referred to as "scale," and the complexation/precipitation process is referred to as "scale formation." Many factors affect the rate and quantity of scale formation. Some of these factors are as follows: temperature, rate of heat transfer, pH of the water, and the character and amount of dissolved solids in the water.

Any aqueous system containing calcium or magnesium cations or any other positive hardness ions in the presence of phosphate, carbonate, sulfate, or any other suitable anions can experience formation and deposition of scale. Historically, circulating water systems were operated under acidic conditions because of the increased solubility of scale forming salts under acidic pH.

However, in the last few decades, the operating conditions for most cooling water systems are now commonly operated at relatively high pH. This conversion to higher pH in water systems has greatly increased the possibility scale formation. Calcium orthophosphate, calcium sulfate, or carbonate scale is particularly problematic and has proven to be very difficult to inhibit. However, *N*-vinyl amide/maleic acid copolymers have proven their utility in this application [52, 53].

Table 5.10 Calcium carbonate/phosphate scale inhibition by *N*-vinyl amide/maleic anhydride copolymers (adapted from [52, 53])

Maleic anhydride alternating comonomer	% scale inhibition @ 20 ppm polymer	@ 30 ppm polymer	@ 40 ppm polymer	@ 50 ppm polymer	@ 75 ppm polymer	@ 100 ppm polymer
N-Methyl vinyl acetamide	13	85	98+	98+	98+	98+
Vinyl pyrrolidone	9	26	45	65	93	94
Vinyl piperidone	18	44	84	96	98+	98+
Vinyl caprolactam	21	53	94	98+	98+	98+
Vinyl pyrrolidone/ caprolactam	17	42	90	93	95	95

N-Vinyl amide/maleic acid copolymers act as polymeric chelating agents in which the maleic functionality complexes the free calcium in solution, while the *N*-vinyl amide imparts water solubility and prevents coprecipitation out of solution. The calcium scale inhibition by these types of copolymers is summarized in Table 5.10 and demonstrates on a weight basis that at 100 ppm dose levels, all of the copolymers are very good scale inhibitors. Conversely, the *N*-vinyl-pyrrolidone comonomer is the least efficient in calcium complexation when compared to other vinyl amide-maleic anhydride copolymers.

5.10 Introduction to Styrene-Maleic Anhydride Copolymers and Their Physical Properties

Since the invention of styrene-maleic anhydride copolymers in the early 1930s by IG Farbenindustrie Ag, German Application Serial No. 545,146, followed by US Patent US 2,047,398 granted in 1936 [54], styrene-maleic anhydride (SMA) resins have created a whole manufacturing industry for their use in countless applications. Almost all of the major chemical manufacturers have patented these resin types that include Dow, DuPont, Monsanto, BASF, Hoechst, Lubrizol, and Georgia-Pacific to name a few, but surprisingly, most of them do not actually produce them anymore [55].

Some styrene-maleic anhydride polymers are formed by a charge-transfer complex that activates the comonomers to form an almost perfectly alternating copolymer (ABABAB) when using free radical polymerization techniques (Fig. 5.4). Alternatively, styrene can be polymerized by free radical polymerization itself so polymers containing much lower levels of maleic anhydride can still be produced.

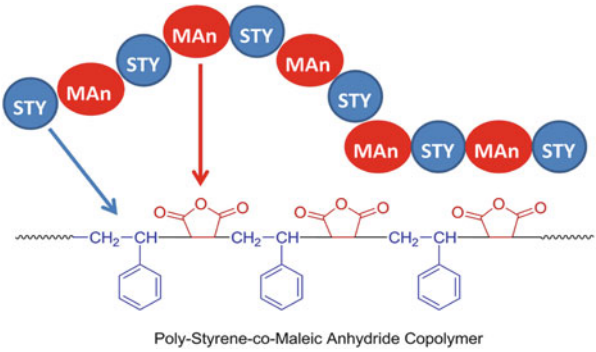

Fig. 5.4 Chemical structure of styrene-maleic anhydride copolymer

Table 5.11 Physical properties of styrene-*co*-maleic anhydride

Property	Value	Property	Value
Acidity	9.1 meq./g	Acid number	510 mg KOH/g
Density (73°F)	1.05 to 1.17 g/cm [3]	Chemical resistance	Good
Apparent density	0.60 g/cm [3]	Clarity	High
Melt mass-flow rate (MFR) (240 °C/ 10.0 kg)	20–22g/10 min	Copolymer processability	Good
T_g	264–320°F	Impact resistance	Good
Vicat softening temperature	230–320°F	Odor	Low to none
Heat resistance	High	Thermal stability	Good
Adhesion	Good	Paintable	Yes
Amorphous	Yes	Copolymer processability	Good
Dimensional stability	Good	Stiffness	High
Stress-crack resistance	High	Filled strength	High
Tensile strength	High	Foamable	Yes

However, poly-maleic anhydride does not readily polymerize by free radical processes, and therefore only low-molecular-weight oligomers are obtained.

The main characteristics of a styrene-maleic anhydride copolymer are its transparency, high dimensional stability, and high heat resistance, along with its reactivity of the anhydride groups for later modification or attachment of specific functionalities post-polymerization (Table 5.11). For example, the styrene-maleic anhydride copolymer can be hydrolyzed under aqueous base forming ammonium or inorganic salts to create clear water-based solutions or can be partially hydrolyzed to form dispersions (Scheme 5.21). They can also be reacted with alcohols to form half-esters or with amines to form amic acids and/or imides. Likewise, the styrene functionality can be sulfonated to increase its hydrophilicity and make the styrene unit more water soluble (Scheme 5.21).

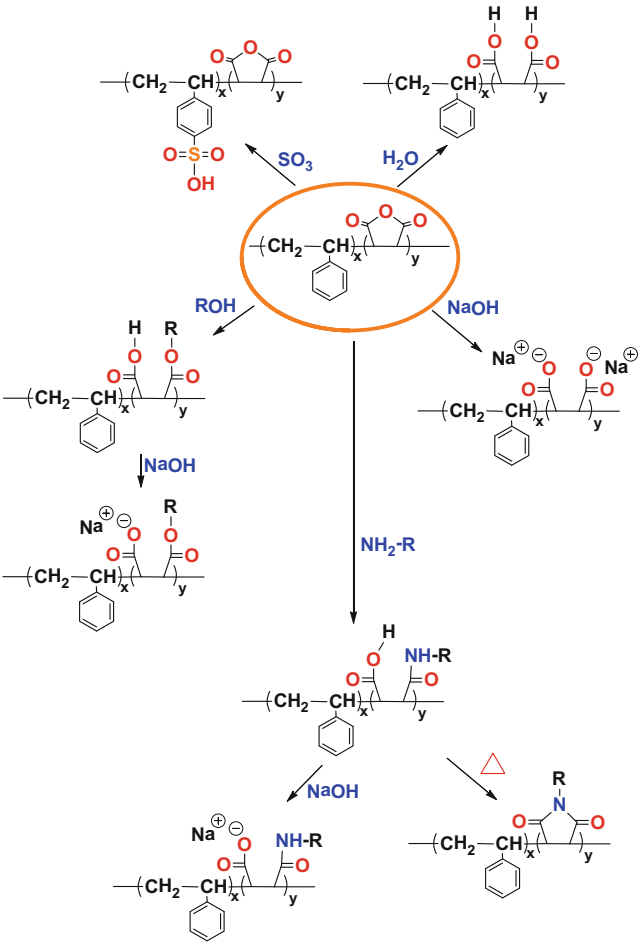

Scheme 5.21 Chemical reactions of styrene-*co*-maleic anhydride copolymer

High-molecular-weight styrene-maleic anhydride polymers are widely employed in engineering plastics, generally in the impact molded or glass fiber-filled variations for automotive parts inside the passenger compartment. Alternatively, styrene-maleic anhydride is employed because of its transparency in combination with other transparent materials such as polymethyl methacrylate (PMMA) or because of its thermal properties to heat-boost other polymeric materials such as polyvinylchloride (PVC) or acrylonitrile/butadiene/styrene (ABS) copolymers.

Additionally, many multifunctional variants of styrene-maleic anhydride copolymers are commercially available from Cray Valley and other manufactures around the world today, and some of their typical properties are summarized in Table 5.11.

These resins are employed in diverse applications such as in adhesives, binders, and coatings, in paper sizing or powder coating, in pigment dispersions or inks, in overprint varnishes, in leather tanning, in microelectronics, in carpet/textile

Table 5.12 Physical properties of styrene-*co*-maleic anhydride copolymers

Styrene: MAn Molar ratio	M_w dalton	PDI	Melt viscosity Poise @ 200 °C	Acid number mg KOH//g sample	T_g (°C)
50:50	5000	2.38	≈60,000	480	155
66:33	7500	2.78	≈6000	355	135
75:25	9500	3.15	≈3000	280	125
80:20	11,000	3.05	≈750	215	115
83:17	11,500	2.09	≈70	156	106
88:12	14,500	1.92	≈100	120	104
Polystyrene	10,000	1.05	ND	0	90
Polystyrene	10 million	1.05	ND	0	100

Table 5.13 Physical properties of styrene-*co*-maleic ester copolymers

SMA polymer	Ester type	M_w kDa	PDI	Melt viscosity Poise @ 200 °C	Acid number mg KOH/g sample	T_g (°C)
A	2-Butoxyethyl	7	2.4	≈300	185	60
B	Cyclohexyl isopropyl	7	2.4	≈10,000	270	125
C	*n*-Propyl	9	2.9	≈1000	220	110
D	C7–C9 Iso-alcohols	10.5	2.6	≈50	117	75
E	C16/C18	17	3.1	≈15	110	45

cleaners, in interior or exterior automotive parts, for food packaging, and in floor care products.

The solubility of styrene-maleic anhydride in alkaline solutions makes it appropriate for numerous applications such as in sizing for paper, in coatings, and in binders. The specific reactivity of styrene-maleic anhydride makes it a suitable agent for compatibilizing normally incompatible polymers such as acrylonitrile/butadiene/styrene copolymers or polyacrylonitrile blends. Table 5.12 summarizes the glass transition temperature of styrene-maleic anhydride copolymers that span approximately 104–155 °C, while polystyrene itself is 90–100°C from 10 kDa to 10 million daltons, respectively.

Styrene-maleic anhydride resins can be esterified with alcohols to form polyesters. The styrene-maleic anhydride ester resins generally exhibit low melt viscosities, improved solubility in many organic solvents, and polymeric surfactant properties, resulting in better compatibility with other polymeric and non-polymeric surfactants (Table 5.13).

Alcohols will react with styrene-maleic anhydride to form monoesters by ring opening of the anhydride groups. For esterification greater than 50 %, or formation of diester groups, excess alcohol is employed with scrupulous removal of water. Diols are sometimes used to cross-link the copolymer as well. Water must be removed, and a catalyst is generally needed to increase reaction rate. For example, 1,4-butanediol will react with styrene-maleic anhydride at room temperature [56–58].

Addition of alkali hydroxides will react with the anhydride or carboxylic acid functionality of styrene-maleic anhydride copolymer to form water-soluble salts. Styrene-maleic ammonium salts are also commercially available as aqueous solutions. These solutions are stable under basic conditions, but tend to exhibit lower viscosity due to charge repulsion of the individual polymer chains. To increase the solution viscosity, the styrene-to-maleic ratio can be varied such that higher styrene content results in higher viscosities when neutralized with ammonia.

Polystyrene-maleic anhydride amic acid resin can be obtained by reaction with the appropriate alkylamine at temperatures around 100 °C. These modified copolymers exhibit polymeric surfactant properties useful in forming stable, low-tarnish metallic pigment dispersions and inks [59].

Polystyrene-maleic anhydride imide resins are prepared from their corresponding amic acid parent but heated to 130 °C or higher. One can lower this ring-closing temperature by forming the mixed anhydride with acetic anhydride. Then, the reaction temperature can be lowered to 60–80 °C for imidation to proceed.

The process for manufacturing these compounds is not as simple as one may envision. In particular, alkylamines react with the anhydride polymer or with the half-ester to form amides below 100 °C. However, a small fraction of the amide population can, and does, ring-close to form its imide. Complete imidization can be accomplished at 150–180 °C for 2 or 3 h. The resultant styrene/dimethyl amino propyl maleimide copolymers usually exhibit higher T_g ranges and higher thermal stability (Table 5.14).

The styrene-maleimide polymers can be useful in adhesives, in alkali-resistant coatings, in polymer modification, in paper manufacture and surface sizing, in pigment dispersions or inks, in overprint varnishes, and in water treatment. Some other uses of styrene-maleic copolymers are summarized in Table 5.15. In fact, it can even be employed as a male contraceptive. Initially, it was conceived as a physical barrier agent when injected into the vas deferens, the tubule responsible for carrying the spermatozoa out of the body, but instead, it removes and disrupts the flagellum from the sperm resulting in loss of motility and hence sterilization. Further, studies proved that the highly acidic maleic acid unit was responsible for this effect [60, 61].

The pendant aromatic groups in polystyrene-maleic anhydride polymers participate in substitution reactions characteristic for aromatic molecules. Sulfonation occurs with sulfur trioxide (or other suitable sulfonation reagents) in an inert solvent. The resultant sodium or potassium sulfonates exhibit surface-active attributes and are useful as dispersants.

Table 5.14 Physical properties of styrene-*co*-maleimide copolymers

Styrene: MAn Molar ratio	Amine index meq/g	M_w dalton	Polydispersity	T_g (°C)
50:50	3.15	5000	2.38	85
66:33	2.50	7500	2.78	88
75:25	2.15	9500	3.15	90
80:20	1.75	11,000	3.05	90

Table 5.15 Application/physical properties of styrene-maleic copolymers

Application/market	Property	Polymer type
Overprint varnishes, ink	Heat resistance	Sty-AN (1:1, 2:1) Cyclo/alkyl esters
	Adhesion to polymer films	BGE ester Fatty esters
	Viscosity stability	Sty-AN(2:1) n-Propyl ester
Powder coatings	Matting agent	Sty-AN(2:1) Alkyl/iso-alkyl esters
Paper making Surface sizing	Water resistance	Sty-AN(2:1) *n*-Propyl-ester
Paper making—wet end Paper coatings for ink jet	Stability in cationic systems	Sty-AN (1:1, 2:1, 3:1) imidized
Waterborne ink, paint pigment Dispersion	Dispersion stability, color development, low viscosity	BGE ester Cyclo/alkyl esters
	Cationic systems	Sty-AN (1:1, 2:1, 3:1, 4:1) imidized
	Carbon black	BGE ester Cyclo/alkyl esters
	Metallics	Sty-AN (1:1) hydrolyzed
Solvent-borne ink, paint Pigment dispersion	Dispersion stability, color development, low viscosity	Iso-alkyl esters Cyclo/alkyl esters
Latex gloves Flame retardant Antioxidant dispersant	Stability of divalent ion containing fillers (calcium, magnesium)	Sty-AN (1:1) Cyclo/alkyl esters
Emulsion polymerization	Particle size control and stability, heat resistance	Sty-AN (1:1, 2:1), Cyclo/alkyl esters
Carpet treatment/ shampoos	Stain/water resistance	Sty-AN (1:1, 2:1), Cyclo/alkyl esters
Wax/floor polish	Coating leveling	*n*-Propyl ester Cyclo/alkyl esters
Printed wiring boards	Improved dielectric properties, heat resistance	Sty-AN (3:1, 4:1, 6:1, 8:1)
Wax emulsions	Hydrophobicity, particle size control and stability	Sty-AN (1:1, 2:1)
Leather tanning	Divalent cation stability	Sty-AN (1:1)
Male reproductive contraceptive	Inert acid donor to remove the flagellum of the sperm	Sty-maleic acid (1:1)

The solubility characteristics of free radical-polymerized polystyrene-maleic anhydride and its derivatives are summarized in Table 5.16. All copolymers regardless of styrene content are insoluble in aliphatic hydrocarbons. In contrast,

Table 5.16 Solubility properties of styrene-maleic copolymers

Solubility of styrene-maleic resins in common solvents at 30 °C							
V = >75 wt%, S = 15–50 wt%, PS = 1–15 wt%, I = <1 wt%							
Styrene-maleic resin	S/M (1:1) An	BGE ester	Cyclohexyl IPA esters	*n*-Propyl ester	S/M (2:1) An	C7-C9 Iso-alkyl esters	S/M (4:1) An
Aliphatic							
Cyclohexane	I	I	I	I	I	I	I
n-Hexane	I	I	I	I	I	I	I
n-Heptane	I	I	I	I	I	I	I
Aromatic							
Toluene	I	I	I	I	PS	S	PS
Xylene	I	I	I	I	PS	S	I
Alcohols							
Methanol	I	PS	PS	PS	I	PS	I
Ethanol, 190 proof	I	PS	I	I	I	PS	I
Ethanol, 200 proof	I	S	PS	PS	I	PS	I
1-Propanol	I	PS	PS	PS	I	PS	I
2-Propanol	I	PS	I	I	I	PS	I
Ketones							
Acetone	V	V	V	V	V	V	V
2-Butanone	V	V	V	V	V	V	V
4-Methyl-2-pentanone	V	V	V	V	V	V	V
Ethers							
Tetrahydrofuran	V	V	V	V	V	V	V
1,4-Dioxane	V	V	V	V	V	V	S
Miscellaneous							
Ethyl acetate	V	V	V	V	V	V	V
Propyl acetate	V	V	V	V	V	V	V
Dimethylformamide	V	V	V	V	V	V	V
Ethoxyethanol	I	S	S	S	I	S	PS
Ethylene glycol	I	I	I	I	I	I	I
Propylene glycol	I	PS	I	I	I	I	I
Propylene carbonate	S	S	S	S	S	I	S

I = insoluble, P = partially soluble, S = soluble, V = very soluble

only the high styrene-containing copolymers, such as styrene-maleic at 2:1 or higher ratios, are partially soluble in aromatic solvents.

The esters of polystyrene-maleic anhydride increase the polarity of the copolymer so that they become partially soluble in lower alcohols, but not in most glycols, while all the anhydride and ester derivatives are soluble in ketones, esters, and amides. Therefore, simple modification of the copolymer due to the anhydride functionality enables one to tailor the properties and solubility of this copolymer for its end use.

Additional modification of polystyrene-maleic anhydride copolymers with small molecules includes attachment of amino-benzoic acids to generate enrichment agents for rare earth elements such as germanium [62]. Hence, modification of the base copolymer resin via the anhydride functionality enables a vast array of different functionalities to be spliced onto the polystyrene-maleic copolymer.

5.11 Graft Copolymers of Styrene-Maleic Anhydride via Chemical Acylation Reactions

Not only can one attach small molecules onto a styrene-maleic anhydride polymer chain, but one can also attach another polymer onto it. These graft copolymers act as block copolymers with hybrid properties. For example, polystyrene-*co*-maleic anhydride is a thermoplastic-type polymer due to the presence of the maleic unit. However, it suffers from poor adhesion to low-energy substrates, due in part to its rather high T_g. Attachment of fatty alcohols to the maleic functionality somewhat improves adhesion, but attachment of a polyolefin significantly improves adhesion and can act as a compatibilizer for other hydrocarbon-rich polymers such as polyethylene, polypropylene, or butadiene/acrylonitrile polymers.

Dharmarajan and coworkers demonstrated that polymer blends of styrene-maleic anhydride copolymer, isotactic polypropylene, and two amino-functionalized polyolefins can form a homogenous dispersion [63]. Blends roughly comprising 25 % styrene-maleic anhydride copolymer exhibited a morphology that comprised a continuous polyolefin medium with a disperse phase of micron-sized particles. The amino-modified polyolefins were predicted to construct graft polymers with the styrene-maleic anhydride copolymer by an amidation process with maleic anhydride (Scheme 5.22). The rheological properties of these blends were complex but not atypical for immiscible polymer blends [63].

The accessibility of the amino-functionalized isotactic polypropylene to the polymeric anhydride functionality suffers due to steric hindrance between the two

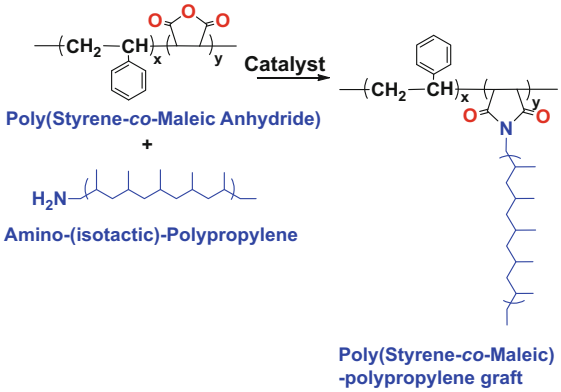

Scheme 5.22 Acylation reactions of styrene-*co*-maleic anhydride copolymer with other polymers (amino-functionalized isotactic polypropylene) (adapted from [63])

polymeric molecules so that a mixture of homopolymers and graft copolymers exists. Despite the low efficiency in coupling of the two polymers, this mixture of graft and individual polymers still exhibits hybrid properties with respect to the overall solubility, thermal stability, and adhesion properties. These properties can be rationalized in part by the development of an interpenetrating polymer network, where the polypropylene section of the graft copolymer preferentially migrates into the hydrocarbon-rich latex, while the hydrolyzed maleic units provide adhesion to metals and provide more water solubility [63, 64].

Many other grafting reactions using the maleic anhydride comonomer unit as a linkage point have been attempted. For instance, styrene-maleic anhydride copolymer or ethylene/maleic anhydride copolymer was attached onto cellulose acetate or methyl cellulose in DMF at 50 °C [63, 64]. The grafting reactions were performed employing cellulose acetate, containing 2.4 degrees of substitution (DS) corresponding to 20 mol% of free hydroxyl groups, or with methyl cellulose (MC), with 1.8 degrees of substitution (40 % free hydroxyl groups) with high-molecular-weight versions of ethylene/maleic anhydride copolymer (EMA) and styrene-maleic anhydride copolymer (Scheme 5.23) [63, 64]. The grafting linkage points between the two polymers were derived by an esterification reaction with the primary OH-group in the C6-position of cellulose reacting with the anhydride moiety of the styrene-maleic anhydride copolymer [65].

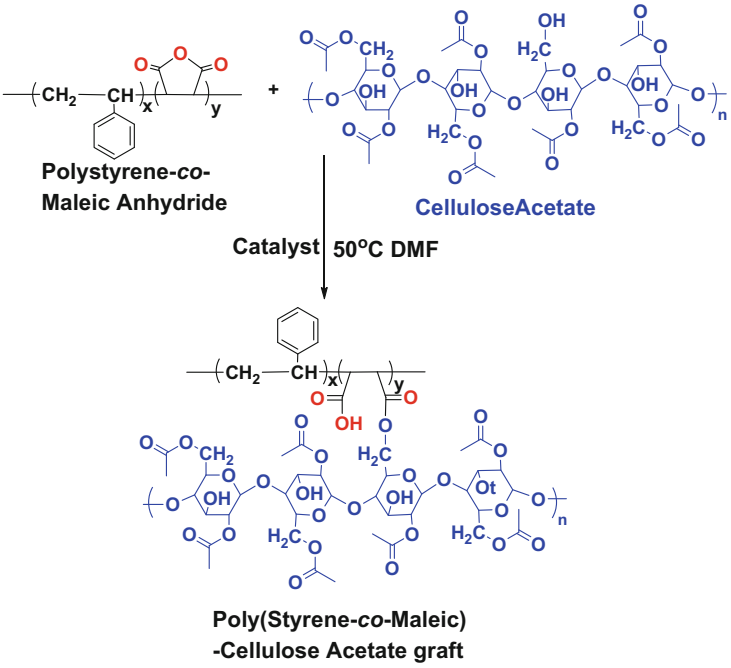

Scheme 5.23 Acylation reactions of styrene-*co*-maleic anhydride copolymer with other polymers (cellulose acetate) (adapted from [64])

Esterification catalysts such as *N*-methylimidazole (NMID) and 4-(*N*,*N*-dimethylamino)-pyridine(DMAP) were found to greatly increase the rate of esterifications. This finding was not unexpected since use of these more powerful catalysts with activities of about 400 and 17,000 times greater than pyridine, respectively, was already known [64].

It was also demonstrated that grafting does not dramatically alter the properties of each copolymer since only a few linkages are involved. Specifically, this process is a means to combine the positive attributes of each copolymer into one, with the possibility of additional synergy between the two copolymers to overcome their individual shortcomings.

Almost all the high-molecular-weight cellulose derivatives used in this study gave gels as the end product [65]. This result underscores the difficulty in controlling grafting reactions with most maleic anhydride-based copolymers. Only one sample did not undergo gelation; this was an oligomeric 1.7 KDa molecular weight styrene-maleic chain containing about six reactive anhydride units per molecule, even after 7 days of reaction at 50 °C with DMAP catalyst.

Grafting of two larger polymer molecules containing multiple reactive sites without cross-linking in a reproducible manner remains challenging and has prevented the use of this approach in industry. Alternatively, this approach is better suited to form insoluble-hybrid substrates, for example, to surface modify polyethylene terephthalate(PET) films [66]. Bigan and coworkers evaluated a coupling approach using a partially hydrolyzed polyethylene terephthalate copolymer that contained terminal hydroxyl groups to react with the anhydride functionality of a polystyrene-maleic anhydride copolymer in order to increase the hot melt properties of the polyethylene terephthalate substrate [66]. A blend of homopolymers and graft copolymers was obtained as a cross-linked mass, as previously observed by Rowland with modified celluloses [65].

Radiation-induced cross-linking such as gamma irradiation, electron beam, or plasma-induced curing is another technique to form insoluble graft copolymers. For instance, Abd-El-Rehim and coworkers grafted low-density polyethylene onto polystyrene-maleic anhydride to form a membrane capable of removing heavy metals from wastewater [67]. Their cross-linked product demonstrated a propensity for binding Fe(III) ions at room temperature, as well as Cu(II) and Cr(III) at 70 °C [67].

In contrast, monosubstituted polymer molecules that contain a single reactive site per chain are more desirable for generating soluble hybrid/grafted polymers instead. Similar findings to the amino-functionalized isotactic polypropylene/styrene-maleic anhydride graft copolymer system were obtained. In particular, Koning and coworkers melt-blended (ɣ-aminopropyl)-polystyrene (PS) with a 71 mol% styrene/29% maleic anhydride copolymer thereby providing the amino group of one polymer to react with the maleic anhydride unit of the other polymer to form imide linkages [68]. It was also noted that as the content of (ɣ-aminopropyl)-polystyrene (PS) increased in the graft copolymer, a larger average particle size was obtained for the dispersion.

This graft copolymer was an effective compatibilizer for polystyrene-maleic anhydride and poly(phenylene oxide) (PPO) blends, as well as blends containing poly(acrylonitrile-*co*-butadiene-*co*-styrene) and poly[styrene-*b*-(ethylene-*co*-butylene)-*b*-styrene] triblock copolymer [68]. The resultant blends exhibited notably improved impact strength in comparison to the control that consisted of just a physical blend of the copolymers [68].

Given the wealth of information on styrene-maleic anhydride copolymers derived from typical thermal free radical initiators available online and in book chapters, the next section will focus on recent advances in the last two decades. For example, newer techniques of "pseudo-living" free radical or controlled polymerization methods by reversible-deactivation radical polymerization techniques have arisen to generate a plethora of graft and block copolymers with unprecedented control over their architecture.

5.12 Recent Advances in the Synthesis of Styrene-Maleic Anhydride Copolymers by Controlled Free Radical Polymerization

Controlled free radical polymerization techniques such as reversible-deactivation radical polymerization methods have significantly advanced over the past 15 years so that sophisticated polymeric architectures can be constructed. These include a predetermined (co)monomer sequence for a particular section along the polymer backbone, followed by the next section or block of monomer(s), and so on. Hence, multiple blocks of different comonomers can be polymerized in sections along the polymer chain. The key to this approach is the controlled switching of a living polymerization between active and dormant states.

A living polymerization will continue until the monomer is completely consumed. Then, the polymer-catalyst chain end enters its dormant state until a fresh monomer is added. It then resumes its active polymerization and continues until the catalyst is removed from the polymer chain end. This approach is limited, however, by the type of monomer that can be employed for a given polymerization methodology, such as atom transfer, nitroxide-mediated, reversible addition-fragmentation, or ring-opening metathesis polymerization, that will be discussed in depth in Chap. 6.

Therefore, multiple approaches have been developed for constructing more complex polymers such as graft and/or block copolymers in order to combine the positive attributes of one polymer combination with another. Desirably, the hybridization of these two polymers into one chain will result in a synergy that is better than the sum of the two parts. To do this requires a functional group that will generate a free radical site by a trigger other than the typical thermal free radical initiation event.

5.12.1 *Nitroxide-Mediated Polymerizations*

One such approach to control free radical polymerization is nitroxide-mediated radical polymerization (NMP). This strategy makes use of an alkoxyamine initiator to produce polymers with narrow polydispersity index [69]. It is a category of the reversible-deactivation radical polymerization (RDRP) mechanism, in which the nitroxide functionality temporarily masks the chain end when no monomer is present. Upon addition of fresh monomer and the right reaction conditions, it reversibly detaches from the polymer chain end to enable polymerization (Scheme 5.24b).

The initiating materials for NMP are a family of compounds referred to as alkoxyamines generally based on TEMPO derivatives [72]. The utility of this

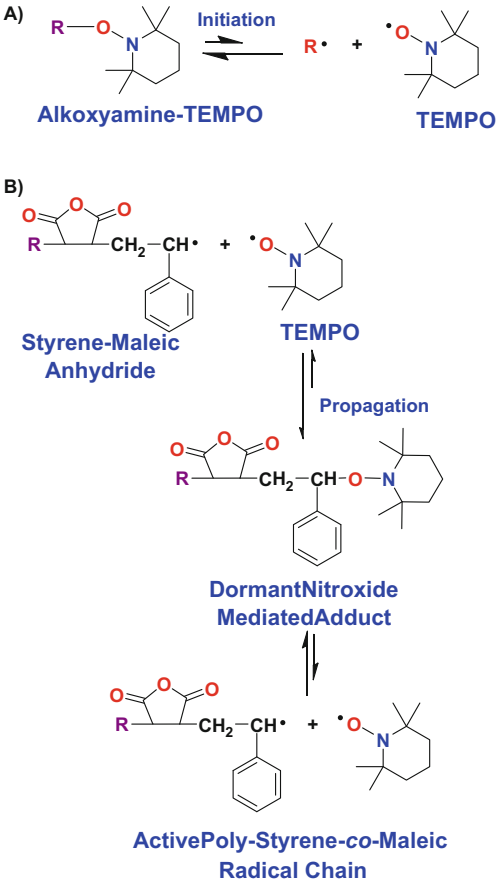

Scheme 5.24 Reversible deactivation of growing polymer radical by nitroxide (adapted from [70, 71])

functional group is that under certain conditions, homolysis of the C–O bond can occur, yielding a carbon radical which serves as an initiator for radical polymerization (Scheme 5.24a) and a stable nitroxide radical that serves to modulate the polymerization (Scheme 5.24b) [72].

The reversible-deactivation radical polymerization (RDRP) mechanism by temporarily end-capping the growing polymer chain end results in controlled molecular weight and polydispersity by SEC. But more importantly, this technique enables the construction of block copolymers that have been very difficult to synthesize by conventional free radical methods.

For the purposes of NMP, the initiator typically contains sterically hindering bulky R groups attached to the nitrogen to aid in bond dissociation, while the alkoxy-amino group undergoes homolysis to generate a stable alkyl radical that initiates polymerization. Once the alkyl radical initiates and the polymerization proceeds, the nitroxide moiety modulates the rate of polymerization by reversible attachment onto the growing chain to form a dormant adduct (Scheme 5.24b). This results in an equilibrium between dormant and active states that preferentially favors the dormant adduct [70, 71].

However, it still directs the repetitive dissociation of the nitroxide group from the growing polymer chain end whenever a monomer is present and guarantees consumption of residual monomers by active chains. Consequently, individual polymer chains dissociate and polymerize at very similar rates, thereby creating a uniform molecular weight and low polydispersity [73]. This rapid equilibrium also inhibits permanent termination, as depicted in Scheme 5.25.

The stability of the nitroxide radical is a result of its unique structure. Typically, the radical is portrayed on the oxygen atom, but another resonance structure exists where the radical is on the nitrogen atom with a double bond to its attached oxygen

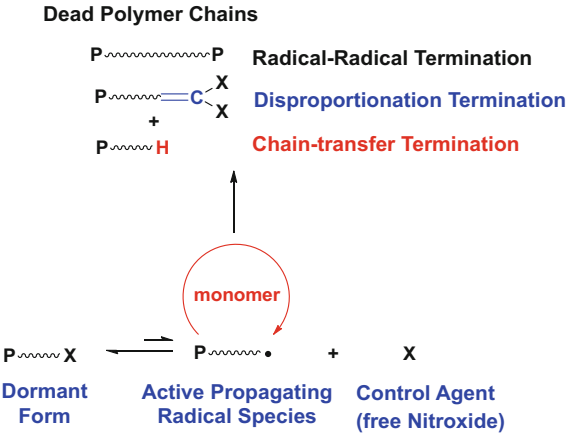

Scheme 5.25 Nitroxide-mediated radical polymerization mechanism (adapted from [73])

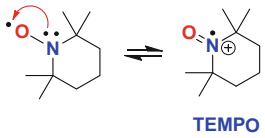

Scheme 5.26 Nitroxide-mediated radical resonance structures (adapted from [74, 75])

(Scheme 5.26). In this form, it is stabilized by the bulky electron-donating groups in the α-position [74, 75]. Electron-donating groups in the α-position help stabilize this species. Therefore, this explains in part the need for methyl groups in the α-position, as in the TEMPO molecule presented in Scheme 5.26.

The utility of this approach to generate polystyrene-maleic anhydride-grafted polybutadiene or polyisoprene copolymers, using nitroxide-mediated processes to graft polybutadiene or polyisoprene onto the Styrene-Maleic anhydride copolymer, did indeed generate the desired graft copolymer; however, the polydispersity values ranged from 2.0 at 30 % conversion versus 5.6 at higher conversion values, clearly indicating that a mixture of unreacted polyolefin, unreacted polystyrene-maleic copolymer, and desired graft copolymer was formed [62].

The nitroxide-mediated polymerization reaction did not perform well from a practical and industrial standpoint for the synthesis of this type of graft copolymer. This behavior may in part be explained by the higher temperatures used for NMP. In particular, the temperature may be as low as 90–115 °C, but are generally higher for larger conversion values. This helps control the equilibrium toward free nitroxide radicals, instead of the dormant species. Therefore, at these higher temperatures, radical backbiting, disproportionation, and other side reactions can occur to broaden the molecular weight distribution. Furthermore, the possible presence of secondary amine impurities that may be present in the nitroxide catalyst precludes its use in the personal care and pharmaceutical arenas because they can be converted to nitrosamines, which are very potent carcinogenic inducers.

In 2010, Lessard and Maric demonstrated that a poly(styrene-*co*-maleic anhydride-block)-polystyrene-block copolymer could be constructed with a polydispersity index of 1.6 in a one-step process utilizing nitroxide-mediated polymerization reaction (Scheme 5.27) [76]. While their polydispersities were improved over those obtained from polyolefin-grafted polystyrene-*co*-maleic anhydride that could be as high as 5.6 [77], they also observed a broadening in the molecular weight distribution/polydispersity from processes such as cross-linking and beta-scission side reactions. The conversions were also typically poor, ranging from 30 to 50 %, and only oligomeric species were obtained in the 6–35 kDa range [76].

Garcia-Valdez and coworkers produced a hybrid polymer comprising chitosan with polystyrene-*co*-maleic anhydride in supercritical carbon dioxide [78]. The goal was to produce a solvent-free biodegradable graft copolymer based on a

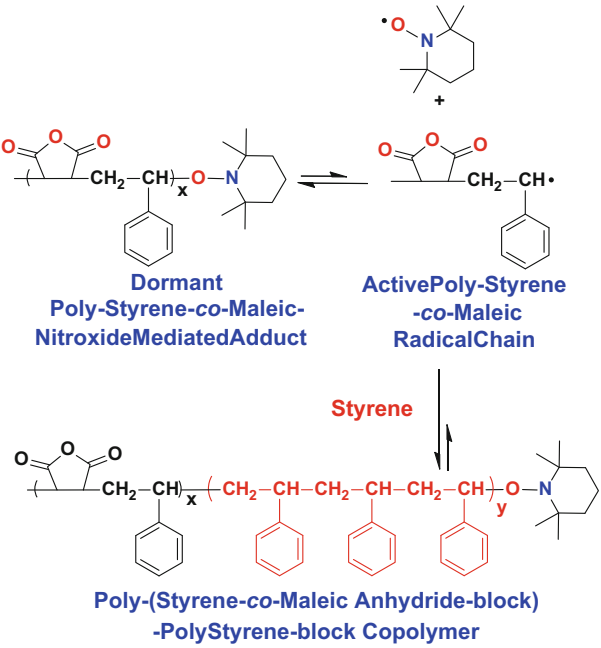

Scheme 5.27 Poly(styrene-*co*-maleic anhydride-block)-polystyrene-block copolymer by nitroxide-mediated radical polymerization (adapted from [76])

chitosan frame with the aim to specifically control the release of acidic drugs. The styrene-maleic copolymer attached to the chitosan scaffold still contains reactive anhydride functionality that can further react with beneficial drugs for controlled release within the human body [79–81].

The graft copolymerization of styrene-maleic anhydride onto chitosan was carried out employing NMP in supercritical CO_2 as the reaction solvent. A preformed macroalkoxyamine TEMPO-functionalized chitosan (chitosan-TEMPO) adduct was produced. This chitosan-TEMPO adduct can act as a macro-initiator and a controller at the same time. The functionalization was performed using a synthetic route recently reported by the Salvidar-Guerra group [77].

Moreover, this strategy targets the primary hydroxyl (OH) groups on the chitosan biopolymer conserving the amino functionality required for complexation to acidic drugs [79]. The graft copolymerization in supercritical CO_2 was performed because of its benign character and provides a solvent-free product without any appreciable VOC content. The resulting material chitosan-graft-poly-styrene-*co*-maleic-TEMPO exhibits a better thermal stability than chitosan itself (Scheme 5.28).

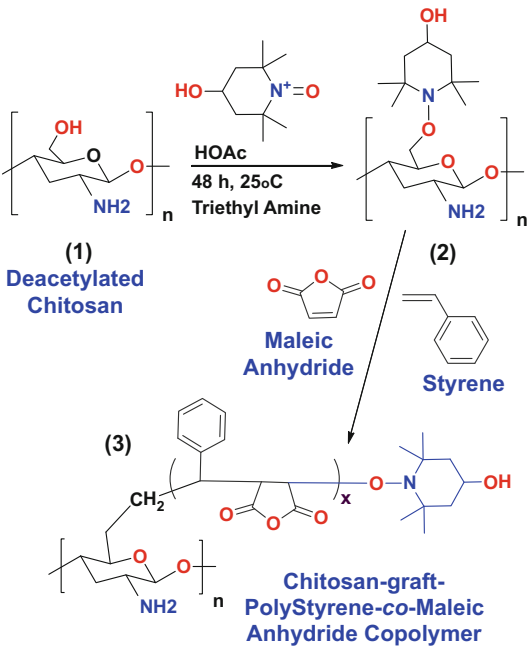

Scheme 5.28 Grafting of chitosan onto polystyrene-*co*-maleic anhydride by nitroxide-mediated polymerization (adapted from [77])

5.12.2 Atom Transfer Radical Polymerization

Atom transfer radical polymerization, known as ATRP, is another strategy to achieve molecular weight and polydispersity control in a free radical polymerization [80]. In particular, it employs transition metal-based catalysts such as Cu, Fe, Ni, Os, or Ru in the presence of an alkyl halide as an initiator (**R-X**).

This reversible process of the carbon-halide scission mediated by the metal catalyst through a one-electron transfer from metal to initiator establishes an equilibrium toward very low radical concentrations. Once the halide is attached to a polymer chain end, the same metal helps catalyze polymer-halide scission to yield an actively growing polymer chain end in the presence of monomers. The molecular weight is dictated by the number of alkyl-halide molecules introduced as these propagate between living/dormant polymer states (**R-Polymer-Halide**), thereby producing polymers with comparable molecular weights and narrow molecular weight distribution (Scheme 5.29) [80].

ATRP processes are very tolerant to different functional groups, such as amino, allylic, epoxy, hydroxyl, or vinyl groups, present in either the monomer or the initiator [82]. ATRP techniques are also useful due to the commercially available reagents and inexpensive catalysts (copper complexes) [80–84]. However, ATRP techniques tend to suffer from incomplete conversion of monomer into polymer, resulting in high residual monomer levels (typically around 5–15 %), so this process has not yet achieved commercial success.

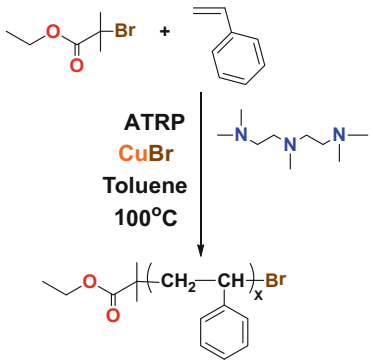

Scheme 5.29 Polystyrene block formed from atom transfer radical polymerization (ATRP) (adapted from [80])

5.12.3 Reversible Addition-Fragmentation Chain Transfer

Yet another approach to control free radical polymerization is reversible addition-fragmentation chain transfer, or RAFT, polymerization. RAFT, like NMP and ATRP, is a form of living radical polymerization employing conventional free radical processes in the presence of a suitable chain transfer (RAFT) reagent. RAFT technology can be employed with a wide range of commercial monomers by all modes of free radical polymerization (solution, emulsion, and suspension).

It employs a reversible chain transfer agent to control the molecular weight and polydispersity. RAFT polymerizations typically employ thiocarbonylthio compounds [85], such as thiocarbamates, xanthates, and dithioesters to control the polymerization by a reversible chain transfer mechanism (Scheme 5.30b).

RAFT has provided a route for the construction of a multitude of polymers with varying functionality and architectures. Synthesis of block copolymers by RAFT has garnered noteworthy attention due to the impediments with conventional methodologies. RAFT polymerization is a versatile route due to its compatibility with many functional monomers and solvents, along with its relative ease of use. This has resulted in the preparation of block copolymers with targeted molecular weight and narrow molecular weight distribution can be achieved (Scheme 5.30) [86–89].

Some disadvantages are that the specific RAFT agent is only suitable for a limited set of monomers; it requires laborious synthetic schemes and requisite purification steps [90]. RAFT agents are also unstable when stored for extended time periods, are highly colored, and are odoriferous yielding sulfur compounds. These shortcomings are unacceptable in certain products and applications such as personal care, oral care, and pharmaceutical industries.

Historically, there is no "universal" RAFT agent capable of preparing block copolymers comprised of lower activity lactam monomers such as *N*-vinylpyrrolidone, *N*-vinylcarbazole, or vinyl acetate, along with more active monomers such as (meth)acrylates or styrene. However, with the development of a new class of stimuli-responsive, "pH-switchable" RAFT agents, polymethyl methacrylate/

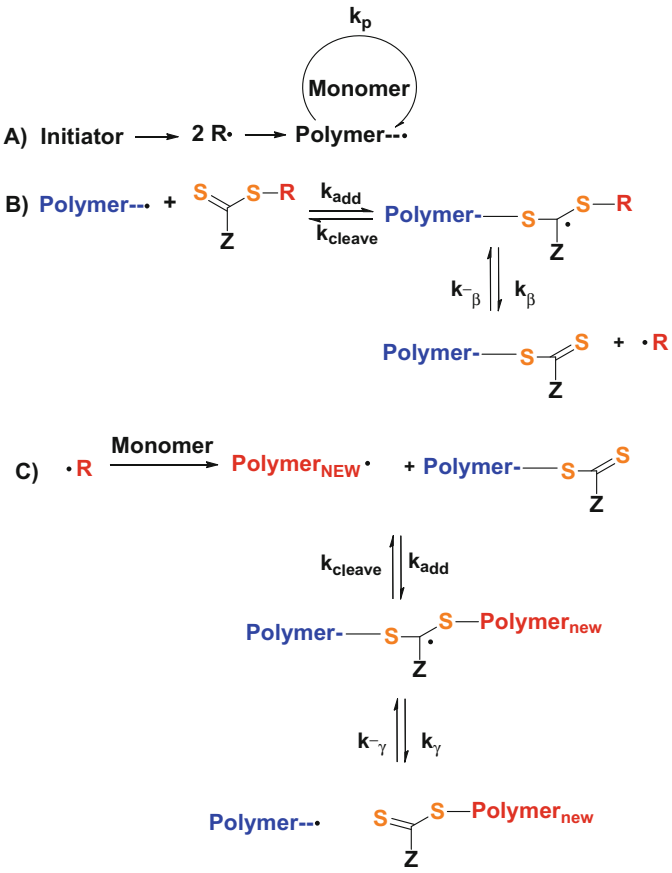

Scheme 5.30 Reversible addition-fragmentation chain transfer (RAFT) mechanism (adapted from [86])

styrene-block-poly(vinyl acetate) copolymers with narrow molecular weight distributions can be readily achieved [91, 92].

The Monteiro group in the Netherlands demonstrated that RAFT could be employed for styrene and maleic anhydride copolymerizations [93]. The product exhibited a narrow polydispersity with a predictable molecular weight. More importantly, they demonstrated that the colored, labile dithioester functionality in the product could be removed by UV irradiation [93]. This tactic eliminates two disadvantages when using RAFT. In particular, the odor and color from the dithioester moiety are removed from the polymer after polymerization is complete.

Tandem techniques using NMP or ATRP followed by RAFT are now generating interest to construct polymers that have previously been problematic [75, 90–96]. Similarly, reactive polymer chain ends that can be further modified to include a RAFT terminus post-polymerization are being constructed, such as that outlined in Scheme 5.31, which provides alternative routes to use RAFT with preformed polymers as macro-initiators.

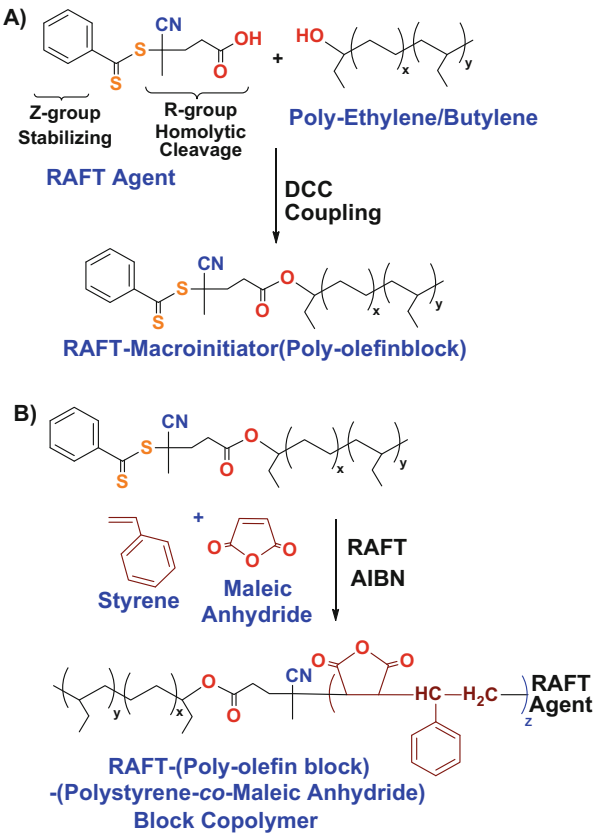

Scheme 5.31 Reversible addition-fragmentation chain transfer (RAFT) for the synthesis of a poly (butylene-ethylene-block)-(styrene-*co*-maleic anhydride) block copolymer. (**a**) Synthesis of macro-initiator-polyolefin block. (**b**) RAFT synthesis of poly(olefin-block)-(styrene-*co*-maleic anhydride) block copolymer (adapted from [89])

Some authors propose that RAFT copolymerization with styrene and maleic anhydride does not require more rigorous polymerization requirements than conventional free radical methodologies [97–99]. For example, a RAFT macroinitiator comprising a polyolefin block was prepared from Kraton L-1203, composed from polyethylene-butylene-(polyethylene-butylene), to prepare block copolymers (Scheme 5.31a). The second block consisted of either polystyrene (PS) or poly(styrene-*co*-maleic anhydride) (Scheme 5.31b) [91]. The labile dithioester was later removed by UV photolysis and further irradiated to produce triblock and star-shaped polymers [89].

Maleic anhydride itself does not homopolymerize, while its copolymerization with styrene favors a more alternating character, as evidenced by the reported reactivity ratios in Chapter 4. Convincing evidence was published in 1994 indicating that the styrene-maleic anhydride copolymerization obeys the penultimate unit model [89]. It was therefore proposed that a substantial mass of the propagating radicals bear a terminal styrene unit during the polymerization because of

Table 5.17 Properties of polyolefin-block-styrene-maleic copolymers by RAFT [89, 91]

Exp #	RAFT agent molar conc.	Styrene molar conc.	Maleic anhydride molar conc.	M_n (kDa)	M_w/M_n	% conversion	Theo. M_n (kDa)
1	1.0	2.0		10	1.18	21	10
2	1.0	4.8		23	1.20	28	20
3	None	1.0	1.0	>2000	–	–	–
4	2.6	1.0	1.0	4.1	1.06	57	4.4
5	1.3	0.5	0.5	11	1.12	62	12

resonance of the terminal radical into the phenyl ring as judged by its slower propagation.

As displayed in Table 5.17 (experiments 3–5), three styrene-maleic anhydride copolymerizations were performed under analogous conditions except to the RAFT agent employed and the monomer concentrations utilized [91]. The control experiment without the RAFT agent became turbid after a minute conversion due to solvent incompatibility (experiment 3). In contrast, the experiment with the RAFT agent remained in solution throughout the entire polymerization (number 4 in Table 5.17). GPC analysis of the final sample indicated a number-average molecular weight of 4.1 kDa, with a polydispersity of 1.06. This molecular weight is close to the expected theoretical value of 4.4 kDa, thereby indicating a well-mannered RAFT polymerization scheme.

The macromolecular RAFT agent (Scheme 5.31b; experiment 5 in Table 5.17) also enabled the preparation of a narrow polydispersity poly(ethylene-*co*-butylene)-block-(styrene-*co*-maleic anhydride) polymer. The final product, a pink powder, has a molecular weight close to the predicted value of 11 kDa and a polydispersity of 1.12.

The examples provided clearly indicate that well-defined molecular weights and narrow polydispersity poly(ethylene-butylene)-block-(styrene-maleic anhydride) copolymers can be prepared by RAFT. Further, UV irradiation also removes the labile dithiobenzoate group thereby providing for less odor and color in the final product. Consequently, it is expected that these types of polymers are to be more useful in coating applications than previous versions.

5.12.4 Production of Styrene-Maleic Anhydride/N-Vinyl Pyrrolidone Gradient Terpolymers by RAFT

In this chapter, the free radical copolymerization of styrene and maleic anhydride with *N*-vinylpyrrolidone will be discussed and compared to the vinyl pyrrolidone-maleic and styrene-maleic copolymers that have been previously discussed in Sects. 5.8 and 5.9. Both proceed through charge-transfer mechanisms to produce alternating copolymers. However, what would happen if you combine the electron donors styrene and *N*-vinylpyrrolidone with the electron acceptor maleic anhydride as illustrated in Scheme 5.32. Do you obtain a blend of individual copolymers or a

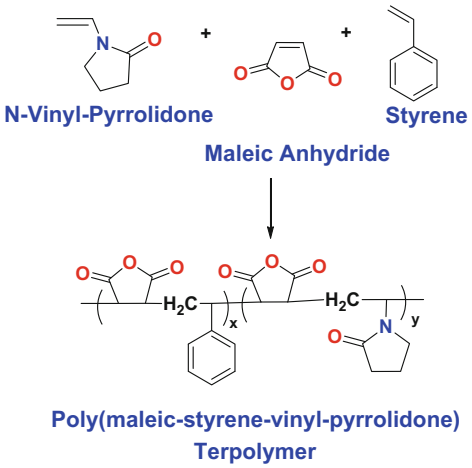

Scheme 5.32 Formation of poly(styrene-*co*-maleic anhydride-*co*-*N*-vinyl-2-pyrrolidone) terpolymer

Table 5.18 Monomer reactivity ratios for maleic anhydride, styrene, and *N*-vinylpyrrolidone (adapted from [101–103])

Copolymer	r_1	r_2	$r_1 \cdot r_2$
Maleic anhydride/styrene	0.005	0.05	2.5×10^{-4}
Maleic anhydride/*N*-vinylpyrrolidone	0.08	0.16	1×10^{-2}
Styrene/*N*-vinylpyrrolidone	15.7	0.05	0.79
Styrene/*N*-vinylpyrrolidone Using γ-ray irradiation	0	0	0

terpolymer? If a terpolymer is produced, is it a statistical distribution of styrene-maleic units to *N*-vinylpyrrolidone-maleic anhydride units, or does one obtain a more complex architecture?

These interesting questions have been answered by several authors using free radical, RAFT, and ATRP polymerization mechanisms [89, 96]. Here we will focus on the RAFT approach since these methods predominantly yield the same end result. One can first start with the individual monomer reactivity toward free radical polymerization to evaluate how a copolymerization will proceed. Measuring the reactivity ratios of the monomers is well known in the literature [100], and these values are summarized in Table 5.18 [101–103].

The monomer reactivity ratios r_1 and r_2 are the ratios of the rate constants for a given radical adding its own monomer (homopropagation/homopolymerization) to that of the other monomer (cross-propagation/copolymerization) (Eq. (5.1)). Thus, $r_1 > 1$ means that the radical M_1 prefers to add to itself rather than monomer M_2; $r_1 < 1$ means that monomer M_1 prefers to add to M_2. In the system maleic anhydride (M_1) and styrene (M_2), for example, where $r_1 = 0.005$ and $r_2 = 0.05$, the maleic anhydride radical prefers to react 200 times faster with the styrene monomer than

itself, while the styrene radical prefers to react 20 times faster with the maleic anhydride monomer than itself:

$$r_1 = \frac{k_{M1-M1}}{k_{M1-M2}} \quad \text{and} \quad r_2 = \frac{k_{M2-M2}}{k_{M2-M1}} \tag{5.1}$$

$$\frac{d[M_1]}{d[M_2]} = \frac{[M_1](r_1[M_1] + [M_2])}{[M_2]([M_1] + r_2[M_2])} \tag{5.2}$$

Note that the reactivity ratio is unit-less (Eq. (5.1)), so it does not indicate the absolute value of the rate, such as how quickly it polymerizes in real time. Likewise, it does not take into consideration the mole fraction of each of the monomers present in the polymerization reaction. These must be included for an absolute rate to be determined as shown in Eq. (5.2). This equation, known as the copolymerization equation or copolymer composition equation, indicates the mole fraction of the two monomers within the bulk copolymer.

Even though the styrene radical would rather add to itself and make blocks of polystyrene rather than copolymerize with vinyl pyrrolidone, (15.7 versus 0.05 in Table 5.18, respectively), Hu and Zhang demonstrated that in the presence of maleic anhydride, styrene and vinyl pyrrolidone homopolymerization/copolymerization were both negligible (<1 %) over 10 h, but both monomers copolymerize to >55 % conversion with maleic anhydride [48].

The authors also determined the equilibrium constants and reactivity ratios for each charge-transfer complex of styrene-maleic anhydride units and *N*-vinylpyrrolidone-maleic anhydride units that they designated as styrene-maleic anhydride charge-transfer complex 1 (CTC1) and *N*-vinylpyrrolidone-maleic anhydride charge-transfer complex 2 (CTC2) (Table 5.19).

The practical relevance of the charge-transfer equilibrium constants in Table 5.19 would indicate that at the start of a batch polymerization containing 0.125 mol% styrene, 0.125 mol% vinyl pyrrolidone, and 0.5 mol% maleic anhydride, the initial polymerization kinetics would favor blocks of styrene-maleic anhydride to be constructed first until this charge-transfer complex (CTC1) was consumed and then vinyl pyrrolidone-maleic (CTC2) blocks would be added. In summary, a gradient copolymer of (styrene-maleic anhydride)-(vinyl pyrrolidone-maleic anhydride) should be formed.

Table 5.19 Charge-transfer equilibrium constants and reactivity ratios for styrene-maleic anhydride charge-transfer complex 1 (CTC1) and *N*-vinylpyrrolidone-maleic anhydride charge-transfer complex 2 (CTC2) (adapted from [48])

Monomer pair forming CTC	K_{eq} (L/mol) at 293.2 K in $CHCl_3$	Reactivity ratio of CTC
Styrene-maleic anhydride-(CTC1)	31×10^{-2}	$r_{CTC1} = 0.17 \pm 0.01$
N-vinyl pyrrolidone-maleic anhydride (CTC2)	3.57×10^{-2}	$r_{CTC2} = 4.20 \pm 0.34$

However, Hu and Zhang obtained the opposite result, where a poly(vinyl pyrrolidone-maleic anhydride) copolymer was formed at earlier conversions [48]. This finding highlighted an oversight in just using the equilibrium constants of the charge-transfer complexes to predict the outcome of the polymerization. In this case, despite the 1000-fold higher concentration of styrene-maleic anhydride (CTC1) over vinyl pyrrolidone-maleic anhydride (CTC2) present in the medium, once vinyl pyrrolidone was incorporated into the polymer, the vinyl pyrrolidone-maleic anhydride CTC2 radical would rather homopropagate than cross-propagate to a styrene-maleic CTC1. Likewise, styrene-maleic CTC1 would rather cross-propagate to vinyl pyrrolidone-maleic anhydride CTC2 than homopropagate with itself, such as styrene-maleic CTC1.

A gradient terpolymer comprised of poly(vinyl pyrrolidone-maleic anhydride) units is formed first, followed by alternating (vinyl pyrrolidone-maleic anhydride)-(styrene-maleic anhydride) units in the center, and lastly (styrene-maleic anhydride) sequences at the end [104–107]. This underscores the importance of not only the equilibrium concentration of the charge-transfer complex present in this reaction but a knowledge of the rate constants and reactivity ratios for each of the charge-transfer complex needs to be known to truly predict the outcome of a particular terpolymerization.

Schematically, this is displayed in Scheme 5.33 where at the beginning of the reaction there is a very high level of styrene-maleic anhydride charge-transfer

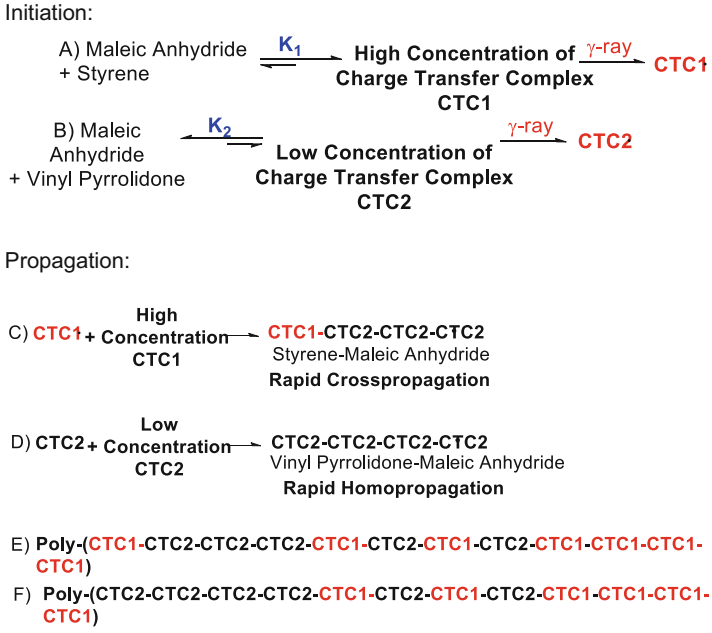

Scheme 5.33 Equilibrium concentration of (maleic anhydride-styrene) CTC1 versus (maleic anhydride-vinyl pyrrolidone) CTC2 during initiation versus propagation (adapted from [48])

complex CTC1 over that of vinyl pyrrolidone-maleic anhydride charge-transfer complex CTC2. Upon γ-irradiation, both charge-transfer complexes enter into their excited triplet state for polymerization to ensue (Scheme 5.33a, b). However, there is a disproportionately higher level of styrene-maleic anhydride charge-transfer complex CTC1 present over vinyl pyrrolidone-maleic anhydride charge-transfer complex CTC2 so that homopropagation of CTC1 should ensue (Scheme 5.33c).

But once the (styrene-maleic) CTC1 cross-propagates to the (vinyl pyrrolidone-maleic anhydride), homopolymerization of CTC2 ensues instead. Likewise, the (vinyl pyrrolidone-maleic anhydride) units would rather homopolymerize with itself then cross-propagate to CTC1 (Scheme 5.33d). In the end, both initiating charge-transfer complexes predominantly make the same polymers (Scheme 5.33e, f), where a gradient distribution of poly(vinyl pyrrolidone-maleic anhydride) blocks, followed by alternating (polystyrene-maleic anhydride-vinyl pyrrolidone-maleic) sequences and by (styrene-maleic anhydride) blocks, is constructed.

In conclusion, this chapter has covered styrene-maleic anhydride copolymers by free radical, ATRP, RAFT, and NMP techniques. The versatile nature of the anhydride functionality within this monomer enables one to derivatize this molecule after copolymerization thereby tailoring the functionality required for a particular application discussed. In general, the maleic unit can be employed as a metal chelant, an adhesive promoter to metals. It can also introduce specific thermoplastic properties into copolymers, such as high heat resistance.

The maleic anhydride monomer does not readily homopolymerize into high-molecular-weight polymers, but rather into oligomers when extremes are employed. However, it does readily copolymerize with electron-donor monomers through a charge-transfer complex by free radical, ATRP, RAFT, and NMP techniques. These donor monomers include styrene, acrylates, methacrylates, acrylamides, methacrylamides, α-olefins (such as ethylene, propylene, and longer-chain analogs), vinyl amides, vinyl lactams, and vinyl esters to name a few.

Under the right set of conditions, this charge-transfer complex can yield a highly alternating comonomer sequence along the whole polymeric backbone or in sections of the polymer if desired. The charge-transfer complex can govern the polymerization kinetics to overshadow the individual monomer's reactivity ratios and completely alter the sequence distribution of terpolymerizations as well.

Since the 1950s, maleic anhydride copolymers have continued to fascinate scientists, and its uses continually rise year after year. This is a testament to the versatility of this monomer and the properties it brings. This simple molecule rests in a very special place for chemists and will continue to generate both small and polymeric materials for years to come!

References

1. Trivedi BC, Culbertson BM (1982) Maleic anhydride. Plenum Press, New York
2. Abd-El-Azim A-AA, Nasr ES, Farhat MS (1994) Polym J 26:423
3. Eisenberg P, Lucas JC, Williams RJJ (1997) J Appl Polym Sci 65(4):755

4. Melville HW, Burnett GM (1954) J Polym Sci 13(71):417
5. Ahamad A, Lubi MC, Mohan A, Safeer M, Thachol ET (2001) Des Monomers Polym 4 (3):260
6. Birley AW, Dawkins JV, Kyriacos D, Bunn A (1981) Polymer 22(6):812
7. Davallo M, Pasdar H, Mohseni M (2010) Int J ChemTech Res 2(4):2113
8. Cherian B, Thachil ET (2004) Int J Polym Mater Polym Biomater 53(10):829
9. Vaidya UR, Nadkarni VM (1987) Ind Eng Chem Res 26(2):1948
10. Cherian B, Thachil ET (2005) Polym Plast Technol Eng 44(5):931
11. Abd-El-Azim A-AA (1995) Polym Bull 35:229
12. Nalampang K, Johnson AF (2003) Polymer 44(19):6103–6109
13. Tong SN, Chen DS, Kwei TK (1985) Polym Eng Sci 25(1):54
14. Qin Y, Jia JR, Zhao L, Huang ZX, Zhao SW, Zhang GW, Dai BF (2011) Adv Mater Res 393:349
15. Jia J, Huang Z, Wang Y (2013) Asian J Chem 25(9):5001
16. Sadler JM, Toulan FR, Nguyen AT, Kayea RV, Ziaee S, Palmese GR, La Scala JJ (2014) Carbohydr Polym 100(16):97
17. Vaidya UR, Nadkarni VM (1988) Ind Eng Chem Res 27(11):2056
18. Potiyaraj P, Klubdee K, Limpiti T (2007) J Appl Polym Sci 104(4):2536
19. Pimpan V, Sirisook R, Chuayjuljit S (2003) J Appl Polym Sci 88(3):788–792
20. Öztürk Y, Güçlü G (2005) Polym Plast Technol Eng 43(5):1539
21. Chen S-A, Wu K-C (1982) J Polym Sci 20(7):1819
22. Zetterlund PB, Weaver W, Johnson AF (2002) Polym React Eng 10(1-2):41
23. Zetterlund PB, Gosden RG, Johnson AF (2003) Polym Int 52(1):104
24. Ashland Inc. [Online] August 07, 2014. [Cited: August 07, 2014.] www.ashland.com
25. DSM [Online] August 07, 2014. [Cited: August 07, 2014.] www.dsm.com
26. CCP Composites [Online] August 07, 2014. [Cited: August 07, 2014.] www.ccpcompositesus.com
27. Jones FN (2003) Alkyd Resins. In: Ullmann's encyclopedia of industrial chemistry. Wiley, Weinheim, p 429
28. Boruah M, Gogoi P, Adhikari B, Dolui SK (2012) Prog Org Coat 74(3):596
29. Bora MM, Gogoi P, Deka DC, Kakati DK (2014) Ind Crop Prod 52:721
30. Dutta N, Karak N, Dolui SK (2004) Prog Org Coat 49(2):146
31. Aydin S et al (2004) Prog Org Coat 51(4):273
32. Crawford RV, Roberts AG, Toseland PA (1968) US Patent No. 3412056
33. Warth H, Mülhaupt R, Hoffmann B, Lawson S (1997) Die Angewandte Makromolekulare Chemie 249(1):79
34. Aigbodion AI, Okiemen FE, Ikhuria EU, Bakare IO, Obazee EO (2003) J Appl Polym Sci 89 (12):3256
35. Poorabdollah M, Beheshty MH, Atai M, Vafayan M (2013) Polym Compos 34(11):1824
36. Saravari O, Phapant P, Pimpan V (2005) J Appl Polym Sci 96(4):1170
37. Murillo EA, López BL (2011) Prog Org Coat 72(4):731
38. Aigbodion AI, Okieimen FE, Obazee EO, Bakare IO (2003) Prog Org Coat 46(1):28
39. Tzoganakis C, Vlachopoulos J, Hamielec AE (1988) Chem Eng Prog 1:47
40. Suwanda D, Lew R, Balke ST (1998) J Appl Polym Sci Part B 35(4):1033
41. Rzayev ZMO (2011) Int Rev Chem Eng 3:153
42. Yang L, Zhang F, Endo T, Hirotsu T (2003) Macromolecules 36(13):4709
43. Abdel-Azim A, Nasser AM, Ahmed NS, Kamal RS (2011) Petrol Sci Technol 29:97
44. Chevron Phillips Online Product Brochure for Poly-anhydrides PA-18 www.cpchem.com/bl/specchem/en-s/Pages/PolyanhydrideResins.aspx
45. Gale DJ (1972) US Patent 3,635,915
46. Bretti C, Crea F, Rey-Castro C, Sammartano S (2005) React Funct Polym 65(3):329
47. Lee CM, Kumler WD (1961) J Am Chem Soc 83(22):4593
48. Wong KF, Eckert CA (1971) J Chem Eng Data 16(1):56

49. Georgiev G, Konstantinov GG, Kabaivanov V (1992) Macromolecules 25:6302
50. Gaylord NG, Mishra MK (1983) J Polym Sci 21:23
51. Veron L, Revol M, Mandrand B, Delair T (2001) J Appl Polym Sci 81:3327
52. Coleman JP, Kvakovsky G, Sikora DJ (1985) EP Patent EP 0172154 B1
53. Konsulov V, Lyapova G, Petrov B, Eremieva B, Saha P (2008) J Chem Technol Metall 43 (3):297
54. Voss A, Dickhauser E (1936) US Patent 2,047,398
55. Gray MH, Sparks Jr HF (1967) US Patent 3,297657
56. Thompson JE (2001) US Patent 20030045605 A1
57. Mabire, F.; Ricker, W.M., Shelton, K., Zweig, A.M., EP Patent EP0889102 A2 (1997).
58. Carroll JB, Shakhnovich AI (2007) US Patent 20090018258 A1
59. Hahn LM, Schmidhauser JC (2001) EP Patent EP1122263 A1
60. Sethi N, Srivastava RK, Singh RK (1989) Contraceptive 39(2):217
61. Lohiya NK, Manivannan B, Mishra PK, Pathak N, Balasubramanian SPA (1998) Contraceptive 58:119
62. Mahmudov KT, Aliyeva RA, Hamidov SZ, Chyragov FM, Mardanova SR, Kopylovich MN, Pombeiro AJL (2012) Am J Anal Chem 3(12):790
63. Dharmarajan N, Datta S, Ver Strate G, Ban L (1995) Polymer 36(20):3849
64. Ku-Lee M, Biermann C (1992) J Wood Chem Technol 12(2):231
65. Rowland SP (1978) Hydroxyl reactivity and availability in cellulose. In: Rowell RM, Young RA (eds) Modified cellulosics. Academic, New York
66. Bigan M, Bigot J, Mutel B, Coqueret X (2008) J Appl Surf Sci 254(8):2300
67. Abd El-Rehim HA, Hegazy EA, El-Hag Ali A (2000) React Funct Polym 43(1):105
68. Koning C, Ikker A, Borggreve R, Leemans L, Moller M (1993) Polymer 1:4410
69. Nicolas J, Guillaneuf Y, Lefay C, Bertin D, Gigmes D, Charleux B (2013) Prog Polym Sci 38:63
70. Bertin D, Gigmes D, Marque SRA, Tordo P (2011) Chem Soc Rev 40:2189
71. Fischer H (2001) Chem Rev 101(12):3581–3610
72. Moad G, Rizzardo E (1995) Macromolecules 28:8722
73. Hawker CJ, Barclay GG, Dao J (1996) J Am Chem Soc 118(46):11467–11471
74. Volodarsky LB, Reznikov VA, Ovcharenko VI (1994) Synthetic chemistry of stable nitroxides. CRC Press, Boca Raton, FL
75. Siegenthaler KO, Studer A (2006) Macromolecules 39(4):1347
76. Lessard B, Maric M (2010) Macromolecules 43:879
77. Bonilla-Cruz J, Guerrero-Sanchez C, Schubert US, Saldivar-Guerra E (2010) Eur Polym J 46:298
78. Garcia-Valdez O, Ramirez-Wong DG, Saldivar-Guerra ES, Luna-Barcenas G (2013) Macromol Chem Phys 214(12):1396
79. Zhang M, Li YH, Gong YD, Zhao N, Zhang XF (2002) Biomaterials 23:2641
80. Kato M, Kamigaito M, Sawamoto M, Higashimura T (1995) Macromolecules 28:1721
81. Cowie JMG, Arrighi V (2008) Polymers: chemistry and physics of modern materials, 3rd edn. CRC Press, Boca Raton, FL, pp 82–84
82. Wang Y, Zhong M, Zhang Y, Magenau AJD, Matyjaszewski K (2012) Macromolecules 45:8929
83. Matyjaszewski K, Xia J (2001) Chem Rev 101(9):2921
84. Wang Y, Soerensen N, Zhong M, Schroeder H, Buback M, Matyjaszewski K (2013) Macromolecules 46:689
85. Yeole N (2010) Synlett 10:1572
86. Keddie DJ (2014) Chem Soc Rev 43:496
87. Moad G, Rizzardo E, Thang SH (2008) Polymer 49(5):1079
88. Moad G, Rizzardo E, Thang SH (2010) Mater Matter 5(1):2
89. Chiefari J, Chong YK, Ercole F, Krstina J, Jeffery J, Le T, Mayadunne R, Meijs GF, Moad CL, Moad G, Rizzardo G, Thang SH (1998) Macromolecules 31(16):5559

90. Moad G, Rizzardo E, Thang SH (2009) Aust J Chem 62(11):1402
91. Benaglia M, Chen M, Chong YK, Moad G, Rizzardo E, Thang SH (2009) Macromolecules 42:9384
92. Benaglia M, Chefari J, Chong YK, Moad G, Rizzardo E, Thang SH (2009) J Am Chem Soc 131:6914
93. De Brouwer H, Schellekens MA, Klumperman B, Monteiro MJ, German AL (2000) J Polym Sci Part A Polym Chem 38(19):3595
94. Schellekens MAJ, Klumperman B (2000) J Macromol Sci Rev Macromol Chem Phys 40:167
95. Jancova K, Kops J, Chen X, Batsberg W (1999) Macromol Rapid Commun 20:219
96. Waterson C, Haddleton DM (1999) Polym Prepr 218:1045
97. Benoit D, Hawker CJ, Huang EE, Lin Z, Russell TP (2000) Macromolecules 33:1505
98. Chen G-Q, Wu Z-Q, Wu J-R, Li Z-C, Li F-M (2000) Macromolecules 33:232
99. Le T, Moad G, Rizzardo E, Thang SH (1998) World Patent WO 9801478 A1 and 980115
100. Chong YK, Le TPT, Moad G, Rizzardo E, Thang SH (1999) Macromolecules 32:2071
101. Sanayei RA, O'Driscoll KF, Klumperman B (1994) Macromolecules 27:5577
102. Billmeyer FW Jr (1984) Textbook of polymer science, 3rd edn. Wiley-Interscience, New York, p 329
103. Sandler SR, Karo W (1995) Polymer synthesis, vol II, 2nd edn. Academic, San Diego, CA, p 271
104. Hu Z, Zhang Z (2006) Macromolecules 39:1384
105. Dao J, Benoit D, Hawker CJJ (1998) Polym Sci 36:2161
106. Greenley RZ (1980) J Macromol Sci Part A Chem 14(4):445
107. Bork JF, Coleman LE (1960) J Polym Sci 18:413

Chapter 6
Ring-Opening Metathesis Polymerization (ROMP) Using Maleic Anhydride-Based Monomers

Michael A. Tallon

6.1 Introduction to Ring-Opening Metathesis Polymerization (ROMP) Using Maleic Anhydride-Based Monomers

In the 1950s, olefin metathesis reactions were intensely investigated as a new route for carbon–carbon bond formation. These reactions used acyclic dienes that were capable of coupling to each other enabling formation of longer linear olefin molecules. Such approaches could also be employed to form simple hydrocarbon-based polymers. This process was referred to as the acyclic diene metathesis (ADMET) polycondensation process that was further developed by the Wagener group [1]. By the 1960s, ring-opening metathesis polymerization, better known as ROMP, was developed as a derivative of these early olefin metathesis reactions [2].

The ROMP polymerization of bicyclic monomers, like norbornene and oxanorbornene, has been intensively studied using a variety of catalysts [3, 4]. Transition metal catalyst systems based on WCl_6, $MoCl_5$, and $OsCl_3$ that were in situ alkylated with Ph_4Sn to activate the catalyst were employed in these earlier catalyst systems. These catalytic methods suffered from poor reproducibility in terms of molecular weight and chain length distribution. In addition, they were especially sensitive to the functional groups present within the monomer [5]. The oxidation state of the catalysts also influenced the level of *cis*/*trans* isomerization products obtained. For instance, $RuCl_5$ produced high *cis* content (54 %) ROMP polymers, while $RuCl_3$ generated highly *trans*-ROMP polymers (89 %) [3, 6].

Newer ROMP catalysts have been developed based on ruthenium [7] and molybdenum [5] for the production of ROMP polymers. Even attachment of the ROMP catalyst to solid supports for easier removal from the medium has been

M.A. Tallon (✉)
Ashland Inc., 1005 Route 202/206, Bridgewater, NJ 08807, USA
e-mail: mtallon@ashland.com

O.M. Musa (ed.), *Handbook of Maleic Anhydride Based Materials*,
DOI 10.1007/978-3-319-29454-4_6

achieved [8]. Reported uses of such polymers include thermosetting resins [6], elevated T_g polymers [3], materials exhibiting high heat impact strength and unique flexural properties [4], new membrane materials [9], new hair care polymers and cosmetic compositions [10], and polymers with potential drug delivery or antimicrobial properties via cell permeability [11].

6.1.1 ROMP Mechanism

In the production of ROMP polymers, a polyunsaturated backbone is constructed. Differing physical properties are expected, often based on the level of *cis* versus *trans* double bonds present within the polymer, which are controlled by the catalyst. Catalyst/monomer systems exhibiting exclusively *cis* double bonds [12–21], or entirely *trans* double bonds [22–25], or mixtures of both have been reported [26–28]. Consequently, one can construct many different polymeric architectures for the same monomer depending on which catalyst is employed.

The microstructure/tacticity of norbornene- and oxanorbornene-based ROMP polymers can also influence the resultant physical properties [5, 8, 29–34]. This section will introduce the reader to ROMP, with all of its intricacies, focusing on maleic anhydride-based ROMP monomers and their resultant polymers.

ROMP is a catalytic polymerization process. This process involves a transition metal catalyst that joins the next incoming cyclic monomer onto the growing polymer end, as depicted in Scheme 6.1 [35–45]. The motivating force for the polymerization process is the release of ring strain. As the process proceeds, the cyclic monomer attaches to the growing polymer end, resulting in ring opening of the cyclic monomer, thereby enhancing the growth of the newly forming linear polyunsaturated polymer. Likewise when bicyclic monomers are used in ROMP, they form a polyunsaturated polycyclic polymer (Scheme 6.2).

Mechanistically, first elucidated by Chauvin and Herisson, the metal alkylidene catalyst complexes the incoming monomer, see Schemes 6.1a and 6.2a. A [2 + 2] cycloaddition involving the metal alkylidene and the monomer establishes the metallocyclobutane transition state as presented in Schemes 6.1b and 6.2b. The orientation of the R-group relative to the incoming monomer will dictate if the new double bond is *cis* or *trans* once the metallocyclobutane transition state is formed; see Schemes 6.1b and 6.2b [46].

Note that the *cis* orientation has been constructed in Scheme 6.1b, while the *trans* configuration has been formed in Scheme 6.2b. Upon cycloreversion and thereby ring opening, the cyclobutane transition state relieves its ring stress. A *cis* double bond is formed along the polymeric backbone in Scheme 6.1c, while a *trans* double bond is formed in Scheme 6.2c.

The subsequent monomers are added by the same mechanism over and over again; see Schemes 6.1d and 6.2d. The polymerization process is complete upon monomer exhaustion; see Schemes 6.1e and 6.2e. Yves Chauvin, Robert H. Grubbs, and Richard R. Schrock were awarded the 2005 Nobel Prize in Chemistry for their

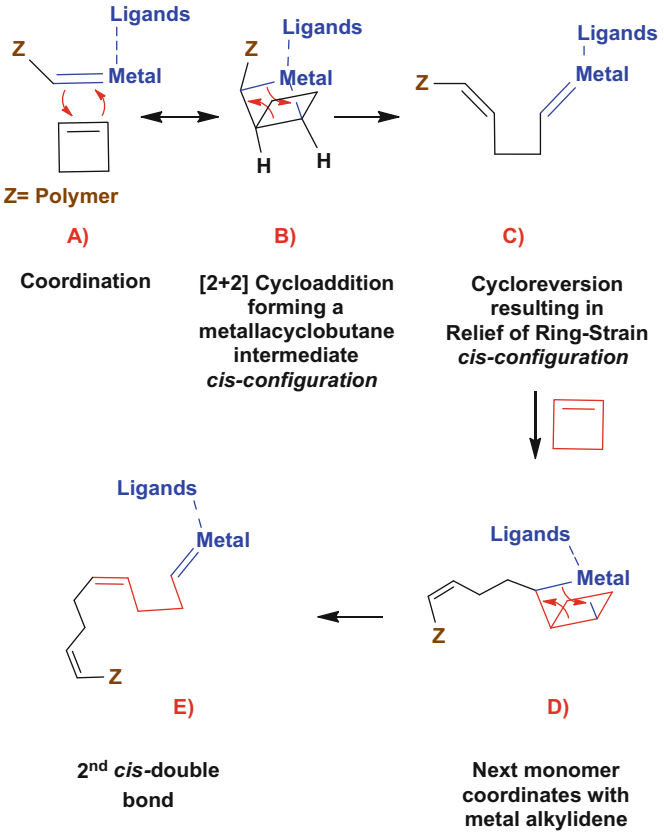

Scheme 6.1 Stepwise ROMP polymerization for monocyclic monomers through a metallocyclobutane transition-state forming *cis* double bonds

efforts in the field of metathesis reactions, further signifying the impact of this field of science.

This deceptively simple reaction scheme can result in rather complex polymeric architectures. The beauty of ROMP arises in the ease of forming these complex block copolymers. Otherwise, such polymeric structures would be extremely difficult to construct with classical free radical, anionic, or cationic polymerization methods.

ROMP does not suffer from a true termination process, unlike classical polymerization methods. ROMP is classified under the reversible activation/deactivation polymerization process, more commonly known, but erroneously defined, as "living polymerization" methods. Such methods include reversible addition–fragmentation transfer (RAFT), atom transfer radical polymerization (ATRP), and nitroxide-mediated polymerization (NMP). Unfortunately, these "living" methods tend to suffer from high residual monomer levels or either toxic, highly colored, and odiferous catalysts species [47–84].

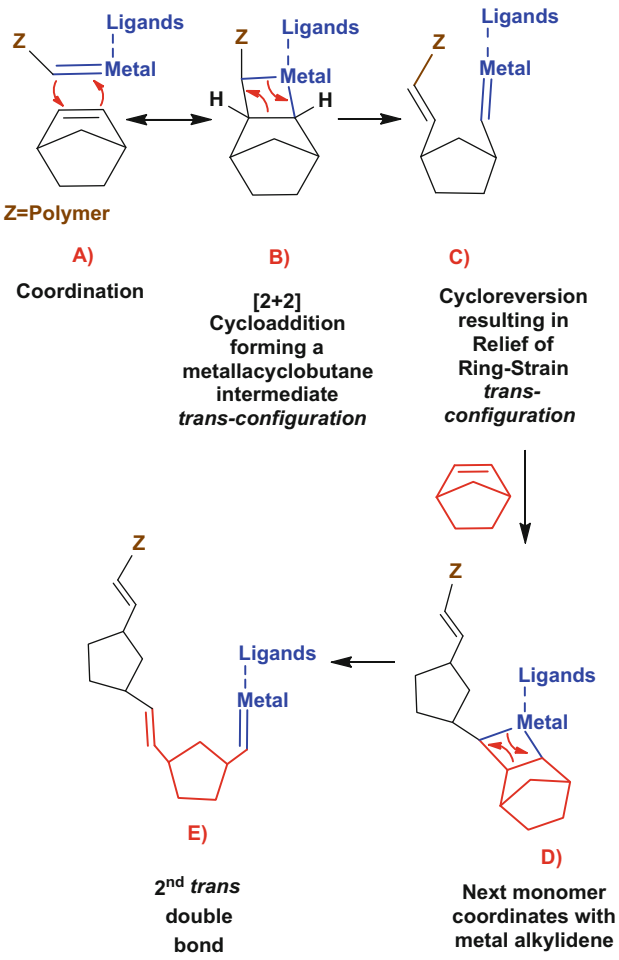

Scheme 6.2 Stepwise ROMP polymerization using a bicyclic monomer norbornene forming a *trans* double bond

6.1.2 Initial Monomers Used in ROMP

Despite being superior in monomer conversion, ROMP can only use a limited number of monomers. These monomers must possess a highly strained cyclic ring structure to demonstrate utility. Examples include cyclobutene, cyclopentene, *cis* cyclooctene, and bicyclic structures like 1,2-cyclopentanyl-cyclobutene, norbornene, and oxanorbornene; see Fig. 6.1. Given this requirement for a highly strained ring structure, typical commercial monomers cannot be employed by ROMP. This has slowed the commercial influence of ROMP polymerization processes.

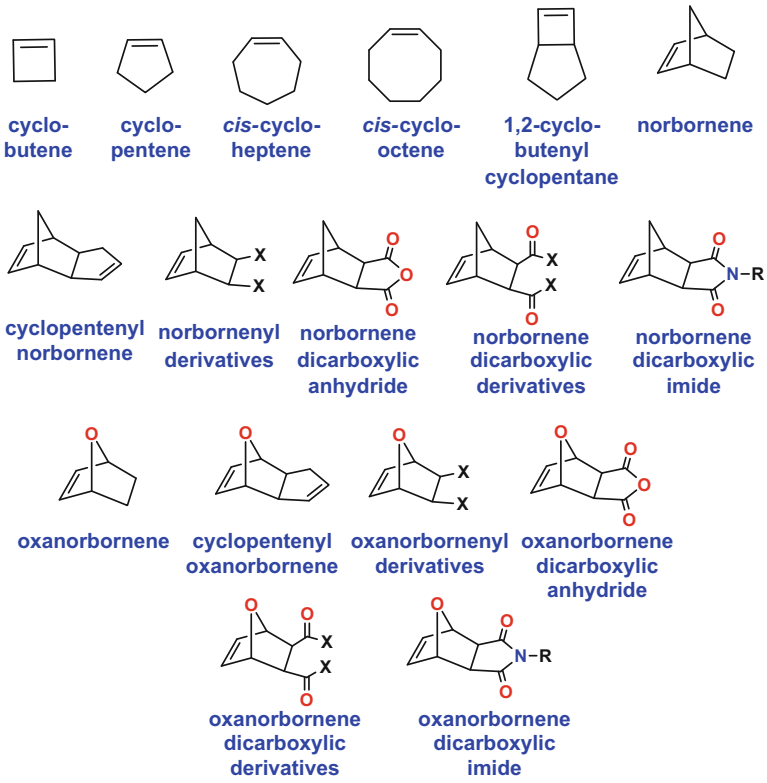

Fig. 6.1 Highly ring-strained monocyclic and bicyclic monomers used in ROMP polymerization (Adapted from [2])

6.1.3 Catalyst Choice

While a number of transition metal-based catalysts have been elucidated for use in ROMP, two major types come to the forefront. First, the highly active Schrock-type catalysts based on tungsten or molybdenum exhibit outstanding cis/trans selectivity. These catalysts are sensitive to the type of functional groups present in the ROMP monomer, as well as to the presence of oxygen and moisture; see Figs. 6.2 and 6.3 [2, 35, 36]. These catalysts can virtually form exclusively *cis* or *trans* double bonds, by the strategic selection of ligands attached to the metal–carbene catalyst.

Second, the Grubbs-type ruthenium catalysts are generally considered superior due to their tolerance of functional groups. However, these catalysts lack cis/trans control [37–43]. Three generations of Grubbs ruthenium catalysts have received much attention. The focus of these catalysts originates from the lack of required special equipment and conditions, such as deoxygenation and scrupulous removal of moisture from reagents.

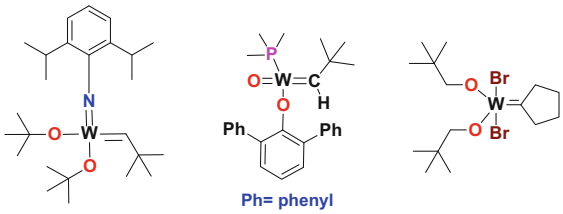

Fig. 6.2 Tungsten carbene Schrock catalysts used in ROMP polymerization (Adapted from [2])

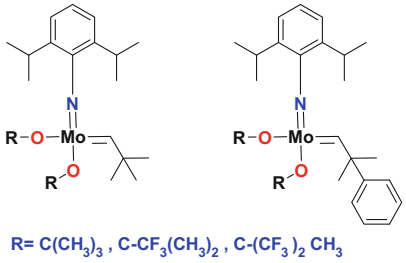

Fig. 6.3 Molybdenum carbene Schrock catalysts used in ROMP polymerization (Adapted from [2])

Depicted in Fig. 6.4 are the chemical structures for first-generation (A), second-generation (B), Hoveyda–Grubbs (C), and third-generation (D) Grubbs catalyst classes.

The first-generation catalyst is known to initiate much slower than second-generation Grubbs catalyst. First-generation catalysts generally form higher trans-containing polymers that are more extended and more accessible to further trans-formations. This accessibility is extremely important since attachment of larger molecules onto ROMP polymers enables the construction of a variety of new polymeric materials. This approach is more facile than trying to polymerize a pre-derivatized monomer comprising this functionality from just steric factors alone. The blue arrows in Fig. 6.4 denote the electron-donating character of the ligand functionality, which promotes the dissociation of one of the ligands, such as tricloco-hexylphosphine or bromopyridine, to produce the activated form of the catalyst.

Another interesting feature of the phosphine ligand is its large cone angle. This spatial arrangement can hinder complexation of the incoming monomer, which can negatively affect the overall rate of initiation, as well as decrease the polymerization rate; see Fig. 6.5. In particular, half of the metal's coordination sphere is occupied by the tris-cyclohexyl groups 179°, whereas smaller ligands like the tris-methyl groups only occupy 118° [85].

Initiation of ROMP can take several hours to days to proceed with first-generation catalyst. Conversely, second-generation Grubbs catalyst only takes several minutes. This disparity arises from slower detachment of the phosphine ligand from the dormant catalyst in the first-generation class. Replacement by a more electron-donating NHC ligand, like that in second-generation catalyst, not

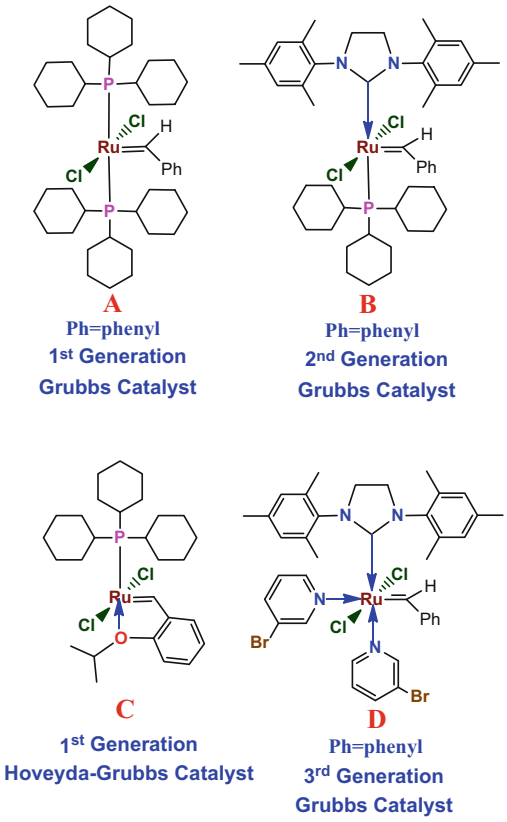

Fig. 6.4 Chemical structures for first-generation, second-generation, Hoveyda–Grubbs, and third-generation Grubbs catalyst

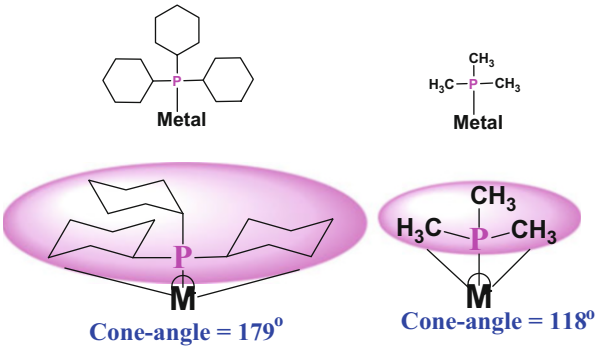

Fig. 6.5 Phosphine cone angle relating to structure of ligand to metal

only promotes the uncoupling of the phosphine ligand from the quiescent catalyst to form the activated catalytic entity involved in ROMP (Fig. 6.6) but also enhances complexation to the olefinic ROMP monomer [41–43, 46].

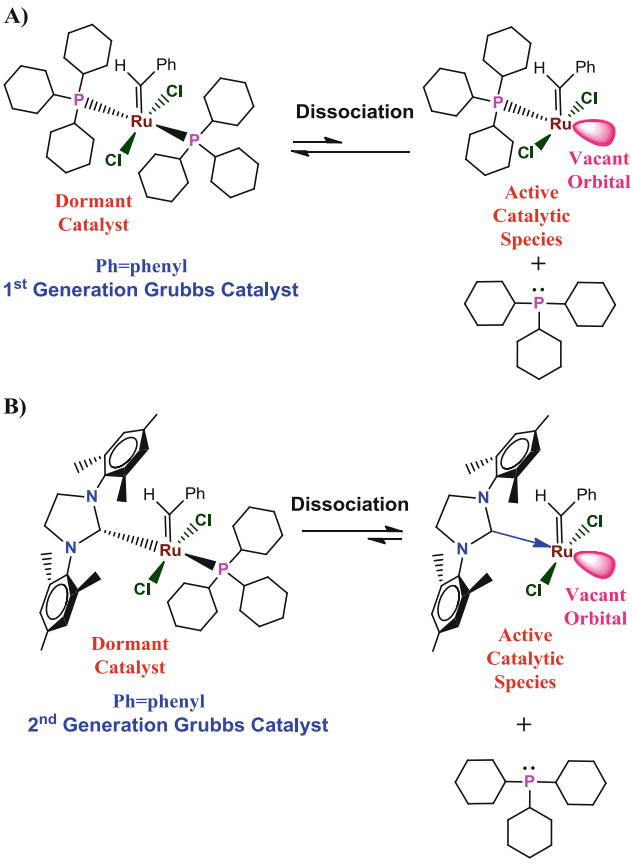

Fig. 6.6 Chemical structures for dormant first-generation catalyst and dissociated form of the active Grubbs catalyst involved in ROMP

This mechanism has been thoroughly studied and was found to proceed by the initial detachment of the phosphine moiety to form a 14-electron Ru intermediate; see Fig. 6.6 [86, 87]. After the ligand dissociates, the olefinic substrate (ROMP monomer) coordinates to the ruthenium to give a 16-electron complex. A metallocyclobutane ring is then formed through coupling of the olefin and the alkylidene moiety within the ruthenium coordination sphere. Note that this dissociation is an equilibrium process as denoted by the double arrows in Fig. 6.6. The phosphine ligand can reunite with the active catalytic entity to restore it to its resting state. Hence, any ligand that stabilizes the active catalytic species will enable an enhanced ROMP initiation. The electron-donating character of the NHC ligand is expected to initiate quicker than first-generation Grubbs catalyst, as illustrated by the blue arrow in Fig. 6.5b.

The first-generation Grubbs catalyst is a five-coordinate, 16-electron, Ru complex exhibiting a slightly distorted square pyramidal geometry with the alkylidene

group occupying the apex; see Fig. 6.6 [86, 87]. Exchange of one phosphine ligand with a bulky N-heterocyclic carbene (NHC) ligand was found to enhance activity and selectivity in several olefin metathesis reactions. Catalysts derived from both unsaturated and saturated NHC ligands were investigated. Both exhibited very good metathesis activity [42]. The electron-donating character of the NHC ligand tends to stabilize the active catalyst as depicted by the blue arrow in Fig. 6.6. Hence, its equilibrium value is further to the dissociated activate form than the first-generation catalyst that is further to its associated dormant form.

Inclusion of the NHC ligands into the catalyst also improves the air and thermal stability of the complexes, enhancing their resistance to oxidation. NHCs ligands tend to provide stronger association to the ruthenium center than their phosphine counterparts and thereby remain attached to the metal center throughout the ROMP process. For several metals, the exchange of phosphines with NHC ligands proceeds readily and doesn't require the NHC ligand to be present in excess. The Hoveyda–Grubbs catalyst provides even more stability; see Fig. 6.4c.

To overcome the slower initiation by first-generation catalysts, larger amounts of first-generation catalyst can be used. Unfortunately, these increased quantities alter the average molecular weight of the resultant polymer, as well as enhance the levels of residual of Ru catalyst present upon reaction completion. High levels of both heavy-metal-based ruthenium and phosphine compounds can be troublesome in certain commercial sectors (such as personal care products and pharmaceutical arenas).

The initiation step of both Grubbs first-generation, second-generation, and Hoveyda–Grubbs catalysts has been further improved by the replacement of the phosphine ligand with weakly bound heterocyclic ligands. This 18-electron bis-pyridine adduct possesses a very high initiation rate and is often referred to as the Grubbs third-generation catalyst; see Fig. 6.7. Under vacuum, one pyridine ligand decoordinates, with formation of the active mono-pyridine complex forming the third-generation Grubbs catalyst class.

It is reported to initiate a millionfold quicker than first-generation catalysts in ROMP [28, 88, 89]. An additional advantage of the strong bonding of NHC ligands to the catalyst metal center is that immobilization of catalysts can be achieved by the use of anchored NHCs ligands. Blechert and coworkers fastened the NHC ligand to a Merrifield resin through an ether linkage, affording the second-generation Grubbs [89] and the Hoveyda–Grubbs [90] catalysts, respectively. Both immobilized catalysts still exhibited moderate activity in ROMP, and their recoverability makes them attractive recyclable alternative catalysts too. Despite the development of over 400 ruthenium catalyst compounds, there continues to be a need for improved ROMP catalysts.

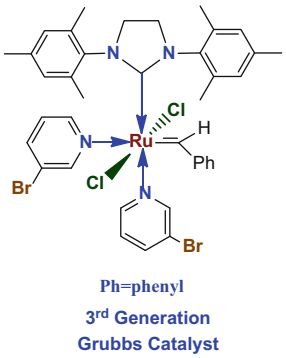

Fig. 6.7 Chemical structure for dormant third-generation Grubbs catalyst involved in ROMP

6.1.4 ROMP Polymerization Stages

The efficiency of ROMP reactions results in >99 % monomer conversion into ROMP polymers, whose molecular weight or chain length can be simply controlled by the monomer/catalyst ratio used. These ROMP polymers typically exhibit low polydispersity (P_d) values, or variability in chain length, approaching two or less. ROMP polymers also contain a polyunsaturated backbone, whose cis/trans levels can be determined by the catalyst selection [2, 35–45]. To increase the thermal and redox stability of ROMP polymers, hydrogenation of the polyunsaturated polymer products is often employed.

Similar to classical polymerization techniques, such as free radical, a ROMP polymerization exhibits three stages: initiation, propagation, and termination; see Scheme 6.3. Under normal circumstances, termination requires a "quenching step," such as an addition of ethyl vinyl ether, to detach the polymer chain end from the metal catalyst. Without this addition, the ROMP polymerization enters a dormant or deactivated stage. Dormancy usually only lasts for days or weeks.

Side reactions can occur that inactivate the catalyst system. For example, cross-metathesis side reactions not only broaden the molecular weight distribution during the polymerization, analogous to chain transfer in classical systems (see Scheme 6.4), but can also lead to the formation of catalyst dimers that are no longer active (see Scheme 6.3b).

Cross-metathesis side reactions can occur between two polymer chains (see Scheme 6.4), which can result in cyclic oligomers and in linear polymer fragments. The net effect is a broadening of the molecular weight distribution. It should be noted that intermolecular cross-metathesis can result in linear polymer fragments, while intramolecular cross-metathesis can result in cyclic oligomers and linear polymer by-products. While these side reactions are slow in the presence of monomer during ROMP polymerizations, they do become more dominant during dormant stages or upon storage where the presence of monomer is minimal. It is critical to remove the metal catalyst as soon as possible to prevent these unwanted by-products [2].

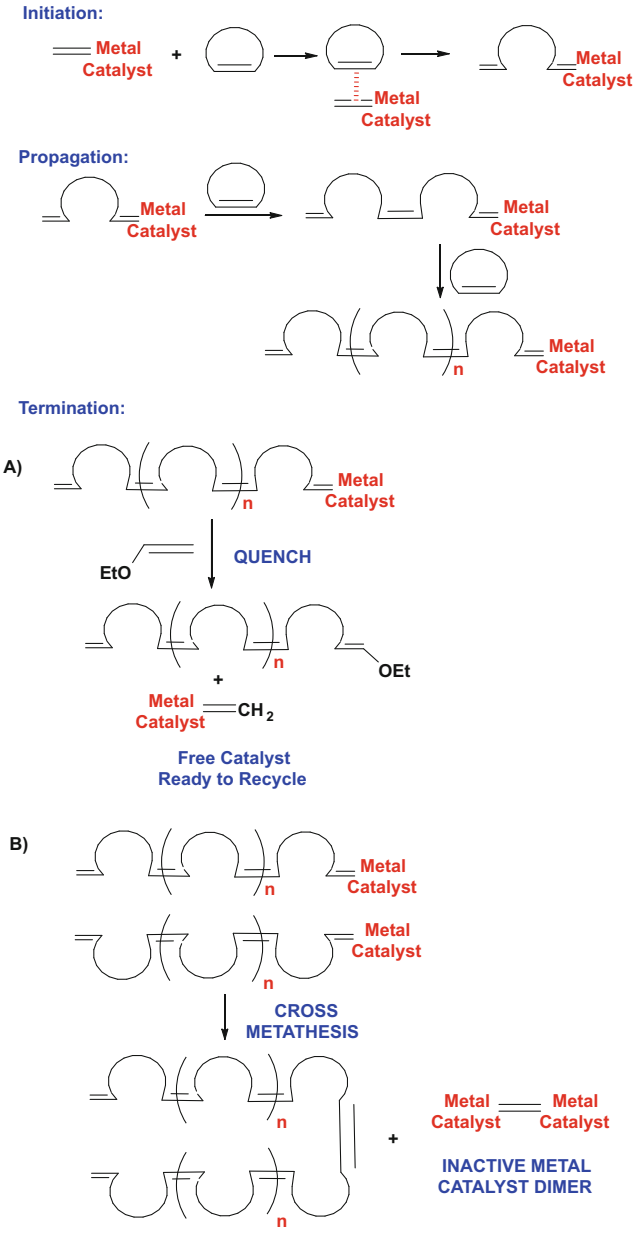

Scheme 6.3 ROMP polymerization stages (Adapted from Sutthasupa, S.; Shiotsuki, M., Sanda, F., *Polymer Journal,* 2010, **42**, p 905. Copyright 2010 with permission from Nature Publishing Group)

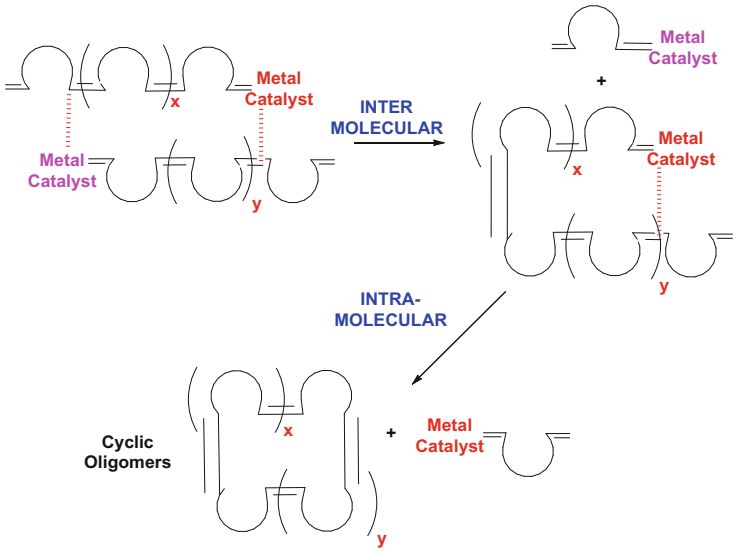

Scheme 6.4 Cross-metathesis side reactions during ROMP and storage (Adapted from Sutthasupa, S.; Shiotsuki, M., Sanda, F., *Polymer Journal,* 2010, **42**, p 905. Copyright 2010 with permission from Nature Publishing Group)

6.1.5 Synthesis of Random Versus Block Copolymers by ROMP

Excellent control over the polymeric hierarchy is possible with ROMP processes. In a representative ROMP process at ambient temperature, monomer is solubilized in solvent, such as THF, and subsequently the catalyst is added with constant stirring. An increase in viscosity of the solution is usually observed during the first 12 h of the reaction. The reaction is quenched by adding ethyl vinyl ether for an additional 30 min; see Scheme 6.5a. The polymer can then be isolated if desired by precipitation and dried.

To obtain a block copolymer, the same protocol is used as outlined above. In this case, the ROMP polymerization is not quenched. The first monomer is allowed to be completely consumed. A second monomer is put into the ROMP polymerization solution to enable the construction of the second block. Because of the living nature of ROMP polymerizations, this process is facile; see Scheme 6.5b. In fact, one can continue to construct a third- or higher-order block sequence in a similar fashion.

In contrast, a random copolymer can be constructed by simply mixing the individual monomers beforehand. The mixed monomers are then added to the ROMP catalyst for polymerization; see Scheme 6.5c. This process continues with the typical protocol of quenching and isolation as described. It becomes readily apparent that ROMP polymers with multiple segments of blocks or random features can be constructed as desired. This flexibility gives synthetic rise to exceptional control of the overall polymer hierarchy in ROMP polymerizations.

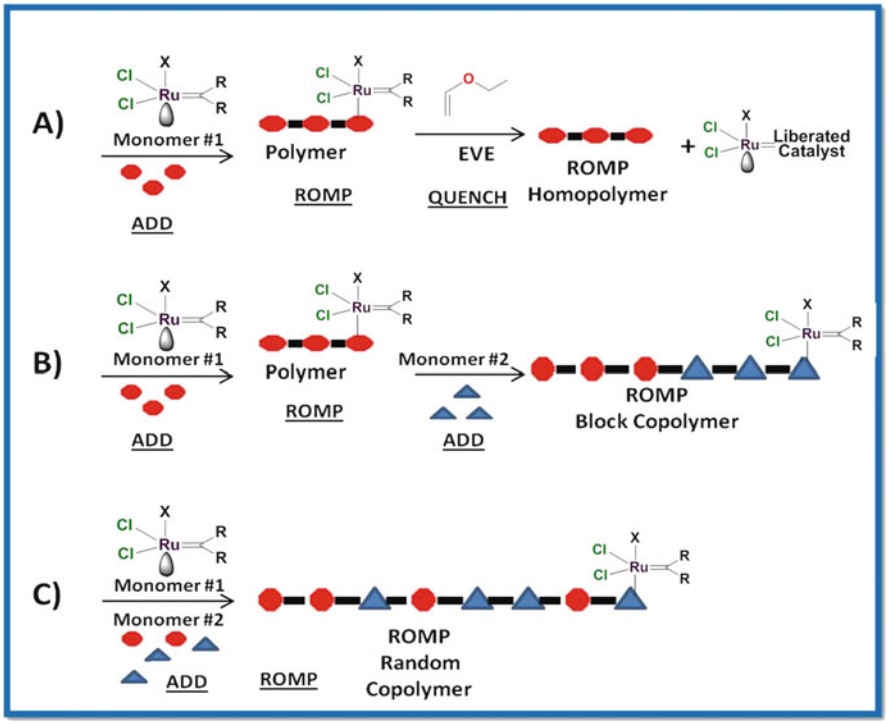

Scheme 6.5 Synthesis of ROMP (**a**) homopolymer, (**b**) ROMP block copolymer, (**c**) ROMP random copolymer

Other tactics include atom transfer radical polymerization (ATRP), reversible addition–fragmentation chain transfer polymerization (RAFT), and nitroxide-mediated polymerization (NMP) which are examples of controlled free radical "living" polymerization techniques. These methods are also described as reversible deactivation techniques. These procedures rely on surrogate molecules, such as nitroxide (NMP), dithioesters or thiocarbamates (RAFT), alkyl halides, and transition metal catalyst (ATRP) systems, to achieve control over the living polymerizations. However, these systems are not as flexible as ROMP for a number of reasons. ROMP can achieve monomer consumption values up to 99+ %, while these techniques are generally around 85–90 %.

The additives employed in NMP, RAFT, and ATRP are sometimes odoriferous as RAFT agents, toxic as nitroxide agents, or corrosive and toxic as ATRP agents, and they are not as attractive as ROMP catalysts that can be selectively removed at the end of polymerization. However, ROMP does require an additional hydrogenation step to produce a saturated oxygen/thermally stable polymer. Nevertheless, ROMP catalysts can be recycled several times to perform multiple polymerization reactions thereby making them more efficient catalytic systems as a whole.

6.1.6 *ROMP Monomers Based on Maleic Anhydride or Its Derivatives*

One strategy to the formation of ROMP monomers is achieved by the Diels–Alder cycloaddition reaction of dienophiles (maleic anhydride or dialkyl maleates), with furan or cyclohexadiene, for the production of 7-oxanorbornene and norbornene derivatives. These (oxa)norbornene monomers contain a highly tensioned bicyclic ring and are mild reagents for ring-opening metathesis polymerization (ROMP), enabling the formation of functionalized unsaturated polymers that can be further derivatized [3–10].

The mechanistic details of Diels–Alder cycloaddition reactions involving relevant derivatives of maleic anhydride were discussed in Sec. 2.6. *Endo* selectivity is usually higher for rigid dienophiles like maleic anhydride (see Schemes 6.6 and 6.7) and is the favorable kinetic isomer. The addition of heat results in isomerization into the thermodynamically favored *exo* isomer.

This arises because of the geometrical orientation of cyclopentadiene with maleic anhydride. The two molecules approach each other as depicted in Scheme 6.6a, as this provides maximal overlap of the *pi*-bonds between the two reactants and favors formation of an initial *pi*-complex resulting in the kinetic *endo* product. In addition, dipolar and van der Waals attractions influence this effect [91, 92].

A multitude of new monomers useful for ring-opening metathesis polymerization can be made from conjugated dienes, such as cyclopentadiene when using maleic anhydride; see Scheme 6.6. Other derivatives such as its esters from dialkyl maleates, amides, or maleimides are also available. 7-Oxanorbornene derivatives from furan are presented in Scheme 6.7. Other useful monomers include thiophene- or pyran-based derivatives; see Scheme 6.8a, b. However, the thiophene adducts require extremes of

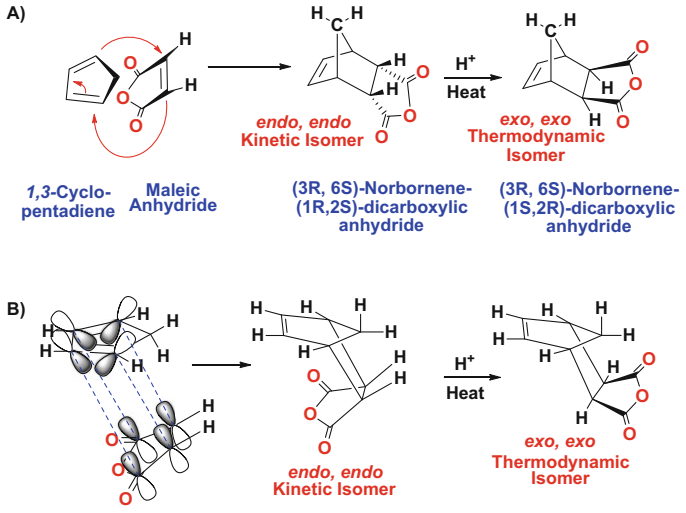

Scheme 6.6 Diels–Alder reaction between cyclopentadiene and maleic anhydride

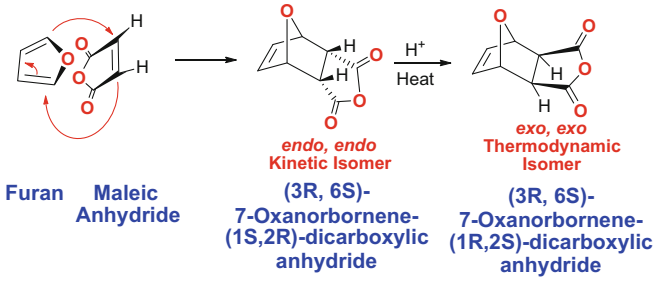

Scheme 6.7 Diels–Alder reaction between furan and maleic anhydride

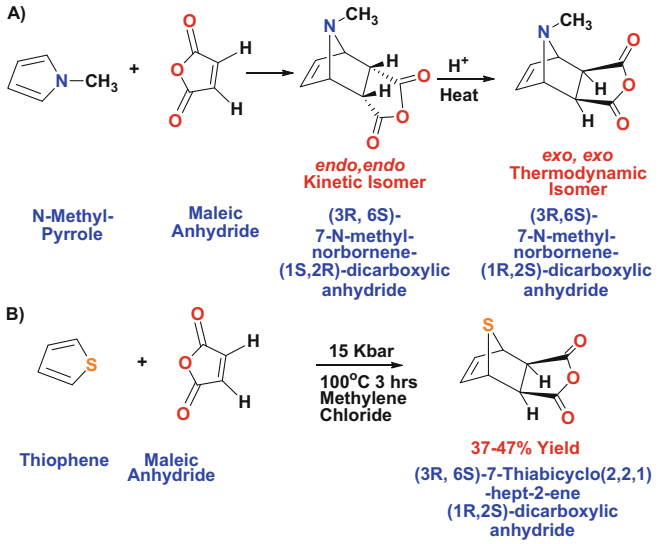

Scheme 6.8 Diels–Alder reaction between *N*-methyl-pyrrole and thiophene with maleic anhydride

temperature and pressure to obtain moderate 37–47 % yields of Diels–Alder adduct [93]. These molecules can be further reacted to form a host of derivatives such as the diacid, mono- and di-alkali salts, esters, amides, imides, and more.

ROMP monomers constructed from maleic anhydride have a fixed geometry such as *endo,endo* or *exo,exo* with respect to the substituent carbonyl groups. Derivatives of either maleic or fumaric can be constructed that are *endo*, *exo*, and *exo*, *endo* that contain acid groups, ester groups, amic acid, and imide functionality. In most cases, these monomers have additional stereochemical complexity. These monomers are either prochiral or chiral and can exist as stereoisomers of each other (Scheme 6.9).

For example, the norbornene diester monomer **M2** exists as a pair of diastereomers, 5-*endo*,6-*exo*, and 5-*exo*,6-*endo*. Similarly, the oxanorbornene monomer **M4** also comprises diastereomers (Scheme 6.9) because of the four stereocenters at carbons 1, 4, 5, and 6, as designated by their R or S configuration in Scheme 6.9.

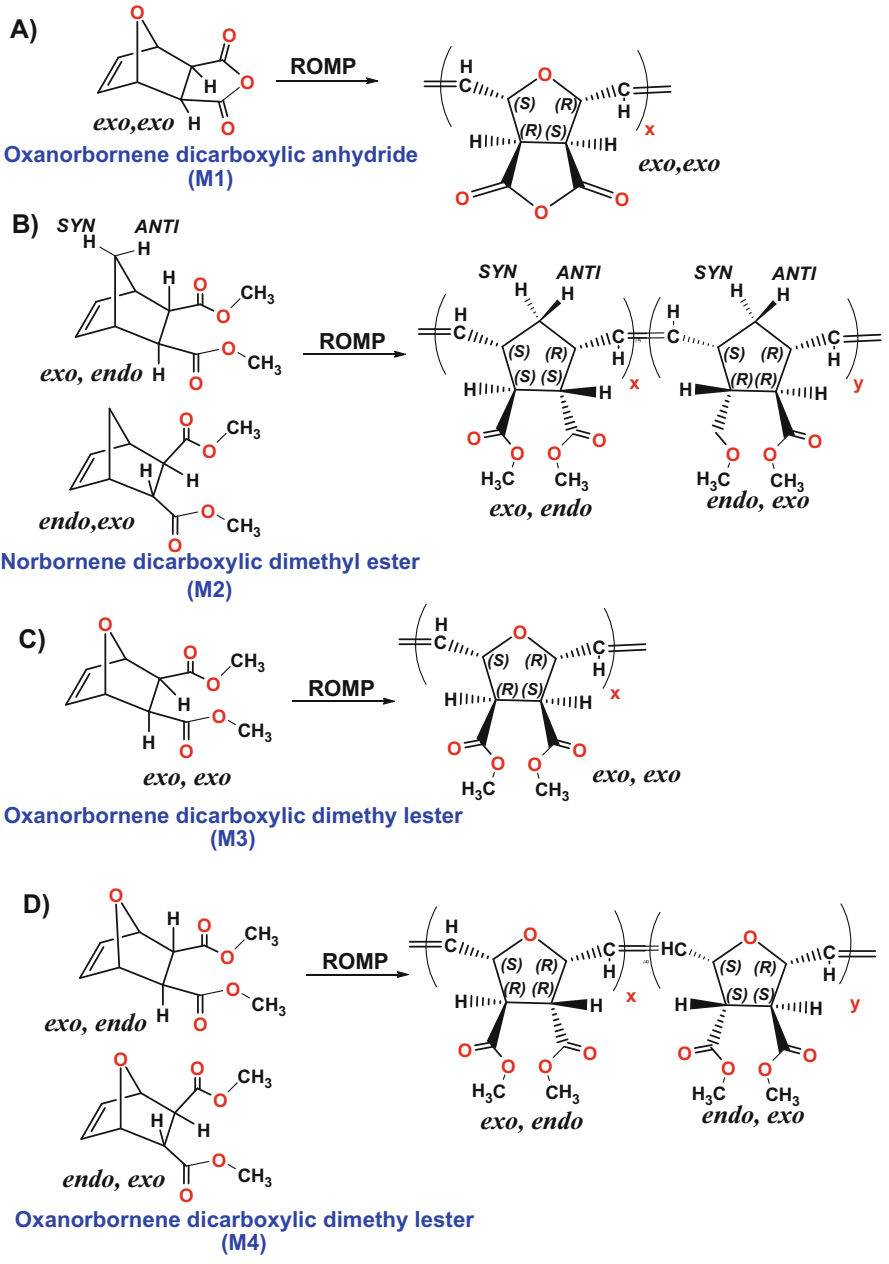

Scheme 6.9 Diastereomers and numbering designation of monomeric units used in this chapter (Adapted from [32])

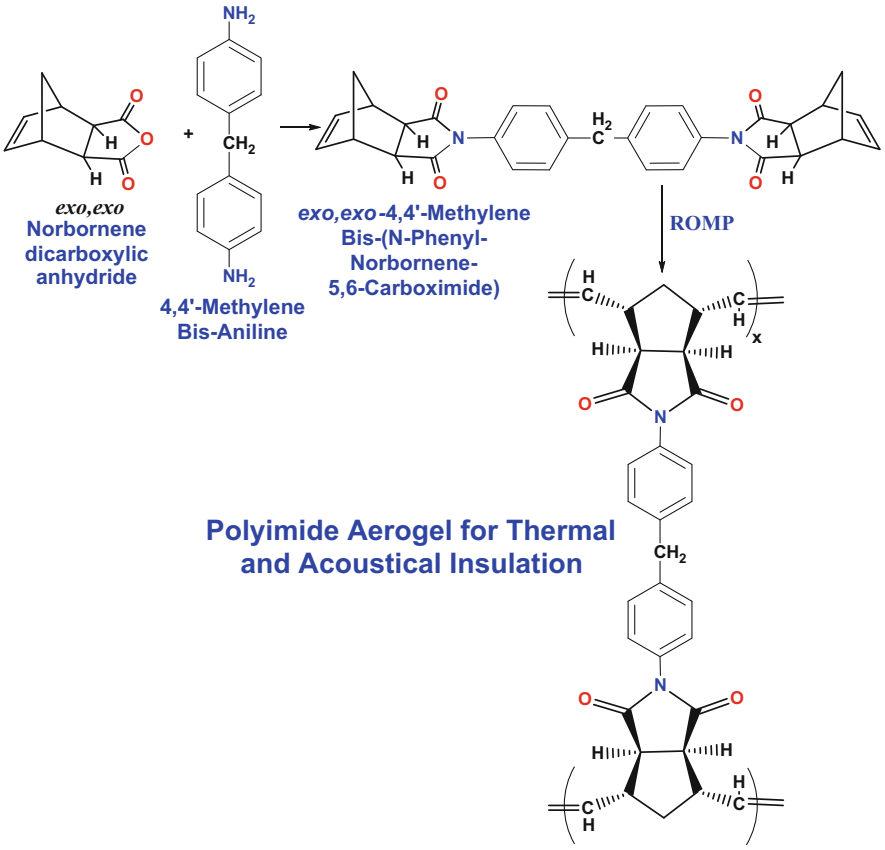

Scheme 6.10 Formation of cross-linkable ROMP monomers from norbornene dicarboxylic anhydride through maleimide chemistry to manufacture polyimide aerogels (Adapted from [34])

ROMP polymers produced from these monomers will translate these stereocenters into the polymer, resulting in the construction of a string of diastereomeric sequences along the polymeric backbone. This additional stereochemistry will affect the overall microstructure and physical properties of the resultant ROMP homopolymer. Forming copolymers from different comonomers can result in even higher-order complexity [32].

ROMP monomers based on maleic anhydride can also be ROMP cross-linkers too. For instance, Leventis and coworkers manufactured polyimide aerogels by utilizing a ROMP cross-linker from 4,4′ methylene bis(aniline) and norbornene dicarboxylic anhydride, as depicted in Scheme 6.10 [34]. This difunctional ROMP monomer generates a nanoporous solid with low thermal conductivity, high surface area, and excellent soundproofing properties. These polymeric materials are known to be very thermally and mechanically stable and could be useful in ballistic armor, and high temperature insulators, due to the rigidity of the molecule as a whole.

6.1.7 Microstructure of ROMP Polymers

The physical and chemical nature of ROMP polymers requires a thorough and comprehensive understanding on how these polymers are constructed on a molecular level. Although the polymerization mechanism is deceptively simple, the resultant ROMP polymers are quite sophisticated. The polyunsaturated backbone can give rise to *cis*/*trans* isomerization, *meso*/*racemic* tacticity, head/tail, tail/tail, or head/head linkages between monomers. All of these linkages or structures result in the polymer's conformation and susceptibility to subsequent derivatization reactions. Therefore, we need to dissect each component, one by one, to gain insight into the structural complexity of these interesting polymeric molecules.

Ring-opening metathesis polymerization using maleic anhydride-based 5,6-disubstituted norbornene or oxanorbornene-type monomers generate polymers with a polyunsaturated main chain; see Scheme 6.9. This backbone unsaturation can be in the *cis* configuration or the *trans* configuration or both. The *cis*/trans content can impact the final properties of the polymer. Utilizing both proton and carbon NMR analyses can quantify the level of *cis* double bonds and *trans* double bonds in the polymer [23, 24].

Generally, the *cis olefinic* proton is located at lower chemical shift than its *trans*-counterpart. In contrast, the *cis-1,4* bridgehead methine protons are located at higher chemical shift than its *trans*- companion [32]. The *cis and trans* content for these ROMP polymers can be resolved and quantified by these variations in proton and carbon NMR profiles.

Additional multiplicity is observed in the carbon spectra for ROMP polymers due to *meso* versus *racemic* dyads that relate to tacticity [23, 24, 94, 95]. Tacticity relates the orientation of the pendant groups relative to the main chain or polymer backbone. In a *meso* dyad, the pendant groups are on the same side relative to the polymer's backbone, while in the *racemic* dyad the pendant side chains are on reverse sides of the polymer's backbone or from the main chain; see Fig. 6.8a. For saturated polymers, this designation is straightforward and can relate to certain physical properties like surfactancy, crystallinity, or density.

Because ROMP polymers contain an unsaturated backbone, the *cis*/*trans* orientations do not directly equate to the *meso*/*racemic* orientations. Instead, tacticity relates to the orientation of either the protons on carbons 1 and 4 or, alternatively, the substituents on carbons 1 and 4 relative to the polymer's backbone or main chain. Each *cis* double bond can be either in the *meso* or *racemic* orientation. The same orientations are also available for the *trans* double bond. These orientations are illustrated in Fig. 6.8b, c.

The difference between the cis and trans double bond orientations can be related to the protons on carbons 1 and 4, highlighted in red in Fig. 6.8. In the *meso* orientation, all the protons on both monomers point in the same direction into the page in this case. All substituents point out of the page. As a result, there is an asymmetry along the chain where all the 1,4-protons are pointing in one direction or toward one face of the polymer molecule, while all the substituents are pointing in the opposite direction relative to the main chain (Fig. 6.8b).

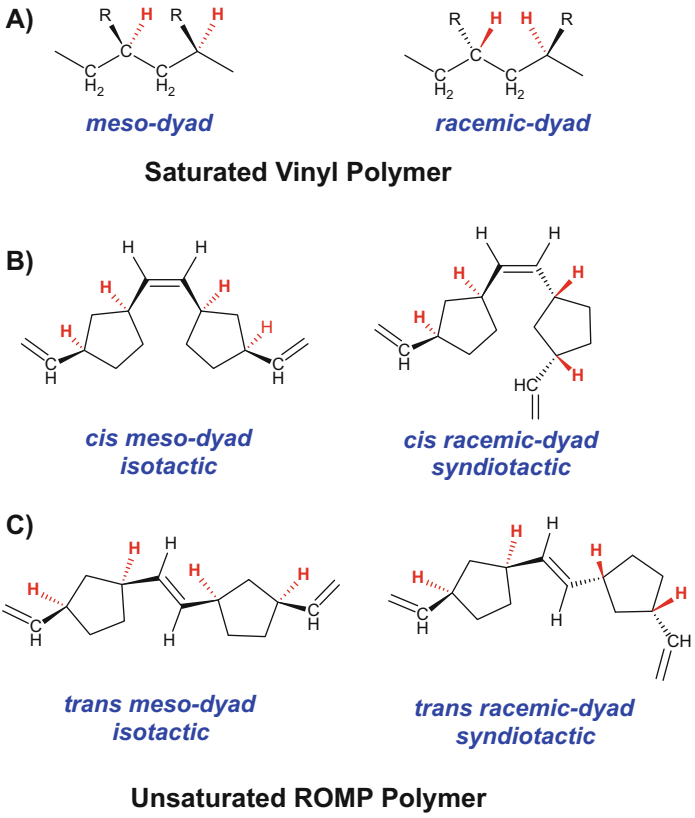

Fig. 6.8 Meso versus racemic dyad for: (**a**) saturated vinyl polymer, (**b**) unsaturated ROMP polymer in the cis-configuration, (**c**) unsaturated ROMP polymer in the trans-configuration

Conversely, the *racemic* dyad reveals one monomer's protons at positions 1 and 4 into the page. The next monomer's protons in positions 1 and 4 are pointing out of the page. This *racemic* orientation has protons or substituents oscillating back and forth in their directionality. Perhaps better described as facing forward or facing backward as one traverses along the main chain of the polymer, Fig. 6.8c. Note that *meso* or *racemic* dyads have nothing to do with the unsaturated double bond being *cis* or *trans*. The four isomeric structures are formed from an achiral ROMP monomer.

Additional complexity arises when head–tail, tail–head, head–head, and tail–ail dyad orientations are taken into account. In this case, an additional eight potential diastereomers are possible (Fig. 6.9). As each new monomer adds to the growing chain end, the number of potential diastereomers exponentially increases. In its simplest representation, with only head–tail linkages, the potential ROMP microstructures for triad sequences are depicted in Fig. 6.10. A detailed discussion on the observed microstructure for maleic anhydride-based ROMP polymers will be presented in the final section of this chapter. Clearly, ROMP polymers contain complex geometric isomers as part of their sequence and microstructure.

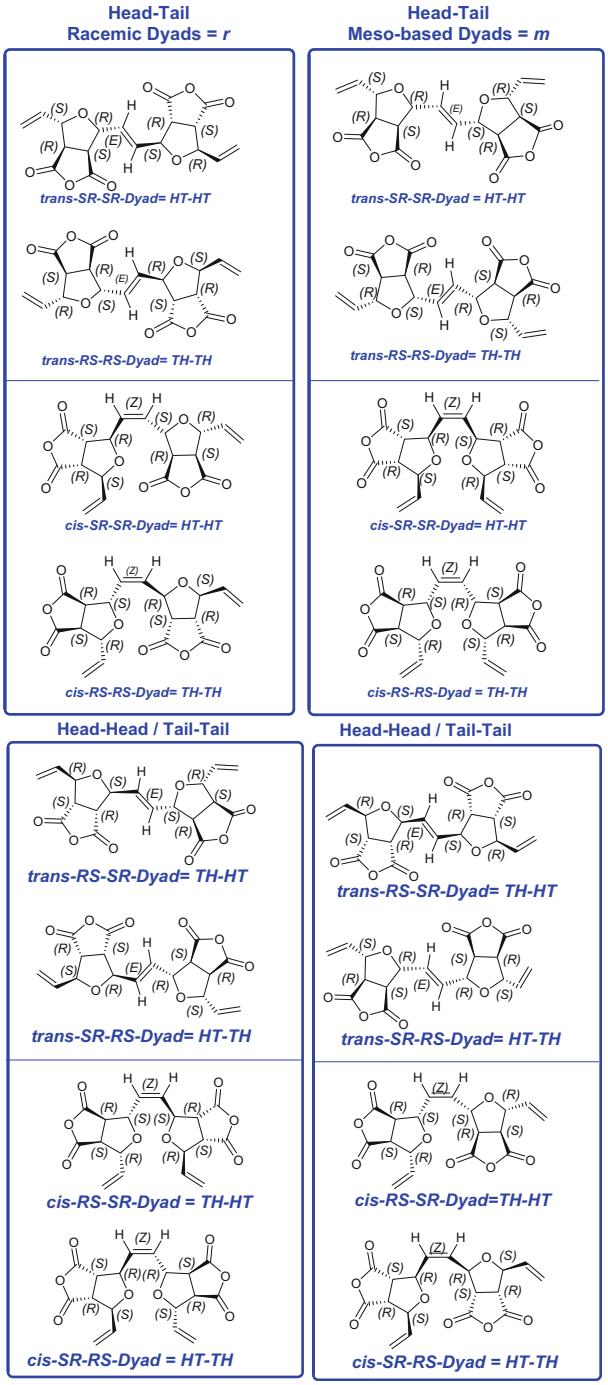

Fig. 6.9 Diastereomeric *cis*/*trans dyads* with head–tail, head–head, and tail–tail linkages (Adapted from [32])

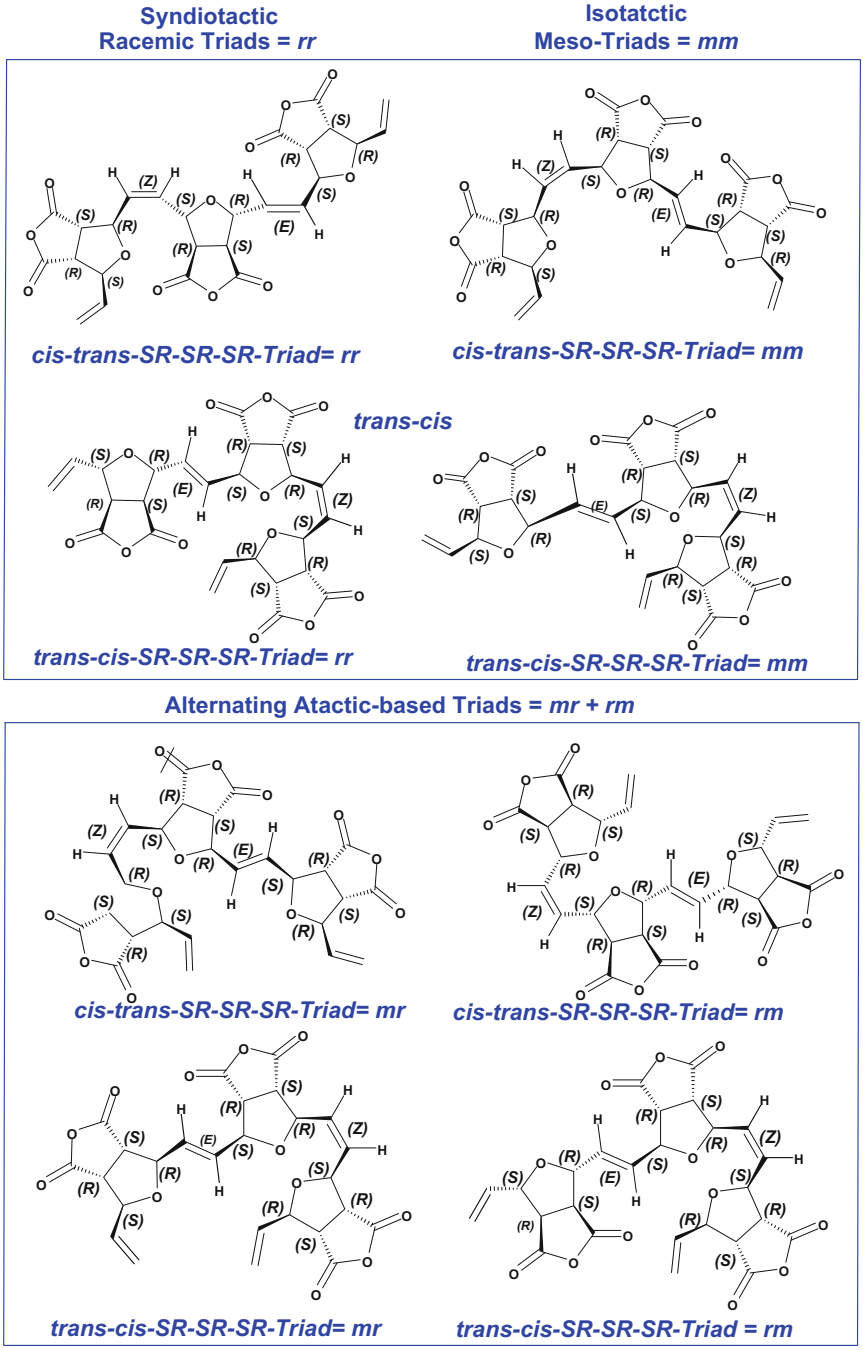

Fig. 6.10 Diastereomeric triads for alternating *cis*/*trans* and *trans*/*cis* adjoined by head–tail linkages (Adapted from [32])

6.1.8 *Aqueous ROMP as Green Chemistry*

As the demand for petroleum-based chemicals increases, while petroleum reserves decrease, an interest has accelerated in the use of chemicals from renewable resources. Furan, a chemical that can be produced from agricultural waste products such as corncobs or grain hulls from rice, oat, wheat bran, sugarcane, and sawdust, is one compound of particular interest. To produce furan, the waste streams from these agricultural products are boiled with dilute sulfuric acid to produce furfural. Furfural can then be decarbonylated by a palladium-catalyzed vapor-phase decarbonylation process and converted into furan, as illustrated in Scheme 6.11 [96].

Once the furan is obtained, a straightforward process to make 7-oxanorbornene dicarboxylic anhydride by its Diels–Alder adduct with maleic anhydride is possible. Many producers of maleic anhydride are also intensively researching ways to make it from renewable resources such as bio-derived 1-butanol or by furfural itself, but currently the processes are too costly to be economically viable [96, 97].

In the future when petroleum reserves are depleted, both of these processes will become more relevant for the synthesis of maleic anhydride and furan. This is an important point because ROMP polymers can be manufactured by totally renewable feedstocks and that by recycling the ruthenium catalyst it can be a way to make polyanhydride polymers using totally ***Green Chemistry*** in the future.

One complication in the ***Green Chemistry*** strategy is that most ROMP polymerizations are run in polar organic solvent, such as THF, DMSO, or methylene chloride. While ionic liquids have shown some promise in ROMP [28, 97], water would be more desirable. Water's low volatility, high heat capacity, thermal stability, and low toxicity make it the perfect solvent. However, most of the catalysts, particularly the Schrock catalyst, cannot be used with water. Many other catalysts exhibit limited water solubility. Similarly, most of the typical maleic anhydride-based ROMP monomers are not water-soluble either.

To overcome these hurdles, 7-oxanorbornene dicarboxylic acid and its water-soluble derivatives were designed for use in aqueous processes. To prevail over the issue of the water-insoluble ruthenium catalysts, water-soluble versions of

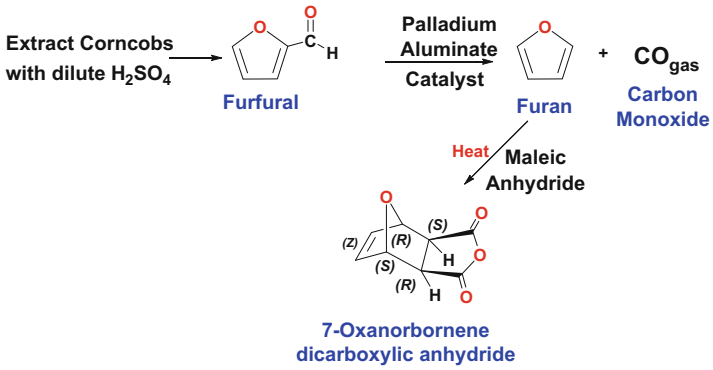

Scheme 6.11 Production of furan from renewable resources like corncobs, enabling the synthesis of *Green* ROMP monomer

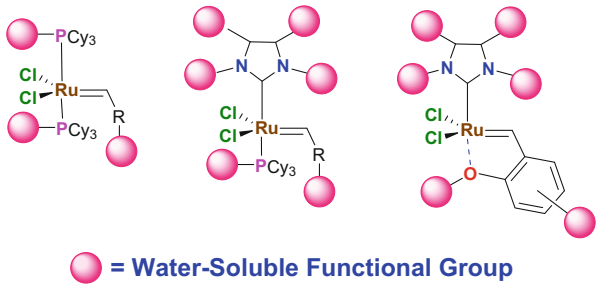

Fig. 6.11 Formation of water-soluble ruthenium catalysts (Adapted from [2])

ruthenium catalyst were developed. The Grubbs group first utilized ruthenium salts like $Ru(H_2O)_6$-di-tosylates [98], while Viswanathan and Jethmaini employed the ruthenium salts, $RuCl_3$-hydrate and $K_2RuC\ l_5$ [99].

While the ruthenium tosylates suffered from slow and inefficient initiation yielding erratic polymers [28], the $RuCl_3$ and K_2RuCl_5 salts did perform extremely well in aqueous ROMP. $RuCl_3$ and K_2RuCL_5 salts could even be recycled multiple times [99]. The authors demonstrated that an emulsion ROMP using 7-oxanornene dicarboxylic anhydride could be obtained in near quantitative yields, with slight preferences for *cis* double bonds over *trans* double bonds.

Given these findings, researchers investigated the use of emulsion polymerization techniques for ROMP employing surfactants, dodecyltrimethylammonium bromide in water, in the form of microemulsions [100–105]. While these polymerizations were successful, they were also prone to flocculation due to the heterogeneous nature of the medium.

To achieve a truly homogenous ROMP system, water-soluble functional groups were attached at various positions within the ruthenium catalyst families. This notion is illustrated in Fig. 6.11. This approach included attachment to the alkylidene group and/or to the ruthenium ligands. For first-generation catalyst, a maximum of three linkage points was constructed. For second- and third-generation catalysts, up to six linkage points to attach water-soluble groups were constructed.

Employing this strategy, the first true homogenous aqueous ROMP reaction was achieved using a water-soluble analog of first-generation Grubbs catalyst. In this case, Lynn, Mohr, and Grubbs synthesized phosphine ligands containing water-soluble quaternary ammonium groups, as depicted in Scheme 6.12 [106]. Although these catalysts significantly decomposed after two days in water, they were found to be somewhat stable in methanol. These catalysts were also very air sensitive in solution and decompose slowly when stored under air as a solid.

These two quaternary catalysts must be stored and used under an inert atmosphere with deoxygenated solvents. In water at pH = 7.0, the ROMP polymerizations do not proceed to complete conversion and yield polymers with a broad polydispersity index (PDI). The addition of hydrochloric acid dramatically increases the rate of polymerization, allowing for quantitative conversion of these monomers to polymers with narrow PDIs [106]. It is possible that the acid stabilizes the propagating species of the Grubbs catalyst by eliminating any hydroxide

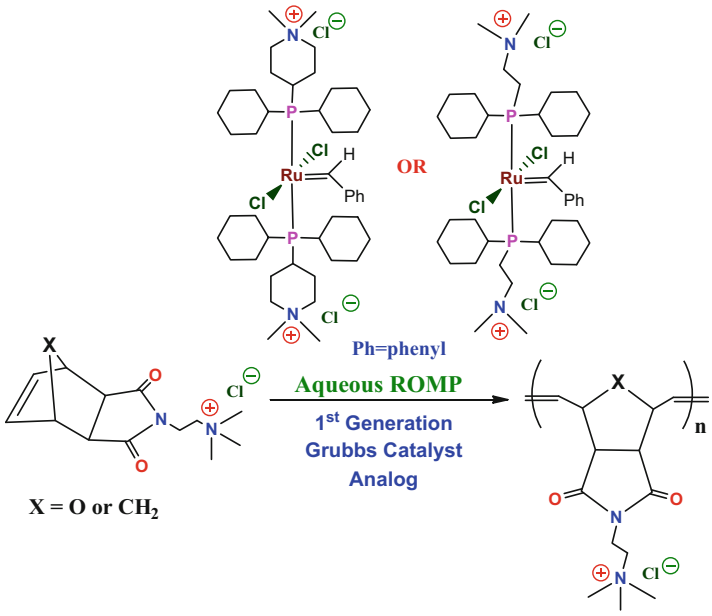

Scheme 6.12 Aqueous ROMP under homogenous conditions with water-soluble catalysts and water-soluble ROMP monomers (Adapted from [106])

produced by the autoprotolysis or phosphine deprotonation of water. Notably, under acidic conditions, ROMP with these catalysts is a living process and can be readily used to generate block copolymers.

In 2005, the first water-soluble second-generation Grubbs catalyst analog containing a PEG-substituted unsaturated NHC ligand was reported by Gallivan, Jordan, and Grubbs, illustrated in Scheme 6.13 [107]. While the initiator did catalyze ROMP, it was slow to initiate and was of limited utility. Once again, upon addition of hydrochloric acid, the polymerization rate dramatically increased. It was postulated that protonation of the free phosphine by the acid resulted in the inhibition of the reunion of the phosphine ligand to the ruthenium center [108].

In 2007, Jordan and Grubbs reported on the use of three new water-soluble first-generation Hoveyda–Grubbs analogs, as depicted in Schemes 6.14, 6.15, and 6.16, to overcome the slow initiation observed with the second-generation Grubbs catalyst analog in Scheme 6.13. To further test these new catalytic systems, they chose a very slow reacting *endo,endo* version of the water-soluble norbornyl-aminoethyl-trimethylammonium chloride monomer to perform ROMP as a demanding benchmark on the efficiency of the catalyst under investigation.

Although the ethoxylated Hoveyda–Grubbs catalyst in Scheme 6.14 did initiate ROMP, it still suffered from slow polymerization rates and flocculation of the catalyst itself out of the medium, similar to that observed with the second-generation Grubbs catalyst analog. It was proposed that the ethoxylated catalysts in Schemes 6.13, 6.14, and 6.15 behave as polymeric entities due to the PEG functionality, and this was responsible for the poor propagation rates observed in ROMP.

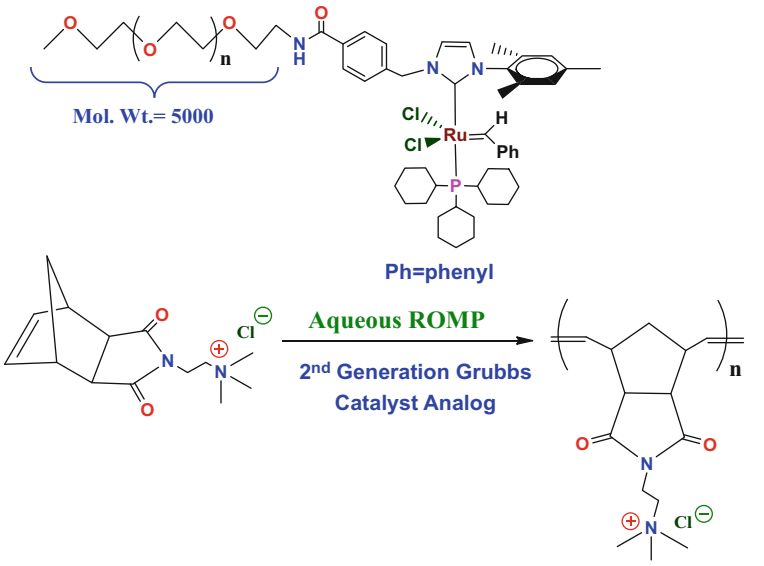

Scheme 6.13 Aqueous ROMP under homogenous conditions with water-soluble catalysts and water-soluble ROMP monomers (Adapted from [107])

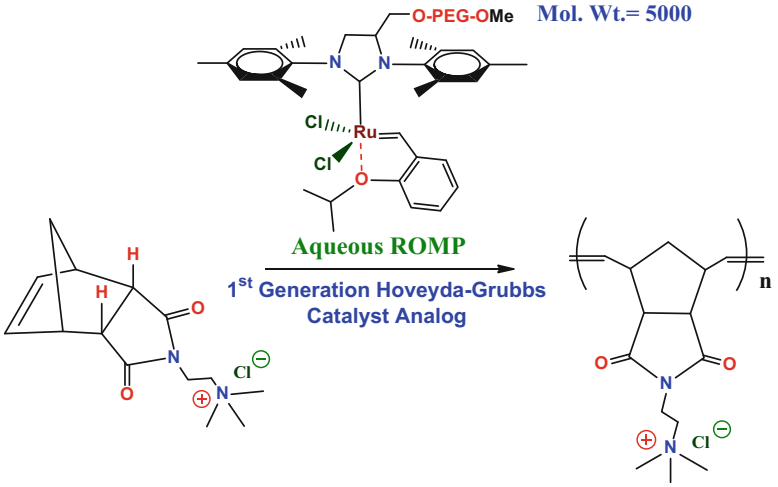

Scheme 6.14 Aqueous ROMP under homogenous conditions with water-soluble catalysts and water-soluble *endo,endo* ROMP monomers (Adapted from [109])

Two smaller analogs that were water soluble were constructed from the Hoveyda–Grubbs-based catalyst system. These are illustrated in Schemes 6.16 and 6.17. They included ammonium-based functionality onto the catalyst as either simple ammonium salts and/or quaternary ammonium salts.

Despite being water soluble, albeit at a very low level in water (<0.01 M in water), the catalyst depicted in Scheme 6.16 rapidly initiated and polymerized the

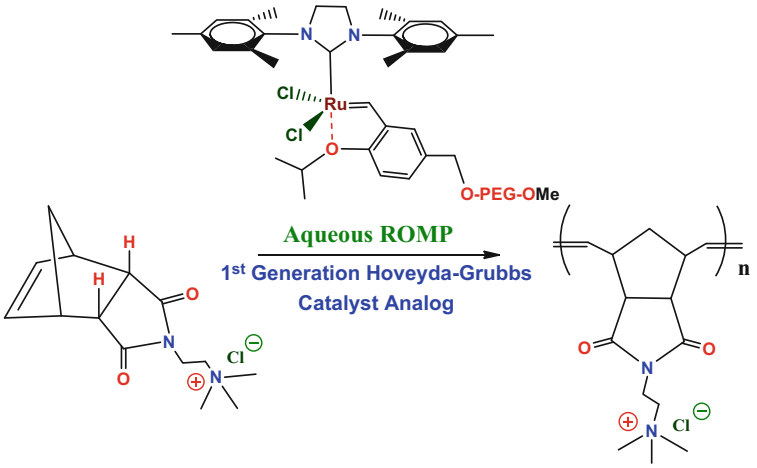

Scheme 6.15 Aqueous ROMP under homogenous conditions with water-soluble catalysts and water-soluble *endo,endo* ROMP monomers (Adapted from [109])

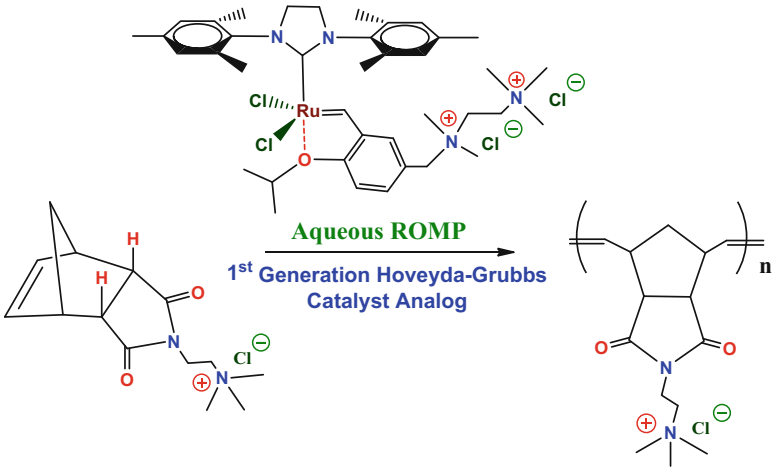

Scheme 6.16 Aqueous ROMP under homogenous conditions with water-soluble catalysts and water-soluble *endo,endo* ROMP monomers (Adapted from [109])

endo,endo-norbornyl analog. In contrast to the solubility behavior of the catalyst in Scheme 6.16, the catalyst illustrated in Scheme 6.17 is completely water soluble and also capable of rapid and efficient polymerization of the *endo,endo*-norbornyl analog by ROMP. This catalyst is phosphine-free and environmentally friendly. While it is challenging to synthesize this catalyst due to the presence of the primary amino group on the NHC ligand, requiring elegant protection and deprotection schemes using the tert-butyloxycarbonyl protection scheme better known as the BOC group, it indeed performed well as a ROMP catalyst.

Despite the superior water solubility of this catalyst, it did not enhance performance versus the poorly water-soluble analog in Scheme 6.16. This result suggests

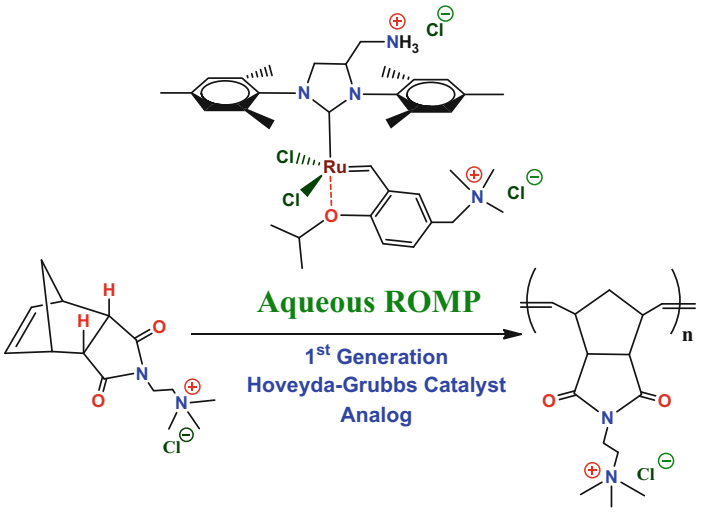

Scheme 6.17 Aqueous ROMP under homogenous conditions with water-soluble catalysts and water-soluble *endo,endo* ROMP monomers (Adapted from [109])

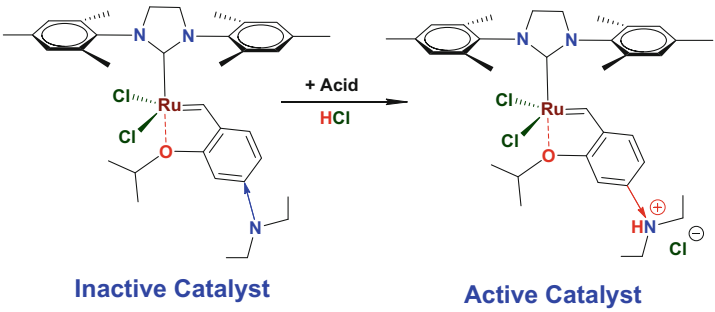

Scheme 6.18 pH-responsive activation of water-soluble ruthenium catalyst (Adapted from [110])

this catalyst may be less efficient. The apparent lower efficiency may be attributed to the presence of the weakly basic primary amine, potentially compromising the catalyst itself by poisoning the ruthenium center by intermolecular complexation with its vacant coordination orbital. It is well known that basic species can poison the ruthenium catalyst by such mechanisms [2, 9, 19].

A pH-responsive catalyst has also been constructed using this weakly basic amine behavior, as illustrated in Scheme 6.18. When unprotonated, the neutral amino group acts as an electron-donating group, and the catalyst is inactive. Lowering the pH enables the catalyst to activate because of the electron-withdrawing character formed upon protonation of the tertiary amino group [42, 110]. It is believed that the electron-withdrawing character of the ammonium group activates the catalyst due to weakening of the O–Ru bond.

Numerous monocationic ruthenium catalysts have been constructed (Fig. 6.12), and all were proficient in ROMP [111–113]. Dicationic betaines were also

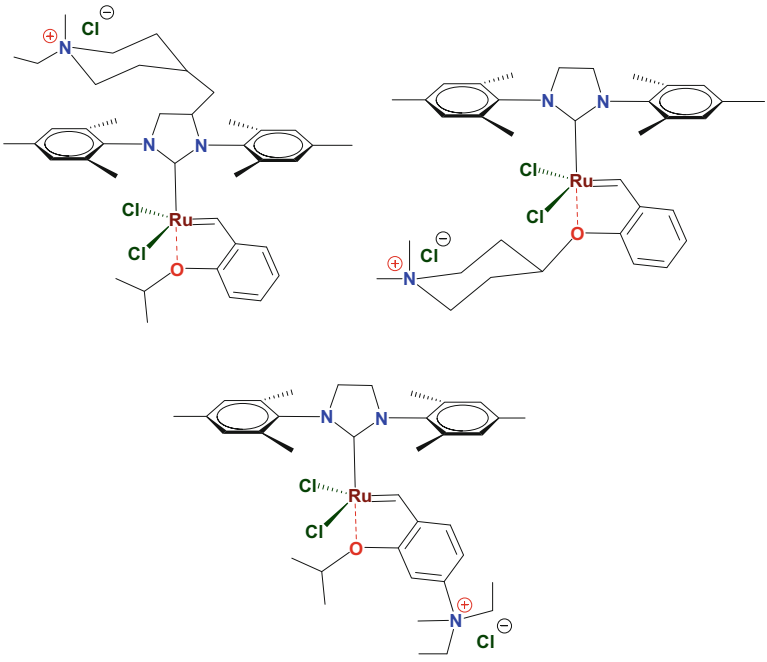

Fig. 6.12 Monocationic water-soluble ruthenium catalysts (Adapted from [110])

constructed where both the alkylidene and the NHC ligand were tagged. These catalysts are more water soluble, and the polar character ensures the water solubility can be maintained with the catalyst after initiation (Fig. 6.13) [42, 109, 114]. The betaine structure is preferred if a broad pH profile for the ROMP catalyst is desired. The amine structure provides for a more pH-responsive catalyst.

In contrast to the numerous cationic catalysts constructed that successfully initiate ROMP, anionic ruthenium catalysts have been slow to develop. Catalysts bearing sulfonate functionality have been constructed but do not participate in ROMP (Fig. 6.14). This has been ascribed to the smaller cone angle of the aromatic-(alkyl)-sulfonate groups, along with the instability of the catalyst itself. Direct addition of the sulfonate functionality to existing catalysts cannot be formed due to the liable halogens attached to the ruthenium center [106, 115]. Cationic ligands have predominated the landscape as useful catalysts for homogenous aqueous ROMP.

The water-soluble ruthenium catalysts, which are successful polymerization catalysts in water, exhibit similar solubility properties to the polymers they construct. Monomers that are water soluble are critical in successful homogenous aqueous ROMP. A number of water-soluble monomers can be constructed from maleic anhydride-based Diels–Alder adducts, most notably, norbornene dicarboxylic anhydride and its sister molecule 7-oxanorbornene dicarboxylic anhydride. These two monomers provide the foundation to numerous water-soluble ROMP monomer derivatives; see Scheme 6.19.

There are a large number of derivatives that can be constructed from the reactive anhydride functionality. These include diacids, diesters, diamides, half-esters, amic

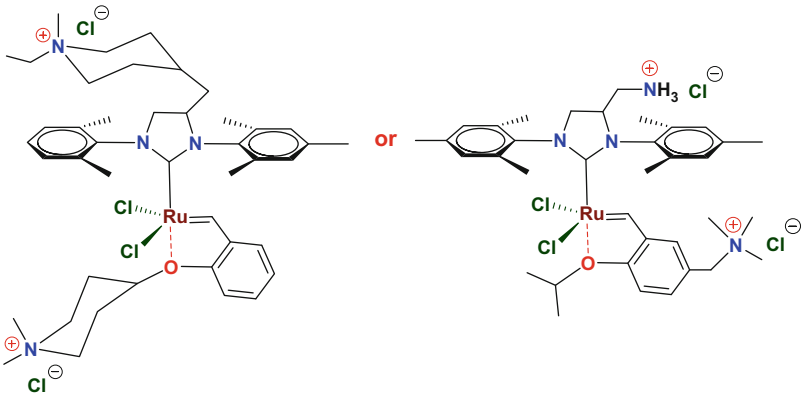

Fig. 6.13 Dicationic water-soluble ruthenium catalysts (Adapted from [109])

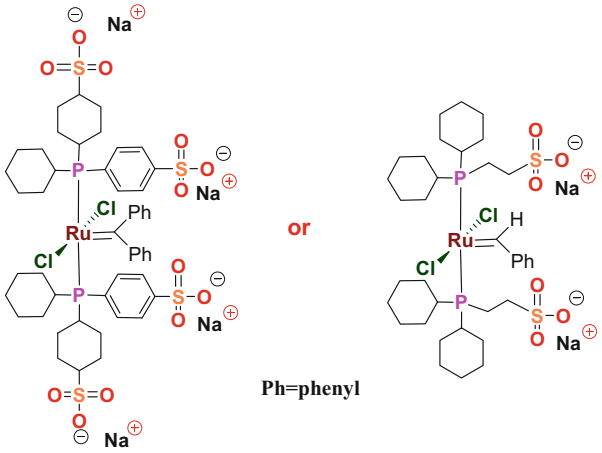

Fig. 6.14 Anionic water-soluble ruthenium catalysts (Adapted from [115])

acids, imides, as well as attachment of amino acids, proteins, polymers, sugars, polysaccharides, oncology agents, etc. These derivatives can be segregated into classes of molecules, as depicted in Fig. 6.15.

While the anhydrides illustrated in Scheme 6.19 are not water soluble, many of their derivatives are water soluble. In particular, if the molecule is water soluble and contains a reactive group (such as NH, OH, SH, etc.), then it can be attached to the fundamental ROMP anhydride and polymerized [2, 32, 41, 116–120]. ROMP polymers bearing anhydride groups have been constructed and further derivatized. This has enabled orthogonal coupling schemes to construct protein–polymer conjugates, polysaccharide–polymer hybrids, polymer–oncology agents, polymer–antibiotic, and polymer–steroid constructs useful in biomedical applications [121–124].

Currently, there are seven orthogonal methodologies for construction of polymer–protein conjugates by chemoselective reactions: Click chemistry, Heck,

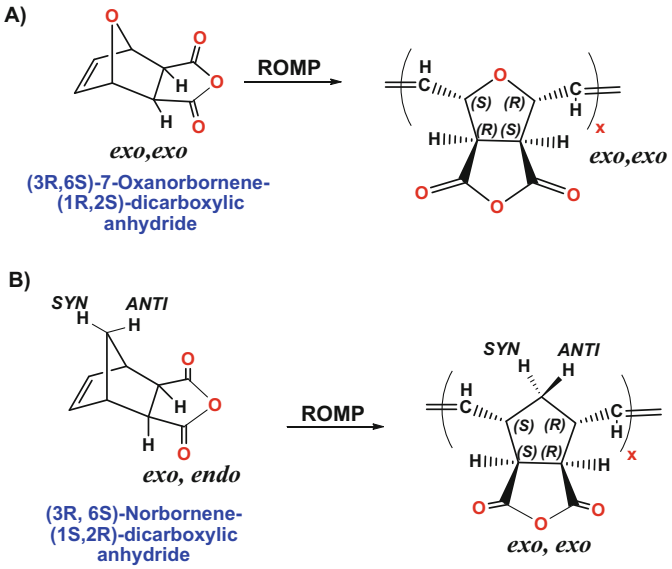

Scheme 6.19 Diels–Alder reactions between (**a**) cyclopentadiene and maleic anhydride and (**b**) furan and maleic anhydride

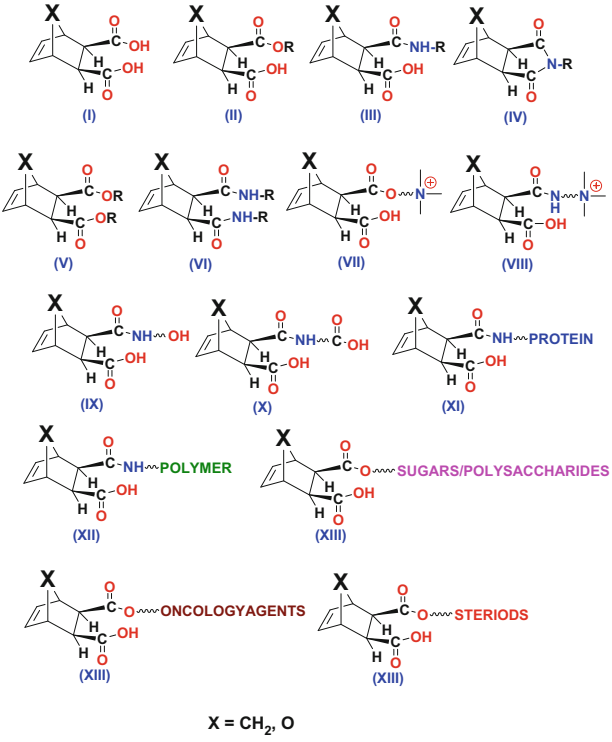

Fig. 6.15 Water-soluble maleic anhydride-based ROMP monomers

Diels–Alder cycloaddition, Sonogashira and Suzuki coupling, Staudinger ligation, Michael's addition, reductive alkylation, and oxime/hydrazone routes for the production of peptide/protein–polymer conjugates [121]. Three have been investigated for use with ROMP monomers and polymers. Schaefer and coworkers demonstrated that maleimide functionalization, active ester groups, and click functionalizations could all reside in the same ROMP polymer. This 3-in-1 ROMP polymer is capable of selectively coupling with three different substrates to form reactive polymer–substrate conjugates or hybrids [121].

6.2 Solid-Phase Supports for ROMP Synthesis

Two important factors have influenced the slow acceptance and use of ROMP technology in the commercial sector: catalyst cost and heavy-metal toxicological properties. To overcome the cost factor, a recyclable catalyst is desirable. Total removal of the transition metal after ROMP is completed would be ideal. If both could be achieved simultaneously, this would be the most preferred ROMP catalytic system.

Attachment of ROMP catalysts to solid supports has been intensively investigated as a means to filter out the ROMP catalyst from the medium after polymerization. This capability should enable the catalyst to be effectively recycled for the next ROMP polymerization, as illustrated in Scheme 6.20.

In Scheme 6.20, the ROMP catalyst is anchored to a solid support. The monomers are added for polymerization to ensue. Once the ROMP process is complete, addition of ethyl vinyl ether enables for detachment of the ROMP polymer from the ROMP catalyst. The catalyst is then taken away by filtration, and the polymer is

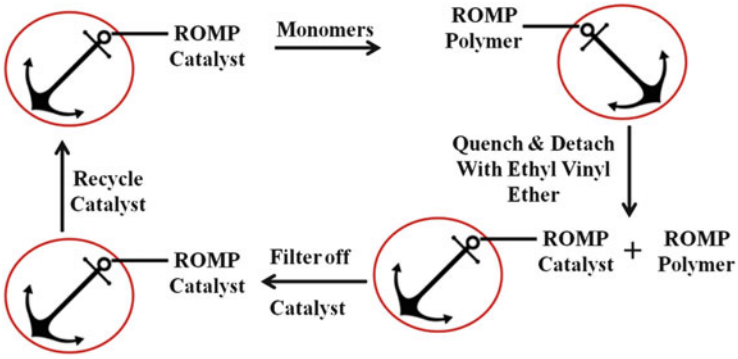

Scheme 6.20 Recyclable ROMP catalyst system attached to solid support

discharged. The free ROMP catalyst is recycled to prepare for the next ROMP polymerization.

While this concept is rather simple to envision, the actual practice is fraught with difficulties. For example, the ROMP catalyst must be anchored to a solid support by a stable bond that is secure throughout the process. Therefore, first-generation catalysts cannot be used. The attachment linkage between the catalyst and solid support must also be far enough away from the catalytic center so that the support does not impede the ROMP polymerization process. As the ROMP polymer forms, the ever increasing size of the polymer and steric hindrance slow down the rate of polymerization. The attachment point onto the solid support favors location on the surface of a solid particle. Attachments located within a swollen gel-like particle are less preferable because monomers must diffuse into the support particle for ROMP to proceed. As the polymer grows, it can plug the pore of the support particle, prematurely terminating the ROMP process.

Since surface modification of the support particle is preferred, the number of available sites is limited. Ideally, these sites don't hinder each other as the ROMP polymer forms. As a result, only a limited catalyst loading is used to properly space the catalytic sites enabling the ROMP process to proceed without interference from other sites. Given the limited number of surface sites for catalysis, more insoluble support particles are required to achieve a practical ROMP polymer yield. Increasing the number of insoluble particles present in the reactor may affect the viscosity of the ROMP slurry, reducing the effectiveness of mixing. Consequently, the use of more insoluble particles inside the reactor vessel can be problematic. If the growing polymer chains become entangled or the polymer is self-aggregating, the polymer can precipitate thereby affecting the solution viscosity. Both effects can be troublesome in batch mode processes.

Mechanical integrity of the support and the ROMP polymer shear stability, as frictional forces increases, are critical. Fracturing of particles into smaller sizes and/or catalyst disruption from the support or polymer by the stress-induced processing environment can be detrimental. Does the support behave like a solid sphere or does it deform easily as mixing pressures rise? How friable is the support?

These practical issues require a thorough process understanding to successfully implement an economically viable manufacturing process. Immobilized polymers onto solid supports have been prepared by either attaching a ROMP monomer, or a ROMP catalyst, onto an insoluble particle [125]. The solid support can be either organic, such as polymers, or inorganic such as surface-treated silica [126]. Early studies focused on attachment of the ROMP catalyst onto polystyrene or silica [127–131].

Barrett and Cramp demonstrated that with a simple cross-metathesis reaction, a vinyl-terminated polystyrene bead could easily attach Grubbs catalysts up to 3 mmol/g loading. Using this catalyst in a ROMP process with additional monomers added yielded a polystyrene core coated with a ROMP polymer. The product formed was a ROMP sphere; see Scheme 6.21. This coated ROMP sphere could be used in ring-closing metathesis reactions [128].

The Grubbs group attached ruthenium catalysts onto insoluble cross-linked polymer supports or silica particles (Fig. 6.16) [42]. These attachment points were on the NHC ligand, enabling the catalyst to remain attached to the insoluble support throughout the

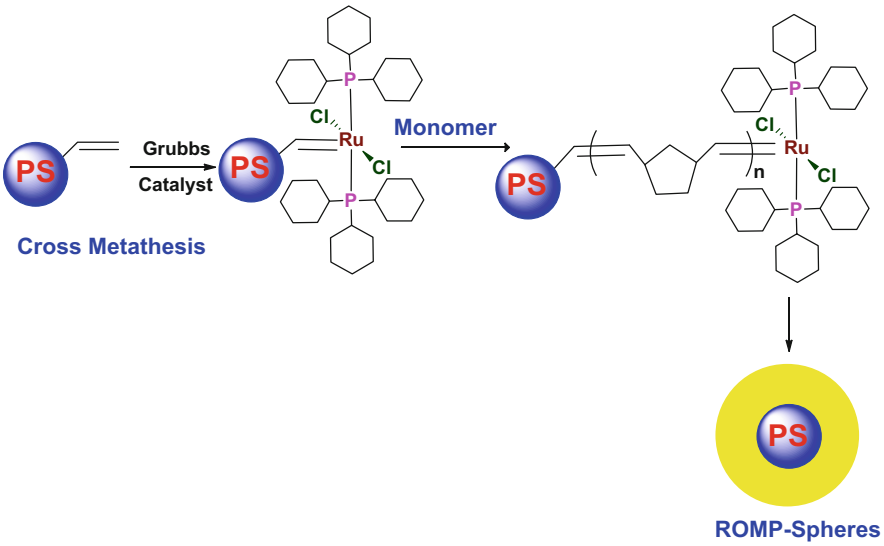

Scheme 6.21 ROMP catalyst system attached to polystyrene solid support in forming ROMP polymer coated polystyrene particles, ROMP-Spheres (Adapted from [128])

ROMP polymerizations, catalyst 15A, B, and D–F. The residual ruthenium level within the polymer product was 70 ppm. The catalyst was recycled from 5 to 20 times. In contrast, attachment of the insoluble support onto the third-generation Grubbs catalyst's isopropyl-benzylidene ligand results in the polymer chain remaining attached to the WANG resin during polymerization, catalyst 15C, while the ruthenium catalyst remains in solution. This effect results in a homogenous polymer product with higher molecular weight because the catalyst is no longer impeded by accessibility and steric factors that result in complex kinetics in ROMP polymerizations.

It was further proposed that the soluble ruthenium species are recaptured after monomer consumption by forming the more stable chelating isopropoxybenzylidenes. This notion gives rise to the boomerang-type catalysts reported in the literature [42]. However, since the polymer is attached to the insoluble support, the catalyst must be cleaved off to produce the desired polymer product. These types of catalyst are more suited for ring-closing metathesis reactions.

In more contemporary strategies for solid-phase ROMP synthesis, a ROMP monomer is attached to the insoluble support, while the ROMP catalyst is in solution. This strategy eliminates the issue of the catalyst accessibility. Since the polymer is attached to the solid support, one can wash out the ruthenium catalyst to much lower levels to less than 10 ppm. The soluble filtrate that contains the ROMP catalyst is more easily recycled and can be supplemented with fresh catalyst to maintain desirable kinetics and molecular weights.

Attachment of maleic anhydride-based ROMP monomers is particularly well suited for this task. For example, cross-linked resins bearing alcohol or amine functionality can be readily reacted with norbornene dicarboxylic anhydride or its 7-oxa analog to form esters or amide/imide linkages, respectively; see Schemes 6.22 and 6.23.

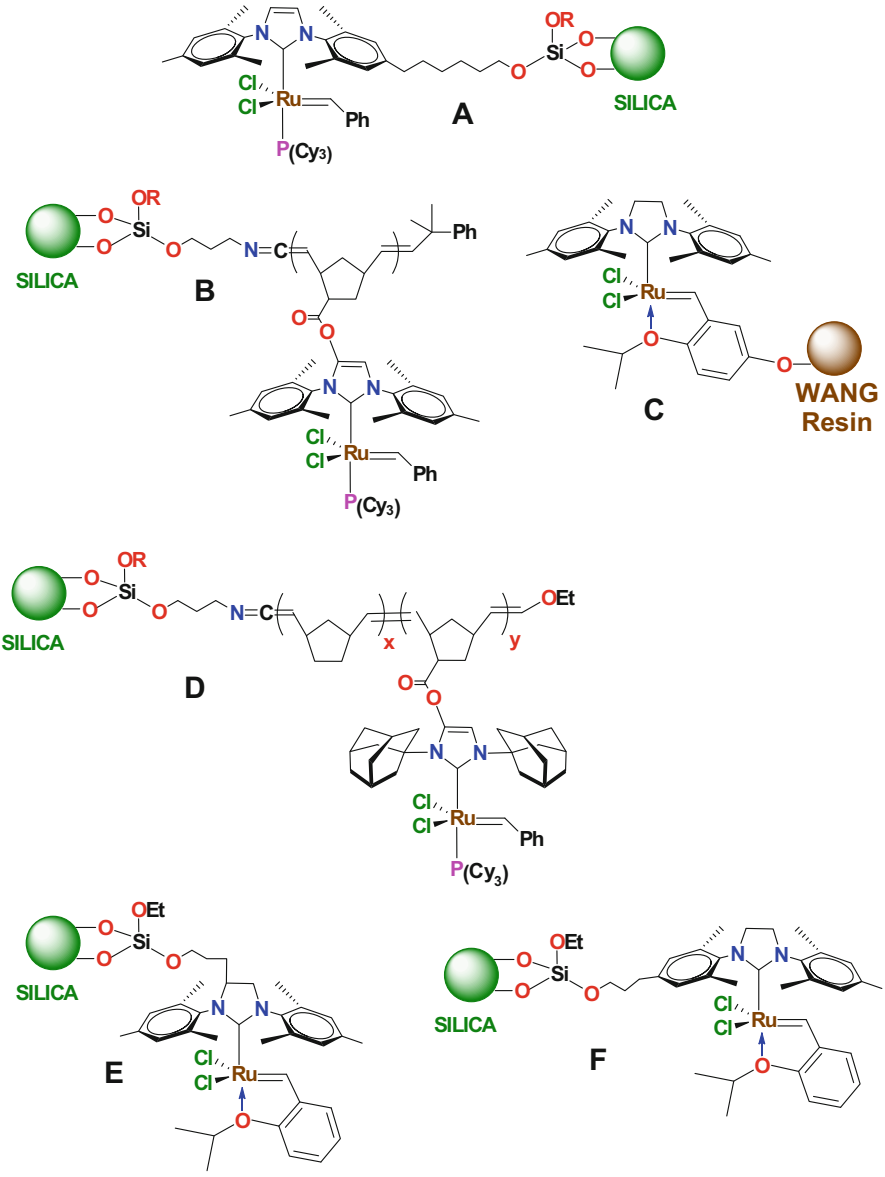

Fig. 6.16 Grubbs catalysts attached to silica or polymer supports (Adapted from [42])

After ROMP polymerization, the polymers can be released by treatment with caustic to free the polymer into solution. Saponification of the ester linkage releases the immobilized ROMP polymer from the silica support; see Scheme 6.22. Treatment with caustic and heat will cleave the amide/imide linkages from the amino-bearing cross-linked resin support; see Scheme 6.23.

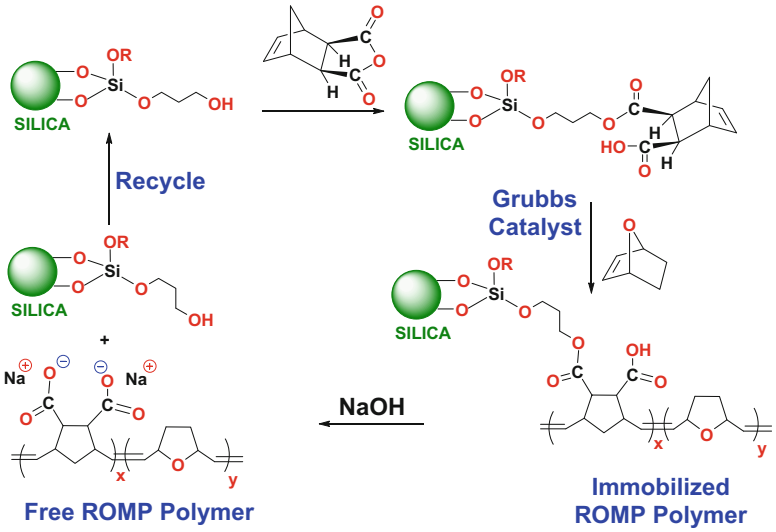

Scheme 6.22 Attachment of ROMP monomer to an insoluble silica support

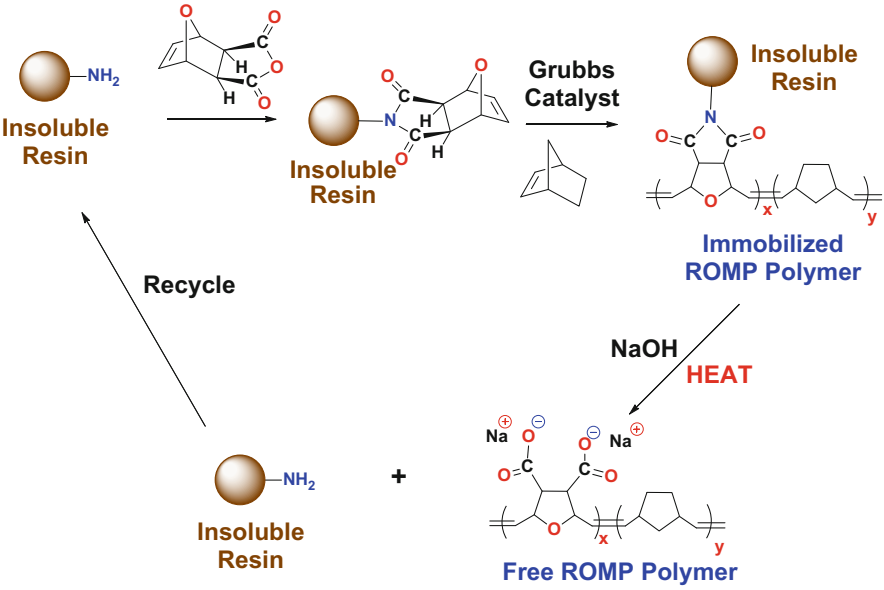

Scheme 6.23 Attachment of ROMP monomer to an insoluble polymer support

In cases where the anhydride or ester functionality needs to be maintained, a more sophisticated capture/release synthetic regime can be applied. This approach was reported by the Kiessling group in 2005 [125]. They used a maleimide-substituted norbornene analog, depicted in Scheme 6.24 as compound 24B, which

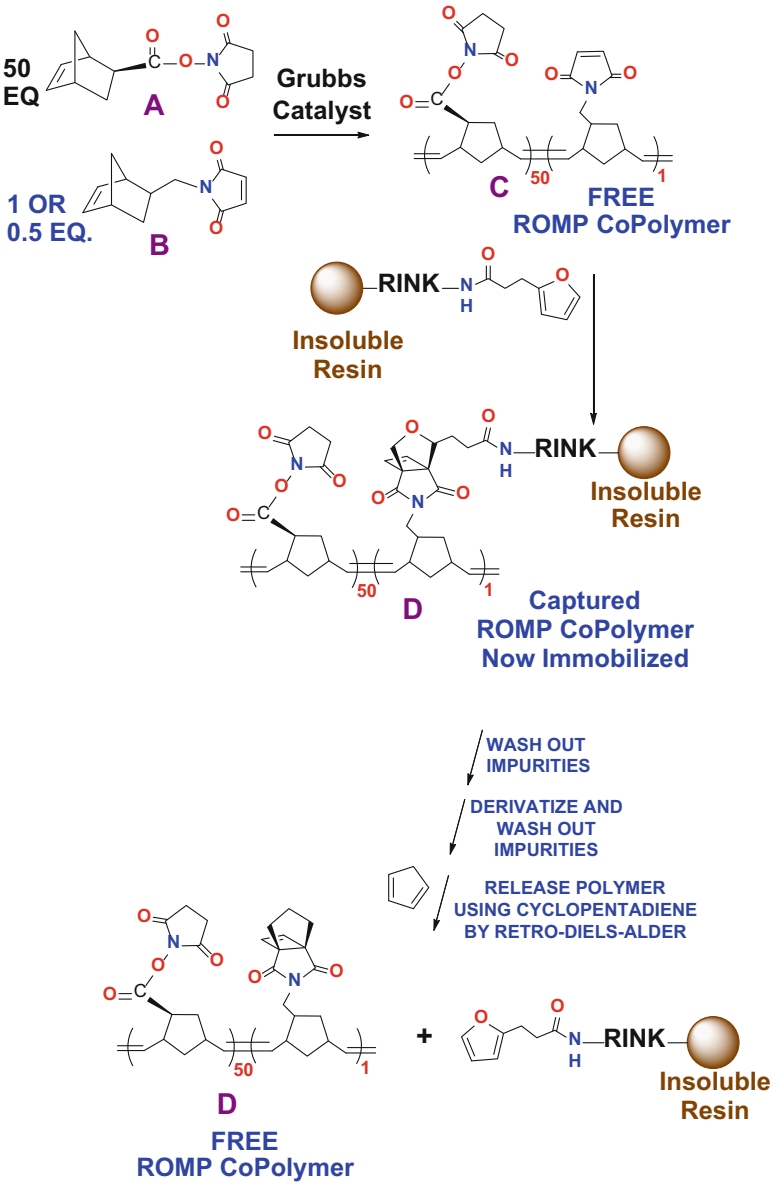

Scheme 6.24 Capture/release of ROMP polymer on an insoluble polymer support (Adapted from [125])

was copolymerized by typical ROMP in solution with Grubbs catalyst, at a level of 1–2 %.

The copolymer constructed now comprises maleimide groups that can be employed to capture the polymer in solution. The polymer is immobilized onto

the insoluble furan containing Rink amide polystyrene resin, compound 24C, by formation of its Diels–Alder adduct [125]. They also used microwave radiation to aid in this attachment and obtained 90 % yield in the capture of ROMP polymer onto their resin, 24 days. They also tested an end-functionalized maleimide derivative as a single-site capture mechanism. This approach only produced a 30 % ROMP polymer yield. Hence, multiple capture points along the ROMP polymer are more efficient when using this regime.

The immobilized ROMP polymer was washed free of ruthenium catalyst and further derivatized with amino-bearing functionality. The immobilized ROMP polymer is released from the insoluble resin support by a retro-Diels–Alder reaction, 24E. The key point is the reversible nature of the furan-based Diels–Alder adduct. These adducts also undergo retro-Diels–Alder reactions. Specifically, attachment of the ROMP polymer occurs because of a reversible Diels–Alder reaction between furan attached to the insoluble support and the maleimide–ROMP polymer for immobilization, and then after washing or further modification, the immobilized ROMP polymer is released from the resin by a retro-Diels–Alder reaction.

This strategy enables the ROMP polymer to be temporarily immobilized onto the insoluble support to remove unwanted impurities or catalyst residues completely. The polymer is then released back into solution while still maintaining its reactive substituents intact. Another important point is that while furan gives a reversible Diels–Alder adduct, cyclopentadiene does not exhibit the same capability. Therefore, a Diels–Alder adduct comprising cyclopentadiene is irreversible. This difference was expected to prove that predominantly all the ROMP polymer was released by this capture and release methodology using the formation and decomposition properties of the Diels–Alder reaction.

Many other solid-phase supports have been constructed for ROMP syntheses. These molecular conjugates are not only for synthetic purposes, but they can also be used for selective solid-phase extraction materials or surface modifiers such as molecularly imprinted polymers (MIPS). Examples employing ROMP polymers attached to an insoluble support include selective extraction of bisphenol A (BPA) from drinking water [132], preparation of chiral beta-cyclodextrin-grafted HPLC stationary phases [133], construction of smooth multilayered polymeric films with nanostructured thickness by solid-phase ROMP on solid surfaces [134], used in self-healing polymer composites [135], solid-phase extraction of trace metals [136], and metathesis polymerization-derived monolithic supports [137].

6.3 Ring-Opening Metathesis Polymerization of Monomers Containing Amino Acids, Peptide, and Protein Mimetics

Proteins are biopolymers constructed from chiral amino acids that mediate every function of biological life. Proteins are not only responsible for structural elements like muscle tissue but serve as catalytic functions responsible for enzymatic processes such as metabolism, anabolism (building up), and catabolism (breaking down) of fuel sources, thereby converting them into required molecules like proteins, polysaccharides, fats, steroids, hormones, and the construction and replication of DNA. While DNA is the informational library in biology, its real value is only truly recognized by the proteins they code for.

Proteins are also natural biodegradable macromolecules. These macromolecules can serve to provide immunity by antibodies, providing for a self-defense mechanism against disease. They influence intracellular and intercellular signaling, conversion of fuel into energy, and homeostasis (control of body temperature, metabolism, replication and repair, neural capacity). A thorough understanding of proteins is necessary to comprehend their function and can be manipulated to influence their function. This understanding can further enable control of all biological processes.

Construction of synthetic proteins to control a particular aspect of human life, or as therapeutic agents, is highly desirable. While proteins may comprise 50–150 amino acids residues in length, often only a handful of amino acids (3–7) are required for its function. The remaining portion is responsible for positioning these critical amino acid residues in the correct 3D orientation for function. Synthetic polymer–protein hybrids composed of amino acids or peptides that can be positioned by a controlled polymeric architecture are desirable [138–142].

Another extremely important factor is that 9 out of the 20 naturally occurring amino acids must be obtained by diet. Biological systems have developed to actively transport these essential amino acids into the cells. These include histidine, lysine, methionine, phenylalanine, tryptophan, threonine, and the alkyl side chains of leucine, isoleucine, and valine. Among these needed amino acids are the basic side chain residues, histidine and lysine. It is believed that the basic side chain and its resulting cationicity aid in its recognition and transport across the cell membrane [138, 139].

This active transport of basic amino acids in the body is important in that it provides a transport system for drug delivery. In one example, HIV (human immunodeficiency virus) responsible for AIDS (acquired immunodeficiency syndrome) capitalizes on this transport system to deliver its si-RNA into the cell for infection. The protein HIV1-TAT protein that complexes the si-RNA contains a sequence of basic amino acid residues based on lysine (designated K) and arginine (designated R), RKKRRQRRR. This amino acid sequence is recognized by the cell surface and actively transported across the cell membrane thereby infecting the cell unknowingly [138].

Incorporation of amino acids or peptide functionality is straightforward with maleic anhydride-based ROMP monomers like norbornene dicarboxylic anhydride and its sister molecule, 7-oxa norbornene dicarboxylic anhydride (Scheme 6.19).

Another advantage of ROMP is its tolerance to the polar groups found in the amino acid side chains, such as hydroxyl, carboxy, amide, and ester functionalities. Temporary protecting groups for the amino, guanidine, imidazole, and thiol functionalities are available from solid-phase peptide synthesis methods [139].

Amino side chains of lysine, arginine, and histidine can be temporarily masked with the t-butoxycarbonyl (BOC) protecting group by the formation of a urethane linkage. The thiol of cysteine can be masked by the S-4-methoxybenzyl group (Scheme 6.25). All of these groups can be cleaved by acid, such as trifluoroacetic acid (TFA)/trifluoromethanesulfonic acid (TFMSA) blend to yield the free amino acid. This strategy enables for regiospecific bond formation with the alpha-amino group, while preventing any side chain side reactions.

Employing this masking strategy, amino acids and peptides attached to ROMP monomers were investigated. The first amino acid monomers tested in ROMP contained nonreactive side chains, like alanine (methyl side chain), glycine (no side chain just H), or isoleucine ($-CH(CH_3)CH_2CH_3$) [140]; see Scheme 6.26. They were constructed from norbornene dicarboxylic anhydride to form the imidized ROMP monomer and then polymerized with Grubbs catalyst.

In addition to actual amino acids bearing ROMP monomers, oxanorbornene-substituted amino acid mimetics were also constructed. These molecules were designed to be simple yet capable of mimicking the essential structure of the amino acid. These types of molecules are usually less costly, easier to synthesize, and more stable than their natural counterparts. For example, a lysine-mimicking ROMP monomer has been constructed using a BOC protection scheme from oxanorbornene dicarboxylic anhydride; see Scheme 6.27 [141, 142].

Utilizing a BOC-protected amino alcohol and oxanorbornene dicarboxylic anhydride produces the monoester ROMP monomer. This monomer can be further esterified with carbodiimide and alcohol, as depicted in Scheme 6.27. ROMP polymerization produces the lysine-like ROMP polymer. Deprotection with trifluoroacetic acid generates the lysine mimetic ROMP polymer [141, 142].

In a similar theme, the Tew group reported on the use of an arginine mimetic specifically designed toward an active transport system [138]. deRonde and Tew synthesized two arginine mimetics based on oxanorbornene dicarboxylic anhydride; see Schemes 6.28 and 6.29.

These arginine mimetic oxanorbornene molecules exhibited controlled molecular weights spanning 5.5–21.8 kDa, with polydispersities ranging 1.08–1.17 and were successful in delivering fluorescently tagged si-DNA into Jurkat T cells [138]. Additionally, the bis-arginine mimetic polymers induced minimal cell death of the T cells.

Other designs followed, such as attachment of whole peptides onto the ROMP monomer [143, 144]. These include cell adhesion promoting amino acid sequences RGD from their one-letter code corresponding to arginine–glycine–aspartic acid tripeptide of elastin onto norbornene dicarboxylic anhydride. These peptide-bearing monomers were then polymerized with second-generation Grubbs catalyst [144]. This ROMP polymer also incorporated polyethylene glycol-norbornene dicarboxamide monomers to ensure water solubility of the whole construct, as well as BOC-protected ethylenediamine–norbornene dicarboxamide units, for post-polymerization cross-linking; see Scheme 6.30.

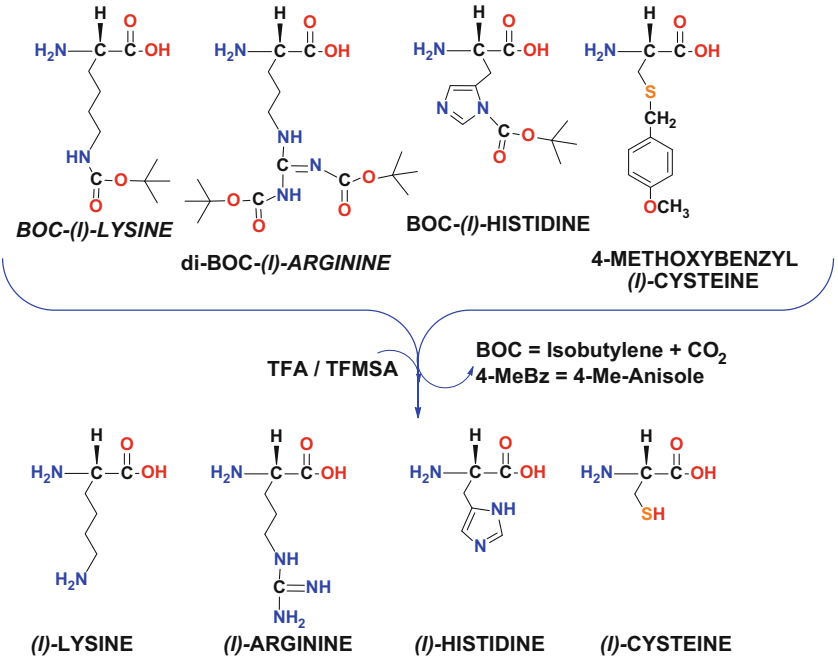

Scheme 6.25 Temporary masking of reactive functionality on amino acid side chains and their removal by TFA/TFMSA

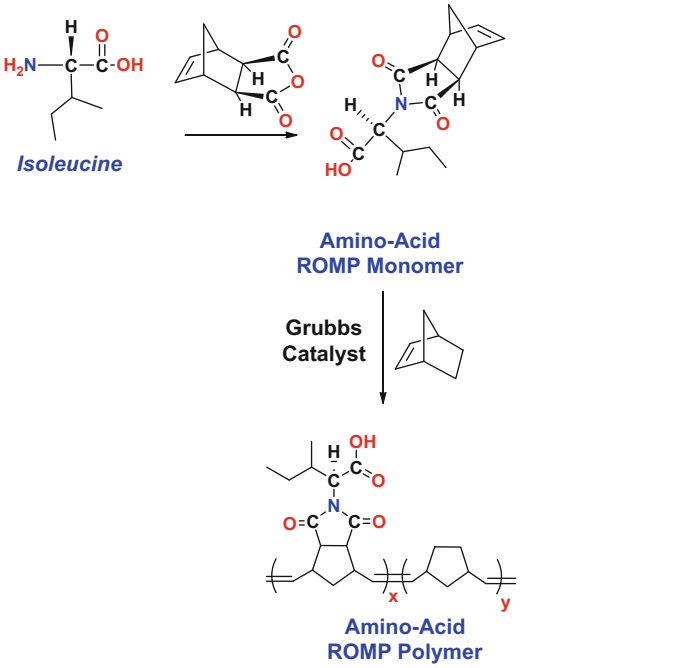

Scheme 6.26 Construction of ROMP polymer with amino acid side chains (Adapted from [140])

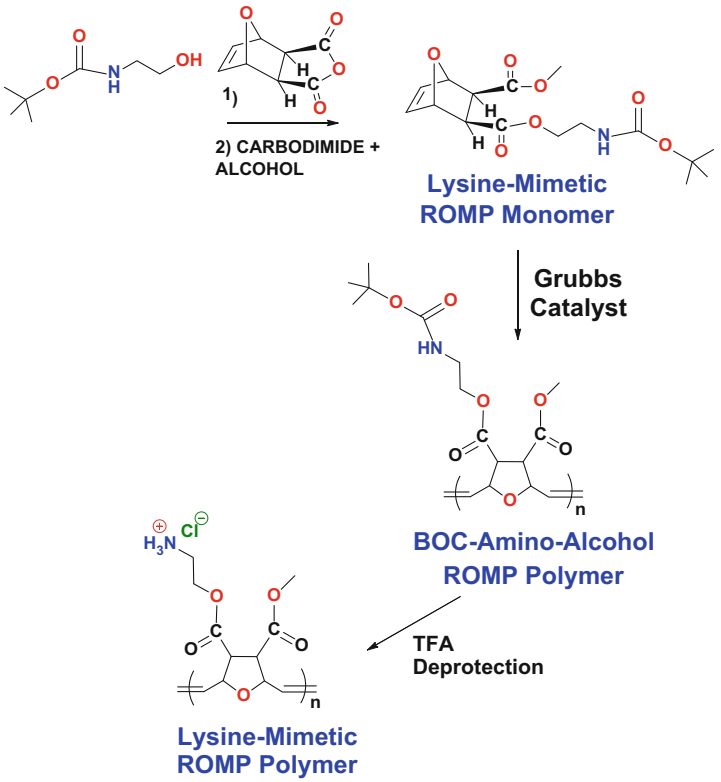

Scheme 6.27 Construction of ROMP polymer with lysine mimetic side chains (Adapted from [141, 142])

This construct exhibited biological recognition to the cells' surface and integrin binding. The construct maybe used as a diagnostic reagent in cell proliferation like that in cancer recognition [144]. Hahn and coworkers attached a series of hydrophobic and hydrophilic peptide sequences onto norbornene dicarboxylic anhydride and copolymerized these monomers by ROMP [145]. The block copolymers still exhibited very low polydispersities spanning 1.05–1.20 with average molecular weights ranging 28–44 kDa. These copolymers still retained their biological activity as evidenced by their ability to be enzymatically processed by a disease-associated enzyme; see Scheme 6.31.

While these studies demonstrated the utility of ROMP to construct polymer–peptide hybrids that retained their biological activity, a simpler approach to these types of conjugates is desirable. A reactive ROMP polymer that could also attach proteins onto ROMP polymers would be ideal.

In 2012, Schaefer and coworkers demonstrated that maleimide groups, active ester groups, and click-functionalized-based monomers could be incorporated into one ROMP polymer. This resulted in a 3-in-1 reactive coupling polymer, Schemes 6.32 and 6.33 [121].

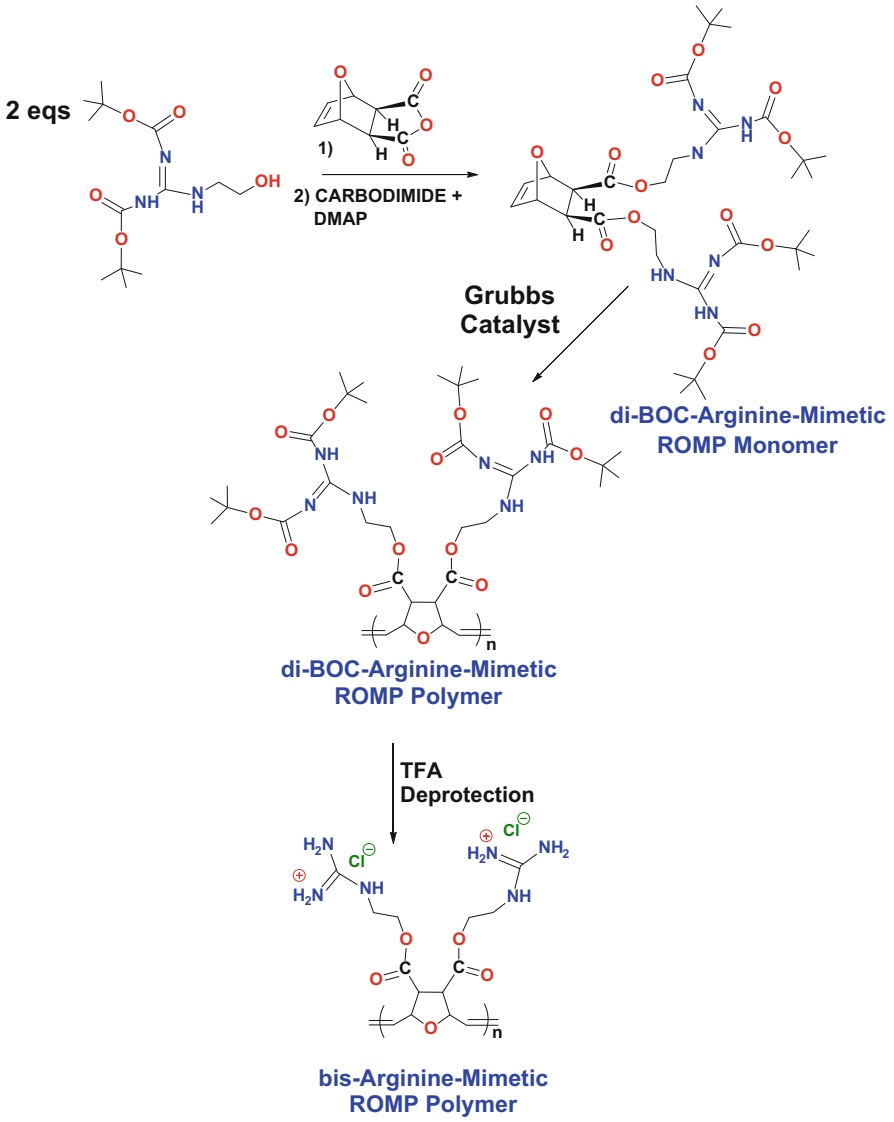

Scheme 6.28 Construction of ROMP polymer with bis-arginine mimetic side chains (Adapted from [138])

Synthesis of the maleimide–norbornene ROMP monomer is achieved by reacting oxanorbornene dicarboxylic anhydride with ethylene diamine and heat to imidize. This is followed by addition of maleic anhydride and heat to complete the second imidation route to produce the maleimide group off norbornene dicarboxamide ROMP monomer (Scheme 6.32a). The active ester moiety was constructed from oxanorbornene dicarboxylic anhydride with hexanol followed

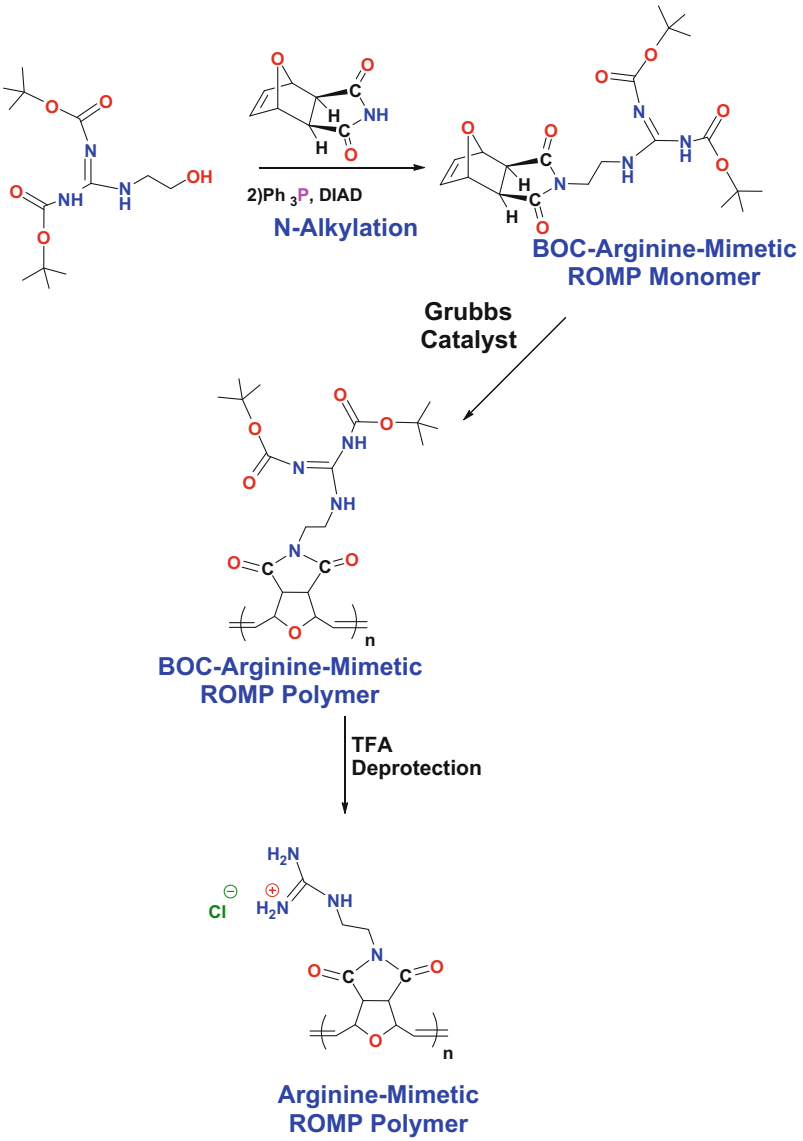

Scheme 6.29 Construction of ROMP polymer with arginine mimetic side chains (Adapted from [138])

by oxalyl chloride coupling with pentafluorophenol (Scheme 6.32b). Lastly, click functionalization was achieved by imidation of oxanorbornene dicarboxylic anhydride with ammonium hydroxide, followed by *N*-alkylation with a tosylated silyl-protected alkyne; see Scheme 6.32c.

ROMP polymerization of these three monomers with first-generation Grubbs catalyst yielded statistically random terpolymers and block copolymers with excellent control over their molecular weight and moderate control over their

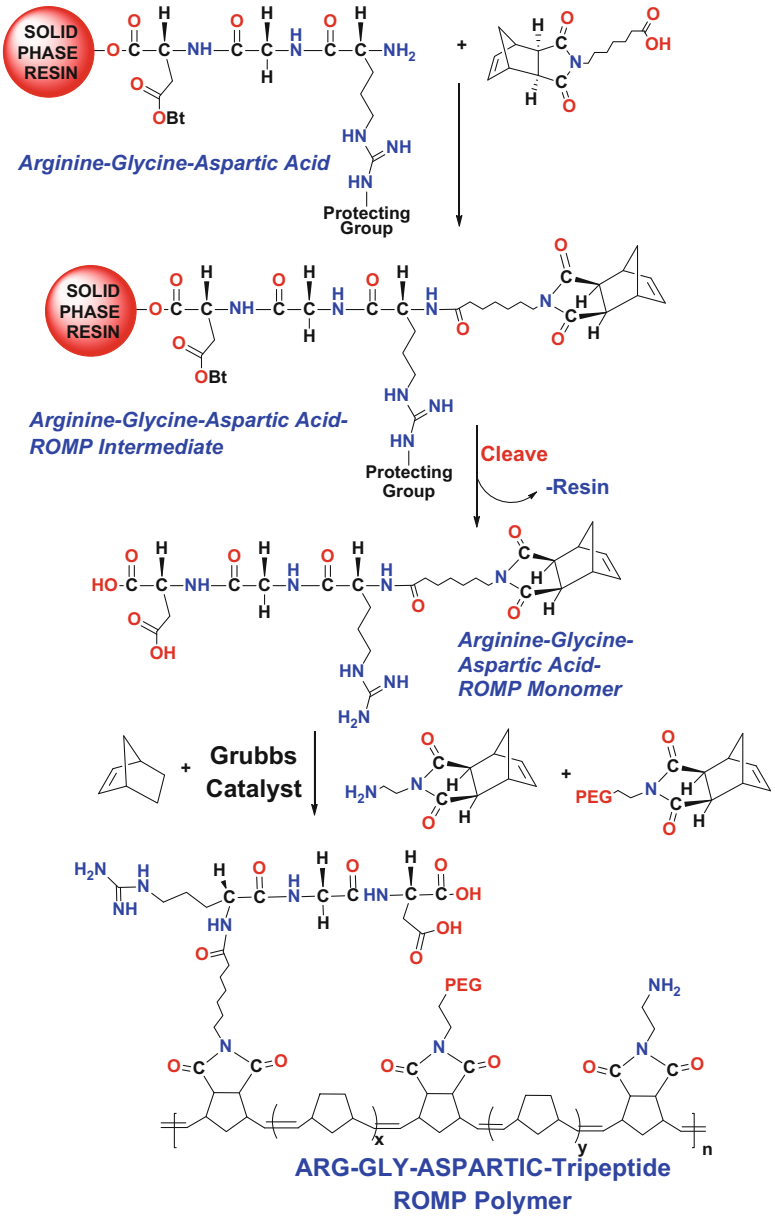

Scheme 6.30 Construction of arginine–glycine–aspartic acid ROMP polymer for cell adhesion to tumor cells (Adapted from [144])

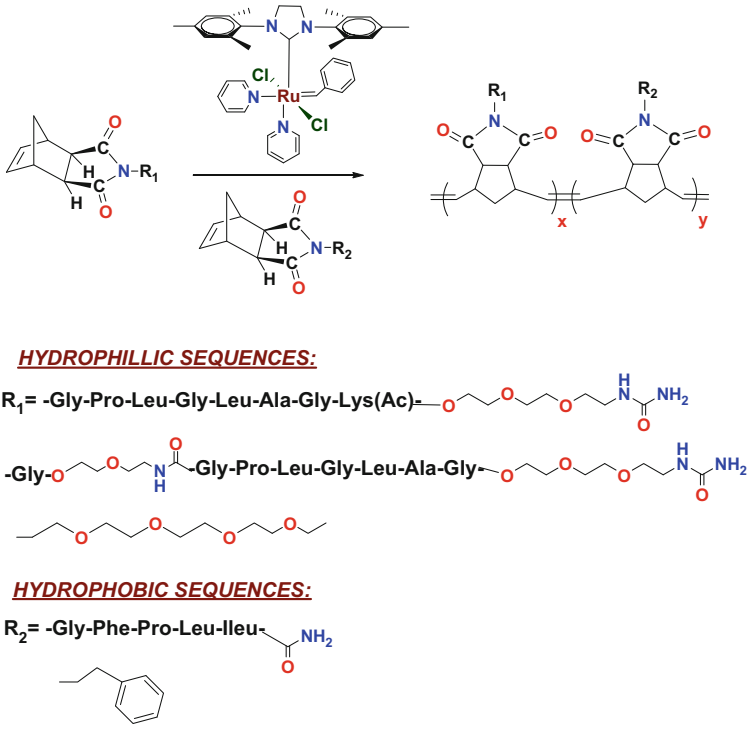

Scheme 6.31 Construction of amphiphilic ROMP block copolymers with hydrophilic and hydrophobic peptide sequences (Adapted from [145])

polydispersity. In particular, average molecular weights spanned 13.7–16.2 kDa, with polydispersity values ranging 1.29–1.48. The terpolymer with all three orthogonal reactive monomers exhibited a molecular weight of 10.8 kDa with a polydispersity of 1.41.

Once this terpolymer was constructed, it was envisioned that the polymer would be capable of selectively coupling with three different substrates to form reactive polymer–substrate conjugates or hybrids. This polymer could be targeted to attachment of proteins with one type of chemistry, attachment of a fluorescent tag with another chemistry, and finally cross-linking to a solid substrate with another chemistry [121]. This 3-in-1 hybrid could be an interesting diagnostic agent, a therapeutic delivery system, and an imaging agent.

To test the compatibility of the three target chemistries within this one polymer, target model compounds were tested. One contained a thiol for maleimide attachment, another comprised of an amine for coupling to the active ester, and finally an azide model compound was reacted with the free alkyne to generate the desired triazole adduct with a copper catalyst as the click attachment.

The authors found that the amine model substrate would react with both the maleimide and the active ester moieties. This finding indicated that the first reaction

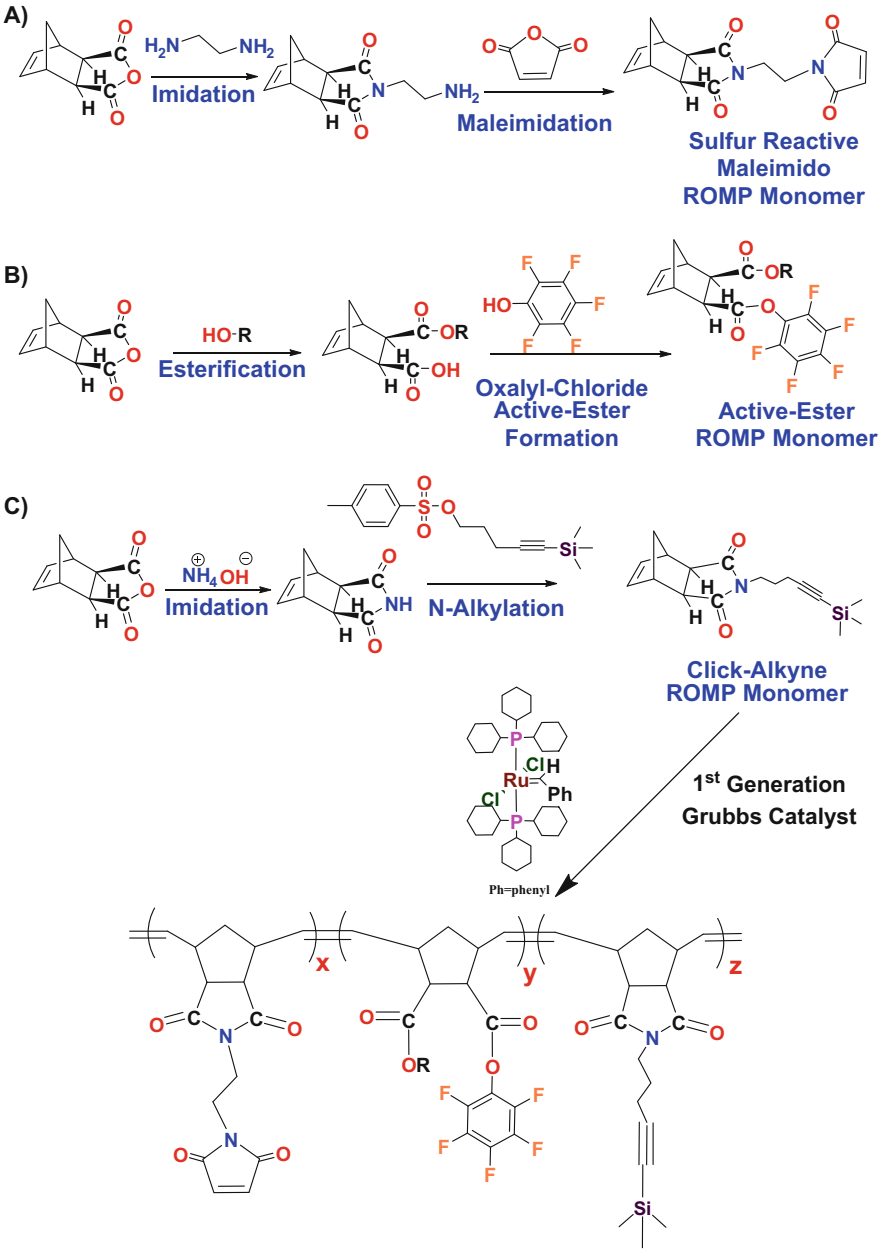

Scheme 6.32 Reactive norbornene ROMP monomers for reactive ROMP polymer construction (Adapted from Schaefer, M.; Hanik, N., Kilbinger, F.M., *Macromolecules*, 2012, **45** p 6807, with permission from ACS Publications)

had to be the maleimide attachment to the thiol. Hence, this polymer has a limitation on the sequential order of what substrates can be attached. In this case, first the thiol attachment, second the amine attachment, and third the click azide attachment.

Accordingly, benzyl mercaptan was reacted first to the maleimide comonomer unit, as depicted in Scheme 6.33a, b. The % attachment to the polymer functionality was determined by gravimetric analysis and calculated to be 91 %. Addition of hexylamine was then added for coupling to the active ester functionality, and the % attached was calculated at 88 %; see Scheme 6.33b, c. Lastly, the formation of the triazole substrate with the copper(I)-catalyzed azide/alkyne "click" chemistry yielded 91 % attachment; see Scheme 6.33c, d. This statistical terpolymer worked very well for attaching three different model substrates to the ROMP polymer in a very selective and high yielding manner.

An alternative approach to forming protein–polymer hybrids, or conjugates, utilizes the strategy of attaching the Grubbs catalyst onto the surface of the protein through its alkylidene moiety and then performing ROMP; see Scheme 6.34. In this approach, the ROMP polymerization would yield an "octopus-like" structure where there is a central proteinaceous core and polymer chains protrude like tentacles [146]. An added benefit of this approach is that it was performed in water.

In the first step, norbornene dicarboxylic anhydride is attached to lysozyme, a protein containing lysine and arginine residues to form a stable amide linkage with the ROMP monomer; see Scheme 6.34a. The second step is the formation of the water-soluble catalyst. Through the use of ligand exchange, third-generation Grubbs catalyst replaces the pyridine moieties that contain polyethylene glycol chains. By combining the lysozyme–ROMP derivative with the highly active third-generation Grubbs catalyst analog, the synthesis of the protein–romp catalyst hybrid is complete; see Scheme 6.34b. Lastly, the addition of ROMP monomer extends the polymer chains from the central proteinaceous core outward, as depicted by the red chains in Scheme 6.34c. Therefore, a protein–ROMP polymer hybrid or conjugate has been constructed [146].

In this section, the versatility of ROMP to construct hybrid or conjugate-type structures that combine polymer to either amino acids, peptides, or proteins has been demonstrated. These linkage points can be on the chain ends of the polymer, or along the main chain of the polymer, or grafted onto, or grafted from, multiple substrates to the polymer chain thereby forming biologically active mimetics. These hybrids have potential in diagnosis, imaging, and construction of enzymatic systems. These studies have underpinned the importance of the ROMP potential in biological systems.

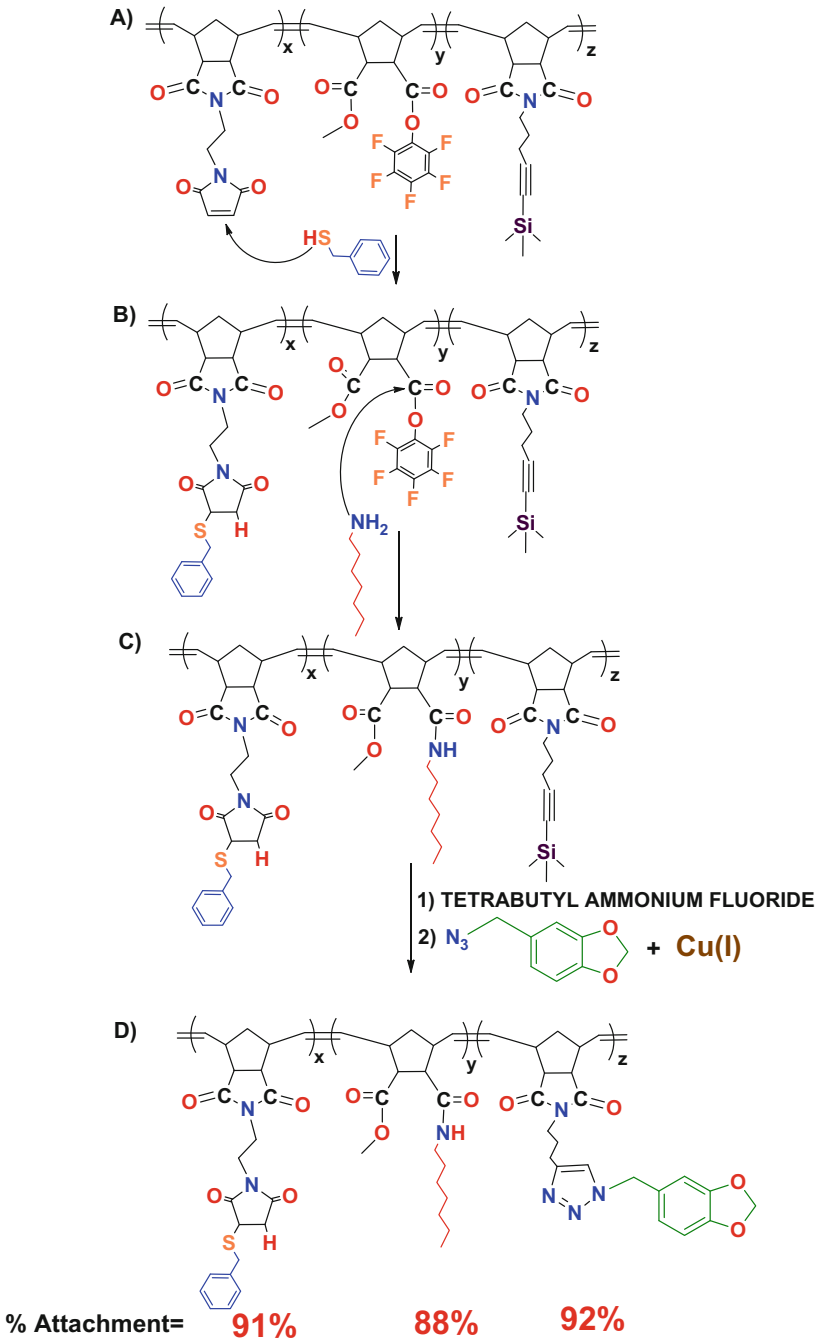

Scheme 6.33 Sequential reactions for 3-in-1 reactive ROMP polymer (Adapted from Schaefer, M.; Hanik, N., Kilbinger, F.M., *Macromolecules*, 2012, **45** p 6807, with permission from ACS Publications)

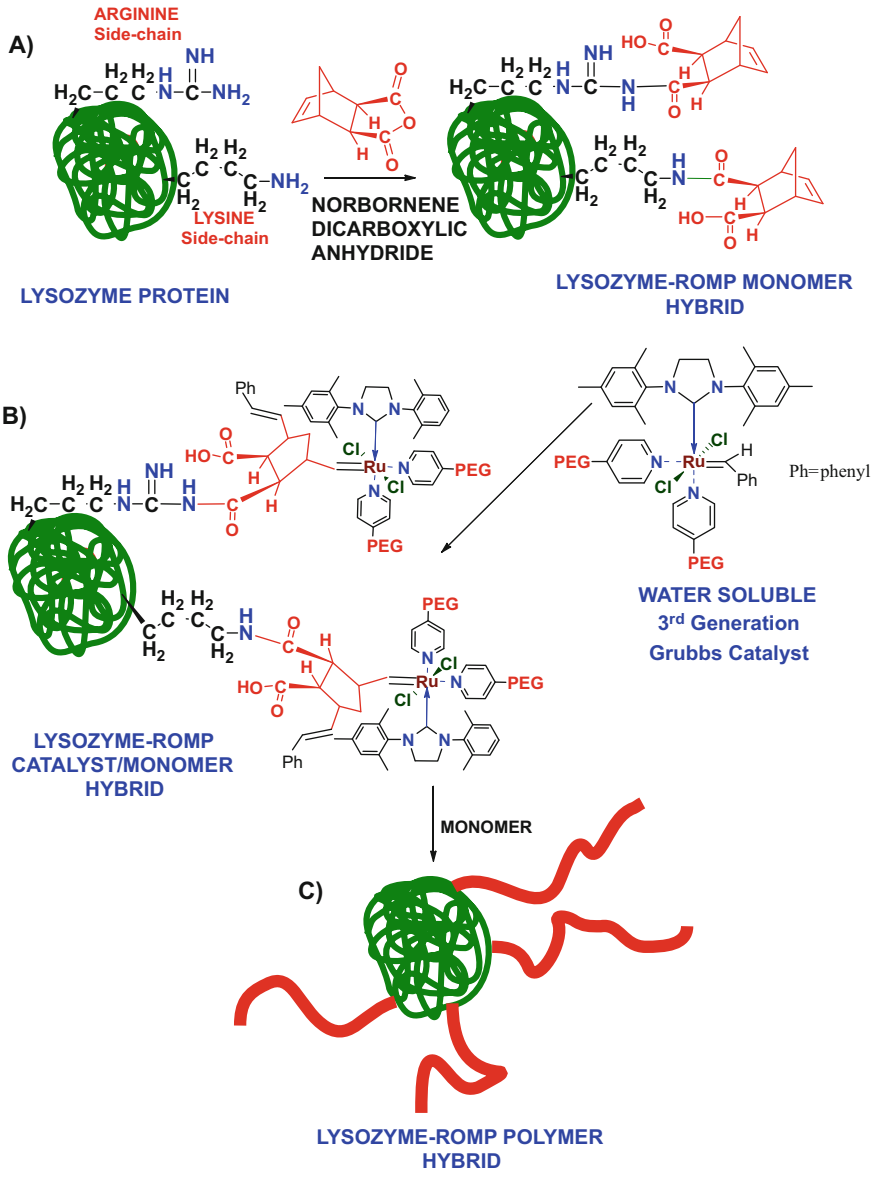

Scheme 6.34 Construction of protein-ROMP-polymer hybrid (Adapted from [153])

6.4 Antimicrobial ROMP Polymers

Another biologically important aspect of ROMP is the construction of antimicrobial polymers. These have found use in hospital environments. The use of soluble antimicrobial agents coated onto a catheter or surface has been found to cause

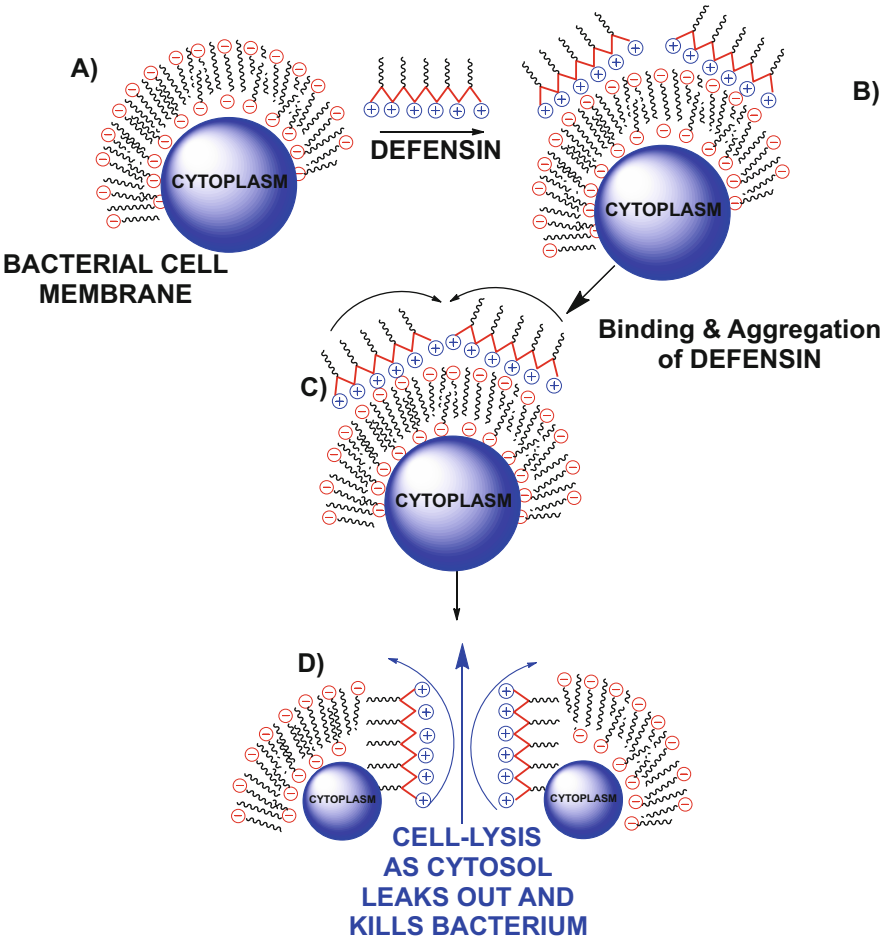

Scheme 6.35 Postulated mode of action for antimicrobial peptides on bacteria by cell lysis and leakage of the cytoplasm out of the bacterium (Adapted from [147])

irritation, swelling, and unwanted seepage into the host cells thereby killing them, and as such, it can compromise the surrounding cells of the host for further infection. It is advantageous to use an antimicrobial polymer coating instead, because the bactericidal agent cannot migrate away from the surface of the device and penetrate into the host's living cells. This causes less irritation, stinging, and damage to the surrounding tissue.

Taking inspiration from nature, the human body uses antimicrobial peptides to defend itself from bacterial infection. One such peptide known as defensin folds in space in such a way as to place cationic groups from lysine and arginine onto one side of the macromolecule and hydrophobic groups onto the opposite surface of the macromolecule (Scheme 6.35a). This arrangement is highly selective to bacterial

cells since their surface is highly anionic, and binding to this peptide is highly favored. In contrast, human cells are more neutral, so binding is less favorable and consequently less toxic [148, 149].

As several of these peptides bind to the surface of the bacterial cell membrane (Scheme 6.35a, b), they aggregate and insert themselves into the membrane (Scheme 6.35c) and form a pore that causes lysis of the membrane (Scheme 6.35d) and leakage of the cellular fluids out of the bacterium thereby killing it [142, 150, 151]. Alternative pathways for disruption of the cell membrane are also known [149].

Employing this simple and elegant approach, polymer molecules that mimic these structural elements, known as mimetics, were constructed using ROMP, as well as conventional methods [142].

Attempts to produce synthetic mimics of antimicrobial peptides (SMAMPs) using polymers by conventional routes of free radical polymerization were not as effective as the ROMP polymers. These included copolymers of poly(ammonium salts of methacrylic acid)/ butyl methacrylate [152], dendritic AMPs [153], polymaleic acid tethered to tetrapeptides [154], AMP's based on lipopeptides [155], and polyacrylamides [147].

In contrast, the ROMP polymers based on oxanorbornene derivatives containing hydrophilic and hydrophobic side chains exhibited a 100x higher activity toward bacteria than human blood cells [155]. Likewise, polynorbornenes containing quaternary pyridinium functionality exhibited selectivities up to 20X toward *Escherichia coli* (*E. coli)* [147]. To further this work, a toolbox of ROMP monomers with a tunable hydrophobic ester moiety and hydrophilic cationic lysine-like moiety were constructed and evaluated for their antimicrobial activity versus their cytotoxicity to mammalian red blood cells [142].

To identify the optimal chain length for the ester to optimize its hydrophobicity, the R-group in Scheme 6.36 was varied from methyl to hexyl, while the hydrophilic lysine-like side chain aminoethyl oxanorbornene was held constant. The overall yields for these monomers were roughly 40 %. The molecular weight was investigated to determine its contribution to antimicrobial activity. Two sets of molecular weights were prepared for all copolymers investigated. A 3 kDa set exhibited an average molecular weight ranging from 9200–11,500 with tight polydispersities spanning 1.08–1.11. A 10 kDa set exhibited molecular weights 11,000–50,000 with polydispersities of 1.04–1.16.

ROMP polymerization was carried out with third-generation Grubbs catalyst using the BOC-protected amines since they hinder the catalyst by ligation [142]. After polymerization, the BOC-polymers were deprotected by trifluoroacetic acid to yield the finished antimicrobial copolymers. The biological results obtained the homopolymers derived from the monoester (Scheme 6.36) were quite interesting. The 3 kDa molecular weight set that revealed the methyl ester was not active toward bacteria nor was it cytotoxic to the host's red blood cells. The propyl-hexyl ester series were extremely active against both gram-negative bacteria especially *E. coli* and gram-positive bacteria such as *Staphylococcus aureus (S. aureus)* but

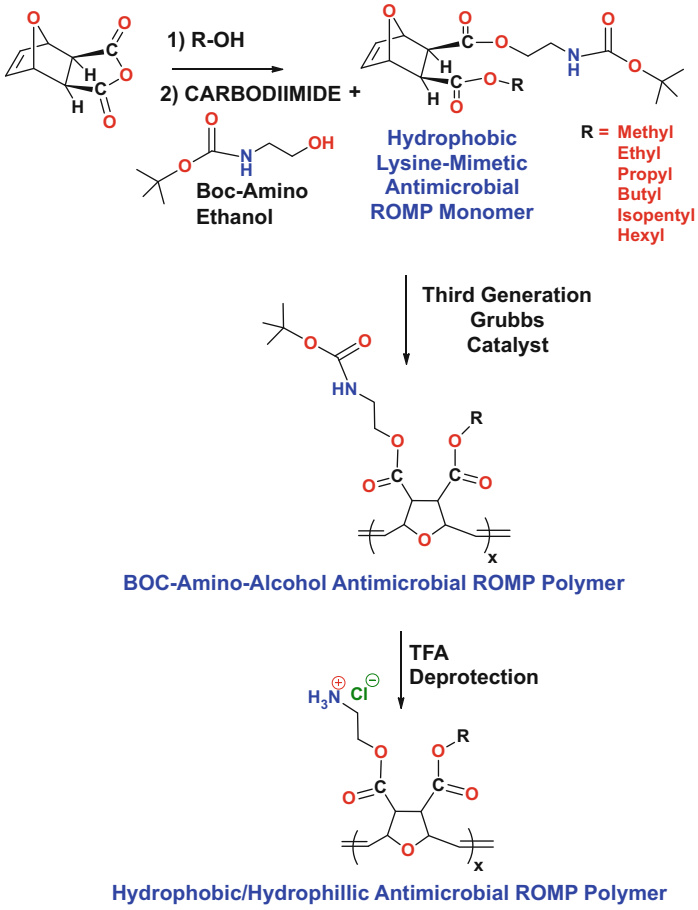

Scheme 6.36 Construction of hydrophobic/hydrophilic antimicrobial ROMP polymer with lysine mimetic side chains (Adapted from [142])

was also cytotoxic to the host's red blood cells. The 3 kDa ethyl ester gave the best of both worlds, in that it was active against both *E. coli* and *S. aureus*, but not cytotoxic to the host's red blood cells.

Since gram-positive *S. aureus* contains a thicker peptidoglycan in its cell wall, it was anticipated that higher molecular weight polymers would not be able to readily diffuse through this cell wall as easily as the thinner peptidoglycan layer of gram-negative *E. coli* (Scheme 6.37). Indeed, the 10 kDa propyl ester exhibited high activity against *E. coli* but was 40-fold less active against *S. aureus*, but this antimicrobial polymer was still cytotoxic to the host. Unfortunately, the ethyl ester 10 kDa homopolymer was not active against *S. aureus* and only modestly active against *E. coli*, despite being noncytotoxic to the host's red blood cells.

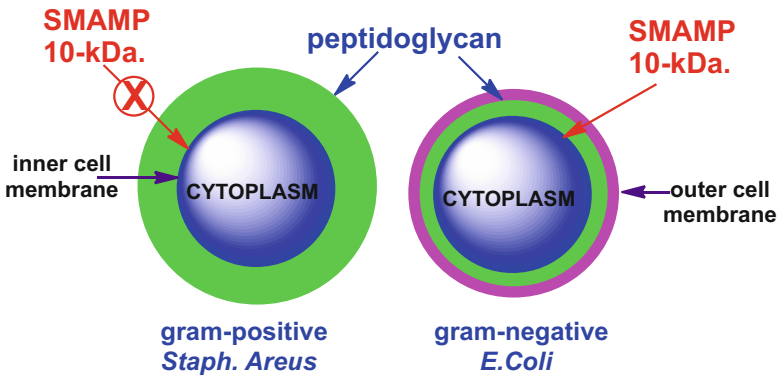

Scheme 6.37 Schematic of gram-positive versus gram-negative bacteria due to the presence of a thicker peptidoglycan cell wall, thereby inhibiting high-molecular-weight antimicrobial polymer (SMAMP) from disrupting inner cell membrane (Adapted from [142])

The molecular weight of the SMAMP polymer was too large to penetrate through the cell wall of this microorganism.

To improve upon these results, copolymers were constructed with a 3 kDa chain length. In this case, employing the nontoxic methyl ester monomer with a highly toxic propyl ester as comonomer, while still retaining the lysine mimetic side chain in both monomers. As little as 10 % propyl ester/amidoethyl comonomer or higher within the methyl ester/amidoethyl copolymer resulted in significant activity against *S. aureus* without cytotoxicity to the host cells. These copolymers were highly selective and toxic to only *S. aureus,* but did not kill *E. coli* or harm the host's red blood cells. This double selectivity is unusual for antimicrobial polymers. In contrast, the 3 kDa ethyl ester/propyl ester copolymers were still highly toxic to both bacteria and the host cells.

The effect of increasing the cationic charge density on the ROMP polymer was evaluated by the synthesis of a double cationic amino alcohol (Scheme 6.38b). Indeed, a higher level of cationicity enhances the selectivity of the SMAMP polymer to bacteria than human host cells, and the most promising candidate polymer for in vivo testing was a 10 % butyl ester (38A)/90 % dicationic (38B) copolymer that was active against multiple strains of gram-positive and gram-negative bacteria [156].

Antimicrobial ROMP polymers can also exhibit selectivity between the two types of bacteria yet do not harm the host cells. Specifically, the ethyl ester homopolymer with 10 kDa molecular weight kills gram-negative *E. coli* bacteria but not *S. aureus* by a size exclusion pathway, while the 3 kDa methyl ester/propyl ester copolymers kill *S. aureus* but not *E. coli*. This double selectivity between bacteria is rare and prompted further analyses. At first, it was thought that the difference in composition of lipids present between two bacteria was responsible, but vesicle studies disproved that hypothesis.

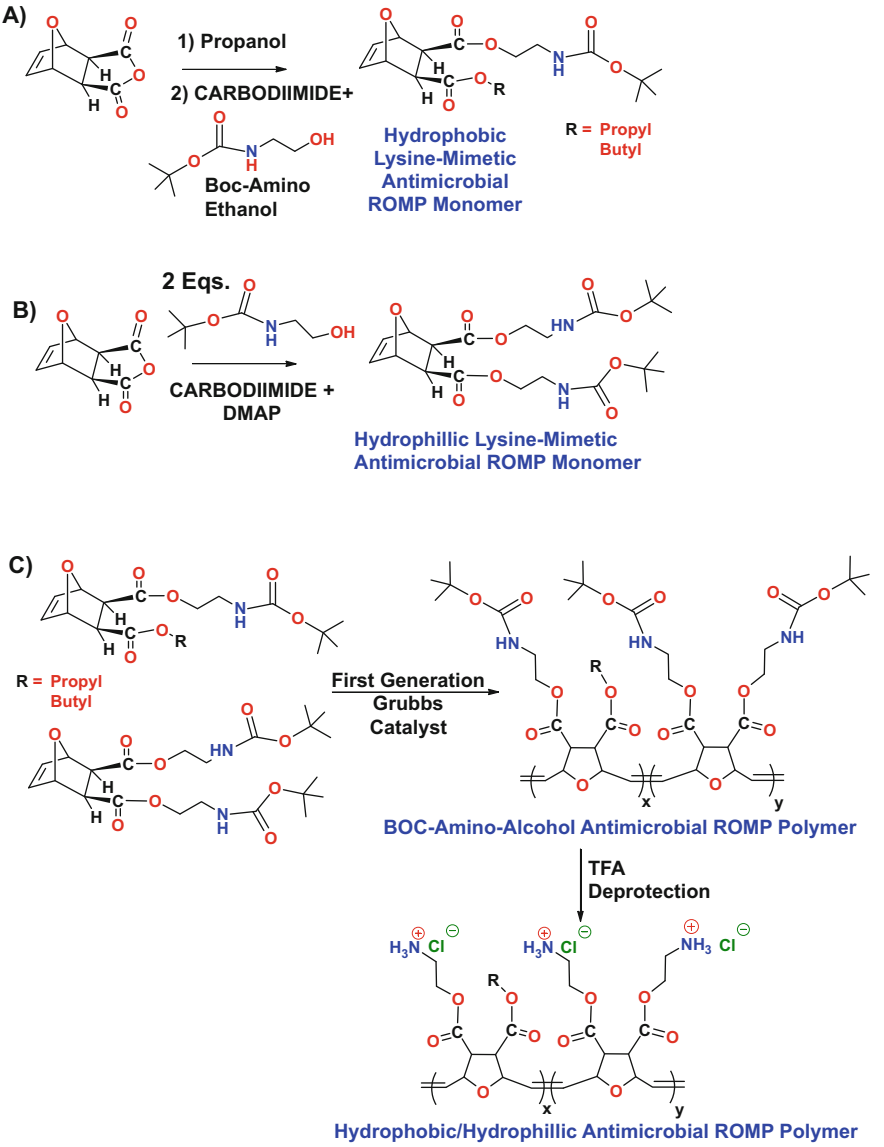

Scheme 6.38 Construction of hydrophobic/hydrophilic antimicrobial ROMP polymer with lysine mimetic side chains (Adapted from [156])

This led to the concept that the outside membrane structure for *E. coli* inhibited the SMAMP from accumulating inside the peptidoglycan layer, so that its actual concentration at the inner cell membrane was significantly less than at the outer cell membrane. To prove this theory, *E. coli* cells were subjected to EDTA for one minute and then quenched with $CaCl_2$. This procedure compromises the outer cell

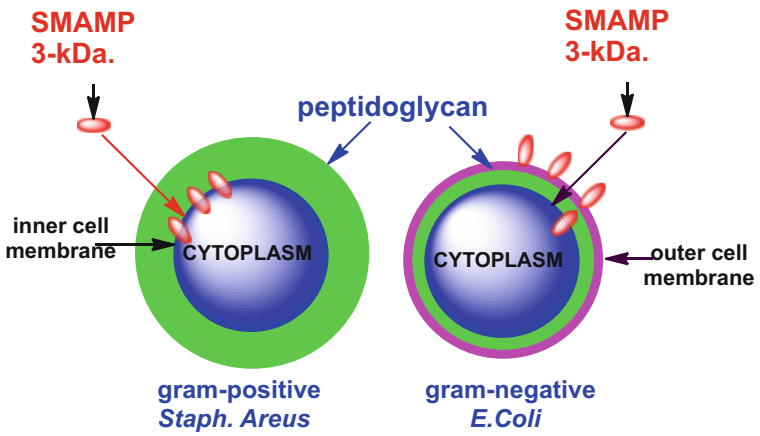

Scheme 6.39 The double membrane structure prevents the SMAMP from accumulating at the inner cell membrane so the 3 kDa SMAMP cannot kill the gram-negative *E. coli* bacteria, by disrupting their inner cell membrane (Adapted from [150])

membrane of *E. coli* but not the inner membrane. When these outer membranes compromised *E. coli* cells were subjected to the SMAMP they were killed, while their untreated counterparts were not compromised [150]. The double membrane structure of *E. coli* appears to prevent the SMAMP from accumulating at the inner membrane. This finding provides insight to how the propyl ester/methyl ester SMAMP would kill *S. aureus* but not *E. coli* bacteria (Scheme 6.39).

6.5 Self-Assembly ROMP Polymers

Self-assembly of individual protein chains, or DNA strands, to come together to form a higher-order configuration or scaffold required for catalysis or structure is ubiquitous throughout nature. This is analogous to protein subunits coming together to form a larger molecular entity required for enzymatic catalysis. These associations are driven by noncovalent forces that include van der Waals interactions, columbic/electrostatic attractions, hydrogen bonding, and pi stacking [157].

A highly specific self-assembly mechanism is DNA base pairing (adenine to thymine and cytosine to guanine) by which the sense strand of DNA (the one that codes for the protein) binds to its antisense strand of DNA (used to stabilize the helix and for repair of damaged sense strand DNA by its complimentary binding pattern), Fig. 6.17. This highly selective complexation of two strands of DNA to each other employs noncovalent forces through hydrogen bonding at a molecular recognition site. The more sites available along the DNA chain results in a higher complexation selectivity [158].

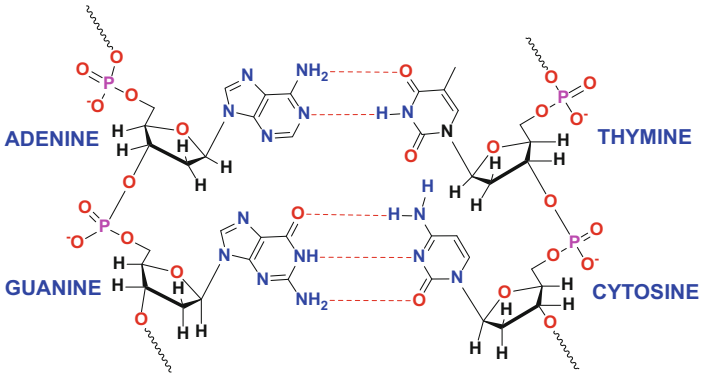

Fig. 6.17 Complimentary base pairing of DNA using hydrogen bonding

The utility of self-assembly to form rods, spheres, or cone-like structures enables formation of larger complexes by use of an external trigger for construction of new architectures. These can be used as biomolecular sensors or delivery agents. Self-assembly is not the same as aggregation or flocculation, because these events lack any particular order or structure within them. These are just a conglomeration of chains with random orientations to each other.

This use of self-assembly with synthetic polymer chains is interesting in that block or random copolymer structures can be constructed, with specific directionality and function. For example, self assembly can be used by the surface modification of metal(gold) nanoparticles to achieve nanometer spacing of these spheres for microelectronic applications [159], enzyme immobilization, biomimetic systems, controlled drug delivery, and in gene therapy [160]; self-healing block copolymers for nanocomposites [161]; reversible hydrogel formation based on either temperature or pH [162, 163]; the construction of polymeric light-emitting diodes [164]; the formation of supramolecular hyperbranched polymers and dendritic polymer assemblies [165, 166]; and the self-assembly of random copolymers into bilayers, vesicles, single-chain nanoparticles, nanogels, and micellar aggregates, as illustrated in Scheme 6.40 [167].

Conventional free radical polymerization has constructed many of these self-assembly polymers [168], including newer methodologies like RAFT [169], ATRP [170], and NMP [171], but now ring-opening metathesis polymerization (ROMP) has also joined the techniques available to synthesize polymeric self-assemblies [172].

Bazzi and Sleiman reported in 2002 on the synthesis of a DNA analog attached to a ROMP monomer [172]. This was easily achieved through the use of the reactive maleic anhydride-based Diels–Alder adduct oxanorbornene dicarboxylic anhydride (Scheme 6.41). Once the DNA base is attached, ROMP polymerization of homopolymers and block copolymers for each of the complimentary base pairs can be produced so that individual polymer chains can self-associate by complimentary base pairing induced by hydrogen bonding like that observed in DNA (Fig. 6.17).

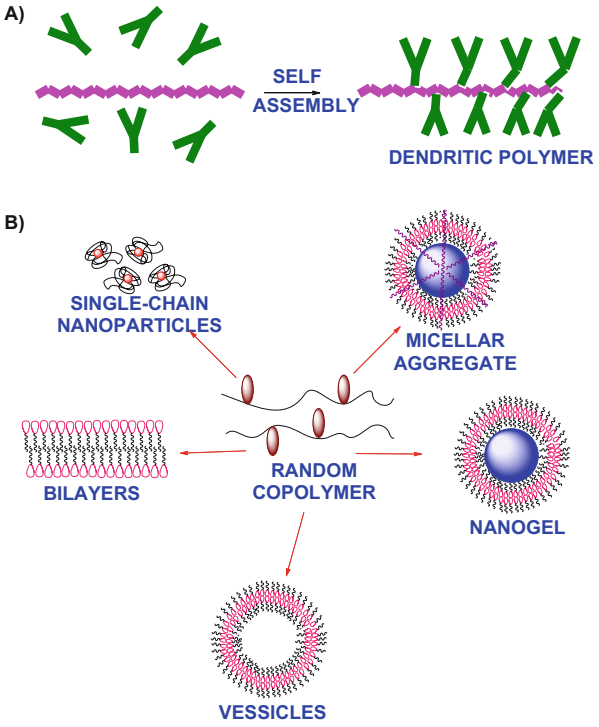

Scheme 6.40 Some of the potential architectures formed by polymeric self-assemblies (Adapted from [167])

In previous studies, the authors described the synthesis of polymers and block copolymers with thymine-based monomer using ROMP [173]. In this study [172], the authors only focused on the adenine self-associating behavior, instead of the typical adenine–thymine association as that in DNA. They attached adenine by first reacting an amino alkyl bromide to oxanorbornene dicarboxylic anhydride (Scheme 6.41). The addition of acetic anhydride catalyzed the ring closure into its imido-alkyl-bromide adduct. This was followed by attachment of adenine that was pretreated with sodium hydride for N-alkylation.

ROMP homopolymerization of this adenine analog with first-generation Grubbs ruthenium catalyst failed to produce any homopolymer. They deduced that the free amino group in adenine was responsible, as it could ligate to the catalyst and deactivate it (Scheme 6.42a). They then tried a more reactive catalyst, second-generation Grubbs catalyst, and indeed obtained the homopolymer, but with only 70 % yield (Scheme 6.42b).

They rationalized the lower yield again to the free amino group in adenine. In response, they attempted complexing this amino group with succinimide before addition of the catalyst. They obtained an increase in conversion of monomer up to 90 % and then quenched the ROMP reaction followed by precipitation of the homopolymer from methanol with a final homopolymer yield of 80 %

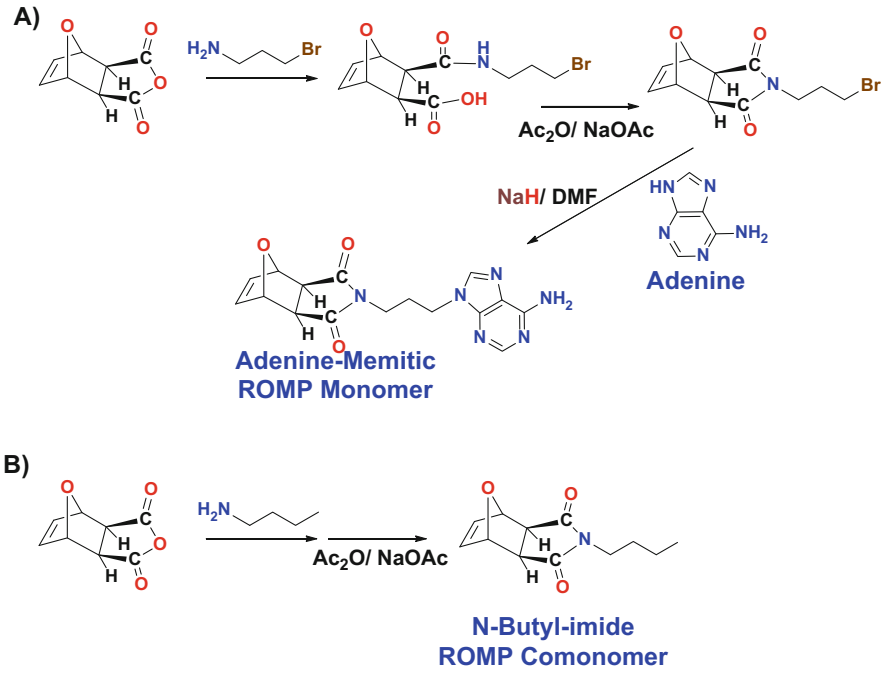

Scheme 6.41 Monomer synthesis of DNA mimetic for polymeric self-assemblies (Adapted from [172])

(Scheme 6.42c). The synthesis of block copolymers based on an *N*-butylmaleimide–oxanorbornene, followed by the adenine mimetic monomer in varying quantities, roughly yielded 85 % block copolymers; see Scheme 6.42c.

The adenine mimetic block copolymer's molecular weight spanned 196–315 kDa and polydispersity values ranging from 1.22 to 1.60. The self-assembly behavior by TEM indicated large, nonspherical aggregates with diameters ranging from 869 to 1238 nm, in addition to well-defined cylindrical rods with average diameters of 30 ± 2 nm. Wide-angle X-ray scattering also indicated some crystallinity for both the adenine homopolymer and the block copolymer aggregates. This attribute was tentatively assigned to the self-binding/assembly process illustrated in Scheme 6.43. This behavior is similar to that observed with DNA base pairing. In this case, it is only related to the adenine moiety (pyrimidine unit) itself, instead of its complimentary (purine) counterpart. Therefore, a self-assembly polymer based on just a pyrimidine foundation was developed and was capable of forming nanorod-like structures.

Many examples of homogenous self-assemblies in solution have been reported. A great deal of work has also been focused on heterogeneous self-assemblies. For example, Lee and coworkers described the self-assembled monolayers (SAMs) onto a gold surface to indirectly place reactive functionalities on the metal's surface for further reaction by Diels–Alder adduct formation or "Click" chemistries [174].

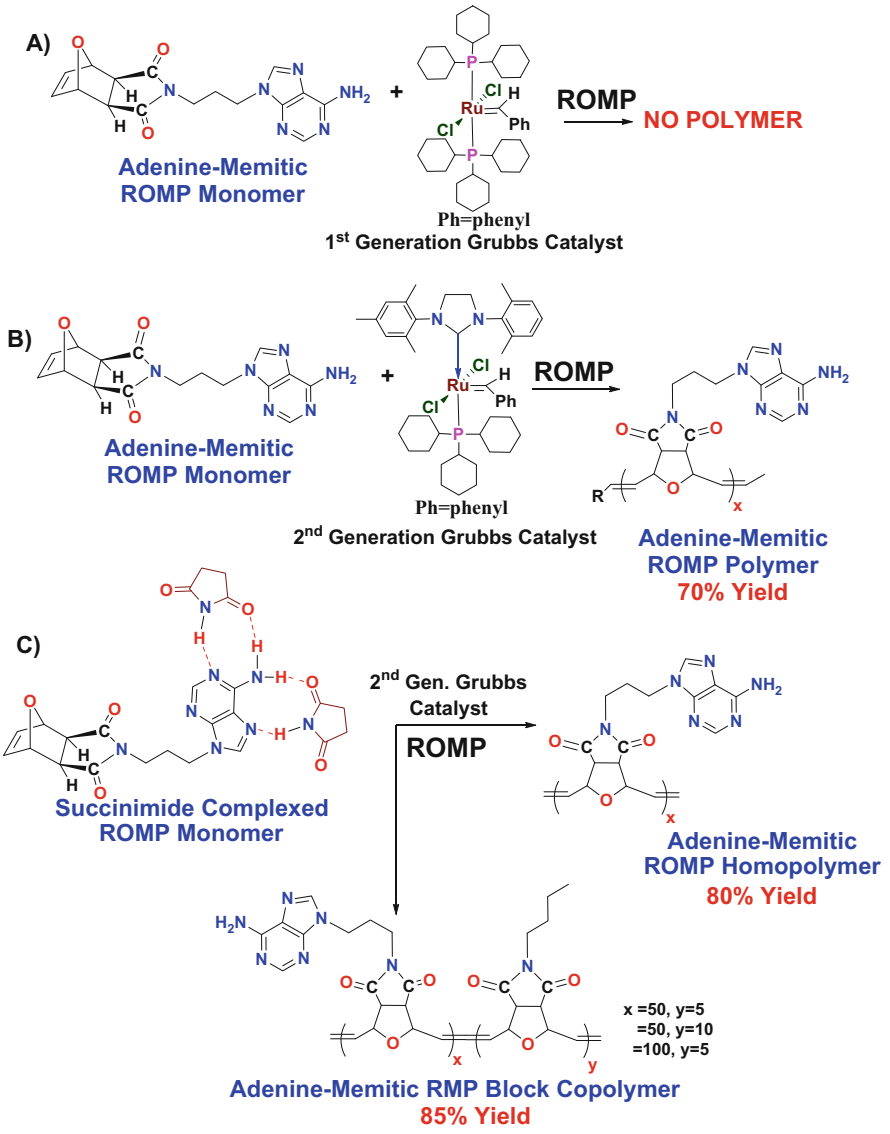

Scheme 6.42 Polymer synthesis of DNA mimetic for polymeric self-assemblies (Adapted from [170])

In particular, the authors reported on the ruthenium-catalyzed cross-metathesis of vinyl-terminated self-assembled monolayers (SAM) to successfully introduce maleic anhydride onto the SAM. During their study, it became apparent that dimerization of the terminal vinyl groups on the surface was problematic and could not be used as a generalized method to introduce reactive functionalities easily.

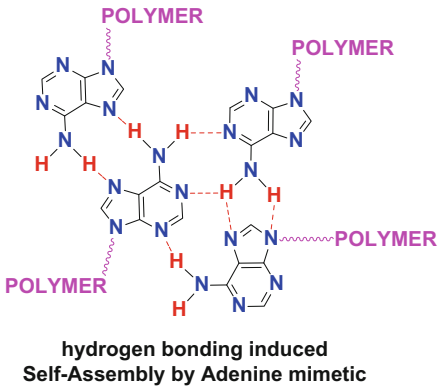

Scheme 6.43 Proposed mechanism for polymeric self-assembly by DNA mimetic (Adapted from [172])

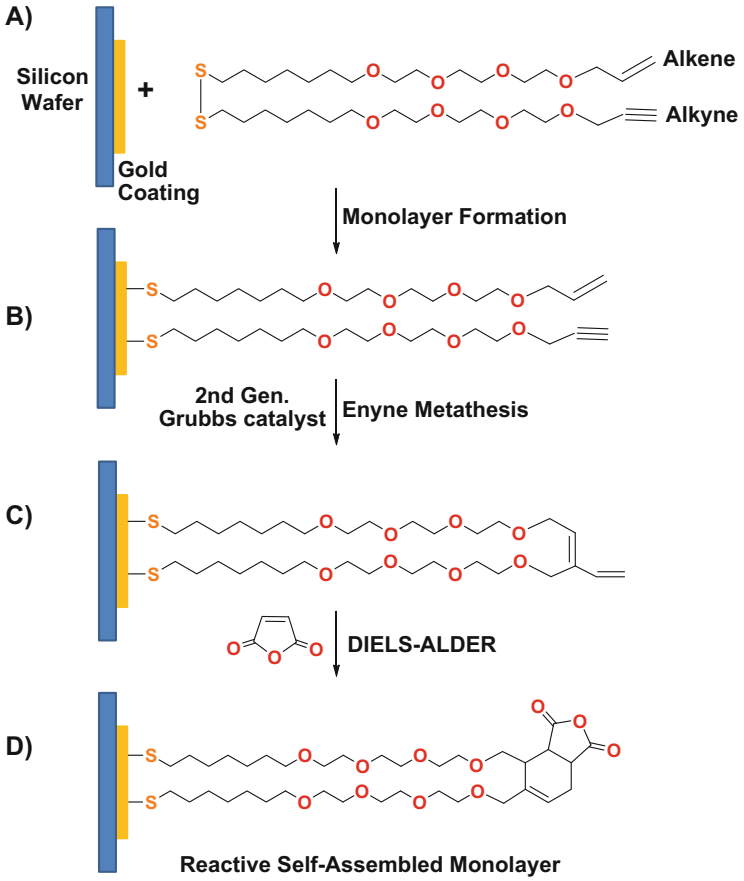

Scheme 6.44 Construction of a reactive self-assembled monolayer using cross-metathesis, followed by Diels–Alder formation (Adapted from [174])

To construct the maleic anhydride-based SAM required several reaction steps, starting with the attachment of an ethoxylated thiol bearing a terminal alkyne and one bearing a terminal vinyl group (Scheme 6.44a). It needs to be recognized that the bond between thiol and gold is not thermally durable and will cleave around 60 °C. So any subsequent reactions must be well below this temperature. Likewise, this bond is also susceptible to cleavage under acidic and basic conditions. The incorporation of the terminal alkyne and vinyl groups needs to be formed prior to attachment to the gold particle. The details of this synthesis can be found in Lee et al. [174].

Once the disulfide bearing the alkyne and vinyl groups was constructed, it was attached to the gold-coated silicon wafer by evaporation from an ethanolic solution (Scheme 6.44a, b). Upon cross-metathesis, employing second-generation Grubbs catalyst in benzene at 50 °C for 4 h, a 1,3-diene is formed (Scheme 6.44c). Addition of maleic anhydride, or its derivatives, forms the desired Diels–Alder adduct and completes the synthesis of the reactive self-assembled monolayer; see Scheme 6.44d. This reactive SAM can now be reacted with a whole host of derivatives, due to the maleic anhydride functionality.

6.6 Thermosetting ROMP Polymers

In general, thermosetting polymers are prepolymers that irreversibly cure upon heating. These polymers are useful in resin transfer molding or reactive injection molding and are capable to thermally cross-link and produce high-mechanical strength materials with excellent thermal stabilities. These processes rapidly produce materials or composites in an extremely efficient manner with little to no waste formed or pollution by solvents to the environment.

However, after the usefulness of the material is over, the currently produced thermosetting polymers are so stable in that they do not degrade and ultimately buildup in trash dumps and eventually pollute the environment for millennia to come. Intense research into thermosetting materials that can be recycled into useful products again is highly desirable in the marketplace today.

The key to this objective is that the thermosetting polymer can still be thermally stable, but that the cross-linking structures should not. A thermally degradable linkage is one strategy capable of recycling thermosetting materials into new useful products. While chemically degradable linkages are available, they do not provide the selectivity to cleave the cross-linking site only. For example, diepoxy monomers containing ester groups [175–177], or carbamate linkages [178, 179], or carbonate functionalities [180, 181], have many drawbacks in that they can degrade before curing is complete so that the mechanical strength of the material is compromised. Maleimide resins have also been used in electronic packaging applications due to their fast cure speed, better adhesion, and low shrinkage after curing [182–185]. They can also copolymerize with other acrylates and styrenics by free radical polymerization; however, the resulting thermoset resins could not be recycled [185].

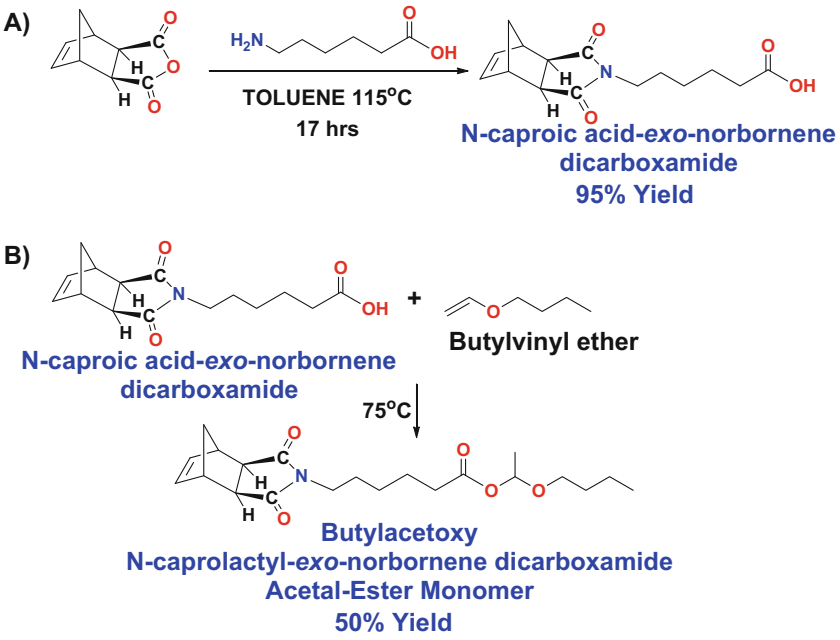

Scheme 6.45 Synthesis of the thermally labile acetal-ester monomer (Adapted from [186])

A newer approach to these types of materials is to use ROMP to construct polymers with well-defined molecular weights, polydispersities, and architectures that are thermally stable and have excellent mechanical strength. It includes superior control over the cross-link density and can use cross-linkers that are thermally labile well below the polymer's decomposition temperature. The crucial aspect of this design is the thermal breakdown of only the cross-linking sites, leaving the main chain intact, allowing for transition of the material from thermo-setting to thermoplastic, thereby facilitating recyclability [186].

In 2010, Khosravi, Iqbal, and Musa reported on ROMP-based polymers with acetal-ester linkages that cleave at 200 °C. This decomposition temperature is well below the polymer's main chain decomposition of 350–400 °C. Only acetaldehyde, butadiene, butenyl alcohol, and pentenoic acid are generated as by-products [186]. The synthesis of the thermally labile cross-linker is summarized in Schemes 6.45 and 6.46.

In particular, *exo*-norbornene dicarboxylic anhydride was reacted with 6-aminocaproic acid in toluene at 115 °C for 17 h to afford the *N*-caproic acid dicarboxamide intermediate in 95 % yield (Scheme 6.45a). This intermediate was then reacted with a solution of butyl vinyl ether and 4-methoxyphenol reacted for 1 h at 75 °C followed by 10 h at 75 °C to generate the acetal-ester monomer (Scheme 6.45b) in 50 % yield. The acetal-ester cross-linker followed the same procedure, using two equivalents of *N*-caproic acid dicarboxamide intermediate with a reaction mixture of 1,4-butanediol and 4-methoxyphenol at 90 °C for 1 h followed by 90 °C for 10 h (Scheme 6.46) in 50 % yield.

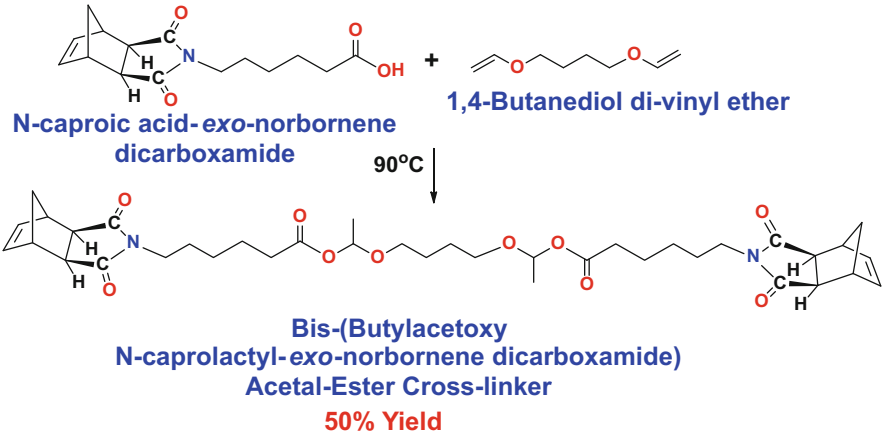

Scheme 6.46 Synthesis of the thermally labile acetal-ester cross-linker (Adapted from [186])

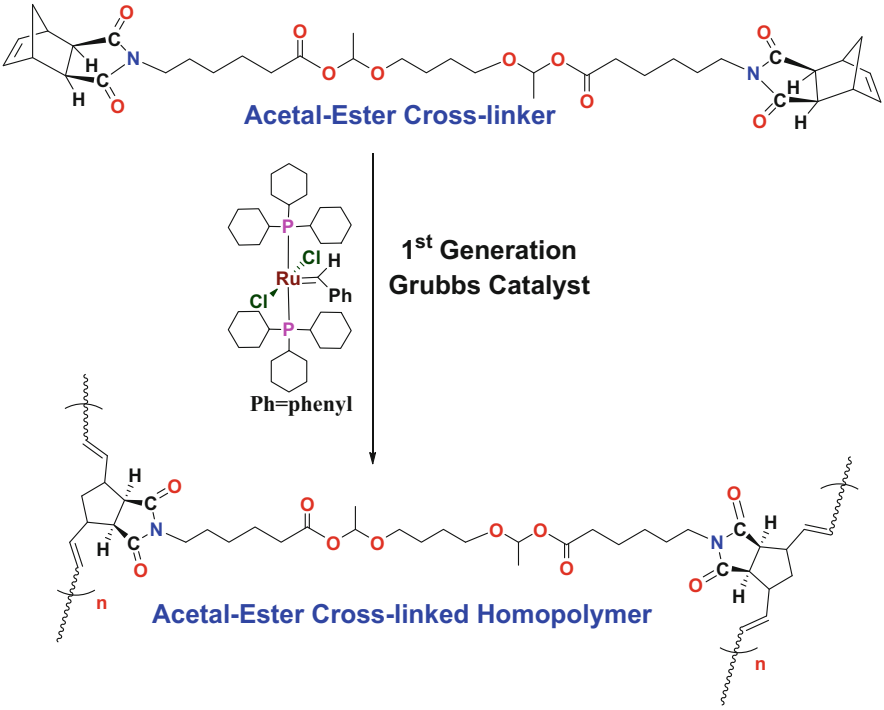

Scheme 6.47 Synthesis of cross-linked thermally labile acetal-ester homopolymer using ROMP (Adapted from [186])

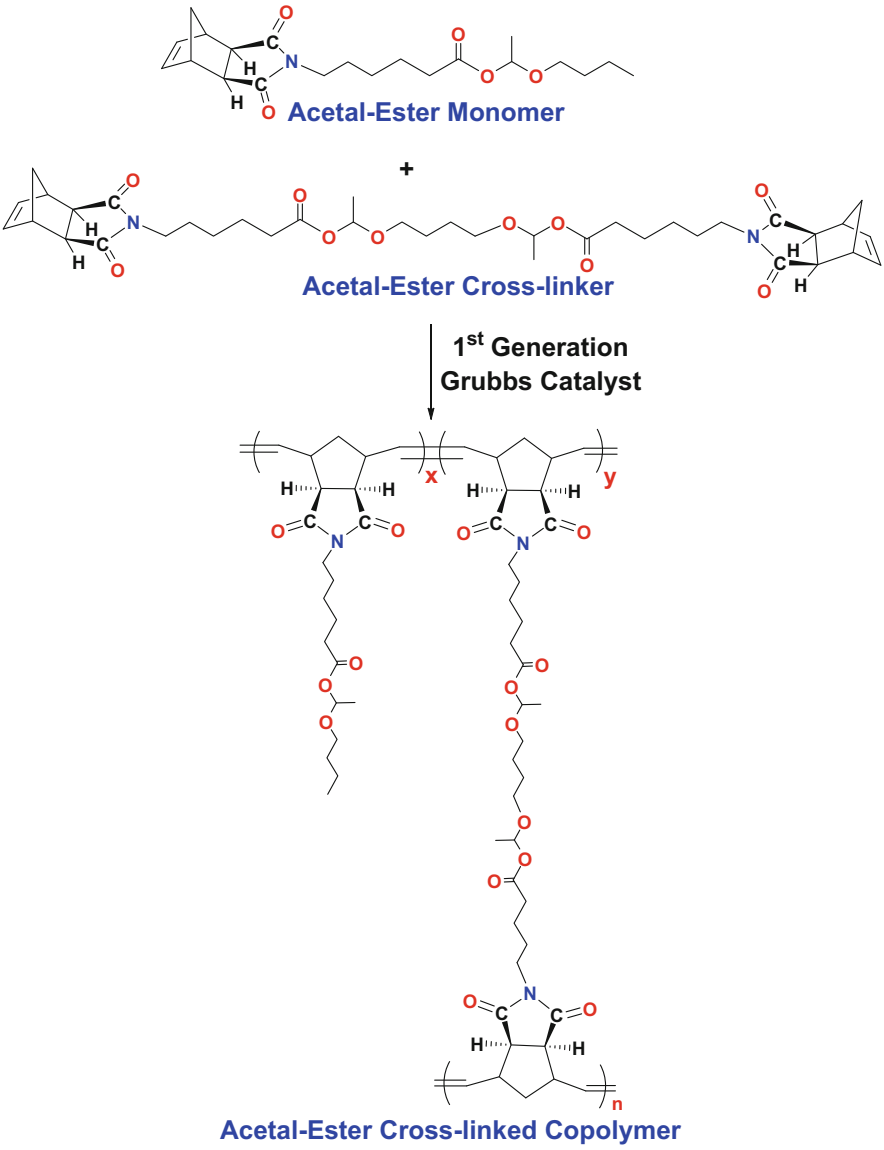

Scheme 6.48 Synthesis of cross-linked thermally labile acetal-ester copolymer using ROMP (Adapted from [186])

Synthesis of ROMP polymers containing the acetal-ester cross-linker (Scheme 6.46) was achieved with first-generation Grubbs catalyst in methylene chloride at ambient temperature. The cross-linked homopolymer was formed soon after the addition of catalyst (Scheme 6.47).

Copolymers based on the monofunctional acetal-ester monomer (Scheme 6.45b) were copolymerized with varying levels of acetal-ester cross-linker. This approach

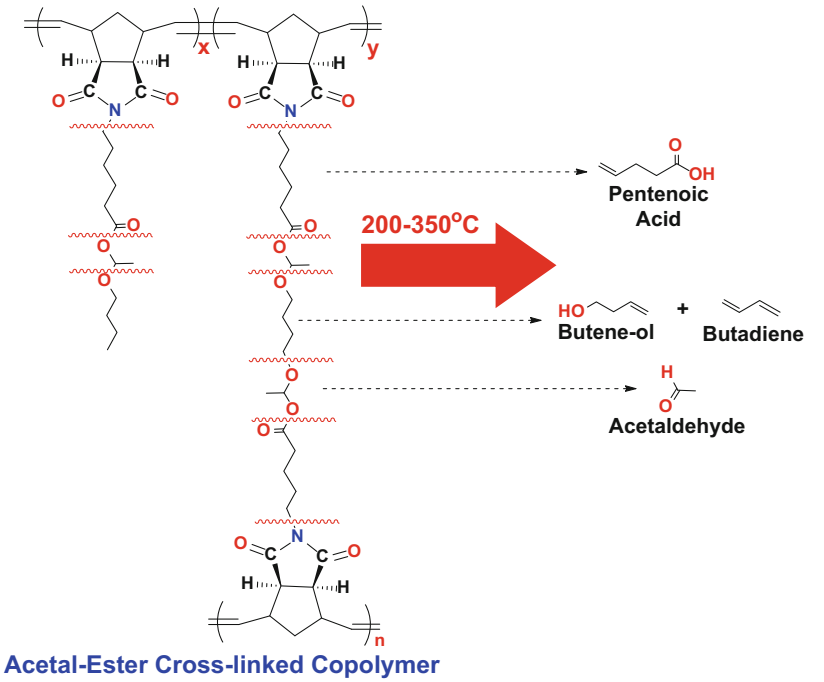

Scheme 6.49 Thermal degradation of cross-linked acetal-ester copolymer indicating labile cleavage points and by-products generated (Adapted from [186])

enabled the determination of the ability to control the cross-link density by the cross-linker concentration (Scheme 6.48).

Sol–gel extractions were performed to determine the percentage of soluble extractable polymer present that failed to undergo the cross-linking ROMP process. All polymers and copolymers in this study yielded low values of soluble polymer. Specifically, the difunctional cross-linker homopolymer has 89 % gel content and 11 % soluble/extractable polymer, while the copolymers varied from 82 to 89 % gel content or 18 to 11 % soluble/extractable uncross-linked polymer.

Employing TGA and TGA-MS, the homopolymer and copolymers were subjected to thermal degradation to evaluate their susceptibility as a function of cross-linker level used. Indeed, the homopolymer using only the acetal-ester cross-linker resulted in 58 % weight loss starting at 200 °C and continued to up to 350 °C. Theoretically, a total decomposition of the acetal-ester cross-linking structure would be 53 %. As a result, complete decomposition of the cross-linker structure was inferred. TGA-MS also determined that the fragmentation of the cross-linker generates pentenoic acid, butadiene, 3-butene-1-ol, and acetaldehyde, as depicted in Scheme 6.49.

Similar results were obtained on the copolymers. Copolymers containing 75 % acetal-ester cross-linker/25 % monofunctional acetal-ester monomer resulted in 45 % weight loss. Theoretically, it should have resulted in roughly 55 % weight loss. The 50/50 and 25/75 copolymers displayed 33 % and 30 %, respectively. Theoretically, they should have corresponded to a weight loss of 55 %.

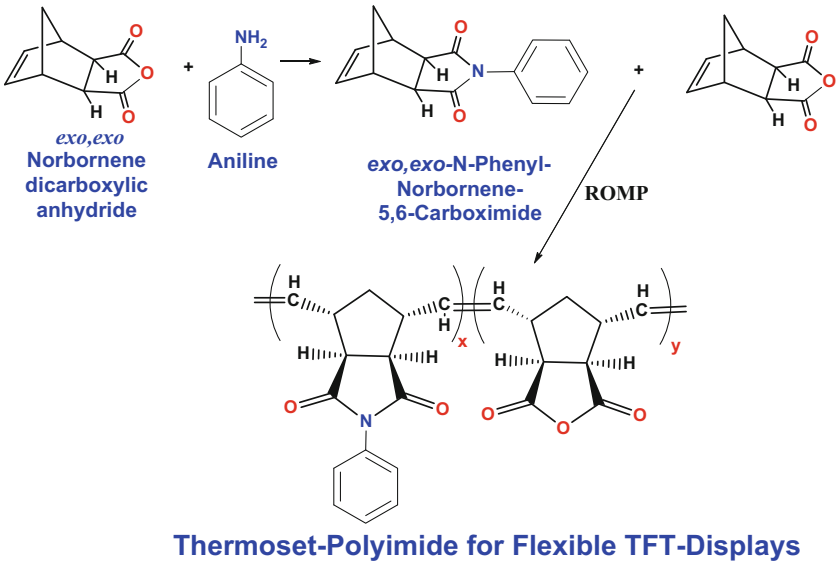

Scheme 6.50 Formation of novel ROMP monomers from norbornene dicarboxylic anhydride through maleimide chemistry (Adapted from [33])

As the monofunctional acetal-ester comonomer increases, less than theoretical weight loss is obtained. This finding suggests that the butyl functionality somehow endows more stability to thermal degradation profile of these copolymers. The reason for this is yet unknown. These cross-linked polymers are not amenable to NMR characterization of the resultant degradation products of the polymer. Despite this finding, the acetal-ester cross-linker demonstrated its utility in degrading almost quantitatively at 200–300 °C, while the main chain of the polymer remained intact.

Other ROMP polymers used in thermosetting-type applications such as aniline-based ROMP polymers used in the aerogel and TFT display industries may be amenable to insertion of this thermally labile acetal-ester cross-linker. For example, thermoset monomers can be constructed from maleic anhydride-based norbornene and oxanorbornene dicarboxylic anhydride. Choi and coworkers synthesized an *exo,exo-N*-phenyl-norbornene 5,6-carboximide monomer from norbornene dicarboxylic anhydride and copolymerized it by ROMP with norbornene dicarboxylic anhydride to form the thermoset polyimide depicted in Scheme 6.50 [33].

The polyimide/polyanhydride copolymer was further reacted with *N*,*N*′-4,4′-diamino-chlorinated biphenyl derivatives to cross-link the polymer matrix for increased thermal stability. This cross-linked polyimide was then impregnated with indium tin oxide to form clear colorless flexible thin-film transistor (TFT) displays [33].

Leventis and coworkers manufactured polyimide aerogels by utilizing a ROMP cross-linker from 4,4′-methylene bis(aniline) and norbornene dicarboxylic anhydride, as depicted in Scheme 6.51 [34]. This difunctional ROMP monomer generates a nanoporous solid with high soundproofing properties, low thermal conductivity, and

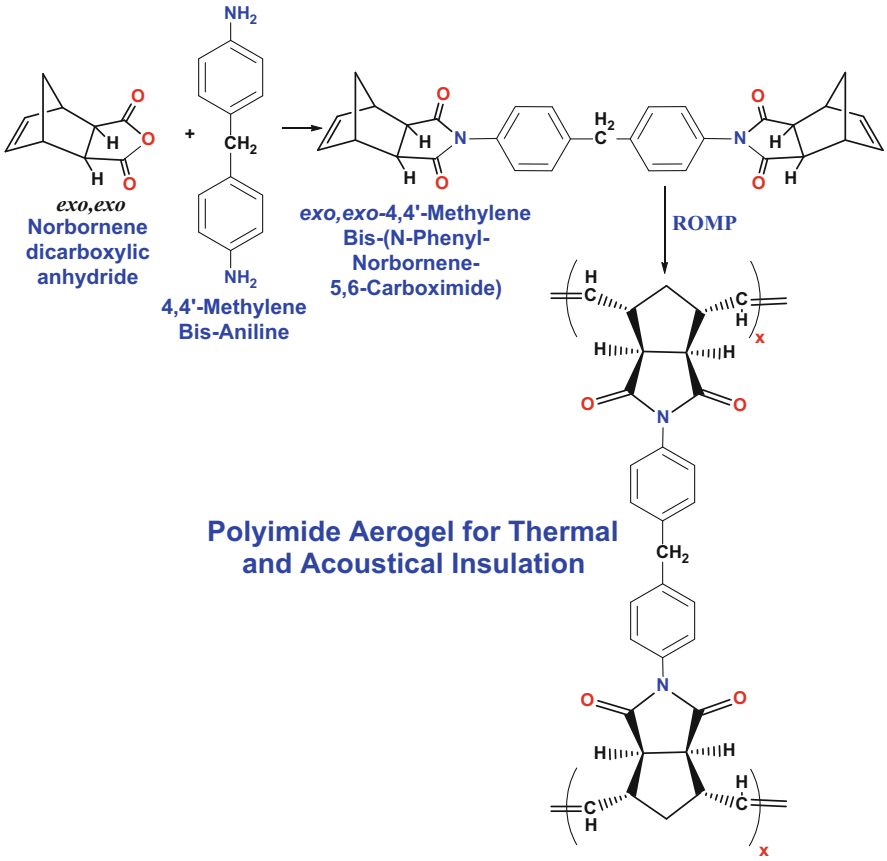

Scheme 6.51 Formation of cross-linkable ROMP monomers from norbornene dicarboxylic anhydride through maleimide chemistry (Adapted from [34])

high surface area. These polymeric materials are known to very thermally and mechanically stable for use in ballistic armor and high temperature insulators.

Even Intel has evaluated and patented the use of specialized ROMP monomers for manufacturing polyimides for their microelectronics industry [186]. They produced ROMP monomers and oligomeric dendrimer/hyperbranched materials that are combined with polyimide to form a low coefficient of thermal expansion material for use as a dielectric substrate layer or an underfill adhesive. These dendrimers/hyperbranched ROMP materials are synthesized to produce low viscosity, high T_g, fast curing, and mechanically and chemically stable materials for imprinting applications.

Given these industrially significant ROMP thermosetting materials, Hou and Khosravi investigated the use of acetal-esters cross-linkers to thermally degrade these materials [187]. 4-Phenyl-aminobutane was used to mimic the aniline functionality as the monofunctional monomer, with the difunctional acetal-ester cross-linker (Scheme 6.52). These materials were subjected to sol–gel extraction (11–26 wt% soluble polymer) and thermal degradation by TGA.

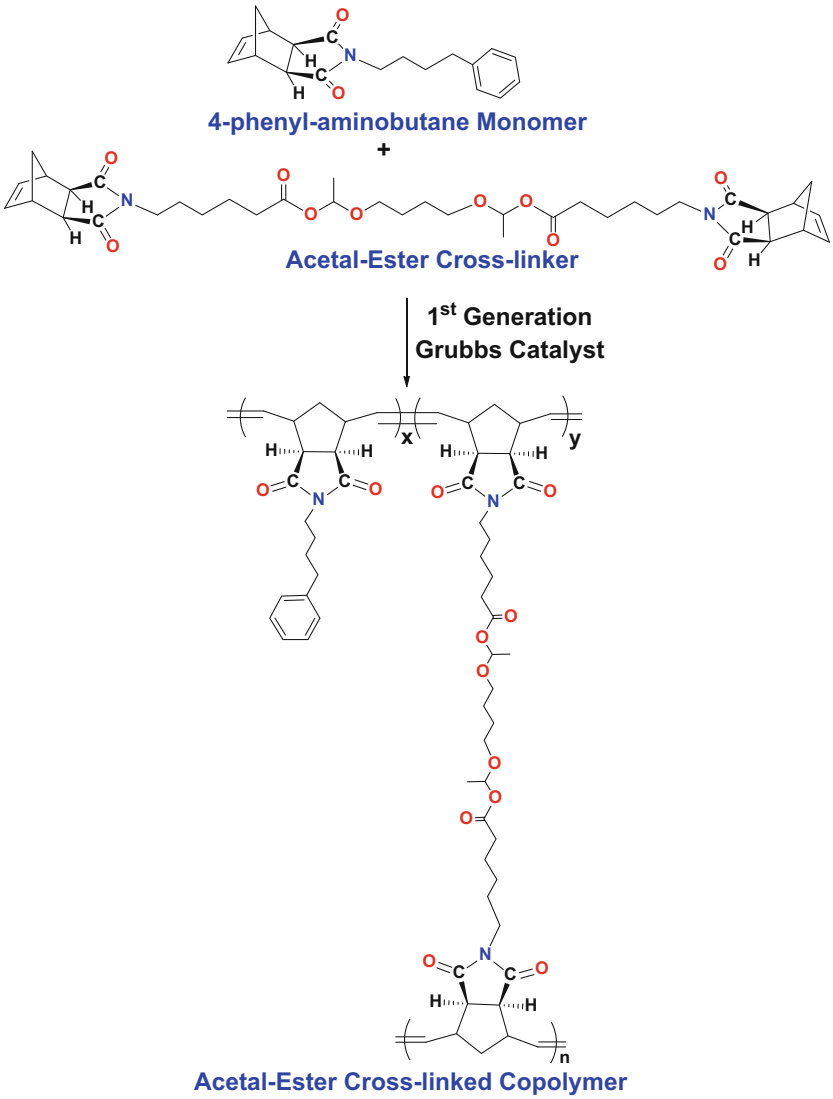

Scheme 6.52 Synthesis of cross-linked thermally labile acetal-ester copolymer using ROMP (Adapted from [187])

The monofunctional homopolymer, *exo*-norbornene-4-phenylbutyl-dicarboxamide thermally degraded by only 2 wt%, while the difunctional acetal-ester homopolymer degraded 23 wt%. In contrast, the 75 mol% monofunctional dicarboxamide/25 % acetal-ester cross-linker, 50/50, and 25/75 polymers decayed 11 %, 16 %, and 22 %, respectively. Indeed, the incorporation of the acetal-ester cross-linker into this thermoset ROMP polymer thermally degrades as expected and lends further support on the use of this cross-linker as a thermally recyclable unit in the thermosetting industry.

6.7 Microstructural Analysis of Maleic Anhydride-Based ROMP Polymers

Recently, a fundamental study on the microstructure of ROMP polymers utilizing maleic anhydride-based ROMP monomers, norbornene dicarboxylic and/or oxanorbornene dicarboxylic derivatives, employing either first- or second-generation Grubbs ruthenium catalysts, was undertaken [32]. Specifically, Grubbs first-generation catalyst (**GC1A**) was compared to the Umicore catalyst, first constructed by Nolan (**GC1B**) (Fig. 6.18) [187]. Both of these first-generation-type catalysts were compared to second-generation Grubbs catalyst (**GC2**), using the monomer derivatives presented in Scheme 6.53 [32].

With respect to the monomers employed, polymers based on monomer **M1**, *exo,exo*-oxanorbornene dicarboxylic anhydride, yield polyanhydride molecules that can be further reacted to generate a myriad of derivatives; see Scheme 6.53a. Comparing the results of Poly-**M1** to those obtained with Poly-**M3**, *exo,exo*-oxanorbornene dicarboxylic dimethyl ester enables one to evaluate how the steric bulk at positions 5 and 6 influences the polymeric hierarchy; see Scheme 6.53c. Evaluating the results of Poly-**M3**, containing the *exo,exo* dimethyl ester structure, to Poly-**M4**, containing the diastereomeric *endo,exo* and *exo,endo* dimethyl esters, enables one to draw conclusions on how the stereostructure impacts the final architecture; see Scheme 6.53d. And lastly, comparing Poly-**M4** (oxanorbornene) to Poly-**M2** (norbornene) enables assessment on how position-7 affects the microstructure; see Scheme 6.53c [12, 13, 23–32, 94, 95, 141, 188–191].

ROMP homopolymers, and both random and block copolymers, were constructed with controlled molecular weight and low polydispersity. All the

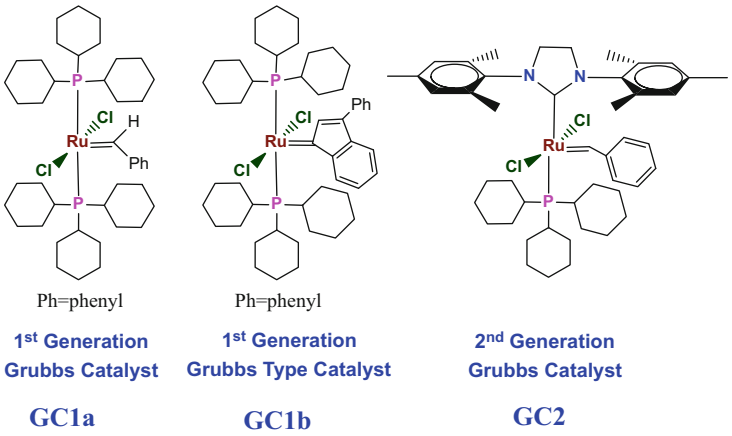

Fig. 6.18 Chemical structures for first-generation Grubbs catalyst (GC1a), first-generation Grubbs-type catalyst (GC1b), second-generation Grubbs catalyst (GC2) (Adapted from [32])

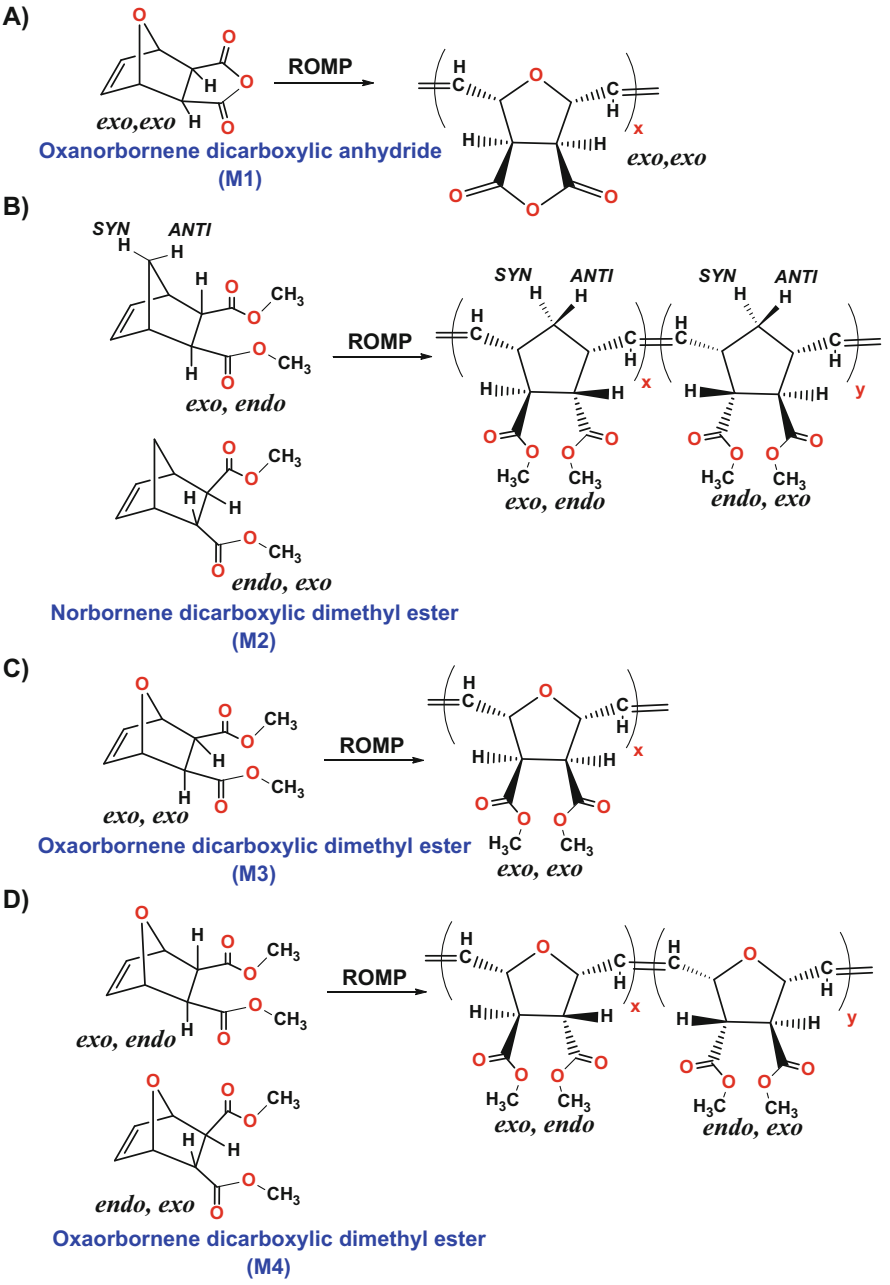

Scheme 6.53 Diastereomers and numbering designation of monomeric units used in this chapter (Adapted from [32])

ROMP polymers were obtained in yields ranging from 92 % to 98 % for the homopolymers and 86 % to 98 % for the copolymers [32]. Regardless of the identity of the monomer(s) used, or the class of catalyst employed, the GPC results clearly demonstrated a reproducible molecular weight range and low polydispersity for all polymers produced. In particular, the relative molecular weight ranged (M_w) from 44 to 37 KDa, with polydispersities from 1.5 to 1.3, for the block copolymers. Homopolymers and random copolymers exhibited relative molecular weights of 45–59 KDa and polydispersities ranging from 1.5 to 1.2.

Spectroscopic analyses on these polymers revealed that both the olefinic double bond and the bridgehead signals at positions 1 and 4 are clearly resolvable for each *cis* or *trans* isomer. A representative proton NMR spectrum for each of the homopolymers is displayed in Fig. 6.19.

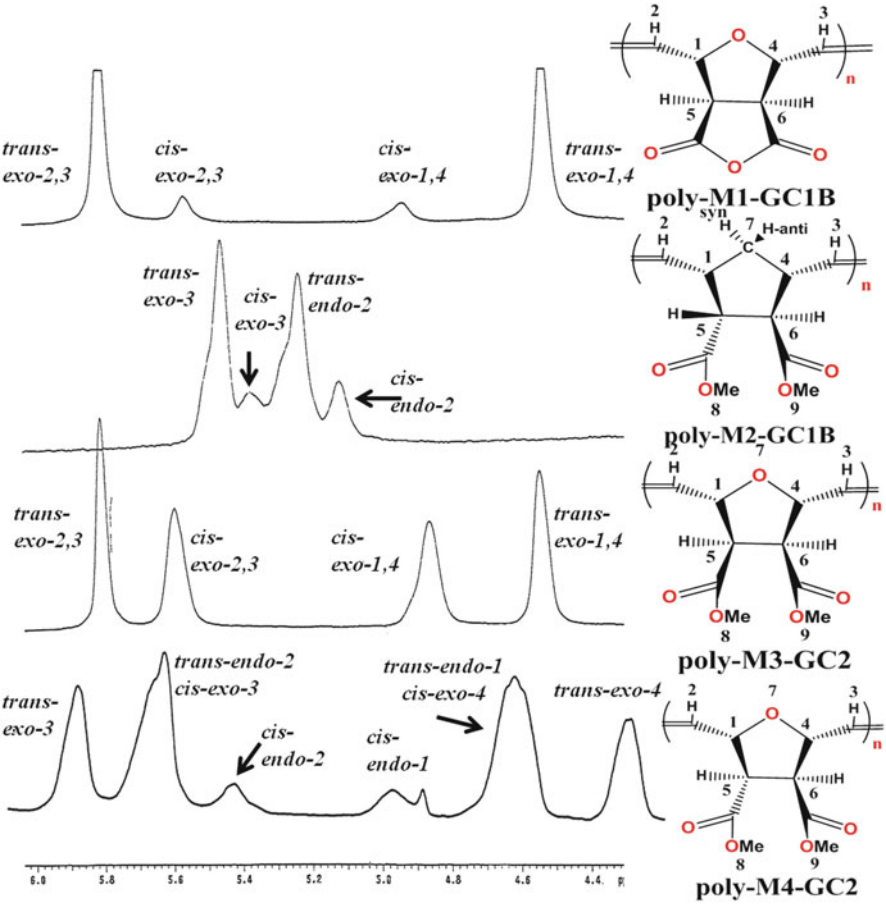

Fig. 6.19 Proton NMR spectra for each ROMP homopolymer

Proton and 13C NMR were used to determine the *cis*/*trans* level in all the polymers produced, and select examples are presented in Table 6.1. These results reveal that first-generation-type Grubbs catalysts **GC1A** and **GC1B** tend to yield high *trans*-containing polymers when using monomers **M1–M3**. Conversely, the second-generation-type Grubbs catalyst **GC2** tends to produce high *cis*-containing polymers; see Table 6.1. There was sufficient resolution to determine the *cis*/*trans* level for each comonomer in the block and random copolymers. These results reveal the exact same trend, in that first-generation catalysts produce high *trans*-containing copolymers, while second-generation catalyst produces high *cis*-containing copolymers, regardless if it was a random or block copolymer; see Table 6.1.

The Poly-**M1** anhydride exhibits the highest *trans* content when using first-generation ruthenium catalysts, ≈92–93 %. Addition of the bulky ester groups in the *exo,exo* configuration significantly decreases the *trans* content in Poly-**M3** as compared to Poly-**M1**, 60 % versus 93 %. A further decrease in *trans* content is observed if one of the esters groups is in the *endo* configuration as in Poly-**M4** versus Poly-**M3**, 50 % versus 60 %; see Table 6.1. Interestingly, when a methylene group is in position-7, as in the norbornene moiety of Poly-**M2**, a higher *trans* content is observed as compared to its oxa analog of Poly-**M4**, 70 % *trans* versus 50 %, respectively. Identical results were obtained for both the random and block copolymers when using first-generation Grubbs ruthenium catalyst; see Table 6.1.

Polymers constructed from second-generation Grubbs ruthenium catalyst exhibit higher *cis* content than their first-generation counterparts when using **M1–M3** monomers. Analogous to the results of first-generation catalysts, incorporation of the exo,exo esters as in Poly-**M3** versus the exo,exo anhydride of Poly-**M1** decreases the *trans* content of the polymer further. In other words, the *cis* content is enhanced when comparing Poly-**M3** (64 % cis) with Poly-**M1** (51 % cis). Incorporation of a methylene group in position-7, as in the norbornene

Table 6.1 Mole % *trans* double bonds in select polymers prepared by ROMP catalysts **GC1A**, **GC1B**, or **GC2** (Adapted from [32])

	Mole % *trans* for given catalyst (first monomer/second monomer)		
Polymer	GC1A	GC1B	GC2
Poly-**M1**	93	92	49
Poly-**M2**	70	75	40
Poly-**M3**	60	64	36
Poly-**M4**	**50**	–	**78**
Poly(**M2**-block-**M1**) 75:25	70/93	73/90	40/40
Poly(**M2**-block-**M1**) 50:50	75/95	67/90	-
Poly(**M2**-block-**M1**) 25:75	75/90	67/83	40
Poly(**M1**-random-**M2**) 50:50	–	75/80	50/40
Poly(**M1**-random-**M3**) 50:50	–	69/68	40/40

– denotes not synthesized

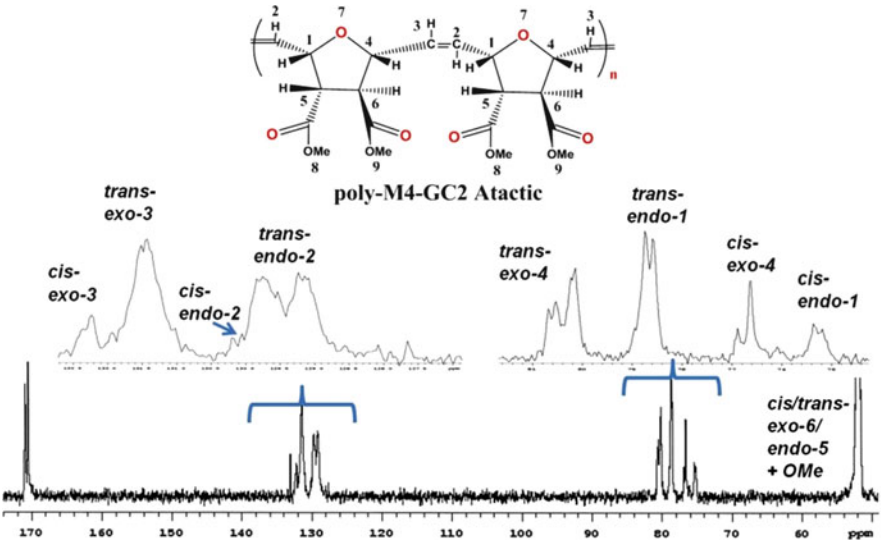

Fig. 6.20 Carbon NMR profile for atactic Poly-**M4–GC2** exhibiting resolvable *trans-exo, trans-endo, cis-exo, cis-endo*-1,4 bridgehead signals (Adapted from [32])

moiety of Poly-**M2**, along with the exo,endo esters, yields roughly the same *cis* content as compared to Poly-**M3**, 60 % *cis* versus 64 % *cis*, respectively. The block and random copolymers generated are virtually identical in their *cis* values when comparing to their homopolymer counterparts constructed by the second-generation Grubbs catalyst.

Results from 1D-13C-NMR and proton-NOESY experiments also indicate that all polymers constructed by either catalyst family are atactic. In other words, the monomer units are in a random distribution of orientations relative to the backbone. This is clearly evident by the multiplicity of each carbon signal attributable to the bridgehead 1,4-carbons of the oxanorbornene ring; see Fig. 6.20.

Astonishing results were obtained when using monomer **M4** and second-generation Grubbs catalyst. The Poly-**M4** constructed by **GC2** catalyst exhibited the complete opposite trend. In this case, the catalyst produced a high *trans*-containing polymer (78 % *trans*), instead of a high *cis*-containing polymer. Structurally, monomer **M4** contains an *endo* substituent in position 5 or 6 and an oxygen atom in position-7; see Scheme 6.54b. This combination results in a significant difference in *cis*/*trans* selectivity by **GC2**. Thus, the interplay of the catalyst with monomer **M4** is different than with all other monomers used. Similarly, the polymer architecture derived for the homopolymer of Poly-**M3** is different than that for Poly-**M4**, when using the second-generation Grubbs catalyst, 36 % *trans* versus 78 % *trans,* respectively; see Schemes 6.54. Structurally, the only difference between these two monomers is the presence of an *endo* substituent in the **M4** monomer versus *exo,exo* in the **M3** monomer.

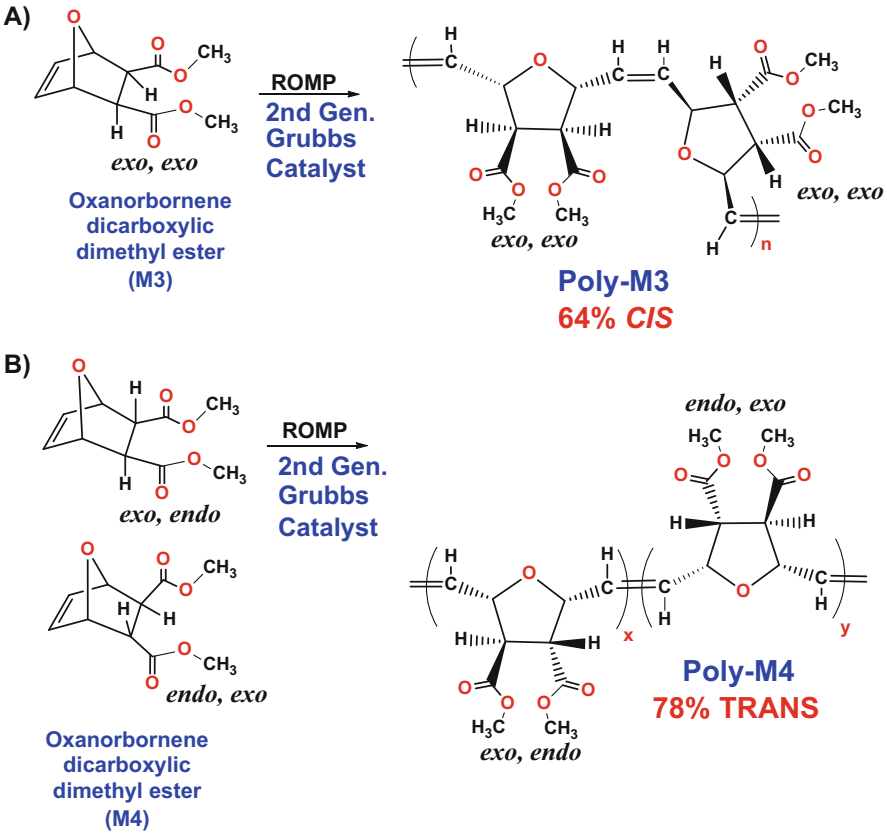

Scheme 6.54 Polymeric architecture comparing Poly-**M3** versus Poly-**M4** using second-generation Grubbs catalyst (Adapted from [32])

A similar trend was observed for Poly-**M2** versus Poly-**M4**, 40 % *trans* versus 78 % *trans,* respectively; see Scheme 6.55. In this case, the only difference is the oxygen atom at position-7 in oxanorbornene versus a methylene group in norbornene, whereas both of the esters are in the *endo,exo*/*exo,endo* configurations. At present, no ultimate rationale can be elucidated for the complete reversal in *cis*/*trans* selectivity between **M4** as compared to **M2** or **M3** monomer with regard to the second-generation catalyst. What is clear is that the presence of an *endo* substituent in either position 5 or 6 and an oxygen atom in position-7 drives the *trans* bias when interacting with second-generation Grubbs catalyst.

Additional microstructural details with respect to the polymeric linkage points between monomers (such as head–tail, head–head, or tail–ail) and the blockiness of the *cis* or *trans* double bonds down the polymer's main chain as well as the determination of the comonomer sequencing for the polymer were obtained through the use of 1H-13C-2D-HSQC–TOCSY NMR experiments, 2D-NOESY, and deuterated analogs of oxanorbornene monomer. These results confirmed

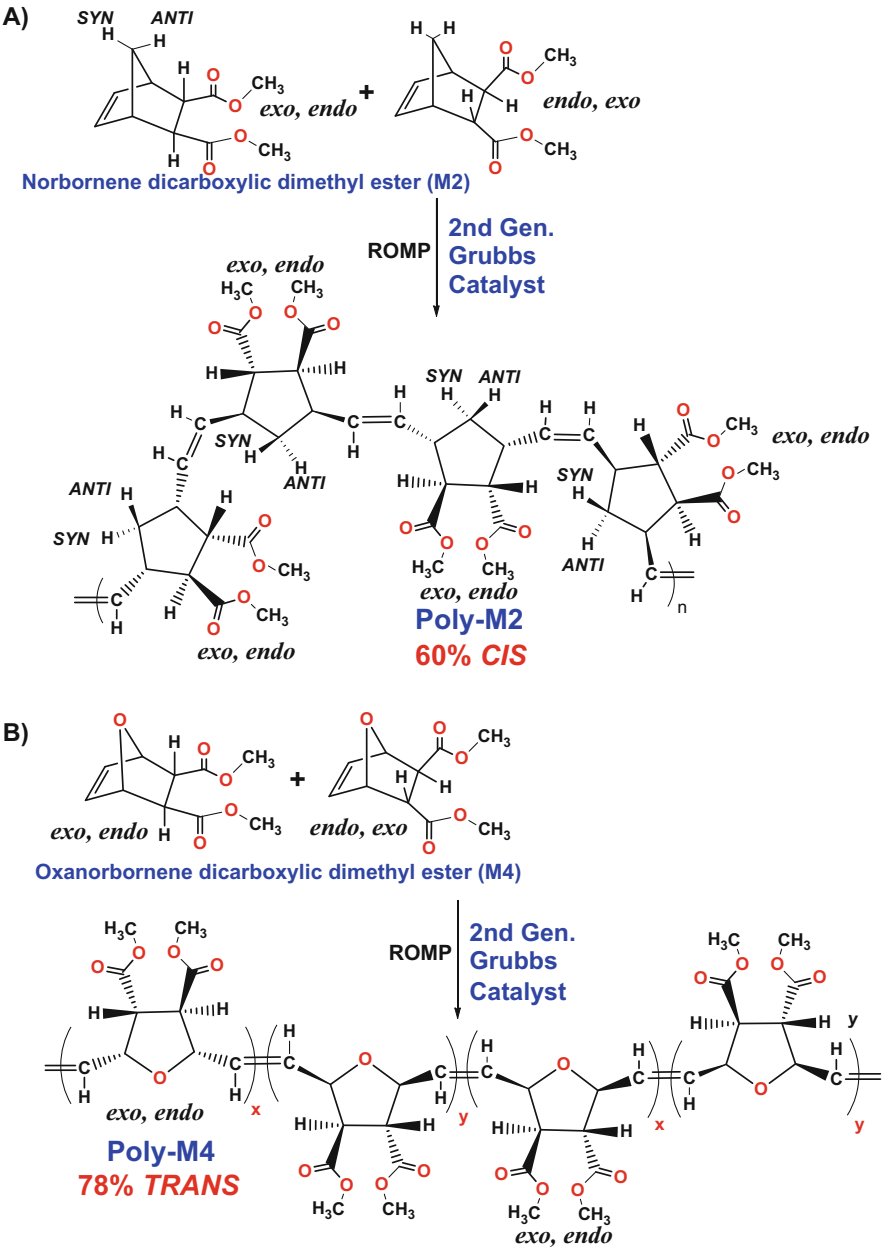

Scheme 6.55 Polymeric architecture for Poly-**M2** versus Poly-**M4** using second-generation Grubbs catalyst (Adapted from [32])

that random or block copolymers were indeed produced, rather than blends of homopolymers.

Given the large dispersion in both the carbon and proton NMR chemical shifts for these ROMP copolymers (Figs. 6.19 and 6.20) prompted further investigation into their comonomer sequence distribution by NMR. When using a 30 millisecond TOCSY mixing time, one obtains a correlation from a specific carbon signal to the proton of its nearest neighbor two bonds away (gold arrow in Fig. 6.22). In contrast, when using an 80 millisecond TOCSY mixing time, one obtains a correlation from the carbon signal to the proton of its next nearest neighbor four bonds away (green or red arrows). If one compares a 2D-HSQC correlating carbons to directly attached protons, to a 2D-HSQC–TOCSY, correlating carbon signals to protons on adjacent carbon atoms, one can construct the whole carbon backbone of the protonated molecule.

This strategy was employed to determine the linkage points between adjacent monomeric units in the ROMP copolymer backbone (Fig. 6.21). The bridgehead 1,4-proton and carbon signals corresponding to the *exo* or *endo* configurations, and the large separation in chemical shift for the *cis* versus *trans* signals are all well resolved from each other in both the Poly-**M4** and Poly-**M2** NMR spectra (Figs. 6.19 and 6.20). These results compelled the authors to further evaluate the polymer's sequence distributions with respect to *endo*,*exo* (H–T), *exo*,*endo* (T–H), *exo*,*exo* (H–H), and *endo*,*endo* (T–T) linkages by directly comparing HSQC–TOCSY results to elucidate the mole fraction for each linkage type present in the ROMP copolymer.

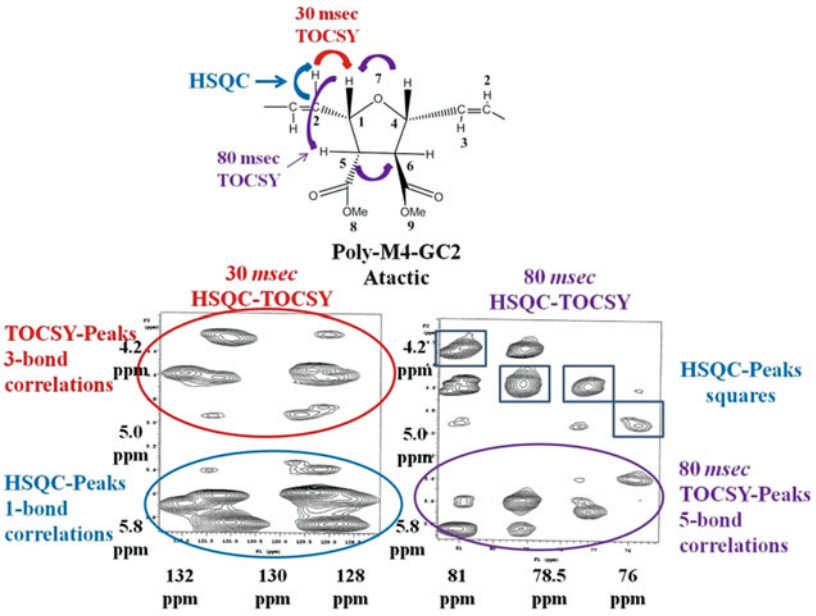

Fig. 6.21 HSQC vs. HSQC–TOCSY analysis for *endo*/*exo* poly M4-I2

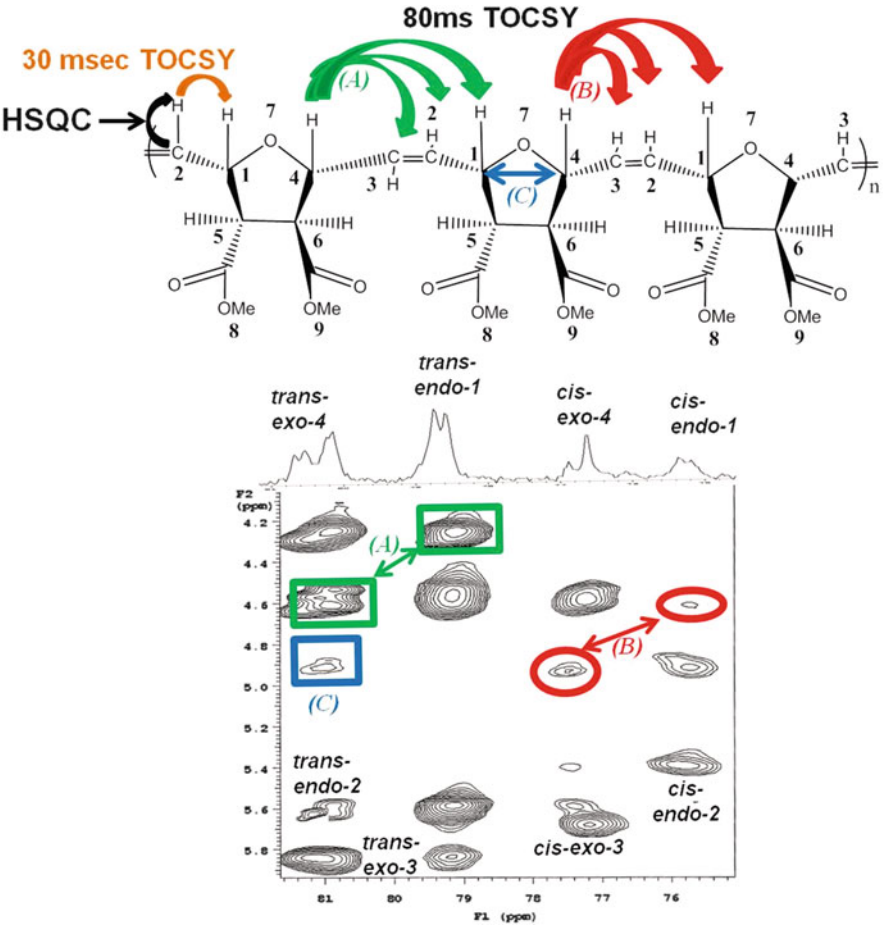

Fig. 6.22 Monomer sequencing analysis using **80 ms HSQC–TOCSY** results on Poly-**M4–GC2** (Adapted from [32])

Sequencing results further reveal that neighboring monomer units in the homopolymers of Poly-**M2** or Poly-**M4** are linked together in a head–tail fashion. In other words, *exo*,*endo* to *exo*,*endo* as judged by the *exo*,*endo* cross peaks is highlighted by green boxes/double-headed arrows for the *trans* comonomer unit versus the red boxes/double-headed arrows for its *cis* counterpart in the 80 ms-TOCSY experiments (Fig. 6.22).

The *cis* double bonds within the first-generation and second-generation-produced homopolymers are not in long blocks but are more homogenously distributed along the polymer backbone. In fact, through the use of a deuterated **M1**-monomer, the authors demonstrated that the second-generation Grubbs catalyst produces 60 % *cis*/40 % *trans* double bonds in Poly-**M1** that are mostly alternating along the polymer backbone, such as *cis-trans-cis-trans*.... This observation is further

supported by the sequencing results on Poly-**M4** using **GC2** catalyst, where the *trans-exo*-4 to *cis-endo*-1 correlation is highlighted by blue arrow/box in Fig. 6.22.

Results further reveal that random copolymers comprising either **M2** or **M4** monomer are statically distributed along the backbone. Neither of the individual comonomer units is in a long block of just one monomer type nor does it form an alternating copolymer. A slight preference of oxanorbornene–oxanorbornene over oxanorbornene–norbornene was observed in the 50/50 **M2/M3** random copolymer.

This discrimination signifies that despite an initial equimolar ratio of **M3** to **M2** monomer at the start of polymerization, there is a slight preference for **M3** to homopolymerize and form 60 % oxa–oxa junctions in comparison to 40 % **M3–M2** oxa–nor links. The *endo* substituent may kinetically decrease random copolymerization for monomer **M2** with monomer **M3**.

These results further confirm that a copolymer is formed by ROMP and not a blend of homopolymers or block copolymer. ROMP random copolymers predominantly exhibit a statistically random sequence distribution of both its cis/trans double bonds and its comonomer units along the main chain for this particular set of norbornene dicarboxylic and oxanorbornene dicarboxylic monomers.

Conformational analyses on maleic anhydride-based ROMP homopolymers were undertaken to elucidate the origin of particular structural features that explain the difficulty of hydrolyzing and hydrogenating Poly-**M1–G2**. All other polymers were less resistant to hydrolysis and hydrogenation processes. These findings implied a compact globular structure that prevents reactants from diffusing into the core of this particular homopolymer. Indeed, a high *cis* content was obtained for Poly-**M1–G2**, inferring that a compact turn could be responsible for this outcome. A head–tail *meso dyad* structure was one potential construct that could account for this behavior for the Poly-**M1–G2** homopolymer.

All other homopolymers could be hydrogenated and hydrolyzed, indicating these particular homopolymers could be in a more extended conformation. To reveal these structural elements, 2D-NOESY experiments were performed to obtain distance constraints between functional groups present within the homopolymer. Proton 2D-NOESY using 200, 300, and 400 ms mixing times reveal several important findings. NOESY results indicate that the *trans* olefinic protons are in close contact with the *cis* olefinic protons [36]. Given the intensity of the NOEs observed for the Poly-**M1–GC2** indicates that a high percentage of alternating *cis*/*trans* double bonds within the main chain is present.

This alternating *cis*/*trans* double bond structural motif is unique for Poly-**M1–G2**. Earlier reports indicated that the *cis* and *trans* double bonds are present in long blocks of each when using these ROMP catalysts [15, 23, 37–45, 94, 192–197]. The NMR results also indicate an overall atactic homopolymer.

Further studies utilizing deuterium isotopic labeling confirmed the original findings, namely, that an alternating *cis*/*trans* turn is responsible for a compact structure, involving three **M1** monomers that place the central **M1** monomer's *cis* and its *trans* double bonds in close special proximity as displayed in Fig. 6.23. Additional interactions observed in the 2D-NOESY experiments are denoted by purple arrows for intra-residue NOEs and red arrows for inter-residue NOEs in

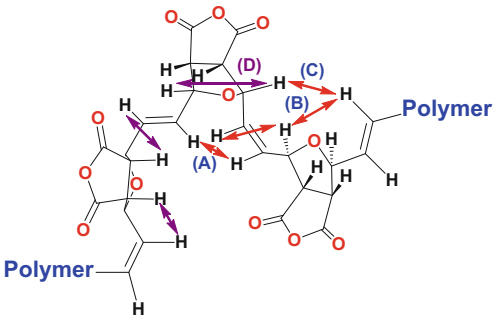

Fig. 6.23 Proton 2D-NOESY correlations observed for **GC2** derived poly(7-oxanorbornene anhydride) (Adapted from Tallon, M.A.; Rogan, Y., Marie, B., Clark, R.B., Musa, O.M., Khosravi, E., *J. Polym. Sci. Part A; Polymer Chemistry,* 2014, **52** (17), pp 2477–2501,Copyright 2014 with permission from John Wiley & Sons)

Fig. 6.23. Molecular modeling results also suggest this turn is energetically attainable as well.

Strong inter-residue NOEs between the *cis* double bond protons to the next residue's *trans* protons are observed denoted as (a) in Fig. 6.23. The *exo-cis* bridgehead proton is in close spatial proximity to the *trans* double bond proton of the next residue (b) in Fig. 6.20. The penultimate bridgehead proton to the *trans* double bond two residues away is also observed denoted by (c). These NOE correlations indicate that a turn structure would be required to obtain them, as presented in Fig. 6.23.

Closer inspection of the molecular modeling results reveals that all seven observed NOEs can be produced by this compact turn construct in Poly-**M1–GC2**. The intensity of the NOE signals further suggests a repetitive pattern of this structural element along the polymer backbone as well. These results would suggest a compact structure for the Poly-**M1–GC2** molecule and would support the problematic issue that this polymer could not be easily hydrolyzed nor hydrogenated as observed.

Utilizing the observed NOEs with molecular modeling and dynamics calculations gives rise to the proposed secondary structural elements that could be present in these polymers. Two distinct models emerge that are coherent with the experimental findings (Fig. 6.24). In particular, Poly-**M1–GC1A** exhibits an extended structure, while Poly-**M1–GC2** contains compact turns (Fig. 6.24). For visual clarity, the yellow atoms signify chain ends.

An identical strategy was applied for Poly-**M2**(*endo,exo*-norbornene dicarboxylic dimethyl ester) derived from first-generation Grubbs catalysts that produced predominantly *trans* atactic Poly-**M2–GC1** homopolymers(70–75 mol% *trans*). The 2D-NOESY results revealed a *trans-isotactic* bias, while the results of the 1D-tacticity studies, Poly-**M2–GC1B**, exhibits an atactic structure (***trans,***

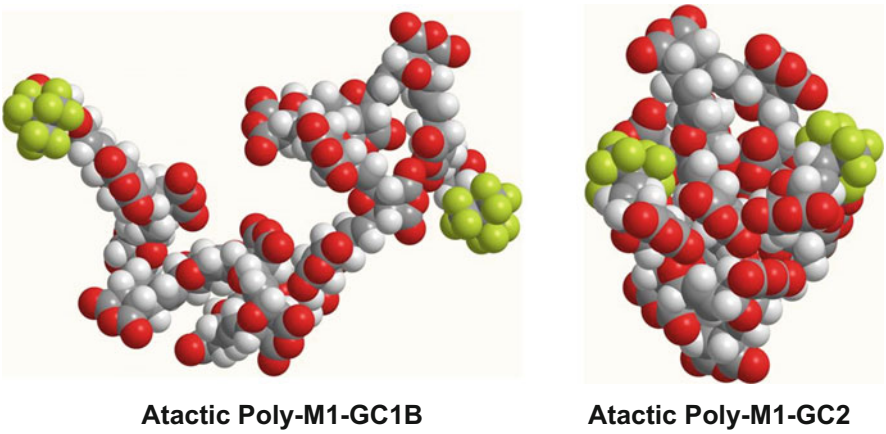

Fig. 6.24 Comparison of secondary structural elements for first-generation vs. second-generation Grubbs catalyst-derived poly(*exo,exo*-oxanorbornene dicarboxylic anhydride), space-filling model of atactic Poly-**M1–GC1B** containing 18 monomer units each (*yellow atoms* denote chain ends) vs. atactic Poly-**M1–GC2**) (Adapted from Tallon, M.A.; Rogan, Y., Marie, B., Clark, R.B., Musa, O.M., Khosravi, E., *J. Polym. Sci. Part A; Polymer Chemistry,* 2014, **52** (17), pp 2477–2501, Copyright 2014 with permission from John Wiley & Sons)

$P_r \approx 0.51/P_m \approx 0.49$; *cis*, $P_r \approx 0.56/P_m \approx 0.44$) with a slight preference or bias to a *trans-isotactic* and *cis-syndiotactic*.

From the correlations derived from the 2D-NOESY experiments and the results from the 1D-tacticity studies, the following secondary structural elements can be elucidated for Poly-**M2–GC1**, as depicted in Fig. 6.25. This extended structure is consistent in that the Poly-**M2** homopolymers, regardless of which catalyst is used, can be hydrogenated.

In contrast to the results obtained by first-generation Grubbs catalyst (Table 6.1), the second-generation Grubbs catalyst produces a predominantly *cis* homopolymer exhibiting 60 mol% *cis* double bonds. 1D-tacticity studies indicated an atactic or heterotactic arrangement with only a slight bias for a *cis-syndiotactic* configuration (*trans*, $P_r \approx 0.50/P_m \approx 0.50$; *cis*, $P_r \approx 0.55/P_m \approx 0.45$).

The 2D-NOESY results reveal that the *cis* double bond between adjoining monomers is arranged such that the rings of each monomer are perpendicular to each other (Fig. 6.25). Conversely, the *trans* monomer's rings are in a parallel or antiparallel orientation. The secondary structural elements of this type of an arrangement still give rise to an extended polymeric backbone structure. The Poly-**M2**-homopolymer, derived by second-generation Grubbs catalyst **GC2,** can be hydrogenated unlike Poly-**M1**-**GC2**, suggesting an extended polymeric backbone.

Combing this information into molecular modeling reveals a very kinky but extended secondary structure. The *cis* double bonds are accessible to hydrogenation as empirically confirmed (Fig. 6.26). Both poly(*endo,exo*-norbornene dicarboxylic dimethyl ester) homopolymers derived from either first- or second-generation

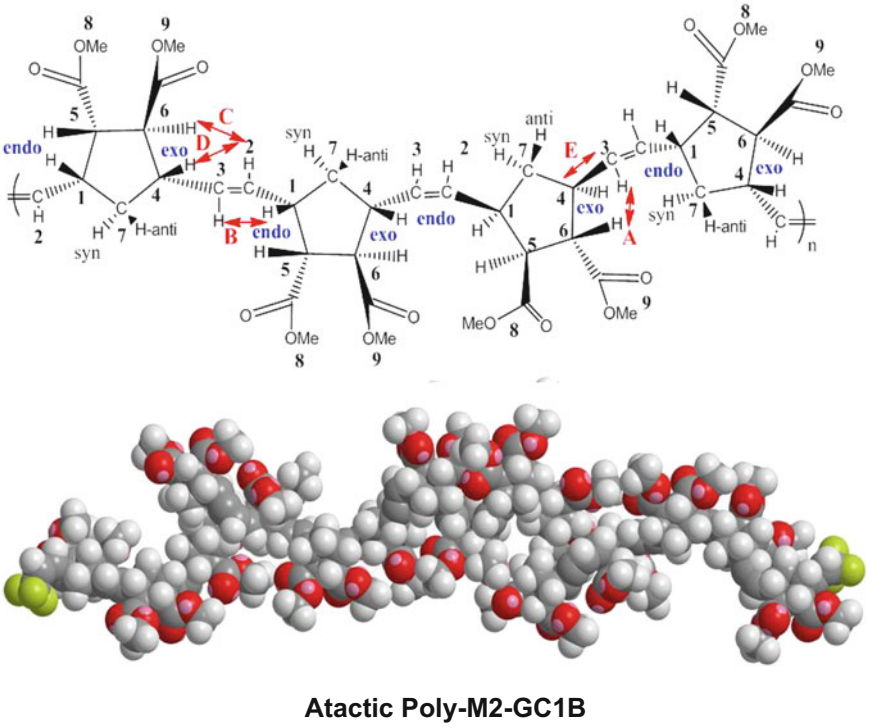

Fig. 6.25 Comparison of secondary structural elements for first-generation Grubbs catalyst-derived poly(*exo,endo-n*orbornene dicarboxylic dimethyl ester) atactic Poly-**M2–GC1B** (Adapted from [32])

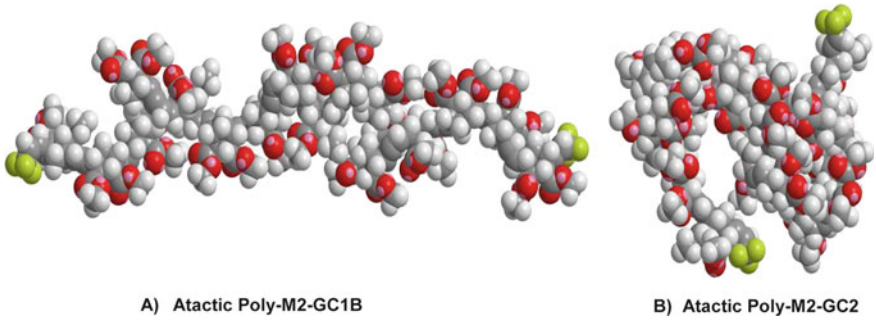

Fig. 6.26 Comparison of secondary structural elements for first-generation Grubbs catalyst vs. second-generation Grubbs catalyst-derived poly(*exo,endo-n*orbornene dicarboxylic dimethyl ester), (**a**) atactic Poly-**M2–GC1B** vs. (**b**) atactic Poly-**M2–GC2** (Adapted from [32])

Grubbs catalyst exhibit a different polymeric architecture, but both homopolymers are still extended and accessible. In contrast, the second-generation Grubbs catalyst fabricated Poly-**M1**-(*exo,exo* 7-oxanorbornene dicarboxylic anhydride) is not.

The results on Poly-**M4**(*endo,exo*-oxanorbornene dicarboxylic dimethyl ester) are the most interesting of all. A complete reversal in the trend for *cis*/*trans* selectivity is observed by both classes of Grubbs catalysts. First-generation Grubbs catalyst is expected to generate an atactic high *trans*-containing homopolymer, while the second-generation Grubbs catalyst is expected to construct an atactic high *cis*-containing homopolymer.

Yet, with the **M4** monomer, both catalysts reverse this trend. The first-generation Grubbs catalyst produces a higher 50 mol% *cis*-containing poly(*endo, exo*-oxanorbornene dicarboxylic dimethyl ester) that exhibits a strong bias for *cis*- and *trans-syndiotacticity,* ***50 mol% trans-(trans,*** $P_r \approx 0.65/P_m \approx 0.35$***; cis,*** $P_r \approx 0.67/P_m \approx 0.33$**.** The second-generation Grubbs catalyst constructs an atactic high *trans*-containing poly(*endo,exo*-oxanorbornene dicarboxylic dimethyl ester) that exhibits a strong bias for *trans-isotacticity* and *cis-heterotacticity,* ***78 mol% trans-(trans,*** $P_r \approx 0.33/P_m \approx 0.67$***; cis,*** $P_r \approx 0.47/P_m \approx 0.53$***)***.

These unusual results must somehow be related to the presence of an oxygen atom in position 7 of the ring system and its interaction with the catalyst/polymer chain end complex. Both classes of catalyst, first or second generation, still construct a homopolymer with an extended but kinky secondary chain structure (Fig. 6.27).

In summary, the following conclusions can be derived. All ROMP polymers exhibit an atactic microstructure. The adjoining monomers are linked in a head–tail fashion, regardless of the monomer identity or the catalyst used. In general, first-generation Grubbs catalyst constructs predominantly *trans* double bonds, while second-generation ruthenium catalyst assembles higher *cis*-containing polymers. A statistically random distribution of *cis* and the *trans* double bonds is predicted along the polymer's main chain from the models portrayed in Figs. 6.25, 6.26, and 6.27.

There are two notable exceptions to this trend. First is the Poly-**M1**, the oxanorbornene anhydride, in which its *cis* and *trans* double bonds are more alternating along the main chain. This results in a tight turn and an overall compact globular tertiary structure when using second-generation Grubbs catalyst. Second is the **M4** monomer. In this case, a complete reversal in *cis*/*trans* selectivity is obtained, where first-generation Grubbs catalyst constructs a high *cis*-containing polymer and second-generation catalyst assembles a highly *trans*-containing polymer with statistical distribution of *cis*/*trans* double bonds along the polymer's main chain.

For random copolymers, sequence distribution studies reveal that most of the comonomers will produce polymers that are statistically random in monomer distribution and not in long blocks of one monomer over the other. Even though a slight bias was observed for the Poly-**M2–M3** copolymer, where **M3–M3** sequences account for 60 % over the 40 % **M3–M2** sequences instead of the theoretical 50/50 ratio.

From these results, it is quite evident that ROMP can construct maleic anhydride-based polymers with variable architectures. These structures can be compact in nature or extended depending upon which catalyst is chosen. The structure of the monomer with regard to its configuration being *exo* or *endo* further influences how

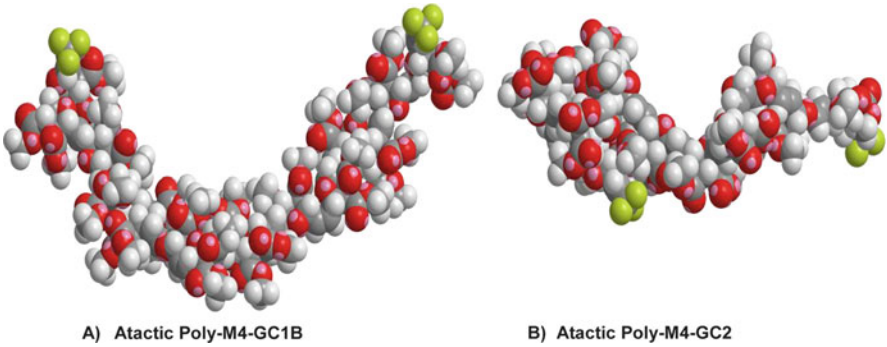

Fig. 6.27 Comparison of secondary structural elements for first-generation Grubbs catalyst vs. second-generation Grubbs catalyst-derived poly(*exo,endo-oxano*rbornene dicarboxylic dimethyl ester), (**a**) atactic Poly-**M4–GC1B** vs. (**b**) atactic Poly-**M4–GC2** (Adapted from [32])

the catalyst will choose the resultant *cis*/*trans* level in the ROMP polymer. This results in greater diversity to the structural isomerization products obtained and greater complexity than one would envision. Nevertheless, block copolymers are easily constructed using ROMP, thereby producing innovative polymers with novel structures.

References

1. Lindmark-Hamberg M, Wagener KB (1987) Macromolecules 20:2949
2. Sutthasupa S, Shiotsuki M, Sanda F (2010) Polym J 42:905
3. Cetinkaya S, Bayram R (2010) Heteroatom Chem 21(1):36–43
4. Asrar J, Hurlbut JB (1993) J Appl Polym Sci 50(10):1727–1732
5. Mukerjee SL, Kyllingstad VL (2002) U.S. Patent Application US 2002/0111446
6. Musa OM (2010) PCT International Application WO/2010/101882
7. Herrmann WA, Schattenmann WC, Nuyken O, Glander SC (1996) Angew Chem Int Ed 35 (10):1087–1088
8. Al-Hashimi M, Abu Bakar MD, Elsaid K, Bergbreiter DE, Bazzi HS (2014) RCS Adv 4:43766
9. Bermeshev MV, Gringolts ML, Starannikova LE, Volkov AV, Finkelstein ES (2009) New smart materials via metal mediated macromolecular engineering. NATO Sci Peace Security Ser A Chem Biol 4:319–326
10. Burry JS (2008) PCT International Application WO/2008/064973
11. Kolonko EM, Pontrello JK, Mangold LM, Kiessling LL, Kolonko EM (2009) J Am Chem Soc 131(21):7327–7333
12. Flook MM, Ng VWL, Schrock RR (2011) J Am Chem Soc 133:1784–1786
13. Flook MM, Gerber LCH, Debelouchina GT, Schrock RR (2010) Macromolecules 43:7515–7522
14. Keitz BK, Fedorov A, Grubbs RH (2012) J Am Chem Soc 134(4):2040–2043
15. Jeong H, Kozera DJ, Schrock RR, Smith SJ, Zhang J, Ren N, Hillmyer MA (2013) Organometallics 32(17):4843–4850
16. Kashif R, Torker S, Hoveyda AH (2013) J Am Chem Soc 135(p):10258–10261

17. Gerber LCH, Schrock RR (2013) Organometalics 32:5573–5580
18. Wang C, Kyle AF, Jakubec AF, Dixon DJ, Schrock RR, Hoveyda AH (2013) Chem Eur J 19 (p):2726–2740
19. Endo K, Grubbs RH (2011) J Am Chem Soc 133:8525–8527
20. Dang Y, Wang ZX, Wang X (2012) Organometalics 31:7222–7234
21. Tuba R, Grubbs RH (2013) Polym Chem 4:3959–3962
22. Roseburgh LE, Marx VM, Keitz BK, Grubbs RH (2013) J Am Chem Soc 135:10032–10035
23. Ivin KJ, Mol JC (1997) Olefin metathesis and metathesis polymerization. Academic, London, pp 238–259
24. Delaude L, Demonceau A, Noels AF (2003) Macromolecules 36:1446–56
25. Bazan GC, Khosravi E, Schrock RR, Feast WJ, Gibson VC, Regan BO, Thomas JT, Davis WM (1990) J Am Chem Soc 112:8378
26. Bazan GC, Oskam JH, Cho NH, Park LY, Schrock RR (1991) J Am Chem Soc 113:6899
27. Ivin KJ, Kenwright AM, Khosravi E, Hamilton JG (2000) J Organomet Chem 606:37–48
28. Leitgeb A, Wappel J, Slugovc C (2010) Polymer 51:2927–2946
29. Schrock RR (2011) Dalton Trans 40:7484–7495
30. Ivin KJ, Kenwright AM, Hofmeister GE, McConville DH, Schorock RR, Amir-Ebrahimir V, Carvill AG, Hamilton JG, Rooney JJ (1998) Macromol Chem Phys 199:547–553
31. Ivin KJ, Lapienis G, Rooney JJ, Stewart CD (1980) J Mol Catal 8:203–218
32. Tallon MA, Rogan Y, Marie B, Clark RB, Musa OM, Khosravi E (2014) J Polym Sci Part A. Polym Chem 52(17):2477–2501
33. Choi MC, Hwang JC, Kim C, Ando S, Ha CS (2010) J Polym Sci A Polym Chem 48:1806
34. Leventis N, Leventis CS, Mohite D, Larimore ZJ, Mang JT, Churu G, Lu H (2011) Chem Mater 23:2250
35. Dubois P, Coulembier O, Raquez JM (eds) (2009) Handbook of ring-opening polymerizations. Wiley-VCH, Weinheim
36. Schrock RR (2014) Acc Chem Res 47:2457
37. Khosravi E et al (2009) New smart materials via metal mediated macromolecular engineering. NATO Sci Peace Security Ser A Chem Biol 4:263–277
38. Nagarkar AA, Kilbinger FM (2014) Chem Sci 5:4687
39. Bielawski CW, Grubbs RH (2007) Prog Polym Sci 32:1
40. Grubbs RH (2003) Handbook of metathesis. Wiley-VCH, Weinheim
41. Grubbs RH, Wenzel AG, O'Leary DJ, Khosravi E (2015) In: Tzur E, Lemcoff G (eds) Handbook of metathesis. Wiley-VCH, Weinheim, Chapter 38
42. Vougioukalakis G, Grubbs R (2010) Chem Rev 110:1746–1787
43. Khosravi E (2003) The impact of well-defined transition metal catalysts on ROMP. Chapter 6 in Novel metathesis chemistry: well-defined catalyst systems for specialty chemical synthesis, tailored polymers, and advanced material applications, Springer, 122 of NATO science series: mathematics, physics, and chemistry
44. Buchmeiser MR (2000) Chem Rev 100:1565–1604
45. Slugovc C (2004) Macromol Rapid Commun 25:1283–1297
46. Herrison J, Chauvin Y (1971) Makromol Chem 141:161–167
47. Nicolas J, Guillaneuf Y, Lefay C, Bertin D, Gigmes D, Charleux B (2013) Prog Polym Sci 38:63
48. Moad G, Rizzardo E (1995) Macromolecules 28:8722
49. Bertin D, Gigmes D, Marque SRA, Tordo P (2011) Chem Soc Rev 40:2189
50. Fischer H (2001) Chem Rev 101(12):3581–3610
51. Hawker CJ, Barclay GG, Dao J (1996) J Am Chem Soc 118(46):11467–11471
52. Volodarsky LB, Reznikov VA, Ovcharenko VI (1994) Synthetic chemistry of stable nitroxides. CRC Press, Boca Raton, FL
53. Siegenthaler KO, Studer A (2006) Macromolecules 39(4):1347
54. Dao J, Benoit D, Hawker CJJ (1998) Polym Sci 36:2161

55. Bonilla-Cruz J, Guerrero-Sanchez C, Schubert US, Saldivar-Guerra E (2010) J Eur Polym 46:298
56. Lessard B, Maric M (2010) Macromolecules 43:879
57. Garcia-Valdez O, Ramirez-Wong DG, Saldivar-Guerra ES, Luna-Barcenas G (2013) Macromol Chem Phys 214(12):1396
58. Zhang M, Li YH, Gong YD, Zhao N, Zhang XF (2002) Biomaterials 23:2641
59. Kato M, Kamigaito M, Sawamoto M, Higashimura T (1995) Macromolecules 28:1721
60. Cowie JMG, Arrighi V (2008) Polymers: chemistry and physics of modern materials, 3rd edn. CRC Press, Boca Raton, FL, pp 82–84
61. Matyjaszewski K, Xia J (2001) Chem Rev 101(9):2921
62. Wang Y, Zhong M, Zhang Y, Magenau AJD, Matyjaszewski K (2012) Macromolecules 45:8929
63. Wang Y, Soerensen N, Zhong M, Schroeder H, Buback M, Matyjaszewski K (2013) Macromolecules 46:689
64. Yeole N (2010) Synlett 10:1572
65. Keddie DJ (2014) Chem Soc Rev 43:496
66. Moad G, Rizzardo E, Thang SH (2008) Polymer 49(5):1079
67. Moad G, Rizzardo E, Thang SH (2010) Mater Matter 5(1):2
68. Chiefari J, Chong YK, Ercole F, Krstina J, Jeffery J, Le T, Mayadunne R, Meijs GF, Moad CL, Moad G, Rizzardo G, Thang SH (1998) Macromolecules 31(16):5559
69. Moad G, Rizzardo E, Thang SH (2009) Aust J Chem 62(11):1402
70. Benaglia M, Chen M, Chong YK, Moad G, Rizzardo E, Thang SH (2009) Macromolecules 42:9384
71. Benaglia M, Chefari J, Chong YK, Moad G, Rizzardo E, Thang SH (2009) J Am Chem Soc 131:6914
72. De Brouwer H, Schellekens MA, Klumperman B, Monteiro MJ, German AL (2000) J Polym Sci A Polym Chem 38(19):3595
73. Schellekens MAJ, Klumperman B (2000) J Macromol Sci Rev Macromol Chem Phys 40:167
74. Jancova K, Kops J, Chen X, Batsberg W (1999) Macromol Rapid Commun 20:219
75. Waterson C, Haddleton DM (1999) Polym Prepr 218:1045
76. Benoit D, Hawker CJ, Huang EE, Lin Z, Russell TP (2000) Macromolecules 33:1505
77. Chen G-Q, Wu Z-Q, Wu J-R, Li Z-C, Li F-M (2000) Macromolecules 33:232
78. Le T, Moad G, Rizzardo E, Thang SH (1998) World Patent WO 9801478 A1 and 980115
79. Chong YK, Le TPT, Moad G, Rizzardo E, Thang SH (1999) Macromolecules 32:2071
80. Sanayei RA, O' Driscoll KF, Klumperman B (1994) Macromolecules 27:5577
81. Billmeyer FW Jr (1984) Textbook of polymer science, 3rd edn. Wiley-Interscience, New York, p 329
82. Sandler SR, Karo W (1995) Polymer synthesis, vol II, 2nd edn. Academic, San Diego, CA, p 271
83. Greenley RZ (1980) J Macromol Sci A Chem 14(4):445
84. Bork JF, Coleman LE (1960) J Polym Sci 18:413
85. Tolman CA (1970) J Am Chem Soc 92(10):2956
86. Dias EL, Nguyen ST, Grubbs RH (1997) J Am Chem Soc 119:3887
87. Love JA, Morgan JP, Trnka TM, Grubbs RH (2002) Angew Chem Int Ed 41(21):4035
88. Choi TL, Grubbs RH (2003) Angew Chem Int Ed 42(15):1743
89. Schurer SC, Buschmann N, Blechert S (2000) Angew Chem Int Ed 40:3898
90. Randl S, Buschmann N, Connon SJ (2001) Synlett 10:1547
91. Carey FA, Sundberg RJ (2007) Advanced organic chemistry: part B: reactions and synthesis, 5th edn. Springer, New York
92. Kobuke Y, Sugimoto T, Furukawa J, Fueno T (1972) J Am Chem Soc 94(10):3633
93. Johnson JS, Evans DA (2000) Acc Chem Res 33(6):325
94. Zenkl E, Stelzer F (1992) J Mol Catal 76:1–14
95. Ho HT, Ivin KJ, Reddy BSR, Rooney J (1989) Eur Polym J 25:805–811

96. Ozer R (2011) PCT International Application WO/2011/026059
97. Csihony S, Fischmeister C, Bruneau C, Horvath IT, Dixnuef PH (2002) New J Chem 23:1667
98. Hillmyer MA, Lepetit C, McGrath DV, Novak BM, Grubbs RH (1992) Macromolecules 25:3345
99. Viswanathan T, Jethmaiani J (1993) J Chem Educ 2:165
100. Burtscher D, Grela K (2009) Angew Chem Int Ed 48:442
101. Monteil V, Wehrmann P, Mecking S (2005) J Am Chem Soc 127:14568
102. Mingotaud AF, Kramer M, Mingotaud CJ (2007) J Mol Catal A Chem 263:39
103. Mingotaud AF, Mingotaud CJ, Moussa W (2008) J Polym Sci A Polym Chem 46:2833
104. Airaud C, Heroguez V, Gnanou Y (2008) Macromolecules 41:3015
105. Airaud C, Ibarboure E, Gaillard C, Heroguez V (2009) J Polym Sci A Polym Chem 47:4014
106. Mohr B, Lynn DM, Grubbs RH (1996) Organometallics 1:4317
107. Gallivan JP, Jordan JP, Grubbs RH (2005) Tetrahedron Lett 46:2577
108. Hong SH, Grubbs RH (2006) J Am Chem Soc 128:3508
109. Jordan JP, Grubbs RH (2007) Angew Chem Int Ed 46:5152
110. Gulajski L, Michrowska A, Bujok R, Grela K (2006) J Mol Catal A Chem 254:118
111. Gulajski L, Michrowska A, Naroznik J, Karczmarska Z, Rupnicki L, Grela K (2008) ChemSusChem 1:103
112. Allaert B, Dieltiens N, Ledoux N, Veracaemst C, Van Der Voort P, Stevens CV, Linden A, Verpoort F (2006) J Mol Catal A Chem 260:221
113. Binder JB, Guzei IA, Raines RT (2007) Adv Synth Catal 349:395
114. Skowerski K, Szczepaniak G, Wierzbicka C, Gulajski L, Bieniek M, Grela K (2012) Catal Sci Technol 2:2424
115. Grubbs RH (1995) In: Horvath IT, Joo F (eds) Aqueous organometallic chemistry and catalysis. Kluwer, Amsterdam, p 15
116. Tew GN, Madkour AE, Alfred SF, King PP, Colak S (2012) US Patent US 8,329,927
117. Tomasek J, Schatz J (2013) Green Chem 15:2317
118. Bertin PA, Smith D, Nguyen ST (2005) Chem Commun 1:3793
119. Ogawa S, Takano S, Fujimon H, Itoh T, Kaita S, Lida T, Wakatsuki Y (2010) React Funct Polym 70(9):565
120. Kilbinger AF (2012) Chimia 66(3):99
121. Schaefer M, Hanik N, Kilbinger FM (2012) Macromolecules 45:6807
122. Kurzhals S, Binder WH. In: Grubbs RH, Wenzel AG, O'Leary DJ, Khosravi E (eds) (2015) Handbook of metathesis. Wiley-VCH Verlag GmbH, p 207, Chapter 35
123. Gauthier MA, Klok HA (2008) Chem Commun 23:2591
124. Gauthier MA, Gibson ML, Klok HA (2009) Angew Chem Int Ed 48(1):48
125. Pontrello JK, Allen MJ, Underbakke ES, Kiessling LL (2008) J Am Chem Soc Commun 127:14356
126. Rolfe A, Loh JK, Maity PK, Hanson PR (2010) Org Lett 13(1):4
127. Ahmed M, Barrett AGM, Braddock DC, Cramp SM, Procopiou PA (1999) Tetrahedron Lett 40:8657
128. Barrett AGM, Cramp SM, Roberts RS (1999) Org Lett 1:1083
129. Weck M, Jackiw JJ, Rossi RR, Weiss PS, Grubbs RH (1999) J Am Chem Soc 121:4088
130. Lindsley CW, Hodges JC, Filzen GF, Watson BM, Geyer AG (1999) Comb Chem 2:550
131. Buchmeiser MR, Wurst K (1999) J Am Chem Soc 121:11101
132. Wang X, Chen L, Xu X, Li Y (2011) Anal Bioanal Chem 401(4):1423
133. Mayr B, Sinner F, Buchmeiser MR (2001) J Chromatogr A 907(1–2):47
134. Nam E, Kim J, Guntari SN, Seyler H, Fu Q, Wong EH, Biencowe A, Jones DJ, Caruso F, Qiao GG (2014) Chem Sci 5:3374
135. Keller MW (2013) In: Hayes W (ed) Healable polymer systems, RSC polymer chemistry series no. 5. Royal Society of Chemistry, Greenland, Chapter 2
136. Camel V (2003) Spectrochim Acta Part B 58:1177
137. Buchmeiser MR (2008) J Separ Sci 31(11):1907

138. deRonde BM, Tew GN (2015) Biopolymers 104:265
139. Bodansky M (1993) Principles of peptide synthesis, 2nd edn. Springer, New York
140. Biagini SCG, Coles MP, Gibson MR, Marshall EL, North M (1998) Polymer 39:1007
141. Sutthasupa S, Terado K, Sanda F, Masuda T (2007) Polymer 48:3026
142. Lienkamp K, Madkour AE, Musante A, Nelson CF, Nusslein K, Tews G (2008) J Am Chem Soc 130(30):9836
143. Conrad RM, Grubbs RH (2009) Angew Chem Int Ed 48:8328
144. Patel PR, Kiser-Conrad RM, Lu YY, Fong E, Ho WC, Tirrell DA, Grubbs RH (2012) Biomacromolecules 13(18):2546
145. Hahn ME, Randolph LM, Adamiak L, Thompson MP, Gianneschi NC (2013) Chem Commun 49(28):2873
146. Isarov SA, Pokorski JK (2015) ACS Macro Lett 4(9):969
147. Eren T, Som A, Rennie JR, Nelson CF, Urgina Y, Nusslein K, Coughlin EB, Tew GN (2008) Macromol Chem Phys 209:516
148. Zasloff M (2002) Nature 415:389
149. Brogden KA (2005) Nat Rev Microbiol 3:238
150. Lienkamp K, Kumar KN, Som A, Nusslein K, Tew GN (2009) Chem Eur J 15:11710
151. Lienkamp K, Madkour AE, Kumar KN, Nusslein K, Tew GN (2009) Chem Eur J 15:11715
152. Kurado K, DeGrado WF (2004) Polym Prepr (Am Chem Soc Div Polym Chem) 84:435
153. Klajnert B, Janiszewska J, Uranczyk-Lipkowska Z, Bryszewska M, Shcharbin D, Labieniec M (2006) Int J Pharm 309:208
154. Liu Z, Deshazer H, Rice AJ, Chen K, Zhou C, Kallenbach NR (2006) J Med Chem 49:3436
155. Makovitski A, Avrahami D, Shai Y (2006) Proc Natl Acad Sci USA 103:15997
156. Al-Ahmad A, Laird D, Zou P, Stienberg T, Lienkamp K (2013) PLoS One 8(9), e73812
157. Ermondi G, Caron G (2006) Biochem Pharmacol 72:1633
158. He Y, Ye T, Su M, Zhang C, Ribbe AE, Jiang W, Mao C (2008) Nature 452:198
159. Hyun J, Chilkoti A (2001) Macromolecules 34:5644
160. Kang Y, Guo K, Li BJ, Zhang S (2014) Chem Commun 50:11083
161. Chen Y, Guan Z (2014) Chem Commun 50:10868
162. Perez CM, Rank LA, Chmielewski J (2014) Chem Commun 50:8174
163. Fleischer M, Schmuck C (2014) Chem Commun 50:10464
164. Zhang J, Dong S, Zhang K, Liang A, Yang X, Huang F, Cao Y (2014) Chem Commun 50:8227
165. Tian YK, Yang ZS, Lv XQ, Yao RS, Wang F (2014) Chem Commun 50:9477
166. Yan J, Li W, Zhang A (2014) Chem Commun 50:12221
167. Li L, Raghupathi K, Song C, Prasad P, Thayumanavan S (2014) Chem Commun 50:13417
168. Ringsdorf H, Schlarb B, Venzmer J (1988) Angew Chem Int Ed 27(1):113
169. Warren NJ, Armes SP (2014) J Am Chem Soc 136(29):10174
170. Couet J, Biesalski M (2006) Macromolecules 39(21):7258
171. Iovu MC, Craley R, Jeffries-EL M, Krankowski AB, Zhang R, Kowalewski T, McCullough RD (2007) Macromolecules 40(14):4734
172. Bazzi HS, Sleiman HF (2002) Macromolecules 35(26):9617
173. Dalphond J, Bazzi HS, Kahrim K, Sleiman HF (2002) Macromol Chem Phys 203:1988
174. Lee JK, Chi YS, Lee JS, Kim YG, Jung YH, Oh E, Ko SB, Jung HJ, Kang PS, Choi IS (2005) Langmuir 21:10311
175. Li H, Wang L, Jacob K, Wong CP (2002) J Polym Sci A Polym Chem 40:1796
176. Yang S, Chem JS, Korner H, Breiner T, Ober CK, Polikis MD (1998) Chem Mater 10:1475
177. Chen JS, Ober CK, Polikis MD (2002) Polymer 43:131
178. Wang L, Wong CP (1999) J Polym Sci A Polym Chem 37:2991
179. Khosravi E, Musa OM (2011) Eur Polym J 47:465
180. Wang L, Li H, Wong CP (2000) J Polym Sci A Polym Chem 38:3771
181. Zhang X, Chen GC, Collins A, Jacobson S, Morganelli P, Dar YL (2008) J Polym Sci A Polym Chem 47:1073

182. Mison P, Sillion B (1999) Adv Polym Sci 140:137
183. Gacal B, Cianga L, Agag T, Takeichi T, Yagei Y (2007) J Polym Sci A Polym Chem 45:2774
184. Lui YL, Hsieh CY (2006) J Polym Sci A Polym Chem 44:905
185. Agag T, Takeichi T (2006) J Polym Sci A Polym Chem 44:1424
186. Khosravi E, Iqbal F, Musa OM (2011) Polymer 52(2):243
187. Hou SH (2012) Synthesis and characterization of durable thermosetting materials. Durham Thesis, Durham University. Available at Durham E-Thesis Online: http://etheses.dur.ac.uk/3563/
188. Ivin KJ, Kress J, Osborn JA (1988) J Mol Catal 46:351–358
189. Amir-Ebrahimi V, Corry DAK, Hamilton JG, Rooney JJ (1998) J Mol Catal A Chem 133:115–122
190. Ho HT, Ivin KJ, Rooney JJ (1982) J Mol Catal 15:245–270
191. Benedicto A, Novack BM, Grubbs RH (1992) Macromolecules 25:5893–5900
192. Manka JT, Douglass AG, Kaszynski P, Friedli AC (2000) J Org Chem 65:5202–5206
193. France MB, Alty LT, Earl TM (1999) J Chem Educ 76:659
194. France MB, Uffelman ES (1999) J Chem Educ 76:661
195. Breitenkamp K, Emrick T (2005) J Polym Sci A Polym Chem 43:5715
196. Lehman Jr SE, Matayabas Jr JC, Jayaraman S (2014) US Patent 8,643,199 B2
197. De Fremont P, Clavier H, Montembault V, Fontaine L, Nolan SP (2008) J Mol Catal A Chem 283:108–113

Chapter 7
Colloidal and Physicochemical Properties of Maleic Anhydride Polymers

Roger L. McMullen

7.1 Introduction

The colloidal and physicochemical properties of maleic anhydride-based polymers are very interesting due to their dynamic conformational behavior. A significant portion of this chapter is dedicated to the topic of conformational behavior of dilute solutions of copolymers of maleic anhydride copolymers. There is a wealth of literature on this topic due to interest in elucidating the colloidal properties of polyacids. Great strides were made in this area utilizing a variety of wet chemistry and instrumental techniques, starting with potentiometric titration, which is a fundamental approach to gaining insight into the chain dynamics of polyacids. Studies based on sophisticated techniques, such as dynamic rheology and spectrofluorescence, help to provide greater insight into conformational phenomena related to maleic anhydride-based polymers. In addition, the interactions of surfactants with maleic anhydride-based polymers are equally intriguing and provide researchers with insights into multicomponent systems, which are commonly found in commercial formulations.

In addition to the solution behavior of maleic anhydride-based polymers, there has been considerable interest in thin films of these polymers deposited on selected substrates. Finally, polymers based on maleic anhydride have been explored for their ability to form polyelectrolyte complexes. These multimolecular complexes have potential applications in a variety of advanced technological fields, and a vast number of studies have been carried out and are reported in the literature.

R.L. McMullen (✉)
Ashland, Inc., 1005 Route 202/206, Bridgewater, NJ 08807, USA
e-mail: rmcmullen@ashland.com

O.M. Musa (ed.), *Handbook of Maleic Anhydride Based Materials*,
DOI 10.1007/978-3-319-29454-4_7

7.2 Conformational Behavior of Dilute Solutions of Maleic Anhydride Copolymers

In the last four decades, there has been a significant amount of interest in understanding the conformational behavior of maleic anhydride polymers in dilute aqueous solution. The earliest work in this area, realized by Ulrich Strauss and Paul Dubin in the late 1960s, focused on understanding hydrophobic microdomain structure of copolymers of maleic anhydride and *n*-alkyl vinyl ethers (Fig. 7.1) [1–3]. Hydrophobic substitution of the vinyl ether monomers of the polymer provide unique behavior characteristic of polysoaps. In summary, it was found that the microdomain structure is composed of micelle-like domains, and the polymer exists in a compact hypercoiled conformation.

A number of techniques have been used to characterize these polymers; however, some of the very first studies were conducted using potentiometric titration allowing researchers to monitor pH as a function of degree of dissociation (α) of the protons from the carboxylic acid functionalities. Upon dissolution in water, maleic anhydride copolymers convert to the diacid form in which each carboxylic acid has a distinct pK_a value. The most commonly studied copolymers of maleic anhydride contained alkyl vinyl ethers with chain lengths ranging from $n = 1$ (methyl substituted) to $n = 16$ (hexadecyl substituted). Overall, it was concluded that the compact conformation exists at low pH for $n = 4$–10; however, as the polymers are neutralized, they undergo a transition to an extended coil form. For polymers where $n = 1$–3, the polymers exist in the random coil state at all dissociation values ($\alpha = 0$–2), and when $n > 10$ they exist in the compact conformation regardless if the carboxylic acid groups are dissociated or not. In addition, the size of the microdomains and the number of hydrophobic units participating in the intramolecular micelles is also an important topic of discussion, which was not adequately addressed until more recently [4–8].

In the paragraphs that follow, a number of techniques are summarized that help shed light on the conformational behavior of copolymers of maleic anhydride and *n*-alkyl vinyl ethers. Utilizing data obtained from potentiometric titrations, viscosity measurements, and fluorescence spectrophotometry, we provide a detailed description of the conformational transitions experienced by these polymers in dilute aqueous solutions. Understanding these phenomena provides us with a more comprehensive structure–function relationship of these materials.

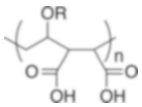

Fig. 7.1 Molecular structure of a copolymer of *n*-alkyl vinyl ether and maleic anhydride, where $R = 1$–16 methylene/methyl groups

7.3 Potentiometric Titration Studies of Polyacids

Acid–base potentiometric titration is one of the most utilized techniques to study the solution behavior of polyacids [9–11]. It allows one to determine pH and other important equilibrium and thermodynamic parameters while the carboxylic acids undergo dissociation. From a conformational perspective, the titration process, starting from low pH and then increasing, leads to the removal of hydrogen ions from the carboxyl groups. Such an event changes the polymer from a neutral molecule to a polyelectrolyte containing negative charges. In a typical polyacid that is not hydrophobically modified, one would expect the polymer chains to transition from a random coil structure to an extended random coil structure. As base is added to the system, the polymer becomes more and more negatively charged, resulting in repulsion of adjacent carboxylate groups, which ultimately leads to extension of the polymer chains.

7.3.1 Treatment of Titration Data

In a potentiometric titration, the degree of neutralization may be expressed as:

$$\alpha = \frac{[\mathrm{NaOH}] + [\mathrm{H}^+] - [\mathrm{OH}^-]}{[\mathrm{Polymer}]} \tag{7.1}$$

in which case [NaOH], [H^+], and [OH^-] are the molarities of added titrant, free hydrogen ion, free hydroxide ion, and polymer.

The Henderson–Hasselbalch equation is commonly used in chemistry to estimate the pH of buffer solutions, determine the extent of ionization state in polypeptides, and study acid–base equilibrium [12]. It is given by the following relationship:

$$\mathrm{pH} = \mathrm{p}K_\mathrm{a} + \log \frac{[\mathrm{A}^-]}{[\mathrm{HA}]} \tag{7.2}$$

where $\mathrm{p}K_\mathrm{a}$ (equivalent to $-\log K_\mathrm{a}$) is the dissociation constant of the weak acid. [HA] and [A^-] are the molarities of the weak acid and its conjugate base. For poly (monoprotic acids), such as poly(acrylic acid), the Henderson–Hasselbalch equation becomes [13]:

$$\mathrm{pH} = \mathrm{p}K_0 - \log\left[\frac{1-\alpha}{\alpha}\right] + \frac{1}{\mathrm{RTln}(10)}\left(\frac{\partial G_\mathrm{el}}{\partial \alpha}\right) \tag{7.3}$$

where $\mathrm{p}K_0$ is the intrinsic dissociation constant of an ionized group in the polyelectrolyte and G_el is the electrostatic free energy change. Most often, this equation

is expressed in terms of the apparent dissociation constant, pK_a, which can be measured from the experiment:

$$pK_a = pH + \log\left[\frac{1-\alpha}{\alpha}\right] + \frac{1}{RTln(10)}\left(\frac{\partial G_{el}}{\partial \alpha}\right) \tag{7.4}$$

In the case of poly(diprotic acids), the Henderson–Hasselbalch equation must take into consideration the dissociation of two carboxylic acids [2]:

$$pH = pK_{1^0} - \log\left\{\frac{1}{2}\left(\frac{1-\alpha}{\alpha}\right) + \frac{1}{2}\left[\left(\frac{1-\alpha}{\alpha}\right)^2 + \frac{4K_{2^0}}{K_{1^0}}\left(\frac{1-\alpha}{\alpha}\right)\right]^{1/2}\right\} + \frac{1}{RTln(10)}\left(\frac{\partial G_{el}}{\partial \alpha}\right) \tag{7.5}$$

in which case K_{1^0} and K_{2^0} are the first and second intrinsic ionization constants of the two carboxylic acid groups in poly(maleic acid) and related copolymers.

As already stated, the apparent dissociation constant, pK_a, is determined from the potentiometric titration. Values of pK_{1^0} are obtained by extrapolating pK_a (Eq. 7.4) to $\alpha = 0$. By performing some algebraic manipulation, pK_{2^0} may then be determined at $\alpha = 1$ by Eq. (7.6), given that pK_{1^0} is already known:

$$\frac{pK_{1^0} + pK_{2^0}}{2} = pH_{\alpha=1} - \frac{1}{RTln(10)}\left(\frac{\partial G_{el}}{\partial \alpha}\right)_{\alpha=1} \tag{7.6}$$

Additional data from potentiometric titration studies may be obtained by calculating the area under the curves. Often, data are presented in the form of pH vs. α, pK_a vs. α, or $[RTln(10)]^{-1}(\partial G_{el}/\partial \alpha)$ vs. α.

7.3.2 *Potentiometric Titration Studies of Hydrophobically Modified Poly(Maleic Acid)*

For illustration, Fig. 7.2 contains a potentiometric titration curve for several copolymers of maleic anhydride and *n*-alkyl vinyl ethers. From the curves, one may note that at low degrees of dissociation ($0 < \alpha < 1$), the methyl- and ethyl-substituted polymers behave similarly. These titration data are very similar to that obtained for poly(maleic acid) [13]. On the other hand, the butyl and hexyl forms have a steeper slope in this region of the plot, which is indicative of the compact conformation in these polymers at low degrees of dissociation. The strength of the intramolecular hydrophobic interactions at low pH allows the hydrophobic forces to overpower those of electrostatic repulsion brought about by the conversion of carboxylic acid to carboxylate functional groups. Interestingly, conductometric titrations were carried out on the same types of polymers, which demonstrated that the

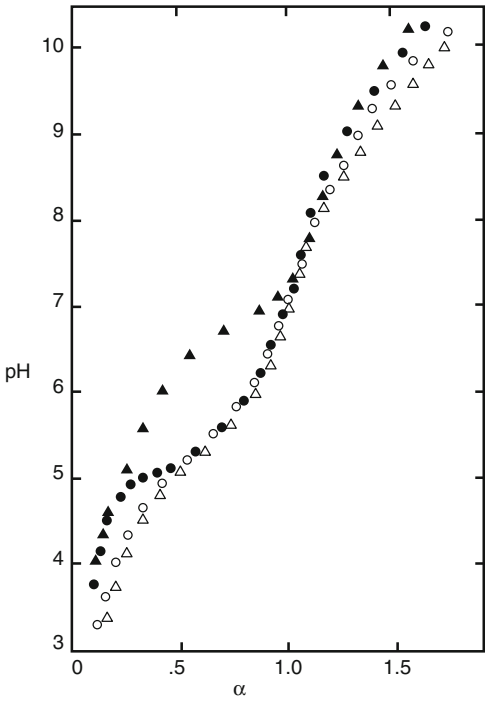

Fig. 7.2 Potentiometric titrations of poly(maleic acid–methyl vinyl ether) (*open triangle*), poly (maleic acid–ethyl vinyl ether) (*open circle*), poly(maleic acid–butyl vinyl ether) (*closed circle*), and poly(maleic acid–hexyl vinyl ether) (*closed triangle*). Experiments were conducted in pure water at 30 °C. Reprinted with permission from P. Dubin and U. Strauss, *J Phys Chem* **1970,** *74* (14), 2842–2847 [2]. Copyright, 1970, American Chemical Society

hydrophobically modified maleic anhydride copolymers [poly(maleic acid–decyl vinyl ether)] have less conductance than polyelectrolyte samples without hydrophobic modification [poly(maleic acid–methyl vinyl ether)] [14].

At a certain point in the potentiometric titration, the curves for both the butyl- and hexyl-substituted polymers flatten due to the transition from the compact to the extended random coil state. It should be noted that the butyl-substituted polymer undergoes the transition at lower dissociation than the hexyl system—a clear demonstration that longer chain lengths provide greater hydrophobic interactions, which to a certain extent are able to counteract electrostatic repulsions. At higher degrees of dissociation ($1 < \alpha < 2$), and after the transition regions for the butyl- and hexyl-substituted polymers, all of the titration curves are similar.

Titration data also provide insight into other structural properties of maleic anhydride-based polymers. For example, since we know the pK_{a^1} and pK_{a^2} of the carboxylic acid groups in poly(maleic acid–alkyl vinyl ether) are 3.47 and 6.47, respectively, we can make several deductions about its local secondary structure. The difference between these two pK_a values is 3.0. For comparison, $\Delta pK_a = 4.2$ for maleic acid, while $\Delta pK_a = 1.4$ for succinic acid. More than likely, the similarity of the ΔpK_a values for maleic acid and poly(maleic acid–alkyl vinyl ether) is probably

related to the similarity of their steric configuration. The two carbon atoms of maleic acid are separated by a double bond, which is not the case for the polymer. In fact, in terms of bonding architecture, the polymer is more like succinic acid. Therefore, the mere fact that the ΔpK_a of the poly(maleic acid–alkyl vinyl ether) polymers is closer in value to maleic acid than succinic acid implies that steric interactions may be involved and that there is restricted motion on the backbone of the polymer chain [15]. It should also be noted that hydrogen bonding occurs between adjacent carboxylic acid groups, and this also affects pK_a values. As a result, the carboxylic acid groups tend to be in the *cis* conformation.

7.4 Thermodynamics of the Ionization Process for Copolymers of Maleic Anhydride

Thermodynamic parameters can provide insight into the polymer chain dynamics during dissociation. Heat of dissociation (ΔH^0) data is particularly intuitive as it can provide some explanation of the local environment of the polymer chains. Likewise, changes in the free energy (ΔG^0) and entropy (ΔS^0) as a function of ionization also yield insight into the physical state of the system. Normally, calorimetry is the preferred method of choice for determining ΔH^0. A calorimeter may be used to measure physical changes as well as phase transitions in the polymer system. The experiment is normally carried out by monitoring temperature, pressure, and volume of the system and utilizing this data to calculate key thermodynamic parameters. Other methods may also be used, often providing a qualitative description of the process of interest.

A typical plot of ΔH^0 as a function of the degree of dissociation of poly(maleic acid–butyl vinyl ether) is provided in Fig. 7.3. A broad transition centered at $\alpha = 0.375$ is clearly evident in the plot. By generating a baseline (dashed line), one may integrate the negative peak to obtain a value for the enthalpy of the polyelectrolyte conformational transition (ΔH_C).

As one might expect, salt concentration influences the thermodynamic transitions. Figure 7.4 includes plots of heat of dissociation as a function of polymer ionization for added salt concentrations of 0.04 M and 0.20 M NaCl. The heat of dissociation in the transition becomes notably smaller (comparing 0.04 M NaCl with the sample in Fig. 7.3, which does not contain salt) resulting in a ΔH_C value significantly smaller, −345 cal/mol for 0.04 M NaCl as compared to −561 cal/mol for 0.0 M NaCl.

Potentiometric titration data may also shed light on thermodynamic parameters related to the transition from the compact to extended random coil form. It has been shown by Strauss and coworkers that a value proportional to the free energy change associated with the transition (ΔG_t°) can be determined by taking the area difference of the potentiometric titration curves between the polymer undergoing the transition and the same hypothetical polymer if it existed in the extended random coil

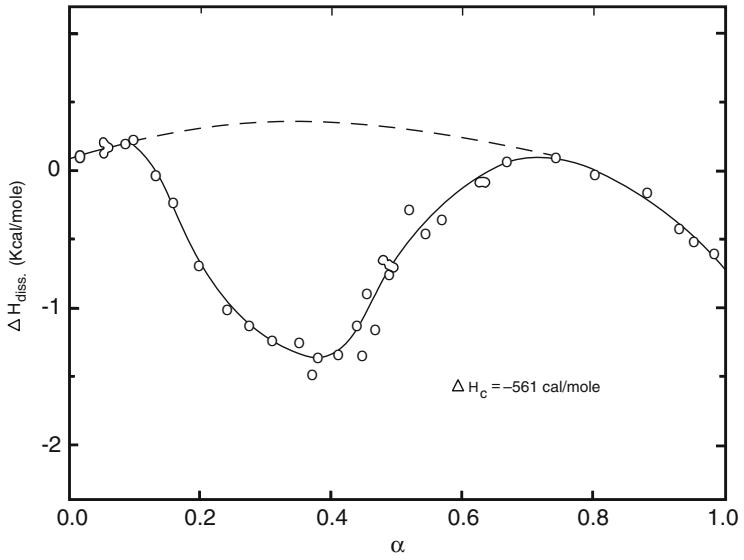

Fig. 7.3 Plot of heat of dissociation as a function of ionization of poly(maleic acid–butyl vinyl ether). Temp = 25 °C; [polymer] = 2.0×10^{-2} eq/mol. Reprinted with permission from Crescenzi et al., *J Polym Sci C* **1972,** *39*, 241–246 [16]. Copyright, 1972, John Wiley & Sons

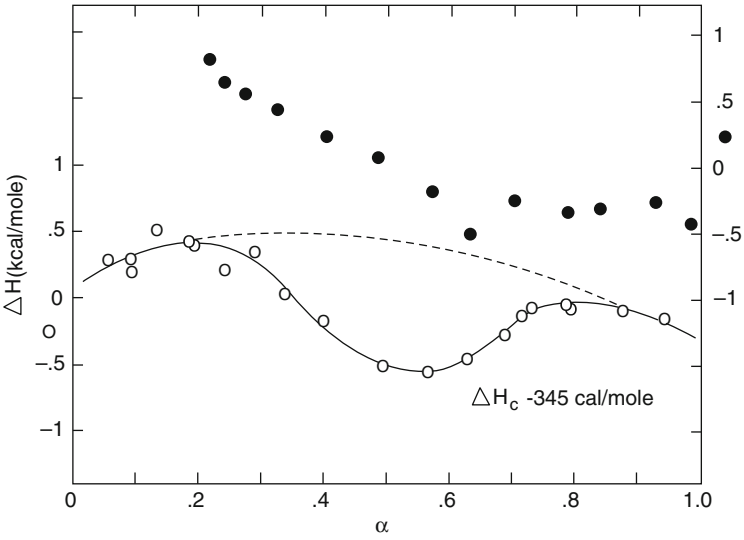

Fig. 7.4 Plot of heat of dissociation as a function of dissociation of poly(maleic acid–butyl vinyl ether) containing two concentrations of salt: 0.04 M NaCl (*closed circle*) (*left* ordinate) and 0.20 M NaCl (*open circle*) (*right* ordinate). Temp = 25 °C; [polymer] = 2.0×10^{-2} eq/mol. Reprinted with permission from Crescenzi et al., *J Polym Sci C* **1972,** *39*, 241–246 [16]. Copyright, 1972, John Wiley & Sons

conformation over all α values. In experiments, data obtained from poly(maleic acid–ethyl vinyl ether) is used as the hypothetical extended random coil polymer across all α values, simply because it behaves in this manner due to its short alkyl chain [17]. Using this methodology, the butyl and hexyl forms of the copolymers yield free energy values (ΔG_t°) of 310 and 1110 cal/mol, respectively. One may further calculate the contribution of each methylene group as 400 cal/mol to the stabilization of the compact conformation.

Another thermodynamic parameter that provides insight into the molecular processes that take place during the dissociation of the polyacid is the entropy difference associated with the transition. As already mentioned, ΔH_c^0 and ΔG_c^0 can be determined by calorimetry and potentiometric titrations. Therefore, one may employ the thermodynamic relationship below:

$$\Delta G_c^0 = \Delta H_c^0 - T\Delta S_c^0 \tag{7.7}$$

To solve for ΔS_c^0:

$$\Delta S_c^0 = -\frac{\Delta G_c^0 - \Delta H_c^0}{T} \tag{7.8}$$

It should be pointed out that the use of this relationship is based on the assumption that conditions are relatively close to standard state.

Studies conducted with poly(maleic acid–butyl vinyl ether) indicate that the entropy change associated with the transition is negative [16]. Such a result suggests that hydrophobic forces are primarily responsible for stabilizing the initial compact conformation.

In similar studies, utilizing both calorimetry and potentiometry, a range of poly (maleic acid–*n*-alkyl vinyl ethers) with varying degrees of hydrophobic modification were studied. These consisted of the methyl, ethyl, propyl, butyl, pentyl, hexyl, and octyl forms of the polymer. A sample of selected data will be presented in terms of the rate of change of ΔG_c^0 as a function of the degree of ionization $(\partial G/\partial \alpha)$. The slope for the polymers with low degrees of hydrophobic modification (methyl, ethyl, propyl, and butyl) slightly increases as a function of dissociation until $\alpha = 1$ where they experience an abrupt increase (see Fig. 7.5). Overall, this group of compounds behaves similarly over the entire ionization range. The initial slight increase in the curves is typical for polyacids and can be ascribed to the increasing electrostatic potential with increasing dissociation [18]. The sharp increase in $(\partial G/\partial \alpha)$, observed at $\alpha = 1$, is believed to arise due to the electrostriction of water by the doubly protonated acid groups [19].

A slightly different picture emerges when we examine poly(maleic acid–*n*-alkyl vinyl ethers) with longer side chains. For the butyl-substituted polymer, at $\alpha = 0.4$, there is a drop in $(\partial G/\partial \alpha)$ until $\alpha = 0.4$, which is believed to be due to the lower affinity of the polymer for hydrogen ion in terms of electrostatic interactions as it becomes deionized and enters the extended conformation. Based on corresponding enthalpy and entropy data obtained from this same region of the deionization curve, it is thought that changes in thermodynamic behavior are caused by the

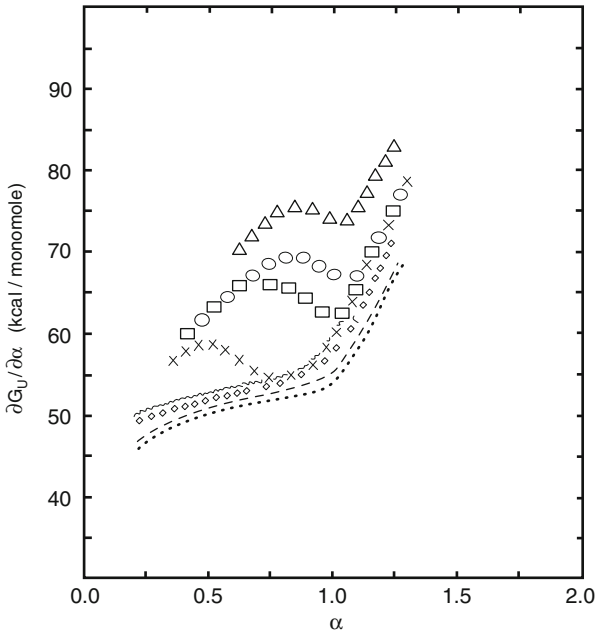

Fig. 7.5 Plot of differential free energy as a function of ionization for variants of poly(maleic acid–*n*-alkyl vinyl ethers): methyl (*dotted line*), ethyl (*dashed line*), propyl (*open diamond*), butyl (*multiplication symbol*), pentyl (*open square*), pentyl baseline (*wavy line*), hexyl (*open circle*), and octyl (*open triangle*). Reprinted with permission from Martin and Strauss, *Biophys Chem* **1980,** *11*, 397–402 [19]. Copyright, 1980, Elsevier

reorganization of water around the newly exposed aliphatic chains [19]. Similar to the butyl-substituted polymer, the pentyl, hexyl, and octyl forms of the polymer show similar transitions in the $(\partial G/\partial \alpha)$ curves, although the transitions are greater in magnitude and slightly shifted. More than likely, this effect is observed due to increasing degrees of hydrophobicity in these polymers.

7.5 Rheological Properties of Polyacids

The rheological performance of polymers in dilute aqueous solutions can provide insight into their conformational behavior. Similar to the potentiometric titration studies, solution viscosity measurements can be carried out at various degrees of deionization for flexible copolymers of maleic anhydride allowing one to make observations about their swelling behavior as a function of pH. The most simple form of the molecule, poly(maleic acid), undergoes changes in viscosity as function of dissociation of the carboxylic acid groups. As elaborated above, these changes in solution behavior are due to conformational changes of the polymers as the negatively charged carboxylate groups begin to repel each other resulting in swelling in which extended random coil conformation prevails.

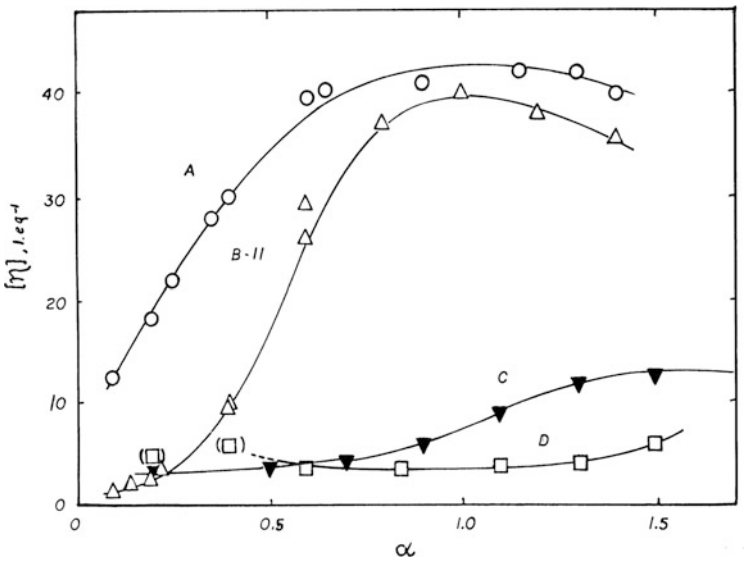

Fig. 7.6 Plot of intrinsic viscosity as a function of degree of dissociation for poly(maleic acid–ethyl vinyl ether) (*open circle*), poly(maleic acid–butyl vinyl ether) (*open triangle*), and poly (maleic acid–hexyl vinyl ether) (*inverted closed triangle*) in 0.04 M NaCl at 30 °C and poly(maleic acid–octyl vinyl ether) (*open square*) in 0.01 M NaCl at 30 °C. Reprinted with permission from Dubin and Strauss, "Hypercoiling in hydrophobic polyacids," published in *Polyelectrolytes and their applications*, Eds. A. Rembaum and E. Sélégny [3]. Copyright, 1975, D. Reidel Publishing Co.

Utilizing the same systems described above, early work concentrated on elucidating the viscosity behavior of copolymers of maleic anhydride and *n*-alkyl vinyl ethers. Figure 7.6 provides a plot of viscosity as a function of dissociation of the carboxyl groups (α). Not surprising, poly(maleic acid–ethyl vinyl ether) portrays typical behavior expected for a weak polyacid. At increasing values of α, the viscosity of the solution increases due to the electrostatic repulsions caused by the anionic carboxylate groups.

Poly(maleic acid–butyl vinyl ether) also undergoes a rheological transition although its viscosity values are much lower at low degrees of deionization. Again, this behavior at low α may be interpreted as resulting from the presence of a highly compact conformation. Once 50 % of the carboxylic acid groups are deprotonated ($\alpha = 1$), the poly(maleic acid–butyl vinyl ether) solution reaches a comparable value to poly(maleic acid–ethyl vinyl ether). The behavior of poly (maleic acid–butyl vinyl ether) at $\alpha = 1$ may be interpreted as the result of the electrostatic repulsion forces becoming greater in magnitude than the van der Waals forces present in the intramolecular stabilized conformation. As shown in Fig. 7.6, poly(maleic acid–hexyl vinyl ether) behaves similar to poly(maleic acid–butyl vinyl ether), although it has much lower viscosity values—again indicative of greater stabilization of the compact conformation by longer alkyl chains.

7.6 Spectrofluorescence Studies of Polymer Conformation

A very informative way to study the colloidal behavior of polymers and surfactants is to utilize fluorescent probe techniques. Typically, molecular fluorescence is extremely dependent on the fluorophore's environment. For example, the maximum emission wavelength (λ_{em}) may shift or change in intensity due to a change in the fluorophore's molecular environment. This is very typical when monitoring fluorescence of a given material in polar versus nonpolar solvents.

Strauss and coworkers took advantage of these properties of fluorophores and attached a dansyl group (1-dimethylamino-naphthalene-5-sulfonyl) to the polymer backbone of several copolymers of maleic anhydride and *n*-alkyl ethers [20, 21]. The reaction takes place between the amino group of the dansyl moiety and the maleic anhydride group of the copolymers (see Scheme 7.1). A relatively small degree of substitution (<10 %) is carried out, as very little modification is required to fluorescently tag the polymer. In a nonpolar environment, the fluorescent probe has a $\lambda_{em} = 500$ nm, which undergoes a shift to longer wavelengths, and a decrease in intensity, in increasingly polar environments.

A plot of fluorescence emission at $\lambda_{em} = 520$ nm versus carboxylic acid dissociation is provided in Fig. 7.7 for the butyl- and methyl-substituted copolymers. Striking, but not surprising, the plot for poly(methyl vinyl ether–maleic acid) is very low in intensity at all carboxylic acid dissociation values ($0 < \alpha < 2$). Such a

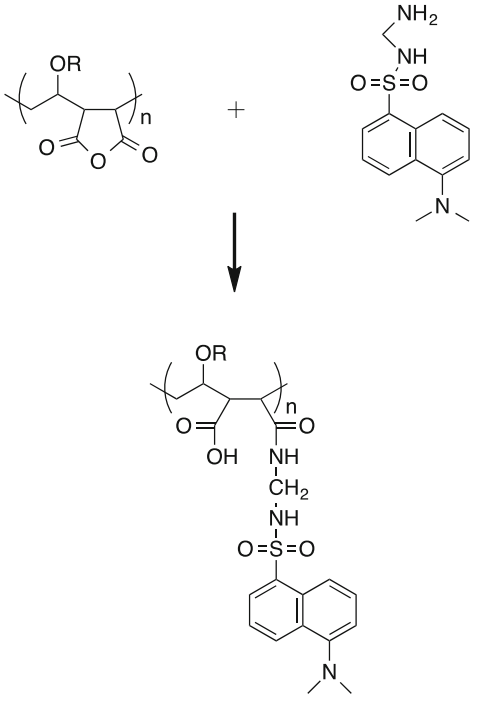

Scheme 7.1 Poly(maleic anhydride–alkyl vinyl ether) labeled with dansyl according to [20, 21]

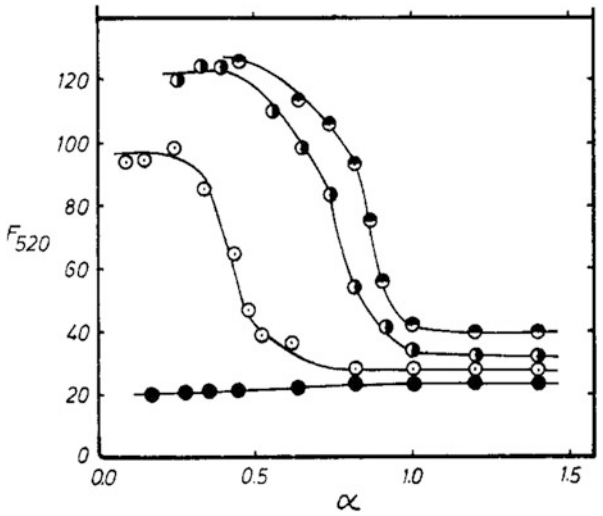

Fig. 7.7 Fluorescence intensity at 520 nm as a function of the degree of dissociation for copolymers of maleic anhydride and *n*-alkyl vinyl ethers derivatized with a fluorescence probe (dansyl group). Higher fluorescence intensity indicates that the dansyl group is in a more hydrophobic environment. Poly(maleic acid–methyl vinyl ether) in water (*closed circle*) is compared to poly(maleic acid–butyl vinyl ether) in water (*open circle*), 0.2 M NaCl (*half-right closed circle*), and 0.5 M NaCl (*half-top closed circle*). Reprinted with permission from U. Strauss and G. Vesnaver, *J Phys Chem* **1975,** *79* (22), 2426–2429 [21]. Copyright, 1975, American Chemical Society

result is in accordance with a dye that is present in a polar environment. Hence, one may surmise that poly(methyl vinyl ether–maleic acid) exists in the extended random coil conformation regardless of the deionization state of the polymer. Poly(butyl vinyl ether–maleic acid) exhibits slightly different behavior, where the fluorescence probe is present in a nonpolar environment (reflected by the high fluorescence intensity) at low dissociation values ($0 < \alpha < 0.4$). This state is indicative of the hypercoiled compact conformation. After undergoing a transition ($0.4 < \alpha < 0.6$), poly(butyl vinyl ether–maleic acid) transforms into the extended random coil conformation.

Two additional trials of poly(butyl vinyl ether–maleic acid), completed at different salt concentrations, demonstrate the role of electrostatic forces in polymer dynamics. At 0.2 M and 0.5 M NaCl, the amount of fluorophore in a hydrophobic environment at the initial state ($0 < \alpha < 0.4$) is significantly greater than in the absence of salt. In addition, the onset of the transition region is shifted to higher degrees of dissociation. It appears that screening the negatively charged electrostatic repulsions of the carboxylate groups with sodium counterions allows the compact conformation to persist until greater degrees of dissociation are reached since the repulsive forces are less powerful than is the case when no salt is added.

Studies carried out at several concentrations of each polymer show equivalent behavior. Such a result demonstrates that the hydrophobic domains are formed as a result of intra-chain, rather than interchain, van der Waals interactions of the alkyl chains [8]. These findings are in contrast with surfactant micelles, which form intermolecular micelles, demonstrating that there is no critical micelle concentration with polysoaps of copolymers of maleic anhydride and *n*-alkyl vinyl ethers.

Other fluorescent probes can also be used to investigate the intramolecular association of copolymers of maleic anhydride and *n*-alkyl vinyl ethers [22, 23]. In particular, pyrene is commonly used as a fluorescence probe to determine the microenvironmental properties of micelles and other higher-order assemblies of molecules (see Scheme 7.2).

Using such methodology, hydrophobically modified poly(maleic acid–octyl vinyl ether) was compared to poly(maleic acid–methyl vinyl ether), also demonstrating that the polysoap undergoes a conformational transition from the compact to extended random coil conformation as the carboxylic acid groups are neutralized (see Fig. 7.8) [22]. This work demonstrated that the long alkyl chains (octyl) from the vinyl ether portion of the polymer form hydrophobic microdomains, and estimates were made that as little as 50 octyl groups could participate in the intra-chain association at low degrees of dissociation. At higher degrees of neutralization,

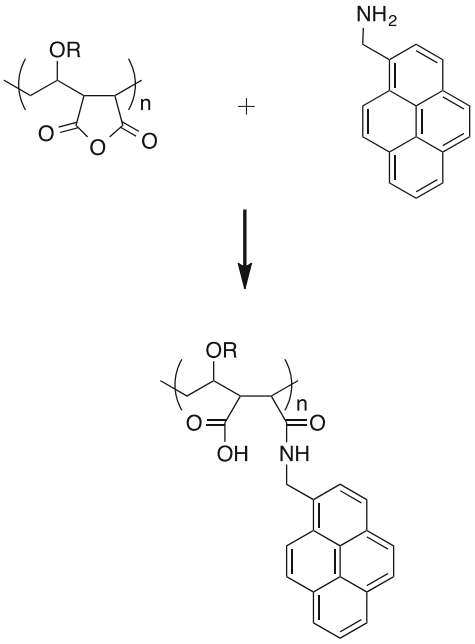

Scheme 7.2 Poly(maleic anhydride–alkyl vinyl ether) fluorescently labeled with pyrene according to [23]. Please note that pyrene is normally supplied in its salt form

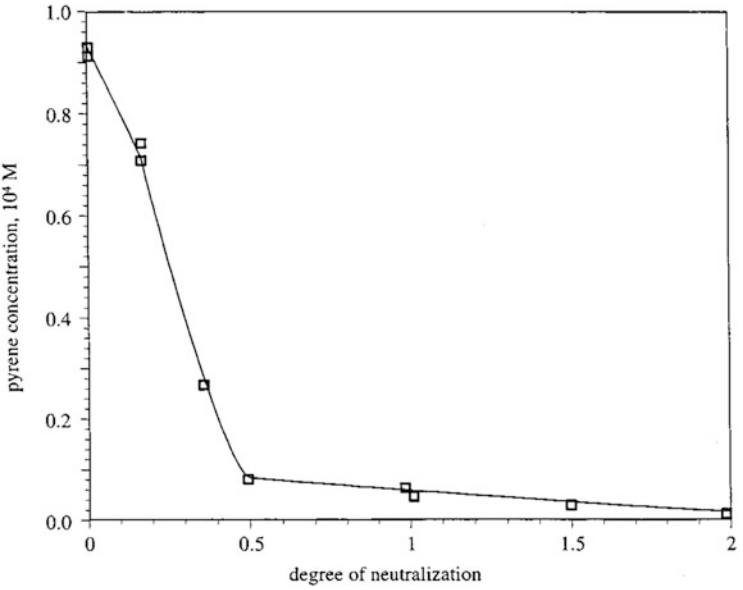

Fig. 7.8 Pyrene solubility in a solution of poly(maleic acid–octyl vinyl ether) (1000 ppm) as a function of dissociation of the polymer's carboxylic acid groups. Reprinted with permission from Q. Qiu et al., *Langmuir* **2002,** *18*, 5921–5926 [22]. Copyright, 2002, American Chemical Society

the polymer extends resulting in a loss of the hydrophobic domains. It should be noted, however, that some compact conformation does remain even at full neutralization ($\alpha = 2$). Also noteworthy, the addition of high concentrations of divalent salts at pH 4.0 to aqueous solutions of poly(maleic acid–octyl vinyl ether) results in the formation of a gel network, which has the properties of a reversibly cross-linked system.

For further illustration, Fig. 7.9 provides an artistic rendition of the polymer chain conformation for hydrophobically modified copolymers of maleic acid and alkyl vinyl ethers. In summary, the (a) compact conformation is shown at low degrees of dissociation in which one may observe a tightly packed chain structure stabilized by intramolecular micelles. In the (b) transition region, there is an intermediate conformation between the compact and extended random coil conformation, illustrating that the intramolecular micelles begin to uncoil. Finally, at high degrees of dissociation, the polymer exists in the (c) extended random coil conformation.

It should be pointed out that these three conformations can be found in different points in the neutralization process—starting at low pH and increasing to higher pH values—for certain hydrophobically modified species of poly(maleic acid–alkyl vinyl ether), specifically poly(maleic acid–butyl vinyl ether), poly(maleic acid–hexyl vinyl ether), and poly(maleic acid–octyl vinyl ether). In the case of more

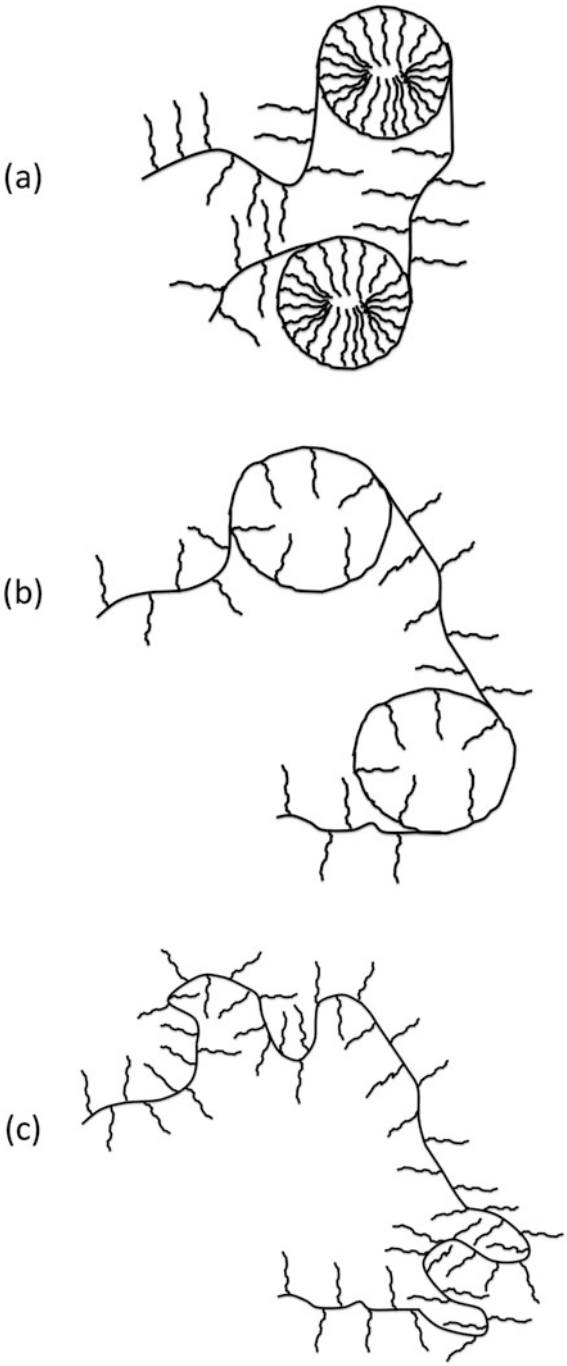

Fig. 7.9 Several conformations that exist for copolymers of maleic acid and alkyl vinyl ether: (**a**) compact conformation, (**b**) transition region, and (**c**) extended random coil

polar species, such as poly(maleic acid–methyl vinyl ether), only the extended random coil conformation is found throughout the neutralization range. Likewise, more nonpolar species, such as poly(maleic acid–hexyl vinyl ether), will exist in the compact hypercoiled conformation at all pH values. An important point to make is that the occurrence of these conformations and transitions as a function of pH is also dependent on the degree of hydrophobic modification of the polymer and any counterions present in the solution [17].

7.7 Conformation Behavior of Copolymers of Maleic Anhydride and Styrene in Water

Similar to the studies carried out on copolymers of maleic anhydride and alkyl vinyl ethers, investigations of the conformational behavior of copolymers of styrene and maleic anhydride have also been of great interest to researchers. Most of the work conducted in this area relied on potentiometric titrations, optical titrations, viscometry, dilatometry, and calorimetric measurements [24–29]. Overall, solution behavior analogous to that described for copolymers of maleic anhydride and alkyl vinyl ethers (Sects. 7.2–7.6) is observed for copolymers of maleic anhydride and styrene. Similar to the studies already described, various physical measurements have been conducted as a function of ionization of the acid groups of poly (styrene–maleic acid) (see Fig. 7.10). Typical experiments are carried out starting at low pH, corresponding to low degrees of ionization (carboxylic acid groups in the uncharged state), while increasing pH results in an increase in the degree of ionization of the polymer's acid groups (carboxylic acid groups in the fully charged state). In general, poly(styrene–maleic acid) in water exists in a compact coil conformation at low degrees of ionization and undergoes a transition with increasing ionization to an extended random coil conformation.

Based on thermodynamic studies of the conformational transition of poly (styrene–maleic acid), evidence suggests that the compact form of the polymer is stabilized by van der Waals and hydrophobic interactions between the phenyl residues of the polymer [29]. Once beyond the conformation transition (greater degree of dissociation), electrostatic forces overcome the hydrophobic and van der Waals forces allowing the molecule to adapt to a more extended coil conformation in which the negatively charged carboxylate groups repel each other.

Titration curves of poly(styrene–maleic acid) are shown in Fig. 7.11. The transition region occurs in the range $0.2 < \alpha_1 < 0.6$ for an ionic strength of $I = 0.03$.

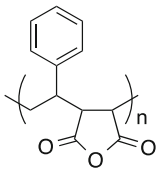

Fig. 7.10 Molecular structure of the anhydrous form of poly(styrene–maleic acid)

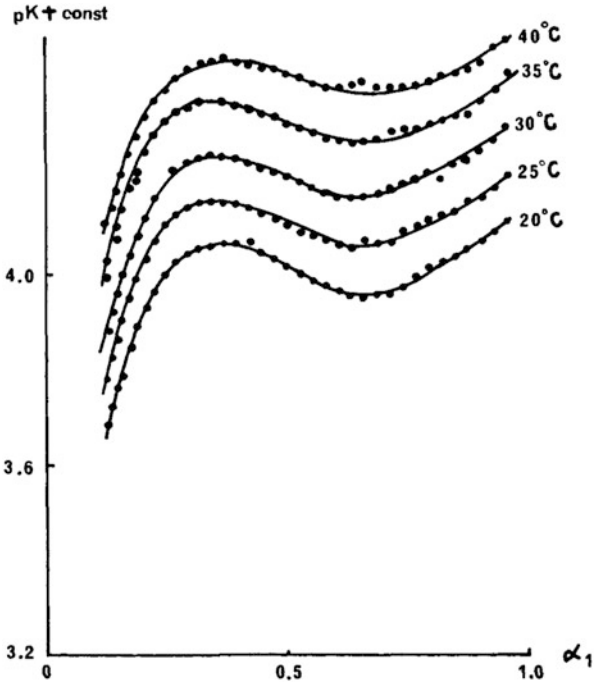

Fig. 7.11 Potentiometric titration *curves* for an aqueous solution of poly(styrene–maleic acid) at $I = 0.03$ and various temperatures. The polymer concentration is 0.0128 mol/L. Plotting constants are 0 at 20 °C, 0.1 at 25 °C, 0.2 at 30 °C, 0.3 at 35 °C, and 0.4 at 40 °C. Reprinted with permission from T. Okuda et al., *J Polym Sci* **1977,** *15*, 749–755 [29]. Copyright, 1977, John Wiley & Sons

Surprisingly, there is very little temperature dependence for this polymer for the range of temperatures tested. This is in contrast to findings with copolymers of hexyl vinyl ether and maleic anhydride where ΔG_t° depends on temperature [2].

For further illustration, Fig. 7.12 contains a plot of the fraction of monomeric units in the extended coil conformation of poly(styrene–maleic acid) as a function of carboxylic acid group dissociation. This data is based on potentiometric titration data in which difference spectra are used to calculate the fraction of monomeric units in the extended coil conformation [30]. The data in Fig. 7.12 clearly show that more monomeric units are involved in the compact conformation at lower degrees of dissociation. As the acid groups of the polymer become more charged, electrostatic repulsion causes more of the molecule to take part in the extended coil conformation. In addition, by varying the salt concentration, one can observe differences caused by ionic strength. The higher the ionic strength, the greater is the observed shift to higher degrees of dissociation. Such a result is within reason since cations from the added salt will interact with negatively charged acid groups of the polymer causing a shielding effect that impedes electrostatic repulsion.

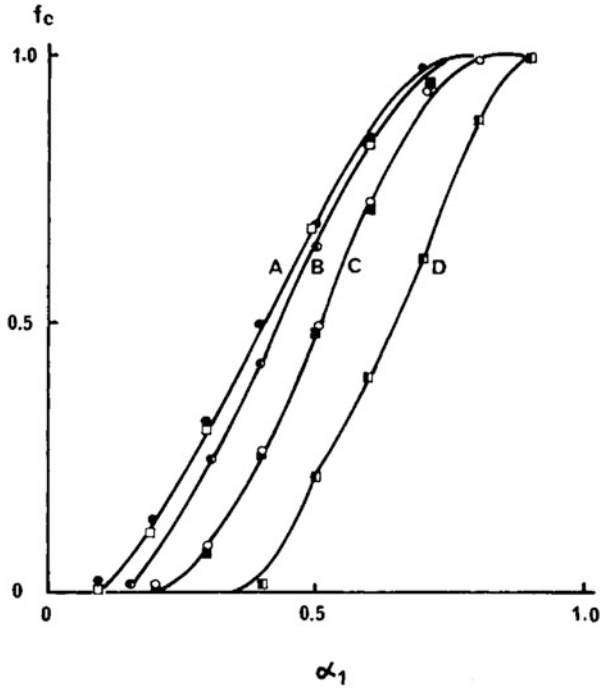

Fig. 7.12 Fraction of monomeric units (f_c) in the extended coil form as a function of dissociation for poly(styrene–maleic acid). Ionic strengths of (A) 0.01, (B) 0.03, (C) 0.10, and (D) 0.27. Reprinted with permission from T. Okuda et al., *J Polym Sci* **1977,** *15*, 749–755 [29]. Copyright, 1977, John Wiley & Sons

7.8 Interactions Between Maleic Anhydride-Based Polymers and Surfactants

A number of key studies shed light on the interactions between maleic anhydride-based polymers and various types of surfactants. The colloidal behavior of nonionic (penta-ethylene glycol mono-*n*-dodecyl ether), cationic (dodecyltrimethyl ammonium bromide), and anionic (sodium dodecyl sulfate) surfactants with poly(octyl vinyl ether–maleic acid) was studied under various conditions, such as surfactant concentration, pH, etc. Specific interest lies in understanding how the hydrophobically modified polymer interacts with the surfactants, either electrostatically or by hydrophobic interactions, often forming mixed micelle systems in which the surfactant tails incorporate themselves into the hydrophobic portions of the polymer. Most of the work in this area was carried out by a group of scientists at Columbia University in New York City under the direction of Professor Somasundaran. Several techniques, discussed to some extent in other sections of this chapter, were used to probe the colloidal and molecular behavior of such systems. In addition, fluorescence spectrophotometry, dynamic light scattering, electron spin resonance, and surface tension measurements were also used to obtain complementary information.

7.8.1 Nonionic Surfactants

The interactions of hydrophobically modified polyelectrolytes with nonionic surfactants is an intriguing topic in colloid science that can be investigated with various physical chemistry measurements. To shed light on polymer–nonionic surfactant interactions, we use the example from the literature of penta-ethylene glycol mono-*n*-dodecyl ether ($C_{12}EO_5$) with poly(octyl vinyl ether–maleic acid) (see Fig. 7.13) [31]. Brief introductions to each of the techniques used to measure phenomena are introduced.

Surface tension measurements are often carried out using the Wilhelmy technique in which a metal (e.g., platinum) plate is dipped into a test solution and removed while monitoring the force required to pull the plate out of solution, which can mathematically be related to the surface tension of the solution. Water has a surface tension of about 72 mN/m, and, in general, adding a monolayer of surfactant onto the water surface would reduce the surface tension. Figure 7.14 contains measurements of surface tension for a control system (water) versus a polymer solution as a function of added nonionic surfactant ($C_{12}EO_5$). As expected, curve (b) initially starts at the surface tension of water and begins to progressively decrease when the critical micelle concentration (cmc) of the surfactant is reached (0.06 mM). In the polymer-containing system (curve (a)), the surface tension starts at a much lower value (ca. 53 mN/m), which can more than likely be attributed to the hydrophobic domains in the polymer. More than likely, they associate together in bulk solution or present themselves at the air–solution interface. Addition of nonionic surfactant to the polymer system results in an initial decrease in surface tension followed by a rise (between 0.0075 and 0.075 mM), which might be explained by considering that the polymer and nonionic surfactant form micelle structures in bulk solution, leaving less surfactants and polymer available at the air–solution interface, where they would influence the surface tension. Further addition of $C_{12}EO_5$ to the solution leads to a decrease in surface tension (starting at 0.075 mM), which eventually reaches a steady value that corresponds to a fully saturated system containing surfactant alone. The surplus of surfactant added to the polymer–surfactant system most certainly causes the system to reach a state in which excess surfactant results in more micelles formed by the nonionic surfactants alone than mixed micelles containing both the surfactant and the polymer. As a result, the properties of nonionic surfactant micelles predominate giving the overall solution a surface tension similar to that obtained in a system containing only the nonionic surfactant above its cmc value.

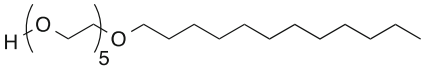

Fig. 7.13 Molecular structure of penta-ethylene glycol mono-*n*-dodecyl ether, referred to as $C_{12}EO_5$ or nonionic surfactant in the text

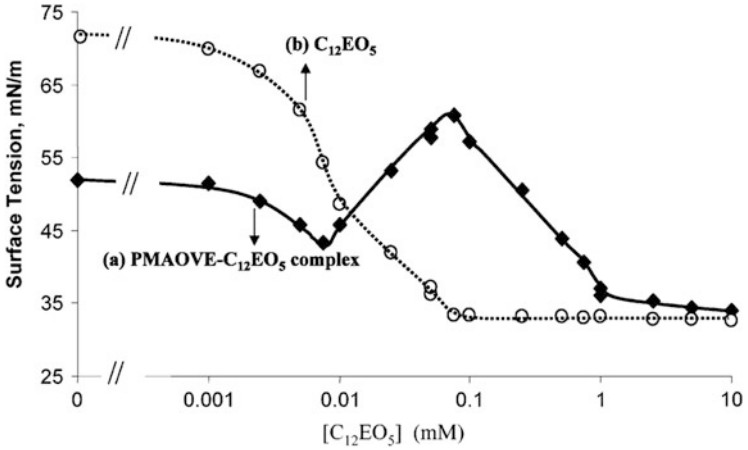

Fig. 7.14 Plot of surface tension as a function of added nonionic surfactant ($C_{12}EO_5$) to (**a**) a polymer solution containing poly(octyl-maleic acid) and (**b**) a control solution (water only). Reprinted with permission from Deo and Somasundaran, *Langmuir* **2005,** *21*, 3950–3956 [31]. Copyright, 2005, American Chemical Society

Equally intuitive, viscosity measurements of the same two aqueous systems described above (water + nonionic surfactant and polymer + nonionic surfactant) yield results consistent with expected behavior. Figure 7.15 includes plots of viscosity for both systems as a function of added $C_{12}EO_5$. Not surprisingly, the polymer solution is more viscous than the corresponding control system. Again, at low surfactant concentrations, the polymer more than likely exists in a highly coiled state stabilized by hydrophobic interactions that would cause a slight increase in viscosity relative to a straight water solution. Increasing the concentration of nonionic surfactant in both systems causes an increase in viscosity; however, it is much greater in the case of the polymer system. The increase in viscosity for the polymer beginning at approximately 0.1 mM provides evidence for the cooperative interactions between the hydrophobic domains of the polymer and, presumably, the aliphatic chains of the nonionic surfactant. The small increases in viscosity of the aqueous solution containing only nonionic surfactant are probably due to micelle structures.

A key learning from studies of $C_{12}EO_5$ with poly(octyl vinyl ether–maleic acid) is that the surfactant integrates into the polymeric hydrophobic nanodomains well below the cmc of the surfactant (see Fig. 7.16). When the surfactant is used in conjunction with the polymer, a critical complexation concentration may be defined as the surfactant concentration where mixed micelles containing the polymer hydrophobic groups and the surfactant are formed. In addition, a saturation point is reached, specific to the particular system under study, in which micelles (surfactant only) and mixed micelles (surfactant + polymer) exist simultaneously. Additional data obtained by electron spin resonance, dynamic light scattering, and spectrofluorescence support these conclusions [31].

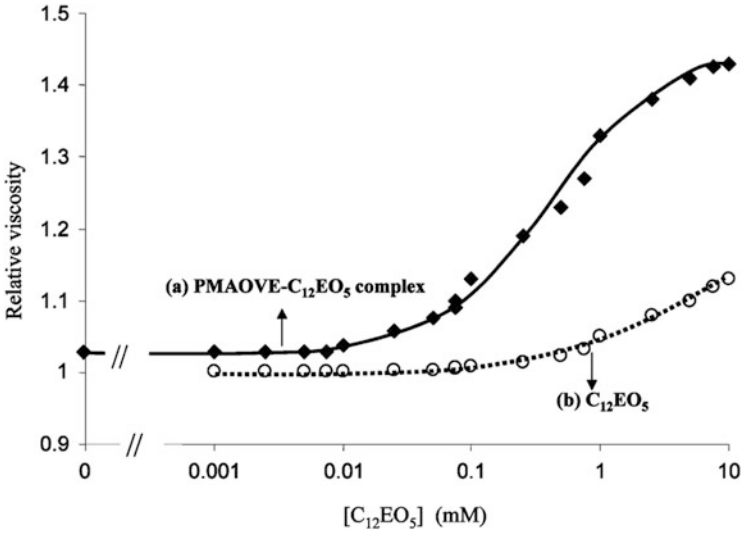

Fig. 7.15 Plot of viscosity as a function of added nonionic surfactant ($C_{12}EO_5$) to a control solution (water only) and a polymer solution containing poly(octyl vinyl ether–maleic acid). Reprinted with permission from Deo and Somasundaran, *Langmuir* **2005,** *21*, 3950–3956 [31]. Copyright, 2005, American Chemical Society

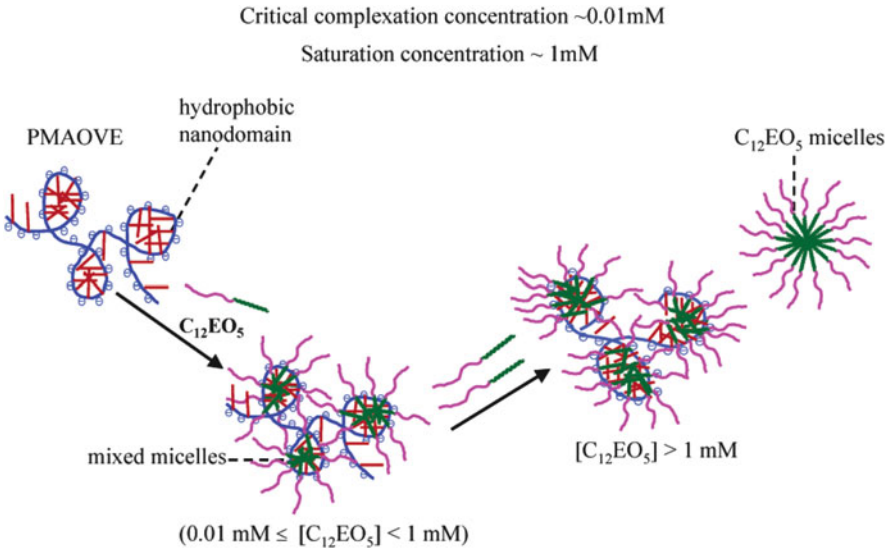

Fig. 7.16 Model of the interactions between $C_{12}EO_5$ and poly(octyl vinyl ether–maleic acid) at various surfactant concentrations. Reprinted with permission from Deo and Somasundaran, *Langmuir* **2005,** *21*, 3950–3956 [31]. Copyright, 2005, American Chemical Society

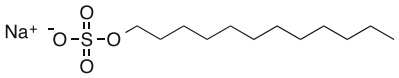

Fig. 7.17 Molecular structure of sodium dodecyl sulfate, referred to as SDS or anionic surfactant in the text

7.8.2 Anionic Surfactants

Sodium dodecyl sulfate (SDS) is a common surfactant used for applications in many different industries (see Fig. 7.17 for its molecular structure). It is particularly well known for its detergency and was employed almost ubiquitously in personal care cleansing formulations for many years. Studies of the interaction of SDS with poly(octyl vinyl ether–maleic acid) are important to understand the colloidal behavior of these molecules when formulated together. Dynamic light scattering, rheological measurements, ultracentrifugation, and pyrene solubility measurements were used to determine the solution behavior of the polymer and anionic surfactant [32].

By adding pyrene crystals to test solutions, one can determine its solubility by UV–visible spectrophotometry, by reading the absorbance of solubilized pyrene at 335 nm. Since pyrene is not soluble in aqueous environments, dissolution of the crystals indicates its incorporation into a lipophilic environment. Figure 7.18 contains a plot of pyrene solubility versus added anionic surfactant for a water (control) system and polymer solution. In the control system (surfactant only), the pyrene solubility is zero until the cmc (8 mM) is reached, where a significant increase corresponds to the formation of micelle structures. In the polymer system, the baseline reading for the poly(octyl vinyl ether–maleic acid) solution is higher than the water system, even at low concentrations of SDS. This indicates that hydrophobic nanodomains exist in the polymer in the absence and presence of SDS. At about 2 mM of SDS, the pyrene solubility begins to increase, most likely corresponding to a restructuring of the polymer hydrophobic domain [32].

Based on dynamic light scattering studies, Fig. 7.19 contains hydrodynamic data as a function of SDS concentration. Up until about 1.5 mM, the size of the polymer–SDS complex remains the same. However, at this point an abrupt increase in the size of the complex occurs at SDS concentrations greater than 2 mM. Finally, a plateau is reached after 12 mM of SDS is added. Together with the pyrene solubility, dynamic light scattering, viscosity, and centrifugation data, Somasundaran and coworkers developed a model of the interaction of SDS with the polymer over the studied concentration range. This is illustrated in Fig. 7.20 and shows that at low concentrations of the surfactant, the polymer exists in a hypercoiled state (similar to its low-pH, deionized state).

More than likely, intra- and interchain interactions of the hydrophobic portion of the polymer result in the formation of hydrophobic nanodomains. At low concentrations of SDS, these are the prominent colloidal interactions. As the concentration of SDS increases—in the range of 2–12 mM—the SDS molecules interact with the

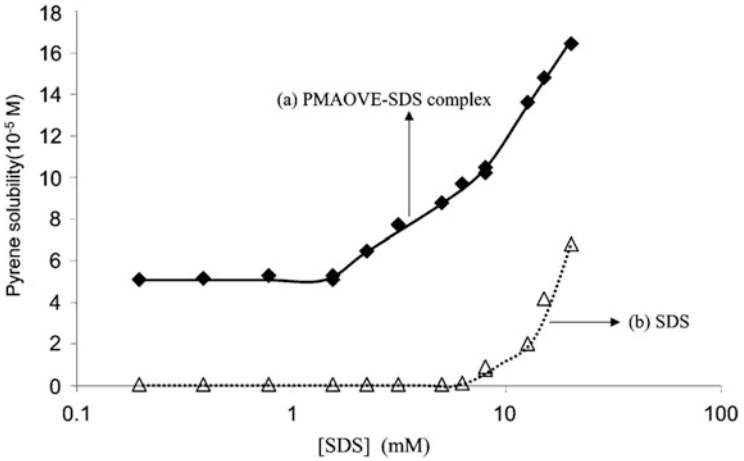

Fig. 7.18 Plot of pyrene solubility as a function of added sodium dodecyl sulfate to (**a**) a polymer solution containing poly(octyl vinyl ether-maleic acid) and (**b**) a control solution (water only). Reprinted with permission from Deo et al., *Langmuir* **2005,** *21*, 9998–10003 [32]. Copyright, 2005, American Chemical Society

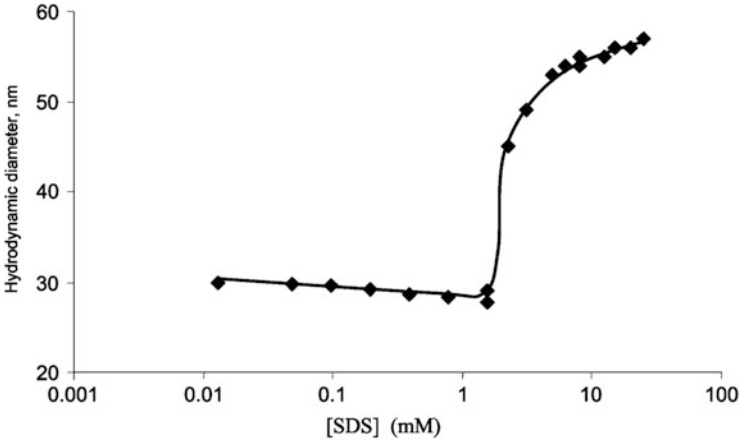

Fig. 7.19 Plot of hydrodynamic radius as a function of added sodium dodecyl sulfate for a solution of poly(octyl vinyl ether–maleic acid). Reprinted with permission from Deo et al., *Langmuir* **2005,** *21*, 9998–10003 [32]. Copyright, 2005, American Chemical Society

hydrophobic portion of the polymer. The resulting complex is best characterized as a combination of both the surfactant and polymer. At higher concentrations of SDS, it is believed that the polymer–SDS complex coexists with SDS micelles that form once all of the possible hydrophobic binding sites on the polymer backbone are occupied. At an SDS concentration of 12 mM, the saturation concentration of the

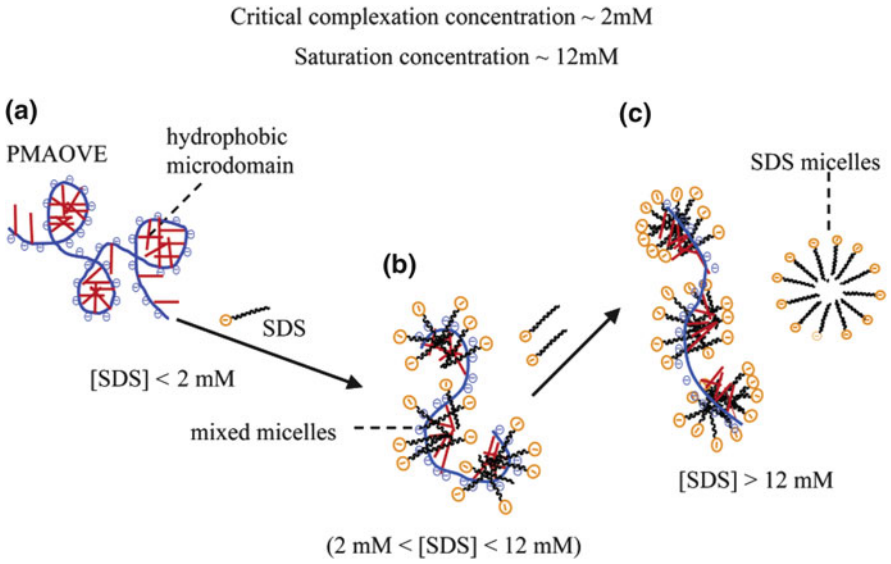

Fig. 7.20 Conformational behavior of poly(octyl vinyl ether–maleic acid) as a result of increasing SDS concentration. Three states may be distinguished falling in the following surfactant concentration ranges: **(a)** [SDS] < 2 mM, **(b)** 2 mM < [SDS] < 12 mM, and **(c)** [SDS] > 12 mM. The polymer concentration is 1 % (w/w). Reprinted with permission from Deo et al., *Langmuir* **2005,** *21*, 9998-10003 [32]. Copyright, 2005, American Chemical Society

surfactant is reached corresponding to about two SDS molecules per one *n*-octyl chain of poly(octyl vinyl ether–maleic anhydride) [32].

7.8.3 Cationic Surfactants

The interactions between oppositely charged species are governed by electrostatics. This is the most long-range force of the non-covalent interactions. However, electrostatics can be influenced by the presence of hydrophobic interactions. In the paragraphs that follow, we discuss the colloidal behavior of poly(octyl vinyl ether–maleic acid) in the presence of the cationic surfactant, dodecyltrimethyl ammonium bromide (DTAB) (see Fig. 7.21). Work conducted in the laboratories of Professor Somasundaran at Columbia University shed light on the behavior of this system at various pH levels [33].

Similar to the sections above—discussing the interactions of poly(octyl vinyl ether–maleic acid) with nonionic and anionic surfactants—surface tension, viscosity, and electron spin resonance were used to provide understanding of the conformation behavior of the polymer with the cationic surfactant, DTAB. Figure 7.22 contains a plot of surface tension versus DTAB concentration for a

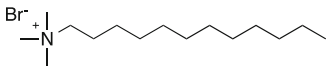

Fig. 7.21 Molecular structure of dodecyltrimethyl ammonium bromide (DTAB)

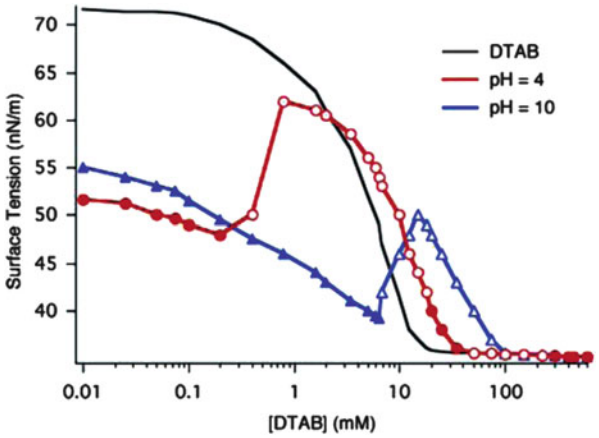

Fig. 7.22 Plot of surface tension as a function of added DTAB for a solution of poly(octyl vinyl ether–maleic acid) at pH 4 (*circles*) and pH 10 (*triangles*) and a solution not containing polymer (line without symbols). Reprinted with permission from Deo et al., *Langmuir* **2007,** *23*, 5906–5913 [33]. Copyright, 2007, American Chemical Society

0.1 % (w/w) solution of poly(octyl vinyl ether–maleic acid) at pH 4 and pH 10 as well as a solution without polymer. The surface tension of the solution without polymer, at low DTAB concentration, is essentially equal to that of pure H_2O. As the concentration of DTAB increases, there is a sharp drop in surface tension starting at 0.5 mM DTAB until it reaches extremely low surface tension values at >10 mM DTAB, which corresponds to the cmc of DTAB (15 mM). The two solutions of poly(octyl vinyl ether–maleic acid) (pH 4 and pH 10) show significantly lower surface tension values (in the range of 50–55 dynes/cm) than pure water (72 dynes/cm). As stated earlier, such a result indicates that hydrophobic moieties of the polymer present themselves at the air–liquid interface (hydrophobic interactions are lower in energy than hydrogen bonding). At pH 4, the surface tension initially decreases when small amounts of SDS are added. However, precipitation is observed between 0.6 and 12 mM, and measurement of the surface tension of the supernatant reveals an abrupt increase between 0.6 and 0.8 mM. Likewise, at pH 10 there is a decrease in surface tension with added DTAB until a concentration of approximately 8 mM is reached. Precipitation occurs between 7 and 100 mM for the solution at pH 10. Similarly, a peak in the surface tension curve is observed in this DTAB concentration range.

Based on surface tension, fluorescence, electron spin resonance, turbidity, and viscosity measurements, Somasundaran and coworkers developed a model for the interaction of DTAB with poly(octyl vinyl ether–maleic acid) at low (pH 4) and

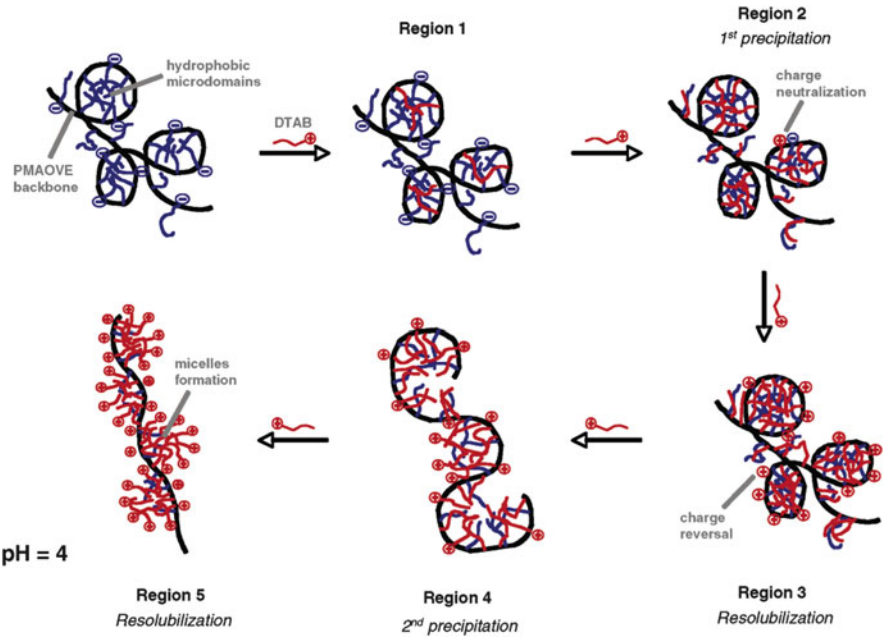

Fig. 7.23 Proposed model of poly(octyl vinyl ether–maleic acid)–DTAB interactions at pH 4 and at various DTAB concentrations. Region 1, 0 mM < [DTAB] < 0.6 mM; Region 2, 0.6 mM < [DTAB] < 0.8 mM; Region 3, 0.8 mM < [DTAB] < 50 mM; Region 4, 50 mM < [DTAB] < 300 mM; Region 5, [DTAB] > 300 mM. Reprinted with permission from Deo et al., *Langmuir* **2007,** *23*, 5906–5913 [33]. Copyright, 2007, American Chemical Society

high (pH 10) pH [33]. At pH 4 (see Fig. 7.23), at low concentrations of DTAB (0 mM < [DTAB] < 0.6 mM), it is proposed that there is some interaction between the positively charged surfactant and negatively charged carboxylic acid groups of the polymer, and hydrophobic tails of DTAB insert themselves into hydrophobic domains of the polymer. Continuing at pH 4, precipitation occurs at concentrations of 0.6 mM < [DTAB] < 0.8 mM, which is presumably due to charge neutralization between the two species. With further increase in DTAB concentration (0.8 mM < [DTAB] < 50 mM), we have additional DTAB being added onto already existing poly(octyl vinyl ether–maleic anhydride)–DTAB complex. This results in a charge reversal and permits the resolubilization of the precipitate. A second precipitation occurs (50 mM < [DTAB] < 300 mM), which more than likely could have resulted from a change in the polymer chain conformation. At [DTAB] > 300 mM, the precipitate dissolves again while maintaining the extended random coil conformation of the polymer with the DTAB interacting with the polymer. In addition, at this concentration the solution properties are dominated by the DTAB micelles.

At pH 10 (which is assumed to be similar to pH 7), in the first concentration range (0 mM < [DTAB] < 7 mM), most of the carboxylic acid groups on the polymer background are ionized, resulting in a more highly extended conformation than at pH 4 (see Fig. 7.24). The addition of DTAB more than likely results in the

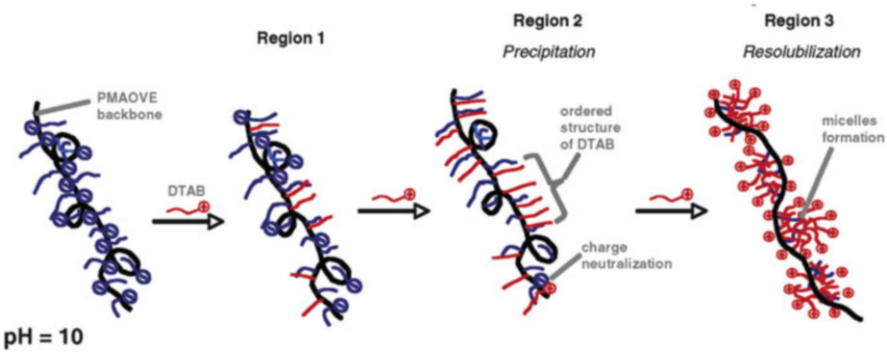

Fig. 7.24 Proposed model of poly(octyl vinyl ether–maleic acid)–DTAB interactions at pH 10 and at various DTAB concentrations. Region 1, 0 mM < [DTAB] < 7 mM; Region 2, 7 mM < [DTAB] < 20 mM; Region 3, [DTAB] > 20 mM. Reprinted with permission from Deo et al., *Langmuir* **2007,** *23*, 5906–5913 [33]. Copyright, 2007, American Chemical Society

interaction between the positively charged surfactant and the negatively charged carboxylic acid groups. Additional stability is provided by van der Waals interactions between the long alkyl chains of the surfactant and the pendant hydrophobe on the polymer chain. At 7 mM < [DTAB] < 20 mM, precipitation occurs due to charge neutralization of the negatively charged polymer by the positively charged surfactant. Further addition of DTAB ([DTAB] > 20 mM) results in a charge reversal of the complex and a resolubilization of the complex.

7.9 Thin Films of Copolymers of Maleic Anhydride

As we have already seen in previous sections, a number of different techniques (e.g., potentiometric titration, NMR studies, and intrinsic viscosity measurements) have been used to probe the behavior of alternating copolymers of maleic anhydride in aqueous solution. Based on the results of these studies, one may conclude that electrostatic forces, hydrogen bonds, and hydrophobic interactions are responsible for the conformational behavior of these polymers. For example, copolymers based on maleic anhydride have been shown to have two distinct pK_a values corresponding to each acid group on the hydrolyzed maleic anhydride monomer unit. This anomaly arises due to electrostatic repulsion between adjacent carboxylate groups and hydrogen bonding between protonated and deprotonated acids [34]. In addition, hydrophobic moieties in copolymers of maleic anhydride are responsible for a compact conformation that exists at low degrees of ionization (acidic conditions). Neutralization of the copolymers results in deionization along with the concurrent transformation of the polymer to an extended random coil.

There has been considerable interest in understanding similar properties of thin films of copolymers of maleic anhydride [35–44]. An innovative approach to investigating thin films is by electrokinetic studies using a microslit streaming

potential instrument to determine the zeta potential and surface conductivity of the films [34]. In this manner, copolymers of maleic anhydride are spin coated on glass or silicon wafers and placed in the electrokinetic cell. Copolymers of poly (octadecene–*alt*-maleic acid), poly(propylene–*alt*-maleic acid), and poly(styrene–*alt*-maleic acid) were investigated as representative examples of very hydrophobic, hydrophilic, and intermediate substrates, respectively. Since these data were generated at various pH values, the information garnered from the experiments provided an overview of structural transitions and ionization potentials that could be explained by electrostatic interactions, hydrogen bonding, and hydrophobic interactions. At low pH or low degrees of ionization, there is a strong repulsion between the anionic acid groups, resulting in expansion of the films (in the x-y direction) of the more hydrophilic copolymers: poly(propylene–*alt*-maleic acid) and poly (styrene–*alt*-maleic acid). However, in the case of the hydrophobic polymer, poly (octadecene–*alt*-maleic acid), the film properties and dimensions remain unchanged as a function of pH, illustrating the dominating force of the hydrophobic interactions. Similar to solution behavior, the half-dissociated state in poly (propylene–*alt*-maleic acid) and poly(styrene–*alt*-maleic acid) is stabilized by hydrogen bonding between the carboxylic acid anion and its non-dissociated carboxylic acid neighbor. Again, this gives rise to two distinct pK_a values, not only in solution but also in thin films of these polymers.

Other experiments to characterize thin films of maleic anhydride copolymers consist of contact angle measurements (drop shape analysis), surface tension (Wilhelmy method), ellipsometry, atomic force microscopy, transmission electron microscopy, X-ray photoelectron spectroscopy, and dynamic light scattering [34, 45, 46]. These experimental techniques provide information about the hydrophobicity/hydrophilicity, thickness, roughness, morphology, and chemical composition of the thin films. Using such techniques, one particular study provides very instructive results on the conformational behavior of maleic anhydride copolymers of varying polarities [45].

Contact angle measurements were carried out in the dry (annealed; maleic anhydride form) and wet (hydrated; maleic acid form) states on a series of copolymers based on maleic anhydride including poly(propene–*alt*-maleic anhydride), poly(styrene–*alt*-maleic anhydride), and poly(octadecene–*alt*-maleic anhydride). Table 7.1 contains molecular weight, film thickness, film roughness, pK_a values, and the surface concentration of maleic anhydride moieties in the films for the three polymers.

The polymers, which possess various degrees of polarity, were covalently bound to silicon (SiO_2) wafers by annealing, thereby forming a monolayer of polymer on the surface. Sessile drop experiments were conducted in the dry state, while captive bubble measurements were carried out in the hydrated state. This type of measurement is an axisymmetric drop shape analysis that determines the liquid–fluid interfacial tension and contact angle by examining the shape of sessile or pendant drops.

Not surprisingly, comparison of the contact angle results in the dry and wet states for thin films of poly(propene–*alt*-maleic anhydride), poly(styrene–*alt*-

Table 7.1 Properties of thin films of maleic anhydride-based copolymers

	M_w (g/mol)	T_{dry} (nm)	rms roughness (nm)	pK_{a^1}/ pK_{a^2}	σ_{free} (10^{13} cm^{-2})
Poly(octadecene-*alt*-maleic anhydride)	50,000	4.5 ± 0.5	0.32	3.7/6.8	6
Poly(styrene–*alt*-maleic anhydride)	100,000	6.5 ± 0.5	0.31	3.0/6.3	8
Poly(propene-*alt*-maleic anhydride)	39,000	3.1 ± 0.5	0.34	2.8/6.5	10

Molecular weight (M_w), film thickness (T_{dry}), film roughness (rms roughness), pK_a values for each carboxylic acid group in maleic acid, and surface concentration of maleic anhydride moieties (σ_{free}) are reported. Reproduced from P. Uhlmann et al. [45] Reprinted with permission from the American Chemical Society, Copyright, 2005

Table 7.2 Contact angle measurements on dry films for the maleic anhydride copolymers described in Table 7.1

	Advancing contact angle (°)
Poly(propene–*alt*-maleic anhydride)	
Annealed	73 ± 1
Hydrolyzed	53.2 ± 12
Poly(styrene–*alt*-maleic anhydride)	
Annealed	84.2 ± 2
Hydrolyzed	82.6 ± 5
Poly(octadecene–*alt*-maleic anhydride)	
Annealed	107.7 ± 2
Hydrolyzed	97.9 ± 7

Data from P. Uhlmann et al. [45]

maleic anhydride), and poly(octadecene–*alt*-maleic anhydride) demonstrated that greater contact angle readings were obtained in the annealed states (maleic anhydride form) than in the hydrolyzed states (maleic acid form). This is illustrated in Table 7.2, where it is also shown that contact angle measurements in both the dry and wet state depend on the degree of polarity of the molecule. For example, poly (propene–*alt*-maleic anhydride), which has the greatest amount of maleic anhydride groups at the surface of the film (see σ_{free} in Table 7.1), yields the lowest contact angle in both the annealed and hydrolyzed samples—a result that is in line with our expectations for the most hydrophilic polymer of the group. Likewise, the most hydrophobic polymer—poly(octadecene–*alt*-maleic anhydride)—yields the greatest contact angle values. Not surprisingly, thin films of poly(styrene–*alt*-maleic anhydride), which is intermittent polarity, provide values somewhere in between the other two polymers.

In another series of experiments, researchers from Karina Grundke's group at the Leibniz Institute of Polymer Research in Dresden measured the contact angle of the same thin films while submerged in water at various ionic strengths and pH levels. These studies were carried out by conducting captive air bubble measurements. Such liquid–fluid contact angle measurements provide insight to the film's behavior

at various degrees of ionization of the maleic acid groups. Overall, these data demonstrated that when the maleic acid groups are ionized (deprotonated), they cause the surface of the film to be more hydrophilic. The data also revealed that contact angle hysteresis—comparing the advancing and receding angle—was the largest for the most hydrophobic polymer and least for the most hydrophilic polymer. Insight to this finding is still forthcoming, although it more than likely has to do with the number of maleic acid moieties on the surface of the film [45].

7.10 Polyelectrolyte Complexes of Maleic Anhydride-Based Polymers

Polyelectrolyte complexes are formed by combining two oppositely charged polymers together resulting in the formation of a polysalt. This complex is stabilized by electrostatic interactions, and while these Coulomb interactions are the principal stabilizing factor of polyelectrolyte complexes, hydrogen bonding, van der Waals forces, and hydrophobic interactions also play important roles in maintaining polyelectrolyte complex integrity. In addition, a number of other factors determine the properties of the polyelectrolyte complex including the characteristics of the polyanions and polycations involved (molecular weight, charge density, and the nature of the ionic groups), solution properties (ionic strength, pH, and temperature), and the method of preparation [47, 48]. There is a great deal of interest in polyelectrolyte complex technology as there are numerous applications in biotechnology, nanotechnology, energy applications, and pharmaceutical technology.

Polyelectrolyte complexes can take on several different morphologies; however, they are normally formed by separation from the solution phase as flocculated precipitates or as complex coacervates [49]. Typically, polyelectrolytes are not soluble in H_2O even though their constituent parts (individual polymers) are H_2O soluble. For this reason, polyelectrolyte complexes tend to absorb water, similar to the manner of a hydrogel. Polyelectrolyte complexes can be classified as: (1) soluble polyelectrolyte complex, meaning that on the macroscale it is a homogenous system that contains small polyelectrolyte aggregates; (2) turbid colloidal systems containing suspended polyelectrolyte complexes; and (3) two-phase systems containing a precipitate (the polyelectrolyte complex) and a supernatant (the remaining solution) [50].

Numerous techniques have been used to characterize polyelectrolyte complexes and consist of measurements of turbidity, pH/ionic strength, viscosity, dynamic and static light scattering, zeta potential, polyelectrolyte titration, and particle size distribution [51, 52]. Of these tests, turbidimetric measurements monitoring the optical density at 500 nm (OD_{500}) are commonly employed as they can be easily instituted in most laboratories. Furthermore, the optical density is affected by a number of the properties of the polyelectrolyte complex including the shape, number of molecules involved (concentration), size, and polydispersity [50].

Table 7.3 Studies of polyelectrolyte complexes involving maleic anhydride copolymers

Polyelectrolyte complex	References
MPEG-grafted poly(styrene–*alt*-maleic acid) with poly(diallyldimethy-lammonium chloride)	[53]
Poly(ethylene oxide)–poly(maleic acid) with chitosan	[54]
Poly(*N*-vinyl pyrrolidone–*alt*-maleic acid) with bovine serum albumin	[55]
Poly(styrene–maleic acid) with gelatin	[56]
Poly(maleic acid–*alt*-*α*-methylstyrene) with poly(diallyldimethylammonium chloride)	[57]
Poly(maleic acid–*co*-*α*-methylstyrene) or poly(maleic acid–*co*-propylene) with poly(L-lysine) or poly(diallyldimethylammonium chloride)	[58]
Poly(maleic acid–*alt*-divinyl ether) with poly(*N*-ethyl-4-vinylpyridinium)	[59]
Poly(ethene–*alt*-maleic acid) or poly(isobutene–*alt*-maleic acid) or poly(styrene–*alt*-maleic acid) with poly(X-*alt*-*N*-(triethylammonium)-sulfonato-ethyl)-maleimide) or poly(X-*alt*-*N*′-trimethylammonium-(iodide)-propyl)-maleimide); X = ethene, isobutene, or styrene	[60]
Poly(maleic acid–*alt*-vinyl acetate) or poly(maleic acid–*alt*-styrene) or poly (maleic acid–*alt*-vinylnaphthalene) with poly(diallyldimethylammonium chloride)	[52]
Poly(maleic acid–*alt*-propene) or poly(maleic acid–*alt*-*α*-methylstyrene) with poly (diallyldimethylammonium chloride)	[47]
Poly(maleic acid–Na-*co*-propene) with poly(diallyldimethylammonium chloride)	[61]
Poly(maleic acid–*co*-*α*-methylstyrene) with poly(diallyldimethylammonium chloride)	[62]
Poly(maleic acid–*co*-propylene) or poly(maleic acid–*co*-styrene) with poly (diallyldimethylammonium chloride)	[63]
Poly(maleic acid–*co*-propene) or poly(maleic acid–*co*-*α*-styrene) with poly (diallyldimethylammonium chloride)	[64]
Poly(maleic acid–*co*-propene) with poly(diallyldimethylammonium chloride)	[50]

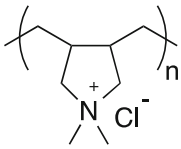

Fig. 7.25 Molecular structure of poly(diallyldimethylammonium chloride), a polycation frequently included in polyelectrolyte complex design

Polyelectrolyte complexes of maleic anhydride copolymers are particularly interesting due to changes in the ionization state of the maleic acid portion of the molecule at various pH values [53–60]. A number of different systems have been investigated and are summarized in Table 7.3. While many different combinations have been explored, poly(diallyldimethylammonium chloride) (Fig. 7.25) is one of the most popular cationic polyelectrolytes used in conjunction with anionic maleic anhydride copolymer polyelectrolytes.

The formation of polyelectrolyte complexes depends on many factors including the order of addition (Is the polyanion or polycation added first?) and if one of the

polyelectrolytes is added in excess as well as molecular weight, charge density, and charge distance within the polyelectrolyte chain. A comprehensive study by Buchhammer and coworkers investigated various preparation parameters on the physical characteristics of polyelectrolyte complexes utilizing quasi-elastic light scattering, polyelectrolyte titration, and turbidity measurements to monitor the particle size, polydispersity, and the degree of complexation [50]. These studies shed light on a number of interesting phenomena involving the formation of polyelectrolyte complexes of poly(diallyldimethylammonium chloride) and poly (maleic acid–*co*-propene); however, the most intriguing—and this is a generalized finding that probably applies to most polyelectrolyte complexes—is that the size and polydispersity of the prepared complex depends if the starting polyelectrolyte solution is deficient or in excess. If the starting solution is deficient, this means that the second polyelectrolyte will be in excess. Therefore, the first polyelectrolyte will be used up entirely, being totally occupied electrostatically with interactions with the added second polyelectrolyte. On the other hand, the second polyelectrolyte will be in excess, meaning that at some point it will run out of partner (i.e., oppositely charged ions) to interact with.

Figure 7.26 contains a visual description of this phenomenon, illustrating one of two possible pathways: (I) the starting polyelectrolyte is deficient or (II) the starting polyelectrolyte is in excess. In this first case, the final polyelectrolyte complex will contain less Polyelectrolyte 1 than Polyelectrolyte 2, while in the second case the opposite will be true, there will be more Polyelectrolyte 1 than Polyelectrolyte 2. When the starting polyelectrolyte solution is deficient, all of the polyions interact with the added second polyelectrolyte. There is, however, remaining Polyelectrolyte 2, which is adsorbed on to the surface. These polyelectrolyte particles are larger, but have much lower polydispersity than particles that were created with the starting solution in excess (i.e., the complex is made by starting with a higher concentration of Polyelectrolyte 1 and a lower concentration of Polyelectrolyte 2 added to the solution). In this case, the polyelectrolyte complex particles will be smaller, but the polydispersity will be higher. It should be noted that polyelectrolyte complexes formed by starting with an excess amount of polycation (deficient amount of polyanion) are more stable than complexes that are created with an excess amount of polyanion (deficient amount of polycation). While the inner core of such polyelectrolyte complexes is hydrophobic, the outer surface containing the charge is rather hydrophilic in nature.

In the experiments by Buchhammer and coworkers, one of the polyelectrolyte systems that they studied, and allowed them to arrive at the conclusions presented in Fig. 7.26, was based on the polycation, poly(diallyldimethylammonium chloride), and the polyanion, poly(maleic acid–*co*-propene) [50]. They were compared to polyelectrolyte complexes of poly(diallyldimethylammonium chloride) and copolymers based on acrylamide and sodium acrylate (polyanion). Their findings demonstrate that the higher the molecular weight (and possibly the lower the anionic charge density), the larger the size of the polyelectrolyte particles. It is also reported that increasing the concentration of the polyelectrolytes results in an increase in the polyelectrolyte complex size, but no change in the size distribution,

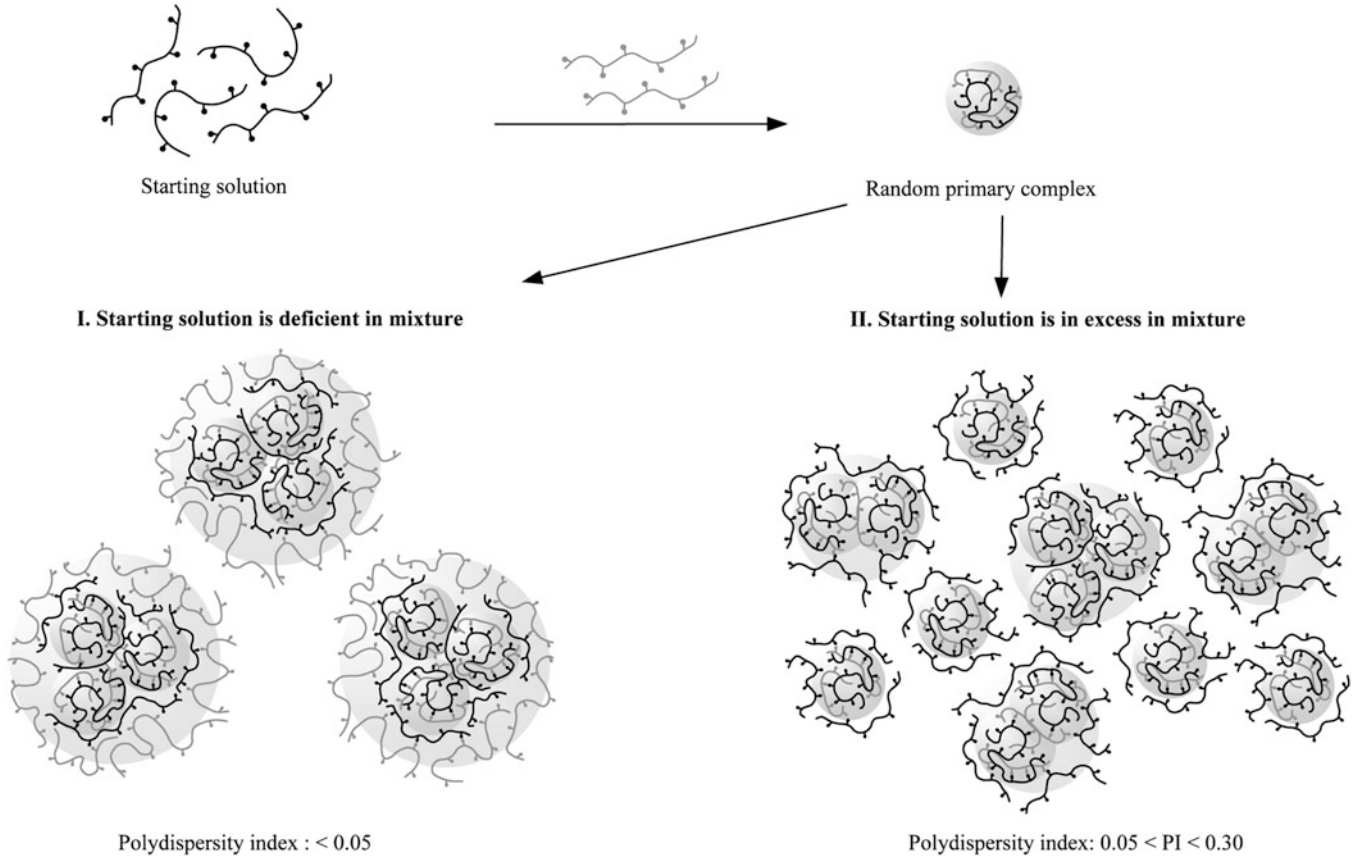

Fig. 7.26 Schematic of the polyelectrolyte complex formation process in which (I) the starting solution is deficient (i.e., one starts with less of the first polyelectrolyte) or (II) the starting solution is in excess (i.e., one starts with more of the first electrolyte). In (I) less of the second polyelectrolyte is added to the solution, while in (II) more of the second polyelectrolyte is added to the solution. Reprinted with permission from Buchhammer et al., *Colloids Surf A* **2003,** *218*, 151–159 [50]. Copyright, 2003, Elsevier

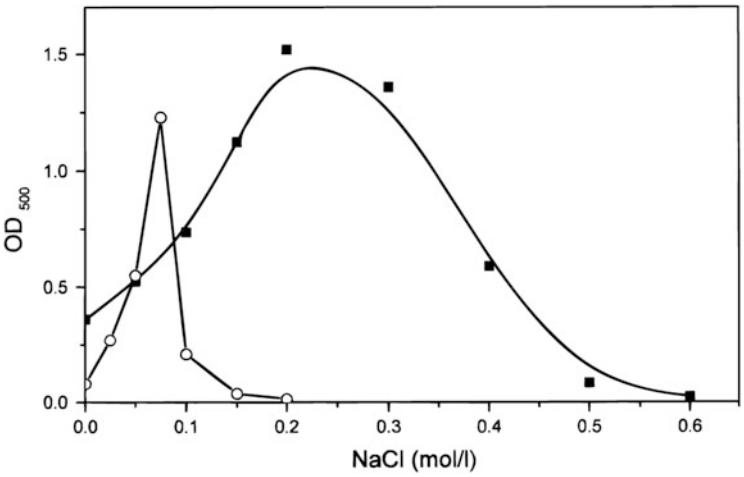

Fig. 7.27 Turbidimetric determination of optical density (OD_{500}) at various NaCl concentrations for polyelectrolyte complexes containing poly(diallyldimethylammonium chloride) and poly (maleic acid–*co*-*α*-methylstyrene) (*closed square*) as well as poly(diallyldimethylammonium chloride) and poly(maleic acid–*co*-propene) (*open circle*), both at mixing ratios ($n-/n+$) of 0.5. Reprinted with permission from Buchhammer et al., *Langmuir* **1999,** *15*, 4306–4310 [47]. Copyright, 1999, American Chemical Society

until a critical polymer concentration is reached, where a large increase in both size and size distribution is observed.

There is also significant interest in understanding the salt tolerance of polyelectrolyte complexes. In fact, studies involving poly(maleic acid–*co*-propene) and poly(maleic acid–*co*-*α*-methylstyrene) in conjunction with poly(diallyldimethylammonium chloride) demonstrate how chemical structural differences influence colloidal behavior of the polyelectrolyte complexes [47, 61]. Not surprising, stability difference is observed when comparing polyelectrolyte complexes based on poly(maleic acid–*co*-propene) and poly(diallyldimethylammonium chloride) with poly(maleic acid–*co*-*α*-methylstyrene) and poly(diallyldimethylammonium chloride). Figure 7.27 provides turbidity data (OD_{500}) as a function of NaCl concentration demonstrating that a complex containing poly(maleic acid–*co*-*α*-methylstyrene) is stable over a much greater concentration range than the same system with poly(maleic acid–*co*-propene). It should be noted that the plot only provides a salt stability profile at one time point. The authors report that at low salt concentrations, both complexes are relatively stable over time; however, as the NaCl concentration is increased, precipitation of the complexes occurs with time leading to low OD_{500} readings [47]. Also, at high salt concentrations, no precipitate is formed, and therefore clear solutions are obtained; thus, low OD_{500} values are observed. Nevertheless, the data in Fig. 7.27 suggest that hydrophobic interactions probably play an important role in the stabilization of polyelectrolyte complexes.

Such an effect may also be related to chain flexibility, depending if the chain is more prone to a compact random coil form or a more extended structure.

Polyelectrolyte complexes are crucial for flocculation applications in the paper industry, water treatment, and mineral processing [65]. Their function is the separation of unwanted particles from dispersions by flocculation. To better understand their flocculation behavior, we can look at their interactions with negatively charged silica particles. Examination of the flocculation capacity of poly(diallyldimethylammonium chloride) alone and in combination with poly(maleic acid–*co*-*α*-methylstyrene) illustrates that flocculation occurs over a much broader polymer concentration range when the polyelectrolyte complex is used, as opposed to the polycation alone [47]. A possible explanation for this behavior is provided in Fig. 7.28. It is very likely that the polycation alone forms a thin layer on the surface of the silica particle, which leads to an overall neutralized charge on the particle surface. Thus, the repulsion forces of the particles will be diminished. Increasing the polymer concentration does help to alleviate this effect, although the polymer has a limited range of efficacy. On the other hand, when a polyelectrolyte complex is utilized for this application, such as that formed from poly(diallyldimethylammonium chloride) and poly(maleic acid–*co*-*α*-methylstyrene), much larger entities will be present on the silica surface leading to greater repulsion between the silica particles over an extended concentration range.

Overall, polyelectrolyte complexes containing maleic anhydride-based copolymers offer many possibilities for industrial and medical applications. This may be attributed to their unique chemical properties, such as alternating copolymerization as well as the ionization potential of the maleic acid portion of the molecule. The studies outlined in Table 7.3 provide sufficient evidence of the academic interest in understanding more about the fundamental properties of polyelectrolyte complexes based on these polymers. We wait with bated breath for more such studies to help guide us in understanding the colloidal behavior of similar systems.

7.11 Concluding Remarks

The physical chemistry of copolymers of maleic anhydride has fascinated scientists for almost 50 years. Early work in this area focused on understanding the pH-dependent conformational behavior of dilute solutions of these polymers with specific emphasis on the influence of hydrophobic modification to these properties. As a result, a great deal of understanding was achieved in terms of the molecular dynamics of the polymers in relation to their structure. More recent studies provide insight into interactions of surfactants with hydrophobically modified maleic anhydride copolymers. Such investigations provide desired knowledge about the colloidal behavior of these systems for a variety of industrial applications. Further, due to the dynamic properties of these polyacid derivatives, there has also been keen interest in their use in thin film applications. Finally, numerous work involving maleic anhydride copolymers has been conducted in the area of polyelectrolyte

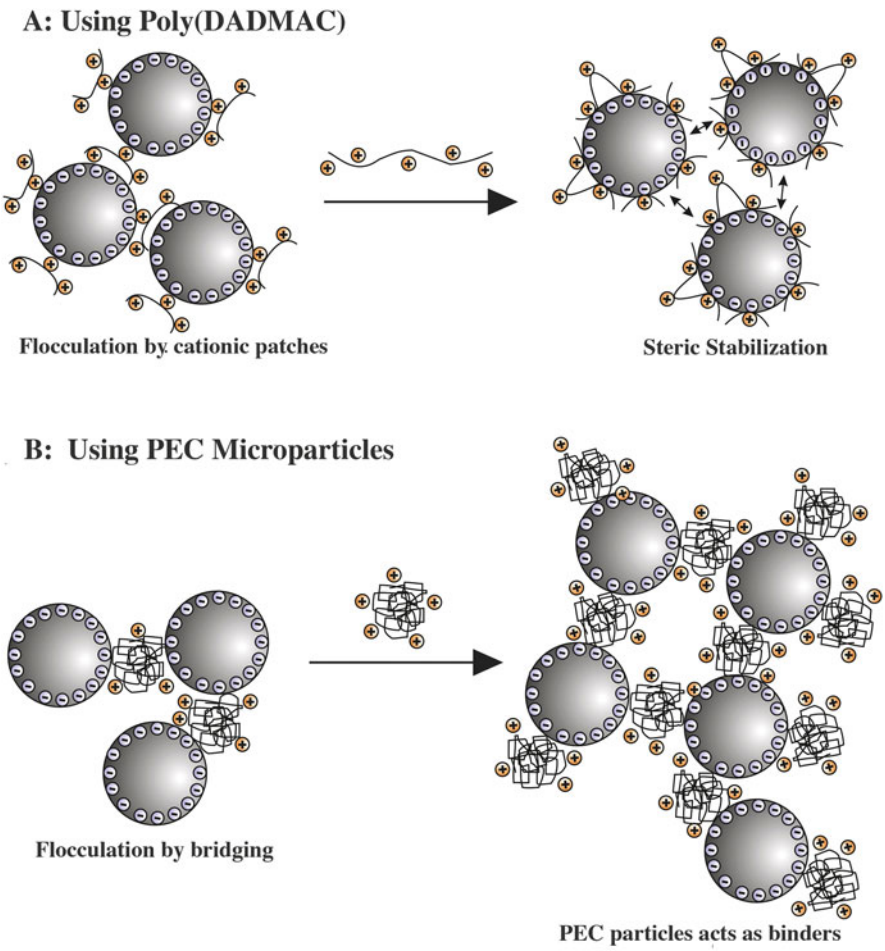

Fig. 7.28 Possible flocculation mechanisms for (**a**) poly(diallyldimethylammonium chloride) alone and (**b**) a polyelectrolyte complex based on poly(diallyldimethylammonium chloride) and poly(maleic acid–*co*-*α*-methylstyrene). Reprinted with permission from Buchhammer et al., *Langmuir* **1999,** *15*, 4306–4310 [47]. Copyright, 1999, American Chemical Society

complexes. This is a contemporary area of research with much promise in bio- and nanotechnology.

Acknowledgments The author would like to acknowledge Dr. Puspendu Deo of The Dow Chemical Company for reviewing this chapter and for providing insight and suggestions. A debt of gratitude is also due to Ms. Mandy Mende of Leibniz Institute for Polymer Research Dresden for providing the high resolution image in Fig. 7.28.

References

1. Dubin P, Strauss U (1967) Hydrophobic hypercoiling in copolymers of maleic acid and alkyl vinyl ethers. J Phys Chem 71(8):2757–2759
2. Dubin P, Strauss U (1970) Hydrophobic bonding in alternating copolymers of maleic acid and alkyl vinyl ethers. J Phys Chem 74(14):2842–2847
3. Dubin P, Strauss U (1975) Hypercoiling in hydrophobic polyacids. In: Rembaum A, Sélégny E (eds) Polyelectrolytes and their applications. D Reidel Publishing Co, Dordrecht, Holland, pp 3–13
4. Strauss U, Barbieri B (1982) Estimation of the cooperative unit size in conformational transitions of hydrophobic polyacids. Macromolecules 15:1347–1349
5. Barbieri B, Strauss U (1985) Effect of alkyl group size on the cooperativity in conformational transitions of hydrophobic polyacids. Macromolecules 18:411–414
6. Hsu J-Y, Strauss U (1987) Intramolecular micelles in a copolymer of maleic anhydride and hexyl vinyl ether: determination of aggregation number by luminescence quenching. J Phys Chem 91:6238–6241
7. Binana-Limbelé W, Zana R (1990) Fluorescence probing of microdomains in aqueous solutions of polysoaps. 2. Study of the size of the microdomains. Macromolecules 23:2731–2739
8. Zdanowicz V, Strauss U (1993) Intramolecular micelle size of polysoaps by luminescence quenching. Role of solubilization. Macromolecules 26:4770–4773
9. de Groot J, Koper G, Borkovec M, de Bleijser J (1998) Dissociation behavior of poly(maleic acid): potentiometric titrations, viscometry, pulsed field gradient NMR, and model calculations. Macromolecules 31:4182–4188
10. Minakata A, Matsumura K, Sasaki S, Ohnuma H (1980) Potentiometric titration of copolymers of maleic acid. 1. A simple theory. Macromolecules 13:1549–1553
11. Delben F, Paoletti S, Porasso R, Benegas J (2006) Potentiometric titrations of maleic acid copolymers in dilute aqueous solution: experimental results and theoretical interpretation. Macromolec Chem Phys 207:2299–2310
12. Po H, Senozan N (2001) The Henderson–Hasselbalch equation: its history and limitations. J Chem Educ 78(11):1499–1503
13. Kitano T, Kawaguchi S, Ito K (1987) Dissociation behavior of poly(fumaric acid) and poly (maleic acid). 1. Potentiometric titration and intrinsic viscosity. Macromolecules 20: 1598–1606
14. Varoqui R, Strauss U (1968) Comparison of electrical transport properties of anionic polyelectrolytes and polysoaps. J Phys Chem 72(7):2507–2511
15. Strauss U, Andrechak J (1985) The effect of molecular weight on the behavior of hydrophobic polyacids. J Polym Sci 23:1063–1075
16. Crescenzi V, Quadrifoglio F, Delben F (1972) Calorimetric studies of polycarboxylic acids in aqueous solution. II. Maleic acid–butyl vinyl ether copolymer. J Polym Sci C 39:241–246
17. Strauss U, Schlesinger M (1978) Effects of alkyl group size and counterion type on the behavior of copolymers of maleic anhydride and alkyl vinyl ethers. 1. Potentiometric titrations. J Phys Chem 82(5):571–574
18. Begala A, Strauss U (1972) Dilatometric studies of counterion binding by polycarboxylates. J Phys Chem 76:254–260
19. Martin P, Strauss U (1980) Thermodynamics of hydrophobic polyacids. Biophys Chem 11: 397–402
20. Strauss U, Vesnaver G (1975) Optical probes in polyelectrolyte studies. I. Acid-base equilibria of dansylated copolymers of maleic anhydride and alkyl vinyl ethers. J Phys Chem 79(15): 1558–1561
21. Strauss U, Vesnaver G (1975) Optical probes in polyelectrolyte studies. II. Fluorescence spectra of dansylated copolymers of maleic anhydride and alkyl vinyl ethers. J Phys Chem 79(22):2426–2429
22. Qiu Q, Lou A, Somasundaran P, Pethica B (2002) Intramolecular association of poly(maleic acid/ octyl vinyl ether) in aqueous solution. Langmuir 18:5921–5926

23. Deo P, Deo N, Somasundaran P, Jockusch S, Turro N (2005) Conformational changes of pyrene-labeled polyelectrolytes with pH: effect of hydrophobic modifications. J Phys Chem 109:20714–20718
24. Sugai S, Ohno N (1980) Conformational transitions of the hydrophobic polyacids. Biophys Chem 11:387–395
25. Garrett E, Guile R (1951) Potentiometric titrations of a polydicarboxylic acid: maleic acid-styrene copolymer. J Am Chem Soc 73(10):4533–4535
26. Sakaguchi Y, Honjyo H, Tamaki K (1971) Formation of acid anhydride, lactonization and potentiometric titration of some copolymers containing maleic acid unit. Kobunshi Kagaku 28(313):423–429
27. Ohno N, Nitta K, Sugai S (1971) The conformational transition of maleic acid-styrene copolymer in aqueous solutions. Kobunshi Kagaku 28(316):671–675
28. Ohno N, Nitta K, Makino S, Sugai S (1973) Conformational transition of the copolymer of maleic acid and styrene in aqueous solution. J Polym Sci 11:413–425
29. Okuda T, Ohno N, Nitta K, Sugai S (1977) Conformational transition of the copolymer of maleic acid and styrene in aqueous solution. II. J Polym Sci 15:749–755
30. Leyte J, Mandel M (1964) Potentiometric behavior of polymethacrylic acid. J Polym Sci A 2: 1879–1891
31. Deo P, Somasundaran P (2005) Interactions of hydrophobically modified polyelectrolytes with nonionic surfactants. Langmuir 21:3950–3956
32. Deo P, Deo N, Somasundaran P (2005) Complexation of hydrophobically modified polyelectrolytes with surfactants: anionic poly(maleic acid/octyl vinyl ether)/anionic sodium dodecyl sulfate. Langmuir 21:9998–10003
33. Deo P, Deo N, Somasundaran P (2007) Interactions of a hydrophobically modified polymer with oppositely charged surfactants. Langmuir 23:5906–5913
34. Osaki T, Werner C (2003) Ionization characteristics and structural transitions of alternating maleic acid copolymer films. Langmuir 19(14):5787–5793
35. Winter C, Tredgold R, Vickers A, Khoshdel E, Hodge P (1985) Langmuir-Blodgett films from preformed polymers: derivatives of octadec-1-ene-maleic anhydride copolymers. Thin Solid Films 134(1–3):49–55
36. Wang M, Zhu X, Wang S, Zhang L (1999) Surface pattern in thin poly(styrene–maleic anhydride) films. Polymer 40(26):7387–7396
37. Tredgold R (1987) Langmuir-Blodgett films made from preformed polymers. Films 152(1–2): 223–230
38. Schmidt U, Zschoche S, Werner C (2003) Modification of poly(octadecene–*alt*-maleic anhydride) films by reaction with functional amines. J Appl Polym Sci 87(8):1255–1266
39. Schiller S, Hu J, Jenkins A, Timmons R, Sanchez-Estrada F, Knoll W, Förch R (2002) Chemical structure and properties of plasma-polymerized maleic anhydride films. Chem Mater 14(1):235–242
40. Pompe T, Zschoche S, Herold N, Salchert K, Gouzy M-F, Sperling C, Werner C (2003) Maleic anhydride copolymers—a versatile platform for molecular biosurface engineering. Biomacromolecules 4(4):1072–1079
41. López-Díaz D, Velázquez M (2008) Evidence of glass transition in thin films of maleic anhydride derivatives: effect of the surfactant coadsorption. Eur Phys J E 26(4):417–425
42. Jenkins A, Hu J, Wang Y, Schiller S, Foerch R, Knoll W (2000) Pulsed plasma deposited maleic anhydride thin films as supports for lipid bilayers. Langmuir 16(16):6381–6384
43. Freudenberg U, Zschoche S, Simon F, Janke A, Schmidt K, Behrens S, Auweter H, Werner C (2005) Covalent immobilization of cellulose layers onto maleic anhydride copolymer thin films. Biomacromolecules 6(3):1628–1634
44. Zhang Y, Cao W (2001) Stable self-assembled multilayer films of diazo resin and poly(maleic anhydride–co-styrene) based on charge-transfer interaction. Langmuir 17:5021–5024
45. Uhlmann P, Skorupa S, Werner C, Grundke K (2005) Characterization of maleic acid/anhydride copolymer films by low-rate dynamic liquid−fluid contact angle measurements using axisymmetric drop shape analysis. Langmuir 21(14):6302–6307

46. Garnier G, Miroslava Duskova-Smrckova M, Vyhnalkova R, van de Ven T, Revol J-F (2000) Association in solution and adsorption at an air-water interface of alternating copolymers of maleic anhydride and styrene. Langmuir 16(8):3757–3763
47. Buchhammer H-M, Petzold G, Lunkwitz K (1999) Salt effect on formation and properties of interpolyelectrolyte complexes and their interactions with silica particles. Langmuir 15: 4306–4310
48. Park K, Shalaby W, Park H (1993) Biodegradable hydrogels for drug delivery. Technomic Publishing Co., Lancaster, PA
49. Booij H, Bungengerg H (1956) Biocolloids and their interactions. Springer, Vienna
50. Buchhammer H-M, Mende M, Oelmann M (2003) Formation of mono-sized polyelectrolyte complex dispersions: effects of polymer structure, concentration and mixing conditions. Colloids Surf A 218:151–159
51. Lankalapalli S, Kolapalli V (2009) Polyelectrolyte complexes: a review of their applicability in drug delivery technology. Ind J Pharm Sci 71(5):481–487
52. Popescu I, Suflet D, Mihai M (2012) Influence of comonomer structure and of the initial pH on the characteristics of polyelectrolyte complexes based on maleic acid copolymers. J Polym Res 19:9958
53. Yin X, Stöver H (2003) Hydrogel microspheres formed by complex coacervation of partially MPEG-grafted poly(styrene–alt-maleic anhydride) with PDADMAC and cross-linking with polyamines. Macromolecules 36:8773–8779
54. Shin-Ya Y, Tsurushima H, Tsurumi T, Kajiuchi T, Leong K (2004) Polyelectrolyte complex films derived from polyethyleneoxide-maleic acid copolymer and chitosan: preparation and characterization. Macromolec Biosci 4(5):526–531
55. Veron L, Revol M, Mandrand B, Delair T (2001) Synthesis and characterization of poly(N-vinyl pyrrolidone–*alt*-maleic anhydride): conjugation with bovine serum albumin. J Appl Polym Sci 81:3327–3337
56. Rong Y, Chen H-Z, Wei D-C, Sun J-Z, Wang M (2004) Microcapsules with contact membrane structure from gelatin and styrene-maleic anhydride copolymer by complex coacervation. Colloids Surf A 242:17–20
57. Müller M, Kessler B, Richter S (2005) Preparation of monomodal polyelectrolyte complex nanoparticles of PDADMAC/poly(maleic acid–*alt*-α-methylstyrene) by consecutive centrifugation. Langmuir 21:7044–7051
58. Müller M, Reihs T, Ouyang W (2005) Needlelike and spherical polyelectrolyte complex nanoparticles of poly(L-lysine) and copolymers of maleic acid. Langmuir 21:465–469
59. Izumrudov V, Gorshkova M, Volkova I (2005) Controlled phase separations in solutions of soluble polyelectrolyte complex of DIVEMA (copolymer of divinyl ether and maleic anhydride). Eur Polym J 41:1251–1259
60. Boyko V, Richter S, Mende M, Schwarz S, Zschoche S, Arndt K-F (2007) Characterization of polyelectrolyte complexes based on maleic anhydride alternating copolymers by static and dynamic light scattering. Macromolec Chem Phys 208:710–717
61. Pergushov D, Buchhammer H-M, Lunkwitz K (1999) Effect of a low-molecular-weight salt on colloidal dispersions of interpolyelectrolyte complexes. Colloid Polym Sci 277:101–107
62. Petzold G, Nebel A, Buchhammer H-M, Lunkwitz K (1998) Preparation and characterization of different polyelectrolyte complexes and their application as flocculants. Colloid Polym Sci 276:125–130
63. Kramer G, Buchhammer H-M, Lunkwitz K (1997) Surface modification by polyelectrolyte complexes: influence of different polyelectrolyte components and substrates. Colloids Surf A 122:1–12
64. Mende M, Buchhammer H-M, Schwarz S, Petzold G, Jaeger W (2004) The stability of polyelectrolyte complex systems of poly(diallyldimethylammonium chloride) with different polyanions. Macromolec Symp 211:121–133
65. Petzold G, Schwarz S (2014) Polyelectrolyte complexes in flocculation applications. Adv Polym Sci 256:25–66

Part IV
Applications

Chapter 8
Maleic Anhydride Applications in Personal Care

Roger L. McMullen

8.1 Introduction

Maleic anhydride and its derivatives are used in many different areas in personal care. They are indispensable ingredients used in hair, skin, and oral care formulations. In hair care applications, copolymers containing maleic anhydride are mostly found in hair fixative and styling formulas. They act as film formers, compatible with a variety of solvent systems, which form polymer-hair fiber assemblies with resistance to high humidity and mechanical insult to the hairstyle. The use of this type of chemistry in hair care has a long history that began in the 1950s and continues to find itself in contemporary products. In skin care, the largest impact of maleic anhydride chemistry is in the form of copolymers of maleic anhydride and methyl vinyl ether that are used in transdermal delivery systems and as bioadhesives for biomedical devices. In addition, there are many innovative uses of maleic anhydride chemistry in the delivery of cosmetic active ingredients as well as adjuvants in antiperspirant formulations. Moreover, copolymers of maleic anhydride function as rheology modifiers in finished skin care formulations providing desirable textural and sensorial properties for the consumer. In oral care, poly (methyl vinyl ether-maleic anhydride) is found in dentifrice formulations, where it acts as a bioadhesive, film former, and delivery vehicle for active ingredients. For many years, the bioadhesive nature of poly(methyl vinyl ether-maleic anhydride) to the oral mucosa has been exploited in denture adhesive formulations as the key active ingredient. In the pages that follow, we provide a summary and critical analysis of both historical and contemporary uses of maleic anhydride in the personal care arena focusing on traditional and innovative approaches.

R.L. McMullen (✉)
Ashland, Inc., 1005 Route 202/206, Bridgewater, NJ 08807, USA
e-mail: rmcmullen@ashland.com

O.M. Musa (ed.), *Handbook of Maleic Anhydride Based Materials*,
DOI 10.1007/978-3-319-29454-4_8

8.2 Applications of Maleic Anhydride Copolymers in Hair Care

Human hair plays an important role in many facets of the consumer's daily life. It is important from a psychological and sociological perspective and often is indicative of the beauty and/or health state of an individual. For these reasons, the hair sector of the beauty industry has grown to colossal scale over the last century. A variety of products are used to shape hair into various desired configurations. Some product categories are permanent (e.g., hair relaxers and permanent waves) and require chemically reactive treatments that change the chemistry of the mature hair shaft. Other treatments, generally oils and polymers, are used to modify the three-dimensional arrangement of the fiber assembly and to fix it in place. This latter category of treatments covers a realm of products consisting of gels, mousses, hair sprays, waxes, and pomades. A major requirement of these treatments is to provide a durable style for a reasonable amount of time (~4–8 h) while withstanding stressful environmental conditions, such as high humidity, as well as mechanical disruption of the assembly, which occurs when the individual touches the hair fiber assembly as well as motion caused by walking and other factors. In the paragraphs that follow, we provide a description of hair structure as well as various applications of maleic anhydride chemistry in hair care.

8.2.1 Structure and Function of Hair

The morphological structure of a mature human hair contains an inner core (cortex) of spindle-shaped cortical cells (5 μm in diameter and 50 μm in length) aligned along the length of the fiber. This is surrounded by overlapping flat cuticle cells that are arranged in a manner analogous to fish scales or shingles [1–4]. The fiber may also contain a medulla, which is located at the center of the cortex. Figure 8.1 contains an illustration of the three principle morphological components of hair, while Fig. 8.2 provides a close-up look of the hair fiber only revealing the outer cuticle structure. In many cases, the first thing that usually comes to mind when we think of hair is alpha-keratin, which is a fibrous-type protein located in the cortical cells of the cortex. The alpha-keratin chains associate together to form a hierarchal quaternary structure. This is the "crystalline" part of the hair fiber known as the intermediate filament (or microfibril). Intermediate filaments (hundreds of them) are embedded in a pseudohexagonal array within a cysteine-rich protein matrix to form the keratin macrofibril. Several tens of macrofibrils are packed longitudinally within each cortical cell. The crystalline phase intermediate filaments play an integral role in the mechanical tensile strength of the fiber. Equally important, the cysteine-rich amorphous phase influences the mechanical properties of the fiber. For example, in the wet state hair is more extensible, although it requires less

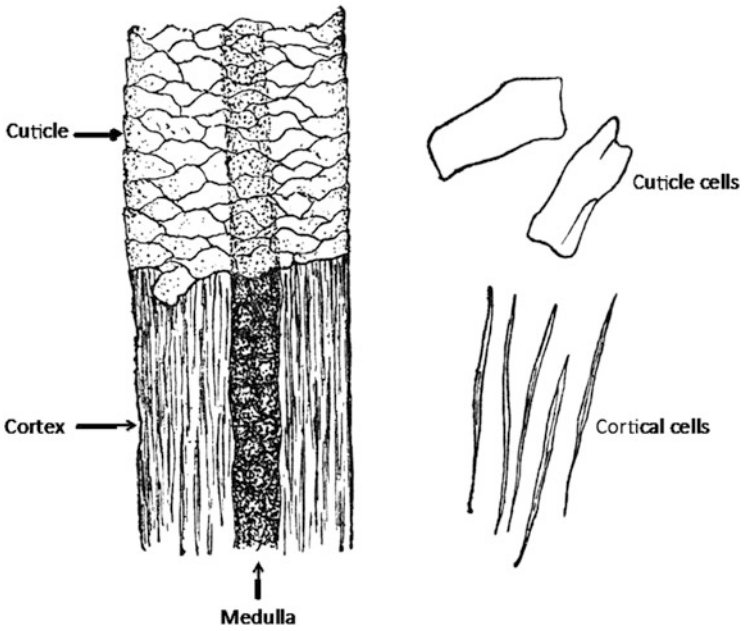

Fig. 8.1 Morphological structure of human hair, which contains three principle components: (1) an internal cortex surrounded by (2) overlapping cuticle cells and (3) the medulla. For demonstration, the cuticle is removed in the lower half of the illustration revealing the underlying cortex structure. Individual cortical and cuticle cells are shown on the *right side* of the drawing. This illustration originally appeared in G.A. Piersol, *Human Anatomy*, Vol. II, J.B. Lippincott Company: Philadelphia, PA (1908) [5]

energy to break than in the dry state. The uptake of water by the amorphous matrix also greatly influences the styling behavior of hair.

The morphological and chemical structure of the hair cuticle is equally complex. Each cuticle cell, which is ca. 0.5 μm thick and 60 μm square, consists of various components known as outer beta-layer, epicuticle, A layer, exocuticle, endocuticle, inner layer, and inner beta-layer. These cuticular subcomponents are lamellar and arranged in the order listed above from the exterior of the fiber to its interior. The outer and inner beta-layers constitute part of what is known as the cell membrane complex, which is unlike most biological phospholipid membranes. It is believed that the outer beta-layer, exposed to the surface and to overlying cuticle cells, consists predominantly of 18-methyleicosanoic acid (18-MEA) [6]. In addition, the cell membrane complex contains a delta layer, which is the intercellular cement that joins the inner beta-layer of one cuticle cell with the outer beta-layer of an underlying cuticle cell. The A layer, exocuticle, and inner layer are thought to be proteinaceous in nature and have been shown to be extremely rich in disulfide bonds [7]. The endocuticle, on the other hand, is generally low in cystine, but is also comprised of proteinaceous material. Human hair usually contains ca. 10 layers of cuticle cells at the root of the fiber; however, this number diminishes along the length of the fiber

Fig. 8.2 Scanning electron microscope (SEM) micrograph of a human hair fiber

toward the tip direction [8]. Overall, it is sufficient to say that undamaged hair has a hydrophobic surface due to the composition of the outer beta-layer as well as sebaceous lipids that do not play a structural role, but lubricate the fiber.

One should bear in mind, however, that chemically treated hair (dyed, bleached, permanent waved, relaxed, etc.) has entirely different surface properties than virgin hair. Contact angle readings can drop from ~98° in the case of virgin hair to ~74° for bleached hair—representative of a hydrophobic surface (virgin hair) that has become extremely hydrophilic (damaged hair). This will greatly influence how fixative and styling agents interact with the hair due to wetting behavior. For example, studies have shown that delipidized hair, which has a much lower contact

angle than virgin hair, is stiffer when treated with a hydroalcoholic solution of fixative polymer. The explanation stems from the greater wettability of delipidized hair, which is allowed to swell to a greater extent, thereby resulting in greater contact area in the weld regions where polymers bind with the fiber [9]. Thus, it is essential to understand the morphological structure of hair to explain the interactions of ingredients with hair and how they affect its cosmetic behavior.

8.2.2 Hair Sprays

A common method for maintaining a temporary hairstyle is manipulating hair into a desired configuration followed by treatment with hair spray, which fixes the hairstyle for an extended period of time. Hair sprays generally fall into one of two categories: pump or aerosol hair sprays. Aerosol hair sprays are often referred to as hydrocarbon or dimethyl ether aerosols, and they contain an alcohol-hydrocarbon solvent-propellant system, polymeric resin, base to neutralize the resin (if acid groups are present on the polymer), plasticizer, surfactant, and fragrance [1]. The polymeric resin is the ingredient responsible for binding/gluing fibers together; the base (the most common is 2-amino-2-methyl-1-propanol) adjusts the solubility of the polymer allowing it to be more easily removed from hair; the plasticizer fine tunes the mechanical properties of the film, such as hardness/flexibility, to the desired state; and surfactant modifies the surface tension making the polymer more/less spreadable on the hair surface. Essentially an aerosol is a suspension of fine particles (solid or liquid) that forms when a liquefied propellant gas is dispensed from a pressurized container. As the propellant reverts to a gas under normal atmospheric pressure, it atomizes the carrier liquid into fine droplets that form the spray. Pump hair sprays refer to similar systems that do not require propellant, but rather are dispensed by a pumping mechanism that contains an atomizer that in conjunction with springs, valves, etc. produces fine droplets of the formulation through the mechanism of mechanical breakup.

Modern-day aerosol systems were invented in the early part of the twentieth century. They were in cans with nozzles and contained a propellant. Following advances made by the military during World War II for the delivery of insecticides to prevent insect-borne diseases in soldiers, the beauty industry took advantage of this technology to deliver polymeric setting resins to hair. The first hair spray systems were based on shellac, a natural resin obtained from secretions by the lac bug. By the 1950s, there was explosive growth in the development of polymeric resins used for hair sprays. It was during this time that the first maleic acid-based polymers were introduced to the marketplace, and the use of these polymers in hair sprays started to appear in the patent literature [10, 11].

The earliest most successful maleic acid-based polymers to be incorporated into these systems were copolymers of methyl vinyl ether and maleic acid (see Fig. 8.3). Later adaptations of these molecules were based on esterification of one of the acid groups on the maleic acid portion of the polymer resulting in either an ethyl or butyl

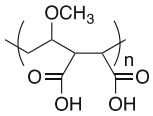

Fig. 8.3 Molecular structure of poly(methyl vinyl ether-maleic acid)

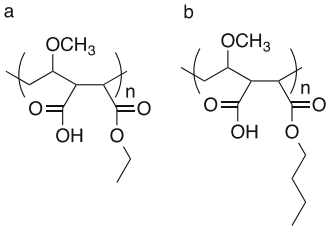

Fig. 8.4 Molecular structure of (**a**) monoethyl ester of poly(methyl vinyl ether-maleic acid) and (**b**) monobutyl ester of poly(methyl vinyl ether-maleic acid)

ester (see Fig. 8.4). Not surprisingly, the butyl ester of poly(vinyl ether-maleic acid) provides more resistance to breakdown of the hair set from high humidity than the ethyl ester derivative. Hydrophobic modification of both hairstyling and fixative polymers makes the polymer-fiber assembly more resistant to humidity and liquid water. Nevertheless, these polymers were originally designed for and are still used in aerosol hair sprays in many countries [12–17].

During the 1970s, the use of hair sprays declined in the United States in part due to changes in hairstyles, but also due to regulatory pressures to reduce the quantity of chlorofluorocarbons (CFCs) in consumer products. CFCs were commonly used propellants in aerosol systems; however, regulatory agencies, such as the Environmental Protection Agency (EPA) in the United States, set guidelines restricting their use due to growing concerns of the role of CFCs in the destruction of ozone in the stratosphere. For this reason, CFCs have largely been replaced with more environmentally friendly propellants, such as dimethyl ether and 1,1-difluoroethane—commonly known as hydrofluorocarbon 152-A. In the late 1980s to early 1990s, there was pressure to reduce the level of volatile organic compounds (VOCs) in consumer products. The push toward 80 % VOC then to 55 % VOC hair spray systems in the United States led to a hair spray market with increasing numbers of pump hair sprays. Polymers that functioned very well in high VOC systems now faced the challenges presented by water-based formulas, such as solubility, difficulty in spraying due to high viscosity, poor high-humidity curl retention, and increased formulation tackiness [18]. Curl droop, or the relaxation of the hair and consequent disturbance of the hairstyle after addition of the fixative agent, is another issue since the hair physically interacts with water. In addition, corrosion in metal aerosol cans also became a significant challenge due to the greater presence of H_2O. Regardless, there was a flurry of patent literature utilizing poly(methyl vinyl ether-maleic anhydride) and its derivatives in low VOC systems.

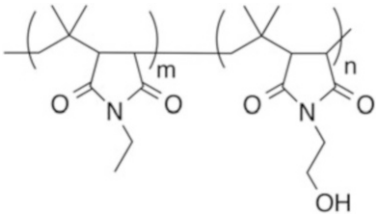

Fig. 8.5 Molecular structure of poly(isobutylene-ethylmaleimide-hydroxyethylmaleimide)

They were formulated in both 80 % VOC compositions [19–21] and 55 % VOC systems [22–25]. There are even examples of 0 % VOC systems in which a microemulsion of these polymers is dispersed in H_2O [26]. Regardless, anhydrous hair spray systems still exist largely in part due to higher use levels of hydrofluorocarbon-152A, which is exempt from the VOC list, as the system propellant and solvent. Overall, the use of this molecule as both propellant and solvent leads to a more expensive formulation, although it offers the salon practitioner and consumer access to anhydrous systems, for quick-drying formulations. In fact, hydrofluorocarbon 152-A allowed aerosol systems to become the prominent form of hair spray once again.

The reduction of VOCs in hair spray formulations led to the development of new polymers that were compatible in these systems and lower molecular weight analogs of polymers already used in the high VOC formulas. Another approach to solve this problem was to utilize lower molecular weight analogs of polymers already used in the high VOC formulas. This evolution eventually led to the development of maleic anhydride polymer derivatives that were more soluble in H_2O and, hence, more suitable for 55 % VOC applications. The best example of a commercially successful polymer in this category is an imidized isobutylene/maleic anhydride copolymer consisting of three monomeric units: isobutylene, ethylmaleimide, and hydroxyethylmaleimide (see Fig. 8.5) [27, 28]. It is found in many modern-day low VOC hair sprays. This polymer has some properties in common with traditional maleic anhydride-based polymers (e.g., ethyl or butyl ester of poly(vinyl ether-maleic acid)). However, the polymeric design leads to more favorable hair fixative properties, such as pH stability, enhanced optical properties (hair shine), no corrosion, no flaking, and increased stiffness of the hair set [29]. Examples of several formulation types (e.g., hair spray, hair setting formula) containing poly(isobutylene-ethylmaleimide-hydroxyethylmaleimide) may be found in the patent literature [30, 31].

8.2.3 Hair Gel and Mousse Applications

Hair gels became popular in the 1960s when companies, such as Dep (California) and Dippity-do (Canada), introduced gel formulations to the marketplace. Gels are

still popular today and are largely comprised of a thickening polymer—cross-linked poly(acrylic acid) is the most popular—used in conjunction with a styling polymer; the most common are poly(vinyl pyrrolidone) and poly(vinyl pyrrolidone-vinyl acetate). On the other hand, hair mousses were introduced in the 1970s, although they did not become extremely popular until the early 1990s, when the grunge look became fashionable [18]. Mousses are available as aerosol or nonaerosol formulations. They are dispensed as a foam, which is then worked through the hair to give a desired style. Typical ingredients in an aerosol mousse consist of solvent, propellant, surfactant, and polymeric resin. In most cases the solvent is H_2O. The most popular propellants are 1,1-difluoroethane and mixtures of propane and isobutane [32]. Surfactant is typically added to aid in the formation of a more stable foam or mousse. Like hair sprays, there are also VOC restrictions on mousses and gels. For mousses, VOC levels as set forth by the EPA in the United States should not exceed 16 % and in some states, such as California, they cannot exceed 6 %. Gel formulations should contain no more than 2 % VOCs [33]. As one might expect, polymers designed for hairstyling applications (hair gel or mousse) are, in general, higher molecular weight species than those employed in hair spray systems. They often also contain cationic or pseudo-cationic polymers.

In general, most polymeric resins designed for anhydrous hair spray systems do not formulate well in mousse or gel systems, since they are usually supplied as alcoholic solutions, making it difficult to achieve the low VOC levels (J. Dallal, Personal communication, 2014). In addition, hair spray polymers are typically lower in molecular weight, allowing for better spray distribution patterns, while styling polymers are generally higher molecular weight species. During the rise of popularity of hair mousse systems in the early 1990s, it was found that higher molecular weight poly(methyl vinyl ether-maleic anhydride) derivatives (~1,000,000 KDa) produce mousses with optimum performance as compared to lower molecular weight versions of this polymer, originally designed for hair sprays [34].

Maleic anhydride-based polymers, more suitable for hairstyling applications, were developed and commercialized into the specialty chemical marketplace beginning in the late 1990s. The monoester of poly(isobutylene-dimethylaminopropryl maleimide-ethoxylated maleimide-maleic acid), sold under the trade name Aquaflex XL-30, was designed for hair gel systems containing a poly(acrylic acid) thickener (see Fig. 8.6 for molecular structure) [35]. Cross-linked poly(acrylic acid), commonly referred to as carbomer, is an anionic thickening agent that forms clear gels. Most developers of finished hair care products require that hairstyling polymers used in conjunction with carbomer in hair gel systems are clear. While the monoester of poly (isobutylene-dimethylaminopropyl maleimide-ethoxylated maleimide-maleic acid) was originally designed for carbomer-based hair gels, there are a number of commercial examples of its use in hair mousses and other types of styling lotions.

So far, our focus in this section has centered on maleic anhydride-based polymers that act as hairstyling agents in formulations. Another key use of this chemistry is in the thickening of hair gel formulations [36, 37]. Water-soluble gels containing hydrolyzed poly(vinyl ether-maleic anhydride) can be formed in combination with various bases, such as mineral bases, aliphatic amines, amino

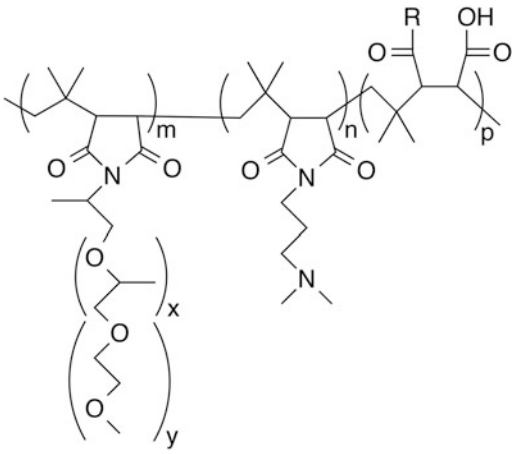

Fig. 8.6 Molecular structure of the monoester of poly(isobutylene-dimethylaminopropyl maleimide-ethoxylated maleimide-maleic acid). It is also known by its INCI name: polyimide-1

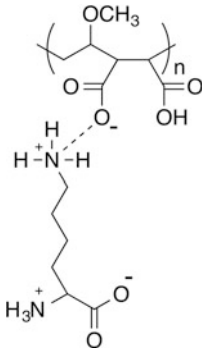

Fig. 8.7 Electrostatic interactions between the carboxylate groups of maleic acid and amino acids containing pendent amino groups (e.g., lysine). At pH 6–7 85–90 % of the hydroxyl groups of maleic acid are protonated, assuming a $pK_{a_1} = 3.47$ and $pK_{a_2} = 6.47$

alcohols, or triethanol amine. Utilization of these neutralizing groups renders a gel that is irritating to the skin. To circumvent such issues, amino acids containing pendant amine groups (e.g., proline, arginine, etc.) have been employed as neutralizing agents for personal care applications (see Fig. 8.7) [38].

More recent studies disclose compositions based on the interactions between poly(methyl vinyl ether-maleic acid) and poly(lysine), which provide better high-humidity curl resistance and anti-frizz benefits [39]. A different approach consists of formulating aqueous solutions of hydrolyzed poly(methyl vinyl ether-maleic anhydride) cross-linked with 1,9-decadiene, producing relatively viscous gels (35,000–180,000 cps) in H_2O at concentrations of 0.5–1.5 % (w/w) within a pH range of 4–11 [40, 41]. This cross-linked analog of poly(methyl vinyl ether-maleic

anhydride) comes in several commercially available forms and is sold under the trade name Stabileze by Ashland, Inc.

8.2.4 Split End Mending with a Polyelectrolyte Complex

Repeated grooming (combing, brushing, etc.) of human hair exposed to chemical treatments (bleaching, perming, and relaxing), UV radiation, and exposure to thermal styling appliances often results in mechanical damage to the protective overlying cuticle cells, leading to their erosion and, further, often to the development of split ends [42]. Technically referred to as trichoptilosis, split ends are a splitting or fraying of the hair shaft. There are several different forms, which are characterized by the degree of splitting, for example, single versus multiple splits. For illustration, Fig. 8.8 contains an SEM micrograph of a split end containing fiber. Hair bears a negative charge, which is thought to increase upon the formation of split ends due to overall increased surface accessibility. Normally, damaged hair is treated with cationic surfactants or polymers, which provide a lubricious feel during wet grooming procedures (e.g., combing or brushing). The electrostatic interactions between hair and the applied cationic species are strong enough to withstand sustained rinsing of hair with water; however, cationic surfactants are usually removed by washing the hair with sodium dodecyl sulfate or similar anionic surfactants. Polymers are usually more tightly bound since one polymer is attached at many different sites on the

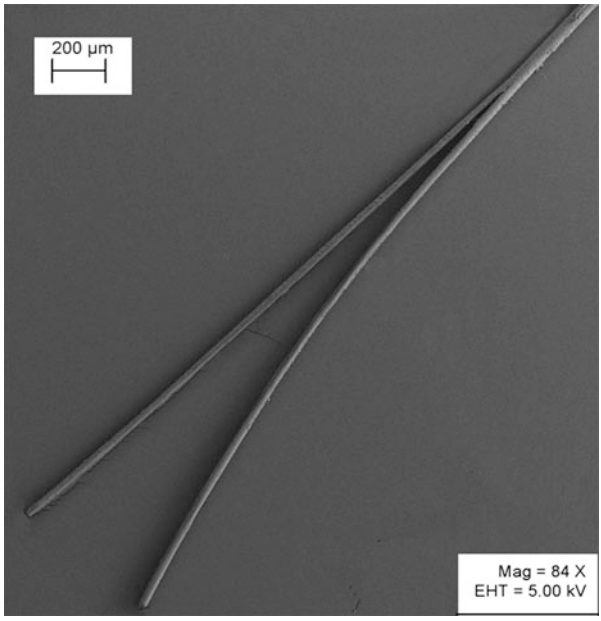

Fig. 8.8 SEM micrograph of a hair fiber containing a split end

hair surface, making it difficult to break all of the electrostatic and van der Waals interactions simultaneously. In the case of hair containing split ends, treatment with a cationic surfactant or polymer will help condition the fiber, but will do nothing to ameliorate the split end. To circumvent such damage, a novel approach is to treat split end containing hair with a polyelectrolyte complex.

Polyelectrolyte complexes are formed when two oppositely charged polymers combine together (see Fig. 8.9). In many cases it is enough to mix a polycation and polyanion in aqueous solution at an appropriate pH to obtain a robust complex that may bear synergistic or unique behavior not observed in the component polymers themselves. Reported studies demonstrate the use of neutralized poly(methyl vinyl ether-maleic acid) in combination with cationic poly(vinyl pyrrolidone-methacrylamido propyl trimethylammonium chloride) to mend split ends (see structures in Fig. 8.10) [43–45].

Evidence for the formation of a polyelectrolyte complex is based on optical microscopy, Malvern particle size analysis, and viscometry. When mixed together, these polymers form a distinguishable microgel structure. One should bear in mind that the charge on the quaternary amine of poly(vinyl pyrrolidone-methacrylamido propyl trimethylammonium chloride) is not dependent on pH, since it contains a quaternary amine group. On the other hand, the acid groups of the diacid moiety of poly(methyl vinyl ether-maleic acid) need to become deprotonated in order to interact with the cationic quaternary amine and form a polyelectrolyte complex. It should be noted that the diprotic maleic acid moiety of this anionic polymer has pK_a values of 3.47 and 6.47 [46]. Figure 8.11 contains a titration curve in which the

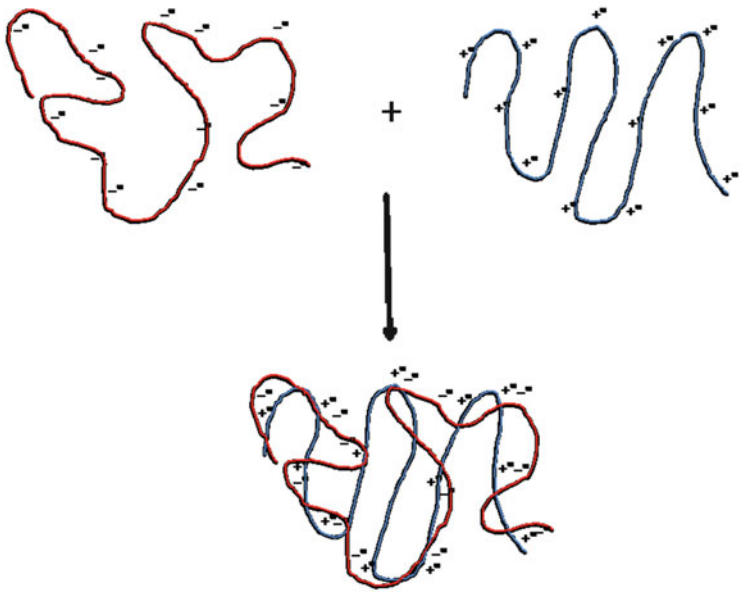

Fig. 8.9 Illustration of the complexation of a polycation and polyanion to form a polyelectrolyte complex

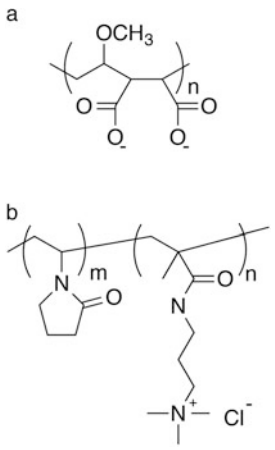

Fig. 8.10 Molecular structures of (**a**) poly(methyl vinyl ether-maleic acid) and (**b**) poly(vinyl pyrrolidone-methacrylamido propyl trimethylammonium chloride). The INCI names for these polymers are PVM/MA copolymer and Polyquaternium-28, respectively

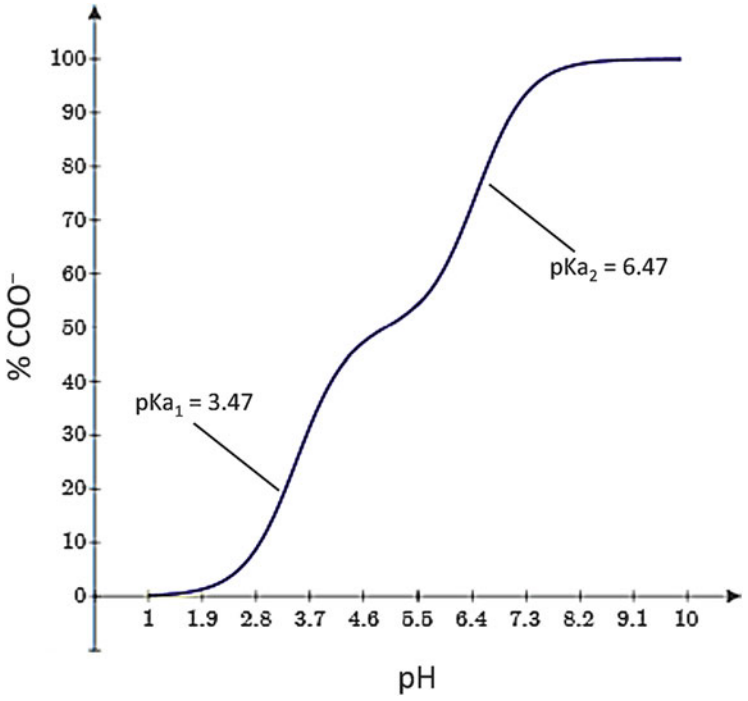

Fig. 8.11 Titration curve of poly(methyl vinyl ether-maleic acid) providing the percentage of negatively charged carboxylate groups (COO^-) in poly(methyl vinyl ether-maleic acid). The plot was obtained using the Henderson-Hasselbalch equation and the literature values of $pK_{a_1} = 3.47$ and $pK_{a_2} = 6.47$

percentage of negatively charged carboxylate groups (COO^-) in poly(methyl vinyl ether-maleic acid) is plotted as a function of pH. Therefore, one may determine the relative number of negatively charged species on the polymer backbone. This is a very useful tool for understanding polyelectrolyte interactions.

Based on viscometry measurements and the analysis of phase diagrams, the optimum stoichiometric charge ratio for the two polymers is 1:1, which results in concentrations of 0.2 % (w/w) poly(methyl vinyl ether-maleic acid) neutralized to pH 7 with NaOH and 0.8 % (w/w) poly(vinyl pyrrolidone-methacrylamido propyl trimethylammonium chloride). A proposed mechanism entails the polyelectrolyte complex in the form of a micron-sized hydrogel which acts as a cross-linking structure to bind the subassemblies of the damaged fiber together. More than likely, the poly(vinyl pyrrolidone-methacrylamido propyl trimethylammonium chloride) interacts with the negatively charged hair. Since poly(methyl vinyl ether-maleic acid) has adhesive properties, it is likely to glue together with itself bringing frayed or split ends together—a form of mending.

8.2.5 Thermal Styling and Protection

Thermal styling has been an integral part of the hair grooming process for many years. Traditionally, hot rollers and curling irons (typical temperatures ranging from 120 to 170 °C) were commonly employed to fix hair into a newly desired configuration while driving water from its internal structure by applying heat. In more recent years, the use of hot flat irons has exploded, often employing temperatures ranging from 180 °C to 235 °C. Their growth in popularity stems from their ability to straighten the fiber, as many individuals prefer straight hair rather than wavy, kinky, or frizzy hair. This trend has even escalated to the use of formaldehyde-containing products in combination with hot irons, resulting in permanent straightening due to alleged cross-linking of the keratin protein within the hair fiber [47]. In general there has been a market need in the personal care industry for thermal protectants and thermal activating agents. Such products began to be introduced in the late 1990s. During this same period, studies investigating the damaging effects of hot curling irons in the temperature range of 130–164 °C concentrated on the damaging effects of heat on hair (e.g., protein damage, color changes, and surface damage) as well as the effect of various treatments when applied to hair in combination with hot irons [48, 49]. While the protective mechanisms investigated in these studies were never clearly identified, it was proposed that coating fibers could provide an insulation effect or, possibly, provide lubrication to the fiber thereby preventing secondary grooming damage, resulting from a combination of thermal and mechanical combing damage. Nevertheless, based on combing force measurements, polymer-heat-treated hair often was more lubricious in the wet state than virgin hair, which persisted even after multiple washing cycles with sodium dodecyl sulfate. More than likely, the polymer became permanently attached to the fiber via cross-linking (likely to occur at such high

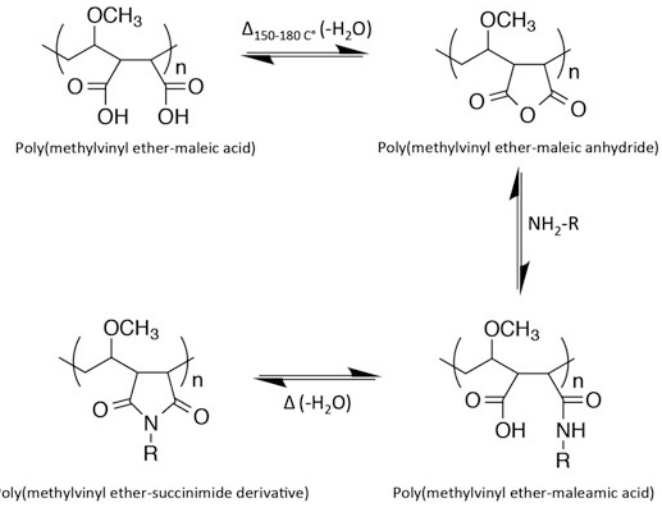

Scheme 8.1 Proposed scheme for the conversion of poly(methyl vinyl ether-maleic acid) to poly (methyl vinyl ether-maleic anhydride) followed by its reaction with protein amino groups on the surface of hair

temperatures) or the formation of a polymer thermal set in which the polymer reacted with itself after repeated treatment, eventually forming an extremely durable coating surrounding the fiber. Further studies demonstrated that poly(methyl vinyl ether-maleic acid) protected hair keratin protein (monitored by measuring the tryptophan content) to a greater extent than other polymers and that the polymer permanently remained on the hair surface [50]. In the absence of spectroscopic data, it was hypothesized that poly(methyl vinyl ether-maleic acid) would likely react with amino groups on the surface of hair fibers by a mechanism proposed in Scheme 8.1. During this process, ring closure of the maleic acid portion of the polymer liberates H_2O, which has an extremely high ΔH_{vap}. Possibly, such an effect could help protect surface proteins from conductive heat transfer from the hot iron to the hair surface.

Another comprehensive study, exploring the protective effects of polymers for thermally treated hair, demonstrates the use of the polyelectrolyte complex, described in the preceding section, in preventing hair thermal damage during exposure to hot flat irons with temperatures exceeding 200 °C [51]. To reiterate, the polyelectrolyte complex consisted of anionic poly(methyl vinyl ether-maleic acid) and cationic poly(vinyl pyrrolidone-methacrylamido propyl trimethylammonium chloride). These researchers demonstrated evidence of its efficacy by conducting FTIR spectroscopic imaging, dynamic scanning calorimetry (DSC), dynamic vapor sorption (DVS), atomic force microscopy (AFM), and scanning electron microscopy (SEM). Cross sections of hair were analyzed by FTIR spectroscopic imaging to monitor the quantities of alpha- and beta-keratin (see Fig. 8.12 for an example). DSC measurements were used to monitor the health state of hair,

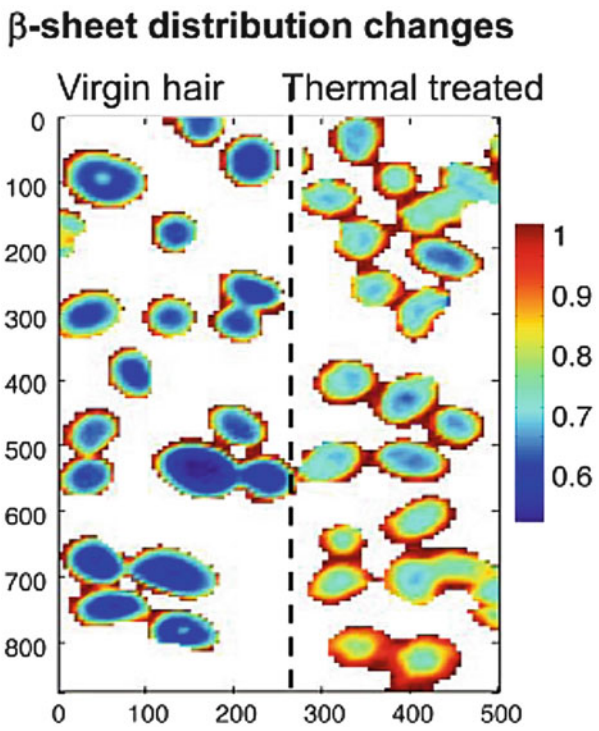

Fig. 8.12 FTIR spectroscopic images of cross sections of (a) undamaged, virgin hair and (b) hair that has been exposed to a thermal styling device. The FTIR image was generated from the ratio of 1516/1548 cm^{-1} obtained from the spectra gathered for each pixel. The representative spectra were obtained from European dark-brown hair. The *color scale* on the *right* indicates the relative levels of beta-keratin in the various morphological regions of hair. In virgin hair, beta-sheet conformation is confined to the cuticle region, with significantly less found in the cortex. This is the natural disposition of the hair fiber. However, after exposure to a thermal styling device, the amount of beta-keratin greatly increases in the cortical region. Image kindly provided by Dr. Guojin Zhang, Ashland, Inc.

providing information about the crystalline phase alpha-keratin and amorphous matrix surrounding the keratin intermediate filaments. DVS of hair provides information about the water management properties of hair. Thermally damaged hair has reduced water regain and overall retention. Pretreating hair with the polyelectrolyte complex prior to thermal exposure led to improvement in both of these parameters. Surface damage to the hair cuticle, as monitored by AFM and SEM, decreased as a result of pretreatment with the polyelectrolyte complex, providing a hair surface with less cracks and other deformities.

In most hair care styling applications, polymeric resins are employed in the form of styling agents, such as hair gels or mousses, or hair fixative agents such as hair sprays. Normally, after application of these materials to hair, they are later removed by shampooing. In some cases, the consumer desires a more semipermanent styling

agent that withstands repeated shampooings. Technologies based on maleic anhydride chemistry were developed as solutions to this consumer-driven durable-styling need [52, 53]. While this invention covers several compositions, its primary commercial application consists of treating frizzy hair with a polymer blend of poly (methyl vinyl ether-maleic acid) and poly(isobutylene-dimethylaminopropyl maleimide-ethoxylated maleimide-maleic acid) in combination with the application of a high-temperature flat iron (ca. 230 °C). As a result, several benefits are delivered to hair including de-frizzing, improved shine, and better fiber alignment, which can withstand up to five wash cycles without reapplication of the polymer blend. While the exact mechanism has yet to be elucidated, evidence suggests that the polymer blend forms a thermoset or may have some reactivity with hair, which could result in cross-linking [50].

8.3 Maleic Anhydride Chemistry in Applications for Skin Care and Transdermal Delivery[1]

Over the last several decades, there have been considerable advances in the use of maleic anhydride chemistry for applications related to the skin. First and foremost, it is an excellent bioadhesive agent. This is important for both the biomedical and personal care industries. It is an imperative component that helps to bind medical devices to the skin, including biosensors, and also serves as an aid in wound healing. In skin care, maleic anhydride polymers are used to remove unwanted debris from facial pores, especially those surrounding the nasal region, and as an aid to help reduce aluminum in antiperspirant formulations. Moreover, polymers based on maleic anhydride are used as transdermal delivery agents in both traditional systems and more innovative designs, such as microneedles. Maleated compounds also play important roles as emollients in skin care formulations and as delivery agents for active ingredients, such as vitamin C. Polymers based on maleic anhydride are used as topical skin-tightening agents and rheology modifiers in various types of cosmetic formulations. Before delving into these exciting topics, we begin this section of the chapter with a thorough review of skin structure and function and follow this with the vast application areas.

8.3.1 Skin Structure and Function

As the largest organ of the body, the skin provides a protective barrier for the body against the external world and also prevents transepidermal water loss (TEWL), permitting an aqueous organism to live in a rather arid environment. In addition,

[1] Portions of this section were previously published in Refs. [54–57].

there are many other functions provided by the skin, which are often overlooked. For example, the skin maintains body temperature through two mechanisms: one in which the body is cooled by the action of sweating, via sweat glands; the other is by the vasoconstriction or vasodilation of the blood vessels in the dermis which either decreases or increases the flow of blood to the dermis from other internal organs. If the internal organs are overheated, vasodilation occurs in the dermis allowing increased blood flow, which in turn releases heat to the environment. Through the combined process of sweating, sebum production, and desquamation, a thin film is present on the surface of skin protecting it from bacterial infections and invasion by foreign substances as well as hydrating and lubricating the surface. Another essential function of the skin is sensation, which is provided by a complex network of nerves located in the dermis and at the base of the epidermis.

Morphologically, the skin is composed of two principal components, the epidermis and dermis, which contain various cell types and structural proteins. The hypodermis—also known as the subcutaneous layer—is often categorized as a third component, located below the dermis. Primarily it is comprised of adipose tissue. The epidermis is a squamous epithelium that contains several appendages: pilosebaceous unit, nail, and sweat gland. The dermis provides the skin with mechanical strength and elasticity, which is brought about by collagen and elastic fibers (e.g., elastin). A diagram of the skin is provided in Fig. 8.13 where the structural components of the dermis and epidermis are shown as well as the various appendages of the skin and its vascular network.

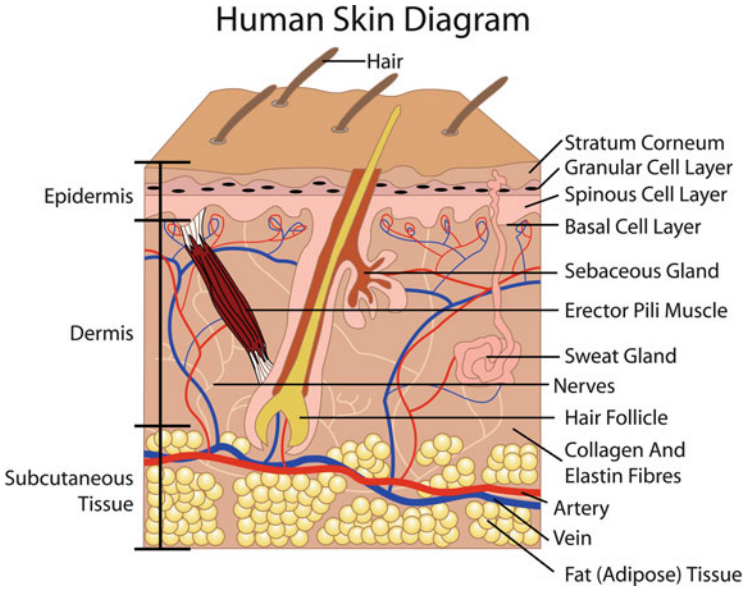

Fig. 8.13 Morphological structure of human skin. Reprinted with permission from R.L. McMullen, Antioxidants and the skin [57]. Copyright, 2013, Allured Business Media

8.3.1.1 Epidermis

This layer of the skin primarily consists of keratinocyte cells, which undergo a process of events leading to terminal differentiation. The keratinocyte begins its journey as a metabolically active cell at the base of the epidermis and eventually makes its way to the outermost layer of the skin where it becomes void of its normal cellular organelles, becomes filled with keratin intermediate filaments (KIF) and matrix proteins, and contains an unusually tough, protein-rich plasma membrane—known as the cell envelope—which is highly cross-linked. Through this process, the keratinocyte drastically changes shape during its voyage from the bottom to the top of the epidermis. Ultimately, a dehydrated morphological component is formed—the stratum corneum—which prevents H_2O loss to the environment and the entry of foreign pathogens into the viable dermis. While keratinocytes make up the majority of epidermal cells, there are also Langerhans cells, melanocytes, and Merkel cells. Langerhans cells carry out an immunological function by seeking out pathogens and presenting them to T cells, ultimately leading to the generation of antibodies. As implied by their name, melanocytes are responsible for the synthesis of melanin, which provides protection for the keratinocytes found in the lower layers of the epidermis. Finally, Merkel cells are a type of nervous system cell found in the lower layers of the epidermis and are responsible for the detection of light touch and allow us to differentiate different textures.

There are several layers of strata within the epidermis, and they are categorized based on the level of differentiation of the keratinocyte cells. Figure 8.14 provides a schematic of the epidermis, which illustrates the different cell types present as well as the histological changes associated with the keratinocyte differentiation. As shown in the figure, the lowermost layer of the epidermis (stratum basale) and the dermis are separated by the dermal-epidermal junction.

As implied by their name, keratinocytes synthesize KIF, which ultimately determine the shape of the cell as it makes its way up the epidermis. At the most fundamental level of KIF structure, two molecules (chains) of alpha-keratin wrap around each other (analagous to a rope) to form a coiled coil. Two coiled coils then associate together to form a protofilament. Two protofilaments pair to form one protofibril. Four protofibrils constitute one intermediate filament. There are about 30 different known members of the keratin family—20 of epithelial origin and 10 from hair. Keratins are classified as type I-acidic (K10–K20) or type II-basic (K1–K9). Coiled coils are formed by the pairing of two alpha-keratins, one from each class.

8.3.1.2 Dermal-Epidermal Junction

This region of the skin, also referred to as the basement membrane zone, provides the connection between the dermis and epidermis. It has an extremely important function, not only to provide a good connection between the two layers of the skin but also because it serves as the link between the vascularized dermis and

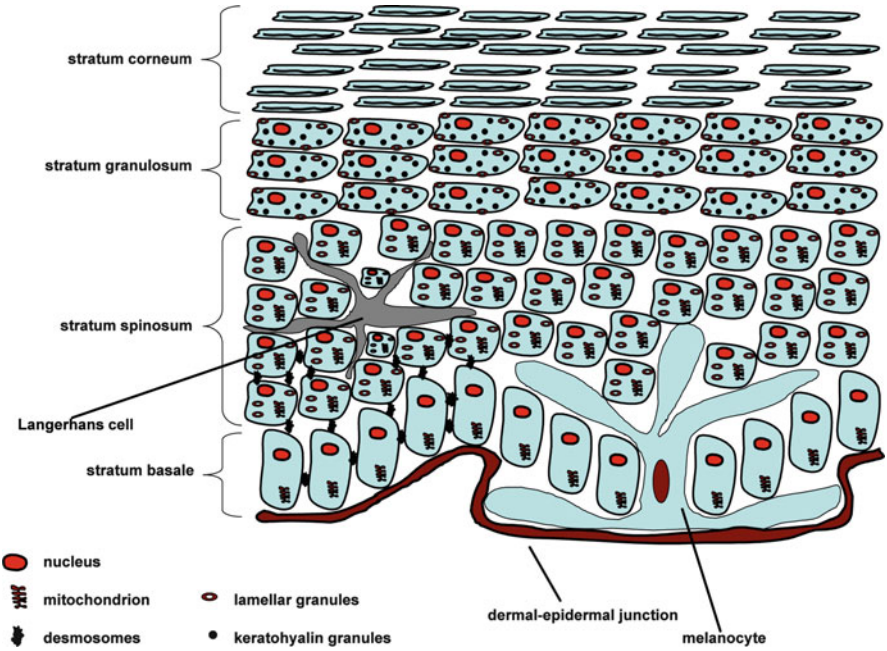

Fig. 8.14 Structure of the epidermis. Reprinted with permission from R.L. McMullen, Antioxidants and the skin [57]. Copyright, 2013, Allured Business Media

nonvascularized epidermis in which nutrients must pass through this junction to arrive at the epidermis. Often, the dermal-epidermal junction is categorized into four distinct layers: the keratinocyte plasma membrane from the stratum basale along with its associated hemidesmosomes, the lamina lucida, the lamina densa, and the sub-lamina densa fibrillar zone. As can be inferred from their names, the lamina lucida is transparent or lucent when viewed through the electron microscope, while the lamina densa is an electron dense layer. Essentially, these two layers represent the constitutive dermal-epidermal junction.

8.3.1.3 Dermis

The dermis of the skin is composed of two distinct regions, namely, the papillary dermis and the reticular dermis, and provides the skin with its structural strength. It primarily consists of connective tissue proteins such as collagen and elastic fibers; however, various other components are found as reported in Fig. 8.15. In addition, the dermis provides residence for the vascular network in which nutrients from the blood supply are fed to the epidermis via the dermal-epidermal junction. A complex nerve network also resides in the dermis and serves various sensory functions such as touch, pressure, heat, and vibration. Moreover, the appendages of the cutaneous

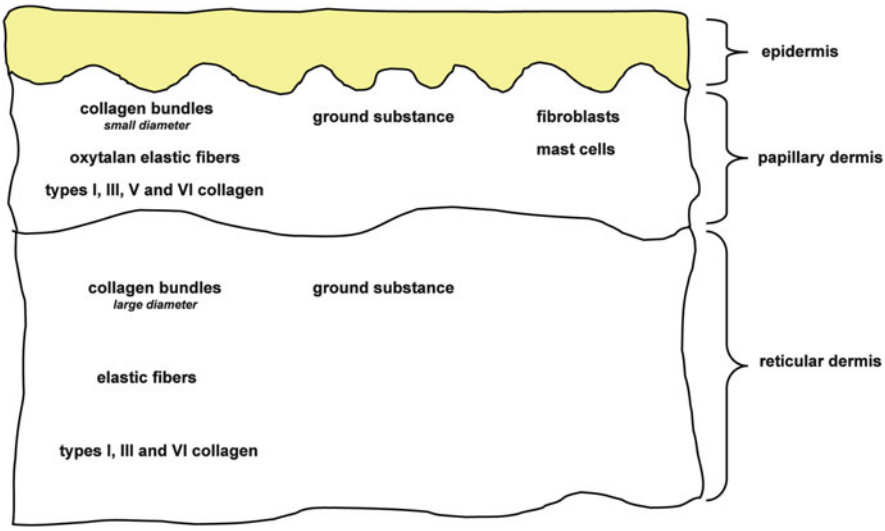

Fig. 8.15 Components of the papillary and reticular dermis. Reprinted with permission from R.L. McMullen, Antioxidants and the skin [57]. Copyright, 2013, Allured Business Media

system inhabit the dermis and consist of the nail, pilosebaceous unit, and sudoriferous glands (eccrine and apocrine sweat glands).

The primary cell types present in the dermis include fibroblasts, mast cells, and tissue macrophages. Fibroblasts are the most abundant cell type and are responsible for the synthesis and structuring of the structural tissue and ground substance. In addition, various cells associated with the immune response are also found in the dermis.

The papillary layer receives its name from the dermal papillae, which are fingerlike projections of the dermis into epidermis (see Fig. 8.13). Such a geometric structure provides increased stability for the binding of the dermis and epidermis as well as an increase in the surface area of the papillary layer which permits greater exchange of nutrients and waste products between the dermis and epidermis. Located just below the dermal-epidermal junction, the papillary layer primarily contains type III collagen, which is arranged into fibrillar bundles. The fibrillar bundles in this layer are smaller than those found in the reticular layer.

The reticular layer of the dermis is bordered above by the papillary layer and below by the hypodermis. Collagen I, which is arranged in large bundles, constitutes the largest population of collagen in this layer. The density of the fibers is much greater in this layer than in the papillary dermis.

Collagen is arranged into fibrils or bundles and the elastic fibers are intertwined within this network. Typically, four different types of collagen are present in the dermis and consists of types I, III, V, and VI, but mostly types I and III. Collagen has a polypeptide sequence that follows the scheme, Gly-X-Y, where X and Y correspond to proline and 4-hydroxyproline, respectively. In terms of secondary structure, collagen contains three alpha chains (not to be confused with alpha helix)

that are supertwisted (protein tertiary structure) together to provide its fibril structure.

The elastic fibers can be categorized into a fibrillar component (fibrillin) as well as an amorphous component (elastin). Elastic fibers are further classified as (1) oxytalan fibers, fibers that are lightly coated with elastin, and (2) elaunin fibers, fibers more heavily coated with elastin.

8.3.1.4 Cutaneous Appendages

Additional components of the gross anatomical structure of the skin consist of the cutaneous appendages: eccrine/apocrine glands, pilosebaceous unit, and nail unit. The sudoriferous glands (eccrine and apocrine) aid in controlling body temperature as well as play a possible role in pheromone signaling. The pilosebaceous unit is comprised of the hair follicle and sebaceous gland, which lubricates the mature hair shaft with sebum and antioxidants, bringing them to the surface of the skin where they can provide protection. Apocrine glands are also associated with the pilosebaceous unit. Their secretions, mostly composed of lipids and proteins, are also brought to the skin surface by the growing hair fiber.

8.3.2 Bioadhesives

The area of adhesives is a very broad field that has applications in many industrial fields. In relation to skin care, adhesives are especially important in the medical device industry. Maleic anhydride polymers are used as bioadhesive agents in many applications including pressure-sensitive tapes and tapes designed for surgical purposes, dermatological tape strips to remove keratotic material from the skin, and wound healing.

Usually, adhesives are categorized as inorganic or organic. Inorganic adhesives are either silicon- (e.g., water glass) or calcium-based (e.g., cement or plaster). These adhesives, of course, are not used in applications related to the skin. On the other hand, organic adhesives, which make the vast majority of adhesives, consist of heat-curing resins, thermoplastic resins, and rubber/elastomer materials. Furthermore, adhesives can be classified by their curing process. Several examples are volatile solvent (curing occurs due to vaporization of organic solvents: polyvinyl acetate or nitrile rubber), moisture curing (curing occurs due to reaction with moisture in the air: cyanoacrylate and silicon rubber), heat curing (curing is attained when a hardener in the resin is activated and cured by heat: epoxy and acrylic resin), UV curing (curing occurs due to activation when exposed to UV light: epoxy and acrylic resins), and, finally, *pressure sensitive* (curing is achieved by applying pressure: acrylic and maleic anhydride-based resins).

Equally important is the manner in which an adhesive bonds to a substrate. Bonding can be chemical (chemical reaction between the adhesive and adherend),

adsorption based (hydrogen bonding occurs between the adhesive and adherend), electrostatic (the opposite charges of the adhesive and adherend cause them to bind together), anchoring effect (the adhesive seeps into grooves and asperities of the adhesive and adherend), and mutual diffusion (the adhesive dissolves the surfaces of the adhesive and adherend and forms a strong junction at the interface of the three components).

Pressure-sensitive adhesives are the most common type of adhesive utilized for application to the skin. They adhere to the surface of the skin by simply applying pressure to the tape while on top of the skin. Tape may contain several components, principally the adhesive resin, a tack agent, pigment, plasticizer, and antioxidant. Usually, these elements are incorporated on top of a backing material made of paper, plastic, or cloth. The plasticizer provides flexibility to the adhesive resin while antioxidants prevent accelerated aging due to exposure to solar radiation, heat, etc.

As already mentioned, maleic anhydride-based polymers are frequently used as bioadhesives for the skin. Early work in this area demonstrated the utility of these materials in pressure-sensitive medical and surgical tapes [58–59]. In general, these materials were based on copolymers of maleic acid and vinyl ether. In particular, several advantages exist to using these resins. Notably, there is no need to employ additional tack agents as the maleic acid-vinyl ether resin itself has a considerable degree of stickiness. Further, such resins bind to a greater degree with substrates than they do to themselves. Throughout the 1970s and 1980s, there was less activity in the patent arena in relation to the use of maleic anhydride-based polymers in adhesives [60]. Regardless, these materials remained in use with some improvements in their formulation and application [61]. Cross-linking of poly(maleic acid-alkyl vinyl ether) resulting in a cross-linked polymeric ester or amide/imide produces a hydrogel with desirable rheological behavior while maintaining bioadhesion to the skin [62]. In addition, maleic acid-based polymers have found utility in ostomy appliances where they serve as an adhesive holding together a medical device and the skin at the point of a stoma—an opening or orifice surgically created to provide a pathway from an internal organ to the surface of the body. While these polymers have enjoyed success in this area, there have been several accounts reporting peristomal allergic contact dermatitis in regions surrounding the stoma [63, 64].

Silicone polymers such as polydimethylsiloxane are also frequently used in the medical device industry as pressure-sensitive adhesives for transdermal delivery, wound dressings, and other biomedical applications. One of the challenges with silicones is the need to improve their adhesion, especially in moist environments. Hydrocolloids can be used to absorb moisture; however, they often comprise the dry peel strength of the adhesive. To circumvent such issues, poly(ethylene glycol) can be grafted to poly(dimethylsiloxane), yielding an amphiphilic polymer that when blended with poly(maleic acid-vinyl ether) provides desirable adhesion properties [65].

8.3.3 Biosensors

In the 1990s, there was considerable excitement in the maleic anhydride community about the use of poly(methyl vinyl ether-maleic anhydride) derivatives in biomedical sensor applications [66–68]. Ag/AgCl inks are used as biosensors for biomedical monitoring, medical diagnostics, and iontophoretic drug delivery. Typically, the inks are printed onto a substrate, which then serves as the biosensor. Bioadhesive polymeric hydrogels provide a very good flexible means for attaching the biosensor to the skin. In addition, the hydrogel can be made conductive by adding electrolyte. In a typical formulation, one could include the bioadhesive component poly(methyl vinyl ether-maleic acid), plasticizer (glycerine), viscosity builder (poly(vinyl pyrrolidone)), and electrolyte (sodium chloride) [68]. A key advantage of the maleic anhydride chemistry for this application lies not only in its bioadhesive properties but also its activation by water in moist environments. This allows the adhesive to remain efficacious even during perspiration and in moist or damp environments. It should be noted that over-wetting the adhesive polymer results in a slimy residue that is difficult to dry.

8.3.4 Wound Healing

In addition to their use as adhesives in medical devices, maleic anhydride-based polymers are also employed in other wound healing applications. Nitric oxide is a known agent that is used topically to promote healing of chronic wounds, such as diabetic ulcers [69]. It functions by regulating collagen formation, cell proliferation, and wound contraction [70]. Unfortunately, the short half-life of nitric oxide and its associated instability have hampered its success in finished pharmaceutical products. To circumvent this problem, a group at the University of Toronto designed a supramacromolecular complex capable of controlled delivery of nitric oxide to wound areas of the skin. The general structure of the complex is provided in Scheme 8.2. As shown in the illustration, poly(methyl vinyl ether-maleic anhydride) is reacted with S-nitrosoglutathione, which becomes esterified to one of the acid groups. S-nitrosoglutathione contains the functionality of the antioxidant, glutathione, and contains nitric oxide embedded in the structure, which is released to the tissue.

Also shown in the scheme is the complexation of poly(vinylpyrrolidone), which associates with poly(methyl vinyl ether-maleic acid) via hydrogen bonds. Overall, the complexation of the two polymers and the esterification with S-nitrosoglutathione result in a functional controlled release vehicle for nitric oxide. The addition of poly(vinylpyrrolidone) to the supramolecular complex causes an increase in the hydrophilicity of the complex, which is accompanied by a decrease in the dissociation rate of nitric oxide due to its delayed release in aqueous mediums. Therefore, it is not surprising that the controlled release of nitric oxide depends on the concentration ratio of poly(vinylpyrrolidone) to poly(methyl

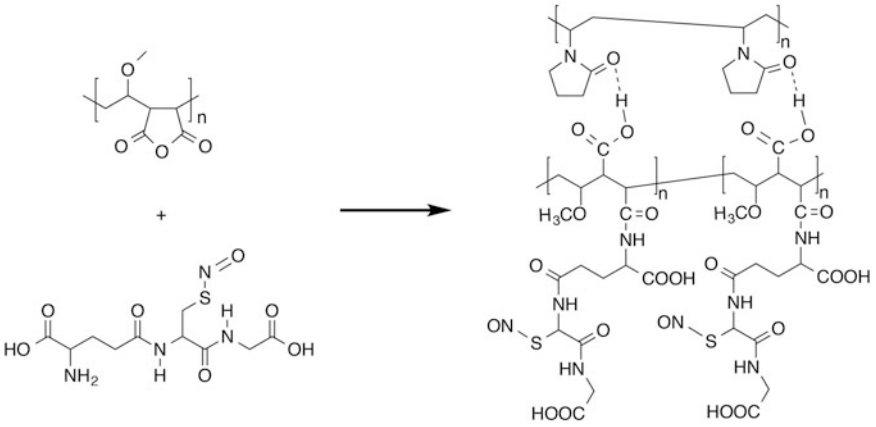

Scheme 8.2 Reaction scheme of nitrosoglutathione with poly(methyl vinyl ether-maleic anhydride). The resulting molecule may complex with poly(vinyl pyrrolidone) by a hydrogen-bonding mechanism

vinyl ether-maleic acid), which is optimal at a one-to-one ratio. The kinetic release profiles also depend on the molecular weight of both poly(maleic acid-methyl vinyl ether) and poly(vinylpyrrolidone). Not surprisingly, higher molecular weight species produce slower nitric oxide release profiles. In this case, higher molecular weight polymers will yield a more structurally extensive complex that undergoes slower dissolution [71].

Disinfection is extremely important during surgical procedures. As a preparatory step, the area of the skin where the incision is to be administered as well as the surrounding regions is treated with an antibacterial agent. Unfortunately this preparatory procedure is not sufficient to completely sterilize the site or to immobilize unwanted bacteria from migrating into the incision. In many instances, an additional step is added to the preparatory procedure that consists of treating the site with incise drapes, which are large sheets of adhesive film. The incise drapes are applied to the site prior to surgery and incisions are made directly through the drapes. Skin sealants are also used for this purpose and essentially are thin-film skin protectants. Due to its exceptional bioadhesivity, poly(vinyl ether-maleic acid) is included in skin sealant formulations. Typically, the sealant components consist of a suitable bioadhesive polymer and antibacterial agent that are soluble in ethanol and form a water-insoluble film designed to immobilize bacteria and prevent infection to the site of incision [72, 73].

8.3.5 Keratotic Plug Removal

Over the last decade, increasing attention has been given to the topic of skin pores—also often referred to as facial pores. In this case, the term “pore” evolved

from the lay population to describe an opening in the skin associated with a pilosebaceous unit, which consists of the sebaceous gland and hair follicle. These "pores" are clearly evident to the human eye and are especially visible in certain anatomical regions of the body, such as the face where they often present themselves in areas adjacent to the nasal region. Such pores are generally associated with excessive sebum production [74]. Comedones may be formed when there is an excess of sebum and keratinocyte cell debris (keratotic plugs). In layman's terms, comedones refer to black heads (open pore) or white heads (closed pore). The dark color of the black heads originates from oxidation of the cell debris and sebum. There has been much effort in the personal care industry to design products to help remove black heads. These products are essentially shaped like a Band-Aid strip and are adhered to the nasal region of the face (see Fig. 8.16). After a certain period of time, the tape strip is removed from the skin and it brings with it all of the gunky dark material from the pore. Looking at the underside of the nose strip, one normally observes something analogous to a range of mountain peaks corresponding to all of the debris collected from the pore. Commercial products based on this technology, were designed based on a high molecular weight (1,500,000 Da) analog of poly(methyl vinyl ether-maleic acid), which serves as the bioadhesive in the nose strip. The nose strip is constructed of a flexible nonocclusive substrate sheet that is impregnated with the bioadhesive [75–77]. Prior to application, the nose strip is immersed in water and placed in the region of interest. After it dries, the nose strip is then removed from the skin site bringing with it unwanted black head debris.

Fig. 8.16 Photograph demonstrating the use of adhesive strips for keratotic plug removal in the skin

8.3.6 Antiperspirant Technology

In *Homo sapiens* the principal mode of thermoregulation is accomplished by evaporative cooling that takes place when sweat is secreted from eccrine glands and evaporated from the surface of the skin. Overall, such a process ensures that the body's core temperature does not significantly rise above 37 °C to levels that can lead to heat exhaustion or hyperthermia. There are about two to five million eccrine glands distributed over the surface of the body that carry out this function. In addition, there are approximately 100,000 apocrine glands localized in specific regions of the body, most notably the axillae (underarm region). Although apocrine glands secrete substances that eventually break down to malodorous compounds, antiperspirant treatments target eccrine glands that are located in the axillae.

For many years, the mechanisms by which antiperspirant salts prevent sweating mystified scientists. There are a number of different strategies to intervene with sweat production. For example, one could impair the neuroglandular junctions using an anticholinergic compound that prevents acetylcholine from reaching the gland [78]. Researchers utilized botulin toxin specifically for this purpose in patients suffering from hyperhidrosis [79]. Another strategy would be to prevent the secretory coil (secretory cells) from mobilizing sweat and/or ions. More than likely, this would require targeting enzymes, such as Na/K-ATPase, or other membrane channels that couple the funneling of ions to the lumen with sweat flow. Antiperspirant treatments could also damage part of the eccrine gland (or possibly apocrine gland), such as the duct, resulting in escape of sweat from the gland unit before it has a chance to reach the surface. This mechanism, originally proposed by Papa and Kligman as the "leaky hose" model, results in the loss of sweat through orifices in the duct allowing it to be reabsorbed in the extracellular space of viable skin [80]. The most common mechanism for sweat prevention occurs due to the formation of a plug in the lumen of the sweat gland duct [78]. In the paragraphs that follow, we discuss the complexities surrounding the issue of plug formation.

Historically, the most frequently employed antiperspirant salts were aluminum chloride ($AlCl_3$), aluminum chlorohydrate (ACH), and aluminum zirconium chlorohydrate complex (AZAP). For this reason, most of our understanding of plug formation comes from studies conducted with these materials. Studies conducted in the 1950s by Shelley and coworkers were among the first to attempt to address the question of plug formation in the eccrine sweat gland duct and introduced the possibility of a biochemical event associated with the plug [81–83]. The authors were studying several forms of miliaria—a disease of the skin resulting from malfunctioning or underdeveloped sweat glands. Shelley and coworkers examined the effects of various treatments of the skin (one being $AlCl_3$). Based on histological studies, they proposed that $AlCl_3$, and the other damaging treatments, produced a hyperkeratotic plug in the lumen of the duct—a form of abnormal keratinization.

For more than 30 years after the initial studies by Shelley and Horvath, a wave of studies cast more light on the unanswered inquiries concerning the mechanism of antiperspirant action. Reller and Luedders are credited as the first to propose that aluminum salts form polymeric hydroxide gels at/below physiological pH, which results in a plug that prevents the flow of sweat to the surface (see Fig. 8.17). It has become known as the "emphraxis" theory [84]. Subsequent work suggests the involvement of plug formation with biochemical events leading to a plug containing both topically applied antiperspirant salt and tissue. One explanation suggests that the eccrine acrosyringium is damaged as a result of complexation between mucopolysaccharides of luminal cells and aluminum [85]. It was later suggested that the secretory portion of the eccrine gland also experienced damage from long-term treatment with $AlCl_3$ [86]. Damage and eventual atrophy of eccrine acini—groups of cells responsible for secretion in the coil—were just one of the clinical manifestations found in their study. Corresponding apocrine glands, on the other hand, appeared normal.

Researchers at Gillette made significant findings demonstrating the location of plug formation in the eccrine gland dependant on the type of aluminum salt employed [78, 87, 88]. For example, $AlCl_3$ was found to form the deepest plugs of the three salts tested, sometimes as far down as the dermal duct. In contrast, treatment with ACH and AZAP, which are far less irritating, results in plugs mostly in the stratum corneum region of the duct [89]. Still, many questions remain as to

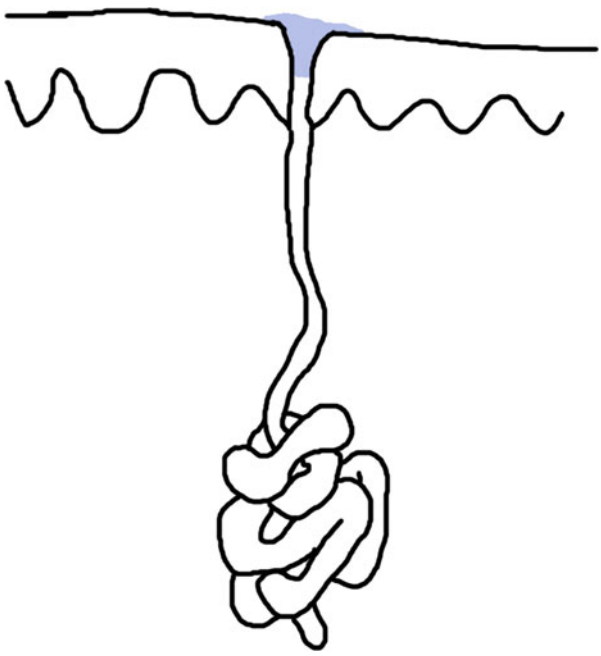

Fig. 8.17 Illustration of an antiperspirant forming a plug (*blue*) in the eccrine gland duct

the nature of the plug. However, we now have a better understanding of the molecular composition, thanks to an infrared study, which confirmed that keratin bound to aluminum is part of the plug [90]. Although it is postulated that luminal cells desquamate, the authors point out that a plug bound to the ductal walls would offer more resistance to the hydraulic pressure exerted by the gland. Another important finding of the infrared spectroscopy study by Strassburger and Coble is that the plug did not contain sweat proteins.

The activity of antiperspirant salts can be affected by various factors [91]. For example, antiperspirant efficacy is enhanced if the treatment is administered at night when the glands are dormant [83]. Also, occlusion during treatment is more efficacious than treatment administered in open air. Treatment carried out before, during, or after sweating yields a variety of results depending on the sweat state of the subject. It is difficult to plug the glands when they are firing. Also, sweat presumably changes the solubility of the antiperspirant formula. The effects of lipids (sebum) on antiperspirant effectiveness yield conflicting results. Some studies demonstrate no difference in antiperspirant efficacy after delipidation [91], while others show enhanced activity [92, 93]. It is likely that irritation is a major factor. Likewise, surfactants were found not to influence sweating behavior; however, surfactant treatment may cause effects if used at concentrations that are irritating to the skin [91]. Studies by Hölzle and Kligman also demonstrate that massaging increases antiperspirant efficacy. Such a treatment protocol could have applications in the mode of antiperspirant application, for example, spray versus roll-on versus stick.

Due to the negative publicity of aluminum-based compounds in consumer products and its association with Alzheimer's disease and breast cancer, considerable efforts have been made to minimize its use in antiperspirant formulations [94–98]. Such compositions can be achieved by supplementing the antiperspirant formulation with polymers that act as co-gellants with the aluminum salts thereby allowing lower levels of the aluminum salt to be employed.

Initial work in this area focused on maintaining the antiperspirant aluminum salt and poly(vinyl ether-maleic acid) in two separate phases in the formulation [94]. Upon application of the antiperspirant to the skin, the formulation mixes allowing the polymer and aluminum salt to interact, resulting in gelation of the ingredients. The mixture fills the sweat pores, which eventually clog, preventing the passage of sweat.

The ability of maleic anhydride in its acid form to complex with Lewis acids, such as aluminum chloride, is well known [99]. While not explained very well in the literature with specific reference to antiperspirant salts, the aluminum/zirconium salts are also believed to complex with the diacid groups of poly(methyl vinyl ether-maleic acid). More than likely, positive charges from the aluminum or zirconium ions are attracted to the negative charge of the deprotonated acid groups of poly(methyl vinyl ether-maleic acid). As already mentioned, this permits the formulator to reduce the amount of aluminum salt in the formulation, which can often reach as high as 10–20 % (w/w).

Another approach to maintaining the antiperspirant salt and the maleic anhydride polymer separate prior to application would be to utilize a water-in-oil emulsion system in which the antiperspirant salt along with an emulsifier would be present in the continuous oil phase and the polymer in the dispersed water phase [96]. Other types of suspension systems could also be employed [95]. Similar to the polyelectrolyte complex already discussed in relation to hair in the preceding section, such compositions are also used in antiperspirant technology [97]. Polyelectrolyte complexes formed between poly(methyl vinyl ether-maleic acid) and poly(vinyl pyrrolidone-methacrylamidopropyl trimethylammonium chloride) exist in the form of microgels and may be utilized in various antiperspirant vehicles, including sticks, aerosols, and roll-ons. A key advantage of the polyelectrolyte system is its low viscosity, allowing it to be used in various product vehicles and its ability to form clear antiperspirant films, which is more aesthetically pleasing to consumers. Furthermore, concentrations as low as 1 % (w/w) of antiperspirant salts can be employed in combination with maleic anhydride-based polyelectrolyte complexes providing the same efficacy as antiperspirant formulations containing 10 % (w/w) of antiperspirant salts.

8.3.7 Transdermal Drug Delivery

There is continued interest in the medical community to develop transdermal delivery vehicles for the administration of medicine. This is a huge area of growth in the pharmaceutical arena. Transdermal delivery offers several advantages to oral delivery and hypodermic injections including bypassing the liver, which can sometimes prematurely metabolize drugs; providing an alternative to hypodermic injections, which are uncomfortable and have the normal risks associated with needle use; and providing very good controlled release systems, which can last on the order of days [100]. One of the challenges with transdermal drug delivery is crossing the stratum corneum barrier, which is extremely efficient at keeping foreign substances from compromising the skin and gaining access to the viable epidermis. First-generation transdermal delivery systems focus on the delivery of small lipophilic molecules to the skin utilizing a patch. Second-generation systems consist of chemical penetration enhancers, non-cavitational ultrasound, and iontophoresis. Third-generation delivery systems are based on microneedles, thermal ablation, microdermabrasion, electroporation, and cavitational ultrasound [100]. While most of the techniques in this third group are still in development, microneedles and thermal ablation offer the most clinically promising prospects.

8.3.7.1 Transdermal Patch Applications

Maleic anhydride copolymers have been incorporated into the most basic transdermal delivery vehicle known as the patch. The essential components of the

bioadhesive patch consist of a bioadhesive polymer in combination with a backing material (e.g., nylon), plasticizer, and pharmaceutical active ingredient to be delivered to the skin. The plasticizer is a key component of this formulation. In the case of poly(methyl vinyl ether-maleic anhydride), the T_g of the dry powder is 151 °C, while in the free acid form (i.e., when the polymer is dissolved in H_2O), the T_g drops to 141 °C due to increased flexibility of the free acid structure [101]. Regardless, films cast from poly(methyl vinyl ether-maleic acid) solution are brittle and not suitable for transdermal delivery applications on their own. Thus, a suitable plasticizer must be employed. Researchers at Queen's University Belfast conducted a great deal of research in this area over a period of a decade. Initial research investigated the use of glycerol as a plasticizing agent. Unfortunately, supporting evidence suggested that glycerol was cross-linking with poly(methyl vinyl ether-maleic acid) [102]. Figure 8.18 provides the structures of five different oligomers, which are likely to form as the result of a condensation reaction between glycerol

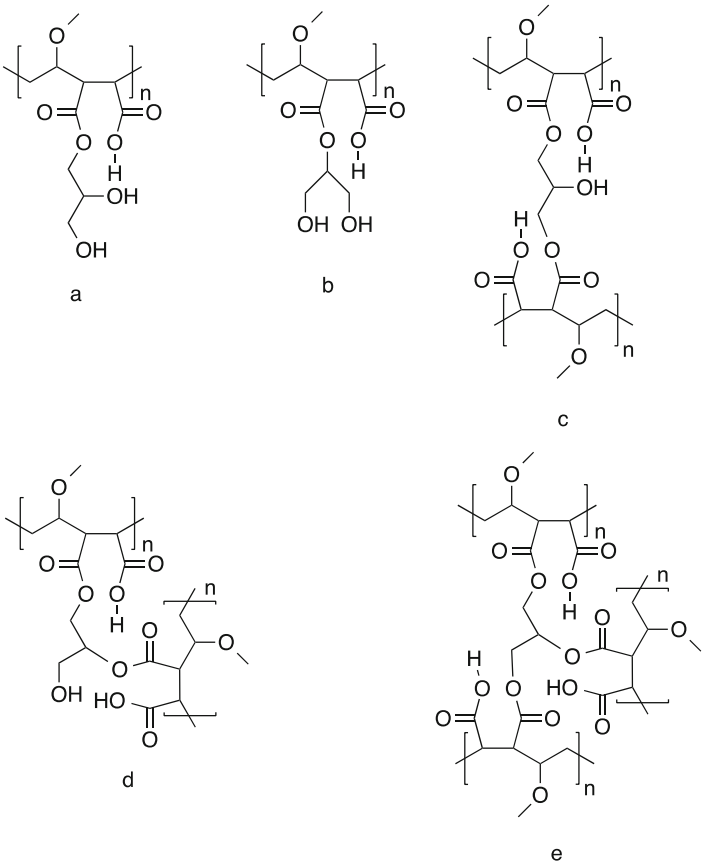

Fig. 8.18 Oligomeric structures formed as the result of cross-linking between glycerol and poly (methyl vinyl ether-maleic acid)

and poly(methyl vinyl ether-maleic acid). In certain cases, cross-linking could produce adverse effects such as decreasing the degree of flexibility of the polymer and reducing its capacity to make intimate contact with the skin surface. Furthermore, in many cases uncontrolled cross-linking could affect the bioadhesive properties of the resin. In any event, attempts to use glycerol as a plasticizer were abandoned due to its high reactivity with the polymer. Other attempts to find a suitable plasticizing agent focused on the use of tripropylene glycol methyl ether, an innocuous compound that only contains one hydroxyl group and no carboxylic acid moieties. Therefore, one would not expect any cross-linking to occur with poly (methyl vinyl ether-maleic acid). There was much promise in the use of tripropylene glycol methyl ether as a plasticizing agent in bioadhesive patch formulations containing poly(methyl vinyl ether-maleic acid). Unfortunately, it is not commercially available in pharmaceutical grade and, therefore, is not suitable for use in transdermal delivery applications. This is unfortunate as the Belfast researchers even completed clinical trials demonstrating the efficacy of this patch formulation [103–105].

Further attempts to plasticize poly(methyl vinyl ether-maleic acid) focused on combining it with poly(ethylene glycol) to obtain bioadhesive films with desirable physicochemical properties [106–111]. In initial studies, researchers investigated the influence of poly(ethylene glycol) molecular weight (200, 1000, and 10,000 Da) on the properties of the films. The structural integrity of the films was determined by mechanical analysis (e.g., tensile strength, elongation at break, Young's modulus, and the work of failure), and the degree of plasticization was monitored by measuring the glass transition temperature with dynamic scanning calorimetry [106]. Not surprisingly, tensile strength, Young's modulus, and work of failure decrease when higher concentrations of poly(methyl vinyl ether-maleic acid) or poly(ethylene glycol) are used in the formula and also when lower molecular weight (200 Da) poly(ethylene glycol) is employed. On the other hand, the elongation at break increases at higher concentrations of poly(methyl vinyl ether-maleic acid) or poly (ethylene glycol) and at lower molecular weights of poly(ethylene glycol). Furthermore, based on T_g data from differential scanning calorimetry, a molecular weight of 200 Da was found to be the most efficient plasticizer of the blended system, as compared to 1000 and 10,000 Da. Also, increasing the concentration of poly(ethylene glycol) results in a greater degree of plasticity of the films. Clearly, polyols such as poly(ethylene glycol) are hydrophilic and cause ambient H_2O to diffuse into the polymer structure. It is also very likely that poly(ethylene glycol) disrupts stabilizing hydrogen bonds found in poly(methyl vinyl ether-maleic acid) (see Fig. 8.19). In any event, plasticization and the increase in flexibility of poly(methyl vinyl ether-maleic acid) occur due to the interpolation of poly(ethylene glycol) and H_2O into the polymer structure and the resulting disruption of intermolecular forces. More than likely, lower molecular poly(ethylene glycol) provides a more plasticized system due to its greater mobility than higher molecular weight variants leading to its ability to diffuse more into the polymer structure. Such an effect can be explained by the small molecular volume of the lower molecular weight species accompanied by a greater number of hydroxyl groups per unit mass [106]. In addition, increases in the

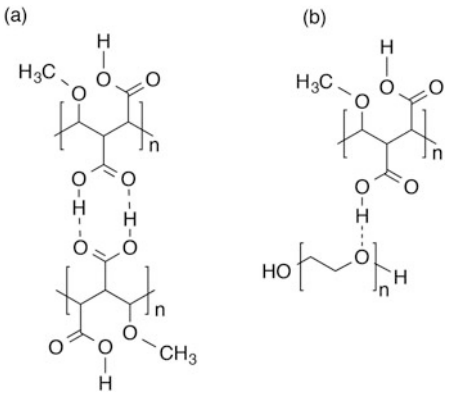

Fig. 8.19 (**a**) Hydrogen bonding of poly(methyl vinyl ether-maleic acid) with itself. (**b**) Hydrogen bonding between poly(methyl vinyl ether-maleic acid) and poly(ethylene glycol)

flexibility of poly(methyl vinyl ether-maleic acid) at increasing concentrations may be explained as a self-plasticizing effect, which is commonly observed in polymers.

After much work in investigating the properties of blends of poly(methyl vinyl ether-maleic acid) and poly(ethylene oxide), considerable evidence (thermal analysis, attenuated total reflectance-FTIR, swelling studies, and scanning electron microscopy) surfaced demonstrating that these polymers cross-link under the employed mixing conditions, which were carried out at slightly elevated temperatures, ultimately forming a hydrogel system [107]. For illustration, Fig. 8.20 contains an SEM micrograph of a hydrogel containing a 2:1 ratio of poly(methyl vinyl ether-maleic acid) to poly(ethylene glycol). The porous nature of the hydrogel is clearly evident in the image.

The same molecular weight samples of poly(ethylene glycol) already described were further investigated to determine the cross-link density imparted to the finished hydrogel. The lowest molecular weight poly(ethylene glycol) (200 Da) yielded the most highly cross-linked hydrogel network. Again, such a result is not surprising, as lower molecular weight compounds will have greater access to the interior structure of poly(methyl vinyl ether-maleic acid), or any polymer for that matter. In any event, a cross-linked hydrogel system works extremely well for transdermal delivery applications. Hydrogels are insoluble and can absorb significant amounts of H_2O without dissolving. At the same time, they serve as good vehicles for pharmaceutical active ingredients and can precisely control its diffusion or permeation into the desired tissue. The diffusion coefficient of the drug depends on a number of factors including hydrogel structure and pore size, water content, molecular weight of the polymer, and degree of ionization [108]. It also depends on the dimensions of the pharmaceutical active. In some instances, one may wish to deliver a larger molecule, such as a peptide or protein. If the inherent pore size of the hydrogel is too small, this will influence the diffusion rate of the

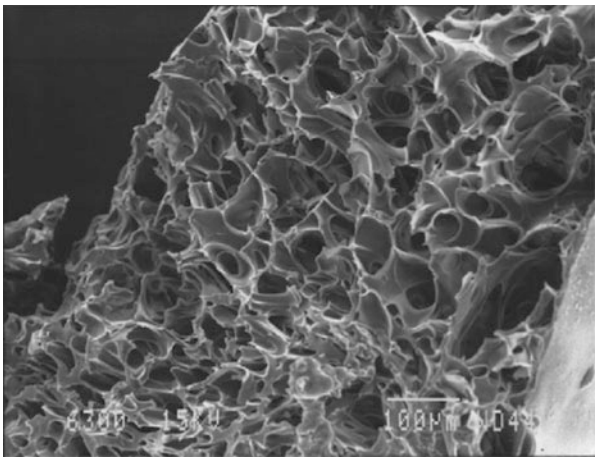

Fig. 8.20 SEM micrograph of a hydrogel containing a 2:1 ratio poly(methyl vinyl ether-maleic acid) to poly(ethylene glycol). Originally published in T.R.R. Singh et al., *Eur Polym J* **2009,** *45*, 1239-1249 [107]. Reprinted with permission from the Royal Pharmaceutical Society of Great Britain, copyright 2010

pharmaceutical active to be delivered. The pore size of the hydrogel can be increased by adding a pore-forming agent. In fact, Donnelly and coworkers used sodium bicarbonate in hydrogels made of poly(methyl vinyl ether-maleic acid) and poly(ethylene glycol) to create large pores in the structure [110]. Increasing the pore size results in higher equilibrium water content and average molecular weight between cross-links. The overall expectation for this type of hydrogel modification is increased permeation of the solute into the skin. Other studies with similar hydrogel systems (without pore-forming agents) demonstrated increased permeability of the drug when the ionic conductivity of the hydrogel is increased by applying an external current [109].

8.3.7.2 Microneedles

The use of microneedles to painlessly bypass the stratum corneum is also a viable route for transdermal drug delivery [112–116]. There are several methods of microneedle administration, which are summarized in Fig. 8.21. A complete description of the various types of microneedle systems is provided in the figure caption. Briefly, these consist of (a) a solid microneedle system that punctures the skin and is followed by treatment with a traditional transdermal patch; (b) a solid microneedle system coated with the drug, which upon penetration the drug dissolves; (c) a soluble microneedle system containing the drug in which both the drug and the microneedles dissolve upon introduction into the skin; and (d) a hollow microneedle system in which the drug is discharged and the microneedles are withdrawn. Historically, microneedles were constructed of silicon-type materials,

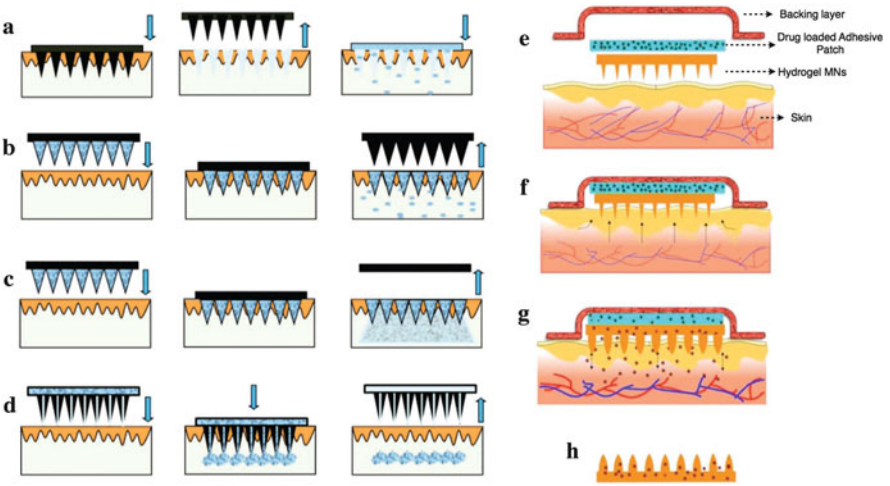

Fig. 8.21 Various methods of microneedle application to the skin during transdermal drug delivery. (**a**) Solid microneedles are used to puncture the skin, which is followed by a second step in which a traditional transdermal patch is used. (**b**) Solid microneedles coated with the drug. The microneedles are removed after the drug dissolves in the skin's interstitial fluid. (**c**) Microneedles fabricated with a soluble polymer/carbohydrate carrying the drug is applied to the skin until the drug and microneedles dissolve in the skin. (**d**) Hollow microneedles containing the drug inside puncture the skin and then discharge the drug. (**e**–**h**) A delivery system based on a backing layer, drug-loaded adhesive patch, and hydrogel microneedle system. (**f**) The hydrogel microneedle-adhesive patch system is in contact with the skin. (**g**) Water diffuses from the skin into hydrogel microneedles, causing them to swell, and then further into the adhesive patch. (**h**) As a result, drug molecules are liberated from the patch and migrate through the hydrogel and into the skin. Originally published in R.F. Donnelly et al., *Adv Funct Mater* **2012**, *22*, 4979-4890 [117]. Reprinted with permission from WILEY-VCH Verlag GmbH & Co. KGaA, Weinheim, copyright (2012)

which could cause issues due to lack of biocompatibility. A modern approach to this problem is to fabricate microneedles with hydrogels [118]. Blends of poly(methyl vinyl ether-maleic acid) ($M_w = 1{,}080{,}000$ Da) and poly(ethylene glycol) ($M_w = 200$; 1000; and 10,000 Da) have been used at concentrations of 15 % (w/w) and 7.5 % (w/w), respectively, together and then cross-linked to form a suitable hydrogel [117]. The utility of a hydrogel system for a particular application depends on its swelling and diffusional properties, which in turn is primarily dependent on its cross-linking density [119].

8.3.7.3 Nanoparticle Technology

Over the last two decades, there have been tremendous efforts to develop polymeric nanoparticles as controlled release agents for pharmaceutical actives. They offer a variety of benefits as delivery agents including high loading efficiency of the drug, ability to target specific organs or tumors, and delivery of proteins, DNA, and other

biomolecules to key tissue sites [120]. Polymeric nanoparticles are generally 10–1000 nm in diameter and delivered via the oral administration route [121]. In recent years there has been increasing interest in developing polymeric nanoparticles as transdermal delivery agents for both pharmaceuticals and cosmetics [122]. With respect to maleic anhydride chemistry, there has been considerable interest in fabricating polymeric nanoparticles for the oral delivery route [123–126]. The general principle behind controlled release when drugs are orally administered is that the polymeric nanoparticles bind to key surfaces in the gastrointestinal tract (e.g., the interior of the stomach or intestinal region) providing the pharmaceutical active with a desired pharmacokinetic release profile over an extended period of time. Since maleic anhydride chemistry is very biocompatible with the skin, it is not surprising that efforts have also been made to utilize maleic anhydride-based nanoparticles as transdermal delivery agents [127, 128].

Cyanoacrylates are a family of adhesive molecules that are used for various applications. The most commonly known products that contain cyanoacrylates are Krazy Glue and Super Glue, two household adhesives with incredible strength. Interestingly, copolymers of polyethylene glycol-modified maleic anhydride and ethyl cyanoacrylate have been used in the fabrication of polymeric nanoparticles designed for transdermal drug delivery [127]. Figure 8.22 contains the structure for poly{[α-maleic acid-ω-methoxy-poly(ethylene glycol)]-*co*-(ethyl cyanoacrylate)} [129, 130].

As already mentioned, the key to any successful controlled release agent is that it releases the drug at a controlled rate. Normally, permeation studies of drugs through the skin are carried out with a Franz diffusion chamber (Fig. 8.23). Ex vivo animal skin (e.g., porcine or rat skin) is placed in the upper portion of the diffusion cell, and the formula or delivery vehicle is placed on top of the skin. As the pharmaceutical or cosmetic active penetrates through the skin, it arrives to the other side (dermis side) and is dissolved in the receptor solution. Then, the amount of drug that has traversed the skin barrier is determined by taking UV/visible spectra (assuming the drug absorbs UV or visible light) at selected time intervals.

Figure 8.24 provides a plot of the cumulative amount of the pharmaceutical agent, D,L-tetrahydropalmatine, that has crossed the skin barrier after treatment with

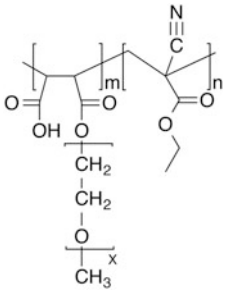

Fig. 8.22 Molecular structure for poly{[α-maleic acid-ω-methoxy-poly(ethylene glycol)]-*co*-(ethyl cyanoacrylate)} used to fabricate polymeric nanoparticles

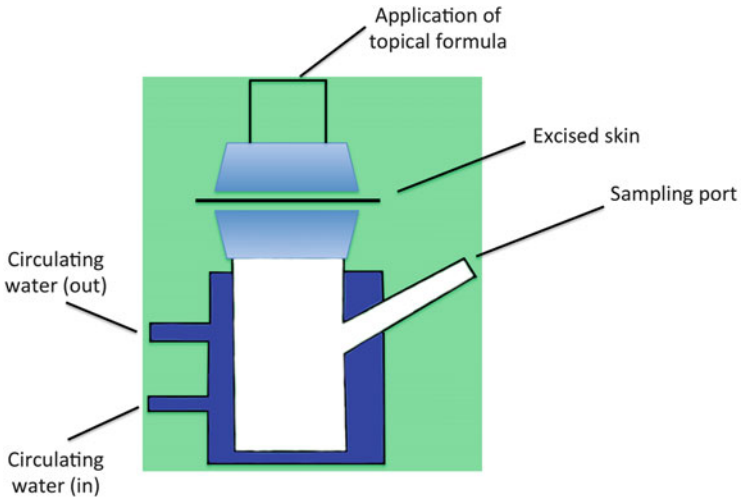

Fig. 8.23 Franz diffusion cell apparatus used for determining the permeation of ingredients through ex vivo skin. Adapted from Kim et al. [131]

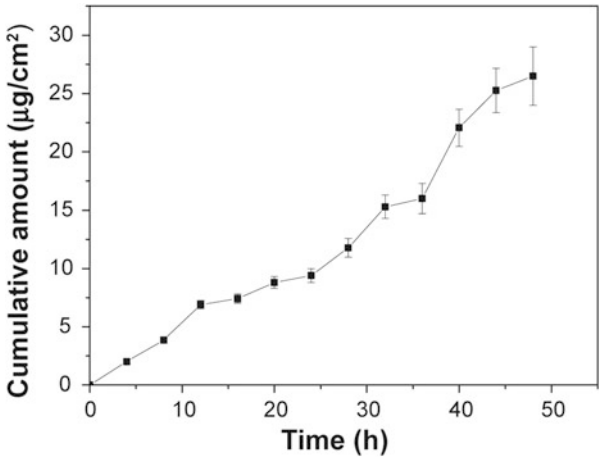

Fig. 8.24 Typical data obtained from the Franz diffusion cell apparatus to determine the permeation of ingredients through ex vivo skin. In this particular case, the skin was treated with poly{[α-maleic acid-ω-methoxy-poly(ethylene glycol)]-*co*-(ethyl cyanoacrylate)} nanoparticles containing the pharmaceutical agent, D,L-tetrahydropalmatine. Originally published in Xing *et al.*, *Int J Nanomed* **2009**, *4*, 227-232 [127]. Reprinted with permission from Dovepress, copyright 2009

nanoparticles based on poly{[α-maleic anhydride-ω-methoxy-poly(ethylene glycol)]-*co*-(ethyl cyanoacrylate)}. It is nearly a linear release of the drug, which is the desired effect.

For illustration, Fig. 8.25 contains a transmission electron micrograph of polymeric nanoparticles, which in this particular case, there is a distribution of sizes.

Another instructive example is the incorporation of Dead Sea minerals in nanoparticles made of poly(maleic acid-*alt*-butylvinyl ether) in which 5 % of the maleic acid portion is grafted with poly(ethylene glycol) ($M_W = 2000$) and 95 % grafted with 2-methoxyethanol (see Fig. 8.26) [128, 132]. Dead Sea minerals are commonly used for the treatment of skin ailments such as psoriasis and atopic dermatitis. Such nanoparticles are made using a mini-emulsion/solvent evaporation process.

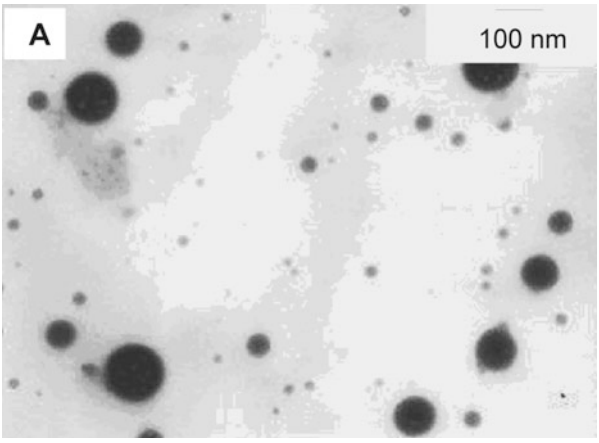

Fig. 8.25 Transmission electron image of polymeric nanoparticles based on poly{[α-maleic acid-ω-methoxy-poly(ethylene glycol)]-*co*-(ethyl cyanoacrylate)}. Originally published in Xing *et al*., *Int. J. Nanomed.* **2009**, 4, 227-232 [127]. Reprinted with permission from Dovepress, copyright 2009

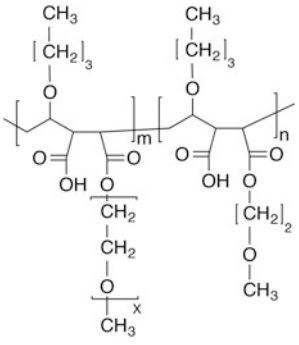

Fig. 8.26 Molecular structure of poly(maleic acid-*alt*-butylvinyl ether) grafted with poly(ethylene glycol) and 2-methoxyethanol to fabricate polymeric nanoparticles

8.3.8 *Delivery of Active Ingredients*

There are many compounds in the cosmetic industry that are used to improve the health state of the skin. These active ingredients typically have some biological activity and can modulate important processes in the skin. Examples of such ingredients include antioxidants, biologically active peptides, and sunless tanning agents. Other active ingredients such as sunscreens, anti-acne agents (e.g., retinol), antiperspirant actives, whitening agents, and dandruff products are regulated by the Food and Drug Administration (FDA) and are considered over-the-counter (OTC) drugs. The delivery of these molecules to the skin is paramount to their ability to be functional. Often times this includes choosing the correct formulation vehicle and sometimes can even mean encapsulating products in a variety of vesicles for effective delivery. The lack of affinity to the skin can hinder the molecule's efficacy. A creative approach to ensuring that agents are delivered in a sustained manner is to utilize a nontoxic, biologically compatible binding agent that has affinity for the skin and is also capable of binding active ingredients that can then be ferried to the skin's surface.

Throughout this chapter we discuss the bioadhesive properties of maleic anhydride chemistry to the skin, although we do not discuss the interactions or possible chemical affinity between maleic acid and the skin. A likely mechanism for the enhanced affinity of maleic acid and its derivatives toward the skin and other biological tissue could likely stem from possible covalent interactions between the hydrolyzed form of succinic anhydride (succinic acid) and various amino acid residues. Scheme 8.3 provides a possible explanation for the binding of maleic acid with proteins via side-chain groups of amino acids, such as amino, sulfhydryl, carboxyl, or hydroxyl functionalities [133].

There are numerous examples of different types of succinate-functionalized materials. For example, Fig. 8.27 demonstrates the attachment of ascorbic acid, an important antioxidant for skin health.

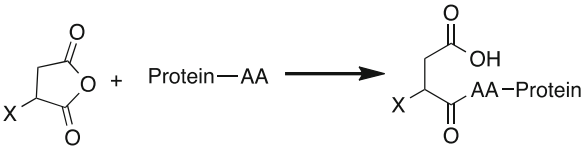

Scheme 8.3 Reaction of succinic anhydride with side chains of amino acids (AA). Various types of pendant groups (X) may be attached to the succinic anhydride molecule

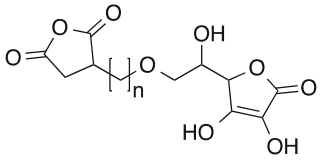

Fig. 8.27 Succinic anhydride covalently linked with ascorbic acid

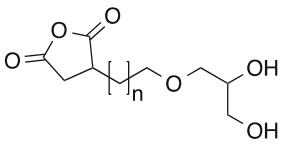

Fig. 8.28 Succinic anhydride covalently linked with glycerol

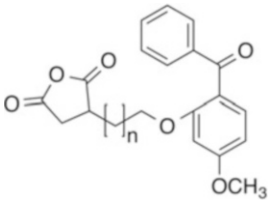

Fig. 8.29 Succinic anhydride covalently linked with benzophenone-3

Other molecules that could similarly serve as functionalizing agents to a succinate framework consist of glycerol (see Fig. 8.28) and benzophenone-3 moieties (see Fig. 8.29). In general, one would expect that with enhanced binding at the surface of the skin via the maleic acid moiety of the molecule, there would be greater probability that these molecules would carry out their function in the skin. For example, glycerol is a humectant that penetrates the skin and binds water, thereby serving as a moisturizing agent that keeps the skin hydrated.

Benzophenone-3, on the other hand, is a sunscreen whose principal mode of action is to remain on the surface of the skin and absorb UV radiation. It should be noted that this type of approach, while inventive, does not discriminate as to the location of the delivery of the cosmetic agent. For example, there may be certain compounds that we want to penetrate deeply into the epidermis, while others would preferentially like to remain on the surface—more or less analogous to the case of glycerol and benzophenone-3.

It is often desirable to deliver lipophilic ingredients to the skin, which have poor aqueous solubility. Normally, this is accomplished by incorporating the ingredient in an oil-in-water or water-in-oil emulsion that is directly applied to the skin in the form of a cream or lotion. In some cases, such compositions can be aesthetically unpleasant or unstable with limited extended shelf life. More sophisticated delivery systems have been gaining popularity in recent years. One example is a polymer/lipid macromolecular complex that is used to deliver oil-soluble, hydrophobic ingredients to the skin [134, 135]. These complexes are engineered utilizing copolymers of poly(styrene-maleic acid) and phospholipids. Normally, an oil-soluble delivery agent is solubilized in a phospholipid micelle (e.g., dilauroyl phosphatidylcholine or dipalmitoylphosphatidylcholine) and then combined with the polymer before adjusting the pH.

It has been postulated that the lipids in combination with the polymer form discoidal (disk-shaped) micelles in which the lipids form a bilayer core. It is

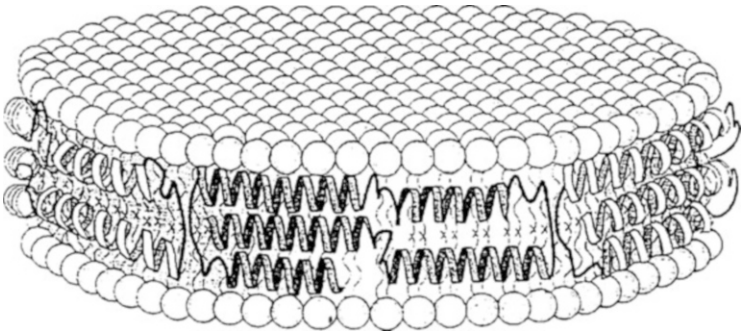

Fig. 8.30 Illustration of a discoidal polymer/lipid macromolecular complex containing poly (styrene-maleic acid) and phospholipids. Reprinted from S. Tonge and B. Tighe, U.S. Patent 6,436,905 B1, 2002 [136]

believed that the polymer is in an alpha-helical conformation with one face occupied by nonpolar groups (styrene monomers) and the other with polar groups (maleic acid monomers) [136]. Figure 8.30 shows an illustration of the macromolecular complex. Evidence of such structures has been confirmed by cryo-TEM measurements [137]. This technology has been proposed for both pharmaceutical and topical cosmetic application. The copolymer can be an alternating or block copolymer of poly(styrene-maleic acid); however this will influence the secondary structure of the polymer.

8.3.9 Skin Care Formulations

Maleic anhydride derivatives are utilized in a variety of skin care formulations where they are used as emulsifiers, emollients, gelling agents, and soap additives. Skin care formulations are usually classified as leave-on or rinse-off. Leave-on treatments usually refer to creams, lotions, body milks, etc. They are applied to the skin and absorbed by the stratum corneum through mechanical manipulation (rubbing and massaging). On the other hand, rinse-off skin care products may consist of soap bars, body washes, foaming cleansers, etc. Usually, the toxicological profile for leave-on products must meet relatively strict guidelines to avoid possible sensitization reactions during use, which could result in contact dermatitis or even more serious skin or ocular conditions.

8.3.9.1 Applications of Skin Care Emollients

Emollients are skin care ingredients that are used in cream, lotion, or gel formulations that, upon treatment, make the skin more soft and supple. With respect to maleic anhydride, research activity in this area has focused on creating adducts of

vegetable oils with maleic anhydride [138, 139]. Specifically, the desire is to create an adduct of maleic anhydride with the principal component of castor oil, ricinolein, which is the triglyceride of ricinoleic acid. Castor oil is obtained from the seeds of the plant, *Ricinus communis*, and is sought after for its therapeutic properties in skin care formulations.

Figure 8.31 provides the structure for the maleated analog of ricinolein where it is shown that one of the triglyceride chains is chemically modified with maleic anhydride. A number of compositions for both rinse-off and leave-in formulations have been described in the literature [140–142]. However, due to skin sensitization, it is usually recommended that maleated castor oil be used in rinse-off applications and at concentrations that do not exceed 0.5 % (w/w). It should be noted, however, that when used in liquid surfactant systems (e.g., body washes), maleated castor oil helps to reduce surfactant-induced irritation and perturbation of the skin's lipid barrier [143]. When combined with palmitic acid, maleated castor oil forms a highly ordered lamellar gel analogous to that found in the lipid barrier (in the stratum corneum) of healthy skin [144]. It is believed that these ordered structures can fortify the lipid matrix of the stratum corneum.

Maleated soybean oil and maleated sunflower oil are also two popular cosmetic ingredients. In general, any oil that is not completely saturated can be maleated such as avocado, coconut, corn, cottonseed, jojoba, linseed, nut, olive, palm, raisin, rapeseed, safflower, sesame, squash, and sunflower [145]. Figure 8.32 provides an example of a triglyceride from vegetable oil that has been maleated. There are numerous examples in the literature demonstrating the modification of natural oils with maleic anhydride [146–149]. Furthermore, maleated oils may be modified by reaction with water ultimately forming a maleic acid derivative or with a hydroxide resulting in the corresponding salt form [145]. Such chemical modification could lead to many additional possibilities in regard to functional moieties that could be included in the oil, while at the same time maintaining a renewable/sustainable molecule. A major advantage of introducing the polar functionality of maleic acid into the backbone is an increase in the molecule's overall water solubility. Moreover, this leads favorably to the ability of the oil to self-emulsify [150].

Other interesting applications in skin care include modification of polysaccharides with maleic anhydride to obtain functional moisturizing ingredients. Chitosan derivatives are a good example of molecules that have been engineered by acylation

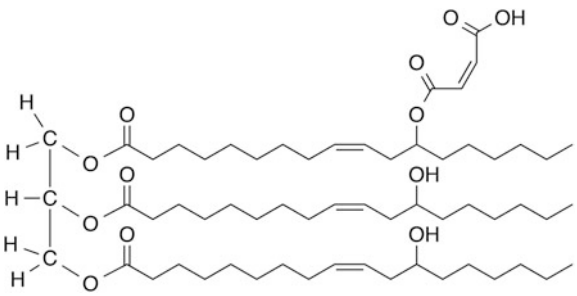

Fig. 8.31 Molecular structure of maleated ricinolein, the chief component of castor oil

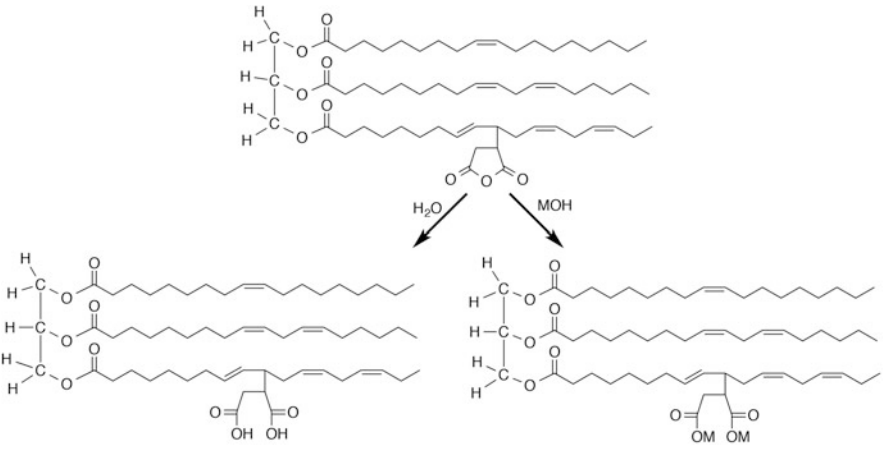

Fig. 8.32 Maleic anhydride grafted onto a triglyceride of a vegetable oil in which treatment with H_2O or base (MOH) results in the opening of the anhydride ring

of chitosan with maleic anhydride [151]. Chitosan is derived from chitin, which is a polysaccharide of N-acetylglucosamine units linked together by a β-1,4′ bond. Chitin is naturally found in the exoskeleton of crustaceans and insects. Chitosan is obtained by a deacetylation reaction of chitin; however the reaction is not complete and chitin is usually a mixture of both glucosamine and N-acetylglucosamine units [152]. Figure 8.33 presents the structure of both chitosan and its maleic anhydride-derivatized counterpart. As shown in the figure, maleic anhydride is attached to chitosan via the amine group at the 2-position on the glucosamine ring. One of the key motivations for modifying chitosan is due to issues with solubility. Unmodified chitosan is insoluble in alkaline medium and, in fact, is only soluble in acid medium in the form of salts.

Maleic anhydride-based materials may also be used as emulsifiers in emulsion systems. An emulsion is a heterogeneous system in which two or more immiscible liquids or semisolid materials are dispersed in another liquid in discrete droplets. The materials that are dispersed (or emulsified) form the dispersed or internal phase, while the rest of materials form the continuous phase or external phase. There are a variety of emulsion types that consist of oil-in-water (o/w), water-in-oil (w/o), multiple (oil-in-water-in-oil; water-in-oil-in-water), nano-, micro-, and Pickering emulsions (a type of oil-in-water emulsion). O/W emulsions are probably the most commonly employed vehicles in skin care formulations, which contain an oil phase dispersed in an aqueous continuous medium. A schematic representation of a dispersed droplet in an o/w emulsion is shown in Fig. 8.34. An emulsifier (or emulsifying agent) is an amphipathic molecule, which arranges itself at the interfaces between the two immiscible phases, thus reducing the surface (interfacial) tension between the two phases, and is able to disperse oil droplets in water. When used with o/w emulsions, they arrange themselves with the

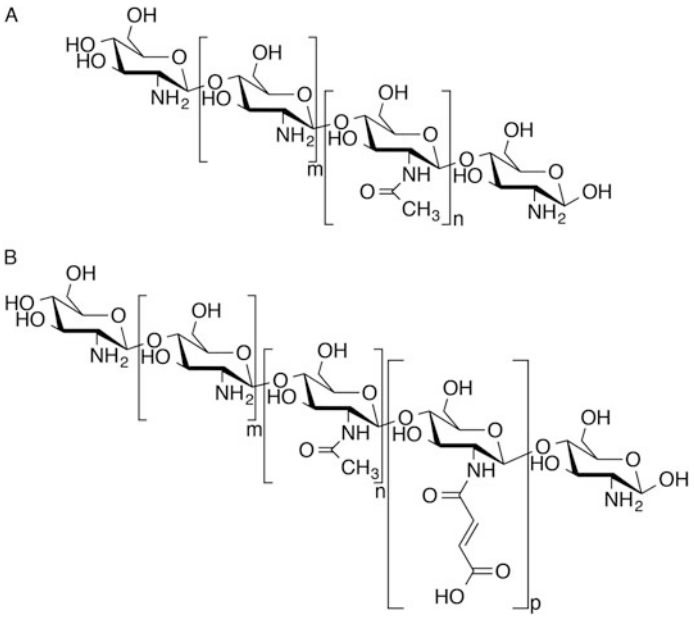

Fig. 8.33 Molecular structure of (**a**) chitosan and (**b**) maleated chitosan

hydrophobic tails in the oil (internal) phase and hydrophilic heads in the water (external) phase.

One example of a polymeric maleic anhydride-based emulsifier is poly(isobutylene) succinic anhydride. This polymer is obtained by reacting poly(isobutylene), which contains vinylidene end groups, with maleic anhydride [153]. As a result, one obtains a polymer with a hydrophobic interior and an end-capped polar functionality. For illustration, Fig. 8.35 contains the structure of poly(isobutylene) and poly (isobutylene) succinic anhydride. One of the benefits of this molecule is its low degree of color. It should be noted that the polyolefin portion of poly(isobutylene) succinic anhydride is extremely hydrophobic, while the maleic anhydride-modified end group is only slightly polar. Further reactions can be carried out with the maleic anhydride portion of the molecule using more highly polar species, resulting in greater surface activity of the polymer.

8.3.9.2 Skin Cleansing Formulations

In general, skin cleansing products are manufactured in the form of solids (bars), liquids, or gels. They function to clean the skin by removing excess oils, dirt, and dead, sloughed skin cells on the surface. Historically, soap was universally used as a cleansing agent. Soaps are fatty acid salts that are manufactured by saponification of vegetable oils or animal fats. There were many safety concerns regarding the use of

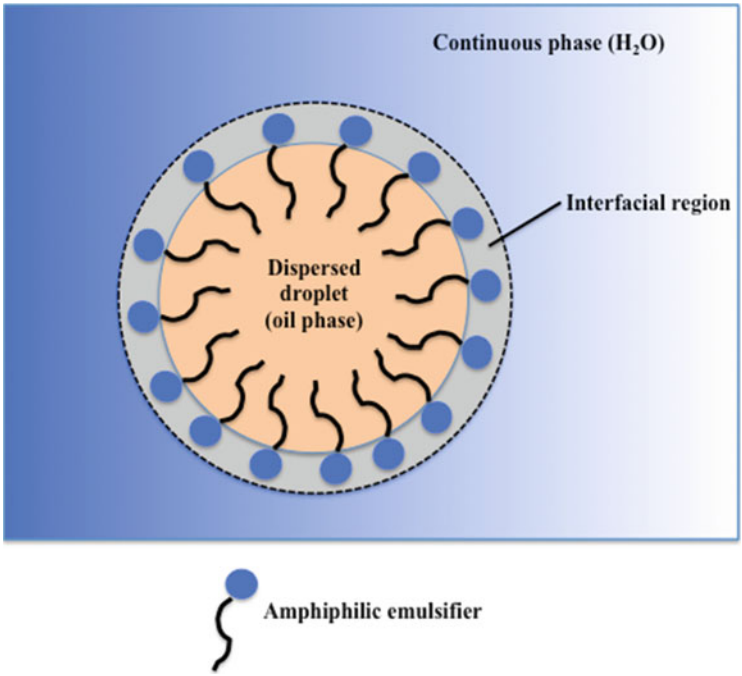

Fig. 8.34 Illustration of a dispersed oil droplet in a typical o/w emulsion stabilized with an emulsifier

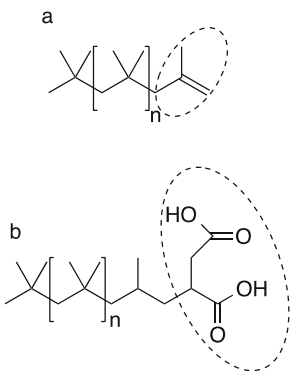

Fig. 8.35 Structure of (**a**) poly(isobutylene) and (**b**) poly(isobutylene) succinic acid. Note that the vinylidene end group in (**a**) can react with maleic anhydride to produce the structure in (**b**). The vinylidene group in (**a**) and maleic acid group in (**b**) are *circled*

soaps and their role in causing irritation, dryness, scaling, and roughness. This led to the development of a variety of anionic, amphoteric, and nonionic surfactants with less skin irritation potential that could be used in skin detergents. In modern skin cleansing formulations, the most commonly used ingredients are anionic surfactants,

which often include acyl phosphates, acyl sarcosinates, alkyl aryl sulfonates, alkyl ether sulfates, alkyl sulfates, isethionates, and olefin sulfonates [154]. Even with the development of this new arsenal of ingredients, there are still many reported cases of skin irritation. Therefore, milder skin cleansing formulations are often sought after. Terpolymers of alpha-olefin and maleic anhydride were suggested irritant-reducing agents in skin cleansing formulations [155]. The alpha-olefin monomers consist of a shorter chain 1-alkene and longer chain 1-alkene having at least 18 carbon atoms. Therefore, the composition consists of a maleic anhydride, short-chain aliphatic, and long-chain aliphatic monomeric components [156]. The polymer is 49–60 mol% of maleic anhydride, 10–40 mol% of shorter chain olefin, and 40–10 mol% of long-chain olefin (see Fig. 8.36). By adjusting the ratio of the shorter and longer aliphatic monomers, one may fine-tune the solubility and waxiness of the polymer. The use of this polymer, which can reach as high as 50 % of the total surfactant concentration in cosmetic detergents, reportedly does not comprise its foaming and cleansing properties [157].

8.3.9.3 Soap Bar Dimensional Stability

Soap bars are used almost universally to clean the skin. There are, of course, inherent problems with the stability of the soap bar during its life in the shower. As the soap bar ages, cracking occurs in its structure due to the presence of water. More than likely, such an effect occurs due to changes in the crystalline phase of the soap bar caused by residual moisture. Studies have shown that incorporation of polymers based on maleic anhydride, specifically poly(methyl vinyl ether-maleic acid) and its esterified form, reduces the number of cracks in the soap bar and helps to maintain its dimensional stability [158]. Further, the author reports an emollient effect for such compositions coupled with a smoothening effect when applied to the skin. In general, other types of polymers have been used in similar applications.

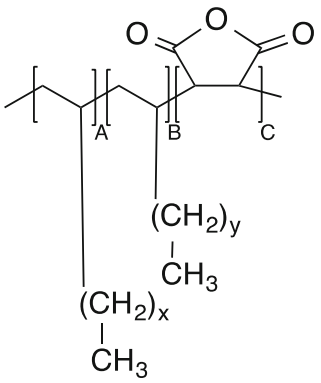

Fig. 8.36 Molecular structure of a terpolymer of alpha-olefin and maleic anhydride with the following mole percent monomer composition: $A = 10–40\,\%$, $B = 40–10\,\%$, and $C = 49–60\,\%$. The aliphatic chains of the olefin monomers are $x < 17$ in A and $y \geq 17$ in B

Unfortunately, the mechanism by which soap bar dimensional stability is conserved is unknown.

8.3.9.4 Stabilization of Vitamin C

Vitamin C, or ascorbic acid, is an important antioxidant in the skin that prevents free radical damage, stimulates collagen synthesis, boosts the immune response, and acts as a synergistic antioxidant with vitamin E (alpha-tocopherol) [159]. Unlike other mammalians, humans lack an enzyme required for vitamin C biosynthesis. Therefore, it must be obtained through the diet or by topical treatment. However, a major issue with formulating ascorbic acid in skin care preparations is its inherent instability. Several approaches to circumvent this instability issue include packaging that provides a more inert atmosphere, thereby preventing oxidation; creating a two-phase formula in which one is a dry powder (containing vitamin C) and the other is liquid—they are combined immediately prior to use; formulating with high concentrations of glycols or polyols to reduce the solubility of oxygen in the formulation; and formulating ascorbic acid in an anhydrous system based on silicones [160]. There have even been numerous attempts to synthesize vitamin C derivatives, such as sodium ascorbyl phosphate or ascorbyl palmitate; however, the bioavailability of these materials is reportedly low [161]. In recent years, there has been some patent activity utilizing low molecular weight poly (styrene-maleic anhydride) chemistry to prevent oxidation of ascorbic acid in skin care formulations [162–167]. Unfortunately, the precise mechanism by which the polymer prevents oxidation is not disclosed.

8.3.9.5 Alpha Hydroxy Acids

Another important class of compounds for the treatment of the skin is hydroxy acids [168]. These consist of alpha hydroxy acids, beta hydroxy acids, and polyhydroxy acids. Alpha hydroxy acids are the most important in this group and have had considerable success in the personal care marketplace. Structurally, alpha refers to the position of a hydroxyl group on the carbon adjacent to the carboxylic acid functional group in these molecules. These agents incur biologically induced changes in the skin resulting in antiaging, antiwrinkle activity, and improved skin tone. The most common alpha hydroxyl acids in skin care preparations are glycolic acid, salicylic acid, citric acid, and lactic acid. After topical application, alpha hydroxy acids function by stimulating proliferation of keratinocytes in the epidermis, which leads to enhanced skin turnover. Treatment with alpha hydroxy acids also improves the condition of collagen and other molecules in the dermis. The mechanism behind the overall enhanced skin renewal is still not well understood, although strong clinical evidence demonstrates the efficacy of these materials in rejuvenating skin. In addition, current evidence suggests that alpha hydroxy acids incite a cascade of cell signaling events involving cytokines secreted by

keratinocytes in the epidermis. The activation of cytokines in the skin leads to many important processes in the skin including immune response, wound healing, and accelerated cell turnover.

In regard to maleic anhydride chemistry, skin care compositions containing poly (methyl vinyl ether-maleic acid) and poly(methyl vinyl ether-maleic acid-isobutylene) are proposed as possible agents that perform like alpha hydroxy acids [169, 170]. One major drawback of alpha hydroxy acids is their high irritation potential. Treatment with polyacids to minimize negative toxicological effects may prove to be an alternative treatment modality, although its commercial relevance has yet to be demonstrated by its incorporation into finished consumer products. In addition, further work to investigate the use of the polymers in conjunction with the alpha hydroxyl acids could prove interesting. Possibly, lower levels of alpha hydroxy acids could be utilized to achieve similar results when the formulation contains maleic anhydride-based polymers.

8.3.10 Incorporation of Maleic Anhydride Derivatives in Sunscreen Formulations

Sunscreens are formulations regulated as an OTC drug by the FDA in the United States. In Europe, on the other hand, they are regulated as cosmetics according to Council Directive 76/768/EEC. Regardless, it is a critical product category for the protection of the skin against harmful ultraviolet rays from the Sun. Exposure to ultraviolet radiation could lead to sunburn reactions characterized by erythema and edema. It is the culprit of many ailments of the skin including photoaging, photoimmunosuppression, and photocarcinogenesis. Sunscreen actives are normally characterized as inorganic or organic filters. Inorganic compounds, such as titanium dioxide or zinc oxide, are particulates that reflect or scatter incoming ultraviolet rays, thereby preventing them from reaching the surface of the skin. On the other hand, organic filters (e.g., benzophenone-4, avobenzone, etc.) absorb the incoming light. In addition to sunscreen active ingredients, other components of a sunscreen formulation are equally important. For example, how well the sunscreen film spreads, whether it is waterproof, and if the formulation is stable, especially at elevated temperatures, are all important considerations when engineering a new product.

Often, it is desirable to create sunscreen formulations with aesthetically pleasing properties, yielding a final product that leaves a nonoily, non-tacky film that is not visible and dries quickly. Such sunscreen products may be formulated using water-soluble maleic anhydride polymeric derivatives. One example is a gel based on poly (ethylene-maleic anhydride) [171]. In this case, the formula is thickened by the polymer and does not require emulsifiers or surfactants. On the other hand, it is also desirable for the sunscreen formula to have waterproofing properties allowing the treatment to remain stable during sweating or swimming. It has been a common

practice to use a cross-linked terpolymer of methyl vinyl ether, tetradecene, and maleic anhydride for this purpose [172]. Due to the long aliphatic chain of tetradecene, this polymer is oil soluble, thereby providing compatibility with organic sunscreens as well as waterproofing properties. More information is provided for this type of polymer technology in the next section on rheology modifiers.

In addition to serving as formulating agents, maleic anhydride derivatives may also provide performance-boosting properties to sunscreen formulations by other means. For example, inherent problems exist with some of the commercially available sunscreen agents. Para-aminobenzoic acid is a very polar molecule making it water soluble, thereby not allowing it to remain on the skin during perspiration and swimming. Likewise, avobenzone undergoes keto-enol isomerization leading to instabilities of the molecule and ensuing reactions that render the sunscreen less efficacious. Providing a more stable environment for the sunscreen agent can circumvent some of these issues. Maleic anhydride functionalities within a molecule readily undergo reactions with primary amines, opening the epoxide ring and yielding a half-acid, half-amide functionality. Two amine functional aromatic compounds that can be incorporated into a maleic anhydride functionality are 2-aminobenzoic acid and 2-aminobenzophenone [173]. These molecules share similar properties to their structural counterparts, para-aminobenzoic acid and avobenzone, which are used universally in sunscreen formulations. Figures 8.37 and 8.38 provide a demonstration of how each of these molecules is incorporated separately and together by grafting them on to the aliphatic chains of the triglyceride component of maleated soybean oil derivatives. At this time, these molecules are not FDA-approved sunscreen compounds; however, they could have possible applications as photostabilizers or SPF boosters.

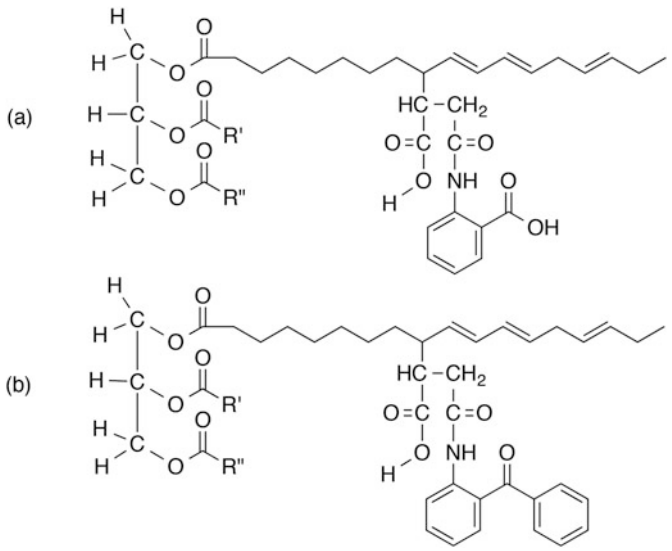

Fig. 8.37 Molecular structure of a maleated triglyceride from vegetable oil that has undergone substitution with (**a**) 2-aminobenzoic acid and (**b**) 2-aminobenzophenone

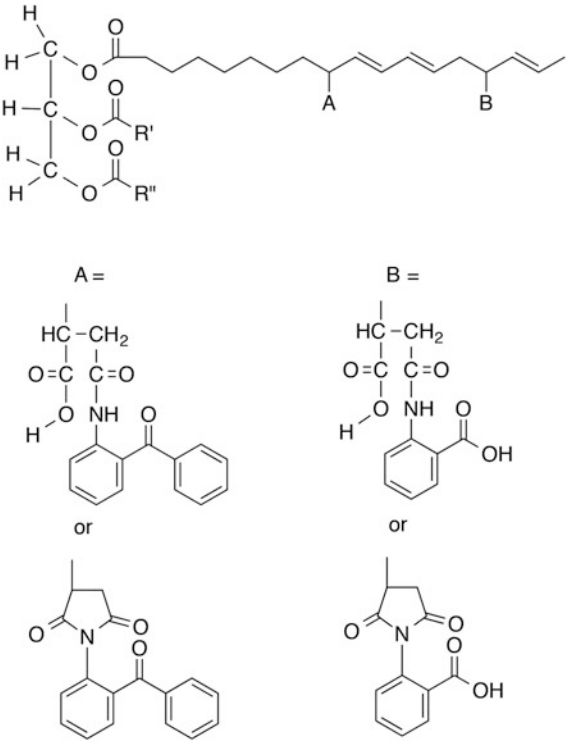

Fig. 8.38 Molecular structure of a maleated triglyceride from vegetable oil that has undergone substitution on the same chain with (**a**) 2-aminobenzophenone and (**b**) 2-aminobenzoic acid

8.3.11 Rheology Modifiers for Skin Care Formulations

Rheology modification is extremely important for skin care. Formulations are often engineered by taking into account the desired yield stress, sheer thinning behavior, thixotropy, viscosity, and mechanical stability. Most of these measured parameters apply to the cosmetic composition when it is applied to the skin. However, equally important is the rheological behavior of a given material when it is dispensed from its packaging element. There has been much interest in the personal care industry to utilize rheology to determine the sensorial properties of cosmetic formulations and to predict a product's stability over long periods of time and at elevated temperatures [174, 175]. A class of cross-linked maleic anhydride polymers are particularly important in this area [176, 177]. They are used as rheology modifiers for many different types of personal care formulations including topical wound healing compositions, sunscreens, surfactant-based systems, nail treatment formulas, and hairstyling gels [178–182].

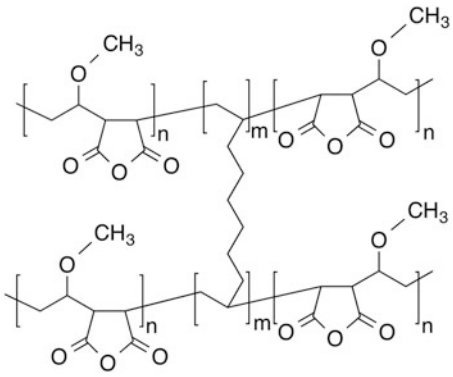

Fig. 8.39 Molecular structure of poly(methyl vinyl ether-maleic anhydride) cross-linked with 1,9-decadiene

In the late 1980s, GAF Chemicals Corporation (later International Specialty Products; currently Ashland, Inc.) developed a series of polymers based on poly (methyl vinyl ether-maleic anhydride) cross-linked with 1,9-decadiene (Fig. 8.39). Originally, there were several grades of the polymer available and sold under the trade names Stabileze 06, Stabileze 12, and Stabileze 15, which were 2.5 %, 2 %, and 3–3.5 % cross-linked, respectively [183]. Today, only Stabilize 06 and Stabileze QM are commercially available. The difference between these two forms of the polymer lies in the particle size of the commercially available powder. Stabileze QM has a smaller particle size and is more quickly dispensed in water and converted into a gel.

In the powder form, the polymer exists as an anhydride. In order to thicken formulations, these polymers must first be hydrolyzed in order to open the anhydride ring resulting in the diacid form of the molecule. Much effort has gone into developing processes for hydrolyzing and simultaneously neutralizing these cross-linked polymers. Hydrolysis can be achieved by three methods: (a) dispersing the polymer in water at room temperature for 24–48 h, (b) heating the polymer in water at 65–80 °C for 30–90 min, or (c) heating the polymer in dilute sodium hydroxide solution at 65 °C for 30 min [183–185]. High-viscosity gels may be obtained when the polymer is fully neutralized with an organic or inorganic base, typically in the pH range of 5.5–9, resulting in the expansion/uncoiling of the polymer chains. The broad thickening pH range is afforded due to the two pK_a values of the acid groups in the polymer, which in pure maleic acid are 1.97 and 6.06 [186]. In poly(methyl vinyl ether-maleic acid), these values are shifted to 3.47 and 6.47. There have been proposals of replacing the conventional organic and inorganic bases used for neutralization with basic amino acids [187]. This mainly stems from concerns that traditional bases cause irritation. Nevertheless, amino acid neutralization is not a common practice employed by formulators.

8.3.12 Skin Tightening

The modification of the rheological properties of the skin by cosmetic treatments is an area of active research and product development in the personal care industry. Often, the aim is to soften the skin by treatment with plasticizers, such as glycerol, or by an occlusive effect of hydrophobic materials such as oils and emollients. As a result, water accumulates in the stratum corneum resulting in plasticization, which ultimately decreases the modulus of the skin, ameliorates the stress between the stratum corneum and underlying skin layers, and softens lines and wrinkles. Another approach to changing the mechanical behavior of the skin is to induce skin tightness, also referred to as skin firming or lifting. This can be accomplished by washing with water or surfactants, which removes low molecular weight materials such as amino acids, urocanic acid, squalene, cholesterol, and lipids from the skin. This results in temporary stiffening of the stratum corneum and causes the sensation of tightness.

Skin tightening can also be produced by surface deposition of certain film-forming agents, including proteins, polysaccharides, and polymers. This area—skin tightening induced by treatment with a film-forming polymer—is what we are most interested in for our current discussion. Quite some time ago, it was reported that ethylene-maleic anhydride copolymers were particularly useful at smoothing the wrinkles of human skin [188]. In fact, this patent was well ahead of its time. It was not until the early 2000s that polymeric skin-tightening treatments really began to make any headway in the marketplace. While a variety of polymeric film formers could induce a slight skin-tightening effect, terpolymers of poly(isobutylene-*alt*-maleic acid) with dimethylaminopropylamine and methoxy-PEG/PPG propylamine (INCI: polyimide-1) have been reported to be exceptionally efficacious (see Fig. 8.6 for molecular structure) [189]. While the precise mechanism is not fully understood, it is very likely that upon dry-down this particular polymer has the ability to act like a shrink wrap while still maintaining its bioadhesive strength [190]. Therefore, the skin will experience an inward force while still maintaining good adhesion to the polymer, overall providing a tightening sensation. Often such ingredients are used in finished products for the temporary effects they produce. For example, many formulas, such as antiaging and skin whitening, require that the consumer repeatedly use the products for an extended period of time (e.g., 1 month or even longer) in order to induce a quantifiable biological effect in the skin. Often times, the consumer may quit the regimen if they do not see an immediate effect. Therefore, many skin care finished good manufacturers will attempt to include a secondary cue, such as skin tightening or a tingling sensation produced from methanol, to maintain the consumer's interest in repeat use of the product.

8.4 Maleic Anhydride Chemistry in Oral Care

Maleic anhydride-based polymers have a long and rich history of use in oral care products. For over three decades, poly(methyl vinyl ether-maleic acid) salts have been used in denture adhesive formulas. As a bioadhesive compound, this polymer helps maintain the denture in place even when strong forces are encountered during mastication. Maleic anhydride chemistry also plays an integral role in oral health. It functions as a bioadhesive delivery agent for active ingredients including antibacterial agents. In this section, we review some basic principles about tooth anatomy and then discuss the details of the oral care health benefits provided by poly(methyl vinyl ether-maleic acid).

8.4.1 Bioadhesive Properties of Poly(Methyl Vinyl Ether-Maleic Acid)

Poly(methyl vinyl ether-maleic acid) polymers are known for their excellent bioadhesive properties and used as denture adhesives and also to substantiate the slow release of hydrophobic therapeutic agents in the oral cavity. The polymer's bioadhesive property is mainly attributed due to its hydrogen-bonding groups (-COOH) that can form strong anionic charges and have excellent wetting characteristics with sufficient flexibility that allows it to penetrate and adhere to mucus/mucosal tissue surfaces [191]. For illustration, Scheme 8.4 demonstrates the protonation and deprotonation of the maleic acid moiety of poly(methyl vinyl ether-maleic acid).

The adsorption kinetics of poly(methyl vinyl ether-maleic acid) can be described as a three-step mechanism [192, 193]. The first step is the mass transport process, in which polymers diffuse to the proximity of the surface. The second step, the attachment onto the mucosal tissue surface, occurs when the polymer chains begin to interact with the mucosal tissue surface through secondary interactions including hydrophobic (or van der Waals), hydrogen bonding, and electrostatic interactions [194–196]. The last step is the rearrangement of adsorbed polymer in order to achieve a more stable state. In order to provide a frame of reference, Table 8.1 describes the relative mucoadhesion force of poly(methyl vinyl ether-maleic acid) in comparison to other bioadhesive polymers.

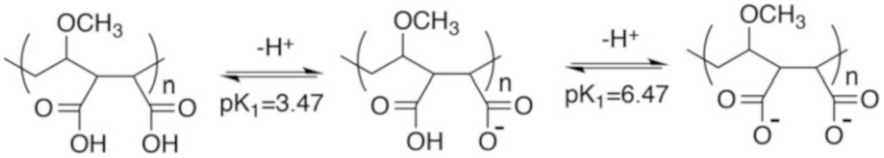

Scheme 8.4 Protonation and deprotonation of the maleic acid moiety of poly(methyl vinyl ether-maleic acid)

Table 8.1 Mucoadhesive forces for various polymers. Assembled by Alexander et al. [197]

Mucoadhesive polymers	Adhesive force
Poly(acrylic acid)	185.0 ± 10.3
Tragacanth	154.4 ± 7.5
Poly(methyl vinyl ether-maleic acid)	147.7 ± 9.7
Poly(ethylene oxide)	128.6 ± 4.0
Methylcellulose	128.0 ± 2.4
Sodium alginate	126.2 ± 12.0
Hydroxypropylmethyl cellulose	125.2 ± 16.7
Karaya gum	125.2 ± 4.8
Methylethyl cellulose	117.4 ± 4.2
Soluble starch	117.2 ± 3.1
Gelatin	115.8 ± 5.6
Pectin	100.0 ± 2.4
Poly(vinyl pyrrolidone)	97.6 ± 3.9
Poly(ethylene glycol)	96.0 ± 7.6
Poly(vinyl alcohol)	94.8 ± 4.4
Poly(hydroxyethyl-methacrylate)	88.4 ± 2.3
Hydroxypropyl cellulose	87.1 ± 13.3

In addition, poly(methyl vinyl ether-maleic acid) possesses the following important characteristics that make it versatile and useful for oral care applications:

- It adheres to oral tissues and forms stable films.
- It has an excellent safety profile.
- It does not irritate the mucous membrane.
- It has a high molecular weight to form strong non-covalent bonds with the mucin-epithelial cells and tooth surfaces.
- It is compatible with oral care products.

8.4.2 Tooth Anatomy[2]

The human tooth is a complex morphological structure, in which part of the tooth is exposed, while a considerable amount is embedded in the gums (gingiva) and extends into the jaw bone (mandibula). An illustration of tooth and its component parts is provided in Fig. 8.40 and can be subdivided into three components: root, neck, and crown.

As already mentioned, the root is embedded in the bone mass of the mandibula—the alveolar bone. The relatively long root structure also contains nerve tissue that extends up until the pulp cavity, which also contains pulp and

[2] Portions of this section were previously published in Ref. [198].

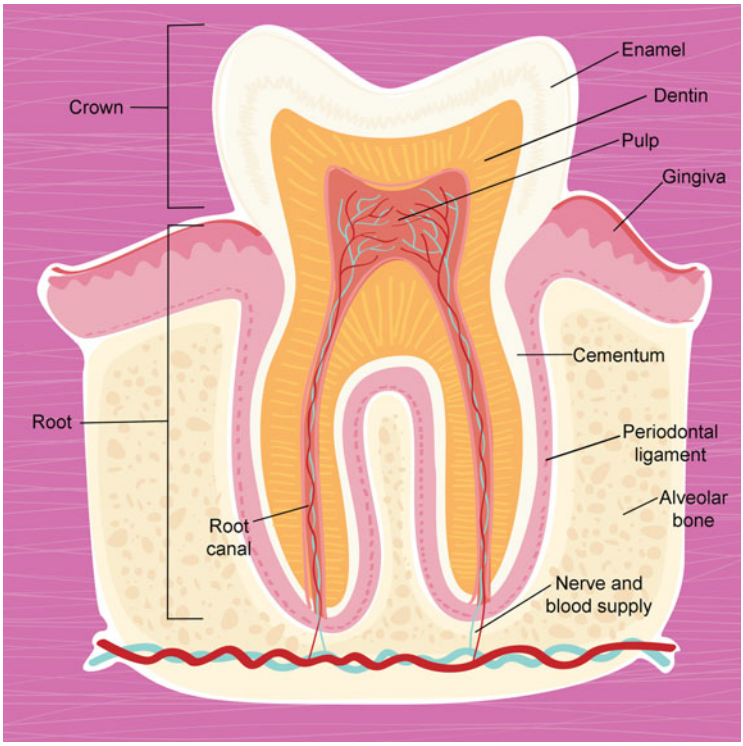

Fig. 8.40 Anatomical structure of the tooth. Reprinted with permission from Ref. [198]. Copyright, 2016, The Cosmetic Chemist LLC

blood vessels. Odontoblast cells in the pulp are responsible for forming dentin. Nutrients are delivered to this region via the blood supply and allow the tooth to sustain itself as a living tissue. The presence of nerves allows for the sensation of pain, which is often caused by extreme temperatures, and is especially noticeable when drinking cold or hot beverages. The root canal (also known as the pulp canal) is the narrow conduit starting at the base of the root and extending up until the pulp cavity, which provides access for vascularization and innervation. Problems in the pulp cavity, such as infection, often require root canal therapy.

Surrounding the root structure, the cementum provides a biological adhesive layer between the main body of the root and the periodontal ligament. It is composed of fibrous tissue, which firmly attaches the teeth to the jaws. One end of the fiber bundle is connected to the cementum and the other into the alveolar socket, which is the connection point to the jaw. The neck of the tooth describes the area where the gingiva (gum tissue) is located and the tooth becomes exposed to the buccal cavity (the region of the oral cavity that is bound by the lips, cheeks, and gums).

Finally, the crown is the visible portion of the tooth and contains a hard, crystalline outer layer of enamel that protects the interior structure of the tooth by preventing demineralization. It also facilitates mastication, as it is a very smooth

surface. Since enamel is a hard structure, it is also very brittle. Enamel is a translucent layer that is susceptible to damage due to eating sugary foods or drinking acidic beverages and is not like the other bone tissue, which the body can self-heal. Staining of teeth usually occurs on the enamel layer and is caused by consuming beverages, such as tea and coffee, as well as by smoking tobacco or even poor oral hygiene. Normal tooth color is not pure white, but a slight off-white, gray, or even yellow color. Below the enamel, most of the tooth structure is composed of dentin, a bone-like substance that provides teeth with their characteristic color.

At the chemical level, tooth is principally comprised of crystalline calcium phosphate, which exists in the mineral form as hydroxyapatite and has the molecular formula $Ca_5(PO_4)_3(OH)$. Enamel, which again is very hard and brittle, contains relatively high levels of hydroxyapatite (ca. 92–94 %) as well as much lower quantities of water (2–3 %), carbonate (2 %), trace elements (1 %) (e.g., sodium, magnesium, potassium, chloride, zinc), fluoride (0.01–0.05 %), and proteins and lipids (<1 %) [199]. Dentin, on the other hand, contains much less hydroxyapatite and is also comprised of collagen and other organic matter (35–50 %).

8.4.3 *Plaque, Calculus, Caries, and Gingivitis and Strategies for Protection*[3]

Poor oral care health can result in a number of unfavorable conditions in the oral cavity that are principally caused by bacteria. There has been considerable interest in the cosmetic and toiletry industry to design and invent products in the form of dentifrices for the treatment and prevention of these ailments. Plaque and calculus (tartar) are principle concerns as well, as they can lead to more serious conditions such as the formation of caries, commonly known as cavities, or the development of gingivitis (inflammation of the gum tissue).

Dental plaque is a yellow biofilm film formed on the surface of the tooth enamel due to bacterial colonization. There can be as many as 1000 bacterial species present, and plaque owes its bacterial diversity due to the lack of a biological self-cleansing system [200]. Initially, the biofilm is soft in nature; however, after several days it begins to harden forming tartar, also known as calculus.

Dental biofilms represent a significant threat to oral health as many of the bacteria present in dental plaque are cariogenic—they cause demineralization of the tooth. Typically, such bacteria are acidogenic (they produce organic acids) and aciduric (they are able to survive in acidic environments). Their degradative activity occurs as a result of fermentation of dietary carbohydrates (e.g., sucrose) into formic, acetic, and propionic acid, which makes the tooth more susceptible to the perils discussed above.

[3] Portions of this section were previously published in Ref. [198].

The enamel pellicle contains a protective layer of proteins that bind to hydroxyapatite. In addition to these proteins, there are other salivary proteins that also deposit on the surface of the enamel pellicle and protect it from metabolic by-products of bacteria that comprise the biofilm [201]. These proteins have a variety of functions in protecting the tooth, such as inhibiting the adhesion of microorganisms and even helping the tooth remineralize by binding important trace elements, such as calcium.

Dental calculus results from the crystallization of dental plaque. As already noted, plaque exists in the form of a soft biofilm, which hardens due to the accumulation of minerals from saliva, such as calcium phosphate. Often, calculus is further classified as supragingival or subgingival, which indicates the location where it is found—supragingival calculus occurs on the crown of the tooth, while subgingival forms lower in pockets of the gingiva. Supragingival calculus has a mineral content of about 37 % and also contains proteins and lipids, which are also believed to be an integral part of calculus formation [202]. It should be noted that calculus cannot be removed simply by brushing and other normal oral hygiene routines. Usually it requires special dental tools such as a traditional or ultrasonic tooth scaler since it is so tightly bound to the tooth surface. Calculus buildup, however, can be prevented when suitable dentifrices are utilized on a routine basis.

Dental caries form as a result of demineralization of the tooth structure. The acidic environment that prevails during the presence of plaque and calculus ultimately leads to damage of the tooth's enamel coating and can extend into the interior dentin structure. Carie formation is usually detected in the early stages during routine dental checkups. However, there are instances when visible pits or holes can be found in the tooth.

Gingivitis is a type of periodontal disease resulting in inflammation and infection of the gum tissue. It is a degenerative disease that is caused by the long-term effects of dental plaque and calculus deposits on the teeth. The bacteria associated with plaque and calculus, along with their metabolites, infect the gum tissue eventually leading to the degeneration of tissue that supports the tooth, such as periodontal ligaments and alveolar bone tissue of the tooth socket.

Despite innate protective mechanisms in the oral cavity against undesired bacteria and other malicious agents, considerable efforts in the oral care industry have aimed to circumvent the development of plaque, calculus, caries, and gingivitis. In most circumstances, this strategy consists of treating the oral cavity with a dentifrice in the form of a toothpaste or mouth rinse. An antibacterial agent, can be employed to combat plaque microflora along with fluoride (usually in the form of sodium fluoride, sodium monofluorophosphate, or stannous fluoride) as a fortifying agent that remineralizes enamel and helps prevent the formation of caries. These ingredients may be formulated in conjunction with poly(methyl vinyl ether-maleic anhydride) in which the polymer acts as a bioadhesive, thereby ensuring that the other key ingredients in the dentifrice are delivered to the site of interest on the surface of the enamel.

The bioadhesive properties of poly(methyl vinyl ether-maleic acid) ensure that the polymer, along with active ingredients, remains on the tooth surface to ward off flora that could otherwise lead to the development of plaque and calculus.

8.4.4 Denture Adhesives

Dentures are false teeth, which are removable prosthetic devices that adhere to the gum. Dentures can be a complete prosthetic design, replacing all of the teeth on one of the arches, or partial replacement of several teeth. Our discussion in this section will focus on complete dentures, as these are the ones most commonly accompanied by the use of an adhesive. For illustration, Fig. 8.41 contains a photograph of conventional dentures for both the maxillary (upper) and mandibular (lower) arches.

In order to ensure proper fixation of the dentures, adhesive materials are commonly placed on the surface of the dentures that comes in contact with the gum tissue (Fig. 8.42). Adhesives are typically formulated as a paste or a powder that can be of natural or synthetic origin. Normally, the adhesive is hydrophilic and absorbs moisture from the saliva resulting in the formation of an adhesive hydrogel with high tack. The denture adhesive formula is usually applied to the denture once a day. Most dentures do not fit in perfect alignment with the gum tissue due to changes that occur in the gum tissue over time. Therefore, by adding a denture adhesive, the interstices between the gum and the prosthetic device are filled. It is desirable that the denture adhesive can withstand the forces encountered during mastication and also that it is resistant to degradation during the consumption of hot and cold beverages. At the same time, the adhesive strength of the adhesive cannot be so strong that the prosthetic device cannot be removed.

Many years ago denture adhesives were formulated with natural ingredients such as karaya gum; however, such compositions did not provide consistent adhesion between the denture and the gum tissue. In 1961, a patent was granted

Fig. 8.41 Photograph of conventional dentures that fit over the maxillary and mandibular region of the oral cavity

Fig. 8.42 Photograph of the application of an adhesive material to a denture prosthetic device

for the use of a synthetic polymer, consisting of mixed or partial salts of copolymers of maleic acid with vinyl ether, for use as a denture adhesive [203]. The salts used included calcium in combination with alkalies, such as sodium and potassium, but quaternary ammonium compounds may also be used as counterions to the acid groups of poly(methyl vinyl ether-maleic acid). There have been a significant number of publications describing their use in denture adhesive formulations [204–209].

A typical denture adhesive formula based on poly(methyl vinyl ether-maleic acid) may be used in combination with either carboxymethyl cellulose or poly (vinylpyrrolidone) [210]. Upon application, carboxymethyl cellulose or poly (vinylpyrrolidone) becomes hydrated and binds via ionic interactions with the gum tissue and the prosthetic device [211]. These interactions are short lived, and poly(methyl vinyl ether-maleic acid) provides the long-term adhesion necessary to ensure proper denture stability.

Acknowledgments I would like to express my sincere gratitude to Joseph Dallal, Raymond B. Clark, and Petros Gebreselassie of Ashland, Inc. for many helpful conversations as well as suggestions for the text. A debt of gratitude is also due to Timothy Gillece and Raymond Rigoletto, also from Ashland, Inc., who reviewed the manuscript and provided guidance and support.

References

Applications of Maleic Anhydride Copolymers in Hair Care

1. Robbins C (2012) Chemical and physical behavior of hair, 5th edn. Springer, Heidelberg
2. Jollès P, Zahn H, Höcker H (1997) Formation and structure of hair. Birkhäuser Verlag, Basel
3. Forslind B, Lindberg M (2004) Skin, hair, and nails: structure and function. Marcel Dekker, New York
4. Bouillon C, Wilkinson J (2005) The science of hair care. Taylor & Francis, Boca Raton
5. Piersol GA (1908) Human anatomy, vol II. J.B. Lippincott, Philadelphia, PA
6. Jones L, Rivett D (1997) Role of 18-methyleicosanoic acid in the structure and formation of mammalian hair fibres. Micron 28:469–485
7. Swift J (2012) The structure and chemistry of human hair. In: Wickett R, Evans T (eds) Practical modern hair science. Allured, Carol Stream, IL
8. Garcia M, Epps J, Yare R, Hunter L (1978) Normal cuticle-wear patterns in human hair. J Soc Cosmet Chem 29:155–175
9. McMullen R, Laura D, Chen S, Koelmel D, Zhang G, Gillece T (2013) Determination of physicochemical properties of delipidized hair. J Cosmet Sci 64:355–370
10. Wright G (1955) Film-forming compositions, US 2,723,248
11. Tarpey C (1964) Maleic anhydride and ethylene oxide copolymers in hair preparations, US 3,130,127
12. Nandagiri A, Tripathi U, Hunter L (1979) Aerosol hairspray containing an ethyl or butyl monoester of a copolymer of maleic acid and a vinyl monomer, US 4,164,562
13. Abegg J-L, Madrange A (1975) Aerosol hair sprays containing ethyl or butyl monoester of copolymer of vinyl monomer and maleic acid, US 3,922,341
14. Varco J, Williams C (1986) Stabilized hair spray composition and process, US 4,567,040
15. Benson A, Hourihan J, Tripathi U (1992) Aerosol hairspray composition, US 5,094,838
16. Gerstein T (1994) Hair setting compositions, US 5,374,420
17. Waxman B, Lin S (1986) Low molecular weight hairspray, US 4,567,035
18. Dallal J, Rocafort C (1997) Hair styling/fixative products. In: Johnson D (ed) Hair and hair care. Marcel Dekker, New York
19. Nandagiri A, Tripathi U, Hunter L (1981) Copolymer of vinyl ether and ester of maleic acid as aqueous spray, CA 1,092,980 A1
20. Hamilton B, Walls E (1996) 80% VOC, single phase aerosol hair spray composition, WO 1996 002 227 A1
21. Rocafort C, Ulmer H (1998) Hair spray composition having 80% or less VOC and advantageous physical and performance characteristics, EP 0 865 273 A1
22. Malawer E, Narayanan K, Cullen J, Rocafort C (1997) Low VOC hair spray composition, US 5,597,551
23. Watling I, Patel D, Petter P (1993) Non-aerosol, low VOC, pump hair spray composition, WO 1993 025 181 A1
24. Chuang J-C, Walls E, Johnson S, Tazi M (1990) Non-aerosol pump hair spray compositions, WO 1990 014 072 A1
25. Chuang J-C, Walls E, Johnson S, Tazi M (1990) Non-aerosol pump hair spray compositions, US 4,954,336
26. Malawer E, Narayanan K, Cullen J, Rocafort C (1995) 0% VOC, single phase hair spray composition, US 5,458,871
27. Blaine A, Foltis L, Gillece T, Katirgis J, Ulmer H (1999) Derivatized polymers of α-olefin-maleic anhydride alkyl half-ester or full acid, WO 1999 067 216 A1
28. Ulmer H, Gillece T, Katirgis J, Foltis L, Blaine A (1999) Derivative polymers of alpha-olefin-maleic anhydride alkyl half-ester or full acid, EP 1,098,877 A4

29. Foltis L (1999) Aquaflex FX-64 – A new stiff polymer for hair sprays and styling products. Spray Tech Market 9(5):26–29
30. Streuli D, Foltis L (2004) Hair spray composition, US 10/643,238
31. Knappe T, Scheffler R, Scheunemann V (2007) Hair-setting composition containing derivatized maleic anhydride polymer and a nonionic homopolymer or copolymer of vinylpyrrolidone, WO 2007 059 829 A1
32. Dallal J (2000) Hair setting products. In: Rieger M (ed) Harry's cosmeticology. Chemical Publishing, New York
33. Rigoletto R, Mahadeshwar A, Foltis L, Streuli D (2012) Advances in hair styling. In: Evans T, Wickett R (eds) Practical modern hair science. Allured, Carol Stream, IL
34. Helioff M, Plochocka K, Tazi M (1991) Mousse hair composition, US 5,066,481
35. Ulmer H, Gillece T, Katirgis J (2006) Maleic compound modified alpha-olefin, US 7,041,281 B2
36. Lee G, Hentrich S (1998) Hair treatment composition, US 5,714,135
37. Jones S, Marchant P (1999) Hair cosmetic composition, US 5,922,312
38. Constantin K, Zabotto A, Contamin J-C (1977) Gels based on vinyl ether-maleic anhydride copolymer neutralized by a basic amino acid, US 4,010,224
39. Dimotakis E, Singer J, Bui H, Simmonnet J-T (2013) Hair cosmetic and styling compositions based on maleic acid copolymers and polyamines, US 2013/0,309,190 A1
40. Helioff M, Kwak Y, Login R, Tazi M (1992) Hair styling gel composition, WO 1992 002 205 A1
41. Helioff M, Kwak Y, Login R, Tazi M (1993) Hair styling gel composition, EP 19 910 912 160
42. Swift J (1997) Mechanism of split-end formation in human hair. J Soc Cosmet Chem 48:123–126
43. Rigoletto R, Zhou Y, Foltis L (2007) semi-permanent split end mending with a polyelectrolyte complex. J Cosmet Sci 58:451–476
44. Rigoletto R, Zhou Y (2010) Mending hair damage with polyelectrolyte complexes, US 7,837,983 B2
45. Wright M, Szerszen M, Cohen J, Petroski D, Eagan D, Felski C, Verboom G (2010) Hair-mending compositions and associated methods, EP 20 110 834 854
46. Ashland, Inc. (2015) Internal technical data property chart
47. Valdez A (2011) Brazilian hair straightening. Cosmetiscope 17(6):1–7
48. McMullen R, Jachowicz J (1998) Thermal degradation of hair. I. Effect of curling irons. J Cosmet Sci 49:223–244
49. McMullen R, Jachowicz J (1998) Thermal degradation of hair. II. Effect of selected polymers and surfactants. J Cosmet Sci 49:245–256
50. McMullen R, Jachowicz J (2001) Thermal protection of hair keratin, US 6,241,977 B1
51. Zhou Y, Rigoletto R, Koelmel D, Zhang G, Gillece T, Foltis L, Moore D, Qu X, Sun C (2011) The effect of various cosmetic pretreatments on protecting hair from thermal damage by hot flat ironing. J Cosmet Sci 62:265–282
52. Cornwell P, Green P, Bullen R (2011) Hair styling composition, WO 2011 030 096 A2
53. Streuli D (2013) Durable styling compositions and the uses thereof, EP 2 646 539 A1

Maleic Anhydride Chemistry in Applications for Skin Care and Transdermal Delivery

54. McMullen RL (2015) Applications of maleic anhydride chemistry in skin care, biomedical devices, and transdermal delivery. Part I. Cosmetiscope 21(1):1, 4–7
55. McMullen RL (2015) Applications of maleic anhydride chemistry in skin care, biomedical devices, and transdermal delivery. Part II. Cosmetiscope 21(2):1, 4–9

56. McMullen RL (2015) Applications of maleic anhydride chemistry in skin care, biomedical devices, and transdermal delivery. Part III. Cosmetiscope 21(5):1, 6–14
57. McMullen RL (2013) Antioxidants and the skin. Allured Books, Carol Stream, IL
58. Sellers J (1958) Method of preparing adhesive composition comprising a maleic anhydride copolymer and product obtained, US 2,866,772
59. Sellers J (1961) Adhesive salt of an ester of a maleic anhydride copolymer, US 3,005,802
60. Lowey J, Frommherz T (1976) Methyl vinyl ether-maleic ester copolymer, US 3,988,495
61. Russell G, Pelesko J (1992) Pressure sensitive adhesive compositions and elements made therefrom, US 5,106,914
62. Plochocka K, Lynn J (2003) Polymeric hydrogels, US 6,583,225 B1
63. Al-Niaimi F, Beck M, Almaani N, Samarasinghe V, Williams J, Lyon C (2012) The relevance of patch testing in peristomal dermatitis. Br J Dermatol 167:103–109
64. Scalf L, Fowler J (2000) Peristomal allergic contact dermatitis due to gantrez in stomahesive paste. J Am Acad Dermatol 42:355–356
65. Sambasivam M, Crivello J (2012) Amphiphilic silicone copolymers for pressure sensitive adhesive applications, EP 2,451,883 A1
66. Woolfson A, McCafferty D, McCallion C, McAdams E, Anderson J (1995) Moisture-activated, electrically conducting bioadhesive hydrogels as interfaces for bioelectrodes: effect of formulation factors on cutaneous adherence in wet environments. J Appl Polym Sci 56:1151–1159
67. Woolfson A, McCafferty D, McCallion C, McAdams E, Anderson J (1995) Moisture-activated, electrically conducting bioadhesive hydrogels as interfaces for bioelectrodes: effect of film hydration on cutaneous adherence in wet environments. J Appl Polym Sci 58:1291–1296
68. Woolfson A (1996) Moisture-activated, electrically conducting bioadhesive interfaces for biomedical sensor applications. Analyst 121:711–714
69. Witte M, Kiyama T, Barbul A (2002) Nitric oxide enhances experimental wound healing in diabetes. Br J Surg 89:1594–1601
70. Witte M, Barbul A (2002) Role of nitric oxide in wound repair. Am J Surg 183:406–412
71. Lee P, Li Y (2009) Supramacromolecular polymer complexes providing controlled nitric oxide release for healing wounds, WO 2009 026 680 A1
72. Schorr P, Hoffman D, Weart I, Yang K (2011) Skin preparation that immobilizes bacteria, WO 2011 077 281 A2
73. Schorr P, Hoffman D, Weart I, Yang K (2012) Skin preparation that immobilizes bacteria, EP 2,515,783 A2
74. Roh M, Han M, Kim D, Chung K (2006) Sebum output as a factor contributing to the pore size of facial pores. Cutan Biol 155:890–894
75. Crotty B, Miner P, Johnson A, Znaiden A (1999) Cosmetic product for removal of keratotic plugs from skin pores, US 5,968,537
76. Crotty B, Miner P, Johnson A, Znaiden A (2001) Cosmetic product for removal of keratotic plugs from skin pores, US 6,174,536 B1
77. Crotty B, Miner P, Johnson A, Znaiden A, Corey J, Vargas A, Meyers A, and Lange B (1998) Cosmetic product, WO 1998 042 303 A1
78. Quatrale RP, Waldman AH, Rogers JG, Felger CB (1981) The mechanism of antiperspirant action by aluminum salts. I. The effect of cellophane tape stripping on aluminum salt-inhibited eccrine sweat glands. J Soc Cosmet Chem 32:67–73
79. Glogau RG (2001) Treatment of palmar hyperhidrosis with botulinum toxin. Semin Cutan Med Surg 20:101–108
80. Papa C, Kligman A (1967) Mechanism of eccrine anhidrosis. II. The antiperspiratory effect of aluminum salt. J Invest Dermatol 49:139–145
81. Shelley WB, Horvath PN (1950) Experimental miliaria in man. II. Production of sweat retention, anhidrosis and miliaria crystallina by various kinds of injury. J Invest Dermatol 14:9–20

82. Shelley WB, Horvath PN (1950) Experimental miliaria in man. III. Production of miliaria rubra (prickle heat). J Invest Dermatol 14:193–204
83. Shelley WB, Hurley HJ (1975) Studies on topical antiperspirant control of axillary hyperhidrosis. Acta Derm Venereol 55:241–260
84. Reller HH, Luedders WL (1977) Pharmacologic and toxicologic effects of topically applied agents on the eccrine sweat glands. In: Marzulli FN, Maibach HI (eds) Advances in modern toxicology, vol 4, Dermatoxicology and pharmacology. Hemisphere Publishing, Washington, DC
85. Hölzle E, Kligman AM (1979) Mechanism of antiperspirant action of aluminum salts. J Soc Cosmet Chem 30:279–295
86. Hölzle E, Braun-Falco O (1984) Structural changes in axillary eccrine glands following long-term treatment with aluminum chloride hexahydrate solution. Br J Dermatol 110:399–403
87. Quatrale RP, Coble DW, Stoner KL, Felger CB (1981) The mechanism of antiperspirant action by aluminum salts. II. Histological observations of human eccrine sweat glands inhibited by aluminum chlorohydrate. J Soc Cosmet Chem 32:107–136
88. Quatrale RP, Coble DW, Stoner KL, Felger CB (1981) The mechanism of antiperspirant action of aluminum salts. III. Histological observations of human eccrine sweat glands inhibited by aluminum zirconium chlorohydrate glycine complex. J Soc Cosmet Chem 32:195–221
89. Quatrale RP, Thomas EL, Birnbaum JE (1985) The site of antiperspirant action by aluminum salts in the eccrine sweat glands of the axilla. J Soc Cosmet Chem 36:435–440
90. Strassburger J, Coble DW (1987) Infrared characterization of human sweat glands inhibited with aluminum chlorohydrate. J Soc Cosmet Chem 38:109–124
91. Hölzle E, Kligman AM (1979) Factors influencing the anti-perspirant action of aluminum salts. J Soc Cosmet Chem 30:357–367
92. Brun R (1959) Studies on perspiration. J Soc Cosmet Chem 10:70–77
93. Schmid U, Hunziker N, Brun R, Jadassohn W (1964) The protective effect of the sebaceous layer. Br J Dermatol 75:307–319
94. Rieley H, Smith K (2002) Antiperspirant products, US 2002/0,119,108 A1
95. Cropper M (2005) Antiperspirant compositions, US 2005/0,100,521 A1
96. Brown N, Rieley H, Smith I, Stockton J (2006) Antiperspirant emulsion compositions, US 2006/0,051,306 A1
97. Gillece T, Foltis L, Koelmel D, Luschen A, Barrett C (2010) Use of polyelectrolyte complexes in antiperspirant technology, US 2010/0,297,201 A1
98. Fares H, Prettypaul D (2013) Antiperspirant/deodorant compositions, WO 2013 052 454 A1
99. Travedi B, Culbertson B (1982) Maleic anhydride. Plenum, New York
100. Prausnitz M, Langer R (2008) Transdermal drug delivery. Nat Biotechnol 26:1261–1268
101. Chung K, Wu C, Malawer E (1990) Glass transition temperatures of poly(methyl vinyl ether-*co*-maleic anhydride) (PMVEMA) and poly(methyl vinyl ether-*co*-maleic acid) (PMVEMAC) and the kinetics of dehydration of PMVEMAC by thermal analysis. J Appl Polym Sci 41:793–803
102. McCarron P, Woolfson A, Donnelly R, Andrews G, Zawislak A, Price J (2003) Influence of plasticizer type and storage conditions on properties of poly(methyl vinyl-*co*-maleic anhydride) bioadhesive films. J Appl Polym Sci 91:1576–1589
103. Zawislak A, McCarron P, McCluggage W, Price J, Donnelly R, McClelland H, Dobbs S, Woolfson A (2004) Successful photodynamic therapy of vulval Paget's disease using a novel patch-based delivery system containing 5-aminolevulinic acid. BJOG 111:1143–1145
104. McCarron P, Donnelly R, Zawislak A, Woolfson A, Price J, McClelland H (2005) Evaluation of a water-soluble bioadhesive patch for photodynamic therapy of vulval lesions. Int J Pharm 293:11–23
105. Donnelly R, Ma L-W, Juzenas P, Iani V, McCarron P (2006) Topical bioadhesive patch systems enhance selectivity of protoporphyrin IX accumulation. Photochem Photobiol 82:670–675

106. Singh T, McCarron P, Woolfson A, Donnelly R (2009) Physicochemical characterization of poly(ethylene glycol) plasticized poly(methyl vinyl ether-*co*-maleic acid) films. J Appl Polym Sci 112:2792–2799
107. Singh T, McCarron P, Woolfson A, Donnelly R (2009) Investigation of swelling and network parameters of poly(ethylene glycol)-crosslinked poly(methyl vinyl ether-*co*-maleic acid) hydrogels. Eur Polym J 45:1239–1249
108. Singh T, Woolfson A, Donnelly R (2009) Investigation of solute permeation across hydrogels composed of poly(methyl vinyl ether-*co*-maleic acid) and poly(ethylene glycol). J Pharm Pharmacol 62:829–837
109. Garland M, Singh T, Woolfson A, Donnelly R (2011) Electrically enhanced solute permeation across poly(ethylene glycol)-crosslinked poly(methyl vinyl ether-*co*-maleic acid) hydrogels: effect of hydrogel cross-link density and ionic conductivity. Int J Pharm 406:91–98
110. Singh T, Garland M, Migalska K, Salvador E, Shaikh R, McCarthy H, Woolfson A, Donnelly R (2012) Influence of a pore-forming agent on swelling, network parameters, and permeability of poly(ethylene glycol)-crosslinked poly(methyl vinyl ether-*co*-maleic acid) hydrogels: application in transdermal delivery systems. J Appl Polym Sci 125:2680–2694
111. Luppi B, Cerchiara T, Bigucci F, Di Pietra A, Orienti I, Zecchi V (2003) Crosslinked poly (methyl vinyl ether-*co*-maleic anhydride) as topical vehicles for hydrophilic and lipophilic drugs. Drug Deliv 10:239–244
112. Boehm R, Miller P, Singh R, Shah A, Stafslien S, Daniels J, Narayan R (2012) Indirect rapid prototyping of antibacterial acid anhydride copolymer microneedles. Biofabrication 4 (1):011002. doi:10.1088/1758-5082/4/1/011002
113. Gomaa Y, El-Khordagui L, Garland M, Donnelly R, McInnes F, Meidan V (2012) Effect of microneedle treatment on the skin permeation of a nanoencapsulated dye. J Pharm Pharmacol 64(11):1592–1602. doi:10.1111/j.2042-7158.2012.01557.x
114. Gomaa Y, Garland M, McInnes F, El-Khordagui L, Wilson C, Donnelly R (2012) Laser-engineered dissolving microneedles for active transdermal delivery of nadroparin calcium. Eur J Pharm Biopharm 82(2):299–307. doi:10.1016/j.ejpb.2012.07.008
115. Donnelly R, Garland M, Morrow D, Migalska K, Singh T, Majithiya R, Woolfson A (2010) Optical coherence tomography is a valuable tool in the study of the effects of microneedle geometry on skin penetration characteristics and in-skin dissolution. J Control Release 147 (3):333–341. doi:10.1016/j.jconrel.2010.08.008
116. Migalska K, Morrow D, Garland M, Thakur R, Woolfson A, Donnelly R (2011) Laser-engineered dissolving microneedle arrays for transdermal macromolecular drug delivery. Pharm Res 28(8):1919–1930. doi:10.1007/s11095-011-0419-4
117. Donnelly R, Singh T, Garland M, Migalska K, Majithiya R, McCrudden C, Kole P, Mahmood T, McCarthy H, Woolfson A (2012) Hydrogel-forming microneedle arrays for enhanced transdermal drug delivery. Adv Funct Mater 22:4879–4890
118. Donnelly R, Mooney K, McCrudden M, Vicente-Pérez E, Belaid L, González-Vázquez P, McElnay J, Woolfson A (2014) Hydrogel-forming microneedles increase in volume during swelling in skin, but skin barrier function recovery is unaffected. J Pharm Sci 103:1478–1486
119. Singh T, Garland M, Migalska K, Salvador E, Shaikh S, McCarthy H, Woolfson A, Donnelly R (2012) Influence of a pore-forming agent on swelling, network parameters, and permeability of poly(ethylene glycol)-crosslinked poly(methyl vinyl ether-*co*-maleic acid) hydrogels: application in transdermal delivery systems. J Appl Polym Sci 125:2680–2694
120. Shroff K, Vidyasagar A (2013) Polymer nanoparticles: newer strategies towards targeted cancer therapy. J Phys Chem Biophys 3:125. doi:10.4172/2161-0398.1000125
121. Soppimath K, Aminabhavi T, Kulkarni A, Rudzinski W (2001) Biodegradable polymeric nanoparticles as drug delivery devices. J Control Release 70:1–20
122. Guterres S, Alves M, Pohlmann A (2007) Polymeric nanoparticles, nanospheres and nanocapsules, for cutaneous applications. Drug Target Insights 2:147–157

123. Arbós P, Arangoa M, Campanero M, Irache J (2002) Quantification of the bioadhesive properties of protein-coated PVM/MA nanoparticles. Int J Pharm 242:129–136
124. Arbós Vila P, Merodio de la Quintana M (2002) Production of nanoparticles from methyl vinyl ether copolymer and maleic anhydride for the administration of hydrophilic pharmaceuticals, more particularly of puric and pyrimidine bases, EP 1 369 110 A1
125. Salman H, Azcarate I (2012) Nanoparticles comprising esters of poly(methyl vinyl ether-co-maleic anhydride) and uses thereof, WO2012 140 252
126. Irache Garreta J, Gamazo de la Rasilla C, Sanz Larruga M, Ferrer Puga M, San Roman Aberasturi B, Salman H, Gomez Martinez S, Ochoa Reparaz J (2007) Immune response stimulating composition comprising nanoparticles based on a methyl vinyl ether-maleic acid copolymer, US 2007/0,224,225 A1
127. Xing J, Deng L, Li J, Dong A (2009) Amphiphilic poly {[α-maleic anhydride-ω-methoxy-poly(ethylene glycol)]-*co*-(ethyl cyanoacrylate)} graft copolymer nanoparticles as carriers for transdermal drug delivery. Int J Nanomed 4:227–232
128. Dessy A, Kubowicz S, Alderighi M, Bartoli C, Piras A, Schmid R, Chiellini F (2011) Dead Sea minerals loaded polymeric nanoparticles. Colloid Surf B Biointerfaces 87:236–242
129. Deng L, Yao C, Li A, Dong A (2005) Preparation and characterization of poly{[α-maleic anhydride-ω-methoxy-poly(ethylene glycol)]-*co*-(ethyl cyanoacrylate)} copolymer nanoparticles. Polym Int 54:1007–1013
130. Zhai Y, Qiao Y, Xie C, Lin L, Ma Y, Dong A, Deng L (2008) Preparation and in vitro release of D, L-tetrahydropalmatine-loaded graft copolymer nanoparticles. J Appl Polym Sci 110:3525–3531
131. Kim K, Kim K-S, Kim H, Lee S, Park J-H, Han J-H, Seok S-H, Park J, Choi Y, Kim Y, Han J, Son J-H (2012) Terahertz dynamic imaging of skin drug absorption. Opt Express 20 (9):9476–9484
132. Chiellini F, Piras A, Gazzarri M, Bartoli C, Ferri M, Paolini L, Chiellini E (2011) Bioactive polymeric materials for targeted administration of active agents: synthesis and evaluation. Macromol Biosci 8:516–525
133. Bekele H (2002) Topical composition comprising a functionalized acid anhydride-based cosmetic bonding agent, US 6,495,150 B2
134. Tonge S (2009) Compositions comprising a lipid and copolymer of styrene and maleic acid, US 2009/0,155,375 A1
135. Tonge S (2014) Compositions comprising a lipid and copolymer of styrene and maleic acid, US 8,623,414 B2
136. Tonge S, Tighe B (2002) Lipid-containing compositions and uses thereof, US 6,436,905 B1
137. Tonge S, Tighe B (2001) Responsive hydrophobically associating polymers: a review of structure and properties. Adv Drug Deliv Rev 53:109–122
138. Force C, Starr F (1986) Vegetable oil adducts as emollients in skin and hair care products, WO 1996 000 800 A1
139. Bertz S, Miksza F, Zucker E (2001) High purity adduct of castor oil and maleic anhydride, US 6,225,485 B1
140. Spina M, Carnelos C, Leo C, Faria J (2008) A non-rinse off cosmetic composition and a cosmetic product comprising said composition, US 2008/0,193,396 A1
141. Potechin K, Boyke C (2013) Foaming cleanser, US 2013/0,137,619 A1
142. Harmalker S, Ash K (2014) Moisturizing compositions, US 8,703,160 B2
143. Lu G, Moore D (2013) Measuring changes in skin barrier function with skin impedance. HPC Today 8(1):28–31
144. Moore D, Orofino S, Antonopoulos P (2006) Maintaining moisturization from rinse-off products. HAPPI (November), 77–81
145. Musa O, Khosravi E (2013) Renewable modified natural compounds, US 2013/0,289,284 A1
146. Coats C (1969) Electrocoating compositions comprising of aromatic amine amidated drying oil copolymer-maleic anhydride adducts, US 3,428,589

147. Thames S, Smith O, Evans J, Dutta S, Chen L (2008) Functionalized vegetable oil derivatives, latex compositions and coatings, US 7,361,710 B2
148. Aydin S, Akçay H, Özkan E, Seniha Güner F, Tuncer Erciyes A (2004) The effects of anhydride type and amount on viscosity and film properties of alkyd resin. Prog Org Coat 51:273–279
149. Seniha Güner F, Yağcı Y, Tuncer Erciyes A (2006) Polymers from triglyceride oils. Prog Polym Sci 31:633–670
150. Musa O, Narayanan K, Shih J, Qu X, Zhang T, Onnembo G (2013) Self-emulsifying oil, US 2013/0,210,630 A1
151. Vanlerberghe G, Sebag H (1976) Cosmetic compositions for the skin containing a chitosan derivative, US 3,953,608
152. Zhong C, Wu J, Reinhart-King C, Chu C (2010) Synthesis, characterization and cytotoxicity of photo-crosslinked maleic chitosan-polyethylene glycol diacrylate hybrid hydrogels. Acta Biomater 6:3908–3918
153. Hollingshurst C, Price D, Steckel T, Filippini B, Huang N (2006) Low color polyisobutylene succinic anhydride-derived emulsifiers, US 2006/0,223,945 A1
154. Rieger M (2000) Skin cleansing products. In: Rieger M (ed) Harry's Cosmeticology. Chemical Publishing, New York
155. Chaussee J (1986) Cleansing compositions containing alpha olefin/maleic anhydride terpolymers, US 4,603,005
156. Verbrugge C (1982) Waxy maleic anhydride alpha olefin terpolymers, US 4,358,573
157. Chaussee J (1985) Cleansing compositions containing alpha olefin/maleic anhydride terpolymers, EP 0 182 369 A2
158. G. Sonenstein (1981) Soap bar, US 4,265,778
159. Chen LH (1989) Interaction of vitamin E and ascorbic acid (review). In Vivo 3:199–209
160. Biatry B (2004) Oxidation-sensitive hydrophilic active principle containing composition and use thereof, US 2004/0,047,824 A1
161. Kameyama K, Sakai C, Kondoh S, Yonemoto K, Nishiyama S, Tagawa M, Murata T, Ohnuma T, Quigley J, Dorsky A, Bucks D, Blanock K (1996) Inhibitory effect of magnesium l-ascorbyl-2-phosphate (VC-PMG) on melanogenesis in vitro and in vivo. J Am Acad Dermatol 34:29–33
162. Biatry B (2004) Cosmetic and/or dermatological use of a composition comprising at least one oxidation-sensitive hydrophilic active principle stabilized by at least one maleic anhydride copolymer, US 2004/0,001,792 A1
163. Biatry B (2004) Composition containing oxidation-sensitive hydrophilic active principle and maleic anhydride copolymer and use thereof, US 2004/0,042,990 A1
164. Biatry B (2004) Process of making and using composition containing oxidation-sensitive hydrophilic active principle and maleic anhydride copolymer, US 2004/0,175,342 A1
165. Biatry B (2004) Cosmetic and/or dermatological use of a composition containing at least one oxidation-sensitive hydrophilic active principle stabilized by at least one maleic anhydride copolymer, US 2004/0,052,739 A1
166. Biatry B (2010) Oxidation-sensitive hydrophilic active principle containing composition and use thereof, US 7,691,903 B2
167. Biatry B (2010) Cosmetic and/or dermatological use of a composition comprising at least one oxidation-sensitive hydrophilic active principle stabilized by at least one maleic anhydride copolymer, US 7,803,354 B2
168. Carrera M, Primavera G, Berardesca E (2006) Alpha hydroxy acids. In: Paye M, Barel A, Maibach H (eds) Handbook of cosmetic science and technology (2nd edn). Taylor & Francis, New York
169. Chaudhuri R, Bower D (1998) Cosmetic composition for rejuvenation of skin without skin irritation, US 5,736,128
170. Prosise W, Plochocka K (2001) Cosmetic composition for rejuvenation of skin without skin irritation, US 6,312,714 B1

171. Black A, Feinstone W (1974) Sunscreen preparation employing ethylene-maleic anhydride copolymers, US 3,821,363
172. Kwak Y, Kopolow S, Helioff M, Tazi M (1992) Sunscreen composition, US 5,145,669
173. Musa O, Shih J (2013) Performance-boosting UV-absorbing compounds, US 8,557,226 B2
174. Ozkan S, Gillece T, Senak L, Moore D (2012) Characterization of yield stress and slip behaviour of skin/hair care gels using steady flow and LAOS measurements and their correlation with sensorial attributes. Int J Cosmet Sci 34:193–201
175. Tadros T (2006) Principles of emulsion stabilization with special reference to polymeric surfactants. Int J Cosmet Sci 57:153–169
176. Goertz H-H, Raubenheimer H-J, Denzinger W (1990) Preparation of copolymers of ethylenically unsaturated dicarboxylic anhydrides and alkyl vinyl ethers, US 4,952,558
177. Gripp A, Helioff M, Kwak Y (1996) Stabileze PVM/MA decadiene crosspolymers: versatile thickeners for skin care formulations. *Cosmet Toilet Manf Worldwide*, 115–118
178. Osborne D (2000) Topical antibiotic composition for rapid wound healing, EP 0,987,019 A1
179. Evison J, Rhowbotham S (2013) Depilatory compositions, US 2013/0,205,514 A1
180. Cauwet D, Dubief C (1998) Cosmetic composition containing at least one surface-active agent of the alkyl polyglycoside and/or polyglycerolated type and at least one crosslinked copolymer of maleic anhydride (C1-C5) alkylvinyl ether, US 5,744,147
181. Helioff M, Tazi M, Kwak Y, Login R (1991) Creamy nail polish remover containing hydrolyzed and neutralized maleic anhydride C1-C4 alkyl vinyl ether copolymer, US 5,024,779
182. Helioff M, Tazi M, Login R, Kwak Y (1991) Hair styling gel composition, US 5,032,391
183. Kwak Y, Kopolow S (1993) Rapid hydrolysis of crosslinked maleic anhydride/lower alkyl vinyl ether copolymers, US 5,254,636
184. Kwak Y, Kopolow S (1996) Process for hydrolyzing and neutralizing a crosslinked polymer of maleic anhydride and a C1–C5 alkyl vinyl ether, optionally with a hydrophobic monomer, substantially instantly at room temperature, US 5,521,256
185. Kwak Y, Kopolow S, Login R (1996) Process for the preparation of stable water based stock solutions of crosslinked lower alkyl vinyl ether and maleic anhydride copolymers and hydrogel product of the process, US 5,516,828
186. Kiatkamjornwong S, Mongkolsawat K, Sonsuk M (2002) Synthesis and property characterization of cassava starch grafted poly[acrylamide-*co*-(maleic acid)] superabsorbent via γ-irradiation. Polymer 43:3915–3924
187. Koulbanis C, Zabotto A, Contamin J-C (1977) Gels based on vinyl ether-maleic anhydride copolymer neutralized by a basic amino acid, US 4,010,254
188. Feinstone W, Black A (1970) Method of wrinkle smoothing, US 3,523,998
189. Jachowicz J, McMullen R, Zolotarsky Y, Prettypaul D (2005) Skin tightening with polymer-containing formulations. Mechanical skin indentation, photography-image analysis, and panel testing. In: Cosmetic science technology. T Four Group, London, pp 206–215
190. Jachowicz J, McMullen R, Prettypaul D (2008) Alteration of skin mechanics by thin polymer films. Skin Res Technol 14:312–319

Maleic Anhydride Chemistry in Oral Care

191. Roy S, Prabhakar B (2010) Bioadhesive polymeric platforms for transmucosal drug delivery systems – a review. Trop J Pharm Res 9(1):91–104
192. Gregory J, Polymers at interfaces, by G.J. Fleer, M.A. Cohen Stuart, J.M.H.M. Scheutjens, T. Cosgrove and B. Vincent. Chapman and Hall, London, 1993, pp xv + 502, price £65.00. ISBN 0-412-58160-4. Polym Int 1995, 36(1):102

193. Guzmán E, Ortega F, Baghdadli N, Cazeneuve C, Luengo G, Rubio R (2011) Adsorption of conditioning polymers on solid substrates with different charge density. ACS Appl Mater Interfaces 3(8):3181–3188
194. Silva R, Urzúab M, Petri D (2009) Lysozyme binding to poly(4-vinyl-N-alkylpyridinium bromide). J Colloid Interf Sci 330(2):310–316
195. Van de Steeg H, Cohen Stuart M, De Keizer A, Bijsterbosch B (1992) Polyelectrolyte adsorption: a subtle balance of forces. Langmuir 8(10):2538–2546
196. Rojas O, Ernstsson M, Neuman R, Claesson P (2002) Effect of polyelectrolyte charge density on the adsorption and desorption behavior on mica. Langmuir 18(5):1604–1612
197. Alexander A, Ajazuddin S, Mukesh S, Tripathi D (2011) Polymers and permeation enhancers: specialized components of mucoadhesives. Stamford J Pharm Sci 4(1):91–95
198. www.TheCosmeticChemist.com
199. Hicks J, Garcia-Godoy F, Flaitz C (2004) Biological factors in dental caries enamel structure and the caries process in the dynamic process of demineralization and remineralization (part 2). J Clin Pediatr Dent 28(2):119–124
200. ten Cate J (2006) Biofilms, a new approach to the microbiology of dental plaque. Odontology 94(1):1–9
201. Van Nieuw Amerongen A, Bolscher J, Veerman E (2004) Salivary proteins: protective and diagnostic value in cariology? Caries Res 38:247–253
202. Jin Y, Yip H-K (2002) Supragingival calculus: formation and control. Crit Rev Oral Biol Med 13(5):426–441
203. Germann D, Krops E, King R, Stickney P (1961) Stabilizer for dentures, US 3,003,988
204. Tazi M, Login R, Kwak Y, Gangadharan B, Haldar R (1991) Denture adhesive, US 5,037,924
205. Schobel AA, Kumar L (1992) Cationic derivative of guar gum, sodium-calcium salt of maleic anhydride-methyl vinyl ether copolymer, sodium carboxymethyl cellulose, US 5,093,387
206. Kumar L, Schobel A (1990) Denture adhesives and methods for preparing same, US 4,980,391
207. Chang AT-S, Zientek L, Viningauz A, Scheps M (1983) Denture fixative composition, US 4,373,036
208. Synodis J, Smetana A, Gasman R, Wong E, Clarke H (1998) Denture adhesive composition, US 5,830,933
209. Borja M (2011) Hydrogel denture adhesive, US 2011/0,065,831
210. Borja M (2013) Gantrez hydrogel with dry tack, US 2013/0,195,771 A1
211. Saunders G, MacCreath B (2010) Analysis of water soluble polymers in denture adhesives by SEC. Agilent Technologies; application note; www.agilent.com/chem

Chapter 9
Application of Maleic Anhydride in Coatings, Adhesives and Printing

David K. Hood and Osama M. Musa

9.1 Introduction

The mass production capabilities coupled with a broad synthetic platform have powered maleic anhydride to an incredibly diverse range of commercial applications. Applications so vast, its broad detailed discussion is well beyond the ability of one book chapter to capture. Consequently, this chapter is written more as a survey, covering many of the most important maleic anhydride applications while discussing a few specific topics in more detail. It is our hope that the reader will finish this chapter with a greater appreciation for the broad applicability and emerging potential for maleic anhydride.

9.2 Coatings

Maleic anhydride's use in coating technology is widespread. From automotive and architectural coatings to antimicrobial and anti-adhesive coatings, there are many opportunities for the use of maleic anhydride chemistry. Most coatings are comprised on several key components. Each component delivers distinctive functionality. Functionalities often perform in concert with the other ingredients to yield the final application performance attributes. Among the most common components are pigments, binders, rheology modifiers, dispersants, and biocides. From these basic ingredients, the various functional features of maleic anhydride will be further elucidated.

D.K. Hood (✉) • O.M. Musa
Ashland Inc., 1005 Route 202/206, Bridgewater, NJ 08807, USA
e-mail: dhood@ashland.com

O.M. Musa (ed.), *Handbook of Maleic Anhydride Based Materials*,
DOI 10.1007/978-3-319-29454-4_9

9.2.1 *Binders: Alkyd Resins*

Alkyd resins are the reaction product of fatty acids, polyols, and dibasic acids. When the applied coating resin is exposed to air, the corresponding film undergoes an auto-oxidative drying process. A common example of an oxidizing alkyd is a composition comprised of soybean fatty acids, glycerol, and phthalic anhydride. The auto-oxidative drying process is a process whereby free radicals abstract hydrogens on methylene groups located between the double bonds, which can be repeated, ultimately forming covalent cross-links, enabling curing of the film. Metal driers, such as cobalt and manganese salts, are often added to these coatings to increase the rate of the auto-oxidation process. With this simple example, maleic anhydride is reported to be added to alkyd resin systems to impart better adhesive properties coupled to increase drying speed [1].

An example of how maleic anhydride is typically incorporated and used in an alkyd-type coating is demonstrated with a modified styrene–acrylic polymer. Firstly, a multicomponent copolymer of styrene, acrylate, and maleic anhydride monomers is prepared via conventional free radical polymerization. Coupled to this copolymer is an additional additive component, the separate reaction product of various unsaturated, olefinic, monocarboxylic acids and an aminoalkyl alcohol. This product is reported to be in the form of a hydroxyalkyl amide. During the complex synthetic process, these additive amide moieties are found to rearrange to ester moieties, where the original amide nitrogen enables the subsequent formation of an imide group. The idealized, final product is represented below [2, 3].

More specifically, the additive component is comprised of a mixture of soybean oil fatty acids, or soya fatty acids, and a conjugated unsaturated C_{18} monocarboxylic acid, such as Konjuvandol fatty acid from Henkel AG, which are further reacted with an aminoalkyl alcohol, i.e., aminoethanol, enabling the formation of hydroxyethyl amide-derived compounds. The polyimide functionality is then obtained by the reaction of these various additive components with the modified styrene–acrylic copolymer, which results in a rearrangement effect enabling the formation of polyimide compositions, as depicted in Scheme 9.1. Note that R is the esterified residues of soybean oil fatty acids as well as the conjugated unsaturated C_{18} monocarboxylic acid. This imide-modified styrene–acrylic copolymer is then combined with naphtha solvent and an oxime-based antiskinning agent (Ascinin R Conz. Bayer AG). The equivalent ratio of anhydride groups to nitrogen was 1:1.13. A comparative system was designed with another similar styrene–acrylic

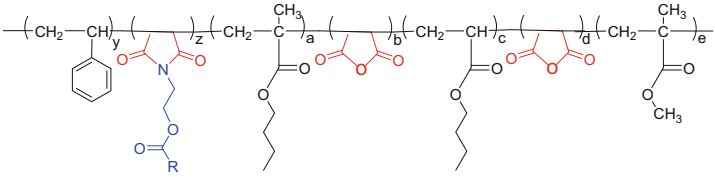

Scheme 9.1 Proposed structure of styrene–acrylate–maleic anhydride imidized alkyd polymer

Table 9.1 Performance properties of resins capable of oxidative cross-linking [2]

Property	Example 1	Example 2
Styrene/maleic anhydride/*n*-butyl methacrylate/*n*-butyl acrylate/methyl methacrylate	27/19/6/15/28[a]	NA
Styrene/maleic anhydride/*n*-butyl methacrylate/*n*-butyl acrylate/methyl methacrylate	NA	22/24.75/x/23.1/26.3[a]
Percent of imide formed in polymer (weight %)	48 %	60 %
Solution viscosity (62 % solids, 23 °C) (mPa s)	1100 (in naphtha)	4500 (in xylenes)
Paint solids	63 %	55 %
Drying hours (180 μm wet film, room temperature)	2.5	3
Gardner gloss (20°)	79	76
Feel	No feel, non-tacky	No feel, non-tacky
Konig pendulum hardness (seconds)		
2 days at room temperature	32	21
7 days at room temperature	52	27
Erichsen elasticity (mm) after 1 day at 70 °C	9.0	9.0
Resistance to premium gasoline (1 min) after 16 h at room temperature (0 = 0 dissolution; 5 = heavily dissolved)	4	2
Adhesion to steel plates after 3 days at room temperature (0 = best value; 5 = worst value)	0	1

[a]Weight percent. Balance is t-butyl peroctoate initiator

copolymer and the additive composition but employing xylene as the coating solvent [2]. To these polymeric compositions, TiO_2 [1–0.8 (binder to TiO_2)] and octoate-based drying aids (calcium, lead, and cobalt) were added. This final coating composition was ground in a bead mill and further diluted with white spirit and xylene mixtures to comparable DIN 4 mm cup flow times, thereby matching the viscosity. Prior to application, the composition was further diluted to enable a spray-applied coating on glass and steel plates. Application results for these coatings are presented in Table 9.1.

In this example, both coatings comprise maleic anhydride, but the first example exhibits improved performance. The performance differences could be attributed to the level of imide present, where results suggest higher imide levels improved overall performance. Other coatings presented in this research, but not in Table 9.1, illustrate acceptable performance with comparably high, ~60 %, imide formation. It is possible that the molecular weight requires some suppression in order to get the proper balance of film formation properties and cross-link density. These results do highlight the importance of balanced compositional and physical properties to achieve required coating performance parameters in a commercially viable finished coating. Nevertheless, these maleic anhydride-based polymers have demonstrated the capability to form an adhesive, insoluble, gasoline-resistant coating through the oxidative cross-linking of unsaturated, olefinic monocarboxylic acid moieties.

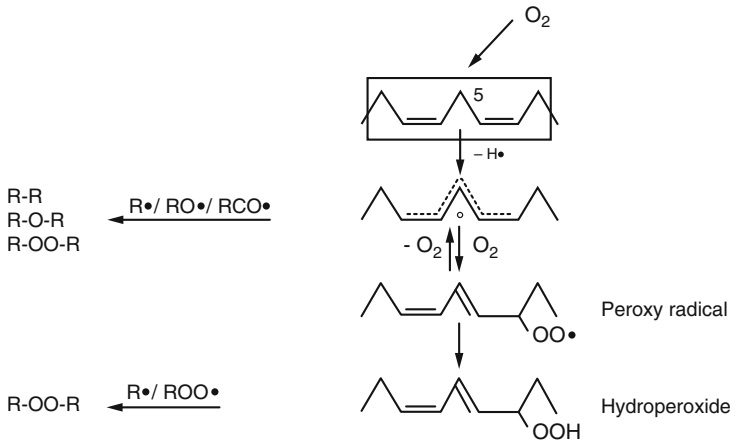

Scheme 9.2 Mechanism of oxidative cross-linking [4]. Reprinted from Progress in Organic Coatings, 35, Zabel, K.H.; Klaasen, R.P.; Muizebelt, W.J.; Gracey, B.P.; Hallett, C.; Brooks, C. D., "Design and incorporation of reactive diluents for air-drying high solids alkyd paints," pages 255–264, Copyright **1999**, with permission from Elsevier

In the alkyd coating oxidation process, a hydrogen atom is easily abstracted from an allylic methylene, resulting in the formation of a free radical. The free radical can proceed to react with atmospheric oxygen, forming peroxy radicals. Ultimately, the peroxy radical forms a hydroperoxide moiety. The net result is the formation of a chain reaction capable of forming new C–O–C, C–O–O–C, and C–C bonds. A schematic of the oxidative cross-linking process is presented in Scheme 9.2.

Once the radical is formed, it can then proceed to form new covalent bonds with other unsaturated moieties. Radical formation initiates the process of polymer network formation and ultimately reduces the solubility and solvent sensitivity of the polymer. This effect is successfully demonstrated with the unsaturated olefin moieties which are incorporated into styrene–acrylate copolymer, via maleimide formation, coupled with esterification of the monocarboxylic acid. The coating product transitions from a soluble polymer to an insoluble, thermoset film which was insoluble to gasoline.

While such coatings are functionally capable of meeting many stringent economic and performance requirements (i.e., cost, functionality, ease of use), there are some significant limitations. The modern trend in coatings is to eliminate heavy metals (i.e., cobalt and especially lead) in addition to minimizing and/or eliminating volatile organic compounds (VOCs) (i.e., naphtha and xylene solvents). Consequently, the prior example is best considered as instructive to a general coating design strategy but of limited practical use. How has maleic anhydride helped scientists successfully meet these current coating trends?

One approach to reducing or eliminating VOC content in alkyd coatings is to employ reactive diluents in place of solvents. In order for this strategy to be effective, the reactive diluents must exhibit the following attributes: (1) high

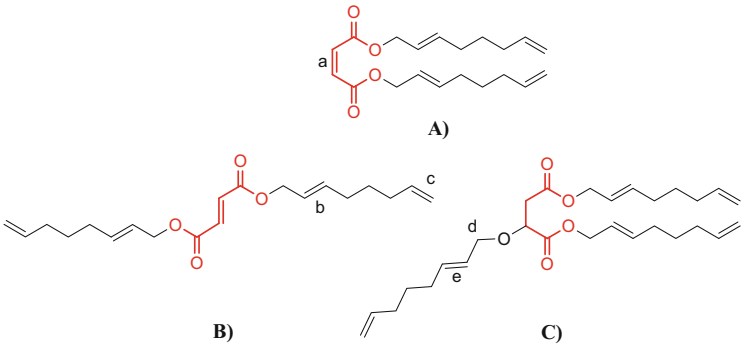

Fig. 9.1 Maleate-, fumarate-, and succinate-derived reactive diluents [4]

boiling point (>300 °C); (2) reactivity comparable to normal alkyd drying rates; (3) capable of polymerization with linoleic acid, either via homo- or copolymerization; (4) low viscosity; (5) good resin compatibility; (6) low order of toxicity; (7) low color; and (8) economical [4, 5]. With these attributes in mind, reactive diluents based upon octadienyl maleate, fumarate, and succinate have been developed. The chemical structures of these reactive diluents are presented in Fig. 9.1.

A few distinct features become readily apparent upon examining the compounds presented in Fig. 9.1. Structures A and B are *cis*/*trans* isomers of the maleic acid ester while maintaining the acrylate-like double bond (a). Both A and B structures also comprise olefinic double bonds (b) and (c). On the other hand, structure C loses the acrylate-like double bond but gains more and different olefinic double bonds (e), as a consequence of the Michael addition of 2,7-octadienol to the (a)-type double bond. Another distinction is the oxidizable C–H bonds (d) that can be an additional source for free radical initiation. The allylic ether group (e) is unique among the olefinic double bonds of these compounds and more reactive than the allylic ester groups (b) [4].

The variation in reactive features of these reactive diluents, in addition to the allyloxysuccinate, enabled an effective paint system to be designed and exhibit excellent performance characteristics [4]. For example, a reactive diluent comprising of 11 % (w/w) di-(2,7-octadienyl) maleate (Fig. 9.1a), 43 % (w/w) di-(2,7-octadienyl) fumarate (Fig. 9.1b), and 41 % (w/w) 2-(2,7-octadienoxy) di-(2,7-octadienyl) succinate (Fig. 9.1c) was added to a high-solid alkyd resin system. Specifically, 30 % (w/w) of the reactive diluent was added to Setal 293®, a long oil alkyd resin with the following properties: min 99 % nonvolatile, viscosity of 1 Pa s at 23 °C, unsaturated fatty acid-type oil, and color =4 [6]. The final coating design is presented in Table 9.2.

The coating drying performance and weight measurements, for additional evidence of the reactive diluents' entrainment to the coated film, are presented in Table 9.3.

These performance results demonstrate acceptable drying rates and negligible weight change of the coating film. Essentially, the reactive diluent-modified alkyd

Table 9.2 Alkyd coating composition employing reactive diluents [7]

Ingredient	Coating 1 (grams)	Coating 2 (grams)
Setal® 293	70	100
Reactive diluents	30	–
Siccarol® 938 drier	6.7	6.7
Methyl ethyl ketoxime	0.5	0.5
Diluent	Reactive diluents to target viscosity	White spirit (Exxon 100) to target viscosity
Application viscosity (Pa s)	0.68 ± 0.03	0.68 ± 0.03

Table 9.3 Performance attributes of alkyd coating with reactive diluents compositions or white spirits [7]

Coating	Drying time (hours) (paint stored for 1 week at 23 °C)	Weight% remaining of coated film after 195 h
1	5.69	100.03
2	3.9	97.28

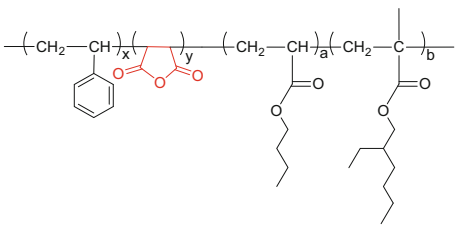

Fig. 9.2 Copolymer of styrene, maleic anhydride, *n*-butyl acrylate, and 2-ethyl hexyl methacrylate (poly(styrene-*co*-maleic anhydride-*n*-butyl acrylate-2-ethyl hexyl methacrylate)

coating performs as a 100 % solid coating, with little or no VOC. While a promising development, later testing reported that these films, when aged, can be susceptible to yellowing and embrittlement. A more recent approach to addressing these issues utilizes reactive diluents based upon derivatives of malonates, but these materials are beyond the scope of this chapter [8].

9.2.2 Binders: Styrene–Acrylic–Maleic Anhydride

Aqueous-based styrene–acrylic–maleic anhydride coatings, which are self-cross-linking, have been developed utilizing maleic anhydride functionality. For example, a copolymer comprising styrene, maleic anhydride, *n*-butyl acrylate, and 2-ethyl hexyl methacrylate was prepared. This copolymer is presented in Fig. 9.2 [9].

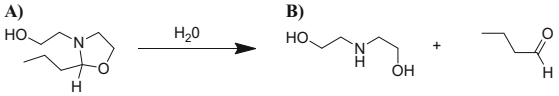

Scheme 9.3 Hydrolysis of oxazolane product of diethanolamine and isobutyraldehyde

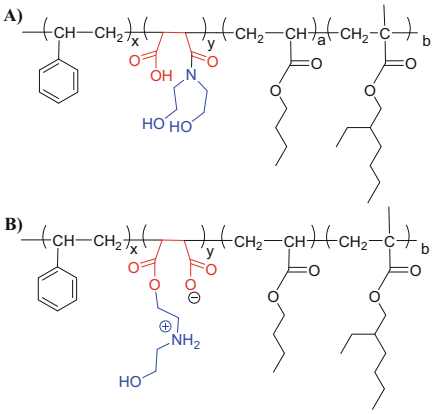

Fig. 9.3 Proposed reaction products of poly(styrene-*co*-maleic anhydride-*n*-butyl acrylate-2-ethyl hexyl methacrylate) with diethanolamine

Targeting the reaction of the anhydride functionality, where succinic anhydride is derived from the maleic anhydride, the copolymer in Fig. 9.2 was combined with the reaction product of diethanolamine and isobutyraldehyde. The corresponding oxazolane reaction product is depicted in Scheme 9.3a [10, 11].

The process to combine oxazolane with poly(styrene-*co*-maleic anhydride-*n*-butyl acrylate-2-ethyl hexyl methacrylate) involves heating in a naphtha and water mixture. As a result, the oxazolane and the succinic anhydride can hydrolyze to yield diethanolamine, isobutyraldehyde (see Scheme 9.3b), and succinic acid. Upon azeotropic removal of the water (with xylenes) (note that the liberated isobutyraldehyde is also expected to be removed at this time), the succinic acid reacts with the diethanolamine to form new amide (Fig. 9.3a) and ester (Fig. 9.3b) bonds. Proposed structures are presented in Fig. 9.3 [12].

Because of the multifunctional nature of succinic acid and diethanolamine, it becomes readily apparent that from beyond the first new covalent bond formations, subsequent covalent bond formations are also possible, either via amidation or esterification reactions. Thus, a self-cross-linking polymer system is formed. This polymer is diluted in water to 30 % solids. This coating system does not require organic solvents, VOC neutralization agents, or blocking agents to yield good performance characteristics [9]. The self-cross-linking polymer was applied to glass, with a wet film thickness of 210 μm, and allowed to air-dry for 15 min at room temperature. Then the coating is placed in an oven for 30 min at 140–150 °C to yield a condensation-type, cross-linked coating that demonstrates high-quality

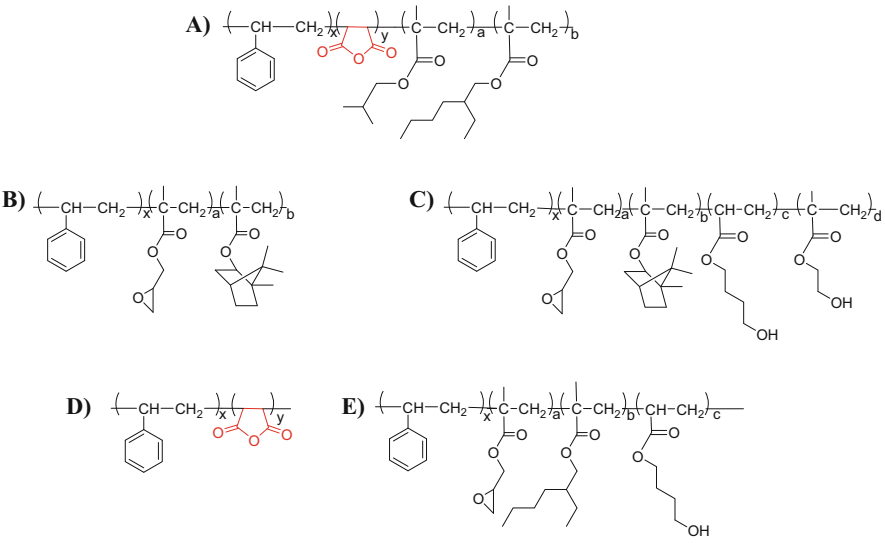

Fig. 9.4 Various copolymer structures suitable for an acid rain-resistant automotive topcoat [13]

water and solvent resistance (i.e., no visible effects after 300 double wipes with acetone), which is further evidence of film cure.

Self-cross-linking styrene–acrylic–maleic anhydride automotive topcoats have also been the subject of renewed interest. Especially where there is a requirement for strong acid rain resistance performance. In one study, half-esters of maleic anhydride copolymers were developed and evaluated in the context of a mar-resistant clear coating. Examples are given for a variety of useful copolymer structures for styrene, maleic anhydride, isobutyl methacrylate, isobornyl methacrylate, 2-hydroxyethyl methacrylate, 2-ethylhexyl methacrylate, 4-hydroxybutyl acrylate, and glycidyl methacrylate. The structures for these copolymers are presented in Fig. 9.4.

The anhydride group is known to react with epoxide groups, resulting in the formation of new ester moieties. Likewise, the anhydride group is also well known to react with hydroxyl groups which also result in the construction of ester bonds and are commonly referred to as "half-ester." This process can proceed rapidly at room temperature. However, recyclization of the half-ester bond to the anhydride requires additional heating. To better understand this effect, a variety of primary alcohols were employed to determine not only suitability for half-ester formation but also capability to efficiently recyclize to anhydride at 120 °C [13]. Specific examples for several alcohols are presented in Scheme 9.4.

In determining the efficiency of formation of half-ester copolymers, three different primary alcohols—half-esters—were prepared and studied. Their subsequent ability to reform the anhydride was also evaluated by heating the polymeric film to 120 °C for 30 min and then analyzing the film composition via IR spectroscopy. The results of these various experiments are presented in Table 9.4.

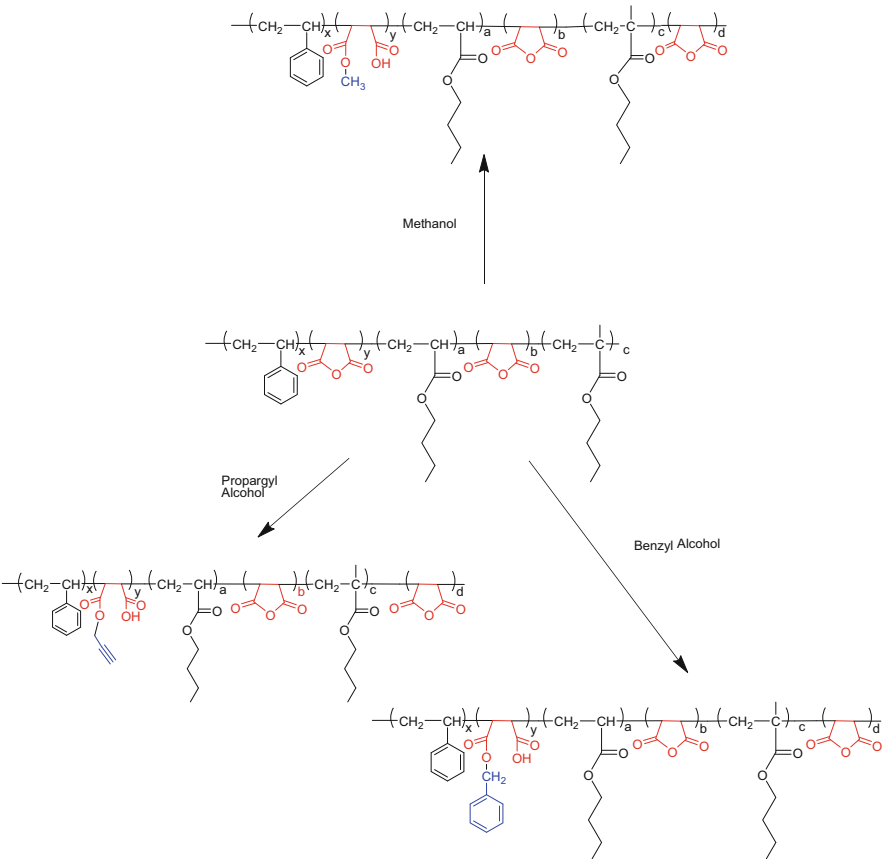

Scheme 9.4 Structures of various half-esters for poly(styrene-*co*-maleic anhydride-*co*-*n*-butyl acrylate-*co*-*n*-butyl methacrylate)

Table 9.4 Results of various primary alcohols ability to form half-esters and recyclize to anhydride [13]

Copolymer	% conversion	% anhydride in polymer after heating	% recyclized
Poly(styrene-*co*-maleic anhydride-*co*-*n*-butyl acrylate-*co*-*n*-butyl methacrylate) with methanol half-ester	95	57	55
Poly(styrene-*co*-maleic anhydride-*co*-*n*-butyl acrylate-*co*-*n*-butyl methacrylate) with methanol half-ester with benzyl alcohol half-ester	81	63	54
Poly(styrene-*co*-maleic anhydride-*co*-*n*-butyl acrylate-*co*-*n*-butyl methacrylate) with methanol half-ester with propargyl alcohol half-ester	62	99	98

Results presented in Table 9.4 highlight a few important effects. First, methanol was determined to be the most efficient in converting the anhydride group to half-ester. Benzyl alcohol was also quite efficient but still noticeably less so than methanol. Interestingly, note that propargyl alcohol was not efficient in converting the anhydride to the half-ester. Second, after heating the half-ester copolymer, results clearly demonstrate that propargyl alcohol half-esters yield the most capable anhydride formation from half-esters. Third, the recyclization ratio was strongest for propargyl alcohol, but basically the same for methanol and benzyl alcohol, in spite of the large difference in boiling points. One possible explanation for this effect is that the propargyl and benzyl alcohol oxyanions are more stable [13]. Similar experiments in the presence of tetrabutyl ammonium bromide (0.2 mol%) catalyst, in this case for the polymeric half-ester formed from methanol, when heated to 140 °C, illustrate a conversion of ~85 % in 20 min. This result suggests the copolymer has suitability for an automotive topcoat.

In formulating an actual automotive clear coat, one system employs three of these copolymers. In first system, 41.4 % of copolymer A (see Fig. 9.4), 11.7 % of copolymer B (see Fig. 9.4), and 46.9 % of copolymer C (see Fig. 9.4) were mixed such that the COOH/epoxy/OH ratio was 1/1/1 in the presence of 0.5 % catalyst (i.e., tetrabutyl ammonium bromide) [13]. This approach enables not only esterification between the carboxylic acid and hydroxyl moieties but also oxirane reactions with carboxylic and hydroxyl moieties. Interestingly, analogous coatings prepared with acrylic acid, in place of maleic anhydride, revealed lower cross-link density (~1) in the coating indicating that the hydroxyl groups did not participate in cross-linking the coating. However, for the present example, the cross-link density was much greater (~2.5) suggesting significant cross-linking contributions from the hydroxyl groups in addition to the glycidyl groups.

Another clear coat formulation employs two copolymers. In formulation #2, 36.8 % of copolymer D (see Fig. 9.4) and 63.2 % of copolymer E (see Fig. 9.4) were mixed such that the COOH/epoxy/OH ratio was 1/1/1 in the presence of 0.5 % catalyst (i.e., tetrabutyl ammonium bromide). The cross-link density for this coating (~3.1) was the largest reported in the study suggesting strong cross-linking contributions from the hydroxyl groups in addition to the glycidyl groups. Such results suggest processing behavior and cross-link densities suitable for clear coating application, a key to development in the implementation of the maleic half-ester approach [13]. Another important feature of this coating design is that the free carboxylic acid group should not react preferentially to a glycidyl moiety. Thus, with these two design elements in mind, a one-package, mar-resistant coating system was developed.

Beyond acid rain resistance, mar resistance is an important feature to the decorative appearance of the automotive topcoat. Especially for vehicles that are likely to pass through cleaning machines equipped with brushing mechanisms. In formulation #2, which exhibited the highest cross-link density (~3.1), demonstrating a T_g (°C) of 86 °C and a gloss retention after marring of 80.5 was best in class. Consequently, by utilizing a strategy of half-ester to anhydride cross-linking of hydroxyl groups, in combination with cross-linking in the presence of glycidyl groups, a higher cross-linking density was achievable resulting in acid rain-resistant

automotive clear topcoat with superior mar resistance. This development was commercialized in the early 1990s and was known as "MACFLOW" [13].

9.2.3 Binders: Corrosion Protection

Corrosion of metals is a significant challenge in many industrial fields. From pipes, ships, locomotives, aircraft to automobiles, buildings, and bridges, there are many metallic structures that require corrosion-resistant coatings to maximize their longevity. Corrosion-resistant primer coatings comprising zinc pigments are often employed. As the industry transitions to water-based paints, a significant challenge with zinc-based pigments is their hydrogen corrosion of the zinc in the aqueous, alkaline paint. Hydrogen gas can build up in the coating container leading to a dangerous pressure build [14]. Approaches that eliminate this issue have included toxic materials, such as chromium (VI) compounds, but such approaches are not favored today. More recently, organic, amphiphilic polymers have been shown to be effective.

One approach employs a copolymer of styrene, maleic anhydride, and *n*-dodecyl methacrylate. This polymer's anhydride group can be hydrolyzed in water with a catalytic amount of dimethylethanolamine. The succinyl dicarboxylic acid, derived from the maleic anhydride unit, is then capable of chelating to the zinc pigment surface [15]. An illustration of this is presented in Fig. 9.5.

Chelating zinc at the surface enables the polymer to protect zinc from hydrogen corrosion. To test this effect, a corrosion medium comprising deionized water, butyl glycol, and a small amount of nonylphenol ethoxylate, to improve surface wetting of the zinc pigment, was prepared. The pH of this solution was adjusted with dimethylethanolamine to achieve pH = 8 and pH = 10. To this solution, 0.5 % (wt %) of the hydrolyzed copolymer was added. Then the hydrocarbon solvent-based zinc pigment paste was added and dispersed. The corrosion reaction was monitored as a function of time for 35 days at room temperature by volumetric measurement of evolving hydrogen gas. Results of this experiment are presented in Fig. 9.6.

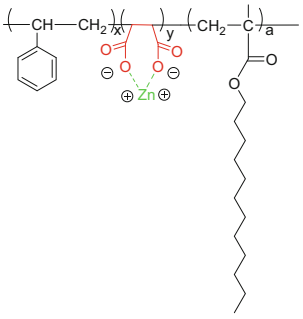

Fig. 9.5 Chelating zinc with poly(styrene-*co*-maleic acid-*co*-dodecyl methacrylate)

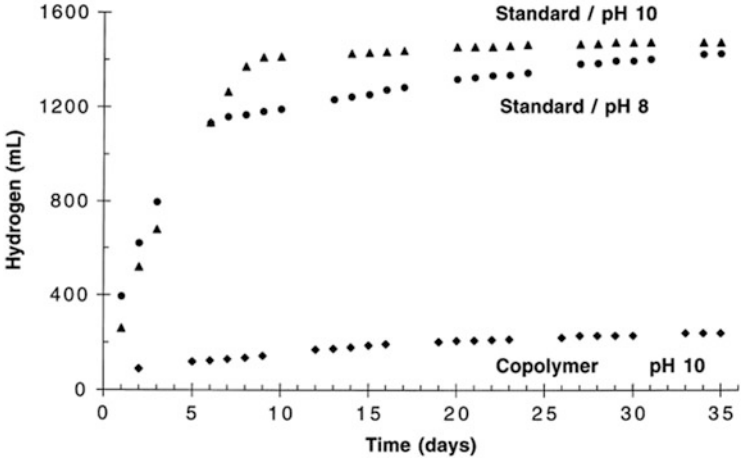

Fig. 9.6 Time dependence (days) of the hydrogen formation from dispersions of the zinc pigment in water/butyl glycol at pH 8 and 10 without polymers (standards) and with addition of 0.50 wt% of copolymer 12 (only at pH 10) [14]. Reprinted from Corrosion Science, Muller, B.; Oughourlian, C.; Schubert, M., "Amphiphilic copolymers as corrosion inhibitors for zinc pigment," pages 577–584, Copyright 2000, with permission from Elsevier

Results in Fig. 9.6 demonstrate that addition of the maleic anhydride-based copolymer significantly reduced, but did not eliminate, the amount of hydrogen gas generated. Apparent is the suggestion of a corrosion inhibition effect. It is also apparent that the initial amount of evolving hydrogen gas is greater at pH = 8 than at pH = 10. In further study of this effect, the following results were produced.

Results in Fig. 9.7 are comparative based upon polymeric compositions where the maleic acid anhydride/styrene/(meth)acrylic ester weight ratio is 15:15:70. The (meth)acrylic esters were varied to be ethyl, *n*-butyl, *n*-hexyl, *n*-dodecyl, and *n*-octadecyl. (see copolymer nos. 2, 4, 6, 12, and 18 in Fig. 9.7, respectively). These results indicate that longer-chain esters are generally less effective at preventing zinc corrosion. The ethyl and butyl chain esters exhibit preferential performance attributes coupled with improved performance at higher pH. Also note that a dosing response to the polymer addition is observed, where results of 0.5 wt% additions are directly compared to 1.0 wt% additions (see Fig. 9.7). Interestingly, these results are opposite to similar evaluations with aluminum-based pigments [14].

Another approach to corrosion-resistant coatings is derived from surfactant-free latexes. In one study, polymeric compounds comprising maleic anhydride were subjected to partial ammonolysis, enabling the formation of surfactant-free latex. Ammonolysis, in this case, describes a process whereby the treatment of anhydride with ammonia results in the formation of amide and carboxylic acid moieties. For example, poly(styrene-*co*-maleic anhydride) partly imidized with *n*-heptylamine, polybutadiene grafted with 17 % (wt%) maleic anhydride, and poly(octadecene-*co*-maleic anhydride) were evaluated after partial ammonolysis [16]. These copolymers were then cross-linked with adipic dihydrazide (ADH), a compound which imparts

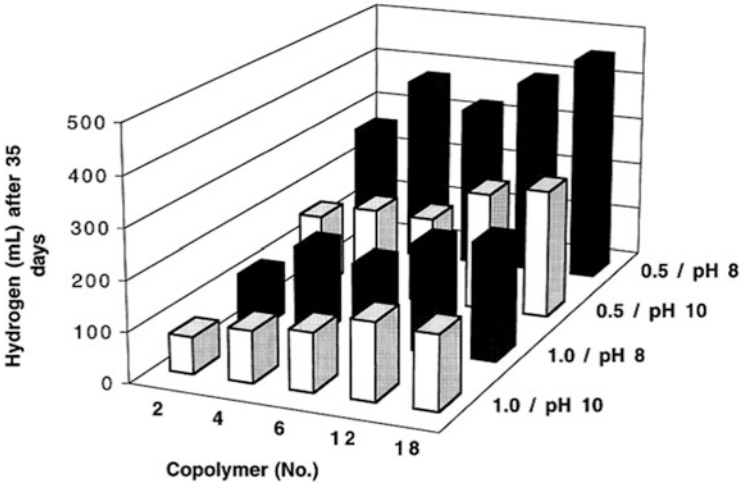

Fig. 9.7 A comparison of hydrogen volumes evolved within 35 days from dispersions of the zinc pigment in water/butyl glycol at pH 8 and 10 with the addition of 0.50 and 1.0 wt% of the different copolymers [14]. Reprinted from Corrosion Science, Muller, B.; Oughourlian, C.; Schubert, M., "Amphiphilic copolymers as corrosion inhibitors for zinc pigment," pages 577–584, Copyright 2000, with permission from Elsevier

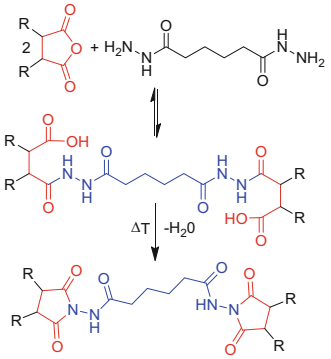

Scheme 9.5 Cross-linking reaction of adipic dihydrazide with anhydride moieties. Adapted from [16, 17]

good adhesive properties to metals such as aluminum, the focus of this particular study. A schematic of the cross-linking reaction is presented in Scheme 9.5.

In Scheme 9.5, "R" indicates a polymer backbone. Upon the addition of ADH, the first step in cross-linking is the formation of an "amic acid"-type structure. This step is reversible. At elevated temperatures though, the "amic acid" condenses, losing water, and forms an irreversible "imide" structure. These coatings were

applied to alkaline pretreated aluminum substrates and dried at temperatures ranging from 100 °C to 160 °C. Upon completion, the coated metal was submitted to a variety of tests: 90° coating pull-off, Electrochemical Impedance Spectroscopy (EIS) measurements (EIS is used to determine the barrier layer properties), and 5 % (wt%) NaCl solution at room temperature (both undamaged and crosshatch coatings). The polybutadiene-based coating exhibited the strongest adhesion (~600–700 N) followed by the poly(styrene-*co*-maleic anhydride) coating (~300 N). Note that the poly(octadecene-*co*-maleic anhydride)-based coating did not exhibit good adhesive properties which was attributed to surface shielding effects from the long aliphatic chains obstructing polymer/surface interaction with acidic groups [16]. The polybutadiene-based 20 μm coating exhibited excellent barrier properties in the NaCl solution. An example of the EIS spectra for this coating is presented in Fig. 9.8.

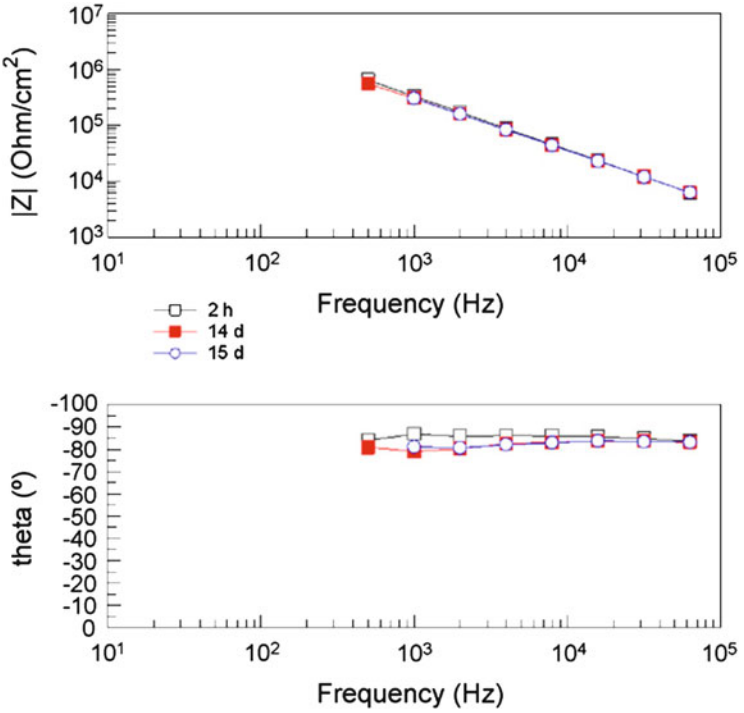

Fig. 9.8 EIS spectra of a 20 μm PBDMA film, cured at 100 °C [16]. Reprinted from Progress in Organic Coatings, 65, 1, Soer, W.J.; Ming, W.; Koning, C.E.; van Benthem, R.A.T.M.; Mol, J.M.C.; Terryn, H., "Barrier and adhesion properties of anti-corrosion coatings based on surfactant-free latexes from anhydride-containing polymers," pages 94–103, Copyright 2008, with permission from Elsevier

In evaluating the barrier layer properties, EIS results presented in Fig. 9.8 demonstrate no decrease in impedance with time, noting that the results nearly overlap. No significant difference was observed for the phase angle (theta) either, which suggests little or no water adsorption by the coating. These results coupled with the lack of any visible damage to either the coating or substrate suggest excellent barrier properties for the cross-linked copolymer coating. The other two coatings did not exhibit similar EIS spectral stability. Salt water immersion results confirm the performance attributes of the poly(butadiene-graft (g)-maleic anhydride) based 20 μm coating. Good protective performance is observed for the aluminum substrate, where the coating exhibits negligible mechanical insult due to the crosshatch test in addition to only small defects indicative of corrosion onset at 4 weeks. Thus, the poly(butadiene-*g*-maleic anhydride)-based coating was found to possess the critical characteristics: adhesion, barrier properties, hydrolytic stability, and corrosion protection [16].

More recently, integrated pretreatment, corrosion-resistant coil coatings were designed to incorporate thioamide moieties onto the copolymer. Thio-based compounds are known to exhibit both corrosion inhibition and adsorption properties to metals. Beyond the importance of adsorption to the surface for effective corrosion inhibition, other critical factors which can influence inhibition effectiveness include temperature, media pH, molecular structure, and metal surface properties [18]. A broad series of maleic anhydride-based materials were prepared and evaluated. In one specific set of examples, a copolymer of maleic anhydride, C_{12} olefin, and $C_{20–24}$ olefin was evaluated with no derivatization and as derivatives of $–CSNH_2$ and –SH functional groups. Examples of the polymeric structures are presented in Scheme 9.6.

The compounds in Scheme 9.6 are then formulated into cross-linkable coating compositions comprising either polyurethane or epoxy-based resins. The components of these two coating systems are presented in Table 9.5.

In comparing the two coating formulations presented in Table 9.5, both coating systems are employing the same fillers (pigment). The epoxy-based coating is comprised of butyl glycol, whereas the polyurethane coating is aqueous based. Because of the aqueous-based nature of the polyurethane coating, additional ingredients, exhibiting functionalities such as dispersing, flow control, and defoaming, are required. To these base formulations, the thio-based poly(maleic anhydride-*co*-olefin) copolymers (see Scheme 9.6) were added [at 5 % (wt%)]. The final coil coating is then applied to the cleaned surface of galvanized steel and dried at 185 °C yielding a dried coating thickness of 6 μm. The corrosion resistance of the coated steel plates was then tested for 10 weeks as per VDA [German Association of the

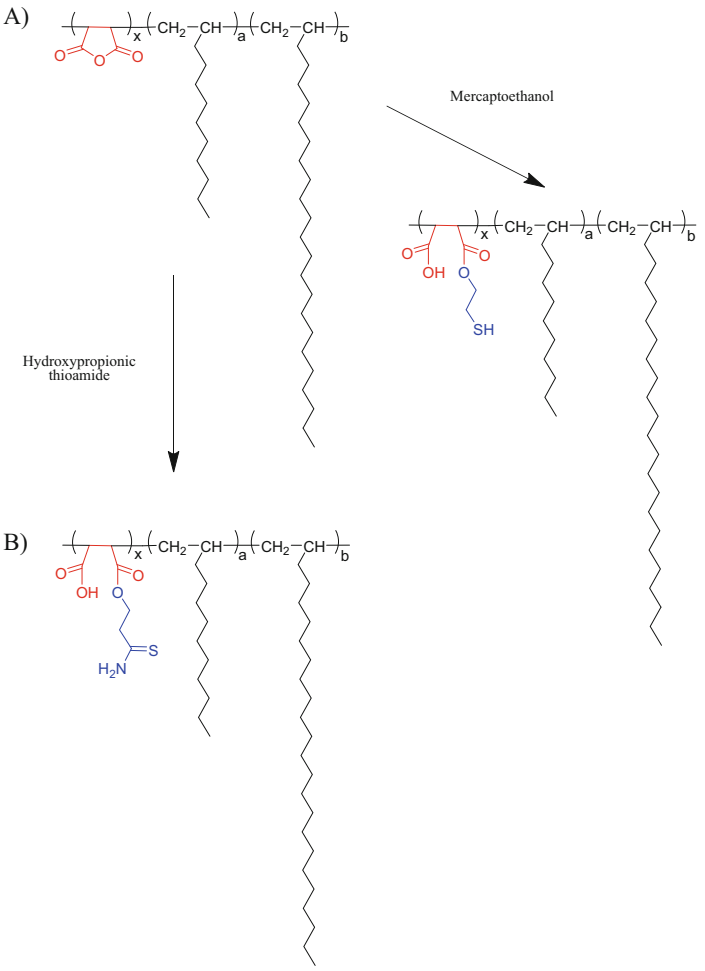

Scheme 9.6 Proposed structures for thio-based poly(maleic anhydride-*co*-olefin) copolymers [19, 20]

Table 9.5 Base formulations for cross-linkable integrated pretreatment coil coatings [19, 21]

Function	Epoxy coating components	Polyurethane coating components
Cross-linking binder	Epoxy bisphenol A binder (molecular weight 1000 g/mol, 50 % solids)	Aqueous polyurethane dispersion (molecular weight 21,000 g/mol (M_w), 44 % solids)
Unspecified additive	–	Dispersing additive
Unspecified additive		Flow control agent with defoamer action
Cross-linker	–	Melamine resin (Luwipal® 072 from BASF Ag
Filler	Hydrophilic pyrogenic silica (Aerosil® 200 V from Degussa)	Hydrophilic pyrogenic silica (Aerosil® 200 V from Degussa)
Filler	Talc Finntalc M5	Talc Finntalc M5
Filler	White pigment titanium rutile 2310	White pigment titanium rutile 2310
Filler	Silica modified with calcium ions (Shieldex® from Grace Davison)	Silica modified with calcium ions (Shieldex® from Grace Davison)
Filler	Zinc phosphate (Sicor® ZP-BS-M, Waardals Kjemiske Fabriken)	Zinc phosphate (Sicor® ZP-BS-M, Waardals Kjemiske Fabriken)
Filler	Black pigment (Sicomix® Schwarz from BASF Ag)	Black pigment (Sicomix® Schwarz from BASF Ag)
Solvent	Butyl glycol	

Automotive Industry] test sheet 621-415 Feb 82) [19, 21]. The 1 week requirements for this test are presented in Table 9.6.

Corrosion test results for various coil coating compositions are presented in Table 9.7.

Table 9.6 Corrosion resistance test parameters for pretreated coil coatings [19, 21]

Stage	Parameters
Initial salt spray test	Sample exposure to 5 % NaCl solution at 35 °C for 1 day
Condensation water test	Exposure to humid conditions (100 % relative humidity at 40 °C for 8 h) followed by dry conditions (60 % relative humidity at 22 °C for 16 h) repeating for four cycles
Room condition	2-day dry conditions (60 % relative humidity at 22 °C)

Table 9.7 Performance test results of thioamide-functionalized maleic anhydride copolymers in coil pretreatment coatings [19, 21]

Molar ratio	Coating system	Functional unit	Coated galvanized steel panel results
1/0.6/0.4	Polyurethane/water	–	Same as blank
1/0.6/0.4	Polyurethane/dioxane/water	$-CSNH_2$	Same as blank
1/0.6/0.4	Epoxy/MEK	–SH	Less corrosion than blank

Results presented in Table 9.7 suggest that for the functionalized –$CSNH_2$ poly (maleic anhydride-*co*-olefin) copolymer, there was no enhancement to the corrosion resistance of the galvanized steel plate when compared to the uncoated plate in a polyurethane-based coating system. However, for the functionalized –SH poly (maleic anhydride-*co*-olefin) copolymer, improvement was noted in corrosion resistance when compared to the blank steel plate for an epoxy-based coating system. It is important to note that there were many other systems tested in this study, and in a few examples, un-functionalized poly(maleic anhydride-*co*-olefin) copolymers, particularly those based on poly(maleic anhydride-*co*-C_{12} olefin-*co*-undecenoic acid), outperformed the functionalized thio-based copolymers [19, 21].

9.2.4 *Binders: Prevention of Marine Fouling*

Another important function of a coating is the prevention of fouling to a structural surface, particularly in marine environments. Fouling of marine paint can lead to significant drag on ship hulls requiring increased energy consumption for transportation goods. In one specific example, researchers designed an amphiphilic surface with a layer-by-layer (LBL) approach employing fluorinated polymers derived from poly(isobutylene-*co*-maleic anhydride) [22]. The synthetic route to this copolymer derivatization in presented in Scheme 9.7.

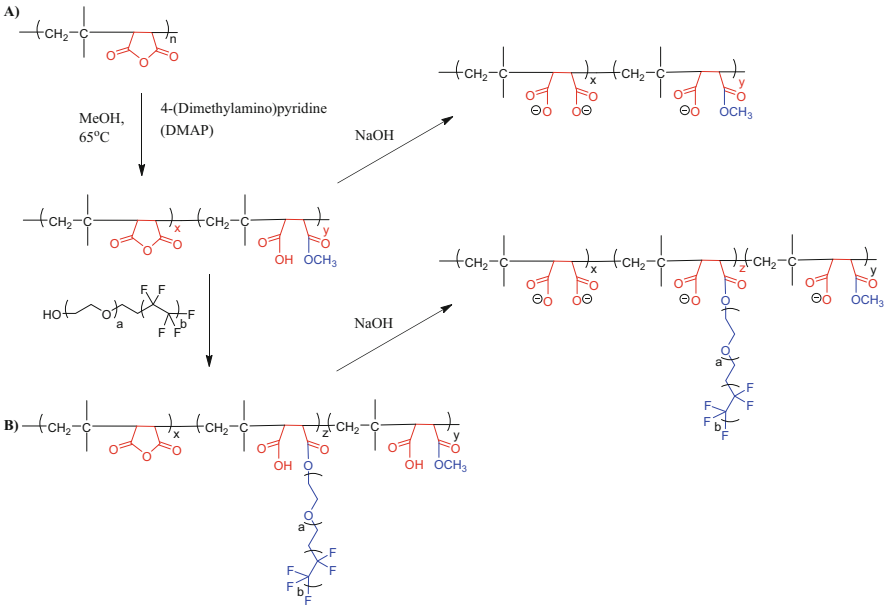

Scheme 9.7 Derivatization scheme for poly(isobutylene-*co*-maleic anhydride) with perfluoroalkyl polyethylene glycol [22]. Adapted with permission from Zhu, X.; Guo, S.; Janczewski, D.; Velandia, F.J.P.; Teo, S.L.M.; Vancso, G.J., *Langmuir*, 30, pp. 288–296, **2014**. Copyright 2013 American Chemical Society

These antifouling coatings were constructed by a LBL technique employed on silicon wafers. The wafer was first submerged in polyanion solutions, either Scheme 9.7a or b, followed by deionized water rinse. The same wafer was submerged into a polyethyleneimine solution followed by a deionized water rinse. This cycle was repeated to make any desired number of layers. Upon completion, the LBL film was dried under nitrogen stream followed by room-temperature vacuum oven drying for 5 h. The final step was to cross-link the film by heating the dried LBL film at 60 °C, in vacuo, for 5 h. To challenge these films, several test protocols were designed, employing different test assays. For example, the LBL wafers were submerged in marine bacterial suspension of *Pseudomonas* strain NCIMB 2021 for up to 6 days, changing the bacterial suspension every 2 days. After exposure, the LBL wafers were fixed in a solution of glutaraldehyde phosphate-buffered saline (PBS), followed by rinsing with fresh PBS and oven drying at 60 °C. Other protocols employed *Amphora coffeaeformis*. Results demonstrate that the untreated wafer exhibits bacterial coverage of ~38 %. Conversely, with the cross-linked LBL system, little or no bacteria is observed at the surface. A reduction in surface settlement by *Amphora coffeaeformis* was also reported, when compared to the untreated silicon wafer [22].

9.2.5 *Reactive Polymeric Surfactants*

Another developing area in coatings is in the field of reactive polymeric surfactants (RPS) [23]. There are many interfaces, such as air–liquid, air–solid, liquid–liquid, and solid–solid, that coating materials must efficiently manage. As we learned in the corrosion coating discussion, for the aqueous-based polyurethane coil coating (see Table 9.5), additional components, such as dispersing and defoaming additives, were required to enable the coating to be applied properly. Building from these basic functionalities, reactive polymeric surfactant materials can tether to latex particles enabling the formation of latex materials with core–shell-type morphology. For example, reactive polymeric surfactant copolymer can be prepared through the polymerization of 5-t-butylperoxy-5-methyl-1-hexen-3-yne and maleic anhydride. The product of this reaction is presented in Fig. 9.9.

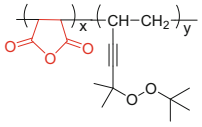

Fig. 9.9 A reactive polymer surfactant derived from maleic anhydride [23]

The copolymer structure in Fig. 9.9 illustrates a peroxide-based moiety coupled with the anhydride group and hydrophobic residues (ethylene backbone). Some refer to these materials as "polyinisurfs" [23]. This type of copolymer can enhance the solubilization of hydrophobic monomers in water and increase the localized proximity of the initiating species to the micellar interface. A schematic representation of these effects is presented in Scheme 9.8.

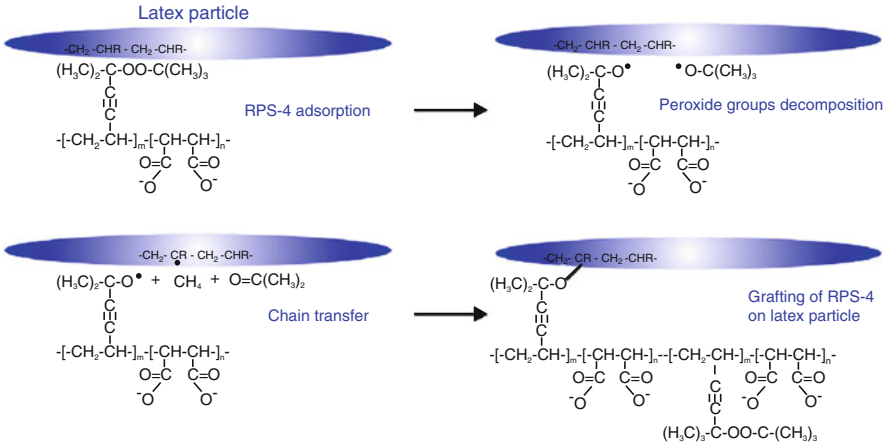

Scheme 9.8 Scheme of reactive polymeric surfactant (RPS)-4 immobilization on the surface of latex particles [23]. Reprinted from Current Opinion in Colloid & Interface Science, 19, Voronov, S.; Kohut, A.; Tarnavchyk, I.; Voronov, A., "Advances in reactive polymeric surfactants for interface modification," pages 95–121, Copyright 2014 with permission from Elsevier

In Scheme 9.8, the reactive polymeric surfactant copolymer physically adsorbs to the surface, with the peroxide moiety oriented to the latex particle. Upon heating, the peroxide decomposes producing two free radicals: one polymeric and one a small molecule. It is possible for chain transfer, or hydrogen abstraction, type processes to occur with the active small-molecule free radical. Subsequently, the newly formed polymeric free radical can proceed to polymerize and/or recombine with radicals to yield a new graft to the latex particle. Essentially, the reactive polymeric surfactant becomes a tethered, covalently bound copolymer to the latex particle.

Another analogous approach is accomplished with reactive polymeric surfactant inisurf copolymer that is structured with an amide-bonded peroxide moiety. The structure for this copolymer is presented in Fig. 9.10.

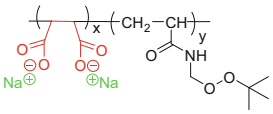

Fig. 9.10 Reactive polymeric surfactant inisurf derived from maleic anhydride and *N*-[(t-butylperoxy)methyl]acrylamide, in the ionized form [23]

Table 9.8 The effect on physical properties with the addition of peroxidized, monodispersed polystyrene latex to an acrylic latex [23]

Property	0 % Reinforcement	1 % Reinforcement	10 % Reinforcement
Impact resistance (intrusion/extrusion), in. lb.	>176/136 ± 8	>176/120 ± 8	>158/24 ± 4
Konig hardness, s	110 ± 5	114 ± 5	126 ± 6
Pencil hardness (gouge)	B	HB	H
# of MEK double rubs	0 ± 1	2 ± 1	8 ± 3
Thickness (μm)	16 ± 2	13 ± 2	13 ± 3

The reactive polymeric surfactant inisurf copolymer presented in Fig. 9.10 yields latex particles that can exhibit localized peroxide groups on the surface, if controlled decomposition of the peroxide moieties is achieved. This effect yields the prospect of further functionalization of the latex particles with exposure to other monomers. In studying the behavior of this reactive polymeric surfactant copolymer, peroxidized, monodispersed polystyrene latex treated with a reactive polymeric surfactant (see Fig. 9.10) was added, at 1 and 10 % (wt%), to an acrylic latex in order to assess the impact of RPS/polystyrene reinforcement to the acrylic latex. These formulations were applied to aluminum panels and placed into an oven for 12 h of curing at 90 °C or 120 °C. Physical test results for these films are presented in Table 9.8.

These physical properties illustrate that the addition of peroxidized latex particles to the acrylic latex results in a hard film that is more solvent resistant. Other studies based upon styrene–butadiene latexes also confirm this effect. However, with the styrene–butadiene systems, the difference in hardness is more pronounced, an effect likely due to the additional unsaturation present within the butadiene comonomer [23].

9.2.6 *Photostabilizers*

Photostability is an important topic in coating science, especially for applications where coatings are likely to experience continuous exposure to sunlight. Coatings that are not photolytically stable can degrade, discolor, and become unable to protect/decorate the object's surface. Photostabilizers based upon maleic anhydride diamines have been developed and evaluated [24]. A few examples are provided in Fig. 9.11.

To determine the effectiveness of the photostabilizer, coating compositions with polystyrene and photostabilizer at 2 % (wt%) were prepared in dry toluene then allowed to vacuum dry in a 60 °C oven to a film thickness of 0.25 ± 0.02 mm. These films were then subjected to a high-pressure mercury lamp ($\lambda_{max} = 365$ nm) for varied time periods. Weight loss during exposure, gel formation, and viscosity average molecular weight were monitored. The end results of the 30 h tests are presented in Table 9.9.

Results in Table 9.9 demonstrate that brominated maleic diamide yields the least amount of weight loss and gel content. The viscosity average molecular was slightly higher for this compound, relative to others. When comparing this result to the pure polystyrene film, the rate and overall magnitude of the molecular weight change is substantially reduced, indicative of a reduction in photodegradation by these compounds. Note that this study also discusses possible mechanistic routes to photolytic degradation and stabilization [24].

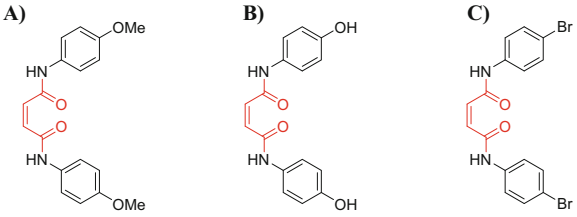

Fig. 9.11 Photostabilizers based upon maleic anhydride diamines [24]

Table 9.9 Test results for aged films of polystyrene and photostabilizer [24]

Compound (Fig. 9.11)	% weight loss	% gel content	M_v ($\times 10^4$)
A	4.1	9.9	10.9
B	4.5	11.0	10.4
C	2.6	6.1	12.1

9.2.7 *Antimicrobial Compositions*

Antimicrobial and biocidal compounds are commonly used in coating applications to reduce or prevent bacterial growth in coating storage container and after application to the surface of the substrate. Most often, low molecular weight compounds are employed in these applications. While effective, there can be challenges. These compounds can leach out of the film, reducing or eliminating the coating's ability to prevent defacement. Some compounds can leach into waterways which can also be environmentally problematic. A common strategy is to develop larger molecules to reduce the leach effect and, potentially, permanently fix the antimicrobial activity into the film to enhance its service life. For example, antimicrobial compounds constructed from poly(styrene-*co*-maleic anhydride) have been designed. Derivatives with 3-dimethylamino-1-propylamine moieties have been developed and demonstrate activity. The process to produce this antimicrobial compound is illustrated in Scheme 9.9.

To produce the antimicrobial polymer depicted in Scheme 9.9, the poly(styrene-co-maleic anhydride) is first treated with 3-dimethylamino-1-propylamine to yield an imidized version of the maleic copolymer. In the second step, the copolymer is treated with ammonia to yield an additional amic acid form to the residual anhydride groups. These copolymers are then employed as a polymeric surfactant [at 1.1 % (total mass)] during the synthesis of styrene/butyl acrylate latex. Wet-state bacterial and yeast challenge testing, using nutrient agar and potato dextrose agar, revealed no contamination after 13 days. Conversely, after 24 h,

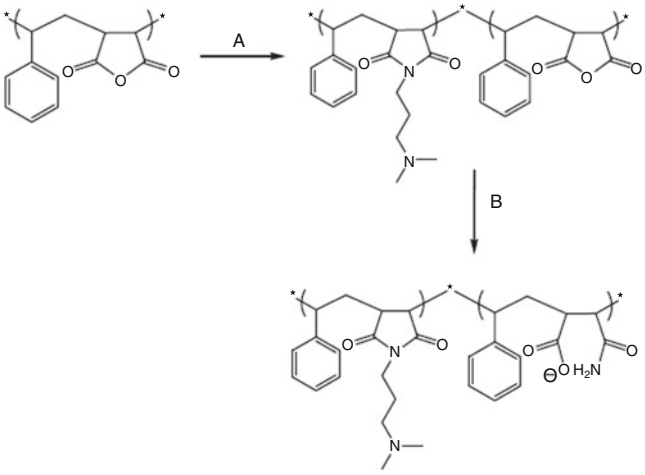

Scheme 9.9 Reaction scheme of partial imidization of SMA (A) and subsequent ring opening of residual maleic anhydride units (B) [25]. Reprinted from European Polymer Journal, 49, Cloete, W.J.; Verwey, L.; Klumperman, B., "Permanently antimicrobial waterborne coatings based on the dual role of modified poly(styrene-*co*-maleic anhydride)," pages 1080–1088, Copyright 2013, with permission from Elsevier

the control exhibited dense growth. Wet-state fungal challenge testing, using fungal spores, also indicates no growth after 28 days for samples with $\geq$1 wt% of antimicrobial polymer. The 0.5 wt% for the antimicrobial polymer and the control were not resistant. This study indicated improved coating microbial resistance for the approach that tested the polymeric surfactant during latex polymerization. It should be noted that as a post-add compound, the antimicrobial polymer demonstrated effectiveness, but, importantly, the inhibition properties were not uniform across the film [25].

9.3 Composite Resins and Adhesives

Composite materials are objects that are comprised of at least two different components. In structural composites, these objects can be fashioned from materials such as fibers and adhesive resins and bi-phase resin systems (with or without fibers). Composite applications have rich diversity, ranging from transportation, electrical, buildings/structures, and electronics to sporting equipment, furniture, and appliances. Composite materials are quite desirable and capable in many wide-ranging applications because of the generally high strength/weight ratio, high stiffness/weight ratio in addition to flexural characteristics, anti-corrosiveness, chemical resistance, and electrical insulation properties. Examples of applications described in more detail below include unsaturated polyester resins in marine applications, bismaleimide resins in aerospace composites, electronic adhesives, and epoxy-based adhesives.

9.3.1 Unsaturated Polyesters

Unsaturated polyester resins are the largest single application, by volume, for maleic anhydride [26, 27]. There are many types of unsaturated polyester resins, including polymers derived from maleic anhydride/acids and diols (condensation-type polymerization), maleic anhydride, and oxiranes (addition polymerization), and two-stage processes that enable incorporation of isophthalic acid [28]. Once the copolymer resin is prepared, it is often solubilized in a monomer (i.e., styrene), which serves as the reactive diluent solvent, to enable the resin to be applied to fibers. This combination is then cured and solidified in order to achieve a fully consolidated composite material comprised of fiber and matrix (cured resin). The curing process typically involves a radical initiator (i.e., peroxide system), monomer polymerization (i.e., styrene), and cross-linking of the double bonds, found in the unsaturated polyester chains, which originate from maleic anhydride.

A specific example of a condensation-type unsaturated polyester is presented in Scheme 9.10.

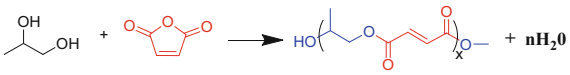

Scheme 9.10 Idealized synthesis of an unsaturated polyester prepared via condensation

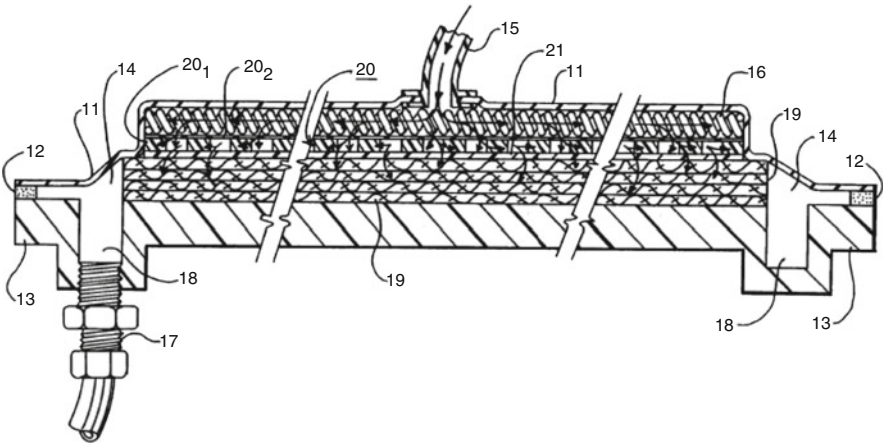

Fig. 9.12 A cross-sectional view of a resin transfer molding assembly [33]

Several structural elements are apparent upon a closer examination of the unsaturated polyester structure. The methyl group, derived from the propylene glycol, serves to enhance the hydrophobic character of the copolymer. The maleic anhydride yields two ester linkages, resulting in a double bond that can be polymerized by free radicals. More subtle is the depiction of *trans* orientation about the double bond. During the esterification, the maleic acid can isomerize to a *cis*-maleate ester moiety or a *trans*-fumarate ester moiety. The degree to which there are *cis* and *trans* orientations is determined by the reaction conditions: time, temperature, diol nature, acidity, and catalysts [29]. Generally, the *trans*-fumarate double bond is more reactive than the *cis*-maleic double bond [30]. At 1580 g/mol, this copolymer would exhibit roughly 10 vinylene bonds per polymer strand couple to a 1:1 molar ratio of propylene glycol/fumarate ester. When dissolving into styrene, at 71 % solids, the molar ratio of vinylene bonds to styrene double bonds is determined to be 1.24. The commercial rendition of this system is the Aropol™ Q6585 product from Ashland Performance Materials [31]. This product is considered a highly reactive closed molding resin suitable for structural sheet molding compound (SMC) fabrication systems, particularly for the transportation market [32].

To fabricate a SMC object, a common approach is to employ a resin transfer molding technique. An example of such a process is often employed in the manufacturing of boats. An illustrated cross-sectional view of the part assembly is presented in Fig. 9.12 to help navigate the following discussion.

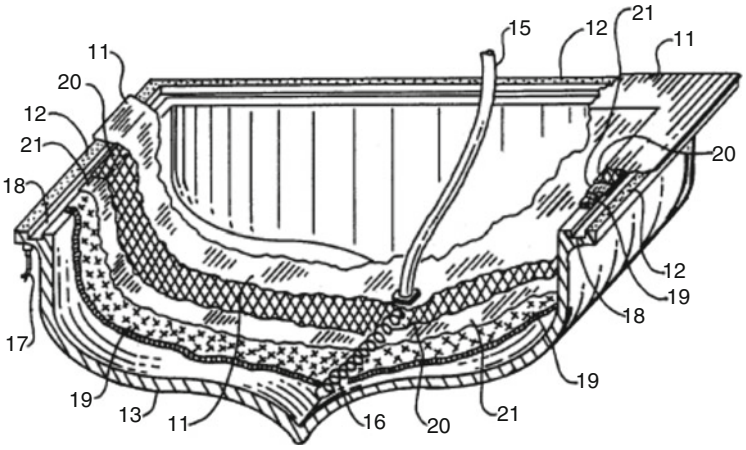

Fig. 9.13 Typical SCRIMP assembly for production of a fiberglass boat hull [33]

The general features describe this process. To a rigid mold surface (**13**), such as a boat hull, which often has a release coating applied to it, numerous fibrous sheets (**19**), or mats, of glass or carbon are laid in a manner to conform to the shape (the fabric lay-up). In addition, a resin distribution medium (**20**, $\mathbf{20_1}$, and $\mathbf{20_2}$) is also applied which comprises strands and helical springs (**16**) placed to prevent direct contact between the peel ply (**21**) and the outer sheet (**11**). Once the lay-up and the resin protection layer have been applied to the mold, a resin impervious outer sheet is applied so as to cover the entire lay-up surface and tightly pressed or sealed with tape (**12**). There is an outer trough (**14**) that surrounds the perimeter of the lay-up. The resin inlet (**15**) and vacuum outlet (**17**) complete the assembly. The prefabrication steps are now completed. A resin inlet is connected to the surface of the part and a vacuum outlet is connected to the bottom of the part. Once the vacuum is applied, the outer film will collapse to the resin distribution layer. The resin is then allowed to flow into the part lay-up. As the resin penetrates into the fibers of the lay-up, it will rapidly distribute throughout as well as vertically descend toward the vacuum inlet. Using this process, the fibers are uniformly wetted to promote physical properties, especially when compared to prepreg autoclave processes. The part is then cured to achieve the final, desired structure. This process is commonly referred to as the Seemann Composites Resin Infusion Molding Process or SCRIMP. An illustrated depiction of the SCRIMP assembly for boat hull production is presented in Fig. 9.13, which employs the same descriptive numbers.

Among the many important elements to these applications are the ability to control viscosity, cure speed, degree of cure as well as residual monomers, and shrinkage. Using the SCRIMP process, Aropol™ Q6585 was studied to determine strategies for controlling volume shrinkage and residual styrene. In the processing of an unsaturated polyester resin system, as the curing process proceeds, the reaction becomes diffusion controlled near and after gelation, essentially due to the decreased mobility of free radicals and reactive double bonds as the network

structure grows, transitioning to a thermoset. Consequently, the unsaturated polyester resin's ability to move is dampened. The net effect is that as the conversion increases, the styrene reaction becomes more dominant primarily due to its greater mobility. However, the rate of homopolymerization for styrene is low, more so at lower temperatures. One approach to overcoming this challenge is to incorporate a comonomer, such as methyl methacrylate (MMA). By using MMA as an additive, this study found that the final product conversion and residual styrene could be enhanced, indicating that styrene and MMA copolymerization is more preferred than just styrene alone. However, this study also found that MMA exhibited a negative effect on shrinkage control, due to the increased challenges of phase separation in which increasing MMA levels tend to make the system more compatible [34].

A typical SMC resin can have numerous additional components. Beyond the unsaturated polyester resin and reactive diluent monomer(s), there will also be an initiator(s), typically a peroxide-based compound. Examples of suitable peroxide include methyl ethyl ketone peroxide, acetylacetone peroxide, benzoyl peroxide, and lauroyl peroxide. Some initiators, such as benzoyl peroxide, require an accelerating agent, which could be dialkyl aniline or dimethyl-*p*-toluidine. The basis for selecting the initiator is typically pot life of the resin, gel time, exotherm behavior, and application temperature. Other typical additives for SMC resins include fillers, calcium carbonate, clay, antimony oxide, glass spheres, aluminum oxide trihydrate, and chlorinated alkanes [29].

As the production capabilities of composite manufacturing advance, greater expectations are placed upon the performance characteristics of these materials. A critical element to the ultimate performance of composite materials is the behavior of the fiber/matrix resin interface. The more intimate this interface becomes, the stronger adhesive forces become at the interface, enabling efficient load transfer properties at the interface between the fiber and matrix resin. In one study, polyalkenyl-poly-maleic-anhydride-ester/amide resin compounds were found to be effective coupling agents (sizing agents) for glass fiber-reinforced polyester composites [35]. A specific example from this study is presented in Fig. 9.14, which is an ester/amide derived from dodecanol and *n*-butylamine.

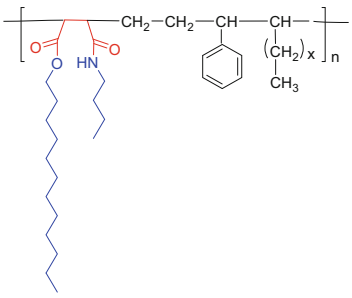

Fig. 9.14 Idealized structure for polyalkenyl-poly-maleic-anhydride-ester/amide coupling additive (CA-4). Adapted from [35]

Table 9.10 Properties of polyalkenyl-poly-maleic-anhydride-ester/amide coupling additive [35]

Property	Result
M_n (number average molecular weight)	2060
M_w (weight average molecular weight)	2470
Polydispersity	1.2
Acid number (mg KOH/g)	15.5

Table 9.11 Properties of Aropol™ M105 TB unsaturated polyester resin [36]

Property	Result
Brookfield viscosity (RV2, 10RPM)	1400 mPa s
Styrene content	41 %
Density	1.1 kg/dm^3
Gel time (1 % MEKP-50)	40 min
Peak exotherm	110 °C

Physical properties of the coupling additive are presented in Table 9.10.

This low molecular weight polymer was then added to hydrocarbon (10 wt%) to enable treatment of glass-woven fibers [0/90°] at 80 °C followed by drying in an air oven at 110 °C for 2 h. After treatment, these glass fibers were then used to produce composites with Aropol™ M105 TB unsaturated polyester resin from Ashland Performance Materials. Aropol™ M105 TB is a thixotropic, pre-accelerated product based on an orthophthalic acid-modified polyester resin. The typical properties of the liquid resin are presented in Table 9.11.

To produce composite samples, five layers of glass fabric were employed in hand lay-up fashion. Curing is accomplished at a fixed temperature yielding laminate structures that were 200 mm × 300 mm. The laminates were then Computer Numerical Control (CNC) machined to dog-bone forms, as required in ASTM D638 type 2, to the following dimensions: overall length 150.0 ± 0.4 mm, width 5.0 ± 0.2 mm, and thickness 2.9 ± 0.4 mm. It is important to note that that this study monitored and controlled the fiber/matrix ratio to 61.4 ± 2.1 %. Results of the mechanical tests are presented in Fig. 9.15.

Results presented in Fig. 9.15 demonstrate that the overall performance of the various coupling agents was similar. The CA-4 coupling agent exhibited similar modulus properties but the highest maximum load and extensional properties. Perhaps more compelling are the Charpy impact test results. Charpy tests are used to measure the resilience of a material and its resistance to damage under shock loading, another critical attribute to composite performance. Results for the Charpy are presented in Fig. 9.16.

Charpy results indicate that coupling agents CA-4 and CA-5 (a similar copolymer employing glycerin and dodecyl amine to achieve the ester/amide derivative) yield significant improvement to the impact strength of glass-woven composite samples, especially when compared to the untreated composite samples [35]. These

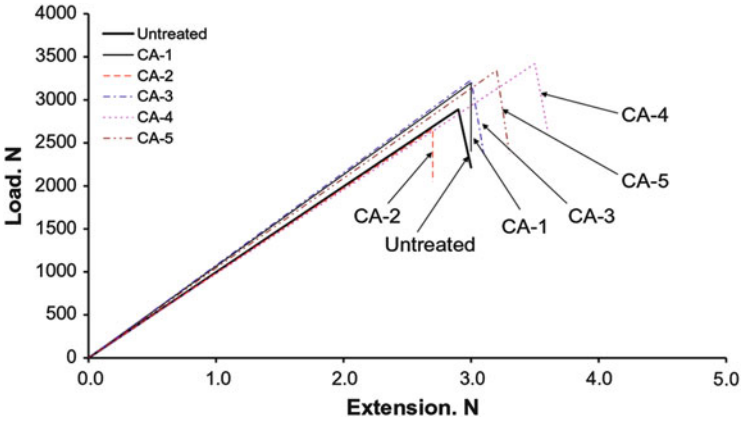

Fig. 9.15 The tensile test diagram of glass-woven [0/90°] fabric-reinforced polyester composites [35]. Reprinted from Materials and Design, 31, Varga, Cs.; Miskolczi, N.; Bartha, L.; Lipoczi, G., "Improving the mechanical properties of glass-fibre-reinforced polyester composites by modification of fibre surface," pages 185–193, Copyright 2009, with permission from Elsevier

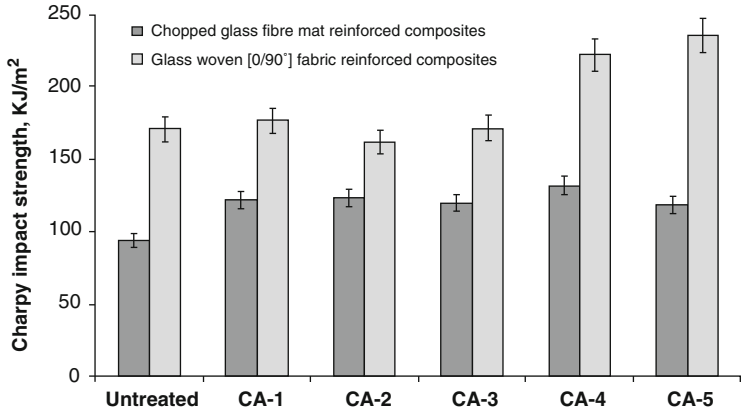

Fig. 9.16 Charpy impact strength of reinforced polyester composites in case of different coupling additives [35]. Reprinted from Materials and Design, 31, Varga, Cs.; Miskolczi, N.; Bartha, L.; Lipoczi, G., "Improving the mechanical properties of glass-fibre-reinforced polyester composites by modification of fibre surface," pages 185–193, Copyright 2009, with permission from Elsevier

series of results led to the proposal of a coupling mechanism for the interfacial interactions of the glass fiber/coupling agent/unsaturated polyester resin surfaces. The proposed scheme for the coupling mechanism is presented in Fig. 9.17.

Figure 9.17 illustrates the coupling agent aromatic rings orienting to the unsaturated polyester, which is known to comprise aromaticity. The coupling agent interacts with the glass fiber surface through the –NH–, –O–, and –OH moieties. Generally, they suggest stronger interaction for the –NH– moiety but to a limit.

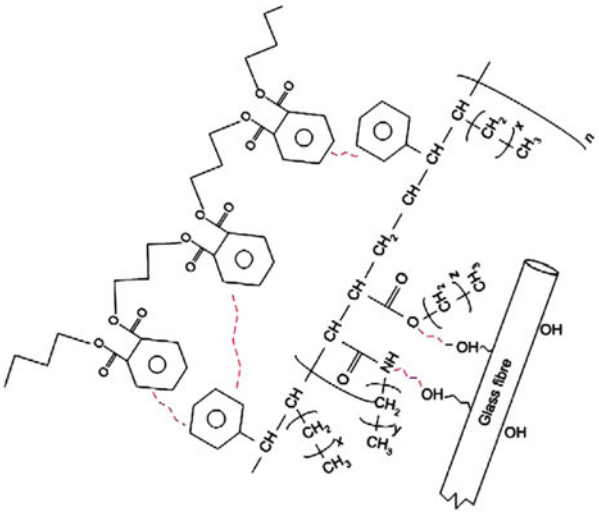

Fig. 9.17 The possible scheme of coupling [35]. Reprinted from Materials and Design, 31, Varga, Cs.; Miskolczi, N.; Bartha, L.; Lipoczi, G., "Improving the mechanical properties of glass-fibre-reinforced polyester composites by modification of fibre surface," pages 185–193, Copyright 2009, with permission from Elsevier

Preferred performance attributes were found with the combination of ester and amide functionality. In a later study, by the same research team, industrial-scale composites were fashioned using a similar experimental design. The results of this work suggest similar performance improvements for Charpy impact tests. However, tensile and elongation results were more mixed, when compared to the earlier laboratory work. It is possible that the relationship between the coupling agent's styrene content and its solubility in the unsaturated polyester resin is a potential influencing factor to these results [37].

Dicyclopentadiene (DCPD) coupled with maleic anhydride is another type of unsaturated polyester resin. When heated to temperatures above 150 °C, DCDP de-dimerizes to yield cyclopentadiene (CPD). CPD undergoes a Diels–Alder reaction with maleic anhydride to yield endomethylene tetrahydrophthalic anhydride (EMTHPA). From EMTHPA, reactions with diols are possible. Also, under particular reaction conditions, such as heating at temperatures below 120–140 °C and acidic mediums, DCPD is capable of reacting with carboxylic acids, glycols, and water via nucleophilic addition [38]. Examples of these various transformations are presented in Scheme 9.11.

Given the variety of possible reactions, there are numerous approaches to preparing dicyclopentadienyl unsaturated polyesters. For example, a synthetic approach where maleic anhydride, phthalic anhydride, diols, and DCPD are all combined and heated to 120–140 °C for a few hours is one possibility. This approach is referred to as the "beginning" method. Another possibility is the

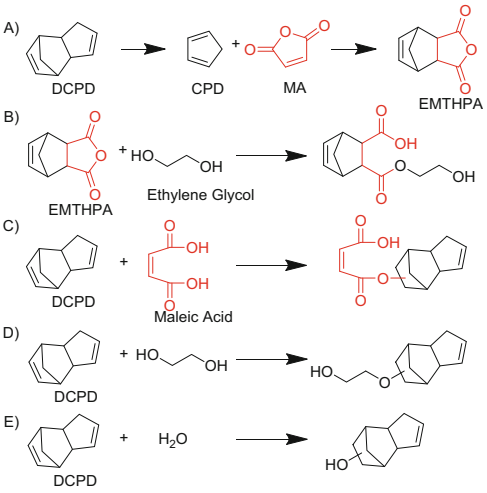

Scheme 9.11 Various dicyclopentadiene reaction possibilities [39]. Reprinted from Polimery, 44, 11–12, Frydrych, A.; Ostrysz, R.; Penczek, "The Effect of Built-in Dicyclopentadiene on Selected Properties of Unsaturated Polyester Resins," pp. 745–749, Copyright 1999, with permission from Polimery

combination of maleic anhydride and DCPD which is heated to 180 °C, in an inert atmosphere, to yield EMTHPA. To this product, phthalic anhydride and diol with heating to 200 °C coupled with water removal were added. This approach is often called the "anhydride" method. In the "end" method, DCPD is added to the unsaturated polyester at the end of the reaction to enable the copolymer to be end capped by DCPD moieties [38, 40].

A current challenge in marine composite industry is to reduce emission of styrene reactive diluents. Because these structures are based upon large and thick composite materials, hand lay-up techniques are still widely employed. As such, there is a trend toward implementation of other manufacturing processes, such as injection and infusion process (i.e., the SCRIMP process), but these processes have not completely eliminated hand lay-up. In parallel, resin suppliers have been working to develop new formulations to reduce or eliminate styrene emission and/or content [41]. Toward that end, resins suppliers have developed unsaturated polyester resin systems with lower styrene emission/content properties, some based upon modifications employing DCPD. DCPD is known to enhance the solubility of the unsaturated polyester resins, which enables higher concentrations of resin to be diluted by styrene reactive diluent [42].

The mechanical properties of glass fiber-reinforced composites based upon low-styrene emission resins have been compared to more conventional systems [41]. The resins evaluated are presented in Table 9.12.

Table 9.12 Resins studied [41]

Reference	Product	Supplier	Resin type	Type
SO1	Polylite 420-731	Reichhold	Polyester orthophthalic	Standard
SO2	Synolite 3785-L1	DSM	Polyester orthophthalic	Standard
LS	Synolite 8388-L7	DSM	Polyester orthophthalic DCPD	Low-styrene content
LE	Polylite 505-M800	Reichhold	Polyester orthophthalic	Low-styrene emission
LES	Synolite 8388-P1	DSM	Polyester orthophthalic DCPD	Low-styrene content and emission
SI	Synolite 3720-I1	DSM	Polyester isophthalic	Standard
SV1	Dion 9100-700	Reichhold	Vinylester	Standard
SV2	Atlac 580 ACT	DSM	Vinylester	Standard

A comparative assessment of the tensile behavior of cast resin plates in addition to degree of cure (DSC) and dynamic mechanical behavior (DMA) measurements is presented in Fig. 9.18 [41].

In Fig. 9.18a, results demonstrate that the low-emission and low-styrene resin systems exhibited both lower failure stress and strain behaviors when directly compared to the other conventional systems. To examine these differences in more detail, stress–strain plots of a three-resin system are presented in Fig. 9.18b. Again, the low-styrene resin system exhibits lower stress failure magnitudes coupled with lower percent elongation. Taking these results into account, this study found that the DCPD resins tend to exhibit a brittleness that is not found in conventional resin systems [41].

Chlorendic unsaturated polyester resins are prepared from the reaction of maleic anhydride and chlorendic anhydride. These resins are typically employed in applications such as corrosion-resistant pultruded pipes, flanges, pumps, pump housing, and mist eliminator blades or other equipment which will be exposed to corrosive gases and liquids. The general structure of this resin type is presented in Fig. 9.19.

The decoration of the unsaturated polyester resin by chlorine atoms enables these resins to be particularly resistant to corrosive wet chlorine gas in addition to strong oxidizing chemicals such as nitric, sulfuric, and chromic acids. These resins are widely employed in the chlorine manufacturing industry [43].

An example of a chlorendic system is Hetron™ 197 from Ashland Performance Materials. The properties of Hetron™ 197 are presented in Table 9.13.

Bisphenol A fumarates are another class of unsaturated polyester resins prepared from the reaction of dipropoxylated bisphenol A and fumaric acid. These materials are also employed in corrosive environments, offering good caustic corrosion resistance, particularly in high-temperature sodium hydroxide applications. They

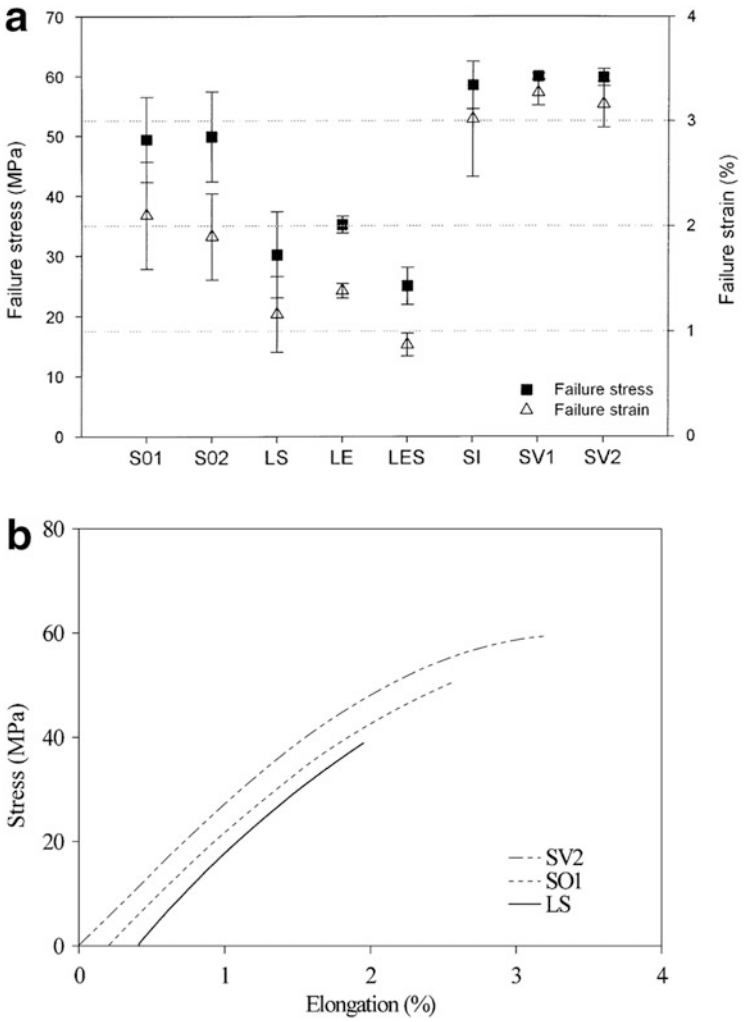

Fig. 9.18 (**a**) Tensile failure stresses and failure strains of the resins studied. (**b**) Tensile behavior. Stress–strain plots for three resins [41]. Springer and Applied Composite Materials, 13, 2006, pages 1–22, "Mechanical Properties of Composites Based on Low Styrene Emission Polyester Resins for Marine Applications," Baley, C.; Perrot, Y.; Davies, P.; Bourmaud, A.; Grohens, Y., Figures 1 and 2, ©2006 Springer with kind permission from Springer Science and Business Media

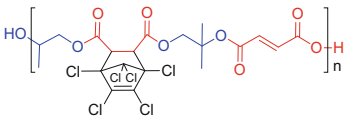

Fig. 9.19 Hetron^{TM} chlorendic unsaturated polyester resin [43]

Table 9.13 Properties of Hetron™ 197, a chlorendic unsaturated polyester resin [44]

Property	Result
Brookfield viscosity (#3, 30RPM)	2000 mPa s
Solids	68.5 %
Specific gravity	1.20 g/cc
Gel time (1 % Lupersol DDM-9, CoNaph6, phr = 0.5)	15 min

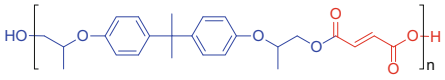

Fig. 9.20 Bisphenol A fumarate unsaturated polyester resin

Table 9.14 Properties of Atlac™ 382, a bisphenol A fumarate unsaturated polyester resin [45]

Property	Result
Viscosity (mPa s)	560–660
Solids	~50 %
Density (kg/m^3)	1030
Gel time (from 25 °C to 35 °C) (1.5 % Butanox, 0.6 % NL51P, 1 % NL 63-10 based on 100 g resin) (min)	5–12
Peak exotherm (°C)	140–170

are also employed in chlorine dioxide storage systems. The general structure on this polyester resin is presented in Fig. 9.20 [43].

An example of a bisphenol A fumarate unsaturated polyester resin is Atlac™ 382 from DSM. The properties of Atlac™ 382 are presented in Table 9.14.

To better understand the behavior of Atlac™ 382 resin when exposed to aggressive environments, its exposure to monochlorobenzene was undertaken [46]. A composite of the resin and glass fiber mat was cured using methyl ethyl ketone peroxide in conjunction with cobalt octoate accelerator. After post-curing the panels at 180 °C for 3 h, the panels were subjected to the aggressive solvent. Dynamic mechanical experimental results for samples exposed to monochlorobenzene at room temperature are presented in Fig. 9.21.

Results in Fig. 9.21 illustrate that the virgin sample shows only a single α_1 relaxation transition, near 137 °C at 1 Hz. After exposure (Sample 2, Fig. 9.21a), in addition to the decreasing magnitude of the α_1 transition, a new broad transition is observed in the lower-temperature region. Additionally, the storage modulus (E') decreases significantly upon exposure (Sample 2, Fig. 9.21b). These effects are ultimately attributed to the possible monochlorobenzene plasticization of the polystyrene regions in the unsaturated polyester [46]. These types of tests can aid scientists in developing a deeper understanding of the fundamental nature of exposure mechanisms and the root cause as to why this solvent is, ultimately, not recommended [47]. All credible resin manufacturers provide significant, detailed

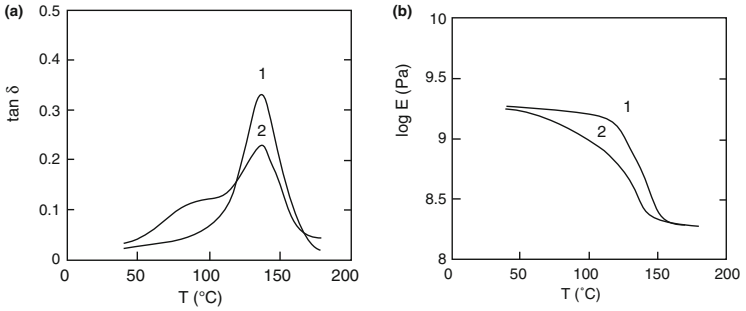

Fig. 9.21 Dynamic mechanical behavior after exposure to MCB (monochlorobenzene) for ATLAC A-382: (**a**) loss factor, (**b**) storage modulus, (1) original sample, (2) after 6 h in MCB [46]. Reprinted with permission from the Journal of Applied Polymer Science, 71, Valea, A.; Gonzalez, M.L., Mondragon, I., "Vinyl Ester and Unsaturated Polyester Resins in Contact with Different Chemicals: Dynamic Mechanical Behavior," pages 21–28. Copyright 1999 John Wiley and Sons

literature to aid in the proper selection of resins suitable for liquid and gas applications (e.g., [47, 48]).

9.3.2 Bismaleimide Resins and Adhesives

For advanced composite materials, where thermal, mechanical, and electrical properties are critical to the performance success criteria, bismaleimide (BMI)-based thermosetting resins have been developed. Bismaleimide resins are primarily based upon low molecular weight oligomers that are capable of homopolymerizing into a highly cross-linked network. This class of resin can be found in composite materials employed in applications ranging from the US Air Force's F-22 aircraft to high-performance automobiles. Perhaps the most compelling attribute of BMI resins is their performance in high-temperature applications, some capable of 230–290 °C service temperatures, coupled with epoxy-like autoclaving process behavior characteristics, a common processing technique in the advanced composite industry [49]. Maleic anhydride is employed in the production of a class of bismaleimides often referred to as addition bismaleimides.

The most widely practiced route to addition bismaleimides is via the condensation reaction of maleic anhydride with difunctional amines. This route is depicted in Scheme 9.12.

This synthetic approach is often referred to as Searle's route [51]. Essentially, maleic anhydride is reacted with a diamine compound, via condensation, to yield the bismaleiamic acid product. A subsequent condensation reaction enables the formation of the bismaleimide compound. What is particularly interesting in these compounds is the reactivity of the maleimide double bond, which is suitable for

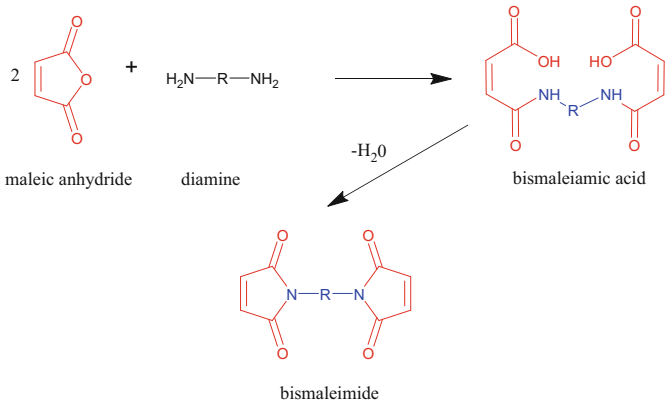

Scheme 9.12 General synthetic route to an idealized addition bismaleimide resin [50]

addition polymerization via free radical catalysis and its susceptibility to primary amines via the Michael addition reaction. This type of Michael addition reaction is represented in Scheme 9.13.

The cross-linking of the bismaleimide as presented in Scheme 9.13 occurs via nucleophilic attack by the primary diamine, which is possible due to the activation of the maleimide double bond by the two neighboring carbonyl moieties. Because of these two separate and powerful reaction pathways, namely, the addition polymerization and Michael addition reaction, there is a significant degree of formulation space. Also note that the polymerization process for the bismaleimide oligomer is temperature induced, which is another attractive feature of these materials. Therefore, there are many options to the modification of the composite resin composition to achieve the most desirable processing behavior and physical properties for the finished composite [49].

One commercial example is Cytec's CYCOM® 5250-4 RTM resin system. The main components of the resin system are presented in Fig. 9.22.

The CYCOM® 5250-4 resin system is comprised of three main components. The first two components are both bismaleimide structures, where the 4,4′-bismaleimidediphenylmethane can be thought of as "para" in arrangement and the bismaleimide-1,3-tolyl can be considered "ortho" when considering the orientation of the maleimide moiety. Interestingly, the o,o'-diallylbisphenol A is also incorporated, while not a maleimide, to enable the BMI resin to be more processable and less brittle [52]. The allylic bonds are known to be less reactive, suggesting that this component essentially functions as reactive plasticizer. This material is a one-part, homogeneous resin system suitable for resin transfer molding. The properties of CYCOM® 5250-4 resin are presented in Table 9.15.

CYCOM® 5250-4 resin is a common bismaleimide resin system in the aerospace industry. Another product form for this material is a prepreg, where the resin is applied to high-performance fibers, including carbon (IM-7) and glass materials. For example, unidirectional, 12K carbon fibers comprising 33 % (wt) resin are

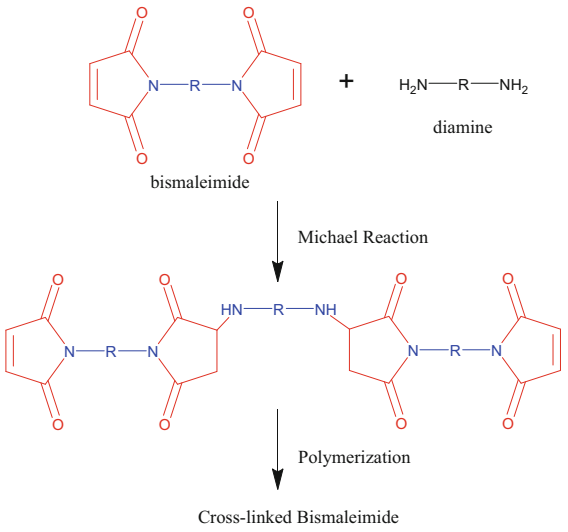

Scheme 9.13 Cross-linking of an idealized bismaleimide with diamines via Michael addition reaction [50]

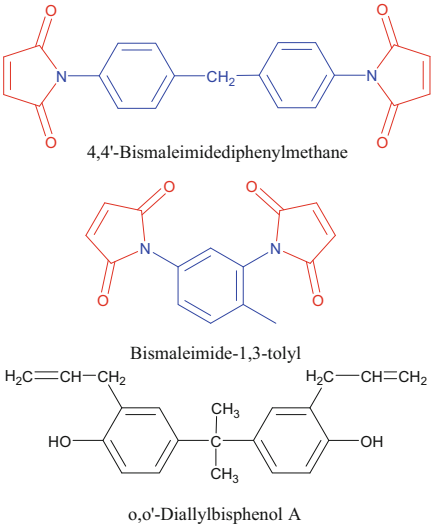

Fig. 9.22 Main components to Cytec's CYCOM® 5250-4 RTM resin system [52]

Table 9.15 Standard properties of neat Cytec's CYCOM® 5250-4 resin [53]

Property	Result at standard cure + standard post-cure[a]
Cured resin density (g/cm^3)	1.25
T_g (°C) dry	271
T_g (°C) wet	207
Gel time at 177 °C (min)	~35

[a]6 h at 177 °C to 191 °C + 4 h at 227 °C

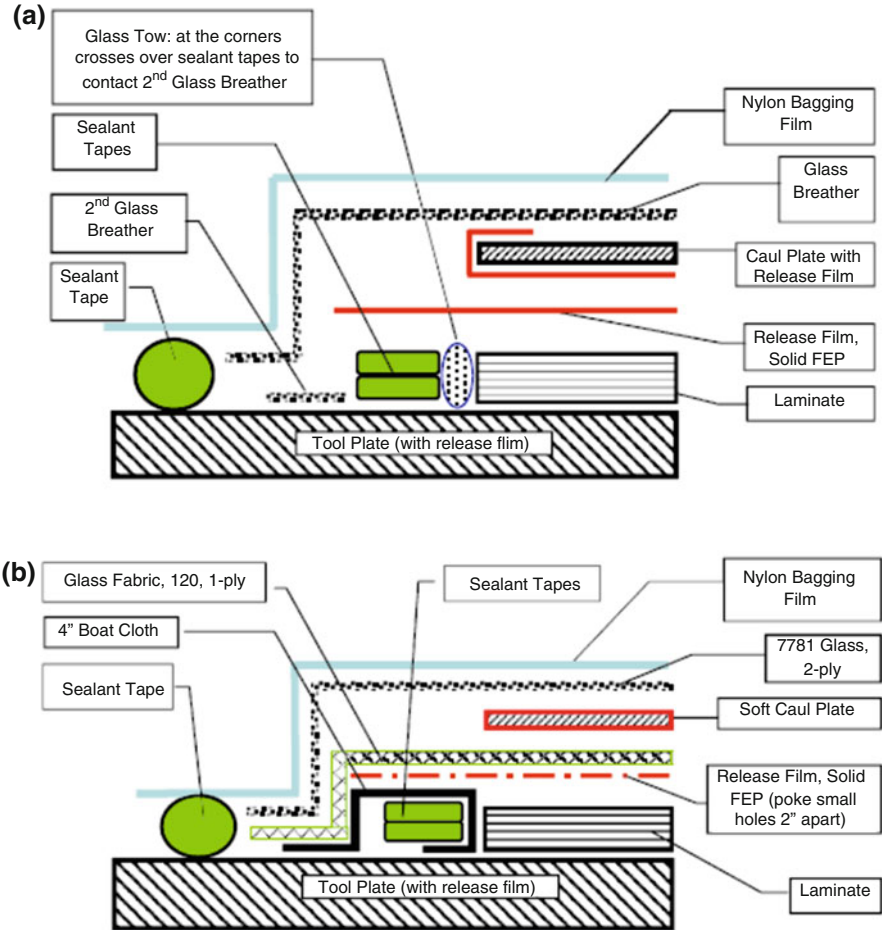

Fig. 9.23 Vacuum bag configuration for (**a**) autoclave and (**b**) vacuum processing of IM7/5250-4 prepreg tape ([54]; see also [55] for additional information). Springer and Applied Composites Materials, 18, **2011**, pages 231–251, "An Enhanced Vacuum Cure Technique for On-Aircraft Repair of Carbon-Bismaleimide Composites," Rider, A.N.; Baker, A.A.; Wang, C.H.; Smith, G., Figure 1, ©2010 Springer with kind permission from Springer Science and Business Media

supplied as a unidirectional tape, up to 152.3 cm wide. This material should be stored in a freezer to minimize resin advancement. Typically, prepreg materials are cut to the proper dimensions and laid up into the desired geometry and fiber pattern, with the number of layers determined by the engineering requirements. This construction is then covered by release film, vacuum bagged (sealing with high-temperature tape), and debulked for up to 30 min. Finally, the vacuum seal of the construction is confirmed by verifying minimal vacuum loss over 10 min, with the vacuum source disconnected from the part. Examples of two-part assembly approaches are presented in Fig. 9.23.

Table 9.16 Some physical properties of IM-7 unidirectional carbon fiber composite (60 % fiber volume) with CYCOM® 5250-4 matrix resin using standard cure and post-cure conditions [56]

Property	Test temperature (°C)	Result
0° Compression strength (MPa) (ASTM D695 MOD)	24	1620
0° Compression modulus (GPa)	24	158
0° Flexural strength (MPa) (ASTM D790)	24	1723
0° Flexural modulus (GPa)	24	157
Neat resin T_g (dry, °C)	–	300

Once properly tested, the part is then positioned into a high-temperature autoclave for curing. In the autoclave, a typical pressure of 15 psi is applied while the assembly remains attached and under vacuum at the laminate edge. The part is then heated from room temperature to 121 °C at 0.6–3 °C/min. This heating reduces the viscosity of the resin for a certain period of time to enable the fiber and resin to consolidate into a continuous composite structure. After about 30 min, when the temperature is 121 °C, the polymerization of the bismaleimide resin begins to advance to the point where the viscosity begins to build, thereby reducing the fluidity of the resin. Once at 121 °C, the part is held isothermally for 45 min. The pressure is then increased to 85 psi, and the vacuum is vented. The part is heated from 121 °C to 177 °C at 0.6–3 °C/min. Once at 177 °C, the part is held isothermally for 6 h. The part is then allowed to cool under pressure to <49 °C at 0.6–3 °C/min. The final part is post-cured in an air oven by heating from room temperature to 227 °C at 0.6–3 °C/min, held isothermally for 6 h, and cooled to <49 °C at 0.6–3 °C/min [56]. Some physical properties of bismaleimide composites fabricated with unidirectional carbon fibers using these cure guidelines are presented in Table 9.16.

Generally, bismaleimide matrix resin properties are superior to unsaturated polyester resins. They are widely used in high-temperature, high-strength applications such as primary aircraft structure like fuselage skins, stiffeners, wing and stabilizer spars, and skins [56]. Their high cross-link density also provides for excellent chemical and solvent resistance. However, this high cross-linked density imparts brittleness to the resin which can lead to composite micro-cracking [57].

Recently, researchers have developed self-healing polymeric materials based upon bismaleimide moieties. This effort highlights two features of these materials: the potential for these materials to be reworkable, remendable and, potentially, recyclable. Such properties would be unusual in thermosetting materials [58]. A schematic of the reaction between bismaleimide and furan-functionalized polyketone (PK-furan) is presented in Scheme 9.14.

In describing the reaction processes presented in Scheme 9.14, the forward path highlights the Diels–Alder reaction between the furfuryl moiety and maleimide double bond. Studying this reaction in solution, gel formation occurred in 2 h at 50 °C. At 150 °C, the retro-Diels–Alder reaction occurred in 5 min. These processes were repeated numerous times without any visible appearance differences. Furthermore, the kinetics of these processes were found to be suitably adjusted by altering

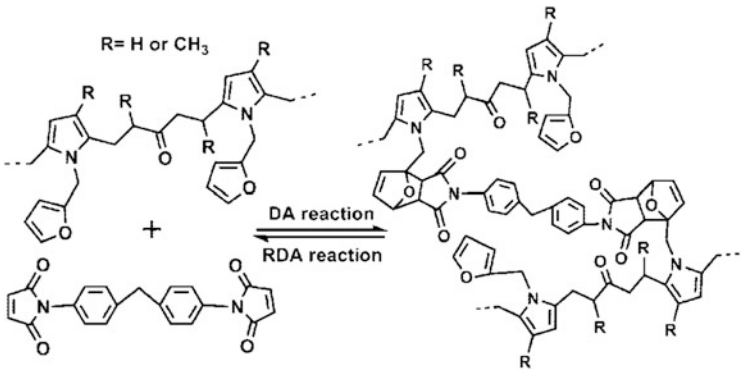

Scheme 9.14 Reversible reactions between furan-functionalized polyketone (PK-furan) and bismaleimide [58]. Reprinted with permission from Zhang, Y.; Broekhuis, A.A.; Picchioni, F., *Macromolecules*, 42, pp. 1906–1912. Copyright 2009 American Chemical Society

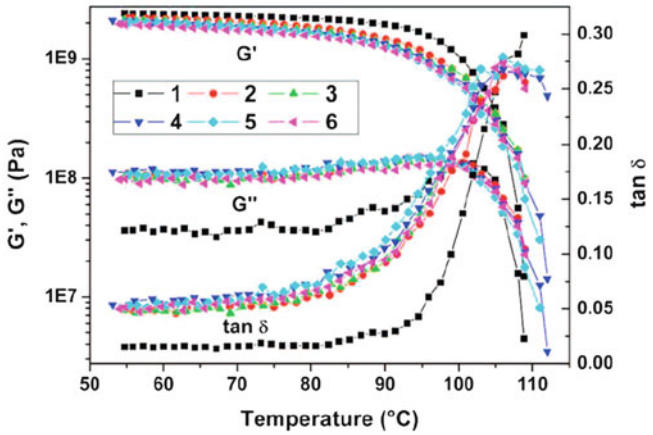

Fig. 9.24 DMA test results for continuous heat cycling of furan-functionalized polyketone and bismaleimide (ratio = 1) [58]. Reprinted with permission from Zhang, Y.; Broekhuis, A.A.; Picchioni, F., *Macromolecules*, 42, pp. 1906–1912. Copyright 2009 American Chemical Society

the molar ratios of the components [58]. In another series of experiments, the self-healing properties of the furan-functionalized polyketone and bismaleimide were demonstrated by compression molding small granules of the cross-linked system into bars, at 110–150 °C for 10–30 min, and then mechanically evaluated by dynamic mechanical analysis (DMA) techniques. One series of these results is presented in Fig. 9.24.

In Fig. 9.24, the re-workability of the furan-functionalized polyketone and bismaleimide (ratio = 1) is demonstrated. Upon the first heating #1, the sample exhibits a softening (T_g) around 100 °C, via an inflection point determination of G'. This sample was cooled and reheated six times. The material's ability to maintain

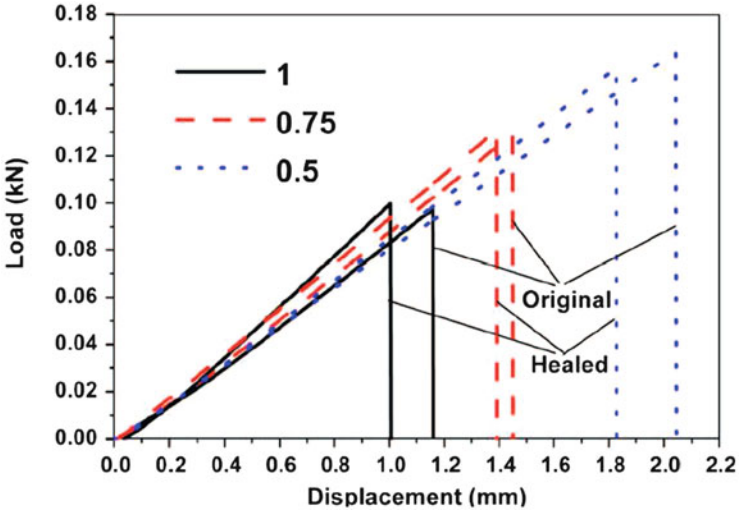

Fig. 9.25 Three-point bending test results for furan-functionalized polyketone and bismaleimide (ratios = 1, 0.75, and 0.5) [58]. Reprinted with permission from Zhang, Y.; Broekhuis, A.A.; Picchioni, F., *Macromolecules*, 42, pp. 1906–1912. Copyright 2009 American Chemical Society

its shape and mechanical properties during thermal cycling is evidence of its reforming capabilities. Note that the slight decrease in G' from cycle 1 to 2 is attributed to discrepancy between DMA measurement time-scaling effects and the kinetics of the cross-linking reaction [58]. Another mechanical evaluation was performed using three-point bending, which then is related to self-healing efficiency by comparison of the remended result to the original fracture load capability. An example of these tests results is presented in Fig. 9.25.

Three-point bending results demonstrate that the relative ratio of bismaleimide to furan-functionalized polyketone has an impact on the mechanical performance of the system. Generally, the lower amounts of bismaleimide generate increased fracture loading capabilities. After the test was completed, the fractured sample was shredded and remolded into the geometry via compression molding at 120 °C for 20 min. Upon retesting these remolded samples, the fracture load capability was completely recovered [58]. In the future, such an approach may prove to have merit in challenges surrounding micro-cracking and damage/repair of bismaleimide materials.

One of the most rapidly changing parts of our world is the field of microelectronics, electronic devices, and telecommunications. Today, portability, appearance, and ease of use are major considerations for the consumer when considering an electronic device. The consumer now expects a new device or capability to be produced every year or even more frequently. It is instructive to see how far the technology has progressed by reflecting, if only for a moment, into the past. The singular technical development that enabled the electronic revolution was that of

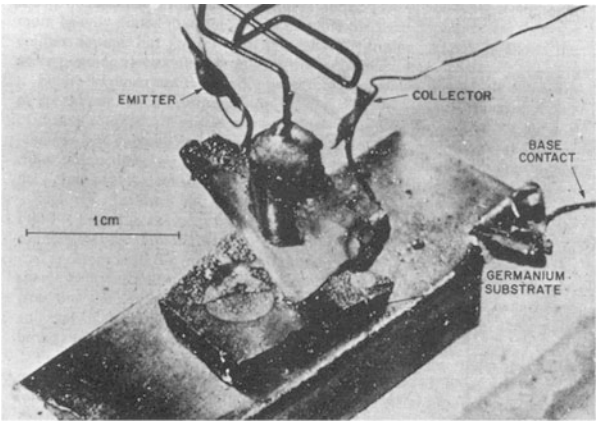

Fig. 9.26 The first transistor, 1947 [59]. Reproduced from Boudenot, J.C., "From transistor to nanotube," Comptes Rendus Physique, 9, pages 41–52. Copyright © 2008, published by Elsevier Masson SAS. All rights reserved

the transistor. In 1947, the transistor, or point-contact transfer resistor, was discovered by Bardeen and Brattain. Not long after, the junction transistor was invented by Shockley [59]. Bardeen, Brattain, and Shockley were awarded the 1956 Nobel Prize in Physics for their "researches on semiconductors and their discovery of the transistor effect" [60]. A picture of the first transistor is presented in Fig. 9.26.

The main components to the transistor are emitter (or source), base (gate), and collector (drain). Essentially, an electrical signal is applied to the base and influences the semiconductive material, in this early example a germanium crystal, which can enable an electrical current to proceed to the collector [61]. The development of the transistor resulted in the replacement of vacuum tube technologies. Early transistors were large in size, as it becomes readily apparent in an early advertisement from Texas Instruments shown in Fig. 9.27. Another early photograph of a the various assembly features of a commercially available transistor, relative to a common match (far left) and tweezer tip (second from left) holding the germanium layer, is shown in Fig. 9.28.

To appreciate the progress made over the last decades, one 1955 silicon transistor is ~1 square inch in size. The Intel® Itanium 2 Processor (9 MB Cache) (2004) comprises 592,000,000 transistors and occupies an area of about seven US postage stamps, an obvious and tremendous leap in manufacturing and technical capability [64].

Another key component of an electronic device is the joining technology employed to connect various device components, i.e., transistors, to a primary structure (printed circuit board). From the earliest days of the electronics industry, the joining technology most commonly applied was tin–lead solder compositions. Tin–lead compositions have been employed as soldering materials for thousands of years, when even the Romans used such compositions in plumbing and art

Fig. 9.27 1954 Texas Instruments' advertisement for the silicon transistor [62], used with permission from Texas Instruments Incorporated

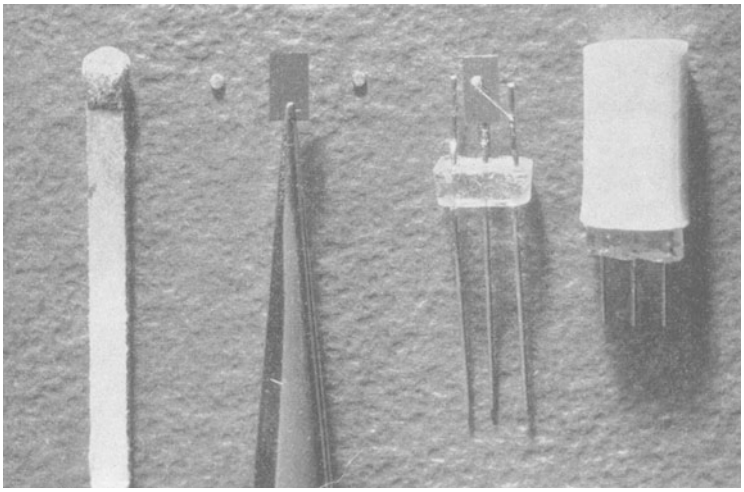

Fig. 9.28 Commercially available alloy junction transistor [63]. Reprinted from Journal of The Franklin Institute, Vol. 259, No. 2, Herold, E.W., "Semiconductors and The Transistor," pages 87–106, **1955**, with permission from Elsevier

applications. More recently, the electronics industry has been experiencing pressure to replace tin–lead solder compositions due to the inherent hazards of these materials and the limited recycling of disposed electronic products [65]. Replacing this technology is difficult, given its long use and manufacturing familiarity coupled with low cost. But there has been important progress.

In developing new joining technologies, conductive organic adhesives have been a focus. Maleic anhydride has enabled new conductive adhesives and approaches to device joining. In other words, conductive adhesives have been developed for use in bonding integrated circuits to lead frames and printed wire boards. This application is often referred to as die attach, where a semiconductor die (or chip) is attached

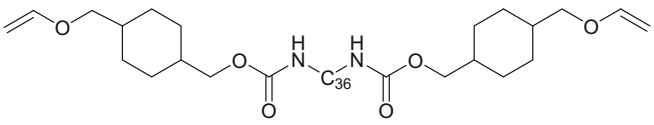

Vinyl ether (electron donor)

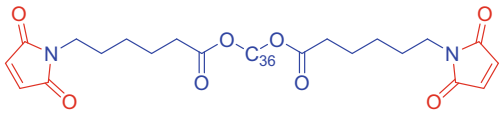

Bismaleimide (electron acceptor)

Fig. 9.29 Chemical structures for key organic components to a die-attach conductive electronic adhesive [67]

Table 9.17 Die attach adhesive formulation [67]

Component	Weight %
Bismaleimide	11.19
Vinyl ether	10.31
Maleic anhydride 8 % (Ricon 131)	2.50
Initiator	0.50
Blend of adhesion promoters	0.50
Silver flakes	75.0

(or bonded) to a substrate [66]. For example, one die-attach adhesive system is designed to function with an electron donor/acceptor strategy, where both a bismaleimide (electron acceptor) and vinyl ether (electron donor) are employed to form the die-attach adhesive. The chemical structures of these two components are presented in Fig. 9.29.

Within these two components are several key properties. First, the polar functionalities, i.e., esters, maleimide, and carbamate moieties, enhance the adhesive properties of the integrated circuit chip to the lead frame. Second, both compounds are difunctional cross-linkers, ensuring a thermosetting, adhesive performance by either thermal or UV cure. Third, both compounds comprise a C_{36} spacer group, which aids in promoting a homogeneous adhesive system and ensuring the adhesive is hydrophobic, minimizing any moisture pickup.

To formulate the conductive, die-attach paste, the compounds in Fig. 9.28 were mixed with several additional ingredients, most important of which is silver flake. The specific formulation is presented in Table 9.17. For comparative purposes, a nonpolar dimer divinyl ether (DDVE) derived from C_{36} was also formulated in a similar fashion.

Table 9.18 Adhesive test results for conductive die-attach formulation [67]

	Room-temp die shear			240 °C die shear		
	Pd (kg)	Ag (kg)	Cu (kg)	Pd (kg)	Ag (kg)	Cu (kg)
Die attach adhesive	13.2	11.1	11.7	4.4	3.8	2.8
DDVE	7.0	7.9	7.2	4.0	3.3	2.2

In evaluating the cure kinetics of this polar formulation, the onset to polymerization was found to be 97.78 °C coupled with a peak exotherm of 113.99 °C. The degree of enthalpy was 239.5 (J/g). The cure kinetics for the nonpolar DDVE formulation are as follows: The onset to polymerization was found to be 101.49 °C coupled with a peak exotherm of 119.01 °C. The degree of enthalpy was 207.2 (J/g) [67]. These results indicate similar curing behaviors.

To evaluate the adhesive properties, the formulation was placed between a 120 mil by 120 mil silicon die and a metal lead frame (i.e., Pd, Ag, and Cu). Each assembly was placed on a 200 °C hot plate and cured for ~60 s. After curing, pressure is applied at a defined temperature until shearing occurs. The results of these tests are presented in Table 9.18.

As indicated by the adhesive test results, the more polar adhesive exhibited a significant improvement in the room-temperature adhesive strength. While not as significant at 240 °C, the adhesion was still improved at the elevated temperature.

In another thermosetting die-attach adhesive strategy, a trifunctional maleimide resin comprising an isocyanurate core was designed. This maleimide resin was then formulated into a conductive adhesive system with an acrylate resin, also with an isocyanurate core. The chemical structures for these two reactive compounds are presented in Fig. 9.30.

An interesting feature to the trifunctional maleimide compound is that at 50 °C, the compound demonstrates a viscosity of 26,000 cPs, whereas most maleimide compounds are solids. Also important to note is this compound has very little volatility, about 0.12 % at 200 °C. To a formulation that was designed around base components, the isocyanurate core compounds were added to assess the adhesive performance. The formulation strategy is presented in Table 9.19.

The adhesive performance was evaluated by testing the shear strength of a 500 mil by 500 mil silicon die on a silver-coated lead frame at 260 °C, after curing the assembly at 200 °C for 2 min. The formulation with the additive components exhibited ~30 % improvement in adhesive strength, when compared to the control formulation [68].

One challenge with thermosetting, die-attach adhesives is their permanence. Integrated circuits and chips are expensive devices. If there is an error in the device placement or an unexpected design change, there is no way to conveniently rework the assembled and cured structure resulting in a significant cost for waste. In the realm of 2D devices, that could mean a loss of one device. A schematic of a circuit

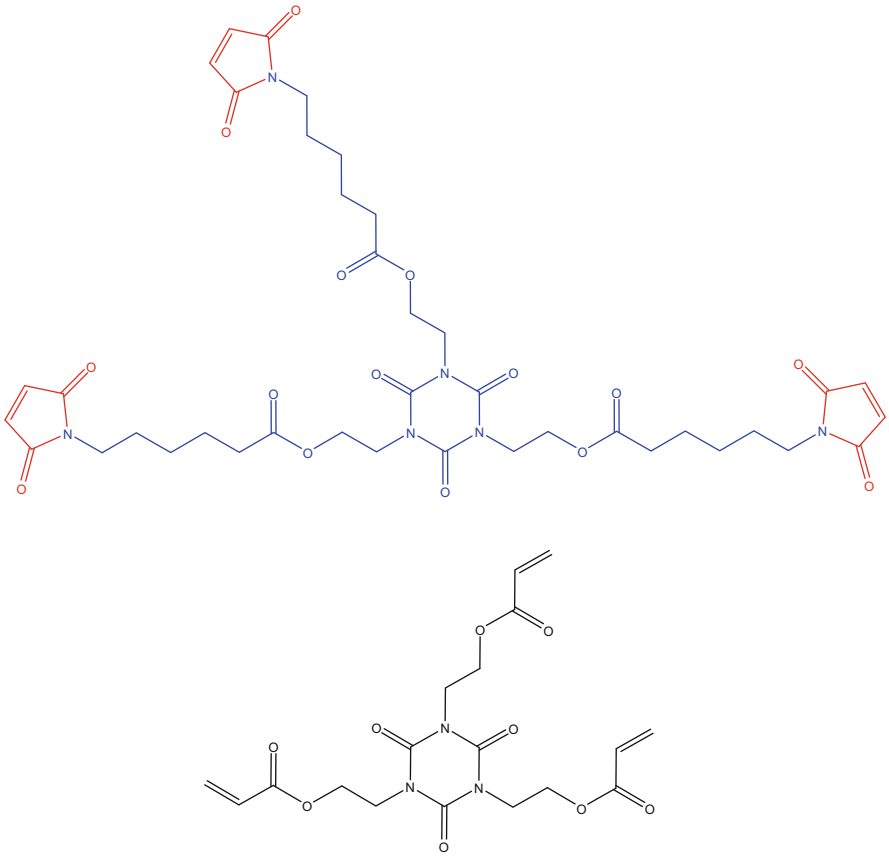

Fig. 9.30 Die attach adhesive compounds designed with an isocyanurate core [68]

Table 9.19 Die attach adhesive based upon an isocyanurate core formulation [68]

Control formulation	Parts by weight
Bismaleimide resin	10
Acrylate resin	10
Epoxy resin	10
Ethylene glycol diethyl methacrylate	15
Curing agent	Effective amount
Adhesion promoter	Effective amount
Silver flakes	45
Additive components	
Trifunctional maleimide resin (isocyanurate core)	2.5
Trifunctional acrylate resin (isocyanurate core)	2.5

panel assembly with individually packaged chips, in two dimensions, is presented in Scheme 9.15.

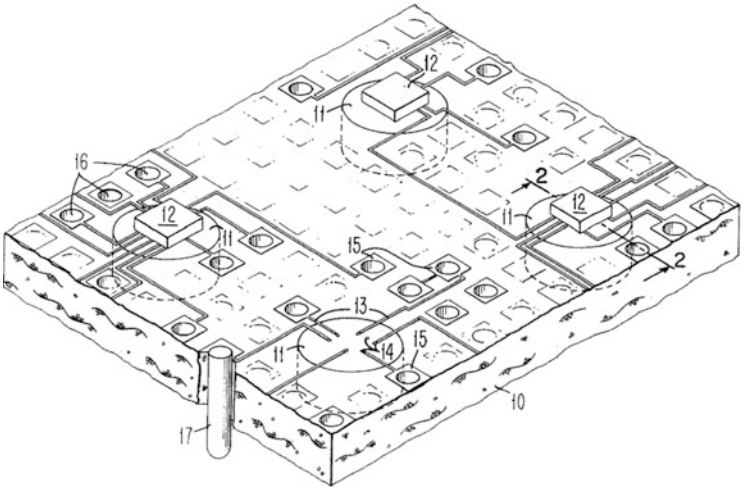

Scheme 9.15 Top view of individually packaged chips on a circuit board [69]

As illustrated in Scheme 9.15, individually packaged chips (12) are placed and bonded onto the circuit panel (10). The chips can be mounted with solder columns (not shown) and interconnected with conductive circuit lines (13). In the early days of circuit board assembly, when tin–lead solder was employed, it would be possible to melt the solder to reposition, repair/replace, or otherwise alter the positioning of the chip on the board. In deploying a thermosetting adhesive, this would not be possible, resulting in a potential loss of the chip or, even worse, the board assembly itself. As the technology has progressed, 3D integrated circuit assemblies are becoming more common. An example of a multiple chip package, or 3D integrated circuit, is presented in Scheme 9.16.

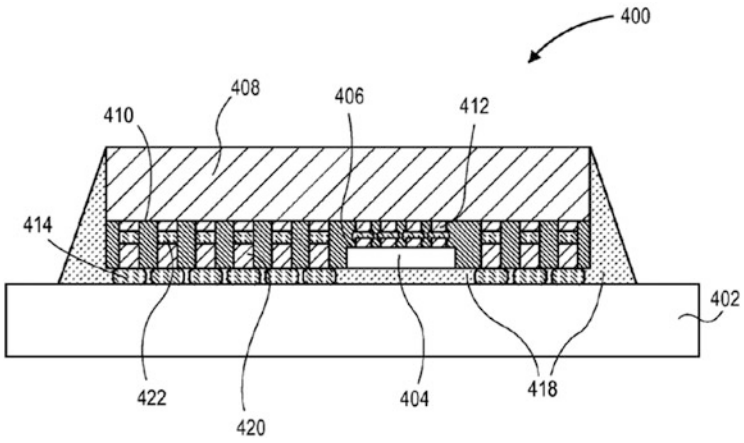

Scheme 9.16 3D integrated circuit package [70]

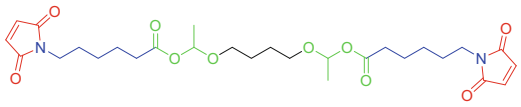

Fig. 9.31 Bismaleimide comprising thermal degradable acetal–ester moieties [71]

In examining the 3D semiconductor package (400) presented in Scheme 9.16, it is readily apparent that multiple chips are assembled on top of the substrate (402). The bottom of the semiconductor die (404), which is connected to the substrate (402), has an active side (406). A top semiconductor (408), with an active side (410), is connected to the substrate (402) via die to die interconnect structures (412) equipped with many bump columns (420) and intermediate solder balls (422). Between these columns are molding layers. These structures are further coupled by an underfill material layer (418). Molding and underfill layers are nonconductive resinous materials such as epoxy comprising silica filler [70]. If the adhesive is a thermoset and there is an assembly issue, it is possible to lose many chips or even an entire board assembly with many more chips than in the past. Increasing the potential cost in production waste. With this challenge in mind, adhesive technology has been developed to help the electronic fabricator or repair person salvage such assemblies.

In designing an adhesive that can be thermally degraded and reworkable, thermosetting bismaleimides incorporating acetal–ester groups were designed. An example of such a compound is presented in Fig. 9.31.

The compound presented in Fig. 9.30 exhibits a viscosity of 5000 cPs at 25 °C. In formulating the compound, 1,1-di(tert-amyl peroxy) cyclohexane (at 2 wt%), the polymerization begins at 105 °C, reaching its pinnacle at 121 °C. The degree of enthalpy was 389 (J/g). In evaluating this compound as an underfill for a standard electronic package, the adhesion was tested after curing for 10 min at 120 °C. The adhesion of the compound at room temperature was found to be 35.2 kg but dropped to 2.3 kg at 150 °C, demonstrating that the thermoset degraded upon exposure to heat. To better conceptualize these various processes, a mechanism is proposed in Scheme 9.17.

As proposed in Scheme 9.17, heating of a maleimide comprised of carboxylic acid functionality in the presence of divinyl ether compounds enables the formation of a new bismaleimide compound composed of acetal–ester linkages. The bismaleimide compound can be free radically polymerized to form a thermoset adhesive. Importantly, upon further applied heat to the thermoset, a thermal degradative process begins, first with decomposition of the C–O bond adjacent to the C=O group, resulting in the formation of a vinyl ether and carboxylic acid moiety, thereby cleaving the thermoset linkages. In an acidic environment, the vinyl ether can hydrolyze to form acetaldehyde and alcohol. The alcohol can backbite the other acetal–ester to form a cyclic acetal and another carboxylic acid moiety. It is possible that the other acetal–ester can also yield butanediol and acetaldehyde, but experimental results indicate this reaction to be less favored [71]. These processes are more clearly represented in Chap. 3 of this book. Bismaleimides

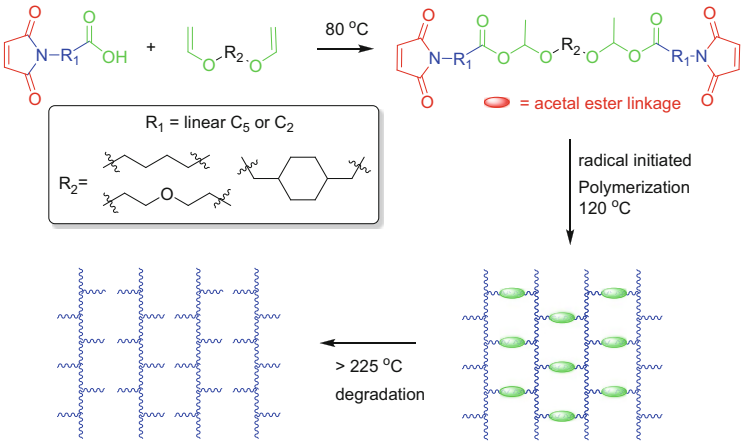

Scheme 9.17 Proposed synthesis, polymerization, and degradation mechanism for bismaleimide comprising thermal degradable acetal–ester moieties [71]. Adapted with permission from Journal of Polymer Science Part A: Polymer Chemistry, 47, Zhang, X.; Chen, G.C.; Collins, A.; Jacobson, S.; Morganelli, P.; Dar, Y.L.; Musa, O.M., "Thermally Degradable Maleimides for Reworkable Adhesives," pages 1073–1084. Copyright 2009 John Wiley and Sons

comprising acetal–ester groups demonstrate an ability, upon heating to high temperature, to facilitate integrated circuit removal, providing innovative opportunities to rework, repair, and, perhaps, even recycle expensive electronic components and assemblies.

9.3.3 Epoxy-Based Adhesives

Adhesives based on epoxy chemistry are found in numerous applications, ranging from aerospace composites to electronics and construction-oriented adhesive products. They can also find utility in potting compounds to protect components from environmental exposure. For example, such compounds have been used to protect wire and cable splices on telecommunication equipment and signal transmission devices. Often these products are two-part systems, where the individual components are mixed, then potted. Once potted, the composition is allowed to cross-link and cure in place. Epoxy compounds are known to generate exothermic reactions during cure, which can damage the wire and cables. By reducing the exothermic behavior, the excellent physical properties of these systems can be used more advantageously.

A two-part epoxy potting system was designed using that which employs maleic anhydride technology. The formulation for this two-part epoxy resin is presented in Table 9.20. Part A is gray shade and Part B is unshaded.

Table 9.20 Two-part epoxy compound for protecting telecommunication equipment and signal transmission devices [72]

Component	Weight Percent	Equivalent Weight (mol fraction)
Polybutadiene with 35% maleic anhydride functionality (Ricon MA, Lithen)	30	0.4
Poly(maleic anhydride-*co*-methyl vinyl ether) Gantrez AN 119 (30% suspension in bis(isopropyl)naphthalene (Ruetasolv DI)	19.7	0.59
Hydrocarbon resin solution (naphthalene) (Nevchem LR)	18.4	---
Bisphenol A epoxy resin (EPON 828)	35.7	0.69
Bis(isopropyl)naphthalene (Ruetasolv DI)	14.7	---
Hydrocarbon resin solution (naphthalene) (Nevchem LR)	25.4	---
100% Active urethane diol (KFlex UD 320-100)	9.2	0.34
Polyol with a high level of primary alcohols (CASPOL 5004)	9.7	0.33
Castor oil polyol (Polycin M365)	5.2	0.3
2,4,6-tris(dimethylaminomethyl)phenol, epoxy accelerator (DMP 30)	7	---

Table 9.21 Ingredients of 3M™ Scotch-Weld™ Industrial Plastic Adhesive 4475 [74]

Ingredient	Weight (%)
Methyl ethyl ketone (MEK)	50–60
Polyurethane polymer	15–25
Poly(vinyl chloride-*co*-vinyl acetate-*co*-maleic acid)	15–25
Epoxy resin	0.1–1

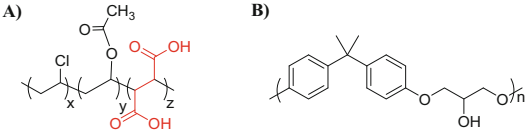

Fig. 9.32 Chemical structure for poly(vinyl chloride-*co*-vinyl acetate-*co*-maleic acid) (**a**) and epoxy resin (**b**)

To prepare the formulations presented in Table 9.20, Part A is prepared by mixing, in order, the first four components until the mixture appears homogeneous. Similarly, Part B is prepared by mixing components five through ten, in order, until the mixture appears homogeneous. Then the two parts are combined and mixed until homogeneous. At 23 °C, it takes about 20 min for the composition to cross-link and cure. The cured composition exhibits a dielectric strength of about 13.5×10^5 V/m, a Shore A hardness of about 80, and a tensile strength of about 2.84×10^6 N/m^2 [72].

Another common examples of an epoxy-based adhesive are general purpose adhesives designed for bonding a wide variety of substrates, i.e., plastic, ceramic, glass, leather, and cloth materials. An example of this product is 3M Scotch-Weld™ Industrial Adhesive 4475 [73]. Adhesive 4475 is comprised of four components, which are presented in Table 9.21.

The chemical structure of the poly(vinyl chloride-*co*-vinyl acetate-*co*-maleic acid) and epoxy resin, respectively, are presented in Fig. 9.32.

The formulation of these polymers in MEK results in a clear viscous product that is 6500–10,500 cPs at ~43 % solids. For some plastic surfaces, the MEK can serve as a softener to enhance the adhesion of the polymer system. However, care must be taken due to the potential flammability of the solvent. In testing the peel strength of canvas to steel, at ~24 °C, the strength continued to build from 13 lbs./in., in 1 day, to 44 lbs./in. after 3 weeks [73]. As the solvent dries, over time, the polymer system can esterify, via carboxylic acid and hydroxyl moieties, to yield cross-linking, in addition to the inherent adhesive behavior of these polymers.

9.4 Printing and Imaging

There are many functional uses for maleic anhydride in printing applications. Beyond purely monolithic requirements, such as adhesion, flexibility, and viscosity, are often found more subtle necessities, such as color, color stability, reactivity/cure speed, and compositional versatility. Maleic anhydride, through its myriad possible transformations, can provide the link required to achieve the requisite product performance.

9.4.1 Adhesion

In thermal transfer imaging processes, the adhesion layer must be carefully designed to enable proper retention of the color image upon heating and peeling of the image during transfer to its final position. To accomplish this complex task, an adhesive layer comprising a maleic anhydride-based copolymer was designed. Specifically, a poly(α-olefin-*co*-maleic acid-*co*-maleic acid anhydride monoisopropyl-ester) (i.e., Ceramer 1608 from Petrolite Corporation) is formulated into a coating solution comprising poly(ethylene-*co*-vinyl acetate), aromatic petroleum resin (i.e., Neopolymer 160 from Nippon Petrochemical), methyl ethyl ketone, cyclohexane, and toluene. This coating solution is applied to the coloring layer at 0.6 g/m^2, on a dry weight basis [75].

For many packaging applications, specially designed printing inks are required to achieve the proper adhesion and flexibility. For example, in printing of uncoated, lightweight paper stocks, high holdout inks are desired. To develop a high holdout, adhesive ink, a modified, carboxylated polyamide ink composition is designed with maleic anhydride in mind. Specifically, in the first example, gum rosin and maleic anhydride are combined and mixed to 200 °C for 2 h. This process enables a Diels–Alder reaction between the gum rosin and maleic anhydride to occur. An amorphous polyamide, such as Versamid® 930, is slowly added, while the heat is raised to 240 °C for 5 min, enabling a condensation reaction between the maleinized gum rosin and amorphous polyamide to occur. Afterward, diethanolamine is added and this mixture heated for 10 min at 180 °C [76].

In a different, second approach, a poly(styrene-*co*-maleic anhydride) and polyamide resin (i.e., GAX-340 from Henkel) are combined. While the mixture appears incompatible, the heat is gradually raised to 240 °C for 1 h. This enables a condensation reaction between the poly(styrene-*co*-maleic anhydride) and amorphous polyamide resins to occur. After 1 h, the heating is turned off and the mixture cooled to room temperature. Water, t-butyl alcohol, and ammonia are added, and the temperature is gradually raised to 80 °C, enabling the solids and pH to be adjusted to the final, aqueous solution [76].

In preparing a base varnish blend, the rosinated polyamide from the first example is blended with a poly(styrene-*co*-acrylic ester-*co*-acrylic acid) (i.e., Lucidene® 604) latex, polyethylene wax, and *n*-propanol. To the base varnish, water, poly (styrene-*co*-maleic anhydride) rubine chip, ammonium hydroxide, glycol (defoamer), and amine are added. This aqueous ink is then printed onto treated stretched polyethylene using an anilox roller at 700–1000 ft/min, revealing a printed image with excellent gloss, adhesion, and no pinholes [76].

Adhesion to polyolefins is a particularly important topic in printing, giving the wide use of polyolefin films in the printing and packaging industry. Chlorinated resins are one option for formulators to evaluate in an effort to boost the adhesiveness of the ink applied to the polyolefin. However, chlorinated resins can suffer from poor weather resistance and less favorable environmental profiles, limiting their use in some applications. Non-chlorinated adhesion promoters have emerged as an important topic and one that is also influenced by maleic anhydride. In one example, poly(ethylene-*co*-propylene-*co*-butene) is placed into an extrusion device. Once the temperature reaches 170 °C, maleic anhydride, styrene, and the peroxide Perbutyl D are added and kneaded for 10 min. This process enables high levels of maleic anhydride, in addition to styrene, to be grafted onto the polyolefin. In this example, 5.4 % maleic anhydride grafting is achieved [77].

The composition previously described was then evaluated as an adhesion promoter in white ink. To test its functionality, the maleic anhydride- and styrene-grafted polyolefin was solubilized in an 80/20 solvent blend of toluene/ethyl acetate. Then this composition was formulated with a urethane resin, titanium dioxide, ethyl acetate, and isopropyl alcohol. This white ink was coated onto oriented polypropylene film (OPP) with a #12 Mayer rod, dried, and then adhesion tested with cellophane tape. This white ink not only exhibited strong adhesive quality to OPP but, in other tests, exhibited strong heat seal, weathering, and oil resistance attributes [77].

In another approach to a non-chlorinated adhesion promoter, poly(propylene-*co*-ethylene-*co*-butene) was added to an extrusion device with maleic anhydride and lauryl methacrylate. Peroxide initiator was added into the extruder, with a total residence time of 10 min at 180 °C; the maleic anhydride and lauryl methacrylate were successfully grafted onto the polyolefin at 5.2 % and 6.2 %, respectively. In evaluating the performance of this adhesion promoter, this grafted composition was solubilized in a 70/30 blend (wt) of ethylcyclohexane/butyl acetate. To this solution urethane resin, titanium dioxide, ethyl acetate, and isopropyl alcohol were added. This white ink was coated onto oriented polypropylene film (OPP), high-density

Table 9.22 Adhesiveness of white ink formulated with poly(propylene-*co*-ethylene-*co*-butene) grafted with maleic anhydride and lauryl methacrylate adhesion promoter [78]

Film	Adhesiveness
OPP	No peeling
HDPE	No peeling
PET	No peeling
NY	No peeling

polyethylene (HDPE), poly(ethylene terephthalate) (PET), and nylon (NY) films with a #12 Mayer rod, dried, and then adhesion tested with cellophane tape [78]. Results of these tests are presented in Table 9.22.

Again, this white ink not only exhibited strong adhesive quality to a variety of synthetic films but, in other tests, exhibited strong heat seal, warm water resistance, and gasoline resistance attributes [78].

9.4.2 Nonaqueous Printing

Phase-change inks, also referred to as solid inks or hot-melt inks, are an increasingly important ink class. Phase-change inks are found in nonimpact printing technologies in either thermal transfer or digital printing via solid ink [79]. An example of this printing process is presented in Scheme 9.18.

In examining the process presented in Scheme 9.18, during the rotation of the anodized aluminum drum heated to 65 °C, the drum is cleaned prior to receiving a thin layer of silicone release oil. Concurrently, the solid ink is melted by an ink melter and allowed to pass into the print head, which is fashioned from stainless steel. The printhead heats the ink to 135 °C to enable spraying of ink droplets, or ink-jets, to the drum in a desired pattern [80]. Concurrently, the paper is moving through the printing web. The paper is preheated and then passes into a gap between the pressure/transfer roller and drum, effectively forming a pressure nip. At this moment, the four-color ink droplets on the drum are transferred to the paper, under heat and pressure. The pressure roller also flattens the ink droplets to reduce any light scattering resulting from the previously spherical surface orientation. After the ink is transferred, the paper is ejected from the machine [80]. This process is depicted in Scheme 9.19.

Because phase-change inks are solid materials at room temperature, there are several advantages to this growing technology. Good storage stabilization of the ink product and reduced nozzle clogging due to lack of solvent evaporation enables the printhead to last for the lifetime of the machine [80, 81]. Other advantages include good image quality and ease of use for solid ink, and the final prints are water-fast. Furthermore, this process enables fast ink dry time enabling rapid printing speeds, with some solid ink-jet printing machines, such as the Xerox® ColorQube® 9302/9303, capable of >50 color pages per minute [82].

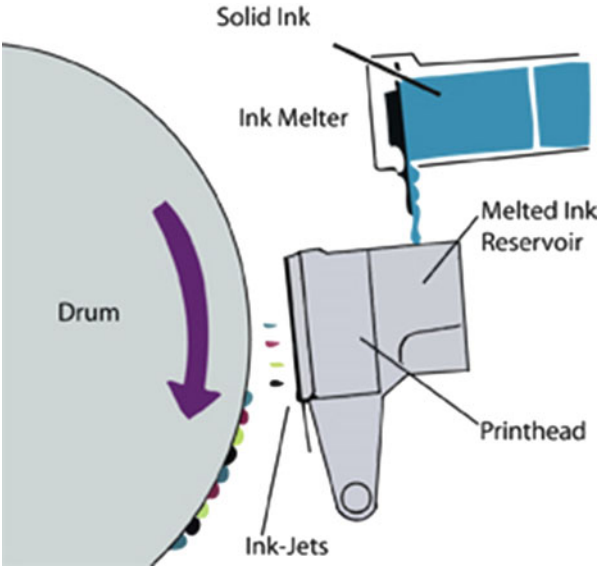

Scheme 9.18 Solid ink printer with offset printing. *Molten color ink* is sprayed onto the drum by an ink-jet printhead [80]. Reprinted with permission of IS&T: The Society for Imaging Science and Technology sole copyright owners of www.imaging.org

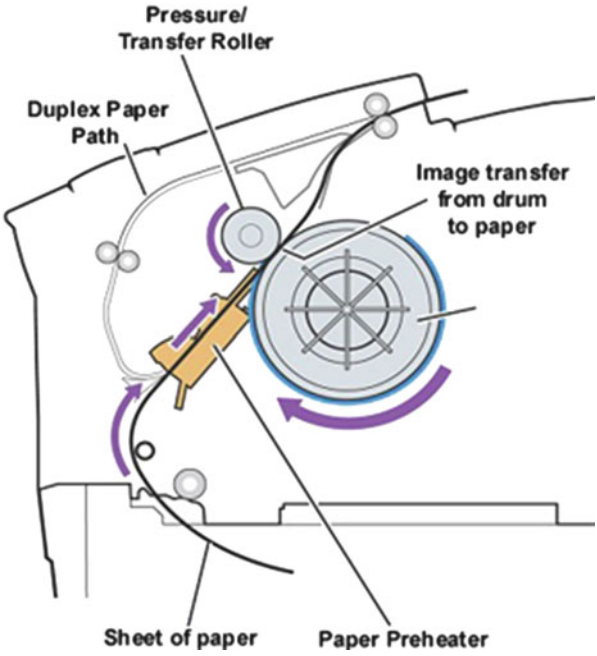

Scheme 9.19 Solid ink printer with offset printing path. Semisolid color ink transfers from the drum onto a heated sheet of paper. The duplex path allows two-sided printing [80]. Reprinted with permission of IS&T: The Society for Imaging Science and Technology sole copyright owners of www.imaging.org

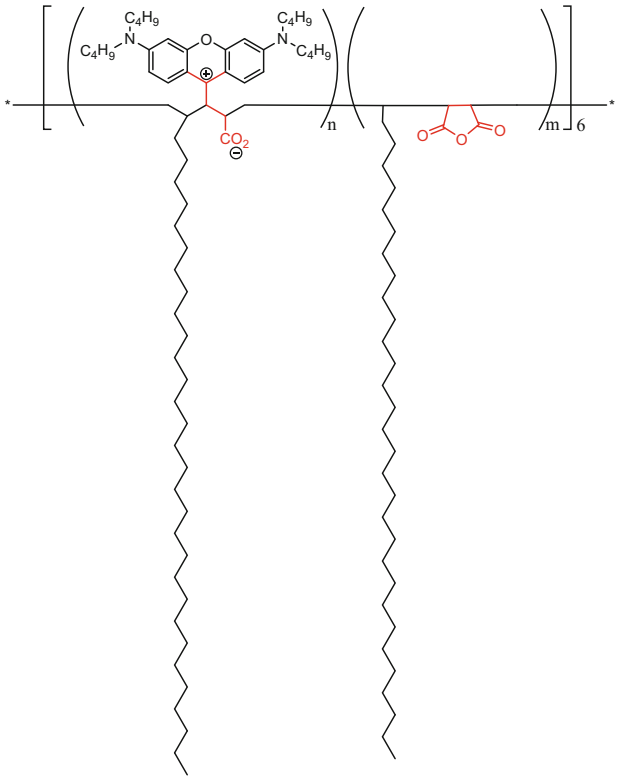

Fig. 9.33 Magenta phase-change ink based upon poly(maleic anhydride-*co*-α-olefin) [81]

On the other hand, the elevated temperature often employed to melt the solid ink has resulted in color stability and color stabilization as important technical challenge topics for phase-change inks. In one approach to developing new magenta ink compositions that exhibit improved color stability, in addition to other required qualities of phase-change inks, ink compositions based upon modified poly(maleic anhydride-*co*-α-olefin) were designed [81]. In the first case, the maleic copolymer was derivatized with *N*,*N*-diethylaminophenol, in the presence of sulfuric acid, to yield a solid magenta zwitterionic copolymer. The proposed chemical structure of this compound is presented in Fig. 9.33.

The composition depicted in Fig. 9.33 was then formulated into a solid ink base. The solid ink base is comprised of a polyethylene wax, a stearyl stearamide wax, a tetra-amide resin (from Example 1 in [83]), a hydroabietyl alcohol derivative (from Example 1 in [84]), a urethane resin derivative (from Example 4 in [85]), and an antioxidant. To prepare this mixture, the components are first melted, mixed, and then filtered. Then the components are mixed at 135 °C in an oven until molten, transferred to a heating mantle, and mixed for 45 min. This final product is then filtered and poured into molds for testing purposes. For laboratory print testing, the

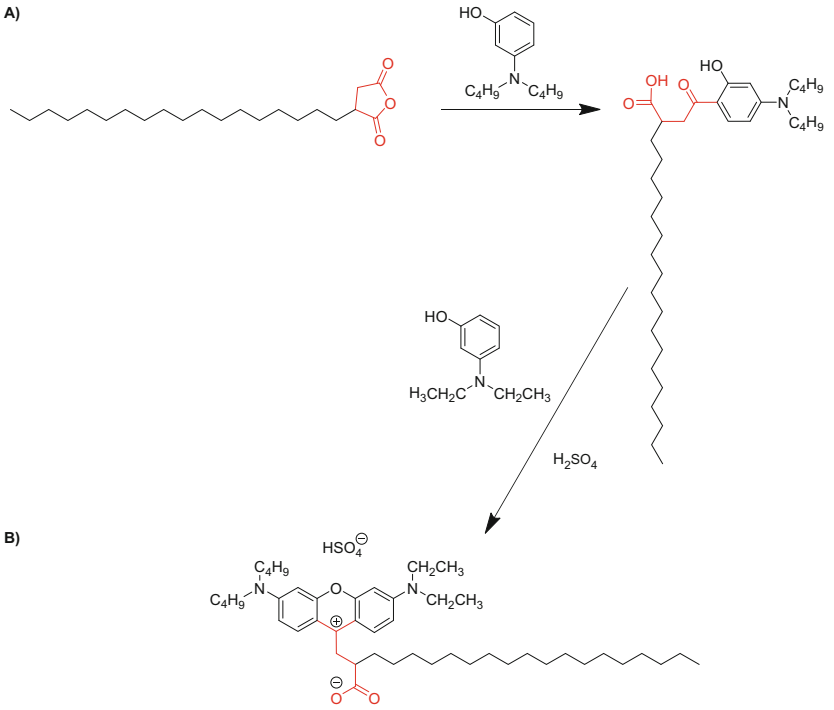

Scheme 9.20 Synthetic approach to a phase-change ink derived from octadecyl succinic anhydride [86]

ink wax molds are melted onto a printing plate at 150 °C. Then a roller bar fitted with paper is rolled over the plate. Once the paper is cooled, the ink was evaluated visually for performance [81].

In another approach to a magenta phase-change ink, octadecyl succinic anhydride is reacted with dibutyl-hydroxybenzoyl benzoic acid to yield the phase-change intermediate depicted in Scheme 9.20a. This intermediate is then reacted with *N*,*N*′-diethyl-m-aminophenol, in the presence of sulfuric acid, to yield a magenta, unsymmetrical solid depicted in Scheme 9.20b [86].

The composition depicted in Scheme 9.20 was then formulated into a solid ink base.

Another important class of ink is liquid toner. Liquid toner inks are found in another offset printing technology that is sometimes referred to as a liquid electrophotography process. This process is depicted in Fig. 9.34 representing HP Indigo printing process.

In a brief overview of this printing process, a uniform electrostatic charge is applied to a charge roller comprising the photo imaging plate (PIP) mounted on the imaging cylinder (**1**). While the imaging cylinder continues rolling and, after charging, the PIP is exposed to laser imaging (**2**), this laser exposure enables the surface charge to be dissipated resulting in the formation of an invisible

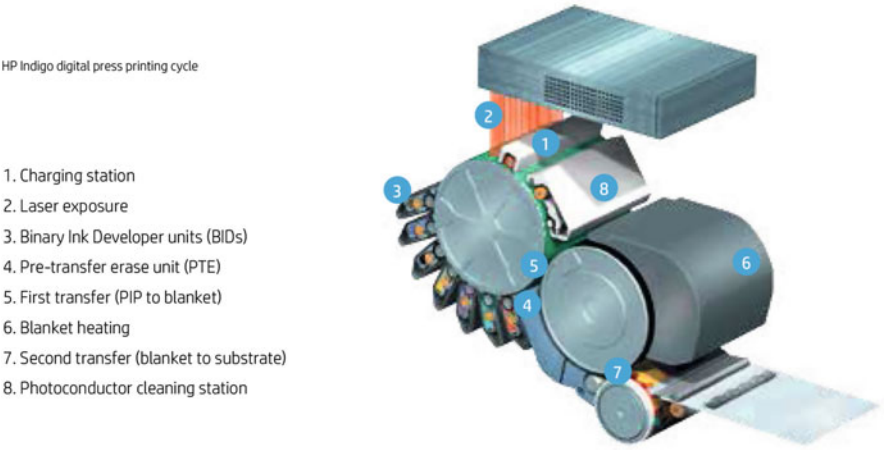

Fig. 9.34 HP Indigo digital press printing process [87]. Reprinted from *HP Indigo Digital Offset Color Technology*, 4AA1-5248ENW, Hewlett-Packard Development Company, **2012**, with permission from The Hewlett-Packard Company

electrostatic image on the PIP surface. As the imaging cylinder continues to rotate, the image is developed by binary ink developer (BID) units, where the ink is attracted to image areas and repelled from nonimage areas (**3**). The imaging cylinder has now transitioned from the invisible image to a clean inked image that is now visible. Immediately prior to the image transfer, the PIP is exposed to diodes to form a uniform surface conductivity to allow for a clean transfer of the image, in the pre-transfer erase unit (**4**). The ink image is then transferred to an electrostatically charged blanket located on the transfer cylinder (**5**). The ink image is now transferred to the heated blanket, resulting in the ink particles partially melting and blending, while, simultaneously, the carrier oil is evaporating and being recycled. The process results in an image that is in the form of an almost dry, hot, adhesive plastic film (**6**). The hot, adhesive ink film then comes into contact with the substrate, which is below the melting temperature of the ink film, which results in 100 % transfer of the ink film from the heat blanket to the substrate (**7**). For the PIP, the final step is a pass through the cleaning station to prepare the PIP for the next image (**8**) [88].

One key to the success of the HP Indigo printing process is the complete transfer of the hot, adhesive ink film to the substrate as indicated in (**7**) above. In one example of preparing an adhesive toner, a composition comprising poly(ethylene-co-methacrylic acid), poly(ethylene-*co*-acrylic acid), and poly(ethylene-*co*-ethyl acrylate-*co*-maleic anhydride) is blended in an isoparaffinic oil (Isopar L). To this pasty blend, pigments, aluminum stearate, and additional Isopar are added to provide for a cyan color after 20 h of mixing. Additional Isopar is added to form a dispersion to which a charge director containing lecithin, basic barium petronate, and isopropylamine dodecylbenzesulfonate is added to yield the final cyan toner.

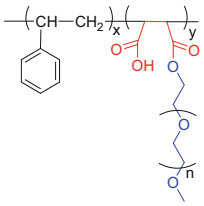

Fig. 9.35 Proposed structure for poly(styrene-*co*-maleic anhydride)-*g*-polyethylene glycol monomethyl ether) (SMA–PEG)

This toner highlights the use of maleic anhydride thermoplastic as exhibiting a higher affinity for paper than other materials [89].

In another approach, a paper coating was designed which includes the reaction product of maleic anhydride, polyethylene glycol monomethyl ether, and styrene which is pH adjusted with sodium hydroxide to yield a dispersion [90]. A proposed structure for the base copolymer reaction product, in un-neutralized form, is presented in Fig. 9.35.

SMA–PEG was added to a solution of oxidized potato starch which was then applied, via size press, to wood-free paper at 0.1–5 g/m^2 (solid). After conditioning the paper for 24 h at 50 % relative humidity and room temperature, the paper was calendared. The paper was then printed on using an Indigo 3000 digital printing press and the toner adhesiveness judged with adhesive tape as a function of time. Test results indicate immediate improvement in adhesiveness of the liquid toner, which the adhesiveness continues to positively build over a 24 h period. Also, coatings which were 100 % SMA–PEG generated even greater immediate adhesive power when compared to either starch or starch/SMA–PEG blends [90].

Recently, a variety of maleic anhydride-based materials were developed and proposed as additives to toner receptive coatings or as adhesion enhancement agents to solvent-based toner systems. Examples of the copolymers are presented in Fig. 9.36. (*Note*: Fig. 9.36 abbreviations are as follows: ODA = octyl/decyl acrylate, IBOA = isobornyl acrylate, MAN = maleic anhydride, VCHE = 4-vinyl-1-cyclohexene 1,2-epoxide).

A key property to the copolymers presented in Fig. 9.36 is their compatibility to hydrophobic oils such as isoparaffinic fluids (ISOPAR^{TM}). To better demonstrate their compatibility with oil such as ISOPAR^{TM}, a polymer solubility study was performed. Results of this oil solubility evaluation are presented in Table 9.23.

9.4.3 Aqueous Printing

For print-receptive surfaces that receive aqueous-based inks, water-soluble and water-sensitive polymers continue to deliver many important properties to the final coated product. Water-soluble polymers such as hydroxyethylcellulose and

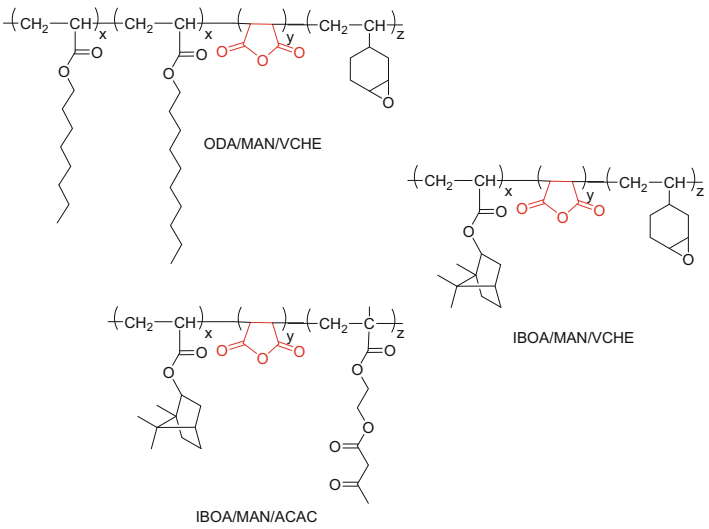

Fig. 9.36 Maleic anhydride copolymers for toner printing application [91]

Table 9.23 Oil solubility of maleic anhydride-based copolymers for toner printing applications [91]

	Isopar H	Isopar K	Isopar L	Isopar M	Isopar V
Polymer	Soluble? (Y, P, N)	Soluble? (Y, P, N)	Soluble? (Y, P, N)	Soluble? (Y, P, N)	Soluble? (Y, P, N)
ODA/MAN/VCHE (80/10/10)	Y	Y	Y	Y	Y
IBOA/MAN/VCHE (80/10/10)	Y−	Y−	Y−	Y	Y−
IBOA/MAN/ACAC (80/10/10)	P	P	P	P+	N
	Linseed oil	Mineral oil	Isopar C	Isopar E	Isopar G
Polymer	Soluble? (Y, P, N)	Soluble? (Y, P, N)	Soluble? (Y, P, N)	Soluble? (Y, P, N)	Soluble? (Y, P, N)
ODA/MAN/VCHE (80/10/10)	Y	Y	Y	Y	Y
IBOA/MAN/VCHE (80/10/10)	Y	Y	Y−	Y−	Y
IBOA/MAN/ACAC (80/10/10)	Y	P	P	Y	P

P partial

sodium carboxymethyl cellulose (HEC and CMC), polyvinyl alcohol (PVOH), polyethylene oxide (PEO), polyethyleneimine (PEI), poly(2-ethyl-2-oxazoline) (PEOX), and polyvinylpyrrolidone (PVP) are commonly employed. Most are capable of forming glossy films suitable for absorbing or displacing the print ink

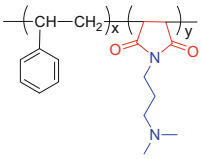

Fig. 9.37 Poly(styrene-*co*-dimethylaminopropylamine maleimide) SMA® 1000I resin [95]

solvent. However, their ability to bind the dyes and pigments, enabling enhanced image resolution and high optical density, is not universal. Often, these materials require further modifications to achieve optimal performance [92, 93].

Paper coatings comprising derivatives of styrene–maleic anhydride resins have been developed to support a growing digital ink-jet printing market. In one example, a poly(styrene-*co*-maleimide) resin neutralized with acetic acid was evaluated in a paper coating [94]. The base chemical structure of the SMA® 1000I resin is presented in Fig. 9.37.

To formulate the paper coating, partially hydrolyzed polyvinyl alcohol, poly (styrene-*co*-maleimide) resin neutralized with acetic acid, and precipitated calcium carbonate were formulated in water. Coatings of 8–9 g/m^2 were applied using a standard laboratory coater. After conditioning the paper for 24 h at 50 % relative humidity and room temperature, the paper was calendared at 100 °C. Anionic, aqueous base ink-jet ink was printed onto coated surface and evaluated. Results of the study indicate that this approach enables chemical fixation of the anionic ink to the cationic, poly(styrene-*co*-maleimide) resin neutralized with acetic acid, resin leading to high optical density and sharpness, Furthermore, water fastness is improved, which is another indicator of dye fixation, coupled to enhance surface and print gloss properties [94].

Beyond print receptivity, enhancing the physical performance properties of coatings often requires cross-linking to develop the film and product performance attributes. Cross-linking, a process forming new bonds or links between polymer and oligomer chains, can result in significant improvements to water/solvent resistance, toughness, and durability, as these new bonds lead to dramatic increases in molecular weight. Cross-linking can also reduce print receptivity, so a targeted approach is required. Another interesting subsegment of cross-linking is in the field of applied temperature. Knowledge and capability in low-temperature cure or curing at ambient temperature is being developed. Ambient curing is interesting, not only because of the ability to form networked, gel structures on heat-sensitive materials but in introducing the possibility of reducing energy consumption during the product production process. Aziridines and carbodiimides are known to be useful in this area, especially for carboxylic acid-containing polymers. The acetoacetyl moiety is also known to be useful for a variety of polymer systems where suitable reactions with functional materials comprised of isocyanate, activated alkenes, aldehydes, and polyfunctional amine moieties are desirable.

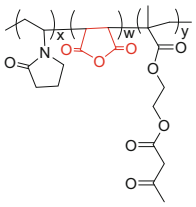

Fig. 9.38 Poly(vinyl pyrrolidone-*co*-maleic anhydride–*co*-acetoacetoxyethyl methacrylate) (PVP/MAN/AAEM) structure [93, 97]

Table 9.24 Physical properties of PVP/MAN/AAEM curable polymer

Property	PVP/MAN/AAEM data
Viscosity (cPs) (50 % in hydroxyethyl acrylate) (DV-III, 100 RPM, #4 spindle)	1580
T_g (°C)	~95 (first heating)
K-value range	~10

Toward this end, a study of multi-reactive features of a terpolymer comprised of poly(vinyl pyrrolidone-*co*-maleic anhydride–*co*-acetoacetoxyethyl methacrylate) (PVP/MAN/AAEM) was designed and evaluated in the context of various curing strategies [96]. The structure of PVP/MAN/AAEM is presented in Fig. 9.38.

The PVP/MAN/AAEM polymer has a number of interesting attributes. The maleic anhydride can hydrolyze upon introduction to water, yielding a vicinal maleic acid terpolymer which can be suitably neutralized with bases such as ammonium hydroxide or sodium hydroxide. Another interesting attribute of this terpolymer is the inherent hydrogen bonding capacity of the pyrrolidonyl carbonyl group coupled with the proton donating group on the maleic group. This coupled functionality results in polymeric, zwitterionic behavior [98]. The physical properties of the terpolymer are presented in Table 9.24. In general, the polymer is a low-viscosity material that exhibits a reasonably high T_g. In addition to the previously mentioned properties, the polymer also exhibits high gloss, transparency, film forming, and dye fixation properties.

To demonstrate the cross-linking functionality of the PVP/MAN/AAEM terpolymer, a variety of cross-linking strategies were evaluated. First, films were constructed, to clearly elucidate the thermal cross-linking between PVP/MAN/AAEM + hydroxyethyl cellulose and PVP/MAN/AAEM + polyvinyl alcohol. The results demonstrate that water-resistive films, which were clear, glossy, and hard films (8H pencil hardness), coupled with good solvent resistance, were observed. Analogous test results for polyvinylpyrrolidone (PVP K-90) were inferior.

Second, other popular printing applications deploy microporous coating technology, where alumina pigments are critical components to the print-receptive layer

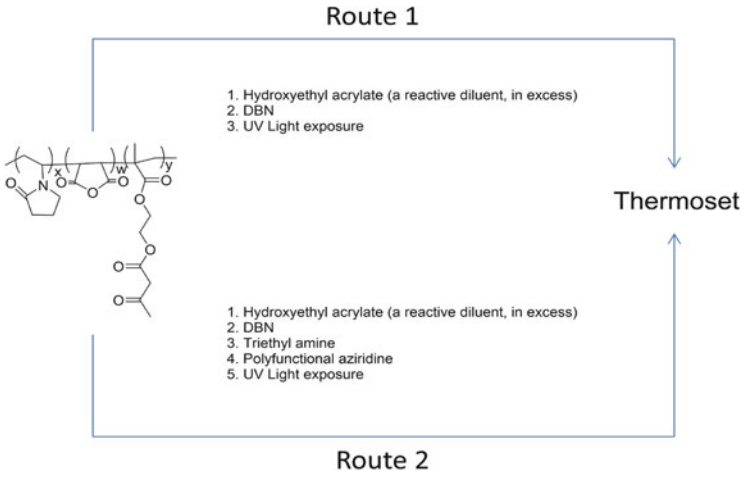

Scheme 9.21 Strategy for dual cure of PVP/MAN/AAEM via the Michael addition and aziridine [92, 93, 97]

[99]. A key feature of the microporous coating pigment loading is that the dry coating comprises ~90 % (by weight) pigment. A common binder employed in these coatings is polyvinyl alcohol, which can cross-link with melamine/formaldehyde, glyoxal, or zirconates. For the PVP/MAN/AAEM terpolymer, AAEM monomer is also known as good chelator of metals such as copper and alumina. A variety of films were made to elucidate the cross-linking potential of PVP/MAN/AAEM terpolymer employing alumina chelation coupled with thermal cross-linking to evaluate the general coating behavior. Water-resistive films were also noted as arising from this approach.

Third, previous work on polymers comprising carboxylic acid and acetoacetyl moieties for dual-cure coatings demonstrated that using a cross-linker blend of dialdehyde and aziridine enabled improvements to water resistance of nonwoven articles, such as paper towels [100]. An interesting feature of this curing approach is the low-temperature cure range (20–40 °C). Utilizing this approach, the cure response of PVP/MAN/AAEM terpolymer was evaluated for both high-temperature and ambient-temperature curing. Excellent water resistance was observed for both temperature ranges. Note that for low-temperature curing, the time was extended to enable the coating to dry [97].

Fourth, to render PVP/MAN/AAEM terpolymer suitable for UV cross-linking, the base polymer was derivatized by employing the "Michael addition" of an acrylate to the acetoacetate moiety in the presence of a base catalyst 1,5-Diazabicyclo[4.3.0]non-5-ene (DBN) (see Route 1 in Scheme 9.21). Such approaches have been thoroughly presented in earlier papers [101, 102]. Mechanistically, the addition of DBN enables the deprotonation of the acetoacetoxy's methylene group to yield an enolate anion. The enolate anion then readily attacks, in the fashion of 1,4-conjugate addition, the olefin of the acrylate. The carbonyl

Table 9.25 Compositions for PVP/MAN/AAEM UV–thermal dual cure

Material	Coating I	Coating II	Coating III	Coating IV
PVP/MAN/AAEM	48.75	48.75	47.25	46
Hydroxyethyl acrylate	48.75	48.75	47.25	46
Darocur 1173	2.5	–	–	–
DBN	–	2.5	2.5	2.4
TEA	–	–	0.5	–
PZ-33 (aziridine)	–	–	2.5	5.6
Total	100	100	100	100

Table 9.26 Properties for PVP/MAN/AAEM UV–thermal dual cure

Property	Coating I	Coating II	Coating III	Coating IV
Appearance	Transparent	Transparent	Transparent	Hazy
Gloss	High	High	High	High
Pencil hardness	2H	2H	3H	6H
Adhesion	100 %	100 %	100 %	100 %
MEK rubs	60	100	180	>200
Water resistance	Water resistant	Water resistant	Water resistant	Water resistant

stabilizes the resulting anion until the base is regenerated from proton transfer. This reaction occurs easily at room temperature. The result is a polymer suitable for further initiating common UV-coating monomer and polymer components. For dual cure, aziridine was also added to enable facile, low-temperature, reactive cross-linking with the acid groups of maleic anhydride (see Route 2 in Scheme 9.21). A schematic of these proposed reactions is presented in Scheme 9.21.

Various nonaqueous coating compositions were made to demonstrate the dual-cure functionality of this system. The coatings are presented in Table 9.25. Table 9.26 presents the final physical coating properties.

The PVP/MAN/AAEM terpolymer in hydroxyethyl acrylate exhibited UV cure in the presence of photo-initiator. Interestingly, the PVP/MAN/AAEM terpolymer exhibited cure, in the absence of photo-initiator, where only the Michael addition product formed by DBN was employed. Films were glossy and transparent and exhibited excellent adhesion. Dual-cure (UV and thermal) performance, in the presence of DBN and aziridine, was also observed. This is demonstrated by the boost in the performance of the film, comparing DBN to DBN + aziridine. The additional aziridine boosts the MEK rub resistance, which is indicative of an additional cure response for this coating system [92, 93, 97].

Acknowledgments The authors would like to express their sincere gratitude to Alan Fernyhough, Frank Fusiak, Randy Johnson, and Laurence Senak, all of Ashland, Inc., for their many helpful conversations/suggestions and thorough review of the manuscript prior to publication.

References

1. Wicks ZW (2004) Alkyd resins. In: Seidel A (ed) Kirk-Othmer encyclopedia of chemical technology, vol 2, 5th edn. Wiley, Hoboken, NJ
2. Blum H, Fleiter L (1993) Polymers capable of oxidative crosslinking. US 5,223,582
3. Jayne DW, Milton DH (1942) Amino alcohol esters. US 2,305,083
4. Zabel KH, Klaasen RP, Muizebelt WJ, Gracey BP, Hallett C, Brooks CD (1999) Prog Org Coatings 35:255–264
5. Muizebelt WJ, Hubert JC, Nielen MWF, Klaasen RP, Zabel KH (2000) Prog Org Coatings 40:121–130
6. Nuplex Resins (2011) Resins for decorative coating. Product Brochure, February
7. Deans H, Gracey BP, Hallett C, Hodgson PKG, Klaasen RP (1997) Reactive diluents. WO 97/02230
8. Meijer MD, Mes GP, Kelders HP, Klaasen RP, Lansbergen AJH, Spierenburg ML (2012) Coating composition comprising a reactive diluent of malonate. US 8,124,688 B2
9. Blum H (1990) Aqueous solutions or dispersions of self-crosslinking binders, a process for their production and their use. US 4,980,412
10. Wamprecht C, Blum H, Pedain J, Hohlein P (1992) Modified copolymers, a process for their production, binders containing the modified copolymers and their use in coating compositions and sealing compounds. US 5,135,987
11. Marrion AR (1994) The chemistry and physics of coatings. Royal Society of Chemistry, Cambridge
12. Knapp GG (1967) Ester-amides of alkenyl succinic anhydride and diethanolamine as ashless dispersants. US 3,324,033
13. Fushimi A, Okude Y, Ishikura S (2001) Prog Org Coating 42:159–166
14. Muller B, Oughourlian C, Schubert M (2000) Corros Sci 42:577–584
15. Lai CT, Hong JL (2009) J Phys Chem C 113:18578–18583
16. Soer WJ, Ming W, Koning CE, van Benthem RATM, Mol JMC, Terryn H (2009) Prog Org Coatings 65(1):94–103
17. Soer WJ, Ming W, Koning CE, van Benthem RATM (2008) Prog Org Coatings 61:224–232
18. Lazarova E, Petkova G, Iankova T, Ivan L, Neikov G (2008) J Appl Electrochem 38:1391–1399
19. Gothlich A, Vandermeulen G, Hickl M, Dornbusch M, Witteler H, Gonzalez MF (2008) Method for applying integrated pre-treatment layers containing dicarboxylic acid olefin copolymers to metallic surfaces. US 2008/0171195A1
20. Gonzalez MF, Hickl M, Mock-Knoblauch C, Essig M, Hennig I, Gothlich A (2008) Method for applying corrosion protection layers comprising thioamides to metallic surfaces. US 2008/0131678A1
21. Gonzalez MF, Hickl M, Mock-Knoblauch C, Essig M, Hennig I, Gothlich A (2012) Method for applying corrosion protection layers comprising thioamides to metallic surfaces. US 8,273,412 B2
22. Zhu X, Guo S, Janczewski D, Velandia FJP, Teo SLM, Vancso GJ (2014) Langmuir 30:288–296
23. Voronov S, Kohut A, Tarnavchyk I, Voronov A (2014) Curr Opin Colloid Interface Sci 19:95–121
24. Rabie ST, Ahmed AE, Sabaa MW, Abd El-Ghaffar MA (2013) J Ind Eng Chem 19:1869–1878
25. Cloete WJ, Verwey L, Klumperman B (2013) E Poly J 49:1080–1088
26. Mirasol F (2012) Chemical profile: maleic anhydride. ICIS.com, 23 April
27. Victory M, Burridge E (2012) Chemical profile: maleic anhydride. ICIS.com, 9 January
28. Jedlinski ZJ (1991) Polyesters. In: Kricheldorf HR (ed) Handbook of polymer synthesis (Part A). Marcel Dekker, New York, NY, pp 645–678

29. Fradet A, Arlaud P (1989) Unsaturated polyesters. In: Comprehensive polymer science, vol 5. Pergamon Press, Oxford, pp 331–344
30. Feuer SS, Bockstahler TE, Brown CA, Rosenthal I (1954) Ind Eng Chem 46(8):1643–1645
31. Grunden BL, Sung CSP (2003) Macromolecules 36:3166–3173
32. *Ashland resins for the transportation market*. Brochure. Ashland Performance Materials (2010)
33. Seeman WH (1990) Plastic transfer molding techniques for the production of fiber reinforced plastic structures. US 4,902,215
34. Cao X, Lee LJ (2003) Polymer 44:1507–1516
35. Varga C, Miskolczi N, Bartha L, Lipoczi G (2010) Mater Des 31:185–193
36. *Aropol™ M 105 TB low styrene emission resin*. Technical datasheet. Ashland Performance Materials (2013)
37. Varga C, Miskolczi N, Szakacs H, Lipoczi G (2011) Mater Des 32:12–20
38. Penczek P, Czub P, Pielichowski J (2005) Adv Polym Sci 184:1–95
39. Frydrych A, Ostrysz R, Penczek P (1999) Polimery 44(11–12):745–749
40. Klang JA, Yang LS (1999) Process for making dicyclopentadiene polyetherester resins. WO99/15574
41. Baley C, Perrot Y, Davies P, Bourmaud A, Grohens Y (2006) Appl Compos Mater 13:1–22
42. Pepper T (2001) Polyester resins. In: ASM handbook, vol 21. pp. 90–96
43. Derakane™ epoxy vinyl ester resins: the Evolution of Corrosion Resistant FRP. Ashland Performance Materials (2012)
44. Hetron® 197. Technical data sheet. Ashland Performance Materials, Document 2127 V2 F2, Approved 2009-6-12 (2011)
45. Atlac 382 (2011) Product data sheet. DSM composite resins, version: 001893/7.0
46. Valea A, Gonzalez ML, Mondragon I (1999) J Appl Polym Sci 71:21–28
47. Guide to chemical resistance: durability and protection, version 12:002_12-4340. DSM (2012)
48. Hetron™ and Aropol™ resin selection guide for corrosion resistant FRP applications. Bulletin 2636-1. Ashland (2003)
49. Stenzenberger H (2001) BMI resins. ASM Handbook 21:97–104
50. De Abajo J (1992) Chapter 15: Polyimides. In: Kricheldorf HR (ed) Handbook of polymer synthesis. Marcel Decker, New York, NY, pp 941–989
51. Searle NE (1948) Synthesis of N-aryl-maleimides. US 2,444,536
52. Link PE (2007) High temperature degradation of 5250-4 polymer resin. Thesis. Air Force Institute of Technology, Wright Patterson AFB, OH
53. CYCOM® 5250-4 RTM resin system, Cytec Engineering Materials. AECM-00019, Rev: 01. (2012)
54. Rider AN, Baker AA, Wang CH, Smith G (2011) Appl Compos Mater 18:231–251
55. Lay-up and bagging guidelines. Technical data sheet, TDS1038_05.13_Issue1a. Cytec (2012)
56. CYCOM® 5250-4 RTM resin system, Cytec Engineering Materials. AECM-00008, Rev: 01. (2012)
57. Mallick PK (1993) Fiber reinforced composites. In: Materials, manufacturing, and design, 2nd edn. Marcel Dekker, New York, NY
58. Zhang Y, Broekhuis AA, Picchioni F (2009) Macromolecules 42:1906–1912
59. Boudenot JC (2008) CR Physique 9:41–52
60. http://www.nobelprize.org/nobel_prizes/physics/laureates/1956/
61. Riordan M (2014) Transistor. Encyclopedia Britannica. Encyclopedia Britannica Online, Web 06 Nov
62. http://www.ti.com/corp/docs/company/history/timeline/semicon/1950/docs/54commercial.htm used with permission – Texas Instruments Incorporated
63. Herold EW (1955) J Franklin Institute 259(2):87–106
64. http://www.intel.com/pressroom/kits/events/moores_law_40th/ downloaded 11/12/2014
65. Gilleo K (1994) Circuits Assembly October:30–34

66. Gilleo K (2001) Chapter 21: Die attach and rework. In: Gilleo K (ed) Area array packaging handbook: manufacturing and assembly. McGraw-Hill, New York, NY
67. Musa OM, Herr DE (2004) Die attach adhesives with vinyl ether and carbamate or urea functionality. US 6,699,929 B2
68. Musa OM (2008) Maleimide resin with cyanurate core. US 7,456,280 B2
69. Tatusko P, Williams R (1973) Circuit panel and method of construction. US 3,777,220
70. Mallik D, Sankman RL (2015) 3D integrated circuit package with through-mold first level interconnects. US 9,099,444
71. Zhang X, Chen GC, Collins A, Jacobson S, Morganelli P, Dar YL, Musa OM (2009) J Polym Sci: Part A: Polym Chem 47:1073–1084
72. Zeller-Pendrey JI (2011) Curable resin composition. US 8,008,422 B2
73. 3M Scotch-Weld™ Industrial Adhesive 4475 Technical Data, 78690002478, 3M (2010)
74. MSDS for 3M Scotch-Weld™ Industrial Plastic Adhesive 4475, August 2 (2010)
75. Hirano T (2003) Thermal transfer sheet, thermal transfer method and thermal transfer system. US 6,646,664 B2
76. Stone E, Wasyliw B, Incontro RC, Giunta JP (1990) Modified polyamide compositions, their preparation and printing inks containing them. EP0359129 A2
77. Fujino K, Fujitaka T, Usui K, Masumoto K, Yoshioka H (2002) Modified polyolefin composition and uses thereof. US 6,426,388 B1
78. Usui K, Fujino T, Fujitaka T, Matsui H, Yoshioka S (2006) Modified polyolefin resin, modified polyolefin resin composition, and use thereof. EP 1321481 B1
79. Pekarovicova A, Bhide H, Fleming PD, Pekarovic J (2003) J Coat Technol 75(936):65–72
80. Jaeger CW (2009) Color solid ink printing. http://www.imaging.org/ist/resources/tutorials/solid_ink.cfm
81. Banning JH (2009) Colorant compounds. US 7,485,728 B2
82. Xerox® ColorQube® 9302/9303. Xerox Product Literature, Q93BR-01UE (2014)
83. Banning JH, Jaeger CW, Titterington RD (2001) Composition of matter, a phase change ink, and a method of reducing a coefficient of friction of a phase change ink formulation. US 6,174,937
84. Bui LV, King CR, Banning JH, Titterington DR (1998) Isocyanate-derived materials for use in phase change ink jet inks. US 5,782,966
85. Banning JH, Titterington, DR, Wedler WG (2001) Colorless compounds, solid inks, and printing methods. US 6,309,453
86. Banning JH (2009) Colorant compounds. US 2009/0099372 A1
87. HP indigo digital offset color technology. 4AA1-5248ENW. Hewlett-Packard Development Company (2012). With permission from The Hewlett-Packard Company
88. HP indigo digital offset color technology. 4AA1-5248ENW. Hewlett-Packard Development Company (2012)
89. Ben-Avraham P, Bossidan B, Landa B (2006) Liquid toner and method of printing using same. US 7,078,141 B2
90. Stein H, Ettl R, Bell HP (2009) Substrates coated with maleic acid for electrophotographic printing method. US 2009/0162624 A1
91. Hood DK, Wasserman CJ, Visscher KB, Sarkar S (2014) Hydrophobic coating compositions for forming toner receptive coatings. WO 2014/160754 A1
92. Hood DK, Kamin S, Visscher KB (2012) American Coatings Conference Session 3.2: Radiation curing, Indianapolis, IN, May 7
93. Hood DK, Visscher KB, Kamin S (2013) Lactamic polymer containing an acetoacetate moiety. US 2013/0261268 A1
94. Sreekumar J, Sain M, Farnood R, Dougherty W (2005) Pulp Paper Can 106(3):38–41
95. Technical data sheet: SMA® 1000I Resin. Cray Valley, USA. LLC (2010)
96. Del Rector F, Blount WW, Leonard DR (1989) J Coat Technol 61(771):31–37
97. Hood DK, Visscher KB, Kamin S, Sarkar S (2012) Lactamic polymers containing an acetoacetate moiety. WO 2012/148533 A1

98. Subotic D, Ferguson J, Warren BCH (1989) Eur Polym J 25(12):1233–1237
99. Schroder H, Schupp G (1984) Recording paper for ink jet recording processes. US 4,474,847
100. Goldstein JE, Pangrazi RJ (2000) Polymers having dual crosslinkable functionality and process for forming high performance nonwoven webs. US 6,117,492
101. Mathur BD, Viswanathan K, Miller KM, Long TE (2006) Prog Polym Sci 31:487–531
102. Gould ML, Narayan-Sarathy S, Hammond TE, Fechter RB (2005) RadTech Europe

Chapter 10
Application of Maleic Anhydride-Based Materials

David K. Hood and Osama M. Musa

10.1 Introduction

Exploration of maleic anhydride's utility continues in this chapter, which is a continuation from Chap. 9. Written as a survey, this chapter addresses the most important maleic anhydride applications while discussing a few more interesting topics in detail. It is our hope that the reader will finish this chapter with a greater appreciation for the broad applicability and emerging potential for maleic anhydride.

10.2 Additives for Automotive Applications

Additive packages for engine oil and automotive fuels are essential components to properly operating equipment, whether for improving fuel efficiency, reducing engine wear, or ensuring compliance with local emission standards. Not unexpectedly, each ingredient found in the additive package serves a different purpose and, in some cases, can interfere with other additive's performance capabilities. Consequently, significant testing is required to ensure proper formulation design and capability prior to market implementation. We will examine only a few examples of additives found in these automotive applications to understand how maleic anhydride fundamentally contributes to this industry.

D.K. Hood (✉) • O.M. Musa
Ashland Inc., 1005 Route 202/206, Bridgewater, NJ 08807, USA
e-mail: dhood@ashland.com

O.M. Musa (ed.), *Handbook of Maleic Anhydride Based Materials*,
DOI 10.1007/978-3-319-29454-4_10

10.2.1 Fuel Additives

Storage and conveyance of diesel fuel and gasoline commonly occurs in vessels and pipes constructed from mild carbon steel. As free water is commonly found in fuel, internal corrosion of pipes and storage vessels is a significant problem. In addition to surface corrosion, fine particles of rust can separate from the steel surfaces and transport in the fuel itself. Such corrosion issues can not only lead to increased drag on fluids, resulting in greater energy consumption during pump operation, but also increase wear on equipment, increasing maintenance issues and downtime. To overcome these challenges, compounds capable of inhibiting rust formation are frequently added to fuel. These compounds are known as rust inhibitors [1]. Examples of low molecular weight corrosion inhibitors are presented in Fig. 10.1.

2-Octadecen-1-ylsuccinic anhydride (ODSA), 2-dodecen-1-ylsuccinic anhydride (DDSA), 2-Octen-1-ylsuccinic anhydride (OSA), and 6-(3-tetrapropenyl-2,5-dioxopyrrolidin-1yl)hexanoic acid (Tetra-PSCA) are all liquid at room temperature [2]. Essentially, these compounds function by the polar head group, i.e., anhydride moiety, anchoring or adhering to the metal surface, enabling the metal surface to be protected. The hydrophobic tail enables the solubilization of the compound in the fuel [3]. In addition, the hydrophobic tail can shield the metal surface from exposure to water molecules.

2-Octadecen-1-ylsuccinic anhydride

2-Dodecen-1-ylsuccinic anhydride

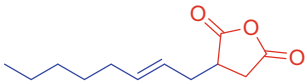

2-Octen-1-ylsuccinic anhydride

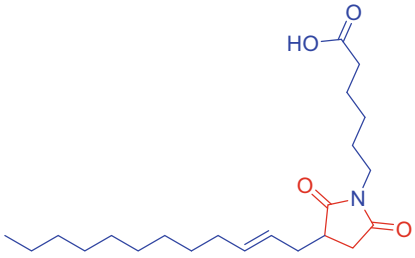

6-(3-tetrapropenyl-2,5-dioxopyrrolidin-1-yl)hexanoic acid

Fig. 10.1 Chemical structures for commercial corrosion inhibitors

In a modification of succinate derivatives, the incorporation of triazole function was evaluated in corrosion inhibition. Specific examples of the triazole compounds studied are presented in Fig. 10.2.

In developing these triazole compounds, DDSA was employed as the foundation to which, through an esterification reaction, the alcoholic triazole compound was constructed. The triazole moieties were first prepared via "click" chemistry. Octyl, dodecyl, and octadecyl substituent derivatives (labeled as R' in Fig. 10.2) were synthesized and evaluated. The dosing effect of rust prevention was evaluated as per ASTM D665 Method where steel coupons are immersed in a seawater/paraffin oil for a period of 1 day. Results of these tests are presented in Table 10.1.

Test results suggest slightly better performance for the mono-functional triazole corrosion inhibitor. This slight improvement is attributed to the presence of the carboxylic acid group, which can react with products of corrosion, thereby increasing the thickness of the protective layer. However, in general, the testing demonstrated good anti-corrosion behavior for both classes of materials. Interestingly, increasing the length of the R' (see Fig. 10.2) alkyl group was found to be a hindrance to performance. This effect was attributed to a reduced number of molecules resulting from an increasing molecular weight, at identical concentrations [4].

In addition to small molecule compounds, polymeric corrosion inhibitors are also well known. For example, polysuccinimide, prepared from maleic anhydride

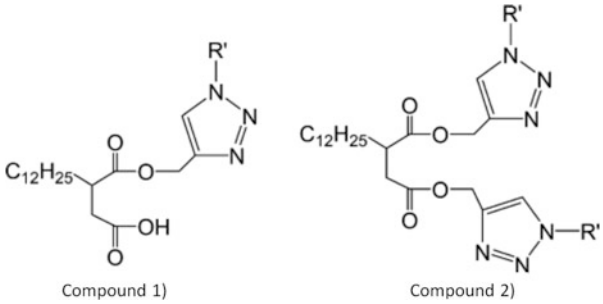

Fig. 10.2 Succinic-based triazole compounds for corrosion inhibition [4]. Adapted with permission from Baek, S.-Y.; Kim, Y.-W.; Yoo, S.-H.; Chung, K.; Kim, N.-K.; Kim, J.-S., *Ind. Eng. Chem. Res*., 51, pp. 9669–9678. Copyright 2012 American Chemical Society

Table 10.1 Dosing effect on performance of succinic-based triazole compounds in rust prevention, where R' is C_8 (adapted from Table 2 in [4])

PPM of triazole compound	Compound 1 (Fig. 10.2)	Compound 2 (Fig. 10.2)
20	Severe	Severe
40	Pass	Light
80	Pass	Pass
150	Pass	Pass
300	Pass	Pass

Adapted with permission from Baek, S.-Y.; Kim, Y.-W.; Yoo, S.-H.; Chung, K.; Kim, N.-K.; Kim, J.-S., *Ind. Eng. Chem. Res*., 51, pp. 9669–9678. Copyright 2012 American Chemical Society

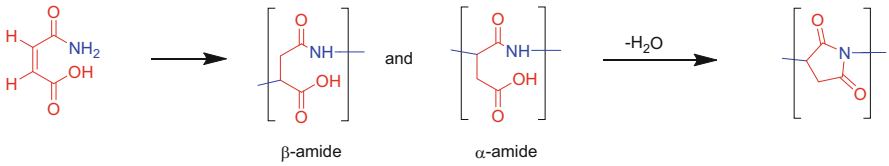

Scheme 10.1 Maleamic acid route to polysuccinimide via maleic anhydride and ammonia [5]

and ammonia, can be employed directly or further hydrolyzed to form polyaspartic acid compounds. An example of these transformations is presented in Scheme 10.1.

There are a wide variety of polymer derivatives that can be constructed from this preparative strategy. Among these are the sodium salt of polyaspartic acid, polysuccinimide, polysuccinic acid octadecylamide, and polysuccinic acid dodecylamide. All of these compounds are reported to exhibit corrosion inhibition properties for carbon steel deployed in sour gas conditions incorporating seawater [6].

10.2.2 Lubricants and Fuels: Detergents and Dispersants

Detergents have a long history of use in engine oils dating back to the 1940s. Their primary function was to reduce the carbonaceous deposits that form on hot, metallic engine components. Overbasing, where additional dispersed basic material (i.e., colloidal $CaCO_3$), significantly improved the performance of these additives [7]. The two common additives in overbased lubricants are alkaline-earth alkylaryl-sulfonates and poly(isobutenyl)succinimides [8]. The alkaline-earth alkylaryl-sulfonate serves to stabilize the colloidal inorganic dispersion in the hydrocarbon oil, where the typical particle size range is 8–16 nm. The poly(isobutenyl) succinimide is deployed to prevent sludge formation in the engine, via steric stabilization where the polar moiety of the succinimide adsorbs onto particulates and enhances their suspending behavior. A schematic of proposed surface interactions of these three components is presented in Scheme 10.2.

Langmuir adsorption experiments demonstrate that the amount of polysuccinimide interaction with the inorganic particle is significant. As reflected in Scheme 10.2, the polysuccinimide, especially for higher chains of polyethylene polyamines (i.e., DETA, TETA, etc.), adsorbs in a ratio of approximately one bis(succinimide) for every four calcium alkylarylsulfonate molecules. The adsorption is attributed to the polar head group which is comprised of both polyamine and succinimide moieties. Consequently, it is believed the particle surface is essentially covered by some type of mixed micelles [8]. Work has also been done in this technical space to develop techniques to probe the neutralization mechanisms for the systems [9].

Typically, when developing such a product for automotive applications, the additive packages must be evaluated in actual automotive engines in order to clearly demonstrate effectiveness. With increasing regulatory pressure to develop engines with improved fuel economy, changes to engine designs are becoming

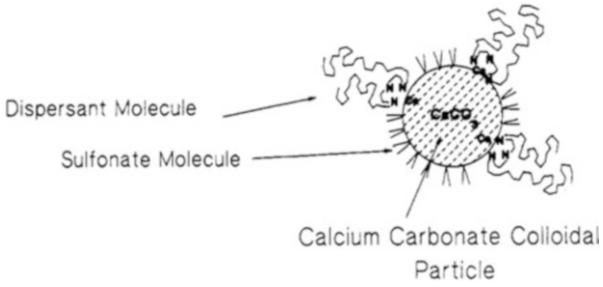

Scheme 10.2 Pictorial representation of hypothesized interactions between a calcium sulfonate colloidal particle and adsorbed poly-(isobutenyl)bis(succinimide) dispersants [8]. Reprinted with permission from Papke, B.L.; Bartley, L.S.; Migdal, C.A., *Langmuir*, 7, pp. 2614–2619. Copyright 1991 American Chemical Society

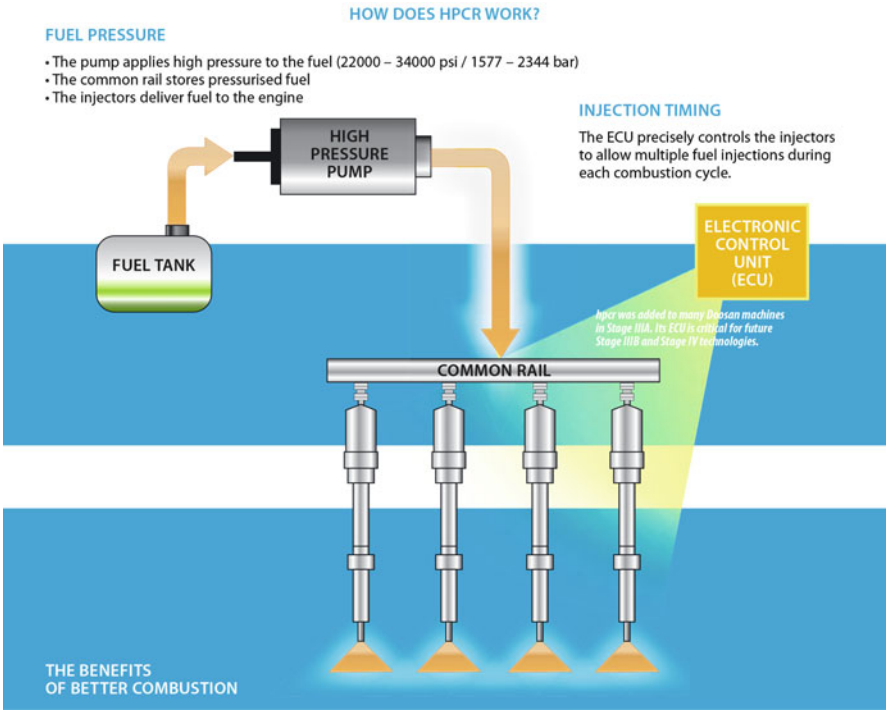

Scheme 10.3 Doosan High Pressure Common Rail (HPCR) system [11]. Reprinted from *Doosan Stage IIIB Tier 4 Interim*, Doosan, D4401500-EN, **2011**, with permission from The Doosan Corporation

more frequent. For example, the High Pressure Common Rail (HPCR), which was first mass produced in 1995, can increase degradation of fuel as a consequence of high-temperature exposure [10]. An illustration of a diesel engine common rail design is presented in Scheme 10.3.

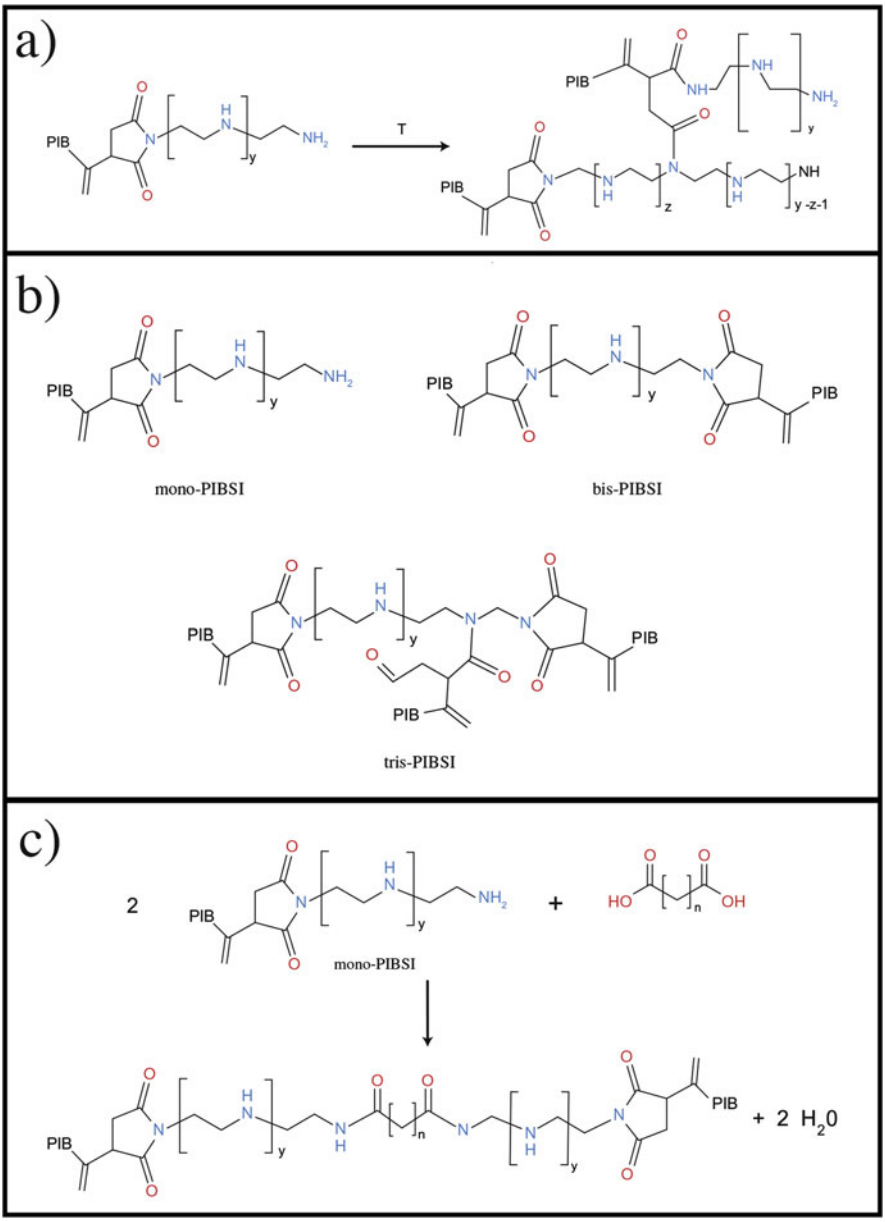

Scheme 10.4 (A) Thermally modified succinicimido-amide (additive A); (B) mono-alkenylsuccinicimide (additive B), bis-alkenylsuccinicimide, tris-alkenylsuccinicimido-amide; (C) chemically modified succinicimido-amide (additive C) [12]. *PIB* polyisobutene. Reprinted from *Fuel*, Volume 122, Zak, G.; Ziemianski, L.; Stepien, Z.; Wojtasik, M., "Engine testing of novel diesel fuel detergent–dispersant additives," Pages 12–20, Copyright 2014, with permission from Elsevier

Table 10.2 Test conditions for diesel engines that simulate city driving [12]

Phase	Time (s)	Engine speed (RPM)	Engine load (Nm)
1	30	1200 ± 30	10 ± 2
2	60	3000 ± 30	50 ± 2
3	60	1300 ± 30	35 ± 2
4	120	1850 ± 30	50 ± 2

In the Doosan HPCR system, diesel fuel is fed from the tank into a high pressure pump, operating at 1577–2344 bar. The high pressure pump then feeds the common rail, which stores the fuel. When demanded, the injectors deliver the fuel in a fine mist to the internal combustion engine. The fine mist ensures a more effective burning of fuel, cleaner exhaust, more energy output due to multiple injections during each cycle, and noise reduction due to reduction in cylinder pressure [11].

Key to the effectiveness of these types of engines is the ability to keep spray nozzle free from deposits. Toward this end, new detergent dispersants were developed in an effort to enhance the cleanliness of the metal surface during engine operation. Several different succinicimido-amides were designed for this purpose and are presented in Scheme 10.4.

The compound "A," in Scheme 10.4, is a thermally modified material. Likewise, the compounds in "B" are unmodified succinicimido-amides and the compound "C" is a chemically modified succinicimido-amide. These materials were evaluated on Peugeot XUD 9A/l, Fiat 2.0 JTD, and Ford Duratorq 2.0i 16V TdCi engine test stands at dosages of 100 mg/kg of fuel. Engines were operated in a manner that simulates city driving conditions for a period of 10 h [12]. The cycling conditions are presented in Table 10.2.

Not surprisingly, the performance results of these different compounds yielded somewhat unique effects in the test engines. For example, the succinicimido-amide compounds exhibited improved detergent properties on the Peugeot engine by demonstrating less impact on air flow restriction. The Ford engine demonstrated a decrease in particulate matter and smoke emission as well as lower fuel consumption. Finally, the Fiat engine exhibited a small decrease in engine power [12]. The results clearly highlight the need for real application testing to ensure optimal product design and implementation.

10.2.3 Anti-static Additive for Fuels

The combustible nature of fuels, in air or oxygen, is well known. A contributing factor to this behavior is their poor electrical conduction behavior which can result in accumulation of charge and discharging of sparks in an unexpected manner. To overcome these effects, the anti-static behavior of fuel is modified by additives

Table 10.3 Additive formulation for fuel anti-static composition [13]

Component	Mass (wt%)
1-Decene-sulfur dioxide copolymer	21
Solvent naphtha heavy	54
Dodecylbenzenesulfonic acid	7
Poly($C_{20/24}$-olefin-*co*-maleic anhydride) converted to imide with tallow fat-1,3-diaminopropane ($M_w \sim 2000–5000$ g/mol)	18

Table 10.4 Effect of anti-static additive package to the electrical conductivity of various fuels [13]

Fuel sample (dosage in mg/L)	Electrical conductivity (pS/m)
Commercial petroleum (3)	890
Commercial diesel fuel (3)	670
Commercial heating oil (3)	690
Commercial turbine fuel (1, 3, 5)	174, 750, 1275
Commercial turbine fuel (1, 3, 5) after 4 days storage	230, 735, 1205
Commercial hydraulic oil (130)	167

capable of enhancing the conductivity of the medium. An example of an anti-static additive formulation is presented in Table 10.3.

Electrical conductivity measurements, using DIN Standard 51412-2 (Field Method), enabled the experimental determination of anti-static properties for the composition presented in Table 10.3. These results can be found in Table 10.4.

In all of the fuels evaluated, the additive package is reported to demonstrate an effective improvement to the electrical conductivity of the fuel, which enhances the anti-static properties of the fuel. The poly($C_{20/24}$-olefin-*co*-maleic anhydride), which was converted to imide with tallow fat-1,3-diaminopropane, is oil soluble. Oil solubility is also an important property for effective activity and storage stability. For these compounds, it has been suggested that the absence of nitrogen, in this particular case imide functionality, would lead to a reduction or even total loss of anti-static performance [14].

10.3 Biologically Active Compounds and Pharmaceutical Compositions

10.3.1 Introduction

Maleic anhydride is employed in a wide variety of biological and pharmaceutical applications. Beyond its highly versatile synthetic capabilities are some attractive

inherent functional features. From an environmental perspective, for example, it is not harmful to aquatic organisms, not bio-accumulative, and readily biodegradable [15]. From a human perspective, the compound is harmful if swallowed and can be a severe irritant but not considered a mutagen, carcinogen, and not expected or anticipated to be a developmental toxic or reprotoxicity material for reproduction [15].

Some compounds consisting of maleic anhydride have approved regulatory status with the US Food and Drug Administration (FDA) for use in various applications. For example, compounds such as pentaerythritol ester of maleic anhydride-modified wood rosin have been approved under the Code of Federal Regulations Title 21 (21 CFR):172.210 for use in coatings of fresh citrus fruit. Another example is the approved use of styrene-maleic anhydride copolymers in 21 CFR Section 177.1820 Subpart B for use as basic components of single and repeated use food contact surfaces. It is important to note that these materials must also meet certain criteria for molecular weight, residual monomers, and extractables to be suitable for such applications. A final example is the approved use of polyvinylmethylether maleic anhydride (PVM-MA), acid copolymer, and carboxymethylcellulose sodium (NaCMC) denture adhesive in 21 CFR Section 872.3500 (Dental Devices) [16]. Given the inherent properties of maleic anhydride and the regulatory familiarity of this compound, we will now examine a few more examples in more detail.

10.3.2 Salt Formation

The formation of salts with pharmaceutically active compounds is a common industrial practice. Salt formation with drug active compounds can result in solubility modification. Enhancing drug active solubility is often critical to its efficacy because many active compounds are, in fact, poorly water soluble. In addition, salt formation enables the alteration of the drug active dissolution rate. Today, many currently available US Federal Drug Administration (US FDA) drugs employ not only this technical strategy, but utilize maleic anhydride chemistry in the salt-forming compounds. Examples of such approved compounds are presented in Table 10.5.

A few chemical structures for pharmaceutical salt compounds employing maleic anhydride-based materials are presented in Fig. 10.3.

During the developmental stages, numerous salts are screened to develop structure–property relationships, in the search for the most effective solid form of the pharmaceutical active. An example of this effort has been reported for (1R, 2S)-(−)-ephedrine salts. The generalized salt structure for this compound is presented in Fig. 10.4.

Among the numerous ephedrine compounds that were evaluated in crystallization experiments are combinations of maleic acid, fumaric acid, and succinic acid. Interestingly, only maleic and succinic acid were capable of forming a crystalline

Table 10.5 US FDA approved pharmaceutical compounds that employ salt formation technology derived from maleic anhydride [17]

Type of administration	Pharmaceutical compound	Salt former
Intravenous	Methylergonovine-hydrogenmaleate	Maleate
Oral	Timolol-hydrogenmaleate	Maleate
Oral	Desvenlafaxine-hydrogensuccinate	Succinate
Oral	Loxapine-hemisuccinate	Succinate
Oral	Bisoprolol-fumarate	Fumarate
Intravenous	Ibutilide-fumarate	Fumarate

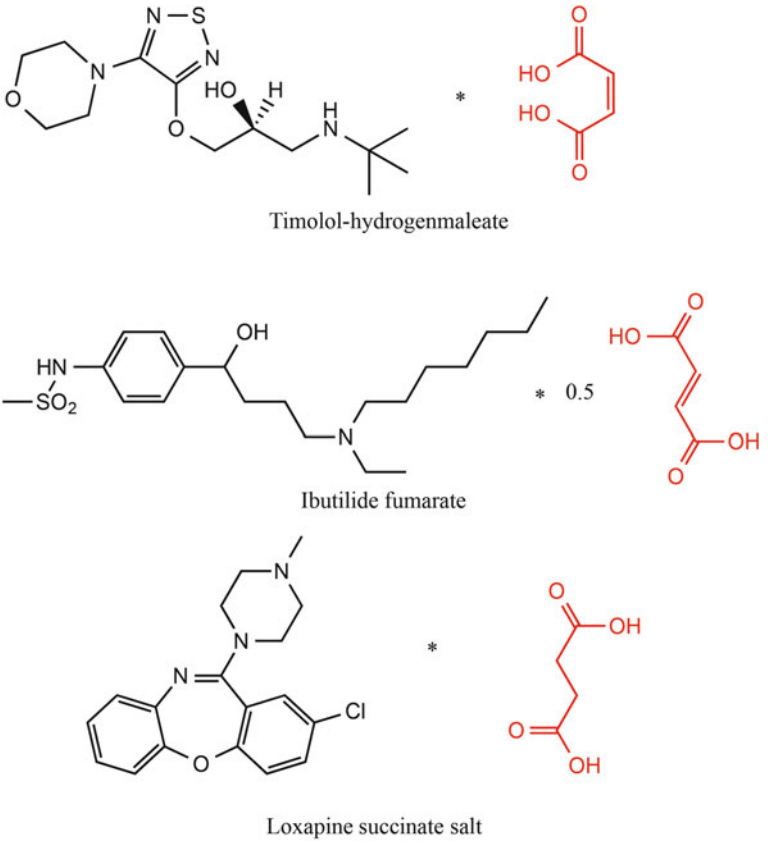

Fig. 10.3 Pharmaceutical salt compounds employing maleic anhydride based materials [18–20]

salt structure. Note that the succinic acid formed a disordered structure via crystallization from an amorphous phase. The researchers point out that the experimental conditions are critical in such crystallization experiments and highlight that stoichiometry for diacids along with water content are especially important.

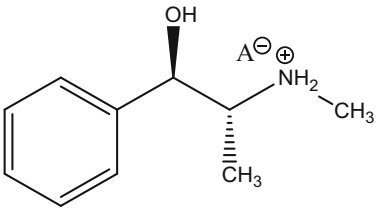

Fig. 10.4 Generalized (1R, 2S)-(−)-ephedrine salt structure [21]. Reprinted with permission from the Journal of Pharmaceutical Sciences, 96, 5, Black, S.N.; Collier, E.A.; Davey, R.J.; Roberts, R. J., "Structure, Solubility, Screening, and Synthesis of Molecular Salts," pages 1053–1068. Copyright 2007 John Wiley and Sons

Table 10.6 Selected properties of ephedrine salt compounds

Compound	T_m (°C)	ΔH_m (kcal/M)	Density (g/cm^3)	Solubility (mol (ephedrine)/L)	pH
Ephedrine	34.7	2.86	1.114	0.345	11.52
Ephedrine-maleate monohydrate salt	Hydrate	Hydrate	1.273	3.792	3.41
Ephedrine-HCl salt	217	8.7	1.229	1.601	3.18

Adapted with permission from the Journal of Pharmaceutical Sciences, 96, 5, Black, S.N.; Collier, E.A.; Davey, R.J.; Roberts, R.J., "Structure, Solubility, Screening, and Synthesis of Molecular Salts," pages 1053–1068. Copyright 2007 John Wiley and Sons

Experimentally determined physical properties of various salts are presented in Table 10.6.

Results presented in Table 10.6 clearly demonstrate the wide variety of physical properties that are possible when forming different salt structures with biologically active compounds. Compounds can change from low melting materials to high melting, or even not exhibit melting behavior. While the salt structures examined in both cases exhibit lower pH, their respective solubility notably differs by a factor of two. This result is a significant observation and clearly reinforces the need to assess active salt structures in a careful systematic manner.

10.3.3 Organophosphates

Malathion is another biologically active material that is made from a maleic anhydride derivative, diethylmaleate or diethyl fumarate. It is classified as an organophosphate. The general synthetic approach to producing Malathion is presented in Scheme 10.5.

This broad-spectrum insecticide is used to control mosquito, boll weevil, and fruit fly insects in both agricultural and residential environments. In addition, it is also used to control head lice as delivered by shampoo [23]. The physical properties of Malathion are interesting and presented in Table 10.7.

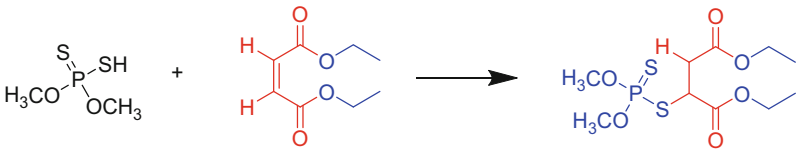

Scheme 10.5 Chemical preparation of Malathion [22]

Table 10.7 Physical properties of Malathion (adapted from [23, 24]

Property	Result
Form	Liquid
Odor	Skunk or garlic odor
Vapor pressure (mmHg at 25 °C)	1.78×10^{-4}
Octanol/water partition coefficient (log K_{ow}) at 25 °C	2.7
Solubility in water (mg/L)	145
Boiling point (°C)	No value determined due to decomposition at 174 °C

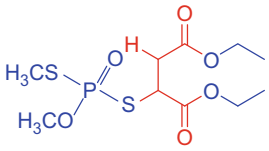

Fig. 10.5 Chemical structure of isomalathion [22]

Malathion was first developed in the early 1950s [25]. Yet, it still receives attention today in efforts to improve product quality. It has been reported that the storage instability of Malathion, where temperatures ≥40 °C, can increase the toxicity of the material. This effect has been attributed to an increase in isomalathion content [22]. The chemical structure for isomalathion is presented in Fig. 10.5.

By reducing not only isomalathion, but other impurities, through new synthetic and purification approaches, has resulted in improved storage stability. These developments have enabled less hazardous materials to be deployed in pharmaceutical formulations, such as lotions, gels, and creams [22].

10.3.4 Polymer-Enhanced Active Compounds

An important derivative of maleic anhydride is succinic anhydride. While it is the case that succinic acid can be produced by bacterial fermentation, it is mostly

produced via catalytic hydrogenation of maleic anhydride [26–28]. Succinic acid is often employed to add important functionality to polymeric materials. One example, which is found in pharmaceutical applications, is hydroxypropyl methyl cellulose acetate succinate (HPMS-AS). HPMC-AS was specifically developed as an enteric coating polymer. An enteric coating provides for a protective layer to a product, such as a pill or tablet, enabling the product to pass through the stomach unaffected but designed to deliver the product in the intestinal tract. The general chemical structure for HPMC-AS is presented in Fig. 10.6.

The key elements of the HPMC-AS structure include a cellulosic ether derivative containing mixed esters of acidic succinyl and aliphatic monoacyl moieties. This composition results in enteric coatings that exhibit increased flexibility without the use of large quantities of plasticizers, dosage forms that exhibit less tack and less tendency for adhering to each other, and coatings that are chemically and physically stable under the influence of moisture over time [30]. Recently, there has been much patent activity in compositional modification of HPMC-AS, illustrating the effect of structure variations (i.e., degree of substitution and molecular weight) on key performance characteristics [31–33].

A popular use of HPMC-AS is in the preparation of pharmaceutical spray-dried dispersions (SDD). Solubility and bioavailability of active compounds, a critical attribute in pharmacology, as illustrated by commercial importance of salt formation as discussed previously, can also be enhanced by spray-dried solid amorphous dispersion processes. In the SDD process, typically the active compounds and the

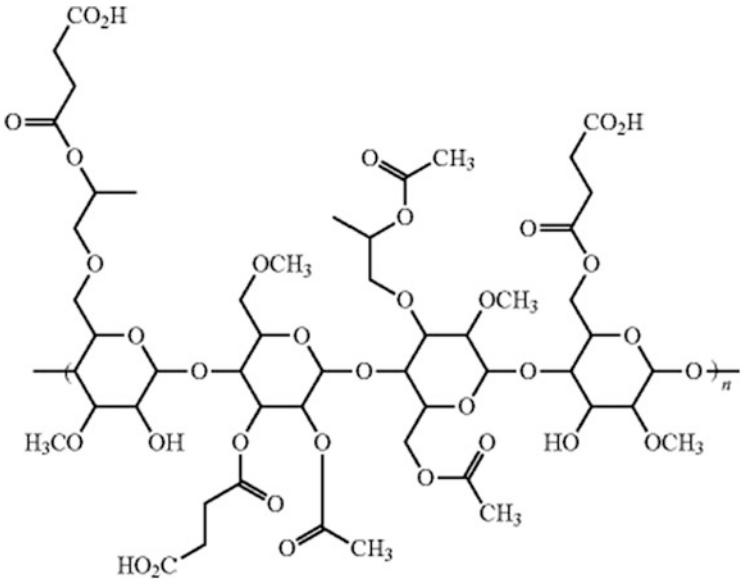

Fig. 10.6 General chemical structure for HPMC-AS [29]

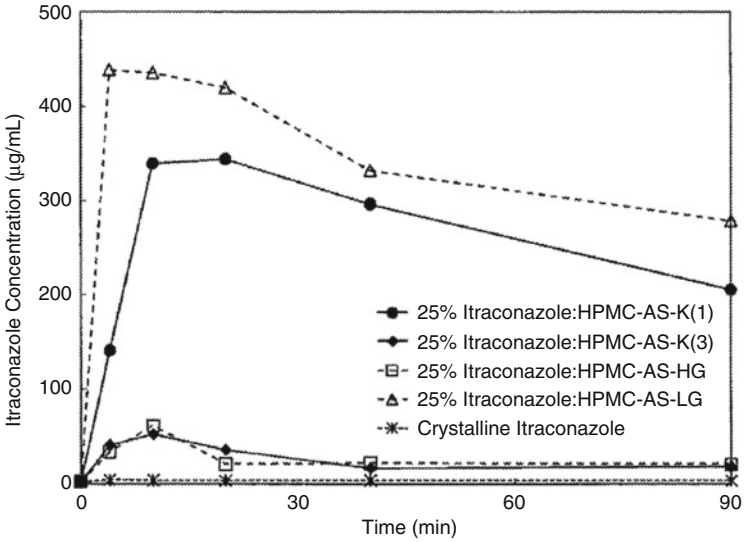

Fig. 10.7 Solubility of various forms of Itraconazole [32]

polymer are dissolved in solvent (i.e., methanol or acetone) and then pumped into an atomizer to be spray dried. The conditions for this process are selected to enable the trapping of the active compound in an amorphous form, which enhances the solubility of the active compound relative to its crystalline analog [34]. An example of the enhancement to bioavailability is presented in Fig. 10.7.

Figure 10.7 presents results of a dissolution study for Itraconazole for materials prepared by SDD or in a bulk, crystalline form via micro-centrifuge dissolution at 37 °C. Itraconazole active compounds are used to treat fungal infections in the lungs that can spread throughout the body [35]. As these results illustrate, the bulk, crystalline active compound exhibits very little solubility. HPMC-AS significantly enhances the solubility of this compound. Importantly, the chemical structure of the polymer is critical to this solubility behavior and can yield a wide array of solubility behaviors. In this particular example, HPMC-AS-LG (aka: Shin Etsu's AQOAT®) resulted in the highest solubility. This grade corresponds to a granular ("G") material containing a methoxyl content of 20.0–24.0, a hydroxypropoxyl content of 5.0–9.0, an acetyl content of 5.0–9.0, and a succinoyl content of 14.0–18.0 [32]. Note that these results will vary, sometimes strongly, depending on factors such as chemical composition of the active compound, polymer structure, SDD process conditions, and formulary strategy.

In 2012, the FDA approved a new cystic fibrosis (CF) treatment called Kalydeco®. This is the first drug targeting the root cause of CF, by improving the function of the defective protein, CFTR [36]. The active compound in Kalydeco® is *N*-(2,4-di-tert-butyl-5-hydroxyphenyl)-1,4-dihydro-4-oxoquinoline-3-carboxamide, *N*-[2,4-bis(l,l-dimethylethyl)-5-hydroxyphenyl]-l,4-dihydro-4-oxoquinoline-3-carboxamide, or ivacaftor. The chemical structure for this compound is presented in Fig. 10.8.

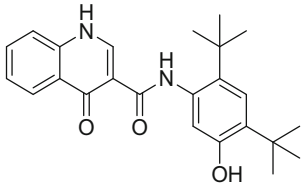

Fig. 10.8 The chemical structure for *N*-[2,4-bis(l,l-dimethylethyl)-5-hydroxyphenyl]-l,4-dihydro-4-oxoquinoline-3-carboxamide or ivacaftor [37, 38]

Table 10.8 SDD ingredients for pre-tablet manufacture of *N*-[2,4-bis(l,l-dimethylethyl)-5-hydroxyphenyl]-l,4-dihydro-4-oxoquinoline-3-carboxamide or ivacaftor [37]

Ingredient	Mass (kg)
N-[2,4-bis(l,l-dimethylethyl)-5-hydroxyphenyl]-l,4-dihydro-4-oxoquinoline-3-carboxamide or ivacaftor	9.00
HPMC-AS	8.91
Sodium lauryl sulfate (SLS)	0.09
MEK	64.80
Water	7.20

Ivacaftor is practically insoluble in water (<0.05 μg/mL). The oral solid tablet comprises colloidal silicon dioxide, hydroxypropyl methyl cellulose acetate succinate or hypromellose acetate succinate HPMC-AS, sodium croscarmellose, lactose monohydrate, magnesium stearate, microcrystalline cellulose, and sodium lauryl sulfate [38]. The tablet is also coated and printed on by other chemical components that are beyond the focus of this discussion. In preparing this tablet, an intermediate SDD composition is prepared. An example of this composition is presented in Table 10.8.

The mixture presented in Table 10.8 is allowed to mix at ~23 °C until it becomes homogeneous and all components have dissolved. Then this mixture is presented to a Niro Mobile Minor Spray Drier equipped with an extended chamber and a two-fluid atomizer (1.3 mm) under processing conditions presented in Table 10.9.

Once the SDD composition is prepared, it is then blended with microcrystalline cellulose, lactose, sodium croscarmellose, SLS, colloidal silicon dioxide, and magnesium strearate and dry mixed and sieved until thoroughly mixed. This mixture is then presented to a mechanical tablet press for producing the final tablet product form [37]. From this point the tablet is then coated and marked prior to distribution to doctors and patients. The commercial product may have a different formulation and product route than the prior discussion; a 150 mg oral dose to healthy patients achieves the peak plasma concentration in approximately 4 h [38].

Table 10.9 Spray drying parameters for *N*-[2,4-bis(l,l-dimethylethyl)-5-hydroxyphenyl]-l,4-dihydro-4-oxoquinoline-3-carboxamide or ivacaftor pre-tablet composition [37]

Processing parameter	Result
Flow rate for atomizer (kg/h)	10.5
Spray solution flow rate (kg/h)	7
Temperature of inlet (°C)	~105
Temperature of outlet (°C)	40 ± 5
Temperature of vacuum dryer (°C)	55
Drying time in vacuum (h)	24

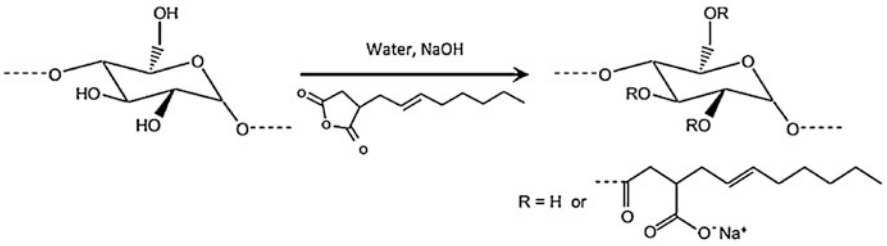

Scheme 10.6 Structure of OSA-modified starches [40]. Reprinted from *Carbohydrate Polymers*, Volume 92 (1), Sweedman, M.C.; Tizzotti, M.J.; Schafer, C.; Gilbert, R.G., "Structure and physicochemical properties of octenyl succinic anhydride modified starches: A review," Pages 905–920, Copyright 2012, with permission from Elsevier

10.4 Microencapsulation

Microencapsulation describes a process where small particles, comprised of a liquid, solid, or gas "payload," are encapsulated, or surface coated, with a thin film. There are numerous excellent reviews on this technology [39]. The process employed to microencapsulate the payload will dictate the form of the final microencapsulated particle. Some of the classic microencapsulated particle forms are core-shell, multi-core, or multi-shell in structure. Maleic anhydride can have a role in the payload and thin film surface coatings. For this part of the discussion, we will focus on examples of various types of surface coatings that employ maleic anhydride technology.

Octenyl succinic anhydride (OSA) starch is a well-established commercial technology for microencapsulation coatings. The structure OSA starch is presented in Scheme 10.6.

OSA is derived from maleic anhydride. Starches known to have been modified by OSA include waxy maize, potato, barley, and rice [40]. A specific example of a linear OSA-modified starch is HI-CAP® 100, a waxy maize-based compound, from Ingredion [41, 42]. By incorporating the OSA functionality to starch, the molecule becomes amphiphilic, comprised of both hydrophilic and hydrophobic regions, and

Table 10.10 Physical properties of HI-CAP® 100, OSA-modified starch (adapted from [41, 43])

Property	Result
Intrinsic viscosity (100 cm^3/g) (20 °C water)	0.1171
Huggins (k') constant (20 °C water)	1.2864
Color	White
Form	Fine powder
Moisture	6 %
pH	4

exhibits surface active behavior. Various physical properties of HI-CAP® 100 are presented in Table 10.10.

The intrinsic viscosity and Huggins parameter (k') provide insight into the polymer behavior in solution. They are determined from the classic Huggins equation (10.1).

$$\frac{\eta_{sp}}{c} = [\eta] + k'[\eta]^2 c \tag{10.1}$$

where η_{sp} is the specific viscosity, c is concentration, and k' is the Huggins coefficient. Interpreting the viscosity results, the Huggins parameter ($k' \geq 1$) is indicative of a tendency of the polymer to aggregate and self-associate [47]. In other words, the polymer prefers itself as opposed to the surrounding water medium. This is an important effect for microencapsulation, especially for flavor, fragrances, and oil encapsulated products.

OSA-modified starch is generally employed to emulsify an oil and/or fragrance in water, followed by a spray-drying process. As starting point for the encapsulation of a flavor, 30 % (wt%) of HI-CAP® 100 is mixed with 5 % (wt%) flavor oil, the balance of this mixture being water. The oil is emulsified using a colloidal mill, homogenizer, or blender and then spray dried [41]. The flavor oil transitions to the "payload," with the OSA-modified starch traveling to the oil–water interface and effectively coating the surface of the oil. This approach was used to encapsulate vanilla extract, a common flavor ingredient in food. A scanning electron microscopic (SEM) image of the surface of a spray-dried, HI-CAP® 100 encapsulated vanilla extract (5 % ethanol content) is presented in Fig. 10.9.

The encapsulated particle exhibits a smooth surface texture coupled with an interesting dimpled surface. While this research actually found that vanilla extract was more effectively encapsulated by another branched OSA-modified starch, Capsul®, but both starches, which are based upon a maleic anhydride modification, were capable of encapsulating the extract oil [42].

Beyond food ingredients, encapsulated products can be found in personal care items, such as antiperspirant sticks. In a separate development, fragrance was

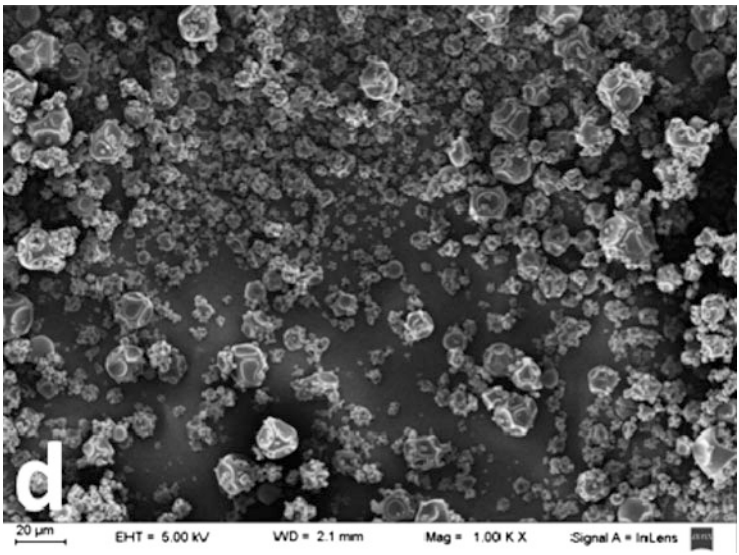

Fig. 10.9 SEM image obtained from S2 samples of HI-CAP® 100 with the addition of 5 % vanilla extract (1000×) [42]. Reprinted from Journal Food Research, Rodriguez, S.D.; Wilderjans, T.F.; Sosa, N.; Bernik, D.L., "Image Texture Analysis and Gas Sensor Array Studies Applied to Vanilla Encapsulation by Octenyl Succinic Anhydride Starches," 2, 2, pages 36–48, **2013** with permission

Table 10.11 HI-CAP® 100 fragrance capsule composition [44]

Ingredient	Dry weight percent (%)
Water	
HI-CAP® 100	41.5
Fragrance	25.0
Poly(vinyl pyrrolidone) (PVP) K-30	3.5
Silica capsule slurry	30.0

encapsulated by HI-CAP® 100 and poly(vinyl pyrrolidone) (PVP K-30). The specific encapsulation formulation is presented in Table 10.11.

To prepare the capsule solution, the fragrance and OSA-modified starch are throughly mixed. In a separate container the PVP and silica are mixed, forming the silica capsule slurry. This slurry is then added to the previously formed fragrance emulsion and continuously mixed until spray dried [44]. Particles prepared by this process will exhibit a structure similar to Fig. 10.10.

These encapsulated particles normally exhibit a centrally located air pocket surrounded by large hole-type structures. In this study, consumer panel testing found that formulating this type of encapsulated fragrance into an antiperspirant stick base resulted in improved fragrance intensity [44].

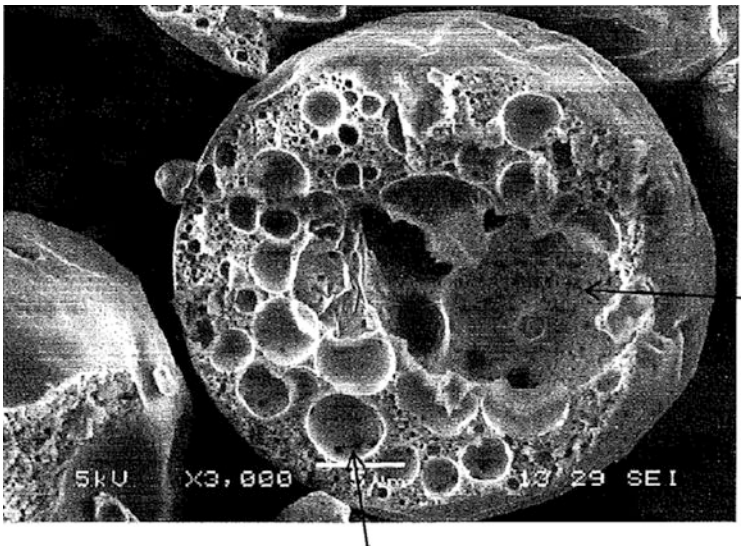

Fig. 10.10 Fragrance encapsulated by HI-CAP® 100, an OSA-modified starch [44]

10.5 Thermoplastics and Films

10.5.1 Molding

Many automotive applications employ thermoplastic resins. Parts such as side rear view mirrors, front and rear bumpers, and fenders are often fabricated from thermoplastic materials. Critical to the success of these components is their ability to resist damage from impact, whether from rocks or other foreign objects. One widely used class of thermoplastic resin is polyamides such as nylon 6. Polyamides have a complex structure comprising amorphous and crystalline domains as a result of the hydrogen bonding originating from the amide bond. These regions can be adjusted by controlling the composition of the amide copolymer itself in addition to blending with other copolymer materials. Critical to improving the toughness of polyamides is the ability to form homogeneous dispersed phases within the polyamide resin, particularly dispersed phases that can react with the functional ends, such as the $-NH_2$ groups, of the polyamide resin. These materials can help to ensure good adhesion between the interface of the dispersed phase and the matrix resin as well as enhancing the quality of the dispersed phase. Examples of effective dispersed phases often incorporate reactive functionalities, such as maleic anhydride and acrylic acid, which can covalently bond the dispersed phase to the polyamide matrix resin. Additionally, these materials enhance the dispersion of other nonreactive materials, such as linear low-density polyethylene and very low-density polyethylene, and poly(ethylene-*co*-vinyl acetate) materials [45]. In the first example, the impact modifier is comprised of poly(ethylene-*co*-butyl

Table 10.12 Physical properties of injection molded impact resistant polyamide [45]

Example	Pressure head (bar)	Melt flow index (235 °C, 2.16 kg)	Notched Charpy Impact at 23 °C (kJ/m^2)	Notched Charpy Impact at −40 °C (kJ/m^2)
1	14	8.7	78	25
2	15	5	47	10
3	17	5.8	99	25

acrylate-*co*-maleic anhydride (3 wt%)) (i.e., Lotader® 3410 from Arkema) and mono-functional –NH_2 polyamide 6, Irgafos® 168 (Ciba, stabilizer). Irganox® 1098 (Ciba, antioxidant) is then added to these components, extruded at 240–280 °C, and pelletized. This composition is then added to low-density polyethylene by compounding and further dry blended with a polyolefin elastomer (density 0.87 g/cm^3) (Engage® 8200) from Dow Chemical Company to be injection molded. In a second example, the impact modifier is poly(ethylene-*co*-ethyl acrylate-*co*-maleic anhydride (1.5 wt%)) (Lotader® 4700 from Arkema). In the third example, the impact modifier is poly(ethylene-*co*-octene)-graft(g)-maleic anhydride (Fusabond® MN493D from DuPont). The physical properties of this injection molded compositions are presented in Table 10.12.

In examining the experimental results presented in Table 10.12, the polyamide-block graft copolymer (Example 1) demonstrated a significant improved in Charpy Impact at 23 °C and −40 °C when compared to the impact modifier (Example 2). Interestingly, results for Example 3 exhibit a similar Charpy Impact, but the melt flow index is reduced which is not ideal for thin and large size objects produced by injection molding. The polyamide-block graft copolymer, which employs an imidization approach to maleic anhydride, provides the most effective route to the impact-resistant polyamide [45].

In another thermoplastic process called roto-molding, or rotational molding, a multi-layer thermoplastic tank can be prepared using maleic anhydride grafted materials to improve the adhesion characteristics between the thermoplastic layers. In a one-shot approach, the thermoplastic, outer layer is added into the mold at the same time as the inner layer thermoplastic. However, the inner layer thermoplastic is encapsulated in a thermoplastic bag to physically separate the two thermoplastics until a desired temperature is achieved which enables the thermoplastic bag to melt and enable the inner layer thermoplastic to coat the inside of the mold. In one example, a blend of medium-density polyethylene and polyethylene grafted with maleic anhydride is added into a roto-mold. To this system, polyamide 11 ($T_m = 190$ °C) encapsulated in a 5 mil thick copolyamide (poly(adipic acid-*co*-hexamethylene diamine-*co*-lactam 6-*co*-lactam 12) bag is added. The bag film exhibits a melting temperature of 150–155 °C. The roto-mold oven temperature is set to 300 °C and an internal air temperature of 215 °C is employed for polyamide 6 materials. Upon heating, the polyethylene materials melt, first coating the inside of the mold. Once the internal air temperature of ~150 °C is achieved, the polyamide bag melts enabling the polyamide 11 to begin melting and coating the mold.

Once cooled, in examining the tank, excellent separation between the layers was observed, with no apparent mixing between the polyethylene and polyamide. This tank also exhibited excellent interlayer adhesion [46].

Another process developed to improve interfacial adhesion performance between polyethylene and fluorinated thermoplastics does not employ a bag element in the roto-molding process. In one example, a blend of polyethylene (density = 0.940 g/cc) and poly(ethylene-*co*-methyl acrylate-*co*-glycidyl methacrylate) is added to a roto-mold and heated using an oven temperature of 300 °C. This step enables the polyethylene resin to become fluid and form the first layer on the inside of the mold. When the internal air temperature reaches 130–170 °C, the 5000 ppm maleic anhydride grafted PVDF is added to the roto-mold. Mixing is continued until the internal air temperature reaches 210–235 °C. The outside of the roto-mold is then cooled with an air/water mist combination to solidify the polyethylene layer prior to the PVDF layer. The result is a two-layer tank, the outer layer being polyethylene based and the internal layer PVDF based, with good adhesion between the two layers. Interestingly, the order of addition for the functionalized polyethylene and PVDF resins is not specific. If this process is repeated, but without the functionalized polyethylene and PVDF thermoplastics, then no adhesion between these materials is displayed [47].

10.5.2 Tubing

Thermoplastic resins are used in tubing applications to transfer fluids and gases in fields such as automotive, medical, municipal, and oil and gas. In many cases, multiple layers of thermoplastic resin are required in order to provide a sufficient barrier for the materials to be conveyed in the tubing.

In automotive applications, for example, polyamide resins find wide utility due to a number of excellent physical attributes. Among these attributes are mechanical strength, toughness, abrasion resistance, chemical resistance (i.e., gasoline resistant), electrical insulative, and arc resistance properties. However, polyamide resins used in automotive tubing and hose applications have been limited due to rubber compatibility, flexibility, viscosity, and processability challenges coupled with low impact resistance at low temperatures, poor appearance, and high price. In developing an improved polyamide thermoplastic system, ethylene/propylene/diene monomer (EPDM) rubber grafted with maleic anhydride was employed to develop a more suitable automotive tube. Specifically, nylon-6, EPDM-*g*-maleic anhydride, sulfonamide plasticizer (i.e., o,p-toluenesulfonamide), caprolactam (plasticizer), ethylene-*co*-vinyl acetate (EVA) resin, thickener (i.e., styrene/maleic anhydride copolymer), and carbon black were dry blended followed by melt-kneading at 240 °C, pelletized, and twice dried at 70–90 °C and then processed in an extruder. This composition was then compared to a similar construct fashioned with nitrile rubber. These compositions are described in detail in Table 10.13. The physical properties of these two compositions are presented in Table 10.14.

Table 10.13 Polyamide tubing for automotive for fuel tubing [48]

Example	Nylon 6	Caprolactam	EPDM-g-MA	Nitrile rubber	Sulfonamide	Thickener	EVA	Master batch of Carbon Black
1	53.3	8.0	30.0	NA	1.5	0.2	5.0	2.0
2	60.0	8.0	NA	30.0	NA	NA	NA	2.0

Table 10.14 Physical properties of polyamide tubing for automotive for fuel tubing [48]

Example	Melt index (g/10 min)	Tensile strength (kg/cm^2)	Elongation (%)	Flexural strength (kg/cm^2)	Flexural modulus (kg/cm^2)	Impact Strength (kg cm/cm)		Appearance	Extrusion behavior
						23 °C (left)	40 °C (right)		
1	0.8	400	290	210	5100	No break	27.6	Excellent	Excellent
2	1.1	400	200	210	4750	No break	10.5	Not uniform	Excellent

In comparing the physical properties of the two tubing compounds, the composition fashioned from EPDM-*g*-maleic anhydride exhibits comparative tensile strength and modulus behavior. Interestingly, this composition is tougher, as reflected in the improved elongation and low-temperature impact strength. In further testing of these materials, these compositions were immersed in gasoline at 50 °C for up to 96 h and then the physical properties reevaluated. Under these harsh conditions, Example 1 exhibited generally superior flexural properties (i.e., flexural strength and modulus) in addition to similar oil adsorption properties. Generally, the appearance of the EPDM-*g*-maleic anhydride composition was better [48].

In another approach to improving the barrier resistance of tubes and hoses constructed from polyamides is to couple to a layer of metal (i.e., aluminum). While sputtering techniques are known for applying metal to plastics surfaces, it does not enhance the barrier properties or impermeability behavior. To improve such properties, foil laminate structures are preferred for such objects as fuel tanks, hoses, and gas rails. To enhance the adhesion between these two dissimilar surfaces, olefin grafted with maleic anhydride is employed. To test the laminate strength, a laminate structure is prepared in the following order: 4 in. diameter (1/8 in. thick) discs of nylon 6,6 (Zytel® 101 NC0101 from DuPont), a layer of adhesive film, aluminum foil, a second layer of the same adhesive film, and nylon 6,6. The assembly is placed into an 180 °C press and 10,000 psi is applied for 5 min. The assembly is removed and cooled. These samples are then cut into 1 in. squares and strength tested and fuel resistance tested. In an example where the adhesive film layer was high-density polyethylene grafted with maleic anhydride (Bynel® 4003 from DuPont), superior laminate strength and fuel resistance properties are observed. Interestingly, while low-density polyethylene was found to be inferior

in both laminate strength and fuel resistance, EPDM elastomer grafted with maleic anhydride was also inferior to fuel resistance despite exhibiting good laminate strength properties [49]. The results highlight the importance of not only the grafted maleic anhydride but also the importance of the base thermoplastic capability to resist the fluid medium.

In municipal applications, thermoplastic tubing is used for transporting water and natural gas. In these applications, the materials need to be resistant to aggressive chemicals, such as chlorinated chemicals (i.e., bleach) and ozone, in addition to being capable of withstanding pressure, sometimes >10 bar. Some chemical additives can be especially damaging to the tubing. To overcome this damage, multi-walled tubing is often deployed to enable the tubing to become more chemically resistant [50]. An example of a suitable construction is presented in Fig. 10.11.

In Fig. 10.11, the first layer (**1**) is a fluoropolymer that is covered by a radiation grafted fluoropolymer layer (**2**). The next layer (**3**) is an adhesion layer which is then covered by polyolefin layer (**4**). Another adhesion tie layer (**5**) follows which is covered by a gas barrier (**6**) layer. Covering the gas barrier is another adhesion tie layer (**7**) with a final outer layer of polyolefin (**8**). In one example of construction, KYNAR® PVDF is modified by radiation grafting of maleic anhydride. The PVDF and maleic anhydride are blended and coextruded at 230 °C at 150 RPM with a throughput of 10 kg/h. The extrudate is then irradiated with gamma radiation by exposing to Co^{60} to 3 Mrad for 17 h which yielded a grafting content of 1 %, as determined by infrared spectroscopy. The PVDF-*g*-maleic anhydride (1) is covered by Lotader® AX 8840 (8 % glycidyl methacrylate/92 % ethylene) (3), which

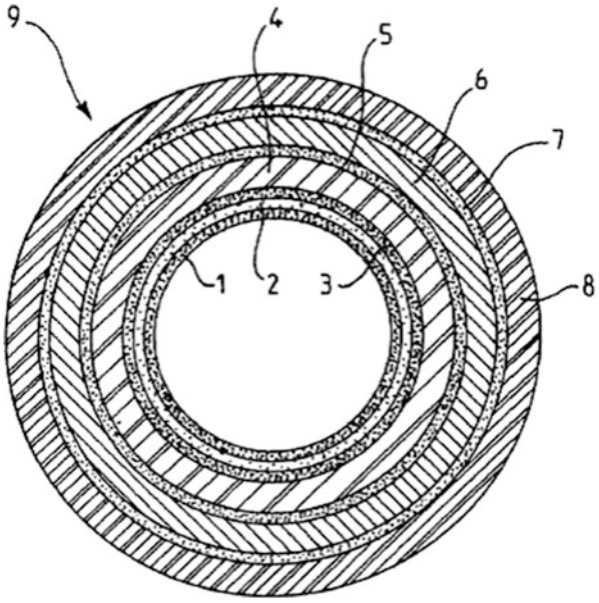

Fig. 10.11 Multi-walled pipe suitable for transporting water or gas [50]

performed as the adhesive tie layer, and finally covered by XPE (i.e., BorPEX ME2510, a silane cross-linked olefin using MB 51 to accelerate the moisture-induced cross-linking reaction) to achieve the final cross-linked polyolefin outer layer [50].

In oil and gas applications, several different tubing approaches are employed which utilize thermoplastic resins. In the first example, thermoplastic resins are used to protect oil and gas pipelines from corrosion [51]. In this application, a multi-walled tube is constructed which is depicted in Fig. 10.12.

In Fig. 10.12, a hollow metal tube is depicted as (**1**). The hollow metal tube is covered with an epoxy resin (**3**), followed by a binder layer (**5**), and then covered by a layer of olefin (**7**). Critically, these layers must exhibit excellent adhesion at high temperatures (80 °C). To fabricate this structure, the metal tubing is heated to 195 °C and then an epoxy resin is spray applied to the hot metal surface. The epoxy quickly forms a gel. An adhesive binder composition is then applied to this epoxy gel. To prepare the olefin binder, a mixture of linear low-density polyethylene (LLDPE) (density = 0.934 and 0.920) is coextruded in the presence of maleic anhydride [1.5 % (wt)] and free radical initiator (2,5-di(t-butylperoxy)-2,5-dimethyl hexane (Luperox® 101). This process enables the maleic anhydride to graft to polyethylene extrudate. To this extrudate, additional polyethylene (density = 0.934) and poly(ethylene-*co*-butyl acrylate) (Lotryl® 30BA02) are mixed and coextruded into a film. This film is then applied to the hot epoxy coated pipe. Finally, a 3 mm thick layer of high-density polyethylene is applied by rolling to the binder layer. The tube is then cooled to room temperature with water and prepared for testing or use. In peel strength testing, this approach enabled excellent room temperature and 80 °C adhesive protective layers to be formed onto the metal pipe [51].

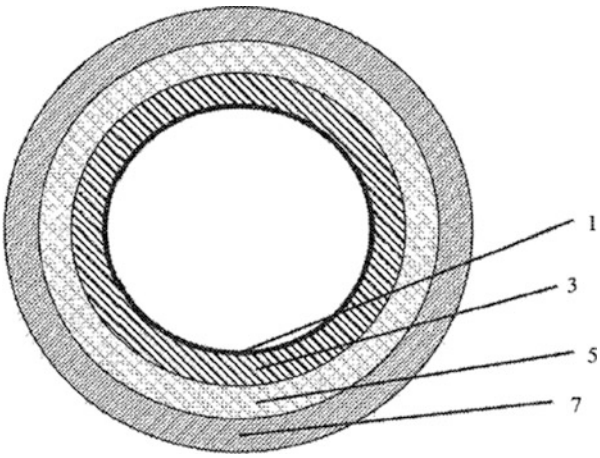

Fig. 10.12 Multi-walled tubing structure for oil and gas pipelines [51]

The ability of thermoplastic materials to replace steel and iron piping is increasing along with continued evolution of their performance properties. In another approach to manufacturing a thermoplastic, flexible pipe, maleic anhydride grafted thermoplastic resins are deployed to improve the overall performance of the flexible pipe. A schematic of the composite pipe is presented in Fig. 10.13.

Figure 10.13a provides for a cross-sectional view of the flexible pipe (**1**). The interlocked tube (**3**) is fashioned from stainless steel configured in an "S" shape and interlocked so as to provide flexibility to the pipe. A resin layer (**5**) is covering the interlocked steel (**3**) which can comprise polyamide (nylon) or PVDF, depending on the ultimate service temperature of the pipe. Covering this layer is an optional seat layer (**13**), comprised of nonwoven fabric to provide a cushion for the uneven layer below. An internal-pressure-resistant layer (**7**) is provided by metal tapes, possessing a C or Z shape cross section for interlocking purposes. The yield strength of these metallic tapes is ~1000 MPa. An axial-force reinforcement layer (**9**) is provided for by reinforcing strips (**15**) and provides a long pitch and deformable behavior with the flexibility of the interlocked tube. In Fig. 10.13c, the reinforcing strip (**30**) provides a closer detailed view where resin layers (**31**) and (**33**) form the outer layer of the strip body (**17**). Layer (**31**) comprises more adhesive power than (**33**) to prevent exfoliation between layers (**31**) and the strip body (**17**).

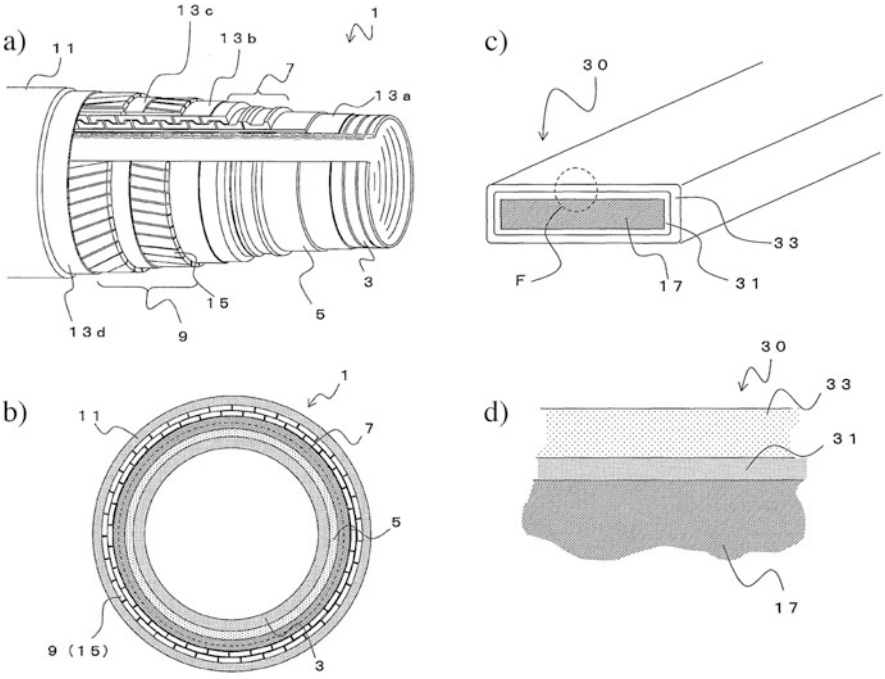

Fig. 10.13 Diagram of flexible tube for fluid transport [52]

To achieve this enhanced adhesion, maleic anhydride-modified polyethylene, maleic anhydride-modified polypropylene, and maleic anhydride-modified ethylene-vinyl acetate copolymers are preferred. Likewise, for PVDF systems, preferred adhesive enhancements are achieved with maleic anhydride-modified polyvinylidene fluoride and maleic anhydride-modified ethylene-tetrafluoroethylene (ETFE) copolymers. For polyamide systems, dimer acid-based polyamides are the preferred adhesion enhancement agents [52]. In assessing the adhesive performance, maleic anhydride-modified resins were found to exhibit good peel strength properties coupled with good corrosion resistance. Both of these properties are critical to flexible pipes, which can be several kilometers in length.

10.5.3 Films

Thermoplastic films are deployed in a wide variety of applications, ranging from safety, security, and medical films to specially designed packaging materials. There are many processes employed to produce these materials, from extrusion and blown film to extrusion coating and thermoforming. Additionally, these films can be composite in construction, incorporating fiber and other fillers to provide the correct physical properties for the application. We will focus on the application of maleic anhydride in two particular film application spaces: air bag (safety) films and packaging films.

10.5.3.1 Airbags

Since the passage of the Intermodal Surface Transportation Efficiency Act (ISTEA) (P.L. **102-240)** in 1991, 100 % of passenger vehicles produced in 1998 model year were required to have airbags to protect vehicle passengers [53]. Typically, airbags are constructed out of synthetic fabrics, such as nylon, polyester, polyethylene, polyaramid, and a barrier film to provide an airtight seal during inflation. This construction enables a flexible laminate bag structure suitable for folding, rapid unfolding, and human impact at high vehicle speed. Critical to the performance of an airbag is the adhesive strength of the lamination film, coupled with permeability, flexibility, thickness, and overall strength of the laminated film [54].

Of particular utility in airbags is polyolefin film, because it exhibits low permeability, has excellent adhesive properties, and is economical. To achieve the required adhesive properties, an adhesive layer consisting of polyolefin grafted with maleic anhydride is employed, for example, poly(ethylene-block(*b*)-octene) grafted with 0.8 wt% maleic anhydride which exhibits a peak melting temperature of 120 °C and a T_g of −60 °C. The maleic anhydride grafted copolymer is blended with two un-grafted polyolefins, a poly(ethylene-*b*-octene) (a peak melting temperature of 120 °C and T_g of −60 °C) and low-density polyethylene (a peak melting

Table 10.15 Physical properties of polyolefin film/nylon fabric airbag structure [54, 55]

Example	Ratio of barrier film to adhesive film	Adhesive film melt temperature (°C)	Film density (g/cm^3)	Film thickness (microns)	Maleic anhydride (g/m^2)	Permeability	Peel failure mode
1	30/70	120	0.903	50	0.054	0.020	Cohesive
2	30/70	120	0.903	50	0.051	0.020	Cohesive

temperature of 108 °C). These materials are extruded into a strand and then pelletized. Then these pellets are processed on a blown film extrusion line, operating to produce a two-layer polyolefin film 50 microns thick. The barrier layer #1 is a polypropylene film and the adhesive layer #2 is comprised of the three thermoplastics described above. This two-layer film is then laminated to nylon fabric by fusing sheets of nylon fabric and the two-layer polyolefin film between two moving belts at 160–177 °C for 30 s at 30 psi [54]. Physical test results on these complex structures are presented in Table 10.15.

In a second approach to producing an airbag structure, a barrier layer consisting of several un-grafted polyolefins is employed. For example, poly(propylene-*co*-ethylene) is blended with an un-grafted polyolefin, a poly(propylene) (a peak melting temperature of 160 °C). These materials are extruded into a strand and then pelletized. The pellets are processed on blown film extrusion line, operating to produce a two-layer polyolefin film 50 microns thick. The barrier layer #1 is a polypropylene film and the adhesive layer #2 is comprised of poly(ethylene-*b*-octene) grafted with 0.8 wt% maleic anhydride. This two-layer film is then laminated to nylon fabric by fusing sheets of nylon fabric and the two-layer polyolefin film between two moving belts at 160–177 °C for 30 s at 30 psi [55]. Physical test results on these complex structures are presented in Table 10.15.

Not surprisingly, results presented in Table 10.15 illustrate that while the maleic anhydride grafting enables the construction of an airbag composite film, the airbag can be fabricated out of an adhesive layer comprised solely of maleic anhydride grafted polyolefin or grafted olefin blends with un-grafted olefin.

10.5.3.2 Tamper Evident Products

Tamper evident, secure films are employed in applications ranging from letter and envelope films to labels for pharmaceutical containers and expensive electronic items. In many cases, these films are composite structures that reveal messages or other indications of changes to indicate counterfeiting and/or tampering of the article [56].

To structure secure films, composite films of different peel strengths are often employed. A schematic of a complex, tamper evident multilayer film structure is presented in Fig. 10.14.

In Fig. 10.14, the composite film (**10**) is comprised of the first film layer (**12**), a second film layer (**14**), and a third film layer (**16**). In designing this composite film

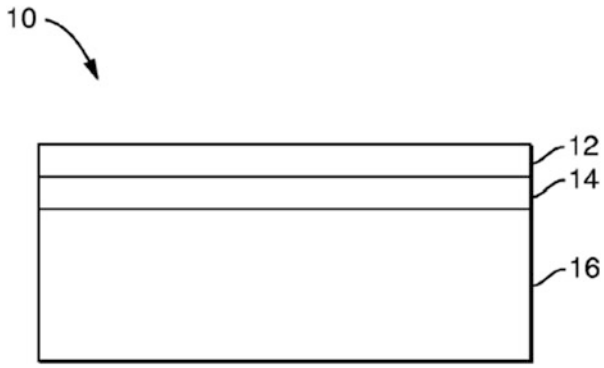

Fig. 10.14 General cross section of a composite, tamper evident multilayer film structure [56]

Table 10.16 Physical properties of polyethylene terephthalate tamper evident films [56]

Sample	Average peel strength (gf/in.)	Maximum peel strength (gf/in.)
1	4.3	4.8
2	36.7	44.5
3	3.1	3.6

structure, de-lamination strategies to indicate an improper use are designed such that layer (**12**) preferentially de-laminates from layer (**14**) or, alternatively, layer (**12**) and layer (**16**) can delaminate from layer (**14**). In one example, layers (**12** and **16**) are comprised of polyethylene terephthalate (PET) film. The middle layer (**14**) is comprised of mixture of low-density polyethylene and poly(ethylene-*co*-methyl acrylate-*co*-maleic anhydride (0.3 wt%)). In a second example, the middle layer (**14**) is comprised of mixture of low-density polyethylene and poly(ethylene-*co*-butyl acrylate-*co*-maleic anhydride (3.1 wt%)). For comparison, a third film was constructed where the middle layer (**14**) was pure low-density polyethylene [56]. Physical test results on these complex structures are presented in Table 10.16.

Interestingly, results presented in Table 10.16 exhibit a wide range of peel strength properties, ultimately depending on the composition of the middle layer. Consequently, in addition to adjusting the composition of this middle layer, the thermoplastic film of the two outside layers can also be altered, resulting in many different, customizable peel behavior possibilities.

10.5.3.3 Packaging

Flexible packaging films serve a variety of functions: gas and water barrier (to enhance food preservation), sealing and weld-ability, re-tort-ability (or hermetically sealed for long-term unrefrigerated storage), mechanical properties

sufficient to protect product from tampering, and visual appeal. The films can be found in applications ranging from pharmaceutical wrappers, to candy bar wrappers, microwave packages, potato chip bags, and flexible wine "bottles." Because of the wide variety of applications, coupled with stringent requirements by both consumer food companies and governmental regulatory agencies, packaging film specifications are typically complex multilayer structures to meet all requirements.

Perhaps the most common application for maleic anhydride in packaging is in the tie layer, for its adhesion functionality. Maleic anhydride-modified polypropylene films are typically found as solvent-free extrusion tie layers. For example, biaxially oriented polyamide film is coated with an aqueous primer layer of poly (ethylene imine). To this poly(ethylene imine) layer an extrusion coated layer of blended polypropylene grafted maleic anhydride is applied. Then a sealant layer of polypropylene is applied to finalize the construction of the packaging film. The resulting structure is inseparable in direct and soaking water tests and no delamination is observed in re-tort testing [57].

Recently, the development of recyclable packaging films has accelerated, as pressure to reduce pollution, reduce dependence on fossil fuels, and reduce accumulation of waste increases. Toward that end, bio-renewable and biodegradable polymers, derived from plant sources, have been developed to meet packaging application requirements. For example, a tie-layer composition consisting of maleic anhydride grafted onto poly(lactic acid), un-grafted poly(lactic acid), and poly (ethylene-*co*-ethyl acrylate-*co*-maleic anhydride) was coextruded between film layers of poly(lactic acid) and poly(ethylene-*co*-vinyl alcohol) [58]. This process yielded a multilayer packaging structure containing significant amounts of bio-renewable and biodegradable materials.

In fashioning blister packs, maleic anhydride grafted olefins, such as poly (ethylene-*g*-maleic anhydride) and poly(ethylene-*co*-vinyl acetate-*g*-maleic anhydride), are typically employed as tie layers between polyesters and polyvinylidene chloride (PVDC) films. In a primary example of a composite film structure, a blend of a copolyester of ethylene 1,2-cyclohexyldimethylene terephthlate (intrinsic viscosity = 0.75 dL/g and 0.52 dL/g), poly(ethylene-*co*-vinyl acetate-*g*- maleic anhydride (0.11 wt%)), a formulated polyvinylidene chloride consisting of magnesium hydroxide, a poly(ethylene-*co*-vinyl acetate-*g*- maleic anhydride (0.11 wt%)), and a blended copolyester of ethylene 1,2-cyclohexyldimethylene terephthlate (intrinsic viscosity = 0.75 dL/g and 0.52 dL/g) (first outer layer, first tie layer, core layer, second tie layer, second outer layer, respectively) is structured. In a second film structure example, a copolyester of ethylene 1,2-cyclohexyldimethylene terephthlate (intrinsic viscosity = 0.73 dL/g), a poly (ethylene-*co*-vinyl acetate-*g*- maleic anhydride (0.11 wt%)), a slightly different formulated polyvinylidene chloride comprising (Ca, Mg, Al)$(OH)_2$ SiO_2 stabilizer, a poly(ethylene-*co*-vinyl acetate-*g*- maleic anhydride (0.11 wt%)), a copolyester of ethylene 1,2-cyclohexyldimethylene terephthlate (intrinsic viscosity = 0.73 dL/g) (first outer layer, first tie layer, core layer, second tie layer, second outer layer, respectively) are all structured. These complex film structures are then processed in a blister pack line resulting in packages of dessicant silica, sealed with foil, for

Table 10.17 Properties of multilayer blister packs [59]

Property	Example 1	Example 2
Gauge, mil	10	10
Percent Haze	14.8	26.5
PVDC layer thickness, mil	0.9	2.3
Water vapor transmission rate ($g/m^2/day$)	0.752	0.27
Oxygen transmission rate ($cc/m^2/day/atm$)	1.353	0.48
Moisture vapor transmission rate (mg/day/blister)	1.12	0.42
Percent shrink	−1.56	−1.0
Elmendorf tear, g	370	250
Modulus, kpsi	180	115
Yellowness index	6	6

evaluating the effectiveness of the final assembly [59]. Testing results are presented in Table 10.17.

Results presented in Table 10.17 illustrate that modest structural changes, such as PVDC thickness, coupled with slight variations in extrusion formulations, such as magnesium oxide thermal stabilizers, can lead to significant changes in film appearance and performance. Specifically, the haze increases by a factor of two while the water vapor transmission, oxygen transmission, and moisture vapor transmission rate decrease by greater than a factor of two. These results are indicative of a strong inter-relationship between the various performance capabilities of each component.

Another approach to improving the barrier properties of packaging films is to employ metalized surfaces. Particularly for applications that require good oxygen barrier properties, it is common to employ thin layers of aluminum film. Generally, polyolefin films poorly bind to metals due to the non-reactive surface. To enhance the affinity of these materials towards metals, functional groups, such as maleic anhydride, are grafted or copolymerized to the polyolefin. Grafting of the maleic anhydride is the more economical route to functionalization of the polyolefin. To demonstrate the utility of this approach, square film thermoplastic coupons consisting of maleic anhydride grafted polyolefin are cut and then placed into a vacuum chamber. Aluminum metal is then vacuum deposited to achieve a thickness to 200 Å and used to form different packaging structures for testing purposes. To test the aluminum metal adhesion, Nucrel® 903 film was heat sealed to the metalize film at 135 °C and 40 psi for 0.5 s. Peel testing on the heat sealed film was then performed. Experimental results demonstrated that the maleic anhydride grafted to linear low-density polyethylene and very low-density polyethylene used as modifiers in polypropylene compositions is an effective approach to developing good bonding between the aluminum metal and the thermoplastic film [60].

Dielectrically heating thermoplastic films, also known as radio frequency welding, is a common technique used to seal products inside of flexible packages. This method is a noncontact method. Polyolefin films are insufficiently lossy to permit efficient welding. Consequently, polyolefins must be formulated to enable

an appropriate response to high-frequency electromagnetic excitation. In one approach, a zeolite is added, at a level of at least 5 wt%, to the polyolefin formulation. For example, a polyolefin composition containing poly(ethylene-*co*-octene) and polyethylene wax grafted with maleic anhydride is blended with Purmol® 4 zeolite (Zeochem) and extruded into a 10 mil film. Using a Callanan Radio Frequency Welder, output frequency of 27.12 MHz, Clayton set for 20, 90 % power, and a weld time of 4 s, weld strength of 9.6 pounds per inch is achievable coupled with a characteristic cohesive failure. Using this approach, structures ranging from inflatable toys, watercraft, furniture and awnings, tents, pool liners are among the many articles that can be produced [61].

10.6 Water Treatment

10.6.1 Desalination of Seawater

Water is an essential part of life. In many arid regions of the planet, there is insufficient freshwater reserve to support the human population. Consequently, to supply freshwater to these regions, desalination of seawater has emerged as a critical technology. One important seawater desalination process is known as multistage flash (MSF) [62]. From the 1960s, where less than 10 plants were operating, the technology has emerged to become the most commonly practiced technology [62, 63]. A schematic of the MSF desalination process is presented in Scheme 10.7.

The MSF desalination process is typically divided into three zones: Heating Section, Heat Recovery Section, and Heat Rejection Section. Seawater is pumped into the plant entering through condenser tubing in the heat rejection (cool side) of the plant. Once through the heat rejection section, the seawater can be mixed with brine discharge, directly discharged, and/or mixed with brine to enter the condenser tubing in the heat recovery section. As the seawater progresses through the condenser tubing, under pressure, its temperature is progressively rising. Once the seawater exits the condenser tubing in the heat recovery section, it enters the feed water heater in the heating section of the plant. At this point, heat is applied to the seawater with steam to achieve an elevated temperature, ranging from 90 °C to 115 °C. The hot seawater/brine solution is then forced back into the heat recovery section, this time into a reduced pressure chamber, which can be up to 20 m wide and 100 m long. The wide expanse of hot seawater/brine enables its partial volatilization and condensation on overhead tubing discussed previously. The condensate then collects in pans as freshwater to be pumped out of the plant for use. As the seawater/brine cascades through the plant, from hot side to cool side, seawater can be added to supplement the flow. Ultimately, the remaining seawater/brine in the heat rejection section is pumped to discharge from the plant or recirculated through the plant for more processing. A large-scale MSF desalination plant can produce between 10,000 and 65,000 m^3 of water per day [64].

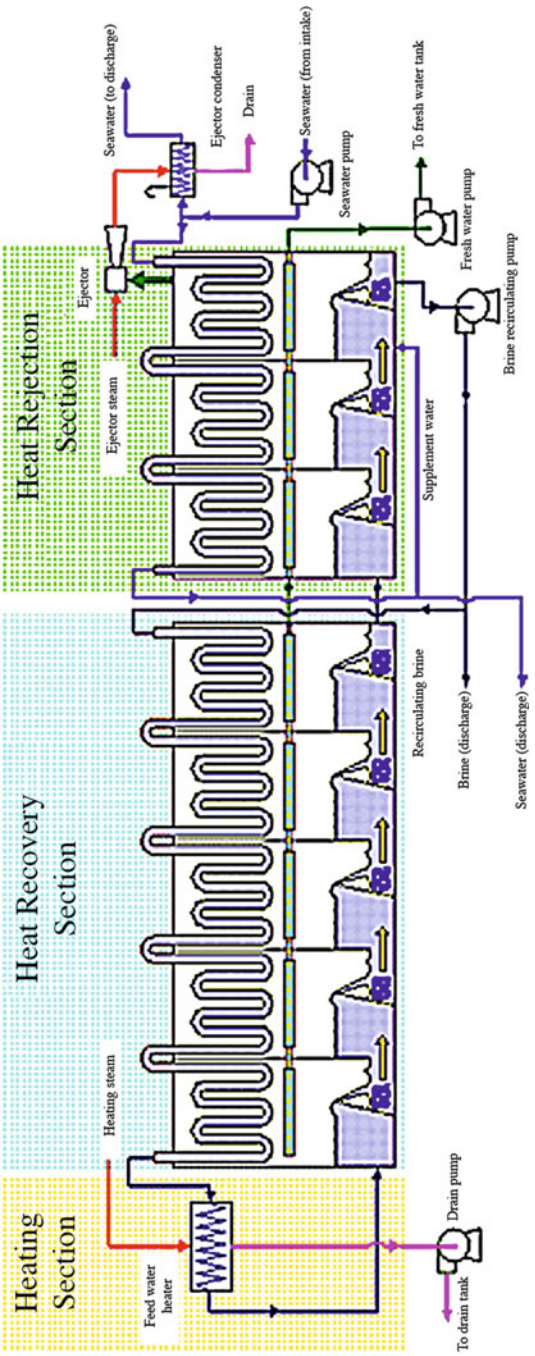

Scheme 10.7 A multistage flash (MSF) desalination process (used with permission)

Table 10.18 Physical properties of Belgard® EV, a poly(maleic acid) solution (from [67])

Property	Result
Viscosity (at 25 °C)	10–25 cSt
Solids	30–60 %
Relative density (at 20 °C)	1.16–1.19
pH value	<2
Boiling point (°C)	100–102 @ 760 mm Hg
Partition coefficient (N-Octanol/Water)	0.73

Key to successfully operating an MSF plant is the minimization of fouling. Seawater is comprised of many elements that are more than capable of forming scale. Additionally, with elevated temperature, pressure, and more concentrated seawater solutions present, fouling must be controlled and minimized to limit downtime in the production of valuable freshwater. Fouling is generally related to two types of scales: alkaline (i.e., calcium carbonates and magnesium hydroxides) and non-alkaline (i.e., calcium sulfates). To alleviate issues originating from these scaling compounds, chemical additives are employed. These chemical additives function by exhibiting an effect on at least one of three general properties: threshold (solubility), crystallization behavior, and dispersion behavior. Interestingly, while polyphosphates exhibit many of these properties, they are infrequently used because they can yield thick sludge in MSF plants that is difficult to remove due to strong adhesive properties to heat transfer surfaces [65].

A variety of water treatment polymers are prepared from maleic anhydride, in an effort to prevent scale formation. As a class, they are commonly referred to as maleates. Maleic anhydride's vicinal carboxylic acid groups are excellent chelation moieties for calcium, magnesium, and other metals commonly found in surface waters in addition to being readily polymerizable with many other monomers. The common polymer design strategies include compositional variation and polymer architecture modification (i.e., molecular weight, co-monomer ratio, charge, etc. . .) coupled with specific, target scaling salt [66]. Established examples of polymer compositions include poly(maleic acid), poly(maleic acid-*co*-acrylic acid), poly (maleic acid-*co*-sodium methallyl sulfonate), poly(maleic acid-*co*-acrylic acid-*co*-acrylamide), poly(maleic acid-*co*-styrene sulfonic acid), and poly(maleic acid-*co*-ethyl acrylate-*co*-vinyl acetate), to name but a few.

In one example of an industrial scale control polymer is poly(maleic acid) which has been evaluated as an anti-foulant in the context of a seawater desalination plant that employs multistage flash and multi-effect desalination processes [65]. The physical properties of a commercial poly(maleic acid) product, known as Belgard® EV, are presented in Table 10.18.

In this study, calcium carbonate control was evaluated for control of deposits and crystal growth inhibition. To evaluate the performance of this polymer, a test rig is assembled to simulate deposition onto metal under suitable process conditions. As schematic of this test rig is presented in Scheme 10.8.

To determine the effectiveness of chemical additives, synthetic seawater containing calcium, magnesium, chloride, sodium, carbonate, sulfate, and

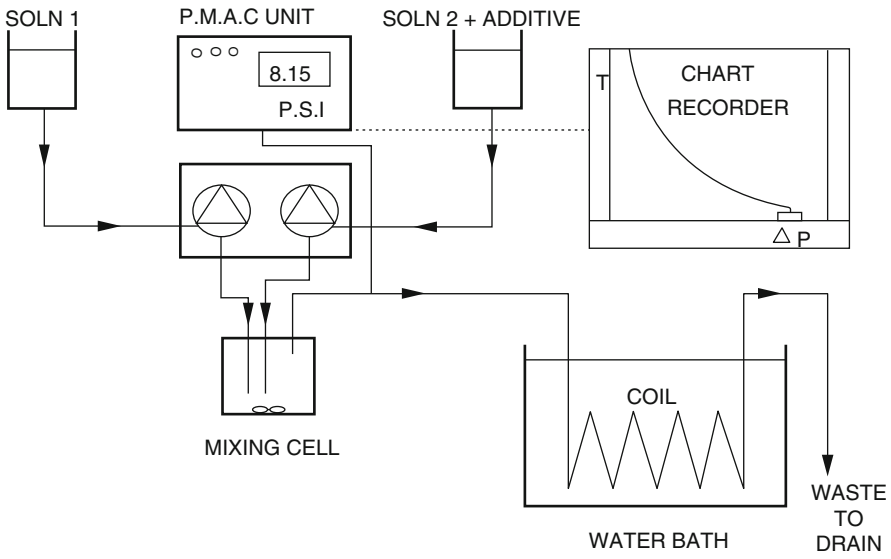

Scheme 10.8 Calcium carbonate deposition test rig [65]. Reprinted from Desalination, 124, Patel, S.; Finan, M.A., "New antifoulants for deposit control in MSF and MED plants," pages 63–74, Copyright 1999, with permission from Elsevier

potassium in water which is pH adjusted to 8.6. To this solution, the polymeric additive is added at 2 mg/L. This solution is pumped through a 316 stainless steel capillary tube which coiled and heated to 90 °C in a water bath. The time for the pressure to exhibit a change of 1 psi is determined. An increase in the length of time indicates an improvement to the inhibition performance of the additive. Using this test method, poly(maleic acid) was determined to be inferior for deposition control. However, poly(maleic acid) exhibits excellent crystal growth inhibition properties. Magnesium hydroxide control was marginal for poly (maleic acid) as well as its dispersion properties for mixtures of calcium carbonate and magnesium hydroxide scale. It was found to be excellent in inhibiting calcium sulfate [65].

To improve the overall anti-fouling performance, an additive approach with "enhanced maleates" incorporating both "polyacrylate and phosphonate" technology was developed [65]. This strategy resulted in a significant improvement in resistance to calcium carbonate deposition coupled with maintaining the good crystal growth inhibition properties. These same trends were observed for magnesium hydroxide as well. However, poly(maleic acid) continued to demonstrate superior performance in calcium sulfate inhibition [65]. Clearly, performance improvements can be realized by developing a clear understanding of each components behavior in the context of a solid blending design strategy.

10.6.2 Oil Spill Dispersants

Given our dependence on crude oil, the risk of oil spills into or onto the Earth's surface waters continues to be a significant concern, especially, given that crude oil is transported in large quantities in most regions of the globe. In recent times, several significant oil spills can be easily recalled: Deepwater Horizon [Gulf of Mexico (2010)], Amoco Cadiz [Off Brittany, France (1978)], Exxon Valdez [Alaska (1989)], and Kuwait [Gulf War (1991)] [68]. In many of these catastrophes, dispersants were applied to the oil slicks to help clean up and minimize the long-term effects on the shore-line, animals, and the environment.

In the specific case of the Deepwater Horizon event, the US EPA received notification from BP that the dispersant Corexit® EC9500A would be applied to the oil spill, from the surface and subsurface, in an effort to minimize the environmental damage and disperse the oil plume [69]. The disclosed information of Nalco's Corexit® 9500 ingredients, and their common use, is presented in Table 10.19. The physical properties of Corexit® EC9500A are presented in Table 10.20.

An important component to Corexit® 9500 is butanedioic acid, 2-sulfo-, 1,4-bis (2-ethylhexyl) ester, sodium salt (1:1), which is derived from maleic anhydride. This compound is also known as AOT, Aerosol® OT, bis(2-ethylhexyl) sulfosuccinate sodium salt, DOSS, and docusate sodium**.** A chemical structure for this compound is presented in Fig. 10.15.

Table 10.19 Nalco's Corexit® 9500 ingredients [70]

Ingredient	Common use
Sorbitan, mono-(9Z)-9-octadecenoate	Personal care products (e.g., skin creams, shampoo, emulsifiers)
Sorbitan, mono-(9Z)-9-octadecenoate, poly (oxy-1,2-ethanediyl) derivatives	Personal care products (e.g., children's bath, oral rinse, face lotion, emulsifiers)
Sorbitan, tri-(9Z)-9-octadecenoate, poly (oxy-1,2-ethanediyl) derivatives	Personal care products (e.g., body lotions)
Butanedioic acid, 2-sulfo-, 1,4-bis (2-ethylhexyl) ester, sodium salt (1:1)	Wetting agent (e.g., personal care products, beverages additives)
Propanol, 1-(2-butoxy-1-methylethoxy)	Household cleaning products
Distillates (petroleum), hydrotreated light	Household air freshener and cleaning products

Table 10.20 Physical properties of Nalco's Corexit® EC9500A [71]

Property	Result
Boiling point (°C)	147
Density (lb/gal)	7.91
pH (100 %)	6.2
Vapor pressure (37.8 °C)	15.5 mm Hg
Viscosity (at 0 °C)	177 cSt

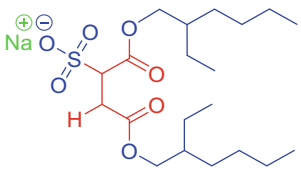

Fig. 10.15 Chemical structure of bis(2-ethylhexyl) sulfosuccinate sodium salt [72]

The surfactant properties of bis(2-ethylhexyl) sulfosuccinate sodium salt (Aerosol® OT) are a result of its chemical structure, where the polar head (organized around the sulfate anion) is neighboring a hydrophobic region (a consequence of branched alkane chains). This structure enables rapid wetting coupled to low critical micelle concentrations (CMC). For Aerosol® OT-S, a 70 % solution of Aerosol® OT in light petroleum distillate (from Cytec Industries), the surface tension in water was determined to be 26 mN/m and the critical micelle concentration (cmc) (%/wt) is 0.12 [73]. There have been many studies related to better understanding of the structure of this compound and how it affects the interfaces of air, water, and oil [74–76]. In one particularly interesting series of studies, by *Eastoe et al*., a variety of molecular structures were prepared to enable an elucidation of the impact of molecular structure to performance properties. The chemical structures of the various compounds are presented in Fig. 10.16.

Fumaryl chloride was used to prepare the compounds presented in Fig. 10.16 and is derived from maleic anhydride [77]. In studying the behavior of these various derivatives, experimental results report a trend of increased hydrophobic chain length coupled with a decrease in molecular area, as reflected in the CMC. As expected, side branching on hydrophobic chains increases the molecular area, when compared to linear sodium sulfosuccinates. Interestingly, the molecular area within a comparison of linear hydrophobic groups changes more dramatically when compared to the variation within the branched compounds. In other words, the branched compound's molecular area is generally less affected by changes to the branching structure [74]. In evaluating the microemulsion behavior of these compounds, results indicate that the structure of the hydrophobic tail determines packing at the interface. However, in assessing the air–water and oil–water interfaces, there was little difference between the molecular behavior. In forming microemulsion systems, disorder (branching) in the hydrophobe was found to be important; the ability to solubilize water can be correlated to the hydrophobe structure, and, in the case of Aerosol® OT, the interfacial film is liquid-like [75].

Beyond the fundamental understanding of Aerosol® OT, work has also been undertaken to study the effect of Corexit® 9500 on dispersing artificially weather Arabian medium crude oil in a near-shore environment [78]. To accomplish this work, numerous tanks suitable for simulating a beach shore-line, outfitted to simulate tidal cycles and various wave patterns, were employed. A profile of the wave tank is presented in Scheme 10.9.

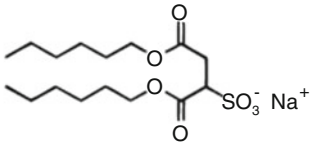

di-C6SS
Sodium bis (1-hexyl) sulfosuccinate

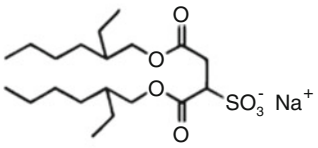

AOT① (Aerosol® OT)
Sodium bis (2-ethyl-1-hexyl)
sulfosuccinate

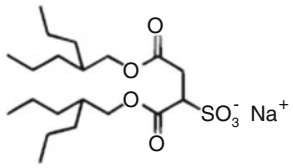

AOT②
Sodium bis (2-propyl-1-pentyl)
sulfosuccinate

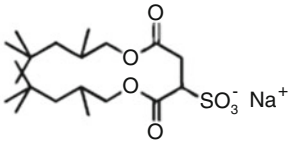

AOT③
Sodium bis (2,4,4-trimethyl-1-pentyl)
sulfosuccinate

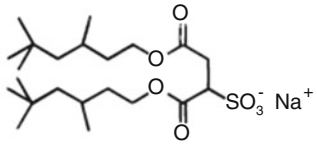

AOT④
Sodium bis (3,5,5-trimethyl-1-hexyl)
sulfosuccinate

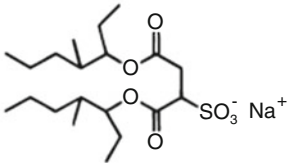

AOT⑤
Sodium bis (1-ethyl-2-methyl-1-pentyl)
sulfosuccinate

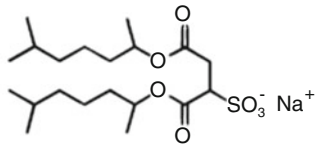

AOT⑥
Sodium bis (1,4-dimethyl-1-hexyl)
sulfosuccinate

Fig. 10.16 Schematic molecular structures of di-C*n*SS and AOT surfactants [74]. Reprinted with permission from Nave, S.; Eastoe, J.; Penfold, J., *Langmuir*, 16, pp. 8733–8740. Copyright 2000 American Chemical Society

As indicated in Scheme 10.9, various locations for sampling are located within each wave tank. Three scenarios were studied: pre-mixed oil and dispersant, oil only, and un-oiled control. Known amounts of materials were added to the tanks to enable a material balance to be determined. Samples of sediment and water are retrieved to establish locations for oil accumulation/location. This study was able to establish that timely application of dispersant can significantly reduce the accumulation of oil on the beach. In this case, less that 1 % remained in the beach sediment, when using a dispersant to oil ratio of 1–10 versus 49 % of oil remaining on beach sediment for the untreated oil [78].

Returning to the Deepwater Horizon incident, Corexit® 9500 was applied at the surface as well as below the surface of the Gulf of Mexico. A depiction of the various modes of dispersant application in the context of the incident is presented in Fig. 10.17.

Clearly, from the depiction presented in Fig. 10.17, fundamental knowledge of chemical structure, properties, and function is critical to success in the context of such complex problems. In carefully examining these images, it is easy to identify parameters such as air–water, oil–water interfaces, wave/wind action, from the image of aerial dispersant application. Likewise, current, density, salinity, emulsification/dispersion kinetics, and fluid flow can easily be anticipated as parameters to understand the subsurface application of dispersant.

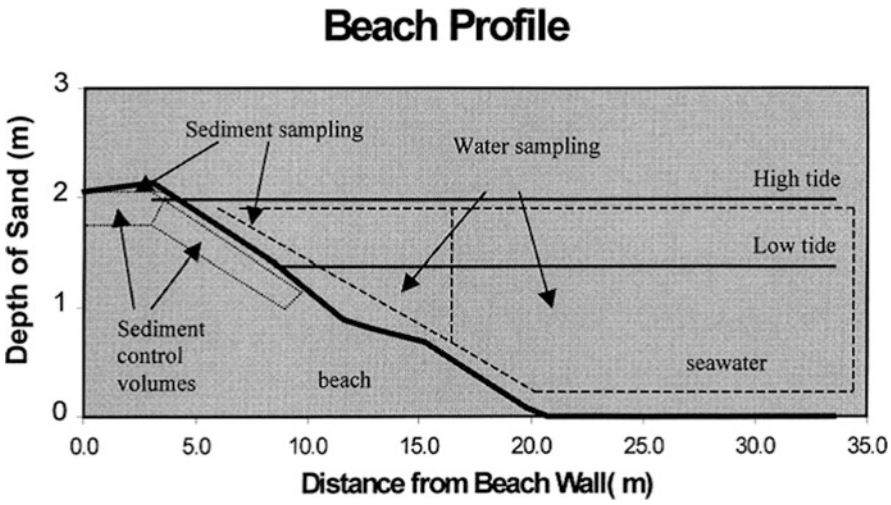

Scheme 10.9 Beach profile in wave tank. Also depicted are sampling locations for sediments and water, low/high tide delineations, and control volumes for sediment and water phases used in mass calculations [78]. Reprinted from Water Research, 34(9), Page, C.A.; Bonner, J.S.; Sumner, P.L.; McDonald, T.J.; Autenrieth, R.L.; Fuller, C.B., "Behavior of a Chemically-Dispersed Oil on a Near-Shore Environment," pages 2507–2516, Copyright 2000, with permission from Elsevier

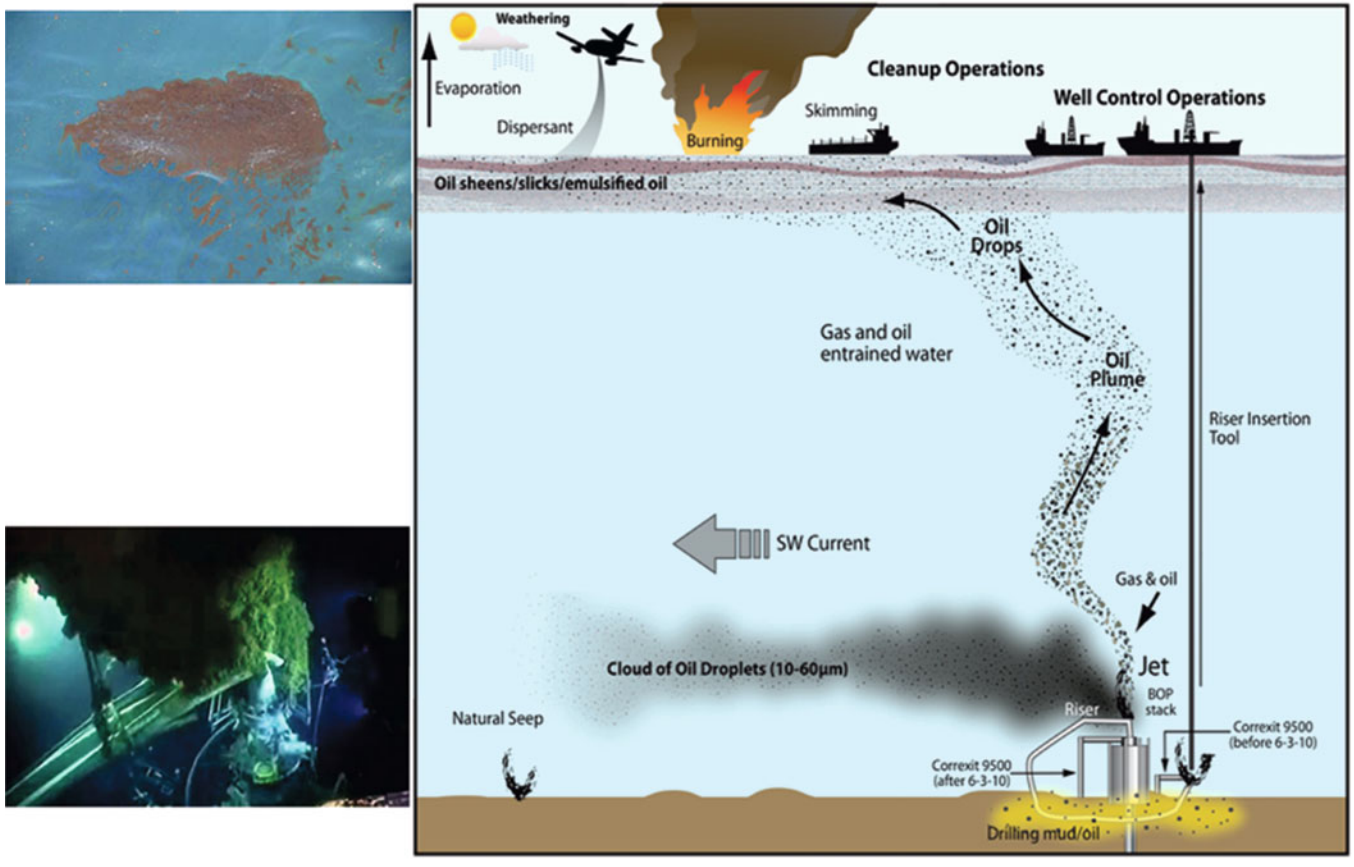

Fig. 10.17 Graphic depiction of Deepwater Horizon spill and cleanup [79]. Reprinted with permission from Atlas, R.M.; Hazen, T.C., *Environmental Science & Technology, 45* (16), pp. 6709–6715, **2011**. Copyright 2011 American Chemical Society

10.6.3 Cleaners and Detergents

The major trend in the household cleaning and detergents industry has been to improve the environmental footprint of these products. As a result, two product development themes have emerged as focus points: phosphate replacement and biodegradability. By July of 2010, all major automatic dishwashing detergent (ADW) cleaning products in the USA had removed phosphates, such as sodium tripolyphosphate (STPP). STPP was a common ingredient to ADW products [80]. STPP had developed a strong position in the ADW application because of its ability to inhibit corrosion, remove oil substances, suspend insolubles, and maintain pH while at the same time sequester calcium and magnesium ions, resulting in a pleasing appearance to clear glasses. With all of the functionalities, replacing phosphate performance in cleaners and detergents has not been an easy task for product manufactures, in terms of performance matching.

Some important phosphate alternatives have been comparatively evaluated for calcium binding power. The binding properties for these compounds are presented in Table 10.21.

In this experimental work, two maleic anhydride compositions were studied: trisodium carboxymethyloxysuccinate and poly(maleic acid). In further analyzing the results presented in Table 10.21, essentially two types of behavior are noted. First, compounds that exhibit calcium binding power <400, which are citric acid, ethylenediaminetetraacetic acid, pentasodium tripolyphosphate, and trisodium carboxymethyloxysuccinate, are all low molecular weight compounds. Conversely, high, only in this context, molecular weight compounds poly(acrylic acid) and poly (maleic acid) exhibit calcium binding power >500. Notably, nitrilotriacetic acid, a

Table 10.21 Calcium binding power of common chelating agents and polymers [81]

Composition	Theoretical calcium binding power (CBP)	Actual calcium binding power (CBP)	Stability constant (log *K*)
Ethylenediaminetetraacetic acid (EDTA)	342	340	7.0
Citric acid	520	391	4.1
Pentasodium tripolyphosphate (STPP—Na 5)	272	269	7.0
Trisodium carboxymethyloxy-succinate (CMOS—Na 3)	240	237	6.8
Nitrilotriacetic acid (NTA)	523	509	6.1
Poly(maleic acid) (Belcene 200) (MAO)	861	539	3.7
Poly(acrylic acid) (Good-rite K-700) (PAA)	695	869/620	5.3

With kind permission from Springer Science and Business Media: Journal of the American Oil Chemists' Society, "The binding of free calcium ions in aqueous solution using chelating agents, phosphates and poly(acrylic acid)," 60, 3, **1983**, pages 618–622, Chang, D.M., Table 1

low molecular weight compound exhibits a high binding power. When investigating the stability constant, however, the low molecular weight compounds are clustered together and the high molecular weight compounds are clustered, but at a lower value. The major finding of this study was to point out that calcium binding at the equivalence point, alone, is not effective at comparing sequestering compounds. Only in unique situations are materials employed at stoichiometric amounts. The author suggests that it is more meaningful to compare materials at particular concentrations. Using this strategy, the utility of polymeric compounds will become apparent because of their suitableness over a wide concentration range coupled with additional electrostatic effects benefits of polyelectrolytes [81].

In 2001, Bayer Corporation (technology acquired by Lanxess) earned the "Greener Synthetic Pathways Award" for Baypure™ CX (Sodium Iminodisuccinate): An Environmentally Friendly and Readily Biodegradable Chelating Agent Baypure™ CX (Sodium Iminodisuccinate): An Environmentally Friendly and Readily Biodegradable Chelating Agent from the U.S. E.P.A. Presidential Green Chemistry Challenge. According to the award statement, sodium iminodisuccinate, along with nearly all other aminocarboxylates, was produced from acetic acid derivatives with amines, formaldehyde, sodium hydroxide, and hydrogen cyanide. Hydrogen cyanide, in particular, is an extreme toxicity hazard. The product and process developed by Bayer is produced from maleic anhydride, water, sodium hydroxide, and ammonia, using only water as a process solvent. The only side product generated in this process is ammonia dissolved in water, which is recycled back into sodium iminodisuccinate production or used in other processes at Bayer [82]. A chemical representation of the Baypure® succinate product forms and chemical structures is presented in Scheme 10.10.

Properties of Baypure® DS100 and CX 100 are presented in Table 10.22.

An important attribute to this succinate platform is biodegradable functionality. In addition, both sodium polyaspartate and sodium iminodisuccinate exhibit strong chelation capabilities, notably for iron(III), copper(II), and calcium(II). From a toxicological and ecotoxicological standpoint, these materials are considered environmentally friendly and nonpolluting. These features have made the technology an attractive phosphate alternative in applications such as builders and bleach stabilizers for laundry and dishwashing detergents, which after use will find their effluents in surface waters around the globe [83].

In one study related to calcite ($CaCO_3$) dissolution, a mechanism for the dissolution of $CaCO_3$ via exposure to polyaspartic acid was proposed. A schematic of this mechanism is presented in Scheme 10.11.

The study proposed different mechanisms of $CaCO_3$ dissolution. In one possibility, the solubilized polymer (H_3L^{-1}) translates from the bulk to the calcite surface interface. Once at the interface, the dissociation occurs, resulting in the formation of H+ and a deprotonated polymeric ligand (H_2L^{-2}). This process enables free calcium, hydrogen carbonate, and calcium–polymer complexes to form. An unstable calcium–polymer complex will collapse in the bulk to reveal Ca^{2+} and free polymer ligands (H_2L^{2-}), resulting in primarily proton transport and

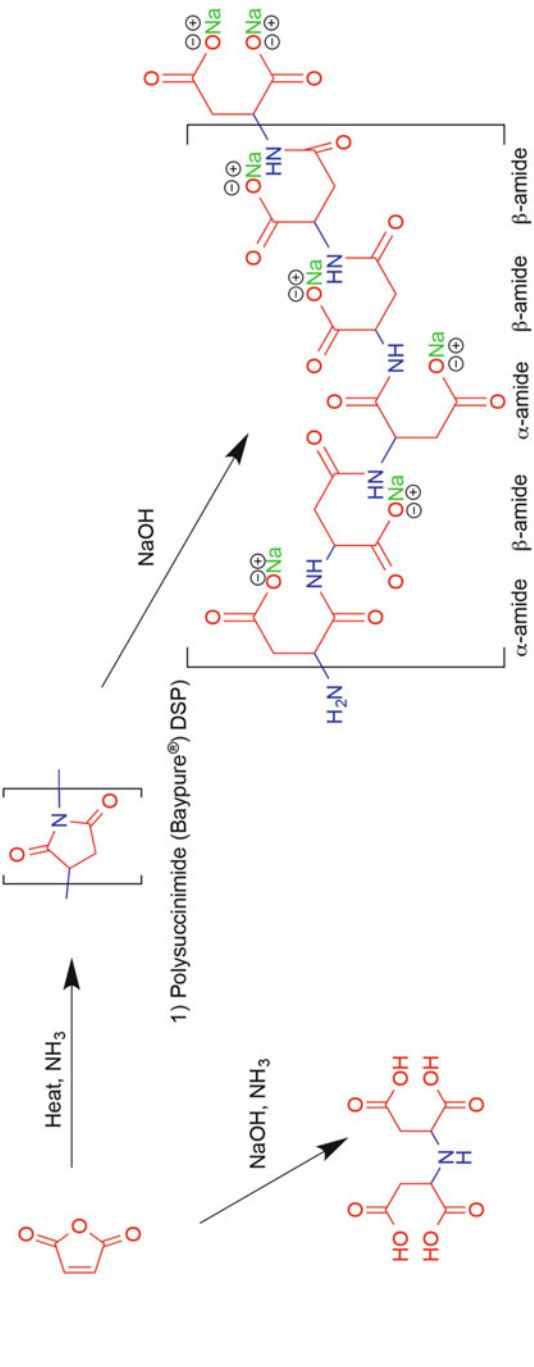

Scheme 10.10 Baypure® chemical routes and structures [83]

Table 10.22 Physical Properties of Baypure® DS 100 and CX 100 [83]

Baypure® property	DSP	DS 100	CX 100
Solids	100	100	100
Solubility in water at 20 °C (g/100 g H_2O)	Insoluble	80	56
Bulk density (kg/L)	0.50–0.60	0.55–0.90	0.5–0.7
pH (10 % solution)	–	~10.5	11.0

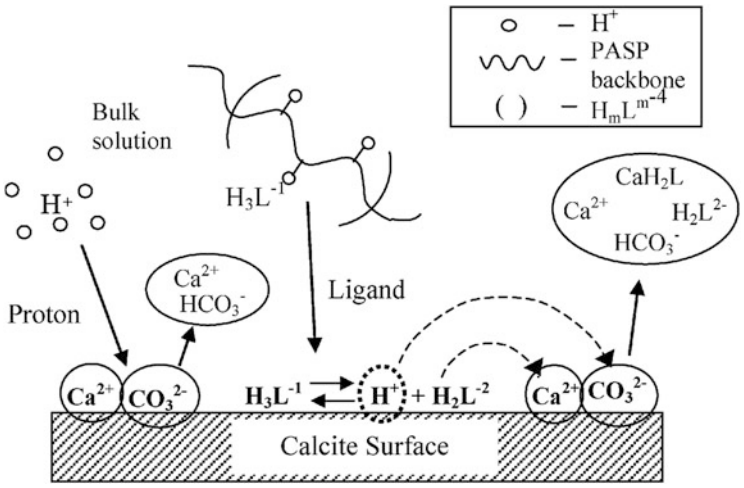

Scheme 10.11 Mechanisms of calcite dissolution in the presence of PASP (polyaspartic acid) [84]. Reprinted with permission from Burns, K.; Wu, Y-T.; Grant, C.S., *Langmuir*, 19, pages 5669–5679, Copyright 2003 American Chemical Society

dissociation functions for the polymer. If the calcium–polymer complex is stable, the complex will remain in solution and chelation is main function [84]. Note that while the chelation properties of polyaspartate is strong, the $CaCO_3$ dispersion properties, at pH = 10, are clearly superior to polycarboxylate type sequestering agents, suggesting that this is a key attribute to the functionality of this polymer [83].

One commercial example of a product that employs sodium polyaspartic acid includes Method's Smarty Dish Plus dishwasher detergent packs, which lists the polymer functionality as chelator and dispersant [85]. Another example is 7th Generation's Free and Clear Natural Dishwasher Detergent Packs, which reports using polyaspartic acid in this product [86]. For the last example, tetrasodium salt of aspartic acid or tetrasodium iminodisuccinate, products such as PortionPac LaundryPac Commercial Strength Laundry Detergent 940 Professional Use laundry detergent employ such technology [87].

10.6.4 Membranes

Seawater can also be desalinated using a membrane process. One of the largest desalination plants is the reverse osmosis (RO) membrane plant located in Ashkelon, Israel. This plant is capable of processed 110 million m^3/year of drinking water by directly pumping seawater into the plant intake to begin the water treatment process. A plant process diagram is present in Scheme 10.12.

In briefly analyzing this plant process, seawater received in the plant is pretreated, using chemicals, such as sodium hypochlorite (chlorination), sulfuric acid (pH modification), ferric chloride (coagulant), and polymers, followed by gravity filtration. Once the pretreatment process is completed, the water is pressurized into the reverse osmosis process. In this plant, a four-pass system has been designed due to the stringent requirement for chloride < 20 ppm and boron < 0.4 ppm. The plant operates $>25{,}000$ seawater and $>15{,}000$ brackish reverse osmosis membranes that are manufactured by FilmTec. Once the water passes through the reverse osmosis process, it is treated with lime to re-mineralize the water to help limit corrosion throughout the distribution network [88]. Typical formats of RO membranes include flat sheet and hollow fibers.

Osmosis takes advantage of natural effects based upon the principle of equilibrium. In a classic osmosis experiment, freshwater and brackish water are separated by a semipermeable membrane, a membrane that is permeable to water but not salt. The freshwater will flow through the semipermeable membrane to the brackish water until a new state of equilibrium is achieved. At this new equilibrium point, there will be a difference in the liquid height, where the brackish water is now elevated relative to the freshwater and the brackish water is now applying a pressure across the semipermeable membrane. This pressure is the osmotic pressure. In reverse osmosis, a pressure is applied to the brackish feed water, forcing the flow of freshwater across the semipermeable membrane to the freshwater (permeate), effectively concentrating the brackish water salt solution. In a modern reverse osmosis processes, a cross-flow filtration technique is employed. A diagram of cross-flow membrane filtration is presented in Scheme 10.13.

This simple process concept does have some significant technical challenges. For example, to maximize the water flux through the membrane, the membrane should exhibit good hydrophilicity for wetting and permeability but still demonstrate effective salt rejection. Fouling of the membrane surface, from salts or other foreign matter found in production feed waters, can lead to "blinding" the membrane surface, requiring more energy (pressure) to yield similar quantities of water. Cleaning is a remedy often employed in these processes, but performance can suffer depending on time and cleaning frequency.

Recognizing the need to improve membrane performance attributes, some researchers have developed technology that employs maleic anhydride compositions in a post-fabrication membrane treatment strategy. For example, partially saponified polyvinyl acetate was modified with maleic anhydride or succinic anhydride to yield modified poly(vinyl acetate-*co*-vinyl alcohol-*g*-maleic acid) or

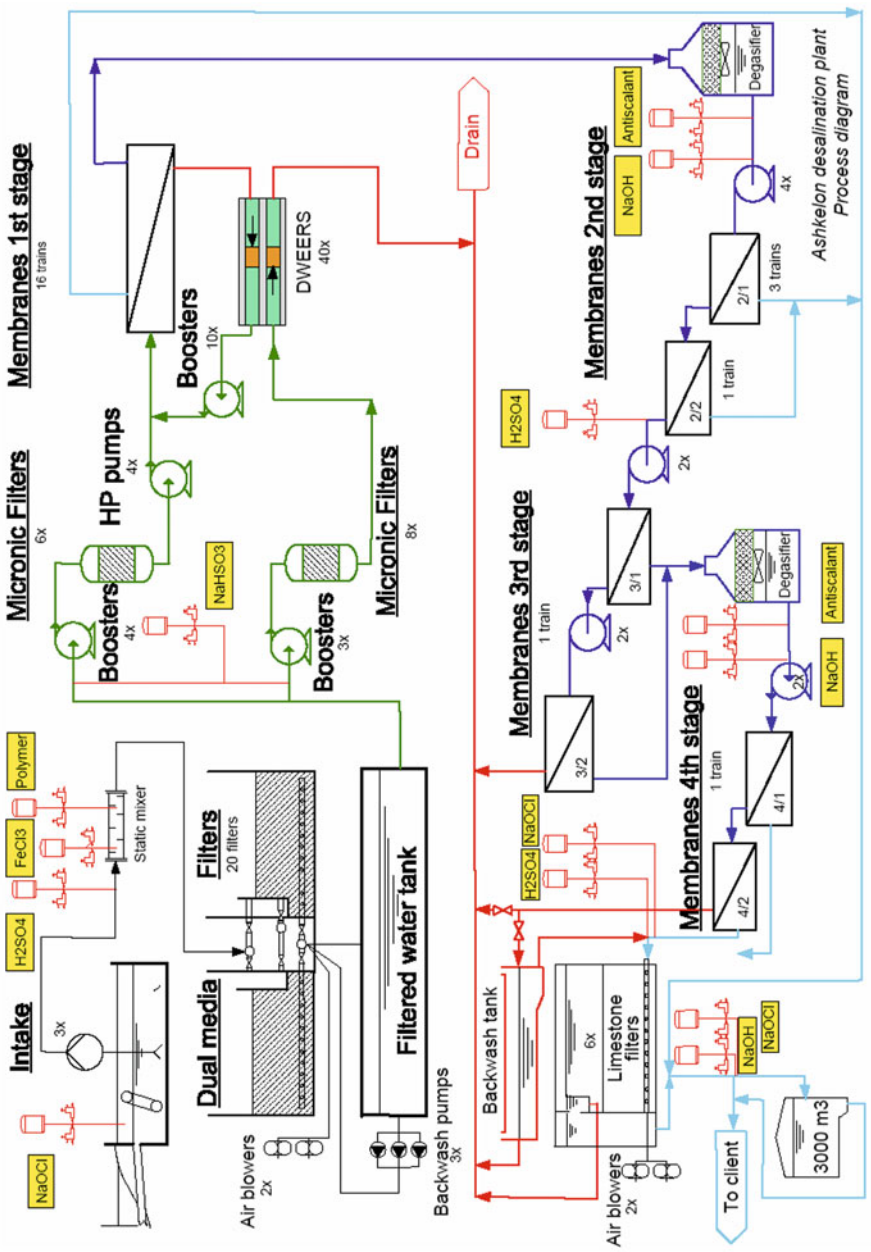

Scheme 10.12 Ashkelon reverse osmosis plant design [88]. Reprinted from Desalination, 203, Sauvet-Goichon, B., "Ashkelon desalination plant – A successful challenge," pages 75–81, Copyright 2007 with permission from Elsevier

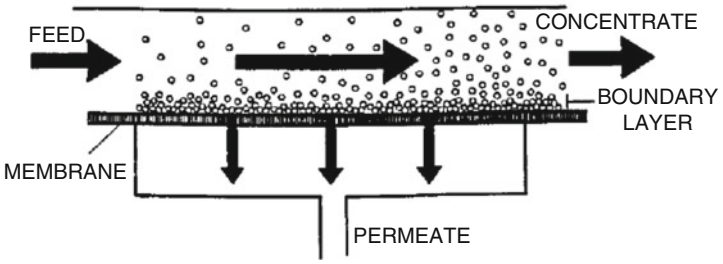

Scheme 10.13 Cross-flow membrane filtration [89]. Reprinted from FILMTEC™ Membranes: Basics of RO and NF: Desalination Technologies and Filtration Processes, Form No. 609-02002-504, with permission from The Dow Chemical Company

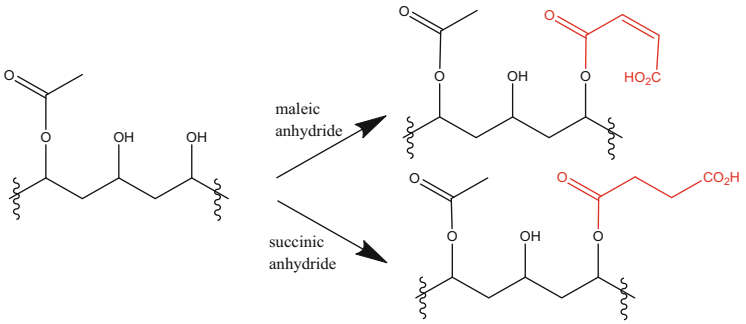

Scheme 10.14 Proposed structures of maleic and succinic anhydride treated partially saponified polyvinyl acetate

poly(vinyl acetate-*co*-vinyl alcohol-*g*-succinic acid) resin. Proposed structures for these compounds are presented in Scheme 10.14.

The impact of these modified polyvinyl acetate resins was evaluated on cellulose acetate asymmetric reverse osmosis membranes by adding the maleic anhydride-based polymer, at 100 ppm, to a 3.5 % sodium chloride feed solution and pumping through the membrane at 0.30 m^3/m^2 day. After an hour of treatment, the salt rejection improved, from 98.7 % to 99.35 % but the water flux was reduced to 0.25 m^3/m^2 day. Returning the feed solution to 3.5 % sodium chloride, the membrane performance was maintained for more than 24 h. In a similar evaluation, the succinic anhydride-based polymer, at 10 ppm, was added to a 3.5 % sodium chloride feed solution and pumped through the membrane. After 24 h of treatment, the salt rejection improved, from 97.27 % to 99.37 %, but the water flux was reduced to 0.33 m^3/m^2 day from 0.36 m^3/m^2 day. This membrane performance was maintained for more than 24 h upon returning the feed solution to just the salt solution [90]. This improvement is also depicted in Fig. 10.18.

Figure 10.18 (1) indicates the original performance of the membrane while (4) indicates the effect of the polymer treatment, which is significant in terms of

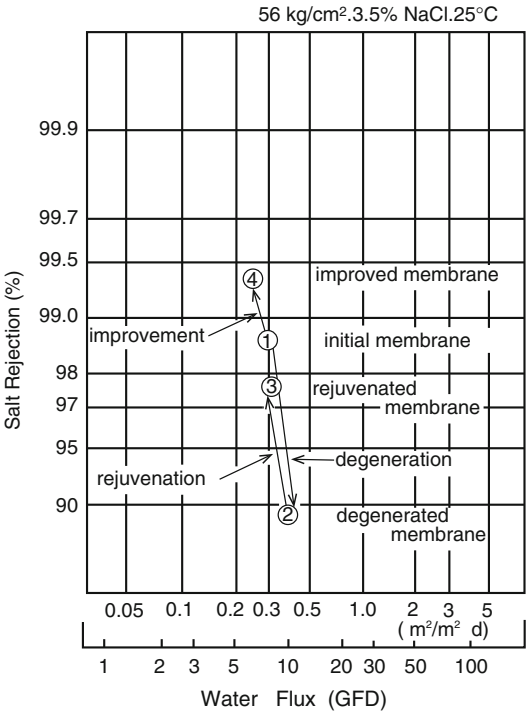

Fig. 10.18 Membrane performance improvement upon modification with maleic anhydride treated partially saponified polyvinyl acetate [90]

Table 10.23 Membrane dope solution for hollow fiber production [91]

Ingredient	Weight percent
PVDF	17
Lithium chloride	3
Poly(vinyl pyrrolidone-*co*-vinyl acetate) (PVP/VA S-630)	2.7
Poly(methyl vinyl ether –*co*- maleic anhydride) (Gantrez®)	3.1
N-methyl-2-pyrrolidone	74.2

salt rejection improvement. In a second series of experiments, the same maleic treated polymer demonstrated an ability to improve the performance of a degenerated membrane (2) to become rejuvenated (3) with a significant recovery in salt rejection [90].

In another approach, this time incorporating a maleic anhydride base polymer, poly(methyl vinyl ether-*co*-maleic anhydride), as an additive to the poly(vinylidene fluoride) (PVDF) membrane dope solution was developed for fabrication in a similar induced phase separation process as previously described [91]. An example of the hollow fiber membrane dope solution is provided in Table 10.23.

Upon finished fiber production of this membrane dope solution, the fibers were subjected to a posttreatment solution consisting of one of the following compounds: tetraethylenepentamine, tris-(hydroxymethyl)aminomethane, sulfuric acid, polyethylene glycol, calcium carbonate, or butanol. The posttreatment is performed to further functionalize the membrane surface by employing the anhydride functionality to achieve surface grafting. Towards that end, the permeability results for poly (ethylene glycol), tris-(hydroxymethyl)aminomethane, and $CaCO_3$, on 0.85 mm (OD) fibers, were most interesting. Also notable was the impact of increasing the molecular weight of the polysulfone on the improvement of mechanical properties for this formulation strategy [91].

Beyond water desalination of seawater, other materials largely consisting of water can be subjected to membrane process. Products such as wine, vegetable juice, and fruit juice are excellent examples. To process such fluids, a hollow fiber microfiltration membrane structure incorporating maleic anhydride was designed [92]. An example of this viscous membrane casting solution is provided in Table 10.24.

Once the casting solution is assembled, it is spun into fibers by passing through a small annular spinneret orifice, a shown in (**14**) in Scheme 10.15. Simultaneously, a bore fluid, consisting of *N*-methyl-2-pyrrolidone, poly(ethylene glycol) (PEG 400), and isopropyl alcohol, is pumped inside the hollow fiber (**16**) to control pore size and prevent the fiber from collapsing. The extruded fiber exits and falls freely into the coagulation bath, consisting of combinations of water, *N*-methyl-2-pyrrolidone,

Table 10.24 Membrane casting solution for hollow fiber production [92]

Ingredient	Weight percent
Polysulfone (degree of polymerization = 1700)	15
N-methyl-2-pyrrolidone	65
Poly(vinyl-2-pyrrolidone) (PVP)	5
Maleic anhydride	15

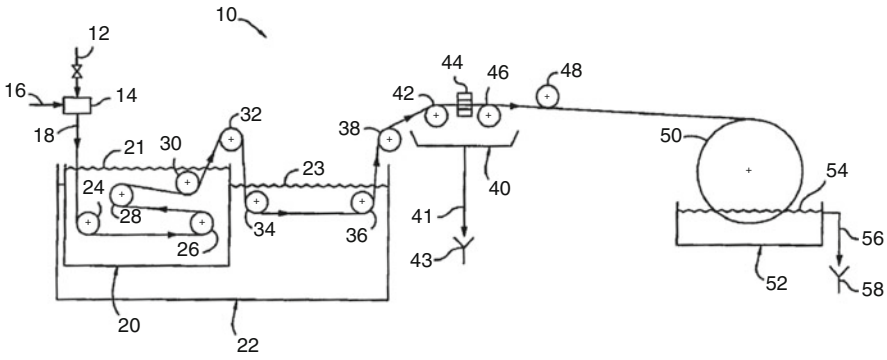

Scheme 10.15 Hollow fiber spinning system [92]

Table 10.25 Hollow fiber properties [92]

Fiber properties	Result
Outside diameter (mil)	61.2
Inside diameter (mil)	33.5
Membrane Thickness (mil)	14.3
Tensile (psi)	563
Elongation (%)	53
Pure water flux (gallons per square foot per day) (gfd) at 20 psi	27
Red wine flux (gfd) at 20 psi	184
525 nm color passage (%)	98.9

isopropyl alcohol, and poly(ethylene glycol). As the fiber travels through the coagulation bath and the leaching bath (**22**), the soluble materials are removed resulting in the formation of the membrane structure.

Once the fiber exits the leaching bath, it travels through the godet station (**40**), where water is removed via line (**41**). The fiber passes through a laser scan micrometer at (**44**). Finally, the fiber is wound onto the take-up wheel (**50**) which is partially submerged in a second leaching bath (**52**). The controlling parameters for the phase inversion and pore size are achieved by the compositions and temperatures of the bore fluid and the coagulation bath coupled with the rates of extrusion for the dope and the flow of the bore fluid, while solidification is achieved by the leaching bath composition and temperature. Maleic anhydride is employed in this process because it is highly soluble in the casting solution, remaining in the membrane during phase inversion, while exhibiting instability towards hydrolysis, contributing to the formation of pores [92].

The properties of the hollow fibers produced as described are presented in Table 10.25.

The color passage test is used to determine how much red pigment from red wine is capable of passing through the hollow fiber. The UV/visible spectrum of the wine feed, when compared to the membrane permeate, indicates nearly overlapping spectra. This test provides an indication of the ability of the membrane to maintain product color through the filtration process.

Acknowledgments The authors would like to express their sincere gratitude to Alan Fernyhough, Frank Fusiak, Randy Johnson, and Laurence Senak, all of Ashland, Inc., for their many helpful conversations/suggestions and thorough review of the manuscript prior to publication.

References

1. Bennett J (2014) In: Folkson R (ed) Alternative fuels and advanced vehicle technologies for improved environmental performance: towards zero carbon transportation. Woodhead Publishing, Waltham, MA, pp 165–194
2. Safety data sheets from Dixie Chemical Company (DDSA, June 28, 2012) and (ODSA, December 09, 2013) and Gulf Bayport Chemicals, L.P. (OSA, October 16, 2009).

(Tetrapropenylsuccinimido)-caproic acid GPS Product Safety Summary from Clariant GPSSR-27, March 2014
3. Fuel additives: use and benefits. Technical Committee of Petroleum Additive Manufacturers in Europe, ATC, ATC Document 113, September 2013
4. Baek S-Y, Kim Y-W, Yoo S-H, Chung K, Kim N-K, Kim J-S (2012) Ind Eng Chem Res 51:9669–9678
5. Groth T, Joentgen W, Linden HW, Muller N, Rother HJ, Wagner P, Kugler M (1996) Process for the preparation of polysuccinimide, polyaspartic acid and salts thereof, and the use of these compounds. US 5,543,490
6. Schmitt G, Saleh AO (2000) Corrosion 2000. Paper No. 00335
7. Seddon EJ, Friend CL, Roski JP (2010) Chapter 7: Detergents and dispersants. In: Mortier RM et al (eds) Chemistry and technology of lubricants, 3rd edn. Springer, Netherlands
8. Papke BL, Bartley LS, Migdal CA (1991) Langmuir 7:2614–2619
9. Hone DC, Robinson BH, Steytler DC, Glyde RW, Galsworthy JR (2000) Langmuir 16:340–346
10. Denso report published on http://www.globaldenso.com/en/technology/product/powertrain/files/common_rail_e.pdf, http://www.globaldenso.com/en/investors/library/annual_report/2014/about/history.html, and Zak G, Ziemianski L, Stepien Z, Wojtasik M (2014) Fuel 122:12–20
11. Doosan (2011) Doosan Stage IIIB Tier 4 Interim. D4401500-EN
12. Zak G, Ziemianski L, Stepien Z, Wojtasik M (2014) Fuel 122:12–20
13. Posselt D, Maehling FO, Lange A, Vinckier A, Kormann C (2013) Additive formulation suitable for antistatic modification and improving the electrical conductivity of inanimate material. US 8,551,365 B2
14. Thompson NES (1983) Antistatic agents for organic liquids. US 4,416,668
15. GPS safety summary, maleic anhydride. BASF, December 1 (2011)
16. http://www.accessdata.fda.gov/scripts/cdrh/cfdocs/cfcfr/CFRSearch.cfm
17. Saal C, Becker A (2013) Eur J Pharm Sci 49:614–623
18. Timolol maleate ophthalmic gel forming solution 0.25% and 0.5% package insert. NDA 20330/SLR-027, Aton Pharma and Laboratories Merck Sharp & Dohme-Chibret, 2009
19. Product Monograph, Corvert™, Pfizer Canada Inc., Control Number 086476, 2003
20. http://www.sigmaaldrich.com/catalog/product/sigma/l106?lang=en&region=US, 2014
21. Black SN, Collier EA, Davey RJ, Roberts RJ (2007) J Pharm Sci 96(5):1053–1068
22. Gutman D, Baidussi W (2009) Process for preparing malathion for pharmaceutical use. US 7,560,445 B2
23. Gervais JA, Luukinen B, Buhl K, Stone D (2009) Malathion technical fact sheet. National Pesticide Information Center, Oregon State University Extension Services
24. World Health Organization (2013) WHO specifications and evaluations for public health pesticides: Malathion. World Health Organization, Geneva
25. Cassaday JT (1951) Addition product of diester of dithiophosphoric acid and maleic acid and its esters, and method of preparation. US 2,578,652
26. Fumagalli C (2007) Succinic acid and succinic anhydride. In: Seidel A (ed) Kirk-Othmer encyclopedia of chemical technology, 5th edn. Wiley-Interscience, New York, NY
27. Song H, Lee S-Y (2006) Enzyme Microbial Technol 39:352–361
28. Alton KM, Richter WR (1941) Manufacture of succinic anhydride. US 2,245,404
29. Babcock WC, Friesen DT, Lyon DK, Miller WK, Smithey DT (2012) Pharmaceutical compositions with enhanced performance. US 8,207,232 B2
30. Onda Y, Muto H, Maruyama K (1980) Ether-ester derivatives of cellulose and their applications. US 4,226,981
31. Kang GD, Park HY, Kang JK (2012) Acetylated cellulose ether and articles comprising the same. US 2012/0296078 A1

32. Miller WK, Lyon DK, Friesen DT, Caldwell WB, Vodak DT, Dobry DE (2013) Hydroxypropyl methyl cellulose acetate succinate with enhanced acetate and succinate substitution. US 2013/0102691 A1
33. Brugel TA, Nguyen TT, Sahoo S, Tewari D, Zong Y (2014) Pharmaceutical compositions with enhanced performance and improved processability. US 2014/0249235 A1
34. Friesen DT, Shanker R, Crew M, Smithy DT, Curatolo WJ, Nightingale JAS (2008) Mol Pharma 5(6):1003–1019
35. http://www.nlm.nih.gov/medlineplus/druginfo/meds/a692049.html
36. http://www.cff.org/treatments/therapies/kalydeco/
37. Rowe W, Hurter P, Young CR, Dinehart K, Verwijs MJ, Overhoff K, Grootenhuis PDJ, Botfield M, Grossi A, Zlokarnik G, Goor FFV (2012) Pharmaceutical composition and administrations thereof. US 2012/0220625 A1
38. Highlights for prescribing information. Kalydeco® (ivacaftor Tablets, for oral use), Vertex Pharmaceuticals Incorporated (2014)
39. Thies C (2005) Microencapsulation, Encyclopedia of polymer science and technology. Wiley, New York, NY
40. Sweedman MC, Tizzotti MJ, Schafer C, Gilbert RG (2013) Carbohydr Polym 92:905–920
41. Ingredion (2012) HI-CAP® 100 technical service bulletin. Ingredion
42. Rodriguez SD, Wilderjans TF, Sosa N, Bernik DL (2013) J Food Res 2(2):36–48
43. Dokic P, Dokic L, Dapcevic T, Krstonosic V (2008) Progr Colloid Polym Sci 135:48–56
44. Lei Y, Imperiale MV, Popplewell LM, Pringgosusanto F, Gencarelli R (2014) Hybrid fragrance encapsulate formulation and method for using the same. US 2014/0044761 A1
45. Hert M, Bouilloux A, Montanari T, Fine T (2013) Impact-resistant composition based on a polyamide resin and on a blend of at least one graft copolymer with polyamide blocks and a low-density ethylene polymer. US 8,410,216 B2
46. O'Brien GS, Clay B, Partridge R (2011) Process for forming multi-layer molded articles. US 8,029,718 B2
47. O'Brien G, Bonnet A (2012) Multi-layer rotational moulding. US 8,129,024 B2
48. Lee CJ, Lee SR, Lee SJ, Seo JH (2011) Polyamide resin composition. EP 1,106,652 A1
49. Fish R (2005) Nylon composite articles of manufacture and processes for their preparation. US 2005/0037214 A1
50. Bonnet A, Werth M (2006) Multilayer pipe for transporting water or gas. US 2006/0275572 A1
51. Gerbaulet A, Devisme S, Quillet L (2012) Adhesive composition containing grafted polyethylene. US 8,247,053 B2
52. Ishii K, Manabe H, Watanabe M (2014) Flexible tube for fluid transport. US 8,636,037 B2
53. Houston DJ, Richardson LE (2000) Policy Stud J 28(3):485–501
54. Van DJ, Mcgee R, Batra A, De WP (2010) Polyolefin film having an improved adhesive layer for airbag applications. WO 2010/042335 A1
55. Van DJ, Mcgee R, Batra A, De WP (2010) Polyolefin film having an improved barrier layer for airbag applications. WO 2010/042334 A1
56. Culbertson EC, Muschelewicz (2012) Tamper evident composite film. US 8,158,230 B2
57. Trouilhet Y (2004) Multilayer film. US 2004/0229058 A1
58. Chopinez F, Laffargue J, Predel JL, Rauline D, Devisme S (2010) Coextrusion binders on a renewable/biodegradable basis. US 2010/0266858 A1
59. Bonekamp JE, Skapik SJ (2012) Coextruded multilayer film structure. WO 2012/037180 A1
60. Leboeuf C (2008) Polypropylene modification for improved adhesion of polypropylene-based multilayer packaging film structure to vaccum deposited aluminum. US 2008/0286586 A1
61. Weaver LB, Hu Y, Rego JM (2013) High frequency weldable polyolefin compositions containing zeolites. WO 2013/096705 A1
62. El-Dessouky H, Alatiqi I, Ettouney H (1998) Desalination 115:155–179
63. National Water Commission (2008) Emerging trends in desalination: a review. National Water Commission, Canberra, Australia, November

64. World Health Organization (2007) Desalination for safe water supply: guidance for the health and environmental aspects applicable to desalination. World Health Organization, Geneva
65. Patel S, Finan MA (1999) Desalination 124:63–74
66. Amjad Z, Zuhl RW, Zibride JF (2003) Factors influencing the precipitation of calcium-inhibitor salts for industrial water systems. Association of Water Technologies, September
67. BWA Water Additives (2012) Material safety data sheet, Belgard® EV. Version No. 4, September 4
68. Casselman A (2010) 10 biggest oil spills in history May 7. popularmechanics.com
69. Suttles DJ (2010) May 19, 2010 Addendum 2 to dispersant monitoring and assessment directive. May 20
70. Schor E (2010) Ingredients of controversial dispersants used on gulf spill are secrets no more. The New York Times, June 9; http://www.nalcoesllc.com/nes/1602.htm
71. Corexit® EC9500A Safety Data Sheet, Version 4.3. Nalco Environmental Solutions, Sugarland, Texas, Date Issued March 1, 2012
72. Screening-level hazard characterization: sulfosuccinates category. USEPA Hazard Characterization Document, September 2009
73. Cytec Industries Inc. (2013) Specialty additive: Aerosol® surfactants. PAT-0005-A-EN-WW-10E. Cytec Industries Inc.
74. Nave S, Eastoe J, Penfold J (2000) Langmuir 16:8733–8740
75. Nave S, Eastoe J, Heenan RK, Steytler D, Grillo I (2000) Langmuir 16:8741–8748
76. Nave S, Eastoe J, Heenan RK, Steytler D, Grillo I (2002) Langmuir 18:1505–1510
77. Kyrides LP (1955) Organic syntheses, Coll vol 3, p 422; (1940) vol 20, p 51
78. Page CA, Bonner JS, Sumner PL, McDonald TJ, Autenrieth RL, Fuller CB (2000) Wat Res 34 (9):2507–2516
79. Atlas RM, Hazen TC (2011) Environ Sci Technol 45(16):6709–6715, http://pubs.acs.org/doi/pdf/10.1021/es2013227
80. McCoy M (2011) Chem Eng News 89(4), January 11
81. Chang DM (1983) JAOCS 60(3):618–622
82. The Presidential Green Chemistry challenge: award recipients 1996–2009. Published by U.S. E.P.A., 744K09002, June 2009
83. Baypure General Product Information. Lanxess, LXS-FCC170, October 2005
84. Burns K, Wu Y-T, Grant CS (2003) Langmuir 19:5669–5679
85. http://methodhome.com/shop/smarty-dish-plus-24ct/
86. http://shop.seventhgeneration.com/dishwasher-tabs/?sku=41
87. Material Safety Data Sheet, LaundryPac Laundry Detergent No. 940, PortionPac Chemical Corporation, No. 900, November 2011
88. Sauvet-Goichon B (2007) Desalination 203:75–81
89. FILMTEC™ membranes: basics of RO and NF: desalination technologies and filtration Processes. Form No. 609-02002-504, Dow Chemical Company
90. Kurihara M, Harumiya N, Uemura T (1984) Semipermeable membrane treated with modified vinyl polymer. US 4,478,717
91. Muller HJ (2007) Modified membranes. US 7,300,022 B2
92. Ji J, Dicecca C, Schulz EM, Mehta M, Stead D, McKinley D, Koch DH (2006) Method of making and using a hollow fiber microfiltration membrane. US 7,070,721 B2

Index

O.M. Musa (ed.), *Handbook of Maleic Anhydride Based Materials*,
DOI 10.1007/978-3-319-29454-4

T